eman ta zabal zazu

Universidad del País Vasco

Euskal Herriko Unibertsitatea

Azobenzene-appended iridium(III) and ruthenium(II) complexes.

Screening of applications.

PhD Thesis

Ainara Telleria Echaniz

2016

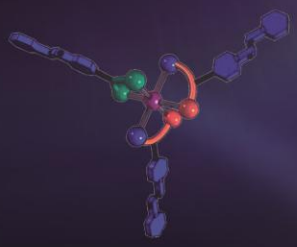

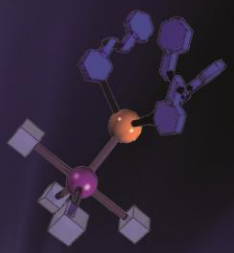

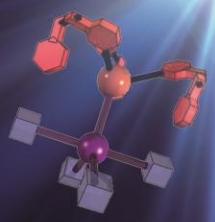

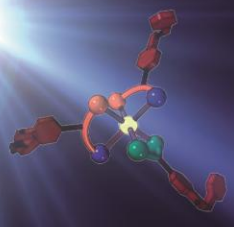

Azobenzene-appended iridium(III) and ruthenium(II) complexes. Screening of applications.

PhD Thesis

Ainara Telleria Echaniz

2016

Dra. Zoraida Freixa Fernández, Profesora de Investigación Ikerbasque en la Universidad del País Vasco,

CERTIFICA:

Que el presente trabajo, titulado "Azobenzene-appended iridium(III) and ruthenium(II) complexes. Screening of applications." que presenta Ainara Telleria Echaniz para la obtención del título de Doctor, ha sido realizado bajo mi dirección.

Donostia, Julio 2016

Dra. Zoraida Freixa

ACKNOWLEDGEMENTS

In this section I would like to thank all the people who helped me during this period.
I hope that I did not forget anyone.

En primer lugar a mi directora de tesis, Zoraida, por darme la oportunidad de realizar este trabajo contigo. Quería decirte que antes de conocerte nunca me había imaginado que pudiese llegar hasta aquí. Gracias por motivarme y animarme cuando las cosas no salían a la primera, por estar siempre ahí para cualquier cosa que he necesitado, en todo momento, a todas horas. Por todo lo que me has enseñado y por confiar en mí.

A Itziar Zumeta, porque si no hubiese sido por ti, esto no habría sido posible. Gracias por pensar en mí y por llamarme aquel día, hace cinco años. Aunque el tiempo pase sigues estando ahí, ayudándome en todo momento. A Jorge, porque hemos estado desde el principio juntos, por todos los momentos que hemos compartido, por esos momentos de risas en el laboratorio y en medio de las charlas. A Martin, por todos los momentos que hemos compartido, esos veranos en el laboratorio y congresos que nos han dejado tan buenos recuerdos. A Virginia, por cuidar de mi y estar siempre dispuesta a escucharme. Arani, zaren bezalakoa izateagatik, bai lanerako eta bai lagun bezala, beti guztia emateko prest zaudelako. A las nuevas incorporaciones del grupo, Borja y Maitane, ha sido un placer trabajar con vosotros, espero que todo os vaya genial en esta nueva etapa. También les quiero agradecer a todos los compañeros con los que he trabajado durante estos años, en especial a Henrik, Abel, Jonathan, Roberto, Miguel, Nacho, Itxaso, Itziar y Susan. Y a todos los profesores de Química Inorgánica.

I want to thank to Piet van Leeuwen, Jairton Dupont and David Mecerreyes, for giving me the opportunity to go to Brazil. It was a pleasure to work in LAMOCA, I want to thank all the people that I met there, especially Jones, Ale and Meike. Eu também queria agradecer as pessoas maravilhosas que me acolheu em sua casa durante esse período, Arthur, Julio, Madelon e Mofo. Foi ótimo morar com vocês, e graças a vocês a minha estadia em Porto Alegre foi muito mais fácil. Durante este estancia también tuve la oportunidad de conocer a dos personas que son muy importantes para mí, Cris y Dayana. Gracias por todos los momentos que pasamos juntas, en especial las fiestas del Basco Loco y la de mi cumple, fueron geniales. A Dayana le quiero agradecer especialmente la despedida del aeropuerto, nunca lo olvidare.

Nire familia guztiari. Aitari, ikasketek duten garrantzia erakutsi, momentu guztietan ikastera animatu eta horretarako aukera emateagatik. Amari, momentu zailetan aurrera egiten laguntzeagatik, beti nire alboan egoteagatik eta beti elkarri laguntzen egongo garelakoan. Nire ahizpari, niretzat oso garrantzitsua zarelako, eta momentu txar nahiz onetan beti hor zaudelako. Oihani, tesi honen diseinu eta irudiekin laguntzeagatik. Tia Olatzi, niretzat oso berezia zarelako eta nitaz asko arduratzen zarelako. Nire lehengusu Mikeli, ordenagailuarekin izandako arazo guztiak konpontzeagatik eta azkenaldian emandako animo guztiengatik. Amama eta attitteri, txiki-txikitatik ni hain ondo zaintzeagatik eta niregatik horrenbeste arduratzeagatik. Amonari, nahiz eta orain gure artean ez egon, beti emandako maitasunarengatik.

Nire lagunei, bereziki Oihanari, beti alboan izan zaitudalako eta tesi honen prozesu guztia jarraitu duzulako. Eskerrikasko momentu guztietan eskainitako arretagatik, beti entzun eta laguntzeko prest egoteagatik. Nire kuadrilla osoari, denboraldi guzti honetan egindako afari eta parranda guztiengatik eta batik bat azken aldiko animoengatik, (ingo al deu? ingo ezteu ba!).

Eta nola ez gure etxeko printzesa txikiari, Nahikariri. Zure irribarrearekin nire egunak alaitu eta arazo guztiak ahazten zaizkidalako. Baita bidean dagoen ilobatxoari ere, etorkizunean igaroko ditugun momentu guztiengatik.

The work performed in the present doctoral thesis has been possible thanks to the funding of:

Ministerio de Economía y Competitividad y Fondo Europeo de Desarrollo Regional (FEDER). Projects: CTQ2011-23333 and CTQ2015-65268-C2.
UPV-EHU. Project: GIU13/06.
Basque Government. Saiotek Program. Projects: S-PE13UN020, S-PE12UN044 and S-PE11UN029.
ICIQ/IKERBASQUE collaboration agreement. Pls Z. Freixa, PWNM van Leeuwen.

GRAPHICAL ABSTRACTS

Chapter 1. Photoswitchable molecules

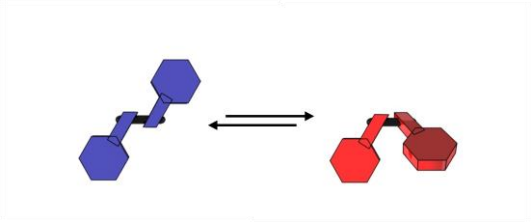

In this chapter a brief overview on photochromic compounds is presented. It focuses on a specific photoswitchable molecule able to change its properties by action of light, the azobenzene. A summary of already published azobenzene-containing bipyridine and phosphine ligands is included.

Chapter 2. Ligands syntheses and characterization

All the azobenzene-containing pyridine, bipyridine and phosphine ligands involved in this thesis are presented in this chapter, together with the study of their photochromic behaviour. Several bipyridines (without photochromic units) with different electronic properties are also presented.

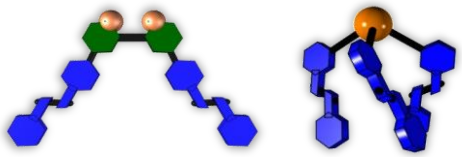

Chapter 3. Cyclometalated Ir(III) bipyridine complexes for dye sensitized solar cells

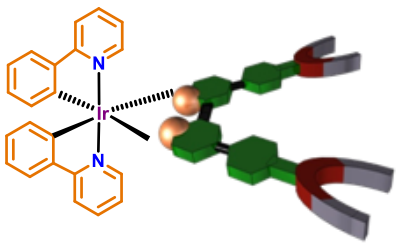

The potential application of iridium(III) complexes containing two phenylpyridine and one 2,2'-bipyridine-type ligands as dyes for DSSC is presented in this chapter. Two different anchoring groups are incorporated at 4,4'-positions of the bipyridine, and the iridium complexes combining them with four different phenylpyridine ligands (one of them containing an azobenzene fragment) are studied. The different stability when anchored on TiO_2 surface together with the performance of DSSCs sensitized with these Ir(III) complexes is discussed.

Chapter 4. Luminescent Ir(III) bipyridine complexes

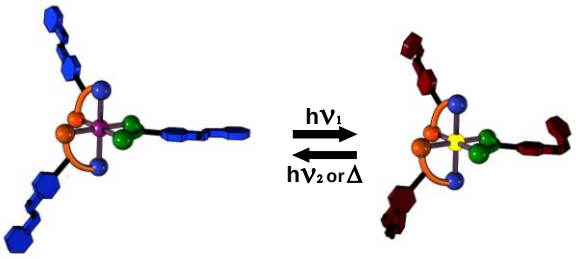

In this chapter, Ir(III) complexes containing two phenylpyridine and one 2,2'-bipyridine ligands are presented. They were intended to be used as phosphors for low energy consumption light-emitting devices. Complexes incorporating azobenzene moieties were synthesized to study the possibility to modify the color of the emission with incident light.

Chapter 5. Ru(II) bipyridine complexes for the solvolytic dehydrogenation of amine-borane adducts

In this chapter, half-sandwich Ru(II) complexes are presented and used as precatalysts for the hydrolytic dehydrogenation of amine-borane adducts. A family of [Ru(*p*-Cym)(bipy)Cl]Cl complexes was synthesized and the efficiency of these precatalysts in the generation of hydrogen by hydrolysis of amine-borane adducts was correlated with Hammett parameters of the substituents on the bipyrdine. Complexes incorporating azobenzene-containing pyridine, bipyridine and phosphine ligands were also tested and the influence of the isomerization of the azobenzene on their catalytic activity was studied.

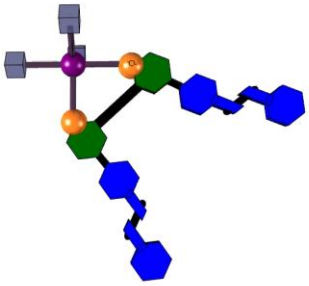

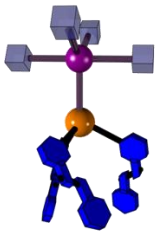

Chapter 6. General conclusions and future work

TABLE OF CONTENTS

GLOSSARY OF TERMS AND ABBREVIATIONS

AB	ammonia-borane
APT	Attached Proton Test
AZO	Azobenzene
azoppy	2-((4-azobenzene)phenyl)pyridine
bipy	2,2'-bipyridine
bipyBr	4,4'-dibromo-2,2'-bipyridine
Brppy	2-(4-bromophenyl)pyridine
COSY	Correlation Spectroscopy
Cp*	pentamethyl cyclopentadienyl
DMAB	dimethylamine-borane
DSSC	Dye-Sensitized Solar Cell
DTE	Dithienylethene
EA	Elemental Analysis
E_{red}	Reduction potential
E_{ox}	Oxidation potential
ESI-MS	Electrospray Ionization Mass Spectrometry
fac	facial
FF	Fill Factor
FG	Fulgimides
Fppy	2-(2,4-difluorophenyl)pyridine
FTO	Fluorine doped Tin Oxide
HAcO	Acetic acid
HSQC	Heteronuclear Single Quantum Correlation
HR-ESI-MS	High Resolution Electrospray Ionization Mass Spectrometry
IPCE	Incident Photon-to-current Conversion Efficiency
I_{SC}	Short circuit current
J_{SC}	Short circuit current density
KIE	Kinetic Isotope Effect
LC	Ligand-Centered
LCD	Liquid-Crystal Display
LEC	Light-emitting Electrochemical Cell
LLCT	Ligand-to-ligand Charge Transfer
MAB	methylamine-borane
mer	meridional
MLCT	Metal to Ligand Charge Transfer

MO	Molecular Orbitals
N3	Black dye
n-BuLi	n-Butyllithium
NMR	Nuclear Magnetic Resonance
OLED	Organic Light-Emitting Diode
Rf	Retardation factor
p-Cym	*para*-cymene
phen	1,10-phenanthroline
Ph	phenyl
ppm	parts per million
ppy	phenylpyridine
PSS	Photostationary State
quat	Quaternary
SOC	Spin-Orbit coupling
SP	Spiropyrans
TBA	tetrabutylammonium cation
TD-DFT	Time-Dependent Density Functional Theory
TBAB	*tert*-butylamine-borane
TEAB	triethylamine-borane
TMAB	trimethylamine-borane
UV	Ultraviolet
UV-Vis	Ultraviolet-Visible
V_{OC}	Open circuit voltage
vs	versus

CHAPTER 1

PHOTOSWITCHABLE MOLECULES

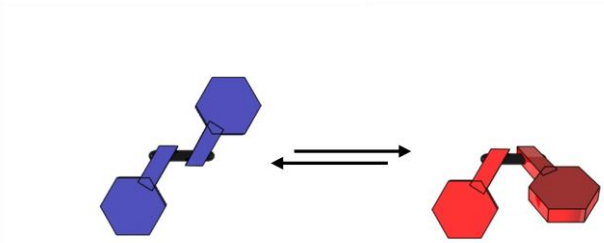

In this chapter a brief overview on photochromic compounds is presented. It focuses on a specific photoswitchable molecule able to change its properties by action of light, the azobenzene. A summary of already published azobenzene-containing bipyridine and phosphine ligands is included.

1.1. INTRODUCTION

Photochromic compounds are those able to reversibly isomerize, being at least one (either the direct or the reverse) process induced by light. These compounds switch, by action of light, between at least two forms, changing their physical and/or chemical properties such as emission intensity or wavelength, refractive index, electronic conduction, electrochemical response, magnetic interactions, self-assembling behaviour of molecules, solubility, etc. In the last decades, photoswitchable materials have been developed by incorporation of photochromic fragments (molecular switches) in their structure. They are intended for the development of a new generation of sophisticated molecular devices named “smart chemical systems”.

Among the so called molecular switches, those that have attracted most interest are dithienylethenes (DTEs), spiropyrans (SPs), fulgimides (FGs) and azobenzenes (AZOs) (Figure 1.1). The photoisomerization of the three first examples implicates reversible cyclization whereas the latter involves the *E*/*Z* isomerization.[1,2]

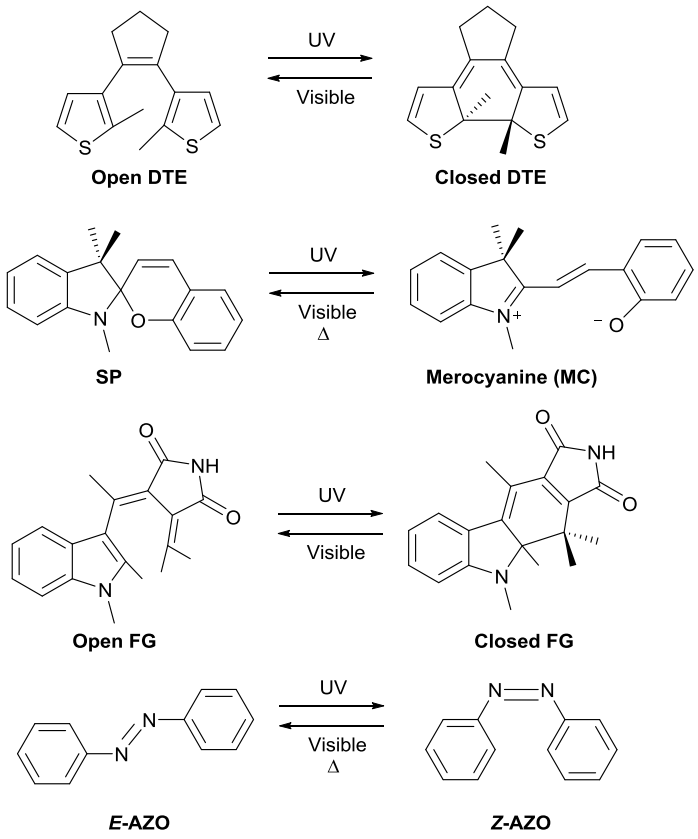

Figure 1.1. Photoswitchable molecules.

Dithienylethenes have attracted special interest due to the high fatigue resistance of the ring closing and opening processes, retaining its photochromic performance over a large number of cycles. The two isomers of DTE (open and closed) have notably different optical and electronic properties, for instance, the open form is colorless and

the closed one is colored. The photoisomerization of spiropyrans, triggered by UV light, leads to a merocyanine zwitterionic molecule. The reverse process can be induced by visible light or heat. The isomerization of fulgimide also involves ring closing and opening processes, implicating the change of the color from colorless or yellow (open) to green (closed). Both fulgimide isomers are thermally stable and as in the case of DTEs, the reverse (opening) isomerization cannot be induced by heating, but by selective visible-light irradiation.[2,3]

1.2. AZOBENZENE

Among the different molecular switches known, probably azobenzene is the one most frequently used for the construction of photochromic materials. It contains two phenyl groups linked through two nitrogen atoms bonded with a double bond (formally a 1,2-diaryldiazene). The photochromicity of azobenzene was discovered in 1937. G. S. Hartley published for the first time that the exposure of an acetone azobenzene solution to sun-light converted it partially to what he identified as the *cis* isomer, which could be selectively extracted due to its different polarity compared to the original *trans*-azobenzene (see Figure 1.2). He also realized, upon evaporation of the solvent, that the reverse *cis*-to-*trans* isomerization was slower in solid state than in solution.[4] Since then, azobenzene (and its derivatives) has been widely studied for different applications, mainly due to its synthetic simplicity, together with the important steric and electronic changes that experiences upon isomerization.

In the thermodynamically most stable form, the azobenzene adopts a planar *trans* (*E*) conformation, exhibiting extended electronic conjugation along the whole molecule. It is well known that when it is irradiated at a specific wavelength, isomerization from the *trans* (*E*) to the *cis* (*Z*) form occurs. The *cis* isomer of the azobenzene is an angular C_2 symmetric molecule, due to the steric repulsion between the *ortho* hydrogen atoms of both aromatic rings, and the electronic conjugation existing in the *trans* form is disrupted. The reverse process (*cis*-to-*trans* isomerization) takes place either by irradiation at a different (specific) wavelength or by heating. Eventually, this *cis*-to-*trans* isomerization occurs spontaneously in the dark (Figure 1.2).[5]

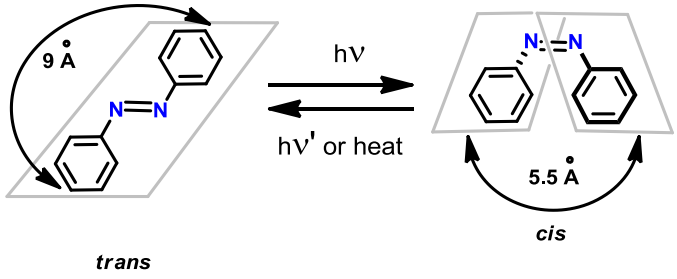

Figure 1.2. Photoisomerization of azobenzene.

Although many studies have been done to clarify the mechanistic pathway of the isomerization of the azobenzene and its derivatives, it still remains unclear and it is subject of controversy. Two main mechanisms have been proposed for the photoisomerization process: they are the so called inversion and rotation mechanisms (Figure 1.3). This description is an oversimplification (the mechanism operative strongly depends on the azobenzene substituents) but it is useful to rationalize most of the experimental observations.

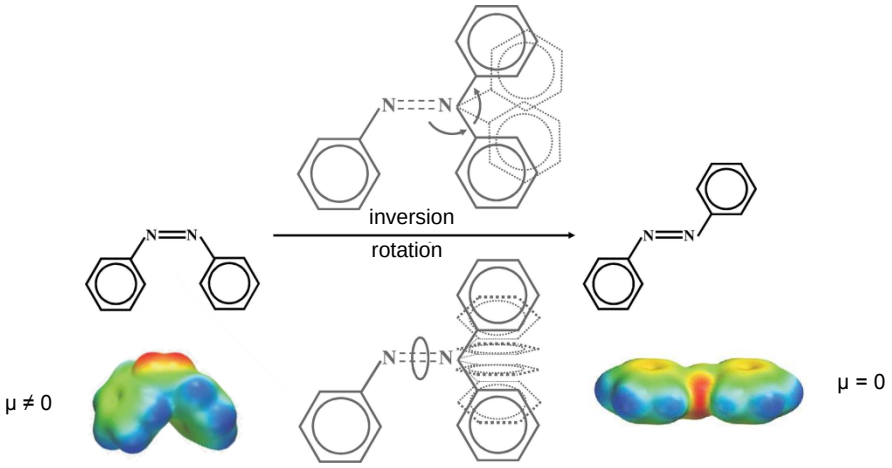

Figure 1.3. Proposed mechanisms for the photoisomerization of the azobenzene and spacefilling models colored by electrostatic potential (red—negative to blue—positive) to highlight the change in dipole moment upon isomerization. Figures extracted from literature.[6,7]

The inversion mechanism can be described as progressive increase of one N–N–C angle (from 120° to 240°, passing through 180°) while the C–N–N–C dihedral angle remains fixed at 0°. In the second one, the rotation changes the C–N–N–C dihedral angle while keeping the N–N–C angle fixed at 120°. Probably, both mechanisms are operative to a larger or lesser extent in many cases, and therefore even a mechanism named inversion-assisted rotation has also been claimed in some examples.[8]

To explain in a simplified manner the electronic transitions involved in the photoisomerization of azobenzene, a qualitative representation of the potential energy diagram of this process is shown in Figure 1.4. Reported studies showed that when the *trans* isomer is excited to the S_1 (n,π*) or S_2 (π,π*) excited states, in both cases there is a rapid decay to the *cis* S_1 (n,π*) excited state potential curve. Then, the relaxation to the *cis* ground state (S_0) occurs. As the *trans* ground state is lower in energy than the *cis* one, and there is a low isomerization barrier, the latter eventually evolves to *trans* S_0 spontaneously or by heat.[6,9]

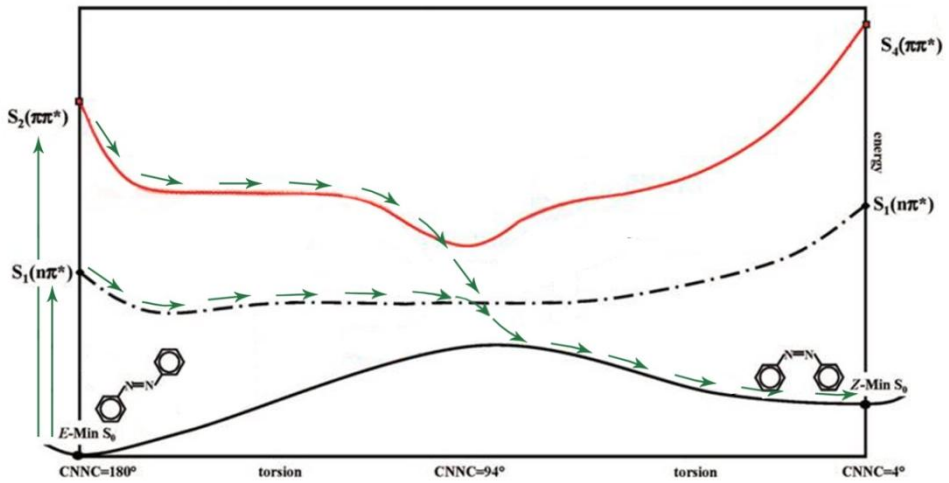

Figure 1.4. Potential energy diagram of the photoisomerization of the azobenzene. Figure extracted from literature.[6]

As mentioned before, with the *trans*-to-*cis* isomerization the distance between the aromatic rings decreases and the planarity of the molecule is lost. With this process, the photophysical properties and dipole moment of the molecule are also modified, which is reflected, for example, in the ^{1}H-NMR spectra. The aromatic signals of *cis* isomer appear at higher fields than the signals of the *trans* isomer, due to the shielding produced for the close-lying aromatic rings.[5] The photoisomerization also alters the absorption spectra of the azobenzene moiety. The *trans* isomer presents two characteristic bands in the UV-Vis region, one intense band around 320 nm, attributed to a symmetry allowed π→π* transition and a weaker band around 450 nm that corresponds to the symmetry forbidden n→π* transition. The symmetry allowed π→π* band is weaker in the *cis* than in the *trans* isomer, and the opposite happens to the symmetry forbidden n→π*. Moreover the π→π* band of the *cis* isomer is slightly blue shifted compared to the band of the *trans* isomer. Therefore, UV-Vis absorption spectroscopy permits monitoring the isomerization process due to the different intensity and small shift of the characteristic absorption bands of the azobenzene in the *E* and *Z* forms. When azobenzene isomerizes from *E* to *Z* the absorption band corresponding to the π→π* absorption decreases gradually while the band corresponding to the n→π* absorption increases (Figure 1.5).[5,8]

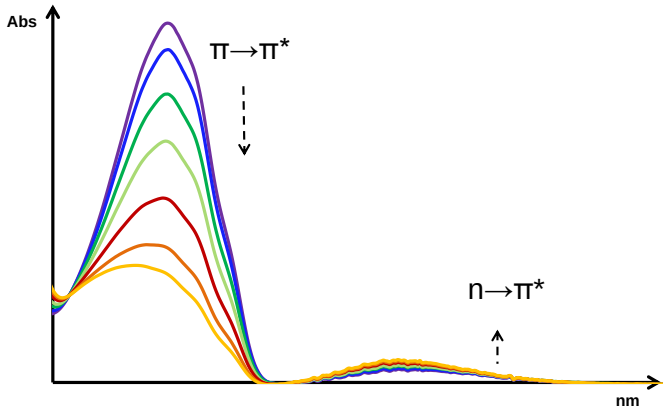

Figure 1.5. Representation of the change in the UV-Vis absorption spectra for the isomerization of the azobenzene from *E* to *Z*.

The wavelength of the light to induce both processes differs with the substituents of the aryl groups, but in general the *trans*-to-*cis* isomerization is prompted by irradiation between 320 and 380 nm (irradiation close to the center of the band π→π*). The reverse process is induced by 400–450 nm wavelength light (irradiation close to the band n→π*).[5,10]

Incorporating electron-withdrawing or electron-donating substituents in the π-system of the azobenzene, produces a shift in the π→π* transition band. The same result is obtained when the azobenzene is linked to a transition-metal. This shift has been of great interest (specially looking for red-shift) to develop photoswitches able to isomerize closer to the visible region.[11,12]

1.3. PHOTOSWITCHING-BASED APPLICATIONS OF AZOBENZENES

The photoisomerization of the azobenzene fragments incorporated into larger molecules has been reported to cause significant changes at the molecular or even macromolecular level, which has been exploited for diverse applications. Many examples are known, and a personal selection of the most appealing ones will be described here.

The first one is a molecular machine constructed with azobenzene fragments that operates as a molecular lift.[13] Azobenzene fragments were adsorbed on the surface of a gold electrode, between a quartz support and a mercury-drop electrode (Figure 1.6). Through the irradiation of azobenzene moieties with a specific wavelength light, *trans*-to-*cis* and the reverse *cis*-to-*trans* photoisomerization was induced at will, producing a up-down movement of the mercury-drop, and a change in the electrodes-distance. This device was described as “both an optoelectronic switch and an optomechanical cargo lifter”.

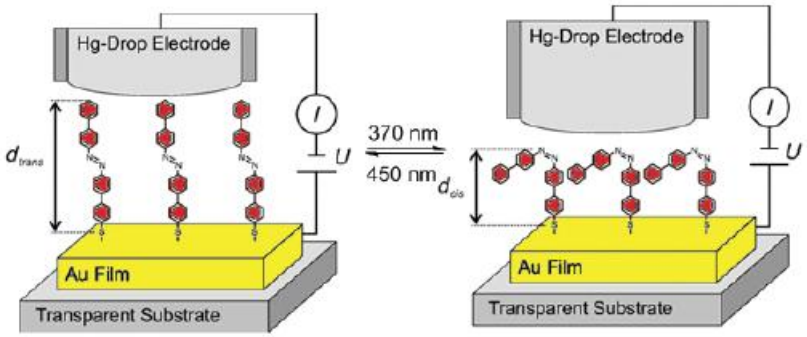

Figure 1.6. Molecular lift based on azobenzene fragments. Figure extracted from literature.[5]

A family of nanovehicles containing azobenzene fragments was also designed to simulate the movement of a worm (Figure 1.7). They were based on the mechanical folding-unfolding process involved in the photoisomerization of the azobenzene fragment that was located in the middle of the molecular machine.[14]

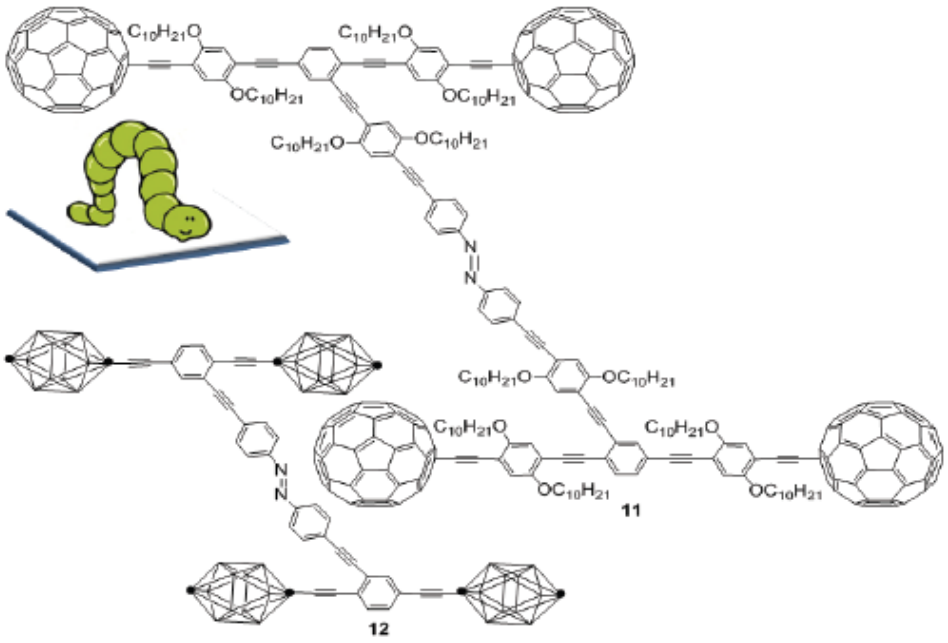

Figure 1.7. Nanovehicles designed to simulate the movement of a worm. Figure extracted from literature.[5]

Another attractive application of azobenzenes is the construction of self-erasable and rewritable materials. The selected example is based on azobenzene coated gold and silver nanoparticles that were reported by Klajn *et al*.[15] These nanoparticles were embedded to a gel matrix and upon irradiation by UV light they formed aggregates changing their color. As it is shown in Figure 1.8, an image can be written into the film irradiating with UV light through a mask. Irradiating with visible light, heating or spontaneously the drawing is erased.

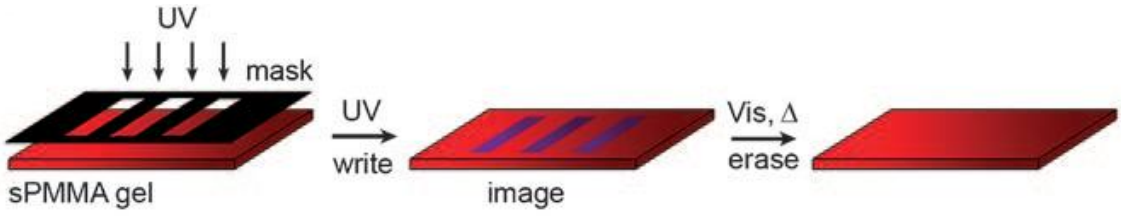

Figure 1.8. Drawing in a self-erasable nanoparticles film. Figure extracted from literature.[15]

After erasure time, it is possible to rewrite into the same film as many times as desired (Figure 1.9). These films can store information temporary using nanoparticles as ink and gel as paper.

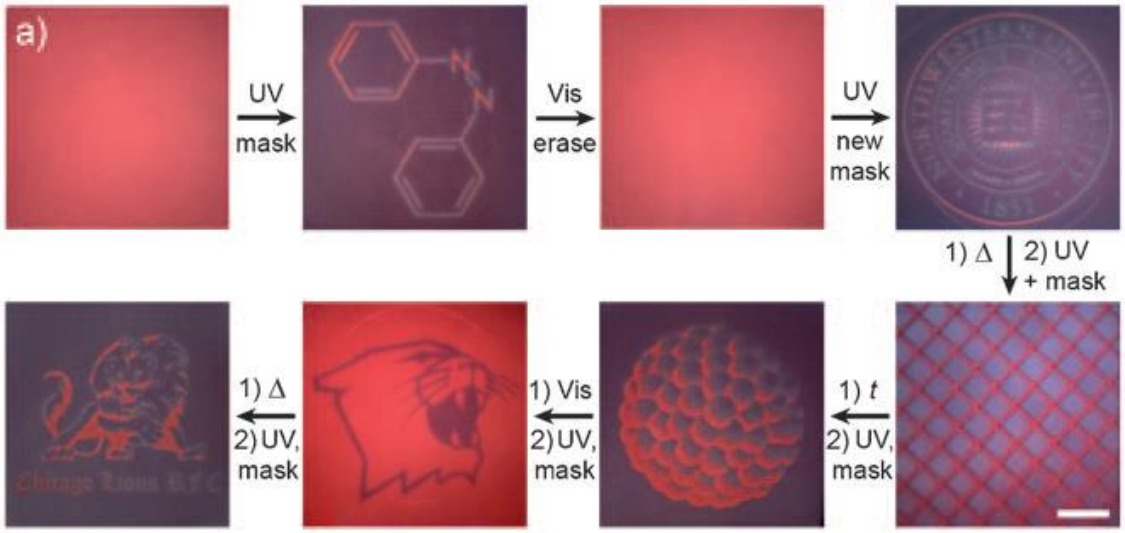

Figure 1.9. Sequential writing into and erasing from Au nanoparticles film. Figure extracted from literature.[15]

One of the most spectacular applications of the azobenzene found in the literature is an azobenzene-containing liquid-crystal film that is bent through *trans*-to-*cis* isomerization and reverted to the initial state through the reverse process.[16] As it is shown in Figure 1.10, the film was irradiated at 366 nm (*trans* to *cis*) to bent it and by irradiation at a wavelength longer than 540 nm (*cis* to *trans*) the film was reverted to the initial state. Even more spectacular was the fact that, when using polarized light, depending on the sense of the polarization of the irradiation, the film was bent in different directions.

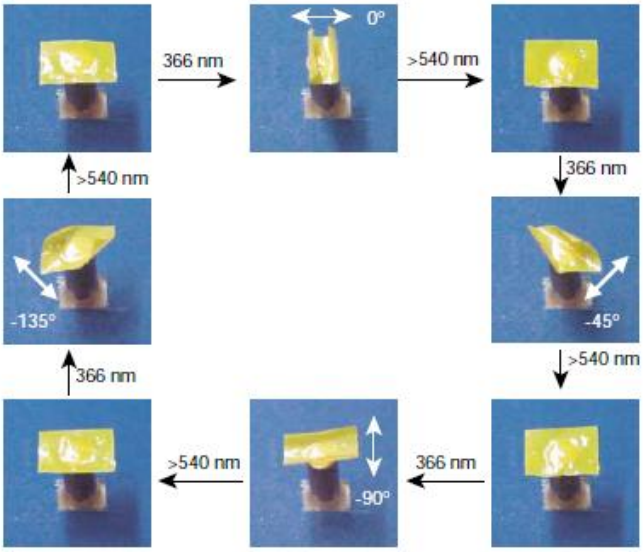

Figure 1.10. Film bending produced by photoisomerization of azobenzene. Figure extracted from literature.[16]

The azobenzene unit has been also incorporated in organometallic compounds for different applications. For example, a molecular machine constituted by an azobenzene fragment and a ferrocene which was able to move as scissors was reported (Figure 1.11).[17,18] The photoisomerization of the azobenzene simulated the opening and closing movements.

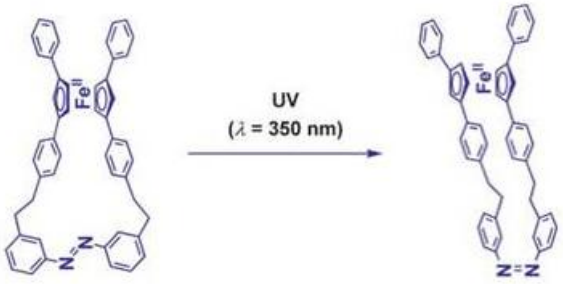

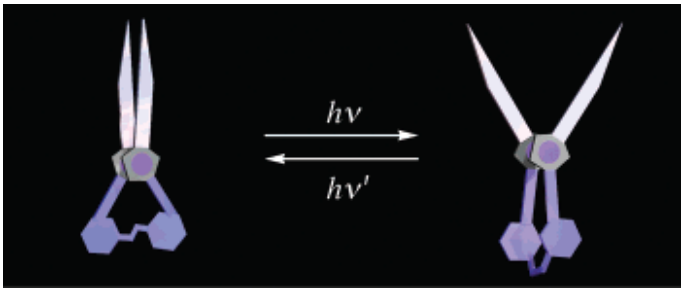

Figure 1.11. Open-close movement induced by photoisomerization of the azobenzene. Figures extracted from literature.[17,18]

A tetranuclear gold(I) macrocyle containing two azobenzene fragments was also reported, in which the photoisomerization of the azobenzenes was controlled by

addition or removal of silver(I) ions.[19] The photoisomerization was inhibited with the addition of silver(I) ions, as a consequence of the coordination of silver(I) to alkynyl units and when silver ions were removed the capacity of azobenzene units to isomerize was recovered (Figure 1.12).

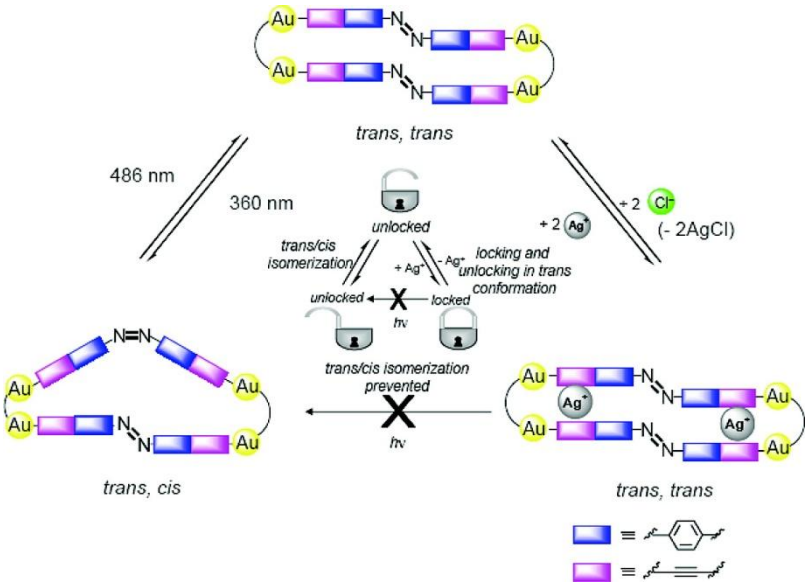

Figure 1.12. The "locking and "unlocking" mechanism of a gold(I) macrocycle induced by photoisomerization of the azobenze. Figure extracted from literature.[19]

The incorporation of photochromic units in metal complexes has attracted great interest for two different reasons, depending on the final purpose of the compound. On the one hand due to the possibility of modifying the isomerization capacity of the photochromic unit as a consequence of the coordination to the metal center and on the other hand, because eventually the properties of metal-complexes can be changed by light.

1.4. COMPLEXES CONTAINING THE AZOBENZENE ON THE BIPYRIDINE

In spite of the wide number of coordination complexes based on 2,2'-bipyridine ligands, to the best of our knowledge, only the groups of Wenger, Nishihara, Otsuki and Amar published examples of transition metal complexes of azobenzene-containing bipyridines.

Wenger *et al*. synthesized a photoswitchable azobenzene-containing bipyridine rhenium tricarbonyl complex.[20] The synthetic route used toward the azobenzene-containing bipyridine is shown in Scheme 1.1. First, 2,2'-bipyridine was oxidized and nitrated to obtain 1-oxide-4-nitro-2,2'-bipyridine. The subsequent reduction of the nitro groups gave the amino substituted bipyridine.[21] Finally, through the condensation of 4-amino-2,2'-bipyridine and nitrosobenzene the desired azobenzene-containing bipyridine was obtained, and it was coordinated to the rhenium center (Scheme 1.1).[22]

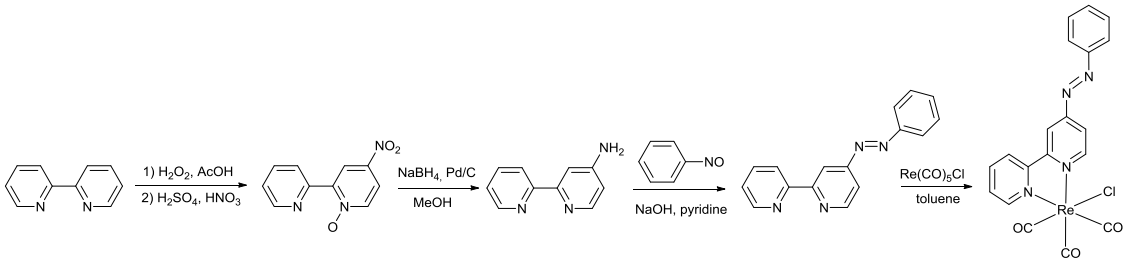

Scheme 1.1. Synthetic route toward rhenium complexes containing the azobenzene fragment in 2,2'-bipyridine ligands.

Unfortunately, when they studied the photoisomerization process on this compound, they realized that it was inhibited, which was attributed to the existence of low-lying energy levels that produced non-productive relaxations from either S_1* or S_2* excited states of the azobenzene.

The group of Nishihara published related 2,2'-bipyridines with either one or two azobenzene fragments. They used synthetic routes based on the same condensation reaction mentioned before.[23a] For the synthesis of 2,2'-bipyridines containing two azobenzene fragments, two steps were necessary prior to the condensation. A Suzuki cross-coupling between 4,4'-dibromo-2,2'-bipyridine and 3-nitro-phenylboronic acid and the reduction of the nitro groups (Scheme 1.2).

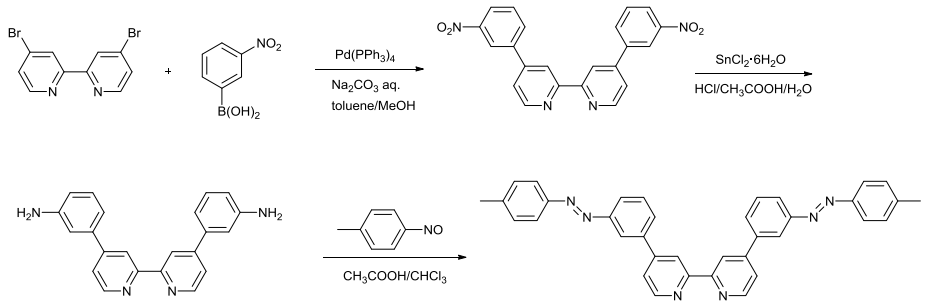

Scheme 1.2. Synthetic route toward bis azobenzene-containing 2,2'-bipyridine ligand.

The synthetic route used by Nishihara's group toward 2,2'-bipyridines containing only one azobenzene fragment was based on the same condensation reaction to form the azobenzene but more steps were needed to obtain the required monosubstituted 4-(3-amino)-phenyl-2,2'-bipyridine that was reacted with nitrosotoluene (Scheme 1.3). Kröhnke´s methodology for the synthesis of pyridines was used to obtain the 4-(3-nitro)-phenyl-2,2'-bipyridine that was reduced to 4-(3-amino)-phenyl-2,2'-bipyridine. Both *meta*- and *para*-substituted ligands containing one azobenzene fragment were synthesized following this methodology.[23,24,25]

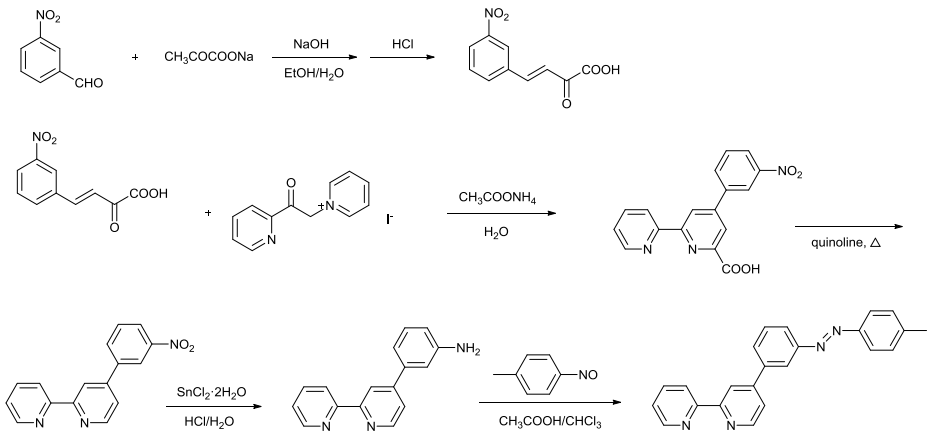

Scheme 1.3. Synthetic route toward mono azobenzene-containing 2,2'-bipyridine ligand.

Tris-bipyridine cobalt complexes containing one or two azobenzenes per bipyridine were synthesized with the aforementioned ligands (Chart 1.1).[23] The photoisomerization of these cobalt complexes was studied and it was demonstrated that the number of azobenzene fragments in the molecule does not affect the ratio of *cis*-azobenzenes in the photostationary state (PSS). However, the isomerization of the azobenzene depends strongly on the oxidation state of the cobalt center. The isomerization from *trans* to *cis* was more efficient for Co(II) than for Co(III) complexes containing either one or two *meta* azobenzene-bipyridine ligands.[23a] Additionally, it was proved that the proportion of *cis*-isomerized azobenzene in the PSS was larger for complexes containing *meta*-substituted azobenzenes than for *para*-substituted complexes.[23b] These results suggest that a stronger electronic communication between the metal center and the azobenzene was established in the latter.

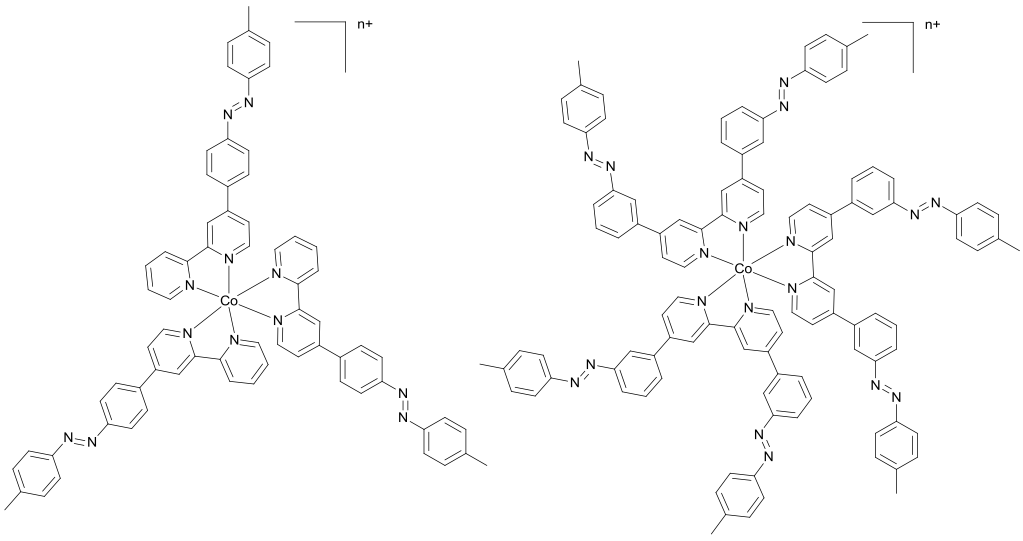

Chart 1.1. Cobalt complexes synthesized by the group of Nishihara.

They also reported azobenzene-appended 2,2'-bipyridine copper and platinum compounds. In the case of copper complexes the photoisomerization was

synchronized with a ligand exchange with 2,2'-bipyridine and a redox reaction of the Cu(II)/Cu(I) redox couple, in a very elegant manner (Figure 1.13).[26]

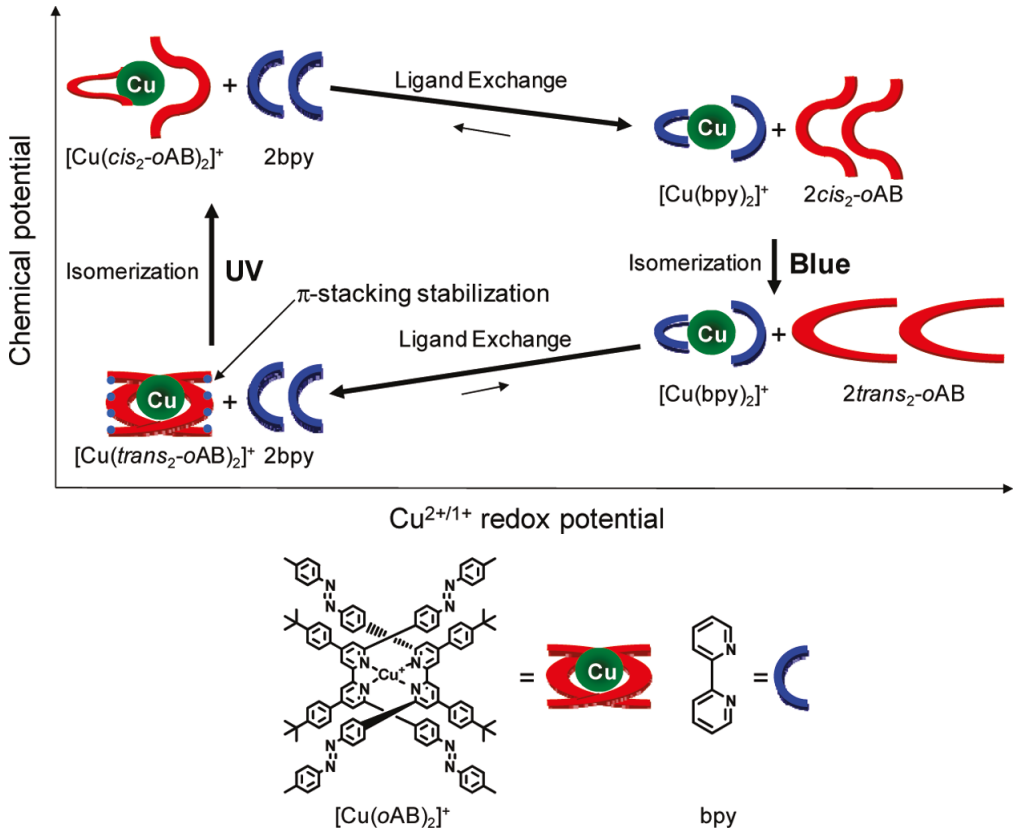

Figure 1.13. Photoelectric conversion system composed for $[Cu(oAB)_2]BF_4$. Figure extracted from literature.[26c]

The photoisomerization of platinum complexes was also studied and, in the case of a compound containing two different azobenzene-appended ligands (Chart 1.2) the azobenzenes from the dithiolate or bipyridine ligand were independently isomerized irradiating at individually optimized light-wavelengths.[27,28]

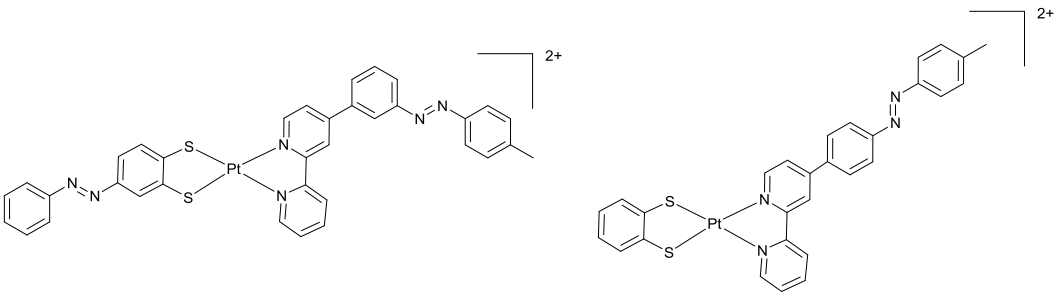

Chart 1.2. Platinum complexes synthesized by the group of Nishihara.

Otsuki *et al*. described switchable ruthenium and osmium bi- and tetranuclear compounds bridged by azobis(bipyridine) ligands, synthesized by reductive coupling of nitro-bipyridine units (Chart 1.3).[29] The synthetic procedure followed in this case to obtain azobenzene containing 2,2-bipyridines is shown in Scheme 1.4.

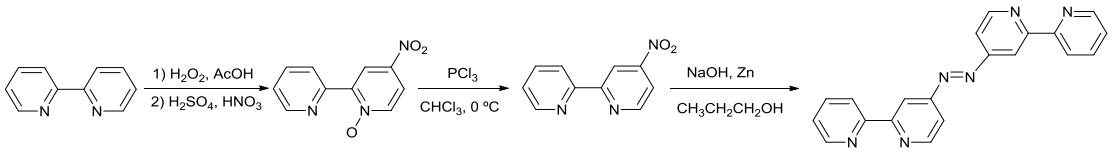

Scheme 1.4. Synthetic route toward one azobenzene containing 2,2'-bipyridine ligand.

Following the same methodology described by the group of Wenger, 1-oxide-4-nitro-2,2'-bipyridine was obtained through the oxidation and nitration of 2,2'-bipyridine. In this case, the pyridine oxide was deprotected by reacting with phosphorus trichloride to give 4-nitro-2,2'-bipyridine.[21] The switchable bridging ligand was obtained by the homocoupling of two of these nitro-compounds.

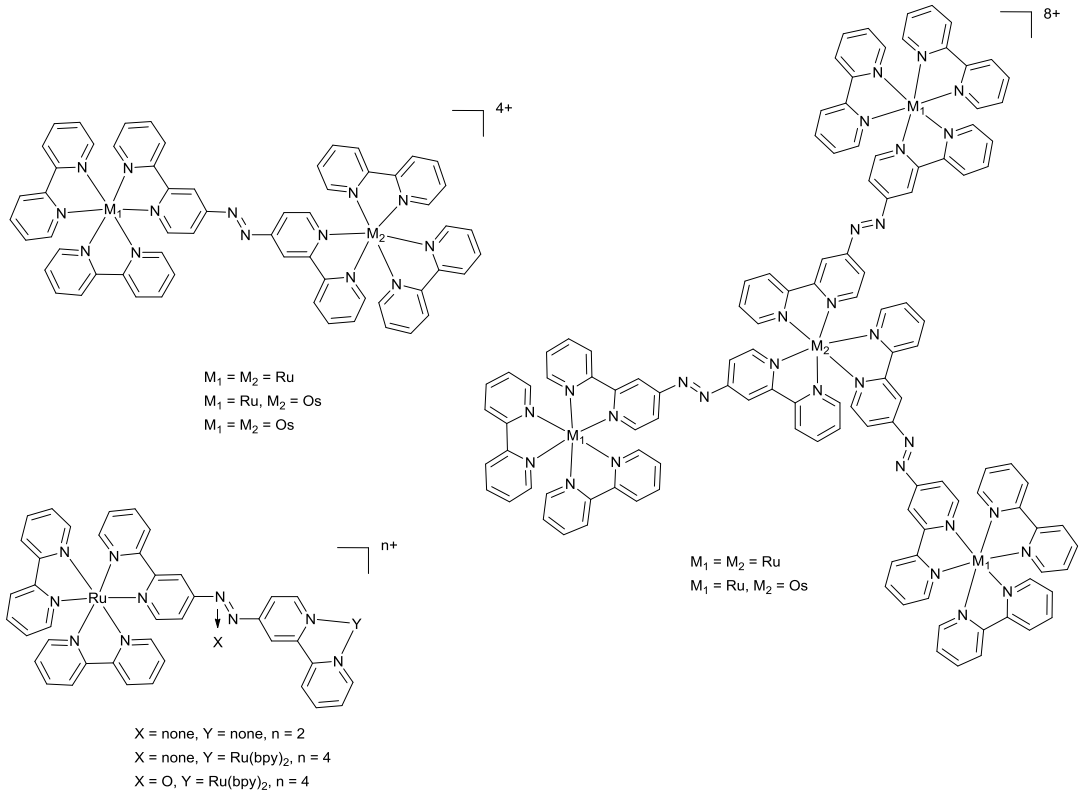

Chart 1.3. Ruthenium and osmium complexes synthesized by Otsuki *et al*.

The emission of these complexes was lower than usual $Ru(bipy)_3$ complexes. The luminescence process was quenched due to low-lying energy levels that permitted the relaxation of the excited states through a non-radiative pathway. When the azo group was reduced, the emission of these complexes was increased.[29d] Only free ligands and one mononuclear complex exhibited notorious changes upon irradiation as consequence of the isomerization of the azo moiety.[29c]

During the course of this thesis in 2015, Amar *et al*. published three new azobenzene-containing Ru(II) complexes with one azobenzene moiety in a bipyridine ligand.[12] They synthesized three different ligands depending on the spacer used to connect the

azobenzene fragment to the bipyridine. In one case (analogue to Nishihara's ligands) an azobenzene was directly part of the bipyridine. In the other two examples an ethynyl or a triazolyl bridge was used between the bipyridine and the azobenzene moiety.

The first one was synthesized through a Negishi cross-coupling between 4-[2-bromopyridin-4-yl)diazenyl]-*N*,*N*-dibutylaniline and pyridine zinc chloride (Scheme 1.5). The synthetic route towards the former involves two steps and the latter was obtained from 2-bromopyridine.

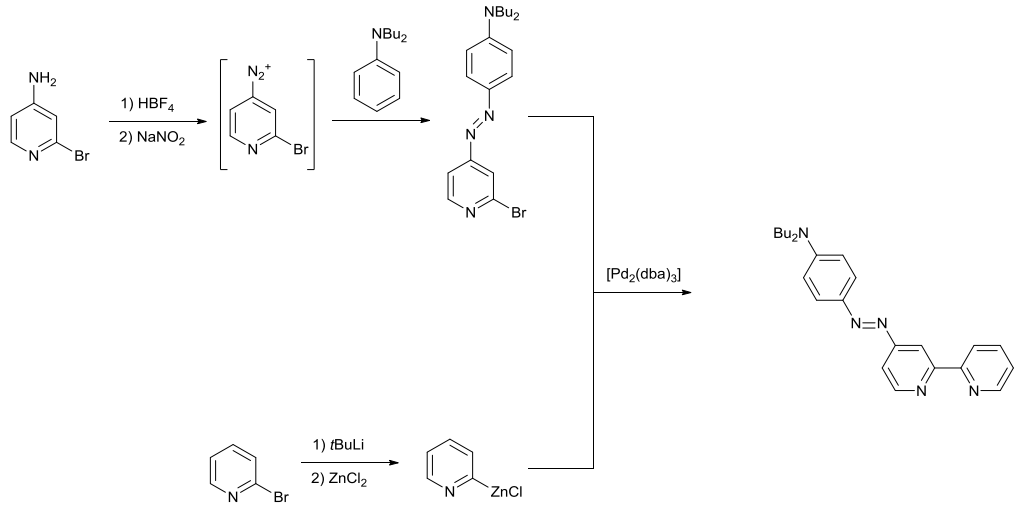

Scheme 1.5. Synthetic route toward one azobenzene containing 2,2'-bipyridine ligand.

Although the synthetic route towards the ethynyl- and triazolyl-bridged ligands looks like an one-step synthesis, this is not strictly the case. For the triazolyl-bridged ligand (synthesized by click chemistry) the required alkyne and azide reacting fragments need to be synthesized (Scheme 1.6, bottom). 3-Ethynyl-2,2'-bipyridine was synthesized following a described methodology that involves 4 steps from 2,5-dibromopyridine[30] and the 4-(*N*,*N*-dibutylamino)-4'-iodoazobenzene was obtained by reaction of *N*,*N*-dibutyl-aniline with iodobenzene diazonium chloride. The azide 4-(*N*,*N*-dibutylamino)-4'-azidoazobenzene was generated *in situ* during the click-coupling.[31] Altogether, five steps were required to obtain the reagents required for the azobenzene synthesis. The synthesis of the ligand with an ethynyl bridge was based on Pd-catalyzed Sonogashira cross-coupling between 3-ethynyl-2,2'-bipyridine and 4-(N,N-dibutylamino)-4'-iodoazobenzene (Scheme 1.6, top).

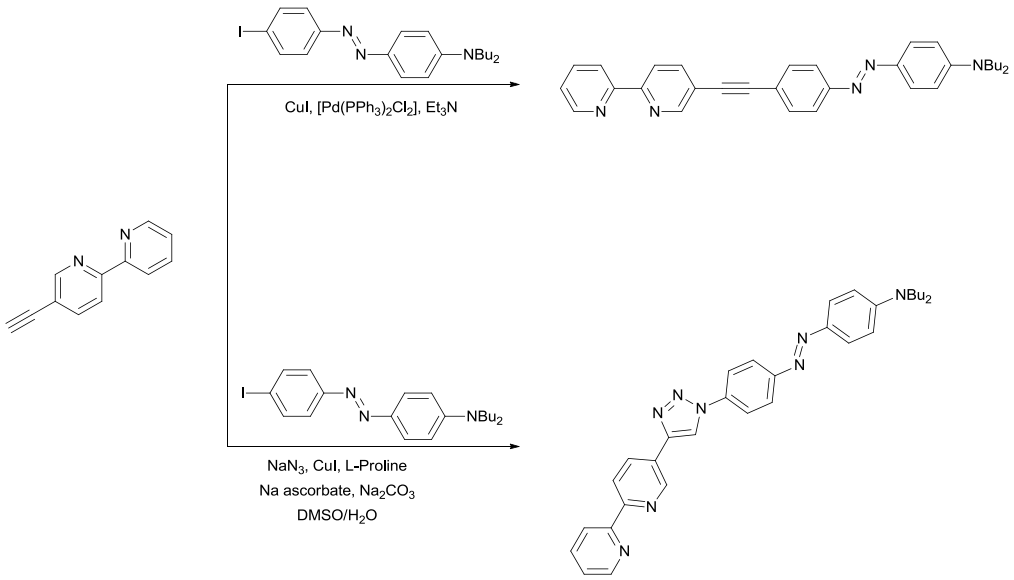

Scheme 1.6. Synthetic routes toward one azobenzene containing 2,2'-bipyridine ligands bridged through ethynyl (top) and triazolyl groups (bottom).

Ruthenium complexes of type $[Ru(bipy)_2(L)](PF_6)_2$ were synthesized with the above described ligands and the extent of the photoisomerization of the azobenzene fragment in these complexes was compared with the one of free ligands. They observed that ruthenium complexation strongly suppressed the *trans*-to-*cis* photoisomerization of the azobenzene moiety. In the case of the complex that contains the ligand without bridging group (analogue to Nishihara's ligands) the photoisomerization was completely inhibited, and in the case of complexes containing bridging groups it was reduced respect to the free ligands. The deactivation of the process was attributed to the fast relaxation pathway (form the S_1^* or S_2^* excited states of the azobenzene) through a metal to ligand charge transfer (MLCT).

All these results clearly point to the fact that the photochromic properties of the azobenzene-appended ligand are not always retained upon metal coordination. Many factors such as oxidation state and electronic accessible states of the metal or electronic conjugation between the metal and the azobenzene play an important role determining the survival of the photoswitching behaviour of the final compound, making the synthesis of photo-switchable complexes a tricky task.

1.5. COMPLEXES CONTAINING THE AZOBENZENE ON THE PHOSPHINE

There are not many examples of azobenzene-containing phosphorus compounds in the literature. The first ones were published in 1953, when phosphonic analogues of methyl orange, ethyl orange and congo red indicators were synthesized (Chart 1.4).[32]

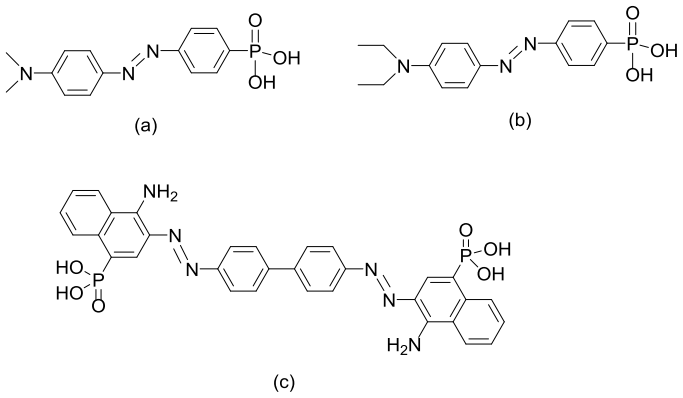

Chart 1.4. First azobenzene-containing phosphorus compounds reported in the literature. Phosphonic acid analogues of a) methyl orange, b) ethyl orange and c) congo red.

In 1995 and 1996, Lequan *et al.* reported azobenzene-containing phosphine oxides (Chart 1.5, a).[33,34] The first azobenzene-containing tertiary phosphine was published by Pritchard and coworkers in 1998 (Chart 1.5, b)[35] and several Cr, W, Mo,[36] Au[37] and Pd[38] complexes incorporating derivatives of this naphthylphosphine were synthesized. They also synthesized azo-containing phosphine sulfides[39] (Chart 1.5, c) and oxides.[40] At the same time, Lambert *et al.* described the synthesis of charged phosphonium salts incorporating up to four azobenzene fragments (Chart 1.5, d).[41] In 2005, Corriu and coworkers synthesized bis-silylated azobenzene phosphonium salts used to stabilize Au nanoparticles (Chart 1.5, e).[42] Irradiating an azide-containing triarylphoshine with a Xe-lamp, an azobenzene bridged diphosphine (Chart 1.5, f) was obtained in 2007.[43]

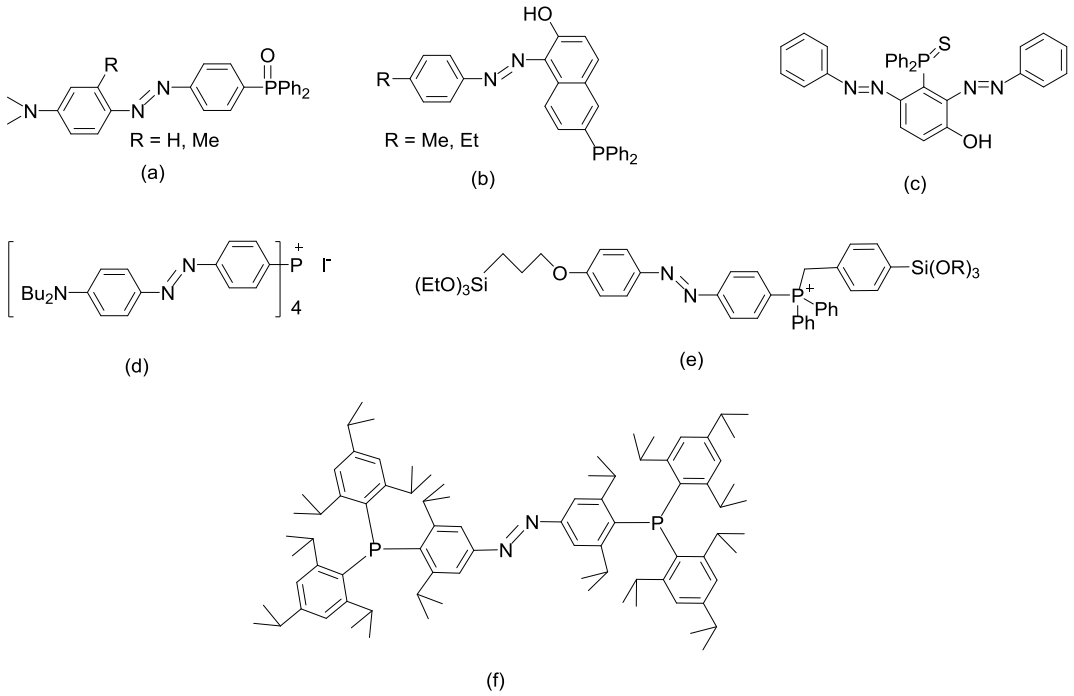

Chart 1.5. Examples of phosphorus-containing azobenzenes reported in the literature.

To the best of our knowledge, the isomerization of the azobenzene-containing phosphines was not studied until 2002, when Kudo and coworkers synthesized chiral azo-phosphines (Chart 1.6, a) and studied the effect of the photoisomerization of the azobenzene on the Pd catalyzed asymmetric allylic alkylation reaction. The isomerization of the azobenzene was effective in the free ligand, but unfortunately they did not observe any influence of the isomerization in their catalytic results.[44] Few years later, Yamamura *et al.* studied the photoisomerization of azobenzenes containing chalcogenphosphines (Chart 1.6, b) where Ch = O, S, Se and the phosphine without chalcogen substitution. The influence of the position of the phosphine group on the photoisomerization of the azobenzene was also analyzed on a family of isomers.[45,46]

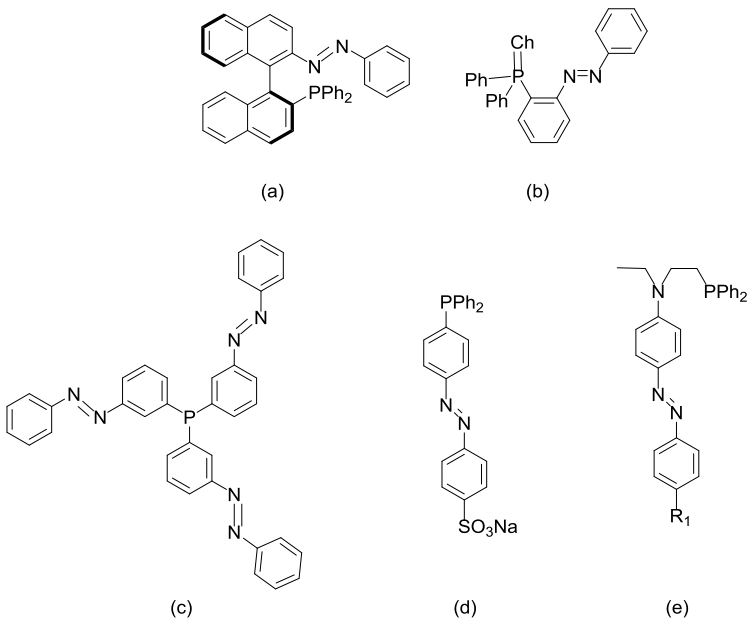

Chart 1.6. Examples of azobenzene-containing phosphines reported in the literature.

In 2010, Freixa and coworkers studied the photoisomerization of triarylphosphines containing one azobenzene in *para* or *meta* positions and the one containing three azobenzene fragments (Chart 1.6, c). They demonstrated that the coordination to Pt did not influence the photoisomerization process of these ligands, being compatible with catalytic applications.[47] In a subsequent work published by Bricout *et al.*, two azobenzene-containing sulfonated phosphines were synthesized. They differed in the position of the photochromic fragment. The one positioned in *para* respect to the phosphorus is shown as an example in Chart 1.6, d. These phosphines were used in Pd-catalyzed cleavage of allylic carbonates, improving the catalytic results with the photoisomerization of the azobenzene. This effect was attributed to a solubility change of the catalyst due to azobenzene isomerization.[48] In 2013, Mirkin and coworkers reported an azobenzene containing phosphine (Chart 1.6, e) that was incorporated in

Pt(II) and Pd(II) complexes.[49] The photoisomerization of free ligands and complexes was studied being effective in most of the cases. They observed that the half-life time of the *cis* isomer was influenced by the coordination mode of the ligand (either P monodentate or P–N chelate), but they were not studied for any application.

To the best of our knowledge, there have not been published examples of effective modification of the activity or selectivity of azobenzene-modified catalysts upon irradiation, up to date.

1.6. GENERAL OBJECTIVES

In view of few examples where the isomerization of azobenzene-containing bipyridines and phosphines has been exploited to change the response of photoswitchable compounds, the general aim of this thesis is the synthesis of photochromic bipyridine and phosphine ligands, for a posteriori coordination to Ir(III) and Ru(II) metal centers, to obtain organometallic complexes able to change their properties by action of an external stimuli, the light.

The influence of the photoisomerization of Ir(III) and Ru(II) complexes will be studied in different applications: dye-sensitized solar cells, light-emitting electrochemical cells and metal-catalyzed hydrogen generation.

1.7. REFERENCES

[1] Y. Hasegawa, T. Nakagawa and T. Kawai, *Coord. Chem. Rev.*, **2010**, *254*, 2643–2651.

[2] A. Fihey, A. Perrier, W. R. Browne and D. Jacquemin, *Chem. Soc. Rev.*, **2015**, *44*, 3719–3759.

[3] B. L. Feringa and W. R. Browne (Eds), **2011**, *Molecular Switches*, Volume 1, Wiley-VCH.

[4] G. S. Hartley, *Nature*, **1937**, *140*, 281–282.

[5] M. Ribagorda, E. Merino, *An. Quím.*, **2009**, *105*, 290–299.

[6] I. Conti, M. Garavelli and G. Orlandi, *J. Am. Chem. Soc.*, **2008**, *130*, 5216–5230.

[7] A. A. Beharry and G. A. Woolley, *Chem. Soc. Rev.*, **2011**, *40*, 4422–4437.

[8] H. M. D. Bandara and S. C. Burdette, *Chem. Soc. Rev.*, **2012**, *41*, 1809–1825.

[9] L. Wang, W. Xu, C. Yi and X. Wang, *J. Mol. Graphics Modell.*, **2009**, *27*, 792–796.

[10] H. Nishihara, *Coord. Chem. Rev.*, **2005**, *249*, 1468–1475.

[11] D. Bléger and S. Hecht, *Angew. Chem. Int. Ed.*, **2015**, *54*, 11338–11349.

[12] A. Amar, P. Savel, H. Akdas-Kilig, C. Katan, H. Meghezzi, A. Boucekkine, J.-P. Malval and J.-L. Fillaut, *Chem. Eur. J.*, **2015**, *21*, 8262–8270.

[13] V. Ferri, M. Elbing, G. Pace, M. D. Dickey, M. Zharnikov, P. Samorì, M. Mayor and M. A. Rampi, *Angew. Chem. Int. Ed.*, **2008**, *47*, 3407–3409.

[14] G. Vives and J. M. Tour, *Acc. Chem. Res.*, **2009**, *42*, 473–487.

[15] R. Klajn, P. J. Wesson, K. J. M. Bishop and B. A. Grzybowski, *Angew. Chem. Int. Ed.*, **2009**, *48*, 7035–7039.

[16] Y. Yu, M. Nakano and T. Ikeda, *Nature*, **2003**, *425*, 145.

[17] T. Muraoka, K. Kinbara, Y. Kobayashi and T. Aida, *J. Am. Chem. Soc.*, **2003**, *125*, 5612–5613.

[18] T. Muraoka, K. Kinbara and T. Aida, *Chem. Commun.*, **2007**, 1441–1443.

[19] H.-S. Tang, N. Zhu and V. W.-W. Yam, *Organometallics*, **2007**, *26,* 22–25.

[20] O. S. Wenger, L. M. Henling, M. W. Day, J. R. Winkler and H. B. Gray, *Polyhedron*, **2004**, *23*, 2955–2958.

[21] R. A. Jones, B. D. Roney, W. H. F. Sasse and K. O. Wade, *J. Chem. Soc. B* , **1967**, 106–111.

[22] E. V. Brown and G. R. Granneman, *J. Am. Chem. Soc.*, **1975**, *97*, 621–627.

[23] a) K. Yamaguchi, S. Kume, K. Namiki, M. Murata, N. Tamai and H. Nishihara, *Inorg. Chem.*, **2005**, *44*, 9056–9067. b) S. Kume, M. Kurihara and H. Nishihara, *J. Korean Electrochem. Soc.*, **2002**, *5*, 189–191. c) S. Kume, M. Kurihara and H. Nishihara, *Chem. Commun.*, **2001**, 1656–1657.

[24] R. A. Kipp, Y. Li, J. A. Simon and R. H. Schmehl, *J. Photochem. and Photobiol. A: Chemistry*, **1999**, *121*, 27–36.

[25] F. Kröhnke, *Synthesis*, **1976**, *1*, 1–24.

[26] a) S. Kume, M. Kurihara and H. Nishihara, *Inorg. Chem.*, **2003**, *42*, 2194–2196. b) S. Kume, M. Murata, T. Ozeki and H. Nishihara, *J. Am. Chem. Soc.*, **2005**, *127*, 490–491. c) S. Umeki, S. Kume and H. Nishihara, *Chemistry Letters*, **2010**, *39*, 204–205. d) S. Umeki, S. Kume and H. Nishihara, *Inorg. Chem.*, **2011**, *50*, 4925–4933.

[27] R. Sakamoto, M. Murata, S. Kume, H. Sampei, M. Sugimoto and H. Nishihara, *Chem. Commun.*, **2005**, 1215–1217.

[28] R. Sakamoto, S. Kume, M. Sugimoto and H. Nishihara, *Chem. Eur. J.*, **2009**, *15*, 1429–1439.

[29] a) J. Otsuki, K. Sato, M. Tsujino, N. Okuda, K. Araki and M. Seno, *Chem. Lett.*, **1996**, 847–848. b) J. Otsuki, A. Imai, K. Sato, D.-M. Li, M. Hosoda, M. Owa, T. Akasaka, I. Yoshikawa, K. Araki, T. Suenobu and S. Fukuzumi, *Chem. Eur. J.*, **2008**, *14*, 2709–2718. c) J. Otsuki, N. Omokawa, K. Yoshiba, I. Yoshikawa, T. Akasaka, T. Suenobu, T. Takido, K. Araki and S. Fukuzumi, *Inorg. Chem.*, **2003**, *42*, 3057–3066. d) J. Otsuki, M. Tsujino, T. Iizaki, T. Araki, M. Seno, K. Takatera and T. Watanabe, *J. Am. Chem. Soc.*, **1997**, *119*, 7895–7896.

[30] A. M. Soliman, D. Fortin, P. D. Harvey and E. Zysman-Colman, *Chem. Commun.*, **2012**, *48*, 1120–1122.

[31] A. K. Feldman, B. Colasson and V. V. Fokin, *Organic Letters*, **2004**, *6*, 3897–3899.

[32] G. M. Kosolapoff, and G. G. Priest, *J. Am. Chem. Soc.*, **1953**, *75*, 4847–4849.

[33] K. Chane-Ching, M. Lequan, R. M. Lequan, C. Runser, M. Barzoukas and A. Fort, *J. Mater. Chem.*, **1995**, *5*, 649–652.

[34] M. Lequan, R. M. Lequan, K. Chane-Ching, P. Bassoul, G. Bravic, Y. Barrans and D. Chasseau, *J. Mater. Chem.*, **1996**, *6*, 5–9.

[35] M. J. Alder, K. R. Flower and R. G. Pritchard, *Tetrahedron Letters*, **1998**, *39*, 3571–3574.

[36] M. J. Alder, W. I. Cross, K. R. Flower and R. G. Pritchard, *J. Organomet. Chem.*, **1998**, *568*, 279–285.

[37] M. J. Alder, K. R. Flower and R. G. Pritchard, *J. Organomet. Chem.*, **2001**, *629*, 153–159.

[38] M. J. Alder, W. I. Cross, K. R. Flower and R. G. Pritchard, *J. Organomet. Chem.*, **1999**, *590*, 123–128.

[39] M. J. Alder, V. M. Bates, W. I. Cross, K. R. Flower and R. G. Pritchard, *J. Chem. Soc., Perkin Trans.*, **2001**, *1*, 2669–2675.

[40] M. J. Alder, W. I. Cross, K. R. Flower and R. G. Pritchard, *J. Chem. Soc., Dalton Trans.*, **1999**, 2563–2573.

[41] C. Lambert, E. Schmälzlin, K. Meerholz and C. Bräuchle, *Chem. Eur. J.*, **1998**, *4*, 512–521.

[42] E. Besson, A. Mehdi, V. Matsura, Y. Guari, C. Reyé and R. J. P. Corriu, *Chem. Commun.*, **2005**, 1775–1777.

[43] S. Sasaki, K. Kato and M. Yoshifuji, *Bull. Chem. Soc. Jpn.*, **2007**, *80*, 1791–1798.

[44] M. Kawamura, R. Kiyotake and K. Kudo, *Chirality*, **2002**, *14*, 724–726.

[45] M. Yamamura, N. Kano and T. Kawashima, *J. Am. Chem. Soc.*, **2005**, *127*, 11954–11955.

[46] M. Yamamura, N. Kano and T. Kawashima, *Inorg. Chem.*, **2006**, *45*, 6497–6507.

[47] M. D. Segarra-Maset, P. W. N. M. van Leeuwen, and Z. Freixa, *Eur. J. Inorg. Chem.*, **2010**, 2075–2078.

[48] H. Bricout, E. Banaszak, C. Len, F. Hapiot and E. Monflier, *Chem. Commun.*, **2010**, *46*, 7813–7815.

[49] J. S. Park, A. M. Lifschitz, R. M. Young, J. Mendez-Arroyo, M. R. Wasielewski, C. L. Stern and C. A. Mirkin, *J. Am. Chem. Soc.*, **2013**, *135*, 16988–16996.

CHAPTER 2

LIGANDS SYNTHESES AND CHARACTERIZATION

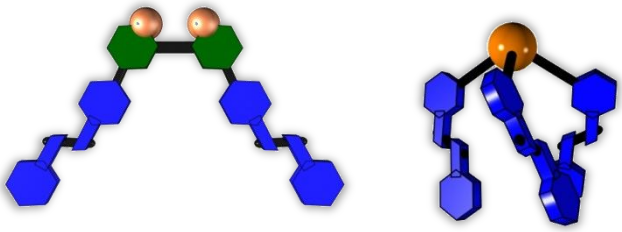

All the azobenzene-containing pyridine, bipyridine and phosphine ligands involved in this thesis are presented in this chapter, together with the study of their photochromic behaviour. Several bipyridines (without photochromic units) with different electronic properties are also presented.

The main properties of transition metal complexes are governed by the nature of their central metal. Nevertheless, ligands coordinated around it can strongly modify them determining, for instance, their solubility or reactivity. Eventually, an accurate selection of both metal and ligands are required to obtain compounds with the desired properties for specific applications. In this work, neutral pyridine, bipyridine and phosphine ligands will be used to induce the desired properties on selected complexes. In this chapter a brief description of the synthetic details towards these ligands, as well as some relevant aspects of their characterization, will be individually discussed.

2.1. AZOBENZENE CONTAINING LIGANDS

Conventionally, ligands were considered as simple spectators that modify the properties of the metal they are coordinated to. Nevertheless, in some modern transition metal complexes, the ligands do not act as steady modifiers. Instead, they contain certain functional groups which make them "dynamic" (*i.e.* able to react to changes in the environment).[1] In this manner, their complexes are also transformed into dynamic entities, and their properties can also eventually be modified by action of an external stimuli, such as pH, light, etc.

As explained before, one of the goals of this thesis is the development of light-responsive transition-metal complexes for different applications. The strategy used is the incorporation of azobenzene units in the structure of the ligands used for their construction. Since this is a preliminary work in the area, the ligands design has been kept as simple as possible, as they will be used as models to study the compatibility of the photochromism of the azobenzene with the metal coordination, and with the conditions required for the specific application of the compound. The synthetic details for their construction will be discussed below.

2.1.1. PYRIDINE AND BIPYRIDINE-BASED LIGANDS

For the studies presented in this thesis four new azobenzene-appended 2,2'-bipyridine ligands (**1**,**3**–**5**) and the well-known 4-phenylazopyridine (**2**) have been synthesized (see Chart 2.1).

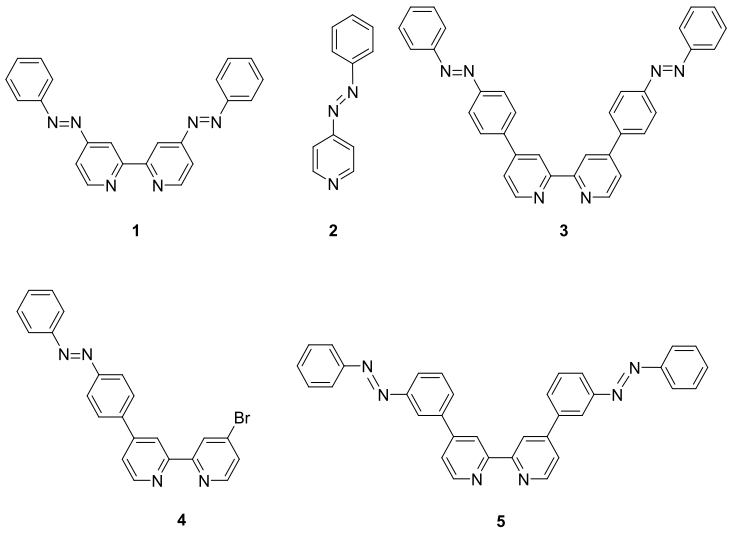

Chart 2.1. Azobenzene-containing pyridine and 2,2'-bipyridine ligands used in this work.

Few azobenzene containing 2,2'-bipyridines have already been reported in the literature.[2] The synthetic strategy most commonly used consists of condensation of nitrosotoluene with the corresponding amino-2,2'-bipyridines. Based on these reports, initially we considered following this methodology to obtain the most simple azobenzene-containing bipyridine of the series, 2,2'-bis(4-phenylazopyridine) ligand **1** (Scheme 2.1). To obtain the starting 4,4'-diamino-2,2'-bipyridine, 2,2'-bipyridine was first protected in the form of 2,2'-bipyridine-*N,N'*-dioxide using H_2O_2/HAcO and then two nitro groups were introduced in 4,4' positions by reaction with H_2SO_4 and fuming HNO_3.[3] The nitro groups were reduced catalytically (Pd/C) with hydrazine monohydrate to obtain 4,4'-diamino-2,2'-bipyridine with an overall yield of 70%.[2] Before testing the condensation with nitrosobenzene with this compound, a preliminary test was run on commercially available 4-aminopyridine. Following this procedure the already described 4-phenylazopyridine (ligand **2**) was obtained as a dark orange microcrystalline solid with a yield of 88% (Scheme 2.1).[4]

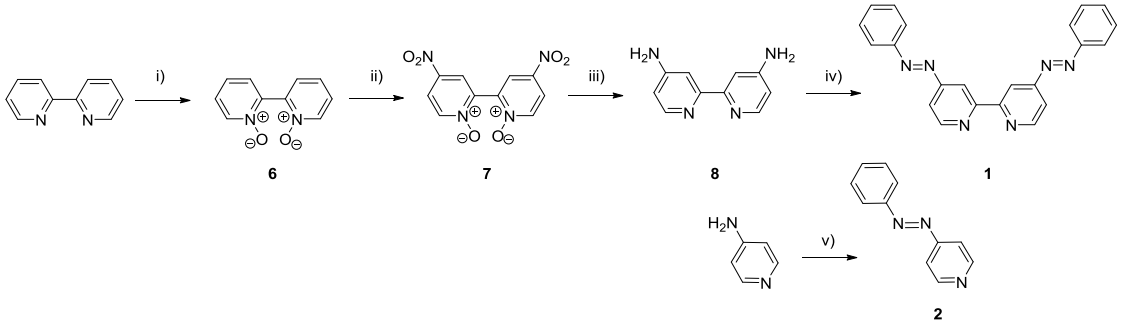

Scheme 2.1. Synthetic routes toward ligands **1** and **2**. i) HAcO, H_2O_2 (30%), 75 ºC, 18 h. Yield: 99%. ii) H_2SO_4, HNO_3, 84 ºC, 72 h. Yield: 53%. iii) Pd/C (0.6 equiv.), $NH_2NH_2{\cdot}H_2O$ (7.8 equiv.), EtOH, 80 ºC, 18 h. Yield: 70%. iv) Nitrosobenzene (2.6 equiv.), NaOH, pyridine, 80 ºC, 18 h. Yield: 56%. v) Nitrosobenzene (1.2 equiv.), NaOH, pyridine, 80 ºC, 1.5 h. Yield: 88%.

When the same procedure was applied for the synthesis of ligand **1** a lower yield (56%) was obtained, even at longer reaction times (full spectra and detailed synthetic procedures are compiled in the Supporting Information). Due to the lower reactivity observed for the condensation of 4,4'-diamino-2,2'-bipyridine with nitrosobenzene compared to the reaction with the more simple 4-aminopyridine, and the long synthetic route needed to obtain the starting 4,4'-diamino-2,2'-bipyridine, the design of an alternative methodology to obtain azobenzene-containing bipyridines was considered. For this reason, a new synthetic route based on palladium-catalyzed cross-coupling of the corresponding azobenzene boronic acids and commercially available 4,4'-dibromo-2,2'-bipyridine was developed (Scheme 2.2).

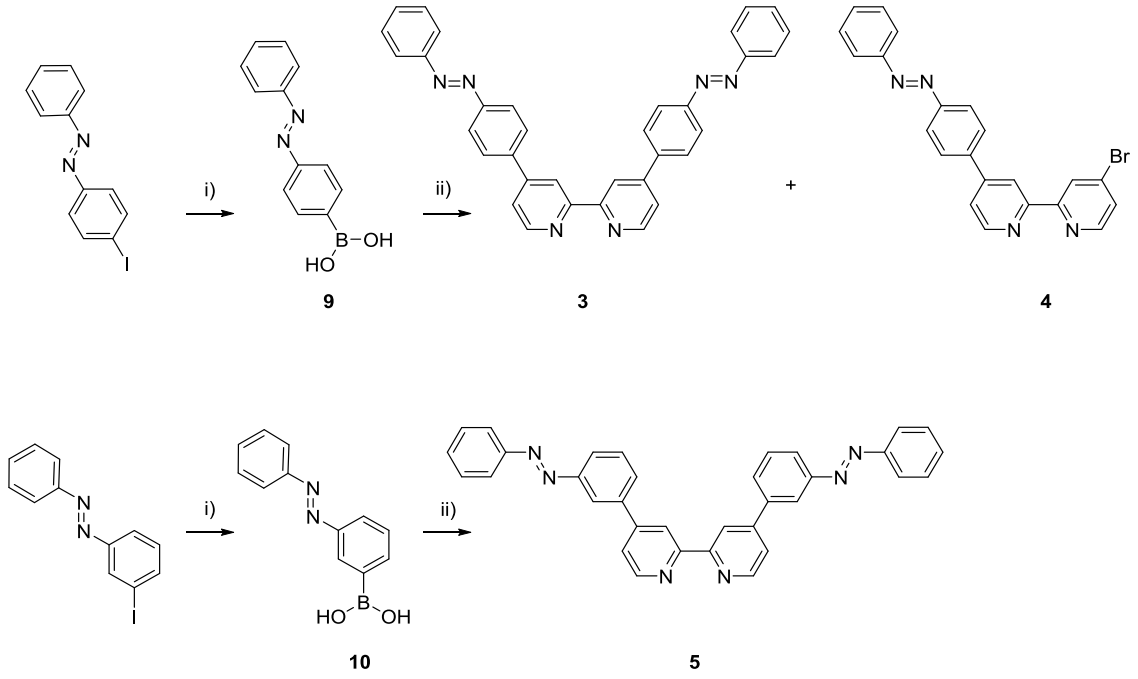

Scheme 2.2. Synthetic route toward ligands **3**–**5**. i) n-BuLi (1.1 equiv.), Et_2O, −112 ºC; $B(OMe_3)_3$ (1.1 equiv.), Et_2O, −112 °C; dil. H_2SO_4, 0 °C. ii) 4,4'-dibromo-2,'2'-bipyridine (0.3–1 equiv.), $Pd(PPh_3)_4$ (1.6–5 mol%), toluene, K_2CO_3 aq (2 M, 0.5–1.7 mol%), 115 °C, 15 h.

The key synthones for this strategy are the corresponding azobenzene-boronic acids 4-(phenylazo)phenyl boronic acid (**9**) and 3-(phenylazo)phenyl boronic acid (**10**), already described in the literature. They were obtained by reaction of the corresponding iodoazobenzenes with n-BuLi and trimethyl borate at –112 ºC and subsequent treatment with diluted sulfuric acid at 0 ºC.[5] Depending on the availability of starting materials 4-(phenylazo)phenyl boronic acid (**9**) or 4-(phenylazo)phenyl boronic acid pinacol ester (**11**) were used indistinctly, without any detrimental effect on the yield of the reaction. 4-(phenylazo)phenyl boronic acid pinacol ester (**11**), that was already reported in the literature, was synthesized via condensation of 4-aniline boronic acid pinacol ester with nitrosobenzene and it was obtained with 82% yield (Scheme 2.3).[6]

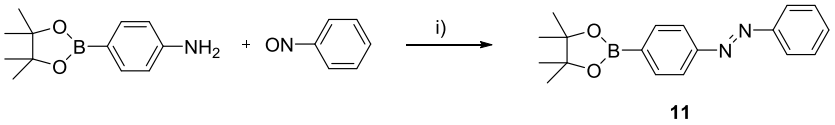

Scheme 2.3. Synthetic route toward [4-(phenylazo)phenyl]boronic acid pinacol ester **11**. i) HAcO, 118 ºC, 3.5 h. Yield: 82%.

Palladium-catalyzed Suzuki cross-coupling of azobenene-containing boronic acids **9** or **11** with 4,4'-dibromo-2,2'-bipyridine in toluene/H_2O, using 1.6 mol% of $Pd(PPh_3)_4$ as catalyst gave a mixture of 4,4'-bis(*p*-azobenzene)-2,2'-bipyridine (ligand **3**) and 4-(*p*-azobenzene)-4'-bromo-2,2'-bipyridine (ligand **4**) (yields 41% and 28%, respectively). These compounds were easily isolated individually because of their different solubility in most common solvents. The reaction mixture, a dark orange suspension, was gravity-filtered. The orange solid obtained was washed with CH_2Cl_2 and acetone. The low solubility of this solid hampered its characterization by NMR spectroscopic techniques in solution. Nevertheless, it was identified as ligand **3** based on its reactivity and analytical evidence. The filtrate was washed repeatedly with equal portions (in volume) of H_2O. After evaporation of the organic phase, the solid residue was purified by column chromatography using CH_2Cl_2 as initial eluent. The first fraction eluted (Rf = 1) was unreacted 4,4'-dibromo-2,2'-bipyridine. Then, the eluent was gradually changed to acetone. A second fraction rendered a light-orange solid, after solvent evaporation. The integration and number of signals observed in the ^{1}H-NMR spectrum of this product were indicative of an asymmetrically 4,4′-disubstituted 2,2′-bipyridine (Figure 2.1). A combined analysis of ^{1}H-, ^{13}C-, COSY- and HSQC-NMR spectra of this sample permitted us to assign some parts of the ^{1}H-NMR spectrum, consistent with a 15H-containing molecule. The signals between 8.2–7.9 ppm (6H) and 7.6–7.5 ppm (3H) were attributed to the azobenzene fragment. Overlapped with the last region described it appeared a signal assigned to one of the hydrogen atoms of the bipyridine. The spectra also presents the five remaining signals characteristic of an 4,4'-asymmetrically substituted 2,2'-bipyridine. A full characterization of this compound (^{1}H-, ^{13}C-NMR, ESI-MS, and EA) permitted its identification as the monoazobenzene-containing ligand **4**, a product of partial cross-coupling, and an intermediate toward ligand **3** (full spectra and detailed synthetic procedures are compiled in the Supporting Information).

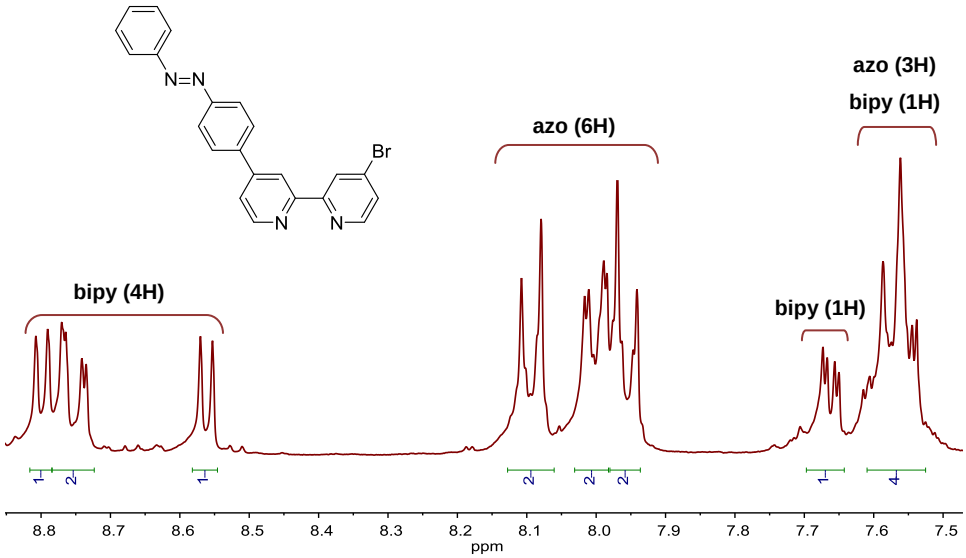

Figure 2.1. ^{1}H-NMR spectrum of ligand **4** in $CDCl_3$, 300 MHz.

When the reaction time was extended to 72 h ligand **3** was obtained in quantitative yield. In an effort to direct the reaction toward monoazobenzene bipyridine **4,** equimolar quantities of 4,4'-dibromo-2,2'-bipyridine and 4-(phenylazo)phenyl boronic acid **9** were used, but a mixture of **3** and **4** was obtained (1:3 ratio), even when the reaction was stopped at 51% of conversion of the dibrominated substrate. This result indicates that it is possible to obtain the ligand **3** as the unique reaction product, but ligand **4** must be extracted from a mixture of both compounds. A similar 2,2'-bipyridine containing only one azobenzene fragment appended was synthesized by the group of Nishihara employing a seven-step route based on the Kröhnke pyridine synthesis, starting from 3-nitrobenzaldehyde.[7] To the best of our knowledge, the experimental details and global yield of such reaction sequence remain unpublished.

As mentioned before, ligand **3** presented very low solubility in all the solvents assayed and it was not possible to characterize it by NMR spectroscopy. Fortunately, a single crystal (only one!) was obtained from a highly diluted solution in $CDCl_3$, which was suitable for X-ray diffraction. The molecular structure of ligand **3** is presented in Figure 2.2, together with selected angles and distances. For comparative purposes, the molecular structure of a related compound reported by Nishihara is shown in Figure 2.2.[7a] As can be observed, the *para* derivative (ligand **3**) presents a roughly planar conformation, whereas in the case of the published *meta* derivative a lack of coplanarity between the azobenzene and bipyridine fragments is evident. This result points to a less effective conjugation between the two moieties in the latter.

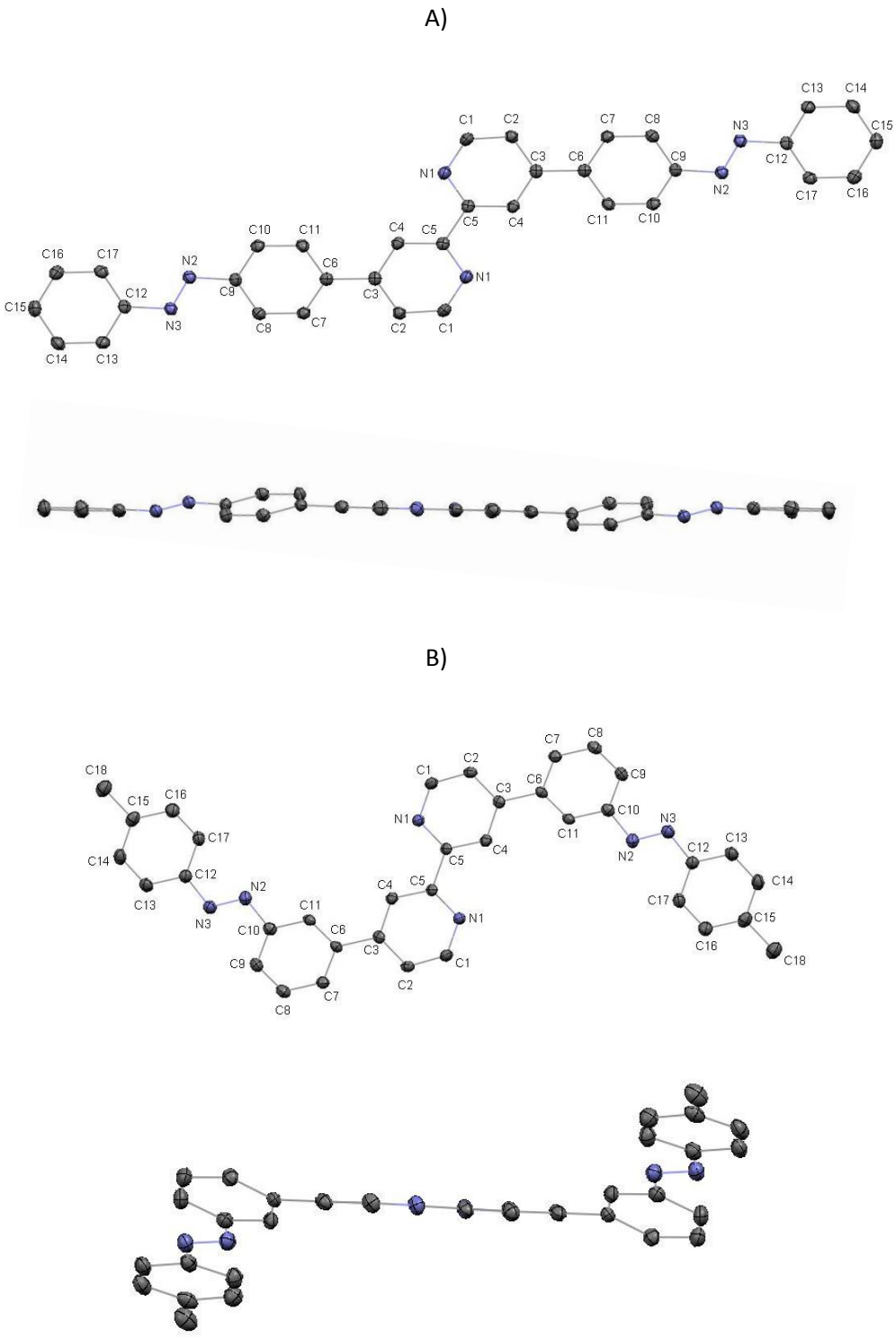

Figure 2.2. A) ORTEP drawing for ligand **3** with ellipsoids at the 50% probability level. Selected bonds-length [Å] and angles [°]: N2–N3 1.2581; C12–N3–N2 114.20; N3–N2–C9 113.60; N1–C5–C5A–N1A 180.00; C2–C3–C6–C11 163.38. B) ORTEP drawing of a ligand published in the literature with ellipsoids at the 50% probability level.[7a] Selected bonds-length [Å] and angles [°]: N2–N3 1.267; C12–N3–N2 114.28; N3–N2–C9 114.68; N1–C5–C5A–N1A 180.00; C2–C3–C6–C11 152.67.

The molecular structure of **3** reveals a flat arrangement, with the two nitrogen atoms of each pyridine fragment in an *anti* disposition around the pyridine-pyridine C–C bond, as observed in previously reported related compounds.[2,7a,8] Only the central ring deviates slightly from this plane (torsion angle 18.06º). This planarity is reflected in the crystal packing, the molecules are stacked in layers showing nearly perpendicular orientations (78.31º) (Figure 2.3).

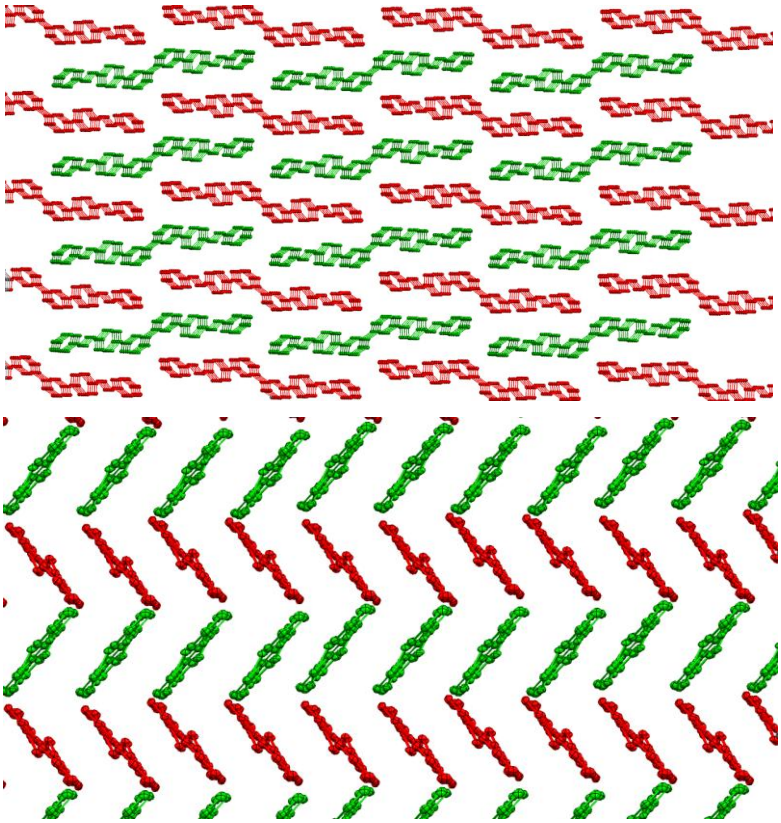

Figure 2.3. Crystal packing of ligand **3**. Different colors have been used to identify layers. Two perpendicular perspectives have been presented to appreciate the angle between layers.

Ligand **5** (4,4'-bis(*m*-azobenzene)-2,2'-bipyridine), containing two *meta*-substituted azobenzene fragments in 4,4'-positions, was obtained with a 71% yield following the same synthetic procedure described for ligand **3**, but using 3-(phenylazo)phenyl boronic acid **10** (Scheme 2.2). In this case the monosubstituted derivative was not obtained, nor detected in the reaction mixture. Ligand **5**, soluble in conventional solvents, was fully characterized by ^{1}H-, ^{13}C-NMR, EA and ESI-MS (full spectra and detailed synthetic procedures are compiled in the Supporting Information). Spectroscopic data of this ligand compare well with those of a similar compound reported by Nishihara.[7a]

It should be noted that in ligands **1**–**5** the azobenzene fragments could be either in *E* or *Z* form. In the case of ligands containing more than one azobenzene fragment (**1**, **3** and **5**) three different isomers are possible (*EE*, *EZ* and *ZZ*). Nevertheless, the symmetry of

the spectra observed in all the cases (confirming the presence only one isomer in solution) together with the larger thermodynamic stability of the *trans* isomer of the azobenzene, and the crystal structure obtained for ligand **3**, permitted us to identify them as the all-*trans* isomers.

2.1.2. PHOSPHINE LIGANDS

Phosphine ligands are among the most widely used ligands for the synthesis of transition-metal compounds. In this work, two azobenzene-containing triarylphosphines were synthesized, tris(*m*-azobenzene)phosphine **12** and tris(*p*-azobenzene)phosphine **13** (Chart 2.2). The *meta*-substituted derivative **12** was already reported by Freixa *et al*.[9] The same methodology described there was adapted for the synthesis of the *para*-substituted triarylphosphine **13**.

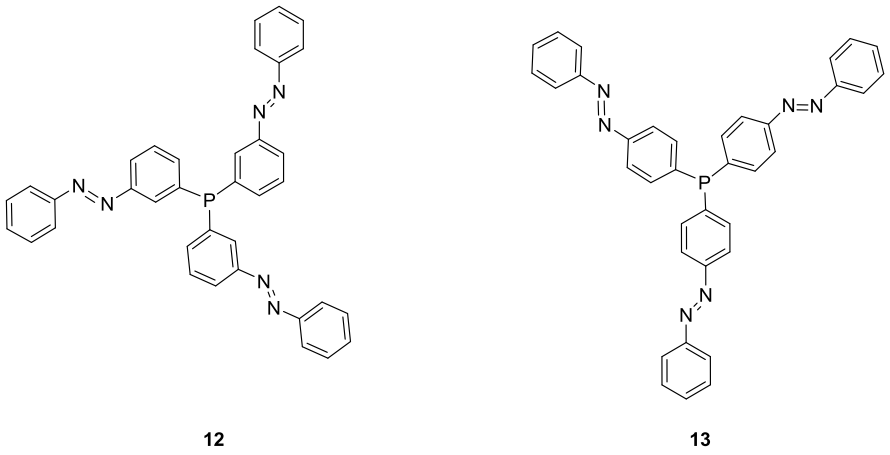

12 **13**

Chart 2.2. Azobenzene-containing phosphine ligands used in this work.

Under a nitrogen atmosphere, 3-iodoazobenzene or 4-iodoazobenzene were reacted at low temperature with BuLi and consecutively with PCl_3 to form the corresponding phosphines containing three azobenzene fragments in their structure (Scheme 2.4). Ligands **12** and **13** were obtained with moderate yields (14% and 10%, respectively).

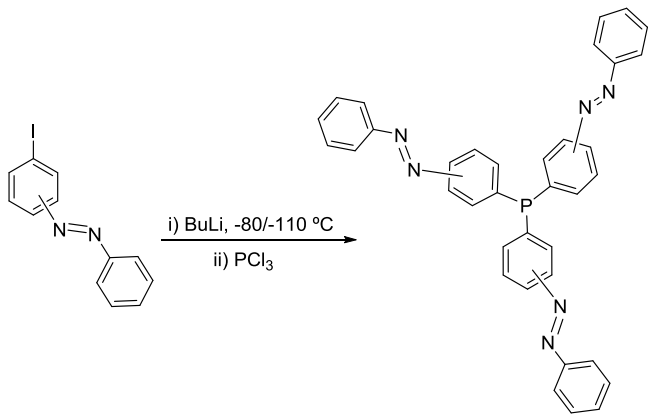

Scheme 2.4. Synthetic route toward ligands **12** and **13**.

Both azobenzene-tethered phosphines (**12** and **13**) were characterized by means of ^{1}H- and ^{31}P-NMR spectroscopy. In the case of *meta*-substituted ligand **12** the spectra matched with literature values, and it sufficed to confirm its identity.[9] Ligand **13**, not described previously in literature, was fully characterized by ^{1}H-, ^{13}C-, ^{31}P-NMR, EA and ESI-MS (full spectra and detailed synthetic procedures are compiled in the Supporting Information). The ^{1}H-NMR (shown in Figure 2.4), exhibits two broad multiplets, in the regions 7.40–7.48 ppm and 7.80–7.88, with relative integrations 5/4, which could correspond with the expected 27 protons in a C_3-symmetric molecule in solution.

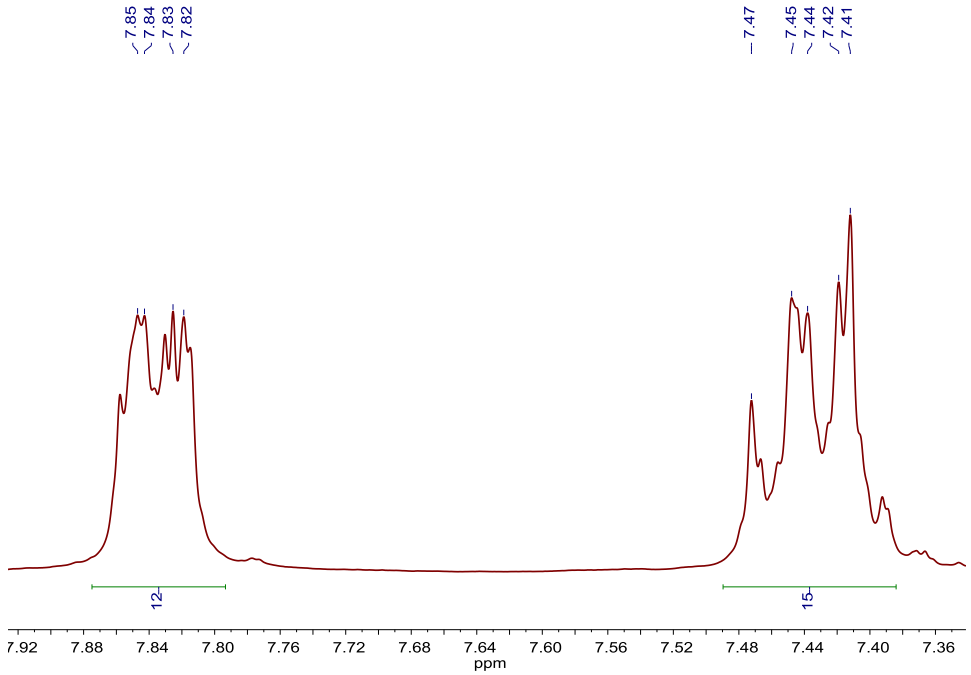

Figure 2.4. ^{1}H-NMR spectrum of ligand **13** in $CDCl_3$, 300 MHz.

^{13}C-APT-NMR spectrum of **13** (shown in Figure 2.5) was more informative to confirm the identity and purity of compound **13**. Assuming that the molecule is C_3 symmetrical in solution, up to 8 signals should appear in the ^{13}C-NMR spectrum. Three picks corresponding to quaternary C atoms and five due to C–H carbon atoms could be distinguished in the ^{13}C-APT-NMR spectrum. The four peaks at lower fields were assigned to the three C_{quat} of the molecule (which was confirmed also by the lack of correlation in the HSQC spectra), one of them (observed at 139.42 ppm) split into a doublet due to the coupling with the P atom. This carbon is most probably the one directly bond to the P atom (1). The seven negative peaks of the spectra were assigned to the 9 C–H units that each azobenzene contains. The four peaks at 134.25, 133.96, 122.54 and 122.46 were in fact attributed to two signals centered at 134.09 and 122.50 ppm, that appeared split into doublets due to coupling with the P atom.

Each signal corresponds to two magnetically-equivalent C–H carbons and they were assigned to the ones of the aromatic ring bonded to the P atom (2 and 3 respectively). The most intense peaks at 128.68 and 122.54 ppm were assigned to 4 C–H from the phenyl ring (grouped in pairs of magnetically equivalent C–H) (6 and 7). Finally the signal at 130.86 ppm was assigned to the C–H of position 8.

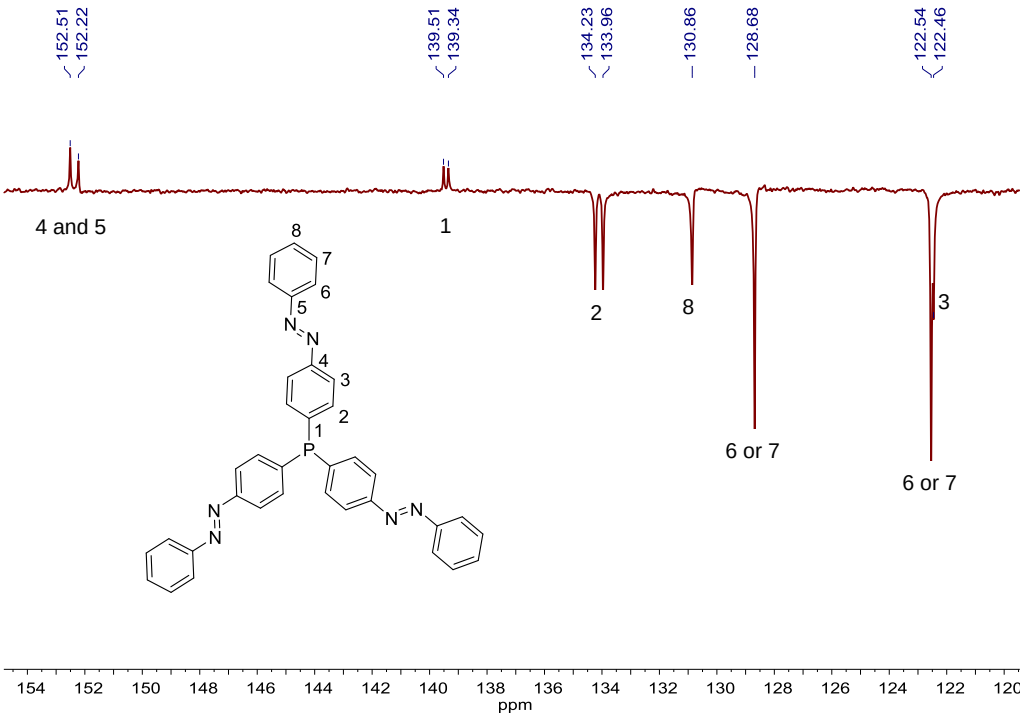

Figure 2.5. ^{13}C-APT-NMR spectrum of ligand **13** in $CDCl_3$, 75 MHz.

The correlation of C and H atoms in the HSQC-NMR (shown in Figure 2.6) confirmed the integration of protons in the ^{1}H-NMR spectra and provide the assignation of them. The multiplet between 7.40–7.48 ppm corresponds to 15 protons on positions 2, 8 and 6 or 7. The multiplet between 7.80–7.88 ppm was assigned to the 12 protons on positions. 3 and 6 or 7.

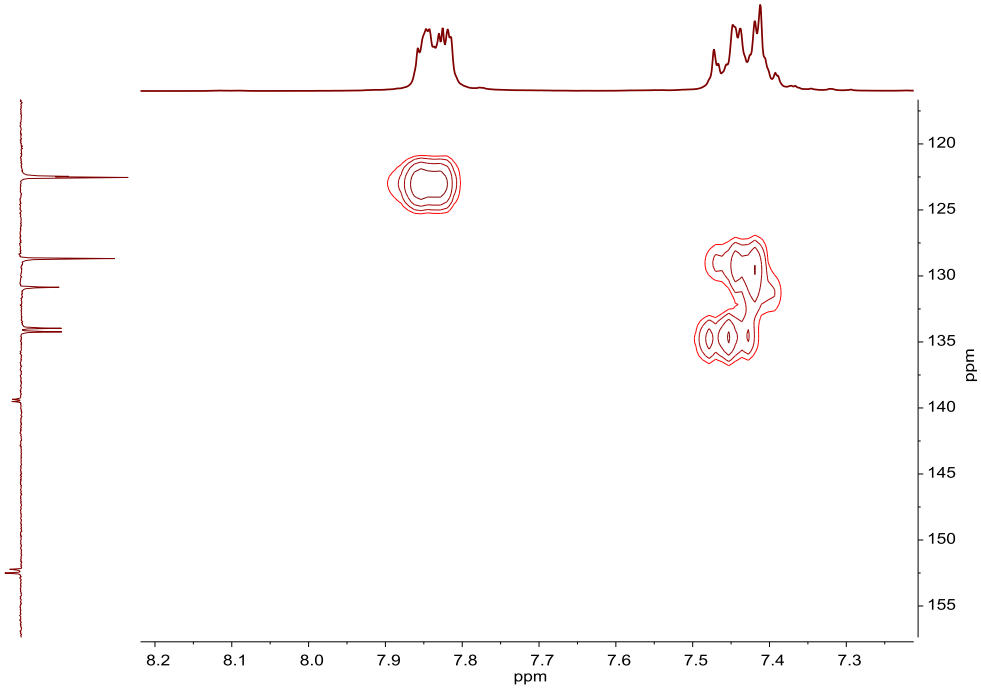

Figure 2.6. HSQC-NMR spectrum of ligand **13** in $CDCl_3$.

The $^{31}P\{^{1}H\}$-NMR spectrum of ligand **13** (shown in Figure 2.7) exhibited a singlet at −3.7 ppm, and only minor (less than 11%) peaks at very similar chemical shifts, indicating that the product is essentially composed by one of the four possible isomers (*ZZZ*, *ZZE*, *ZEE* and *EEE*). The symmetry observed in the molecule exclude the presence of isomers with mixed azobenzene-conformations. The compound was assigned then as *EEE*-**13** due to the larger thermal stability of *trans*-azobenzene derivatives compared to *cis* ones.

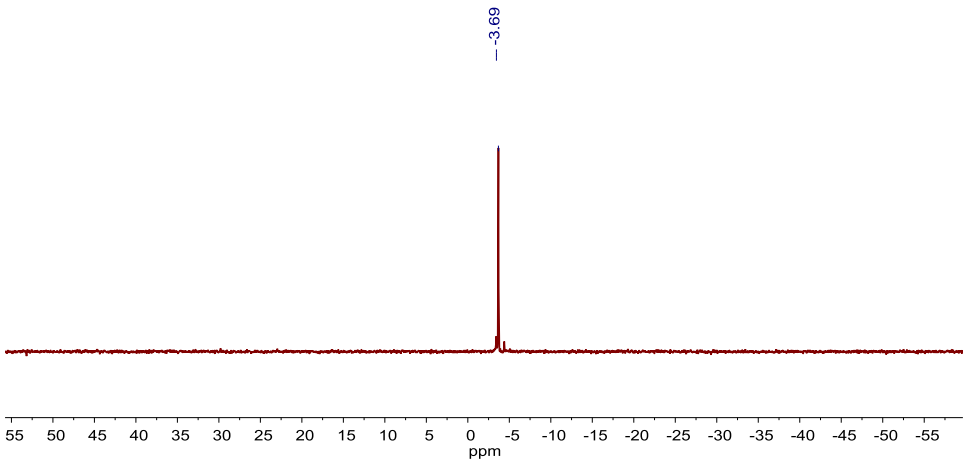

Figure 2.7. $^{31}P\{^{1}H\}$-NMR spectrum of ligand **13** in $CDCl_3$, 202.5 MHz.

2.1.3. PHOTOISOMERIZATION STUDIES

As already mentioned in the introduction, light-triggered azobenzene *trans*-to-*cis* isomerization can be reversed either by light or spontaneously in the dark, due to the thermodynamic stability of the *trans* isomer. Both processes can be easily monitored by UV–Vis absorption spectroscopy due to the different spectroscopic pattern of both isomers. As explained in Chapter 1, when the azobenzene is isomerized from *E* to *Z* the absorption band attributed to π→π* transition is shifted to lower wavelengths and its intensity decreases. On the contrary, the intensity of the band attributed to n→π* transition increases, but it is less noticeable due to the much weaker intensity of this band.[10]

In this section, the studies of the photoisomerization of the azobenzene unit in the free ligands by UV-Vis absorption spectroscopy will be presented. These results will be used along the thesis as reference-data to determine the effect that coordination of these ligands to the metal centre has on the effectiveness of the photoisomerization process.

UV–Vis absorption spectroscopy of diluted CH_3CN solutions of ligands **1**, **2**, **4**, **5**, **12** and **13** were used to get an insight on the extent of the light-triggered isomerization of the azobenzene in free ligands. To maximize the population of the *cis* form in the PSS the irradiation light-wavelength should be individually optimized, as described by Monkovious.[11] According to this methodology, the optimal wavelength to maximize the extent of the photoisomerization can be extracted from the spectra before and after irradiation, as it corresponds to the light-wavelength (close to the π→π* transition band) where a larger difference between both spectra is observed. To calculate it, initially, the UV–Vis absorption spectra of all the compounds were registered to locate the position of their main absorption bands. Then, the same solutions were irradiated for 30 min at the wavelength attributed to π→π* transition, which was individually selected for each compound, and new spectra were registered. Both spectra (before and after irradiation) were used to determine individually the optimal irradiation-wavelength to maximize the population of the *Z* form in the PSS. A practical example is depicted in Figure 2.8 for ligand **4**. In this figure, the spectra of compound **4** before (green line) and after 30 min irradiation at 334 nm (red line), which is the wavelength attributed to its π→π* transition. The difference between both spectra is the dashed blue line, and the maximum of this difference was selected as $\lambda_{optimal}$ for this compound (337 nm). It can be clearly observed that when the sample was irradiated at $\lambda_{optimal}$ (337 nm) for additional 30 min (orange line) it produces a larger proportion of *Z* isomer compared with irradiation at $\lambda_{\pi\rightarrow\pi}$ (334 nm).

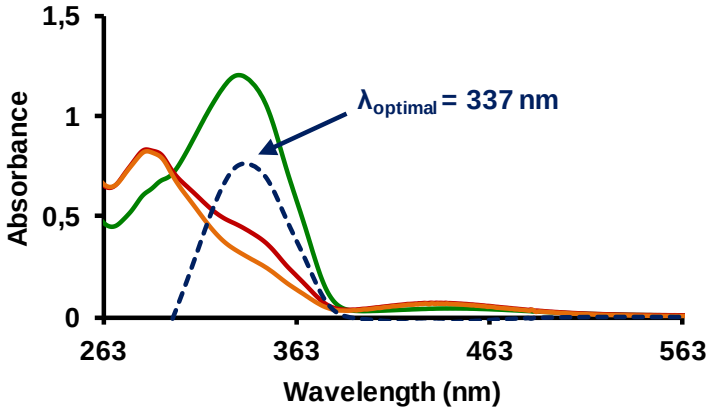

Figure 2.8. UV-Vis absorption spectra of ligand **4**, before irradiation (green line), after 30 min irradiation at the wavelength attributed to π→π* transition (334 nm) (red line), difference between before and after irradiation at 334 nm (dashed blue line) and after 30 min irradiation at $\lambda_{optimal}$ (337 nm) (orange line).

Although lacking the spectra of pure *cis* and *trans* species it is not possible to quantify the extent of the photoisomerization process, in general a small change in the UV-Vis spectra upon irradiation at the optimized light-wavelength is indicative of a rather small population of *cis* form in the PSS, *i.e.* an inefficient photoisomerization. On the contrary, large differences in the spectra are associated to very efficient *trans*-to-*cis* isomerization processes.

All the azobenzene-containing ligands studied **1**, **2**, **4**, **5**, **12** and **13** presented, as expected, a substantial change in their electronic absorption spectra upon irradiation at the appropriate light wavelength (Figure 2.9). The expected decrease in intensity of the band attributed to the π→π* transition of the azobenzene was clearly observed in all the ligands, together with a less notorious increase in the intensity of the less energetic n→π* transition band. From this observation, we assume that in all the cases a considerably large proportion of azobenzene fragments are in the *cis*-form in the PSS.

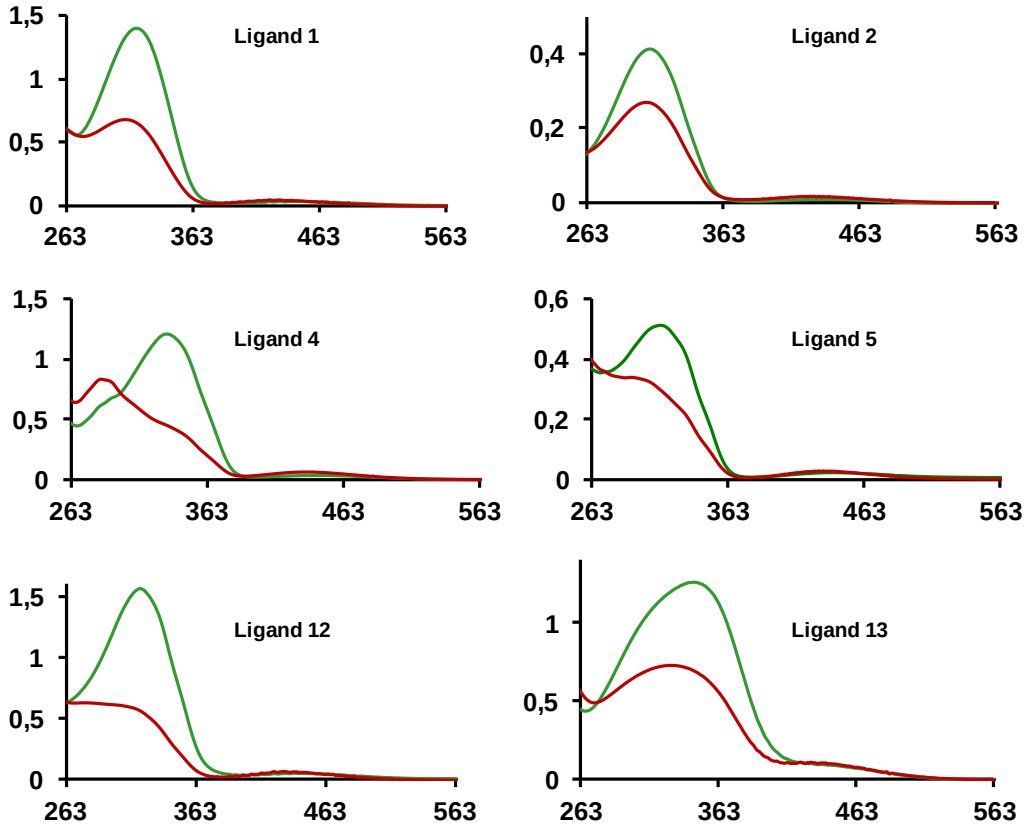

Figure 2.9. UV-Vis spectra (absorbance vs. wavelength (nm)) before (green line) and after (red line) irradiation of ligands after 30 min irradiation at $\lambda_{azo\ \pi\rightarrow\pi^*}$ and 30 min irradiation at $\lambda_{optimal}$. CH_3CN.

To measure the stability of the *cis* form, the reverse process (thermally-induced *Z*→*E* isomerization) was monitored by UV-Vis absorption spectroscopy at 55 ºC. For this purpose, once the PSS was reached, spectra were acquired at regular time intervals, to monitor the reverse process, until the original spectrum was recovered. A representative example of the thermal *cis*-to-*trans* isomerization is shown in Figure 2.10 (ligand **4**).

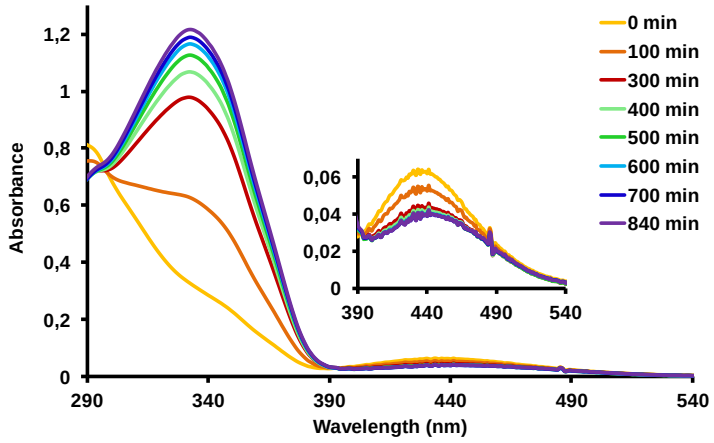

Figure 2.10. UV-Vis spectral changes during thermal *cis*-to-*trans* isomerization of ligand **4**, $3.46 \cdot 10^{-5}$ M solution in CH_3CN (55 ºC) after 30 min irradiation at 334 nm and 30 min irradiation at 337 nm.

Since this process responds to a first-order kinetics, the corresponding rate constants can be easily obtained from absorption vs. time plots. The value of absorbance at $\lambda_{\pi\rightarrow\pi^*}$ was used to follow this process. As an example, the absorbance versus time plot obtained for the ligand **4** as well as the first order plot obtained and used to calculate the rate constant of the process is shown in Figures 2.11 and 2.12.

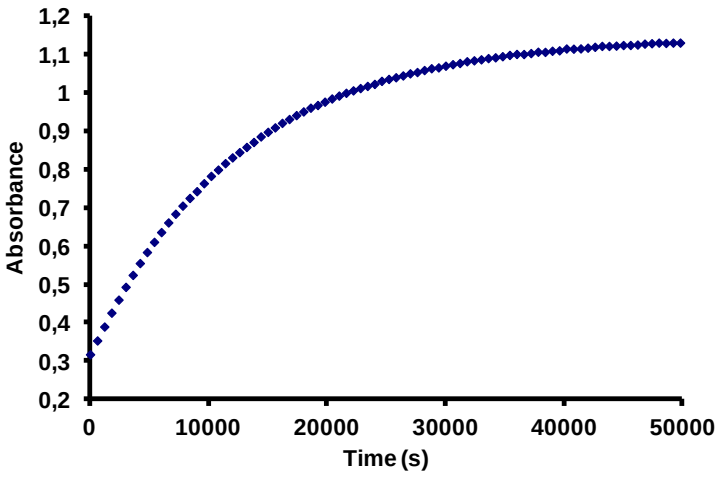

Figure 2.11. Absorbance of the band 334 nm versus time plot obtained for the *Z*→*E* isomerization process in the dark at 55 ºC for 3.46 × 10^{-5} M CH_3CN solution of ligand **4**.

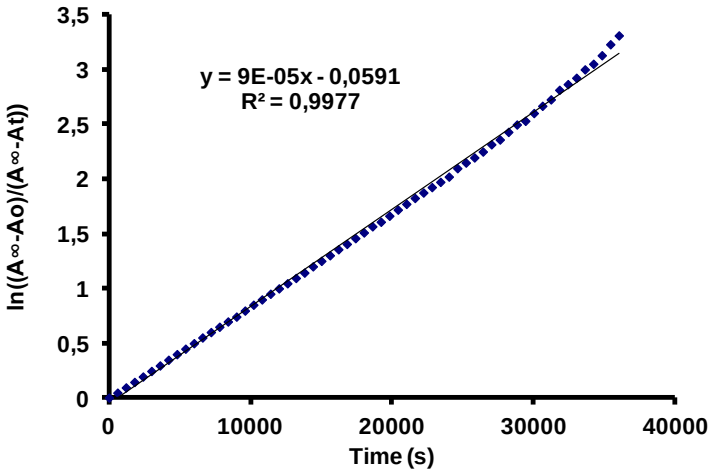

Figure 2.12. The first-order plot obtained for the for the *Z*→*E* isomerization process in the dark at 55 ºC for a 3.46 × 10^{-5} M CH_3CN solution of ligand **4**, based on the absorbance values at 334 nm.

The light-induced trans-to-cis and the reverse isomerization processes of all the azobenzene-containing ligands was studied following the methodology described above. The photoisomerization of ligand **3** was not studied due to its low solubility in common solvents. The UV-Vis spectra before and after irradiation at the individually optimized light wavelength of all the ligands are presented in Figure 2.9, and the calculated $\lambda_{optimal}$, first-order rate constants (k) and half-life times ($\tau_{1/2}$) for the *Z*→*E*

isomerization are shown in Table 2.1 (all absorbance *versus* time and first order plots obtained are compiled in the Supporting Information).

Ligands	$\lambda_{optimal}$ [a] [nm]	k [s^{-1}]	$\tau_{1/2}$ [min]
1	325	4.0×10^{-4}	29
2	312	4.0×10^{-4}	29
4	337	9.0×10^{-5}	128
5	320	5.0×10^{-5}	231
12[b]	323	7.0×10^{-5}	165
13[b]	354	1.0×10^{-4}	115

Table 2.1. Kinetic data for the *Z*→*E* isomerization process at 55 ºC. [a] Optimized light-wavelength for the *E*→*Z* photoisomerization. [b] The *Z*→*E* isomerization process at 65 ºC.

It is worth mentioning, that in all the examples described above the isomerization of each azobenzene fragment has been considered as an independent event (even when more than one azobenzene moieties are present per molecule). We are aware that the presence of more than one azobenzene fragments in the same molecule could perturb (either favour or inhibit) the isomerization of contiguous moieties. This behaviour was not observed in the studied ligands, as can be inferred from the first-order plots obtained in all the cases. Additionally, when the reverse process was monitored, an overlap of all the spectra show a clear isosbestic point (around 400 nm) which is also indicative of independent azobenzene isomerization processes. See Figure 2.13 for a representative example.

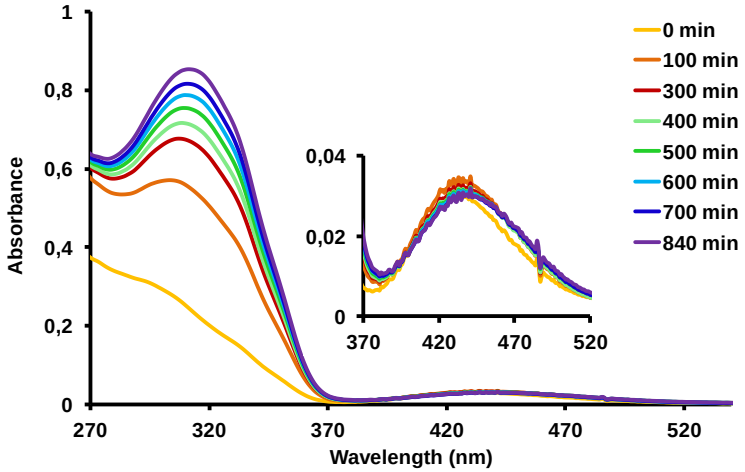

Figure 2.13. UV-Vis spectral changes during thermal *cis*-to-*trans* isomerization of ligand **5**, $3.00 \cdot 10^{-5}$ M solution in CH_3CN (55 ºC) after 30 min irradiation at 314 nm and 30 min irradiation at 320 nm.

As mentioned before, the rate of the reverse process, the thermal *Z*→*E* isomerization, gives an indication of the stability of the *cis* isomer of the azobenzene in the compound. Comparing the rates measured for the different azobenzene-containing bipyridine

ligands, we observed that azophenylpyridine derivatives **1** and **2** presented one order of magnitude faster *Z*→*E* isomerization compared to azobenzene derivatives **4** and **5**.

Ligand **1** that contains two 2,2'-linked 4-phenylazopyridine moieties (two ligands **2**) and ligand **2** itself exhibited the same rate constant, demonstrating that the number of azobenzene moieties does not influence the isomerization process and that in fact they do behave as independent units (as it was already inferred from the inspection of the evolution of their UV-Vis spectra) as already observed for related ligands.[7a] Ligand **4**, containing only one azobenzene moiety in *para* position, presented a faster rate constant than ligand **5** that contains two azobenzene moieties in *meta* positions. If we assume than in this case also the azobenzenes behave as independent photochromic units, the different rate of isomerization observed should be attributed to their substitution pattern. The faster isomerization observed in the case of ligand **4** could be due to an increased stability of the *trans*-form of the azobenzene in this case due to a more effective conjugation along the molecule (*vide supra*).

Compared to the pyridine-based ligands, in the case of azobenzene-substituted phosphines **12** and **13** the *cis* form was considerably more stable. In fact, the *Z*→*E* isomerization process was measured at slightly higher temperatures than the former (65 ºC) to reduce the analysis time and keep it within reasonable acquisition times. Also in this case, the ligands containing *para*-substituted azobenzene moieties (**13**), showed a higher rate constant value than the *meta*-substituted ligand **12**.

The higher stability observed for the *cis* isomer in phosphine ligands makes these ligands specially interesting to achieve the main objective of the thesis.

2.2. SYNTHESES OF BIPYRIDINE LIGANDS WITH DIFFERENT ELECTRONIC PROPERTIES

As mentioned before, the electronic properties of transition metal complexes can be tuned by using appropriate ligands. In order to study the effect of this variation on the properties of the compounds, it is important to construct families of ligands in which this is the only parameter that changes. For this purpose, a series of 2,2'-bipyridine ligands in which the electronic properties were systematically modified by using different groups in 4,4'-positions were synthesized in this work. The introduction of the substituent in *para* respect to the donor N atom facilitates the analysis of the results as it minimizes other effects (such as steric) on the reactivity of the final compound while maximizing the transfer of electronic information to the metal center trough conjugation effects.

The Hammett parameter (σ) is commonly used as a measure of the electronic properties of substituents in organic molecules. It is defined as positive for electron-

acceptor substituents and negative for electron-donors. This parameter was originally determined experimentally based on the ionization constants of *meta*- and *para*-substituted benzoic acids (Scheme 2.5).

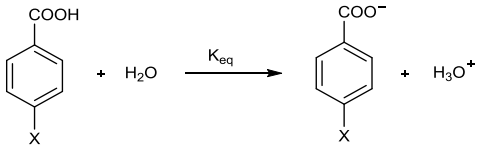

Scheme 2.5. Equilibrium of *para*-substituted benzoic acids used by Hammett to define σ values.

The value of the Hammet parameter (σ) was calculated from the equation shown below, where K_H is the ionization constant for benzoic acid in water at 25 °C and K_x is the corresponding constant for a *meta*- or *para*-substituted benzoic acid.[12]

$$\sigma_x = \log K_x - \log K_H$$

Hammett was able to correlate these values with the reaction rates of the hydrolysis of the corresponding esters. Since then, the Hammett parameter has been used to analyze the electronic influence of different substituents on reaction rates, facilitating the study of reaction mechanisms.[13]

Due to the poor correlations obtained with σ_m (*meta*) and σ_p (*para*) values when extended conjugation was present in the molecule, new parameters (σ_p^- and σ_p^+) were defined.[12] From a practical point of view, when the electronic effects of certain reaction need to be studied, the parameter that renders a better correlation is eventually used. In our case (*vide infra*) σ_p^+ will be the parameter of choice.

The series of 4,4'-functionalized 2,2'-bipyridine ligands used in this thesis is shown in Chart 2.3.

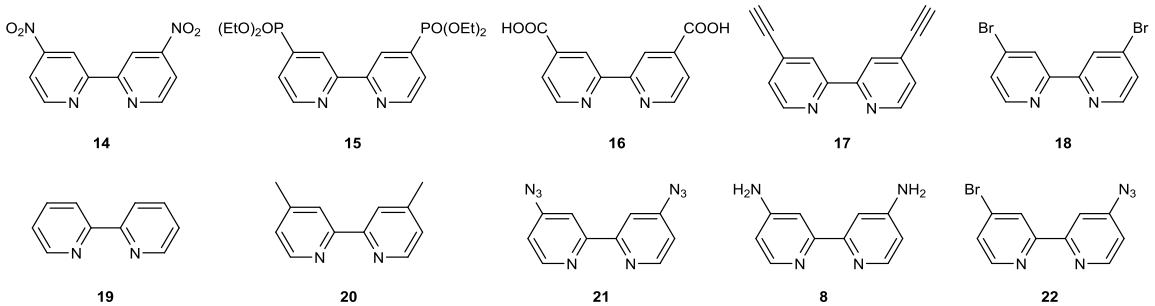

Chart 2.3. 4,4'-disubstituted-2,2'-bipyridine ligands **14**–**22** and **8**.

All these ligands were already reported in the literature. 4,4'-dibromo-2,2'-bipyridine (**18**), 2,2'-bipyridine (**19**) and 4,4'-dimethyl-2,2'-bipyridine (**20**) were obtained from commercial sources. 4,4'-diamino-2,2'-bipyridine (**8**) was an intermediate of the synthesis of ligand **1**.

4,4'-Dinitro-2,2'-bipyridine (**14**) was synthesized according to the procedure described in the literature starting from 4,4'-dinitro-2,2'-bipyridine-N-oxide (**7**), an intermediate for

the synthesis of ligand **1**.[14] The N-oxide moiety of 4,4'-dinitro-2,2'-bipyridine-N-oxide (**7**) was reduced with PCl_3 (Scheme 2.6). The desired ligand was obtained with a yield of 50%.

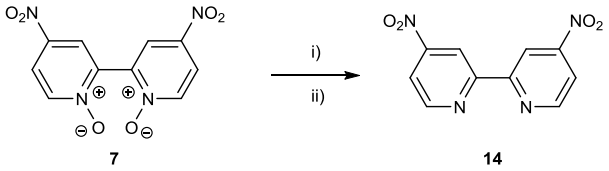

Scheme 2.6. Synthetic route toward ligand **14**. i) 36.5 equiv. PCl_3, CH_2Cl_2, reflux, 16 h. ii) NaOH aq..

4,4'-Bis(diethylphosphonate)-2,2'-bipyridine (**15**) was obtained by Pd-catalyzed coupling of 4,4'-dibromo-2,2'-bipyridine and diethyl phosphite (Scheme 2.7). The product was obtained with a yield of 60%.[15]

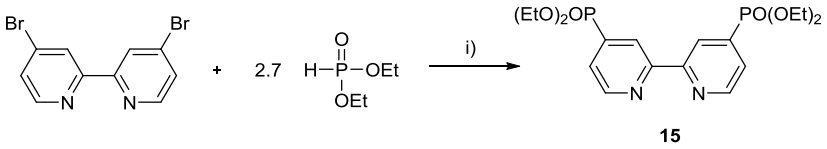

Scheme 2.7. Synthetic route toward 4,4'-bis(diethylphosphonate)-2,2'-bipyridine (**15**) i) 10 mol % $Pd(PPh_3)_4$, NEt_3, toluene, 90 ºC, 4 h.

For the synthesis of 4,4'-bis(carboxy)-2,2'-bipyridine (**16**) a procedure described in the literature was followed (Scheme 2.8).[16] 4,4'-dimethyl-2,2'-bipyridine was added slowly over a solution of $Na_2Cr_2O_7{\cdot}2H_2O$ in concentrated H_2SO_4 and the mixture was stirred for 30 min. After this period of time, the reaction mixture was added over cold water and the yellow solid that precipitated was filtered. The solid was dissolved in 10% NaOH aqueous solution. Then, 10% HCl aqueous solution was added until pH = 2 and the product precipitated. It was obtained in a quantitative yield.

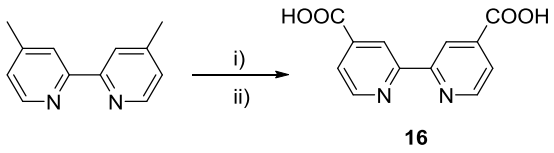

Scheme 2.8. Synthetic route toward 4,4'-bis(carboxy)-2,2'-bipyridine (**16**) i) 4.6 equiv. $Na_2Cr_2O_7{\cdot}2H_2O$, H_2SO_4, H_2O. ii) 10% aq. NaOH, 10% aq. HCl.

4,4'-bis(ethynyl)-2,2'-bipyridine (**17**) was also synthesized according to published methodologies (Scheme 2.9). The intermediate 4,4'-bis(trimethylsilylethynyl)-2,2'-bipyridine derivative was obtained by Sonogashira coupling of 4,4'-dibromo-2,2'-bipyridine and (trimethylsilyl)acetylene with a yield of 76%.[17] Subsequent hydrolysis using K_2CO_3 rendered the desired ethynyl derivative in 86% yield.[18]

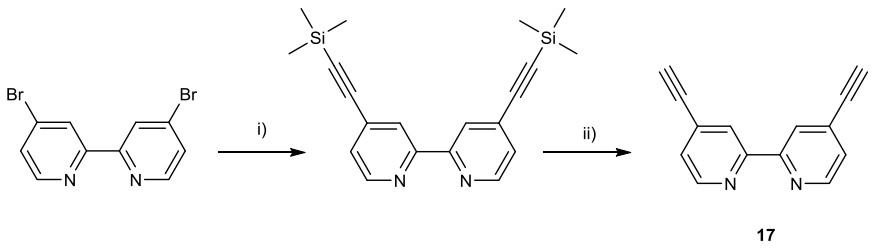

Scheme 2.9. Synthetic route toward ligand **17**. i) (trimethylsilyl)acetylene (3 equiv.), CuI (4 mol%), $Pd(PPh_3)_2Cl_2$ (2 mol%), Et_3N, reflux, 16 h. ii) K_2CO_3 (3.3 equiv.), MeOH, 16 h, rt.

To obtain 4,4'-diazido-2,2'-bipyridine (**21**), a solution of 4,4'-dibromo-2,2'-bipyridine and NaN_3 in DMF was heated for 18 h, as described in the literature (Scheme 2.10).[19] After adding H_2O, the product was extracted with Et_2O and purified by column chromatography (CH_2Cl_2). An asymmetric product was eluted before the desired product that was identified as the intermediate 4-bromo-4'-azido-2,2'-bipyridine (**22**), resulting from the substitution at only one of the bromine atoms of 4,4'-dibromo-2,2'-bipyridine. Subsequently, disubstituted product 4,4'-diazido-2,2'-bipyridine (**21**) was eluted.

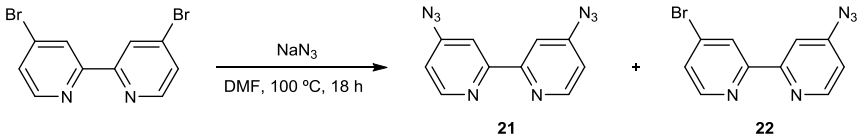

Scheme 2.10. Synthetic route toward ligands **21** and **22**. Yields: **21** (35%) and **22** (13%).

The ^{1}H-NMR spectrum of both ligands and the one of the starting compound (ligand **18**) are presented in Figure 2.14. In the case of the asymmetric ligand **22**, six different proton signals were observed in the ^{1}H-NMR spectra. However, symmetrically substituted ligands **18** and **21** showed only 3 signals, as the protons of both pyridine fragments are magnetically and chemically equivalent for symmetry reasons. It is also worth noticing that spectra of compound **22** corresponds roughly with the overlapped spectra of **18** and **21**.

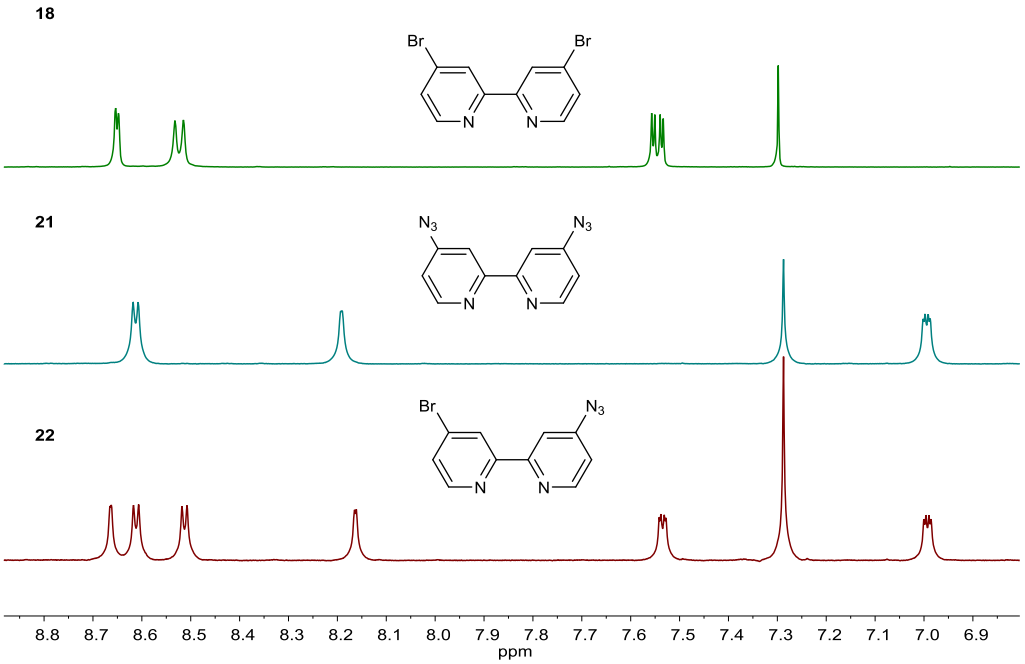

Figure 2.14. ^{1}H-NMR spectrum of **18** (300 MHz), **21** (500 MHz) and **22** (500 MHz) in $CDCl_3$.

All the 4,4'-disubstituted-2,2'-bipyridine ligands were characterized by ^{1}H-NMR and the obtained spectra match with literature values. In Figure 2.15 the ^{1}H-NMR spectrum of all the ligands (except **16** that is not soluble in $CDCl_3$ and **22** that is asymmetric) are shown. The spectrum have been stacked according to the Hammett value (σ_p^+) of their substituents.

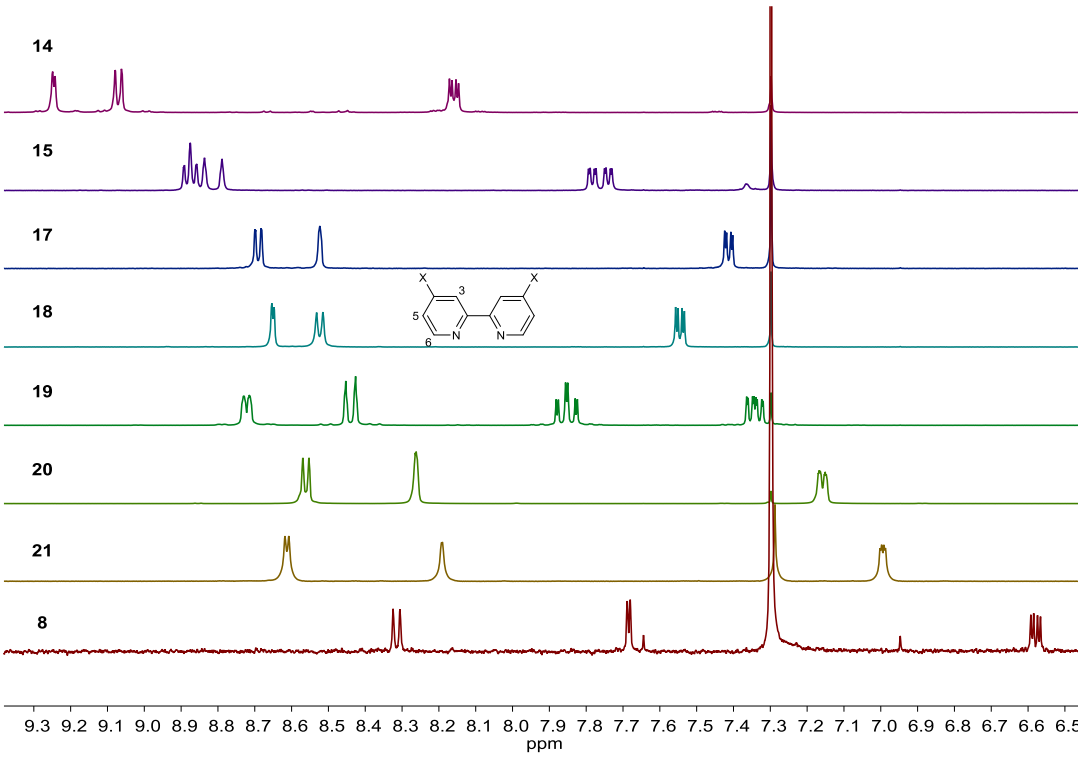

Figure 2.15. ^{1}H-NMR spectrum of **14**, **15**, **17–21** and **8** in $CDCl_3$.

As expected, the electronegativity of the substituent in 4,4'-position of the 2,2'-bipyridine influences the chemical shift of their signals in the ^{1}H-NMR spectrum. In principle, the signals of the 2,2'-bipyridines with electron-acceptor substituents should experience a low-field shift compared with those of the 2,2'-bipyridines substituted with electron-donor groups. In Table 2.2 the chemical shift of the three aromatic signals of the 2,2'-bipyridine in their ^{1}H-NMR spectra, and the tabulated σ_p^+ values of their substituents are summarized.[12]

Ligand	σ_p^+	H_6	H_3	H_5
14	0,79	9.24	9.07	8.16
15	Unknown	8.87	8.81	7.76
17	0,18	8.69	8.53	7.41
18	0,15	8.65	8.52	7.55
19	0	8.72	8.44	7.33
20	-0,31	8.56	8.26	7.16
21	Unknown	8.62	8.20	6.99
8	-1,3	8.31	7.68	6.58

Table 2.2. σ_p^+ values of the substituents and ^{1}H-NMR chemical shifts of **14**, **15**, **17**–**21** and **8** in $CDCl_3$.

To the best of our knowledge, the σ_p^+ values of diethylphosphonate and azido substituents are not published in the literature.[18] Nevertheless, we considered that they could be interpolated from the chemical shift of their signals in the ^{1}H-NMR spectra. For this purpose the chemical shifts of the "known" compounds were plotted against their Hammett values (σ_p^+) (Figure 2.16). As it can be observed, a quite acceptable correlation was obtained for the three signals, being the one obtained with chemical shifts of H_3 the one that presented a better linear fit. For this reason the equation from this proton was chosen to interpolate the missing values of σ_p^+ using the chemical shift of H_3 in compounds **15** and **21**.

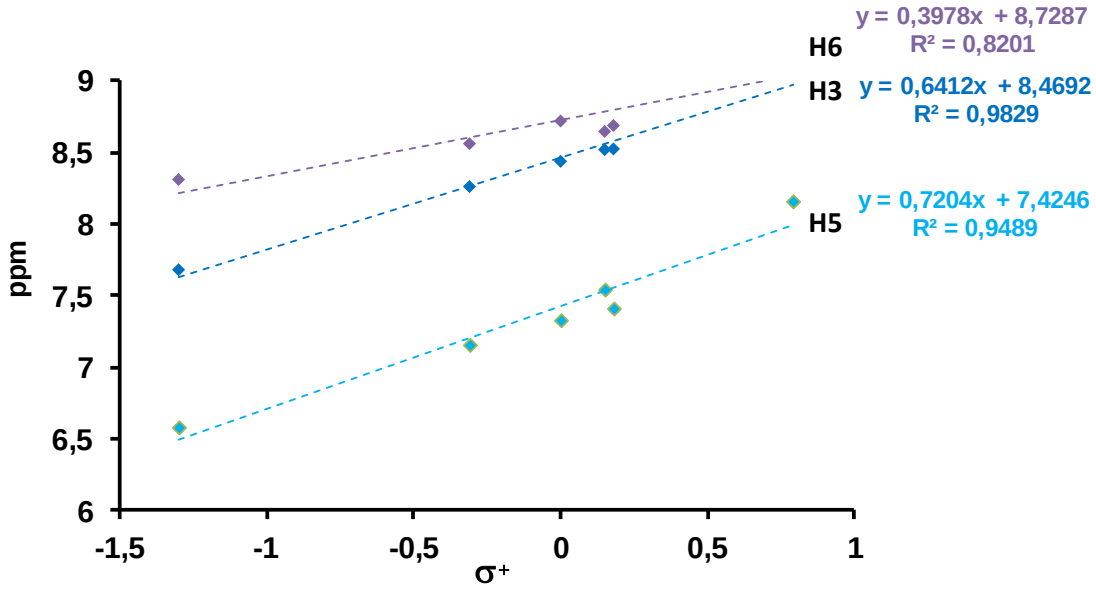

Figure 2.16. σ_p^+ versus chemical shifts plot.

Following the above described procedure, the calculated σ_p^+ values for diethylphosphonate and azido substituents were 0,54 and −0,42, respectively, and they will be used when required along the work presented in this manuscript.

Considering the calculated values of the substituents that were not reported in the literature, the electronegativity of the subsituents can be ordered from the most electron-acceptor to the most electron-donating:

$$NO_2 > PO(OEt)_2 > COOH > C{\equiv}CH > Br > H > CH_3 > N_3 > NH_2$$

2.3. REFERENCES

[1] R. H. Crabtree, *New J. Chem.*, **2011**, *35*, 18–23.

[2] O. Maury, J-P. Guégan, T. Renouard, A. Hilton, P. Dupau, N. Sandon, L. Toupet and H. Le Bozec, *New J. Chem.*, **2001**, *25*, 1553–1566.

[3] D. Zhang, J. P. Telo, C. Liao, S. E. Hightower and E. L. Clennan, *J. Phys. Chem. A*, **2007**, 13567–13574.

[4] M. Busby, P. Matousek, M. Towrie and A. Vlček Jr, *Inorg.Chim.Acta*, **2007**, *360*, 885–896.

[5] N. Kano, J. Yoshino and T. Kawashima, *Organic Letters*, **2005**, *7*, 3909–3911.

[6] J. H. Harvey, B. K. Butler and D. Trauner, *Tetrahedron Lett.*, **2007**, *48*, 1661–1664.

[7] a) K. Yamaguchi, S. Kume, K. Namiki, M. Murata, N. Tamai and H. Nishihara, *Inorg. Chem.*, **2005**, *44*, 9056–9067. b) S. Kume, M. Kurihara and H. Nishihara, *J. Korean Electrochem. Soc.*, **2002**, *5*, 189–191. c) S. Kume, M. Kurihara and H. Nishihara, *Chem. Commun.*, **2001**, 1656–1657.

[8] R. A. Jones, B. D. Roney, W. H. F. Sasse and K. O. Wade, *J. Chem. Soc. (B) Phys. Org.*, **1967**, 106–111 and references therein.

[9] M. D. Segarra-Maset, P. W. N. M. van Leeuwen, and Z. Freixa, *Eur. J. Inorg. Chem.*, **2010**, 2075–2078.

[10] M. Ribagorda, E. Merino, *An. Quím.*, **2009**, *105*, 290–299.

[11] M. Kaiser, S. P. Leitner, C. Hirtenlehner, M. List, A. Gerisch and U. Monkowius, *Dalton Trans.*, **2013**, *42*, 14749–14756.

[12] C. Hansch, A. Leo and R. W. Taft, *Chem. Rev.*, **1991**, *91*, 165–195.

[13] D. Lupp, N. J. Christensen and P.Fristrup, **2015**, Combined Use of Both Experimental and Theoretical Methods in the Exploration of Reaction Mechanisms in Catalysis by Transition Metals, In V. P. Ananikov (Ed), *Understanding Organometallic Reaction Mechanisms and Catalysis: Computational and Experimental Tools*, Wiley-VCH.

[14] H. Arzoumanian and R. Bakhtchadjian, *Transition Met. Chem.*, **2006**, *31*, 681–689.

[15] M. Montalti, S. Wadhwa, W. Y. Kim, R. A. Kipp and R. H. Schmehl, *Inorg. Chem*., **2000**, *39*, 76–84.

[16] K. F. Lin, J. S. Ni, C. H. Tseng, C. Y. Hung and K. Y. Liu, *Mater. Chem. Phys*., **2013**, *142*, 420–427.

[17] P. V. James, K. Yoosaf, J. Kumar, K. G. Thomas, A. Listorti, G. Accorsi and N. Armaroli, *Photochem. Photobiol. Sci.*, **2009**, *8*, 1432–1440.

[18] T. R. Kelly, Y.–J. Lee and R. J. Mears, *J. Org. Chem.*, **1997**, *62*, 2774–2781.

[19] P. Fabbrizzi, B. Cecconi and S. Cicchi, *Synlett*, **2011**, *2*, 223–226.

CHAPTER 3

CYCLOMETALATED Ir(III) BIPYRIDINE COMPLEXES FOR DYE-SENSITIZED SOLAR CELLS

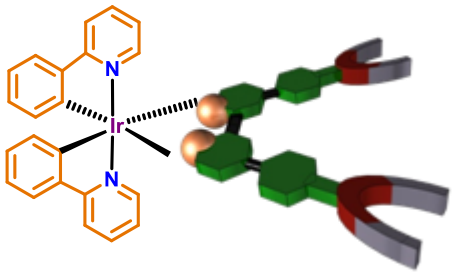

The potential application of iridium(III) complexes containing two phenylpyridine and one 2,2'-bipyridine-type ligands as dyes for DSSC is presented in this chapter. Two different anchoring groups are incorporated at 4,4'-positions of the bipyridine, and the iridium complexes combining them with four different phenylpyridine ligands (one of them containing an azobenzene fragment) are studied. The different stability when anchored on TiO_2 surface together with the performance of DSSCs sensitized with these Ir(III) complexes is discussed.

Part of the work described in this chapter has been published: A. Telleria, E.C. Kohlrausch, RdC. Duarte, F.S. Rodembusch, J. Dupont, Z. Freixa, M.J.L. Santos, Chemistry Select., 2016, accepted.

3.1. INTRODUCTION

A renewable energy source is required to respond to the energy consumption demand of our society, nowadays largely based on limited fosil resources. Dye-sensitized solar cells (DSSCs) are considered the best solution for converting the solar light into electrical energy. A DSSC is composed by a working and a counter electrodes and a redox couple. In the working electrode a mesoporous semiconductor metal oxide (often TiO_2) is deposited on a transparent conducting material (the most commonly used is fluorine-doped tin oxide (FTO)). The mesoporous film is sensitized with a dye, that acts as a light harvesting material. The first solar cell was reported by Grätzel and O'Regan in 1991, composed by TiO_2 films modified with trimeric ruthenium complexes that were deposited on a conducting glass.[1] Since then, numerous ruthenium polypyridine complexes have been used as dyes, because of their intense metal-to-ligand charge-tranfer bands (MLCT) in the visible range. Ru(II) complexes most used as dyes are the called N3 and "black dye" (Chart 3.1). They suffer from poor long-term stability due to the presence of labile isothiocyanate groups. These dyes show efficiencies of around 10%. Further developments are somehow restricted due to the synthetic difficulties encountered that limited the number of ligands that can be introduced easily.[2] That is why iridium complexes gained attention as dyes for DSSCs. Ir(III) easily forms bis- and tris-cyclometalated complexes with high thermal and chemical stability and long excited-state lifetimes. The drawback is that low efficiencies are obtained with these complexes. One of the best iridium complexes used as dye, shown in Chart 3.1, reached an efficiency of only 2.2%, probably because of the weak light absorbance in the visible region.[3]

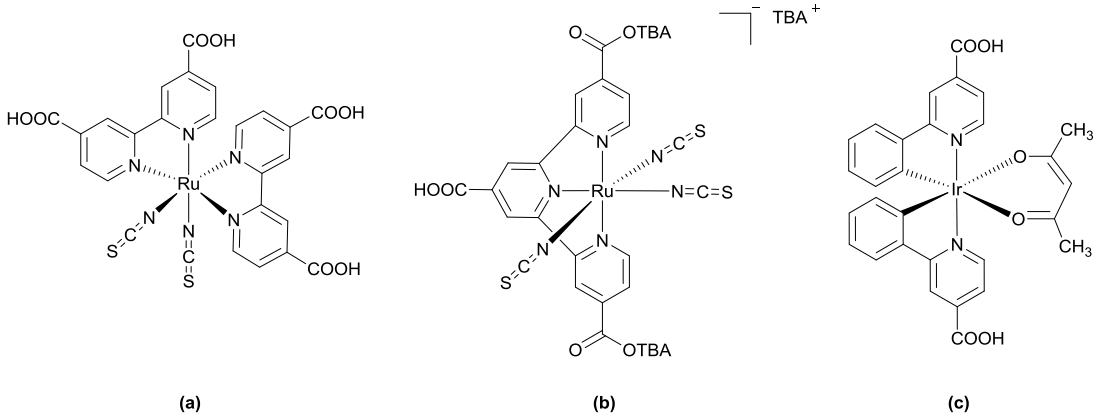

Chart 3.1. Ru(II) and Ir(III) photosensitizers: (a) N3, (b) "black dye" (TBA = tetrabutylammonium cation), (c) one of the best Ir(III) dyes known up to date.

A schematic representation of the operating mode of the DSSC is shown in Figure 3.1. Visible light is absorbed by the sensitizer (dye), which after excitation is oxidized injecting electrons to the conduction band of the TiO_2. The sensitizer, on its oxidized

ground state, is reduced to original form by electron donation from the electrolyte, commonly composed by the iodide/triiodide (I^-/I_3^-) redox system. From the conduction band, electrons flow through the external load to the counter electrode immersed into the electrolyte solution, which is reduced to complete the circuit. Altogether, electrical current is generated harvesting energy from the sun.[4]

In the dark, the Fermi level of the electrons in the TiO_2 is equilibrated with the redox energy level of the electrolyte, but when the cell is exposed to light, this energy difference splits and the driving force that is necessary to generate the electron flow is obtained. The difference between the Fermi level under illumination and the electrolyte redox potential is called open circuit voltage (V_{OC}).[5]

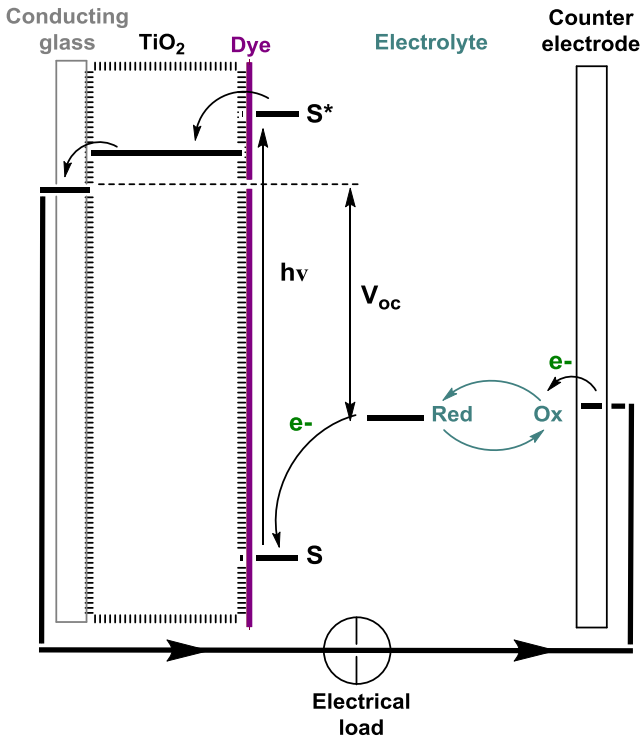

Figure 3.1. Schematic representation of a dye-sensitized solar cell (DSSC).

An efficient sensitizer has to fulfill some requirements:[3]

- A broad and strong absorption capacity, preferably from the visible to the near-infrared.
- Minimal deactivation of the excited state by an emissive relaxation or heat.
- Irreversible adsorption to the semiconductor's surface and a strong electronic coupling between its excited state and the semiconductor conduction band.
- High chemical stability in the ground, excited and oxidized states.
- The LUMO (Lowest Unoccupied Molecular Orbital) of the dye must be located sufficiently high in energy compared to the conduction band of the TiO_2 to prompt an effective electron injection.

- The HOMO (Highest Occupied Molecular Orbital) of the dye must be sufficiently low in energy compared to the redox level of the electrolyte for an efficient regeneration of the dye.

There are some processes that lower the efficiency of a solar cell. For example, the recombination of the injected electrons with the oxidized sensitizer or with the redox couple at the TiO_2 surface. A large surface area of the TiO_2 should benefit the absorption of the solar irradiation through the dye, but the aforementioned undesirable charge recombination processes could be also favored.

To avoid these processes, the separation between the dye and the electrode surface has to be considered. Nevertheless, complexes with MLCT transitions are sensitive to this separation and if the separation is too large it may be prejudicial for the injection efficiency. Altogether, this separation should be large enough to reduce the recombination processes, but still permit an effective injection of the electrons from the dye to the electrode. Complexes with ligand-centered (LC) transitions, as cyclometalated iridium(III) complexes, are less sensitive to this separation, containing both injection pathways, from MLCT and LC transitions (Figure 3.2), and make them good candidates for their use as dyes in DSSC.[4,6]

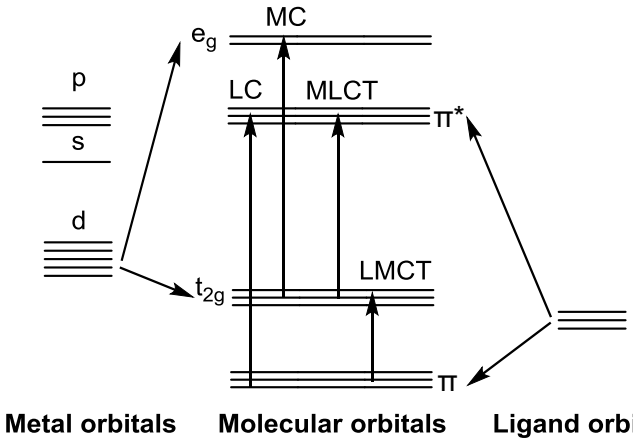

Figure 3.2. Simplified molecular orbital diagram for an octahedral d^6 metal complex with 2-phenylpyridine as ligand and possible electronic transitions.

In addition, variations on the ligands modify the HOMO-LUMO gap of these complexes (this will be extensively explained in Chapter 4) and consequently they can cover a wide range of the absorption spectrum. To improve the efficiency of the electron transfer from the dye to the TiO_2 surface, it is convenient to have the anchoring group of the complex directly linked to the ligand where the LUMO is mostly localized.[7]

Carboxylates have been widely used as anchoring groups between photosensitive complexes and TiO_2 surfaces due to the exceptional electron injections obtained with them.[8,9] The main drawback for their use is that carboxylates are not stable in aqueous

media and get desorbed from the TiO_2 surface by hydrolysis, being unsuitable for the construction of water oxidation photoelectrochemical cells.[10] Several anchoring groups have been studied to replace carboxylates, such as phosphonic acids,[11,12] hydroxamates,[13,14] silanes,[15] silatrane[16] or amides.[17] The phosponate group has gained much attention due to the stronger binding capacity with the TiO_2 surface compared with carboxylates. Both carboxylate and phosphonate have been also combined to anchor a Ru(II) dye to the TiO_2 surface, taking advantage of the efficient electron injection achieved by carboxylate linkers and the more stable binding obtained with phosphonates on the TiO_2 surface.[18]

There are different anchoring modes of carboxylate to the TiO_2 surface (Figure 3.3): through the interaction of one oxygen atom to one Ti(IV) (monodentate (a)) and through the coordination of two oxygen atoms to two Ti(IV) centers (bridging bidentate (b)).[19] In previous works, the adsorption of formate and acetate on TiO_2 surfaces was studied supporting the bidentate binding mode as shown in Figure 3.3b.[20,21,22]

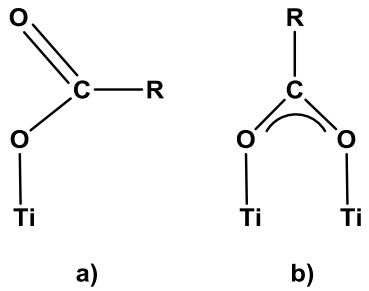

Figure 3.3. Bonding modes of carboxylate on TiO_2 surface. a) η^1 coordination, b) η^2 coordination.

Pechy *et al.* synthesized the first ruthenium sensitizer with a phosphonic acid as anchoring group in 1995.[23] This complex that contains only one phosphonic acid group showed 80 times stronger binding to the TiO_2 surface compared to the previously published N3 sensitizer (Chart 3.1) that contains four carboxylate anchoring groups.[8] Furthermore, the one with the phosphonic acid group was not desorbed from the TiO_2 surface in an aqueous solution of pH 0 to at least pH 9, whilst N3 was desorbed above pH 5.

The linkage of phosphonates to the TiO_2 surface can be through a monodentate, bidentate or tridentate binding mode (Figure 3.4). Although, the most preferred one seemed to be the bidentate, both bidentate and tridentate linkages have been found.[19,24]

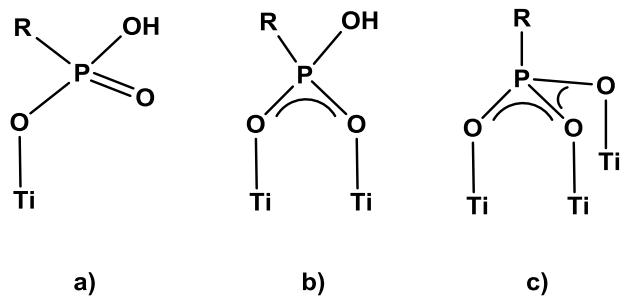

Figure 3.4. Bonding modes of phosphonate on TiO_2 surface. a) monodentate linkage, b) bidentate linkage, c) tridentate linkage.

The problem of phosphonic acids is that they are not compatible with acid-sensitive functional groups and their low solubility in organic solvents. That is why phosphonic esters have been also used as anchoring groups on TiO_2 surfaces. Commonly, phosphonic acids are synthesized from phosphonate esters that are silylated to be more easily hydrolyzed. So the use of phosphonate esters directly as anchoring groups also simplifies the synthetic procedure.[25] Phosphonic esters have been used to modify the TiO_2 surface and although better results were obtained for DSSC with dyes anchored through phosphonic acids, it was demonstrated that phosphonic esters could also be used as anchoring groups.[26]

The performance of a DSSC is evaluated by current *versus* potential diagrams, where the corresponding current (*I*) at rising voltage (*V*) is plotted (Figure 3.5). The overall energy conversion efficiency of a solar cell η is the percentage of solar energy converted into electrical energy, and is calculated by the equation shown below:[27,28]

$$\eta = \frac{I_{SC} V_{OC} \mathrm{FF}}{P_{in}}$$

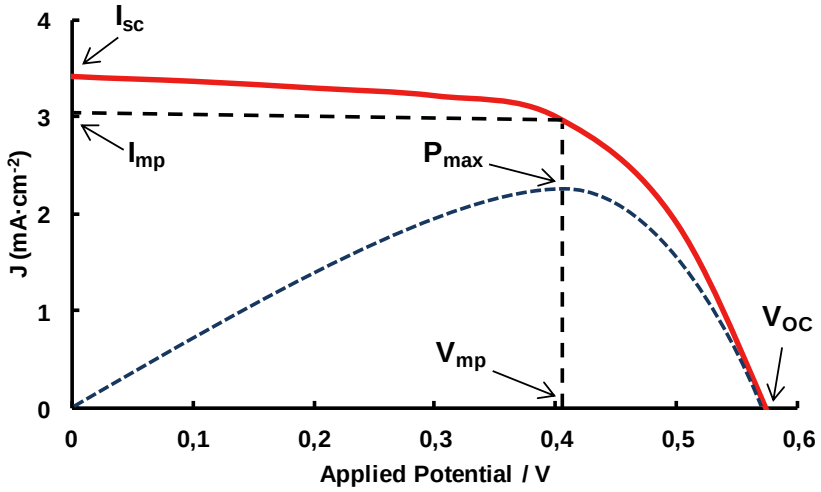

Figure 3.5. Example of current-voltage (I-V) and power-voltage curves.

The short circuit current (I_{SC}) is the current through the solar cell when the voltage across the solar cell is zero and the open circuit voltage (V_{OC}) is the maximum voltage available from a solar cell. P_{in} is the intensity of the incident light. The fill factor of the cell (FF) is defined by the maximum power (P_{max}) of the solar cell divided by the V_{OC} and I_{SC} as it is shown in the next equation:

$$\mathrm{FF} = {}^{P_{max}}\!/_{(I_{SC}V_{OC})}$$

The maximum power (P_{max}) generated by a DSSC is reached when the product of the current and the voltage is maximal. It is calculated by the current at maximal power (I_{mp}) and the voltage at maximal power (V_{mp}), following the next equation:

$$P_{\max} = I_{mp}\, x\, V_{mp}$$

To compare measurements of different solar cells, the current (I) is generally stated as current density (J) [mA/cm^2], then I_{SC} and I_{mp} become J_{SC} and J_{mp}, respectively, and are independent from the photoactive area.

There is another measurement that is called the incident photon-to-current conversion efficiency (IPCE) to measure the spectral response of DSSCs. It is calculated by the photocurrent density produced by the cell in the external circuit under monochromatic illumination divided by the intensity of the incident light and a specific wavelength, following the next equation:

$$IPCE = \frac{J_{SC}(\lambda)}{e\Phi(\lambda)} = 1240\ \frac{J_{SC}(\lambda)[Acm^{-2}]}{\lambda\,[nm]P_{in}(\lambda)[Wcm^{-2}]}$$

The IPCE spectrum normally matches with the absorption spectrum of the dyes. As an example, a IPCE curve for two different dyes are shown in Figure 3.6.

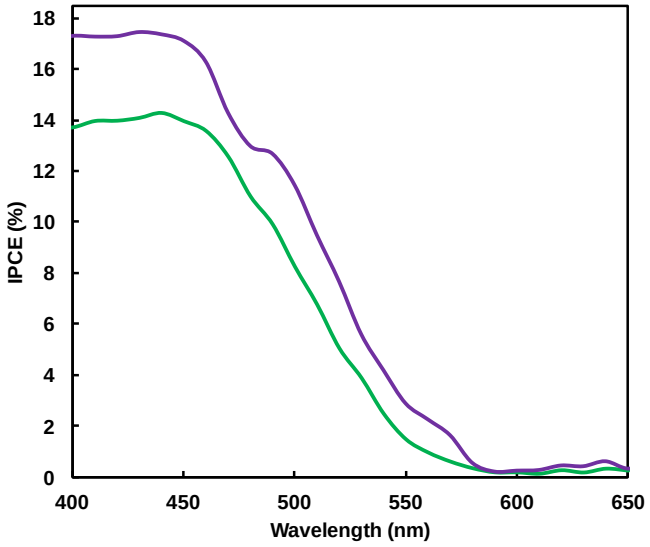

Figure 3.6. Example of IPCE curve for two different dyes.

In this chapter, Ir(III) complexes of type $[Ir(C–N)_2(bipy)]PF_6$ will be synthesized with 4,4'-bis(diethylphosphonate)-2,2'-bipyridine and 4,4'-bis(carboxy)-2,2'-bipyridine as ancillary ligands. Phenylpyridines containing different substituents (H, F and Br) will be used and complexes containing photochromic units (azobenzenes) on phenylpyridines will be also synthesized.

The performance of four DSSCs sensitized with these complexes will be studied to compare the anchoring to the TiO_2 surface with diethylphosphonate and carboxy groups. The influence of electron-withdrawing substituents on the phenylpyridine will be also discussed.

The studies on the performance of the photochromic complexes as dyes on DSSCs is currently under progress through a collaboration with the group of Dr. Marcos Jose Leite Santos at Universidade Federal do Rio Grande do Sul. Therefore, these results will not be presented here.

3.2. RESULTS AND DISCUSSION

3.2.1. SYNTHESES OF IRIDIUM COMPLEXES

Iridium(III) bis-cyclometalated complexes with two phenylpyridines and bipyridines **15** or **16** as ancillary ligands were synthesized following well-known synthetic procedures. Three phenylpyridine ligands with different substituents were used to obtain the iridium dimers used as metal precursors. 2-phenylpyridine and 2-(2,4-difluorophenyl)pyridine were obtained from commercial sources and 2-(4-bromophenyl)pyridine (**23**) was synthesized according to published methodologies.[29,30] The synthetic route for the brominated phenylpyridine **23** consists of CuI-catalyzed coupling reaction of (4-bromo)aryl iodide and pinacolborane to obtain (4-bromo)boronic acid pinacol ester followed by Suzuki cross-coupling with 2-bromopyridine (Scheme 3.1).

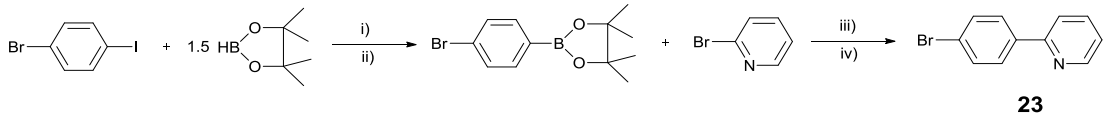

23

Scheme 3.1. Synthetic route toward 2-(4-bromophenyl)pyridine (**23**) i) 10 mol % CuI, 1.5 equiv. NaH, THF, rt, 15 h. ii) NH_4Cl sat. Yield: 82%. iii) 2.3 mol % $Pd(PPh_3)_4$, DME/EtOH. iv) Na_2CO_3 (2 M), 95 ºC, 15 h. Yield: 36%.

Neutral iridium(III) dimers of the form $[Ir(C–N)_2Cl]_2$ (C–N = cyclometalated phenylpyridine-type ligand) were obtained by reaction of $IrCl_3 \cdot 3H_2O$ with two equivalents of the C–N ligands in 2-ethoxyethanol.[31] $[Ir(ppy)_2Cl]_2$,[32] $[Ir(Fppy)_2Cl]_2$[33] and $[Ir(Brppy)_2Cl]_2$[34] were obtained with good yields (Scheme 3.2).

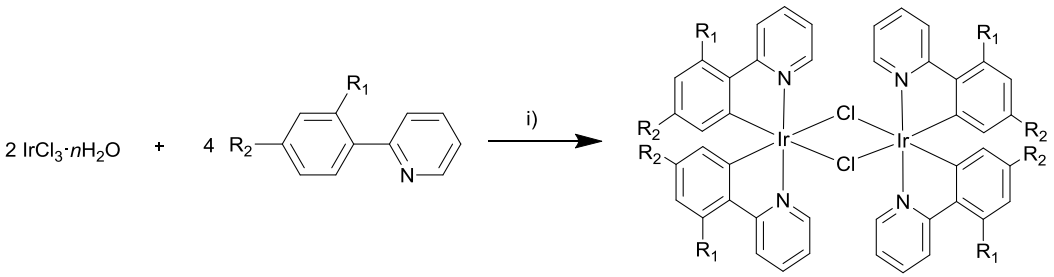

[Ir(ppy)$_2$Cl]$_2$: R_1 = H; R_2 = H
[Ir(Fppy)$_2$Cl]$_2$:R_1 = F; R_2 = F
[Ir(Brppy)$_2$Cl]$_2$:R_1 = H; R_2 = Br

Scheme 3.2. Synthetic route toward neutral dinuclear iridium intermediate. i) 2 equiv. phenylpyridine derivatives, $EtOCH_2CH_2OH/H_2O$, 120 ºC, 24 h. Yields: **[Ir(ppy)$_2$Cl]$_2$**(88%), **[Ir(Fppy)$_2$Cl]$_2$**(73%), **[Ir(Brppy)$_2$Cl]$_2$**(92%).

The general procedure to synthesize biscylometalated bipyridine iridium(III) complexes consists of cleavage of the corresponding chloride-bridged dimer in presence of two equivalents of the diimine ligand in a refluxing mixture CH_2Cl_2:MeOH 2/1.[35] This procedure was used for the synthesis of complexes with ligand **15**, but it did not work to introduce **16** as ancillary ligand. To obtain these complexes an halide abstractor (silver salt) was necessary, as reported for other cyclometalated Ir(III) complexes.[36,37] In both type of compounds KPF_6 was added *in situ* during the purification by column chromatography to the eluent to obtain complexes of general formula $[Ir(C–N)_2(bipy)]PF_6$ (Scheme 3.3). Complexes without substituents on the phenylpyridine are labeled as **A**, complexes with fluorine substituents as **B** and complexes with bromine substituents on the phenylpyridine as **C**.

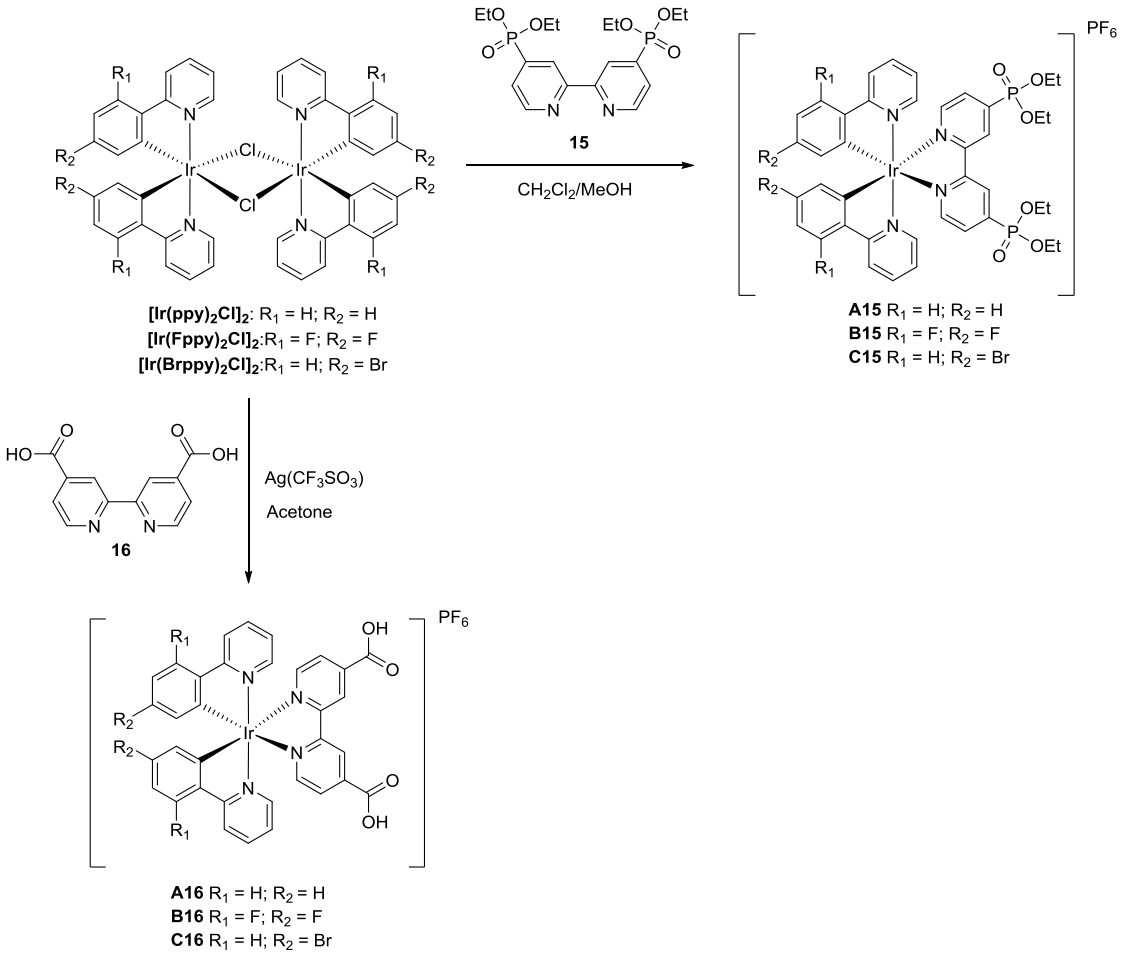

Scheme 3.3. Synthetic route toward cationic Ir(III) complexes with **15** and **16** as ancillary ligands. Yields: **A15** (40%), **B15** (40%), **C15** (68%), **A16** (72%), **B16** (52%), **C16** (41%).

Complexes with **15** as ancillary ligand were characterized by ^{1}H-, ^{13}C- and ^{31}P-NMR spectroscopy (full spectra and detailed synthetic procedures are compiled in the Supporting Information). To exemplify the spectra obtained, the ^{1}H-NMR spectra of **B15** (not described in the literature before) is shown in Figure 3.7. The C_2 symmetry of the compound in solution was reflected in the spectra. It exhibited the 9 aromatic protons in the range 5.5–9.5 ppm, due to the 6 phenylpyridine and 3 assigned to the bipyridine different aromatic protons. The signal around 4.0 ppm, that integrates for 4 protons, was assigned to two CH_2 of the ethyl groups. And around 1 ppm, the most intense peak assigned to two CH_3 of the ethyl groups was identified.

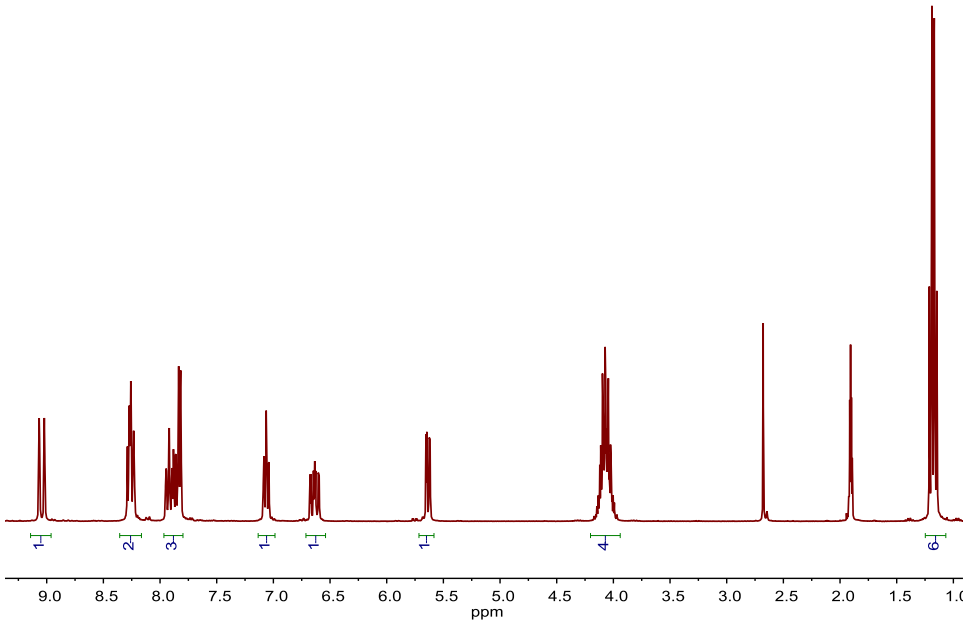

Figure 3.7. ^{1}H-NMR spectrum of **B15** in acetone-d_6, 300 MHz.

In Figure 3.8 the ^{13}C-APT-NMR of **B15** is shown. The negative peaks of the 9 aromatic CH appeared between 95–155 ppm. The signal at 98 ppm was assigned to the CH from the phenylpyridine located between two fluorine atoms that was split into a triplet due to the coupling of the C atom with two F atoms. The signals of another 5 aromatic CH were also split into doublets due to the coupling with one of the F atoms from the phenylpyridine or with the P atom from the phosphonic ester. The positive signals between 125–165 ppm were assigned to the seven quaternary carbons present in the complex. Two of these signals were split into double doublets due to coupling with two F atoms and were assigned to C atoms that are bond to them. Four other signals were split into doublets due to the coupling with one of the F atoms from the phenylpyridine or with the P atom from the 4,4'-substituted bipyridine. Only one quaternary carbon was not coupled with any other nucleus and appeared as a singlet. The non-aromatic region of the NMR showed two signals assigned to the diethyl groups of the bipyridine. The positive signal corresponds to two CH_2 groups and the negative one to two CH_3 groups of the diethylphosphonate.

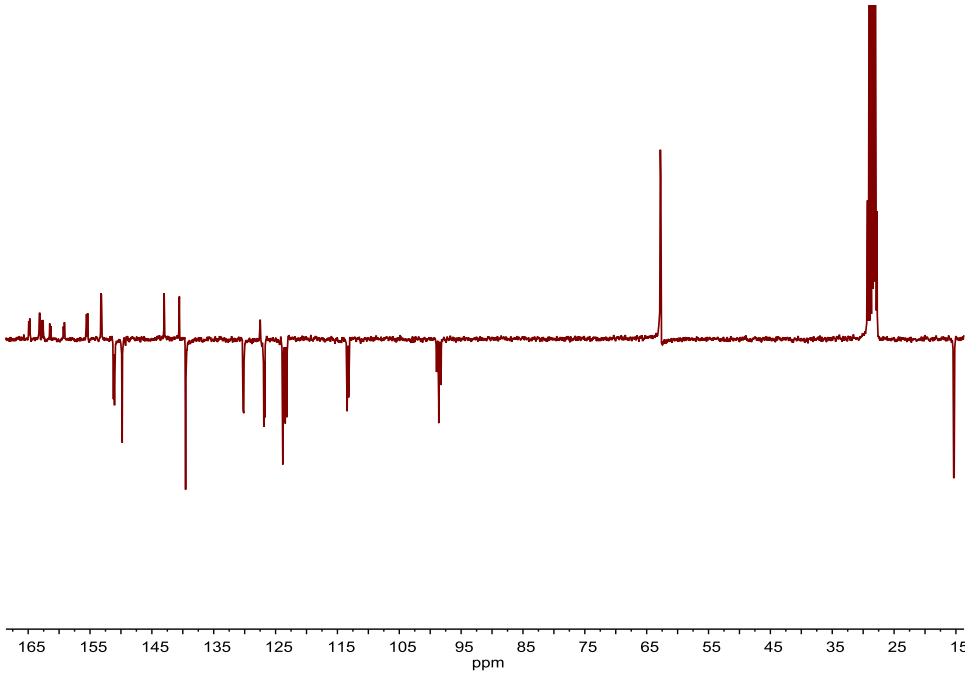

Figure 3.8. ^{13}C-APT-NMR spectrum of **B15** in acetone-d_6, 75 MHz.

The ^{31}P-NMR of **B15**, shown in Figure 3.9, exhibited two signals, one at 11 ppm that corresponds to the P atom of the diethylphosphonate and at -144 ppm the one of the counterion (PF_6). The latter was split into a septuplet due to the coupling of the P atom with six F atoms.

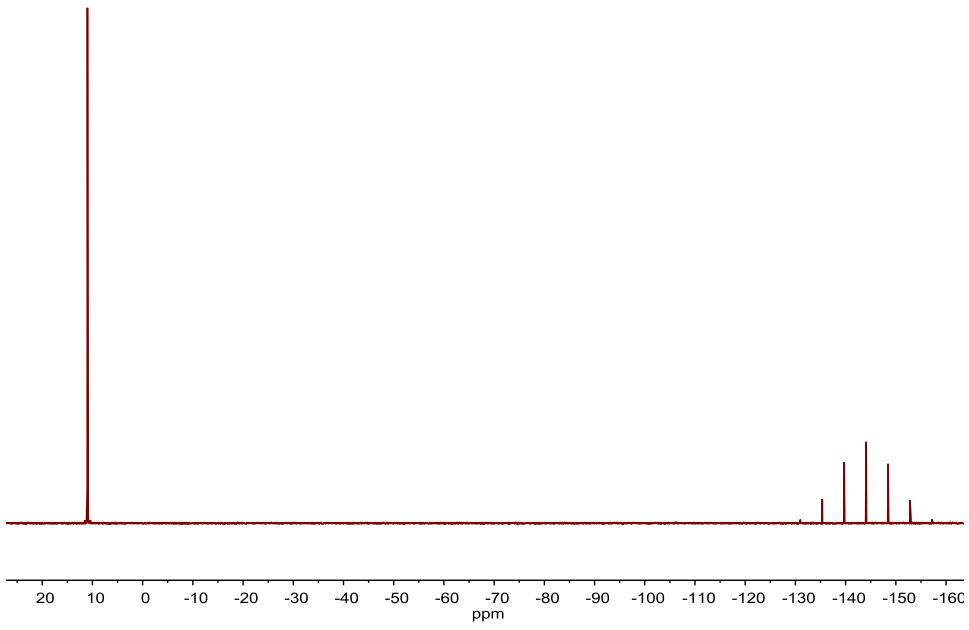

Figure 3.9. ^{31}P-NMR spectrum of **B15** in acetone-d_6, 162 MHz.

Complexes **A16** and **B16** were already reported and the ^{1}H-NMR match literature values.[38,39] **C16** was only characterized by ^{1}H-NMR because of its low solubility in common solvents prevented its full characterization by NMR spectroscopy, which

would require too long acquisition times, but ^{1}H-NMR analysis together with EA and ESI-MS confirmed its identity (full spectrum and detailed synthetic procedures are compiled in the Supporting Information).

Complexes with bromine substituents on the phenylpyridine (derivatives **C**) were synthesized to introduce *a posteriori* azobenzene fragments to obtain photochromic Ir(III) complexes able to change their properties with light. For that purpose, palladium-catalyzed Suzuki cross-coupling reactions of [4-(phenylazo)phenyl]boronic acid pinacol ester **11** with complexes **C15** and **C16** were attempted, but unfortunately the desired compounds were not obtained.

To surpass the aforementioned lack of reactivity, an alternative pathway to obtain azobenzene-containing Ir(III) complexes with 4,4'-bis(diethylphosphonate)-2,2'-bipyridine and 4,4'-bis(carboxy)-2,2'-bipyridine as ancillary ligands was considered. For this purpose, the azobenzene moiety was introduced in the brominated dimer (used as starting compound for complexes type **C**) by palladium-catalyzed Suzuki cross-coupling with [4-(phenylazo)phenyl]boronic acid pinacol ester **11** (Scheme 3.4) on this dimeric compound. This azobenzene-containing dimer **[Ir(azoppy)$_2$Cl]$_2$** was previously synthesized in our laboratory for another project.

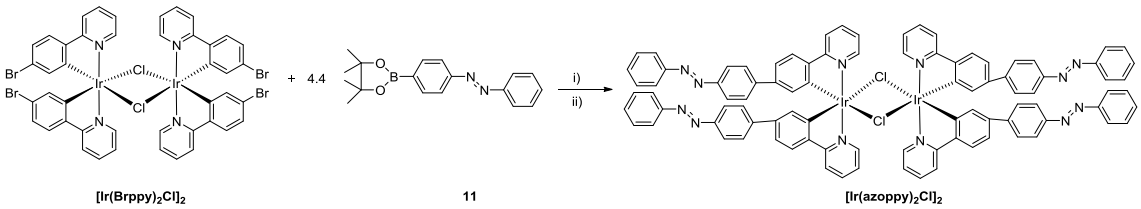

Scheme 3.4. Synthetic route toward azobenzene-containing Ir(III) dimer **[Ir(azoppy)$_2$Cl]$_2$**. i) solvent 2/1 THF:Na_2CO_3 aq. (1 M), $Pd(PPh_3)_4$ (10 mol%), 80 ºC, over-night. Yield: 44%.

The same methodology used previously to obtain complexes **A15**, **B15** and **C15** was used to obtain **D15**. Complex **D16** was obtained with the same procedure used for complexes **A16**, **B16** and **C16**, using a halide abstractor. Both compounds were obtained with moderate yields (Scheme 3.5).

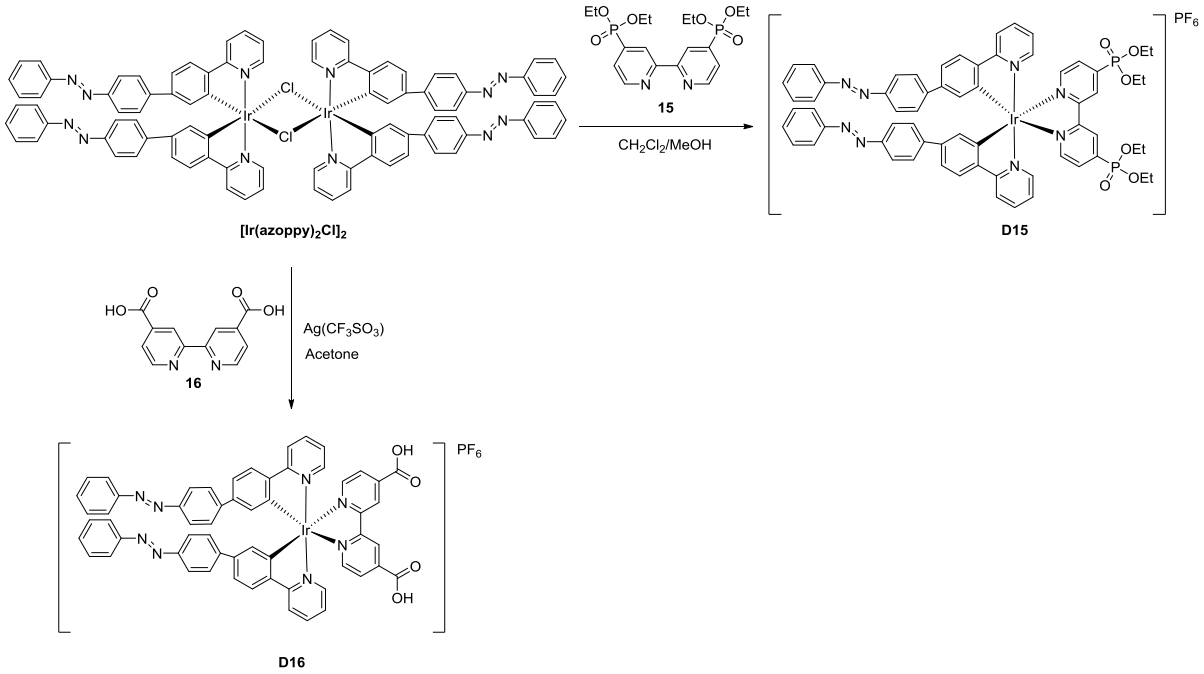

Scheme 3.5. Synthetic route toward cationic azobenzene-containing Ir(III) complexes with **15** and **16** as ancillary ligands. Yields: **D15**(33%), **D16**(63%).

D15 was characterized by ^{1}H-, ^{13}C- and ^{31}P-NMR. Only the ^{1}H-NMR of **D16** was registered because of the low solubility of this complex in common solvents (full spectra and detailed synthetic procedures are compiled in the Supporting Information). As expected, azobenzene-containing complexes **D15** and **D16** exhibited more complicated spectra than ones without azobenzenes due to the overlap of aromatic signals. In Figure 3.10 is shown the ^{1}H-NMR of **D15** to exemplify this complexity.

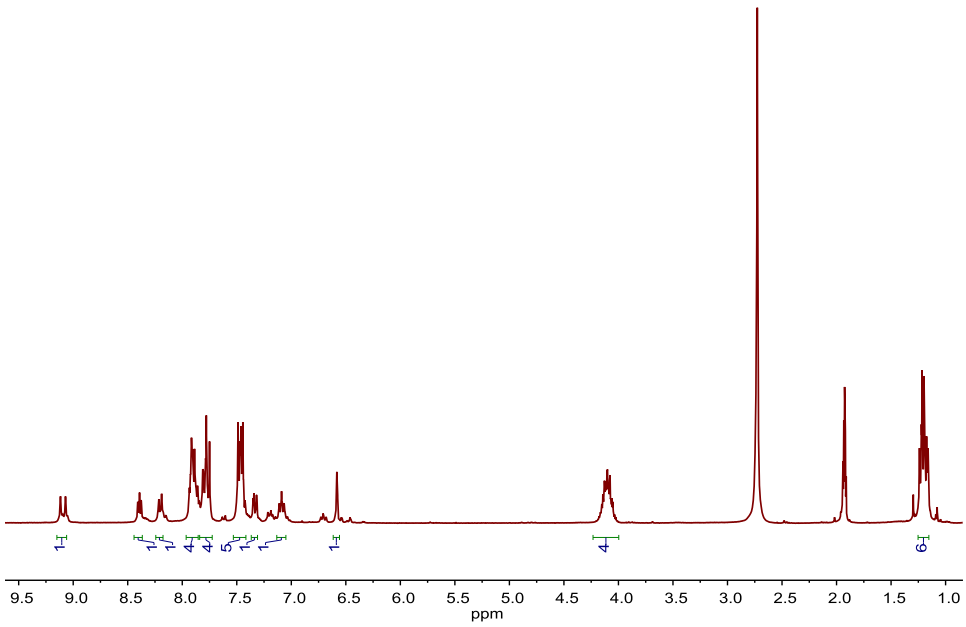

Figure 3.10. ^{1}H-NMR spectrum of **D15** in acetone-d_6, 300 MHz.

3.2.2. UV-VIS CHARACTERIZATION

UV-Vis absorption spectra of all the Ir(III) complexes synthesized were registered in diluted EtOH solutions at room temperature (spectra are shown in Figures 3.11 and 3.12). In the spectra of complexes **A**–**C** the characteristic bands of cationic complexes of the type $[Ir(ppy)_2(bipy)]^+$ were observed. However, for complexes **D15** and **D16** containing two azobenzene fragments on the phenylpyridines, these bands were overlapped with the characteristic bands of the azobenzene fragment, being hardly identified.

The main transitions for these type of complexes are ligand centered π−π* transitions (^{1}LC) where both cyclometalated and ancillary ligands are involved and therefore they exhibit intense absorption bands in the UV region between 250–350 nm (ε~3−5 × 10^4 $M^{-1}cm^{-1}$). Transitions attributed to metal-to-ligand (^{1}MLCT) and ligand-to-ligand (^{1}LLCT) charge transfer are responsible of weaker bands between 350–450 nm.[40,41]

Complexes with the ancillary ligand 4,4'-bis(diethylphosphonate)-2,2'-bipyridine (**15**), presented slightly more intense absorptivity than complexes with 4,4'-bis(carboxy)-2,2'-bipyridine (**16**). In the case of complexes **A15**−**C15** the complex with fluorine substituents (**B15**) is the one with the most intense absorptivity and the complex with bromine subtituents (**C15**) showed the lowest. However, for complexes **A16**−**C16** the derivative without substituents on the phenylpyridine (**A16**) is the one with the highest absorptivity and the one with bromine substituents (**C16**) exhibit the lowest, as in the case of complexes with 4,4'-bis(diethylphosphonate)-2,2'-bipyridine (**15**) as ancillary ligand.

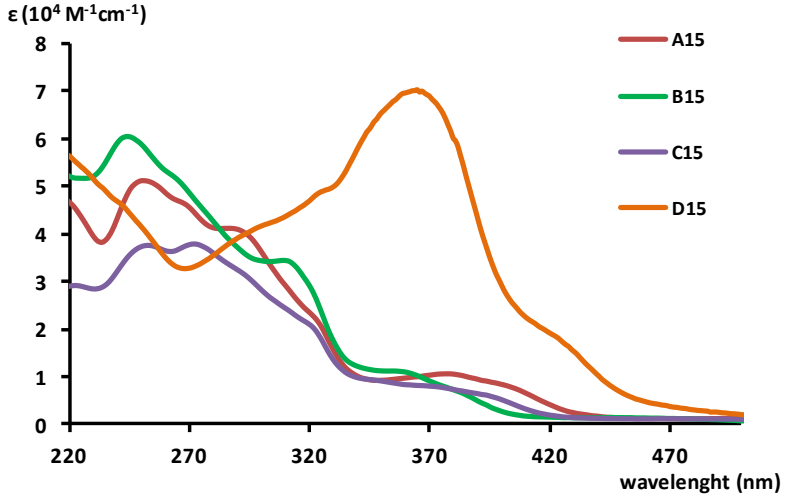

Figure 3.11. UV-Vis absorption spectra of complexes **A15**−**D15**.

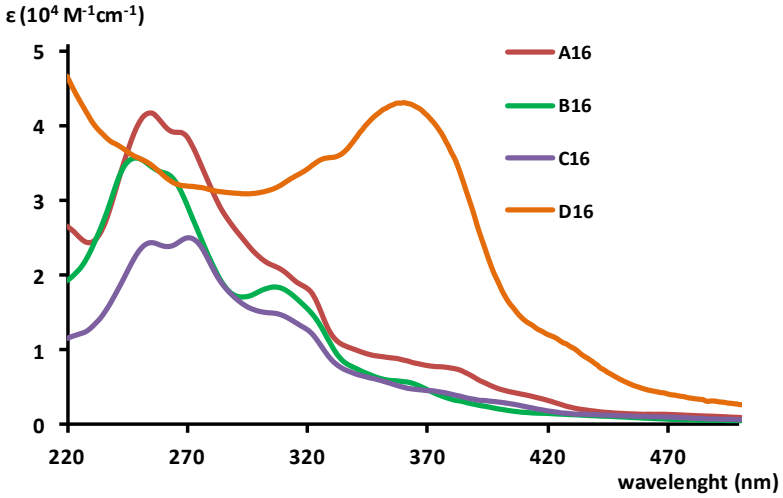

Figure 3.12. UV-Vis absorption spectra of complexes **A16**–**D16**.

Complexes that contain two azobenzene fragments on the phenylpyridines (**D15** and **D16**) presented the intense band attributed to the π−π* transition between 330–390 nm characteristic of the azobenzene fragment.[42] The other characteristic band of the azobenzene that corresponds to the n−π* transition was not clearly observed due to overlapping with the absorptions of the $[Ir(C–N)_2(bipy)]^+$ core (Table 3.1).

	λ [nm] (ε [$10^4 \cdot M^{-1}$ cm^{-1}])	
Compound	$\lambda_{azo\ \pi\rightarrow\pi^*}$	$\lambda_{azo\ n\rightarrow\pi^*}$
D15	365 (7.0)	nd
D16	360 (4.3)	nd

Table 3.1. UV-Vis spectra in EtOH. Selected absorption data.

Complexes **D15** and **D16**, containing two azobenzene fragments, absorb at longer wavelengths than complexes without azobenzene, near the visible region. In addition, these complexes showed higher absorptivities than complexes without azobenzene. The complex **D15** has the highest absorptivity, as shown in Figure 3.13, even higher than the analogous carboxylated **D16**.

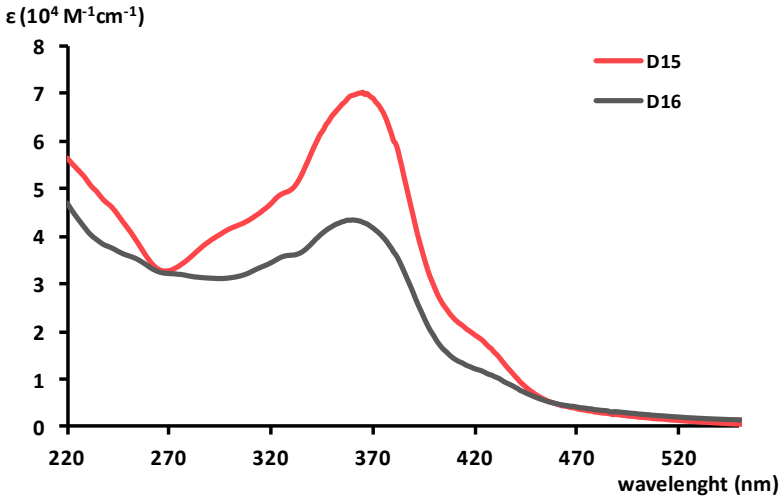

Figure 3.13. UV-Vis absorption spectra of complexes **D15** and **D16**.

3.2.3. PHOTOISOMERIZATION STUDIES

The isomerization of the azobenzene fragment in complexes **D15** and **D16** has been studied by UV–vis absorption spectroscopy. EtOH solutions of both complexes were irradiated for 30 min at the wavelength of the absorption previously attributed to the π→π* transition of the azobenzene (Table 3.1). When it was confirmed that the photoisomerization was active, the samples were irradiated at the optimal wavelength calculated following the Monkowius' methodology (described in Chapter 2).[43] In Figures 3.14 and 3.15 are shown the initial and the obtained UV-Vis spectra after irradiation of complexes **D15** and **D16**.

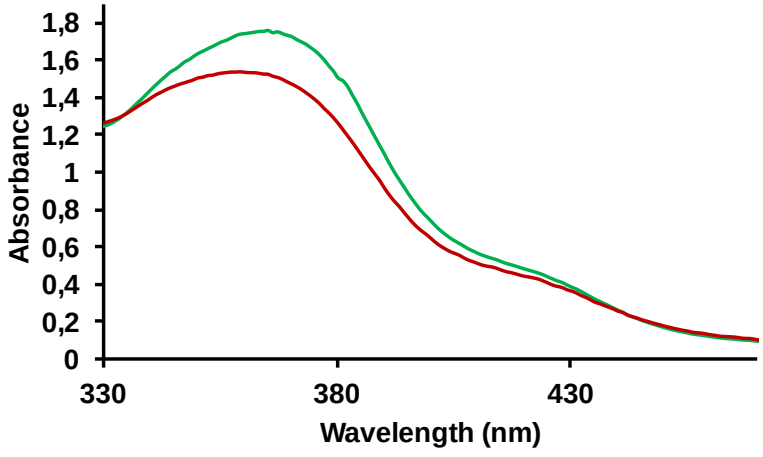

Figure 3.14. UV-Vis absorption spectra of complex **D15**, before (green line) and after (red line) 30 min irradiation at the wavelength attributed to π→π* transition (365 nm) and for additional 30 min at $\lambda_{optimal}$ (377 nm).

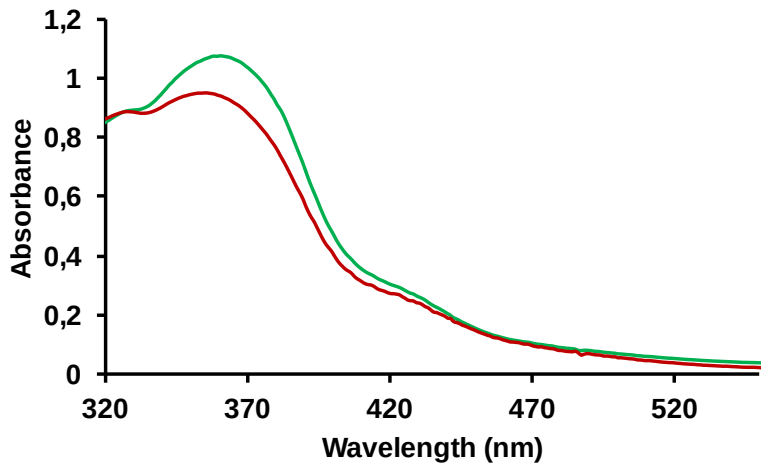

Figure 3.15. UV-Vis absorption spectra of complex **D16**, before (green line) and after (red line) 30 min irradiation at the wavelength attributed to π→π* transition (360 nm) and for additional 30 min at $\lambda_{optimal}$ (374 nm).

The reverse thermal isomerization (from *Z* to *E*) was followed by UV-Vis absorption spectroscopy at 55 °C, registering spectra at regular time intervals until the original spectrum were obtained. The value of absorbance at $\lambda_{\pi\rightarrow\pi^*}$ was used to follow this process. The calculated first order rate constants (k) and half-life times ($\tau_{1/2}$) for this process are presented in Table 3.2 (absorbance *versus* time and first order plots obtained are compiled in the Supporting Information).

Compound	$\lambda_{optimal}$ [a] [nm]	k [s^{-1}]	$\tau_{1/2}$ [min]
D15	377	2.0×10^{-4}	58
D16	374	2.0×10^{-4}	58

Table 3.2. Kinetic data for the *Z*→*E* isomerization process at 55 ºC for complexes **D15** and **D16**.
[a]Optimized light-wavelength for the E→Z photoisomerization.

The calculated first order rate constants (k) and half-life times ($\tau_{1/2}$) of both complexes are identical, and comparable with previously reported values for azobenzene-containing iridium,[44] platinum,[45] silver and gold[43] complexes.

3.2.4. PREPARATION AND CHARACTERIZATION OF DYE-SENSITIZED SOLAR CELLS

The work described in this section has been performed by the group of Dr. Marcos Jose Leite Santos at Universidade Federal do Rio Grande do Sul.

3.2.4.1. DYE-SENSITIZED SOLAR CELLS ASSEMBLY

TiO_2 nanoparticles of ca. 20 nm in diameter and the paste containing 25% w/w of nanoparticles were obtained as previously described in the literature.[46] To

prepare the dye sensitized TiO_2 electrode, the transparent conductive substrates (FTO) were previously soaked in 40 mM $TiCl_4$ aqueous solution at 60 ^oC for 30 minutes. This treatment improves the binding strength between the FTO and the porous TiO_2 layer and it blocks the charge recombination between electrons from the FTO and the redox pair.[47] Then, the TiO_2 paste was screenprinted on the FTO, firstly heating at 125 ^oC for 20 minutes and then the temperature was increased to 450 ^oC for 30 minutes. Afterwards, the TiO_2 electrode was immersed into ethanolic solutions (0.5 mM) of the selected complexes (**A15**, **B15**, **A16** and **C16**) during 12 hours.

The counter-electrodes were prepared by coating the FTO surface with a 30 µL of 1 mM hexachloroplatinic acid and heating at 500 ^oC. The electrolyte (0.6M BMII, 0.03M I_2, 0.10M guanidinium thiocyanate and 0.5M 4-tertbutylpyridine solution in a mixture of acetonitrile and valeronitrile) was placed between the dye sensitized photoanode and the counter-electrode. Finally, the solar cell was sealed using a polymeric film of low melting (Meltonix). The obtained solar cells are shown in Figure 3.16.

Figure 3.16. Photographs of the mesoporous films of TiO_2 sensitized with the dyes **A15**, **B15**, **A16** and **B16**.

3.2.4.2. PHOTOPHYSICAL PROPERTIES OF MODIFIED TiO_2 SURFACES

UV-Vis absorption spectra of the Ir(III) complexes adsorbed on TiO_2 were obtained by diffuse reflectance. The absorption spectra in the solid state of the complexes **A15**, **B15**, **A16** and **B16** adsorbed on the TiO_2 mesoporous film are shown in Figure 3.17. All Ir(III) complexes anchored on the TiO_2 presented relatively intense absorption bands in the visible region.

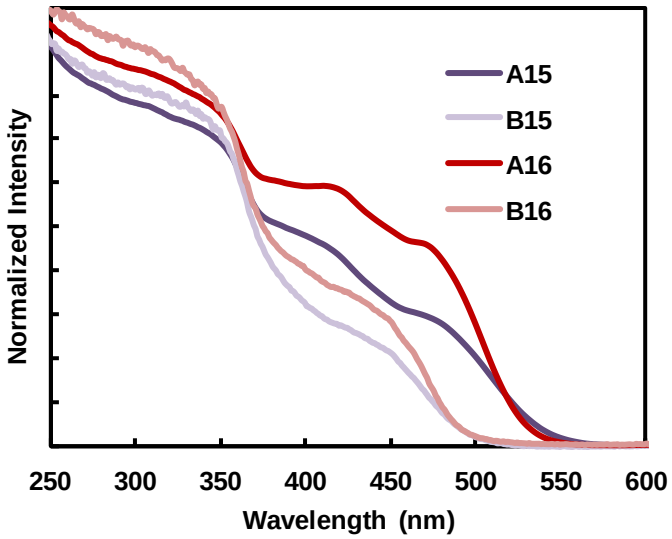

Figure 3.17. UV-Vis absorption spectra obtained by diffuse reflectance of Ir(III) complexes **A15**, **B15**, **A16** and **B16** adsorbed on the mesoporous TiO_2 film.

In solution, the main absorption bands were located below 400 nm (UV region), but the UV–Vis absorption spectra of Ir(III) complexes adsorbed on TiO_2 present absorptions in the blue-green regions (visible region). According to the results obtained, it seems that the environment plays a fundamental role in the absorptivity.

As mentioned before, complexes containing 4,4'-bis(diethylphosphonate)-2,2'-bipyridine (**15**) as ancillary ligand presented higher absorptivities than complexes with 4,4'-bis(carboxy)-2,2'-bipyridine (**16**) in solution. Nevertheless, in the solid state, **A16** that contains 4,4'-bis(carboxy)-2,2'-bipyridine (**16**) as ancillary ligand presented the most intense absorption bands in the visible region. This means that the most effective adsorption on the TiO_2 surface was obtained with the complex **A16**. Also the complex **B16** that contains the 4,4'-bis(carboxy)-2,2'-bipyridine showed higher absorptivities than the analogous **B15** with 4,4'-bis(diethylphosphonate)-2,2'-bipyridine, indicating that the linkage of complexes with carboxylate groups have been more effective. It was also notorious that both fluorinated complexes **B15** and **B16** presented the lowest absorption bands, indicating that the adsorption of the non-fluorinated complexes **A15** and **A16** was more effective. These results indicate that the presence of fluorine substituents play a more important role than the nature of the anchoring groups.

According to the intensity of the spectra, more effective linkage was obtained with carboxylated complexes. The reason could be that the phosphonated Ir(III) complexes studied in this work contain ethyl phosphonic esters and to anchor to the TiO_2 surface an *in situ* deprotection of the ethyl groups to monoester or phosphonic acids is required.[26]

3.2.4.3. SURFACE BINDING EXPERIMENTS

The desorption of the Ir(III) complexes from the TiO_2 surface in aqueous media was studied by diffuse reflectance UV-Vis absorption spectroscopy. The dye sensitized photoanodes were immersed in water in the dark for 1 h up to 32 h. The absorption spectra were registered at different time intervals after drying the samples prior to each measurement. In Figure 3.18 are shown the absorption spectra of the photoanodes containing complexes **A15**, **B15**, **A16** and **B16** adsorbed on the TiO_2 surface.

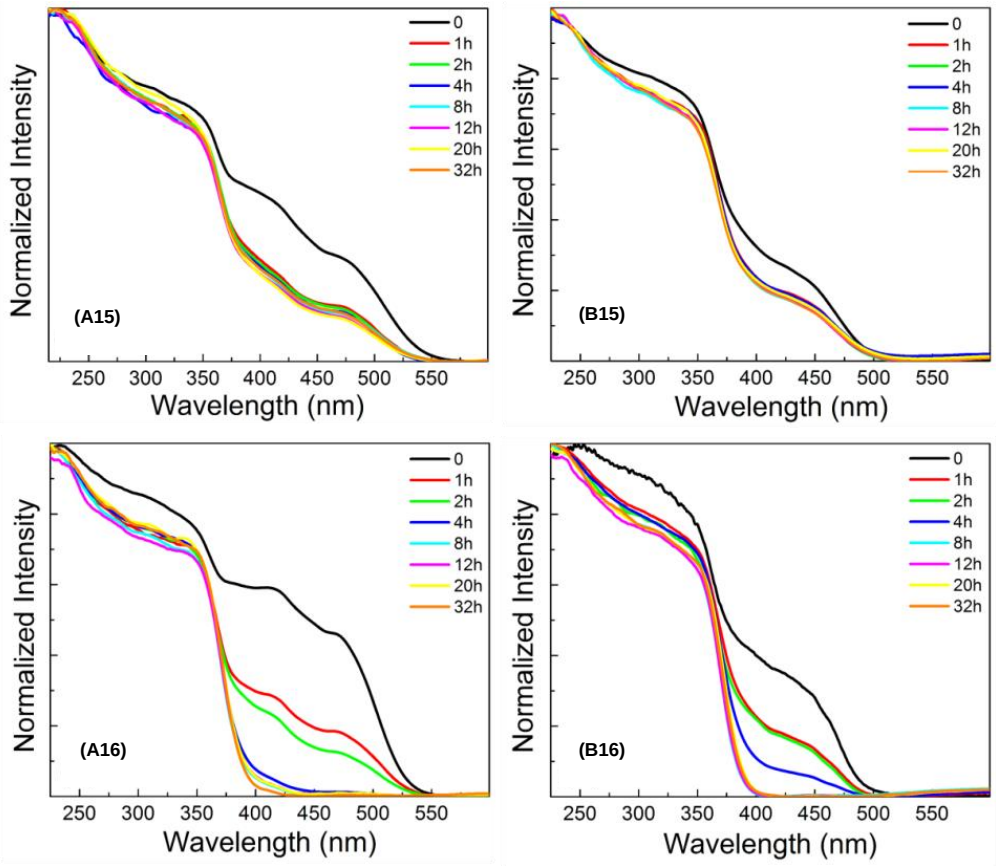

Figure 3.18. Diffuse reflectance UV–vis absorption spectra of complexes **A15**, **B15**, **A16** and **B16** anchored to TiO_2 films in different times.

All the Ir(III) complexes present a decrease in the intensity of the bands in the visible region upon water immersion. A more significant decrease was observed for complexes containing carboxylate anchoring groups than for complexes containing diethylphosphonates. Complexes incorporating diethylphosphonates on the ancillary ligands showed an initial lowering but then complexes remain anchored to the TiO_2 surface. These results demonstrate that, although initially the carboxylate derivatives were anchored more efficiently on the TiO_2 surface, the ethyl phosphonate ester anchorage was more stable in aqueous solution than the one of carboxylate group, as already demonstrated previously in the literature.[19]

The phosphonate group contains three oxygen atoms to anchor to the TiO_2 surface, one more than the carboxylates and could anchor to the metal oxide surface through a monodentate, bidentate or tridentate mode. The carboxylates only have two possibilities, through the monodentate and bidentate mode. These could be the reason why the anchoring of the phosphonates to the TiO_2 surface is stronger. Nevertheless, in case of derivatives of **15**, the ethyl groups should prevent a strong O–Ti interaction. Surprisingly, a strong binding has been observed for these derivatives, pointing to strong partial deprotection of the phosphonate groups. Whether the phosphonate remains protected with the ethyl groups when anchored on the surface, or *in situ* cleavage of the phosphone occurs during the anchoring process remains unclear. Further studies on the use of deprotected derivatives **A–C 15** should be run to confirm this hypothesis.

3.2.4.4. CELL MEASUREMENTS

The performance of the DSSCs was evaluated by current *versus* potential measurements and Incident photon-to-current efficiency. The measurements were carried out using a 300 W Xenon arc lamp with an AM1.5 filter. The power of the simulated light was calibrated to 100 mW/cm^2. The photoelectrochemical properties of the Ir(III) sensitized solar cells are listed in Table 3.3. The current *versus* potential curves of the solar cells assembled with the Ir(III) complexes **A15**, **B15**, **A16** and **B16** are shown in Figure 3.19.

Ir(III) complex	J_{sc} (mA/cm^2)	V_{oc}	FF (%)	η (%)
A15	2.88	0.60	55	1.0
B15	2.84	0.60	55	1.0
A16	3.40	0.57	62	1.2
B16	3.50	0.57	61	1.3

Table 3.3. Relevant electrical parameters of the devices assembled with the Ir(III) complexes **A15**, **B15**, **A16** and **B16**, where J_{sc} is the short-circuit current, V_{oc} is the open circuit voltage, FF is the fill factor and η is the cell efficiency.

The highest photocurrent density and efficiency was obtained with complexes containing carboxylate anchoring groups. Complexes **A16** and **B16** showed very similar values, although the complex **B16** showed slightly higher values than the non-fluorinated complex **A16**. The obtained values are comparable to the electrical parameters described in the literature for devices assembled with similar iridium complexes.[4]

The lower photocurrent generated with complexes containing phosphonic acids was already described in the literature and was attributed to the lower visible light absorption and less effective electrons injection compared to complexes with carboxylic groups.[19,24]

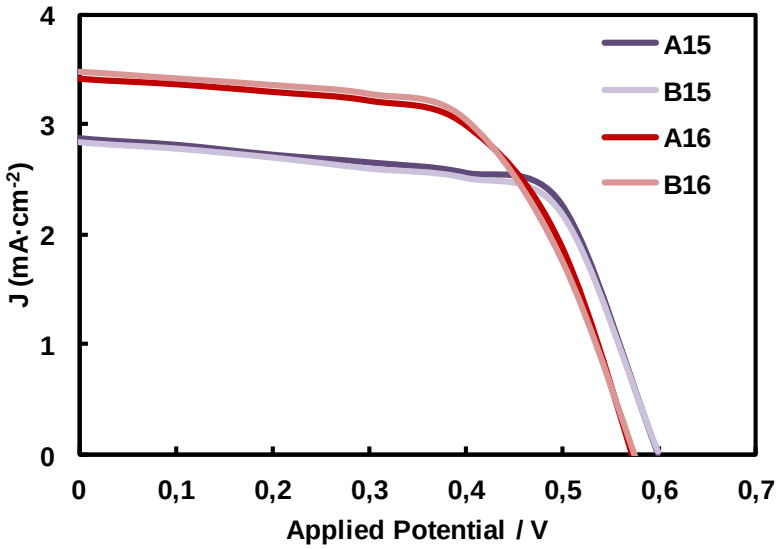

Figure 3.19. Current *versus* potential curves of the devices assembled with complexes **A15**, **B15**, **A16** and **B16**.

The open circuit voltage (V_{oc}) values of the devices sensitized with complexes **A15** and **B15** were slightly higher than devices sensitized with **A16** and **B16**. The higher V_{oc} values were attributed to the higher difference between the Fermi level of the semiconductor conduction band and the electrolyte redox potential in cells containing complexes **A15** and **B15** anchored to the TiO_2 surface.

Incident monochromatic photon-to-current conversion efficiency IPCE spectra of assembled devices are shown in Figure 3.20. The IPCE spectra are consistent with the absorption spectra of the dyes adsorbed on the mesoporous film of TiO_2 (Figure 3.17) and with the results obtained from the I-V curves.

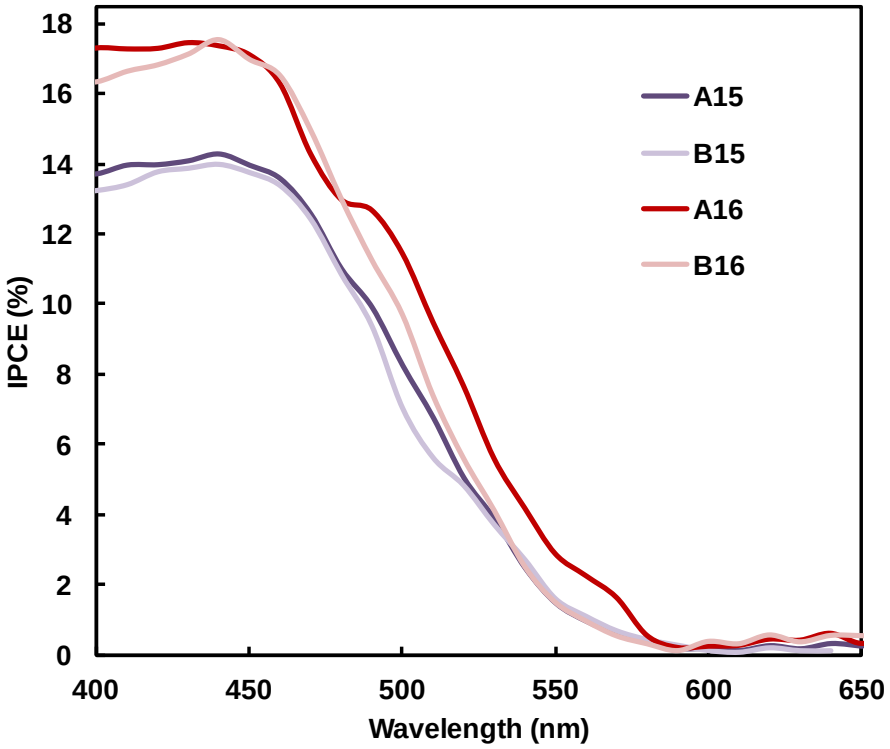

Figure 3.20. IPCE action spectra of the devices assembled with complexes **A15**, **B15**, **A16** and **B16**.

As expected, the IPCE values are higher in the range where the complexes anchored to the TiO_2 absorb light. The highest conversion efficiencies were obtained with complexes with carboxylate anchoring groups but the IPCE response of all the devices was detected beyond 600 nm. The low photocurrent efficiencies are related to the weak absorption spectra of the dyes within the visible region.

3.3. CONCLUSIONS

In this work eight Ir(III) complexes containing carboxy or diethylphosphonate anchoring groups have been synthesized and fully characterized, six of which were not described previously in the literature. In addition, two complexes containing two photoswitchable azobenzene fragments have been synthesized.

The absorptivity of all the complexes was studied in solution by UV-Vis. Phosphonated complexes showed higher absorptivities than the carboxylated and the highest absorptivity was obtained with the azobenzene containing phosphonated complex **D15**. Moreover, complexes incorporating azobenzene fragments, absorb at longer wavelengths, near the visible region. The photoisomerization of these complexes was studied by UV-Vis and the same isomerization rate constants were obtained for **D15** and **D16**.

The TiO_2 surface was sensitized with complexes **A15**, **B15**, **A16**, **B16** and the absorptivity in the solid state was analyzed by diffuse reflectance. Unlike the results

obtained in solution, the carboxylated complex **A16** adsorbed on TiO_2 surface showed the highest absorptivity. Therefore, it was concluded that the anchorage of carboxylate complexes on the TiO_2 surface was more effective than the one of diethylphosphonate. The influence of fluorine substituents on the phenylpyridines was also notorious, as the fluorinated complexes **B15** and **B16** showed the lowest absorptivities. In addition, in the solid state, complexes absorb in longer wavelengths, in the visible region. Surprisingly, when the stability in aqueous media of TiO_2 surfaces modified with these dyes was studied by UV-Vis absorption spectroscopy, less dye-leaching was observed when phosphonated were used as anchoring groups compared to carboxylated, which is rather surprising considering that the protecting ethyl groups of the phosphonate. Partial deprotection of the diethylphosphonate during the anchoring process cannot be discarded.

Four DSSCs were assembled with Ir(III) complexes and their efficacy was analyzed. Complexes **A16** and **B16** containing carboxylate anchoring groups showed better efficiencies than the analogous complexes with diethylphosphonate groups.

Although lower efficiencies were obtained with complexes containing diethylphosphonates, the linkage of these groups to the TiO_2 surface showed to be more stable than carboxylates in aqueous media. Therefore, Ir(III) complexes incorporating mixed ligands with both phosphonate and carboxylates, combining both stability of the anchorage to the TiO_2 and effective electrons injection might be good candidates to use as dyes for DSSCs, an strategy already used for the design of some Ru-based dyes. Nevertheless, the appropriate design of the complex should be used to avoid ending up with a weakly anchored dye with a poor electron injection efficacy.

The construction and evaluation of DSSC using **C15**, **C16** and azobenzene-containing dyes **D15**, **D16** is currently under development. As mentioned before, azobenzene-appended complexes present important absorption near the visible region, which makes them appropriate to be used as dyes in DSSC.

3.4. REFERENCES

[1] O'Regan and M. Grätzel M., *Nature*, **1991**, *353*, 737–740.

[2] S. I. Bezzubov, Y. M. Kiselev, A. V. Churakov, S. A. Kozyukhin, A. A. Sadovnikov, V. A. Grinberg, V. V. Emets and V. D. Doljenko, *Eur. J. Inorg. Chem.*, **2016**, 347–354.

[3] C. A. Bignozzi, R. Argazzi, R. Boaretto, E. Busatto, S. Carli, F. Ronconi and S. Caramori, *Coordination Chemistry Reviews*, **2013**, *257*, 1472–1492.

[4] E. Baranoff, J. H. Yum, M. Graetzel and M. K. Nazeeruddin, *J. Organomet. Chem.*, **2009**, *694*, 2661–2670.

[5] L. Pellejá i Puxeu, **2014**, *Exploring novel dye concepts in Dye Sensitized Solar Cells*, Institut Català d'Investigació Química-Universitat Rovira I Virgili, Tarragona.

[6] C. Dragonetti, A. Valore, A. Colombo, S. Righetto and V. Trifiletti, *Inorg. Chim. Acta*, **2012**, *388*, 163–167.

[7] E. Baranoff, J. H. Yum, I. Jung, R. Vulcano, M. Grätzel and M. K. Nazeeruddin, *Chem. Asian J.*, **2010**, *5*, 496–499.

[8] M. K. Nazeeruddin, A. Kay, I. Rodicio, R. Humphry-Baker, E. Müller, P. Liska, N. Vlachopoulos and M. Grätzel, *J. Am. Chem. Soc.*, **1993**, *115*, 6382–6390.

[9] K. F. Lin, J. S. Ni, C. H. Tseng, C. Y. Hung and K. Y. Liu, *Mater. Chem. Phys*., **2013**, *142*, 420–427.

[10] M. R. Norris, J. J. Concepcion, C. R. K. Glasson, Z. Fang, A. M. Lapides, D. L. Ashford, J. L. Templeton and T. J. Meyer, *Inorg. Chem*., **2013**, *52*, 12492–12501.

[11] I. Gillaizeau-Gauthier, F. Odobel, M. Alebbi, R. Argazzi, E. Costa, C. A. Bignozzi, P. Qu and G. J. Meyer, *Inorg. Chem.*, **2001**, *40*, 6073–6079.

[12] K. Hanson, M. K. Brennaman, H. Luo, C. R. K. Glasson, J. J. Concepcion, W. Song and T. J. Meyer, *Appl. Mater. Interfaces*, **2012**, *4*, 1462–1469.

[13] W. R. McNamara, R. L. Milot, H. Song, R. C. Snoeberger III, V. S. Batista, C. A. Schmuttenmaer, G. W. Brudvig and R. H. Crabtree, *Energy Environ. Sci*., **2010**, *3*, 917–923.

[14] T. P. Brewster, S. J. Konezny, S. W. Sheehan, L. A. Martini, C. A. Schmuttenmaer, V. S. Batista and R. H. Crabtree, *Inorg. Chem*., **2013**, *52*, 6752–6764.

[15] P. Ghosh and T.G. Spiro, *J. Am. Chem. Soc*., **1980**, *102*, 5543–5549.

[16] B. J. Brennan, A. E. Keirstead, P. A. Liddell, S. A. Vail, T. A. Moore, A. L. Moore and D. Gust, *Nanotechnology*, **2009**, *20*, 505203(10pp).

[17] P. R. Moses and R. W. Murray, *J. Electroanal. Chem*., **1977**, *77*, 393–399.

[18] D. G. Brown, P. A. Schauer, J. Borau-Garcia, B. R. Fancy and C. P. Berlinguette, *J. Am. Chem. Soc.*, **2013**, *135*, 1692–1695.

[19] E. Bae, W. Choi, J. Park, H. S. Shin, S. B. Kim and J. S. Lee, *J. Phys. Chem. B*, **2004**, *108*, 14093–14101.

[20] K. Fukui, H. Onishi, and Y. Iwasawa, *Chemical Physics Letters*, **1997**, *280*, 296–301.

[21] Q. Guo, and E. M. Williams, *Surface Science*, **1999**, *433–435*, 322–326.

[22] F. P. Rotzinger, J. M. Kesselman-Truttmann, S. J. Hug, V. Shklover and M. Grätzel, *J. Phys. Chem. B*, **2004**, *108*, 5004–5017.

[23] P. Péchy, F. P. Rotzinger, M. K. Nazeeruddin, O. Kohle, S. M. Zakeeruddin, R. Humphry-Baker and M. Grätzel, *J. Chem. Soc. Chem. Commun.*, **1995**, *1*, 65–66.

[24] B. J. Brennan, M. J. L. Portolés, P. A. Liddell, T. A. Moore, A. L. Moore and D. Gust, *Phys. Chem. Chem. Phys.*, **2013**, *15*, 16605–16614.

[25] G. Guerrero, P. H. Mutin, E. Framery and A. Vioux, *New J. Chem.*, **2008**, *32*, 1519–1525.

[26] F. J. Malzner, S. Y. Brauchli, E. Schönhofer, E. C. Constable and C. E. Housecroft, *Polyhedron*, **2014**, *82*, 116–121.

[27] A. Hagfeldt, G. Boschloo, L. Sun, L. Kloo and H. Pettersson, *Chem. Rev.*, **2010**, *110*, 6595–6663.

[28] H. Hug, M. Bader, P. Mair and T. Glatzel, *Applied Energy*, **2014**, *115*, 216–225.

[29] W. Zhu and D. Ma, *Org. Lett.*, **2006**, *8*, 261–263.

[30] H.-Y. Yang, J.-M. Son, W.-J. Joo, US Patent, 2010/0133992.

[31] S. Sprouse, K. A. King, P. J. Spellane and R. J. Watts, *J. Am. Chem. Soc.*, **1984**, *106*, 6647–6653.

[32] A. A. Rachford, R. Ziessel, T. Bura, P. Retailleau and F. N. Castellano, *Inorg. Chem.*, **2010**, *49*, 3730–3736.

[33] F. Dumur, M. Lepeltier, H. Z. Siboni, D. Gigmes and H. Aziz, *Synthetic Metals*, **2014**, *198*, 131–136.

[34] A. J. Sandee, C. K. Williams, N. R. Evans, J. E. Davies, C. E. Boothby, A. Köhler, R. H. Friend and A. B. Holmes, *J. Am. Chem. Soc.*, **2004**, *126*, 7041–7048.

[35] C. Dragonetti, A. Valore, A. Colombo, S. Righetto, G. Rampinini, F. Colombo, L. Rocchigiani and A. Macchioni, *Inorg. Chim. Acta*, **2012**, *382*, 72–78.

[36] M. C. DeRosa, D. J. Hodgson, G. D. Enright, B. Dawson, C. E. B. Evans and R. J. Crutchley, *J. Am. Chem. Soc.*, **2004**, *126*, 7619–7626.

[37] M. Lepeltier, T. K. M. Lee, K. K. W. Lo, L. Toupet, H. L. Bozec and V. Guerchais, *Eur. J. Inorg. Chem.*, **2005**, 110–117.

[38] Z. Ning, Q. Zhang, W. Wu and H. Tian, *J. Organomet. Chem.*, **2009**, *694*, 2705–2711.

[39] W. Jiang, Y. Gao, Y. Sun, F. Ding, Y. Xu, Z. Bian, F. Li, J. Bian and C. Huang, *Inorg. Chem.*, **2010,** *49*, 3252–3260.

[40] S. Ladouceur and E. Zysman-Colman, *Eur. J. Inorg. Chem.*, **2013**, 2985–3007.

[41] R. D. Costa, F. Monti, G. Accorsi, A. Barbieri, H. J. Bolink, E. Ortí and N. Armaroli, *Inorg. Chem.*, **2011**, *50*, 7229–7238.

[42] a) C. L. Forber, E. C. Kelusky, N. J. Bunce and M. C. Zerner, *J. Am. Chem. Soc.*, **1985**, *107*, 5884–5890. b) M. Dubecký, R. Derian, L. Mitas and I. Štich, *J. Chem. Phys.*, **2010**, *133*, 244301–244305.

[43] M. Kaiser, S. P. Leitner, C. Hirtenlehner, M. List, A. Gerisch and U. Monkowius, *Dalton Trans.*, **2013**, *42*, 14749–14756.

[44] J. Pérez-Miqueo, A. Telleria, M. Muñoz-Olasagasti, A. Altube, E. García-Lecina, A. de Cózar and Z. Freixa, *Dalton Trans.*, **2015**, *44*, 2075–2091.

[45] M. E. Moustafa, M. S. McCready and R. J. Puddephatt, *Organometallics*, **2013**, *32*, 2552–2557.

[46] C. J. Barbé, F. Arendse, P. Comte, M. Jirousek, F. Lenzmann, V. Shklover and M. Grätzel, *J. Am. Ceram. Soc.*, **1997**, *80*, 3157–3171.

[47] S. Ito, T.N. Murakami, P. Comte, P. Liska, C. Grätzel, C., M.K. Nazeeruddin and M. Grätzel, *Thin Solid Films*, **2008**, *516*, 4613–4619.

CHAPTER 4

LUMINESCENT Ir(III) BIPYRIDINE COMPLEXES

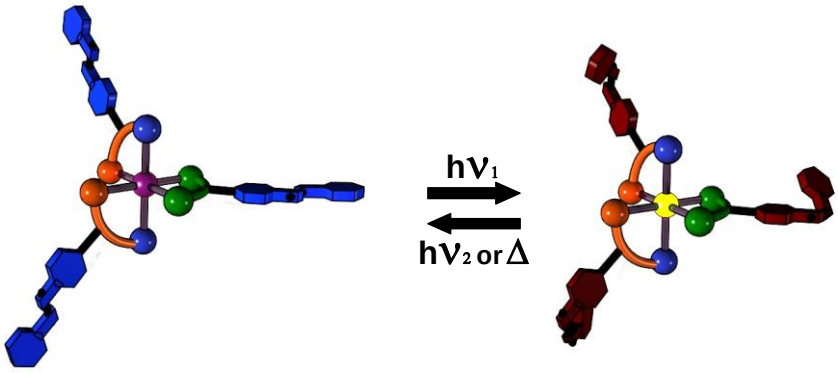

In this chapter, Ir(III) complexes containing two phenylpyridine and one 2,2'-bipyridine ligands are presented. They were intended to be used as phosphors for low energy consumption light-emitting devices. Complexes incorporating azobenzene moieties were synthesized to study the possibility to modify the color of the emission with incident light.

The work described in this chapter has been published: A. Telleria, J. Pérez-Miqueo, A. Altube, E. García-Lecina, A. de Cózar and Z. Freixa, Organometallics, 2015, 34, 5513–5529.

4.1. INTRODUCTION

Cyclometalated Ir(III) complexes have attracted great interest in lighting technologies. In organometallic complexes, light absorption and emission processes are related with electronic transitions between different energy states that are associated with both central metal atom and ligands. The existence of metal-to-ligand charge-transfer (MLCT) and ligand centered (LC) π−π* transitions is responsible of emissive relaxation processes where both metal and ligands are implicated, which facilitates the emission wavelength tunability. Because of this, the selection of the metal and the ligands is a critical issue to be addressed. Cyclometalated aromatic ligands form strong bonding interactions with transition metals, increasing the d–d energy gap and decreasing radiationless metal-centered (MC) transitions. Additionally, octahedral iridium complexes show large splitting energy (Δ_0) values due to the high oxidation state of the metal, and the size of its 5d orbitals.[1,2] The octahedral geometry also permits to introduce specific ligands in a controlled manner changing the photophysical and electrochemical properties of these complexes in a predictable way. Furthermore, these complexes contain stable and accessible oxidation and reduction states and have high triplet quantum yields. Altogether makes phosphorescent iridium(III)-cyclometalated complexes exceptional candidates for many lighting applications.[3]

For all the reasons explained above neutral and charged Ir(III) complexes have been investigated for the construction of electroluminescent devices. The archetype complexes studied for these applications are shown in Chart 4.1. An important drawback of the neutral tris-cyclometalated complexes is the existence of two possible isomers, facial and meridional. Usually, the facial isomer shows better performance but its synthesis requires harsh conditions and a difficult purification processes. Milder conditions are used to obtain charged complexes with neutral bidentate ligands and pro-meridional compounds (easily synthesized) usually present good performance. Furthermore, the solubility in polar solvents is also favored.[4]

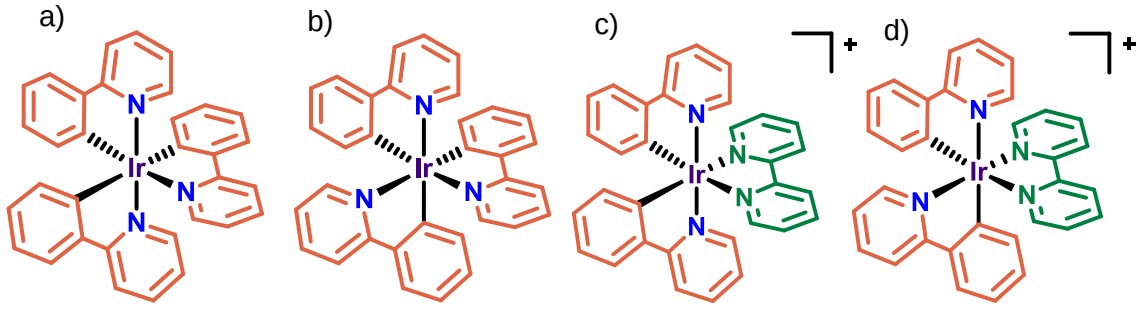

Chart 4.1. Archetypical iridium complexes, a) mer-[Ir(C–N)$_3$], b) fac-[Ir(C–N)$_3$], c) pro-mer-[Ir(C–N)$_2$(bipy)]$^+$, d) pro-fac-[Ir(C–N)$_2$(bipy)]$^+$.

Cationic bis-cyclometalated iridium(III) complexes containing two phenylpyridines and 2,2'-bipyridine or 1,10-phenanthroline as ancillary ligands have been extensively applied in different light-emitting devices. These complexes show intense phosphorescence at room temperature and they have been widely investigated as phosphors in the construction of low energy consumption devices like organic light-emitting diodes (OLEDs)[5] and light-emitting electrochemical cells (LECs)[6] used in many screen devices, such as computers, mobile phones, TVs, watches, etc. OLEDs are LEDs composed of organic materials and are replacing the actual liquid-crystal displays (LCDs) because of their higher efficiencies, improved brightness and longer lifetimes.[7]

OLEDs present multilayered structures with an emissive layer between charge transport layers sandwiched between two electrodes (Figure 4.2). Applying a voltage, holes and electrons are injected and recombined in the emission layer forming approximately 25% singlet and 75% triplet excitons. The emissive layer contains compounds, called emitters, able to absorb the excitation energy and release it as light, either by fluorescence or phosphorescence. Fluorescent emitters absorb singlet excitons and emit light transferring an electron from an excited singlet state to the singlet ground state, but they do not absorb triplet excitons and these decay in a radiationless manner (*i.e.* by heat). Phosphorescent emitters (phosphors) absorb both singlet and triplet excitons and emit light through a transference of an electron from an excited triplet state to the singlet ground state (Figure 4.1). Although the last one is a formally forbidden transition, in heavy metal-containing complexes this transition may become allowed due to the spin-orbit coupling (SOC) induced by the metal. In addition, SOC prompts the transfer from the populated excited singlet states to emissive triplet states.[3]

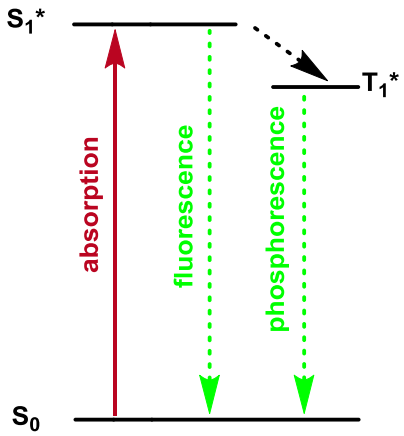

Figure 4.1. Fluorescence and phosphorescence processes.

OLEDs constructed with phosphorescent transition metal emitters exhibit four times better efficiency than ones with organic singlet emitters. When these triplet emitters are ionic transition metal complexes, charge transport layers are not necessary, mobile ions prompt the charge transport and light emission, and the device is called LEC. LECs have many advantages comparing with OLEDs. Their simplicity, easy fabrication and the use of air-stable electrodes make their production cheaper.[8,9]

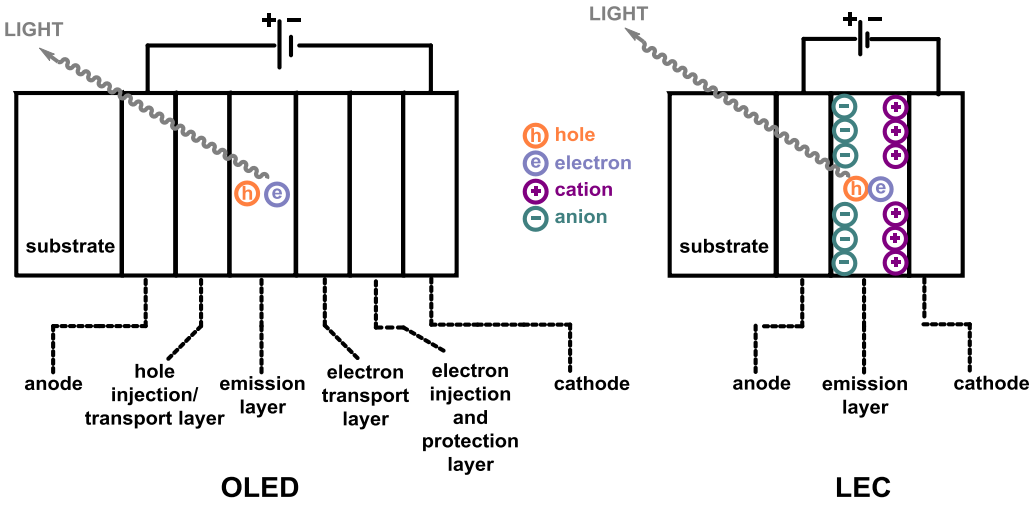

Figure 4.2. Basic structures of OLEDs and LECs.

The first LEC was reported in 1995 by Pei *et al*. and was based on a combination of a light emitting polymer, an ion-conducting polymer and an inorganic salt.[10] Almost a decade later the first ionic iridium complex based LEC was published.[11] The selected iridium(III) complex had two cyclometalating ligands (2-phenylpyridine), one 4,4'-di-*tert*-butyl-2,2'-bipyridine, and (PF_6^-) as a counterion (Figure 4.3).

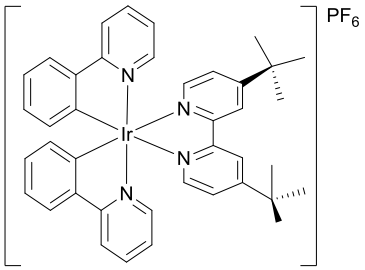

Figure 4.3. First ionic Ir(III) complex used to fabricate a LEC.

The structure of a LEC consists of a luminescent layer of an ionic transition metal complex, between two electrodes (Figure 4.2). As in OLEDs, when a voltage is applied in the system, ions that are in the light-emitting layer migrate to the cathode and anode, forming double layers contiguous to the electrodes. At that point, holes and electrons that are injected from the electrodes recombine in the emissive layer releasing singlet or triplet excitons. As it was explained before, phosphorescent ionic iridium(III)

complexes are able to harvest both excitons originating a very efficient light emission.[12,13,14]

At the molecular level, when the emitter absorbs energy, an electron from the highest occupied molecular orbital (HOMO) is promoted to the lowest unoccupied molecular orbital (LUMO) creating a singlet excited state. For Ir(III) complexes containing two phenylpyridine and one bipyridine ligands, the HOMO is located mainly on the phenyl groups of the cyclometalated ligands and the iridium center, while the LUMO is mostly located on the ancillary ligand. So the two main transitions can be described as a mixture of metal-to-ligand charge transfer (MLCT), where an electron is excited from a singlet metal d orbital to the singlet π* orbital of the bipyridine and ligand centered (LC) transitions, where an electron is transferred from the singlet π orbital of the phenylpyridine to the singlet π* orbital of the bipyridine. The high SOC of the iridium metal center facilities a fast relaxation of singlet excited states to less energetic triplet excited states. When the electron relaxes to the singlet ground state light is emitted in a phosphorescent process (Figure 4.4).[13,15]

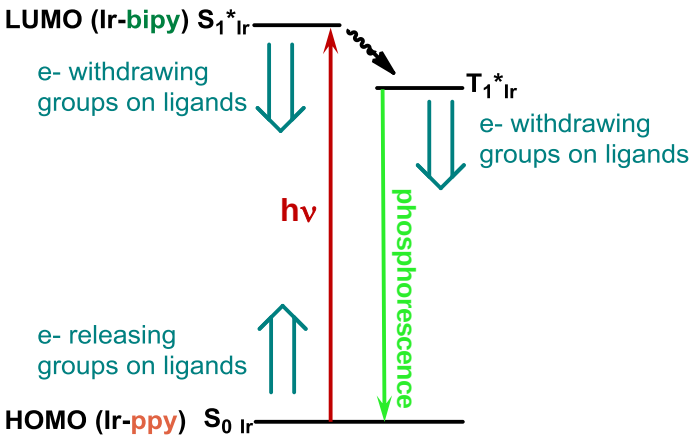

Figure 4.4. Orbital description and electronic transitions for $[Ir(ppy)_2(bipy)]^+$ complexes.

Eventually, the color of the emission is related to the energy gap between the HOMO and LUMO orbitals of the complexes, so stabilization or destabilization of these orbitals causes changes in the color. In these compounds, the HOMO could be stabilized introducing electron-withdrawing substituents on the phenyl fragment of the phenylpyridine ligand, decreasing the electron donation to the metal and so the HOMO-LUMO gap is increased. The inverse effect is obtained with electron-releasing groups and HOMO-LUMO gap is decreased. On the other hand, the LUMO could be destabilized with electron-releasing substituents on the bipyridine ligand and the HOMO-LUMO gap is increased as consequence.[15]

The aim of the work presented in this chapter consists of synthesizing new azobenzene-containing phosphorescent iridium (III) cationic complexes with two

phenylpyridines and 2,2'-bipyridine or 1,10'-phenanthroline as ancillary ligands. Light-induced photoisomerization of the appended azobenzenes should produce a temporary change on the energy of the LUMO molecular orbital (when the azobenzene fragment is appended on the bipyridine ligand) and of the HOMO (if they are also appended on the cyclometalated phenylpyridines), modifying the HOMO-LUMO gap and eventually the color of the emission. The photochromic moiety would be introduced on both, 2,2'-bipyridines and also on phenylpyridine fragments (Figure 4.5).

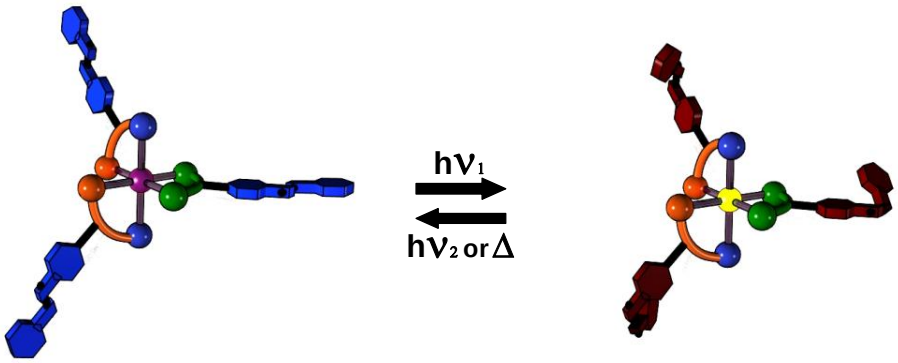

Figure 4.5. Conceptual drawing of the photoisomerization of azobenzene in a tris-azobenzene-containing Ir(III) complex.

The final goal is to combine the properties of phosphorescent iridium complexes with photochromic units creating a new generation of multifunctional metallic compounds able to respond to an external stimuli, the light.

4.2. RESULTS AND DISCUSSION

4.2.1. SYNTHESES OF IRIDIUM COMPLEXES

The azobenzene-appended ligands **1**–**5** described in Chapter 2, were intended to be used as ancillary ligands in cationic Ir(III) bis-cyclometalated complexes. Initially, model compounds using commercially available, 2,2'-bipyridine (**bipy**), 1,10-phenanthroline (**phen**) and 4,4'-dibromo-2,2'-bipyridine (**bipyBr**) were synthesized. These were obtained by cleavage of the corresponding dimeric bis-cyclometalated iridium(III) chloride-bridged complex (see previous chapter) in presence of two equivalents of the corresponding ancillary bipyridine ligand in refluxing CH_2Cl_2:MeOH 2/1. After completion of the reaction, an excess of KPF_6 was added to obtain cationic complexes of the type $[Ir(C–N)_2(N–N)]PF_6$ (C–N = phenylpyridine ligand, N–N = bipyridine ligand) with good yields (Scheme 4.1).[16]

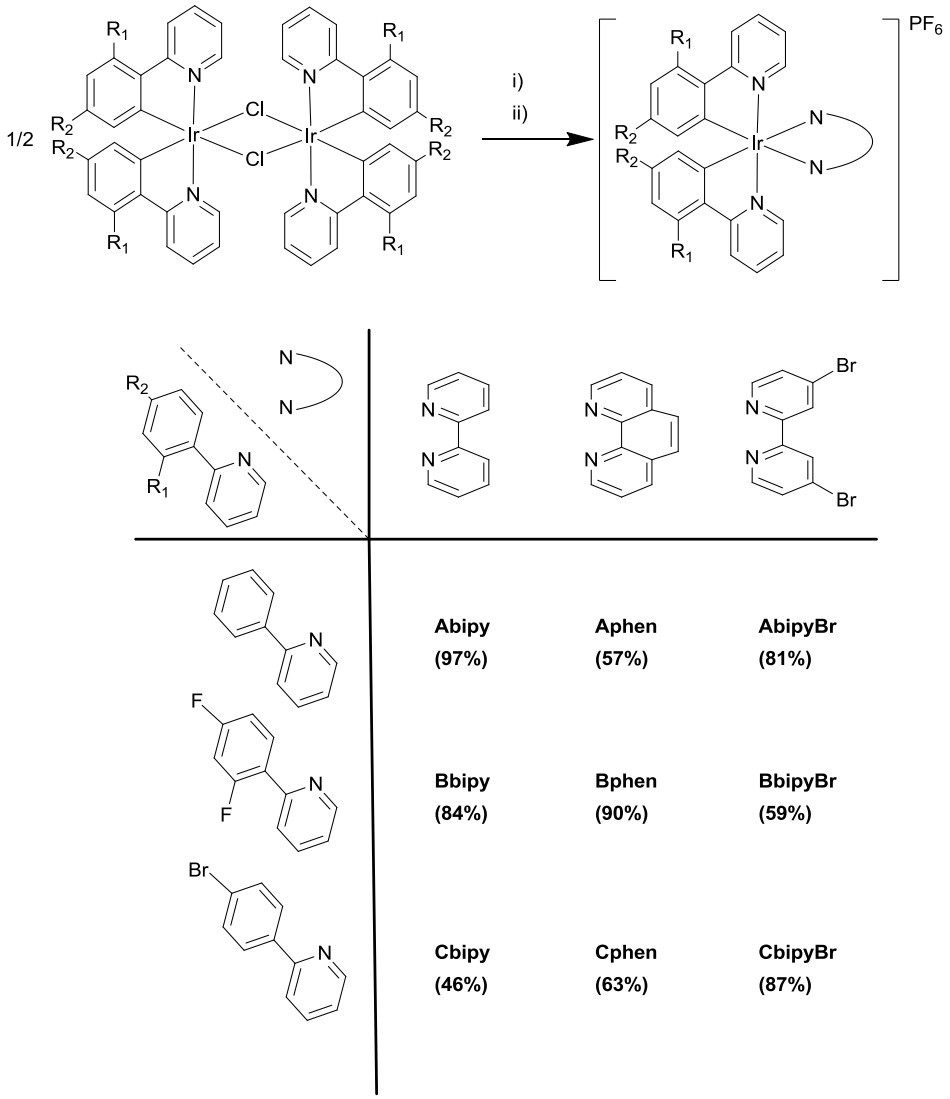

Scheme 4.1. Synthetic route toward cationic iridium model complexes. i) 2 equiv. ancillary bipyridine ligand, CH_2Cl_2/MeOH 2/1, reflux 15 h. ii) KPF_6. Yields are indicated in brackets.

Attending to the cyclometalated ligands used, three different families of complexes have been synthesized. They have been labeled as **A** (phenylpyridine), **B** 2-(2,4-difluorophenyl)pyridine and **C** 2-(4-bromophenyl)pyridine, respectively. **Abipy**[17], **Bbipy**[4], **Aphen**[18] and **Bphen**[19] were previously reported in the literature. The molecular structures of **Aphen**, **Cphen**, **BbipyBr** and **CbipyBr** were confirmed by X-ray diffraction of crystalline samples (full spectra and detailed synthetic procedures are compiled in the Supporting Information).

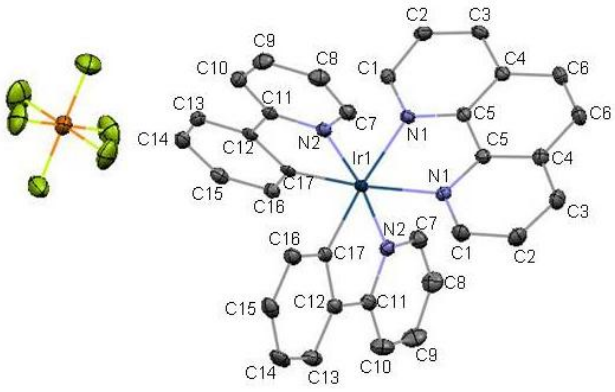

Figure 4.6. ORTEP representation of the molecular structure of **Aphen** according to X-ray diffraction. Hydrogens have been omitted for clarity. Ellipsoids at 50% probability.

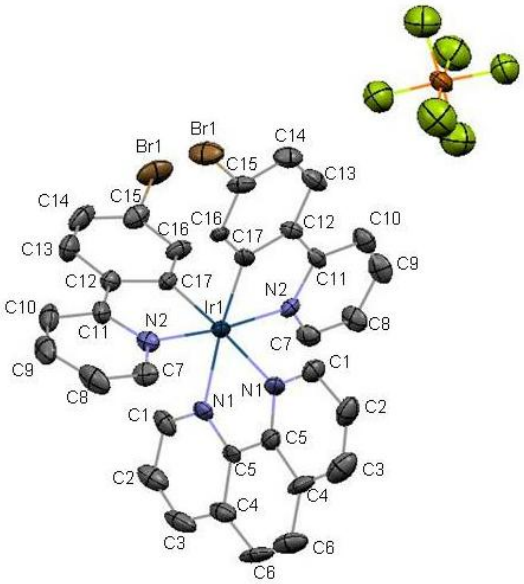

Figure 4.7. ORTEP representation of the molecular structure of **Cphen** according to X-ray diffraction. Hydrogens have been omitted for clarity. Ellipsoids at 20% probability.

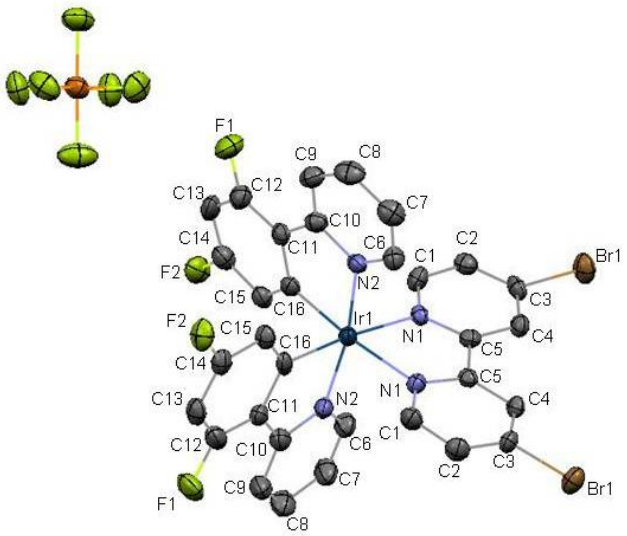

Figure 4.8. ORTEP representation of the molecular structure of **BbipyBr** according to X-ray diffraction. Hydrogens have been omitted for clarity. Ellipsoids at 50% probability.

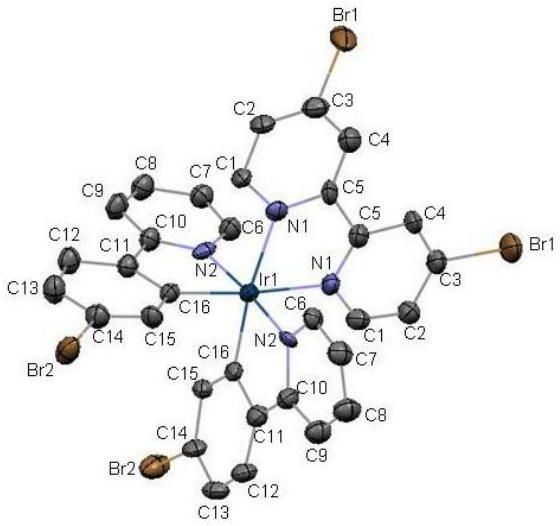

Figure 4.9. ORTEP representation of the molecular structure of the cation of **CbipyBr** according to X-ray diffraction. Hydrogens have been omitted for clarity. Ellipsoids at 50% probability. The counterion PF_6 was omitted due to the high level of disorder that presented.

Molecular structures of the complexes confirmed the octahedral coordination of the iridium center, with the ligands arranged in a pro-meridional configuration (with two nitrogen atoms of the phenylpyridine ligands in mutually *trans* positions). Although these compounds are chiral, due to the two possible arrangements of the phenylpyridine ligands around the metal (Λ and Δ), as expected, the crystals were obtained as racemates.

The same procedure described above for the synthesis of model iridium complexes was used for the synthesis of cationic compounds with azobenzene-containing bipyridine ligands **1** and **3**–**5**. All the compounds were obtained with good yields, except **B3** and **C3**, but this should be attributed to punctual experimental errors rather than to any systematic trend (Scheme 4.2).

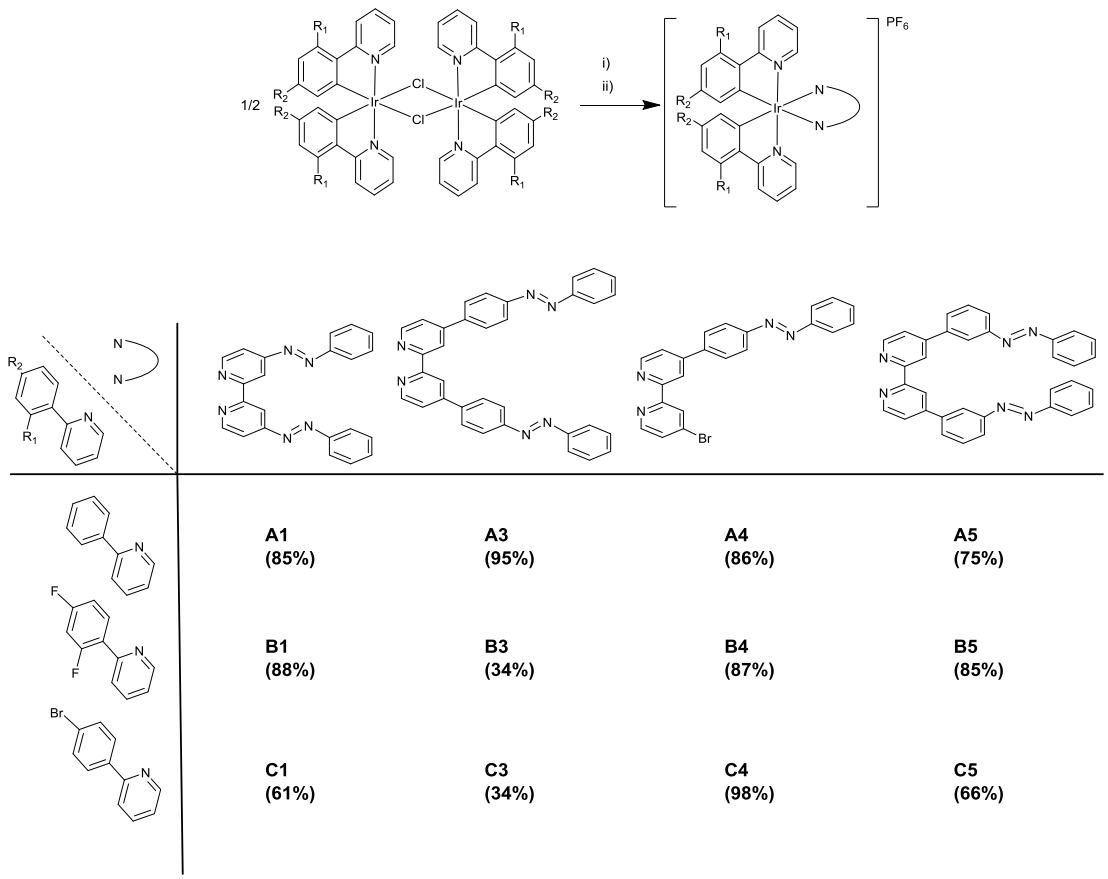

Scheme 4.2. Synthetic route toward azobenzene-containing iridium complexes with ligands **1**,**3**–**5**. i) 2 equiv. bipyridine, CH_2Cl_2/MeOH 2/1, reflux 15 h. ii) KPF_6. Yields are indicated in brackets.

The ^{1}H-NMR of these complexes showed fully aromatic spectra. As a representative example, in Figure 4.10 is shown a comparison of the three derivatives of ligand **1**. Signals integrating 16H, 14H and 15H were observed for **A1**, **B1** and **C1**, respectively, indicating that, as expected, these complexes are C_2-symmetric in solution. It is worth mentioning that the most high-field shifted signal, assigned to the proton that is in *ortho* position to the carbon that is bonded to the metal, experiences a clear up-field shift in the case of derivative **B1** (compared to **A1** and **C1**). It is well known that the fluorine atom produces a low-field shift in aliphatic systems due to the electron-withdrawing effect, but in aromatic systems the opposite effect is observed as consequence of the dominating mesomeric effect.[20] Additionally, the spectra of derivative **B1** shows the additional splitting due to F–H coupling.

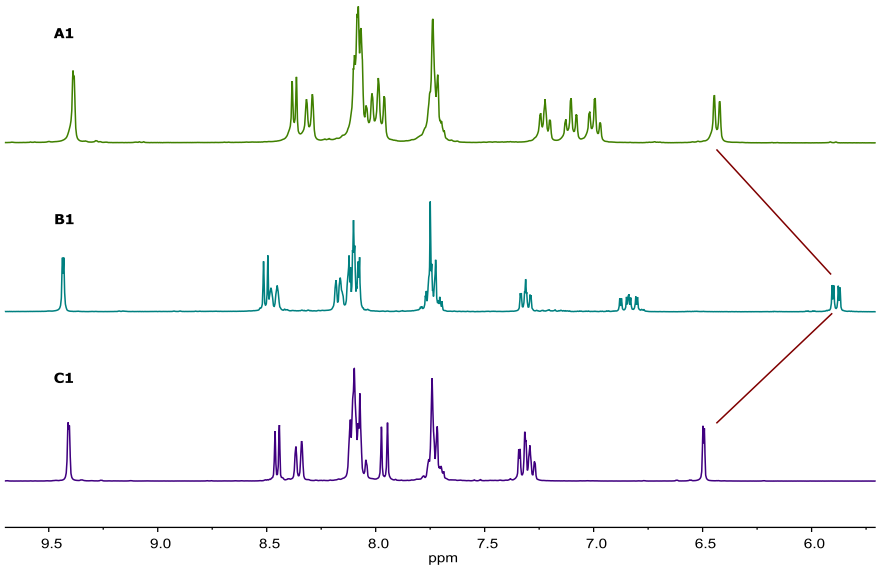

Figure 4.10. ^{1}H-NMR spectrum of **A1**, **B1** and **C1** in acetone-d_6, 300 MHz. The position of the most shielded proton is highlighted with a red line.

Initially, the same synthetic procedure was followed to obtain cationic Ir(III) biscyclometalated complexes containing two monodentate 4-phenylazopyridine ligands **2** instead of a chelating 2,2'-bipyridine as ancillary ligand. The same three families, labeled as **A**, **B** and **C** to indicate the nature of the phenylpyridine ligands used, were synthesized. Unfortunately, **A2** (derived from 2-phenylpyridine) was obtained with very low yield (13%). When the dimeric $[Ir(Fppy)_2Cl]_2$ (Fppy = 2-(2,4-difluorophenyl)pyridine) was used, **B2** was obtained as a 2 to 1 mixture together with a new compound (labeled as **B2'**) (Scheme 4.3), and when the synthesis of **C2** was attempted, the unreacted dimer $[Ir(Brppy)_2Cl]_2$ (Brppy = 2-(4-bromophenyl)pyridine) was recovered at the end of the reaction. The undesired compound **B2'** which was formed together with **B2**, was obtained as the only reaction product when the ligand to metal ratio was lowered to 1/1 (87% yield). The ^{1}H-NMR of the product corresponds to an asymmetric neutral complex of the type $[Ir(Fppy)_2(\mathbf{2})]$ in which the 4-phenylazopyridine ligand was not coordinating as a neutral donor through the pyridine nitrogen, but acted as a monoanionic C−N_{azo} chelate, formed by C–H activation of the *meta* position of the pyridine. In the ^{1}H-NMR, 20 protons are observed and unlike in symmetric complexes, different signals are identified for protons of different phenylpyridine fragments. This coordination mode, resulting from the ortho-metalation of an aromatic metal-azo compound, is extensively described in the literature for related azobenzenes.[21] In Figure 4.11 the ^{1}H-NMR spectrum of **B2** and **B2'** are shown and is notorious that the most high fielded signals attributed to protons from the phenyl part of the phenylpyrdine are duplicated (non equivalent).

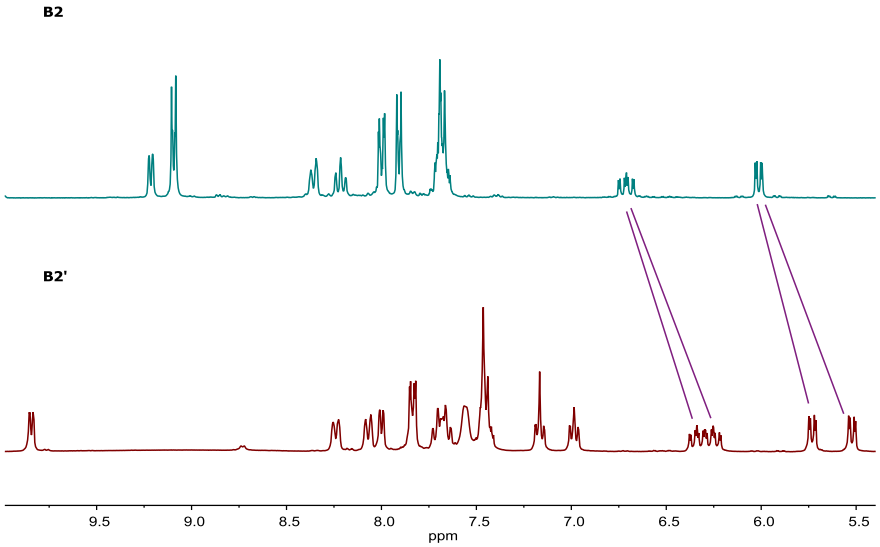

Figure 4.11. ^{1}H-NMR spectrum of **B2** in acetone-d_6, 300 MHz (Top). ^{1}H-NMR spectrum of **B2'** in $CDCl_3$, 300 MHz (Bottom).

Due to the lower reactivity of monodentate ligand **2**, it was considered the use of a halide abstractor (a silver salt) to obtain the desired compounds. The corresponding iridium dimer and 4 equivalents of the monodentate ligand **2** were refluxed in acetone, using AgOTf. Following this procedure, complexes **A2**, **B2** and **C2** were obtained with reasonable yields (Scheme 4.3).[22]

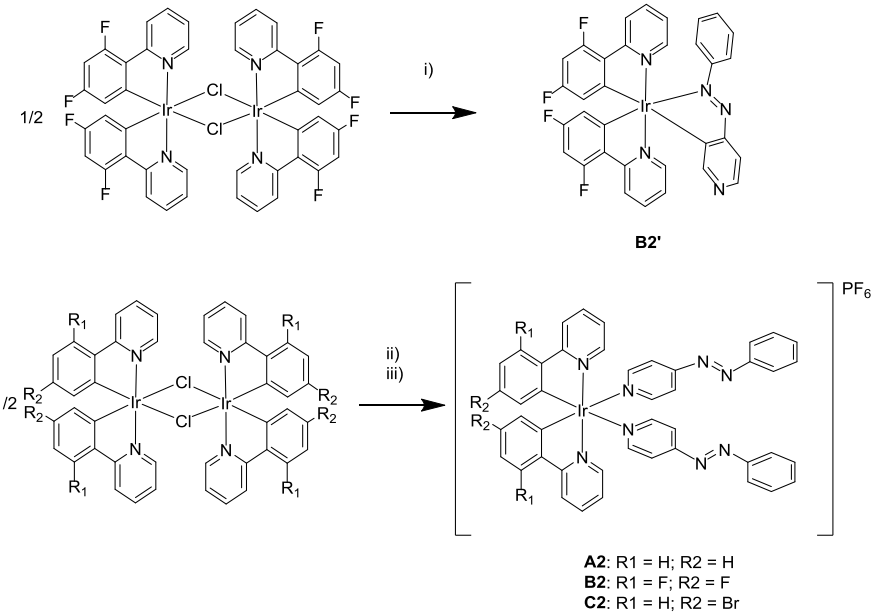

Scheme 4.3. Synthetic route toward azobenzene-containing iridium complexes **B2'**, **A2**, **B2** and **C2**. i) ligand **2** (2 equiv.), CH_2Cl_2/MeOH 2/1, reflux 15 h. ii) AgOTf (3.5–4.6 equiv.), acetone (56 ºC, 2h). iii) ligand **2** (4 equiv.), NEt_3 (8 equiv.), acetone (56 ºC, 15 h). Yields: **A2**(50%), **B2**(48%), **C2**(48%); **B2'**(87%).

Although ligands **1** and **3–5** could potentially also coordinate as monoanionic C–N_{azo} chelates, this coordination was not observed. The coordination as bipyrdiyl five-membered ring chelates is preferred for these ligands.

All the complexes **A**–**C** described above were fully characterized by ^{1}H- and ^{13}C-NMR spectroscopy, elemental analysis and HR-MS spectrometry (full spectra and detailed synthetic procedures are compiled in the Supporting Information). As expected, in all the compounds the two nitrogen atoms of the phenylpyridine ligands occupy mutually *trans* positions. Complexes derived from ligands **1**–**3** and **5** are C_2-symmetric in solution, as confirmed by the number of signals observed in the ^{1}H- and ^{13}C-NMR spectra. Compounds **A4**, **B4** and **C4**, derived from 4-(*p*-azobenzene)-4'-bromo-2,2'-bipyridine ligand **4** present a rather complicated fully aromatic ^{1}H- and ^{13}C-NMR spectra. All the expected signals were observed although they could not be unequivocally assigned. The molecular structures of **B1**, **A2**, **C3**, and **A4** were confirmed by X-ray diffraction of crystalline samples (see Figures 4.12–4.15 and Table 4.1).

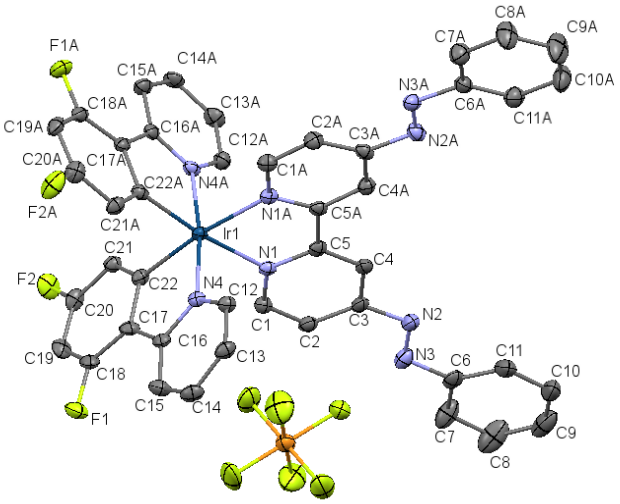

Figure 4.12. ORTEP representation of the molecular structure of **B1** according to X-ray diffraction. Hydrogens have been omitted for clarity. Ellipsoids at 50% probability.

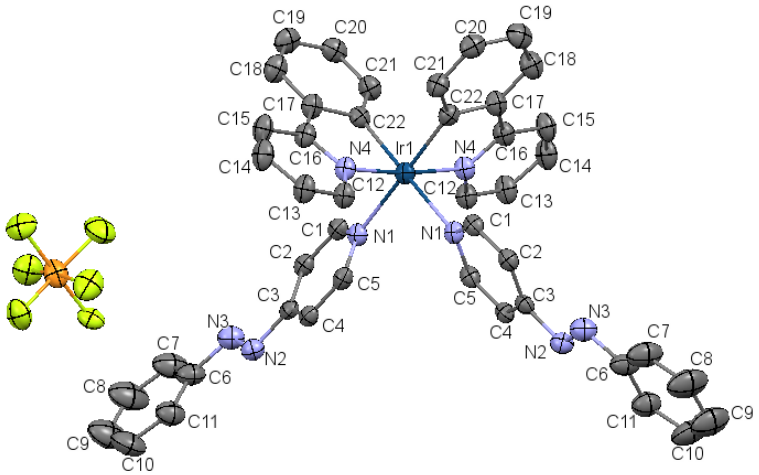

Figure 4.13. ORTEP representation of the molecular structure of **A2** according to X-ray diffraction. Hydrogen atoms have been omitted for clarity. Ellipsoids at 50% probability.

A)

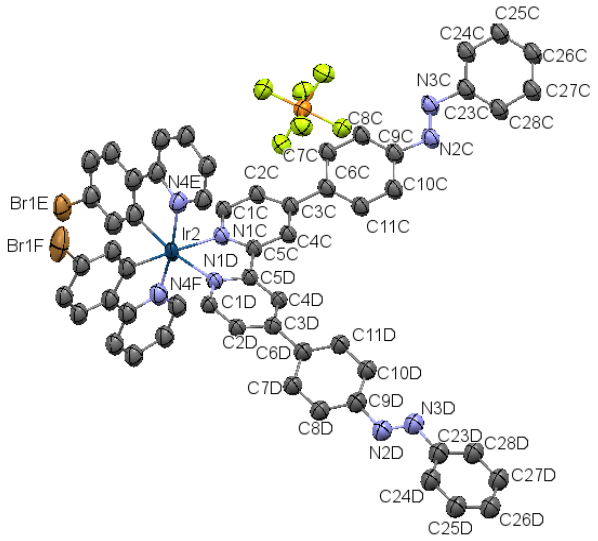

B)

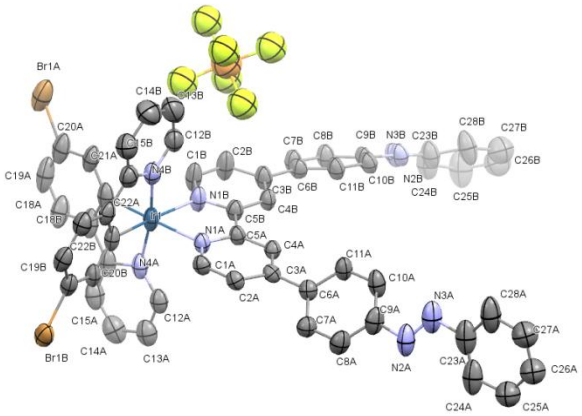

C)

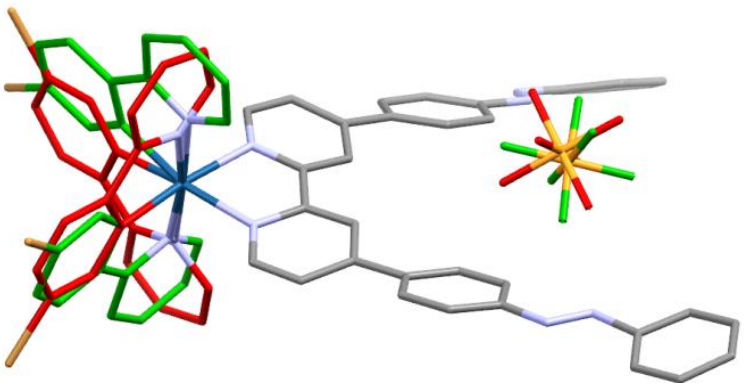

Figure 4.14. A) and B) ORTEP representation of the molecular structure of **C3** according to X-ray diffraction. Hydrogen atoms have been omitted for clarity. Ellipsoids at 50% probability. C) Superposed image of both enantiomers, in green and red respectively.

A)

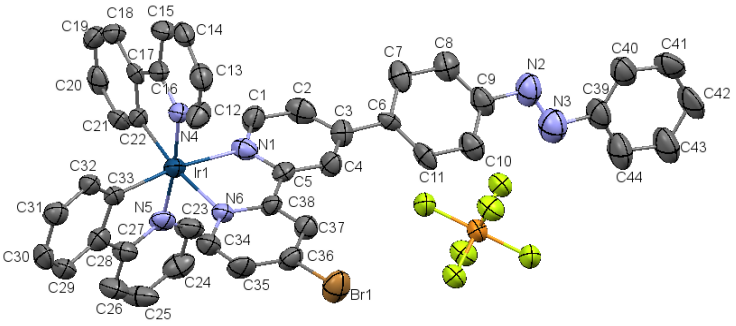

B)

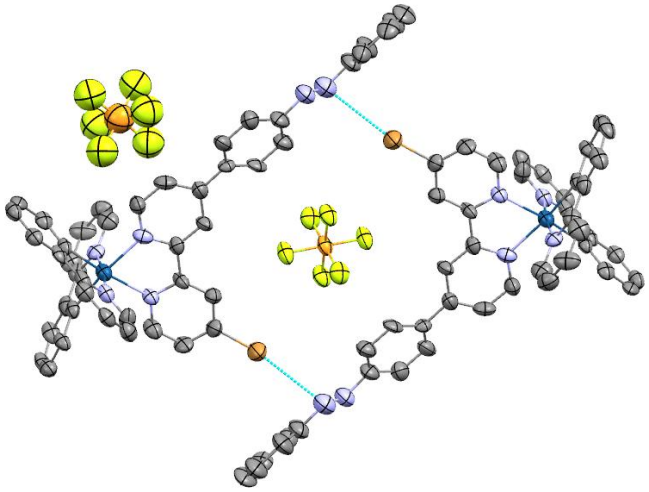

C)

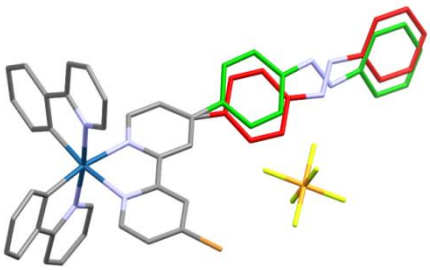

Figure 4.15. A) ORTEP representation of the molecular structure of the **A4** according to X-ray diffraction. Hydrogen atoms have been omitted for clarity. Ellipsoids at 50% probability. B) Selected view of the crystal to show the existing interaction between the two enantiomeric forms. C) Two different arrangements (shown in green and red) with 50% probability have been detected.

As already observed in the molecular structures of the model complexes described above, also the azobenzene-appended complexes present in solid state an octahedral coordination of the iridium center, with two nitrogen atoms of the phenylpyridine ligands in *trans* positions, as observed in solution by NMR spectroscopy. Also in these examples (as in all the compounds synthesized in this chapter) although these compounds are chiral, the crystals were obtained as racemates. For **C3** both enantiomers were packed in a non-patterned manner, which was reflected in the X-ray structure as a disorder in the phenylpyridine ligands (Figure 4.14). In the case of **A4**, the crystal packing showed an interaction between the two enantiomeric forms of the compound through Br−N nonbonding interactions. One counterion was contained in the space defined between a pair of enantiomers, while another one was localized outside and presented more disorder. For this structure some disorder was also observed in the disposition of the azobenzene unit. Two different arrangements with 50% probability each have been detected (Figure 4.15). The same type of crystallographic disorder was previously reported for other azobenzene-containing complexes.[23]

As expected, all the complexes presented the azobenzene fragments in the thermodynamically most stable *E* form. The N–N distances observed are similar to the ones of the free ligand **3**, which confirms the integrity of the azo functionality. An examination of the dihedral angles of the azoaromatic ligands in these complexes showed that in the case of compounds **B1** and **A2** the ligand can be described as planar (with extended π-conjugation), but for derivatives **A4** and **C3** the twist between aromatic rings is in the range 30–40°. Similar values were observed previously for azobenzene-containing bipyridine and terpyridine complexes (see Table 4.1).[24,25]

Unfortunately, we did not obtain any structure of derivatives of ligand **5**, but according to the large dihedral angle observed by Nishihara in the molecular structure of an analogue free ligand (see Chapter 2), a large distortion from the planarity was expected for ligand **5** also upon metal coordination.

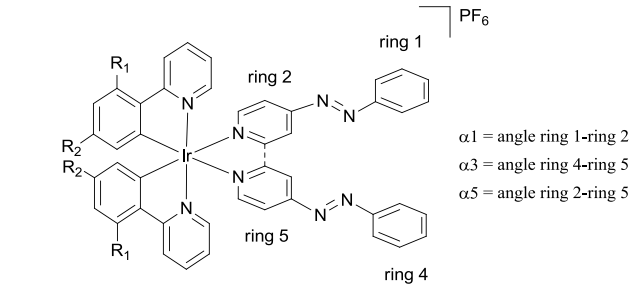

B1, A2

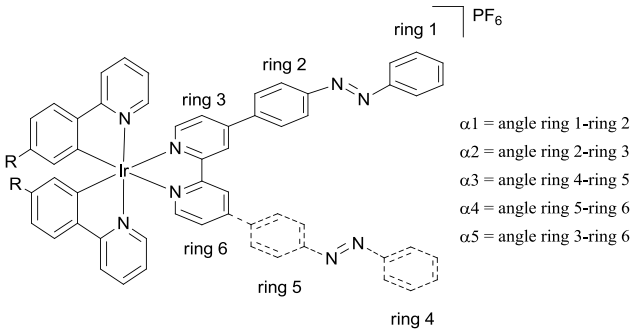

C3, A4

	N–N	N–N	α1	α2	α3	α4	α5
B1	1.257	1.260	9.15	–	10.01	–	4.51
A2	1.255	1.255	0.40	0.40	–	–	57.82
C3	1.269	1.254	40.42	36.37	23.29	26.68	0.36
A4	1.256	–	39.71	29.63	–	–	9.04

Distances are expressed in Å and angles in degrees.

Table 4.1. Most relevant angles and distances extracted from molecular structures of complexes **B1**, **A2**, **C3** and **A4**, determined by X-ray diffraction.

Complexes type **C** were synthesized for *a posteriori* introduction of photochromic azobenzene fragments on the phenylpyridine units by palladium-catalyzed Suzuki cross-coupling. [4-(phenylazo)phenyl]boronic acid **9** or [4-(phenylazo)phenyl]boronic acid pinacol ester **11** used previously for the synthesis of ligands **3** and **4** were catalytically coupled to **C** compounds to obtain **Dbipy**, **Dphen**, **D1–D3** and **D5** containing up to four azobenzene groups, with rather modest yields (Scheme 4.4). This reaction was not carried out with **DbipyBr** nor **C4** because the products would be **D3**, due to the cross-coupling also through the bromines present in the bipyridine ligands.

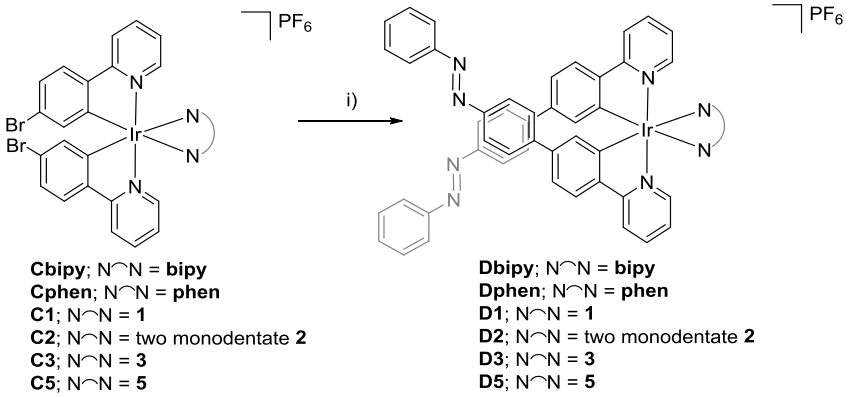

Scheme 4.4. Synthetic route toward azobenzene-containing iridium complexes **D** with 2,2'-bipyridine, 1,10'-phenanthroline and ligands **1**, **2**, **3**, **5**. i) (E)-[4-(phenylazo)phenyl]boronic acid **9** or [4-(phenylazo)phenyl]boronic acid pinacol ester **11** (2.4 equiv.), solvent 2/1 THF:Na_2CO_3 aq. (1 M), $Pd(PPh_3)_4$ (10 mol%), 80 ºC, over-night. Yields: **Dbipy**(10%), **Dphen**(50%), **D1**(34%), **D2**(14%); **D3**(24%); **D5**(26%).

Complexes labeled as **D** were fully characterized by ^{1}H- and ^{13}C-NMR spectroscopy, elemental analysis and HR-MS spectrometry (full spectra and detailed synthetic procedures are compiled in the Supporting Information). As expected, the obtained NMR spectra were even more complicated than the previously described ones. As an example, the ^{1}H- and ^{13}C-NMR of **D5** are shown in Figure 4.16 and Figure 4.17 respectively.

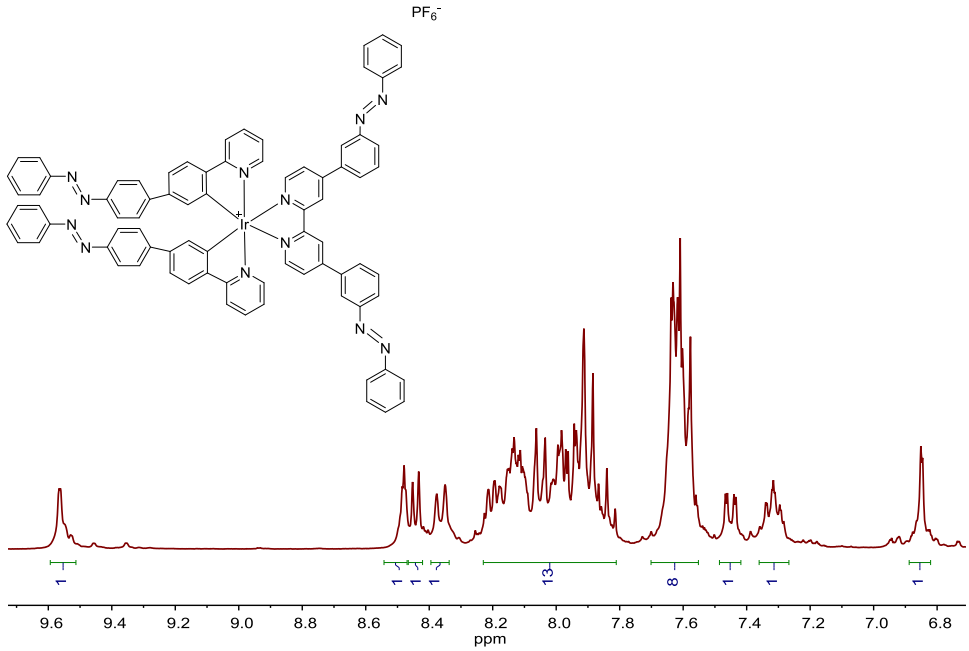

Figure 4.16. ^{1}H-NMR spectrum of **D5** in acetone-d_6, 300 MHz.

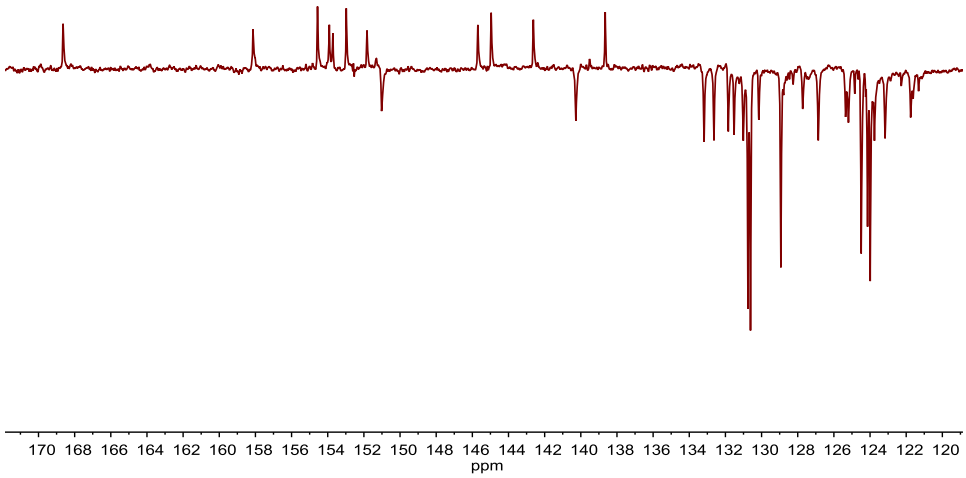

Figure 4.17. ^{13}C-APT-NMR spectrum of **D5** in acetone-d_6, 75 MHz.

This complex contains a total of four azobenzene units, two more than complexes **A**–**C**, resulting in a very complex aromatic region in both ^{1}H- and ^{13}C-NMR spectra. On the ^{1}H-NMR spectrum, 20H were identified and on the ^{13}C-NMR, 20CH and 12C_{quat} but they could not be unequivocally assigned. The number of protons and carbons exhibited are coherent with C_2-symmetric arrangement in solution of the expected compound.

4.2.2. CYCLIC VOLTAMMETRY

The work described in this section has been performed at the laboratories of CIDETEC under the supervision of Dr. A. Altube and Dr. E. García-Lecina.

Cyclic voltammetry measurements of the compounds studied in this chapter are relevant because they can be used to evaluate the HOMO–LUMO energy gap, which could eventually be related to the emission color of such compounds for their potential applications. The electrochemical properties of azobenzene-containing iridium cationic complexes were studied in anhydrous acetonitrile (ACN) solutions, complexes **Abipy**–**Cbipy** containing 2,2'-bipyridine as ancillary ligand were used as model complexes for comparative purposes. The measured half-wave potentials are summarized in Table 4.2 (Complexes **D1**–**D3** and **D5** were not studied, because these complexes were synthesized after performing these measurements). The necessary data was extracted from the obtained reduction/oxidation waves. E_{red} and E_{ox}, are the reduction and oxidation potential values read at the midpoint of each peak. Otherwise, $E_{onsetred}$ and $E_{onsetox}$, are the values obtained considering the starting point of the peak. The HOMO

and LUMO levels of all complexes have been deduced by the equation E_{HOMO}/E_{LUMO} (eV) = −(4.8 + E_{onset}), E_{HOMO} with the oxidation potential and E_{LUMO} with the reduction potential.[26] Under the premise that the energy level of ferrocene/ferrocenium is 4.8 eV below the vacuum level.[27] ΔE has been obtained as the difference LUMO–HOMO.

	E_{red}[a] (V)	E_{ox}[a] (V)	$E_{onsetred}$[a] (V)	LUMO[b] (eV)	$E_{onsetox}$[a] (V)	HOMO[b] (eV)	ΔE[b] (eV)
Abipy	−1.75	1.02	−1.61	−3.19	0.9	−5.70	2.51
Bbipy	−1.65	1.33	−1.51	−3.29	1.15	−5.95	2.66
Cbipy	−1.70	1.21	−1.56	−3.24	1.08	−5.88	2.64
A1	−1.03	1.02	−0.92	−3.88	0.92	−5.72	1.84
B1	−1.00	1.34	−0.88	−3.92	1.24	−6.04	2.12
C1	−1.00	1.22	−0.88	−3.92	1.11	−5.91	1.99
A2	−1.24	1.05	−1.07	−3.73	0.95	−5.75	2.02
B2	−1.20	1.42	−1.01	−3.79	1.28	−6.08	2.29
C2	−1.19	1.26	−1.00	−3.80	1.16	−5.96	2.16
A3	−1.42	1.02	−1.15	−3.65	0.85	−5.65	2.00
B3	−1.40	1.36	−1.27	−3.53	1.18	−5.98	2.45
C3	−1.47	1.10	−1.20	−3.60	0.94	−5.74	2.14
A4	−1.43	1.02	−1.30	−3.50	0.88	−5.68	2.18
B4	−1.40	1.38	−1.25	−3.55	1.22	−6.02	2.47
C4	−1.37	1.28	−1.24	−3.56	1.12	−5.92	2.36
A5	−1.62	1.02	−1.42	−3.38	0.87	−5.67	2.29
B5	−1.58	1.35	−1.39	−3.41	1.22	−6.02	2.61
C5	−1.60	1.23	−1.40	−3.40	1.00	−5.80	2.40

Table 4.2. Electrochemical properties of the Ir complexes. [a] Potential values are reported *versus* Fc/Fc+. [b] HOMO and LUMO levels have been deduced by the equation E_{HOMO}/E_{LUMO} (eV) = −(4.8 + E_{onset}), and ΔE has been obtained as the difference LUMO–HOMO.

According to the literature, the voltammograms of model complexes $[Ir(ppy)_2(bipy)]PF_6$ (**Abipy**) and $[Ir(Fppy)_2(bipy)]PF_6$ (**Bbipy**) exhibit a reversible reduction peak assigned to the reduction of the bipyridine ligand. They also present a reversible oxidation wave attributed to the Ir^{IV}/Ir^{III} redox couple.[28] The obtained ΔE values obtained for the model compounds measured are comparable to those found in the literature for similar Ir complexes.[29] As reported before, the values of the redox potentials of iridium complexes containing phenylpyridine ligands depend on the electron-donating or electron-withdrawing nature of their substituents. The HOMO, that is located basically on the metal and the phenyl ring of the phenylpyridine, is stabilized by electron-withdrawing groups on the phenyl ring of the phenylpyridine, which is reflected in larger oxidation potentials.[30 31]

When looking at the results obtained, the effect of electron-withdrawing groups (F or Br) on the phenyl moiety of the phenylpyridine fragment on the oxidation potentials of iridium derivatives **B** and **C** was notorious in both model complexes and azobenzene-

containing compounds. Comparing the values of the oxidation potentials measured for model compounds **Abipy**, **Bbipy** and **Cbipy** it was observed that the presence of fluorine and bromine groups on the ppy lead to larger values for the oxidation peak (1.33 V and 1.21 V respectively), compared to the unsubstituted **Abipy**. As expected, the reduction wave was less affected, but **B** (−1.65 V) and **C** (−1.70 V) showed more positive reduction potentials than **A** (−1.75 V), which is attributed to a small inductive effect. This shift of the oxidation potential produces that complexes with fluorine and bromine substituents on the phenyl ring of the phenylpyridine showed larger ΔE values than complexes without these substituents (Figure 4.18).

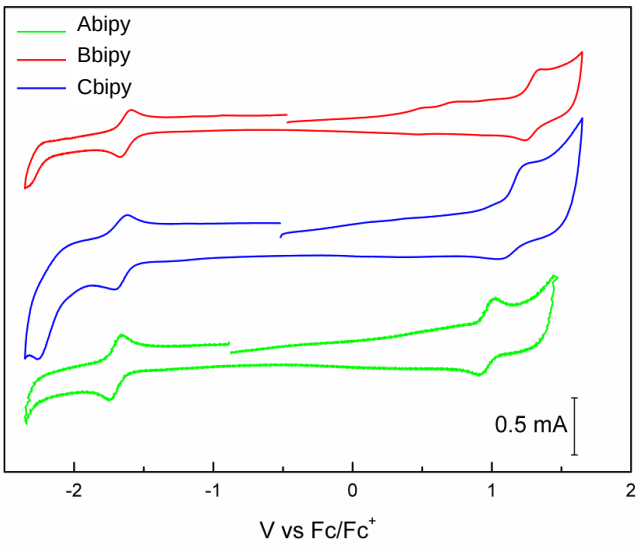

Figure 4.18. Cyclo-voltammograms (10^{-3} M, dry ACN) of **Abipy**, **Bbipy** and **Cbipy** containing 0.1 M $TBAPF_6$ as the supporting electrolyte, scan rate of 100 mV s^{-1}.

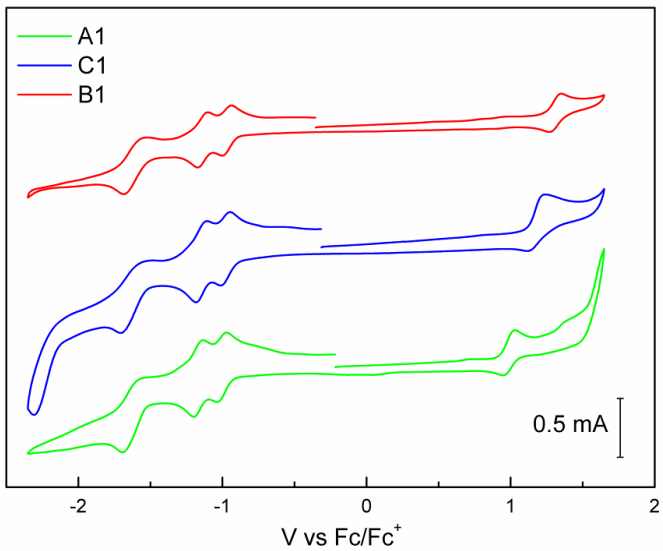

Figure 4.19. Cyclo-voltammograms (10^{-3} M, dry ACN) of **A1**, **B1** and **C1** containing 0.1 M $TBAPF_6$ as the supporting electrolyte, scan rate of 100 mV s^{-1}.

Azobenzene-containing complexes also presented this broadening of the HOMO–LUMO energy gap when electron-withdrawing substituents are present on the

phenylpyridine ligands (Figure 4.19). On the one hand, when we compared the data obtained for three derivatives of each ligand (**A1**–**A5, B1**–**B5, C1**–**C5**) it was clear that the oxidation potential is basically identical to that of **Abipy**, **Bbipy** and **Cbipy**, which confirmed that the anodic peak potentials are not affected by the nature of the ancillary bipyridine ligand. On the other hand, their first reduction peak potentials were between −1.62 and −1.00 V. They are anodically shifted with respect to those of the model compounds. According to the literature, azo groups are electron-withdrawing in nature and trap electrons in the metal-to-ligand charge-transfer (MLCT) excited state.[32a] These observations are in agreement with the general description of the frontier orbital for $[Ir(ppy)_2(bipy)]^+$ complexes. It is generally accepted that for such compounds, the LUMO, is localized essentially at the bipy ancillary ligand and could be stabilized by electron-withdrawing groups.[15] The LUMO of complexes containing azobenzenes in the ancillary ligand is stabilized and as consequence, the ΔE values of these complexes are lower than ΔE values of model compounds.

A comparative analysis of the azobeneze-appended derivatives showed that the presence of an additional benzene ring in the structure of the bipyridine ligand reduced the electron-withdrawing effect of the azo substituent, see for instance the reduction potential values found for derivatives of ligand **3** (−1.43 V for **C3**) compared to derivatives of ligand **1** (−1.00 V for **C1**).[33] On the other hand, by comparing derivatives of ligand **3** (−1.43 V for **C3**) and ligand **5** (−1.60 V for **C5**), we observed that the effect of the azo group is also reduced when it has a *meta*-substitution. Finally, derivatives of ligand **4** presented very similar values to that of derivatives of ligand **3** (−1.37 V for **C4** and −1.47 V for **C3**) indicating that both bromine and azo substituents have a similar electron-withdrawing effect.

Comparison of ligands **1** and **2** permitted us to study the chelate effect. The use of bidentate or monodentate ancillary ligand have a strong influence on the cathodic peak, being more negative for derivatives of the monodentate ligand **2**. The anodic shift induced by azo groups is less effective for derivatives of ligand **2** (−1.19 V for **C2**) than for derivatives of ligand **1** (−1.00 V for **C1**). This behaviour could be attributed to the lower rigidity and conjugation present in the monodentate ligand **2** compared to bidentate ligand **1**.

Altogether, cyclic voltammetry measurements let us conclude that azobenzene appended bipyridines render compounds with smaller HOMO-LUMO gap than parent unsubstituted compounds. But this energy difference can be tuned depending on the substitution pattern of the azobenzene, the extended aromaticity, the chelate effect, and eventually by using electron-withdrawing or electron-donating groups on the phenylpyridine ligands.

4.2.3. UV-VIS CHARACTERIZATION

UV-Vis absorption spectra of **A**–**Dbipy**, **A**–**Dphen**, **A**–**CbipyBr**, ligands (**1**–**5**) and their iridium(III) complexes **A**–**D** were registered at room temperature in CH_3CN solution. Absorption spectra of some model compounds were also recorded for comparative purposes.

Cationic complexes of the type $[Ir(ppy)_2(bipy)]^+$ typically present intense absorption bands in the UV region of the spectra between 250–350 nm (ε~3−5 × 10^4 $M^{-1}cm^{-1}$) assigned to singlet spin-allowed ligand centered (^{1}LC) π→π* transitions involving both cyclometalated and ancillary ligands. At longer wavelengths around 350–450 nm one order of magnitude weaker bands attributed to transitions with mixed metal-to-ligand (^{1}MLCT) and ligand-to-ligand (^{1}LLCT) charge transfer character are observed.[2,34]

The characteristic absorption bands of cationic complexes of the type $[Ir(ppy)_2(bipy)]^+$ described above were difficult to identify in azobenzene-containing complexes due to the overlapping with bands attributed to the azobenzene fragment. To study the influence of the different substitution pattern in both the phenylpyridines and ancillary ligands on this absorption bands, we focused initially on complexes without azobenzenes. Selected absorption maxima and the corresponding molar extinction coefficients of complexes without azobenzene fragments are presented in Table 4.3. The most intense band of the ancillary ligand attributed to a ^{1}LC π→π* transition was shifted to lower energies when they were coordinated to the metal, as it was already observed for related 4,4'-bisstyryl-2,2'-bipyridine Ir(III) complexes.[35] This effect was attributed to a lowering of the LUMO energy level upon coordination of the pyridyl ring (see Figure 4.20).

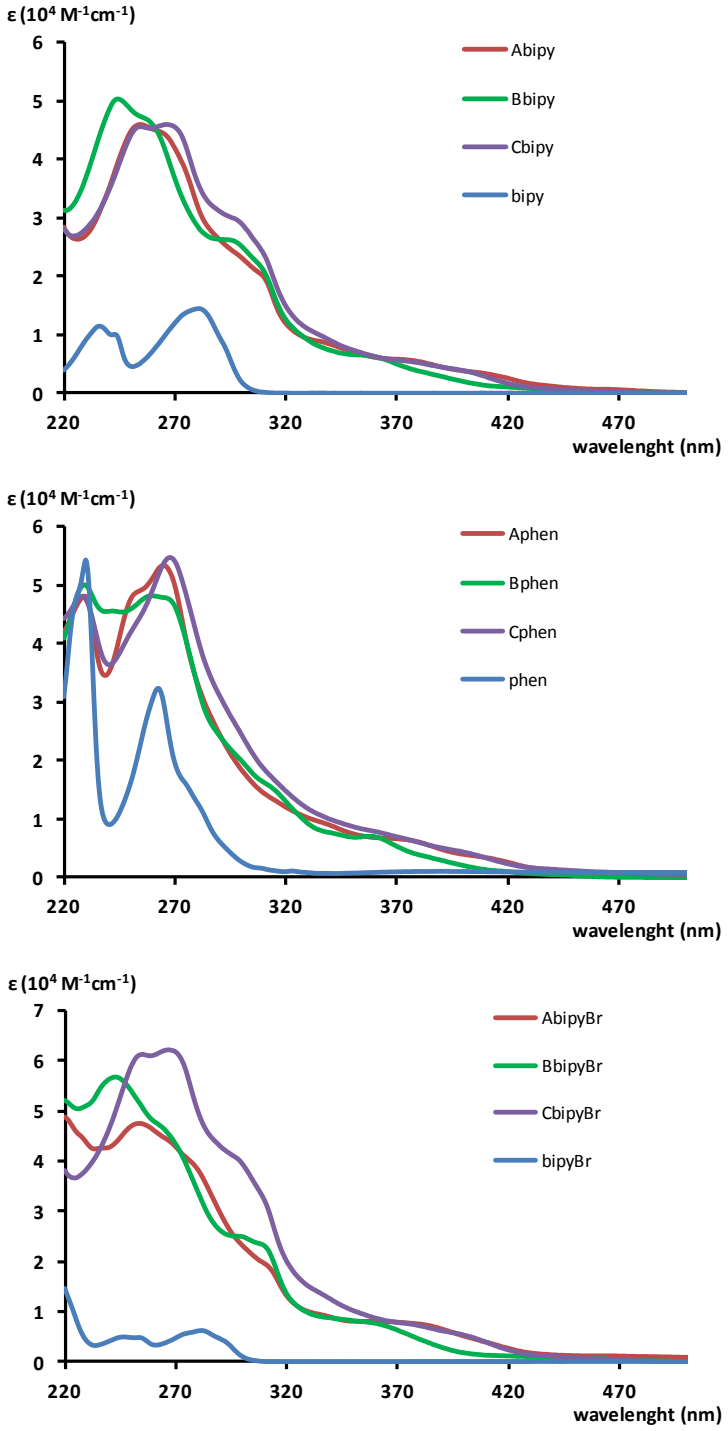

Figure 4.20. UV-Vis absorption spectra. Top: UV-Vis absorption spectra of 2,2'-bipyridine and complexes **A−Cbipy**. Middle: UV-Vis absorption spectra of 1,10-phenanthroline and complexes **A−Cbphen**. Bottom: UV-Vis absorption spectra of 4,4'-dibromo-2,2'-bipyridine and complexes **A−CbipyBr**.

It was not observed any significant difference when comparing the position of the less energetic bands of the complexes incorporating 2,2'-bipyridine or 1,10-phenanthroline (Figure 4.21). Although in a published work they state that the HOMO−LUMO gap decreased when increasing the number of conjugated units on the ancillary ligand.[4] As mentioned before, electron-withdrawing groups on the bipyridine ligand may stabilize

the LUMO, which is reflected in a red-shift of the bands. In our results, when comparing **A−Cbipy** complexes with **A−CbipyBr** complexes, this effect was not observed. Nevertheless it should be noticed that it is difficult to assign a clear maxima to such broad low intense bands. In accordance with our results, the effect of electron-releasing substituents on the bipyridine in Ir(III) complexes was analyzed in a previous publication and it was not observed any significant shift in the UV-Vis spectra.[36]

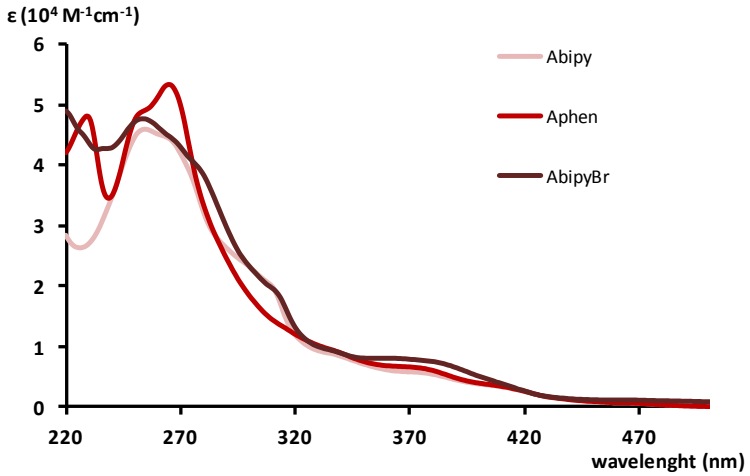

Figure 4.21. UV-Vis absorption spectra of complexes **A** with ligands **bipy**, **phen** and **bipyBr**.

However, complexes with fluorine substituents on the phenylpyridines (derivatives **B**) showed more energetic transitions than unfluorinated analogues, due to the stabilization of HOMO as observed before for related complexes.[37] This results are in agreement with the cyclic voltammetry observations described before. Complexes with bromine substituents on the phenylpyridine presented more energetic transitions than complexes without substituents on the phenylpyridine but less energetic than fluorinated complexes. It is remarkable that in the case of the fluorinated complexes there are two substituents and brominated complexes contain only one bromine in each phenylpyridine. In a previous work the effect of the substituents on phenylpyridine ligands for similar Ir(III) complexes with two phenylpyridines and a picolinate as ancillary ligand was also analyzed, but they did not observe the bands of brominated complexes at smaller wavelengths.[38]

	λ_{max} [nm] (ε [$10^4 \cdot M^{-1}$ cm^{-1}])
Compound	$\lambda_{\pi\rightarrow\pi^*}$
Abipy	412 (0.33)
Bbipy	361 (0.62)
Cbipy	401 (0.38)
Aphen	413 (0.32)
Bphen	360 (0.71)
Cphen	401 (0.42)
AbipyBr	410 (0.39)
BbipyBr	361 (0.76)
CbipyBr	399 (0.54)

Table 4.3. UV-Vis spectra. Selected absorption data.

Azobenzene and its derivatives present two type of low-lying singlet excited states; n→π* (S_1) and π→π* (S_2), which is reflected in their absorption spectra by a weak (symmetry forbidden) broad visible absorption at about 445 nm, and a strong (symmetry allowed) UV band around 315 nm, respectively.[39] In accordance with this general description, almost all free ligands (as described in Chapter 2) and the azobenzene-appended complexes studied here showed one intense band between 290−355 nm ($\lambda_{azo\ \pi\rightarrow\pi^*}$), and a weaker red-shifted band, between 430−513 nm ($\lambda_{azo\ n\rightarrow\pi^*}$) confirming the presence of azobenzene fragments (Table 4.4). In complexes **D** the less energetic band was not determined because it was too broad and weak to locate unequivocally its maxima. In the case of ligand **3**, its low solubility did not allow the determination of this band. A representative example of the series of spectra obtained for the azobenzene-containing derivatives is presented in Figure 4.22 (overlapped spectra of all the ligands and their complexes are compiled in the Supporting Information).

	λ [nm] (ε [$10^4 \cdot M^{-1}$ cm^{-1}])	
Compound	$\lambda_{azo\ \pi\rightarrow\pi^*}$	$\lambda_{azo\ n\rightarrow\pi^*}$
1	317 (3.9)	430 (0.08)
2	309 (1.6)	435 (0.03)
3[b]	340	nd
4	334 (3.5)	443 (0.13)
5[b]	314	435
azoppy[a]	348 (4.2)	441 (0.19)
azobenzene	316 (1.9)	440 (0.06)
A1	327 (5.3)	513 (0.26)
B1	328 (4.5)	479 (0.31)
C1	325 (5.3)	481 (0.32)
D1	349 (9.3)	nd
A2	312 (4.7)	460 (0.37)
B2	318 (4.8)	433 (0.37)
C2	315 (5.2)	446 (0.43)
D2	347 (9.0)	nd
A3	338 (7.2)	467 (0.44)
B3	343 (7.3)	443 (0.47)
C3	336 (6.6)	449 (0.24)
D3	350 (12.7)	nd
A4	333 (4.4)	465 (0.30)
B4	339 (4.3)	440 (0.33)
C4	336 (4.7)	453 (0.35)
A5	290 (6.5)	462 (0.21)
B5	311 (6.1)	436 (0.26)
C5	320 (6.4)	450 (0.25)
D5	337 (9.9)	nd
Dbipy	355 (7.44)	nd
Dphen	355 (6.9)	nd

Table 4.4. UV-Vis spectra. Selected absorption data. [a] **azoppy** = 2-((4-azobenzene)phenyl)pyridine. Data from reference[33]. [b] The solubility of these ligands in CH_3CN was too small for an accurate determination of the corresponding extinction coefficients.

A comparative analysis of the absorption spectrum of ligands **1**–**5** reveals that the absorption band attributed to a π→π* transition observed for ligand **1** (a chelating analogue of two ligands **2**) showed, as expected, a molar absorption approximately double than that of ligand **2**, and it was shifted to lower energy probably due to the extended conjugation present in this molecule (in accordance with the cyclic-voltammetry results). When looking at the same transition band for ligands **3** and **4**, a clear red-shift compared to that of pristine azobenzene was observed, consistent with the existence of extended conjugation between the bipyridine and the azobenzene fragments, as observed in the X-ray structure of ligand **3** (see Chapter 2). Nearly no shift of this band was observed for ligand **5** when compared to azobenzene, which

indicates a weak conjugation of both bipyridine and azobenzene fragments in this ligand. The same influence of the conjugation mentioned for the free ligands was also observed comparing absorption spectra of their corresponding complexes (Figure 4.22). This observation is also consistent with the non planar structure described by Nishihara for a related ligand (see Chapter 2).[40]

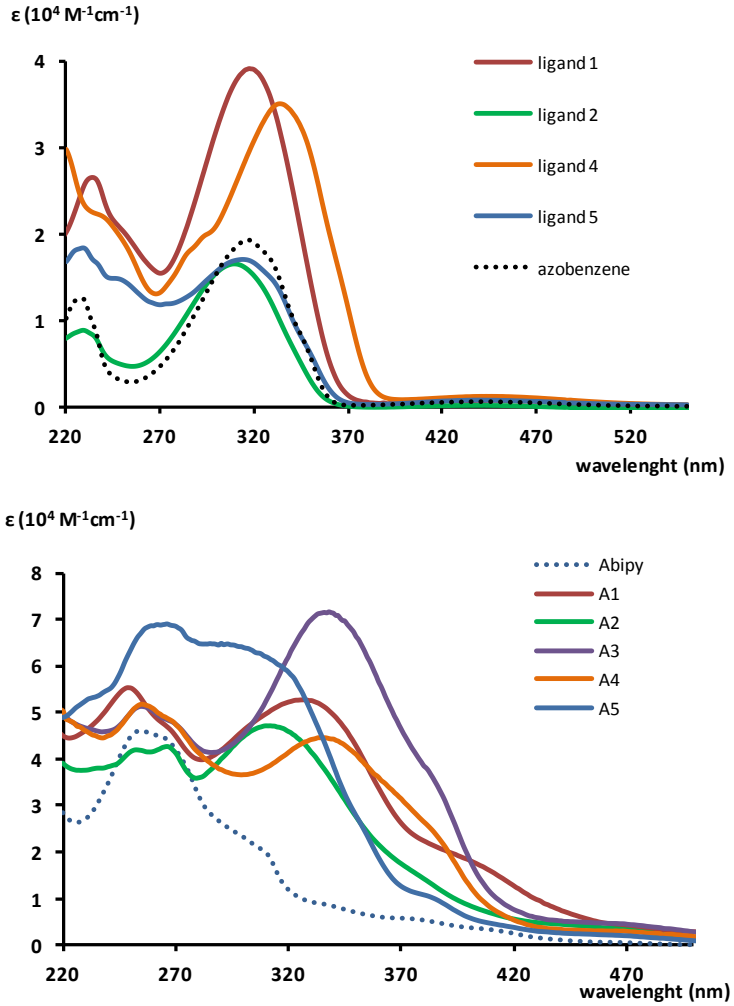

Figure 4.22. UV-Vis absorption spectra. Top: UV-Vis absorption spectra of ligands **1, 2, 4** and **5**. The azobenzene is also shown for comparative purposes. Bottom: UV-Vis absorption spectra of complexes **A** with ligands **1**−**5**. **Abipy** is also shown for comparative purposes.

The effect of the coordination to the metal on the ^{1}LC π→π* transition band observed previously for complexes without azobenzene fragment was not clear in all the azobenzene-containing complexes. The most intense bands of ligands **1** and **2** attributed to these transitions were shifted to lower energies when they were coordinated to the metal (Figure 4.23), but for derivatives of ligands **3**−**5** it was not observed any clear trend. Probably the long distance between the coordinating nitrogen atoms and the azobenzene fragments in these compounds could be responsible for this effect.

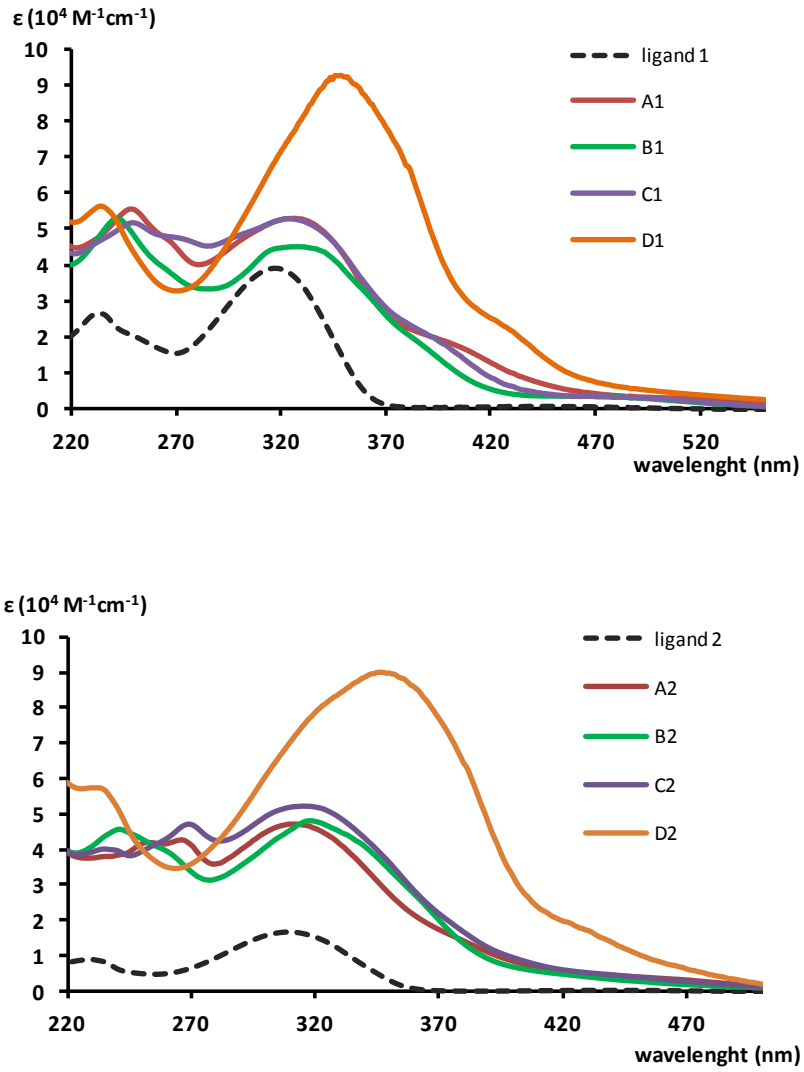

Figure 4.23. UV-Vis absorption spectra. Top: UV-Vis absorption spectra of ligand **1** and its iridium derivatives **A**–**D**. Bottom: UV-Vis absorption spectra of ligand **2** and its iridium derivatives **A**–**D**.

For derivatives **D**, containing azobenzene groups also in the cyclometalated phenylpyridine ligands, this absorption band is clearly red-shifted compared to compounds **A**–**C**, and closer to the absorption of the free 2-((4-azobenzene)phenyl)pyridine **azoppy** ligand (Table 4.4). In these compounds, the extinction coefficient at λ_{max} (azobenzene-centered π→π* transition) is proportional to the number of azobenzene fragments present in the molecule. This observations are in concordance with our previous report on **azoppy**-Ir(III) derivatives.[33]

4.2.4. TD-DFT CALCULATIONS

The work described in this section has been performed by Dr. Abel de Cózar at the University of the Basque Country.

A computational study within the DFT framework was made in order to further analyze the electronic properties of ligands **1**–**4** and their complexes **A**–**C** (unfortunately, no

calculations were performed on derivatives of ligand **5**). Simulations of the absorption spectra of previously optimized structures at TD-CAM-B3LYP(PCM)/6-31+G*&LANL2DZ level of theory have been performed. This computational method has been proven to give reliable results on the study of vertical excitations of azobenzene-iridium complexes.[33] The data associated with the main transitions computed and HOMO-LUMO gaps of these compounds are collected in Table 4.6. Representations of the most relevant molecular orbitals is depicted in Figures 4.24 and 4.25. The optimized structures of ligands **2**−**4** present a planar *trans* conformation on the azo and bipyridine moieties, as observed experimentally in the X-ray structure of ligand **3** (Figure 2.2, Chapter 2). The optimized structures of the complexes showed similar bond distances and angles of the ones obtained by X-ray diffraction (Table 4.5).

	N–N	N–N	α1	α2	α3	α4	α5	RMS
B1	1.26 (1.25)	1.26 (1.25)	9.15 (3.66)	-	10.01 (4.60)	-	4.51 (3.46)	0.27
A2	1.25 (1.25)	1.25 (1.25)	0.40 (0.13)	0.40 (0.13)	–	–	57.82 (60.7)	0.36
C3	1.27 (1.25)	1.25 (1.25)	40.42 (2.54)	36.37 (37.1)	23.29 (1.03)	26.68 (36.3)	0.36 (3.94)	0.51
A4	1.26 (1.25)	1.26 (1.25)	39.71 (1.28)	29.63 (36.4)	-	–	9.04 (3.15)	0.49

Table 4.5. Comparison between X-ray and DFT (between brackets) most relevant geometrical bond distances (Å) and angles (°), and RMS deviation of complexes **B1**, **A2**, **C3** and **A4**.

Moreover, the simulated wavelength values for the main absorptions are similar to the experimental ones, thus pointing out the reliability of the chosen computational method for this family of compounds. The computed main absorption bands are mainly associated with π → π* transitions (Figure 4.24). Actually, in the case of ligands **1** and **2**, the vertical excitations start from an orbital allocated on the nitrogen atoms, with a lower participation of the orbital delocalized in the aromatic system. On the contrary, in conjugated ligands **3** and **4**, all the orbitals involved in the transitions are located in the latter π system. Focusing on the structure of the ligands, a bathochromic displacement in the simulated maximum is observed when extended conjugation is present. Ligand **2** has the most energetic absorption band (305 nm, 4.0 eV), and an increase of 7 nm in the wavelength is found in its dimeric counterpart **1**. Introduction of two additional phenyl groups on the latter (namely, ligand **3**) implies an even higher reduction in the band gap, and therefore an increase in the computed wavelength to 333 nm (3.71 eV). Noteworthy, comparing ligands **3** and **4**, it can be seen that the effect on the wavelength due to the bromine in the 4′ position of the bipyridine moiety is similar to the presence of an azobenzene at the same position, even though only inductive and not

extended conjugation can be addressed for the former substituent. These observations are in agreement with the experimental data described above.

	λ_{max} [nm] (E [eV])	f	Transition	$\Delta E_{HOMO-LUMO}$ [a] [eV]
1	312.3 (3.96)	1.89	HOMO-1➔LUMO (51%) HOMO-2➔LUMO+1 (42%)	
2	305.3 (4.06)	0.83	HOMO➔LUMO (67%) HOMO-1➔LUMO (18%)	
3	333.5 (3.71)	2.87	HOMO➔LUMO (49%) HOMO-1➔LUMO+1 (47%)	
4	330.47 (3.75)	1.41	HOMO➔LUMO (68%)	
A1	322.6 (3.84)	0. 99	HOMO-6➔LUMO (49%) HOMO-7➔LUMO+1 (24%)	1.26
B1	336.6 (3.68)	1.00	HOMO-3➔LUMO (56%) HOMO-1➔LUMO (25%)	1.53
C1	320.1 (3.87)	0.79	HOMO-6➔LUMO (51%) HOMO-3➔LUMO+1 (27%)	1.43
A2	317.3 (3.91)	0.78	HOMO-6➔LUMO (27%) HOMO-2➔LUMO (25%) HOMO-3➔LUMO+1 (25%)	1.50
B2	327.7 (3.78)	1.28	HOMO-3➔LUMO (38%) HOMO➔LUMO+1 (34%) HOMO-4➔LUMO+1 (30%)	1.77
C2	321.5 (3.85)	0.68	HOMO➔LUMO+2 (52%) HOMO-3➔LUMO (22%) HOMO-4➔LUMO+1 (21%)	1.68
A3	333.7 (3.71)	2.11	HOMO-2➔LUMO (43%) HOMO-3➔LUMO+1 (37%) HOMO-1➔LUMO (20%)	1.65
B3	338.9 (3.65)	0.73	HOMO-1➔LUMO+1 (37%) HOMO➔LUMO (36%) HOMO➔LUMO+2 (20%)	1.94
C3	332.8 (3.72)	2.21	HOMO-2➔LUMO (46%) HOMO-1➔LUMO (33%)	1.94
A4	339.9 (3.64)	1.21	HOMO-2➔LUMO (46%) HOMO-3➔LUMO+1 (41%)	1.59
B4	329.4 (3.76)	1.67	HOMO-1➔LUMO+1 (55%) HOMO-2➔LUMO+2 (17%)	1.99
C4	335.4 (3.69)	1.71	HOMO-2➔LUMO (60%) HOMO-2➔LUMO+1 (22%)	1.88

[a] Computed at M06L(PCM)/6-31+G*&LANL2DZ//CAM-B3LYP(PCM)/6-31+G*&LANL2DZ level.

Table 4.6. Main transitions of ligands **1**–**4** and their complexes **A**–**C** computed at TD-CAM-B3LYP(PCM)/6-31+G*&LANL2DZ level of theory.

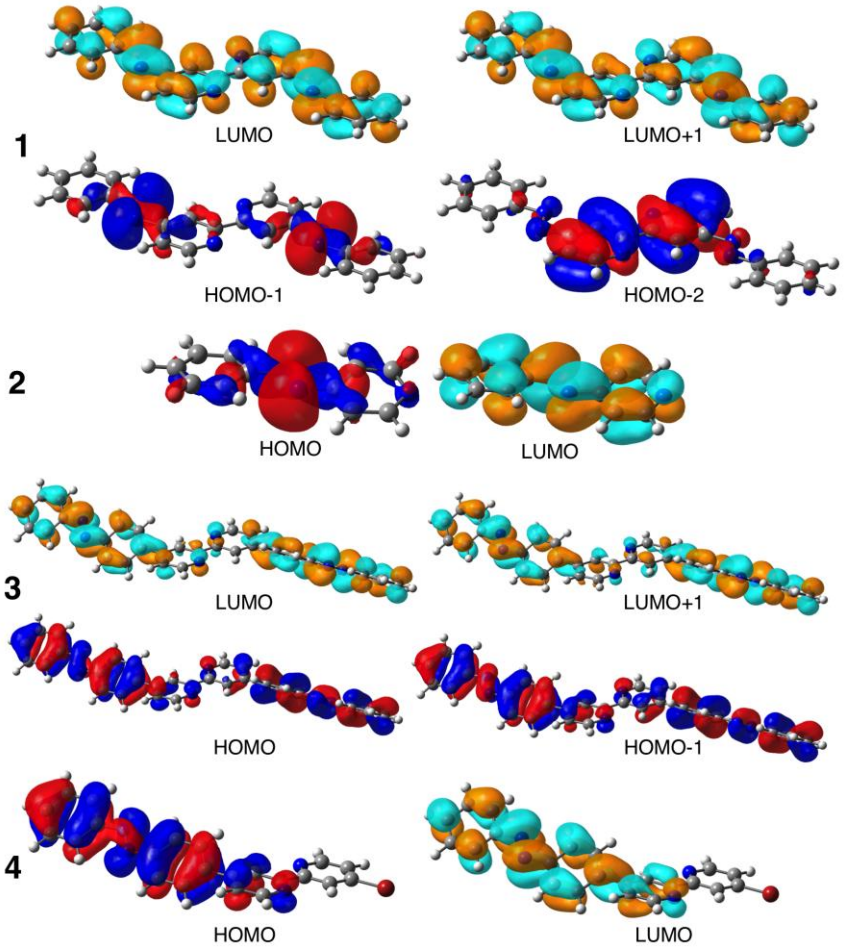

Figure 4.24. Most relevant MO of ligands **1–4** associated with the vertical excitations shown in Table 4.6. Occupied and unoccupied orbitals are represented by red & blue or yellow & green surfaces respectively.

As far as complexes are considered, as experimentally observed by UV-Vis, there is a red-shift on the computed wavelength associated with the chromophores **1**–**4** band due to coordination to the metal. These bands are assigned to the spin-allowed π→π* transitions, which mainly correspond to an intraligand charge transfer (^{1}ILCT) centered on the functionalized azobenzene moieties with no negligible participation of metal to ligand (^{1}MLCT) transitions. In the case of **C3** and **A**–**C4**, this latter ^{1}MLCT becomes the most important process since the vertical excitation involves an occupied orbital located on the [Ir(ppy)$_2$] moiety and an unoccupied orbital lying on the azobenzene ligands (Figure 4.25).

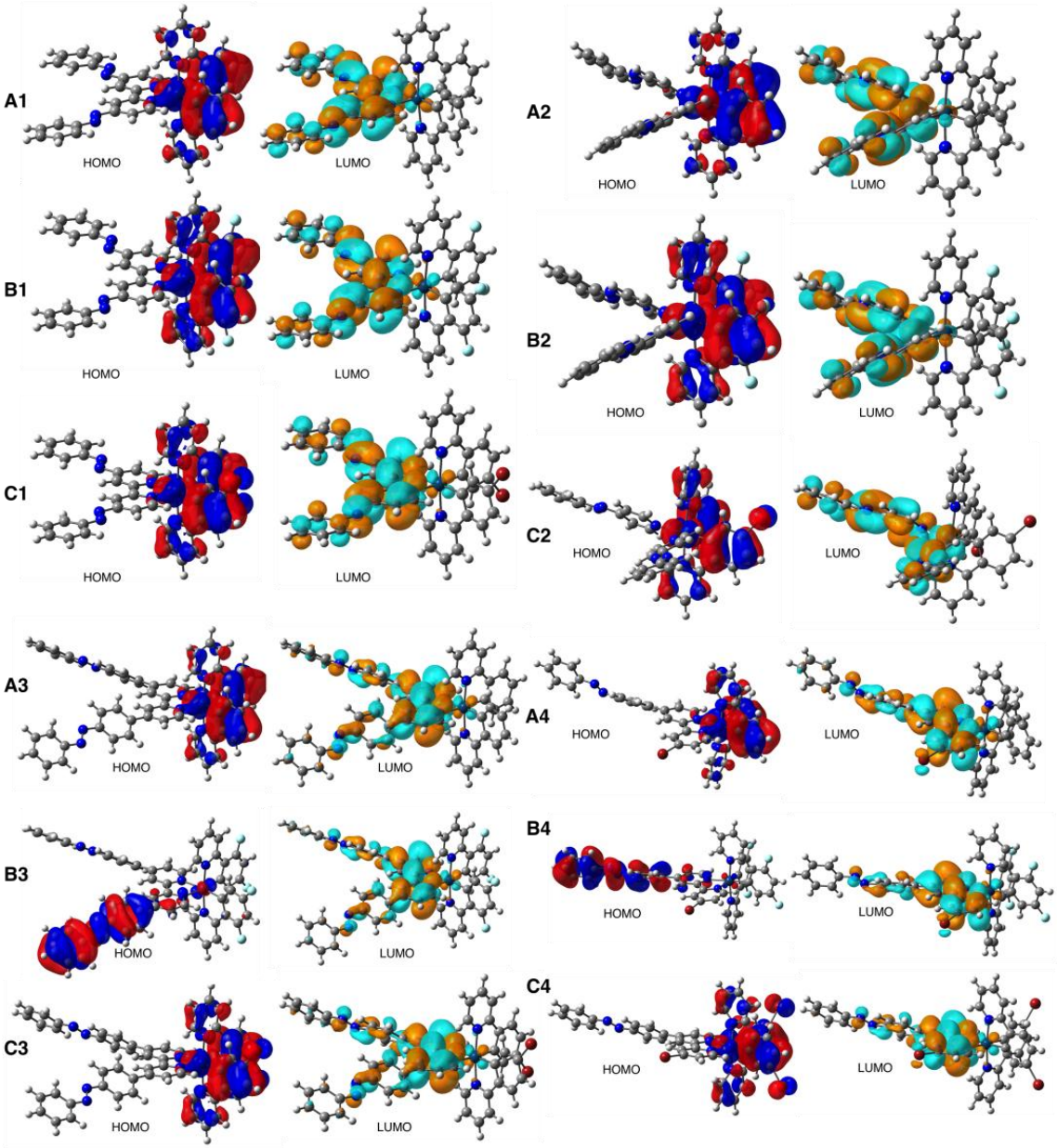

Figure 4.25. Frontier orbitals HOMO-LUMO of complexes **AC1–4**.

On the other hand, within a set of complexes, a monotonic increase of the computed wavelength was observed when extended conjugation is present on the ligand structure. This trend was also observed on the isolated ligands analysis (*vide supra*). Moreover, for a given ligand, a dependence upon the computed wavelength with the halogen substitution in the phenylpyridine moieties was found. In general, presence of fluorine in the structure (**B** set of complexes) implies a bathochromic displacement of the band compared to their non-fluorinated counterparts (**A** complexes). Whereas presence of bromine in the phenylpyridine ligands has a hypsochromic effect (**C** complexes).

The HOMO-LUMO energetic gap ($\Delta E_{HOMO-LUMO}$) of these complexes have been calculated at M06L(PCM)/6-31+G*&LANL2DZ//CAM-B3LYP(PCM)/6-31+G*&LANL2DZ level. This method has been proven to give accurate results on energy calculations by proper consideration of dispersion effects on organometallic complexes.[41] In general, the highest occupied molecular orbital is located in the [Ir(ppy)$_2$] moiety whereas the LUMO is placed on the azobenzene ligands.[31a] Only on complexes **B3** and **B4** both orbitals lie on the azobenzene fragment (see Figure 4.25). Therefore, the conjugated structure of the ligands has a small effect on the computed $\Delta E_{HOMO-LUMO}$ values. Actually, for a given set of compounds, the $\Delta E_{HOMO-LUMO}$ gap increases following the trend **1** < **2** < **3** < **4** where the lowest gap is associated with complexes **A**–**C1** instead of the ones with the simpler ligand structure (namely **A**–**C2)**. The effect of the [Ir(ppy)$_2$] moiety on these gaps was clearly pointed out if complexes with the same ligand are compared. In general, presence of electron-withdrawing groups on the [Ir(ppy)$_2$] moiety (compounds **B** and **C**) implies an increase on the gaps compared to their non-halogenated counterparts (compounds **A**). Noteworthy, the effect on fluorinated compounds **B** is higher than in the brominated ones (**C**), thus presenting the highest $\Delta E_{HOMO-LUMO}$ gaps. However, a general underestimation on the HOMO-LUMO gap values was observed maybe as consequence of the small deviations on the planarity of ligands in the computed structures (*vide supra*).

4.2.5. PHOTOISOMERIZATION STUDIES

The capacity of the azobenzene unit to isomerize in the complexes has been studied by UV-Vis absorption spectroscopy. Diluted CH_3CN solutions of all the compounds were irradiated for 30 min at the wavelength of the absorption previously attributed to the π→π* transition of the azobenzene (see Table 4.4), to confirm if the isomerization process was active. Later on, the solutions were irradiated for additional 30 min at the optimal wavelength calculated individually for each compound, following Monkowius' procedure, as already explained in detail in Chapter 2 (see Table 4.7).[42] Then, the reverse *Z*→*E* isomerization was monitored by UV-Vis absorption spectroscopy at 55 ºC, registering spectra at regular time intervals until the original spectrum was recovered. The value of absorbance at $\lambda_{\pi\rightarrow\pi^*}$ was used to follow this process. The calculated first order rate constants (k) and half-life times ($\tau_{1/2}$) for this process are presented in Table 4.7, and a representative example of the *Z*→*E* process is shown in Figure 4.26 (all absorbance *versus* time and first order plots obtained are compiled in the Supporting Information).

Compound	$\lambda_{optimal}$[a] [nm]	k [s^{-1}]	$\tau_{1/2}$ [min]
A1	348	1.0×10^{-5}	1155
B1	326	–	–
C1	341	6.0×10^{-6}	1925
D1	364	1.0×10^{-4}	115
A2	327	3.0×10^{-4}	38
B2	328	–	–
C2	344	3.0×10^{-4}	38
D2	350	9.0×10^{-6}	1284
A3	345	9.0×10^{-5}	128
B3	354	1.0×10^{-4}	115
C3	355	6.0×10^{-5}	192
D3	355	9.0×10^{-5}	128
A4	343	7.0×10^{-5}	165
B4	351	1.0×10^{-4}	115
C4	336	1.0×10^{-4}	115
A5	319	3.0×10^{-5}	385
B5	319	4.0×10^{-5}	289
C5	318	5.0×10^{-5}	231
D5	327	6.0×10^{-5}	192

Table 4.7. Kinetic data for the *Z*→*E* isomerization process at 55 ºC. [a] Optimized light-wavelength for the E→Z photoisomerization.

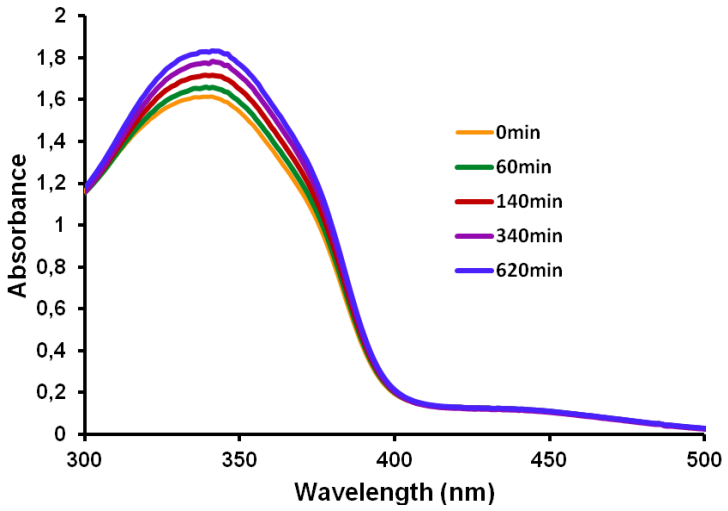

Figure 4.26. UV-Vis spectral changes during thermal *cis*-to-*trans* isomerization of complex **B3**, $2.5 \cdot 10^{-5}$ M solution in CH_3CN (55 ºC) after 30 min irradiation at 343 nm and 30 min irradiation at 354 nm.

When the extent of the photoisomerization of the corresponding Ir(III) derivatives was studied, it was clearly observed that, unfortunately, the isomerization of the azobenzene was not as efficient in the complexes as it was in the free ligands, according to the relatively small change observed in the UV-Vis absorption spectra before and after irradiation (see Figure 4.27).

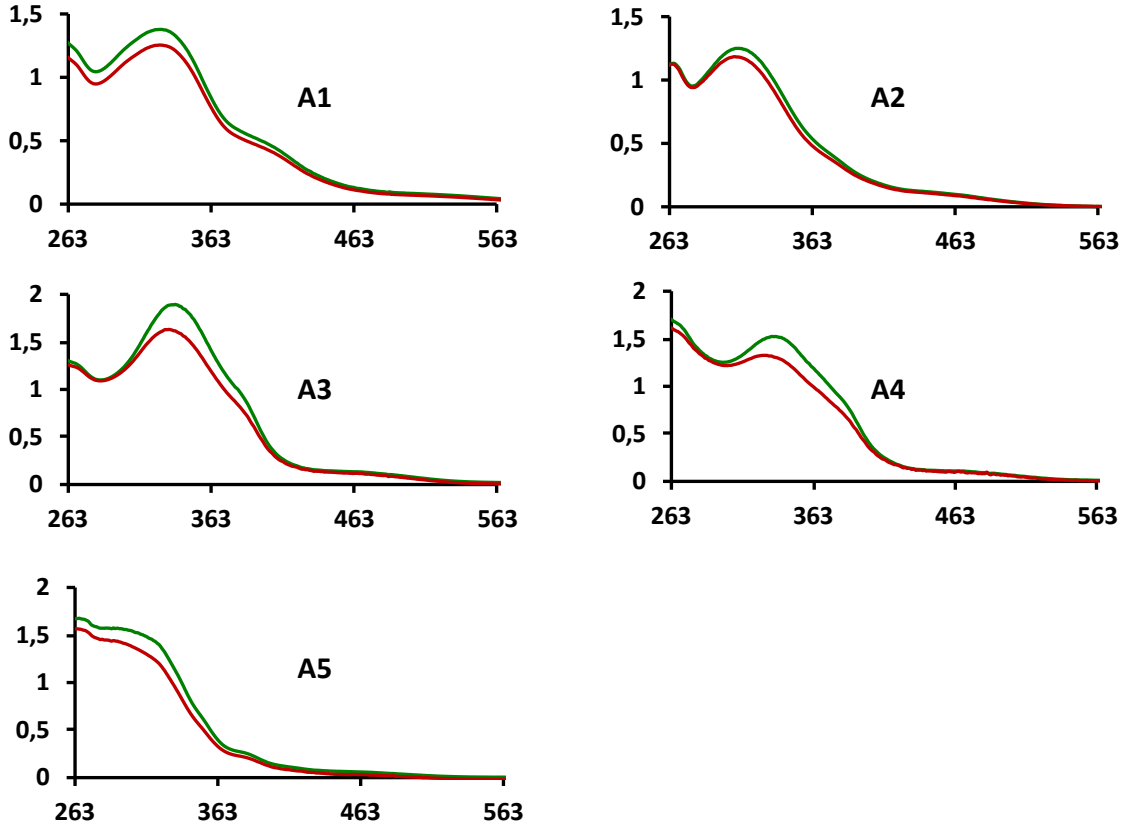

Figure 4.27. UV-Vis spectra (absorbance *vs*. wavelength (nm)) before (green line) and after (red line) irradiation of derivatives **A** after 30 min irradiation at $\lambda_{azo\ \pi\rightarrow\pi^*}$ and 30 min irradiation at $\lambda_{optimal}$. (CH_3CN).

It is well known that metal coordination can affect[33,40] or strongly inhibit[32,43] the photoisomerization of azobenzene-containing bipyridines. The reason for this inhibition in these complexes could be that after irradiation at the light-wavelength to favour the π–π* IL transition of the azobenzene, and promote one electron to the singlet excited state centered at the azobenzene, instead of isomerization to the singlet excited state of the *cis*-azobenzene, the compound relaxes through ligand-to-metal and metal-to-ligand charge transfer processes involving triplet excited states, and decaying eventually to the ground state in a non productive manner. In fact, TD-DFT calculations showed the existence of less energetic MLCT Ir(d)–π* bands. The existence of these low-energy MLCT bands could imply a fast depopulation of the π* azo orbital after irradiation, thus inhibiting the isomerization process (Figure 4.28).

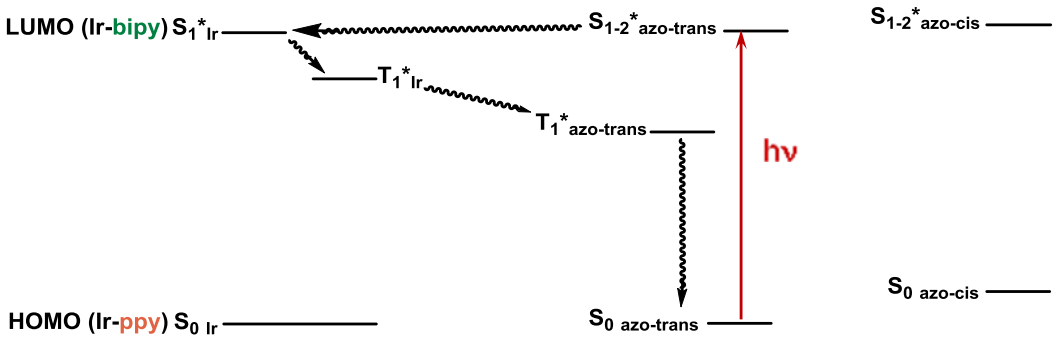

Figure 4.28. Proposal of a relaxation pathway for the isomerization of azobenzene-containing Ir(III) complexes.

In the examples studied here, although the isomerization process was significantly inhibited for all the complexes, it was more effective for derivatives of ligands **3** and **4**, which can be described as *para*-azobenzene-2,2'-bipyridines. For derivatives of ligands **1** and **2**, in which the azophenylpyridine is directly coordinated to the metal center, the change in the spectra was minimal. Surprisingly, for derivatives of **5**, in which the azobenzene is not conjugated with the bipyridine fragment (according to UV-Vis data and X-ray analysis of a related ligand), the photoisomerization was also rather small (Figure 4.27). This result is not in agreement with the observations of Nishihara for *meta*- and *para*-substituted cobalt-azobipyridine complexes.[40] In that case, as expected, light-triggered *trans*-to-*cis* isomerization was more effective when *meta*-azobipyridines were used. In that case the effect was most evident for the Co(II) derivatives than in the analogous Co(III) compounds, for which the photoisomerization was strongly inhibited. Nevertheless, in all the cases studied here the extent of the photoisomerization process was not large enough to permit a conclusive comparison. It is worth mentioning that in all cases the original spectra, assigned to the *trans* isomers, were recovered upon thermal *cis*-to-*trans* isomerization, which proofs the stability of the complexes during the irradiation. Although we tried to corroborate these results by a quantitative NMR spectroscopic analysis, it was not possible due to the overlap of signals (all aromatic).

A systematic study of the luminescent properties of these compounds, and how they change upon light irradiation (which was the original goal of this chapter) has not been performed for two reasons; on the one hand the already explained small extent of the photoisomerization on the azobenzene-appended iridium complexes, and on the other hand the very weak phosphorescence observed in qualitative experiments.

The strong phosphorescene of Ir(III) complexes without azobenzene fragment can be appreciated visually by irradiating diluted solutions with an UV-Vis lamp at 365 nm. Unfortunately, in the case of azobenzene-containing complexes this phosphorescence was strongly inhibited (Figure 4.29).

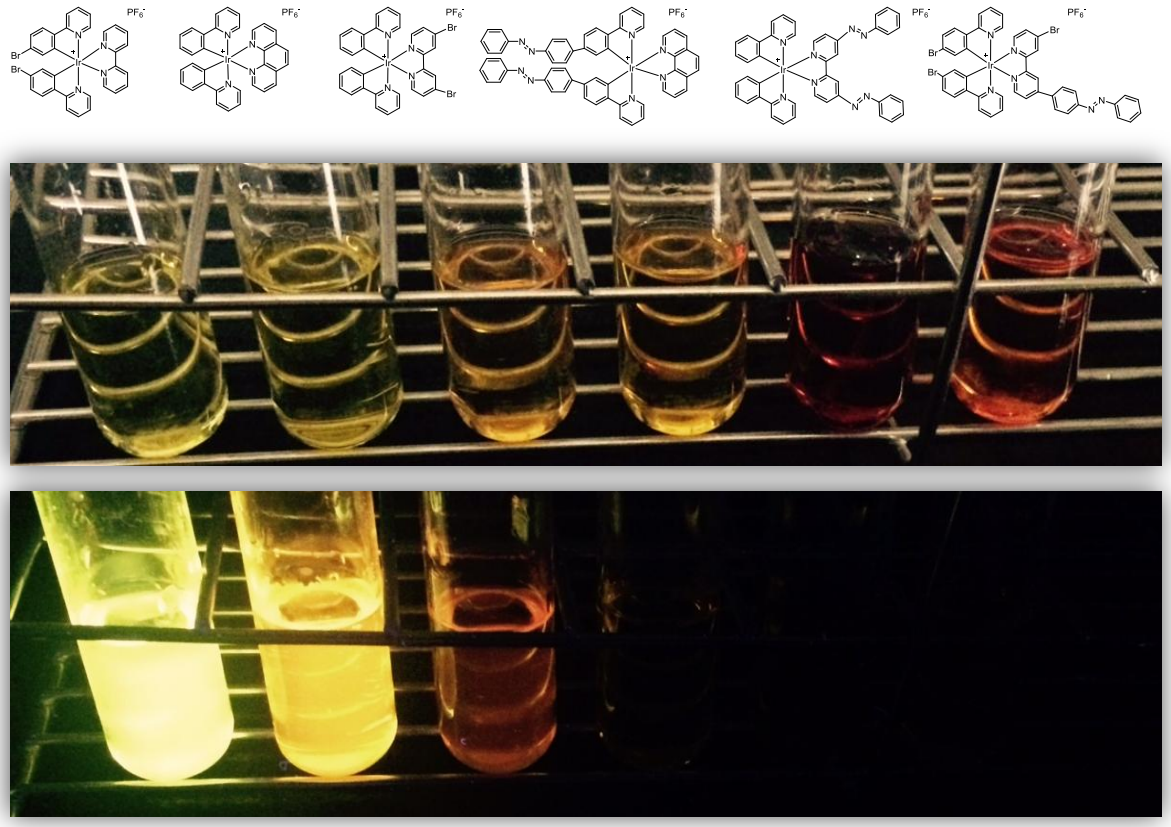

Figure 4.29. Comparison of some DMSO solutions of representative examples of complexes without and with azobenzene-apended ligands. Before irradiation (top) and upon irradiation at 365 nm (bottom).

A tentative explanation of these discouraging results have been proposed based on the same MO diagram used to explain the inhibition of the photoisomerization process. In this case, it is proposed that the phosphorescence could be inhibited because the emissive triplet excited state could be relaxed through the low-lying triplet excited state of the azobenzene (Figure 4.30).

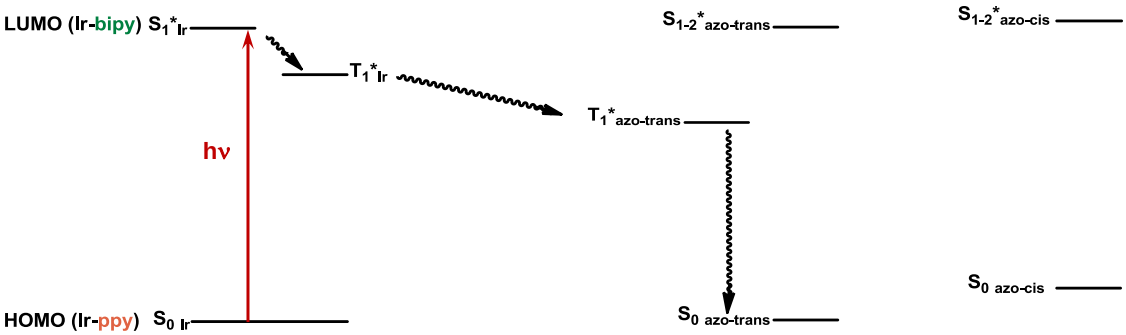

Figure 4.30. Proposal of a relaxation pathway for the emissive triplet excited state of azobenzene-containing Ir(III) complexes.

In some reports published during the elaboration of this work, closely related Ir(III) azobenzene-appended complexes were described. In those examples the emission of the complexes was also strongly inhibited due to the presence of the azobenzene unit (in agreement with our observations). But it was reestablished by *in situ* reduction of

the azo group in presence of sulphite or bisulphite. This permitted them to use these compounds as very sensitive luminescent sensors for the detection *in vivo* of these reducing agents (Figure 4.31).[32a,44]

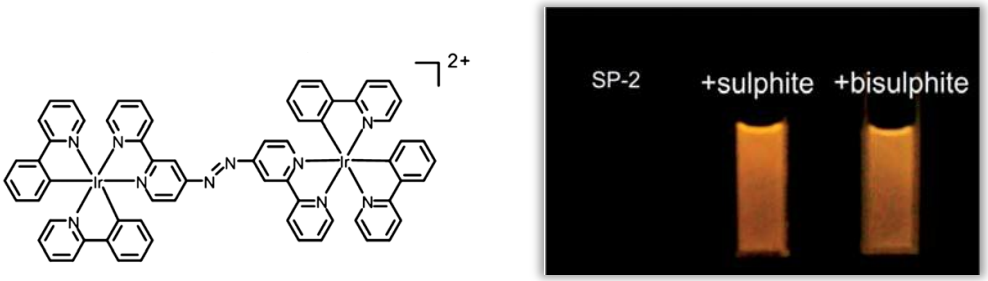

Figure 4.31. Visualisation of the phosphorescent response toward sulphite and bisulphite under 365 nm lamp. Figures extracted from literature.[32a]

A preliminary study of our complexes was carried out to see if they were experiencing the same response to reducing agents. To diluted solutions of several azobenzene-containing complexes described in this chapter, sodium sulphite or bisulphite was added. It was not perceived any qualitative change in their phosphorescence, although a more systematic and detailed study is required to confirm their behaviour.

4.3. CONCLUSIONS

Twenty-one new azobenzene-containing iridium(III) complexes have been synthesized and fully characterized. The molecular structure of four of them has been determined by X-ray diffraction. Four compounds containing up to four azobenzene fragments were obtained

Model complexes, without azobenzene moieties were synthesized for comparative purposes, five of which were not described before in literature. The molecular structure of four of them has been determined by X-ray diffraction.

Stabilization of the LUMO energy level upon coordination of the ligands to the metal was observed by comparison of their absorption spectra before and after coordination. The influence of different substituents on the phenylpyridine and bipyridine in the HOMO–LUMO energy gap was analyzed by UV-Vis and cyclic voltammetry, obtaining the highest energy gap values for fluorinated compounds. The values obtained by TD-DFT calculations showed the same tendency. It was also notable that the extended conjugation of ligands **1**–**4** was lost in the case of ligand **5**.

The photoisomerization process of the azobenzene-containing complexes has been studied by UV-Vis. The results obtained show that it was very effective for all the free ligands (Chapter 2) but rather inhibited for the complexes. For iridium derivatives of ligand **1** and **2**, in which the coordinated pyridyl unit is part of the photochromic fragment, and for derivatives of ligand **5**, where the azobenzene is appended in the

meta position, the photoisomerization is almost suppressed. For ligands **3** and **4**, where the azobenzene is appended in the *para* position in one or both pyridyl units, the isomerization is more notorious and the isomerization rates are comparable to the one observed for other azobenzene-containing complexes.[33,42,45]

It was also visually observed that azobenzene-containing complexes are not as emissive as complexes without the photochromic fragment. Nevertheless this family of compounds could encounter other applications, for instance as selective sensors for reducing agents,[32a,44] and served us to learn about future designs.

4.4. REFERENCES

[1] Y. Chi and P.-T. Chou, *Chem. Soc. Rev.*, **2010**, *39*, 638–655.

[2] S. Ladouceur and E. Zysman-Colman, *Eur. J. Inorg. Chem.*, **2013**, 2985–3007.

[3] H. Yersin and W. J. Finkenzeller, **2008**, Triplet Emitters for Organic Light-Emitting Diodes: Basic Properties, In H. Yersin (Ed), *Highly Efficient OLEDs with Phosphorescent Materials*, Wiley-VCH.

[4] F. Lafolet, S. Welter, Z. Popovic and L. De Cola, *J. Mater. Chem.*, **2005**, *15*, 2820–2828.

[5] C. Sahin, I. Oner and C. Varlikli, *RSC Adv.*, **2014**, *4*, 46831.

[6] I. González, P. Dreyse, D. Cortés-Arriagada, M. Sundararajan, C. Morgado, I. Brito, C. Roldán-Carmona, H. J. Bolink and B. Loeb, *Dalton Trans.***, 2015**, *44*, 14771–14781.

[7] E. Holder, B. M. W. Langeveld and U. S. Schubert, *Adv. Mater.*, **2005**, *17*, 1109–1121.

[8] M. Chandran, Y. Kwon and Y. Choe, *Mol. Cryst. Liq. Cryst.*, **2014**, *601*, 173–181.

[9] F. Dumur, G. Nasr, G. Wantz, C. R. Mayer, E. Dumas, A. Guerlin, F. Miomandre, G. Clavier, D. Bertin and D. Gigmes, *Organic Electronics*, **2011**, *12*, 1683–1694.

[10] Q. Pei, G. Yu, C. Zhang, Y. Yang and A. J. Heeger, *Science*, **1995**, *269*, 1086–1088.

[11] J. D. Slinker, A. A. Gorodetsky, M. S. Lowry, J. Wang, S. Parker, R. Rohl, S. Bernhard and G. G. Malliaras, *J. Am. Chem. Soc.*, **2004**, *126*, 2763–2767.

[12] R. D. Costa, E. Ortí, H. J. Bolink, F. Monti, G. Accorsi and N. Armaroli, *Angew. Chem. Int. Ed.*, **2012**, *51*, 8178–8211.

[13] Y. Kwon, Y. Choe, *J. Solution Chem.*, **2014**, *43*, 1710–1721.

[14] S. B. Meier, D. Tordera, A. Pertegás, C. Roldán-Carmona, E. Ortí and H. J. Bolink, *Materials Today*, **2014**, *17*, 217–223.

[15] M. S. Lowry and S. Bernhard, *Chem. Eur. J.*, **2006**, *12*, 7970–7977.

[16] C. Dragonetti, A. Valore, A. Colombo, S. Righetto, G. Rampinini, F. Colombo, L. Rocchigiani and A. Macchioni, *Inorg. Chim. Acta*, **2012**, *382*, 72–78.

[17] R. D. Costa, E. Ortí, H. J. Bolink, S. Graber, S. Schaffner, M. Neuburger, C. E. Housecroft and E. C. Constable, *Adv. Funct. Mater.*, **2009**, *19*, 3456–3463.

[18] J. I. Kim, I. Shin, H. Kim and J. Lee, *J. Am. Chem. Soc.*, **2005**, *127*, 1614–1615.

[19] Y. You, S. Lee, T. Kim, K. Ohkubo, W. Chae, S. Fukuzumi, G. Jhon, W. Nam, S. J. Lippard, *J. Am. Chem. Soc.*, **2011**, *133*, 18328–18342.

[20] F. A. Bovey, **1987**, The Chemical Shift, *Nuclear Magnetic Resonance Spectroscopy*, Academic Press.

[21] See for instance: a) J. F. van Baar, K. Vrieze and D. J. Stufkens, *J. Organomet. Chem.*, **1975**, *85*, 249–263. b) J. M. Hoover, J. Freudenthal, F. E. Michael and J. M.

May, *Organometallics*, **2008**, *27*, 2238–2245. c) M. I. Bruce, B. Goodall, F. G. A. Stone and B. J. Thomson, *Aust. J. Chem.*, **1974**, *27*, 2135–2138. d) M. Curic, D. Babic, A. Visnjevac and K. Molcanov, *Inorg. Chem.*, **2005**, *44*, 5975–5977. e) C. H. Zambrano, P. R. Sharp, C. L. Barnes, *Organometallics*, **1995**, *14*, 3607–3610. f) N. Deibel, M. G. Sommer, S. Hohloch, J. Schwann, D. Schweinfurth, F. Ehret and B. Sarkar, *Organometallics*, **2013**, 32, 7366–7375. g) J. L. Pratihar, P. Pattanayak, D. Patra, R. Rathore and S. Chattopadhyay, *Inorg. Chim. Acta*, **2011**, *367*, 182–186. h) L.-Y. Huang, U.-R. Aulwurm, F. W. Heinemann, F. Knoch and H. Kisch, *Chem. Eur. J.*, **1998**, *4*, 1641–1646.

[22] M. C. DeRosa, D. J. Hodgson, G. D. Enright, B. Dawson, C. E. B. Evans and R. J. Crutchley, *J. Am. Chem. Soc.*, **2004**, *126*, 7619–7626.

[23] A. Kumar, R. Pandey, R. K. Gupta, V. Mishra, S. M. Mobin and D. S. Pandey, *Dalton Trans.*, **2014**, *43*, 6365–6376.

[24] R. Sakamoto, M. Murata, S. Kume, H. Sampei, M. Sugimoto and H. Nishihara, *Chem. Commun.*, **2005**, 1215–1217.

[25] a) T. Yutaka, I. Mori, M. Kurihara, J. Mizutani, N. Tamai, T. Kawai, M. Irie and H. Nishihara, *Inorg. Chem.*, **2002**, *41*, 7143–7150. b) T. Yutaka, I. Mori, M. Kurihara, N. Tamai and H. Nishihara, *Inorg. Chem.*, **2003**, *42*, 6306–6313.

[26] Q. Zhao, C.-Y. Jiang, M. Shi, F.-Y. Li, T. Yi, Y. Cao and C.-H. Huang, *Organometallics*, **2006**, *25*, 3631–3638.

[27] J. Pommerehne, H. Vestweber, W. Guss, R. F. Mahrt, H. Bässler, M. Porsch and J. Daub, *Adv. Mater.*, **1995**, *7*, 551–554.

[28] S. Ladouceur, D. Fortin, E. Zysman-Colman, *Inorg. Chem.*, **2010**, *49*, 5625–5641.

[29] a) J. I. Goldsmith, W. R. Hudson, M. S. Lowry, T. H. Anderson and S. Bernhard, *J. Am. Chem. Soc.*, **2005**, *127*, 7502–7510. b) A. Singh, K. Teegardin, M. Kelly, K. S. Prasad, S. Krishnan and J. D. Weaver, *J. Organomet. Chem.*, **2015**, *776*, 51–59.

[30] J. Frey, B. F. E. Curchod, R. Scopelliti, I. Tavernelli, U. Rothlisberger, M. K. Nazeeruddin and E. Baranoff, *Dalton Trans.* **2014**, *43*, 5667–5679.

[31] a) R. Terki, L.-P. Simoneau and A. Rochefort, *J. Phys. Chem. A*, **2009**, *113*, 534–541. b) S. Okada, K. Okinaka, H. Iwawaki, M. Furugori, M. Hashimoto, T. Mukaide, J. Kamatani, S. Igawa, A. Tsuboyama, T. Takiguchi and K. Ueno, *Dalton Trans.*, **2005**, 1583–1590. c) M. S. Lowry, J. I. Goldsmith, J. D. Slinker, R. Rohl, R. A. Pascal, G. G. Malliaras and S. Bernhard, *Chem. Mater.*, **2005**, *17*, 5712–5719.

[32] a) G. Li, Y. Chen, J. Wang, Q. Lin, J. Zhao, L. Ji and H. Chao, *Chem. Sci.*, **2013**, *4*, 4426–4433. b) T. Yutaka, I. Mori, M. Kurihara, J. Mizutani, K. Kubo, S. Furusho, K. Matsumura, N. Tamai and H. Nishihara, *Inorg. Chem.*, **2001**, *40*, 4986–4995.

[33] J. Pérez-Miqueo, A. Telleria, M. Muñoz-Olasagasti, A. Altube, E. García-Lecina, A. de Cózar and Z. Freixa, *Dalton Trans.*, **2015**, *44*, 2075–2091.

[34] R. D. Costa, F. Monti, G. Accorsi, A. Barbieri, H. J. Bolink, E. Ortí and N. Armaroli, *Inorg. Chem.*, **2011**, *50*, 7229–7238.

[35] V. Aubert, L. Ordronneau, M. Escadeillas, J. A. G. Williams, A. Boucekkine, E. Coulaud, C. Dragonetti, S. Righetto, D. Roberto, R. Ugo, A. Valore, A. Singh, J. Zyss, I. Ledoux-Rak, H. Le Bozec and V. Guerchais, *Inorg. Chem.*, **2011**, *50*, 5027–5038.

[36] S. Ladouceur, D. Fortin and E. Zysman-Colman, *Inorg. Chem.*, **2011**, *50*, 11514–11526.

[37] P. Coppo, E. A. Plummer and L. De Cola, *Chem. Commun.*, **2004**, 1774–1775.

[38] E. Baranoff, B. F. E. Curchod, F. Montí, F. Steimer, G. Accorsi, I. Tavernelli, U. Rothlisberger, R. Scopelliti, M. Grätzel and M. K. Nazeeruddin, *Inorg. Chem.*, **2012**, 799–811.

[39] a) C. L. Forber, E. C. Kelusky, N. J. Bunce and M. C. Zerner, *J. Am. Chem. Soc.*, **1985**, *107*, 5884–5890. b) M. Dubecký, R. Derian, L. Mitas and I. Štich, *J. Chem. Phys.*, **2010**, *133*, 244301–244305.

[40] a) K. Yamaguchi, S. Kume, K. Namiki, M. Murata, N. Tamai and H. Nishihara, *Inorg. Chem.*, **2005**, *44*, 9056–9067. b) S. Kume, M. Kurihara and H. Nishihara, *J. Korean Electrochem. Soc.*, **2002**, *5*, 189–191. c) S. Kume, M. Kurihara and H. Nishihara, *Chem. Commun.*, **2001**, 1656–1657.

[41] Y. Zhao and D. G. Truhlar, *J. Chem. Phys*., **2006**, *125*, 194101–194116.

[42] M. Kaiser, S. P. Leitner, C. Hirtenlehner, M. List, A. Gerisch and U. Monkowius, *Dalton Trans.*, **2013**, *42*, 14749–14756.

[43] O. S. Wenger, L. M. Henling, M. W. Day, J. R. Winkler and H. B. Gray, *Polyhedron*, **2004**, *23*, 2955–2958.

[44] G. Li, Y. Chen, J. Wang, J. Wu, G. Gasser, L. Ji and H. Chao, *Biomaterials*, **2015**, *63*, 128–136.

[45] M. E. Moustafa, M. S. McCready and R. J. Puddephatt, *Organometallics*, **2013**, *32*, 2552–2557.

CHAPTER 5

Ru(II) BIPYRIDINE COMPLEXES FOR THE SOLVOLYTIC DEHYDROGENATION OF AMINE-BORANE ADDUCTS

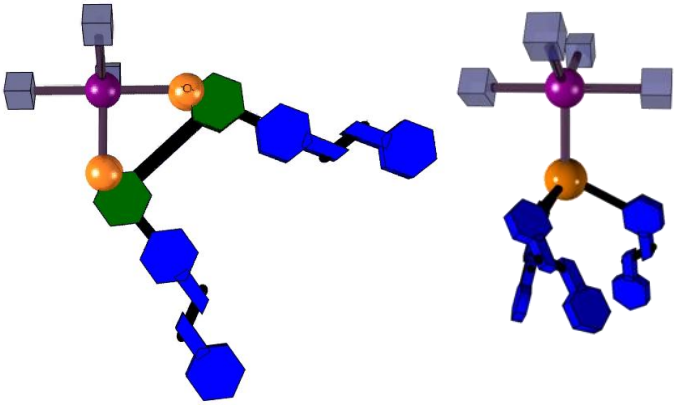

In this chapter, half-sandwich Ru(II) complexes are presented and used as precatalysts for the hydrolytic dehydrogenation of amine-borane adducts. A family of [Ru(*p*-Cym)(bipy)Cl]Cl complexes was synthesized and the efficiency of these precatalysts in the generation of hydrogen by hydrolysis of amine-borane adducts was correlated with Hammett parameters of the substituents on the bipyrdine. Complexes incorporating azobenzene-containing pyridine, bipyridine and phosphine ligands were also tested and the influence of the isomerization of the azobenzene on their catalytic activity was studied.

Part of the work described in this chapter has been published: M. Muñoz-Olasagasti, A. Telleria, J. Pérez-Miqueo, M. A. Garralda and Z. Freixa, Dalton Trans., 2014, 43, 11404–11409.

5.1. INTRODUCTION

Nowadays, carbon-based fuels supply most of the energy demand of the world. Harmful carbon particulates and sulfur and nitrogen oxides are released together with water and carbon dioxide by the combustion of these energy sources. An alternative clean energy carrier is required to avoid world's energy, climate and environmental problems. When considering these alternatives, several aspects should be taken into account, such as a clean production and/or regeneration, a high gravimetric and volumetric energy-concentration and their safe and economical storage and delivery. Hydrogen is a promising and clean energy carrier considering that only water is the byproduct of its combustion and that it can be obtained from different sources such as water, glycerol, biomass, etc. An efficient energy-source material should have high energy content in the minimum volume, to make its storage and transport economically-viable (especially for transport applications). Although hydrogen contains more energy than petroleum per mass (120 $MJ \cdot kg^{-1}$ for hydrogen and 44 $MJ \cdot kg^{-1}$ for petroleum), it contains less energy per volume (0.01 $kJ \cdot L^{-1}$ at standard conditions (gas) and 8.4 $MJ \cdot L^{-1}$ for liquid hydrogen) compared to the 32 $MJ \cdot L^{-1}$ calculated for petroleum.[1] In Table 5.1 the energy contents per mass of different fuels are shown and compared with the energy content of the hydrogen.[2]

Fuel	Energy content (MJ/kg)
Hydrogen	120
Liquefied natural gas	54.4
Propane	49.6
Aviation gasoline	46.8
Automotive gasoline	46.4
Automotive diesel	45.6
Ethanol	29.6
Methanol	19.7
Coke	27
Wood (dry)	16.2
Bagasse	9.6

Table 5.1. Energy contents of different fuels.

Safety is also a key issue, since for the storage of hydrogen as gas or liquid, high pressures and strong tanks are required (cryogenic tanks are needed in the case of liquid hydrogen in order to minimize the loss by evaporation), which constitutes a real handicap to implement it for locomotive applications. Altogether, unless new engineering solutions come to market, hydrogen cannot be stored and handled as such

(in its molecular form), because safety and/or economical issues would be compromised.

There are four methods to store hydrogen: physical means, sorbents, metal hydrides and chemical hydrides. The physical mean, the storage in the gas form, requires tanks enough to support high pressures, but light in weight to maintain the high gravimetric capacity. One option is the use of carbon-fibre reinforced composites tanks that are able to store hydrogen at high pressures, but their cylindrical shape makes them inappropriate for car designs. Whereas if it is stored as liquid hydrogen, additional components to maintain low temperatures are required and even then 1% of the hydrogen is lost per day. Different alternatives have been studied to use hydrogen as energetic vector without the need to transport or store it in its molecular form. For this purpose the so call “hydrogen-storage materials” are being considered. Nanoporous materials, such as, nanotubes, zeolites, organic polymers and metal-organic frameworks (MOFs) are capable to adsorb hydrogen in their structures. The drawback of these materials is that low temperatures are required to obtain efficient adsorptions. Metal hydrides (*i.e.* $NaAlH_4$, $LiNH_2$, $Ca(BH_4)_2$) establish stronger chemical interactions with hydrogen than sorbents, making possible to store it at higher temperatures. Another type of hydrogen storage materials are the called “chemical hydrides”. They have attracted much attention due to the higher gravimetric storage capacity achieved with lighter atoms, compared to metal hydrides. Among them B–N based compounds are the most promising ones because boron and nitrogen atoms are lightweight elements able to contain multiple hydridic (B–H) and protic (N–H) hydrogens that could be easily released.[1] Differing on the substituents on B and N, various amine-borane derivatives have been studied as potential hydrogen storage compounds (Chart 5.1).

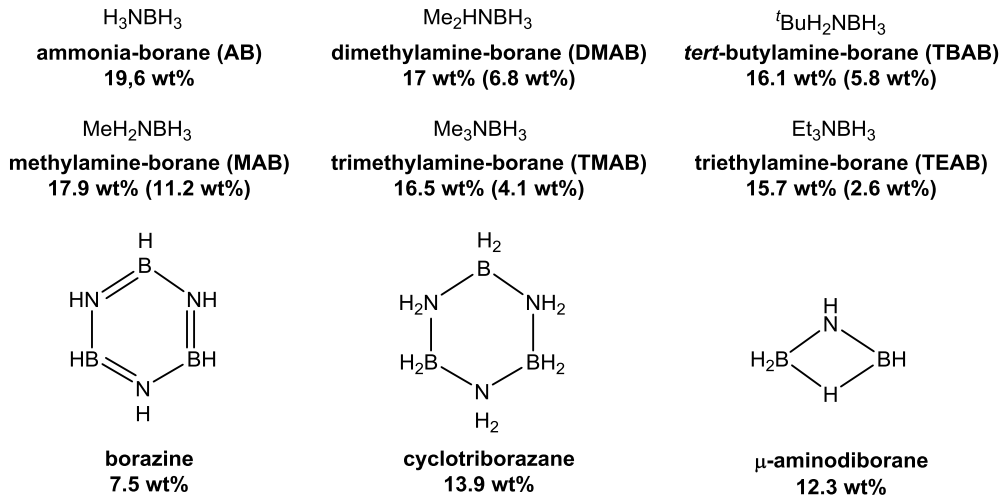

Chart 5.1. Hydrogen content of some B-N-based hydrogen storage materials. The value in brackets is the maximum “releasable” hydrogen content from the total hydrogen content.

Ammonia-borane (NH_3BH_3, AB), the most simple one from the series, presents the highest hydrogen content 19.6 wt%. AB, is a colorless solid, stable at room temperature and soluble in water and other relatively polar solvents. Its melting point is between 110–114 °C and it decomposes thermally through the three reactions shown below:[3]

$$xNH_3BH_3 \rightarrow [NH_2BH_2]_x + xH_2$$

$$[NH_2BH_2]_x \rightarrow [NHBH]_x + xH_2$$

$$[NHBH]_x \rightarrow BN + xH_2$$

The first equivalent of H_2 can be released melting AB between 107–117 °C, the second one at around 150 °C and to liberate the last equivalent temperatures above 500 °C are required.[1] Certainly, these highly energy-consuming conditions are not the most suitable for energy production. For this reason, the use of catalytic amounts of metals was considered to induce a controlled release of H_2 from AB at milder conditions.

There are two different catalytic pathways for a controlled liberation of H_2 from amine-borane adducts: dehydrogenation and hydrolysis (Scheme 5.1).

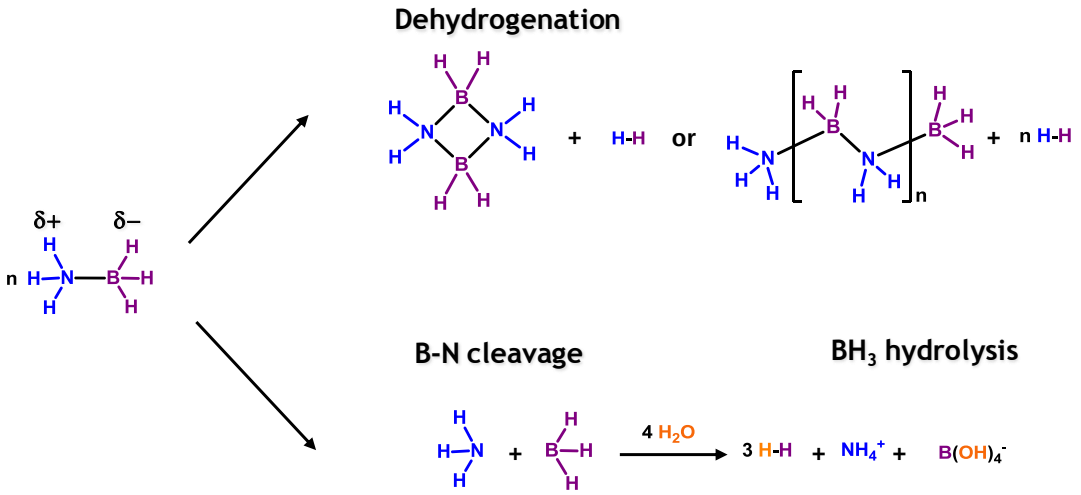

Scheme 5.1. Catalytic pathways for the liberation of H_2 from amine-borane adducts.

Some metallic nanoparticles or clusters,[4,5] and organometallic complexes (*i.e.* based on Rh,[6,7] Ru,[8,9,10] Ir,[11,12] Os,[13] Fe[14] or Pd[15]) are known catalyst for the liberation of one equivalent of H_2 per mole of substrate following a dehydrogenative mechanism. Through this process, each molecule of hydrogen originates from coupling of one protic hydrogen atom of the amine and one hydric hydrogen atom of the borane, and the amine-borane adducts end up as oligomeric or polymeric materials. For this reason, this process is also called dehydrocoupling. For instance, AB ends up in the form of $[H_2NBH_2]_n$. Only some Ru nanoclusters,[10] two homogeneous catalysts based on Ru[16,17,18,19] and one based on Ni[20] are able to further dehydrogenate the formed

polyamineboranes (in case that some N–H and B–H functionalities are still present) liberating up to 2.8 equiv. of H_2, if AB was used as substrate.

In the hydrolytic route the hydrogen is supposed to be formed by a direct hydrolysis reaction of the borane (BH_3). A metal-catalyzed adduct excision, and subsequent (and very fast) BH_3 solvolysis is presumed as reaction mechanism.[21] According to this mechanism, 3 equiv. of H_2 can be released per mole of AB, but none of it comes from the amine-part of the adduct. Instead, the released H_2 originates 50% from the solvent, and 50% from BH_3, as it is shown in the following reaction:[22]

$$NH_3BH_3 + 2H_2O \rightarrow NH_4^+ + BO_2^- + 3H_2$$

Several metal-nanoparticles showed to be efficient catalysts for the hydrolysis of AB.[23,24,25,26] To the best of our knowledge few homogeneous catalytic systems for the hydrolytic cleavage of the AB for H_2 production have been reported up to date. Garralda and coworkers published in 2010 an Ir(III) hydrido-β-diketone complex able to generate 3 equiv. of H_2 per mole of AB, using THF–H_2O mixtures, through an hydrolytic pathway (Chart 5.2 (a)).[27,28] At the same time, an *in situ* formed ruthenium catalyst also able to liberate 3 equiv. of H_2 per mole of substrate in aqueous media was published by Djukic (Chart 5.2 (b)).[29] One year later, two other efficient systems based on iridium(III) were reported: a bis-ortho-metalated Ir(III) NHC[21,30] (Chart 5.2 (c)) and an Ir(III) P-N-P pincer (Chart 5.2 (d)).[31] In 2014, Garralda and coworkers published hydridoacylphosphinorhodium(III) complexes capable of liberating 3 equiv. of H_2 in THF–H_2O mixtures (Chart 5.2 (e)).[32] Last year, Bertrand and coworkers reported copper complexes of type [(CAAC)$CuBH_4$] (CAAC = cyclic(alkyl)(amino)carbene) (Chart 5.2 (f)) claiming that it efficiently promoted the hydrolytic dehydrogenation of AB.[33] Nevertheless, the homogeneity of this system was not stated and most surprisingly they used mixtures of acetone/water (20 wt% of water) as solvent, not taking into account that AB immediately reduces aldehydes and ketones to alcohols in water.[34]

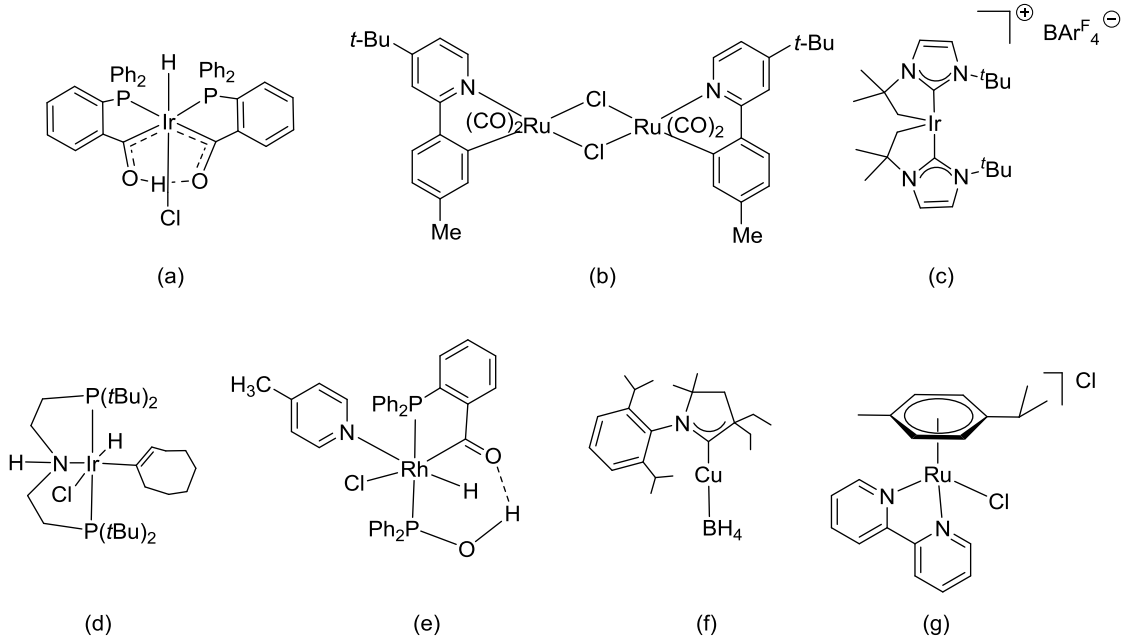

Chart 5.2. Examples of effective catalysts and precatalysts for the hydrolitic dehydrogenation of ammonia-borane.

In 2014, our group published a readily accessible [Ru(*p*-Cym)(bipy)Cl]Cl (*p*-Cym = *para*-cymene, bipy = 2,2'-bipyridine) precatalyst for the hydrolytic dehydrogenation of amine-boranes (Chart 5.2 (g)).[35] The lower price of the ruthenium compared to iridium and the simplicity of the ligands are the main characteristics that made this system appealing. This complex showed to be an efficient catalyst for the dehydrogenation of amine-borane adducts in aqueous mixtures, able to release ~2.8 equiv. of H_2 per AB within 18 minutes at room temperature.

Several aqueous solvent mixtures with different proportions of THF, iPrOH and MeOH in water were assayed, and the use of tap-water was not detrimental for the reaction outcome. The best results were obtained with mixtures THF–H_2O 1/3 and iPrOH–H_2O 1/1. When MeOH was used as the only solvent 1.4 equiv. of H_2 per AB were released and 2.9 equiv. were evolved from iPrOH solutions, but in almost four hours. When only H_2O was used as reaction solvent 2.7 equiv. of H_2 were released in less than an hour, and with pure freshly distilled THF no H_2 generation was detected. These results pointed to a hydrolytic mechanism rather than a dehydrogenation as responsible of the gas liberated. Furthermore, after evaporation of the reaction solvent ^{11}B-NMR spectra of the residues were registered in DMSO-d_6 and the NMR showed a sharp singlet at 1.54 ppm which is consistent with a tetrahedral, negatively-charged boron center, corroborating that the reaction proceeds by an hydrolytic mechanism.[21] To confirm the homogeneity of the catalytic system, at 33% conversion, excess of Hg was added. No

effect on the reaction profile was detected which confirmed the homogeneous nature of the active species.[4]

The recyclability and robustness of [Ru(*p*-Cym)(bipy)Cl]Cl were also assessed by running consecutive reactions. The results obtained showed that the catalyst remained active for at least 6 consecutive cycles, liberating 3360 equiv. of H_2 per mole of Ru. The activity of the catalyst was decreased in the course of the cycles, which was attributed to a change on the reaction medium during the addition of more substrate and solvent and the accumulation of formed salts (see Figure 5.1).

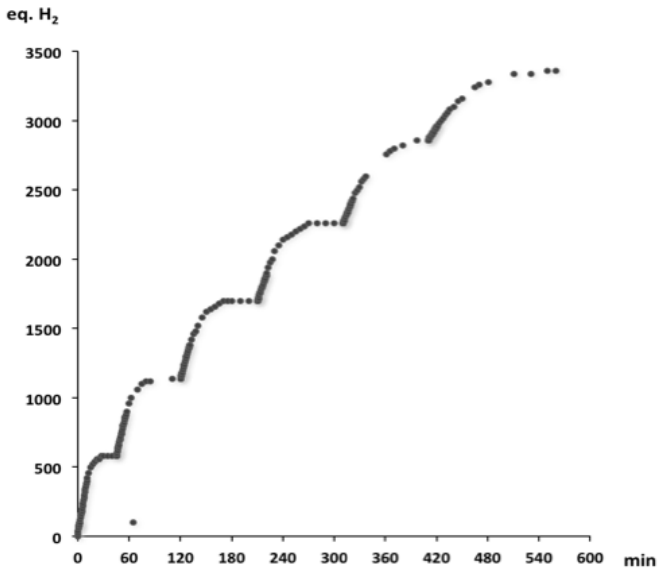

Figure 5.1. Reaction profile (equiv. of H_2 per mole of Ru evolved *vs*. time) in 6 successive cycles of hydrolytic dehydrogenation of AB. Reaction conditions (first cycle): 1.38 mmol AB, 0.5 mol% [Ru(*p*-Cym)(bipy)Cl]Cl, 3 mL THF–H_2O 1/3, rt. Successive additions of 1.38 mmol AB dissolved in 0.5 mL of THF–H_2O 1/3.

The [Ru(*p*-Cym)(bipy)Cl]Cl also showed to be an efficient catalyst for the hydrolytic dehydrogenation of TBAB and DMAB, whereas it was not able to generate H_2 from trisubstituted amine-boranes (TEAB or TMAB). The same lack of reactivity of trisubstituted amine-boranes as substrates for hydrolytic dehydrogenation was also observed by Garralda and coworkers for iridium-based catalysts.[27,28] Although it is appealing to infer from these results that at least one N–H functionality is required on the substrate for the hydrolytic dehydrogenation of AB adducts, this evidence is not enough to confirm this hypothesis. No mechanistic study for the solvolytic dehydrogenation of amine-borane adducts using homogeneous catalysis has been published yet, but presumably the activation of the substrate by the catalyst should proceed through a similar mechanism as that reported for dehydrogenative processes. For those, all the studies published claimed that the responsible for the activation and dehydrogenation of AB is the interaction of the hydric hydrogen atoms of the borane

with the metal center,[14,29,36,37,38,39,40,41,42] without the protic N–H being involved on a first stage (except for bifunctional catalysts).[43] Altogether the lack of reactivity of these substrates, and the apparent need of a protic N–H on the substrate could constitute important clues to unravel the actual reaction mechanism.†

To analyze the species involved on the hydrolytic dehydrogenation of amine-borane adducts promoted by [Ru(*p*-Cym)(bipy)Cl]Cl, ^{1}H-NMR spectra of the precatalyst [Ru(*p*-Cym)(bipy)Cl]Cl in D_2O were performed and the spectrum showed that it exists in equilibrium with the complex [Ru(*p*-Cym)(bipy)(H_2O)]$^{2+}$ in aqueous solutions, indicating that the latter could be the actual catalytic species. In fact, when pure [Ru(*p*-Cym)(bipy)(H_2O)](OTf)$_2$ was tested as precatalyst in hydrolytic dehydrogenation of AB, it showed identical activities compared to the parent chloride compound. *In situ* ^{1}H- and ^{11}B-NMR experiments (in mixtures THF-d_8/D_2O) showed that during the course of the reaction most of the ruthenium is in the form of the hydride [Ru(*p*-Cym)(bipy)H]$^+$ (considered the resting state of the catalyst), and a compound of the type [Ru(*p*-Cym)(bipy)L]$^{n+}$ was obtained after venting the reaction solutions.[35] The mentioned compound was identified as [Ru(*p*-Cym)(bipy)(NH_3)]$^{2+}$ in a subsequent publication by Freixa (Scheme 5.2).[44] Adding more substrate to this species, it was possible to reactivate the hydrolysis and regenerate the hydride. For this reason the amino species [Ru(*p*-Cym)(bipy)(NH_3)]$^{2+}$ was considered a dormant state of the catalyst, which is formed only when high conversions are achieved and the hydrogen pressure is released.

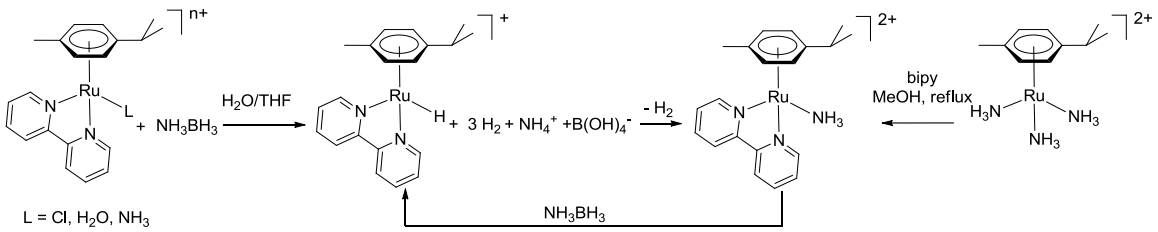

Scheme 5.2. Formation of Ru(II)-NH_3 and schematic proposal of its involvement in the catalytic process.

Initial experiments with this system showed a lack of reproducibility, which was solved by an activation process of the substrate and the precatalyst in freshly distilled THF. Following this procedure, first order plots of reaction profiles were obtained and either the chloro-, aquo- or amino-coordinated ruthenium complexes showed comparable activities, indicating that the same species is formed from any of them (NMR experiments pointed to the formation of the Ru-H complex after the activation period).

† A difference in the strength of the B–N bond in these substrates cannot be ruled out as plausible explanation for their lack of reactivity. Currently, in our group, this hypothesis is being investigated by widening the range of substrates under study, and by theoretical calculations on different mechanistic proposals.

Kinetic experiments confirmed the first order dependence of the rate law on both [Ru] and [AB].

Based on these results, this chapter covers two different objectives:

On the one hand, in view of the high efficiency of the [Ru(*p*-Cym)(bipy)Cl]Cl for the hydrolytic dehydrogenation of AB adducts, and to help unraveling the ultimate reaction mechanism, we decided to study the effect of electronic modifications on the activity of the catalytic system. For this purpose ruthenium(II) half-sandwich complexes containing 4,4'-functionalized 2,2'-bipyridine ligands will be synthesized and evaluated as precatalysts. The electronic influence of each substituent will be quantified using the corresponding Hammett parameter (σ_p^+). The appropriateness of this parameter to evaluate electronic effects in organometallic catalysis is validated by a publication of Himeda's group, where the catalytic activity of iridium catalyst for hydrogen evolution through the decomposition of formic acid was correlated with the electronic effect of the substituents of the 2,2'-bipyridine ligand in $[Ir(Cp^*)(bipy)(H_2O)]^{2+}$ catalysts (Cp* = pentamethyl cyclopentadienyl).[45]

The results obtained will be discussed in combination with theoretical (DFT) and experimental (*in situ* MS spectroscopy), and a reaction mechanism compatible with these observations will be proposed.

On the other hand, the relatively fast reaction rates obtained with the model system (even at relatively low temperatures), made us consider developing photochromic compounds analogues to the model [Ru(*p*-Cym)(bipy)Cl]Cl but containing azobenzene moieties, and analyze the influence of the isomerization of the azobenzene on the catalytic activity for the hydrolytic dehydrogenation of AB. The azobenzene moiety will be introduced either in bipyridine, pyridine or phosphine ligands and standard experiments will be compared with results obtained irradiating the catalytic systems.

5.2. RESULTS AND DISCUSSION

As mentioned before, one of the objectives of this chapter is to evaluate the importance of electronic parameters in the activity of ruthenium-catalyzed hydrolysis of AB. To make a fair comparison, a series of catalysts were only electronics change within the family needs to be used. For this purpose we designed a series of catalysts related to the model [Ru(p-Cym)(bipy)Cl]Cl in which substituents with different electronic properties were incorporated on 4,4' positions of the bipyridine. In this manner, not only the electronic effects of the substituent are maximized, but also the steric difference among the series is minimal.

The ligands used are 2,2'-bipyridines **8** and **14**–**22** described in Chapter 2.

5.2.1. SYNTHESES OF RUTHENIUM COMPLEXES WITH BIPYRIDINE LIGANDS

Complexes of the type [Ru(*p*-Cym)(bipy)Cl]Cl (bipy = 4,4'-disubstituted-2,2'-bipyridine ligand) were synthesized by reaction of two equivalents of the corresponding 4,4'-disubstituted-2,2'-bipyridine with $[Ru(p\text{-Cym})Cl_2]_2$, following the standard methodology (Scheme 5.3).[46] In general, acetone was used as solvent, although for some complexes, CH_2Cl_2 or EtOH were used, as better yields were obtained.

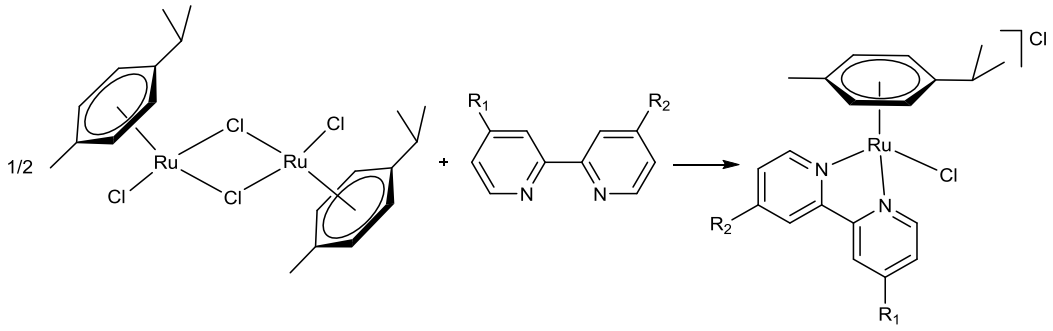

[Ru(*p*-Cym)(14)Cl]Cl, $R_1 = R_2 = NO_2$
[Ru(*p*-Cym)(15)Cl]Cl, $R_1 = R_2 = PO(OEt)_2$
[Ru(*p*-Cym)(16)Cl]Cl, $R_1 = R_2 = COOH$
[Ru(*p*-Cym)(17)Cl]Cl, $R_1 = R_2 = C{\equiv}CH$
[Ru(*p*-Cym)(18)Cl]Cl, $R_1 = R_2 = Br$
[Ru(*p*-Cym)(19)Cl]Cl, $R_1 = R_2 = H$
[Ru(*p*-Cym)(20)Cl]Cl, $R_1 = R_2 = CH_3$
[Ru(*p*-Cym)(21)Cl]Cl, $R_1 = R_2 = N_3$
[Ru(*p*-Cym)(8)Cl]Cl, $R_1 = R_2 = NH_2$
[Ru(*p*-Cym)(22)Cl]Cl, $R_1 = Br$, $R_2 = N_3$

Scheme 5.3. Synthetic route toward [Ru(*p*-Cym)(bipy)Cl]Cl complexes. Yields: [Ru(*p*-Cym)(**14**)Cl]Cl (63%), [Ru(*p*-Cym)(**15**)Cl]Cl (92%), [Ru(*p*-Cym)(**16**)Cl]Cl (71%), [Ru(*p*-Cym)(**17**)Cl]Cl (77%), [Ru(*p*-Cym)(**18**)Cl]Cl (85%), [Ru(*p*-Cym)(**19**)Cl]Cl (93%), [Ru(*p*-Cym)(**20**)Cl]Cl (78%), [Ru(*p*-Cym)(**21**)Cl]Cl (53%), [Ru(*p*-Cym)(**8**)Cl]Cl (60%), [Ru(*p*-Cym)(**22**)Cl]Cl (49%).

Following this methodology all complexes were obtained with acceptable yields (49–93%). The identity and purity of the already published complexes [Ru(*p*-Cym)(**16**)Cl]Cl,[47] [Ru(*p*-Cym)(**19**)Cl]Cl[46] and [Ru(*p*-Cym)(**20**)Cl]Cl[48] was confirmed by comparison of their spectroscopic data with the reported data. All the new complexes were fully characterized by EA, NMR and HR-ESI-MS (full spectra and detailed synthetic procedures are compiled in the Supporting Information). In the case of [Ru(*p*-Cym)(**17**)Cl]Cl, [Ru(*p*-Cym)(**21**)Cl]Cl and [Ru(*p*-Cym)(**22**)Cl]Cl, crystals suitable for X-ray diffraction were obtained by slow diffusion of Et_2O on MeOH ([Ru(*p*-Cym)(**17**)Cl]Cl) or $CDCl_3$ ([Ru(*p*-Cym)(**21**)Cl]Cl and [Ru(*p*-Cym)(**22**)Cl]Cl) solutions (Figures 5.2, 5.3 and 5.4).

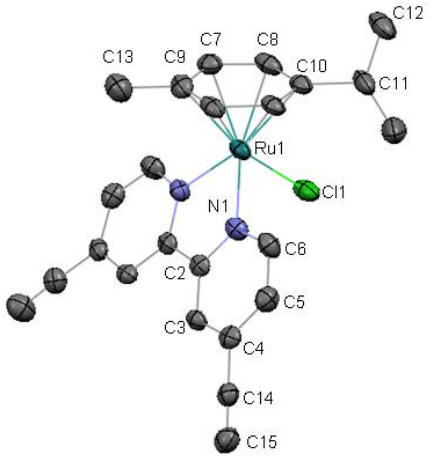

Figure 5.2. ORTEP representation of the molecular structure of [Ru(*p*-Cym)(**17**)Cl]Cl according to X-ray diffraction. Hydrogens have been omitted for clarity. Ellipsoids at 50% probability.

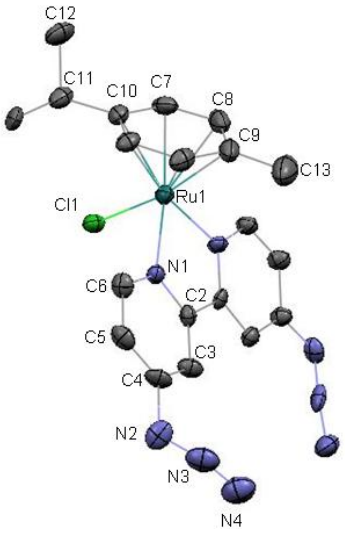

Figure 5.3. ORTEP representation of the molecular structure of [Ru(*p*-Cym)(**21**)Cl]Cl according to X-ray diffraction. Hydrogens have been omitted for clarity. Ellipsoids at 50% probability.

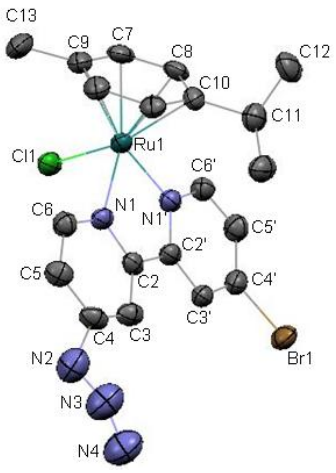

Figure 5.4. ORTEP representation of the molecular structure of [Ru(*p*-Cym)(**22**)Cl]Cl according to X-ray diffraction. Hydrogens have been omitted for clarity. Ellipsoids at 50% probability.

^{1}H-NMR spectra of all the complexes showed the three expected aromatic signals for the 4,4'-disubstituted bipyridine ligands between 6.5 and 10 ppm (except in the case of the unsubstituted model compound [Ru(*p*-Cym)(**19**)Cl]Cl which presents four signals and the asymmetrically substituted [Ru(*p*-Cym)(**22**)Cl]Cl that presents six). In Figure 5.5 is presented a stack-plot of all the ^{1}H-NMR spectra of complexes containing symmetric bipyridine ligands (except the one of [Ru(*p*-Cym)(**14**)Cl]Cl due to its low solubility in MeOD-d_4). Between 5.5 ppm and 6.5 ppm the two doublets corresponding to the aromatic protons of the coordinated *p*-Cymene are observed. Finally, in the high-field area of the spectra appear the three characteristic aliphatic signals of the *p*-Cymene, with multiplicities of septuplet (C*H*$(CH_3)_2$), singlet (CH_3) and doublet (CH(CH_3)$_2$).

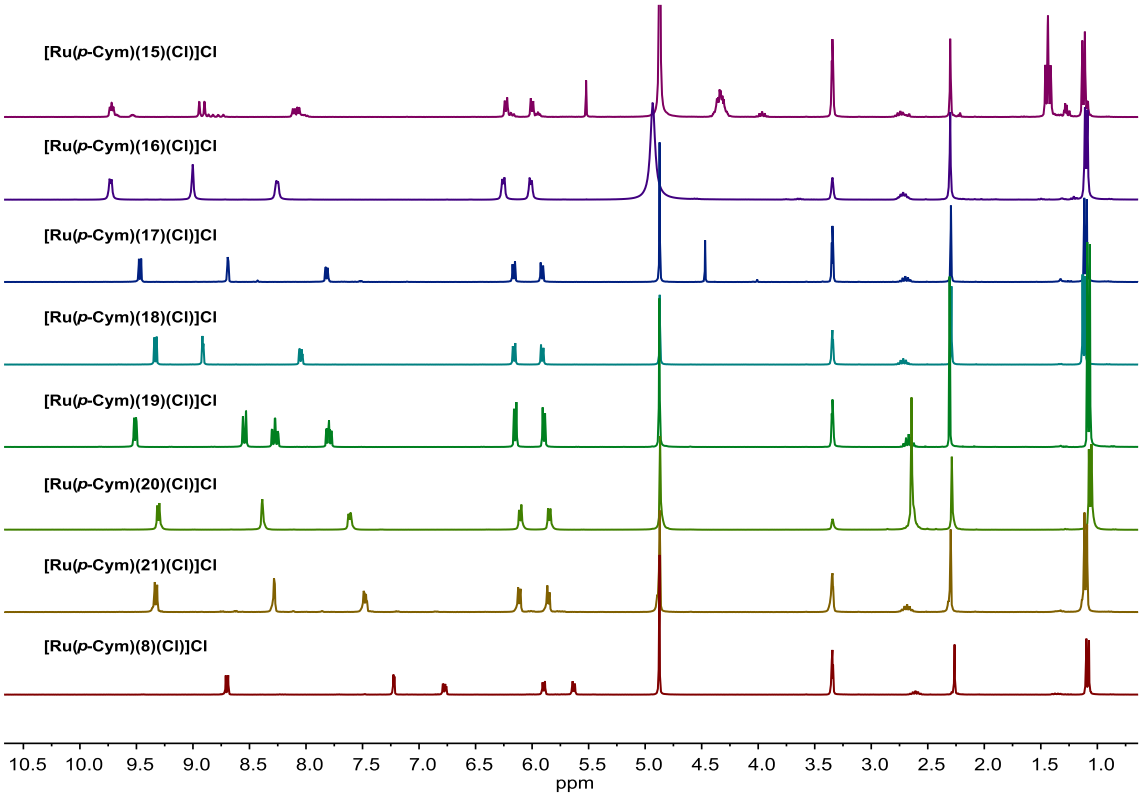

Figure 5.5. ^{1}H-NMR spectra of complexes [Ru(*p*-Cym)(**L**)Cl]Cl (**L** = **15**–**21** and **8**) in MeOD-d_4.

The ^{1}H-NMR spectra of [Ru(*p*-Cym)(**15**)Cl]Cl showed two additional aliphatic signals assigned to the CH_2 and CH_3 of the ethyl groups of diethylphosphonate substituents, and [Ru(*p*-Cym)(**17**)Cl]Cl presents an additional proton of the alkyne group as a singlet at 4.47 ppm. Finally, also the ^{1}H-NMR spectra of [Ru(*p*-Cym)(**20**)Cl]Cl presents one more aliphatic signal that corresponds to the methyl substituent of the bipyridine ligand, which appears overlapped to the signal of the isopropylic CH of the *p*-Cymene.

As expected, the chemical shifts of the ^{1}H-NMR signals were influenced by the electronic properties of the substituents on 4,4' positions of the bipyridine ligand. In Chapter 2 the same effect was already observed in ^{1}H-NMR spectra of the free ligands.

Also when coordinated to the metal center, the signals of the bipyridine ligand are low-field shifted when electron-withdrawing groups were appended on the 4,4'-positions. This linear correlation existing between the chemical shift of the signals and the electronic properties of the substituents was used to calculate the Hammett parameters (σ_p^+) for the azide and diethylphosphonate substituents (not published in the literature). To facilitate the analysis of the results, the most representative chemical shifts of the ^{1}H-NMR spectra of the complexes were plotted against the corresponding Hammett values (σ_p^+) of the substituents on 4-4' positions of the bipyridine ligand (see data in Table 5.2 and plot in Figure 5.6).[49]

Compound	σ_p^+	H_6	H_3	H_5	H_8	H_7	H_{11}	H_{13}	H_{12}
[Ru(*p*-Cym)(**15**)Cl]Cl	Unknown	9.72	8.92	8.09	6.23	6.00	2.74	2.30	1.12
[Ru(*p*-Cym)(**16**)Cl]Cl	0.42	9.73	9.00	8.25	6.25	6.01	2.72	2.30	1.10
[Ru(*p*-Cym)(**17**)Cl]Cl	0.18	9.47	8.69	7.82	616	5.91	2.70	2.29	1.10
[Ru(*p*-Cym)(**18**)Cl]Cl	0.15	9.33	8.91	8.05	6.16	5.91	2.72	2.29	1.12
[Ru(*p*-Cym)(**19**)Cl]Cl	0	9.51	8.54	7.80	6.15	5.90	2.67	2.31	1.07
[Ru(*p*-Cym)(**20**)Cl]Cl	-0.31	9.31	8.39	7.71	6.10	5.85	2.64	2.29	1.06
[Ru(*p*-Cym)(**21**)Cl]Cl	Unknown	9.33	8.28	7.48	6.11	5.85	2.68	2.30	1.10
[Ru(*p*-Cym)(**8**)Cl]Cl	-1.3	8.70	7.22	6.77	5.90	5.63	2.61	2.26	1.08

Table 5.2. σ_p^+ values of the substituents in positions 4,4' of the bipyridine ligand and most representative ^{1}H-NMR chemical shifts of complexes [Ru(*p*-Cym)(**L**)Cl]Cl (**L** = **15**–**21** and **8**) in MeOD-d_4.

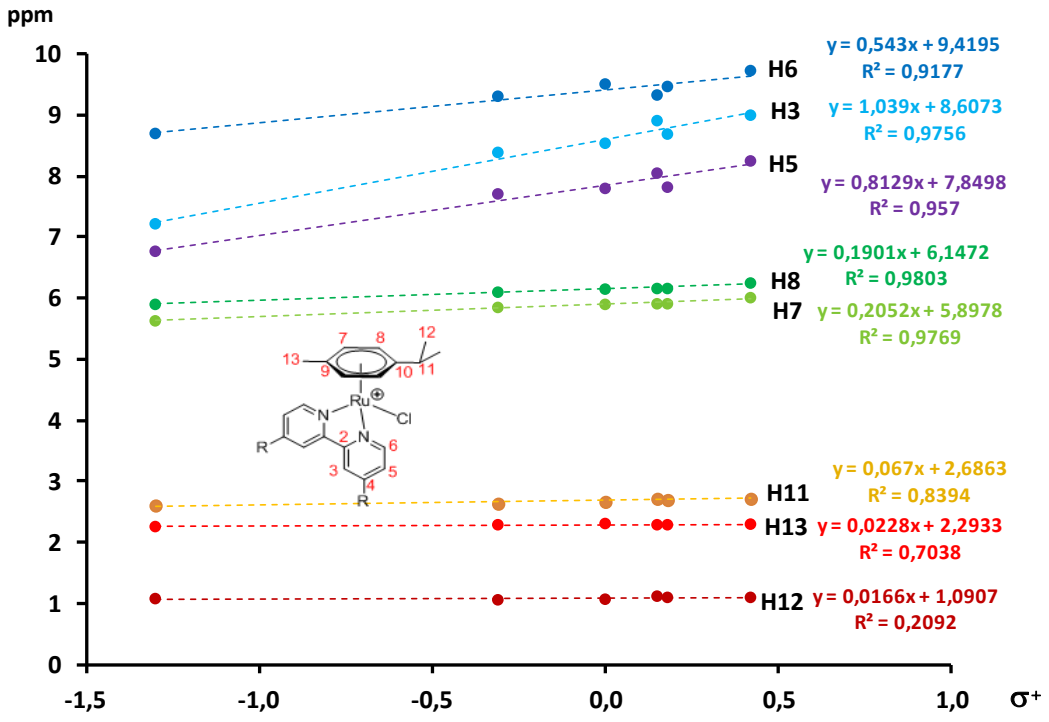

Figure 5.6. Most representative ^{1}H-NMR chemical shifts of complexes [Ru(*p*-Cym)(**L**)Cl]Cl (**L** = **15**–**21** and **8**) in MeOD-d_4 *versus* σ_p^+ values of the corresponding substituents in positions 4,4' of the bipyridine ligand. Equations for the corresponding linear fits are also presented.

Looking at the results, the best correlation between the chemical shift and the Hammet parameter was obtained for the signal assigned to proton H3 (of the bipyridine) and H7 and H8 (assigned to the aromatic atoms of the p-Cymene). Since the variation of the peaks of H7 and H8 within the range was too small to be used for an accurate interpolation, the equation obtained from the plot of H3 was used to calculate the unknown σ_p^+ values. From these data, values of 0,30 and -0,31 were obtained for diethylphosphonate and azido substituents, respectively.

5.2.2. SYNTHESES OF AZOBENZENE-CONTAINING RUTHENIUM COMPLEXES

The second objective of this chapter was the study of photochromic organometallic compounds as potential light-tunable catalysts. For this purpose azobenzene-appended Ru(II) complexes containing ligands **1**–**5**, **12** and **13** (described in Chapter 2) were synthesized to study the influence of the irradiation in their catalytic activity for the hydrolysis of AB.

Complexes of type [Ru(*p*-Cym)(**L**)Cl]Cl where L is an azobenzene-appended bipyridine ligand (**1**, **3**–**5**) were synthesized following the same methodology previously described for complexes of type [Ru(*p*-Cym)(bipy)Cl]Cl.[46] Two equivalents of the corresponding azobenzene-containing bipyridine and [Ru(*p*-Cym)$(Cl)_2]_2$ were refluxed in acetone to obtain the Ru(II) complexes shown in Chart 5.3.

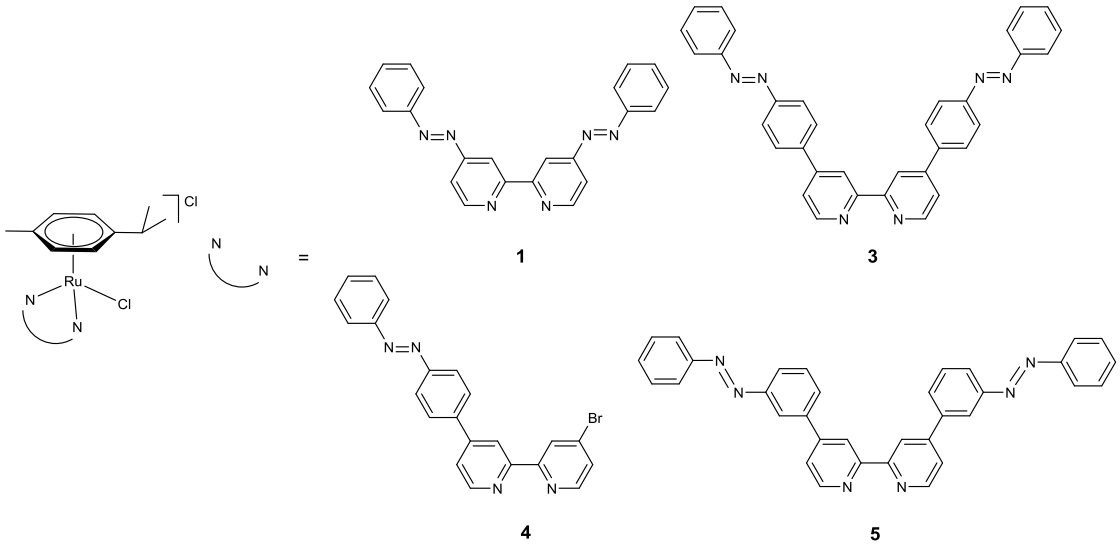

Chart 5.3. Synthesized azobenzene-appended complexes. Yields: [Ru(*p*-Cym)(**1**)Cl]Cl (73%), [Ru(*p*-Cym)(**3**)Cl]Cl (70%), [Ru(*p*-Cym)(**4**)Cl]Cl (65%), [Ru(*p*-Cym)(**5**)Cl]Cl (54%).

All complexes were obtained with quite high yields (54–73%) and were fully characterized by EA, NMR and HR-ESI-MS (full spectra and detailed synthetic procedures are compiled in the Supporting Information).

With ligand **2** (already described in the literature), complexes of type [Ru(*p*-Cym)(**L**)Cl_2] containing one 4-phenylazopyridine and [Ru(*p*-Cym)(**L**)$_2$Cl]PF_6 containing two 4-phenylazopyridines were synthesized (Scheme 5.4). The latter was used to study the chelate effect (by comparison with complex [Ru(*p*-Cym)(**1**)Cl]Cl).

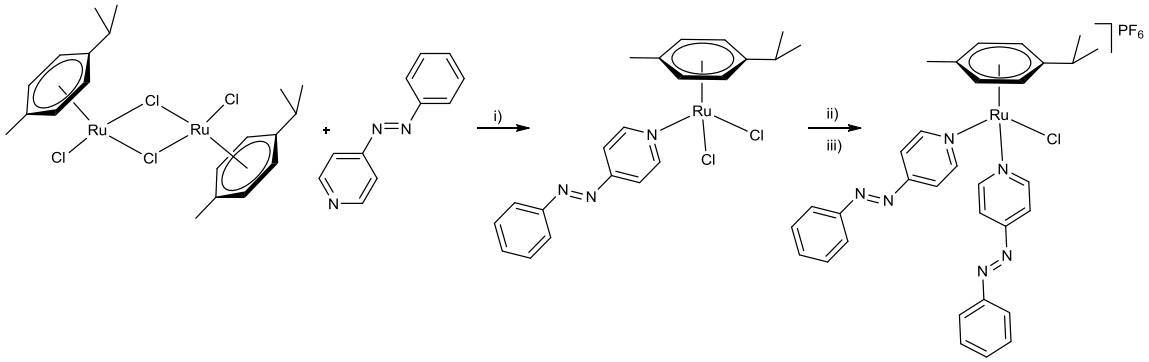

Scheme 5.4. Synthetic route toward complexes [Ru(*p*-Cym)(**2**)Cl_2] (yield: 71%) and [Ru(*p*-Cym)(**2**)$_2$Cl]PF_6 (yield: 55%). i) Acetone, reflux, 15 h. ii) $AgPF_6$ (1 equiv.), acetone/methanol 1/1, 1 h. iii) 4-phenylazopyridine (1 equiv.), 15 h.

The synthetic route followed to obtain the complex containing one 4-phenylazopyridine was the general methodology used to synthesize [Ru(*p*-Cym)(bipy)Cl]Cl complexes.[46] To introduce the second 4-phenylazopyridine, the use of a silver salt as halide abstractor was required (as described in the literature for related ruthenium compounds containing two pyridine ligands).[50]

For comparative purposes, analogous complexes containing one or two pyridine ligands (Chart 5.4) were synthesized, based on the same synthetic procedures.[46,50] As it happened for complexes containing ligand **2**, much higher yield was obtained for the former (89%) than for the latter (45%).

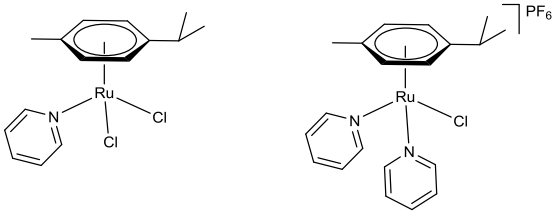

Chart 5.4. Ru(II) complexes containing one and two pyridines.

The neutral complex [Ru(*p*-Cym)(pyridine)Cl_2] was characterized by ^{1}H-NMR and the obtained spectra was coincident with the one described in the literature.[51] The other three new compounds were fully characterized by EA, NMR and ESI-MS (full spectra and detailed synthetic procedures are compiled in the Supporting Information). In the case of the compound containing two coordinated ligands **2**, [Ru(*p*-Cym)(**2**)$_2$Cl]PF_6, a crystalline sample suitable for X-ray diffraction was obtained (Figure 5.7).

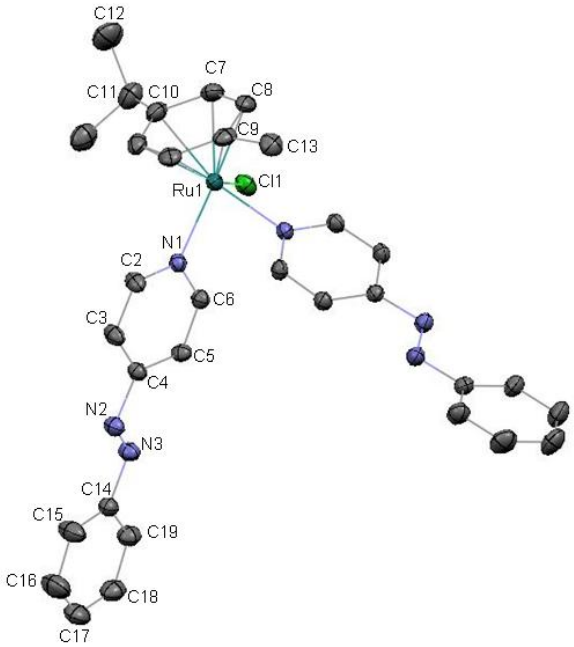

Figure 5.7. ORTEP representation of the molecular structure of [Ru(*p*-Cym)(**2**)$_2$Cl]PF$_6$ according to X-ray diffraction. Hydrogens have been omitted for clarity. Ellipsoids at 20% probability.

Tris(*m*-phenylazobenzene)phosphine (**12**) and tris(*p*-phenylazobenzene)-phosphine (**13**) described in Chapter 2, were also used as ligands to obtain azobenzene-containing complexes of type [Ru(*p*-Cym)(**L**)Cl$_2$] (Chart 5.5). The same synthetic methodology used before for complexes of type [Ru(*p*-Cym)(bipy)Cl]Cl was followed to synthesize phosphine-containing Ru(II) complexes, but in this case hexane was used as solvent, according to the procedure described in the literature for the model complex [Ru(*p*-Cym)(PPh$_3$)Cl$_2$].[52] This known complex was also synthesized for comparative purposes.

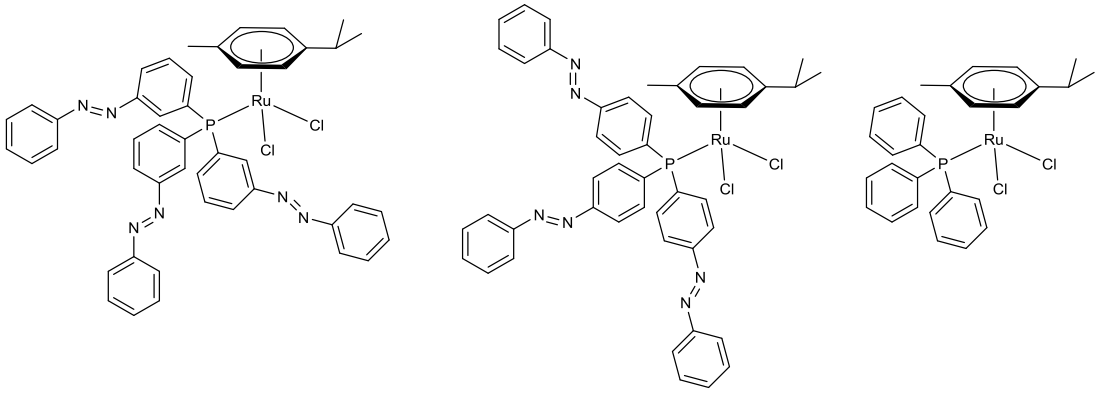

Chart 5.5. Ru(II) complexes containing phosphine ligands.

The complex containing PPh$_3$ was characterized by ^{1}H- and ^{31}P-NMR and the obtained spectra were coincident with the ones described in the literature. Complexes containing ligands **12** and **13** were fully characterized by EA, NMR and HR-ESI-MS (full spectra

and detailed synthetic procedures are compiled in the Supporting Information). The coordination of ligands **12** and **13** to the metal center was reflected in the ^{31}P-NMR spectra obtained. In Figure 5.8, ^{31}P-NMR spectra of ligand **12** (top) and complex [Ru(*p*-Cym)(**12**)Cl_2] (bottom) are shown, as an example.

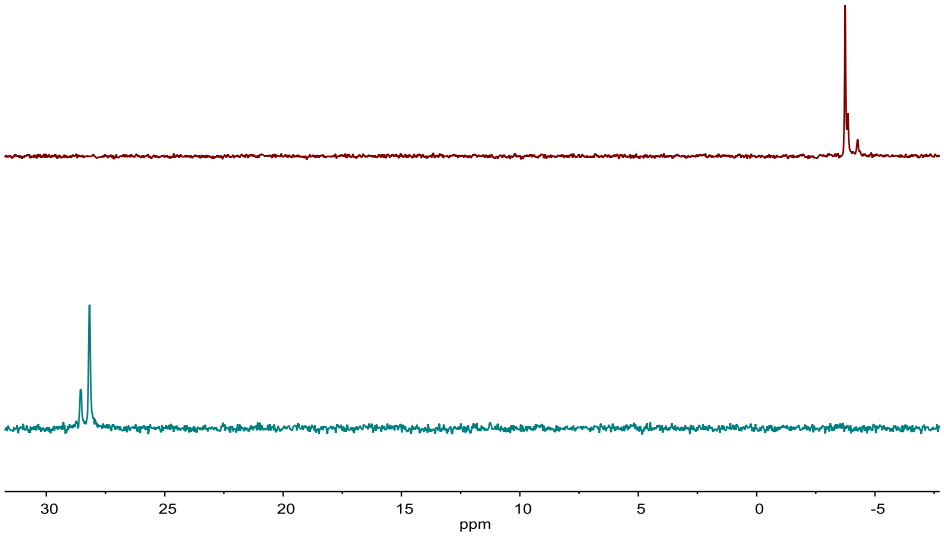

Figure 5.8. ^{31}P-NMR spectra of ligand **12** (top) and complex [Ru(*p*-Cym)(**12**)Cl_2] (bottom) in $CDCl_3$ (202.5 MHz).

A significant change of the chemical shift upon coordination to the Ru(II) was observed by ^{31}P-NMR. As expected, the signal of the phosphorus atom is low-field shifted upon coordination to the metal center. In addition, the spectra of the free ligand showed an intense peak at –3.7 ppm and two small peaks in close proximity, indicating that more than one specie is present (as explained in Chapter 2). The intense peak was assigned to the complex containing all the azobenzene fragments on *trans* conformation (*EEE*), being the thermodynamically most stable isomer. The small peaks were assigned to the other three possible isomers, *ZZZ*, *EZZ* and *EEZ*. These possible isomers could also be present in the complex [Ru(*p*-Cym)(**12**)Cl_2], although only one little peak was observed in this case.

As expected, the same effect upon metal coordination was also observed in the ^{31}P-NMR spectra of ligand **13** and the ruthenium complex [Ru(*p*-Cym)(**13**)Cl_2], exhibiting the latter the signal of the coordinated phosphorus atom at around 26 ppm (Figure 5.9).

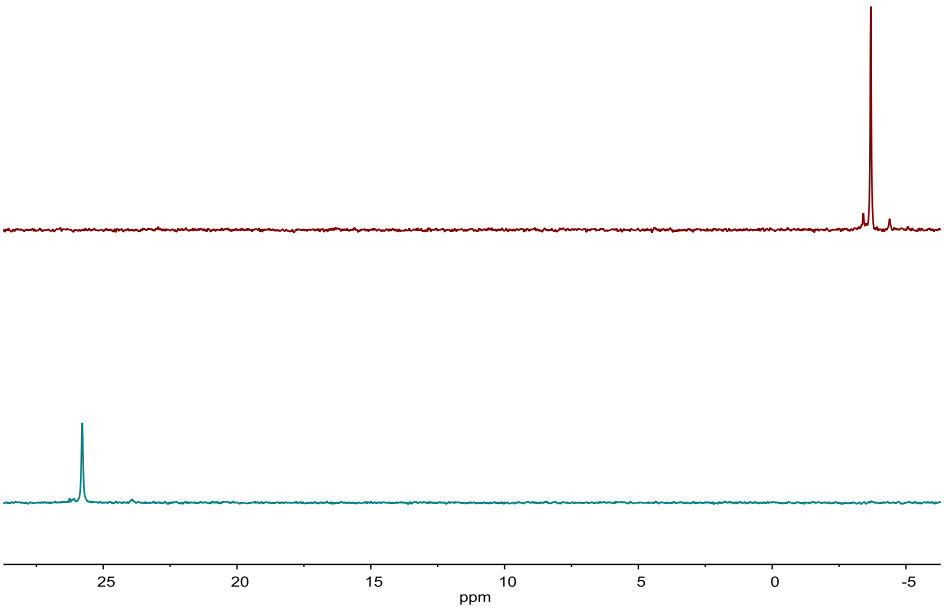

Figure 5.9. ^{31}P-NMR spectra of ligand **13** (top) and complex [Ru(*p*-Cym)(**13**)Cl_2] (bottom) in $CDCl_3$ (202.5 MHz).

In comparison with derivatives of ligand **12**, ligand **13** and its complex [Ru(*p*-Cym)(**13**)Cl_2] present only minor peaks in addition to the most intense one. For this reason it was deduced that in both cases the products are composed essentially by the *EEE* isomer.

5.2.3. PHOTOISOMERIZATION STUDIES

The light-induced isomerization process of complexes containing azobenzene fragments was studied by UV-Vis absorption spectroscopy. Following the same methodology described in previous chapters, diluted CH_3CN solutions of the complexes were irradiated for 30 min at the wavelength attributed to the π→π* transition of the azobenzene (Table 5.3). Then, the solutions were irradiated for additional 30 min at the optimal wavelength individually calculated for each compound, following the Monkowius' procedure (described in detail in Chapter 2).[53] The spectra of all the complexes studied before and after irradiation are shown in Figure 5.10. Once the PSS was reached, the back *Z*→*E* isomerization was monitored by UV-Vis absorption spectroscopy registering spectra at regular time-intervals until the original spectrum was recovered (this process was run in the dark at 65 ºC). The value of absorbance at $\lambda_{\pi\rightarrow\pi^*}$ was used to follow this process. As explained in Chapter 2, the analysis of these spectra permitted us to calculate the first order rate constants (k) and half-life times ($\tau_{1/2}$) for this process. The results obtained are presented in Table 5.3 (all absorbance *versus* time and first order plots obtained are compiled in the Supporting Information).

Compound	$\lambda_{azo\ \pi\rightarrow\pi^*}$ [nm]	$\lambda_{optimal}$[a] [nm]	k [s^{-1}]	$\tau_{1/2}$ [min]
[Ru(*p*-Cym)(**1**)Cl]Cl	332	316	–	–
[Ru(*p*-Cym)(**2**)Cl_2]	312	311	5.0×10^{-5}	231
[Ru(*p*-Cym)(**2**)$_2$Cl]PF_6	320	347	5.0×10^{-5}	231
[Ru(*p*-Cym)(**3**)Cl]Cl	341	350	2.0×10^{-4}	58
[Ru(*p*-Cym)(**4**)Cl]Cl	338	344	3.0×10^{-4}	38
[Ru(*p*-Cym)(**5**)Cl]Cl	309	322	7.0×10^{-5}	165
[Ru(*p*-Cym)(**12**)Cl_2]	321	324	8.0×10^{-5}	144
[Ru(*p*-Cym)(**13**)Cl_2]	328	334	1.0×10^{-4}	115

Table 5.3. Kinetic data for the *Z*→*E* isomerization process at 65 ºC. [a] Optimized light-wavelength for the *E*→*Z* photoisomerization.

Although all the ligands experienced a large extent of *trans*-to-*cis* photoisomerization (according to the difference in their UV-Vis spectra), they showed a different behaviour when coordinated to ruthenium(II). Irradiation of [Ru(*p*-Cym)(**1**)Cl]Cl and [Ru(*p*-Cym)(**2**)Cl_2] produces a minimal change in their UV-Vis spectra (Figure 5.10). Therefore an inhibition of the isomerization upon coordination should be inferred. It is worth mentioning that precisely these two ligands showed, before metal coordination, the shortest half-life times of the *cis* form (less stable *Z* isomers) (see Chapter 2), which combined with the fact that in these ligands the azo presents the strongest electronic communication to the metal center (occupying directly a *para* position of the coordinated pyridine) could be responsible of the lack of photoisomerization. In the rest of the cases a clear effect of the irradiation is reflected in their UV-Vis spectra, which is remarkable, taking into account that in most of the examples of the literature, coordination of an azobenzene-appended ligand to a transition metal center quenches this process (this is more evident when conjugation exists between the donor atom and the azobenzene).[54,55,56] Comparing the series, it can be observed that the *cis*-to-*trans* isomerization rate of the complex containing ligand **3** showed similar values than the one with ligand **4**, although the former that contains two azobenzenes was slightly slower. The first order plot obtained in both cases confirmed that both azobezene units behave as independent chromophores (the isomerization of the first one did not influence the isomerization of the second).

The difference between complexes [Ru(*p*-Cym)(**3**)Cl]Cl and [Ru(*p*-Cym)(**5**)Cl]Cl is only the coordination point of the azobenzene to the bipyridine ligand. The latter, containing two azobenzene fragments on *meta* positions, showed one order magnitude slower *Z*→*E* isomerization compared to the former, in which the azobenzene fragments are in *para* positions respect to the anchoring carbon, indicating that *Z*→*E* isomerization is slower (*cis* form more stable, and with longer half-life times) when the azobenzene is in *meta* position, as already observed for Ir(III) complexes in Chapter 4.

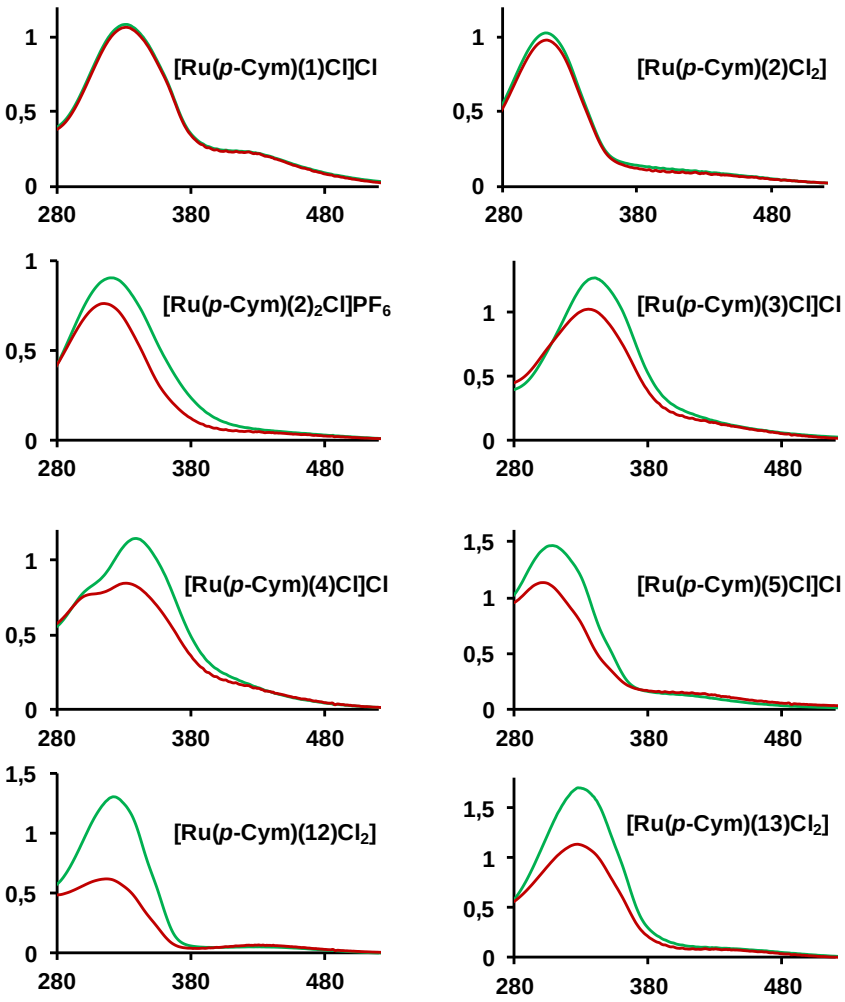

Figure 5.10. UV-Vis spectra (absorbance *vs*. wavelength (nm)) before (green line) and after (red line) irradiation of azobenzene-containing Ru(II) complexes after 30 min irradiation at $\lambda_{azo\ \pi\rightarrow\pi^*}$ and 30 min irradiation at $\lambda_{optimal}$. (CH_3CN).

The most remarkable behaviour was the one observed for phosphine containing complexes [Ru(*p*-Cym)(**12**)Cl_2] and [Ru(*p*-Cym)(**13**)Cl_2], which exhibited a larger degree of photoisomerization compared to pyridine and bipyridine derivatives (according to the difference in their UV-spectra before and after irradiation) and very similar k values for the reverse process to the ones obtained for free ligands **12** and **13**, (identical in the case of the latter!). The complex that contains three azo groups in *meta* positions, showed a slower *Z*→*E* isomerization process than the analogous with three azo groups in *para* positions. Also in these case, linear plots of the reverse process suggest that the three azobenzene fragments behave as independent chromophores.

5.2.4. CATALYTIC EXPERIMENTS

All the complexes already described were synthesized to use as precatalysts for the hydrolytic dehydrogenation of AB. The electronic influence of substituents on 4,4'-

position of the bipyridine in the catalytic activity will be analyzed in the first part of this section. On a second part, the catalytic activity of precatalysts containing photoswitchable azobenzene-appended bipyridine, pyridine and phosphine ligands will be studied and the influence of the irradiation will be analyzed.

5.2.4.1. RUTHENIUM(II) COMPLEXES CONTAINING BIPYRIDINE LIGANDS AS PRECATALYSTS

Complexes [Ru(*p*-Cym)(**L**)Cl]Cl (**L** = **14**–**21** and **8**) were studied as precatalysts for the hydrolytic dehydrogenation of AB, using the experimental conditions optimized previously in our group for the model complex [Ru(*p*-Cym)(**19**)Cl]Cl.[44]

The experimental catalytic procedure implies a pre-treatment of the precatalyst (necessary to obtain reproducible results), that consists of mixing it with the substrate for 5–10 min with the appropriate quantity of freshly distilled THF in a closed reaction vessel. The consecutive addition of H_2O was considered initial reaction time and the gas evolution was measured by and electronic pressure transducer, all set up in a device named "Man on the moon" (Figure 5.11).[57]

Figure 5.11. Man on the moon X102 kit.

In a standard experiment, a 1:3 v/v THF/H_2O mixture was used as solvent and 0.5 mol% of precatalyst were used. The experiments were carried out at 27 °C. The reaction profiles obtained for the hydrolytic dehydrogenation of AB with different precatalysts are presented in Figure 5.12 (the estimated final pressure corresponding to the liberation of 3 equivalents of gas per mol of substrate was considered 100% conversion). To confirm the fate of the boron species after reaction, ^{11}B-NMR of the reaction residue in DMSO-d_6 were registered. In all cases it showed a sharp singlet at 1.54 ppm as the only boron-containing species, which is consistent with a tetrahedral, negatively charged boron centre with four B-O sigma bonds, corroborating that all the AB was consumed and that no dehydrocoupling compounds were formed.[21]

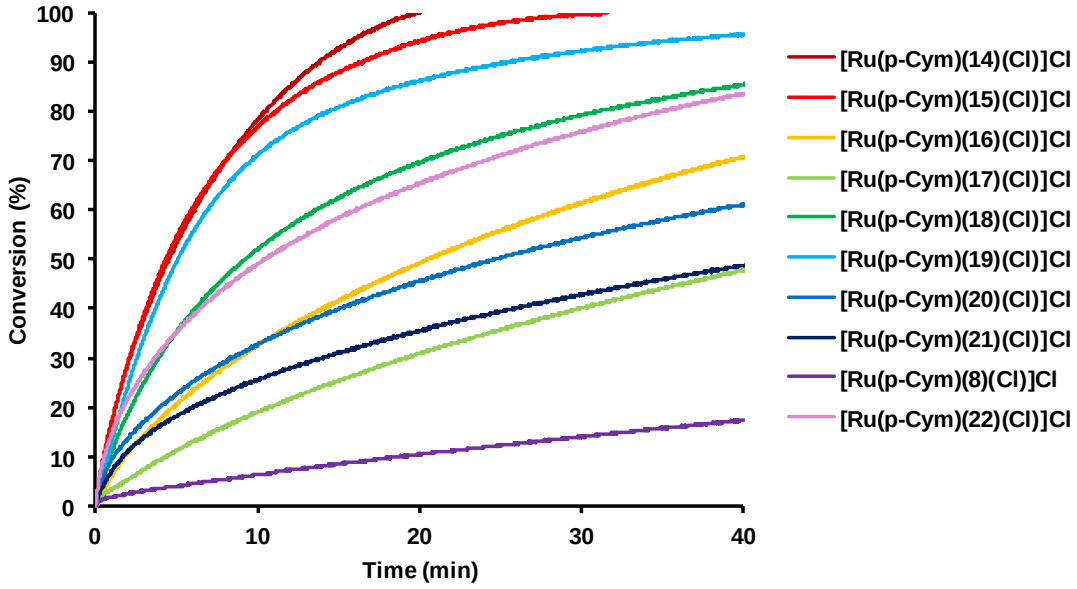

Figure 5.12. Reaction profiles (conversion *vs* time) of the hydrolytic dehydrogenation of AB using as precatalysts [Ru(*p*-Cym)(**L**)Cl]Cl (**L** = **14**–**22** and **8**). Incubation in 0.375 mL of distilled THF, reaction solvent 1.5 mL THF/H_2O = 1/3, [AB] = 0.46 M, catalyst 0.5 mol%, 27 °C.

From these results the different TOF values were individually calculated as mol AB converted/(mol catalyst·hour) at different reaction conversions (initial, one half-life time, and three half-life times). The values obtained at different conversions are summarized in Table 5.4. The conversions obtained with all the precatalysts at the end of the reaction and the time required to achieve full conversion are also shown.

precatalyst	$TOF_{10\%}$ (h^{-1})	$TOF_{50\%}$ (h^{-1})	$TOF_{87.5\%}$ (h^{-1})	max conv. (%) (time (min))
[Ru(*p*-Cym)(**14**)Cl]Cl	2454	1336	819	100 (20)
[Ru(*p*-Cym)(**15**)Cl]Cl	2442	1380	716	100 (31)
[Ru(*p*-Cym)(**16**)Cl]Cl	665	293	154	100 (120)
[Ru(*p*-Cym)(**17**)Cl]Cl	391	195	114	100 (157)
[Ru(*p*-Cym)(**18**)Cl]Cl	1357	650	238	100 (103)
[Ru(*p*-Cym)(**19**)Cl]Cl	1602	1183	486	100 (63)
[Ru(*p*-Cym)(**20**)Cl]Cl	1081	243	92	100 (205)
[Ru(*p*-Cym)(**21**)Cl]Cl	722	142	58	99 (340)
[Ru(*p*-Cym)(**8**)Cl]Cl	64	30	10[a]	83 (650)
[Ru(*p*-Cym)(**22**)Cl]Cl	2386	579	226	98 (78)

Table 5.4. TOF and conversions obtained in the hydrolytic dehydrogenation of AB using as precatalysts [Ru(*p*-Cym)(**L**)Cl]Cl (**L** = **14**–**22** and **8**). Incubation in 0.375 mL of distilled THF, reaction solvent 1.5 mL THF/H_2O = 1/3, [AB] = 0.46 M, catalyst 0.5 mol%, 27 °C. [a] TOF at maximum conversion.

A first-glance analysis of these results indicates that there is a clear influence of the electronic properties of the ligand on the catalytic reaction rate. The use of substituents with increased electronegativity on 4,4' positions of the bipyridine has a beneficial effect on catalytic activity of the system. The best results were obtained with the precatalyst [Ru(*p*-Cym)(**14**)Cl]Cl that contains electron-withdrawing NO_2 substituents on the bipyridine, which is able to release 3 equivalents of H_2 per mole of AB in 20 min. Not surprisingly, [Ru(*p*-Cym)(**15**)Cl]Cl, that contains diethylphosphonate groups also exhibited good results, liberating 3 equivalents in ~30 min. The precatalyst [Ru(*p*-Cym)(**19**)Cl]Cl published previously by us required ~1 hour at this temperature.

Nevertheless, a more careful inspection of these results revealed some inconsistencies:

Based on the Hammett parameter of the ligand-substituent (*vide infra*), a better activity was expected for [Ru(*p*-Cym)(**16**)Cl]Cl that contains carboxylate substituents (as the σ_p^+ of the COOH group is quite positive). According to its Hammett parameter, it should be as efficient as [Ru(*p*-Cym)(**15**)Cl]Cl or at least more efficient than [Ru(*p*-Cym)(**19**)Cl]Cl, which does not fit with the experimental observation. Considering the basic pH of the reaction media, we realized that the σ_p^+ value of CO_2^- (-0.02) would be more adequate to describe the electronic influence of this ligand under catalytic conditions.

Also the activity obtained for the precatalyst [Ru(*p*-Cym)(**17**)Cl]Cl (containing alkyne substituents) was not as good as predicted by the value of its Hammett parameter (*vide infra*). In this case, the reason could be the *in situ* hydrogenation of the alkyne during the reaction curse, generating the diethenyl or diethyl bipyridine derivatives whose σ_p^+ values are -0.16 and -0.30, respectively. To confirm this hypothesis, the dehydrogenation of AB was monitored by *in situ* NMR spectroscopy. ^{1}H-NMR of the complex [Ru(*p*-Cym)(**17**)Cl]Cl (0.019 mmol) in a mixture THF-d_8/D_2O 1/3 was registered and the variation of the spectra after addition of one equivalent of AB was analyzed (Figure 5.13).

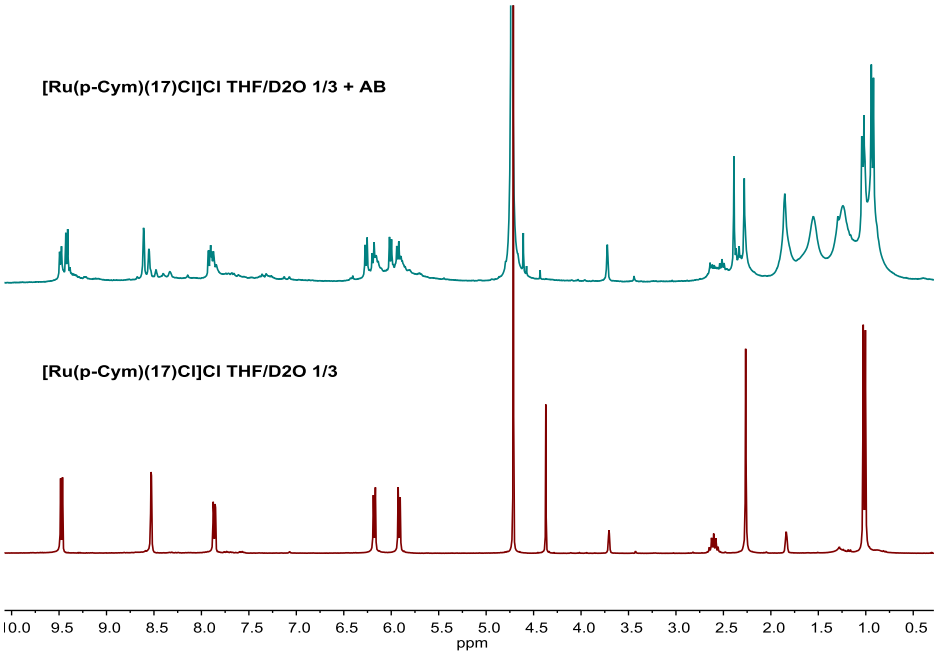

Figure 5.13. ^{1}H-NMR spectra of complex [Ru(*p*-Cym)(**17**)Cl]Cl in THF-d_8/D_2O 1/3 before (bottom) and after adding AB (up) (300 MHz).

With the addition of AB, a new set of signals corresponding to a coordinated *p*-Cymene and bipyridine ligands appeared and the signal of the alkyne at 4.38 ppm disappeared. Although it was not possible to confirm the hydrogenation of alkyne groups (which should be a mixture of products of hydrogenation with the H-D generated by hydrolysis of AB in D_2O), the new species formed and the disappearance of the alkyne signal gave support for this theory. As inferred by comparison with the spectrum of [Ru(*p*-Cym)(bipy)$(NH_3)]^{2+}$, the new species observed could be the amino [Ru(*p*-Cym)(**17**)$(NH_3)]^{2+}$. This is not surprising since the NMR experiment was performed after venting the tube.[44]

Finally, in the case of [Ru(*p*-Cym)(**22**)Cl]Cl (containing an asymmetrically-substituted bipyridine), the activity observed was rather surprising. As it contains one bromine and one azido substituents, its effectiveness was expected to be in the middle of the results obtained for [Ru(*p*-Cym)(**18**)Cl]Cl and [Ru(*p*-Cym)(**21**)Cl]Cl, but it was identical to the former (Figure 5.14). We have been unable to find a logical explanation to this fact.

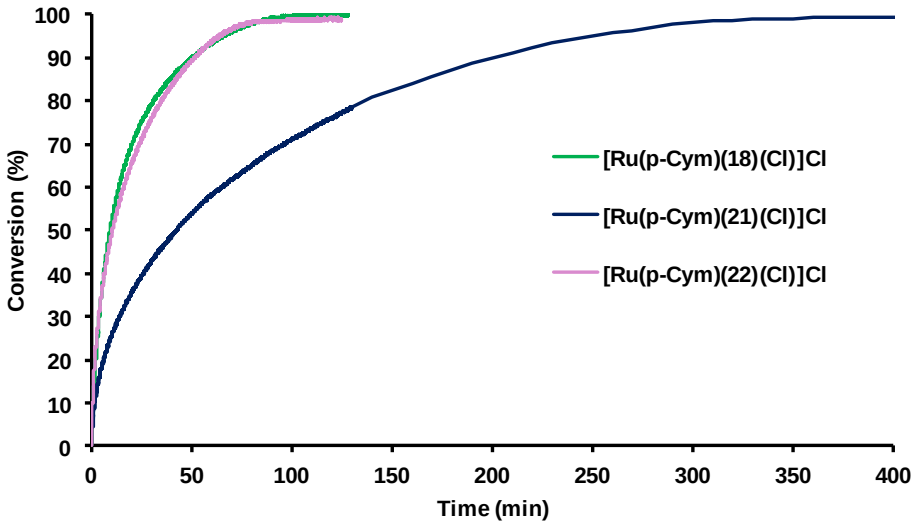

Figure 5.14. Reaction profiles (conversion *vs* time) of the hydrolytic dehydrogenation of AB using as precatalysts [Ru(*p*-Cym)(**L**)Cl]Cl (**L** = **18**, **21** and **22**). Incubation in 0.375 mL of distilled THF, reaction solvent 1.5 mL THF/H_2O = 1/3, [AB] = 0.46 M, catalyst 0.5 mol%, 27 °C.

In order to better understand the correlation existing between the electronic properties of the ligands and the catalytic activity of their ruthenium complexes, the σ_p^+ values of the complexes containing symmetric bipyridines and their activities are shown in Table 5.5. The Hammett values (σ_p^+) were obtained from literature.[49] The activity of each system is presented through the reaction rate constant (k_{obs}) observed plotting the natural logarithm of the AB concentration *versus* time of the data at 3 half-lives (87.5 % conversion) or at maximum conversion for compound [Ru(*p*-Cym)(**8**)Cl]Cl.

precatalyst	σ_p^+	k_{obs} (min^{-1})
[Ru(*p*-Cym)(**14**)Cl]Cl	0.79	0.153
[Ru(*p*-Cym)(**15**)Cl]Cl	Unknown	0.138
[Ru(*p*-Cym)(**16**)Cl]Cl	-0.02[a]	0.029
[Ru(*p*-Cym)(**17**)Cl]Cl	0.18	0.021
[Ru(*p*-Cym)(**18**)Cl]Cl	0.15	0.043
[Ru(*p*-Cym)(**19**)Cl]Cl	0	0.095
[Ru(*p*-Cym)(**20**)Cl]Cl	-0.31	0.016
[Ru(*p*-Cym)(**21**)Cl]Cl	Unknown	0.010
[Ru(*p*-Cym)(**8**)Cl]Cl	-1.3	0.002

Table 5.5. σ_p^+ values of the subsituents on 4,4' position of bipyridine ligand and k_{obs} in the hydrolytic dehydrogenation of AB using as precatalysts [Ru(*p*-Cym)(**L**)Cl]Cl (**L** = **14**–**21** and **8**). Incubation in 0.375 mL of distilled THF, reaction solvent 1.5 mL THF/H_2O = 1/3, [AB] = 0.46 M, catalyst 0.5 mol%, 27 °C. [a] This value corresponds to CO_2^-.

The logarithmic representation of the activity of these systems (normalized k_{obs}) *versus* the Hammett parameter of the substituents was constructed (Figure 5.15). As

explained before, the alkyne substituent of the complex [Ru(*p*-Cym)(**17**)Cl]Cl could be hydrogenated *in situ* during the catalytic process. For this reason the three σ_p^+ values of alkyne (0.18), diethenyl (-0.16) and diethyl (-0.30) substituents were represented (red dots). The σ_p^+ values for diethylphosphonate and azido substituents were extracted from the ones calculated for the free ligands (Chapter 2), because better correlation was obtained with these values than with the ones extracted from the NMR spectra of the ruthenium complexes.

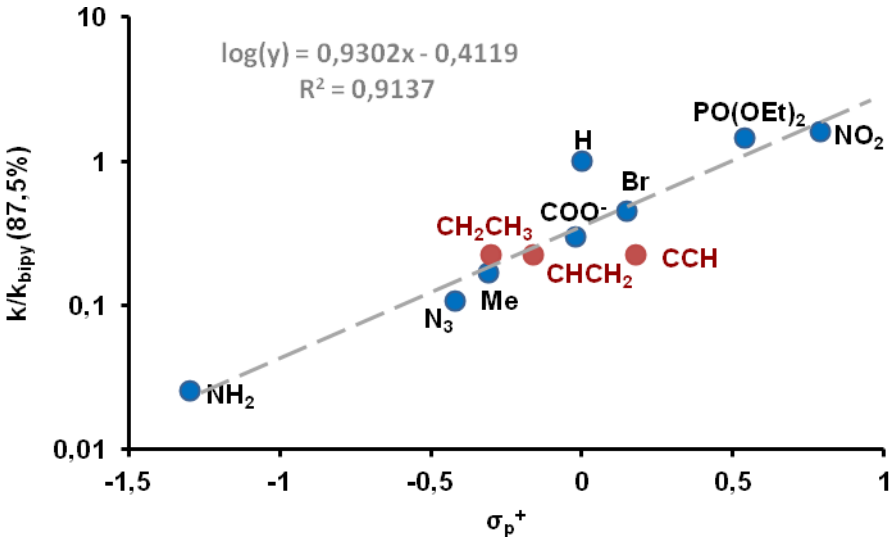

Figure 5.15. Logarithmic representation of $k_{obs}/k_{obs(\mathbf{bipy})}$ at 87.5% conversion *vs*. σ_p^+ for the hydrolytic dehydrogenation of AB using precatalysts [Ru(*p*-Cym)(**L**)Cl]Cl (**L** = **14**–**21** and **8**).

The obtained correlation was good, although the values obtained with [Ru(*p*-Cym)(**17**)Cl]Cl were excluded as it has not been possible to confirm which was the real nature of the catalyst during the catalytic cycle. The catalytic activity obtained with these precatalyst is in accordance with the values of diethenyl or diethyl substituents.

Altogether, a good fit was obtained for the correlation of activities *vs*. Hammett electronic parameter. Only the value of the unsubstituted complex [Ru(*p*-Cym)(**19**)Cl]Cl is slightly over its predicted activity. Since steric effects of the substituents in 4,4'-positions should not have any influence on the reaction rate, the exceptional activity observed for [Ru(*p*-Cym)(**19**)Cl]Cl remains unclear. Nevertheless, the clear correlation observed confirms that electronic effects are important in determining the activity of the system. The positive slope of the curve indicates that the rate determining step of the reaction is accelerated when electron-withdrawing ligands are used, which indicates that a more electrophilic metal center facilitates this step.

As the best results were obtained with the dinitro derivative [Ru(*p*-Cym)(**14**)Cl]Cl, the reaction with this precatalyst was analyzed in more detail, studying several reaction

parameters. Initially, the use of different solvent mixtures THF:H_2O ranging from pure THF to pure H_2O was studied (Figure 5.16).

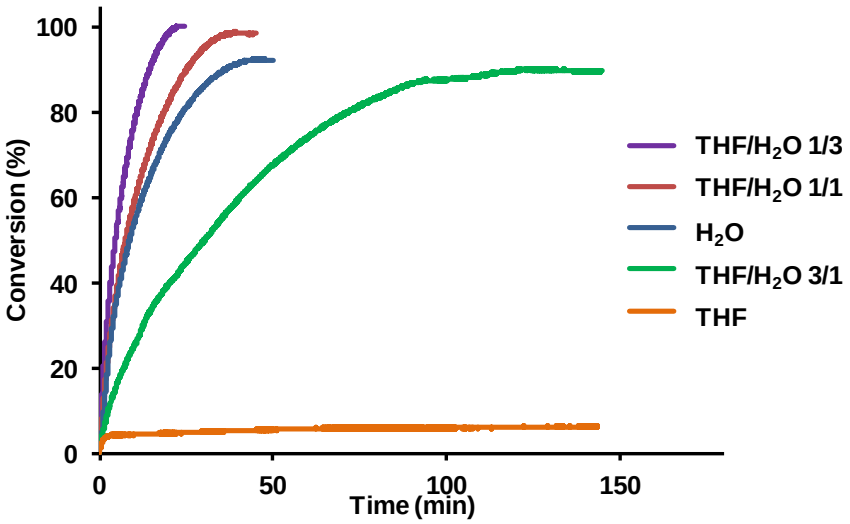

Figure 5.16. Reaction profile (conversion *vs.* time) obtained in the hydrolysis of AB with precatalyst [Ru(*p*-Cym)(**14**)Cl]Cl, with different solvent mixtures, [AB] = 0.46 M, catalyst 0.5 mol%, 27 °C.

The obtained results showed that the best activities were obtained with the mixture THF/H_2O 1/3 v:v, as already observed for the model system [Ru(*p*-Cym)(**19**)Cl]Cl in our previous publication.[35] As expected, insignificant catalytic activity was observed when only freshly distilled THF was used, indicating that the AB dehydrocoupling is not the mechanism operating in the hydrogen liberation. When only H_2O was used, quite good catalytic activity was observed, but only 2.7 equivalents of H_2 per mole of AB were released.

Using the optimized solvent mixture, five catalytic experiments were conducted at different temperatures, in the range of 10–55 °C. The reaction profiles obtained at different temperatures are shown in Figure 5.17 and first order plots of the catalytic hydrolysis of AB at these temperatures are shown in Figure 5.18. As expected, the reaction is faster when the temperature was increased, and at the highest temperature assayed (55 °C), 3 equivalents of H_2 per mole of AB were released in only 3.7 min.

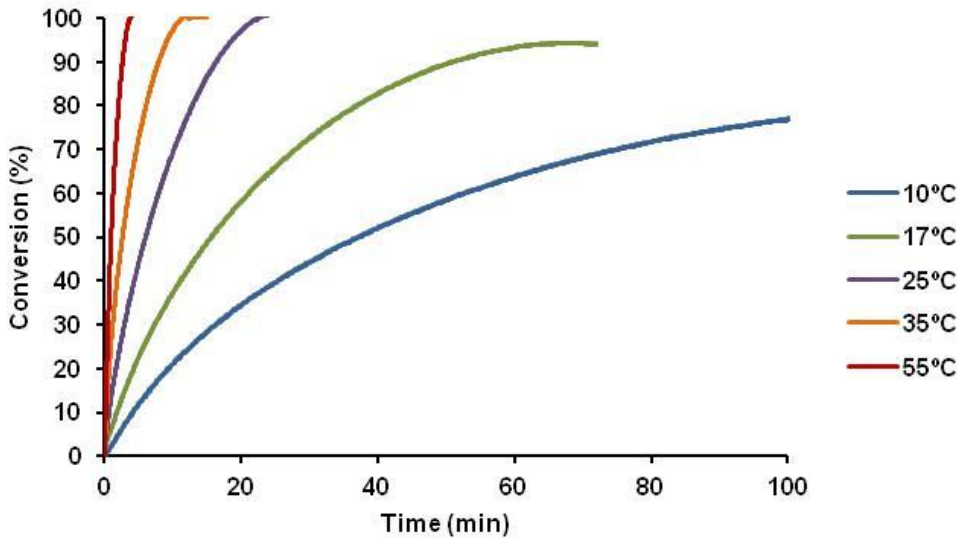

Figure 5.17. Reaction profiles for the hydrolytic dehydrogenation of AB with precatalyst [Ru(*p*-Cym)(**14**)Cl]Cl at different temperatures. Reaction conditions: incubation for 10 min in 0.375 mL of THF; reaction solvent 1.5 mL THF/H_2O = 1/3 (v/v), [AB] = 0.46 M, catalyst 0.5 mol%.

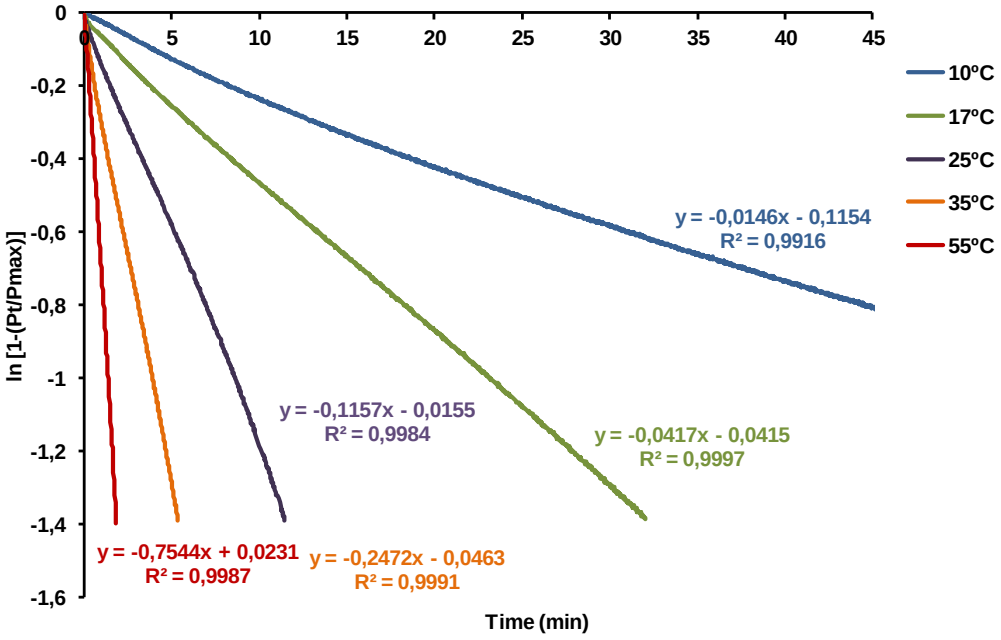

Figure 5.18. First order plot of the catalytic hydrolysis of AB with precatalyst [Ru(*p*-Cym)(**14**)Cl]Cl, at different temperatures, [AB] = 0.46 M, [AB]/[cat] = 200, THF:H_2O = 1/3. Data of 2 half lives.

Since the hydrolytic dehydrogenation of AB is a pseudo-first order reaction, the observed reaction rate constants include the concentration of the precatalyst. Then, the calculated k_{obs} were divided by the concentration of the precatalyst ($2.3 \cdot 10^{-3}$ M) to obtain the actual kinetic k value. All the rate constant values and TOF values obtained at two half-life times are collected in Table 5.6.

Temperature (K)	$t_{75\%}$ (min)	$TOF_{75\%}$ (h^{-1})	k_{obs} (s^{-1})	k ($L \cdot mol^{-1} \cdot s^{-1}$)
283	92	98	$2.4 \cdot 10^{-4}$	0,106
290	32	281	$6.9 \cdot 10^{-4}$	0,302
298	11.5	787	$1.9 \cdot 10^{-3}$	0.838
308	5.3	1685	$4.1 \cdot 10^{-3}$	1.791
328	1.8	4929	$1.2 \cdot 10^{-2}$	5.467

Table 5.6. Time required for 2 half -lives, TOF values, k_{obs} values extracted from the first order plots at different temperatures and calculated k values for the data at 2 half-lives (75 % conversion).

Through the Eyring plot of the calculated reaction rate constants, enthalpy and entropy values comparable to those reported before for the compound [Ru(*p*-Cym)(**19**)Cl]Cl were obtained (Figure 5.19).[44] The negative sign of $\Delta S^{\neq}$ points to an organized transition state for the rate-determining step of the catalytic cycle.

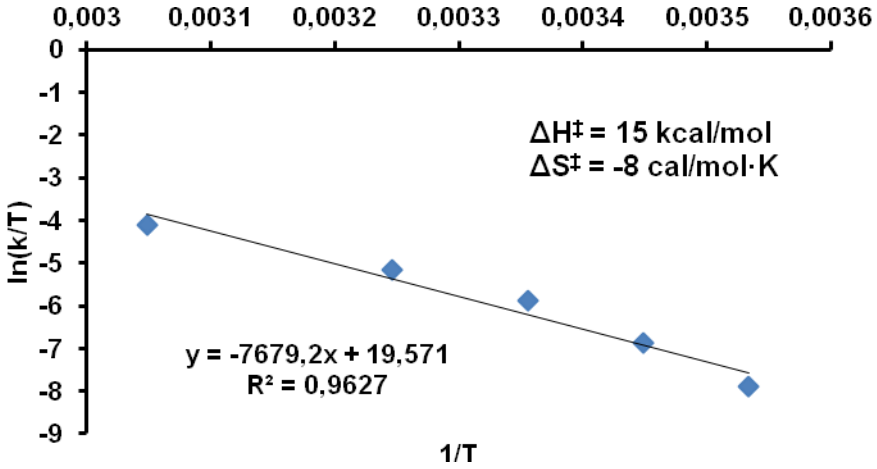

Figure 5.19. Eyring plot. Catalytic hydrolysis of AB with precatalyst [Ru(*p*-Cym)(**14**)Cl]Cl. Reaction conditions: incubation for 10 min in 0.375 mL of THF; reaction solvent 1.5 mL THF/H_2O = 1/3 (v/v), [AB] = 0.46 M, catalyst 0.5 mol%.

The catalytic hydrolytic dehydrogenation of several substituted amine-borane adducts was studied, using the precatalyst [Ru(*p*-Cym)(**14**)Cl]Cl. These substrates were selected to confirm the hydrolytic nature of the process (and to discard a dehydrogenation-based mechanism). The maximum quantity of hydrogen per mole of substrate that can be obtained through a dehydrogenative pathway is determined by the number of N−H groups present in the $R^1R^2R^3N{-}BH_3$ substrate. If the mechanism is based on a hydrolysis of the BH_3 (formed by excision of the adduct), up to 3 equivalents of hydrogen can be liberated independently of the amine fragment. Three substrates, namely *tert*-buthylthylamine-borane (TBAB), dimethylamine-borane (DMAB) and trimethyl-amine-borane (TMAB) were used for this study, and the reaction profiles obtained are shown in Figure 5.20.

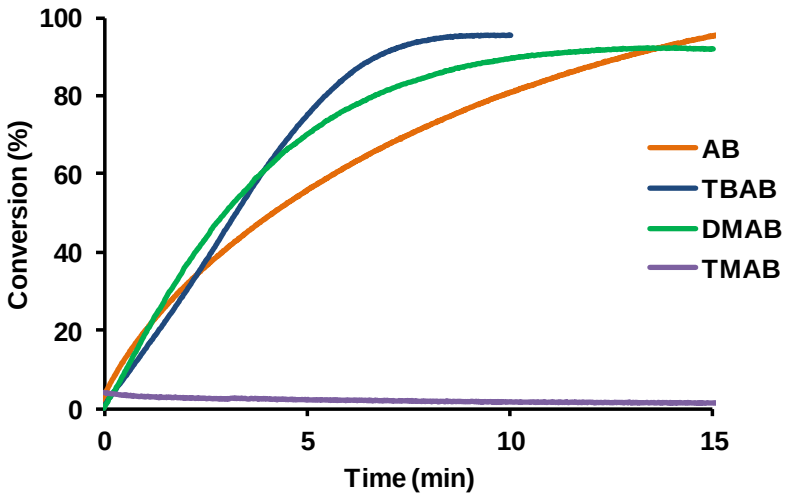

Figure 5.20. Reaction profiles (conversion *vs*. time) obtained for the hydrolytic dehydrogenation of different substrates with precatalyst [Ru(*p*-Cym)(**14**)Cl]Cl. 27 °C, [cat] = $2.3 \cdot 10^{-3}$ M, [AB]/[cat] = 200, THF/H_2O = 1/3 (v/v).

Mono- and disubstituted amine-boranes were able to liberate almost 3 equivalents of H_2 per mole of substrate: DMAB liberated 2.76 and TBAB 2.85 equivalents. This results confirmed that the reaction mechanism of this catalytic system is the hydrolysis of the borane, and not a direct dehydrogenation of the adduct.

As already observed for the precatalyst [Ru(*p*-Cym)(**19**)Cl]Cl, the hydrogen release is slightly faster when substituted amine-boranes are used than with unsubsituted AB and no hydrogen release was observed from trisubstituted TMAB.[35] As mentioned before, the lack of reactivity of the trisubstituted amine-borane could be due to the absence of N–H functionality if necessary in the catalytic cycle or to the larger strength of the B–N bond in TMAB compared to other substrates.

To get some insight on the actual reaction mechanism for the hydrolytic dehydrogenation of amine-borane adducts, a detailed kinetic isotope effect (KIE) study was performed.

Initially, the adduct $H_3N–BD_3$ (synthesized following the synthetic procedure described in the literature)[52] was used as substrate in catalytic experiments in THF/H_2O mixtures. The measured reaction profile was very similar to the one obtained with the non-deuterated AB under the same catalytic conditions ($k_{H3N–BH3}/ k_{H3N–BD3}$ = 1.1). This result indicates that most probably the rupture of the bond B–H is not involved in the rate-determining step of the catalytic process. This is a rather surprising result, as most of the authors point to a B–H-directed mechanism for the rate-determining activation of the substrate in AB dehydrogenation reactions.[14,29,36,37,38,39,40,41,42]

Different experiments were also carried out using D_2O and THF-d_8 as solvents, to analyze their influence on the reaction rates. In Figure 5.21 are shown the reaction

profiles obtained with the different solvent mixtures assayed. When THF-d_8 was used instead of THF an identical reaction profile obtained using non-deuterated solvents was obtained. Consequently, the $k_{THF\text{-}D8}/k_{THF\text{-}H8}$ = 1 observed confirmed that, as expected, the rupture of C–H bonds of THF is not involved in the catalytic process. When D_2O was used instead of H_2O, a much slower reaction rate was observed. The analysis of the kinetic data permitted to determine that k_{H2O}/k_{D2O} = 4.

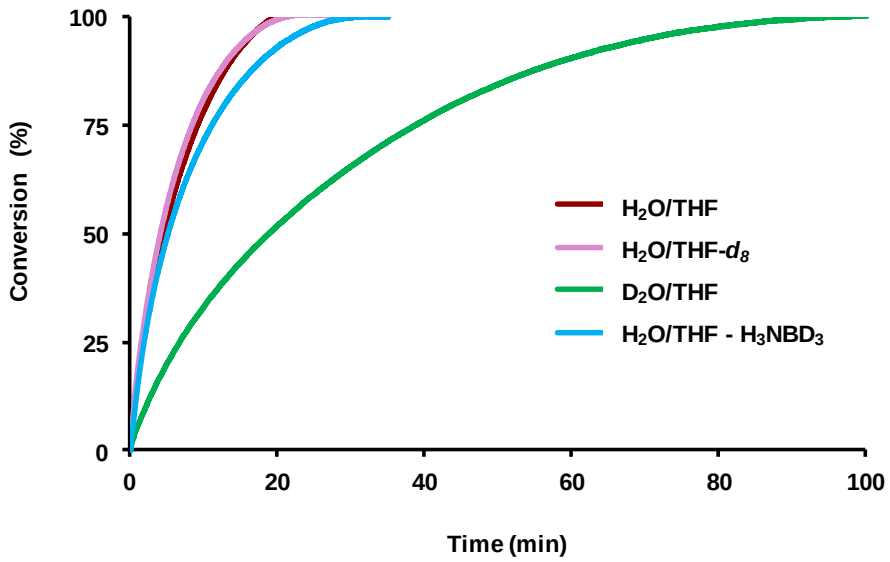

Figure 5.21. Reaction profiles (conversion *vs*. time) obtained for the hydrolytic dehydrogenation of AB with precatalyst [Ru(*p*-Cym)(**14**)Cl]Cl. Incubation in 0.375 mL of distilled THF, reaction solvent 1.5 mL THF/H_2O = 1/3 (v/v), [cat] = $2.3 \cdot 10^{-3}$ M, [AB]/[cat] = 200, 27 °C.

Several hypotheses could explain the first-order KIE observed. In order to rationalize the results obtained, some facts need to be taken into account:

In D_2O media:

- the protic N–H hydrogens of AB experience a fast D↔H exchange, [58] so most of the original H_3N–BH_3 is actually in the form of D_3N–BH_3.
- the hydric B–H atoms AB do not experience D↔H exchange.
- the hydric Ru–H experiences a fast D↔H exchange,[59] so most of the Ru–H is in the form of Ru–D. This species is the main Ru compound during the catalytic cycle, and therefore most probably is the resting state of the catalyst.

Consequently, to explain the observation of an important KIE when H_2O was replaced by D_2O we considered the following hypotheses:

1- O–H bond-cleavage is involved in the rate-determining process, and the KIE observed is because the non-catalyzed hydrolysis of the released BH_3 (see reaction below) is slower than the metal-catalyzed cleavage of the adduct.

$$NH_3{\cdot}BH_3 + 4H_2O \rightarrow 3H_2 + NH_4^+ + B(OH)_4^-$$

2- O–H bond-cleavage is involved in the rate-determining process, but it is due to a metal-catalyzed hydrolysis of the adduct.

3- O–H bond-cleavage is involved in the rate-determining process, because metal-catalyzed H_2O excision is crucial for the catalytic process.

4- Ru–H bond-cleavage is involved in the rate-determining step.

5- N–H bond-cleavage is involved in the rate-determining process, suggesting a N–H–Ru bond formation as part of the activation mechanism of the substrate.

The first hypothesis was discarded on the bases of the kinetics of the reaction, which showed a first-order dependence on catalyst concentration. Hypothesis 2–5 (or combinations of them) are considered to propose the actual reaction mechanism. It is worth mentioning that hypothesis 5 would be in agreement with the experimental observation that the presence of an N–H bond in the substrate for the reaction to proceed.

In situ MS spectroscopic analysis were performed by Cristian V. Barrera at the UJI (Castellón) to identify the species that are present during the hydrolytic dehydrogenation of AB. In Chart 5.6, are shown the most relevant species detected when the catalytic reaction of [Ru(*p*-Cym)(bipy)H_2O](OTf)$_2$ ($1{\cdot}10^{-4}$ M) and AB (~5 equiv.) in a mixture THF/H_2O 3/1 was analyzed.

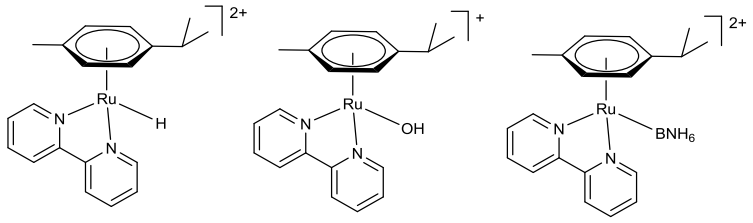

Chart 5.6. The most interesting species detected by *in situ* MS spectroscopy in the reaction of [Ru(*p*-Cym)(bipy)H_2O](OTf)$_2$ ($1{\cdot}10^{-4}$ M) and AB (~5 equiv.) in a mixture THF/H_2O 3/1.

Taking into account all the results explained before, Dr. Abel de Cózar (UPV-EHU) performed theoretical calculations (DFT) and proposed a preliminary reaction mechanism shown below (Figure 5.22). Calculated transition states are also shown in the figure.

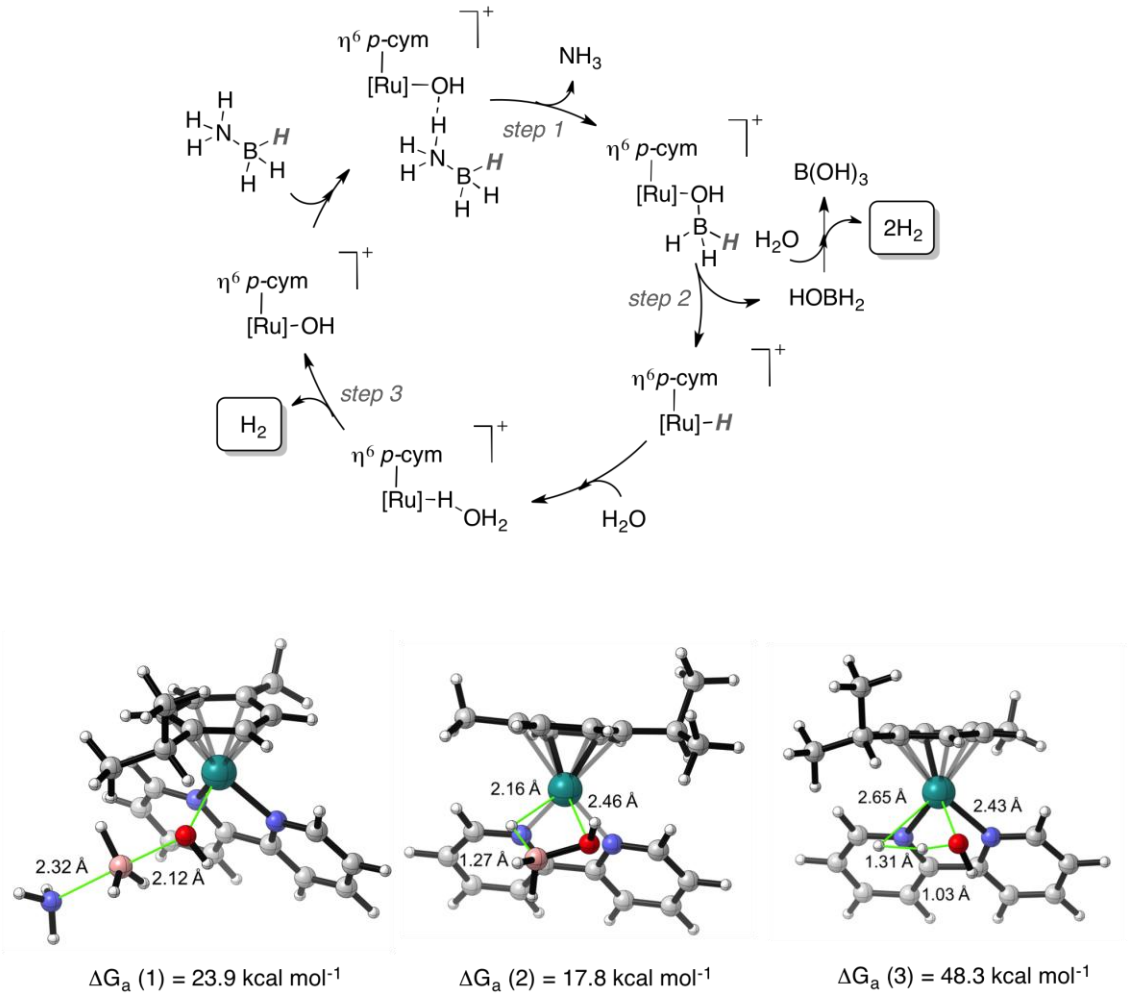

Figure 5.22. Proposed reaction mechanism for the hydrolytic dehydrogenation of AB.

More calculations are currently under development to confirm this reaction mechanism which is very preliminary, and compatible with most of the experimental observations.

5.2.4.2. AZOBENZENE-CONTAINING RUTHENIUM(II) COMPLEXES AS PRECATALYSTS

Azobenzene-containing Ru(II) complexes were synthesized to be used as precatalysts for the hydrolytic dehydrogenation of AB and study the influence of the photoisomerization of the azobenzene in their activity. For this purpose, two catalytic experiments were performed with each precatalyst, one without irradiation and the other one irradiating with an UV immersion lamp.

The experimental catalytic procedure for azobenzene-containing precatalysts was the same followed in the previous section. The precatalyst (0.5 mol%) was mixed with the substrate for 5–10 min in 0.375 mL of freshly distilled THF in a closed reaction vessel. The consecutive addition of 1.125 mL of H_2O was considered initial reaction time.

Nevertheless, some additional precautions need to be taken. Due to the heating of the system caused by prolonged irradiation times, the reaction vessel was immersed in a

water bath, that was maintained at the desired temperature (±4 ºC) by means of a thermostated external cooling jacket. When required, the reaction mixture was irradiated during the catalytic process by means of an immersion lamp (125 W, 365 nm), which was also refrigerated by means of an external cooling jacket made of quartz. The reaction vessel used for these reactions was also made of quartz. The experimental setup is presented in Figure 5.23.

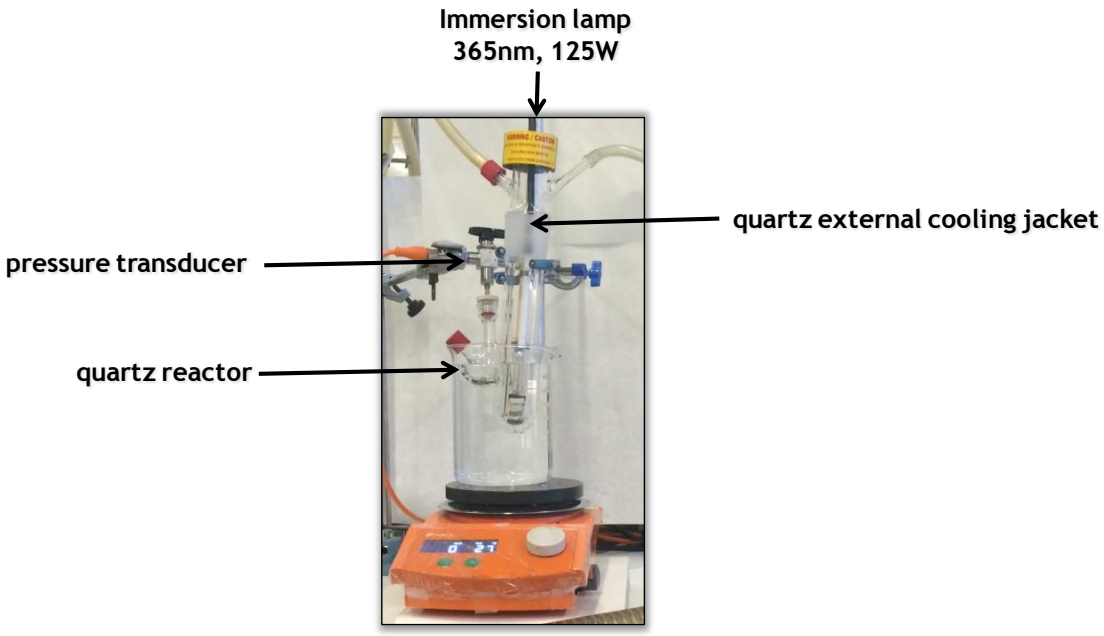

Figure 5.23. Setup for catalytic experiments under irradiation.

Several experiments before testing azobenzene-containing precatalyts were necessary to analyze the influence of the irradiation on the catalytic process and optimize the reaction conditions. Initially, a blank experiment (without catalyst) was carried out, with continuous irradiation to confirm that light-induced AB cleavage and hydrolysis of the released BH_3 was not competing with the catalyzed process (Figure 5.24, red-dashed line). The slight slope observed should be attributed an unavoidable temperature increase (~4 ºC). To select the temperature at which the thermostatic bath should be fixed to avoid overheating of the system, several experiments were performed with the precatalyst [Ru(*p*-Cym)(**19**)Cl]Cl, which does not contain any azobenzene fragment. The catalytic activity of this precatalyst with the thermostatic bath at different temperatures was compared with the reaction profile obtained at 25 °C (without irradiation) until similar reaction profiles were obtained. In this manner, the ideal temperature of the thermostatic bath was set at 10 ºC. By setting the thermostat temperature at 10 ºC, the initial temperature measured for irradiated catalysis was 21 °C and it never exceeded the 25 °C, (Figure 5.24, green (not irradiated) and red (irradiated) lines). For comparative purposes, not irradiated reactions were performed

at 25 °C (the maximum temperature achieved upon irradiation), to guarantee that any outperformance of the irradiated processes was not an artifact caused by temperature. Consequently, as it can observed in Figure 5.24, the activity of the precatalyst [Ru(*p*-Cym)(**19**)Cl]Cl (not light-sensitive) was slightly lower when the reaction was irradiated, due to the lower initial temperature. This small difference in profiles will be assumed as the experimental error inherent to the methodology.

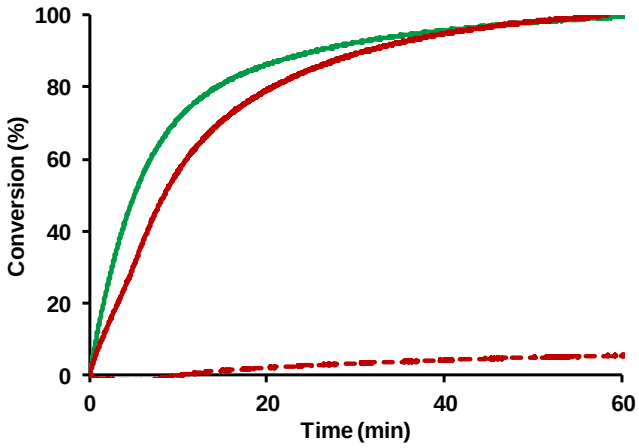

Figure 5.24. Reaction profiles (conversion *vs*. time) obtained for the hydrolytic dehydrogenation of AB without precatalyst (red dashed line), with [Ru(*p*-Cym)(**19**)Cl]Cl not irradiated (green line) and with [Ru(*p*-Cym)(**19**)Cl]Cl irradiated (red line). Incubation in 0.375 mL of distilled THF, reaction solvent 1.5 mL THF/H_2O = 1/3 (v/v), [cat] = $2.3 \cdot 10^{-3}$ M, [AB]/[cat] = 200.

The influence of the irradiation on the catalytic activity of complexes [Ru(*p*-Cym)(**L**)Cl]Cl (**L** = **1**, and **3–5**) was studied and the reaction profiles obtained for these precatalysts are shown in Figure 5.25. All of them showed slightly higher activities when the reactions were irradiated, so the hydrolytic dehydrogenation of AB is favored by the irradiation, presumably due to isomerization of the azobenzene units. The influence of the irradiation was more significant for complexes [Ru(*p*-Cym)(**3**)Cl]Cl, [Ru(*p*-Cym)(**4**)Cl]Cl and [Ru(*p*-Cym)(**5**)Cl]Cl. Only a slight difference was observed for the complex [Ru(*p*-Cym)(**1**)Cl]Cl but considering the lower initial temperature of the irradiated catalysis, it seems that the irradiation favored its activity. The minor effect of the irradiation in the case of derivative of ligand **1** is in agreement with the small degree of photoisomeriztion observed for this complex (*vide supra*).

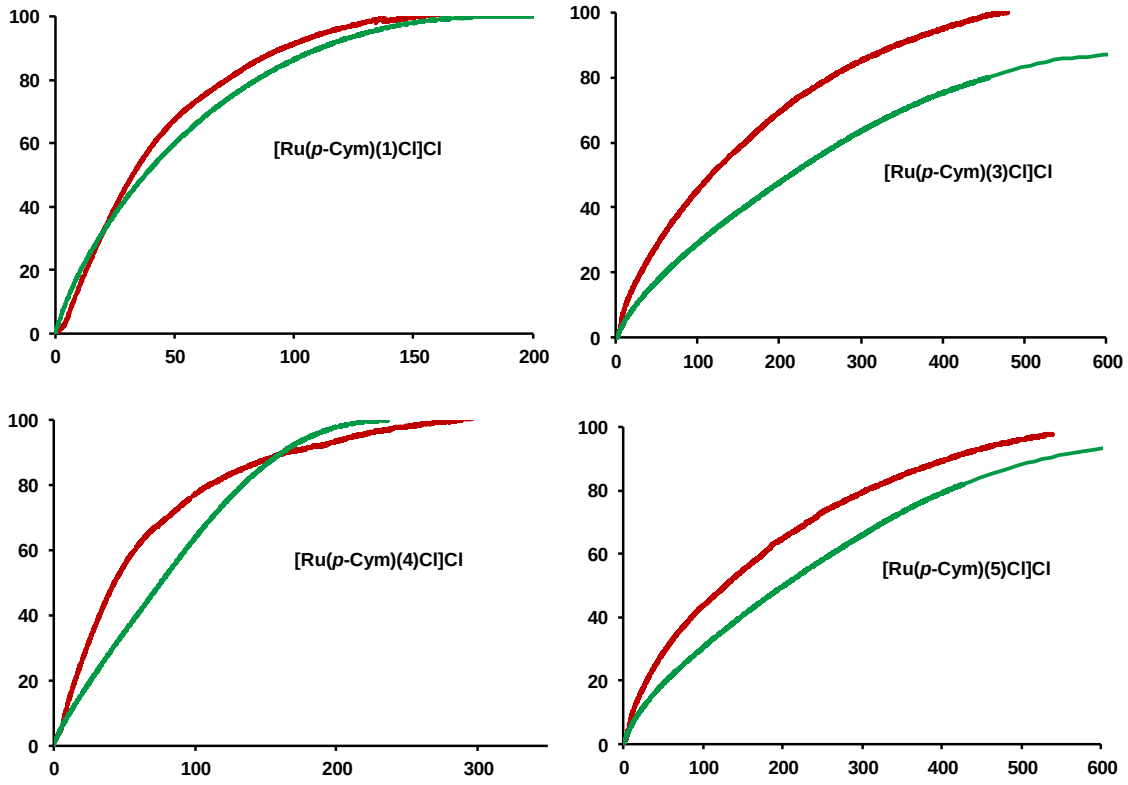

Figure 5.25. Reaction profiles (conversion *vs*. time) obtained for the hydrolytic dehydrogenation of AB with [Ru(*p*-Cym)(**L**)Cl]Cl (**L** = **1**, and **3–5**) not irradiated (green line) and irradiated (red line). Incubation in 0.375 mL of distilled THF, reaction solvent 1.5 mL THF/H_2O = 1/3 (v/v), [cat] = $2.3 \cdot 10^{-3}$ M, [AB]/[cat] = 200.

The activity for complexes containing non chelating pyridine ligands [Ru(*p*-Cym)(**2**)Cl_2] and [Ru(*p*-Cym)(**2**)$_2$Cl]PF_6 upon irradiation was also analyzed and compared with the reaction profiles obtained without irradiation at 25 °C (Figure 5.26). In the case of the cationic complex containing two pyridine ligands, the obtained reaction profiles with or without irradiation were surprisingly similar (which in fact indicates that the irradiated process was slightly faster, due to the lower initial temperature employed). In the case of the neutral complex [Ru(*p*-Cym)(**2**)Cl_2] containing only one 4-phenylazopyridine, there was a considerable difference between the reaction profiles of irradiated and not irradiated catalytic systems. When the reaction was run with irradiation, the shape expected for a catalyzed process following a first-order dependence on substrate was obtained. Surprisingly, without irradiation it presented the sigmoidal shaped profile characteristic of a process that requires catalyst-incubation. This different behaviour could not be attributed to azobenzene isomerization, since the photoisomerization studies showed the inhibition of the photoisomerization in this derivative.

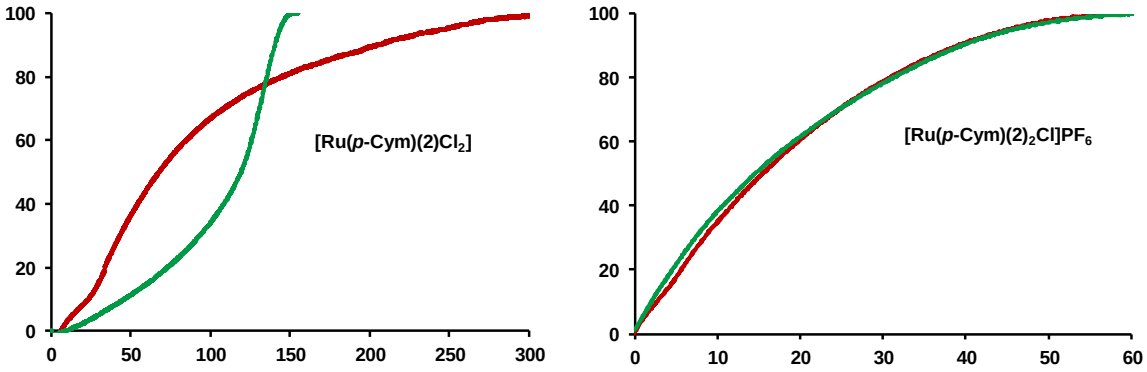

Figure 5.26. Reaction profiles (conversion *vs*. time) obtained for the hydrolytic dehydrogenation of AB with [Ru(*p*-Cym)(**2**)Cl_2] and [Ru(*p*-Cym)(**2**)$_2$Cl]PF not irradiated (green line) and irradiated (red line). Incubation in 0.375 mL of distilled THF, reaction solvent 1.5 mL THF/H_2O = 1/3 (v/v), [cat] = $2.3 \cdot 10^{-3}$ M, [AB]/[cat] = 200.

The peculiar reaction profile obtained for the complex [Ru(*p*-Cym)(**2**)Cl_2], and to confirm that it was not due to the photoisomerization process of the azobenzene, the influence of the irradiation for the hydrolytic dehydrogenation of AB for precatalysts [Ru(*p*-Cym)(pyridine)Cl_2] and [Ru(*p*-Cym)(pyridine)$_2$Cl]PF_6 was studied. The complex [Ru(*p*-Cym)(pyridine)$_2$Cl]PF_6 showed similar activity with or without irradiation (Figure 5.27), being the not irradiated process slightly more active, due to the experimental restrictions.

As it can observed in Figure 5.27, the complex [Ru(*p*-Cym)(pyridine)Cl_2] showed the same behaviour as the complex [Ru(*p*-Cym)(**2**)Cl_2], demonstrating that the photoisomerization of the azobenzene was not the cause of the variation of the reaction profile upon irradiation. Similar S-shaped curves have been reported in the literature for heterogeneous catalysts for hydrolytic dehydrogenation of AB, where the induction period was attributed to the time required to form the active nanoparticle-based catalysts.[5,6,60] To test if formation of active Ru-nanoparticles was responsible of the shape observed, a mercury-test to confirm the homogeneity of the catalytic system was performed. At 50% of conversion of the precatalyst [Ru(*p*-Cym)(pyridine)Cl_2] ~1000 equivalents of Hg were added. The addition of mercury did not affect in the reaction profile, confirming the homogeneity of the catalytic reaction.

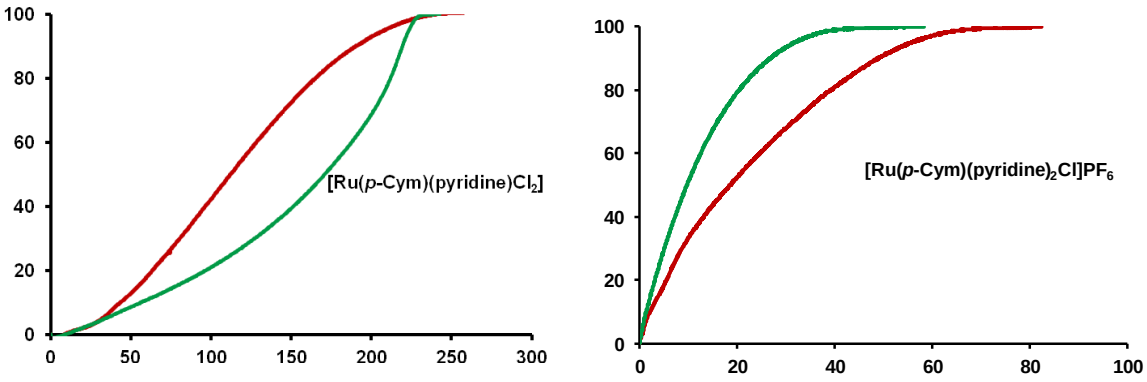

Figure 5.27. Reaction profiles (conversion *vs*. time) obtained for the hydrolytic dehydrogenation of AB with [Ru(*p*-Cym)(pyridine)Cl_2] and [Ru(*p*-Cym)(pyridine)$_2$Cl]PF not irradiated (green line) and irradiated (red line). Incubation in 0.375 mL of distilled THF, reaction solvent 1.5 mL THF/H_2O = 1/3 (v/v), [cat] = $2.3 \cdot 10^{-3}$ M, [AB]/[cat] = 200.

In the view of these results we contemplated the possibility that these profiles were due to dissociation of the Ru–pyridine and Ru–(4-phenylazopyridine) bonds induced by irradiation. It is known that the dissociation of the pyridine fragment occurs irradiating Ru(II) arene complexes of type [Ru(*p*-Cym)(bipy)(py)]$^{2+}$ with UV-Vis light.[61] The displacement of the *p*-Cym was also observed in a complex of this family upon continuous irradiation.[62]

To analyze this hypothesis, two additional experiments were carried out, combining irradiation and non-irradiation periods (Figure 5.28). The obtained reaction profiles showed that if the catalytic process was not irradiated initially and the lamp was switched on after activation period (light-green line), the results were identical to the obtained when the process was not irradiated at all (dark green line). This result suggests that irradiation after the activation period was not producing any effect on the catalytic system. It is worth noticing that after 30 minutes irradiating the lamp was switched off again. As described before, if the reaction was irradiated initially nearly no activation period was observed (red lines). If at 30 % conversion the lamp was switched off, (light-red line) the most effective results were obtained. Using this on/off procedure, the activation period was not required and the activity of the catalytic system did not suffer deactivation al longer reaction times as it was observed when the system was continuously irradiated.

So, according to these results, irradiation favors the initial activation of these catalytic systems, probably through dissociation of a pyridine ligand, but a continuous irradiation is detrimental. The eventual displacement of the *p*-Cym and catalyst decomposition could be the reason for the lowering of the activity of precatalysts [Ru(*p*-Cym)(**2**)Cl_2]

and [Ru(*p*-Cym)(pyridine)Cl_2] upon continuous irradiation. *In situ* NMR irradiation experiments to confirm this hypothesis are currently under progress.

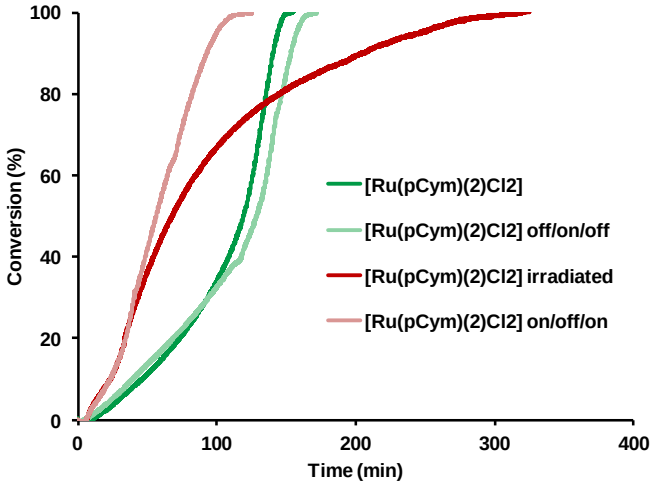

Figure 5.28. Reaction profiles (conversion *vs*. time) obtained for the hydrolytic dehydrogenation of AB with [Ru(*p*-Cym)(**2**)Cl_2]. Incubation in 0.375 mL of distilled THF, reaction solvent 1.5 mL THF/H_2O = 1/3 (v/v), [cat] = $2.3 \cdot 10^{-3}$ M, [AB]/[cat] = 200.

The influence of the irradiation on the catalytic activity for the hydrolytic dehydrogenation of AB using precatalysts [Ru(*p*-Cym)(**12**)Cl_2] and [Ru(*p*-Cym)(**13**)Cl_2], incorporating azobenzene-containing triarylphosphines was also studied. Both complexes showed much higher activity when the catalytic system was irradiated (Figure 5.29). These results are in accordance with the large extent of the azobenzene photoisomerization observed for these compounds (*vide supra*). As explained in a former section, according to the difference in UV-Vis spectra before and after irradiation, these compounds showed the most efficient photoisomerization of the azobenzene from the series, and also the slowest reverse *Z*→*E* process (they contain the most stable *cis* isomers).

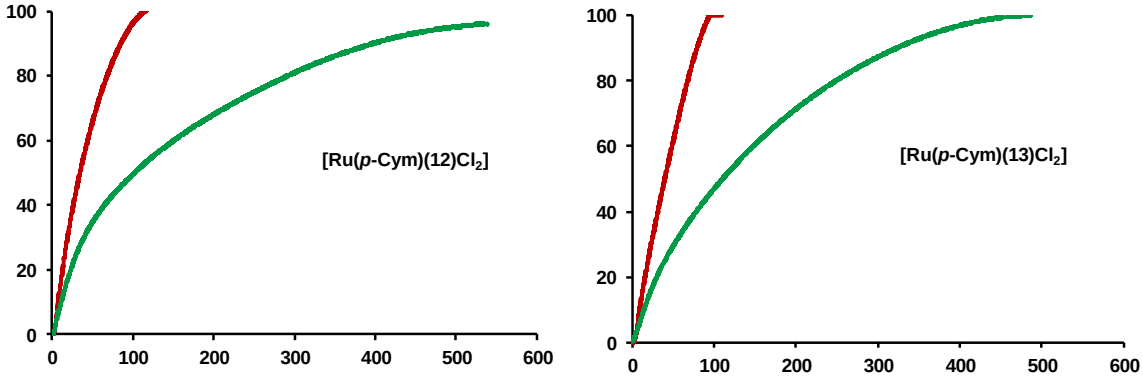

Figure 5.29. Reaction profiles (conversion *vs*. time) obtained for the hydrolytic dehydrogenation of AB with [Ru(*p*-Cym)(**L**)Cl_2] (**L** = **12** and **13**) not irradiated (green line) and irradiated (red line). Incubation in 0.375 mL of distilled THF, reaction solvent 1.5 mL THF/H_2O = 1/3 (v/v), [cat] = $2.3 \cdot 10^{-3}$ M, [AB]/[cat] = 200.

To confirm that the origin of the higher activity of this precatalysts was the isomerization of the azobenzene fragments, and not the dissociation of the phosphine ligand (as postulated for the pyridine derivatives) the catalytic activity of the model precatalyst [Ru(*p*-Cym)(PPh_3)Cl_2] was studied. This precatalyst does not contain azobenzene fragments and exhibited very similar activities under irradiation and without it, which confirms that azobenzene isomerization is responsible of the different activities (Figure 5.30).

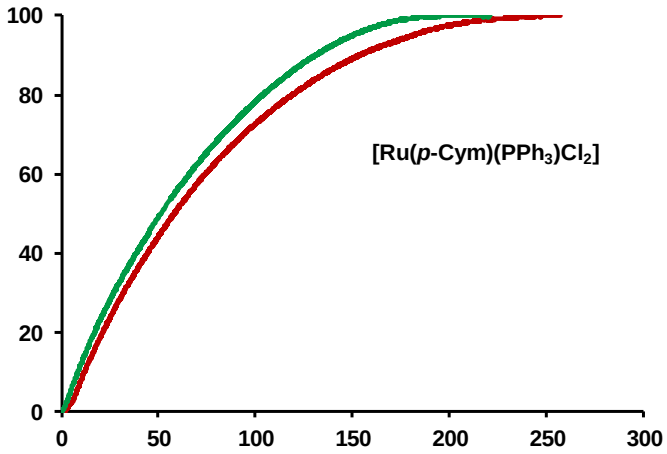

Figure 5.30. Reaction profiles (conversion *vs*. time) obtained for the hydrolytic dehydrogenation of AB with [Ru(*p*-Cym)(PPh_3)Cl_2] not irradiated (green line) and irradiated (red line). Incubation in 0.375 mL of distilled THF, reaction solvent 1.5 mL THF/H_2O = 1/3 (v/v), [cat] = $2.3 \cdot 10^{-3}$ M, [AB]/[cat] = 200.

Once it was confirmed that the catalytic activity of complexes incorporating azobenzene-appended triarylphosphines was increased due to the photoisomerization of azobenzene fragments, additional experiments were carried out for precatalysts [Ru(*p*-Cym)(**12**)Cl_2] and [Ru(*p*-Cym)(**13**)Cl_2], combining irradiation and no irradiation periods (Figures 5.31 and 5.32).

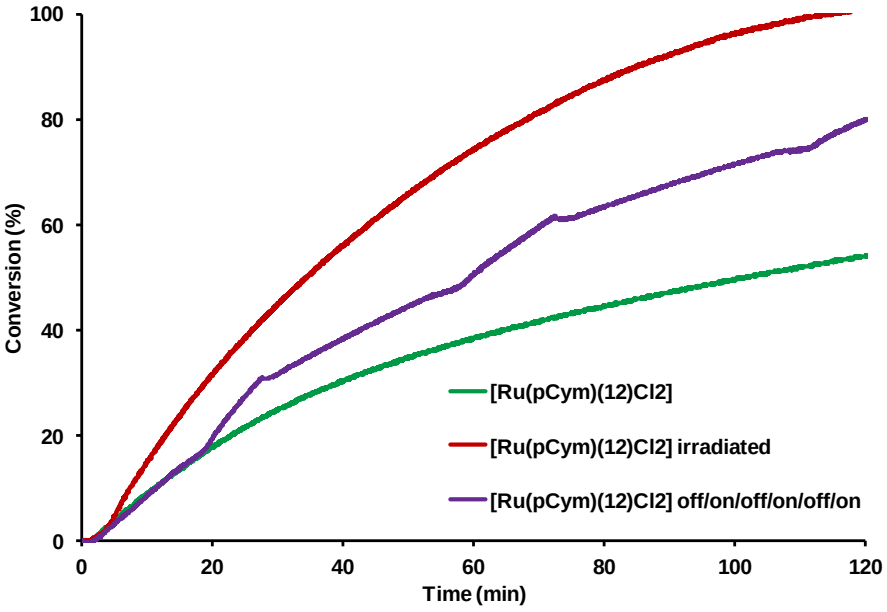

Figure 5.31. Reaction profiles (conversion *vs*. time) obtained for the hydrolytic dehydrogenation of AB with [Ru(*p*-Cym)(1**2**)Cl_2] without irradiation (green line), under continuous irradiation (red line) and combining irradiation and no irradiation periods (purple line). Incubation in 0.375 mL of distilled THF, reaction solvent 1.5 mL THF/H_2O = 1/3 (v/v), [cat] = $2.3 \cdot 10^{-3}$ M, [AB]/[cat] = 200.

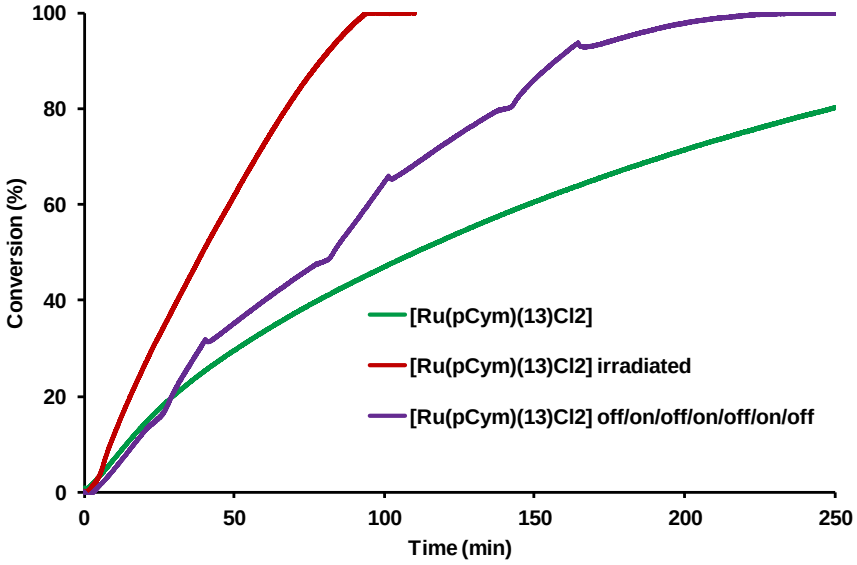

Figure 5.32. Reaction profiles (conversion *vs*. time) obtained for the hydrolytic dehydrogenation of AB with [Ru(*p*-Cym)(1**3**)Cl_2] without irradiation (green line), under continuous irradiation (red line) and combining irradiation and no irradiation periods (purple line). Incubation in 0.375 mL of distilled THF, reaction solvent 1.5 mL THF/H_2O = 1/3 (v/v), [cat] = $2.3 \cdot 10^{-3}$ M, [AB]/[cat] = 200.

The reaction profiles obtained for catalytic systems irradiated at different periods of time, show alternating slopes (rates) consistent with the reaction profiles corresponding to irradiated and no irradiated experiments. Consequently these Ru(II) systems containing azobenzene-appended phosphine ligands behave as phototunable hydrogen generation catalysts.

5.3. CONCLUSIONS

On the one hand, ten complexes of the type [Ru(*p*-Cym)(bipy)Cl]Cl (bipy = 4,4'-disubstituted-2,2'-bipyridine ligand) were synthesized, from which seven were not described before, and were fully characterized. The influence of the electron affinity of different substituents that is determined with the Hammett parameter was reflected in ^{1}H-NMR spectra of the complexes. A correlation between the Hammett parameters and chemical shifts was used to calculate Hammett parameters that were not published in the literature. The activity of these precatalysts for the hydrolytic dehydrogenation of AB was analyzed and a good correlation was obtained between the catalytic results and the Hammett parameter of each substituent, demonstrating the importance that electronic factors have on the reaction rate, being the complex containing 4,4'-dinitro-2,2'-bipyridine the most active from the series. With this compound several reaction parameters have been optimized, and first order KIE effects were observed when D_2O was used as co-solvent. Altogether constitute important key-information to unravel the reaction mechanism.

On the other hand, eight new photoswitchable Ru (II) complexes with azobenzene-containing bipyridine, pyridine and phosphine ligands were synthesized and fully characterized. The photoisomerization of these complexes was studied by UV-Vis spectroscopy and the influence of this process was reflected in their catalytic activity for the hydrolytic dehydrogenation of AB.

Complexes containing the photochromic unit in the bipyridine ligand did not exhibited significant differences in the catalytic activities, but they were slightly more effective when the catalytic systems were irradiated.

The catalytic activity of the complex containing two monodentate 4-phenylazopyridines was not influenced by irradiation, but the neutral complex containing two 4-phenylazopyridines showed a peculiar reaction profile when it was not irradiated. To explore the nature of this unusual activity, [Ru(*p*-Cym)(pyridine)Cl_2] and [Ru(*p*-Cym)(pyridine)$_2$Cl]PF were synthesized and used as precatalysts, obtaining the same results of the analogous complexes containing photochromic units. The homogeneity of the catalytic system of [Ru(*p*-Cym)(pyridine)Cl_2] was confirmed by mercury poisoning experiment. Additional experiments were carried out with the precatalyst [Ru(*p*-Cym)(**2**)Cl_2] combining irradiation and no irradiation periods. Results showed that these precatalysts required an activation period that was accelerated with irradiation, probably due to light-induced ligand dissociation.

The complexes incorporating azobenzene-containing triarylphosphines showed the most significant changes in their catalytic activities upon irradiation, in accordance with

results obtained for the photoisomerization studies (these complexes showed important changes in their absorption spectra through irradiation and presented longer half-life time of the *cis* form). To confirm that the improved catalytic activity observed for these complexes under irradiation was due to the photoisomerization of the azobenzene fragment, the complex [Ru(*p*-Cym)(PPh_3)Cl_2] was synthesized and used as precatalyst for the hydrolytic dehydrogenation of AB. The irradiation did not affect its catalytic activity, proving that the catalytic activity of [Ru(*p*-Cym)(**12**)Cl_2] and [Ru(*p*-Cym)(**13**)Cl_2] was improved because of the isomerization of the azobenzenes and light-induced displacement of the PPh_3 ligand was discarded. An additional experiment was carried out combining irradiation and no irradiation periods, confirming this hypothesis and the reversibility of the process.

5.4. REFERENCES

[1] C. W. Hamilton, R. T. Baker, A. Staubitz and I. Manners, *Chem. Soc. Rev.*, **2009**, *38*, 279–293.

[2] S. Dutta, *J. Ind. Eng. Chem.*, **2014**, *20*, 1148–1156.

[3] P. Wang and X.-D. Kang, *Dalton Trans.*, **2008**, 5400–5413.

[4] M. Zahmakiran, T. Ayvali and K. Philippot, *Langmuir*, **2012**, *28*, 4908–4914.

[5] C. A. Jaska, K. Temple, A. J. Lough and I. Manners, *J. Am. Chem. Soc.*, **2003**, *125*, 9424–9434.

[6] M. E. Sloan, T. J. Clark and I. Manners, *Inorg. Chem.*, **2009**, *48*, 2429–2435.

[7] L. J. Sewell, M. A. Huertos, M. E. Dickinson and A. S. Weller, *Inorg. Chem.*, **2013**, *52*, 4509–4516.

[8] N. Blaquiere, S. Diallo-Garcia, S. I. Gorelsky, D. A. Black and K. Fagnou, *J. Am. Chem. Soc.*, **2008**, *130*, 14034–14035.

[9] D. F. Schreiber, C. O'Connor, C. Grave, Y. Ortin, H. Müller-Bunz and A. D. Phillips, *ACS Catal.*, **2012**, 2505–2511.

[10] S. Duman and S. Özkar, *International Journal of Hydrogen Energy*, **2013**, *38*, 180–187.

[11] M. C. Denney, V. Pons, T. J. Hebden, D. M. Heinekey and K. I. Goldberg, *J. Am. Chem. Soc.*, **2006**, *128*, 12048–12049.

[12] A. Staubitz, A. P. Soto and I. Manners, *Angew. Chem. Int. Ed. Eng.*, **2008**, *47*, 6212–6215.

[13] M. A. Esteruelas, I. Fernández, A. M. López, M. Mora and E. Oñate, *Organometallics*, **2014**, *33*, 1104–1107.

[14] J. R. Vance, A. Schäfer, A. P. M. Robertson, K. Lee, J. Turner, G. R. Whittell and I. Manners, *J. Am. Chem. Soc.*, **2014**, *136*, 3048–3064.

[15] A. Rossin, G. Bottari, A. M. Lozano-Vila, M. Paneque, M. Peruzzini, A. Rossi and F. Zanobini, *Dalton Trans.*, **2013**, *42*, 3533–3541.

[16] B. L. Conley and T. J. Williams, *Chem. Commun.*, **2010**, *46*, 4815–4817.

[17] B. L. Conley, D. Guess and T. J. Williams, *J. Am. Chem. Soc.*, **2011**, *133*, 14212–14215.

[18] Z. Lu, B. L. Conley and T. J. Williams, *Organometallics*, **2012**, *31*, 6705–6714.

[19] X. Zhang, L. Kam and T. J. Williams, *Dalton Trans.*, **2016**, *45*, 7672–7677.

[20] R. J. Keaton, J. M. Blacquiere and R. T. Baker, *J. Am. Chem. Soc.*, **2007**, *129*, 1844–1845.

[21] G. C. Fortman, A. M. Z. Slawin and S. P. Nolan, *Organometallics*, **2011**, *30*, 5487–5492.

[22] T. Umegaki, J. M. Yan, X.-B. Zhang, H. Shioyama, N. Kuriyama and Q. Xu, *Int. J. Hydrogen Energy*, **2009**, *34*, 2303–2311.

[23] Q. Xu and M. Chandra, *Journal of Alloys and Compounds*, **2007**, *446–447*, 729–732.

[24] Q. Xu and M. Chandra, *J. Power Sources*, **2006**, *163*, 364–370.

[25] M. Chandra and Q. Xu, *J. Power Sources*, **2006**, *156*, 190–194.

[26] H. Wang, Y. Zhao, F. Cheng, Z. Tao and J. Chen, *Catal. Sci. Technol.*, **2016**, *6*, 3443–3448.

[27] R. Ciganda, M. A. Garralda, L. Ibarlucea, E. Pinilla and M. R. Torres, *Dalton Trans.*, **2010**, *39*, 7226–7229.

[28] M. A. Garralda, C. Mendicute-Fierro, A. Rodríguez-Diéguez, J. M. Seco, C. Ubide and I. Zumeta, *Dalton Trans.*, **2013**, *42*, 11652–11660.

[29] C. Boulho and J.-P. Djukic, *Dalton Trans.*, **2010**, *39*, 8893–8905.

[30] D. J. Nelson, B. J. Truscott, J. D. Egbert and S. P. Nolan, *Organometallics*, **2013**, *32***,** 3769–3772.

[31] T. W. Graham, C.-W. Tsang, X. Chen, R. Guo, W. Jia, S.-M. Lu, C. Sui-Seng, C. B. Ewart, A. Lough, D. Amoroso and K. Abdur-Rashid, *Angew. Chem. Int. Ed. Eng.*, **2010**, *49*, 8708–8711.

[32] V. San Nacianceno, L. Ibarlucea, C. Mendicute-Fierro, A. Rodríguez-Diéguez, J. M. Seco, I. Zumeta, C. Ubide and M. A. Garralda, *Organometallics*, **2014**, *33*, 6044–6052.

[33] X. Hu, M. Soleilhavoup, M Melaimi, J. Chu and and G. Bertrand, *Angew. Chem. Int. Ed.*, **2015**, *54*, 6008–6011.

[34] L. Shi, Y. Liu, Q. Liu, B. Wei and G. Zhang, *Green Chem.*, **2012**, *14*, 1372–1375.

[35] M. Muñoz-Olasagasti, A. Telleria, J. Perez-Miqueo, M. A. Garralda and Z. Freixa, *Dalton Trans.*, **2014**, *43*, 11404–11409.

[36] R. Kumar and B. R. Jagirdar, *Inorg. Chem.*, **2013**, *52*, 28–36.

[37] G. Alcaraz and S. Sabo-Etienne, *Angew. Chem. Int. Ed. Eng.*, **2010**, *49*, 7170–7179.

[38] C. Y. Tang, A. L. Thompson and S. Aldridge, *J. Am. Chem. Soc.*, **2010**, *132*, 10578–10591.

[39] H. C. Johnson, A. P. M. Robertson, A. B. Chaplin, L. J. Sewell, A. L. Thompson, M. F. Haddow, I. Manners and A. S. Weller, *J. Am. Chem. Soc.*, **2011**, *133*, 11076–11079.

[40] C. J. Stevens, R. Dallanegra, A. B. Chaplin, A. S. Weller, S. A. Macgregor, B. Ward, D. McKay, G. Alcaraz and S. Sabo-Etienne, *Chem. Eur. J*, **2011**, *17*, 3011–3020.

[41] T. M. Douglas, A. B. Chaplin and A. S. Weller, *J. Am. Chem. Soc.*, **2008**, *130*, 14432–14433.

[42] T. M. Douglas, A. B. Chaplin, A. S. Weller, X. Yang and M. B. Hall, *J. Am. Chem. Soc.*, **2009**, *131*, 15440–15456.

[43] A. N. Marziale, A. Friedrich, I. Klopsch, M. Drees, V. R. Celinski, J. Schmedt auf der Günne and S. Schneider, *J. Am. Chem. Soc.*, **2013**, *135*, 13342–13355.

[44] Z. Freixa and M. A. Garralda, *Inorg. Chim. Acta*, **2015**, *431*, 184–189.

[45] Y. Himeda, *Green Chem.*, **2009**, *11*, 2018–2022.

[46] R. R. Dykeman, K. L. Luska, M. E. Thibault, M. D. Jones, M. D. Jones, M. Schlaf, M. Khanfar, N. J. Taylor, J. F. Britten and L. Harrington, *Journal of Molecular Catalysis A: Chemical*, **2007**, *277*, 233–251.

[47] A. Kopecky, G. Liu, A. Agushi, A. G. Agrios, E. Galoppini, *Tetrahedron*, **2014**, *70*, 6271–6275.

[48] C. E. Welby, G. K. Armitage, H. Bartley, A. Wilkinson, A. Sinopoli, B. S. Uppal, C. R. Rice, P. I. P. Elliott, *Chem. Eur. J.* **2014**, *20*, 8467–8476.

[49] C. Hansch, A. Leo and R. W. Taft, *Chem. Rev.*, **1991**, *91*, 165–195.

[50] S. J. Dickson, M. J. Paterson, C. E. Willans, K. M. Anderson and J. W. Steed, *Chem. Eur. J.*, **2008**, *14*, 7296–7305.

[51] C. A. Vock, C. Scolaro, A. D. Phillips, R. Scopelliti, G. Sava and P. J. Dyson, *J. Med. Chem.*, **2006**, *49*, 5552–5561.

[52] E. Hodson and S. J. Simpson, *Polyhedron*, **2004**, *23*, 2695–2707.

[53] M. Kaiser, S. P. Leitner, C. Hirtenlehner, M. List, A. Gerisch and U. Monkowius, *Dalton Trans.*, **2013**, *42*, 14749–14756.

[54] A. Amar, P. Savel, H. Akdas-Kilig, C. Katan, H. Meghezzi, A. Boucekkine, J.-P. Malval and J.-L. Fillaut, *Chem. Eur. J.*, **2015**, *21*, 8262–8270.

[55] T. Yutaka, I. Mori, M. Kurihara, J. Mizutani, K. Kubo, S. Furusho, K. Matsumura, N. Tamai and H. Nishihara, *Inorg. Chem.*, **2001**, *40*, 4986–4995.

[56] O. S. Wenger, L. M. Henling, M. W. Day, J. R. Winkler and H. B. Gray, *Polyhedron*, **2004**, *23*, 2955–2958.

[57] www.manonthemoontech.com

[58] X. Yang, T. Fox and H. Berke, *Chem. Commun.*, **2011**, *47*, 2053–2055.

[59] M. C. Carrión, M. Ruiz-Castañeda, G. Espino, C. Aliende, L. Santos, A. M. Rodríguez, B. R. Manzano, F. A. Jalón and A. Lledós, *ACS Catal.*, **2014**, *4*, 1040–1053.

[60] C. A. Jaska and I. Manners, *J. Am. Chem. Soc.*, **2004**, *126*, 9776–9785.

[61] S. Betanzos-Lara, L. Salassa, A. Habtemariam and P. J. Sadler, *Chem. Commun.*, **2009**, 6622–6624.

[62] F. Barragán, P. López-Senín, L. Salassa, S. Betanzos-Lara, A. Habtemariam, V. Moreno, P. J. Sadler and V. Marchán, *J. Am. Chem. Soc.*, **2011**, *133*, 14098–14108.

CHAPTER 6

GENERAL CONCLUSIONS AND FUTURE WORK

According to the main objectives proposed during the thesis, general conclusions and future work are presented in this chapter.

CHAPTER 2

- A new synthetic procedure was developed to obtain azobenzene-appended bipyridines, which was much direct than previously reported methodologies.
- Bipyridyl type ligands were synthesized incorporating either one or two azobenzene fragments per ligand.
- A new azobenzene-containing phosphine ligand was synthesized (**13**), besides the already reported ligand **12**, both incorporating three photochromic moieties.
- All the azobenzene-containing ligands showed important changes upon irradiation but phosphine ligands **12** and **13** were the ones that presented the lowest reaction rate constants for the *Z*→*E* isomerization, indicating the larger stability of the *cis* form in these ligands compared to azobenzene-containing bipyridines and pyridine.
- The ^{1}H-NMR chemical shifts of 4,4'-functionalized 2,2'-bipyridines were correlated with the Hammett values (σ_p^+) of the substituent on 4,4'-position.
- The Hammett values (σ_p^+) of diethylphosphonate and azido substituents (not published in the literature) were interpolated from their ^{1}H-NMR chemical shifts.

➢ As the most promising results were obtained for azobenzene-containing phosphines, in the future related ligands will be synthesized, but incorporating functionalized-azobenzene fragments.

CHAPTER 3

- The synthesized Ir(III) complexes incorporating diethylphosphonate or carboxy anchoring groups showed to be effective linkers to anchor organometallic dyes on the TiO_2 surface.
- Complexes containing diethylphosphonate anchoring groups exhibited more stable linkage to the TiO_2 surface than the carboxy analogous. Nevertheless the latest showed higher absorptivities when they were anchored to TiO_2 surfaces.
- Better efficiencies were obtained for cells sensitized with carboxylate complexes than for cells sensitized with diethylphosphonates.
- Although it was not possible to construct cells sensitized with photochromic compounds during the time-frame of this thesis, these complexes should be good candidates because they absorb at longer wavelengths and exhibit higher absorptivities than parent complexes without azobenzene fragments.

- The synthesis of Ir(III) complexes incorporating mixed ligands with both phosphonate and carboxylates is currently under development to use as dyes for DSSCs.

- The efficiency of DSSCs based on the azobenzene-appended dyes is currently being evaluated.

CHAPTER 4

- The photoisomerization of Ir(III) complexes studied by UV-Vis was inhibited in most of the cases. Complexes incorporating ligands **3** and **4** showed the most notorious changes upon irradiation, concluding that the isomerization is favored when the azobenzene is further from the metal center.
- A qualitative analysis of the compounds indicated that the characteristic phosphorescence of this type of compounds was inhibited due to the presence of the azobenzene.
- The incompatibility of the azobenzene and the photoluminescence in these compounds was attributed to alternative relaxation pathways of the excited states.

- To analyze if the photoluminescence of these complexes could be recovered, a preliminary experiment of *in situ* reduction of the azobenzene fragment was carried out, with unclear results. A more accurate study is required to determine if, as reported in the bibliography for related compounds, they could be used as phosphorescent sensors for reducing agents.

- New designs with less electronic communication (not conjugated) between the azobenzene and the metal center should be developed to achieve compounds both phosphorescent and photoswitchable.

CHAPTER 5

- A good correlation was obtained between the catalytic results obtained in hydrolysis of ammonia borane and the Hammett parameter of substituents on 4,4'-position of the 2,2'-bipyridines. So the catalytic activity of these type of precatalysts can be predicted (on a qualitative manner) with the Hammett value of the substituents on 4,4'-position of the 2,2'-bipyridines.
- The photoisomerization of photochromic Ru(II) complexes was strongly inhibited for complexes which contain the azobenzene as part of the bipyridine or pyridine ligand. However it was effective for complexes containing other

bipyridines (where the azobenzene was appended to the bipyridine) and even more effective for Ru(II) derivatives of azobenzene-containing phosphine ligands.

- The complexes incorporating azobenzene-containing triarylphosphines showed the most significant changes in their catalytic activities upon irradiation, in accordance with results obtained for the photoisomerization studies, and constitute our first example of phototunable catalysts.

- Some experiments to study the light-induced dissociation of a pyridyl ligand, in order to rationalize some of the reaction profiles observed are currently under development.
- New complexes containing azobenzene-appended phosphines incorporating additional functionalities on the substituents, in order to maximize the effect of the photoisomerization will be developed.
- The study of these compounds in related reactions (such us transfer hydrogenation, selective deuterations, etc.) will be pursued in the future.

Although it was not included in this manuscript, currently two side-projects are under development:

1- **Application of ruthenium containing azobenzene-appended ligands as anticancer drugs**. Some of the compounds developed in this thesis are being studied as potential drugs for cancer therapy. Preliminary results showed outstanding activities for some of the derivatives, and indicate that the presence of azobenzene units conjugated through a bipyridyl units responsible of such activity. More detailed studies to confirm the mechanism of action and the scope of these compounds as anti-cancer drugs are currently being developed in collaboration with Prof. Luca Salassa (UPV-EHU) and Prof Walter Berger (Medical University of Vienna).

2- Bipyridines incorporating the 2,1,3-benzothiadiazole (BTD) fragment. Currently, as part of a Final Degree Project, new bipyridine ligands incorporating both the highly phosphorescent BTD fragment and azobenzenes, are being developed. Their iridium(III) and Ru(II) derivatives are being synthesized and studied for potential applications. This work is performed by Maitane Vázquez, and supervised by Zoraida Freixa and Ainara Telleria, and is developed in the frame of a collaboration with the group of Prof. Jairton Dupont (University of Nottingham).

SUMMARY

Photochromic compounds have been used for long time for the construction of photoswitchable materials able to change their properties (*e. g.* emission intensity or wavelength, refractive index, electronic conduction, electrochemical response, magnetic interactions, self-assembling behaviour of molecules, solubility, etc.) by action of light. In spite of the large number of applications that known for organometallic complexes, the examples of metal complexes that incorporate photochromic units in their structures are rather limited compared to the organic counterparts. This is a relatively recent area of research, that has attracted great interest for two different reasons, depending on the final purpose of the compound. On the one hand due to the possibility to modify the isomerization capacity of the photochromic unit as a consequence of the coordination to the metal center and on the other hand, because by incorporation of photochromic units, eventually the properties of metal-complexes can be changed by light. The latter opens a full range of possibilities. Eventually, all the areas where organometallic compounds are applied could be transformed into light-controlled applications.

This thesis focuses on the development of photochromic-organometallic compounds, and constitutes a preliminary study of potential applications.

The photochromic unit chosen for this study is the azobenzene, which is probably the most widely used molecular switch. The azobenzene undergoes a reversible photoisomerization process from its most stable isomer *E* (*trans*) to the *Z* (*cis*) form upon irradiation with a specific wavelength light. The reverse process takes place by irradiation with a different specific wavelength light, heating or spontaneously in the dark. This isomerization process induces important steric and electronic changes in the molecule. The *E* isomer is planar and the electronic conjugation that exists in this form is disrupted with the *trans*-to-*cis* photoisomerization. As a consequence, photophysical properties and the dipole moment of the azobenzene also change, modifying for example its solubility, ^{1}H-NMR, UV-Vis spectra, etc., which can be used to monitor the extent of the photoisomerization process.

The main objective of this thesis is to develop organometallic complexes incorporating the azobenzene moiety in the structure of the coordinated ligands. The aim is to modify the properties of these complexes through the photoisomerization of the photochromic unit. Eventually, the modification of their properties should affect the behaviour of organometallic complexes in different applications. Namely organometallic Ir(III) and Ru(II) complexes containing azobenzene fragments have been synthesized, and

studied in different applications: as dyes for dye-sensitized solar cells (DSSCs), as phosphors for light-emitting electrochemical cells (LECs) and as catalysts for hydrogen generation. However, model complexes not incorporating the azobenzene fragment have also been synthesized and studied for comparative purposes.

In Chapter 1 a brief introduction of photochromic compounds that have attracted most interest and a more extended description of the azobenzene unit are presented. As in this thesis the azobenzene moiety is mainly incorporated in organometallic complexes as a part of bipyridine and phosphine ligands, an overview of already reported examples of transition metal complexes incorporating azobenzene-containing bipyridines and phosphines is included. Few azobenzene-containing bipyridines are reported in the literature. To the best of our knowledge, only four research groups have published this type of ligands and in most of the cases the photoisomerizaton of the azobenzene is reduce or even inhibited upon coordination to metal complexes. There are also few examples of azobenzene-containing phosphines but there is only one example in which the photoisomerization of the azobenzene in oraganometallic azobenzene-appended phosphines has been successfully exploited.

In Chapter 2 all the ligands involved in the thesis are presented. This chapter is divided in two parts. In the first one the synthetic procedures to obtain azobenzene-containing bipyridines, pyridines and phosphines are described, together with the photoisomerization study of all these ligands monitored by UV-Vis spectroscopy. Reaction rate constants and half-life times of the *Z* to *E* isomerization process of the azobenzenes are calculated to know the stability of the *Z* form in each ligand. For further applications it is essential to have stable *cis* forms, to produce significant and long-term lasting changes which are required for most of the applications.

In the second part of this chapter, the syntheses of 4,4'-disubstituted-2,2'-bipyridines is described. These ligands are designed to obtain bipyridines containing substituents with different electronic properties, used for the study of model compounds in some of the studied applications. The electron affinity of each substituent is quantified by the Hammett parameter (σ_p^+), and the influence of this parameter is reflected in ^{1}H-NMR of different ligands. Through the correlation obtained between the σ_p^+ and selected ^{1}H-NMR chemical shifts it is possible to calculate unknown σ_p^+ values of different substituents.

Once described the general aim of the thesis and all the ligands used to achieve this goal, as well as other ligands for additional purposes, in subsequent chapters the

synthesis and screening of applications of Ir(III) and Ru(II) complexes incorporating these ligands are presented.

In Chapter 3 complexes of type $[Ir(C–N)_2(bipy)]PF_6$ are synthesized to be used as dyes for DSSCs. In an introductory part the operating mode of DSSCs and fundamental measurements that are performed to analyze their performance is explained. These cells are able to convert solar light into electrical energy using light harvesting materials (dyes). The most widely used dyes are Ru(II) complexes, but because of the limited type of ligands that can be introduced easily in this class of compounds, in recent years Ir(III) complexes gained much attention. Ir(III) easily forms bis- and tris-cyclometalated complexes with high thermal and chemical stability and long excited-state lifetimes. The drawback is that low efficiencies are obtained with Ir(III) complexes. Although there is still much to improve on Ir(III) based dyes, they are promising candidates that eventually could replace the Ru(II) complexes as dyes in DSSCs.

Complexes of type $[Ir(C–N)_2(bipy)]PF_6$ containing two phenylpyridine ligands and one bipyridine as ancillary ligand have been synthesized. On one hand, complexes containing specific functionalities (diethylphosphonates and carboxy groups) were synthesized. The anchoring functionality was introduced on the bipyridine to immobilize the potential dyes on the surface of TiO_2. On the other hand, iridium(III) complexes containing azobenzene fragments on the cyclometalated phenylpyridine ligands have been also synthesized. As an important characteristic of light harvesting materials is that they have to absorb strongly and preferably in the visible region, the absorption of the synthesized complexes is studied by UV-Vis. Additionally, the group of Dr. Marcos Jose Leite (Universidade Federal do Rio Grande do Sul) has studied the anchoring of our complexes to TiO_2 surfaces and constructed DSSCs sensitized with some of our complexes. They also analyzed their performance and compared the performance of complexes incorporating either diethylphosphonates and carboxy groups. The methodology used to assemble these cells is described in this chapter. The absorptivities of the dyes are compared with absorptivities of dyes adsorbed on TiO_2 surfaces. The desorption of Ir(III) complexes from the TiO_2 surface in aqueous media is also studied.

Complexes containing diethylphosphonate anchoring groups exhibited more stable linkage to the TiO_2 surface than the carboxy analogous. Nevertheless the latest showed higher absorptivities when they were anchored to TiO_2 surfaces and better efficiencies were obtained for cells sensitized with these complexes than for cells sensitized with diethylphosphonates.

Similar complexes are synthesized in Chapter 4, but for a different application. In this case, to use as luminescent compounds on LECs, that are low energy consumption devices used in many screen devices (computers, mobile phones, TVs, watches, etc.). These devices are actually replacing the liquid-crystal displays (LCDs), because of the higher efficiencies, improved brightness and longer lifetimes. Phosphorescent cationic iridium(III)-cyclometalated complexes are exceptional candidates for this application, because they are able to originate a very efficient light emission when are placed between two electrodes and a voltage is applied. The color of the emission can be tuned by little variations on these ligands. In this chapter, $[Ir(C–N)_2(bipy)]PF_6$ type complexes incorporating photochromic fragments are synthesized intended to change the color of the emission with the isomerization of the azobenzene.

This chapter is divided in two parts. In the first one, model complexes of type $[Ir(C–N)_2(bipy)]PF_6$ have been synthesized, with different ancillary ligands: 2,2'-bipyridine, 1,10-phenanthroline and 4,4'-dibromo-2,2'-bipyridine. As in Chapter 3, different cyclometalated ligands have been used and azobenzene fragments have been introduced in (C–N) ligands by *posteriori* reactions over the complexes.

In the second part, azobenzenes are introduced in the ancillary bipyridine type ligand before the synthesis of Ir(III) complexes and the photochromic units are introduced in the complex as part of the ancillary ligand. Once Ir(III) complexes are synthesized, additional azobenzene moieties are also incorporated through *a posteriori* reactions over the complexes. In this way, Ir(III) complexes containing up to four azobenzene fragments have been synthesized. The photoisomerization of the complexes has been studied and compared with the results obtained for the free ligands in Chapter 2, to analyze the effect of metal-coordination on the photochromic behaviour of the azobenzene unit. As the color of the emission of these type of complexes is related to the energy gap between HOMO and LUMO orbitals, cyclic voltammetry measurements, UV-Vis characterization and TD-DFT calculations were performed to analyze the influence of different ancillary ligands and substituents on the cyclometalated ligands on the HOMO and LUMO orbitals.

Unfortunately, the photoisomerization of Ir(III) complexes studied in this chapter was inhibited in most of the cases. It was a bit more efficient when the azobenzene was further from the metal center. The phosphorescence of these complexes was also inhibited. The incompatibility of the azobenzene and the photoluminescence in these compounds was attributed to alternative relaxation pathways of the excited states.

In Chapter 5 complexes of type [Ru(*p*-Cym)(bipy)Cl]Cl are synthesized to use as precatalysts for the hydrolytic dehydrogenation of amine-borane adducts. These adducts have been used as hydrogen storage materials because they contain high hydrogen content and light-weight elements. In the introduction of these chapter, different amine-borane adducts are presented and different pathways for the controlled hydrogen liberation from these adducts are described (dehydrogenation and solvolysis). An overview of precedent reports of both dehydrogenation and solvolysis of amine-borane adducts is included in the introduction of this chapter. A more detailed description of our publications of hydrolytic dehydrogenation of amine-borane adducts with the precatalyst [Ru(*p*-Cym)(bipy)Cl]Cl is also presented. The lower price of the ruthenium compared to iridium and the simplicity of the ligands are the main characteristics that made this system appealing.

This chapter covers two different objectives. On one hand, in view of the high efficiency of the [Ru(*p*-Cym)(bipy)Cl]Cl, previously described in our group, the effect that electronic modifications have on its activity for the hydrolytic dehydrogenation of AB adducts is studied. For this purpose, [Ru(*p*-Cym)(bipy)Cl]Cl complexes are synthesized with 4,4'-functionalized 2,2'-bipyridine ligands. The electron affinity of different substituents is determined with the Hammett parameter (σ_p^+) and the catalytic activity of precatalysts containing different substituents on the bipyridine ligand is correlated with σ_p^+ values of the corresponding substituents. Using the most effective precatalyst, a detailed kinetic isotope effect (KIE) study is performed to get some insight on the reaction mechanism for this catalytic system. All the results obtained will be combined with theoretical calculations (DFT) and *in situ* MS experiments to propose a reaction mechanism compatible with all the experimental observations.

On the other hand, photochromic compounds analogues to the [Ru(*p*-Cym)(bipy)Cl]Cl but containing azobenzene moieties are synthesized, intended to develop phototunable catalysts. The azobenzene moiety is introduced either in bipyridine, pyridine or phosphine ligands presented in Chapter 2. All the photochromic ligands described in Chapter 2 are used to construct the ruthenium(II) complexes described in Chapter 5. They are compounds of type [Ru(*p*-Cym)(bipy)Cl]Cl, [Ru(*p*-Cym)(py)Cl_2], [Ru(*p*-Cym)(py)$_2$Cl]PF_6 and [Ru(*p*-Cym)(phosphine)Cl_2]. The influence of the isomerization of the azobenzene on the catalytic activity for the hydrolytic dehydrogenation of AB is analyzed comparing standard experiments with results obtained irradiating the catalytic systems.

Complexes containing the azobenzene fragments on the bipyridine ligands showed similar activities upon irradiation. A peculiar change was observed for the complex of

type [Ru(*p*-Cym)(py)Cl_2] containing one phenylazopyridine. Complexes incorporating azobenzene-containing triarylphosphines showed the most significant changes in their catalytic activities upon irradiation. To confirm that the reason of changing the activities of these complexes is the photoisomerization of azobenzene fragments, [Ru(*p*-Cym)(pyridine)Cl_2], [Ru(*p*-Cym)(pyridine)$_2$Cl]PF_6 and [Ru(*p*-Cym)(PPh_3)Cl_2] model complexes have been synthesized and their activities obtained upon irradiation have been compared with standard experiments (not irradiation). The complex [Ru(*p*-Cym)(pyridine)Cl_2] showed the same results of the analogous complexes containing photochromic units, demonstrating that the azobenzene was not the responsible of changing the activity of these complexes. However irradiation did not affect the catalytic activity of the precatalyst [Ru(*p*-Cym)(PPh_3)Cl_2], proving that the catalytic activity of precatalysts incorporating azobenzene-containing triarylphosphines was modified because of the isomerization of the azobenzenes. Therefore, these are our first examples of phototunable catalysts.

According to the main objectives proposed, the general conclusions and future work are presented in Chapter 6.

RESUMEN

Los compuestos fotocrómicos se han utilizado desde hace mucho tiempo para la construcción de los llamados interruptores moleculares. Son compuestos capaces de cambiar sus propiedades (p. ej. la intensidad o longitud de onda de emisión, el índice de refracción, la conductividad, la respuesta electroquímica, interacciones magnéticas, el comportamiento de auto-ensamblaje de las moléculas, la solubilidad, etc.) por acción de la luz. Sorprendentemente, a pesar del gran número de aplicaciones conocidas para los complejos organometálicos, hay pocos ejemplos de complejos organometálicos que incorporen fragmentos fotocrómicos en comparación con el gran número de derivados orgánicos estudiados. Esta es, por lo tanto, una área poco estudiada pero muy interesante, y que ha despertado gran interés en los últimos años. Los estudios publicados pueden dividirse en dos tipos: los que analizan la variación en la capacidad de isomerización del grupo fotocrómico por la coordinación al metal, o bien los estudios relacionados con cómo estos compuestos organometálicos pueden cambiar sus propiedades por acción de la luz. Esta última abre un amplio abanico de posibilidades. En principio, todas las áreas en las que los compuestos organometálicos encuentran aplicación podrían evolucionar hacia aplicaciones fotocontroroladas.

Esta tesis se basa en el desarrollo de complejos organometálicos fotocrómicos y constituye un estudio preliminar de sus posibles aplicaciones.

Para el desarrollo de este trabajo se ha escogido el que probablemente es el interruptor molecular más utilizado, el azobenceno. Esta molécula experimenta una isomerización de la forma *E* (*trans*) a la forma *Z* (*cis*) con la irradiación de la luz de una determinada longitud de onda. El proceso opuesto se puede dar tanto irradiando con luz de una longitud de onda determinada, con calor o en la oscuridad (puesto que la forma *trans* es la termodinámicamente más estable). Este proceso produce importantes cambios estéricos y electrónicos en la molécula, ya que el isómero *E* es plano y en esta forma existe conjugación electrónica extendida a lo largo de toda la molécula, la cual se pierde con la isomerización a la forma *Z*. De este modo, cambian muchas de sus propiedades, por ejemplo sus propiedades fotofísicas o el momento dipolar de la molécula, modificando por ejemplo su solubilidad, los espectros de RMN y UV-Vis, etc. Por esta razón estas técnicas espectroscópicas se pueden utilizar para seguir el proceso de isomerización del azobenceno.

El objetivo principal de esta tesis es desarrollar complejos organometálicos que incorporen el fragmento azobenceno en los ligandos, para modificar las propiedades de los complejos a través de la fotoisomerización. En principio, el cambio de las

propiedades de estos complejos debería influir también en su comportamiento de estos complejos en distintas aplicaciones. Para ello, se han sintetizado complejos de Ir(III) y Ru(II) que incorporan el azobenceno y se han estudiado en distintas aplicaciones: como pigmentos en celdas solares, como fosfores para celdas electroquímicas de emisión de luz y como catalizadores para la generación del hidrógeno.

En el Capítulo 1 se hace una pequeña introducción presentando algunos de los compuestos fotocrómicos más interesantes y se describe más detalladamente el azobenceno, que es el interruptor molecular en el que se basa este trabajo. Como el azobenceno se incorpora en complejos organometálicos como parte de los ligandos bipiridina y fosfina, se muestran los complejos organometálicos publicados anteriormente que contienen el azobenceno en este tipo de ligandos. Existen pocos ejemplos de bipiridinas que contienen el azobenceno, solamente cuatro grupos de investigación han publicado este tipo de ligandos. Además, en la mayoría de los casos se ha observado una inhibición de la fotoisomerizacion del azobenceno con la coordinación al metal. Tampoco hay muchos ejemplos de fosfinas que contengan azobencenos y en tan solo un caso se ha conseguido explotar la fotoisomerización del fragmento fotocrómico para aplicaciones catalíticas.

En el Capítulo 2 se presentan todos los ligandos involucrados en esta tesis. En la primera parte de este capítulo se muestran las bipiridinas, piridinas y fosfinas que contienen el grupo azobenceno y se estudia la fotoisomerización del azobenceno en dichos compuestos. El proceso de isomerización se estudia por espectroscopia de UV-Vis y se calculan la velocidad y el tiempo de vida media de la isomerización de la forma *cis* a la forma *trans* para cada ligando, de esta forma se analiza la estabilidad de la forma *cis* en distintos ligandos. Idealmente la forma *cis* debe ser estable para que la isomerización produzca cambios útiles para las distintas aplicaciones. Si la forma *cis* no fuese muy estable la molécula pasaría enseguida a la forma más estable, que es el *trans* y sería necesaria una irradiación continua para observar sus efectos.

En la segunda parte de este capítulo se explica la síntesis de bipiridinas que contienen distintos sustituyentes en las posiciones 4 y 4' para formar una familia de ligandos donde únicamente varíen sus propiedades electrónicas. Para cuantificar la afinidad electrónica de cada sustituyente se ha utilizado el parámetro de Hammett (σ_p^+) el cual se encuentra tabulado en la literatura para la mayoría de los sustituyentes. Este parámetro se ha correlacionado con las posiciones de las señales observadas para cada ligando en espectro de ^{1}H-RMN y así se han podido calcular los valores de σ_p^+ que no se encontraban en la literatura.

Después de explicar el objetivo general de la tesis y presentados todos los ligandos que se utilizaran a lo largo de la tesis, se procede a la síntesis de complejos y el estudio de las posibles aplicaciones.

En el Capítulo 3 se sintetizan complejos de tipo $[Ir(C–N)_2(bipi)]PF_6$ para utilizarlos como pigmentos en celdas solares. En la parte de la introducción de este capítulo se explica cómo funcionan las celdas solares y las medidas básicas que se realizan para analizar su rendimiento. Dichas celdas son capaces de crear corriente eléctrica a partir de la luz solar, absorbiendo la luz solar a través de los pigmentos. Los pigmentos más utilizados son complejos de Ru(II), aunque en los últimos años se ha mostrado mucho interés por reemplazarlos por complejos de Ir(III). El Ir(III) forma complejos ciclometalados con mayor facilidad que el Ru(II). Además los complejos ciclometalados de Ir(III) suelen ser muy estables y muestran tiempos de vida media de los estados excitados largos. La desventaja de estos últimos es que nos se consiguen rendimientos tan buenos como con los que contienen pigmentos de Ru(II), aun así son complejos prometedores pero que todavía hay que optimizar.

En este capítulo se sintetizan complejos de tipo $[Ir(C–N)_2(bipi)]PF_6$ que contienen dos ligandos de tipo fenilpiridina y una bipiridina. Por un lado se han sintetizado complejos que contienen grupos específicos (dietilfosfonato y carboxilato) en el ligando bipiridina para inmovilizar los complejos en una superficie de TiO_2. Por otro lado, se han sintetizado complejos que contienen el grupo azobenceno en el ligando fenilpiridina. Se ha estudiado la absorción de los complejos sintetizados por espectroscopia UV-Vis, ya que para esta aplicación es importante confirmar que los complejos absorben cerca de la región visible. Además, en el grupo de Dr. Marcos Jose Leite (Universidade Federal do Rio Grande do Sul) han estudiado el anclaje de algunos de nuestros complejos en superficies de TiO_2 y los han utilizado como pigmentos en celdas solares. Han estudiado la eficiencia de estas celdas, comparando entre sí aquellas en las que el complejo está anclado mediante grupos dietilfosfonato y carboxilato. En este capítulo se muestra el procedimiento que siguieron para la construcción de estas celdas. Las absortividades de los complejos en disolución se comparan con la capacidad de absorción de los pigmentos anclados en superficies de TiO_2 y se estudia la estabilidad de los dos grupos de anclaje en medio acuoso.

Los resultados obtenidos muestran que el anclaje de los complejos dietilfosfonato es más estable que el de los complejos carboxilato. Sin embargo los complejos que contienen grupos carboxilato absorben más luz cuando están anclados en superficies de TiO_2 y presentan mayores rendimientos que los complejos análogos que contienen grupos dietilfosfonato.

En el Capítulo 4 se sintetizan complejos muy parecidos a los del capítulo anterior pero con otro fin. En este caso, los complejos que se sintetizan son para utilizarlos como compuestos luminiscentes en celdas electroquímicas de emisión de luz (LECs). Estos son dispositivos de bajo consumo que se usan en dispositivos de pantalla (ordenadores, teléfonos móviles, televisores, relojes, etc.). En estos dispositivos se están reemplazando las pantallas actuales llamadas LCD (pantalla de cristal liquido) por las basadas en tecnología LEC, porque presentan mayor eficacia, mejor brillo y son más duraderos. Los complejos fosforescentes catiónicos de Ir(III) ciclometalados son candidatos apropiados para esta aplicación, ya que son capaces de emitir intensamente cuando están entre dos electrodos y se aplica un voltaje. El color de la emisión se puede cambiar con pequeñas modificaciones en los ligandos. En este capítulo se sintetizan complejos de tipo $[Ir(C–N)_2(bipi)]PF_6$ que incorporan fragmentos fotocrómicos con el objetivo final de cambiar el color de la emisión de los complejos con la isomerización del azobenceno.

Este capítulo se divide en dos partes. Por un lado se sintetizan los complejos modelo de tipo $[Ir(C–N)_2(bipi)]PF_6$, con distintos ligandos auxiliares: 2,2'-bipiridina, 1,10-fenantrolina y 4,4'-dibromo-2,2'-bipiridina. Como en el Capítulo 3, se han utilizado fenilpiridinas con distintos sustituyentes y se ha introducido el fragmento azobenceno en los ligandos fenilpiridina.

En la segunda parte, el azobenceno se introduce en el ligando bipiridina antes de la coordinación al metal. En algunos casos, después de la coordinación al metal se introducen más azobencenos en los ligandos fenilpiridina, llegando a obtener complejos que contienen hasta cuatro moléculas fotocrómicas por metal. Se ha estudiado la influencia de la coordinación al metal en la capacidad de fotoisomerización de los azobencenos en los complejos comparando con los resultados obtenidos en el Capítulo 2 para los ligandos libres. Como el color de la emisión de estos complejos está relacionado con la diferencia energética entre los orbitales HOMO y el LUMO de los complejos, se han realizado medidas de voltamperometría cíclica, espectroscopia UV-Vis y cálculos TD-DFT para analizar la influencia del ligando auxiliar y de los distintos sustituyentes en los ligandos ciclometalados en los orbitales HOMO y LUMO.

Desafortunadamente la fotoisomerización de la mayoría de los complejos de Ir(III) sintetizados en este capítulo es casi nula. Los complejos que han mostrado más capacidad de isomerización son los que contienen el azobenceno más alejado del metal. Los complejos fotocrómicos sintetizados tampoco presentan propiedades luminiscentes. La incompatibilidad del fragmento azobenceno y la fotoluminiscencia se

ha atribuido a distintas transiciones posibles que existen para los procesos de relajación de los estados excitados.

En el Capítulo 5 se han sintetizado catalizadores de tipo [Ru(*p*-Cym)(bipi)Cl]Cl para la deshidrogenación hidrolítica de aductos de amino-borano. Estos aductos se utilizan para el almacenaje de hidrogeno, por la gran cantidad de hidrogeno que contienen debido a que contienen elementos ligeros. En la introducción de este capítulo se presentan los distintos aductos de amino-borano y las distintas rutas que existen para la liberación del hidrogeno a partir de estos aductos (deshidrogenación y solvólisis). Se explican los precedentes que hay tanto de deshidrogenación como de solvólisis de aductos de amino-borano y se explica más detalladamente los precedentes de nuestro grupo en deshidrogenación de aductos de amino-borano mediante hidrólisis utilizando [Ru(*p*-Cym)(bipi)Cl]Cl como precatalizador. Este catalizador es muy prometedor, ya que el rutenio es más barato que el iridio y los ligandos que contiene este complejo son muy simples.

Este capítulo se divide en dos partes. Por un lado, a la vista de los resultado obtenidos por nuestro grupo para el catalizador [Ru(*p*-Cym)(bipi)Cl]Cl, se estudia la influencia que tiene la alteración electrónica en su actividad catalítica para la deshidrogenación de amino-borano mediante hidrólisis. Para ello se ha sintetizado una familia de complejos de [Ru(*p*-Cym)(bipi)Cl]Cl que solamente se diferencian en los sustituyentes de las posiciones 4 y 4' de la bipiridina. Se estudia la actividad catalítica de cada complejo y se correlaciona con el parámetro de Hammett (σ_p^+), que es el parámetro que se utiliza para determinar la afinidad electrónica de cada sustituyente. Para conocer más el mecanismo de esta reacción se realiza un estudio del efecto isotópico cinético con el catalizador que ha dado los mejores resultados. Todos los resultados obtenidos se combinaran con cálculos DFT y experimentos *in situ* de masas para proponer un mecanismo de reacción acorde a todas las observaciones.

Por otro lado se sintetizan complejos fotocrómicos análogos a los anteriores, que contienen fragmentos azobenceno en el ligando bipiridina, piridina o fosfina. Estos complejos se han diseñado para desarrollar catalizadores fotomodulables que cambien su actividad catalítica con la luz. Se han sintetizado complejos de tipo [Ru(*p*-Cym)(bipi)Cl]Cl, [Ru(*p*-Cym)(piridina)Cl_2], [Ru(*p*-Cym)(piridina)$_2$Cl]PF_6 y [Ru(*p*-Cym)(fosfina)Cl_2] utilizando todos los ligandos fotocrómicos descritos en el Capítulo 2. Se analiza el efecto de la isomerización del azobenceno en la actividad catalítica de estos sistemas comparando los resultados obtenidos en experimentos estándares de la deshidrogenación del amino-borano mediante hidrolisis, con los obtenidos cuando

los sistemas catalíticos son irradiados con una luz de una determinada longitud de onda.

Los catalizadores que incorporan el azobenceno en el ligando bipiridina no muestran cambios significantes en sus actividades catalíticas por la irradiación. En cambio el catalizador de tipo [Ru(*p*-Cym)(piridina)Cl_2] que contiene el azobenceno en un ligando de piridina, muestra un cambio peculiar al comparar los resultados estándares con los resultados obtenidos al irradiar el sistema catalítico. Pero entre todos, los cambios más significativos se observan para los que contienen fragmentos azobenceno en ligandos fosfina. Para confirmar que la razón por la que cambian la actividades catalíticas de estos compuestos es la isomerización del azobenceno, se han sintetizado complejos análogos que no incorporan ningún fragmento fotocrómico, [Ru(*p*-Cym)(piridina)Cl_2], [Ru(*p*-Cym)(piridina)$_2$Cl]PF_6 y [Ru(*p*-Cym)(PPh_3)Cl_2] y se ha estudiado el cambio de la actividad de estos complejos con la irradiación.

Se han obtenido los mismos resultados para el complejo [Ru(*p*-Cym)(piridina)Cl_2] y el análogo que contiene un azobenceno en la piridina, por lo que la isomerización del azobenceno no es el responsable de la peculiar actividad catalítica de este sistema bajo irradiación. Sin embargo, la irradiación del sistema catalítico no influye en los resultados obtenidos para el catalizador [Ru(*p*-Cym)(PPh_3)Cl_2], demostrando que los catalizadores que contienen azobencenos en las fosfinas cambian sus actividades catalíticas por la isomerización del azobenceno. Por lo tanto, estos son nuestros primeros ejemplos de catalizadores fotomodulables.

En el capítulo 6 se describen las conclusiones generales de esta tesis y el trabajo de futuro que se está desarrollando en la actualidad o queda pendiente.

APPENDIX

Publications

“Insights into the mechanism of the hydrolytic dehydrogenation of ammonia-borane using ruthenium(II) half-sandwich catalysts”, A. Telleria, C.V. Barrera, A. de Cózar, Z. Freixa. Manuscript in preparation.

“Synthesis and photophysical characterization of diethylphosphonate and carboxylate-appended iridium complexes for application on dye-sensitized solar cells” A. Telleria, E.C. Kohlrausch, RdC. Duarte, F.S. Rodembusch, J. Dupont, Z. Freixa, M.J.L. Santos, *Chemistry Select.,* **2016**, accepted.

"Azobenzene-functionalized iridium(III) triscyclometalated complexes", J. Pérez-Miqueo, A. Telleria, M. Muñoz-Olasagasti, A. Altube, E. García-Lecina, A. de Cózar and Z. Freixa, *Dalton Trans.*, **2015**, *44*, 2075–2091.

"Azobenzene-appended bis-cyclometalated Iridium(III) bipyridyl complexes", A. Telleria, J. Pérez-Miqueo, A. Altube, E. García-Lecina, A. de Cózar and Z. Freixa, *Organometallics*, **2015**, *34*, 5513–5529.

"A readily accessible ruthenium catalyst for the solvolytic dehydrogenation of amine–borane adducts", M. Muñoz-Olasagasti, A. Telleria, J. Pérez-Miqueo, M. A. Garralda and Z. Freixa, *Dalton Trans.*, **2014**, *43*, 11404–11409.

Conferences

A. Telleria, C. M. Davidson, L. T. Gibson, **"Microwave extraction techniques for polycyclic aromatic hydrocarbons (PAHs) removal from soil"**, SETN Annual Environmental Technology Conference, June 2010, Glasgow, United Kingdom. Poster communication.

A. Arzac, A. Ibarnavarro, A. Telleria, Z. Freixa, R. Tomovska, **"Water-borne graphene-plymer composites"**, 1st nanoIKER Workshop, March 2012, San Sebastian, Spain. Poster communication.

J. Pérez-Miqueo, A. Telleria, M. Muñoz-Olasagasti, Z. Freixa, **"Complejos ciclometalados de iridio (III) fotomodulables"**, XXX Reunión del GEQO, June 2012, Castellón, Spain. Poster communication.

A. Telleria, J. Pérez-Miqueo, M. Muñoz-Olasagasti, A. Ibarnavarro, R. Tomovska, Z. Freixa, **"Compuestos organometálicos fotosensibles para la modificación de la superficie del grafeno"**, XXX Reunión del GEQO, June 2012, Castellón, Spain. Poster communication.

J. L. Aceña, D. Houck, A. Telleria, J. Pérez-Miqueo, Z. Freixa and V. A. Soloshonok, **"Asymmetric Synthesis of Bis-α-Amino Acids through Bis-Alkylations of Chiral Glycine Equivalents"**, XXIV Reunión Bienal de Química Orgánica, July 2012, San Sebastian, Spain. Oral communication.

J. Pérez-Miqueo, A. Telleria, M. Muñoz-Olasagasti, J. M. Seco, Z. Freixa, **"Photocromic iridium (III) phosphors"**, XXV International conference on organometallic chemistry, September 2012, Lisboa, Portugal. Poster communication.

A. Telleria, J. Pérez-Miqueo, M. Muñoz-Olasagasti, Z. Freixa, **"Complejos catiónicos de iridio(III) fotomodulables"**, IX Simposio de Investigadores Jovenes, November 2012, Zaragoza, Spain. Poster communication.

J. Pérez-Miqueo, A. Telleria, M. Muñoz-Olasagasti, Z. Freixa, **"Fotointerruptores organometálicos derivados de azobencenos"**, IX Simposio de Investigadores Jovenes, November 2012, Zaragoza, Spain. Poster communication.

A. Telleria, J. Pérez-Miqueo, M. Muñoz-Olasagasti, J. M. Seco, Z. Freixa, **"Photosensitive cationic iridium (III) complexes"**, 20th EuCheMS Conference on Organometallic Chemistry, July 2013, St Andrews, United Kingdom. Poster communication.

J. Pérez-Miqueo, A. Telleria, M. Muñoz-Olasagasti, J.M. Seco, Z. Freixa, **"Photoswitching behaviour of iridium(III) complexes containing azobenzene"**, 20th EuCheMS Conference on Organometallic Chemistry, July 2013, St Andrews, United Kingdom. Poster communication.

A. Telleria, J. Pérez-Miqueo, M. Muñoz-Olasagasti, J.M. Seco, Z. Freixa, **"Complejos cationicos de iridio (III) fotosensibles"**, XXXIV Reunión Bienal Real Sociedad Española de Química, September 2013, Santander, Spain. Poster communication.

J. Pérez-Miqueo, A. Telleria, M. Muñoz-Olasagasti, J.M. Seco, Z. Freixa, **"Complejos ciclometalados de iridio (III) derivados de azobenceno"**, XXXIV Reunión Bienal Real Sociedad Española de Química, September 2013, Santander, Spain. Poster communication.

Z. Freixa, J. M. Seco, J. Pérez-Miqueo, A. Telleria, M. Muñoz-Olasagasti, **"Compuestos organometálicos fotomodulables"**, XXXIV Reunión Bienal Real Sociedad Española de Química, September 2013, Santander, Spain. Poster communication.

M. Muñoz-Olasagasti, A. Telleria, J. Pérez-Miqueo, Z. Freixa, **"Obtención de hidrógeno a partir de aductos de amino borano catalizada por complejos de rutenio"**, XXXI Reunión del GEQO, September 2014, Tarragona, Spain. Poster communication.

J. Pérez-Miqueo, A. Telleria, M. Muñoz-Olasagasti, Z. Freixa, **"Complejos fotocrómicos de iridio (III) derivados de azobenceno"**, XXXI Reunión del GEQO, September 2014, Tarragona, Spain. Poster communication.

J. De Tovar, X. Sala, J. García-Antón, R. Bofill, A. Telleria, Z. Freixa, K. Philippot, C. Amiens, D. Ciuculescu, P. Lecante, **"Nanomaterials for the photoctalytic splitting of water: towards a sustainable way of producing dihydrogen"**, Fourth International Conference on Multifunctional, Hybrid and Nanomaterials, March 2015, Sitges, Spain. Poster communication.

A. Telleria, M. A. Garralda, Z. Freixa, **"Ru(II) complexes for the solvolytic dehydrogenation of amine-borane adducts"**, IX International School On Organometallic Chemistry Marcial Moreno Mañas, July 2016, Donostia, Spain. Poster communication.

F. B. Urquiola, M. Barquín, A. Telleria, Z. Freixa, **"Influence of the ligand electronic properties on the [IrCp*(bipy)(H_2O)]SO_4 catalyzed formic acid decomposition"**, IX International School On Organometallic Chemistry Marcial Moreno Mañas, July 2016, Donostia, Spain. Poster communication.

M. Vázquez, A. Telleria, Z. Freixa, **"Organometallic complexes containing luminescent ligands"**, IX International School On Organometallic Chemistry Marcial Moreno Mañas, July 2016, Donostia, Spain. Poster communication.

Tutoring bachelor students (final project)

July 2015-February 2016	**Borja Urquiola**. Development of iridium(III) half-sandwich compounds, and study of their catalytic activity in the generation of hydrogen by decomposition of formic acid. Final mark 9.5
July 2015-September 2016	**Maitane Vázquez**. New bipyridine ligands incorporating the BTD (2,1,3-benzothiadiazole) fragment. Study of their iridium(III) and ruthenium(II) derivatives. To be defended in September 2016.

Research stages

July 2014-December 2014	Laboratory of Molecular Catalysis in the Universidade Federal do Rio Grande do Sul (Brazil) in collaboration with Prof. Jairton Dupont. Syntheses and characterization of new benzothiadiazoles.
June 2012-July 2012	Laboratory of Inorganic Chemistry in the Universitat Autònoma de Barcelona in collaboration with Dr. Xavier Sala. Cyclic voltammetry measurements.

eman ta zabal zazu

Universidad del País Vasco

Euskal Herriko Unibertsitatea

ikerbasque

Basque Foundation for Science

Supporting Information

Azobenzene-appended iridium(III) and ruthenium(II) complexes. Screening of applications.

PhD Thesis

Ainara Telleria Echaniz

2016

TABLE OF CONTENTS

Chapter 4

Chapter 5

General experimental conditions and instrumentation

All solvents were dried and purified by known procedures and freshly distilled under nitrogen from appropriate drying agents prior to use. All manipulations and reactions involving air and/or moisture-sensitive organometallic compounds were performed under an atmosphere of dry nitrogen using standard Schlenk techniques.

NMR spectra were recorded on a Bruker Avance DPX 300 or 400 MHz and Bruker Avance 500 spectrometers.

EA of the complexes were performed on a microanalizer Leco CHNS-932.

Electrospray ionization Mass Spectrometry (ESI-MS) experiments were carried out on a ultra high performance liquid chromatograph (UPLC) coupled to a high resolution quadrupole-time of flight mass spectrometer (QTOF).

UV-Vis and photoisomerization studies

UV−vis absorption measurements were performed with an Agilent 8453 diode-array spectrophotometer utilizing 10 mm cell-path quartz cuvettes (110 QS).

Measurements of thermal *cis* to *trans* isomerization rates were performed using 10-40 μM solutions of ACN or EtOH. To maximize the initial population of Z derivatives on the PSS, it was followed the procedure described by Monkowius:[1] Using a Shimadzu RF-540 fluorimeter, a 3 mL portion of each sample was irradiated at the corresponding λ_{max} (associated with its π–π* transition band) for 30 min. The λ of the maximum observed after subtracting the first and last spectra of the series was considered as the optimal light wavelength to promote the *Z*–*E* photoisomerization (λ_{opt}). Fresh samples were irradiated at (λ_{opt}) for 30 min, and then placed in a UV−vis spectrophotometer. Their absorbance spectral changes were measured as a function of time for 14 hours. Temperature was controlled with a HP 89090A Peltier temperature control accessory.

Cyclic voltammetry

All electrochemical measurements were carried out in a sealed glass cell under N_2 atmosphere on 10^{-3} M solutions of in anhydrous ACN (containing 0.1 M $TBAPF_6$ as the supporting electrolyte) at a scan rate of 100 mVs^{-1}. The working electrode was a glassy–carbon rod (5 mm diameter) and a Pt wire encapsulated on a porous glass tube was used as counter electrode. The potentials were controlled using a Metrohm Ag/AgCl reference electrode. On the other hand ferrocene/ferrocenium couple (+0.352 V vs Ag/AgCl) was used as the internal standard (10^{-3} M) and all potentials are related to it. The measurements were performed using a Bio-Logic VMP3 potentiostat-galvanostat.

[1] M. Kaiser, S. P. Leitner, C. Hirtenlehner, M. List, A. Gerisch and U. Monkowius, *Dalton Trans.*, **2013**, *42*, 14749–14756.

Computational details

All the calculations were performed with the GAUSSIAN09 suite of programs.[2] Optimization and TDDFT simulation of the absorption processes were carried by using the coulombic-attenuating method developed by Handy et al.[3] named CAM-B3LYP with the standard 6-31+G* and the Hay-Wadt core effective potential (ECP) LANL2DZ[4] basis sets. Solvent effects were estimated using the polarizable continuum model (PCM) within the self-consistent reaction field (SCRF) approach.[5] This method was successfully optimized for vertical excitations and excited estates[6] and was previously proven to give reliable results on the calculation of iridium complexes.[7]

X-ray crystallography

Intensity data were collected on an Agilent Technologies Super-Nova diffractometer, wich was equipped with monochromated Cu kα radiation (λ= 1.54184 Å) and Atlas CCD detector or with monochromated Mo kα radiation (λ= 0.71073 Å) and Eos CCD detector. Data frames were processed (united cell determination, analytical absorption correction with face indexing, intensity data integration and correction for Lorentz and polarization effects) using the Crysalis software package.[8] The structure was solved using Olex2[9] and refined by full-matrix least-squares with SHELXL-97.[10] Final geometrical calculations were carried out with Mercury[11]. and PLATON[12] as integrated in WinGX. [13]

Procedure for the solvolytic dehydrogenation of AB adducts

Catalytic reactions were carried out in a glass reactor connected to an electronic pressure transducer (Man on the moon). 0.69 mmol of the substrate and 0.0034 mmol of the precatalyst were stirred in 0.375 mL of freshly distilled THF for 5–10 min (until no further gas evolution was detected). Addition of 1.125 mL of distilled water to this mixture was considered initial reaction time.

For catalytic reaction under irradiation, the reactor used was made of quartz, and it was immersed in a water bath during the catalytic process. The irradiation lamp used was a an immersion lamp (125 W, 365 nm) thermostated by an external quartz cooling jacket, which temperature was set to 10 °C.

---

[2] Gaussian09, Revision A.02, M. J. Frisch et al., Gaussian Inc., Wallingford CT, **2009**.
[3] T. Yanai, D. P. Tew and N. C. Handy, *Chem. Phys. Lett.*, **2004**, *393*, 51–57.
[4] P. J. May and W. R. Wadt, *J. Chem. Phys.*, **1985**, *82*, 299–303.
[5] R. Cammi, B. Mennucci and J. Tomasi, *J. Phys. Chem. A*, **2000**, *104*, 5631–5637.
[6] A. Charaf-Eddin, A. Planchat, B. Mennucci, C. Adamo and D. Jacquemin, *J. Chem. Theor. Comput.*, **2013**, *9*, 2749–2760.
[7] J. Pérez-Miqueo, A. Telleria, M. Muñoz-Olasagasti, A. Altube, E. García-Lecina, A. de Cózar, Z. Freixa, *Dalton Trans.*, **2015**, *44*, 2075–2091.
[8] CrysAlisPro, Agilent Technologies,Version 1.171.37.31 (release 14-01-2014 CrysAlis171 .NET)(compiled Jan 14 2014,18:38:05).
[9] O. V. Dolomanov, L. J. Bourhis, R. J. Gildea, J. A. K. Howard and H. Puschmann, OLEX2: A complete structure solution, refinement and analysis program, *J. Appl. Cryst.,* **2009**, *42*, 339–341.
[10] G. M. Sheldrick, *Acta Cryst. A64,* **2008**, 112.
[11] C. F. Macrae, *J. Appl. Cryst.*, **2008**, *41*, 466.
[12] A. L. Spek (2010) PLATON, A Multipurpose Crystallographic Tool, Utrecht University, Utrecht, The Netherlands; A. L. Spek, *J. Appl. Cryst.*, **2003**, *36*, 7.
[13] L. J. Farrugia, *J. Appl. Cryst.*, **1999**, *32*, 837.

Immediately, the reactor containing 0.69 mmol of the substrate and 0.0034 mmol of the precatalyst in 0.375 mL of freshly distilled THF the precatalyst was immersed in the bath and stirred for 10 min. The the irradiation lamp was immersed, and immediate addition of 1.125 mL of distilled water to this mixture was considered initial reaction time.

For catalytic experiments where irradiation and no irradiation periods were combined, the lamp was immersed in the water bath only when was it switched on, at not irradiation periods the lamp was pulled out, otherwise the reaction temperature would decrease, due to the external cooling of the lamp.

Synthesis and characterization

Ligand 1 (2,2'-bis(4-phenylazopyridine). Synthesis, characterization and photoisomerization studies.

SYNTHESIS

Under a N_2 atmosphere, 4,4'-diamino-2,2'-bipyridine (0.500 g, 2.68 mmol) were dissolved in 4 mL of NaOH (2 g/4 ml H_2O) and 2 ml of pyridine. The mixture was heated to 80 °C for 45 min and nitrosobenzene (0.750 g, 7 mmol) were added. The reaction mixture was heated to 80 °C for another 15 h. The resulting mixture was cooled down to room temperature. The solid was filtrated, washed with CH_2Cl_2 and H_2O. The product was obtained as an orange solid. Yield 56%.

Elemental Analysis: calculated for ($C_{22}H_{16}N_6$): C, 72.51; H, 4.43; N, 23.06. Found: C, 72.12; H, 3.97; N, 23.04.

Exact Mass: ESI-MS $[C_{22}H_{16}N_6+H]^+$: calculated: m/z= 365.1515, found: m/z= 365.1515.

^{1}H NMR (300 MHz, $CDCl_3$): δ 8.96 (d, J = 5.2 Hz, 1H), 8.92 (d, J = 1.4 Hz, 1H), 8.07 (brd, J = 4.0 Hz, 1H), 8.05 (d, J = 2.2 Hz, 1H), 7.81 (dd, J = 1.9 Hz, J = 5.2 Hz, 1H), 7.60 (m, 3H).

^{13}C APT NMR (75 MHz, $CDCl_3$): δ 158.52 (C_{quat}), 157.74 (C_{quat}), 152.46 (C_{quat}), 150.76 (CH), 132.34 (CH), 129.26 (2CH), 123.48 (2CH), 116.44 (CH), 114.18 (CH).

UV/Vis (CH_3CN), λ, nm (ε, 10^4 M^{-1} cm^{-1}): 317 (3.9), 430 (0.08).

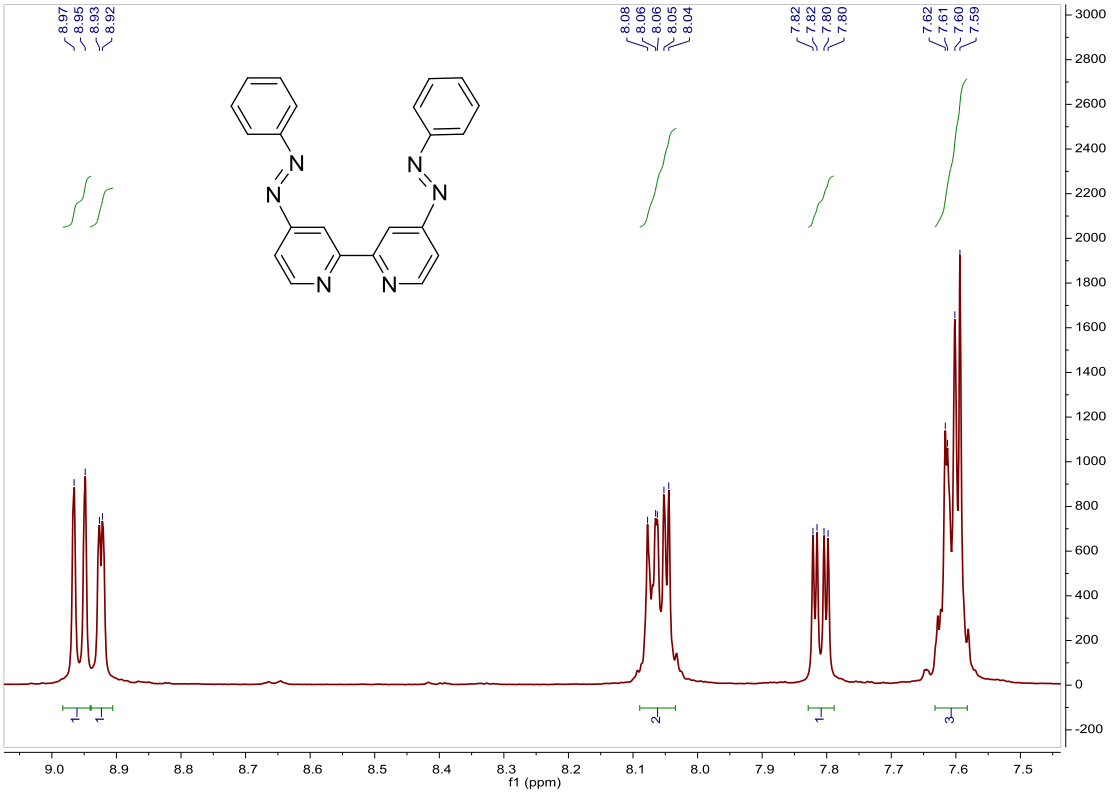

Fig. S1. ^{1}H NMR spectrum of **Ligand 1** in $CDCl_3$, 300 MHz.

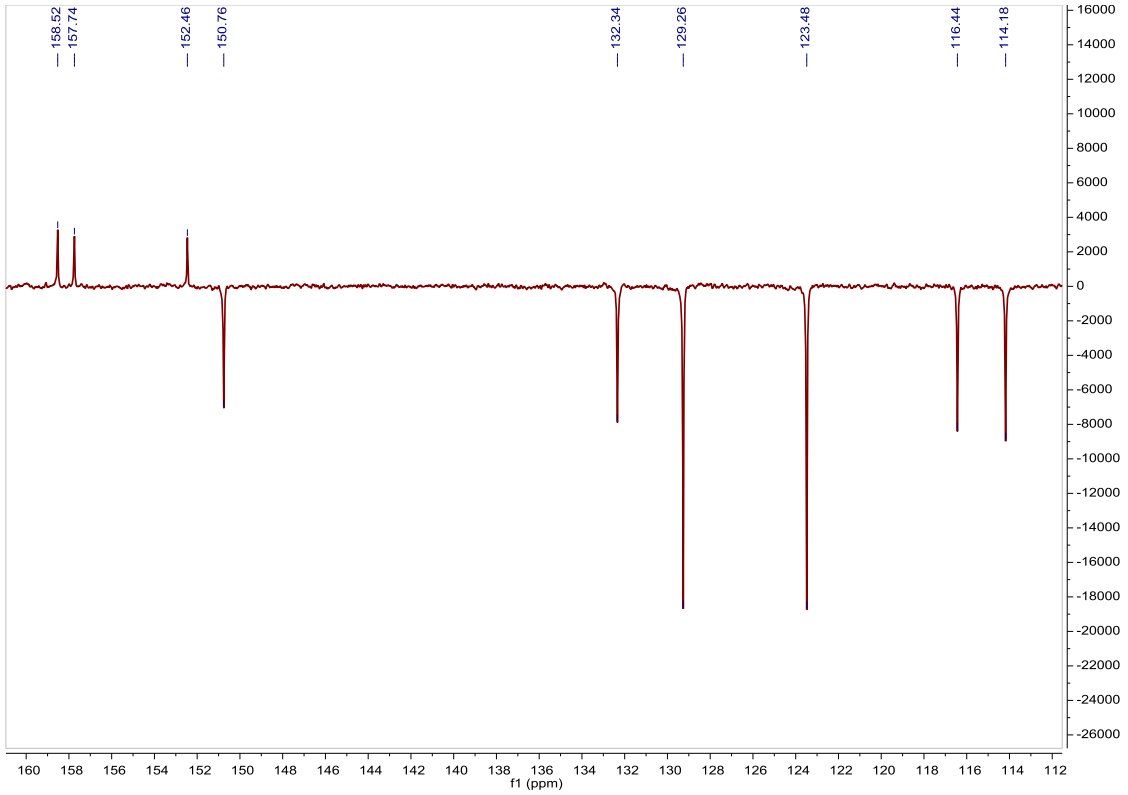

Fig. S2. ^{13}C APT NMR spectrum of **Ligand 1** in $CDCl_3$, 75 MHz.

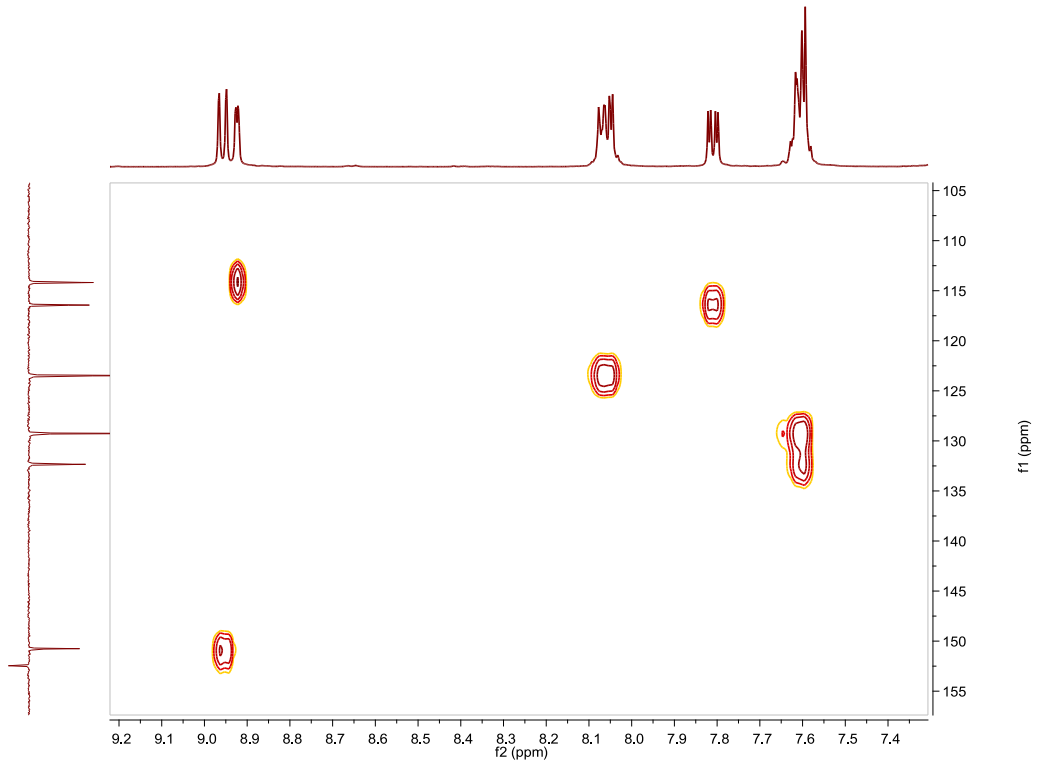

Fig. S3. HSQC NMR spectrum of **Ligand 1** in $CDCl_3$.

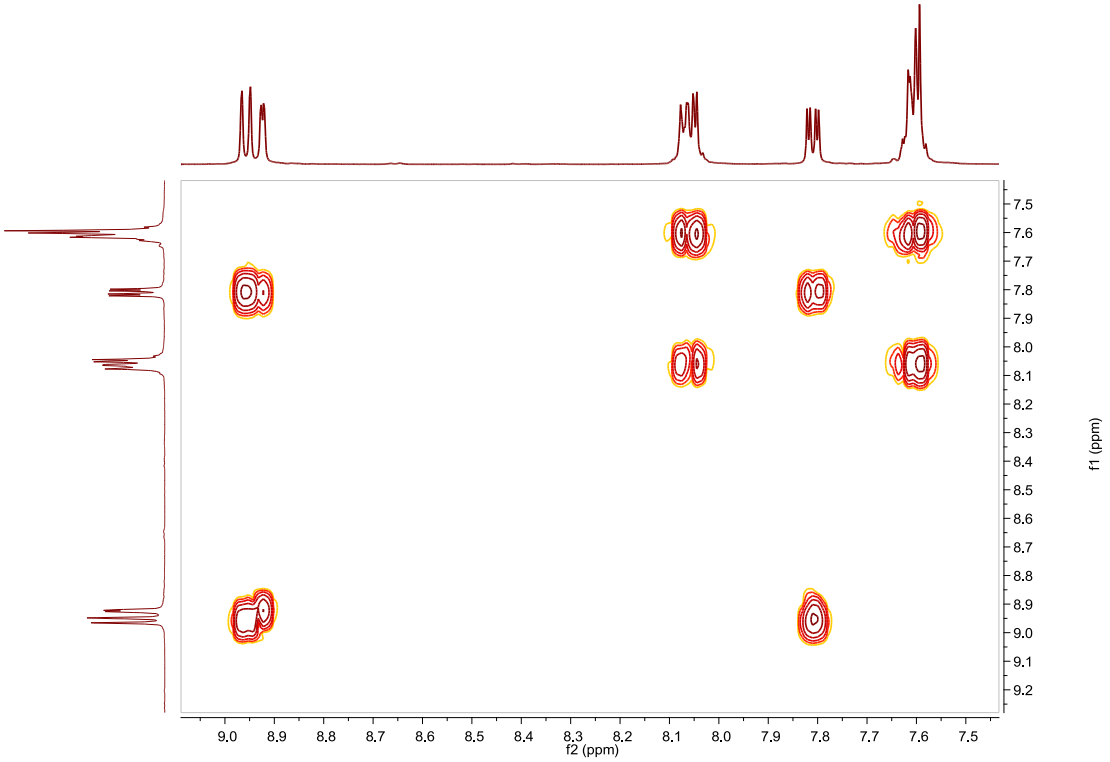

Fig. S4. COSY NMR spectrum of **Ligand 1** in $CDCl_3$.

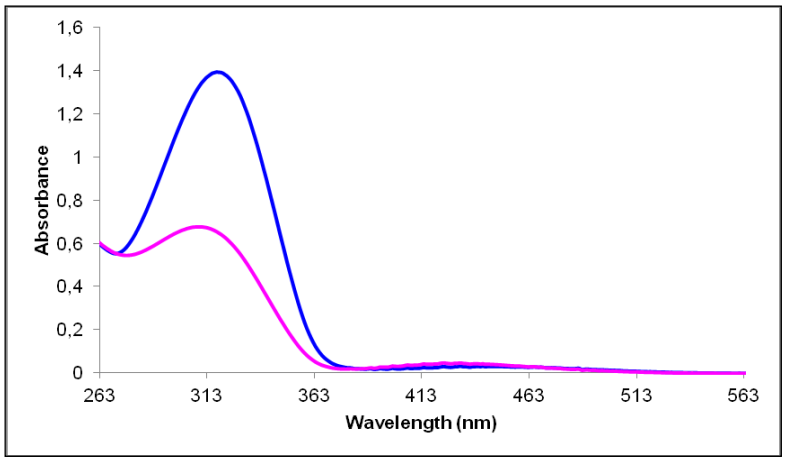

Fig. S5. UV/Vis spectra of **Ligand 1** in CH_3CN. Before (blue line) and after (pink line) irradiation at 325nm, $3.56 \cdot 10^{-5}$ M.

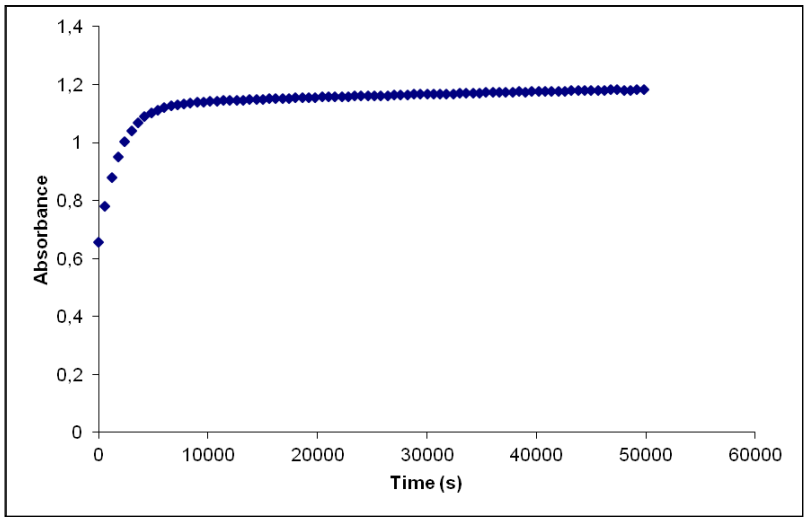

Fig. S6. Cis to trans thermal isomerization kinetics of **Ligand 1**. Absorption change of the band 317nm at 328 K in CH_3CN after irradiation at 325 nm. ($3.56 \cdot 10^{-5}$ M).

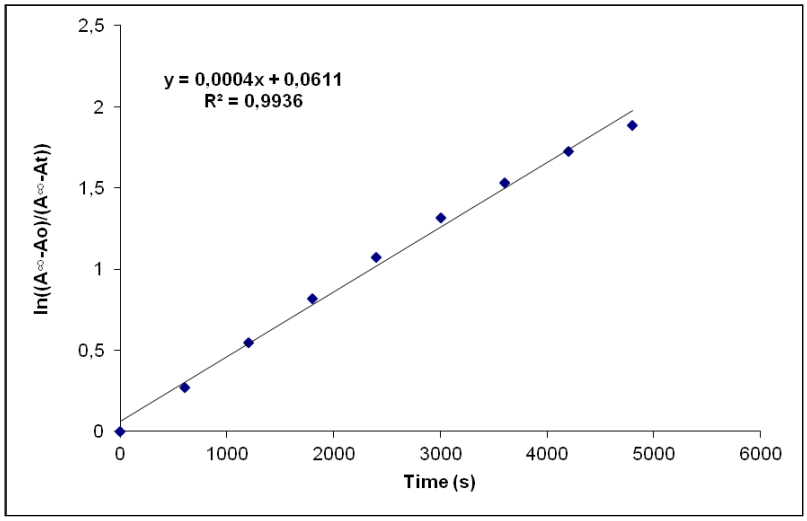

Fig. S7. Cis to trans thermal isomerization kinetics of **Ligand 1**. First-order plot. k (s^{-1}) = $4.0 \cdot 10^{-4}$. Half-life (min) = 29.

Ligand 2, 4-phenylazopyridine. Synthesis, characterization and photoisomerization studies.

SYNTHESIS[14]

Under a N_2 atmosphere, 4-aminopyridine (2.22 g, 23.6 mmol) were dissolved in 10 mL of NaOH (6.5 g/12 ml H_2O) and 7 ml of pyridine. The mixture was heated to 80 °C and nitrosobenzene (3.00 g, 28.0 mmol) were added. The reaction mixture was heated to 80 °C for another 1.5 h. The resulting mixture was cooled down to room temperature and the product was extracted with CH_2Cl_2. To remove the pyridine, the product was dissolved in hexane at 80 °C and cooled down with an ice bath. The product was filtered and was obtained as an orange solid. Yield 88%. The spectroscopic data are coincident with those described in the literature.

^{1}H NMR (300 MHz, $CDCl_3$): δ 8.86 (brd, J = 6.2 Hz, 2H), 8.01 (m, 2H), 7.77 (brd, J = 6.2 Hz, 2H), 7.59 (m, 3H).

UV/Vis (CH_3CN), λ, nm (ε, 10^4 M^{-1} cm^{-1}): 309 (1.6), 435 (0.03).

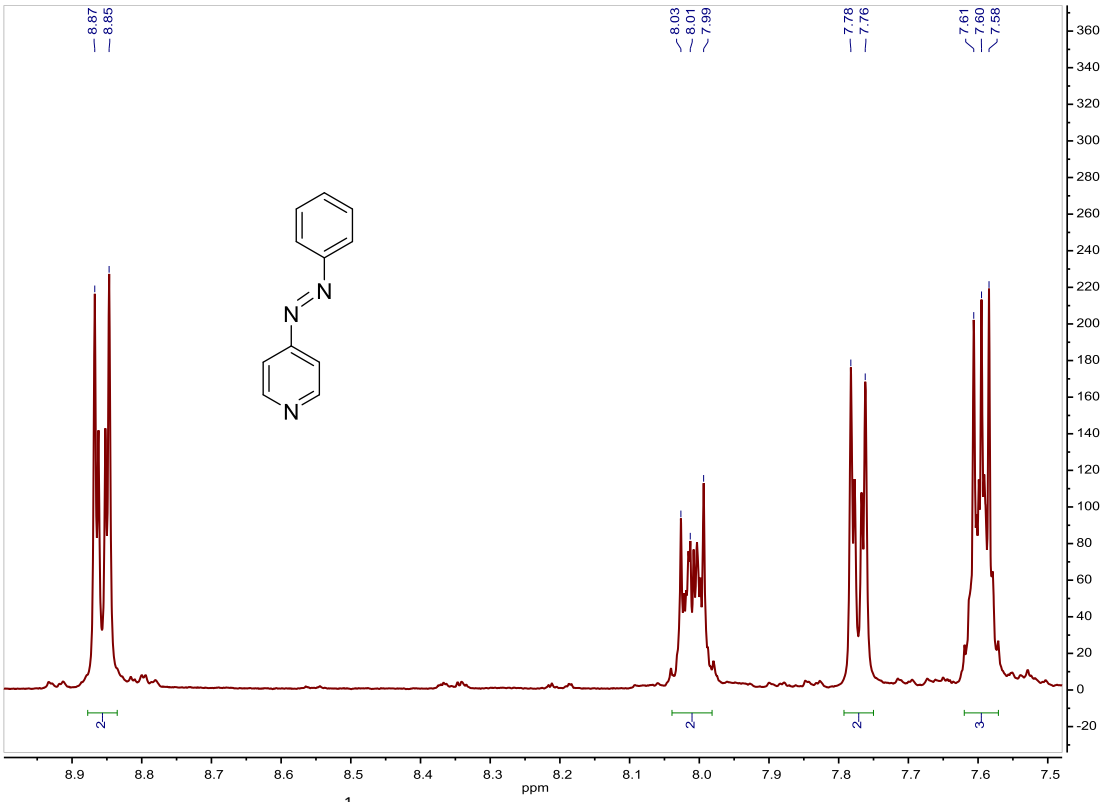

Fig. S8. ^{1}H NMR spectrum of **Ligand 2** in $CDCl_3$, 300 MHz.

[14] Busby, M.; Matousek, P.; Towrie, M.; Vlcek Jr., A., *Inorg. Chim. Acta*, **2007**, *360*, 885–896.

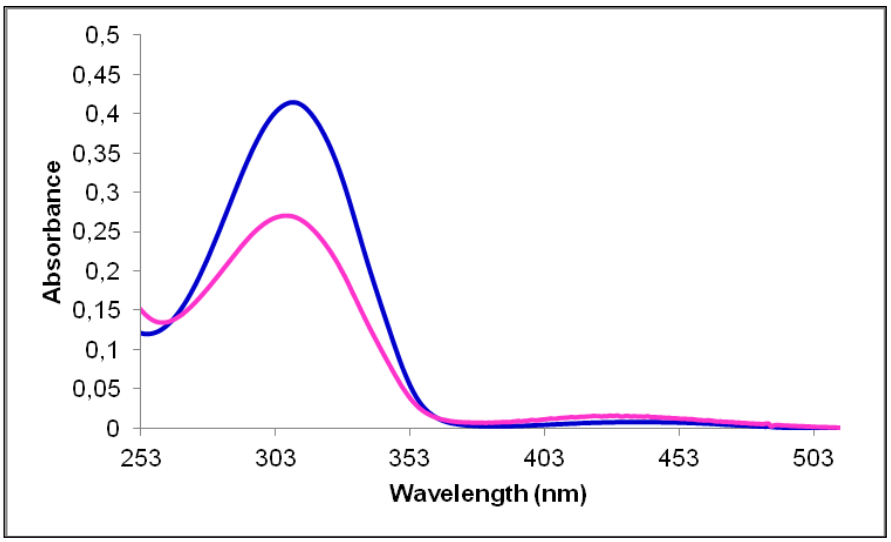

Fig. S9. UV/Vis spectra of **Ligand 2** in CH_3CN. Before (blue line) and after (pink line) irradiation at 312nm, $2.50 \cdot 10^{-5}$ M.

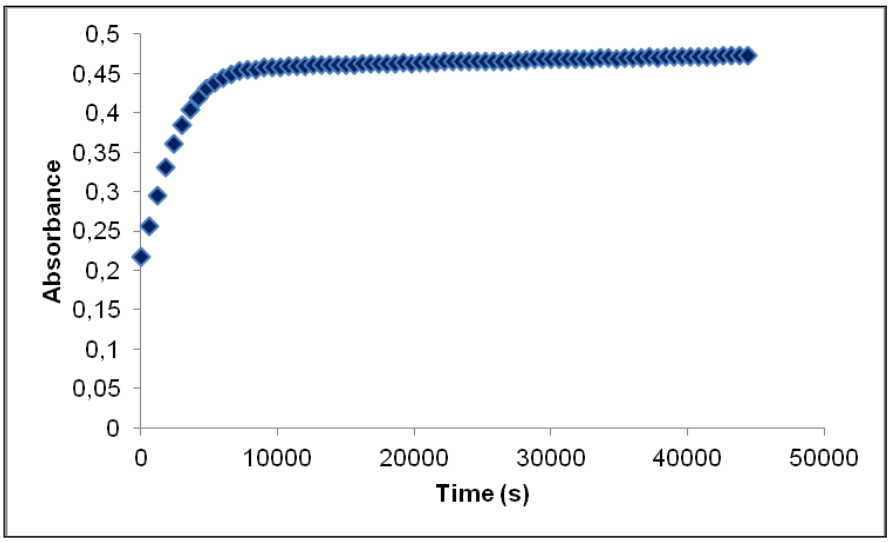

Fig. S10. Cis to trans thermal isomerization kinetics of **Ligand 2**. Absorption change of the band 309nm at 328 K in CH_3CN after irradiation at 312 nm. ($2.50 \cdot 10^{-5}$ M).

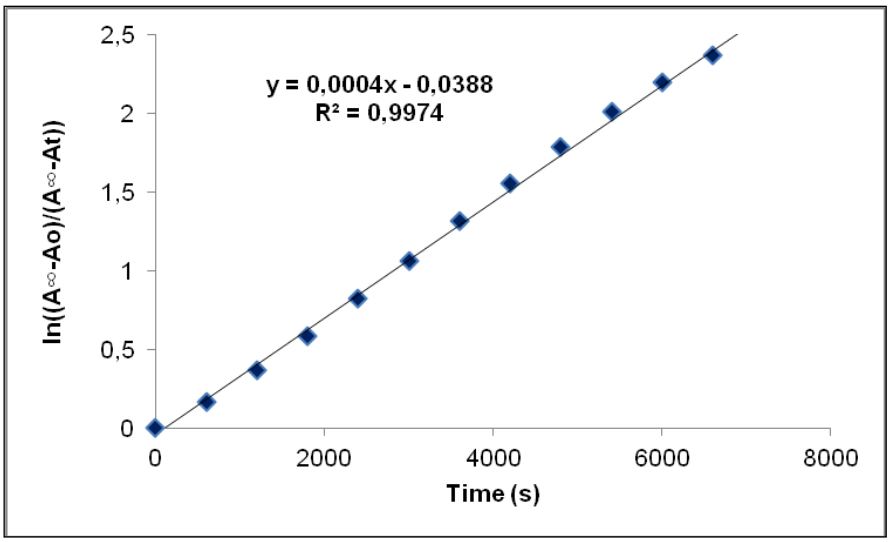

Fig. S11. Cis to trans thermal isomerization kinetics of **Ligand 2**. First-order plot. k (s^{-1}) = $4.0 \cdot 10^{-4}$. Half-life (min) = 29.

Ligand 3, 4,4'-bis(*p*-azobenzene)-2,2'-bipyridine. Synthesis and characterization.

SYNTHESIS.

Under a N_2 atmosphere, 4-4'-dibromo-2,2'-bipyridine (0.6 g, 1.91 mmol) and 4-(phenylazo)phenyl]boronic acid **9** (1.43 g, 6.33 mmol) were dissolved in 35 mL of toluene. K_2CO_3 (16 mL, 2 M,in H_2O) and $Pd(PPh_3)_4$ (0.12 g, 0.104 mmol) were added and the mixture was degassed by N_2 bubbling for 15 min. The reaction mixture was heated to 115 °C for 72 h. The resulting mixture was cooled down to room temperature. The solid was filtrated and washed with CH_2Cl_2 and acetone. The product was obtained as an orange solid. Quantitative yield.

Elemental Analysis: calculated for ($C_{34}H_{24}N_6 \cdot CH_2Cl_2$): C, 69.89; H, 4.36; N, 13.97. Found: C, 70.03; H, 4.45; N, 14.25.

Exact Mass: ESI-MS $[C_{34}H_{24}N_6+H]^+$: calculated: m/z= 517.2141, found: m/z= 517.2147.

Ligand 4, 4-(*p*-azobenzene)-4'-bromo-2,2'-bipyridine. Synthesis, characterization and photoisomerization studies.

SYNTHESIS.

Under a N_2 atmosphere, 4-4'-dibromo-2,2'-bipyridine (1.00 g, 3.18 mmol) and [4-(phenylazo)phenyl]boronic acid pinacol ester **11** (0.98 g, 3.18 mmol) were dissolved in 60 mL of toluene. K_2CO_3 (27 mL, 2 M in H_2O) and $Pd(PPh_3)_4$ (0.184 g, 0.159 mmol) were added and the mixture was degassed by N_2 bubbling for 15 min. The reaction mixture was heated to 115 °C for 15 h. The resulting mixture was cooled down to room temperature and the orange solid (ligand **3**) was removed by filtration. The product was extracted from the filtrated with CH_2Cl_2. The organic phase was dried with $MgSO_4$ and the solvent was evaporated. The product was purified by column chromatography (silica gel, 100% CH_2Cl_2 to 100% acetone), and it was obtained as an orange solid. Yield 38%.

Elemental Analysis: calculated for ($C_{22}H_{15}BrN_4$): C, 63.63; H, 3.64; N, 13.49. Found: C, 63.42; H, 3.62; N, 13.23.

Exact Mass: ESI-MS $[C_{22}H_{15}BrN_4+H]^+$: calculated: m/z= 415.0558, found: m/z= 415.0566.

^{1}H NMR (300 MHz, $CDCl_3$): δ 8.80 (d, J = 5.1 Hz, 1H), 8.75 (dd, J = 1.7 Hz, J = 8.8 Hz, 2H), 8.56 (d, J = 5.2 Hz, 1H), 8.09 (d, J = 8.5 Hz, 2H), 8.00 (dd, J = 1.8 Hz, J = 8.3 Hz, 2H), 7.96 (d, J = 8.4 Hz, 2H), 7.66 (dd, J = 1.8 Hz, J = 5.0 Hz, 1H), 7.56 (m, 4H).

^{13}C APT NMR (75 MHz, $CDCl_3$): δ 157.25 (C_{quat}), 155.44 (C_{quat}), 152.90 (C_{quat}), 152.66 (C_{quat}), 149.84 (2CH), 148.49 (C_{quat}), 140.35 (C_{quat}), 134.03 (C_{quat}), 131.32 (CH), 129.14 (2CH), 127.95 (2CH), 127.06 (CH), 124.74 (CH), 123.56 (2CH), 122.99 (2CH), 122.07 (CH), 119.24 (CH).

UV/Vis (CH_3CN), λ, nm (ε, 10^4 M^{-1} cm^{-1}): 334 (3.5), 443 (0.13).

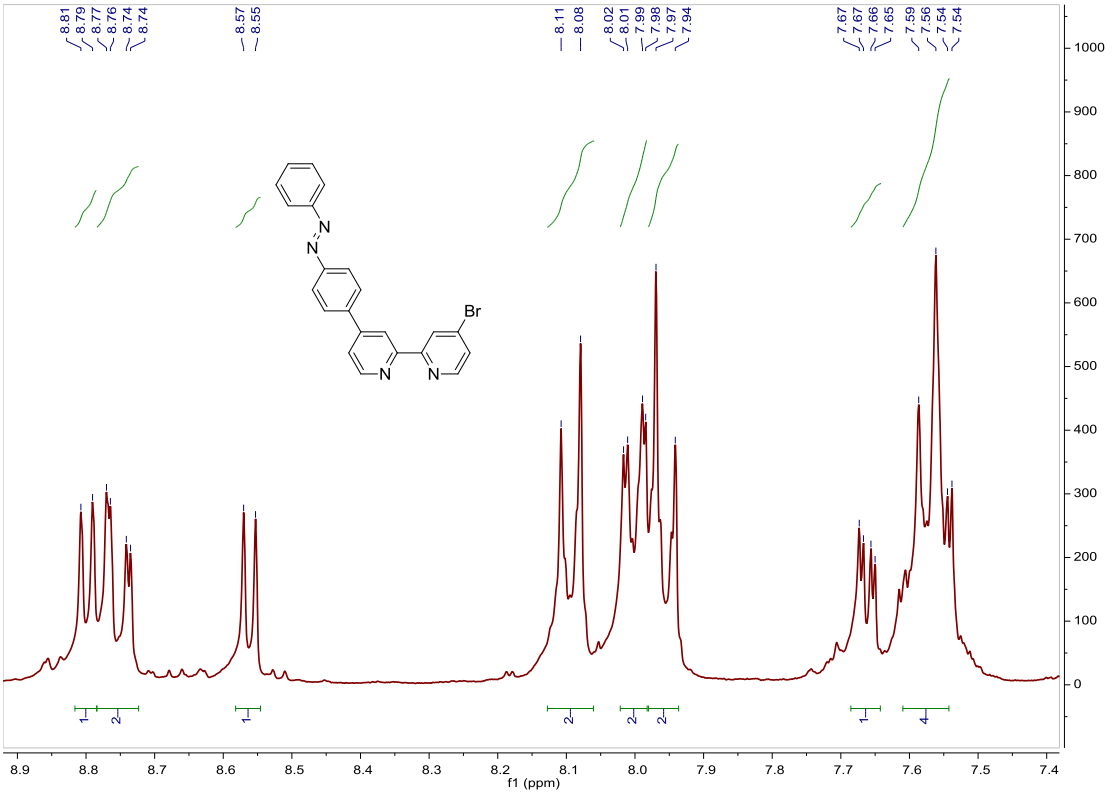

Fig. S12. ^{1}H NMR spectrum of **Ligand 4** in $CDCl_3$, 300 MHz.

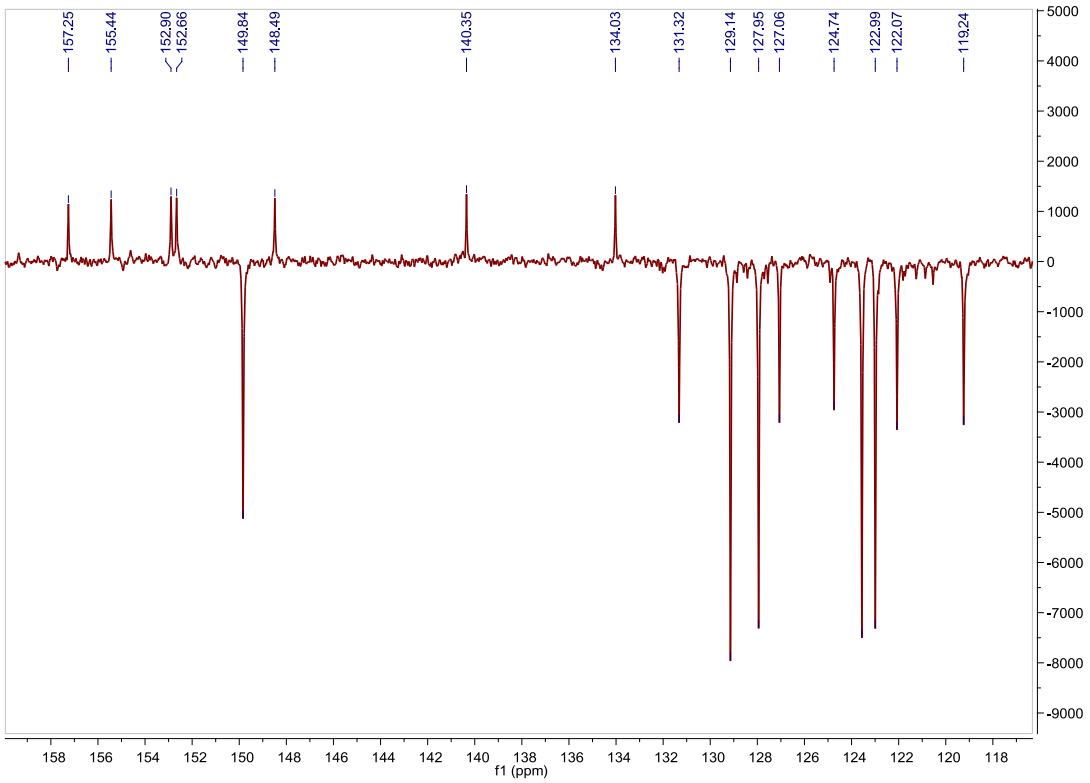

Fig. S13. ^{13}C APT NMR spectrum of **Ligand 4** in $CDCl_3$, 75 MHz.

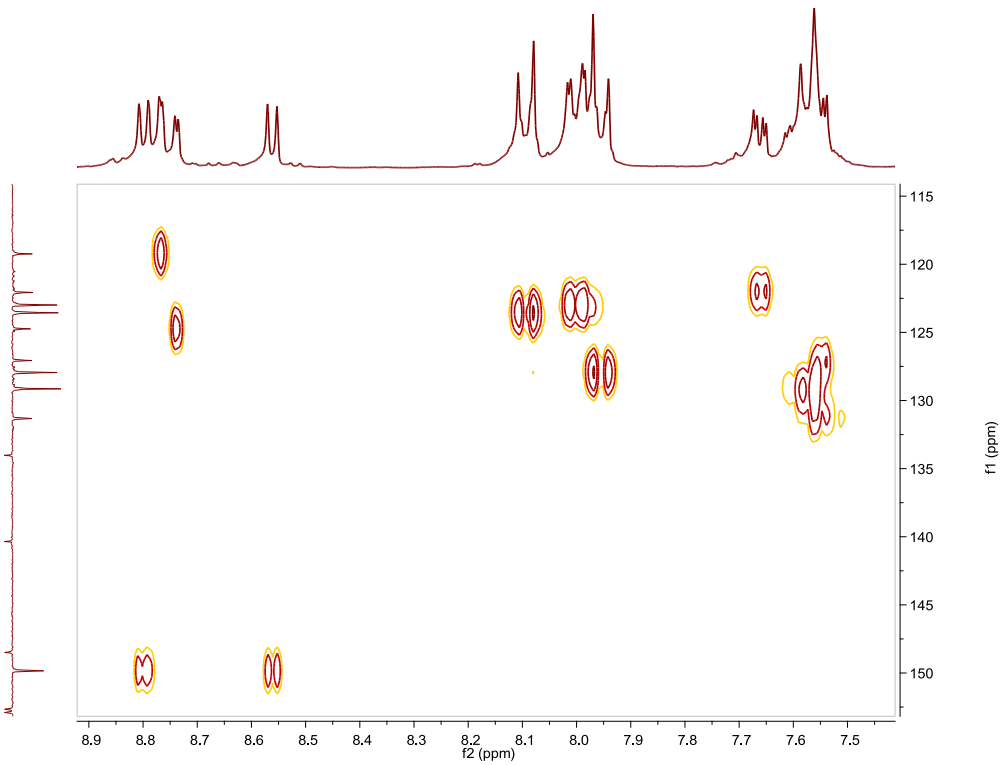

Fig. S14. HSQC NMR spectrum of **Ligand 4** in $CDCl_3$.

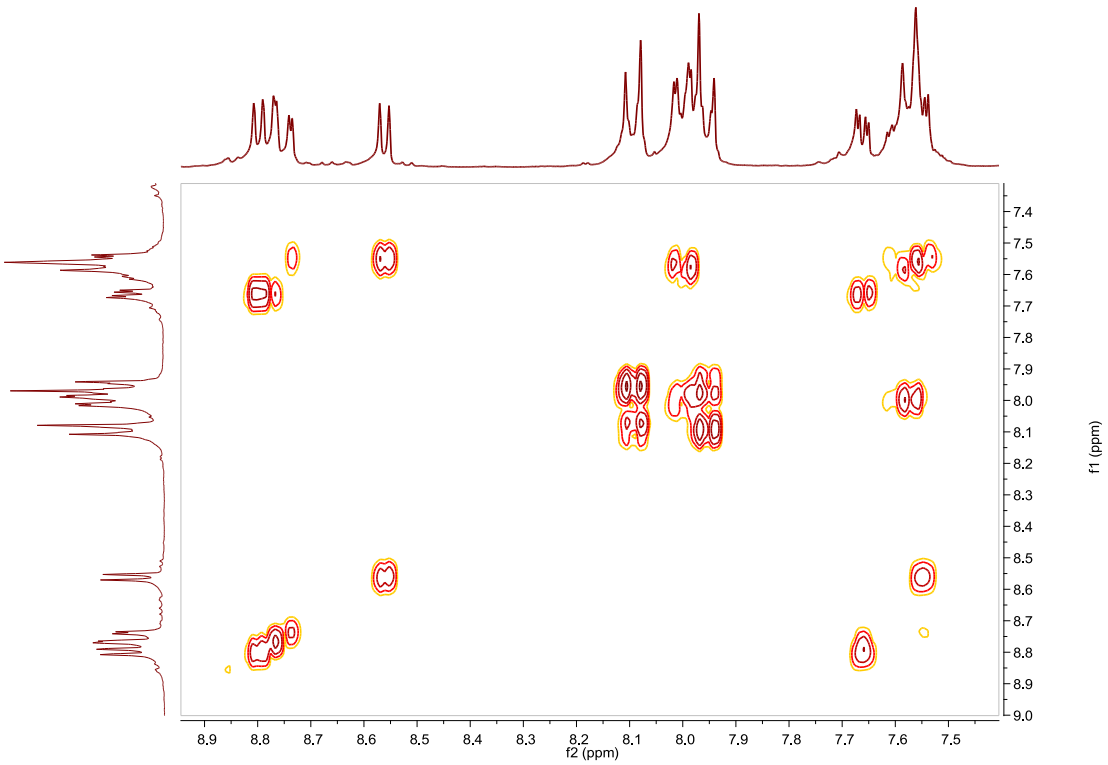

Fig. S15. COSY NMR spectrum of **Ligand 4** in $CDCl_3$.

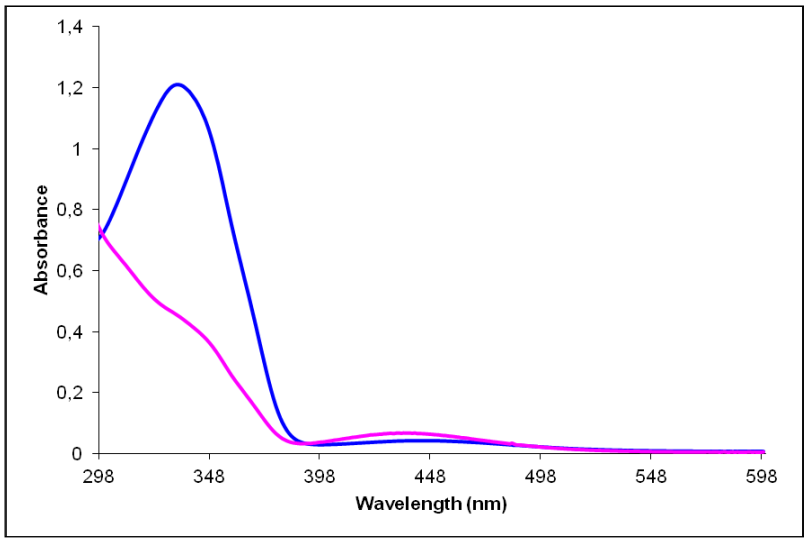

Fig. S16. UV/Vis spectra of **Ligand 4** in CH_3CN. Before (blue line) and after (pink line) irradiation at 337nm, $3.46 \cdot 10^{-5}$ M.

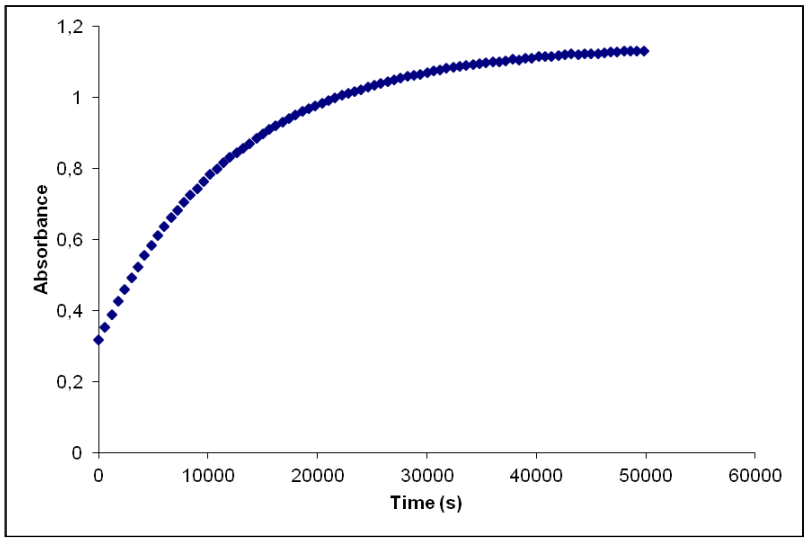

Fig. S17. Cis to trans thermal isomerization kinetics of **Ligand 4**. Absorption change of the band 334nm at 328 K in CH_3CN after irradiation at 337 nm. ($3.46 \cdot 10^{-5}$ M).

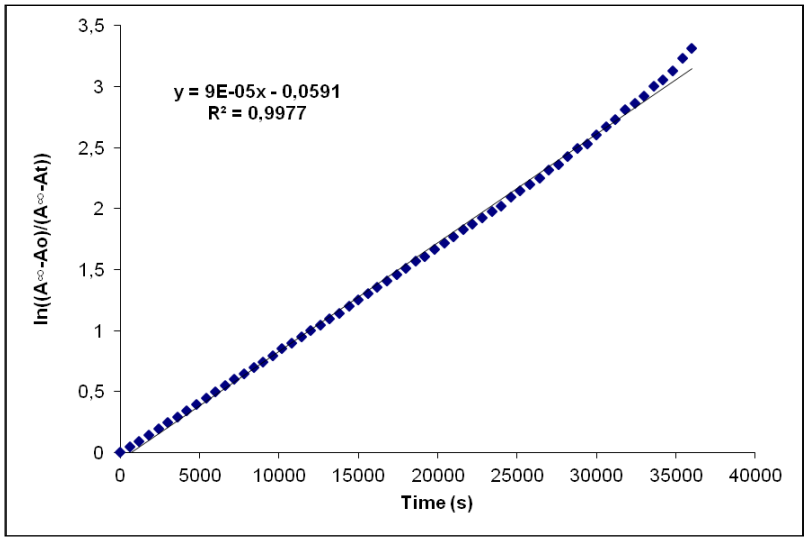

Fig. S18. Cis to trans thermal isomerization kinetics of **Ligand 4**. First-order plot. k (s^{-1}) = $9.0 \cdot 10^{-5}$. Half-life (min) = 128.

Ligand 5, 4,4'-bis(*m*-azobenzene)-2,2'-bipyridine. Synthesis, characterization and photoisomerization studies.

SYNTHESIS

Under a N_2 atmosphere, 4-4'-dibromo-2,2'-bipyridine (0.436 g, 1.39 mmol) and [3-(phenylazo)phenyl]boronic acid **9** (0.785 g, 3.47 mmol) were dissolved in 26 mL of toluene. K_2CO_3 (12 mL, 2 M in H_2O) and $Pd(PPh_3)_4$ (0.08 g, 0.07 mmol) were added and the mixture was degassed by N_2 bubbling for 15 min. The reaction mixture was heated to 115 °C for 15 h. The resulting mixture was cooled down to room temperature and the product was extracted with CH_2Cl_2. The organic phase was dried with $MgSO_4$ and the solvent was evaporated. The product was obtained as an orange solid. Yield 71%.

Elemental Analysis: calculated for ($C_{34}H_{24}N_6 \cdot H_2O$): C, 76.39; H, 4.90; N, 15.72. Found: C, 75.92; H, 4.42; N, 15.28.

Exact Mass: ESI-MS $[C_{34}H_{24}N_6+H]^+$: calculated: m/z= 517.2141, found: m/z= 517.2146.

^{1}H NMR (300 MHz, $CDCl_3$): δ 8.89 (d, J=1.2 Hz, 1H), 8.85 (d, J=5.1 Hz, 1H), 8.39 (pst, J=1.7 Hz, 1H), 8.06 (dpst, J=7.9 Hz, J=1.0 Hz, 1H), 8.02 (brdd, J=8.2 Hz, J=1.8 Hz, 2H), 7.96 (dpst, J=8.1 Hz, J=1.1 Hz, 1H), 7.71 (m, 2H), 7.57 (m, 3H).

^{13}C APT NMR (75 MHz, $CDCl_3$): δ 156.71 (C_{quat}), 153.19 (C_{quat}), 152.58 (C_{quat}), 149.80 (CH), 148.68 (C_{quat}), 139.38 (C_{quat}), 131.29 (CH), 129.82 (CH), 129.53 (CH), 129.15 (2CH), 123.25 (CH), 122.98 (2CH), 121.84 (CH), 121.77 (CH), 119.32 (CH).

UV/Vis (CH_3CN), λ, nm: 314 , 435. (The low solubility of these ligand in CH_3CN was too small for an accurate determination of the corresponding extinction coefficients).

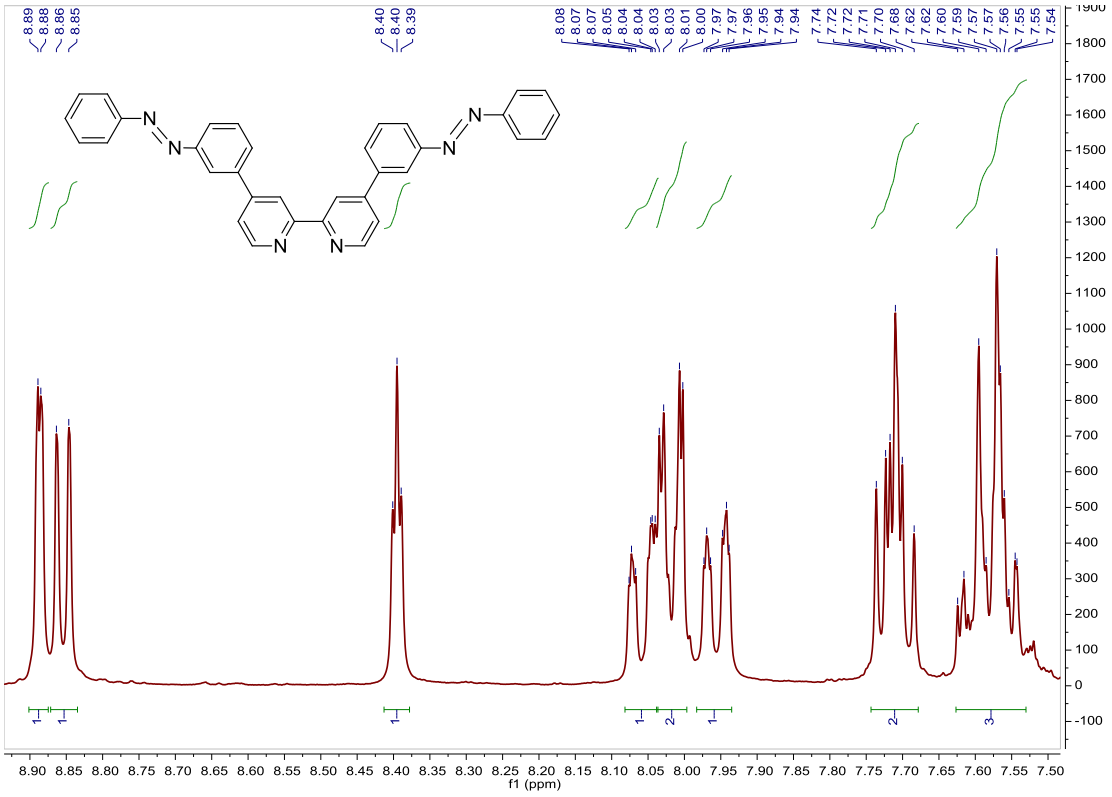

Fig. S19. ^{1}H NMR spectrum of **Ligand 5** in $CDCl_3$, 300 MHz.

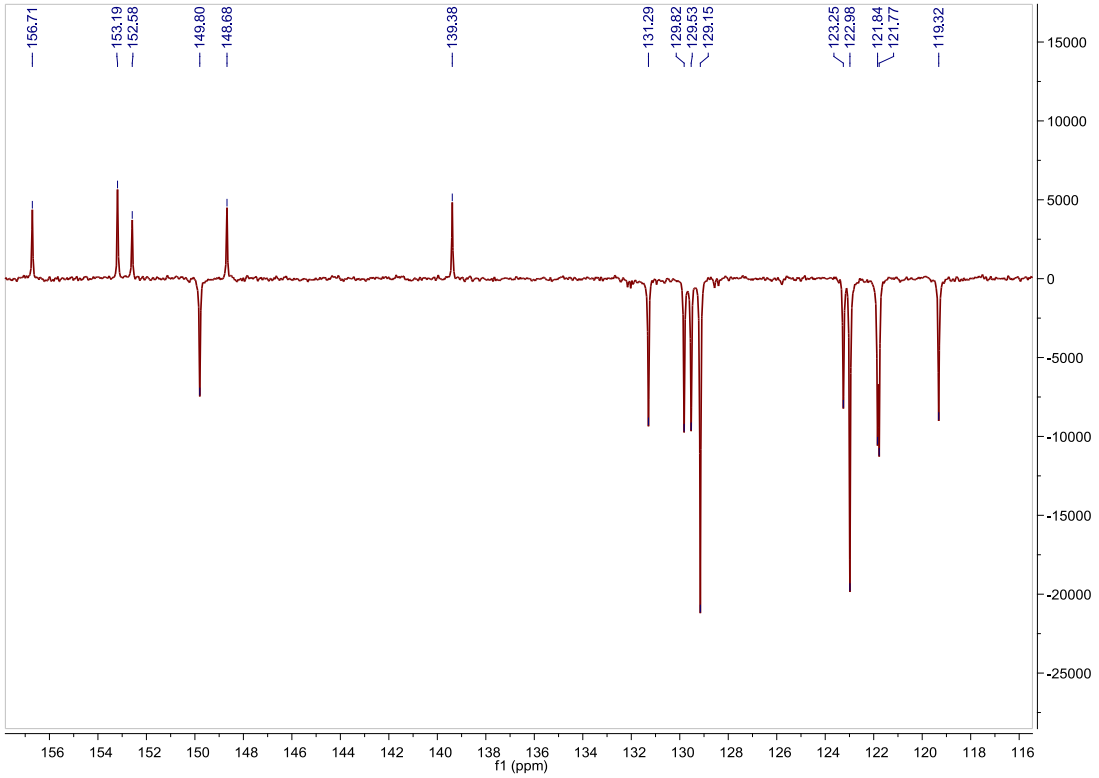

Fig. S20. ^{13}C APT NMR spectrum of **Ligand 5** in $CDCl_3$, 75 MHz.

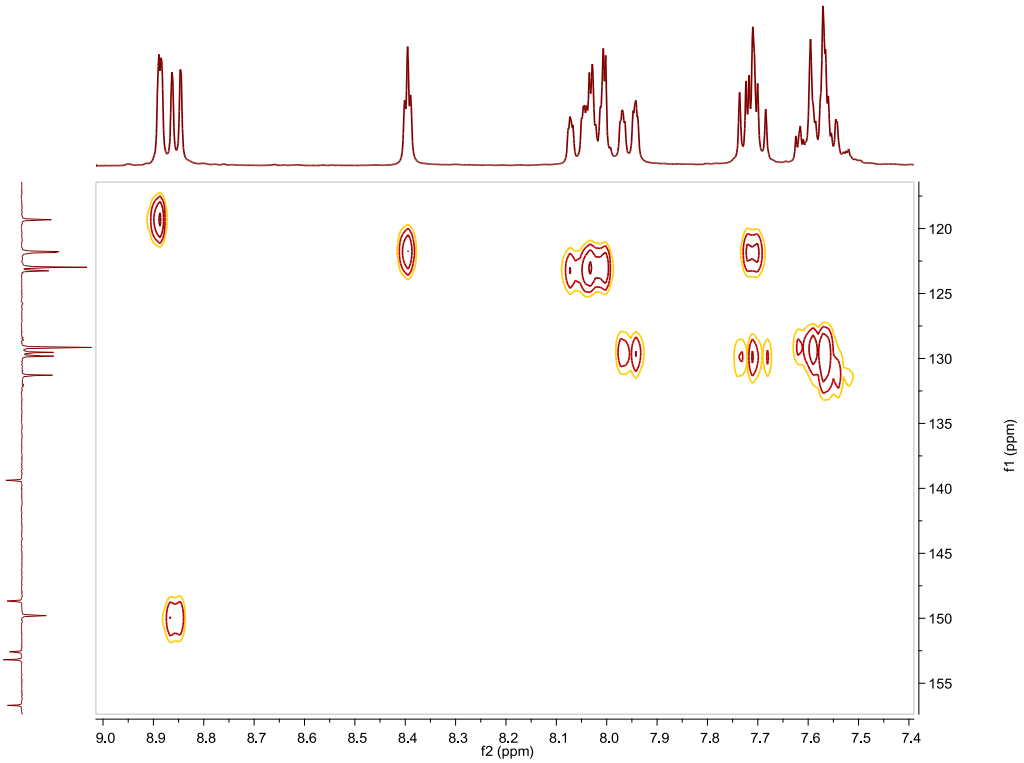

Fig. S21. HSQC NMR spectrum of **Ligand 5** in $CDCl_3$.

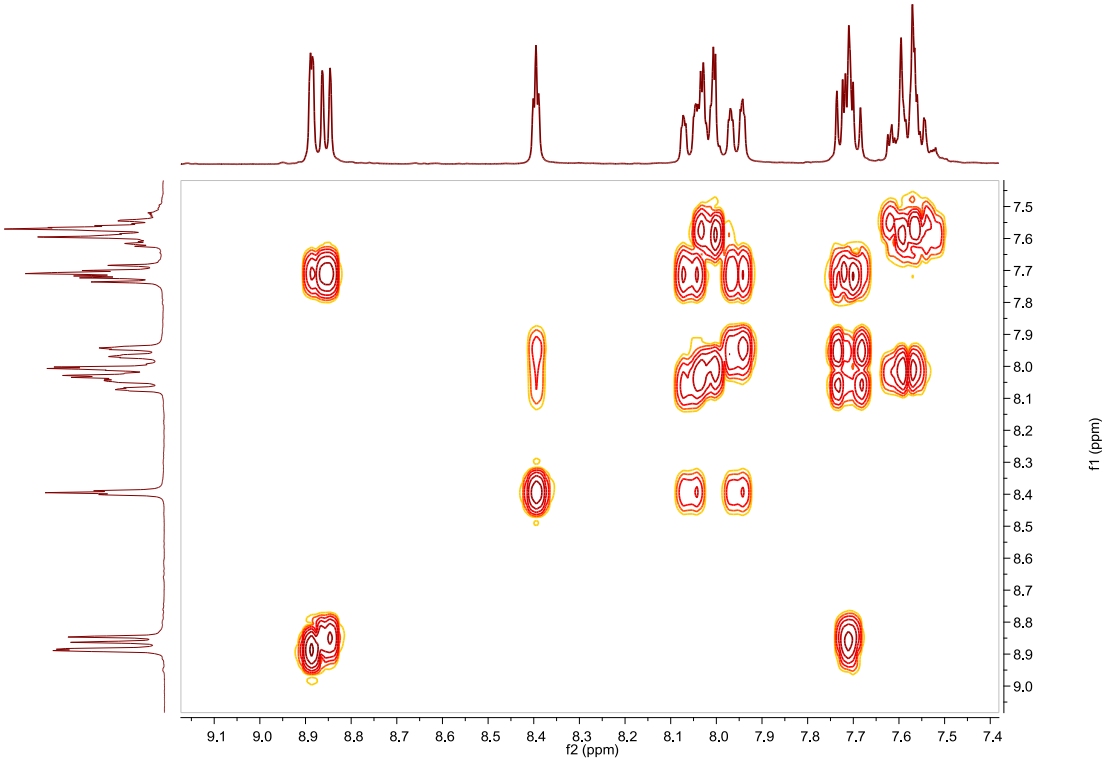

Fig. S22. COSY NMR spectrum of **Ligand 5** in $CDCl_3$.

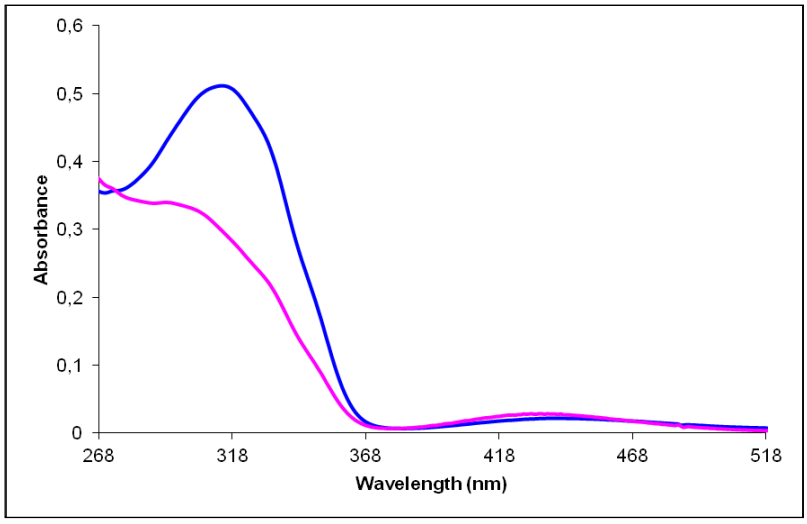

Fig. S23. UV/Vis spectra of **Ligand 5** in CH_3CN. Before (blue line) and after (pink line) irradiation at 320nm, $3.00 \cdot 10^{-5}$ M.

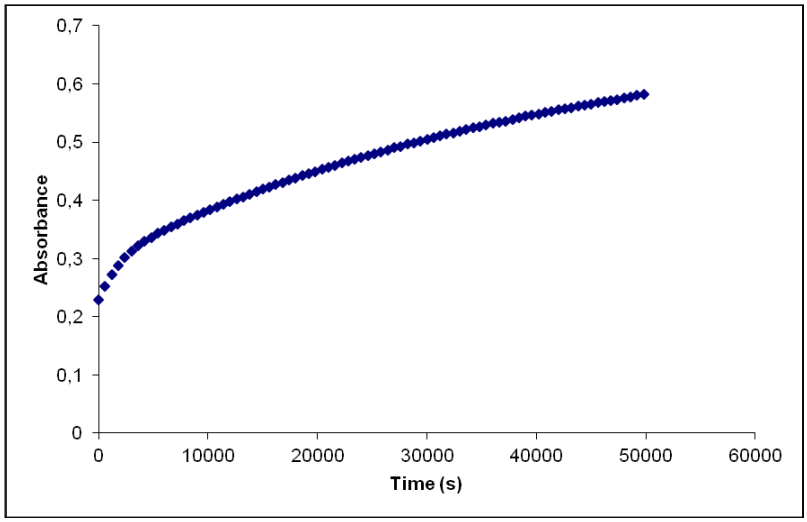

Fig. S24. Cis to trans thermal isomerization kinetics of **Ligand 5**. Absorption change of the band 314nm at 328 K in CH_3CN after irradiation at 320 nm. ($3.00 \cdot 10^{-5}$ M).

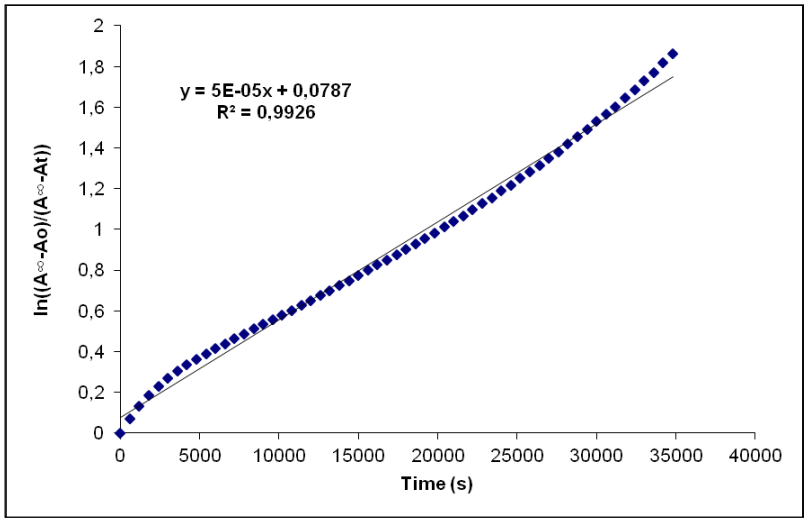

Fig. S25. Cis to trans thermal isomerization kinetics of **Ligand 5**. First-order plot. k (s^{-1}) = $5.0 \cdot 10^{-5}$. Half-life (min) = 231.

2,2'-bipyridine-*N*,*N*'-dioxide, 6. Synthesis and characterization.

SYNTHESIS[15]

2,2'-bipyridine (20.0 g, 128.2 mmol) were dissolved in glacial acetic acid (140 mL) and 30% H_2O_2 (50 mL) was added. The reaction mixture was refluxed at 80 °C for 16 h. After cooling to room temperature acetone (400 mL) was added and the product was precipitated as a white solid. The product was obtained by filtration and concentrating the mother liquor. Yield 97%. The spectroscopic data are coincident with those described in the literature.

^{1}H NMR (300 MHz, D_2O): δ 8.46–8.40 (m, 2H), 7.85–7.77 (m, 2H), 7.76–7.68 (m, 4H).

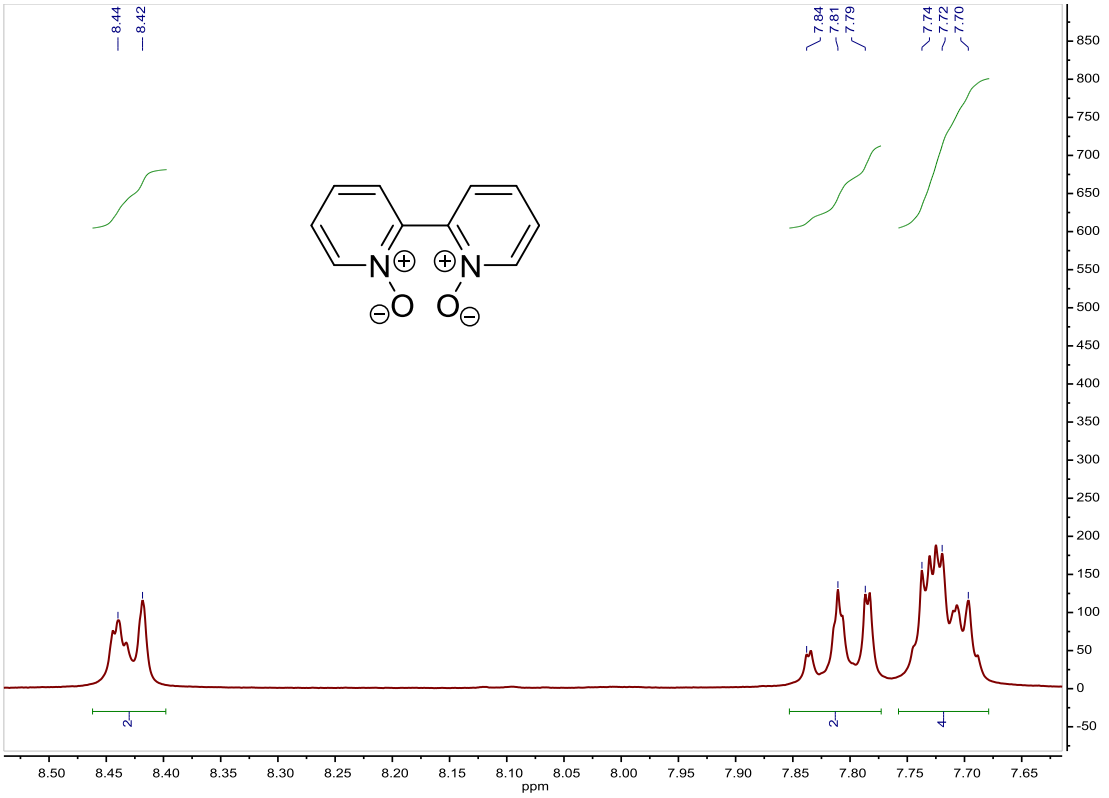

Fig. S26. ^{1}H NMR spectrum of 2,2'-bipyridine-*N*,*N*'-dioxide **6** in D_2O, 300 MHz.

[15] D. Zhang, J. P. Telo, C. Liao, S. E. Hightower and E. L. Clennan, *J. Phys. Chem. A*, **2007**, 13567–13574.

4,4'-dinitro-2,2'-bipyridine-N,N'-dioxide, 7. Synthesis and characterization.

SYNTHESIS[15]

A solution of 2,2'-bipyridine (20.0 g, 106.4 mmol) in 64 mL of sulfuric acid were cooled to 0 °C and fuming HNO_3 (34 mL) was added dropwise. The mixture was heated at 77 °C for 2 days. After cooling to room temperature the solution was poured into a mixture of ice and liquid N_2 (200 mL). The mixture was stirred until all the red fumes were liberated. The yellow solid was filtered off. Yield 53%. The spectroscopic data are coincident with those described in the literature.

^{1}H NMR (300 MHz, DMSO-d_6): δ 8.70 (d, J = 3.3 Hz, 2H), 8.60 (d, J = 7.2 Hz, 2H), 8.38 (dd, J = 3.3 Hz, J = 7.2 Hz, 2H).

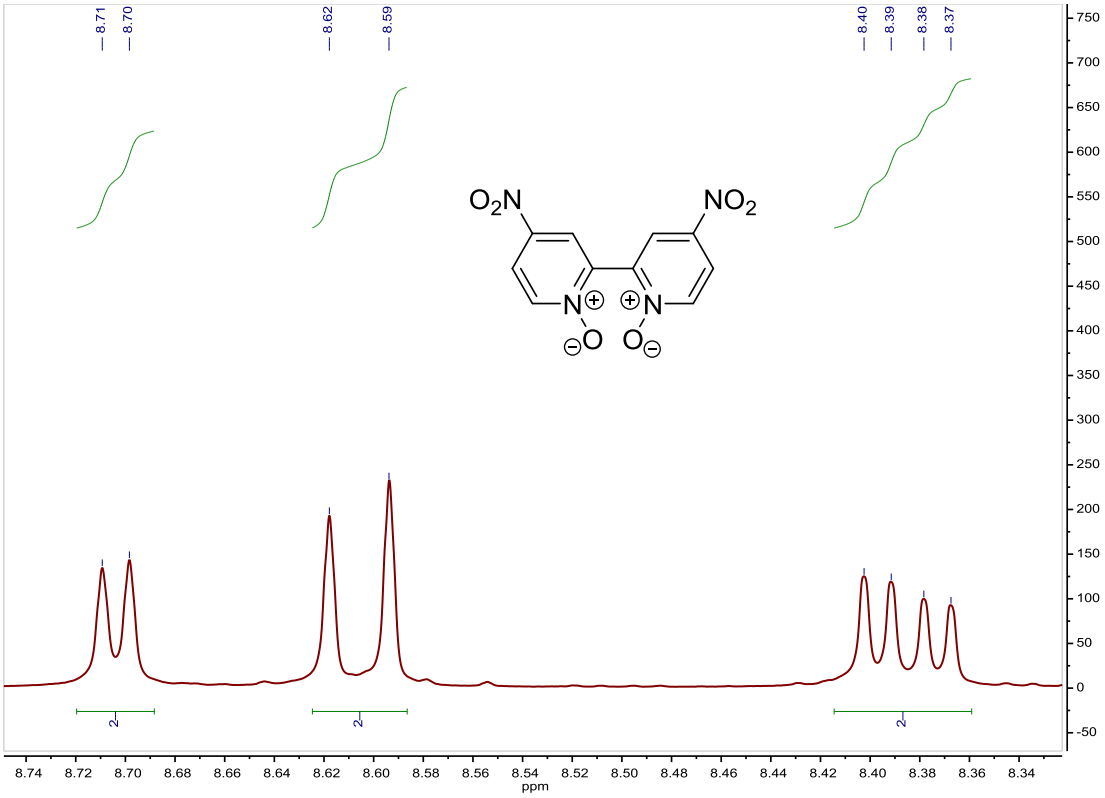

Fig. S27. ^{1}H NMR spectrum of 4,4'-dinitro-2,2'-bipyridine-N,N'-dioxide **7** in DMSO-d_6, 300 MHz.

4,4'-diamino-2,2'-bipyridine, 8. Synthesis and characterization.

SYNTHESIS[16]

4,4'-dinitro-2,2'-bipyridine-N,N'-dioxide **7** (4.0 g, 14.4 mmol) were dissolved in EtOH (133 mL) and 10% palladium on carbon (0.96 g, 9.03 mmol) were added. A solution of hydrazine monohydrate (5.4 mL, 112 mmol) in EtOH (27 mL) was added dropwise and the mixture was refluxed at 80 °C for 16 h. The mixture was filtered hot and washed with cold diethyl ether. The solvent of the filtrate was evaporated and the product was obtained as a brown solid. Yield 65%. The spectroscopic data are coincident with those described in the literature.

^{1}H NMR (300 MHz, DMSO-d_6): δ 8.04 (d, J = 5.5 Hz, 2H), 7.55 (d, J = 2.2 Hz, 2H), 6.46 (dd, J = 2.3 Hz, J = 5.5 Hz, 2H).

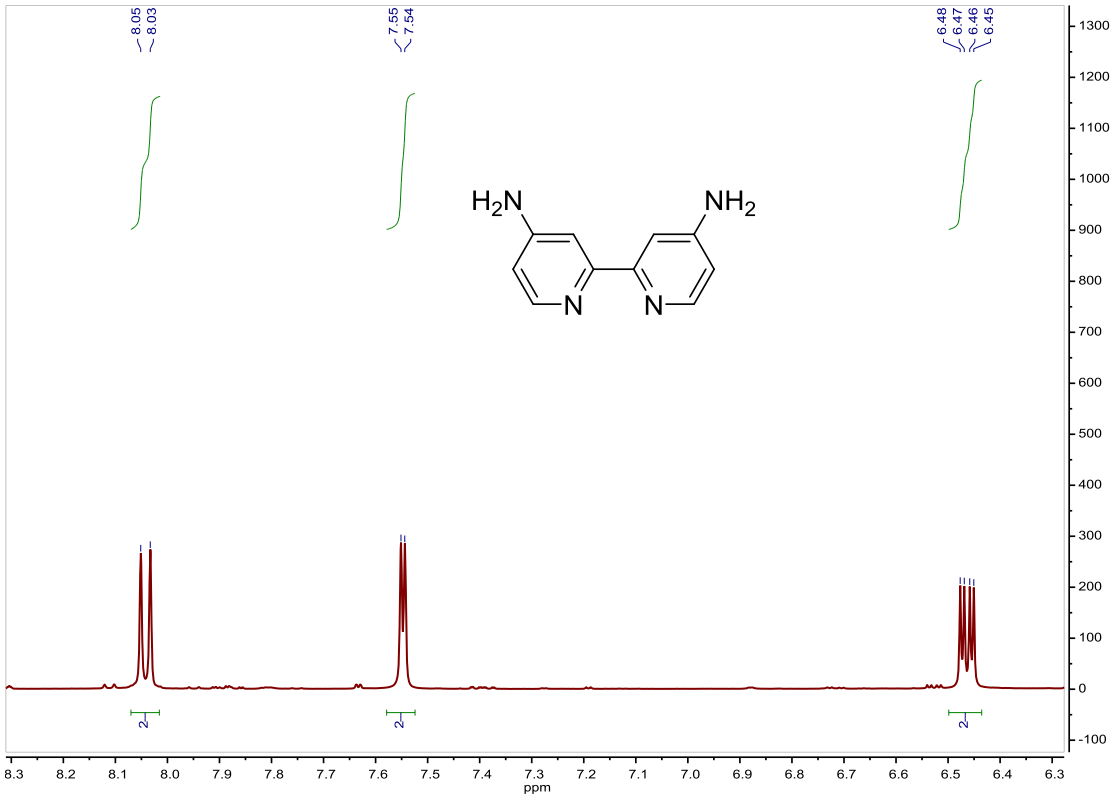

Fig. S28. ^{1}H NMR spectrum of 4,4'-diamino-2,2'-bipyridine **8** in DMSO-d_6, 300 MHz.

[16] O. Maury, J-P. Guégan, T. Renouard, A. Hilton, P. Dupau, N. Sandon, L. Toupet and H. Le Bozec, *New J. Chem.*, **2001**, *25*, 1553–1566.

[4-(phenylazo)phenyl]boronic acid 9. Synthesis and characterization.

SYNTHESIS[17]

The starting 4-iodoazobenzene (1.5 g, 4.87 mmol) was azeotropically dried with toluene under a N_2 atmosphere and dissolved in 40 mL of freshly distilled THF. The solution was cooled to -100 °C, *n*-BuLi 1.6 M in hexanes (3.5 mL, 5.6 mmol) were added and it was stirred for 30 min. The mixture was added to a solution of trimethyl borate (0.6 mL, 5.38 mmol) in 5 mL of freshly distilled THF at -100 °C. The reaction temperature was gradually raised up to room temperature and it was stirred overnight. A mixture of H_2SO_4/H_2O 1/10 (55 mL) was added at 0 °C. The organic layer was separated and the aqueous layer was extracted with Et_2O. An aqueous NaOH solution was added to the combined organic solution and the aqueous layer was washed with Et_2O. A mixture of H_2SO_4/H_2O 1/10 (100 mL) was added to the aqueous layer and an orange product precipitated. The product was purified by column chromatography (silica gel, CH_2Cl_2) and was obtained as an orange solid. Yield 20%. The spectroscopic data are coincident with those described in the literature.[18]

Elemental Analysis: calculated for ($C_{12}H_{11}BN_2O_2$): C, 63.76; H, 4.91; N, 12.39. Found: C, 64.61; H, 4.81; N, 12.30.

^{1}H NMR (300 MHz, $CDCl_3$): δ 8.27 (d, J = 8.1 Hz, 2H, (2 or 3)), 7.91 (d, J = 8.3 Hz, 2H, (2 or 3)), 7.88 (d, J = 9.1 Hz, 2H, (6)), 7.50–7.39 (m, 3H, (7+8)).

^{13}C APT NMR (75 MHz, $CDCl_3$): δ 154.85 (C_{quat}), 152.23 (C_{quat}), 136.14 (2CH, (2 or 3)), 130.96 (CH, (8)), 128.68 (2CH, (7)), 122.66 (2CH, (6)), 121.79 (2CH, (2 or 3)), (carbon bearing boron substituent not observed).

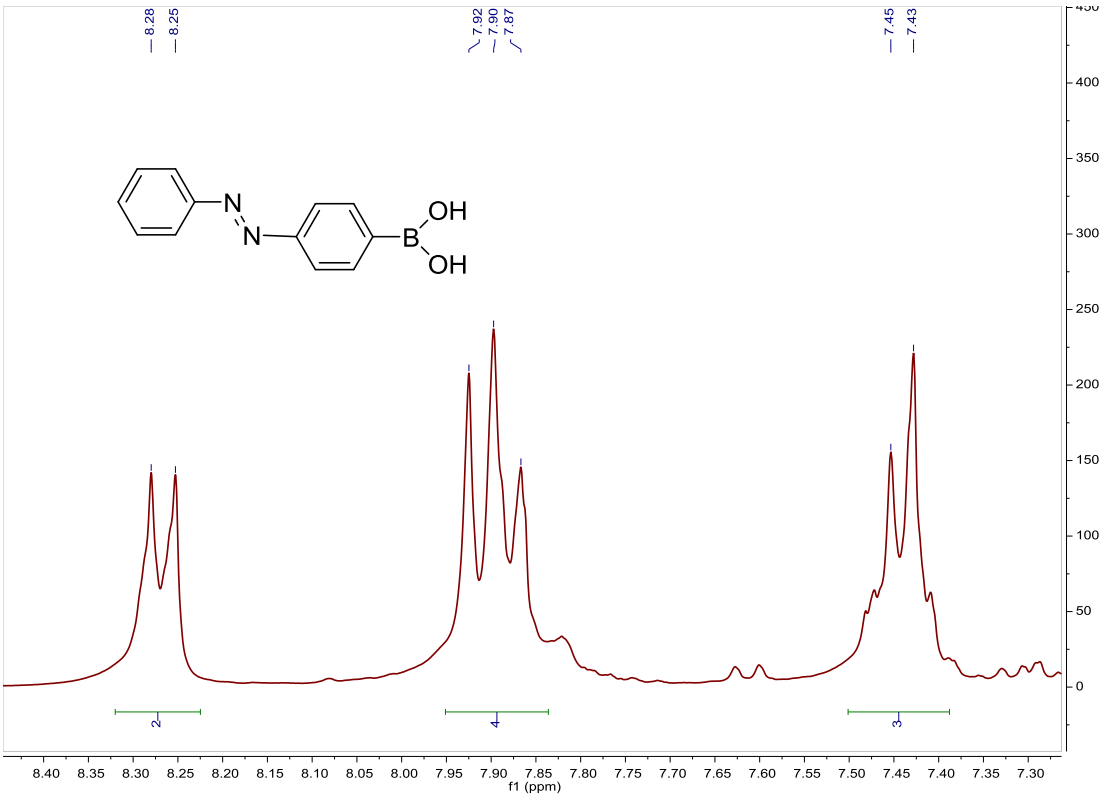

Fig. S29. ^{1}H NMR spectrum of [4-(phenylazo)phenyl]boronic acid **9** in $CDCl_3$, 300 MHz.

[17] N. Kano, J. Yoshino and T. Kawashima, *Org. Lett.*, **2005**, *7*, 3909–3911.

[18] K. Owashi, K. Ueno, T. Satomi, G. Chen and H. Otsuka, *Trans. Mater. Res. Soc. Japan,* **2007**, *32*, 777–780.

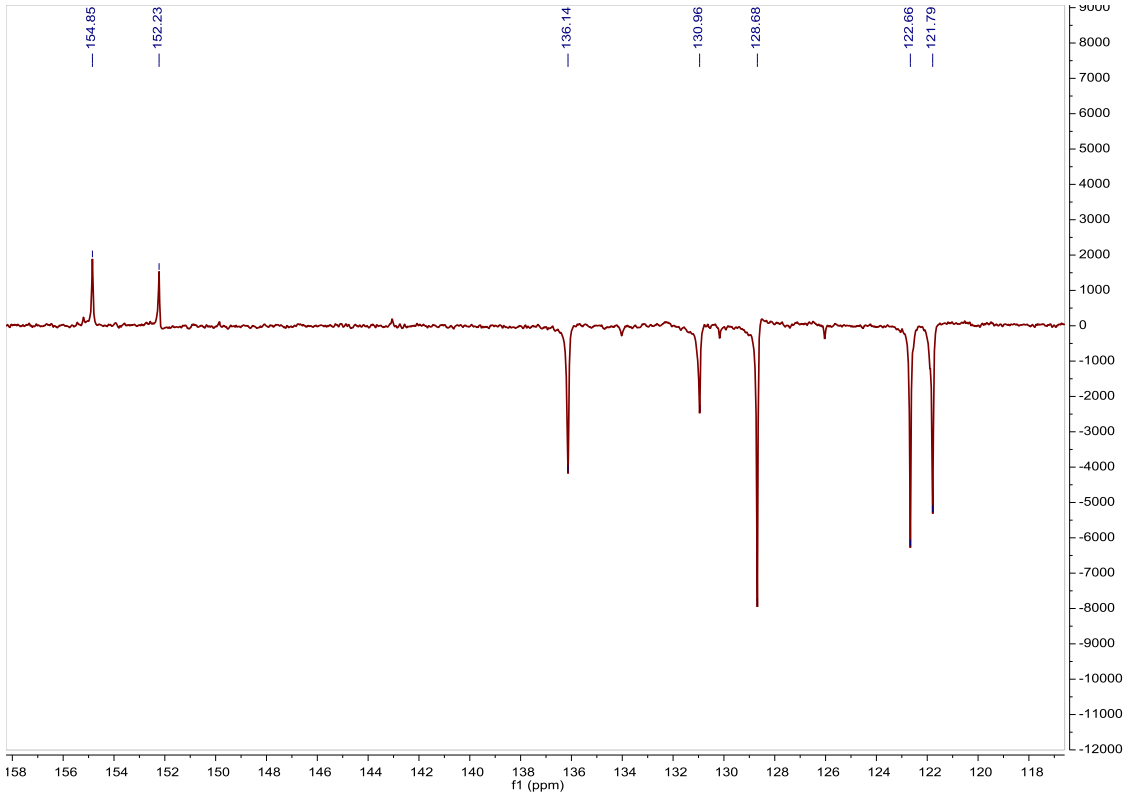

Fig. S30. ^{13}C APT NMR spectrum of [4-(phenylazo)phenyl]boronic acid **9** in $CDCl_3$, 75 MHz.

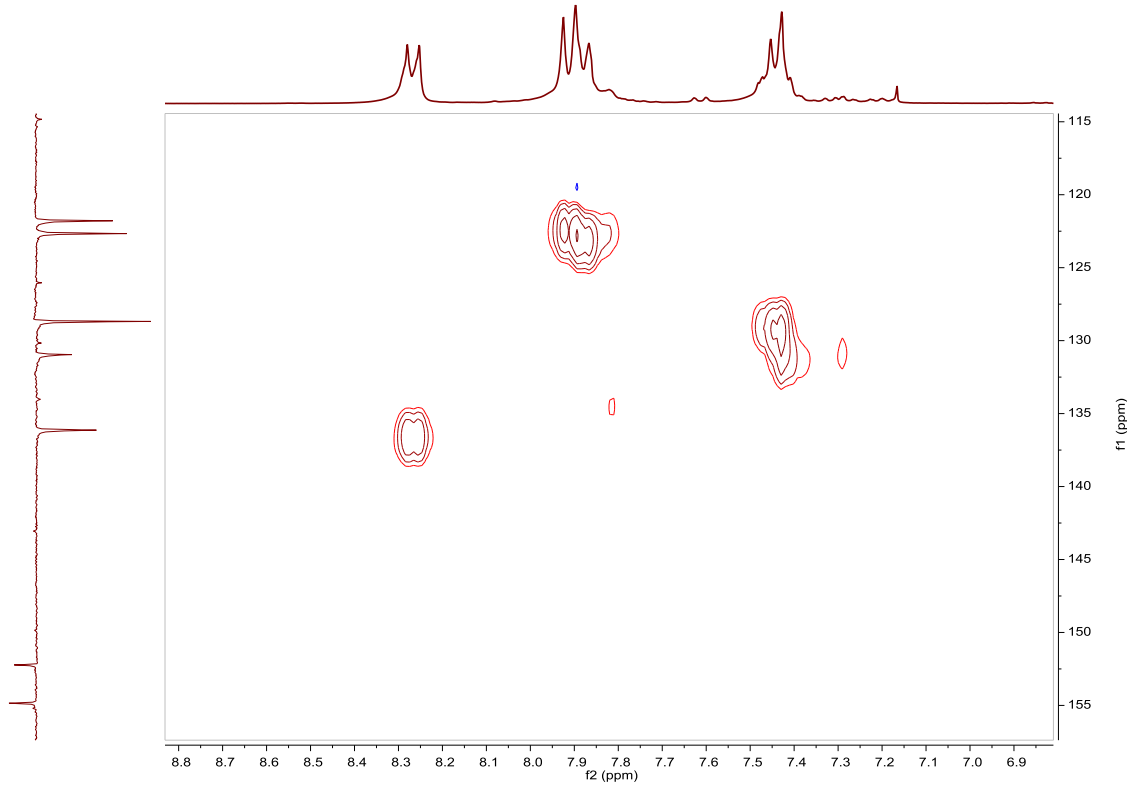

Fig. S31. HSQC spectrum of [4-(phenylazo)phenyl]boronic acid **9** in $CDCl_3$.

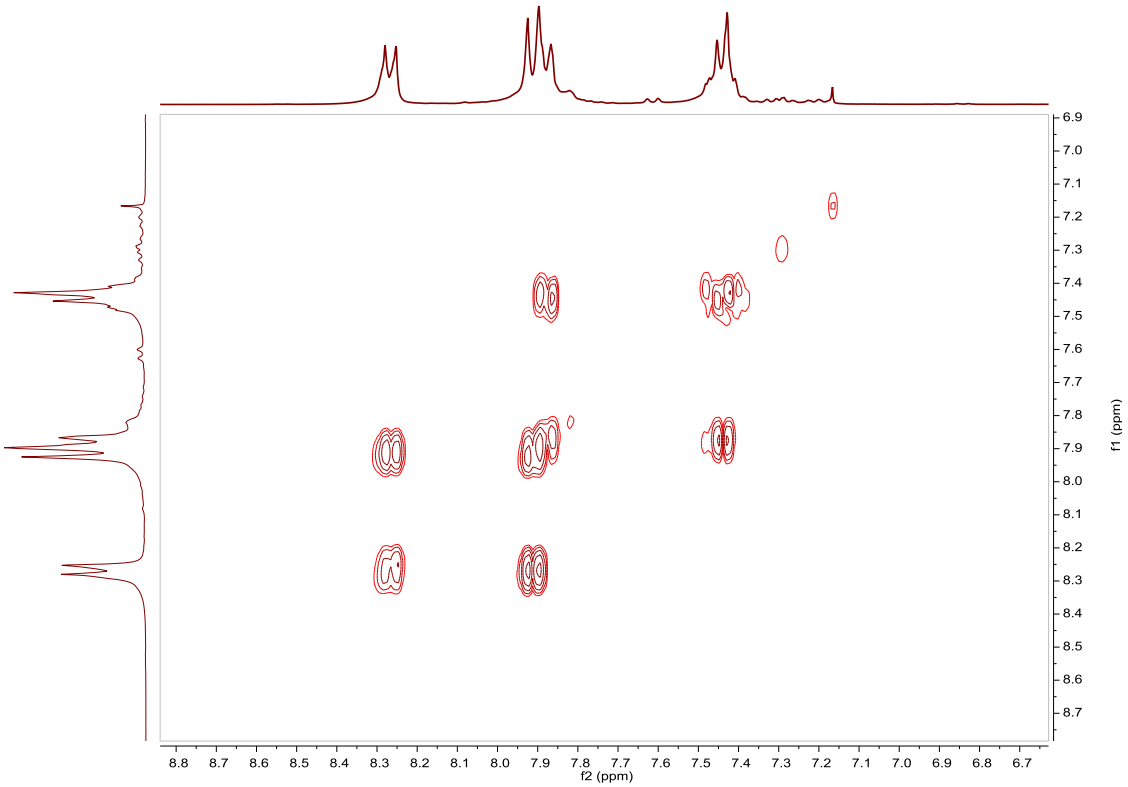

Fig. S32. COSY spectrum of [4-(phenylazo)phenyl]boronic acid **9** in $CDCl_3$.

[3-(phenylazo)phenyl]boronic acid 10. Synthesis and characterization.

SYNTHESIS[17]

The starting 3-iodoazobenzene (3.0 g, 9.74 mmol) was azeotropically dried with toluene under a N_2 atmosphere and dissolved in 80 mL of freshly distilled THF. The solution was cooled to -100 °C, *n*-BuLi 1.6 M in hexanes (7.0 mL, 11.2 mmol) were added and it was stirred for 30 min. The mixture was added to a solution of trimethyl borate (1.20 mL, 10.76 mmol) in 10 mL of freshly distilled THF at -100 °C. The reaction temperature was gradually raised up to room temperature and it was stirred overnight. A mixture of H_2SO_4/H_2O 1/10 (110 mL) was added at 0 °C. The organic layer was separated and the aqueous layer was extracted with Et_2O. An aqueous NaOH solution was added to the combined organic solution and the aqueous layer was washed with Et_2O. A mixture of H_2SO_4/H_2O 1/10 (200 mL) was added to the aqueous layer and a brown product precipitated. The product was filtrated and was obtained as a brown solid. Yield 61%. The spectroscopic data are coincident with those described in the literature.[18]

^{1}H NMR (300 MHz, $CDCl_3$): δ 8.31 (s, 1H), 8.09–8.04 (m, 1H), 7.97 (brd, J = 1.8 Hz, J = 8.3 Hz, 2H), 7.95–7.90 (m, 1H), 7.65–7.50 (m, 4H).

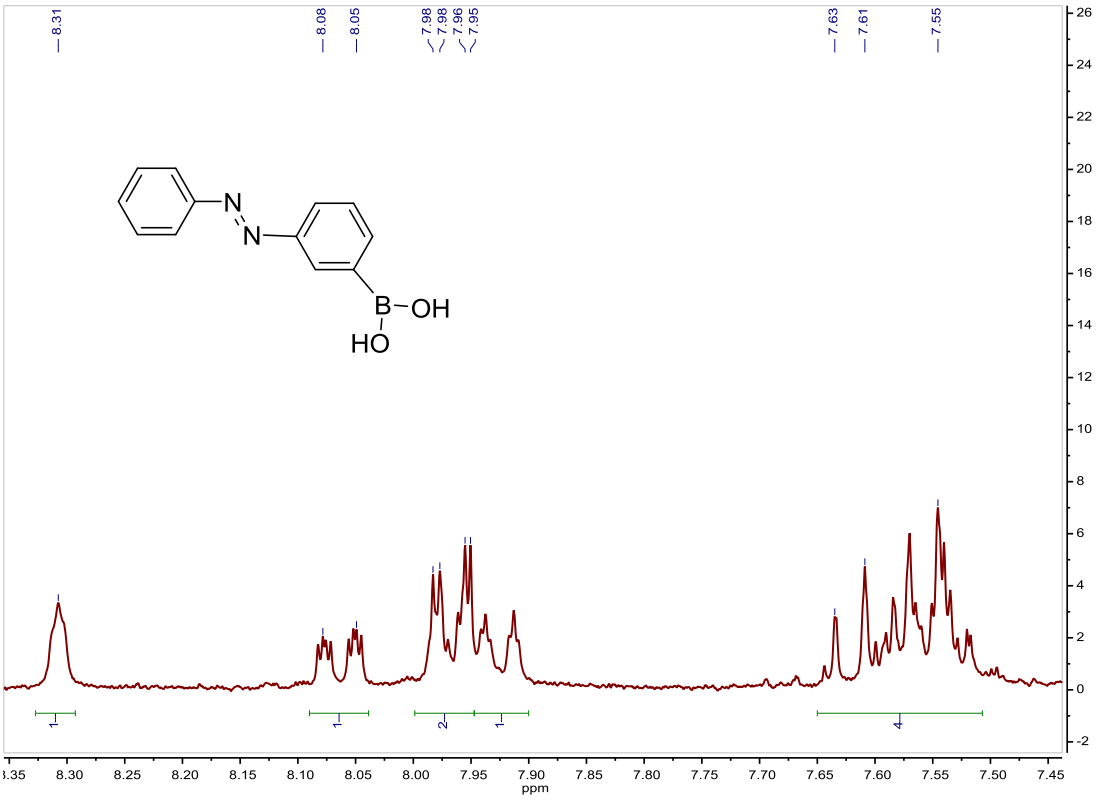

Fig. S33. ^{1}H NMR spectrum of [3-(phenylazo)phenyl]boronic acid **10** in $CDCl_3$, 300 MHz.

[4-(phenylazo)phenyl]boronic acid pinacol ester 11. Synthesis and characterization.

SYNTHESIS[19]

Nitrosobenzene (2.49 g, 23.25 mmol) were dissolved in glacial acetic acid (84 mL) to give a green solution. (4,4,5,5-Tetramethyl-1,3,2-dioxaborolan-2-yl)aniline (3.5 g, 15.98 mmol) were added and the mixture was refluxed at 118 °C for 3.5 h. After cooling to room temperature, H_2O (100 mL) were added and the solution was neutralized with $NaHCO_3$. The product was extracted with CH_2Cl_2 and purified by column chromatography (silica gel, CH_2Cl_2). It was obtained as an orange solid. Yield 82%. The spectroscopic data are coincident with those described in the literature.

^{1}H NMR (300 MHz, $CDCl_3$): δ 8.03–7.91 (m, 6H), 7.60–7.50 (m, 3H).

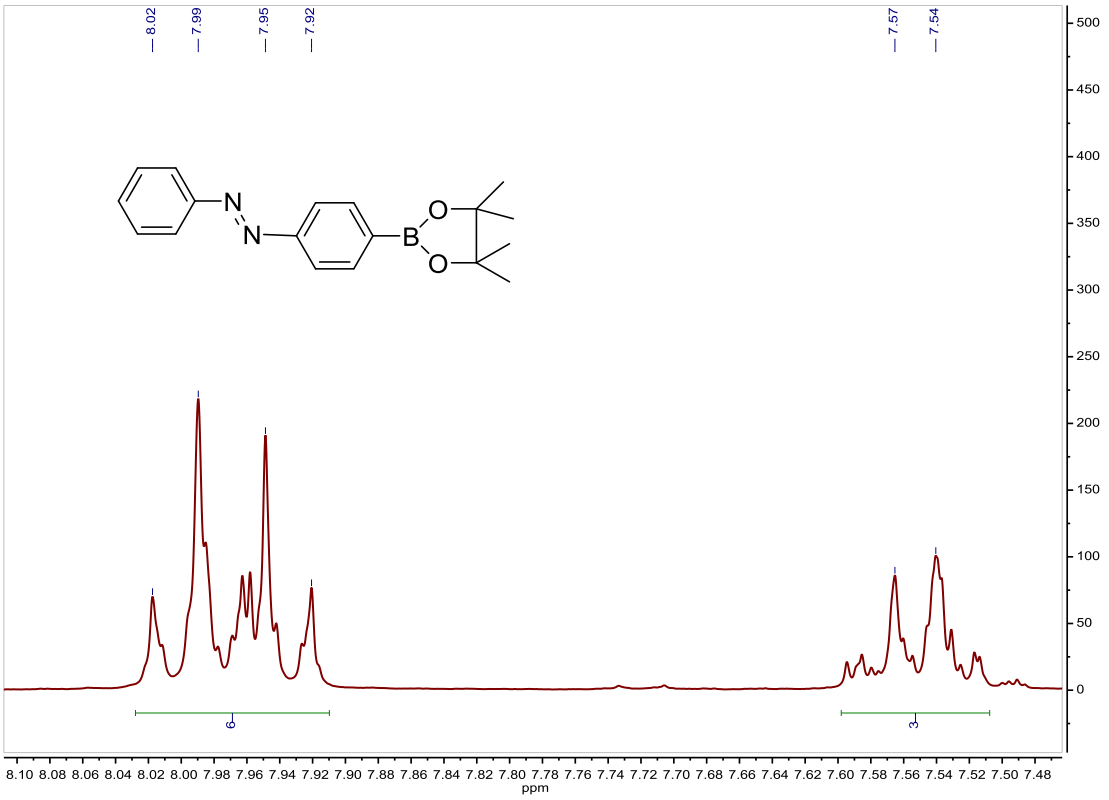

Fig. S34. ^{1}H NMR spectrum of [4-(phenylazo)phenyl]boronic acid pinacol ester **11** in $CDCl_3$, 300 MHz.

[19] J. H. Harvey, B. K. Butler and D. Trauner, *Tetrahedron Lett.*, **2007**, *48*, 1661–1664.

Ligand 12, tris(*m*-azobenzene)phosphane. Synthesis, characterization and photoisomerization studies.

SYNTHESIS[20]

The starting 3-iodoazobenzene (3.0 g, 9.74 mmol) was azeotropically dried with toluene under a N_2 atmosphere and dissolved in 60 mL of freshly distilled THF. The solution was cooled to -110 °C, *n*-BuLi 1.6 M in hexanes (6.0 mL, 9.6 mmol) were added and it was stirred for 30 min. PCl_3 (285 µL, 3.28 mmol) were added, the reaction temperature was gradually raised up to room temperature and it was stirred overnight. The solvent was evaporated and the product was purified by column chromatography (silica gel, CH_2Cl_2/Hexane 1/1). The product was obtained as an orange solid. Yield 14%. The spectroscopic data are coincident with those described in the literature.

^{1}H NMR (500 MHz, $CDCl_3$): δ 7.86–8.13 (m, 12H), 7.45–7.60 (m, 15H).

^{31}P NMR (202.5 MHz, $CDCl_3$): δ -3.74.

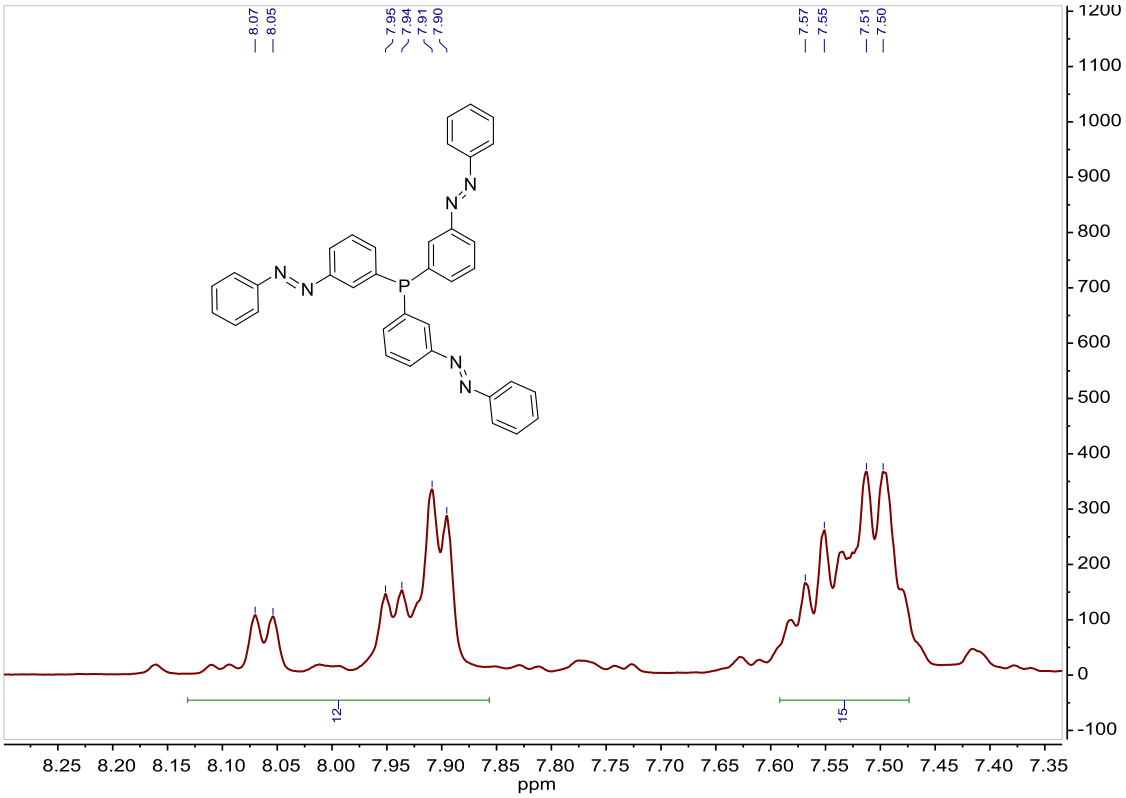

Fig. S35. ^{1}H NMR spectrum of tris(*m*-azobenzene)phosphane **Ligand 12**, in $CDCl_3$, 500 MHz.

[20] M. D. Segarra-Maset, P. W. N. M. van Leeuwen, and Z. Freixa, *Eur. J. Inorg. Chem.*, **2010**, 2075–2078.

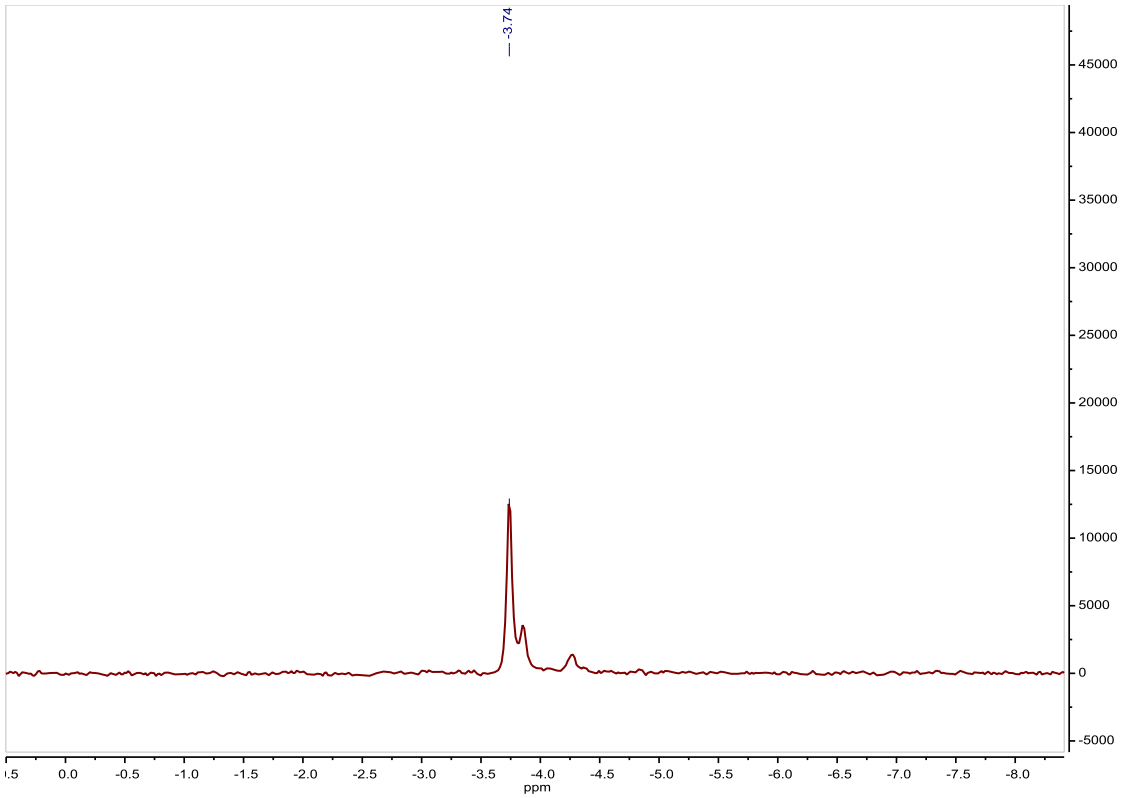

Fig. S36. ^{31}P NMR spectrum of tris(*m*-azobenzene)phosphane **Ligand 12**, in $CDCl_3$, 202.5 MHz.

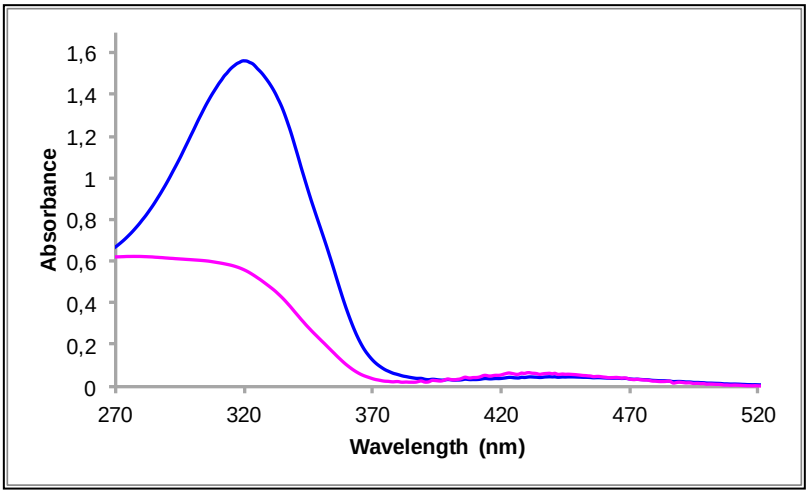

Fig. S37. UV/Vis spectra of tris(*m*-azobenzene)phosphane **Ligand 12** in ACN. Before (blue line) and after (pink line) irradiation at 323 nm, $2.57 \cdot 10^{-5}$M.

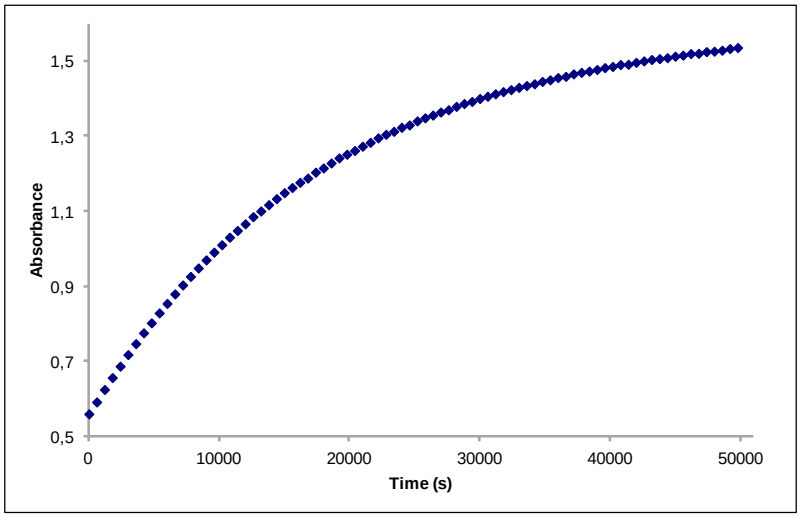

Fig. S38. Cis to trans thermal isomerization kinetics of tris(*m*-azobenzene)phosphane **Ligand 12**. Absorption change of the band 320 nm at 338 K in ACN after irradiation at 323 nm. ($2.57 \cdot 10^{-5}$M).

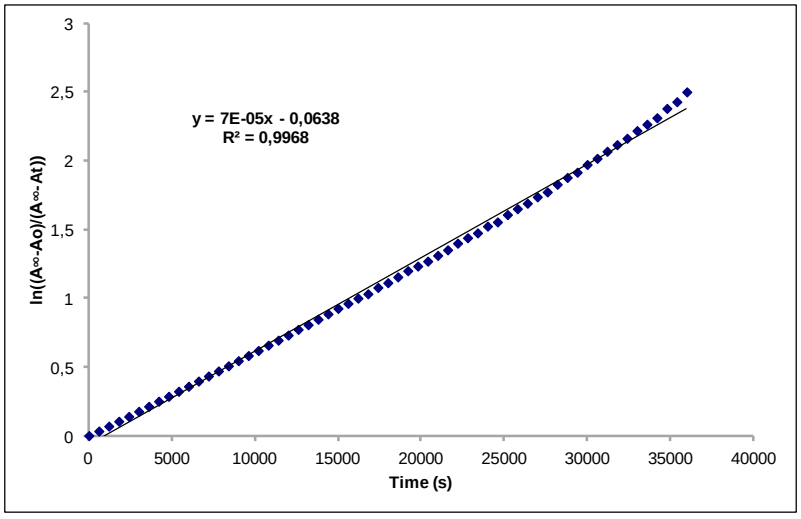

Fig. S39. Cis to trans thermal isomerization kinetics of tris(*m*-azobenzene)phosphane **Ligand 12**. First-order plot. k (s^{-1}) = $7.0 \cdot 10^{-5}$. Half-life (min) = 165.

Ligand 13, tris(*p*-azobenzene)phosphane. Synthesis, characterization and photoisomerization studies.

SYNTHESIS[20]

The starting 4-iodoazobenzene (1.5 g, 4.87 mmol) was azeotropically dried with toluene under a N_2 atmosphere and dissolved in 30 mL of freshly distilled THF. The solution was cooled to -80 °C, *n*-BuLi 1.6 M in hexanes (4.5 mL, 7.3 mmol) were added and it was stirred for 30 min. PCl_3 (142 µL, 1.63 mmol) were added, the reaction temperature was gradually raised up to room temperature and it was stirred overnight. The solvent was evaporated, the residue was washed with EtOH and the product was obtained as an orange solid. Yield 10%.

Elemental Analysis: calculated for ($C_{36}H_{27}N_6P$·EtOH): C, 73.53; H, 5.36; N, 13.54. Found: C, 73.88; H, 4.98; N, 13.85.

Exact Mass: ESI-MS $[C_{36}H_{27}N_6P + H]^+$: calculated: m/z= 575.2113, found: m/z= 575.2123.

^{1}H NMR (300 MHz, $CDCl_3$): δ 7.88–7.79 (m, 12H), 7.49–7.38 (m, 15H).

^{13}C APT NMR (75 MHz, $CDCl_3$): δ 152.51 (s, $3C_{quat}$), 152.22 (s, $3C_{quat}$), 139.42 (d, J = 12.7 Hz, $3C_{quat}$), 134.09 (d, J = 20.2 Hz, 6CH), 130.86 (s, 3CH), 128.68 (s, 6CH), 122.54 (s, 6CH), 122.50 (d, J = 6.0 Hz, 6CH).

^{31}P NMR (202.5 MHz, $CDCl_3$): δ -3.69 (s, 1P).

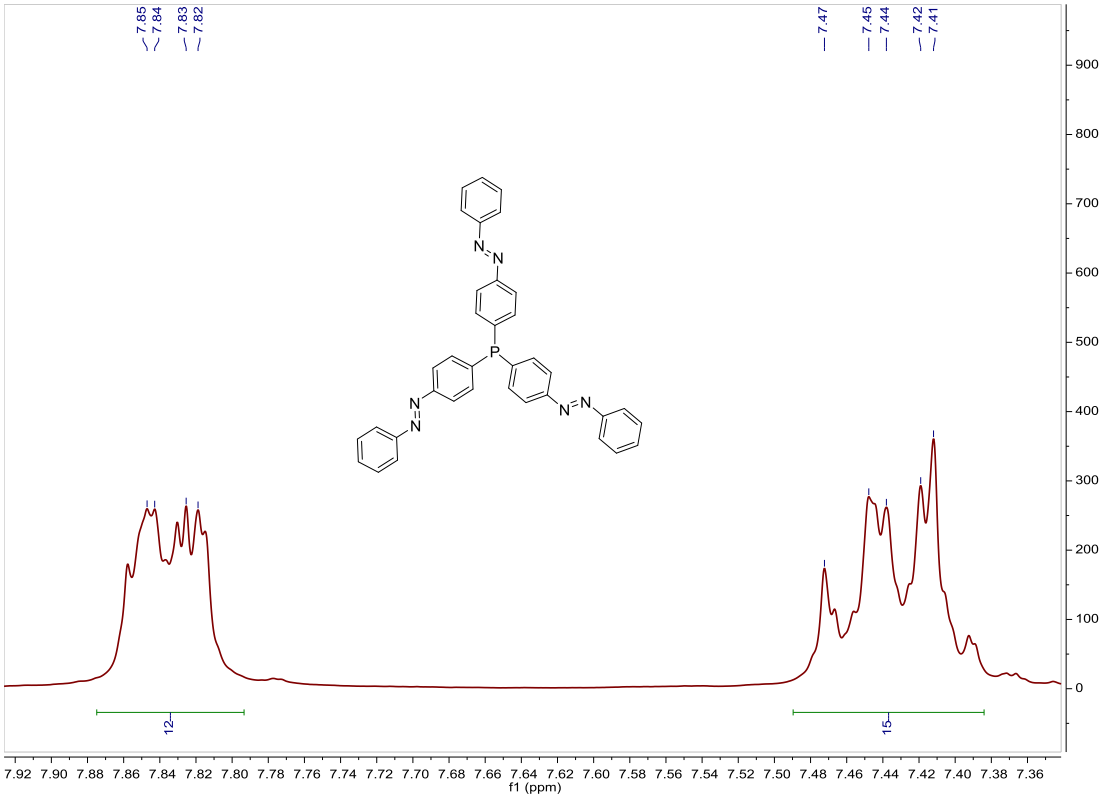

Fig. S40. ^{1}H NMR spectrum of tris(*p*-azobenzene)phosphane **Ligand 13** in $CDCl_3$, 300 MHz.

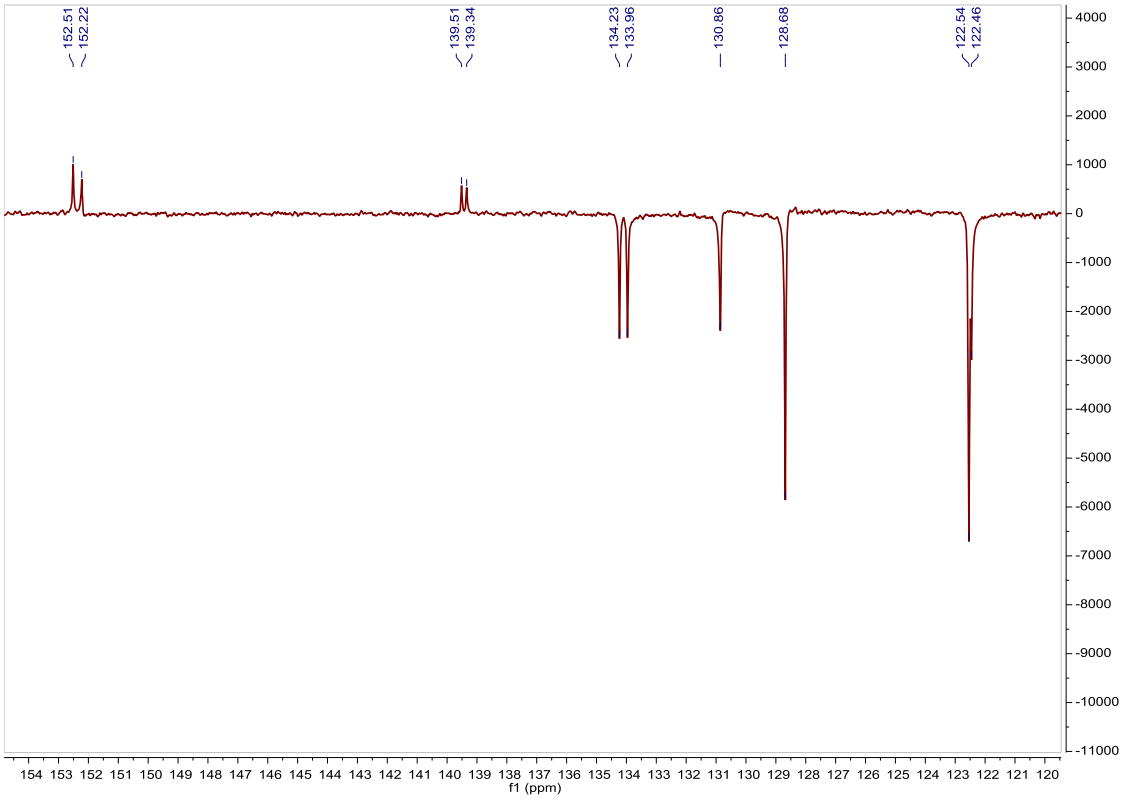

Fig. S41. ^{13}C APT NMR spectrum of tris(*p*-azobenzene)phosphane **Ligand 13** in $CDCl_3$, 75 MHz.

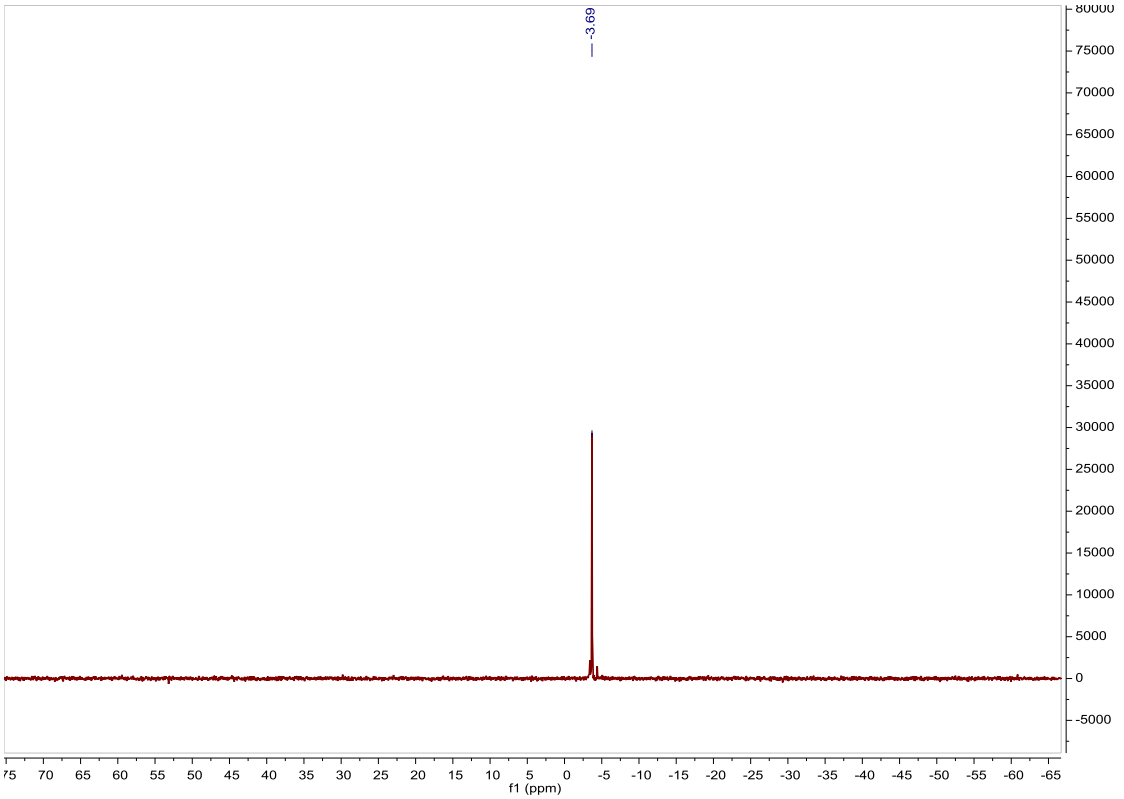

Fig. S42. ^{31}P NMR spectrum of tris(*p*-azobenzene)phosphane **Ligand 13** in $CDCl_3$, 202.5 MHz.

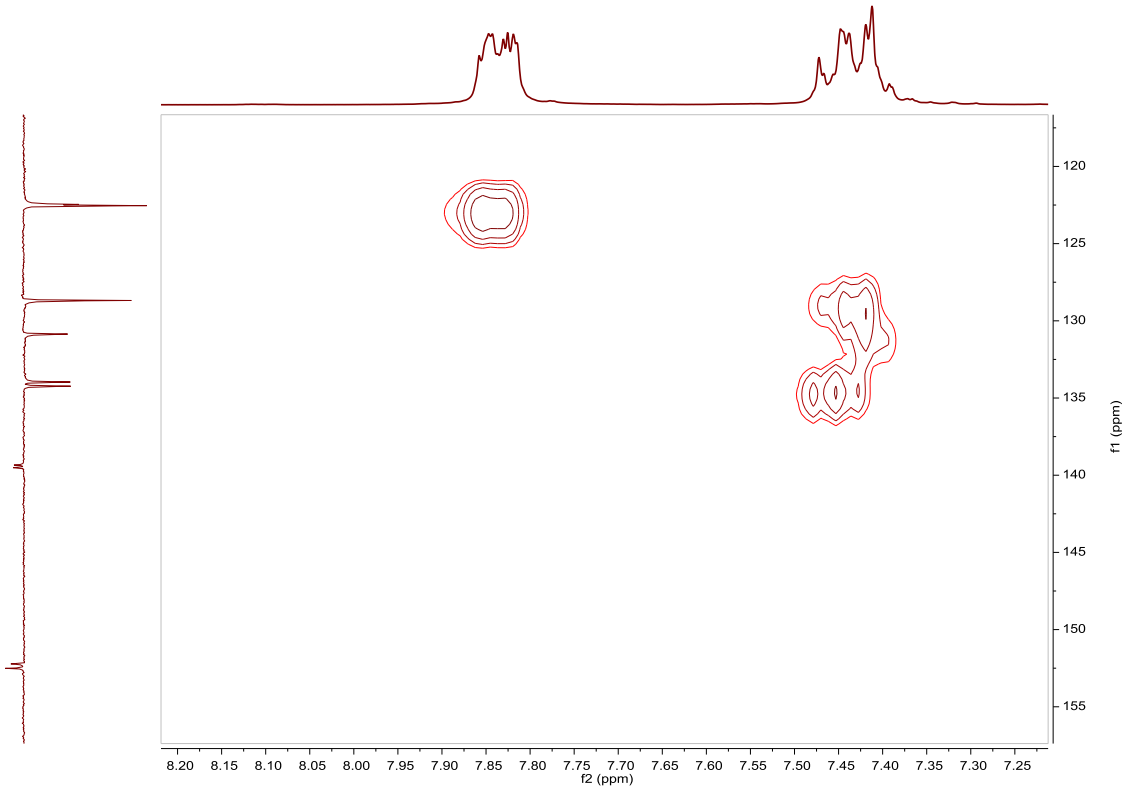

Fig. S43. HSQC NMR spectrum of tris(*p*-azobenzene)phosphane **Ligand 13** in $CDCl_3$.

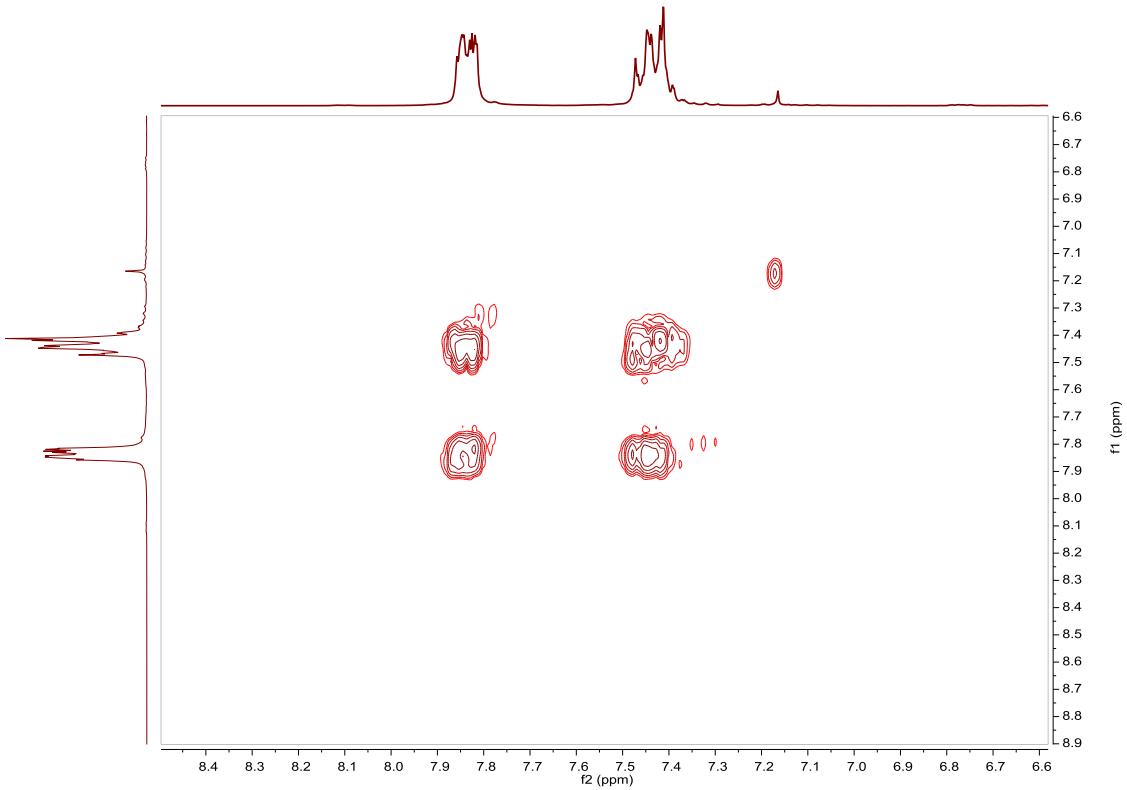

Fig. S44. COSY NMR spectrum of tris(*p*-azobenzene)phosphane **Ligand 13** in $CDCl_3$.

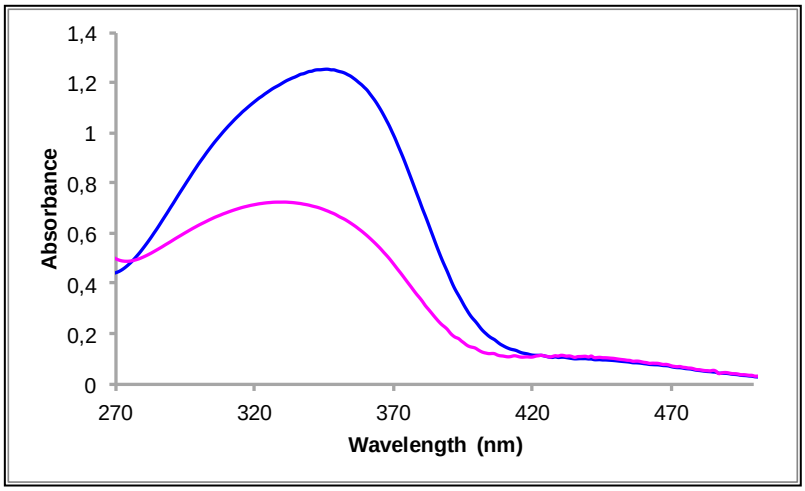

Fig. S45. UV/Vis spectra of tris(*p*-azobenzene)phosphane **Ligand 13** in ACN. Before (blue line) and after (pink line) irradiation at 354nm, $2.72 \cdot 10^{-5}$M.

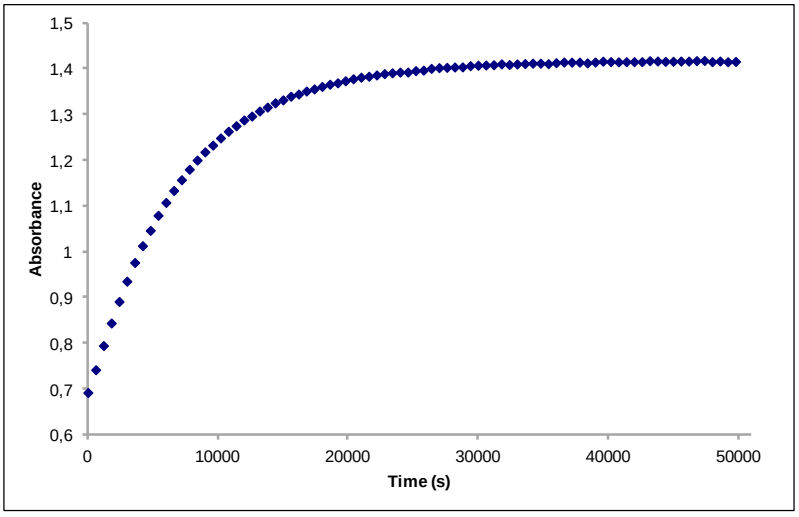

Fig. S46. Cis to trans thermal isomerization kinetics of tris(*p*-azobenzene)phosphane **Ligand 13**. Absorption change of the band 345nm at 338 K in ACN after irradiation at 354 nm. ($2.72 \cdot 10^{-5}$M).

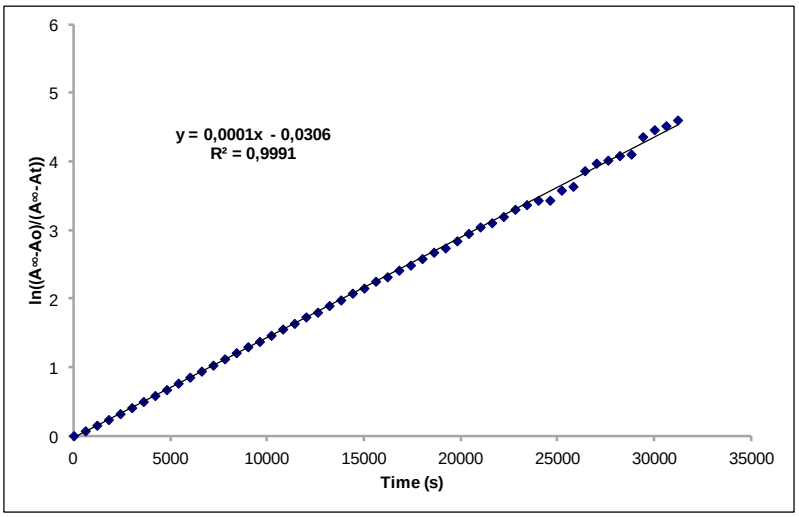

Fig. S47. Cis to trans thermal isomerization kinetics of tris(*p*-azobenzene)phosphane **Ligand 13**. First-order plot. k (s^{-1}) = $1.0 \cdot 10^{-4}$. Half-life (min) = 115.

Ligand 14, 4,4'-dinitro-2,2'-bipyridine. Synthesis and characterization.

SYNTHESIS[21]

4,4'-dinitro-2,2'-bipyridine-N-oxide (1,40 g, 5.03 mmol) were dissolved in freshly distilled CH_2Cl_2. To the solution PCl_3 (16 mL, 183.42 mmol) were added dropwise and the mixture was refluxed for 14 h. After cooling to room temperature, the white solid was removed by filtration and the solution was poured into ice/water (200 mL). An aqueous solution of NaOH was added until pH = 8 and the product was extracted with CH_2Cl_2. The product was redissolved in CH_2Cl_2 and obtained as a yellow solid. Yield 50%. The spectroscopic data are coincident with those described in the literature.

^{1}H NMR (300 MHz, $CDCl_3$): δ 9.24 (d, J = 1.7 Hz, 2H), 9.07 (d, J = 5.3 Hz, 2H), 8.16 (dd, J = 2.2 Hz, J = 5.3 Hz, 2H).

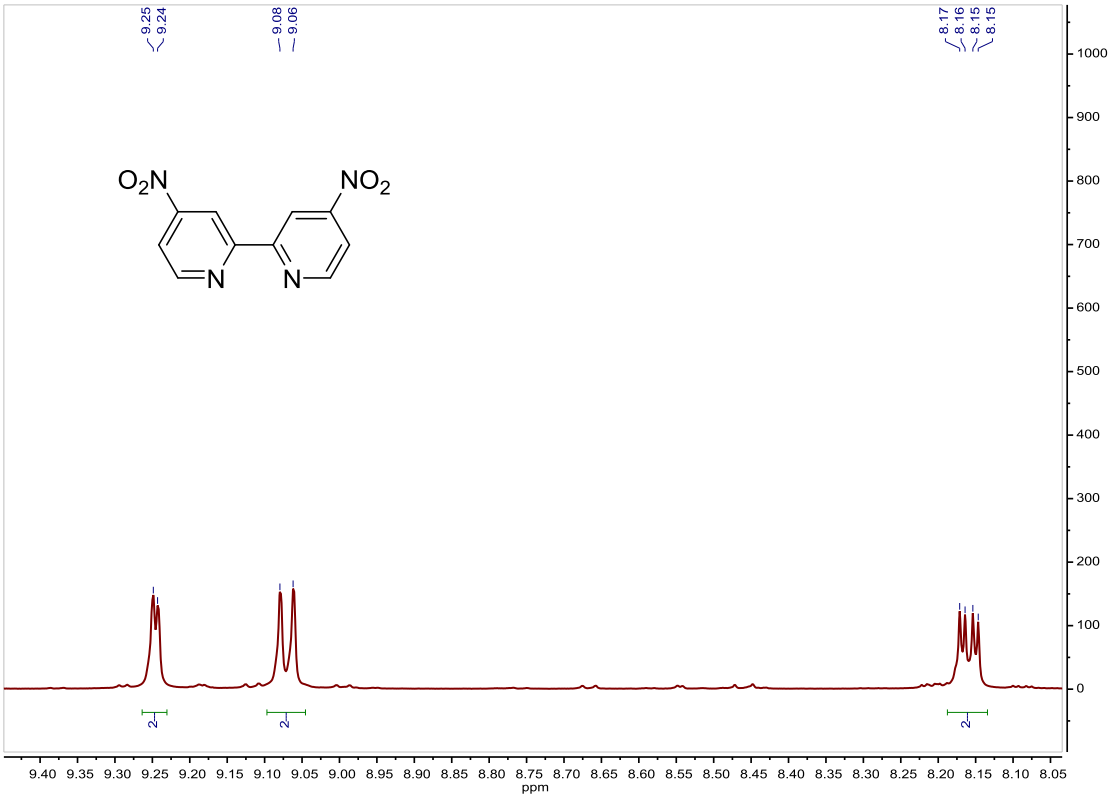

Fig. S48. ^{1}H NMR spectrum of **Ligand 14** in $CDCl_3$, 300 MHz.

[21] H. Arzoumanian and R. Bakhtchadjian, *Transition Metal Chemistry*, **2006**, *31*, 681–689.

Ligand 15, 4,4'-bis(diethylphosphonate)-2,2'-bipyridine. Synthesis and characterization.

SYNTHESIS[22]

4,4'-dibromo-2,2'-bipyridine (0.5 g, 1.6 mmol) was dissolved in 5 ml of freshly distilled toluene and stirred under nitrogen for 20 min. Diethyl phosphite (0.56 ml, 4.35 mmol) and distilled $N(Et)_3$ (0.61 ml) were added and the mixture was stirred for 10 min. The catalyst, $Pd(PPh_3)_4$ (0.18 g, 0.16 mmol), was added and the mixture was heated at 90 °C for 4 h. After cooling to room temperature ether was added and the precipitated was removed by filtration. The product was purified by column chromatography (silica gel, 100% CH_2Cl_2 to 100% acetone) to yield (60%) of the diethylphosphonate bipyridine. The spectroscopic data are coincident with those described in the literature.

^{1}H NMR (300 MHz, $CDCl_3$): δ 8.88 (t, J = 5.5 Hz, 1H), 8.81 (d, J = 14.2 Hz, 1H), 7.76 (ddd, J = 1.4 Hz, J = 4.8 Hz, J = 13.0 Hz, 1H), 4.24 (m, 4H), 1.40 (t, J = 7.0 Hz, 6H).

UV/Vis (EtOH), λ, nm (ε, 10^4 M^{-1} cm^{-1}): 240 (1.2), 292 (1.45).

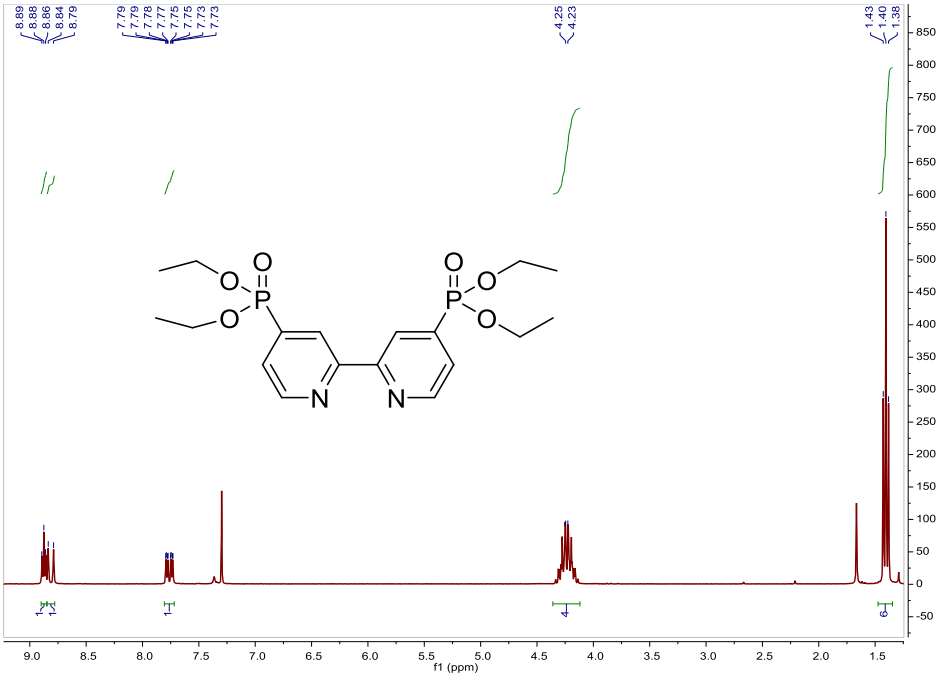

Fig. S49. ^{1}H NMR spectrum of **Ligand 15** in $CDCl_3$, 300 MHz.

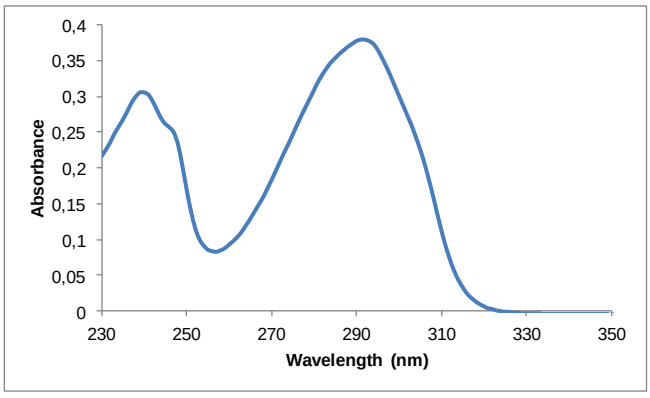

Fig. S50. UV/Vis spectra of **Ligand 15** in EtOH, $2.62 \cdot 10^{-5}$M.

[22] M. Montalti, S. Wadhwa, W. Y. Kim, R. A. Kipp and R. H. Schmehl, *Inorg. Chem.*, **2000**, *39*, 76–84.

Ligand 16, 4,4'-bis(carboxy)-2,2'-bipyridine. Synthesis and characterization.

SYNTHESIS[23]

4,4'-dimethyl-2,2'-bipyridine (0.74 g, 4 mmol) was added slowly and with a vigorous stirring to a solution of $Na_2Cr_2O_7 \cdot 2H_2O$ (5.52 g, 18.5 mmol) in 25 ml concentrated sulfuric acid. After 30 min stirring, the mixture was poured into 200 ml of cold water and the precipitated was filtered. The obtained solid was dissolved in 10% NaOH aqueous solution and 10% HCl aqueous solution was added to reach pH = 2. The precipitated was filtered to yield (100%) of the desired compound as a white solid. The spectroscopic data are coincident with those described in the literature.

^{1}H NMR (300 MHz, DMSO-d_6): δ 8.93 (d, J = 5.0 Hz, 1H), 8.86 (s, 1H), 7.93 (dd, J = 1.5 Hz, J = 5.0 Hz, 1H).

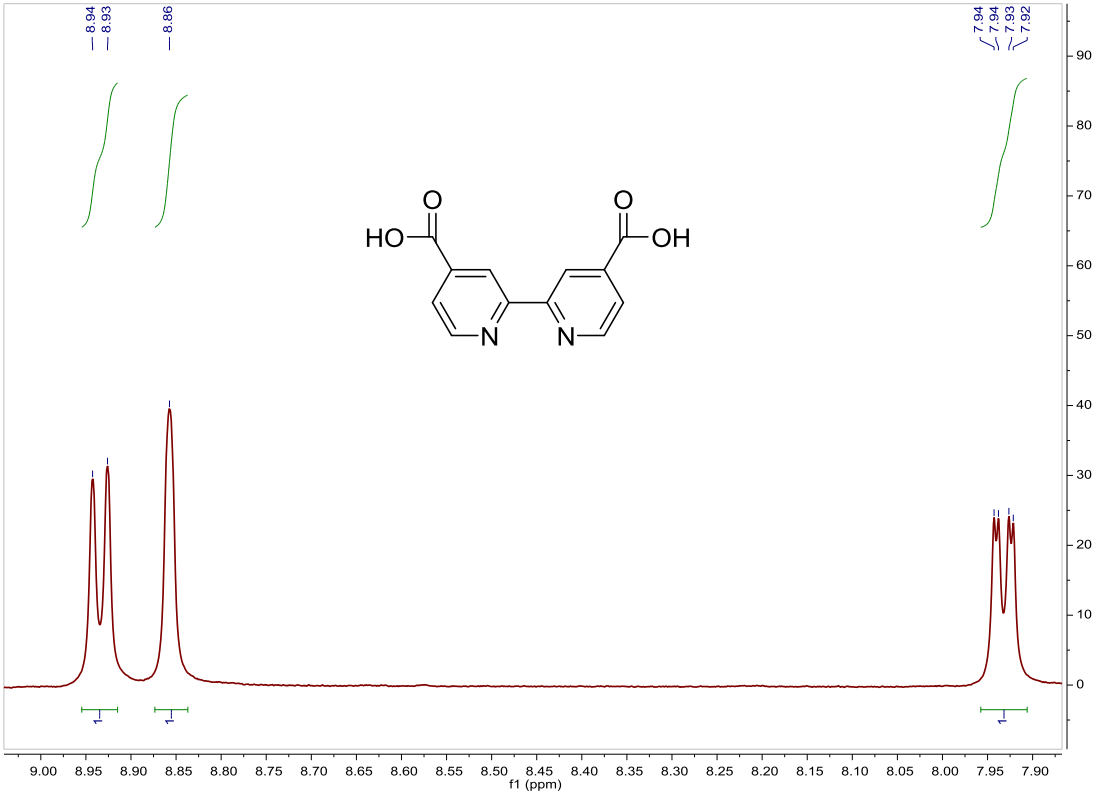

Fig. S51. ^{1}H NMR spectrum of **Ligand 16** in DMSO-d_6, 300 MHz.

[23] K. F. Lin, J. S. Ni, C. H. Tseng, C. Y. Hung and K. Y. Liu, *Mater. Chem. Phys.*, **2013**, *142*, 420–427.

Ligand 17, 4,4'-bis(ethynyl)-2,2'-bipyridine. Synthesis and characterization.

SYNTHESIS[24,25]

4,4'-dibromo-2,2'-bipyridine (1.00 g, 3.18 mmol), CuI (0.02 g, 0.11 mmol) and $Pd(PPh_3)_4$ (0.04 g, 0.06 mmol) were dissolved in freshly distilled NEt_3 (20 mL). (trimethylsilyl)acetylene (1 mL, 7.08 mmol) were added and the mixture was refluxed for 3.5 h. The solvent was evaporated and 4,4'-bis(trimethylsilyl)ethynyl)-2,2'-bipyridine was obtained after purification by column chromatography (alumina, CH_2Cl_2). The product was dissolved in MeOH (50 mL) and K_2CO_3 (1.14 g, 8.26 mmol) were added, the mixture was stirred overnight. The solvent was evaporated and the residue was partitioned between ethyl acetate and water. The ethyl acetate was evaporated and the product was obtained after purification by column chromatography (alumina, CH_2Cl_2) as a white solid. Yield: 77%. The spectroscopic data are coincident with those described in the literature.

^{1}H NMR (500 MHz, $CDCl_3$): δ 8.69 (d, J = 4.9 Hz, 2H), 8.52 (s, 2H), 7.41 (d, J = 5.0 Hz, 2H), 3.35 (s, 2H).

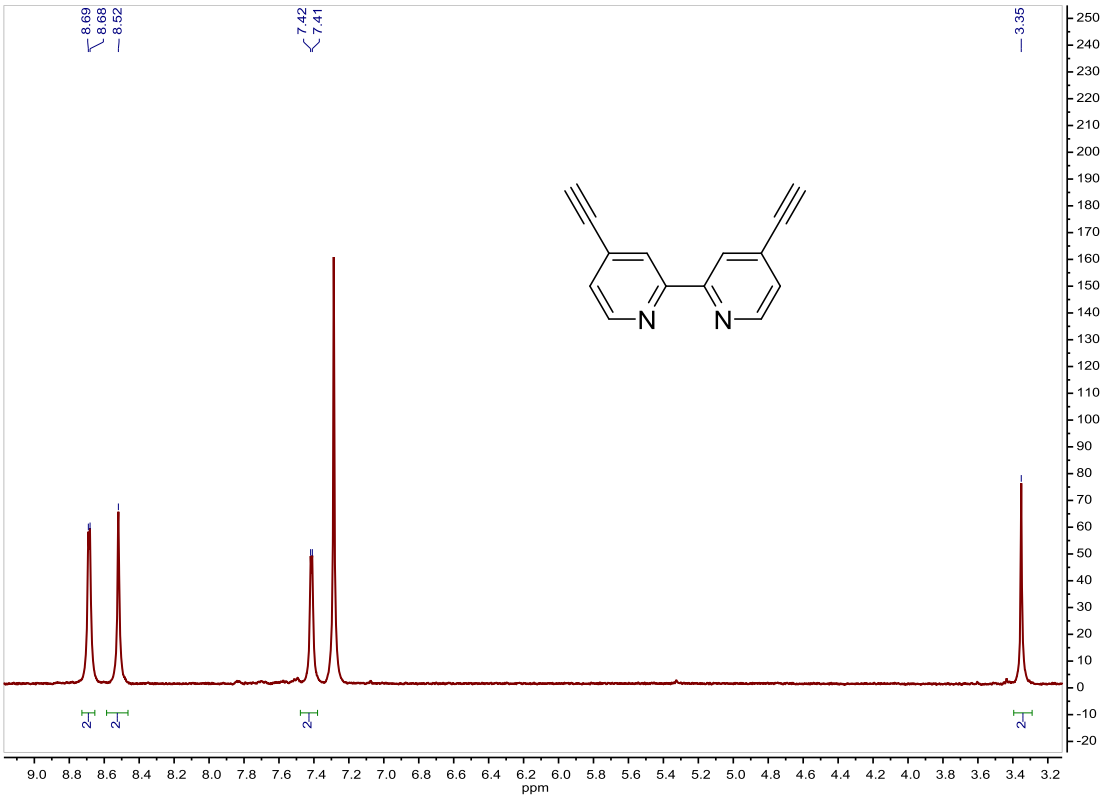

Fig. S52. ^{1}H NMR spectrum of **Ligand 17** in $CDCl_3$, 500 MHz.

[24] P. V. James, K. Yoosaf, J. Kumar, K. G. Thomas, A. Listorti, G. Accorsi and N. Armaroli, *Photochem. Photobiol. Sci.*, **2009**, *8*, 1432–1440.

[25] T. R. Kelly, Y.–J. Lee and R. J. Mears, *J. Org. Chem.*, **1997**, *62*, 2774–2781.

Ligand 21, 4,4'-diazido-2,2'-bipyridine. Synthesis and characterization.

SYNTHESIS[26]

4,4'-dibromo-2,2'-bipyridine (2.00 g, 6.37 mmol) and NaN_3 (2.46 g, 37.8 mmol) were dissolved in DMF (70 mL). The mixture was refluxed for 2 days. After cooling to room temperature, H_2O was added and the product was extracted with Et_2O. It was purified by column chromatography (silica, CH_2Cl_2) and it was obtained as a white solid. Yield: 35%. The spectroscopic data are coincident with those described in the literature.

^{1}H NMR (500 MHz, $CDCl_3$): δ 8.61 (d, J = 5.2 Hz, 2H), 8.19 (s, 2H), 7.41 (dd, J = 2.1 Hz, J = 5.2 Hz, 2H).

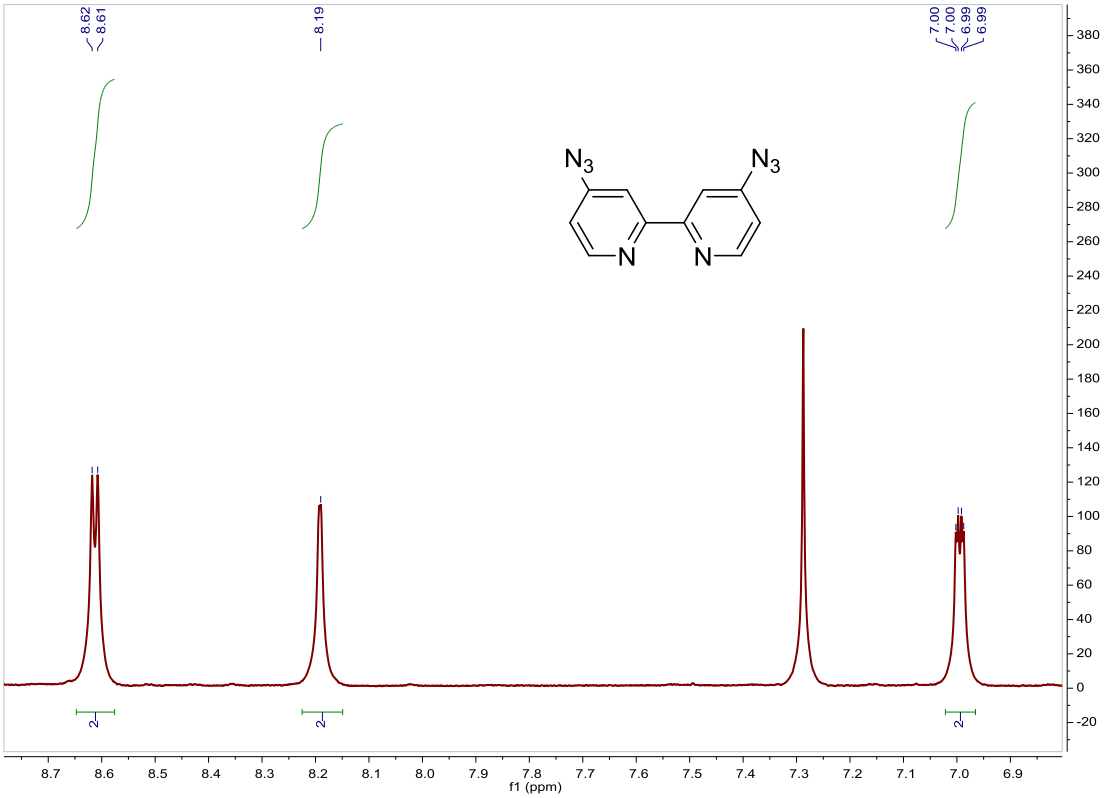

Fig. S53. ^{1}H NMR spectrum of **Ligand 21** in $CDCl_3$, 500 MHz.

[26] P. Fabbrizzi, B. Cecconi and S. Cicchi, *Synlett*, **2011**, *2*, 223–226.

Ligand 22, 4-bromo-4'-azido-2,2'-bipyridine. Synthesis and characterization.

SYNTHESIS[26]

4,4'-dibromo-2,2'-bipyridine (2.00 g, 6.37 mmol) and NaN_3 (2.46 g, 37.8 mmol) were dissolved in DMF (70 mL). The mixture was refluxed for 2 days. After cooling to room temperature, H_2O was added and the product was extracted with Et_2O. It was purified by column chromatography (silica, CH_2Cl_2) and it was obtained as a white solid. Yield: 13%. The spectroscopic data are coincident with those described in the literature.

^{1}H NMR (500 MHz, $CDCl_3$): δ 8.66 (d, J = 1.6 Hz, 1H), 8.61 (d, J = 5.4 Hz, 1H), 8.51 (d, J = 5.1 Hz, 1H), 8.16 (d, J = 2.3 Hz, 1H), 7.53 (dd, J = 2.0 Hz, J = 5.2 Hz, 1H), 6.99 (dd, J = 2.3 Hz, J = 5.4 Hz, 1H).

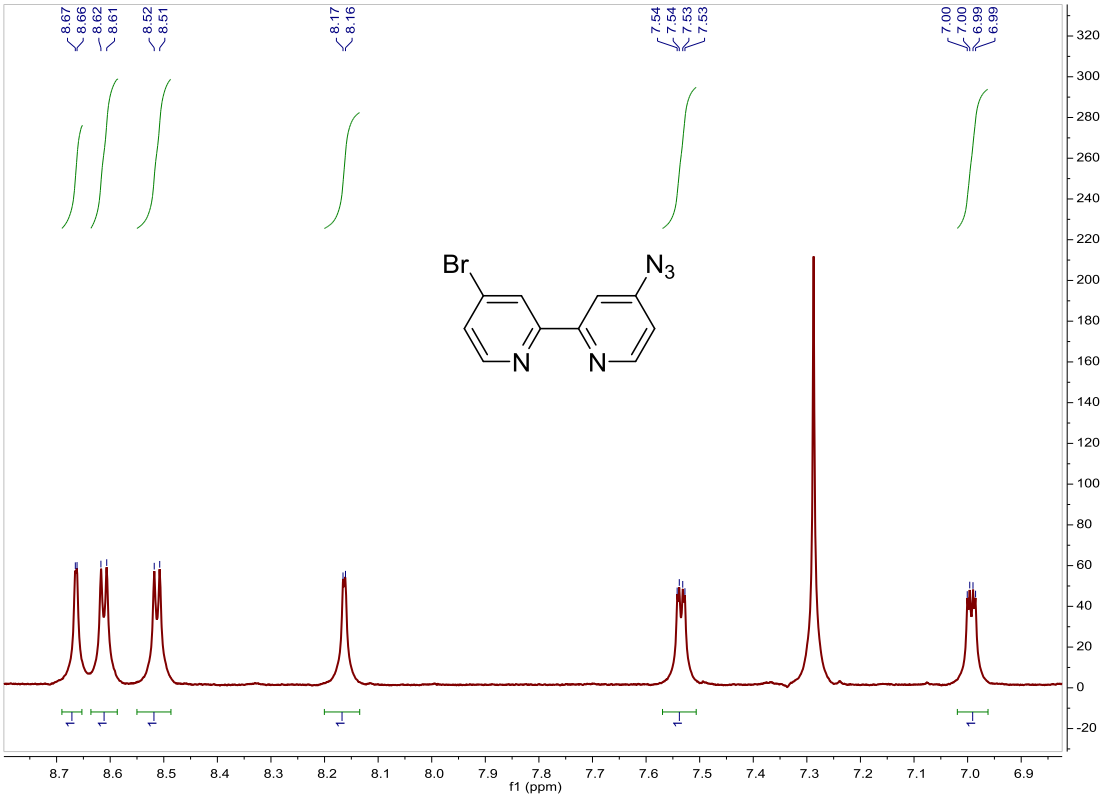

Fig. S54. ^{1}H NMR spectrum of **Ligand 22** in $CDCl_3$, 500 MHz.

[Ir(ppy)$_2$Cl]$_2$. Synthesis and characterization.

SYNTHESIS[27]

Under a N_2 atmosphere, $IrCl_3 \cdot 3H_2O$ (1.00 g, 2.84 mmol) and 2-phenylpyridine (0.81 mL, 5.67 mmol) were dissolved in 30 mL of ethoxyethanol/water 2/1. The reaction mixture was refluxed at 120 °C, under N_2, for 15 h. After cooling to room temperature, the product was filtered and washed with water, hexane and diethyl-ether. The product was obtained as a yellow solid. Yield 88%. The spectroscopic data are coincident with those described in the literature.[28]

^{1}H NMR (300 MHz, $CDCl_3$): δ 9.28 (d, J = 5.8 Hz, 1H), 7.90 (d, J = 8.1 Hz, 1H), 7.77 (ddd, J = 1.6 Hz, J = 7.4 Hz, J = 8.9 Hz, 1H), 7.52 (dd, J = 1.2 Hz, J = 7.8 Hz, 1H), 6.84–6.73 (m, 2H), 6.59 (ddd, J = 1.3 Hz, J = 7.7 Hz, J = 8.8 Hz, 1H), 5.97 (dd, J = 0.8 Hz, J = 7.7 Hz, 1H).

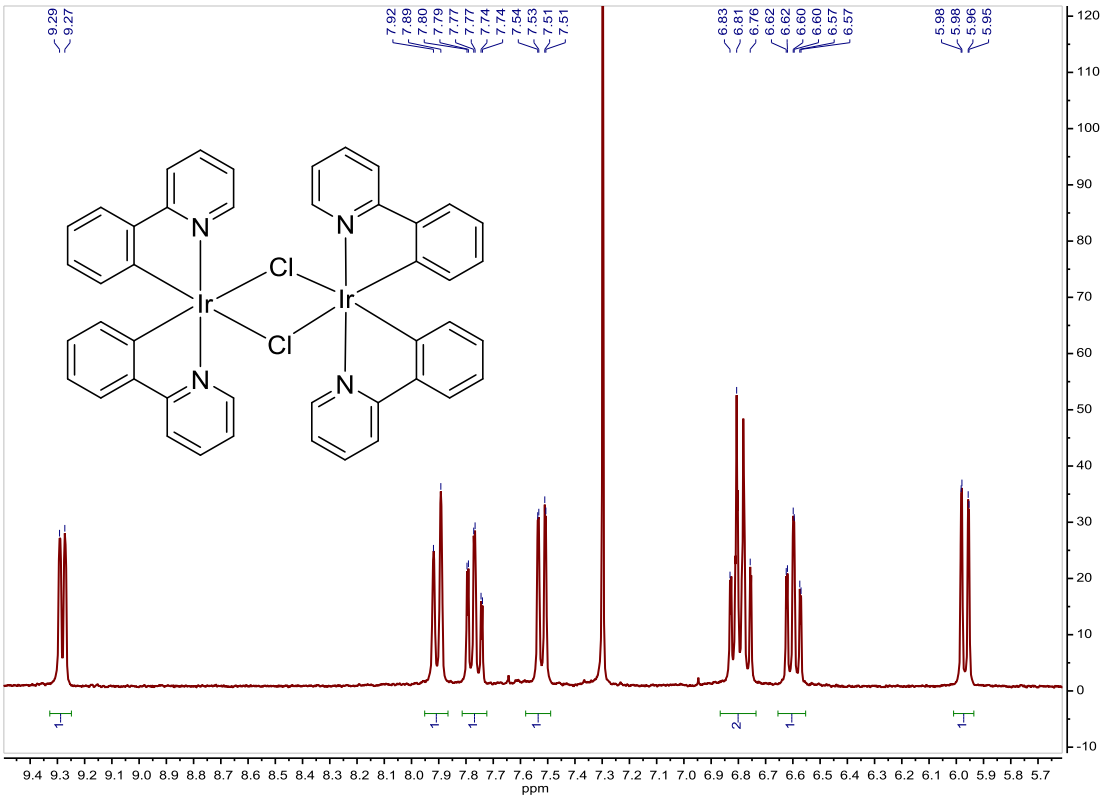

Fig. S55. ^{1}H NMR spectrum of **[Ir(ppy)$_2$Cl]$_2$** in $CDCl_3$, 300 MHz.

[27] S. Sprouse, K. A. King, P. J. Spellane and R. J. Watts, *J. Am. Chem. Soc.*, **1984**, *106*, 6647–6653.

[28] A. A. Rachford, R. Ziessel, T. Bura, P. Retailleau and F. N. Castellano, *Inorg. Chem.*, **2010**, *49*, 3730–3736.

[Ir(Fppy)$_2$Cl]$_2$. Synthesis and characterization.

SYNTHESIS[27]

Under a N_2 atmosphere, $IrCl_3 \cdot 3H_2O$ (2.31 g, 6.56 mmol) and 2-(2,4-difluorophenyl)pyridine (2.0 mL, 13.12 mmol) were dissolved in 60 mL of ethoxyethanol/water 2/1. The reaction mixture was refluxed at 120 °C, under N_2, for 15 h. After cooling to room temperature, the product was filtered and washed with water, hexane and diethyl-ether. The product was obtained as a yellow solid. Yield 73%. The spectroscopic data are coincident with those described in the literature.[29]

^{1}H NMR (300 MHz, $CDCl_3$): δ 9.16 (d, J = 5.8 Hz, 1H), 8.34 (d, J = 8.4 Hz, 1H), 7.86 (t, J = 8.1 Hz, 1H), 6.91–6.82 (m, 1H), 6.37 (ddd, J = 2.3 Hz, J = 9.1 Hz, J = 11.5 Hz, 1H), 5.32 (dd, J = 2.4 Hz, J = 9.1 Hz, 1H).

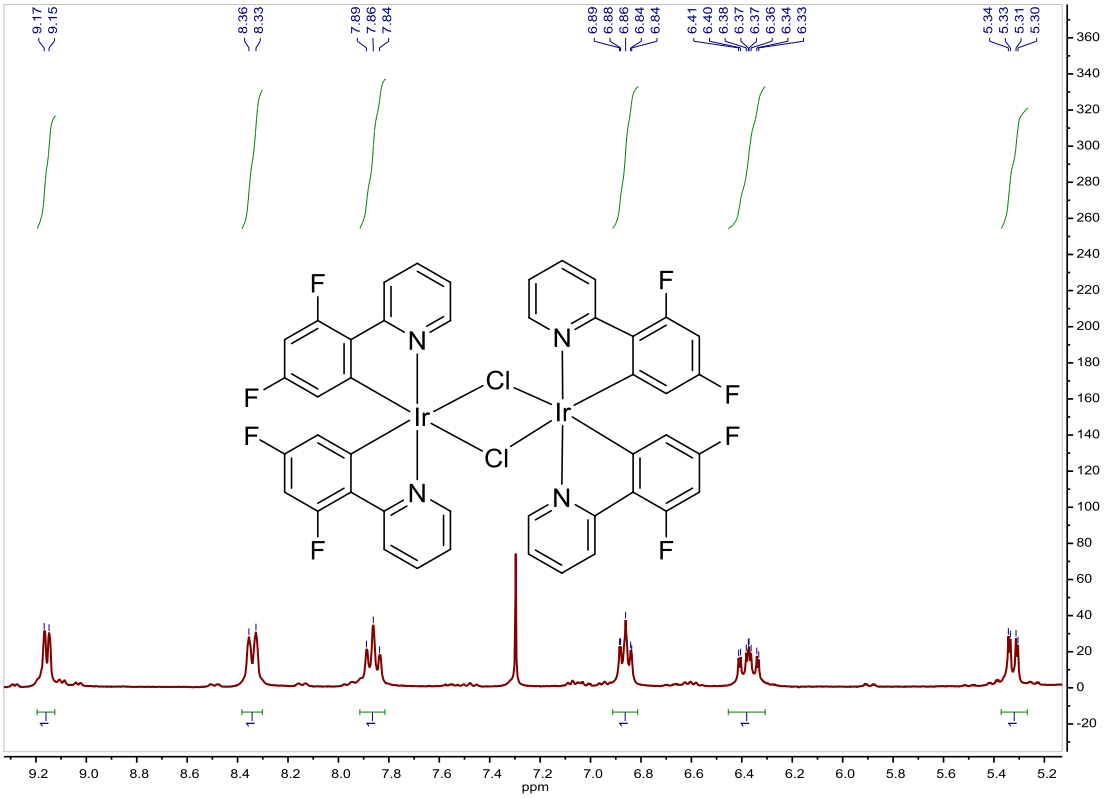

Fig. S56. ^{1}H NMR spectrum of **[Ir(Fppy)$_2$Cl]$_2$** in $CDCl_3$, 300 MHz.

[29] F. Dumur, M. Lepeltier, H. Z. Siboni, D. Gigmes and H. Aziz, *Synthetic Metals*, **2014**, *198*, 131–136.

2-(4-bromophenyl)-4,4,5,5-tetramethyl-[1,3,2]dioxaborolane. Synthesis and characterization.

SYNTHESIS[30]

Under a N_2 atmosphere, to a solution of aryl iodide (8.0 g, 28.3 mmol), CuI (0.54 g, 2.83 mmol) and NaH (1.02 g, 42.5 mmol) in freshly distilled THF (110 mL), pinacolborane (6.6 mL, 42.43 mmol) were added and the reaction mixture was stirred for 15 h at room temperature. A saturated NH_4Cl (140 mL) solution was added and the product was extracted with ethyl acetate. The organic phase was dried over $MgSO_4$ and the solvent was evaporated. The product was purified by column chromatography (silica, 100% hexane to 100% ethyl acetate) and it was obtained as a yellow liquid. Yield 82%. The spectroscopic data are coincident with those described in the literature.

^{1}H NMR (300 MHz, $CDCl_3$): δ 7.70 (brd, J = 8.2 Hz, 2H), 7.54 (brd, J = 8.3 Hz, 2H), 1.37 (s, 12H).

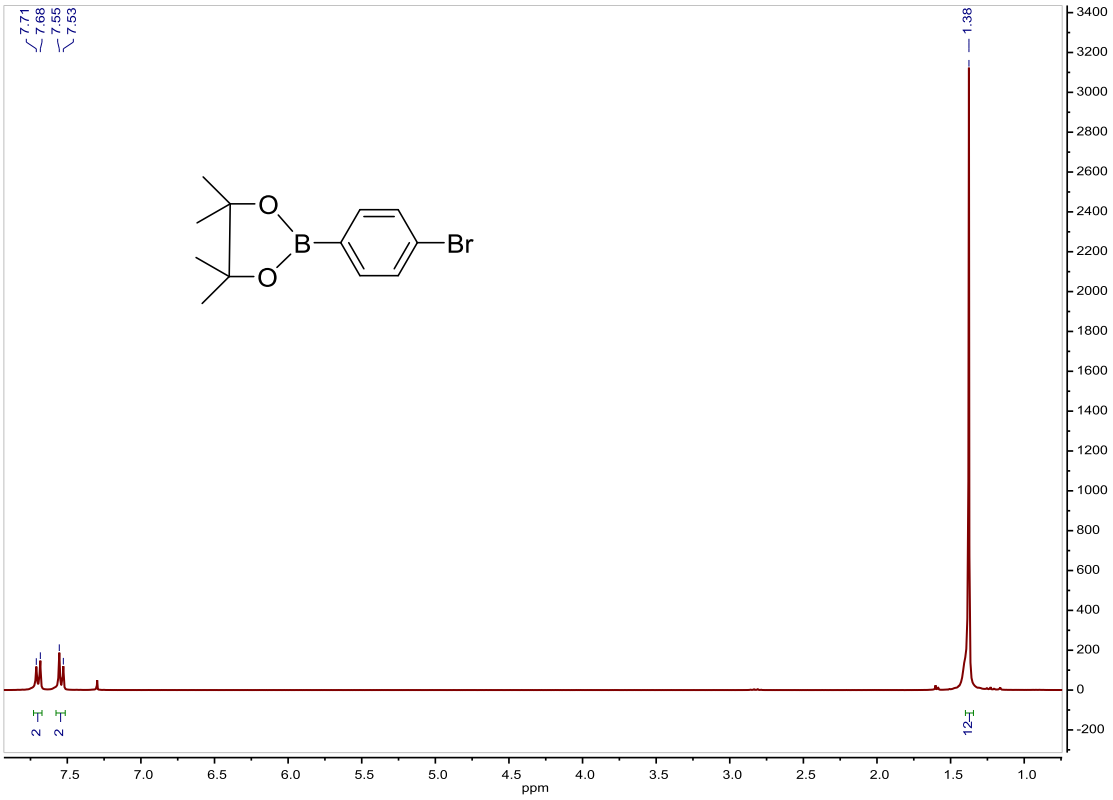

Fig. S57. ^{1}H NMR spectrum of **2-(4-bromophenyl)-4,4,5,5-tetramethyl-[1,3,2]dioxaborolane** in $CDCl_3$, 300 MHz.

[30] W. Zhu and D. Ma, *Org. Lett.*, **2006**, *8*, 261–263.

2-(4-bromophenyl)pyridine. Synthesis and characterization.

SYNTHESIS[31]

Under a N_2 atmosphere, a solution of 2-bromopyridine (2.22 mL, 23.3 mmol) and $Pd(PPh_3)_4$ (0.61 g, 0.53 mmol) in DME (66 mL) was added to a solution of 2-(4-bromophenyl)-4,4,5,5-tetramethyl-[1,3,2]dioxaborolane (6.6 g, 23.3 mmol) in EtOH (66 mL). Na_2CO_3 (2M, 36 mL) was added and the reaction mixture was heated to 95 °C for 15 h. After cooling to room temperature, the solid was removed by filtration and the solvent was evaporated. The impurities that were not soluble in EtOAc and hexane were also removed. The product was obtained as a yellow solid. Yield 36%. The spectroscopic data are coincident with those described in the literature.[32]

^{1}H NMR (300 MHz, $CDCl_3$): δ 8.70 (ddd, J = 1.0 Hz, J = 1.8 Hz, J = 4.8 Hz, 1H), 7.89 (brd, J = 8.7 Hz, 2H), 7.80–7.68 (m, 2H), 7.62 (brd, J = 8.7 Hz, 2H), 7.30–7.23 (m, 1H).

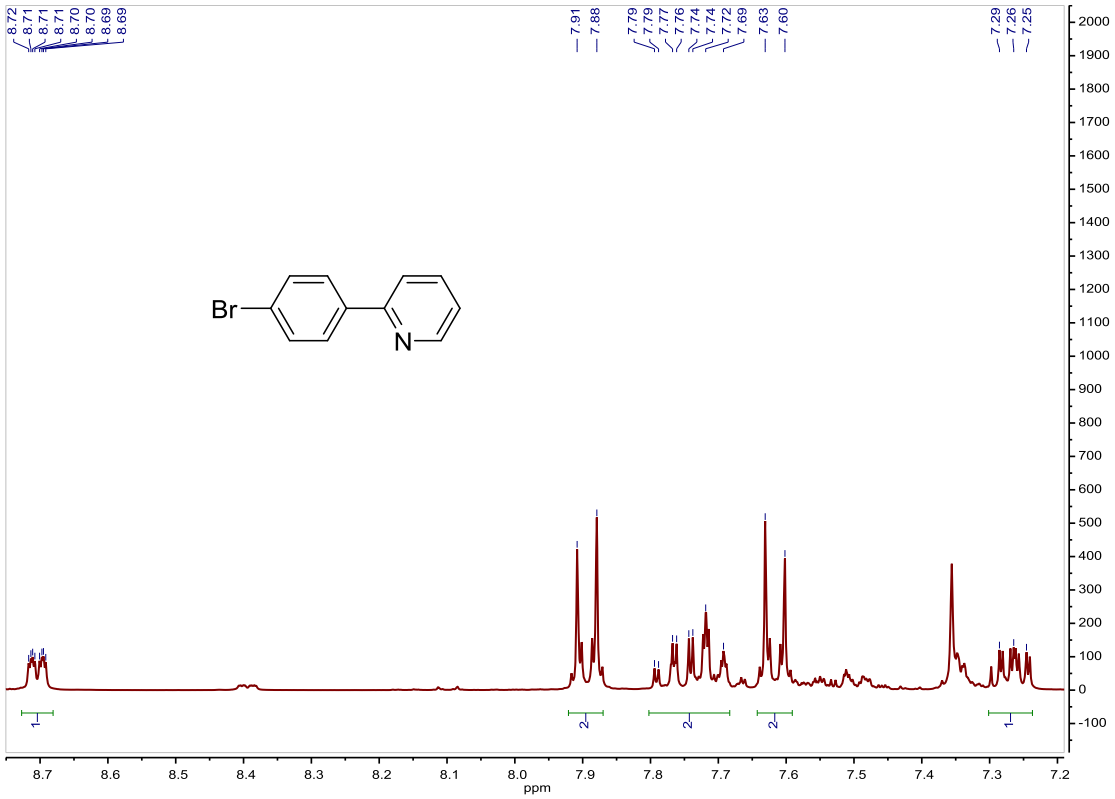

Fig. S58. ^{1}H NMR spectrum of **2-(4-bromophenyl)pyridine** in $CDCl_3$, 300 MHz.

[31] H.-Y. Yang, J.-M. Son and W.-J. Joo, US Patent, 2010/0133992.

[32] A. J. Sandee, C. K. Williams, N. R. Evans, J. E. Davies, C. E. Boothby, A. Köhler, R. H. Friend and A. B. Holmes, *J. Am. Chem. Soc.*, **2004**, *126*, 7041–7048.

[Ir(Brppy)$_2$Cl]$_2$. Synthesis and characterization.

SYNTHESIS[27]

Under a N_2 atmosphere, $IrCl_3 \cdot 3H_2O$ (1.50 g, 4.26 mmol) and 2-(4-bromophenyl)pyridine (2.0 g, 8.53 mmol) were dissolved in 45 mL of ethoxyethanol/water 2/1. The reaction mixture was refluxed at 120 °C, under N_2, for 15 h. After cooling to room temperature, the product was filtered and washed with water, hexane and diethyl-ether. The product was obtained as a yellow solid. Yield 92%. The spectroscopic data are coincident with those described in the literature.[32]

^{1}H NMR (300 MHz, $CDCl_3$): δ 9.14 (d, J = 5.8 Hz, 1H), 7.90 (d, J = 7.4 Hz, 1H), 7.83 (ddd, J = 1.5 Hz, J = 7.2 Hz, J = 8.7 Hz, 1H), 7.41 (d, J = 8.3 Hz, 1H), 7.00 (dd, J = 1.9 Hz, J = 8.2 Hz, 1H), 6.86 (ddd, J = 1.6 Hz, J = 5.9 Hz, J = 7.3 Hz, 1H), 5.98 (d, J = 1.9 Hz, 1H).

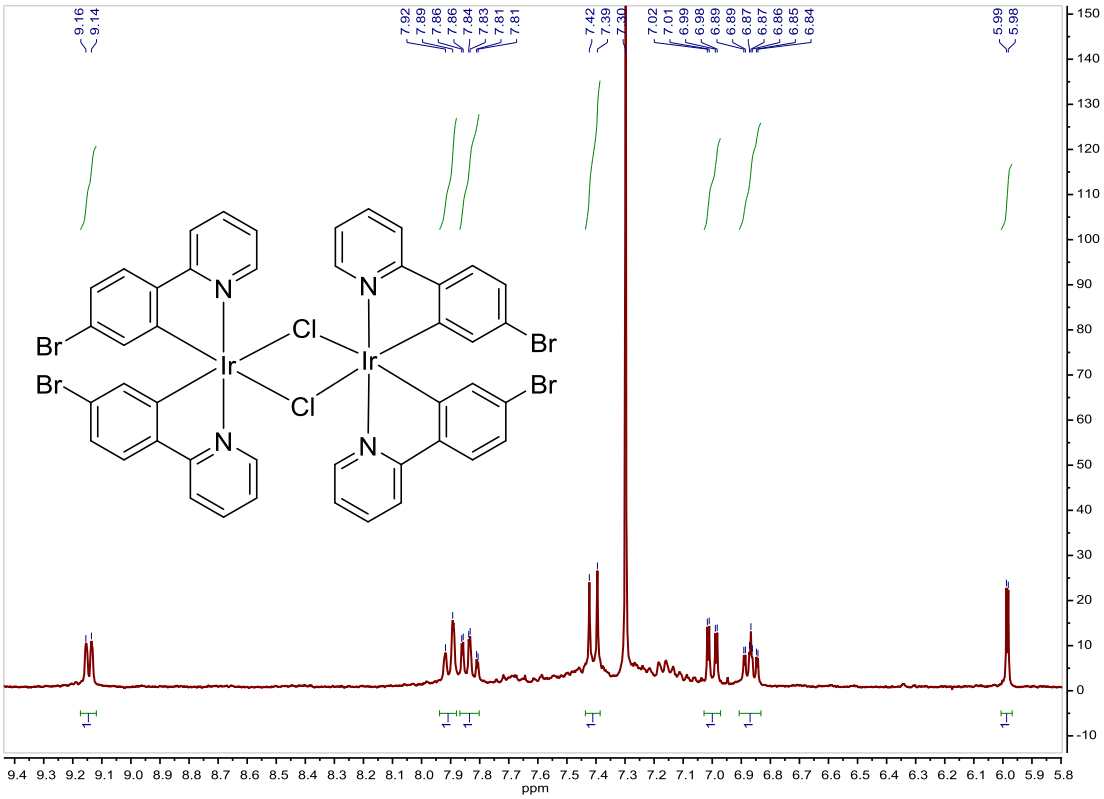

Fig. S59. ^{1}H NMR spectrum of **[Ir(Brppy)$_2$Cl]$_2$** in $CDCl_3$, 300 MHz.

Compound A15, [Ir(ppy)$_2$(4,4'-bis(diethylphosphonate)-2,2'-bipyridine)]PF$_6$. Synthesis and characterization.

SYNTHESIS

Under a N_2 atmosphere, $[Ir(ppy)_2Cl]_2$ (0.100 g, 0.093 mmol) were added over a suspension of 4,4'-bis(diethylphosphonate)-2,2'-bipyridine (0.08 g, 0.186 mmol) in 8 ml CH_2Cl_2–MeOH 2/1. The reaction mixture was refluxed, under N_2, for 15 h. After solvent evaporation the product was purified by column chromatography (silica gel, CH_2Cl_2). When the unreacted $[Ir(ppy)_2Cl]_2$ eluted, 0.05 g of KPF_6 were added on top of the column and the polarity of the eluent was gradually increased to 100% acetone to elute $[Ir(ppy)_2$(4,4'-bis(diethylphosphonate)-2,2'-bipyridine)]PF_6 together with the excess of KPF_6. The desired compound was precipitated with ether after filtration through a celite path in CH_2Cl_2 and it was obtained as a red solid. Yield 40%.

Elemental Analysis: calculated for ($C_{40}H_{42}IrN_4O_6P_3F_6$): C, 44.74; H, 3.94; N, 5.22. Found: C, 44.44; H, 4.06; N, 5.21.

Exact Mass: ESI-MS $[C_{40}H_{42}IrN_4O_6P_2]^+$: calculated: m/z= 929.2209, found: m/z= 929.2216.

^{1}H NMR (300 MHz, acetone-*d*$_6$): δ 9.01 (d, J = 13.7 Hz, 1H), 8.16 (t, J = 4.8 Hz, 1H), 8.09 (d, J = 8.1 Hz, 1H), 7.89–7.70 (m, 4H), 6.98 (ddd, J = 1.3 Hz, J = 5.9 Hz, J = 7.3 Hz, 1H), 6.90 (ddd, J = 1.3 Hz, J = 7.4 Hz, J = 8.6 Hz, 1H), 6.79 (ddd, J = 1.4 Hz, J = 7.4 Hz, J = 8.8 Hz, 1H), 6.19 (d, J = 7.4 Hz, 1H), 4.19 –3.95 (m, 4H), 1.18 (dt, J = 6.7 Hz, J = 6.8 Hz, 6H).

^{13}C APT NMR (75 MHz, acetone-*d*$_6$): δ 167.16 (s, C_{quat}), 155.94 (d, J = 13.6 Hz, C_{quat}), 150.95 (d, J = 13.9 Hz, CH), 149.50 (s, CH), 149.42 (s, C_{quat}), 143.82 (s, C_{quat}), 141.35 (d, J = 187.5 Hz, C_{quat}), 138.72 (s, CH), 131.33 (s, CH), 130.27 (s, CH), 130.13 (d, J = 8.6 Hz, CH), 126.83 (d, J = 9.8 Hz, CH), 124.83 (s, CH), 123.55 (s, CH), 122.63 (s, CH), 119.85 (s, CH), 63.00 (d, J = 5.7 Hz, $2CH_2$), 15.60 (d, J = 5.8 Hz, $2CH_3$).

^{31}P NMR (162 MHz, acetone-*d*$_6$): δ 11.29 (s, 1P), -144.07(sep, J = 707.8 Hz, 1P).

UV/Vis (EtOH), λ, nm (ε, 10^4 M^{-1} cm^{-1}): 250 (5.1), 290 (4.1), 378 (1.0).

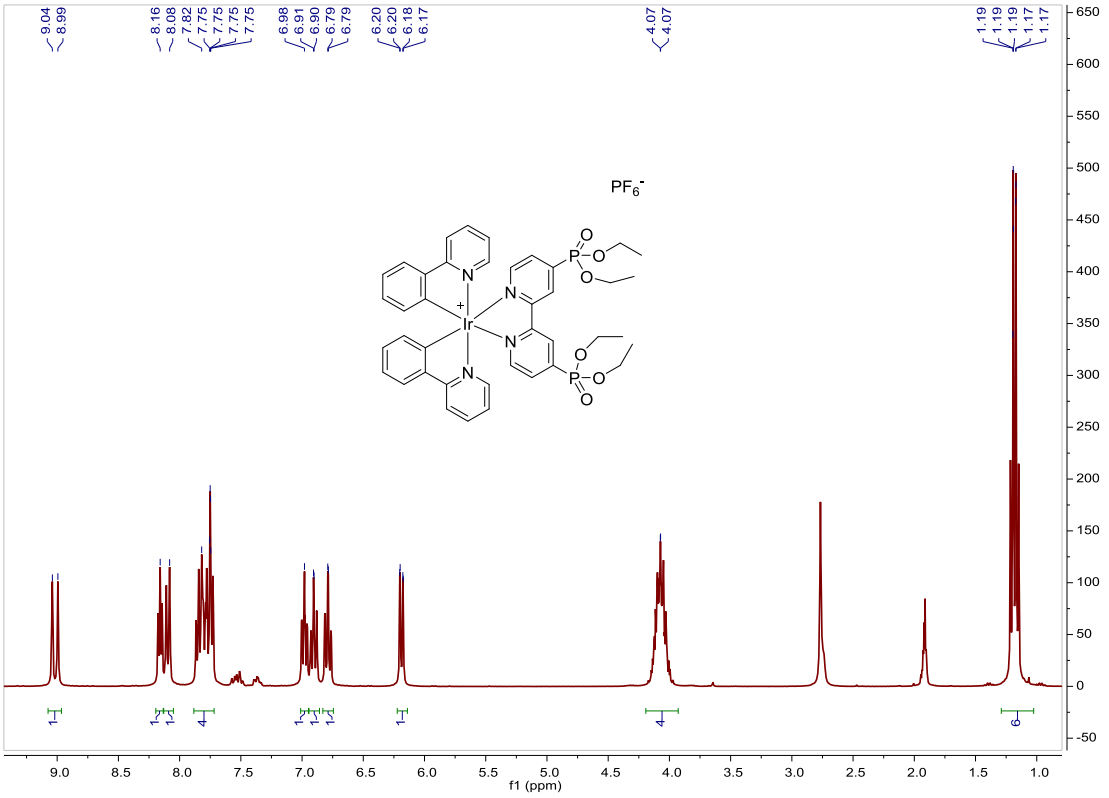

Fig. S60. ^{1}H NMR spectrum of **A15** in acetone-*d*$_6$, 300 MHz.

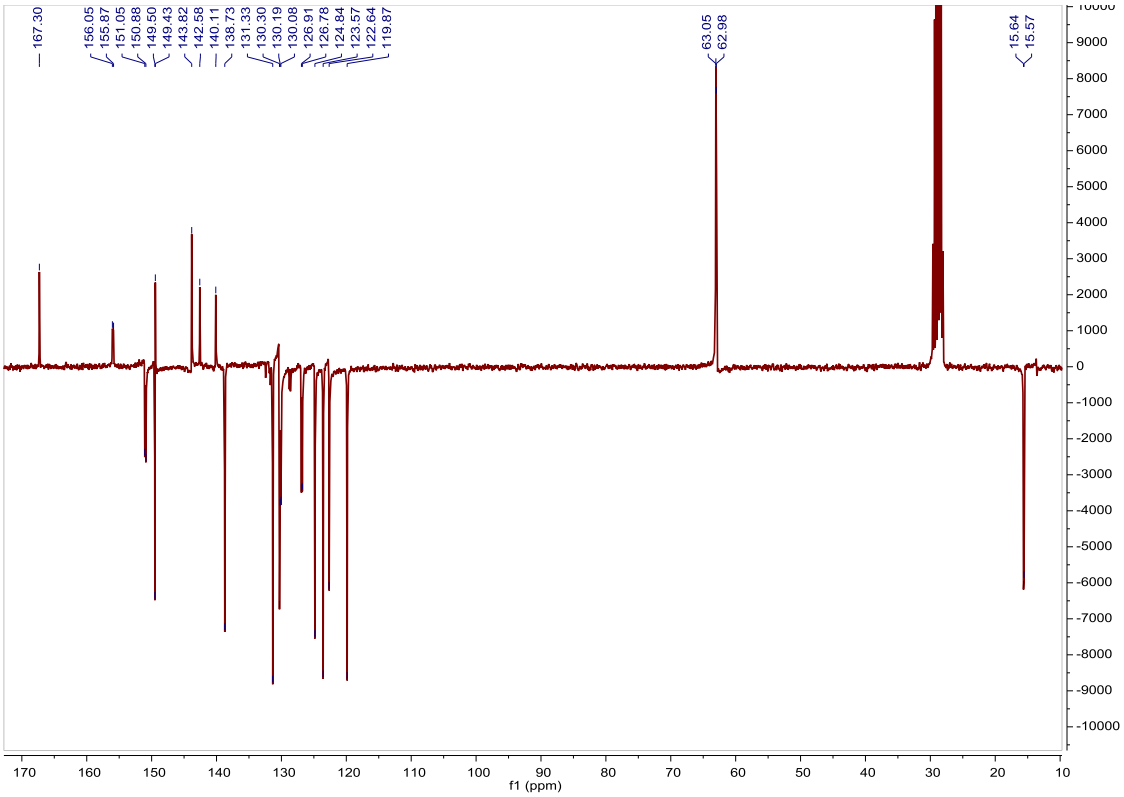

Fig. S61. ^{13}C APT NMR spectrum of **A15** in acetone-d_6, 75 MHz.

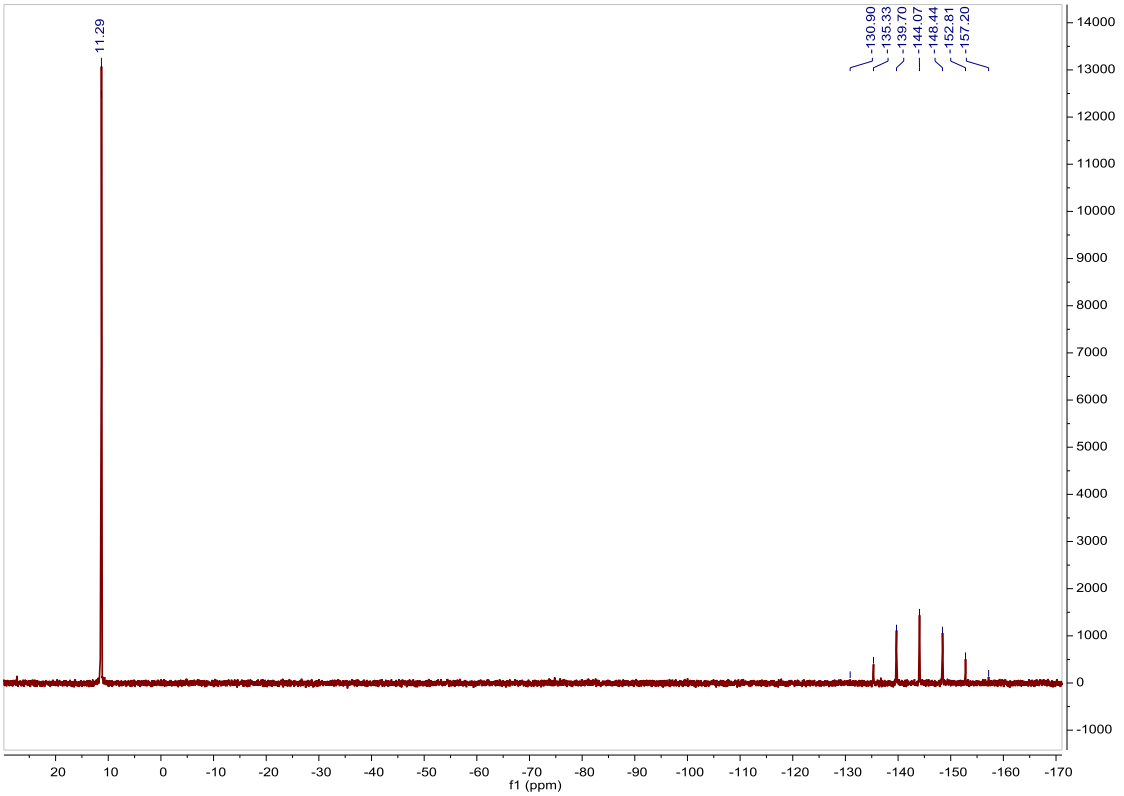

Fig. S62. ^{31}P NMR spectrum of **A15** in acetone-d_6, 162 MHz.

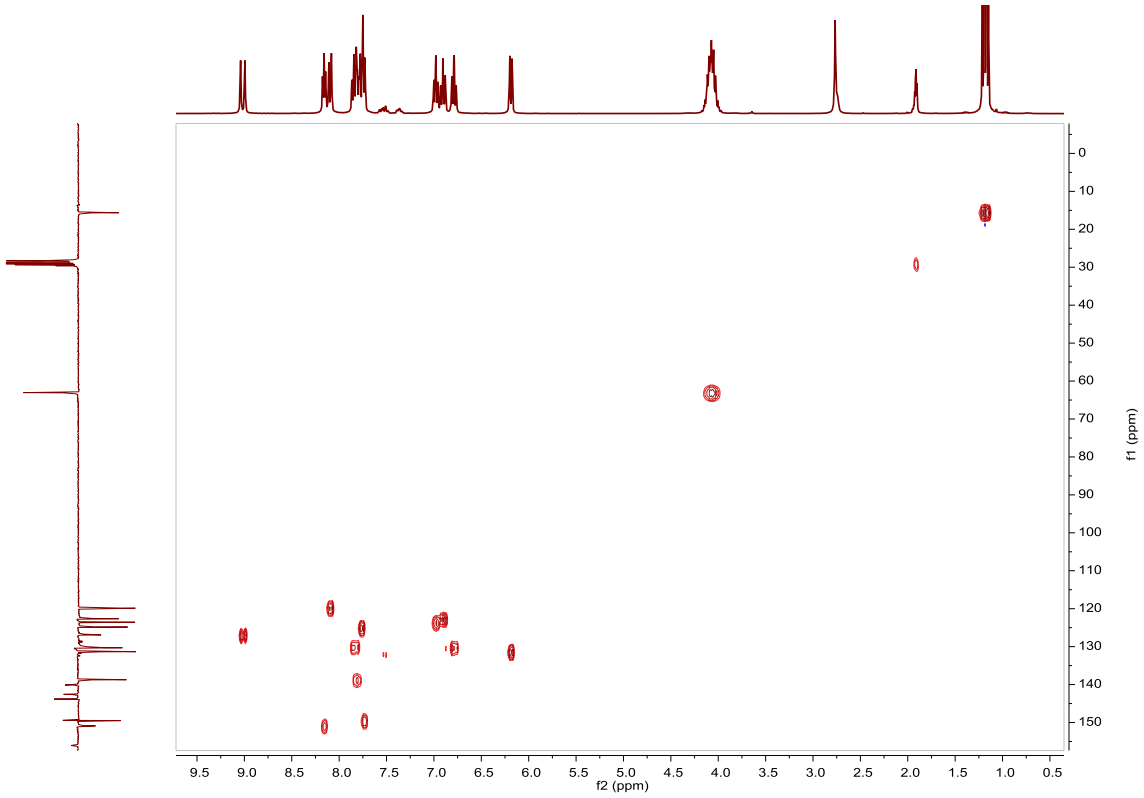

Fig. S63. HSQC NMR spectrum of **A15** in acetone-d_6.

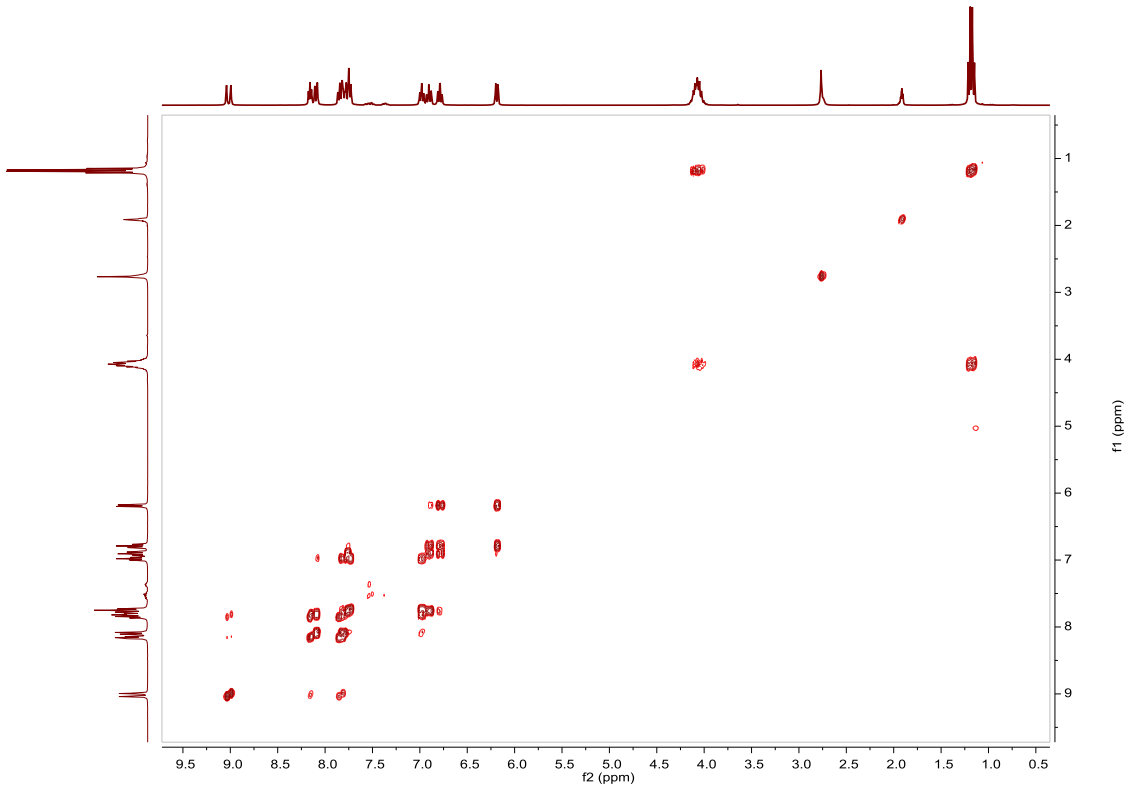

Fig. S64. COSY NMR spectrum of **A15** in acetone-d_6.

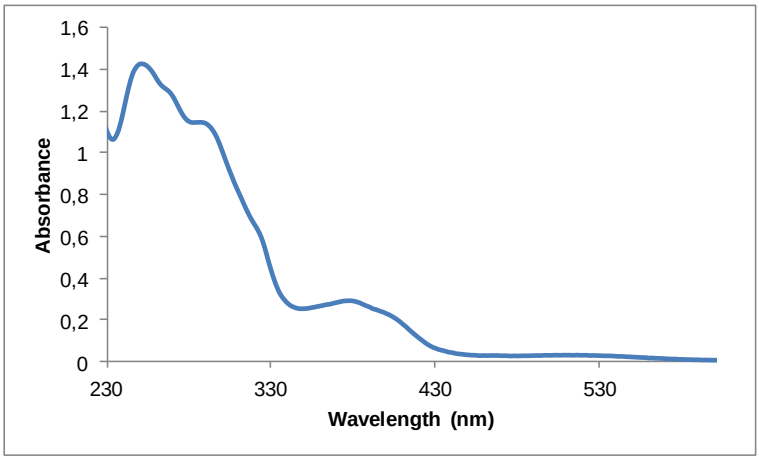

Fig. S65. UV/Vis spectra of **A15** in EtOH, $2.79 \cdot 10^{-5}$M.

Compound B15, [Ir(ppy-F_2)$_2$(4,4'-bis(diethylphosphonate)-2,2'-bipyridine)]PF_6. Synthesis and characterization.

SYNTHESIS

Under a N_2 atmosphere, [Ir(ppy-F_2)$_2$Cl]$_2$ (0.100 g, 0.082 mmol) were added over a suspension of 4,4'-bis(diethylphosphonate)-2,2'-bipyridine (0.07 g, 0.164 mmol) in 8 ml CH_2Cl_2–MeOH 2/1. The reaction mixture was refluxed, under N_2, for 15 h. After solvent evaporation the product was purified by column chromatography (silica gel, CH_2Cl_2). When the unreacted [Ir(ppy-F_2)$_2$Cl]$_2$ eluted, 0.05 g of KPF_6 were added on top of the column and the polarity of the eluent was gradually increased to 100% acetone to elute [Ir(ppy-F_2)$_2$(4,4'-bis(diethylphosphonate)-2,2'-bipyridine)]PF_6 together with the excess of KPF_6. The desired compound was precipitated with ether after filtration through a celite path in CH_2Cl_2 and it was obtained as a yellow solid. Yield 40%.

Elemental Analysis: calculated for ($C_{40}H_{38}F_4IrN_4O_6P_3F_6$): C, 41.93; H, 3.34; N, 4.89. Found: C, 41.97; H, 3.38; N, 5.13.

Exact Mass: ESI-MS $[C_{40}H_{38}F_4IrN_4O_6P_2]^+$: calculated: m/z= 1001.1832, found: m/z= 1001.1854.

^{1}H NMR (300 MHz, acetone-d_6): δ 9.04 (d, J = 13.8 Hz, 1H), 8.33–8.19 (m, 2H), 7.92 (t, J = 7.6 Hz, 1H), 7.87 (dd, J = 1.4 Hz, J = 5.5 Hz, 1H), 7.83 (dd, J = 1.4 Hz, J = 5.7 Hz, 1H), 7.06 (ddd, J = 1.4 Hz, J = 5.8 Hz, J = 7.4 Hz, 1H), 6.64 (ddd, J = 2.4 Hz, J = 9.3 Hz, J = 12.7 Hz, 1H), 5.63 (dd, J = 2.3 Hz, J = 8.5 Hz, 1H), 4.17–3.97 (m, 4H), 1.18 (dt, J = 6.5 Hz, J = 6.2 Hz, 6H).

^{13}C APT NMR (75 MHz, acetone-d_6): δ 163.20 (dd, J = 12.5 Hz, J = 254.0 Hz, C_{quat}), 163.14 (d, J = 7.0 Hz, C_{quat}), 161.03 (dd, J = 12.8 Hz, J = 258.4 Hz, C_{quat}), 155.46 (d, J = 13.6 Hz, C_{quat}), 153.19 (d, J = 6.6 Hz, C_{quat}), 151.12 (d, J = 12.7 Hz, CH), 149.79 (s, CH), 141.78 (d, J = 184.1 Hz, C_{quat}), 139.54 (s, CH), 130.20 (d, J = 8.4 Hz, CH), 127.47 (s, C_{quat}), 126.82 (d, J = 10.4 Hz, CH), 123.82 (s, CH), 123.30 (d, J = 19.9 Hz, CH), 113.29 (d, J = 20.1 Hz, CH), 98.61 (t, J = 27.1 Hz, CH), 62.75 (d, J = 5.0 Hz, $2CH_2$), 15.33 (d, J = 5.8 Hz, $2CH_3$).

^{31}P NMR (162 MHz, acetone-d_6): δ 10.99 (s, 1P), -144.08 (sep, J = 707.8 Hz, 1P).

UV/Vis (EtOH), λ, nm (ε, 10^4 M^{-1} cm^{-1}): 244 (6.0), 312 (3.4), 358 (1.1).

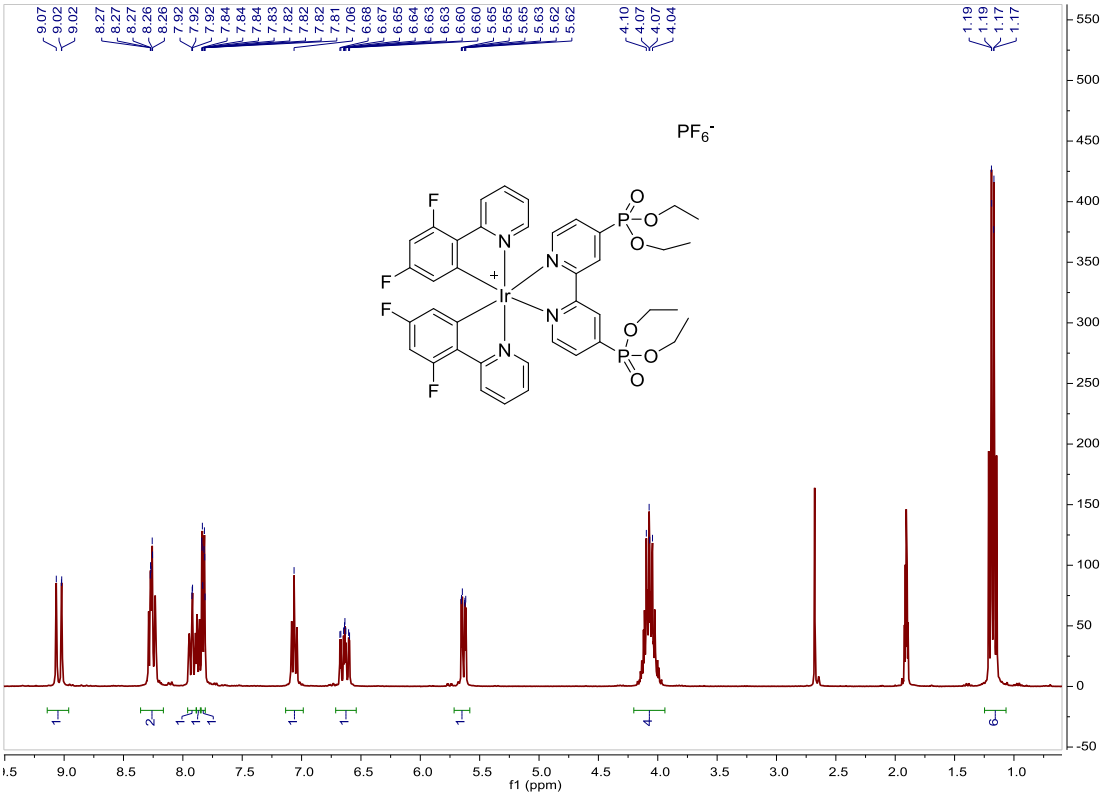

Fig. S66. ^{1}H NMR spectrum of **B15** in acetone-d_6, 300 MHz.

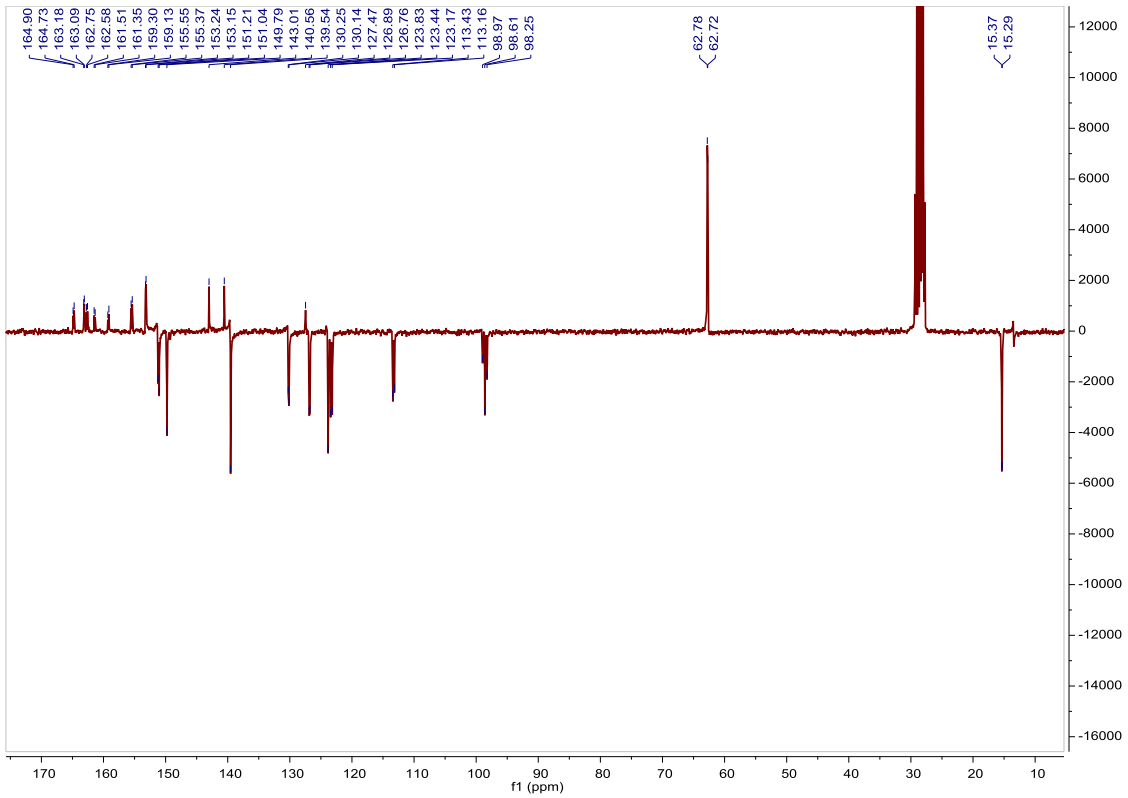

Fig. S67. ^{13}C APT NMR spectrum of **B15** in acetone-d_6, 75 MHz.

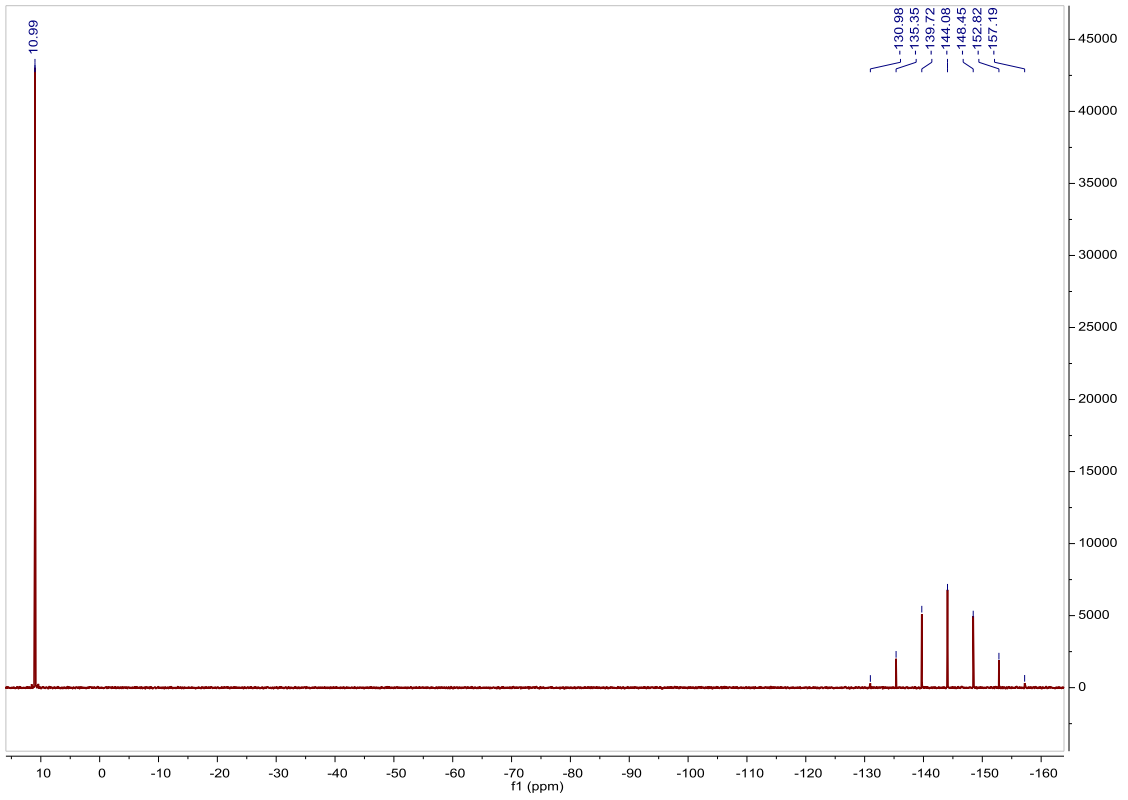

Fig. S68. ^{31}P NMR spectrum of **B15** in acetone-d_6, 162 MHz.

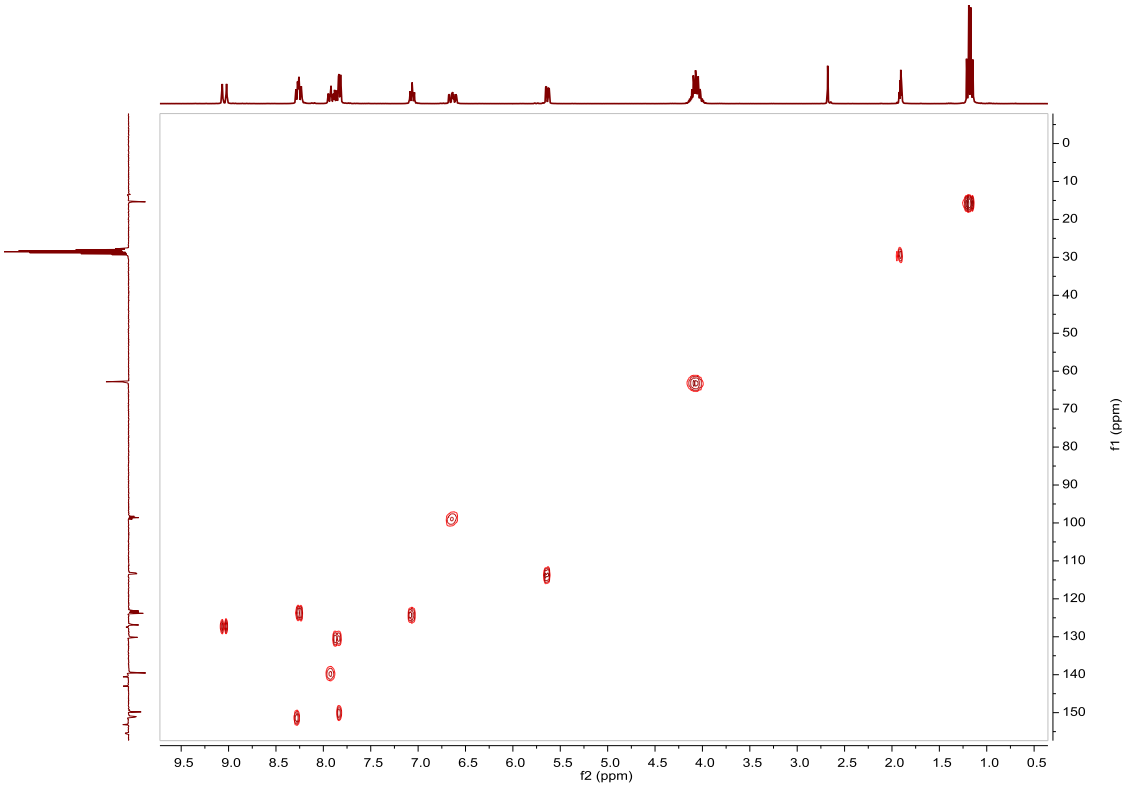

Fig. S69. HSQC NMR spectrum of **B15** in acetone-d_6.

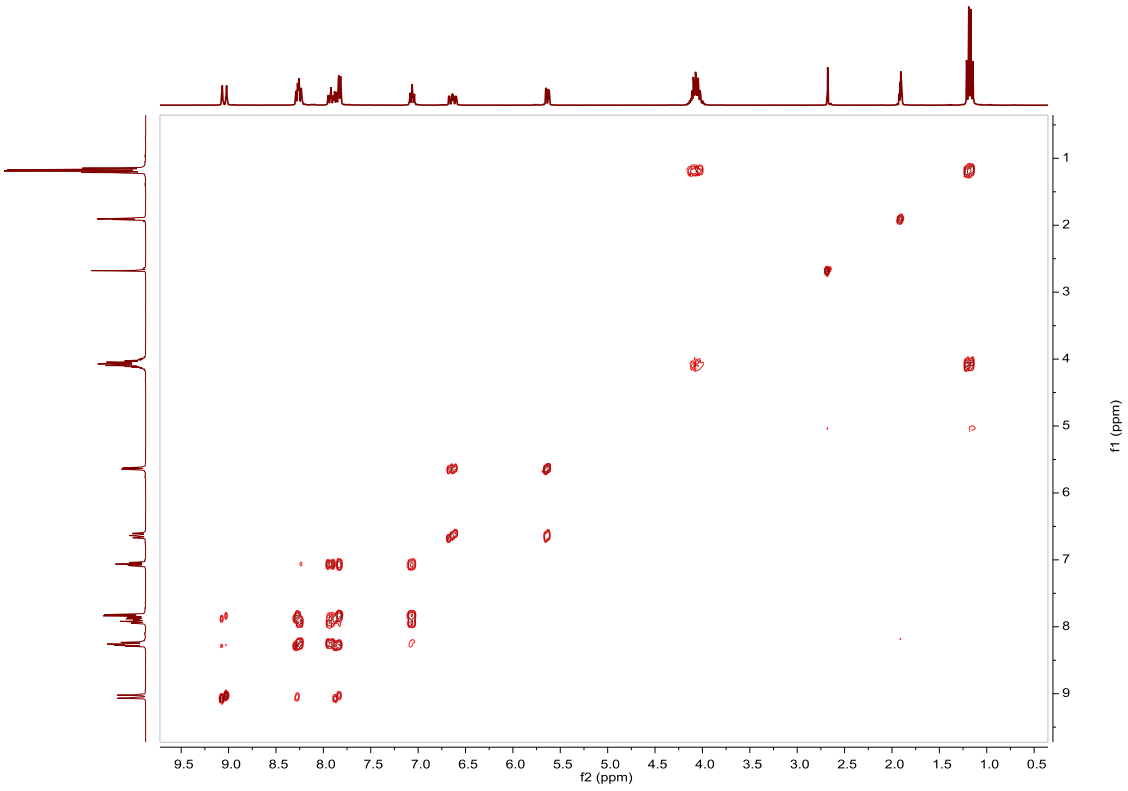

Fig. S70. COSY NMR spectrum of **B15** in acetone-d_6.

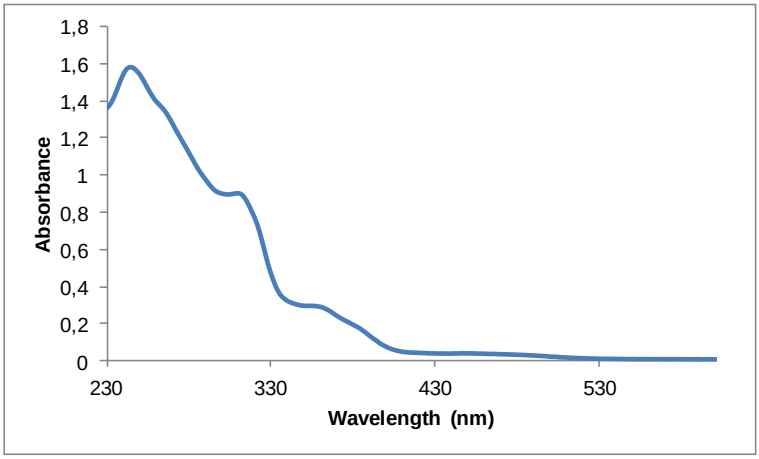

Fig. S71. UV/Vis spectra of **B15** in EtOH, $2.62 \cdot 10^{-5}$M.

Compound C15, [Ir(ppy-Br)$_2$(4,4'-bis(diethylphosphonate)-2,2'-bipyridine)]PF$_6$. Synthesis and characterization.

SYNTHESIS

Under a N_2 atmosphere, $[Ir(ppy\text{-}Br)_2Cl]_2$ (0.200 g, 0.144 mmol) were added over a suspension of 4,4'-bis(diethylphosphonate)-2,2'-bipyridine (0.123 g, 0.288 mmol) in 16 ml CH_2Cl_2–MeOH 2/1. The reaction mixture was refluxed, under N_2, for 15 h. After solvent evaporation the product was purified by column chromatography (silica gel, CH_2Cl_2). When the unreacted $[Ir(ppy\text{-}Br)_2Cl]_2$ eluted, 0.05 g of KPF_6 were added on top of the column and the polarity of the eluent was gradually increased to 100% acetone to elute $[Ir(ppy\text{-}Br)_2$(4,4'-bis(diethylphosphonate)-2,2'-bipyridine)$]PF_6$ together with the excess of KPF_6. The desired compound was precipitated with ether after filtration through a celite path in CH_2Cl_2 and it was obtained as a red solid. Yield 68%.

Elemental Analysis: calculated for ($C_{40}H_{40}Br_2IrN_4O_6P_3F_6{\cdot}CH_2Cl_2$): C, 37.40; H, 3.22; N, 4.26. Found: C, 37.05; H, 3.24; N, 4.41.

Exact Mass: ESI-MS $[C_{40}H_{40}Br_2IrN_4O_6P_2]^+$: calculated: m/z= 1085.0419, found: m/z= 1085.0454.

^{1}H NMR (300 MHz, acetone-d_6): δ 9.20 (d, J = 13.6 Hz, 1H), 8.40 (t, J = 4.9 Hz, 1H), 8.32 (d, J = 7.9 Hz, 1H), 8.05 (brd, J = 6.2 Hz, 1H), 8.03–7.99 (m, 1H), 7.94 (brd, J = 5.1 Hz, 1H), 7.92 (d, J = 8.5 Hz, 1H), 7.30 (dd, J = 2.0 Hz, J = 8.3 Hz, 1H), 7.21 (ddd, J = 1.4 Hz, J = 5.8 Hz, J = 7.3 Hz, 1H), 6.41 (d, J = 1.9 Hz, 1H), 4.41–4.10 (m, 4H), 1.35 (dt, J = 6.6 Hz, J = 7.1 Hz, 6H).

^{13}C APT NMR (75 MHz, acetone-d_6): δ 165.79 (s, C_{quat}), 155.61 (d, J = 14.74 Hz, C_{quat}), 151.21 (s, C_{quat}), 151.03 (d, J = 12.6 Hz, CH), 149.52 (s, CH), 142.91 (s, C_{quat}), 141.58 (d, J = 184.3 Hz, C_{quat}), 139.03 (s, CH), 133.28 (s, CH), 130.13 (d, J = 8.4 Hz, CH), 126.76 (d, J = 10.4 Hz, CH), 126.43 (s, CH), 125.71 (s, CH), 124.54 (s, C_{quat}), 124.01 (s, CH), 120.23 (s, CH), 62.77 (d, J = 4.0 Hz, $2CH_2$), 15.38 (d, J = 5.8 Hz, $2CH_3$).

^{31}P NMR (162 MHz, acetone-d_6): δ 11.10 (s, 1P), -144.07 (sep, J = 707.7 Hz, 1P).

UV/Vis (EtOH), λ, nm (ε, 10^4 M^{-1} cm^{-1}): 252 (3.7), 272 (3.8), 376 (0.7).

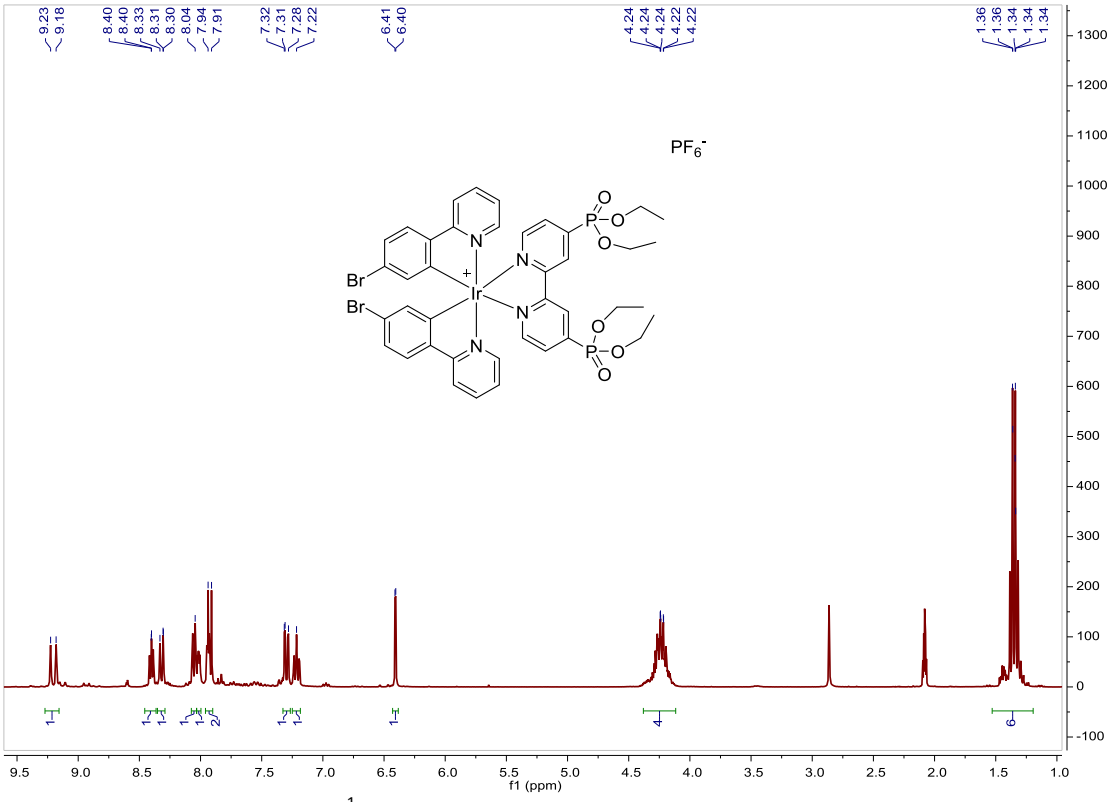

Fig. S72. ^{1}H NMR spectrum of **C15** in acetone-d_6, 300 MHz.

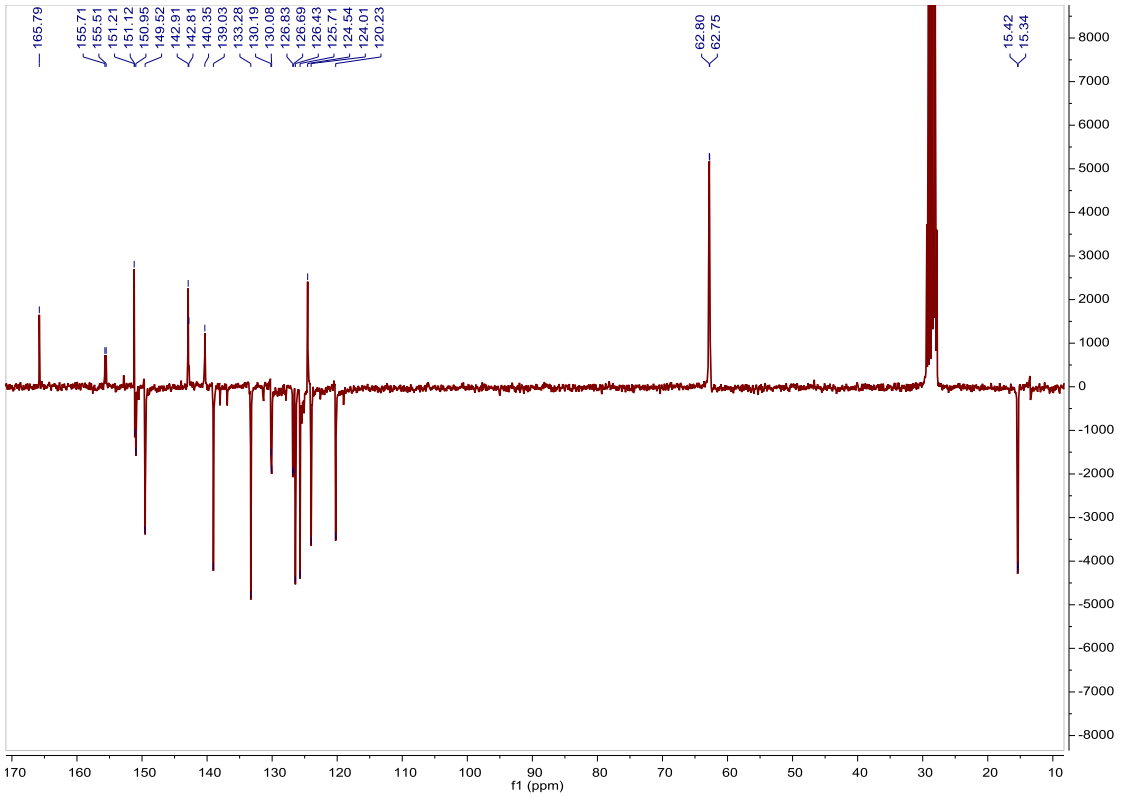

Fig. S73. ^{13}C APT NMR spectrum of **C15** in acetone-d_6, 75 MHz.

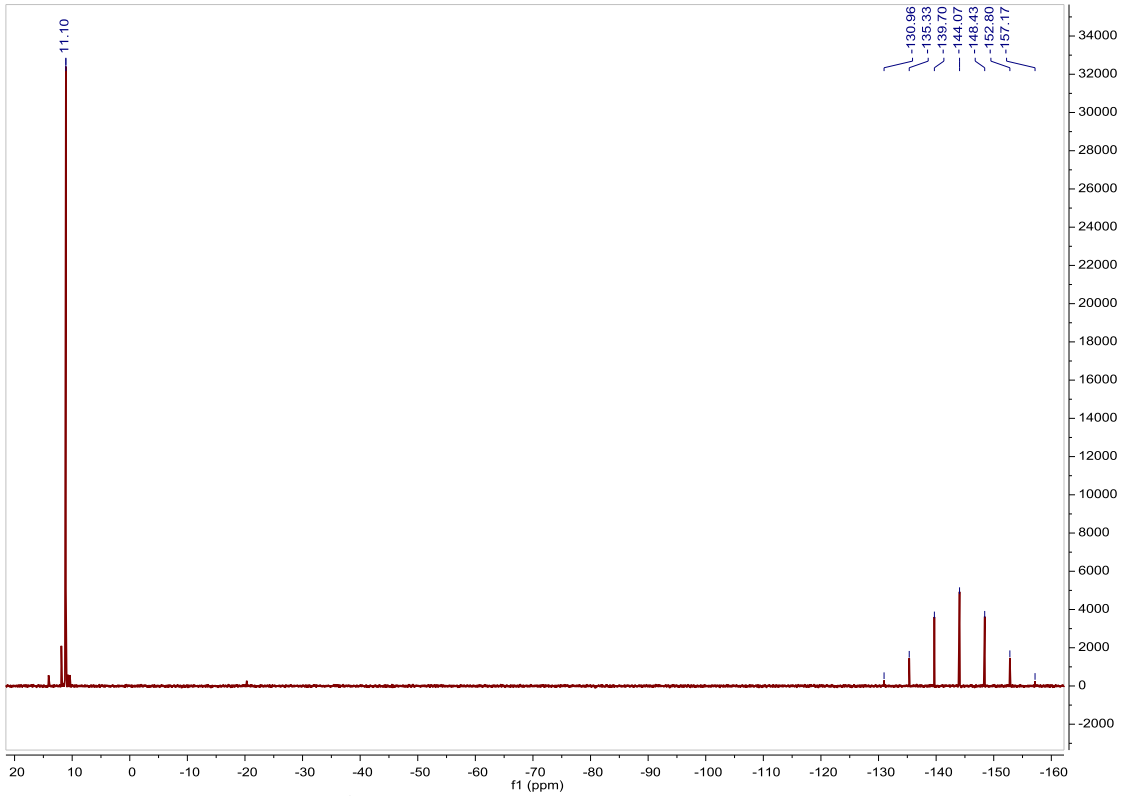

Fig. S74. ^{31}P NMR spectrum of **C15** in acetone-d_6, 162 MHz.

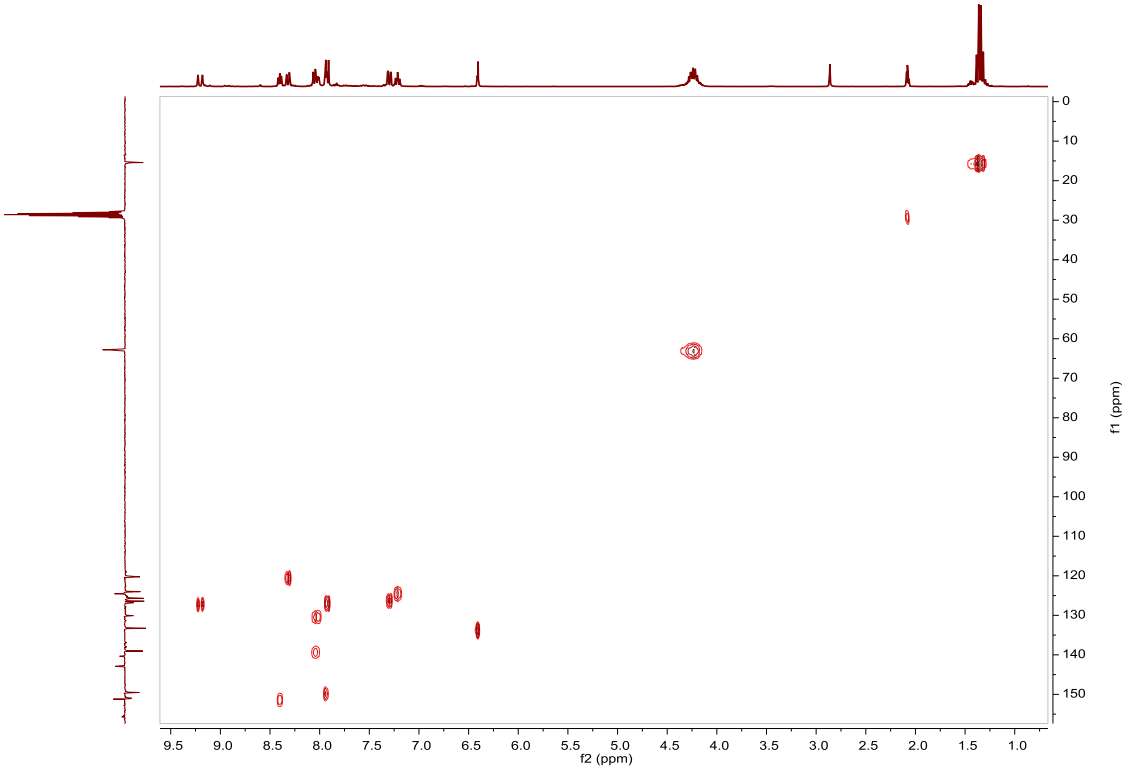

Fig. S75. HSQC NMR spectrum of **C15** in acetone-d_6.

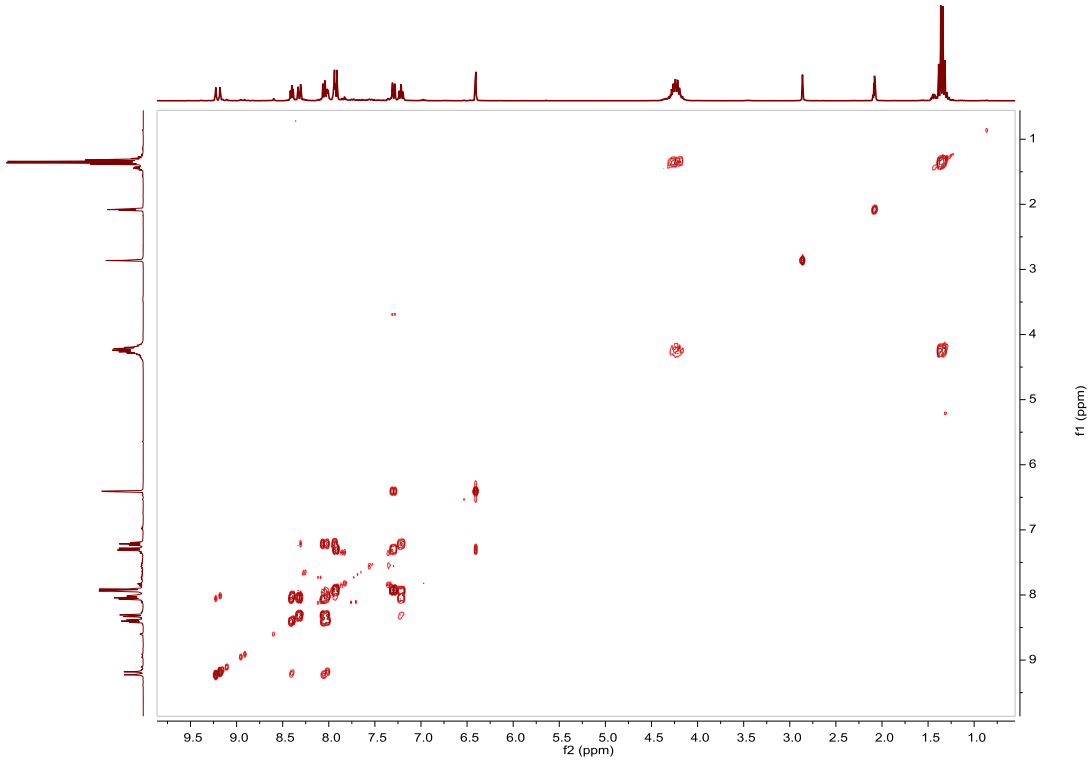

Fig. S76. COSY NMR spectrum of **C15** in acetone-d_6.

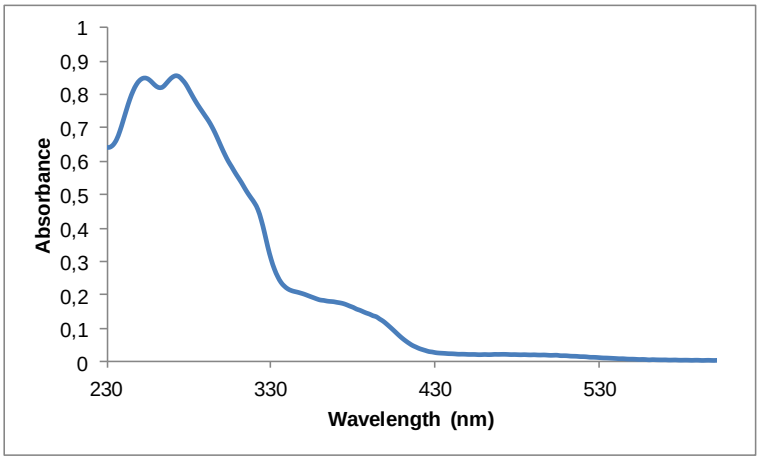

Fig. S77. UV/Vis spectra of **C15** in EtOH, $2.27 \cdot 10^{-5}$M.

Compound D15, [Ir((5-azobenzyl-2-pyridyl)phenyl)2(4,4'-bis(diethylphosphonate)-2,2'-bipyridine)]PF_6. Synthesis, characterization and photoisomerization studies.

SYNTHESIS

Under a N_2 atmosphere, $[Ir((5\text{-azobenzyl-2-pyridyl})phenyl)_2Cl]_2$ (0.03 g, 0.017 mmol) were added over a suspension of 4,4'-bis(diethylphosphonate)-2,2'-bipyridine (0.014 g, 0.033 mmol) in 3 ml CH_2Cl_2–MeOH 2/1. The reaction mixture was refluxed, under N_2, for 15 h. After solvent evaporation the product was purified by column chromatography (silica gel, $CH_2Cl_2/CH_3(CO)CH_3$ 1/9). 0.007 g of KPF_6 were added on top of the column to elute $[Ir((5\text{-azobenzyl-2-pyridyl})phenyl)_2(4,4'\text{-bis(diethylphosphonate)-2,2'-bipyridine})]PF_6$ together with the excess of KPF_6. The desired compound was precipitated with hexane after filtration through a celite path in CH_2Cl_2 and it was obtained as an orange solid. Yield 33%.

Elemental Analysis: calculated for ($C_{64}H_{58}IrN_8O_6P_3F_6 \cdot 2CH_2Cl_2$): C, 49.42; H, 3.90; N, 6.99. Found: C, 48.72 ; H, 3.66 ; N, 6.97.

Exact Mass: ESI-MS $[C_{64}H_{58}IrN_8O_6P_2]^+$: calculated: m/z= 1289.3584, found: m/z= 1289.3606.

^{1}H NMR (300 MHz, acetone-d_6): δ 9.09 (d, J = 13.6 Hz, 1H), 8.39 (t, J = 5.0 Hz, 1H), 8.20 (brd, J = 7.6 Hz, 1H), 7.96–7.85 (m, 4H), 7.83–7.73 (m, 4H), 7.53–7.42 (m, 5H), 7.33 (dd, J = 1.8 Hz, J = 8.1 Hz, 1H), 7.09 (ddd, J = 1.3 Hz, J = 5.8 Hz, J = 7.3 Hz, 1H), 6.58 (d, J = 1.7 Hz, 1H), 4.21–4.01 (m, 4H), 1.26–1.14 (m, 6H).

^{13}C APT NMR (75 MHz, acetone-d_6): δ 166.85 (C_{quat}), 152.45 (C_{quat}), 151.51 (C_{quat}), 151.28 (CH), 149.99 (C_{quat}), 149.85 (CH), 144.02 (C_{quat}), 143.40 (C_{quat}), 142.71 (C_{quat}), 141.19 (C_{quat}), 140.24 (C_{quat}), 138.91 (CH), 131.14 (CH), 130.16 (CH), 129.39 (CH), 129.12 (2CH), 127.43 (2CH), 126.93 (CH), 125.35 (CH), 123.80 (CH), 122.96 (2CH), 122.47(2CH), 121.88 (CH), 120.29 (CH), 62.99 (d, J = 5.6 Hz, $2CH_2$), 15.59 (d, J = 5.8 Hz, $2CH_3$).

^{31}P NMR (202 MHz, acetone-d_6): δ 12.28 (s, 1P), -143.03 (sep, J = 705.0 Hz, 1P).

UV/Vis (EtOH), λ, nm (ε, 10^4 M^{-1} cm^{-1}): 365 (7.0), 420 (1.9).

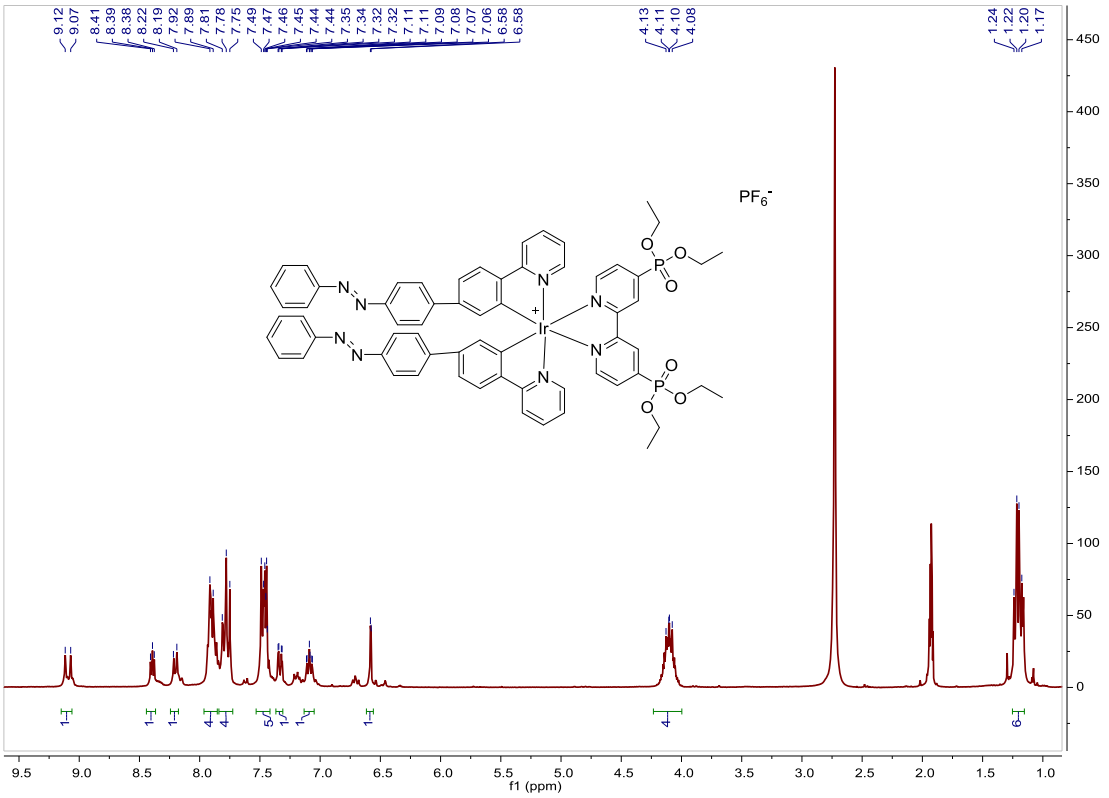

Fig. S78. ^{1}H NMR spectrum of **D15** in acetone-d_6, 300 MHz.

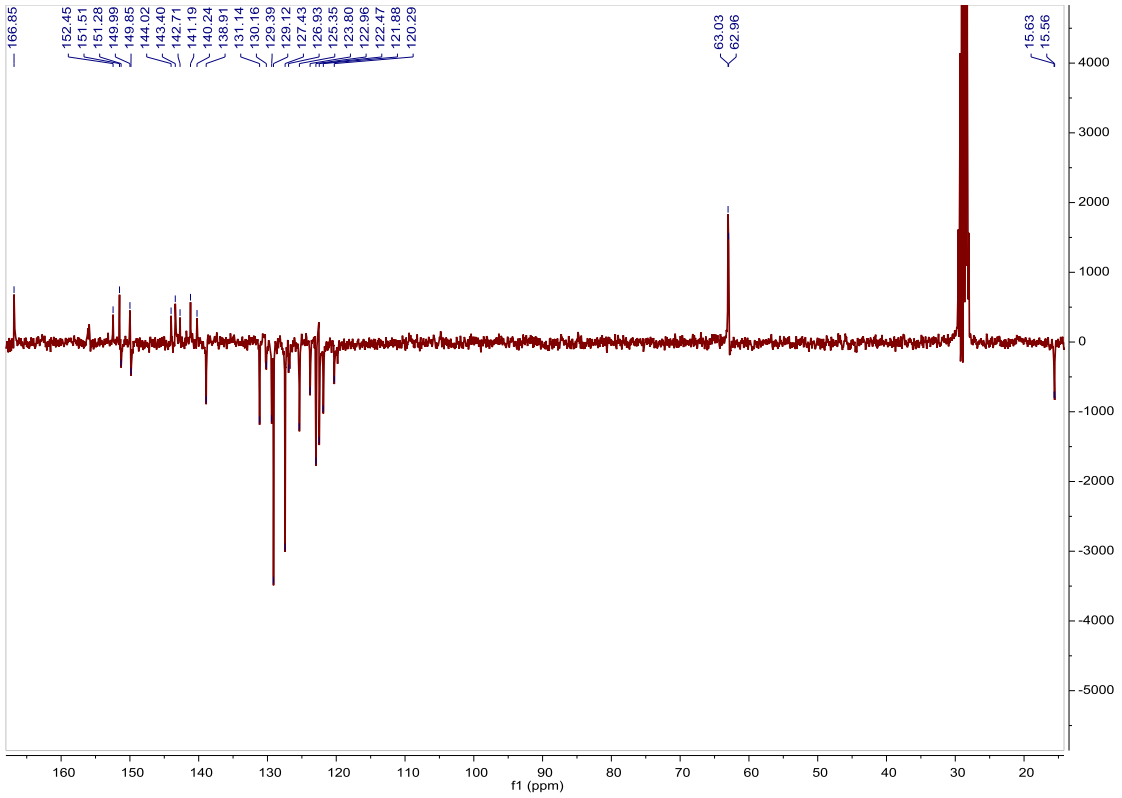

Fig. S79. ^{13}C APT NMR spectrum of **D15** in acetone-d_6, 75 MHz.

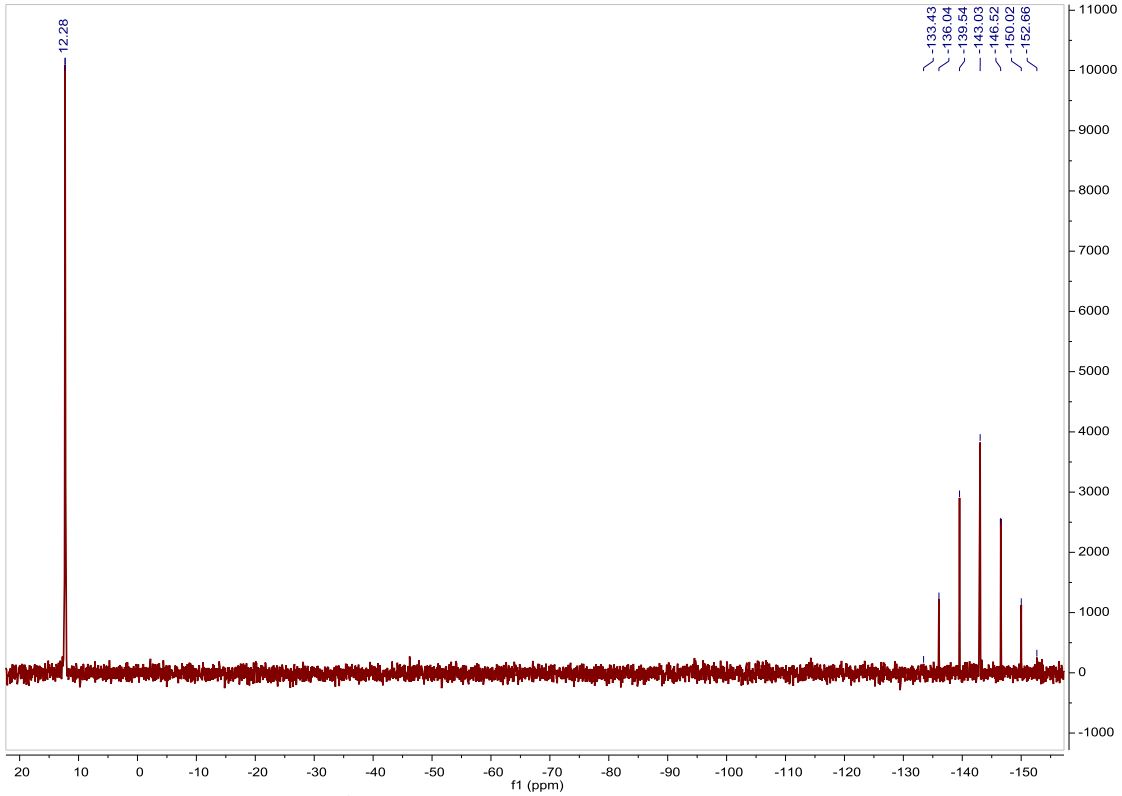

Fig. S80. ^{31}P NMR spectrum of **D15** in acetone-d_6, 162 MHz.

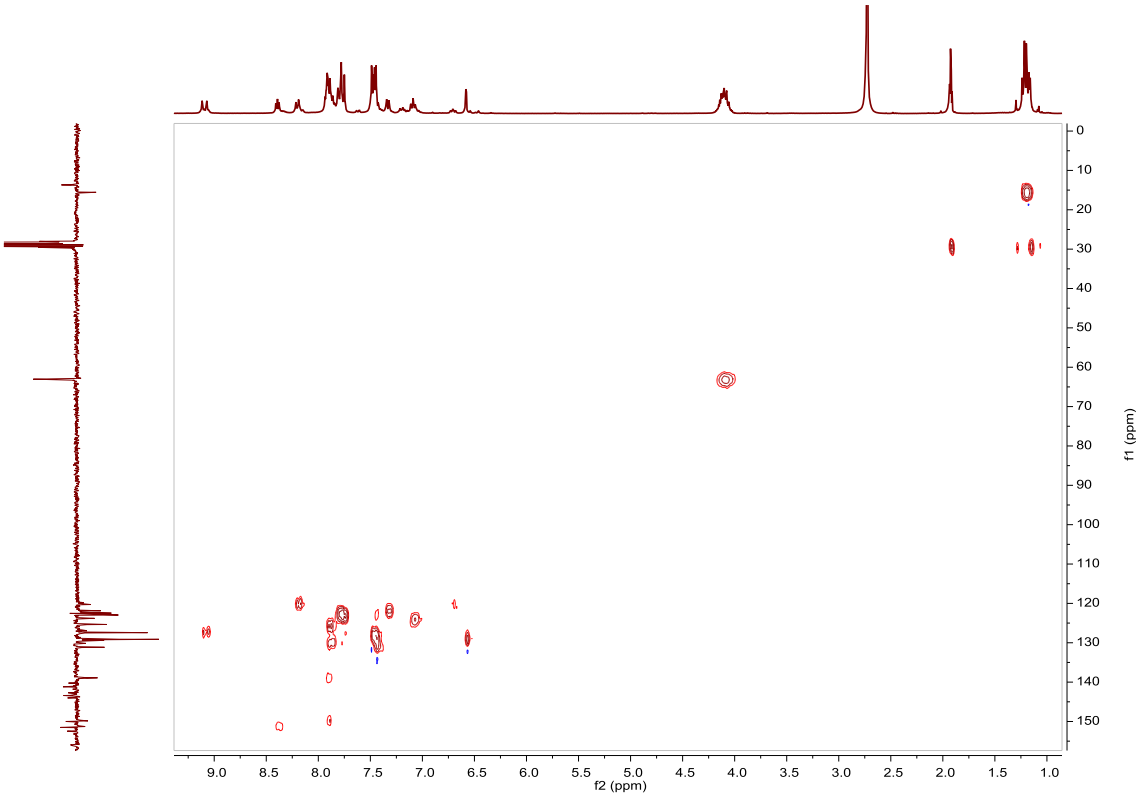

Fig. S81. HSQC NMR spectrum of **D15** in acetone-d_6.

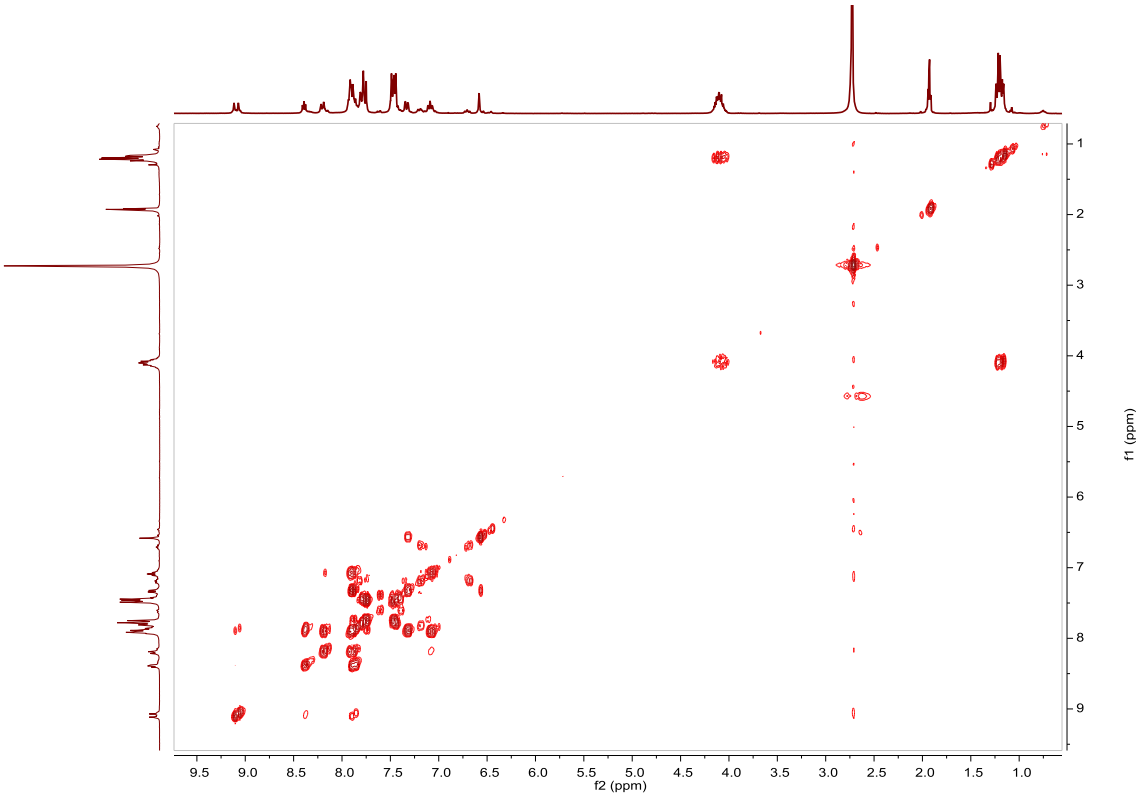

Fig. S82. COSY NMR spectrum of **D15** in acetone-d_6.

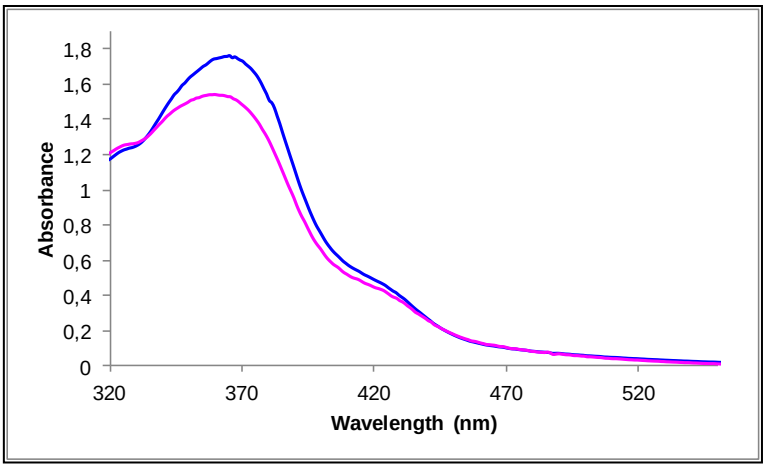

Fig. S83. UV/Vis spectra of **D15** in EtOH. Before (blue line) and after (pink line) irradiation at 377nm, $2.51 \cdot 10^{-5}$M.

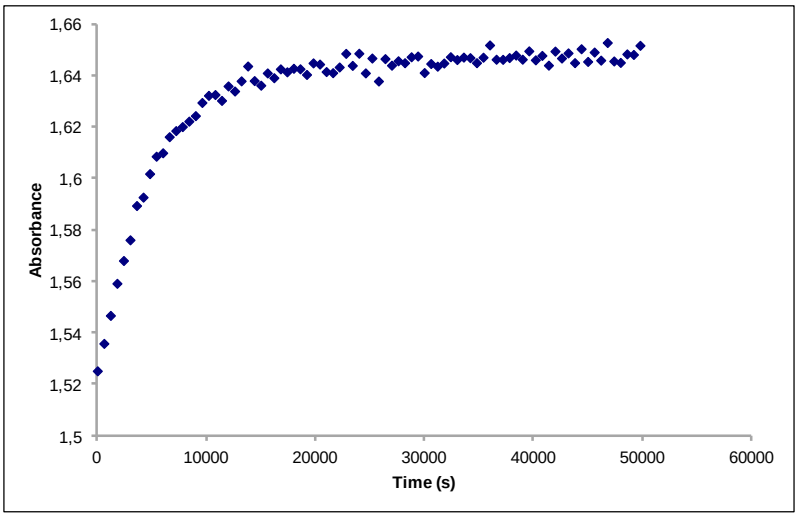

Fig. S84. Cis to trans thermal isomerization kinetics of **D15**. Absorption change of the band 365nm at 328 K in EtOH after irradiation at 377 nm. ($2.51 \cdot 10^{-5}$M).

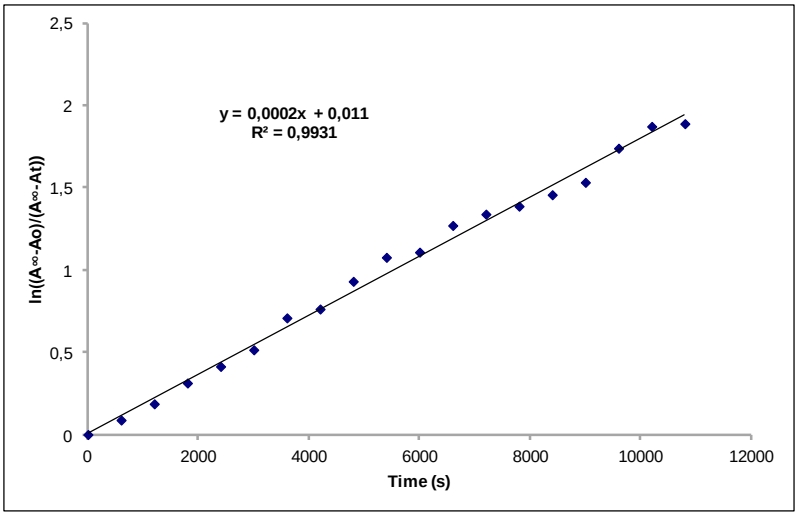

Fig. S85. Cis to trans thermal isomerization kinetics of **D15**. First-order plot. k (s^{-1}) = $2.0 \cdot 10^{-4}$. Half-life (min) = 58.

Compound A16, [Ir(ppy)$_2$(4,4'-bis(carboxy)-2,2'-bipyridine)]PF$_6$. Synthesis and characterization.

SYNTHESIS

Under a N_2 atmosphere, $[Ir(ppy)_2Cl]_2$ (0.100 g, 0.093 mmol) were dissolved in 6 ml of acetone and $Ag(CF_3SO_3)$ (0.096 g, 0.372 mmol) were added. The mixture was heated to 56 °C for 2 h and after cooled down to room temperature, AgCl was removed by centrifugation. The resulting solution was added over a 1 h refluxed suspension of 4,4'-bis(carboxy)-2,2'-bipyridine (0.057 g, 0.232 mmol) in 3 ml of acetone and 102 µl of $N(Et)_3$. The reaction mixture was refluxed, under N_2, for 15 h. After solvent evaporation the product was purified by column chromatography (silica gel, CH_2Cl_2). When the unreacted $[Ir(ppy)_2Cl]_2$ eluted, 0.05 g of KPF_6 were added on top of the column and the polarity of the eluent was gradually increased to 100% methanol to elute $[Ir(ppy)_2(4,4'\text{-bis(carboxy)-2,2'-bipyridine})]PF_6$ together with the excess of KPF_6. The desired compound washed with acetone was obtained as an orange solid. Yield 72%. The spectroscopic data are coincident with those described in the literature.[33]

Exact Mass: ESI-MS $[C_{34}H_{24}IrN_4O_4]^+$: calculated: m/z= 745.1427, found: m/z= 745.1447.

^{1}H NMR (300 MHz, DMSO-*d*$_6$): δ 8.90 (s, 1H), 8.26 (d, J = 7.9 Hz, 1H), 7.97–7.78 (m, 4H), 7.63 (d, J = 4.7 Hz, 1H), 7.16 (t, J = 5.9 Hz, 1H), 7.03 (t, J = 6.9 Hz, 1H), 6.91 (t, J = 7.0 Hz, 1H), 6.21 (d, J = 7.3 Hz, 1H).

UV/Vis (EtOH), λ, nm (ε, 10^4 M^{-1} cm^{-1}): 254 (4.2), 268 (3.9), 320 (1.8), 380 (0.8).

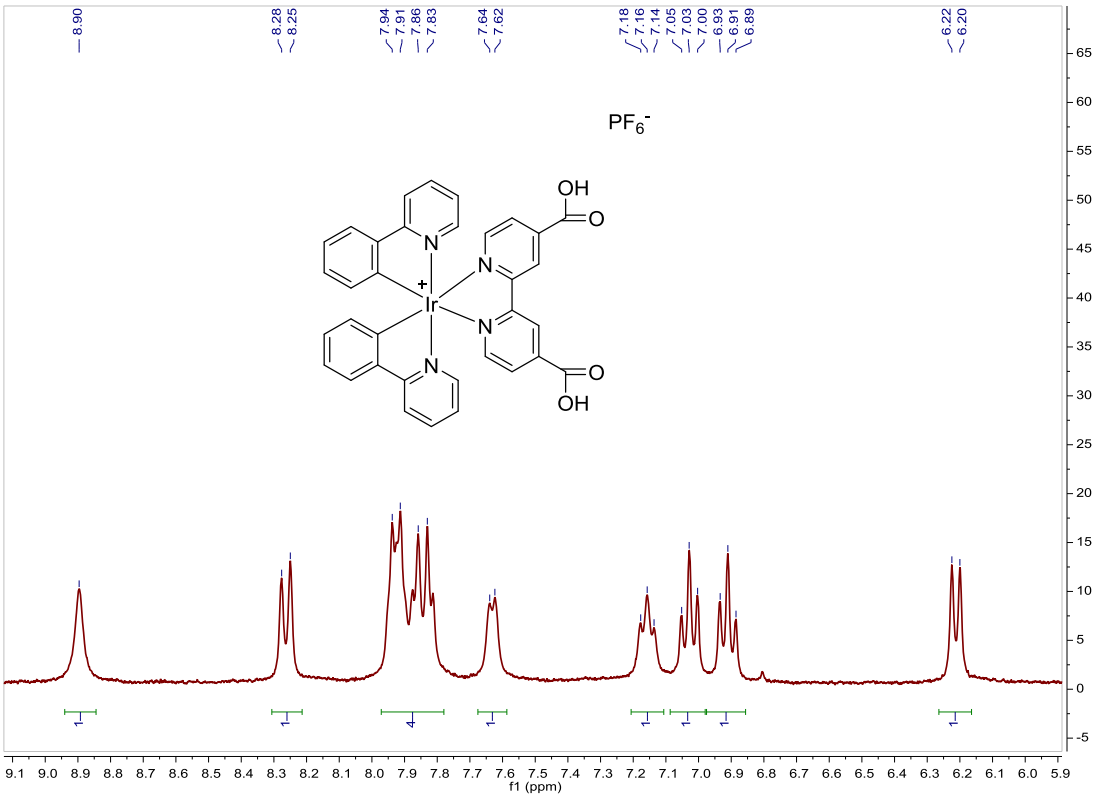

Fig. S86. ^{1}H NMR spectrum of **A16** in DMSO-*d*$_6$, 300 MHz.

[33] Z. Ning, Q. Zhang, W. Wu and H. Tian, *J. Organomet. Chem.*, **2009**, *694*, 2705–2711.

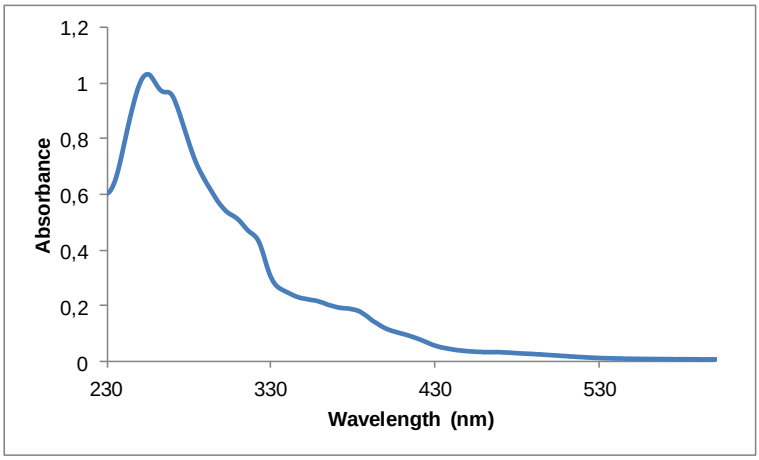

Fig. S87. UV/Vis spectra of **A16** in EtOH, $2.47 \cdot 10^{-5}$M.

Compound B16, [Ir(ppy-F_2)$_2$(4,4'-bis(carboxy)-2,2'-bipyridine)]PF_6. Synthesis and characterization.

SYNTHESIS

Under a N_2 atmosphere, $[Ir(ppy\text{-}F_2)_2Cl]_2$ (0.100 g, 0.082 mmol) were dissolved in 6 ml of acetone and $Ag(CF_3SO_3)$ (0.084 g, 0.328 mmol) were added. The mixture was heated to 56 °C for 2 h and after cooled down to room temperature, AgCl was removed by centrifugation. The resulting solution was added over a 1 h refluxed suspension of 4,4'-bis(carboxy)-2,2'-bipyridine (0.05 g, 0.206 mmol) in 3 ml of acetone and 90 µl of $N(Et)_3$. The reaction mixture was refluxed, under N_2, for 15 h. After solvent evaporation the product was purified by column chromatography (silica gel, CH_2Cl_2). When the unreacted $[Ir(ppy\text{-}F_2)_2Cl]_2$ eluted, 0.05 g of KPF_6 were added on top of the column and the polarity of the eluent was gradually increased to 100% methanol to elute $[Ir(ppy\text{-}F_2)_2$(4,4'-bis(carboxy)-2,2'-bipyridine)]PF_6 together with the excess of KPF_6. The desired compound washed with acetone was obtained as a yellow solid. Yield 52%. The spectroscopic data are coincident with those described in the literature.[34]

Exact Mass: ESI-MS $[C_{34}H_{20}F_4IrN_4O_4]^+$: calculated: m/z= 817.1050 , found: m/z= 817.1060 .

^{1}H NMR (300 MHz, DMSO-d_6): δ 8.88 (s, 1H), 8.30 (d, J = 8.4 Hz, 1H), 8.03 (t, J = 7.3 Hz, 1H), 7.88 (brd, J = 6.4 Hz, 2H), 7.71 (s, 1H), 7.24 (t, J = 6.3 Hz, 1H), 6.97 (ddd, J = 1.9 Hz, J = 2.3 Hz, J = 11.8 Hz, 1H), 5.64 (d, J = 6.7 Hz, 1H).

UV/Vis (EtOH), λ, nm (ε, 10^4 M^{-1} cm^{-1}): 248 (3.6), 262 (3.4), 306 (1.8), 362 (0.6).

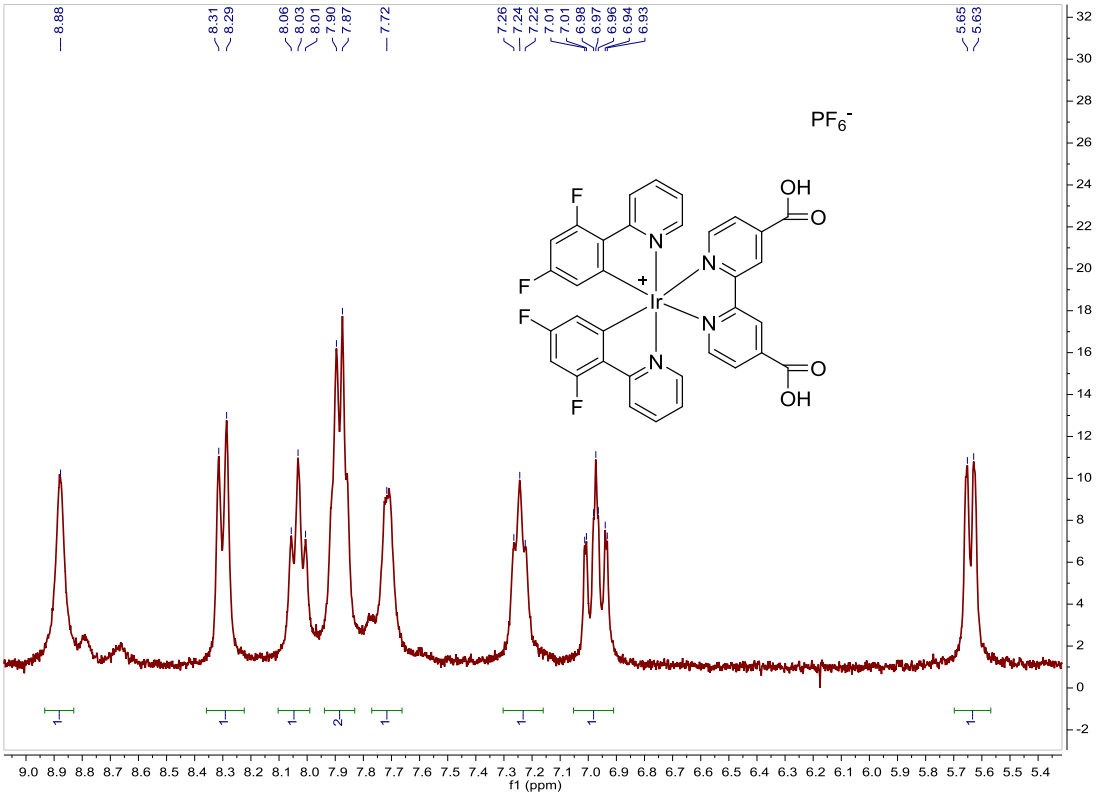

Fig. S88. ^{1}H NMR spectrum of **B16** in DMSO-d_6, 300 MHz.

[34] W. Jiang, Y. Gao, Y. Sun, F. Ding, Y. Xu, Z. Bian, F. Li, J. Bian and C. Huang, *Inorg. Chem.*, **2010,** *49*, 3252–3260.

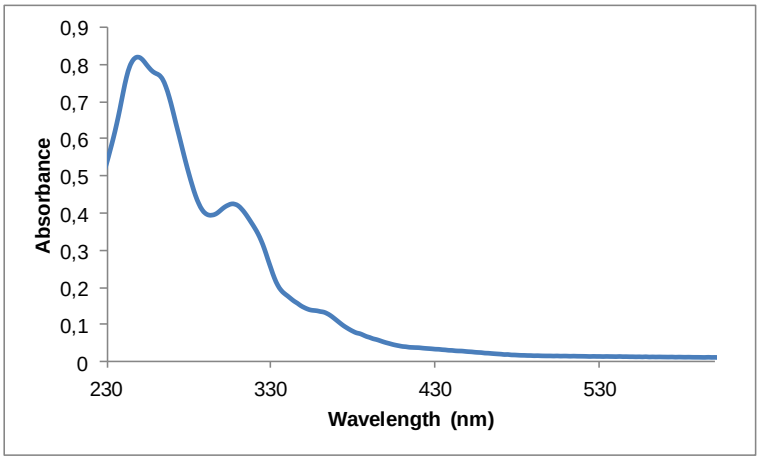

Fig. S89. UV/Vis spectra of **B16** in EtOH, $2.29 \cdot 10^{-5}$M.

Compound C16, [Ir(ppy-Br)$_2$(4,4'-bis(carboxy)-2,2'-bipyridine)]PF$_6$. Synthesis and characterization.

SYNTHESIS

Under a N_2 atmosphere, $[Ir(ppy\text{-}Br)_2Cl]_2$ (0.150 g, 0.108 mmol) were dissolved in 8 ml of acetone and $Ag(CF_3SO_3)$ (0.111 g, 0.432 mmol) were added. The mixture was heated to 56 °C for 2 h and after cooled down to room temperature, AgCl was removed by centrifugation. The resulting solution was added over a 1 h refluxed suspension of 4,4'-bis(carboxy)-2,2'-bipyridine (0.066 g, 0.270 mmol) in 4 ml of acetone and 119 µl of $N(Et)_3$. The reaction mixture was refluxed, under N_2, for 15 h. After solvent evaporation the product was purified by column chromatography (silica gel, CH_2Cl_2). When the unreacted $[Ir(ppy\text{-}Br)_2Cl]_2$ eluted, 0.05 g of KPF_6 were added on top of the column and the polarity of the eluent was gradually increased to 100% methanol to elute $[Ir(ppy\text{-}Br)_2(4,4'\text{-bis(carboxy)-2,2'-bipyridine)}]PF_6$ together with the excess of KPF_6. The desired compound washed with acetone and ether was obtained as a yellow solid. Yield 41%.

Elemental Analysis: calculated for $(C_{34}H_{22}Br_2IrN_4O_4PF_6{\cdot}CH_3COCH_3)$: C, 40.19; H, 2.55; N, 5.07. Found: C, 39.99; H, 2.62; N, 5.47.

Exact Mass: ESI-MS $[C_{34}H_{22}Br_2IrN_4O_4]^+$: calculated: m/z= 900.9637 , found: m/z= 900.9625.

^{1}H NMR (300 MHz, DMSO-d_6): δ 8.80 (s, 1H), 8.23 (d, J = 8.2 Hz, 1H), 7.93–7.78 (m, 3H), 7.74 (d, J = 5.4 Hz, 1H), 7.57 (d, J = 5.5 Hz, 1H), 7.21–7.06 (m, 2H), 6.09 (s, 1H).

UV/Vis (EtOH), λ, nm (ε, 10^4 M^{-1} cm^{-1}): 254 (2.4), 270 (2.5), 310 (1.5).

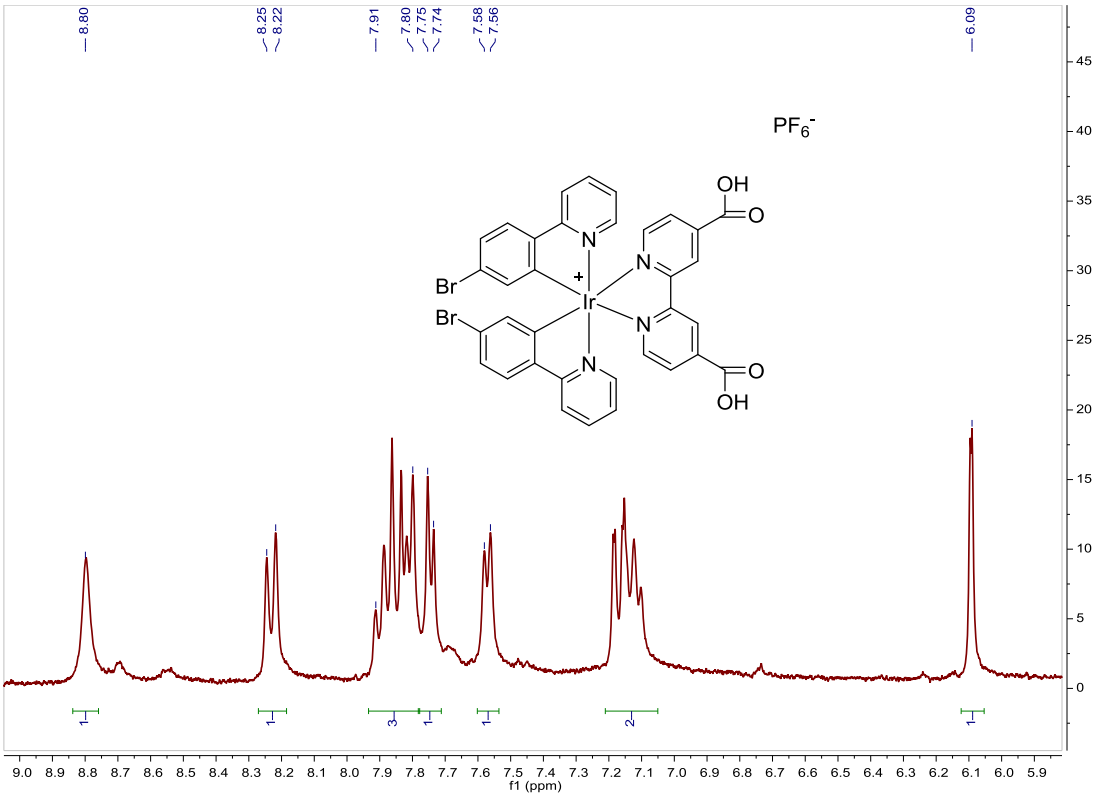

Fig. S90. ^{1}H NMR spectrum of **C16** in DMSO-d_6, 300 MHz.

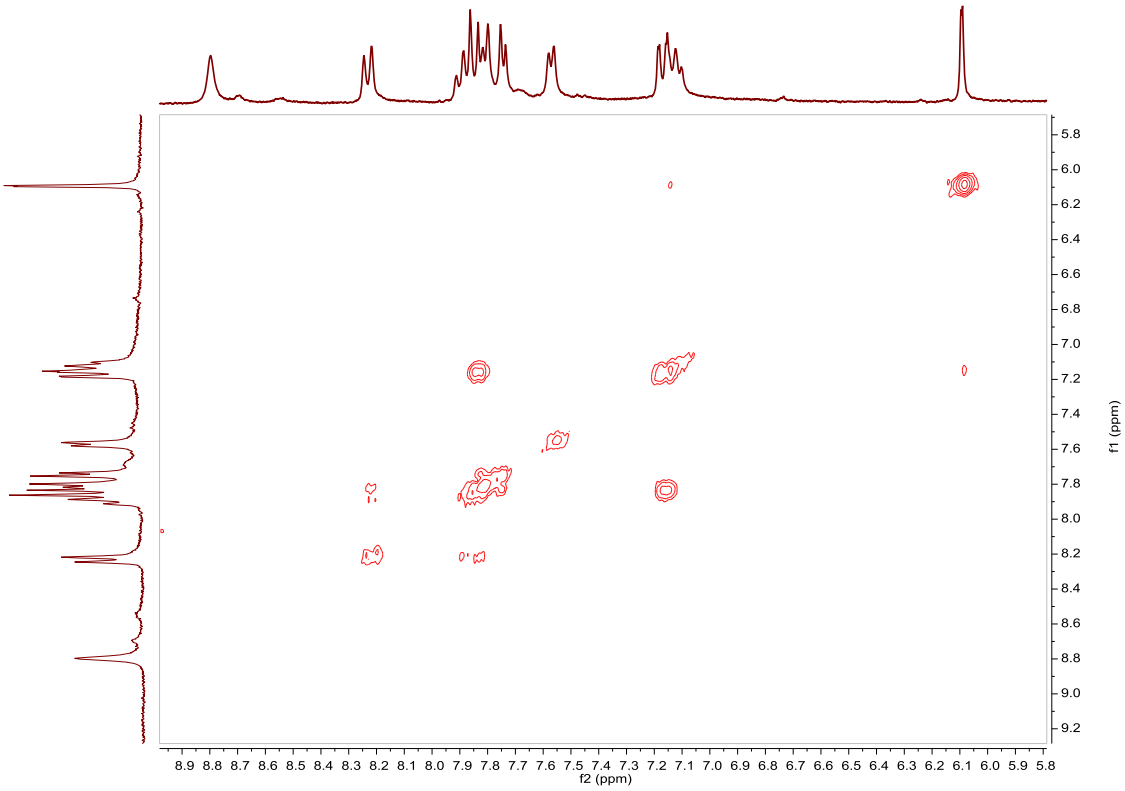

Fig. S91. COSY NMR spectrum of **C16** in DMSO-d_6.

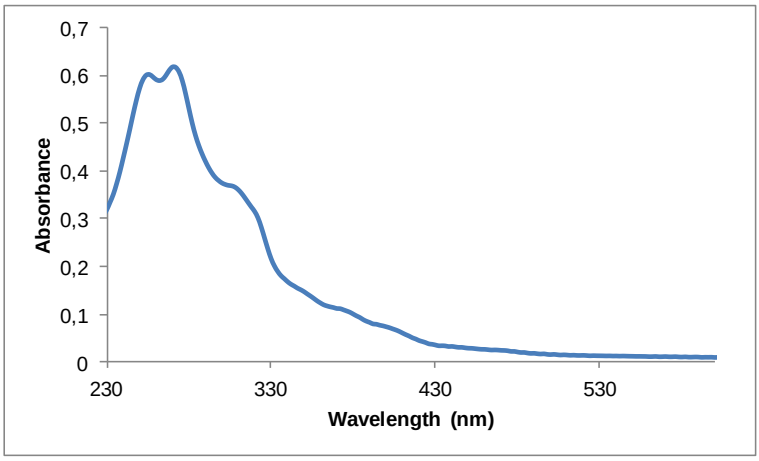

Fig. S92. UV/Vis spectra of **C16** in EtOH, $2.48 \cdot 10^{-5}$M.

Compound D16, [Ir((5-azobenzyl-2-pyridyl)phenyl)$_2$(4,4'-bis(carboxy)-2,2'-bipyridine)] PF_6. Synthesis, characterization and photoisomerization studies.

SYNTHESIS

Under a N_2 atmosphere, [Ir((5-azobenzyl-2-pyridyl)phenyl)$_2$Cl]$_2$ (0.100 g, 0.056 mmol) were dissolved in 4 ml of acetone and Ag(CF_3SO_3) (0.057 g, 0.224 mmol) were added. The mixture was heated to 56 °C for 2 h and after cooled down to room temperature, AgCl was removed by centrifugation. The resulting solution was added over a 1 h refluxed suspension of 4,4'-bis(carboxy)-2,2'-bipyridine (0.034 g, 0.141 mmol) in 2 ml of acetone. The reaction mixture was refluxed, under N_2, for 15 h. After solvent evaporation the solid that was not soluble in MeOH was removed, NH_4PF_6 (0.02 g, 0.123 mmol) were added and the solution was stirred during 1 h. The desired compound was obtained after precipitation with hexane as an orange solid. Yield 63%.

Exact Mass: ESI-MS $[C_{58}H_{40}IrN_8O_4]^+$: calculated: m/z= 1105.2802 , found: m/z= 1105.2839.

^{1}H NMR (300 MHz, DMSO-d_6): δ 9.32 (s, 1H), 8.41 (d, J = 7.6 Hz, 1H), 8.24 (d, J = 5.5 Hz, 1H), 8.19–8.00 (m, 3H), 7.91 (d, J = 7.6 Hz, 3H), 7.83 (d, J = 5.4 Hz, 1H), 7.72–7.53 (m, 5H), 7.49 (d, J = 6.4 Hz, 1H), 7.24 (t, J = 6.7 Hz, 2H), 6.50 (s, 1H).

UV/Vis (EtOH), λ, nm (ε, 10^4 M^{-1} cm^{-1}): 360 (4.3), 425 (1.1).

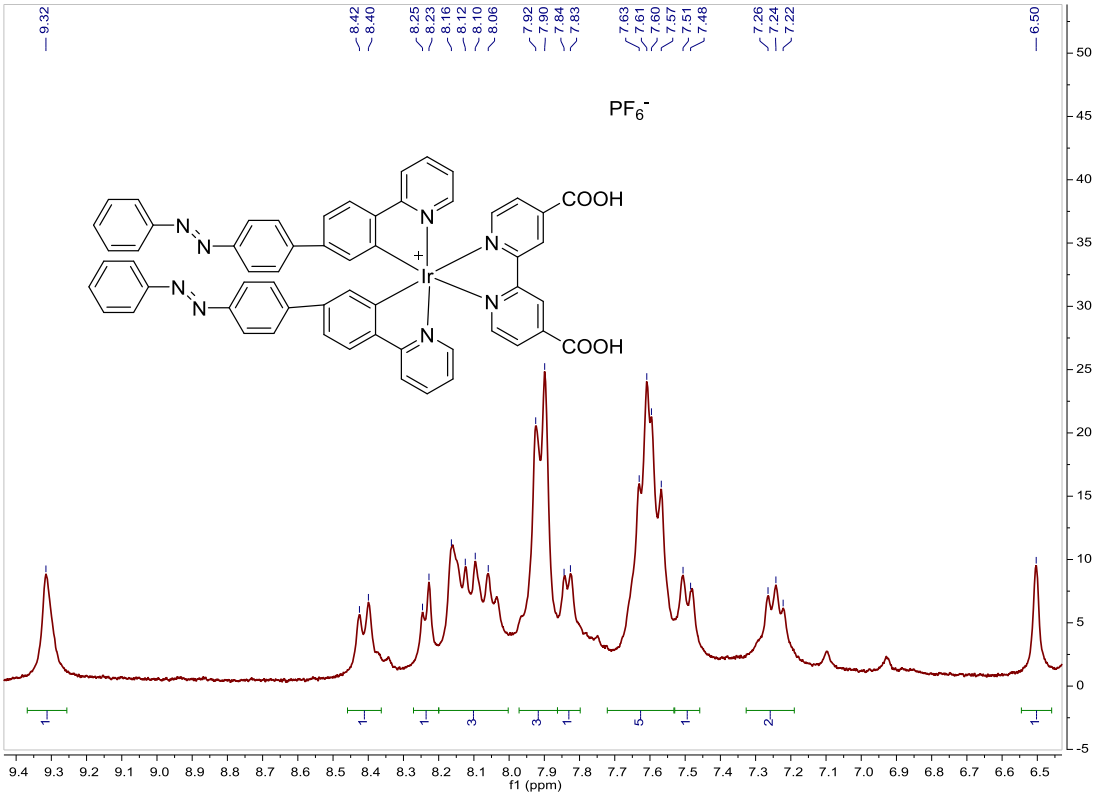

Fig. S93. ^{1}H NMR spectrum of **D16** in DMSO-d_6, 300 MHz.

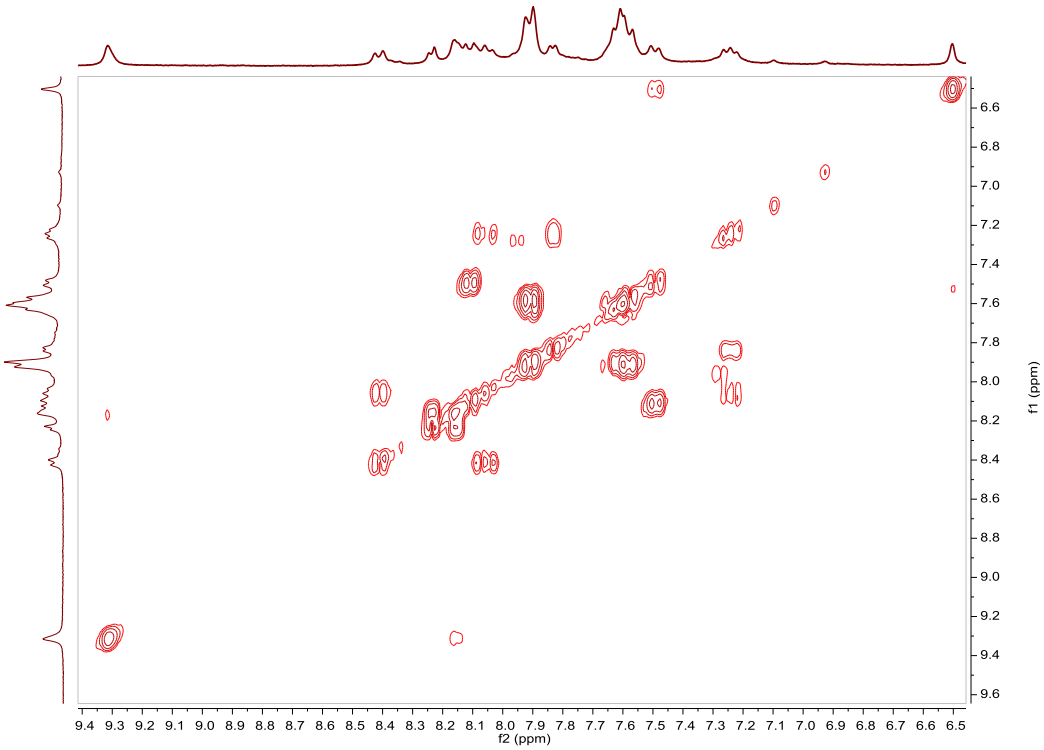

Fig. S94. COSY NMR spectrum of **D16** in DMSO-d_6.

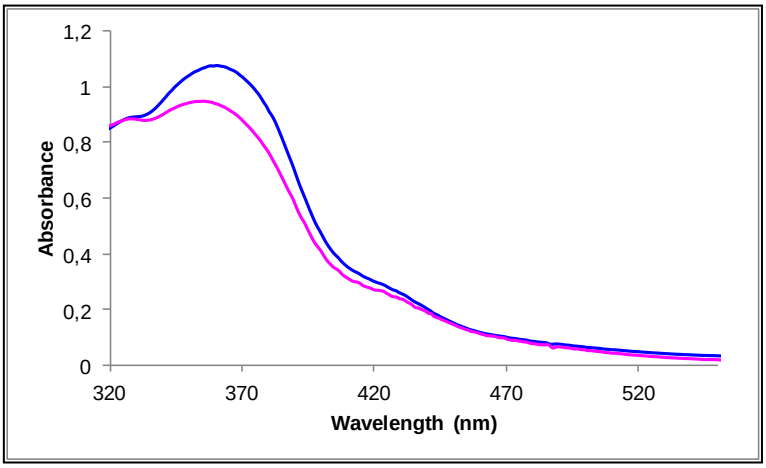

Fig. S95. UV/Vis spectra of **D16** in EtOH. Before (blue line) and after (pink line) irradiation at 374nm, $2.49 \cdot 10^{-5}$M.

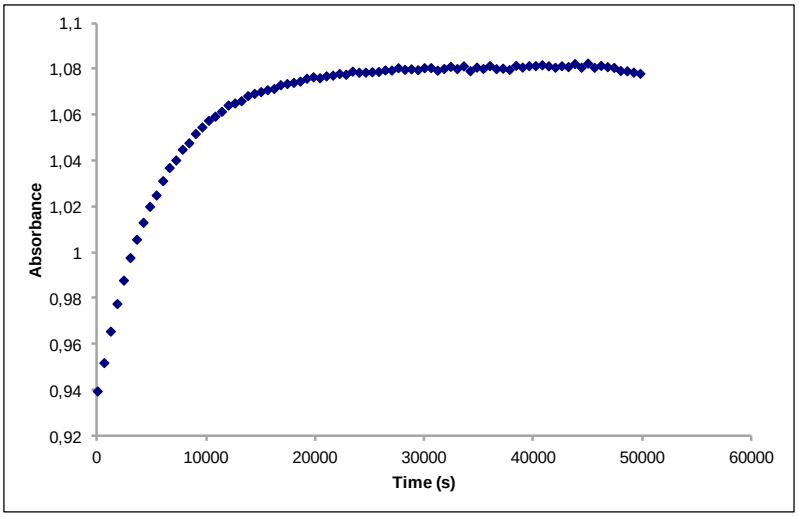

Fig. S96. Cis to trans thermal isomerization kinetics of **D16**. Absorption change of the band 360nm at 328 K in EtOH after irradiation at 374 nm. ($2.49 \cdot 10^{-5}$M).

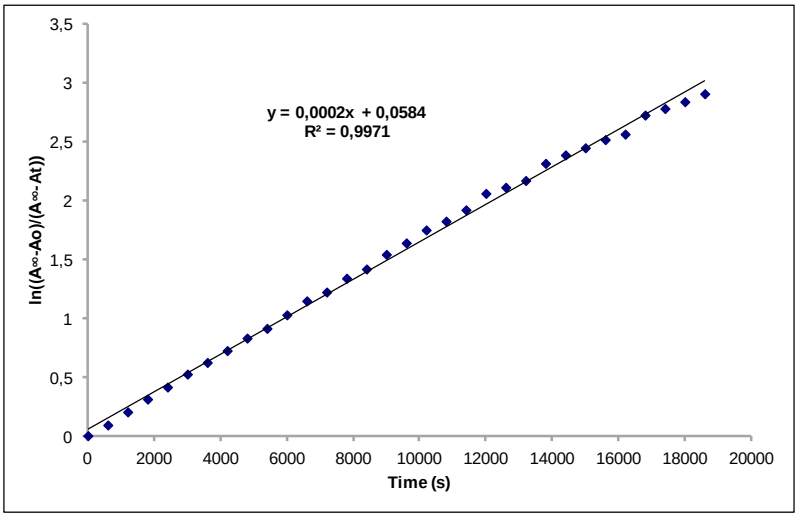

Fig. S97. Cis to trans thermal isomerization kinetics of **D16**. First-order plot. k (s^{-1}) = $2.0 \cdot 10^{-4}$. Half-life (min) = 58.

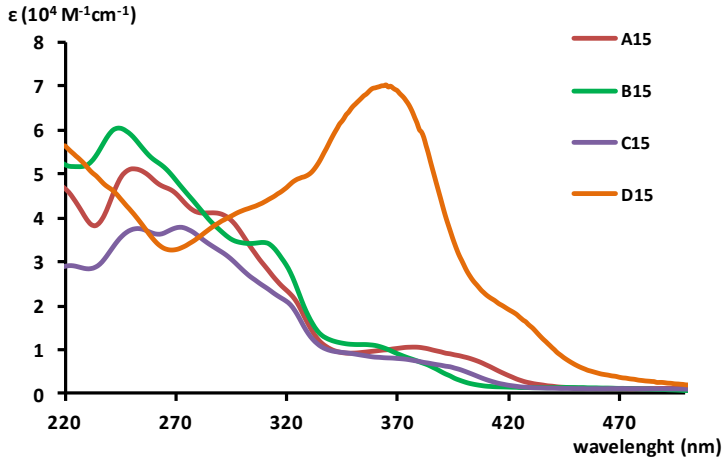

Fig. S98. UV-Vis absorption spectra of complexes **A**–**D** with 4,4'-bis(diethylphosphonate)-2,2'-bipyridine.

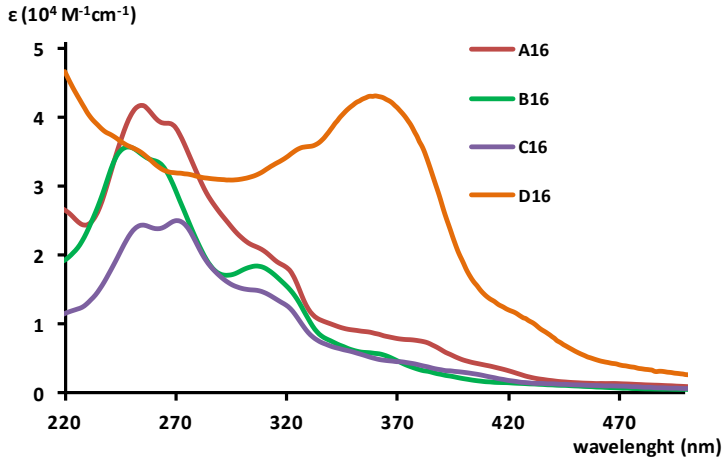

Fig. S99. UV-Vis absorption spectra of complexes **A**–**D** with 4,4'-bis(carboxy)-2,2'-bipyridine.

Compound Abipy, $[Ir(ppy)_2(bipy)]PF_6$. Synthesis and characterization.

SYNTHESIS

Under a N_2 atmosphere, $[Ir(ppy)_2Cl]_2$ (0.200 g, 0.186 mmol) were added over a suspension of 2,2'-bipyridine (0.058 g, 0.371 mmol) in 15 mL CH_2Cl_2–MeOH 2/1. The reaction mixture was refluxed, under N_2, for 15 h. To the resulting orange solution, 0.07 g of KPF_6 were added and the solution was stirred for an 1 h. The solvent was evaporated and the desired compound was obtained after filtration through a celite path in CH_2Cl_2 as a yellow solid. Yield 97%. The spectroscopic data are coincident with those described in the literature.[35]

^{1}H NMR (500 MHz, CD_2Cl_2): δ 8.56 (d, J = 8.1 Hz, 1H), 8.15 (t, J = 7.7 Hz, 1H), 8.05 (d, J = 4.5 Hz, 1H), 7.99 (d, J = 8.1 Hz, 1H), 7.81 (t, J =7.4 Hz, 1H), 7.77 (d, J = 7.7 Hz, 1H), 7.52 (d, J = 5.5 Hz, 1H), 7.49 (t, J = 5.9 Hz, 1H), 7.11 (t, J = 7.3 Hz, 1H), 7.02 (t, J =6.0 Hz, 1H), 6.97 (t, J = 7.4 Hz, 1H), 6.34 (d, J = 7.6 Hz, 1H).

^{13}C NMR (126 MHz, CD_2Cl_2): δ 168.16 (C_{quat}), 156.10 (C_{quat}) , 151.12 (CH), 150.26 (C_{quat}) , 148.89 (CH), 144.06 (C_{quat}), 139.84 (CH), 138.60 (CH), 132.02 (CH), 131.11 (CH), 128.67(CH), 125.30 (CH), 125.03 (CH), 123.69 (CH), 123.12 (CH), 120.25 (CH).

UV/Vis (CH_3CN), λ, nm (ε, 10^4 M^{-1} cm^{-1}): 254 (4.6), 265 (4.4), 309 (2.0), 376 (0.57).

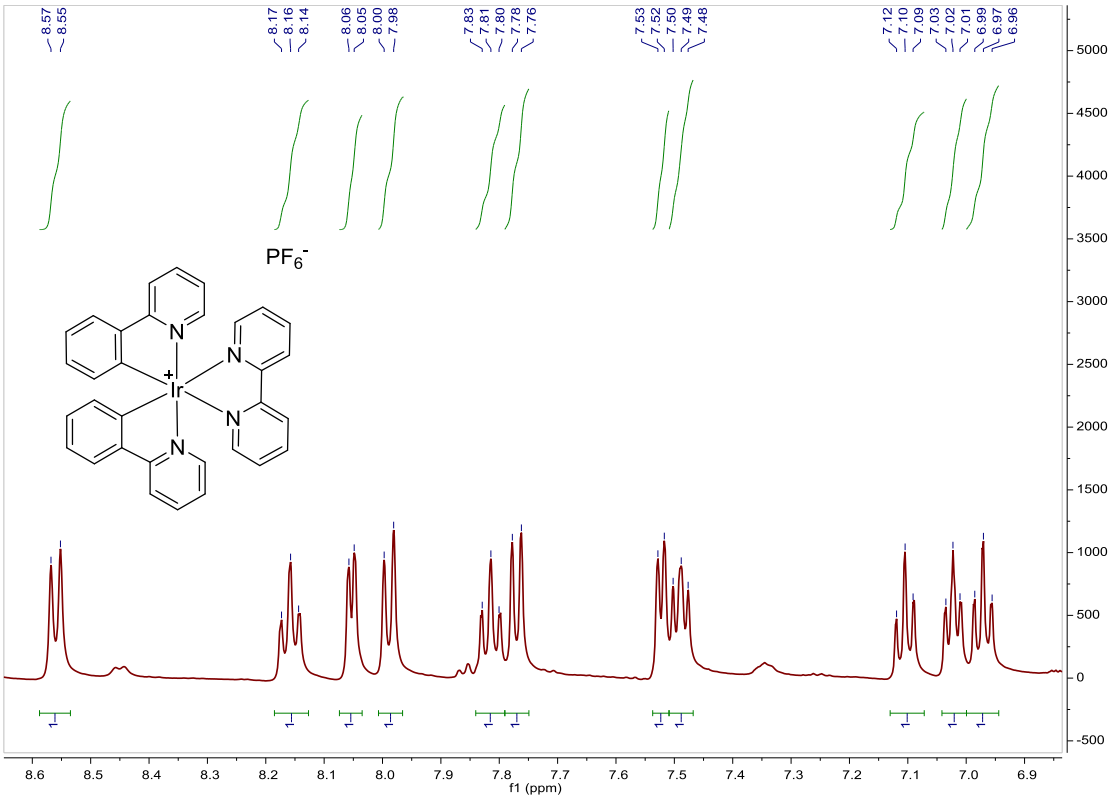

Fig. S100. ^{1}H NMR spectrum of **Abipy** in CD_2Cl_2, 500 MHz.

[35] R. D. Costa, E. Ortí, H. J. Bolink, S. Graber, S. Schaffner, M. Neuburger, C. E. Housecroft and E. C. Constable, *Adv. Funct. Mater.*, **2009**, *19*, 3456–3463.

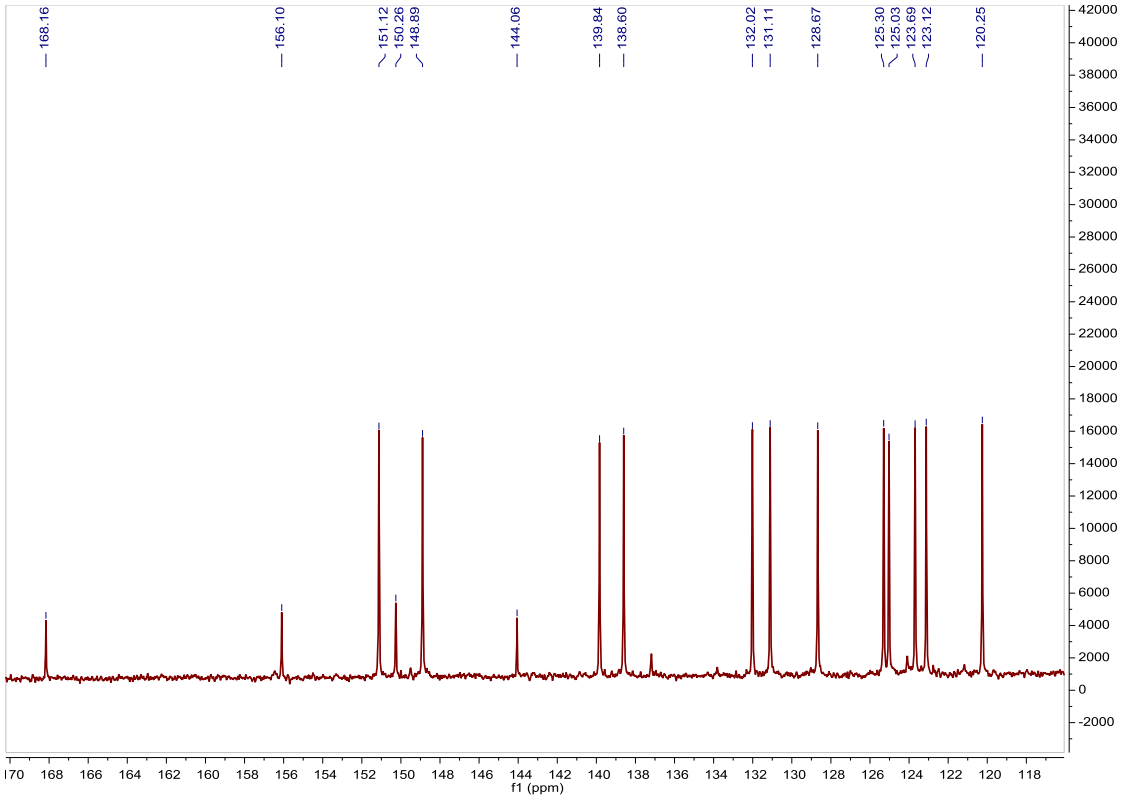

Fig. S101. ^{13}C NMR spectrum of **Abipy** in CD_2Cl_2, 126 MHz.

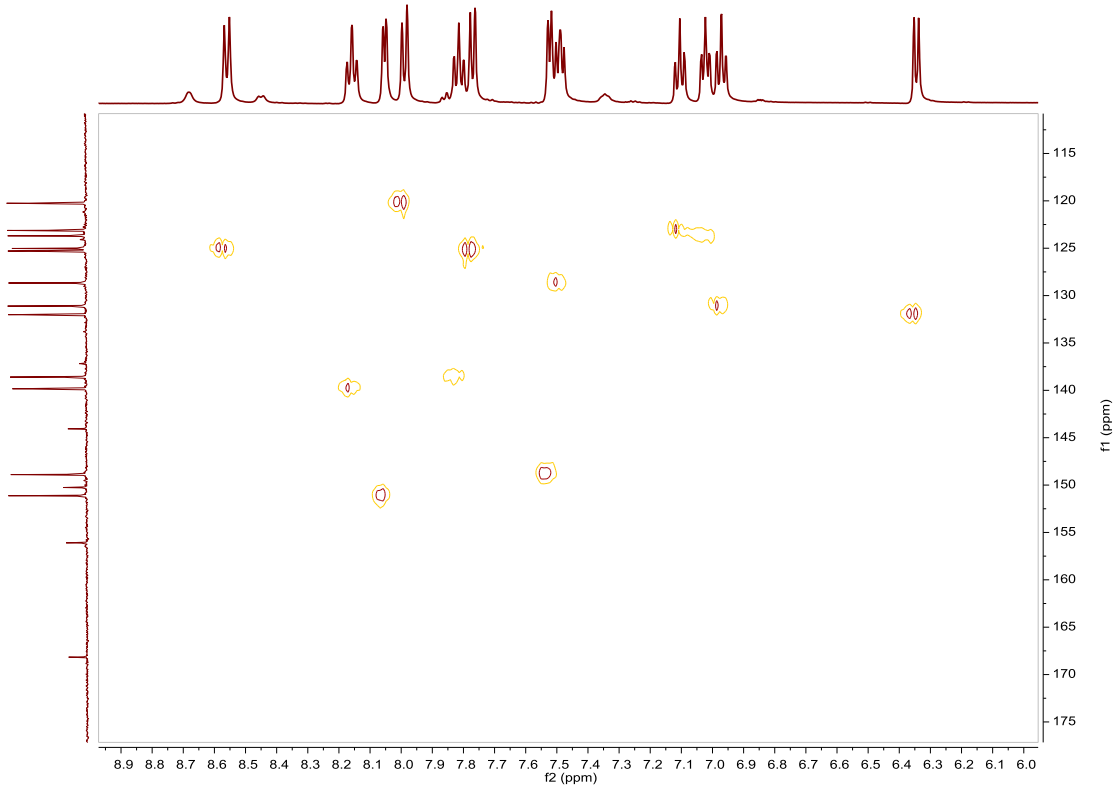

Fig. S102. HSQC NMR spectrum of **Abipy** in CD_2Cl_2.

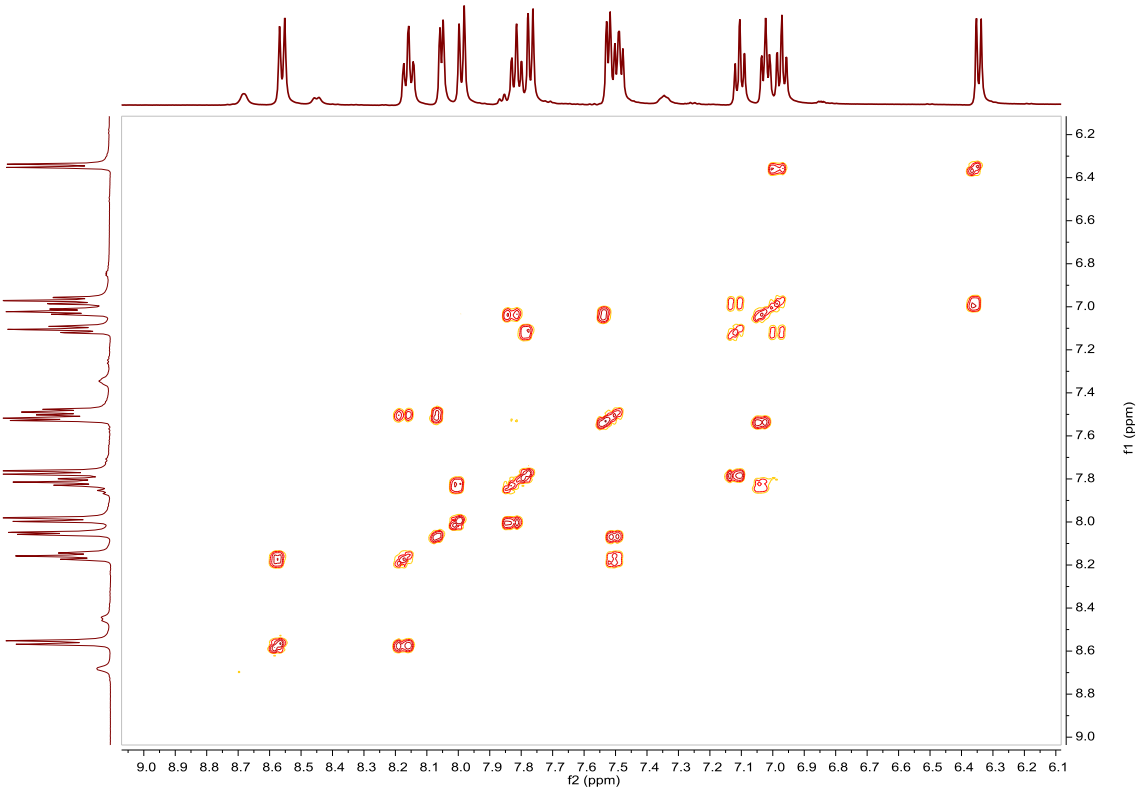

Fig. S103. COSY NMR spectrum of **Abipy** in CD_2Cl_2.

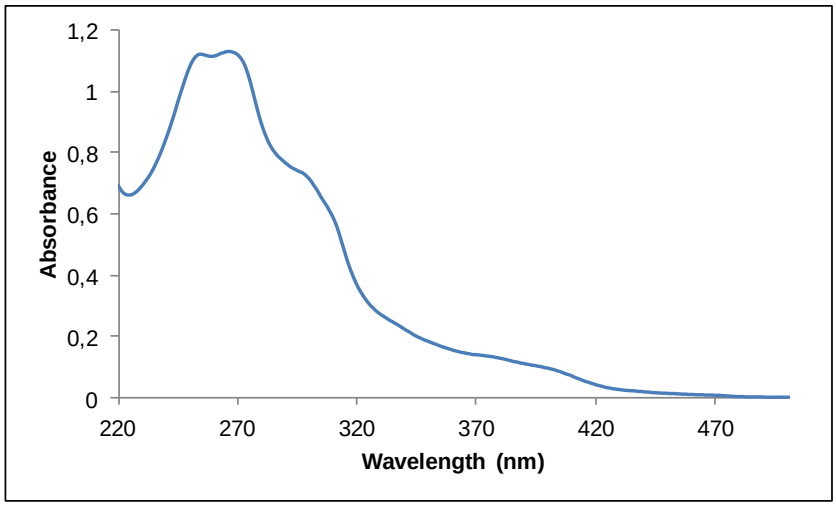

Fig. S104. UV/Vis spectra of **Abipy** in CH_3CN, $2.45 \cdot 10^{-5}$M.

Compound Bbipy, $[Ir(Fppy)_2(bipy)]PF_6$. Synthesis and characterization.

SYNTHESIS

Under a N_2 atmosphere, $[Ir(Fppy)_2Cl]_2$ (0.231 g, 0.190 mmol) were added over a suspension of 2,2'-bipyridine (0.059 g, 0.38 mmol) in 15 mL CH_2Cl_2–MeOH 2/1. The reaction mixture was refluxed, under N_2, for 15 h. To the resulting orange solution, 0.07 g of KPF_6 were added and the solution was stirred for an 1 h. The solvent was evaporated and the desired compound was obtained after filtration through a celite path in CH_2Cl_2 as a yellow solid. Yield 84%. The spectroscopic data are coincident with those described in the literature.[36]

^{1}H NMR (400 MHz, CD_2Cl_2): δ 9.08 (d, J = 8.2 Hz, 1H), 8.37 (d, J = 8.4 Hz, 1H), 8.28 (t, J = 7.1 Hz, 1H), 8.03 (d, J = 5.2 Hz, 1H), 7.89 (t, J = 7.8 Hz, 1H), 7.55 (m, 2H), 7.10 (t, J = 7.1 Hz, 1H), 6.65 (ddd, J = 2.3 Hz, J = 9.2 Hz, J = 11.8 Hz, 1H), 5.80 (dd, J = 2.3 Hz, J = 8.4 Hz, 1H).

^{13}C NMR (100 MHz, CD_2Cl_2): δ 164.24 (d, J = 6.9 Hz, C_{quat}), 163.74 (dd, J = 12.3 Hz, J = 256.3 Hz, C_{quat}), 161.53 (dd, J = 12.6 Hz, J = 259.4 Hz, C_{quat}), 155.67 (s, C_{quat}), 153.77 (d, J = 6.5 Hz, C_{quat}), 150.24 (s, CH), 148.65 (s, CH), 140.43 (s, CH), 139.20 (s, CH), 128.48 (s, CH), 127.68 (s, C_{quat}), 126.19 (s, CH), 123.86 (d, J = 20.1 Hz, CH), 123.68 (s, CH), 113.96 (dd, J = 2.0 Hz, J = 17.6 Hz, CH), 99.06 (t, J = 26.7 Hz, CH).

UV/Vis (CH_3CN), λ, nm (ε, 10^4 M^{-1} cm^{-1}): 245 (5.0), 261 (4.6), 296 (2.6), 359 (0.64).

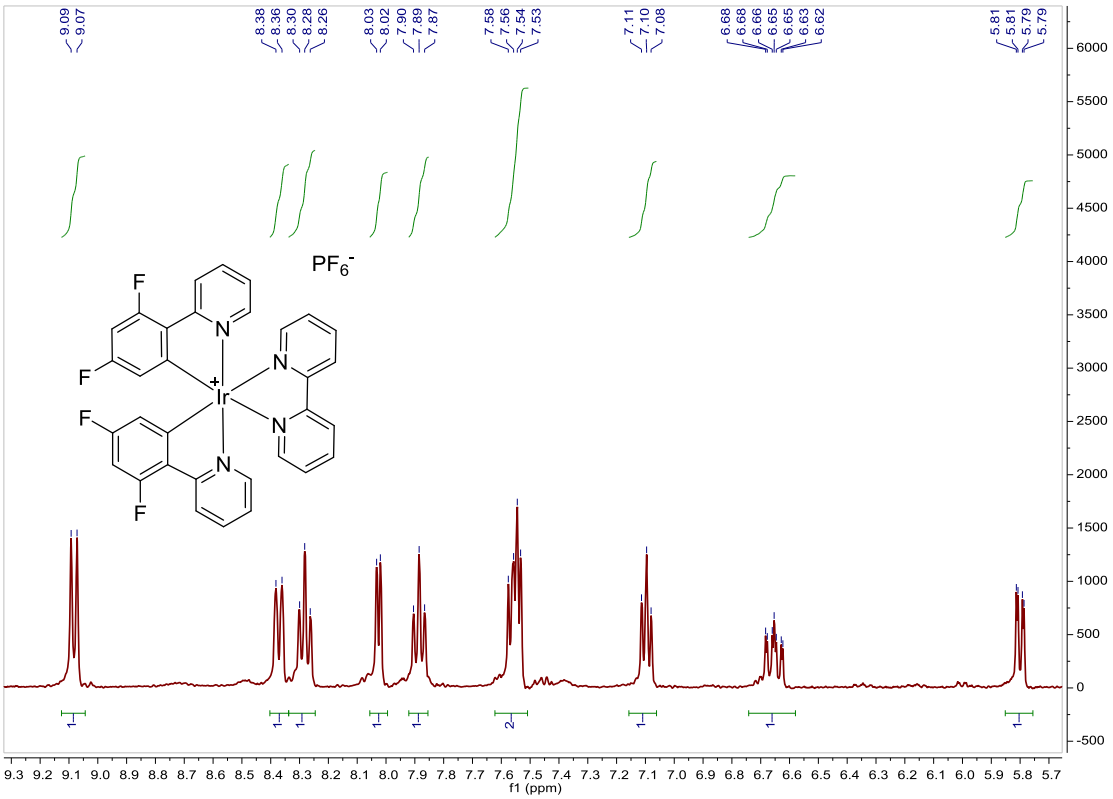

Fig. S105. ^{1}H NMR spectrum of **Bbipy** in CD_2Cl_2, 400 MHz.

[36] F. Lafolet, S. Welter, Z. Popovic and L. De Cola, *J. Mater. Chem.*, **2005**, *15*, 2820–2828.

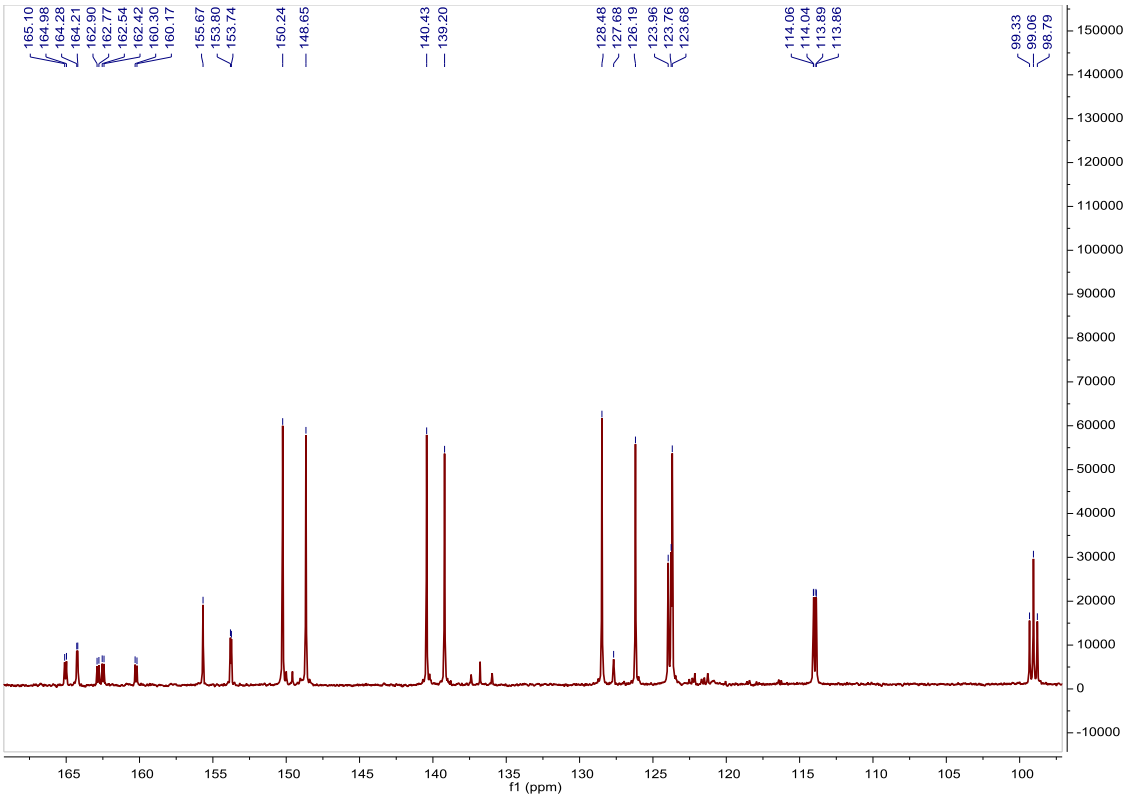

Fig. S106. ^{13}C NMR spectrum of **Bbipy** in CD_2Cl_2, 100 MHz.

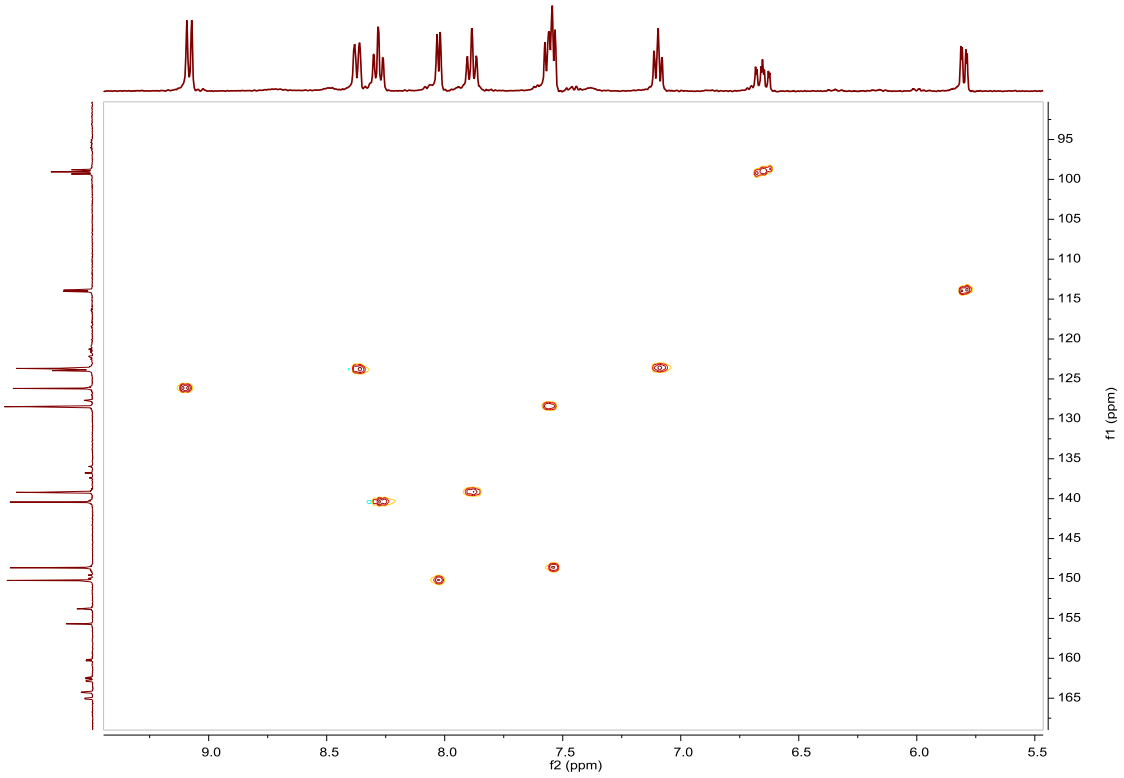

Fig. S107. HSQC NMR spectrum of **Bbipy** in CD_2Cl_2.

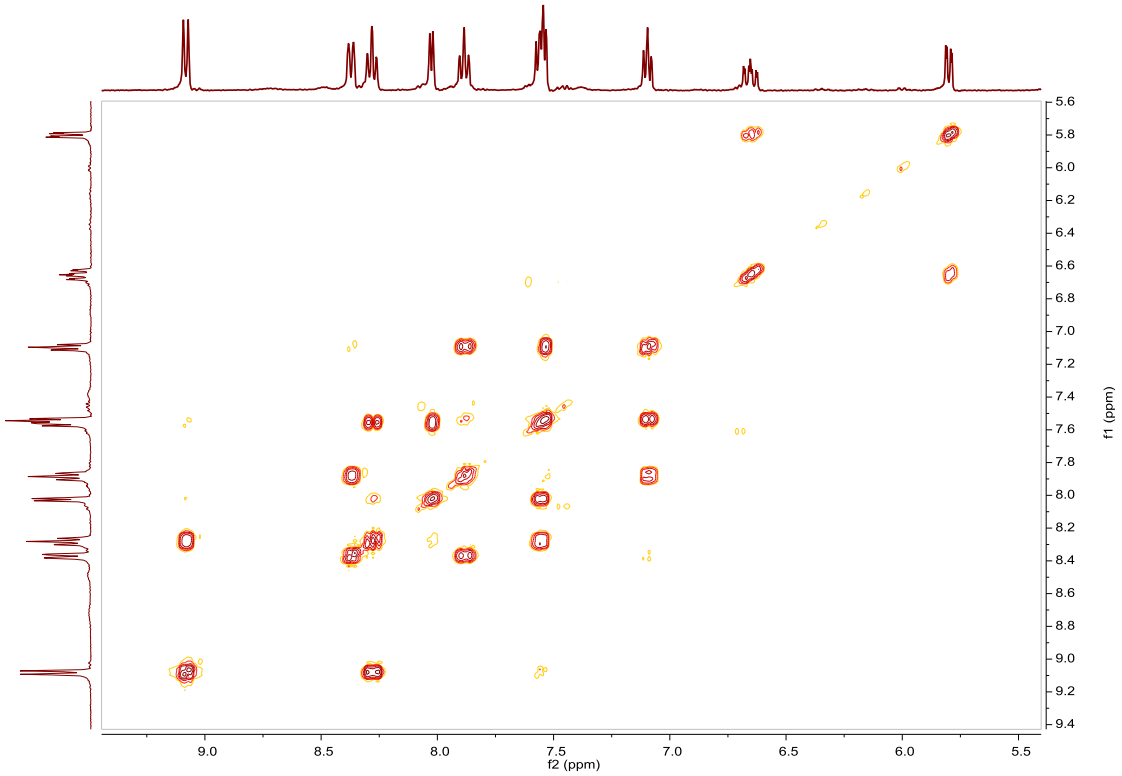

Fig. S108. COSY NMR spectrum of **Bbipy** in CD_2Cl_2.

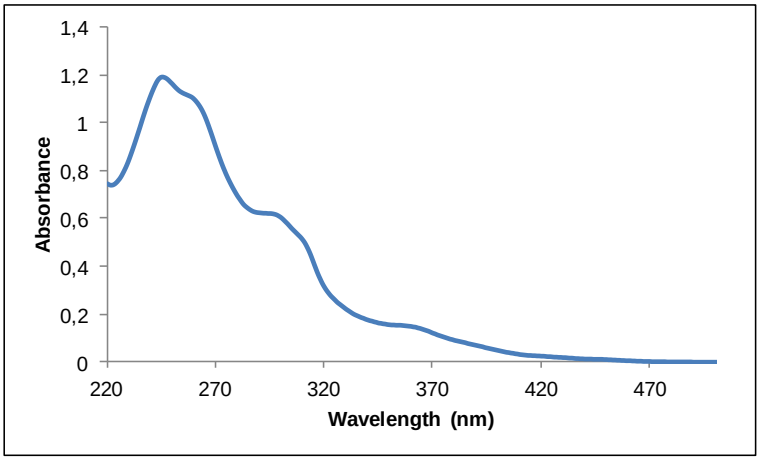

Fig. S109. UV/Vis spectra of **Bbipy** in CH_3CN, $2.37 \cdot 10^{-5}$M.

Compound Cbipy, $[Ir(Brppy)_2(bipy)]PF_6$. Synthesis and characterization.

SYNTHESIS

Under a N_2 atmosphere, $[Ir(Brppy)_2Cl]_2$ (0.200 g, 0.144 mmol) were added over a suspension of 2,2'-bipyridine (0.045 g, 0.288 mmol) in 16 mL CH_2Cl_2–MeOH 2/1. The reaction mixture was refluxed, under N_2, for 15 h. After solvent evaporation the product was purified by column chromatography (silica gel, CH_2Cl_2). When the unreacted $[Ir(ppy\text{-}Br)_2Cl]_2$ eluted, 0.10 g of KPF_6 were added on top of the column and the polarity of the eluent was gradually increased to 100% acetone to elute $[Ir(Brppy)_2(bipy)]PF_6$ together with the excess of KPF_6. The desired compound was precipitated with ether after filtration through a celite path in CH_2Cl_2 and it was obtained as a yellow solid. Yield 46%.

Elemental Analysis: calculated for ($C_{32}H_{22}Br_2IrN_4PF_6$): C, 40.06; H, 2.31; N, 5.84. Found: C, 40.11; H, 2.45; N, 5.37.

Exact Mass: ESI-MS $[C_{32}H_{22}Br_2IrN_4]^+$: calculated: m/z= 812.9840, found: m/z= 812.9813.

^{1}H NMR (300 MHz, acetone-d_6): δ 8.89 (d, J = 8.2 Hz, 1H), 8.35 (ddd, J = 1.6 Hz, J = 7.9 Hz, J = 9.4 Hz, 1H), 8.32 (d, J = 8.0 Hz, 1H), 8.20 (d, J = 5.4 Hz, 1H), 8.04 (ddd, J = 1.5 Hz, J = 7.5 Hz, J = 9.0 Hz, 1H), 7.90 (m, 2H), 7.77 (ddd, J = 1.2 Hz, J = 7.0 Hz, J = 7.6 Hz, 1H), 7.27 (m, 2H), 6.44 (d, J = 1.9 Hz, 1H).

^{13}C APT NMR (75 MHz, acetone-d_6): δ 167.76 (C_{quat}), 157.25 (C_{quat}), 153.80 (C_{quat}), 152.19 (CH), 150.79 (CH), 144.69 (C_{quat}), 141.31 (CH), 140.54 (CH), 135.08 (CH), 130.14 (CH), 128.08 (CH), 127.12 (CH), 126.34 (CH), 126.21 (C_{quat}), 125.63 (CH), 121.84 (CH).

UV/Vis (CH_3CN), λ, nm (ε, 10^4 M^{-1} cm^{-1}): 255 (4.5), 267 (4.6), 295 (3.0), 378 (0.53), 402 (0.37).

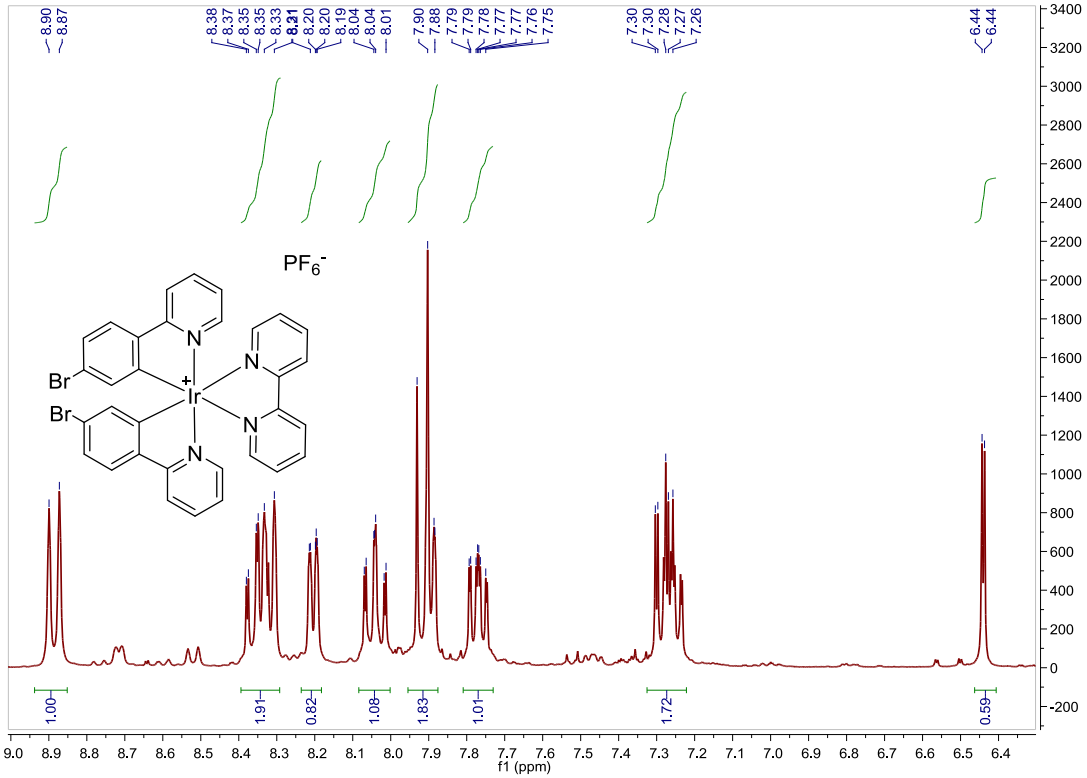

Fig. S110. ^{1}H NMR spectrum of **Cbipy** in acetone-d_6, 300 MHz.

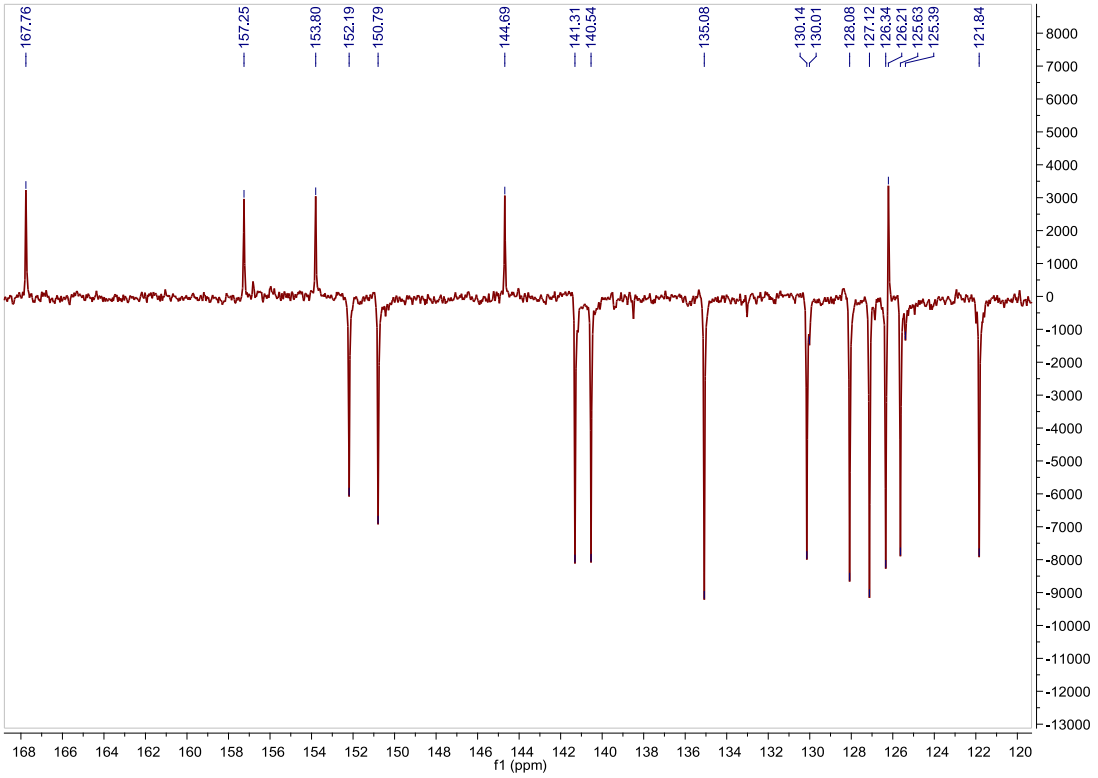

Fig. S111. ^{13}C APT NMR spectrum of **Cbipy** in acetone-d_6, 75 MHz.

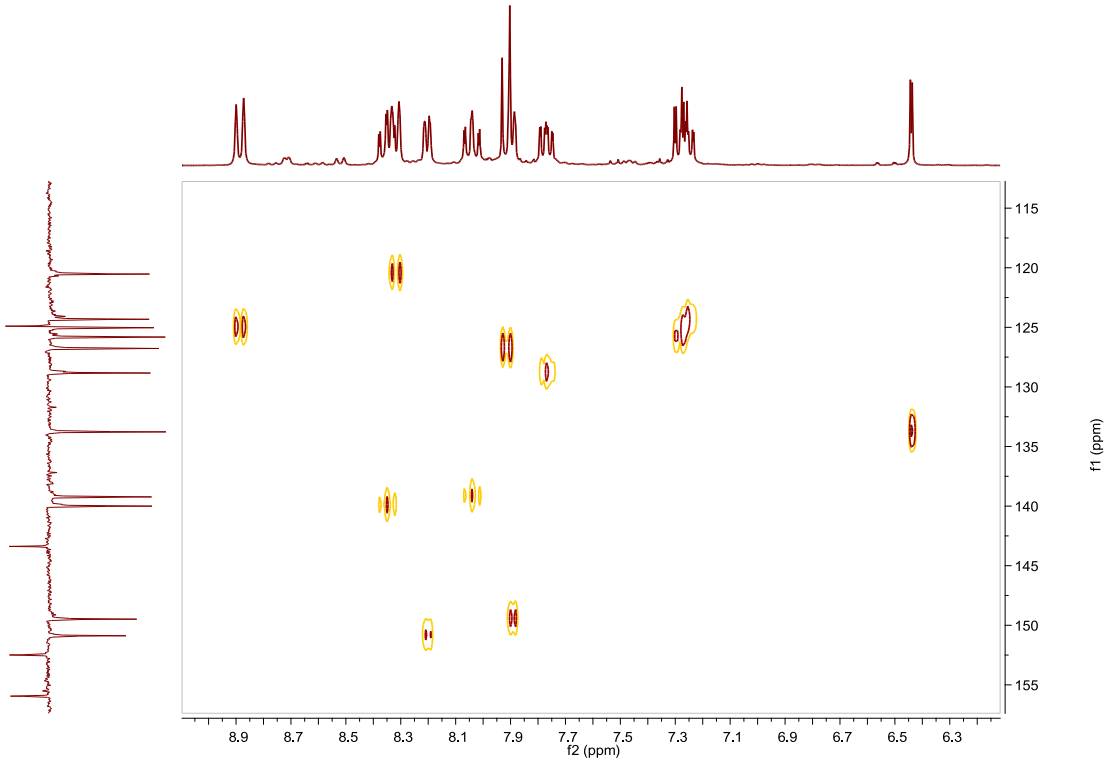

Fig. S112. HSQC NMR spectrum of **Cbipy** in acetone-d_6.

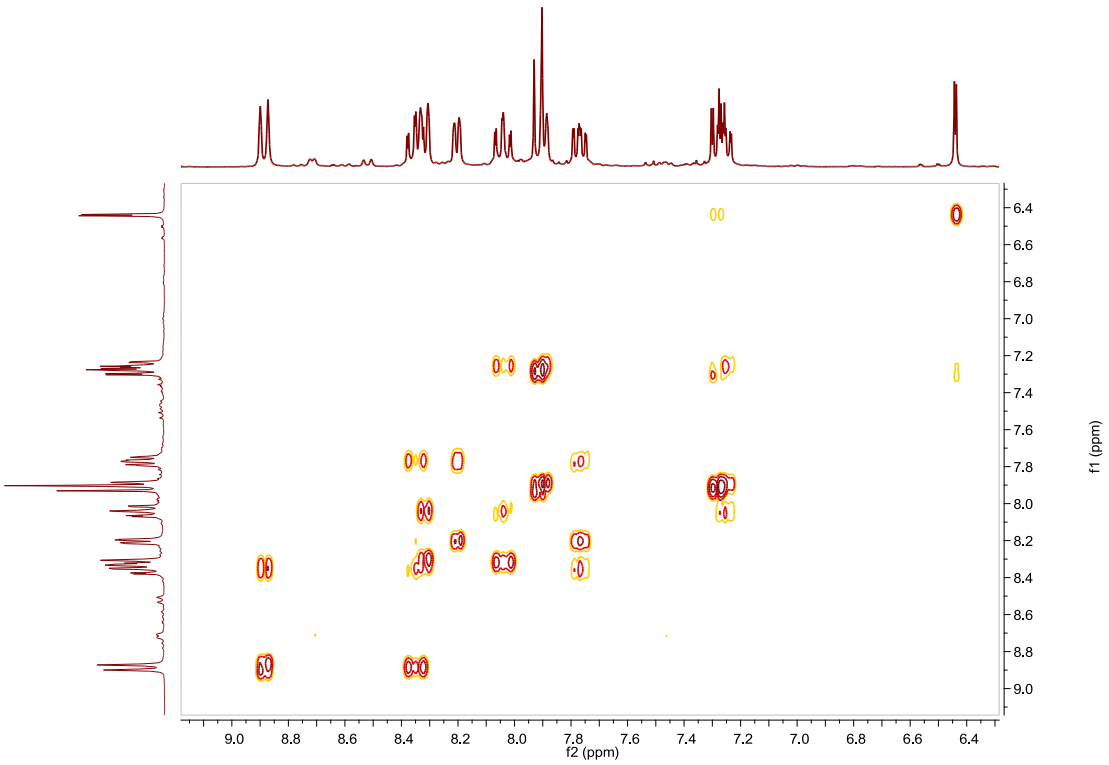

Fig. S113. COSY NMR spectrum of **Cbipy** in acetone-d_6.

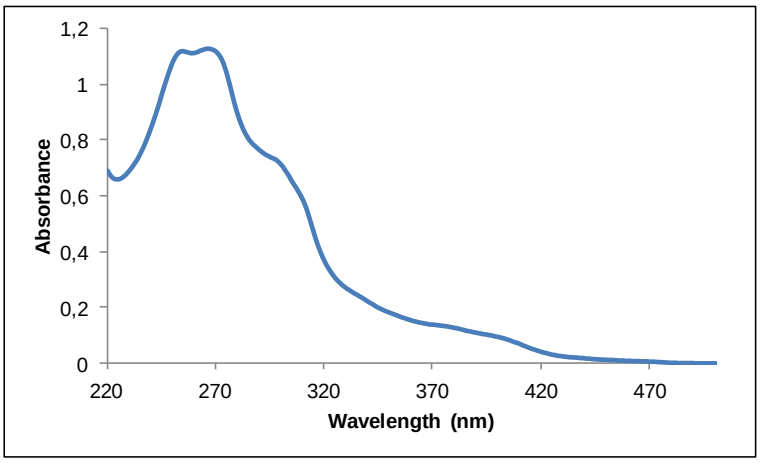

Fig. S114. UV/Vis spectra of **Cbipy** in CH_3CN, $2.46 \cdot 10^{-5}$M.

Compound Dbipy, [Ir(azoppy)$_2$(bipy)]PF$_6$. Synthesis, characterization and photoisomerization studies.

SYNTHESIS

Under a N_2 atmosphere, **C-bipy** (0.065 g, 0.068 mmol) and [4-(phenylazo)phenyl]boronic acid **6** (0.036 g, 0.160 mmol) were dissolved in 4 mL of THF. Na_2CO_3 (1M (aq), 2 mL) and $Pd(PPh_3)_4$ (0.0079 g, 0.0068 mmol) were added and the solution was degassed by bubbling N_2 for 15 min. The reaction mixture was refluxed (80 °C) for 15 h. The resulting mixture was cooled down to room temperature and the product was extracted with CH_2Cl_2. The organic phase was dried with $MgSO_4$, filtered off and the solvent was evaporated. The residue was purified by column chromatography (silica gel, CH_2Cl_2). To the fraction containing the eluted complex, 0.05 g of KPF_6 were added and the resulting solution was filtered through a celite path. The title compound was obtained as an orange solid. Yield 10%.

Elemental Analysis: calculated for ($C_{56}H_{40}IrN_8PF_6 \cdot CH_3COCH_3$): C, 57.88; H, 3.47; N, 9.64. Found: C, 58.03; H, 3.68; N, 9.09.

Exact Mass: ESI-MS $[C_{56}H_{40}IrN_8]^+$: calculated: m/z= 1017.3005, found: m/z= 1017.3036.

^{1}H NMR (300 MHz, acetone-d_6): δ 8.93 (d, J = 7.9 Hz, 1H), 8.42–8.33 (m, 3H), 8.11–8.01 (m, 3H), 7.98–7.89 (m, 4H), 7.79 (ddd, J = 1.1 Hz, J = 5.4 Hz, J = 7.4 Hz, 1H), 7.68–7.57 (m, 5H), 7.50 (dd, J = 1.9 Hz, J = 8.1 Hz, 1H), 7.28 (ddd, J = 1.3 Hz, J = 5.9 Hz, J = 7.3 Hz, 1H), 6.76 (d, J = 1.7 Hz, 1H).

^{13}C APT NMR (75 MHz, acetone-d_6): δ 168.60 (C_{quat}), 157.43 (C_{quat}), 153.94 (C_{quat}), 153.00 (C_{quat}), 152.35 (CH), 152.28 (C_{quat}), 150.88 (CH), 145.61 (C_{quat}), 144.99 (C_{quat}), 142.59 (C_{quat}), 141.00 (CH), 140.20 (CH), 132.63 (CH), 130.97 (CH), 130.61 (2CH), 130.03 (CH), 128.93 (2CH), 126.79 (CH), 126.20 (CH), 125.21 (CH), 124.45 (2CH), 123.97 (2CH), 123.09 (CH), 121.70 (CH).

UV/Vis (CH_3CN), λ, nm (ε, 10^4 M^{-1} cm^{-1}): 355 (7.4).

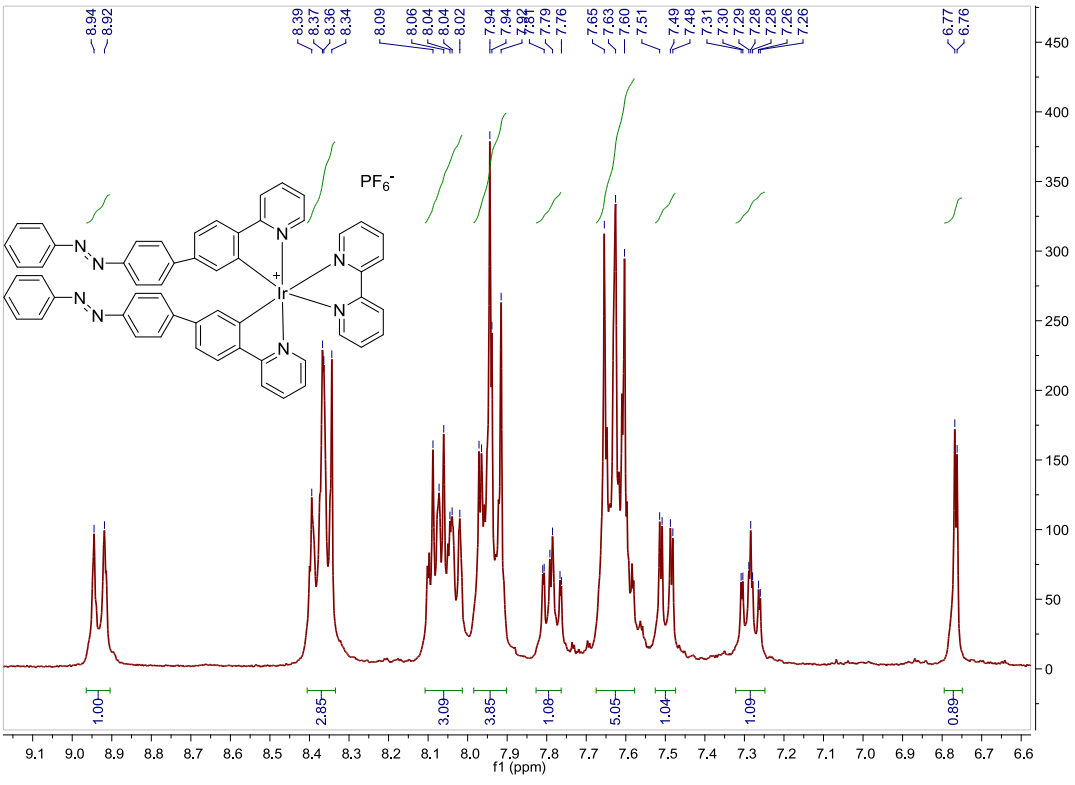

Fig. S115. ^{1}H NMR spectrum of **Dbipy** in acetone-d_6, 300 MHz.

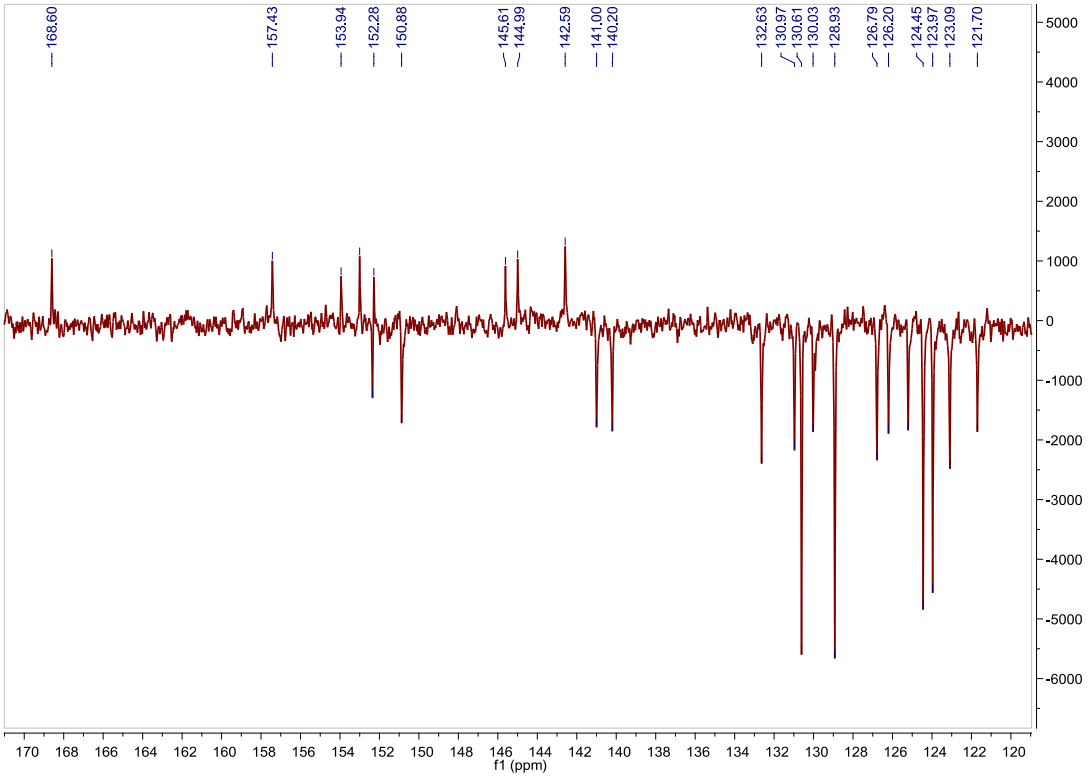

Fig. S116. ^{13}C APT NMR spectrum of **Dbipy** in acetone-d_6, 75 MHz.

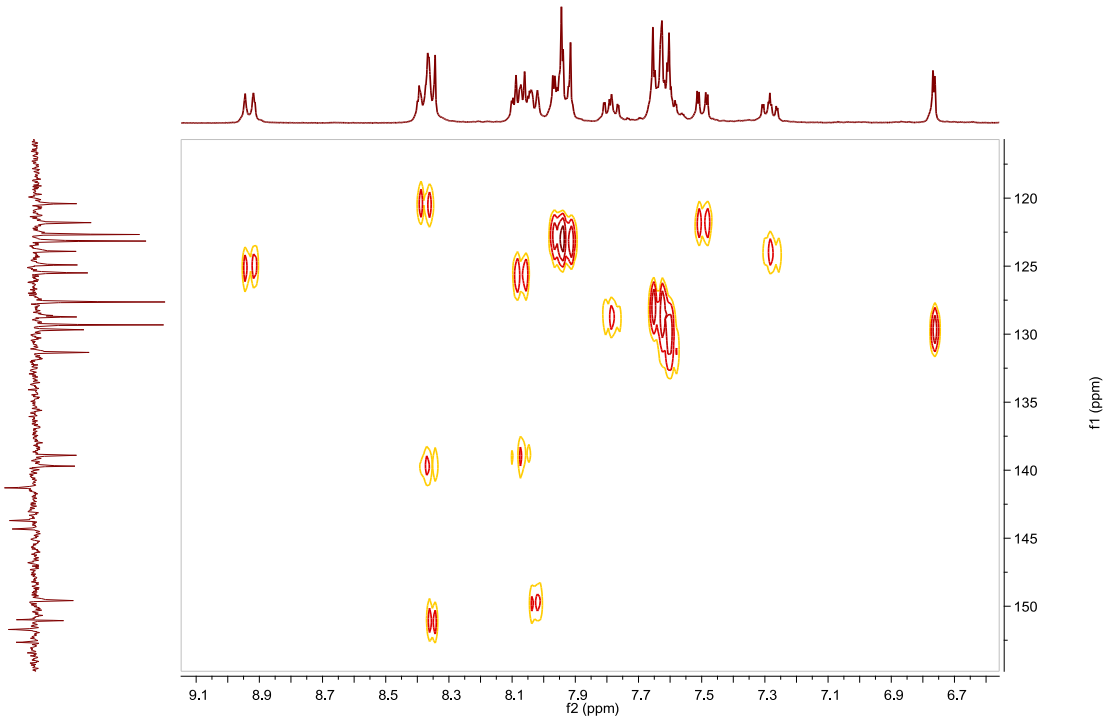

Fig. S117. HSQC NMR spectrum of **Dbipy** in acetone-d_6.

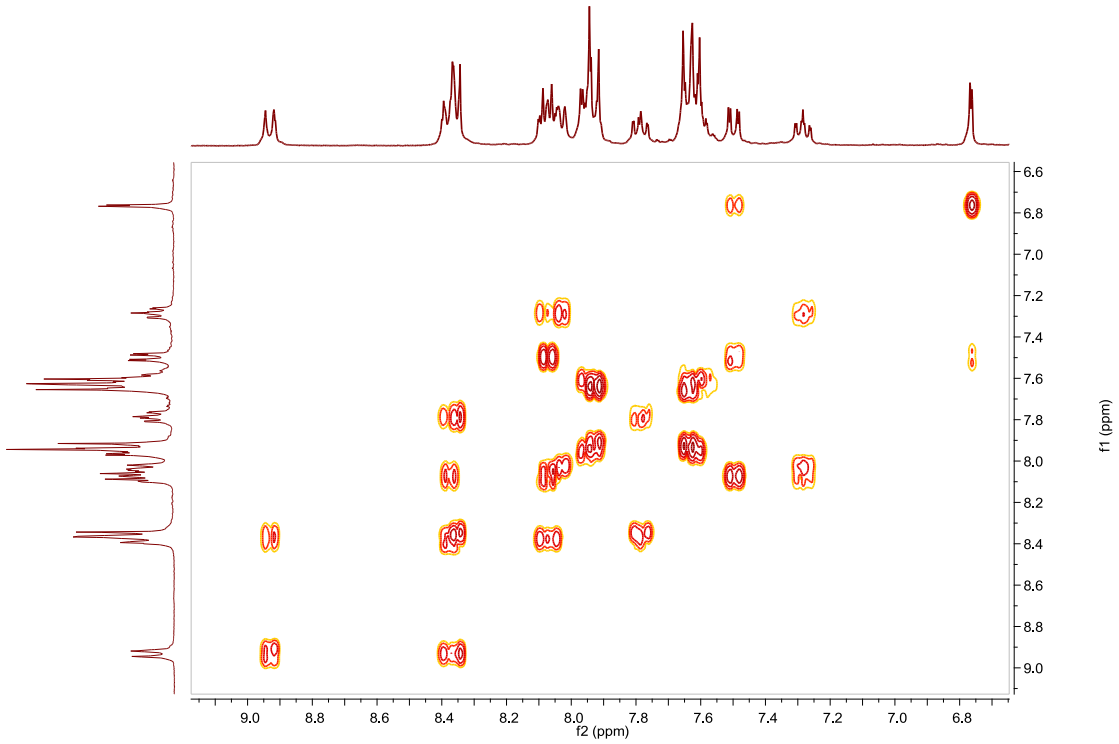

Fig. S118. COSY NMR spectrum of **Dbipy** in acetone-d_6.

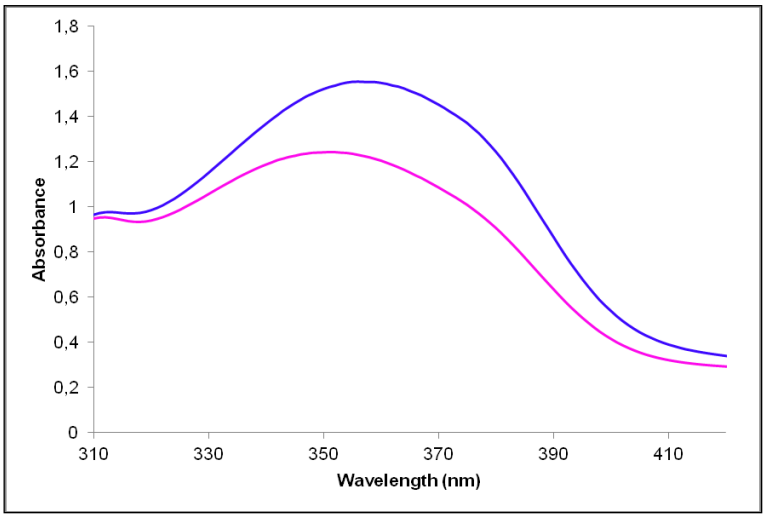

Fig. S119. UV/Vis spectra of **Dbipy** in CH_3CN. Before (blue line) and after (pink line) irradiation at 373nm, $2.09 \cdot 10^{-5}$M.

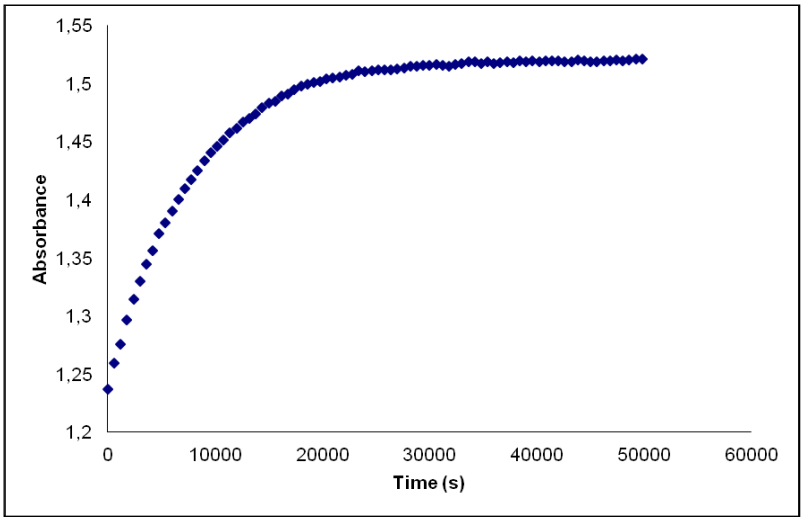

Fig. S120. Cis to trans thermal isomerization kinetics of **Dbipy**. Absorption change of the band 355nm at 328 K in CH_3CN after irradiation at 373 nm. ($2.09 \cdot 10^{-5}$M).

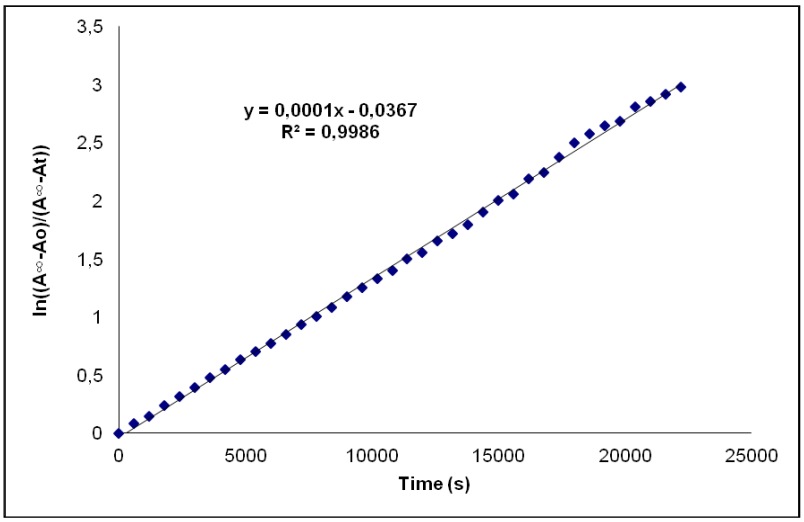

Fig. S121. Cis to trans thermal isomerization kinetics of **Dbipy**. First-order plot. k (s^{-1}) = $1.0 \cdot 10^{-4}$. Half-life (min) = 115.

Compound Aphen, $[Ir(ppy)_2(phen)]PF_6$. Synthesis and characterization.

SYNTHESIS

Under a N_2 atmosphere, $[Ir(ppy)_2Cl]_2$ (0.200 g, 0.186 mmol) were added over a suspension of 1,10-phenanthroline (0.140 g, 0.777 mmol) in 15 mL CH_2Cl_2–MeOH 2/1. The reaction mixture was refluxed, under N_2, for 15 h. To the resulting orange solution, 0.07 g of KPF_6 were added and the it was stirred for an 1 h. The solvent was evaporated and the desired compound was obtained after filtration through a celite path in CH_2Cl_2 as a yellow solid. Yield 57%. The spectroscopic data are coincident with those described in the literature.[37]

^{1}H NMR (500 MHz, DMSO-d_6): δ 8.91 (dd, , J = 1.1 Hz, J = 8.3 Hz, 1H), 8.40 (s, 1H), 8.27 (d, J = 8.2 Hz, 1H), 8.22 (dd, J = 1.0 Hz, J = 5.1 Hz, 1H), 8.06 (dd, J = 5.1 Hz, J = 8.2 Hz, 1H), 7.96 (d, J = 7.6 Hz, 1H), 7.88 (t, J = 8.1 Hz, 1H), 7.47 (d, J = 5.6 Hz, 1H), 7.07 (t, J = 7.3 Hz, 1H), 6.99 (t, J = 6.2 Hz, 1H), 6.96 (t, J = 6.6 Hz, 1H), 6.31 (d, J = 7.4 Hz, 1H).

^{13}C NMR (126 MHz, DMSO-d_6): δ 167.40 (C_{quat}), 151.18 (CH), 150.37 (C_{quat}), 149.64 (CH), 146.64 (C_{quat}), 144.59 (C_{quat}), 139.36 (CH), 139.23 (CH), 131.80 (CH), 131.69 (C_{quat}), 130.74 (CH), 128.89 (CH), 127.67 (CH), 125.59 (CH), 124.39 (CH), 122.91 (CH), 120.50 (CH).

UV/Vis (CH_3CN), λ, nm (ε, 10^4 M^{-1} cm^{-1}): 229 (4.8), 253 (4.9), 265 (5.3), 376 (0.64).

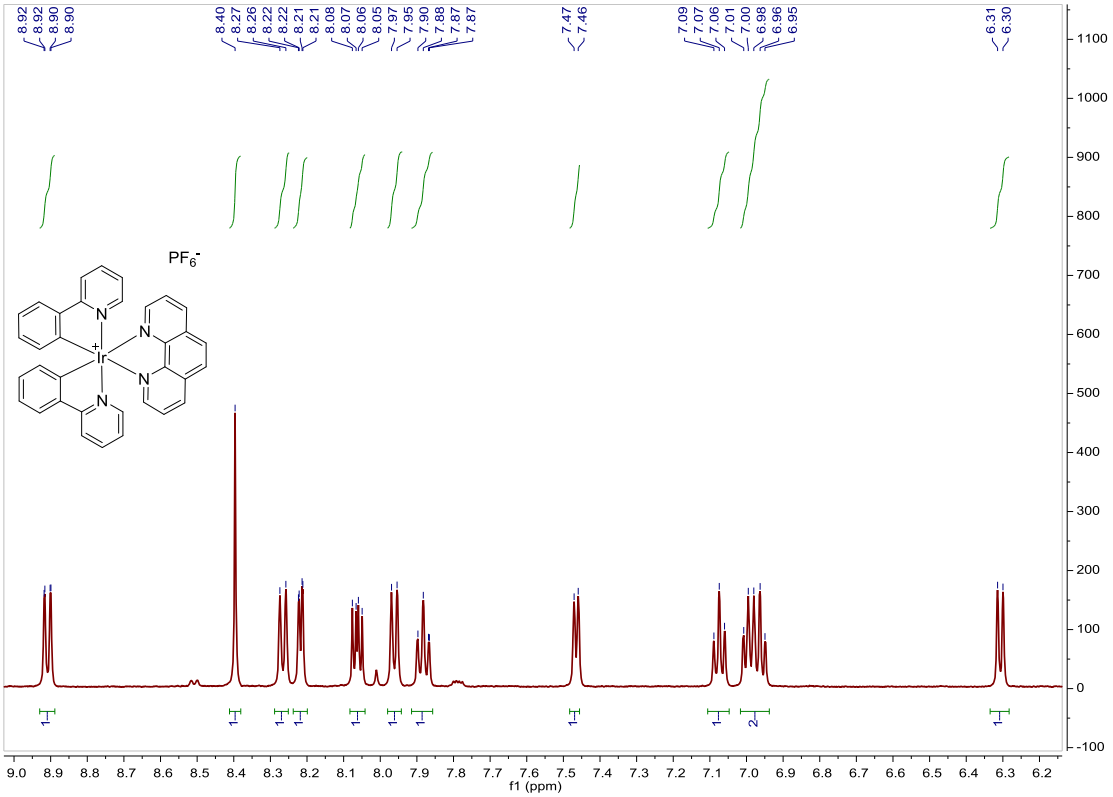

Fig. S122. ^{1}H NMR spectrum of **Aphen** in DMSO-d_6, 500 MHz.

[37] J. I. Kim, I. Shin, H. Kim and J. Lee, *J. Am. Chem. Soc.*, **2005**, *127*, 1614–1615.

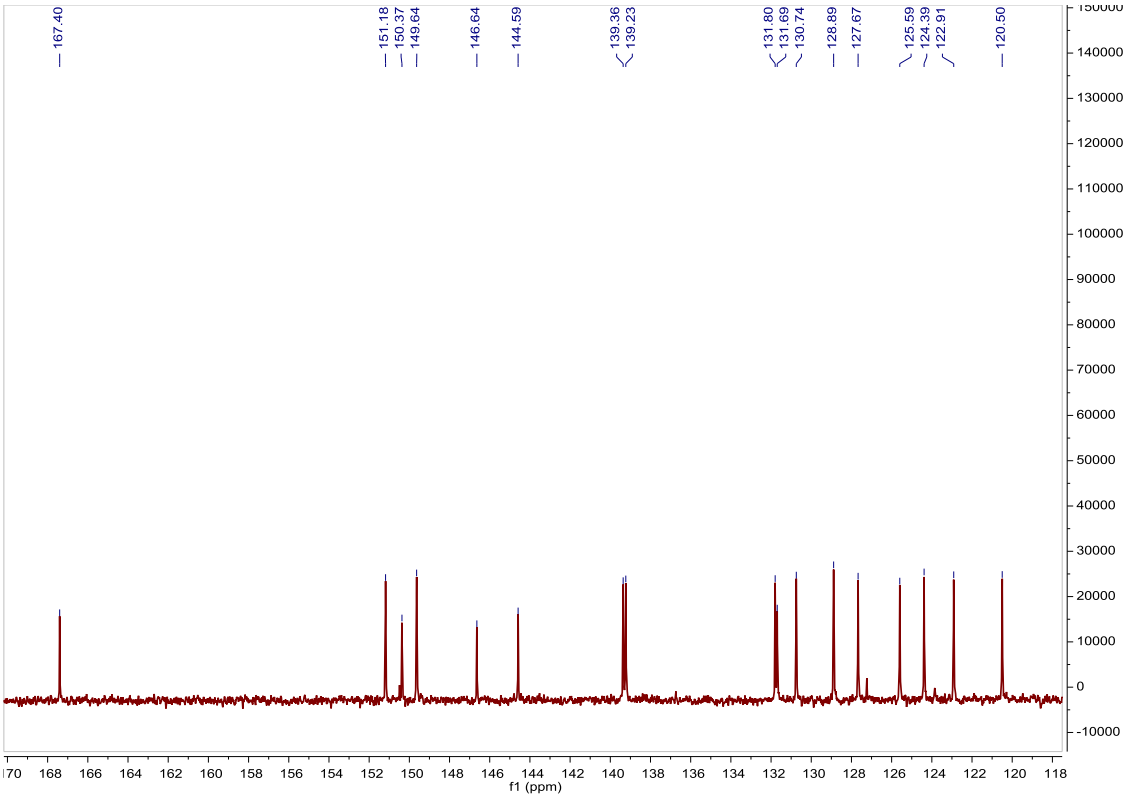

Fig. S123. ^{13}C NMR spectrum of **Aphen** in DMSO-d_6, 126 MHz.

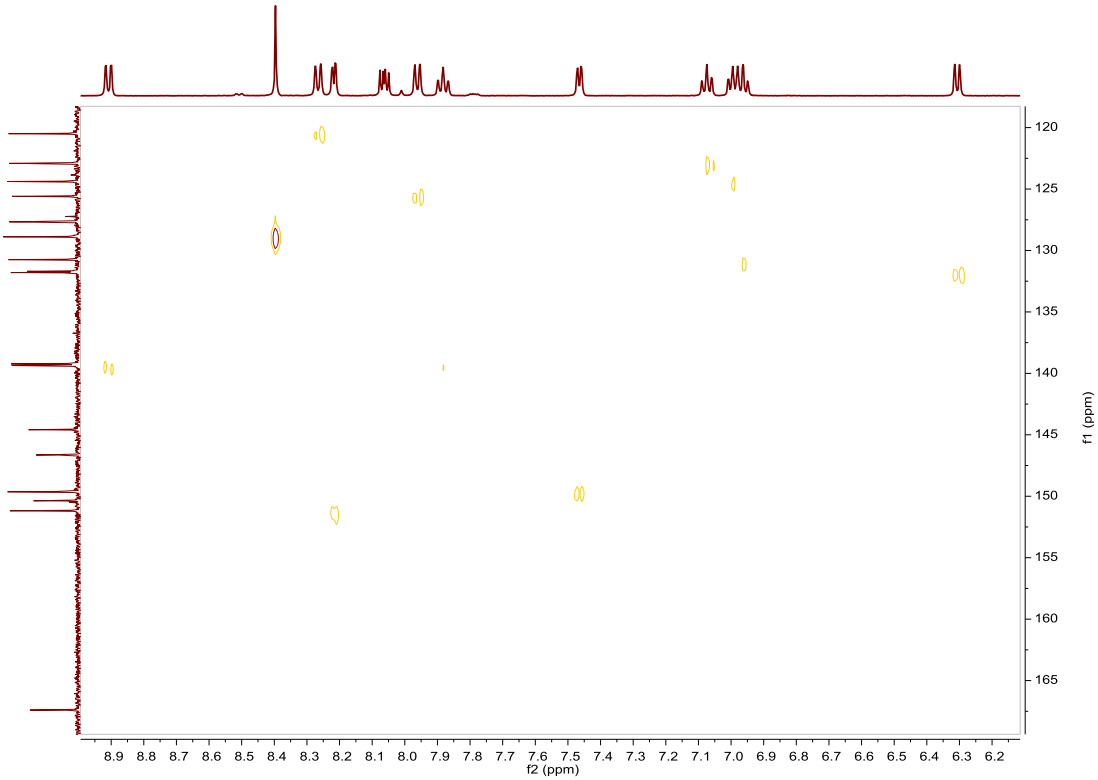

Fig. S124. HSQC NMR spectrum of **Aphen** in DMSO-d_6.

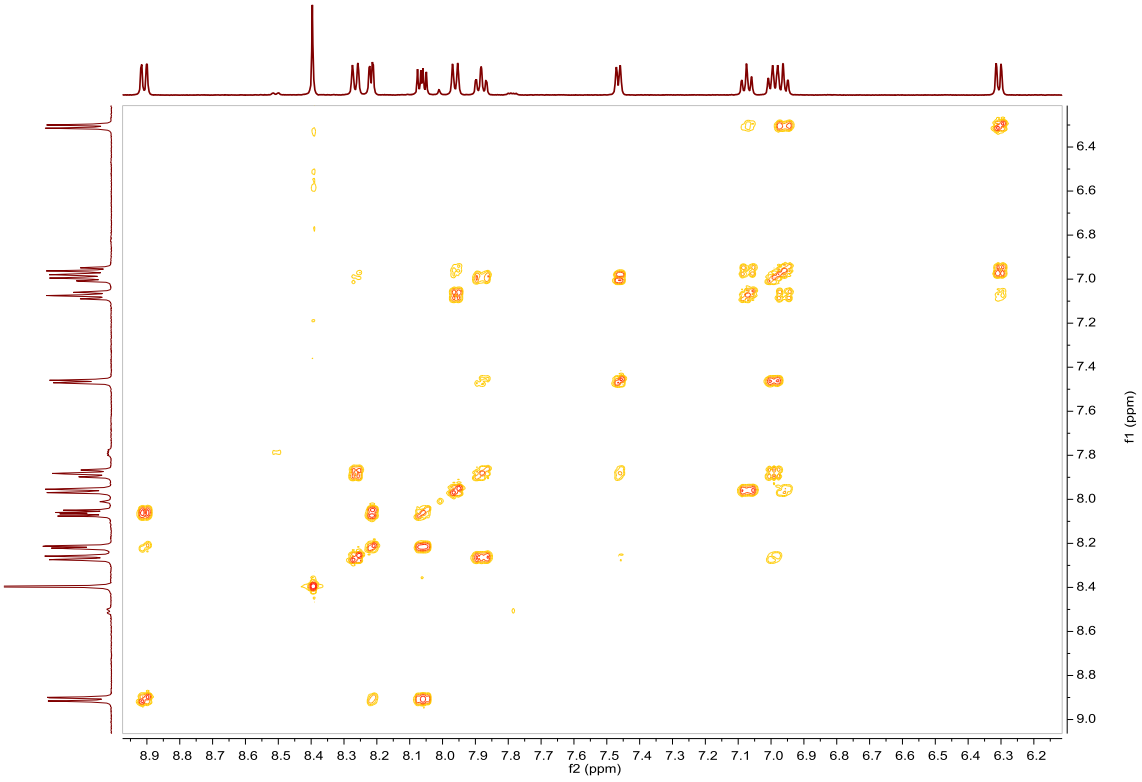

Fig. S125. COSY NMR spectrum of **Aphen** in DMSO-d_6.

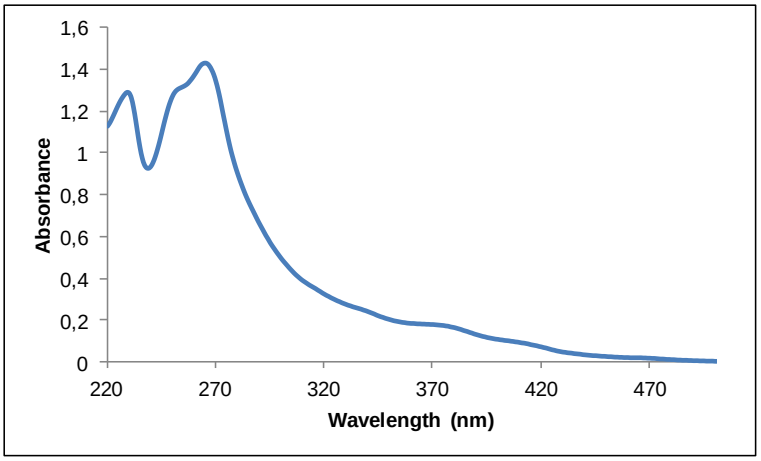

Fig. S126. UV/Vis spectra of **Aphen** in CH_3CN, $2.67 \cdot 10^{-5}$M.

Compound Bphen, [Ir(Fppy)$_2$(phen)]PF$_6$. Synthesis and characterization.

SYNTHESIS

Under a N_2 atmosphere, $[Ir(Fppy)_2Cl]_2$ (0.231 g, 0.190 mmol) were added over a suspension of 1,10-phenanthroline (0.057 g, 0.32 mmol) in 15 mL CH_2Cl_2–MeOH 2/1. The reaction mixture was refluxed, under N_2, for 15 h. To the resulting yellow solution, 0.07 g of KPF_6 were added and the it was stirred for an 1 h. The solvent was evaporated and the desired compound was obtained after filtration through a celite path in CH_2Cl_2 as a yellow solid. Yield 90%. The spectroscopic data are coincident with those described in the literature.[38]

^{1}H NMR (500 MHz, DMSO-*d*$_6$): δ 8.94 (dd, J = 1.1 Hz, *J* = 8.2 Hz, 1H), 8.41 (s, 1H), 8.29 (t, *J* = 10.5 Hz, 2H), 8.06 (dd, J = 5.1 Hz, *J* = 8.2 Hz, 1H), 7.96 (t, *J* = 8.05 Hz, 1H), 7.52 (d, *J* = 5.1 Hz, 1H), 7.06 (t, *J* = 6.15 Hz, 1H), 7.01 (t, J = 10.5 Hz, 1H), 5.71 (dd, J = 2.2 Hz, *J* = 8.3 Hz, 1H).

^{13}C NMR (126 MHz, DMSO-*d*$_6$): δ 162.78 (dd, *J* = 12.5 Hz, J = 252.5 Hz, C_{quat}), 162.77 (d, *J* = 7.5 Hz, C_{quat}), 160.68 (dd, J = 12.5 Hz, J = 257.5 Hz, C_{quat}), 153.90 (d, J = 6.25 Hz, C_{quat}), 151.21 (s, CH), 149.80 (s, CH), 145.73 (s, C_{quat}), 139.91 (s, CH), 139.32 (s, CH), 131.25 (s, C_{quat}), 128.40 (s, CH), 127.83 (s, C_{quat}), 127.44 (s, CH), 124.45 (s, CH), 123.27 (d, J = 20.0 Hz, CH), 113.42 (d, J = 16.25 Hz, CH), 99.11 (t, J = 26.25 Hz, CH).

UV/Vis (CH_3CN), λ, nm (ε, 10^4 M^{-1} cm^{-1}): 230 (5.0), 264 (4.8), 310 (1.6), 359 (0.71).

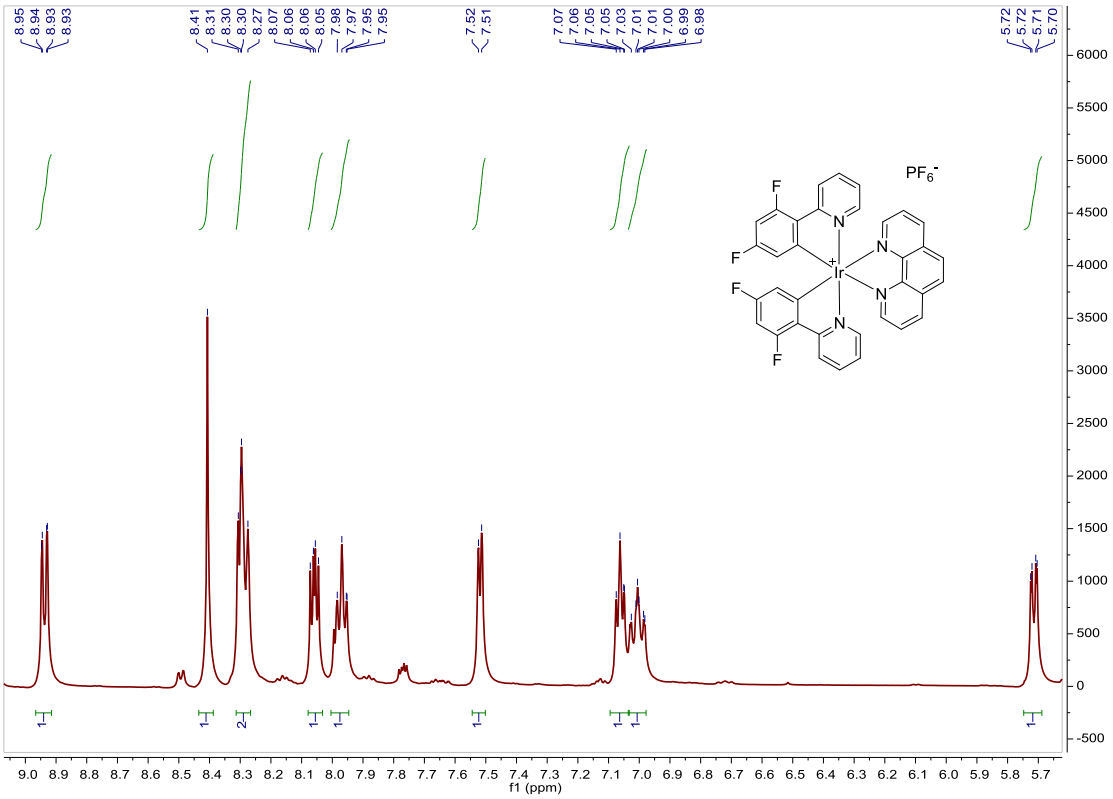

Fig. S127. ^{1}H NMR spectrum of **Bphen** in DMSO-*d*$_6$, 500 MHz.

[38] Y. You, S. Lee, T. Kim, K. Ohkubo, W. Chae, S. Fukuzumi, G. Jhon, W. Nam, S. J. Lippard, *J. Am. Chem. Soc.*, **2011**, *133*, 18328–18342.

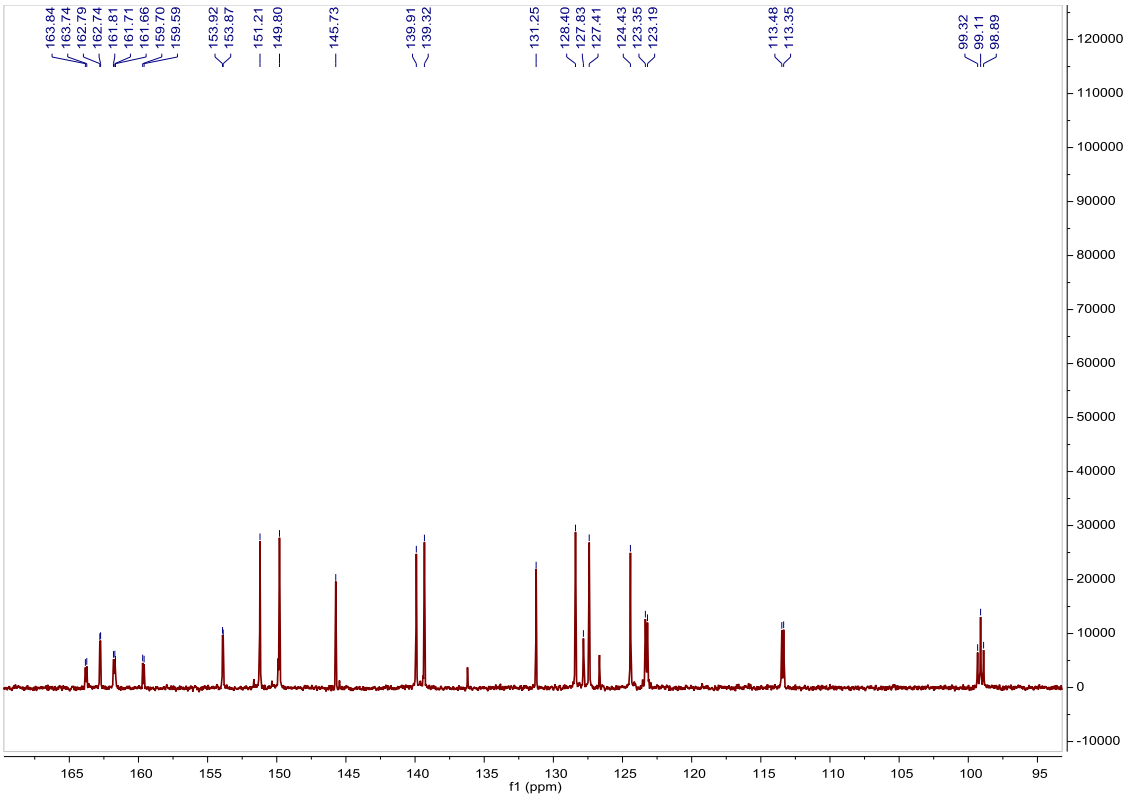

Fig. S128. ^{13}C NMR spectrum of **Bphen** in DMSO-d_6, 126 MHz.

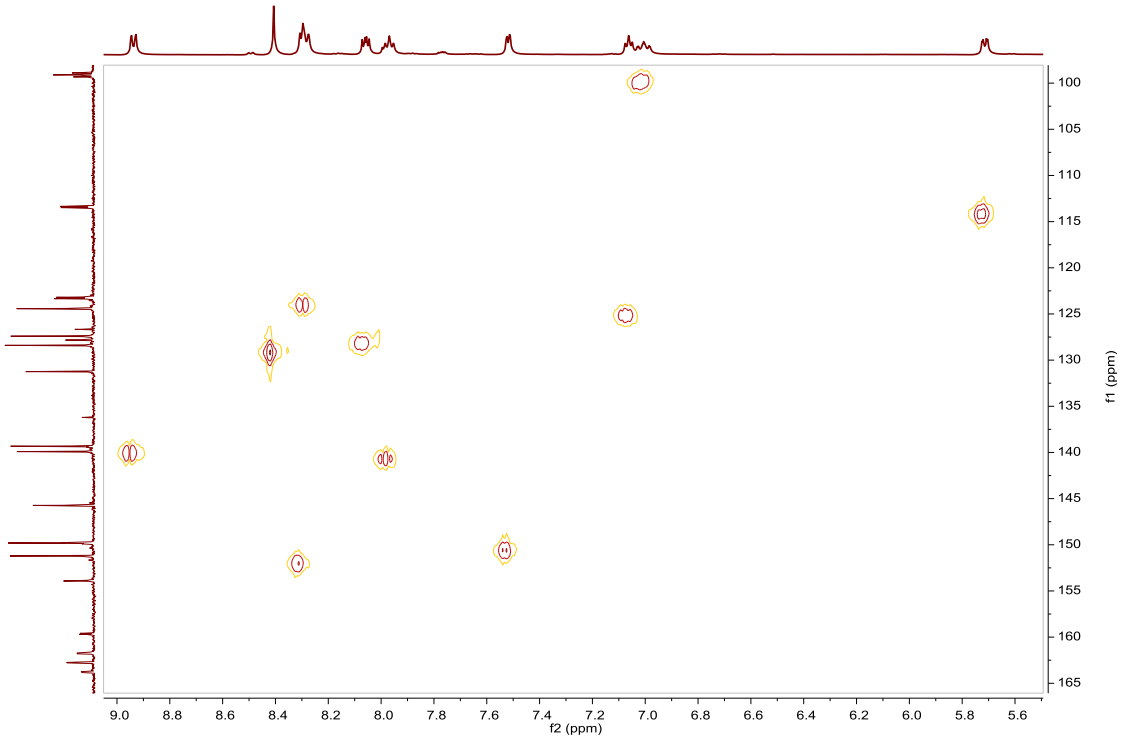

Fig. S129. HSQC NMR spectrum of **Bphen** in DMSO-d_6.

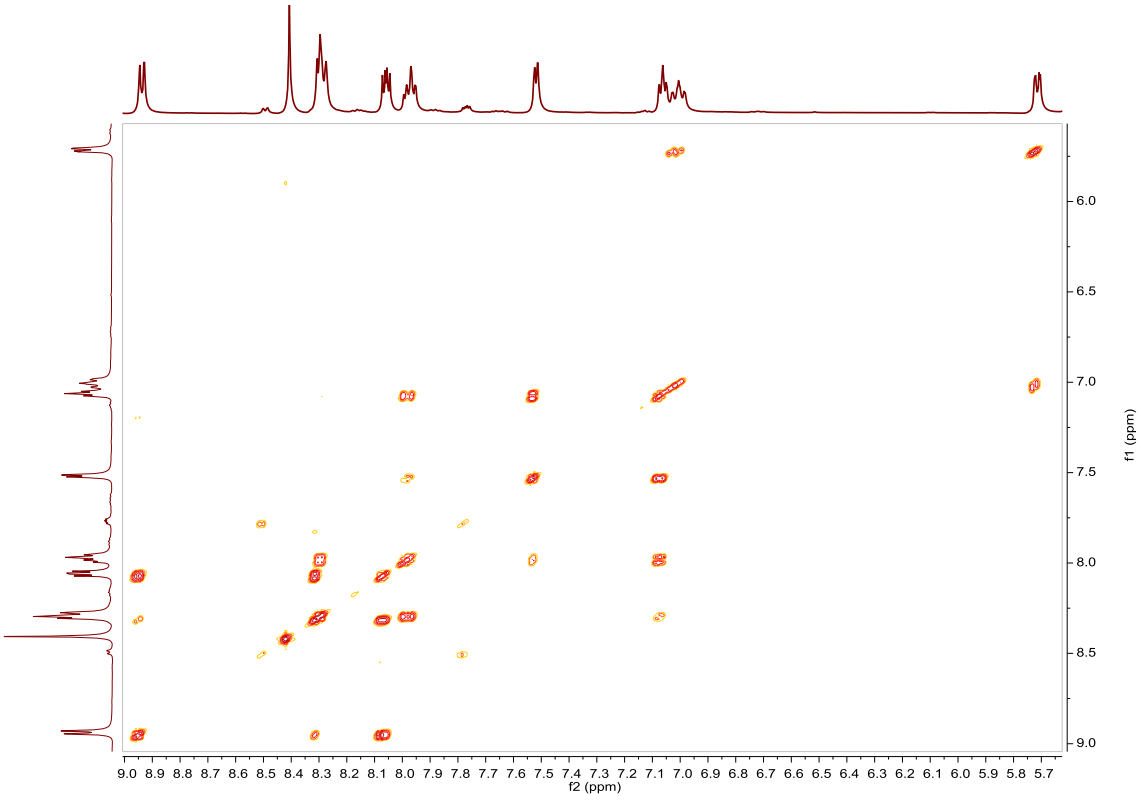

Fig. S130. COSY NMR spectrum of **Bphen** in DMSO-d_6.

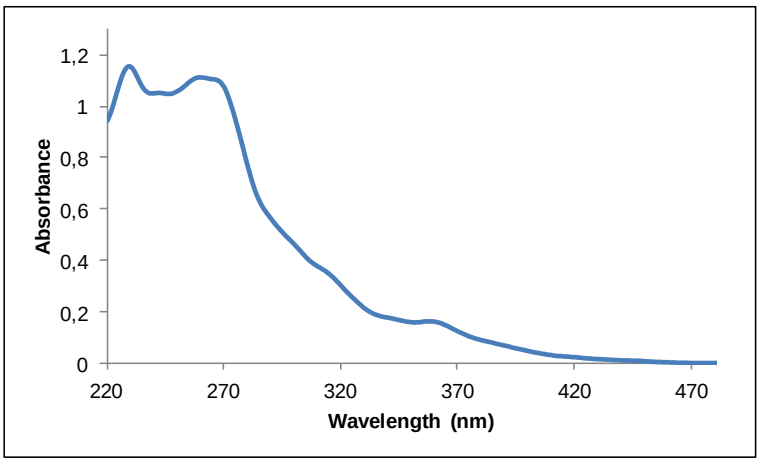

Fig. S131. UV/Vis spectra of **Bphen** in CH_3CN, $2.31 \cdot 10^{-5}$M.

Compound Cphen, $[Ir(Brppy)_2(phen)]PF_6$. Synthesis and characterization.

SYNTHESIS

Under a N_2 atmosphere, $[Ir(Brppy)_2Cl]_2$ (0.100 g, 0.072 mmol) were added over a suspension of 1,10-phenanthroline (0.026 g, 0.144 mmol) in 8 mL CH_2Cl_2–MeOH 2/1. The reaction mixture was refluxed, under N_2, for 15 h. After solvent evaporation the product was purified by column chromatography (silica gel, CH_2Cl_2). When the unreacted $[Ir(ppy\text{-}Br)_2Cl]_2$ eluted, 0.05 g of KPF_6 were added on top of the column and the polarity of the eluent was gradually increased to 100% acetone to elute $[Ir(Brppy)_2(phen)]PF_6$ together with the excess of KPF_6. The desired compound, purified by filtration through a celite path in CH_2Cl_2, was obtained as a yellow solid. Yield 63%.

Elemental Analysis: calculated for $(C_{34}H_{22}Br_2IrN_4PF_6{\cdot}2CH_3COCH_3)$: C, 43.69; H, 3.12; N, 5.09. Found: C, 43.89; H, 3.42; N, 5.01.

Exact Mass: ESI-MS $[C_{34}H_{22}Br_2IrN_4]^+$: calculated: m/z= 836.9840, found: m/z= 836.9802.

^{1}H NMR (300 MHz, acetone-d_6): δ 8.96 (dd, J = 1.4 Hz, J = 8.3 Hz, 1H), 8.56 (dd, J = 1.4 Hz, J = 5.0 Hz, 1H), 8.45 (s, 1H), 8.31 (d, J = 7.9 Hz, 1H), 8.13 (dd, J = 5.1 Hz, J = 8.3 Hz, 1H), 7.97 (ddd, J = 1.5 Hz, J = 7.5 Hz, J = 9.0 Hz, 1H), 7.95 (d, J = 8.4 Hz, 1H), 7.73 (d, J = 5.8 Hz, 1H), 7.33 (dd, J = 2.0 Hz, J = 8.3 Hz, 1H), 7.07 (ddd, J = 1.4 Hz, J = 5.8 Hz, J = 7.3 Hz, 1H), 6.54 (d, J = 1.9 Hz, 1H).

^{13}C APT NMR (75 MHz, acetone-d_6): δ 167.83 (C_{quat}), 153.26 (C_{quat}), 152.92 (CH), 150.95 (CH), 148.10 (C_{quat}), 144.94 (C_{quat}), 140.44 (2CH), 135.27 (CH), 133.14 (C_{quat}), 129.85 (CH), 128.63 (CH), 128.05 (CH), 127.20 (CH), 126.18 (C_{quat}), 125.47 (CH), 121.76 (CH).

UV/Vis (CH_3CN), λ, nm (ε, 10^4 M^{-1} cm^{-1}): 228 (4.8), 268 (5.5), 356 (0.81), 395 (0.46).

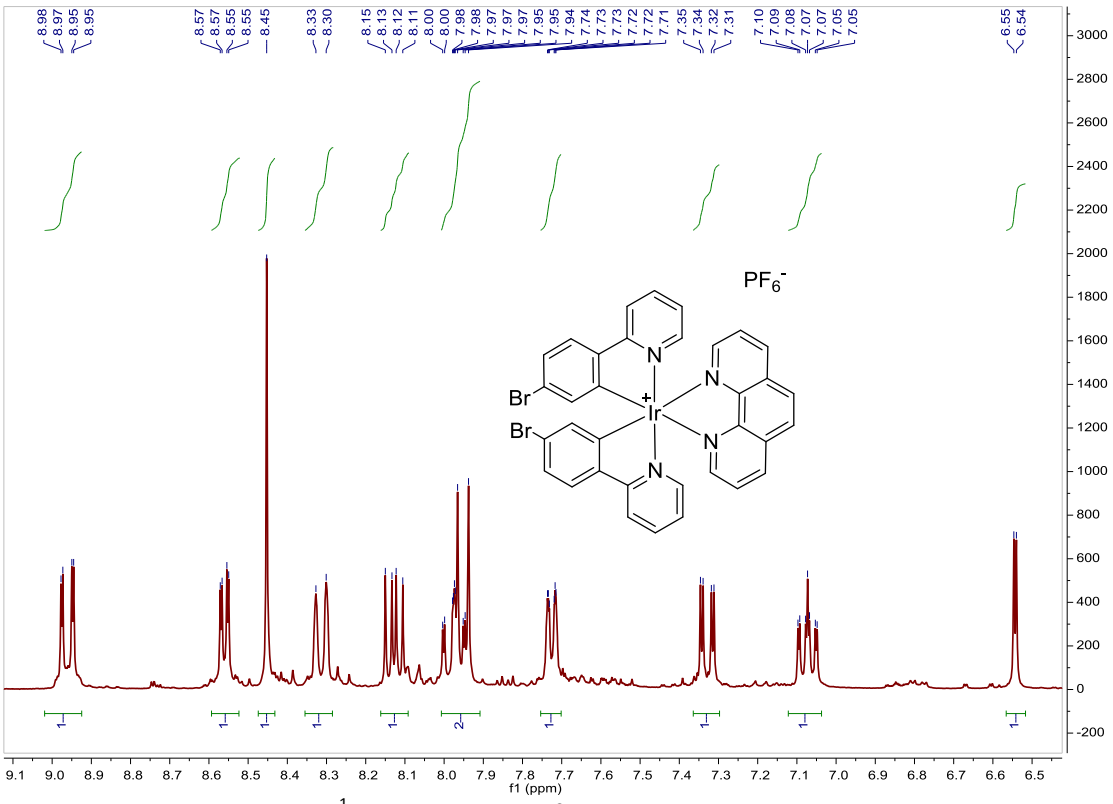

Fig. S132. ^{1}H NMR spectrum of **Cphen** in acetone-d_6, 300 MHz.

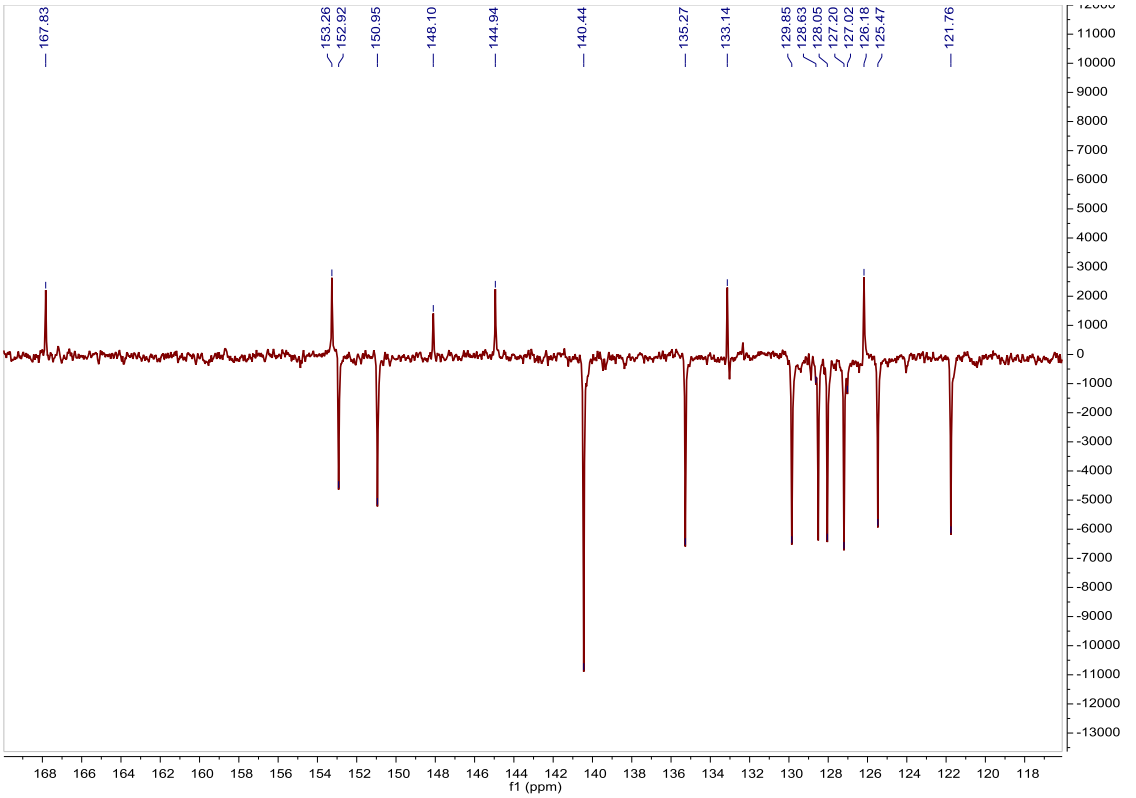

Fig. S133. ^{13}C APT NMR spectrum of **Cphen** in acetone-d_6, 75 MHz.

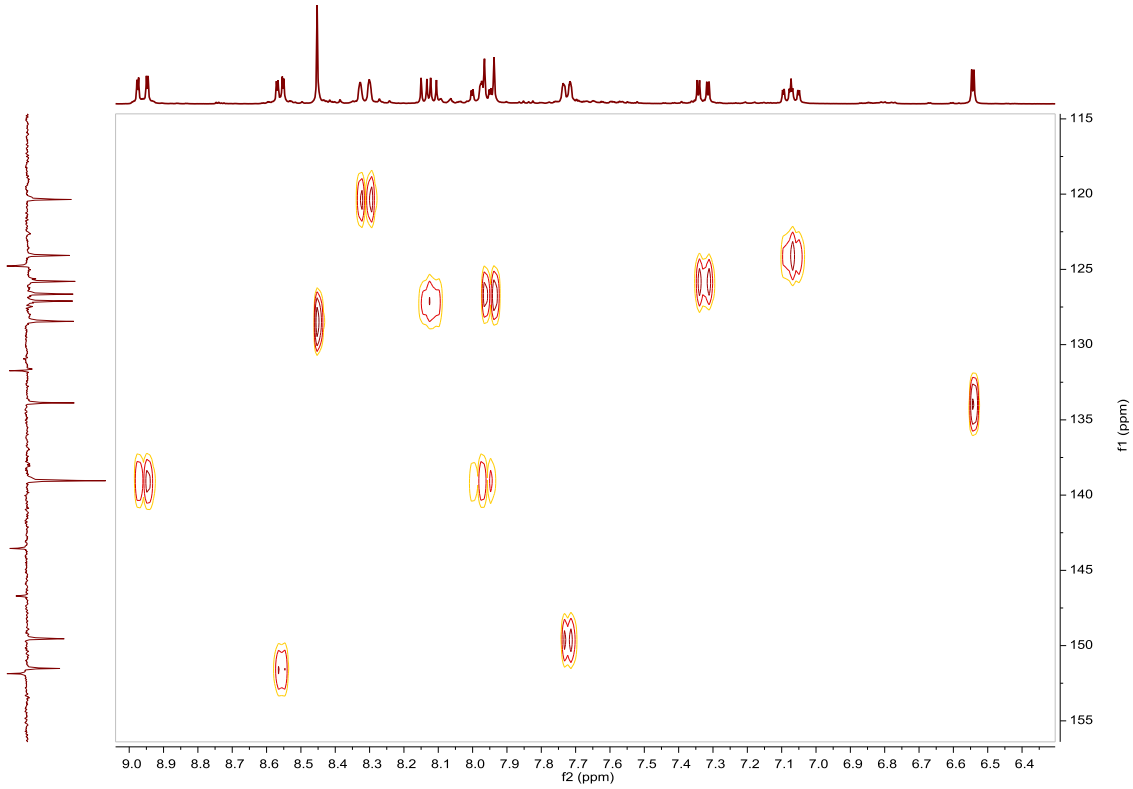

Fig. S134. HSQC NMR spectrum of **Cphen** in acetone-d_6.

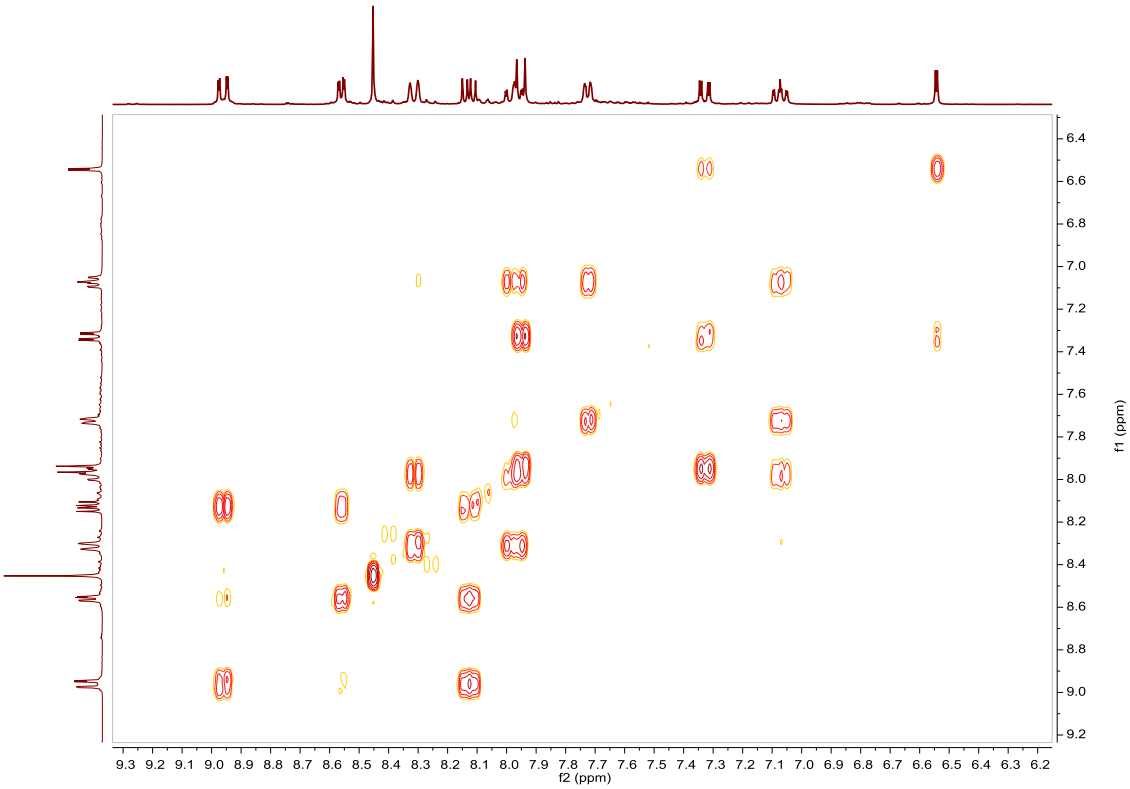

Fig. S135. COSY NMR spectrum of **Cphen** in acetone-d_6.

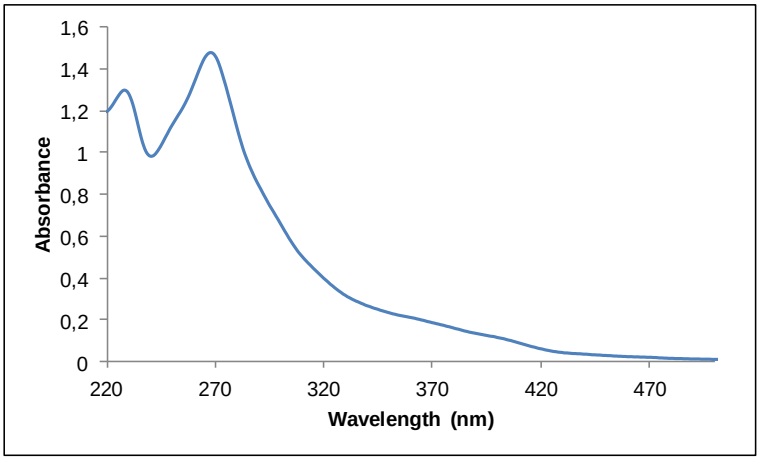

Fig. S136. UV/Vis spectra of **Cphen** in CH_3CN, $2.70 \cdot 10^{-5}$M.

Compound Dphen, [Ir(azoppy)$_2$(phen)]PF$_6$. Synthesis, characterization and photoisomerization studies.

SYNTHESIS

Under a N_2 atmosphere, **Cphen** (0.1 g, 0.102 mmol) and [4-(phenylazo)phenyl]boronic acid **6** (0.056 g, 0.247 mmol) were dissolved in 4 mL of THF. Na_2CO_3 (1M (aq), 2 mL) and $Pd(PPh_3)_4$ (0.012 g, 0.010 mmol) were added and the solution was degassed by bubbling N_2 for 15 min. The reaction mixture was refluxed (80 °C) for 15 h. The resulting mixture was cooled down to room temperature and the product was extracted with CH_2Cl_2. The organic phase was dried with $MgSO_4$, filtered off and the solvent was evaporated. The residue was purified by column chromatography (silica gel, CH_2Cl_2). To the fraction containing the eluted complex, 0.05 g of KPF_6 were added and the resulting solution was filtered through a celite path. The title compound was obtained as an orange solid. Yield 50%.

Elemental Analysis: calculated for ($C_{58}H_{40}IrN_8PF_6$): C, 58.73; H, 3.40; N, 9.45. Found: C, 58.69; H, 3.07; N, 9.35.

Exact Mass: ESI-MS $[C_{58}H_{40}IrN_8]^+$: calculated: m/z= 1041.3005, found: m/z= 1041.3031.

^{1}H NMR (300 MHz, acetone-*d*$_6$): δ 8.97 (dd, J = 1.4 Hz, J = 8.3 Hz, 1H), 8.69 (dd, J = 1.4 Hz, J = 5.0 Hz, 1H), 8.47 (s, 1H), 8.36 (d, J = 8.0 Hz, 1H), 8.17–8.08 (m, 2H), 8.04–7.91 (m, 5H), 7.87 (d, J = 5.8 Hz, 1H), 7.67 (brd, J = 8.6 Hz, 2H), 7.64–7.57 (m, 3H), 7.53 (dd, J = 1.9 Hz, J = 8.1 Hz, 1H), 7.11 (ddd, J = 1.3 Hz, J = 5.9 Hz, J = 7.3 Hz, 1H), 6.87 (d, J = 1.8 Hz, 1H).

^{13}C APT NMR (75 MHz, acetone-*d*$_6$): δ 168.65 (C_{quat}), 157.33 (C_{quat}), 153.94 (C_{quat}), 153.02 (CH), 151.77 (C_{quat}), 151.06 (CH), 148.32 (C_{quat}), 145.87 (C_{quat}), 145.06 (C_{quat}), 142.56 (C_{quat}), 140.15 (CH), 140.10 (CH), 133.10 (C_{quat}), 132.63 (CH), 131.17 (CH), 130.61 (2CH), 129.82 (CH), 128.95 (2CH), 128.44 (CH), 126.76 (CH), 125.07 (CH), 124.46 (2CH), 123.97 (2CH), 123.16 (CH), 121.61 (CH).

UV/Vis (CH_3CN), λ, nm (ε, 10^4 M^{-1} cm^{-1}): 355 (6.9).

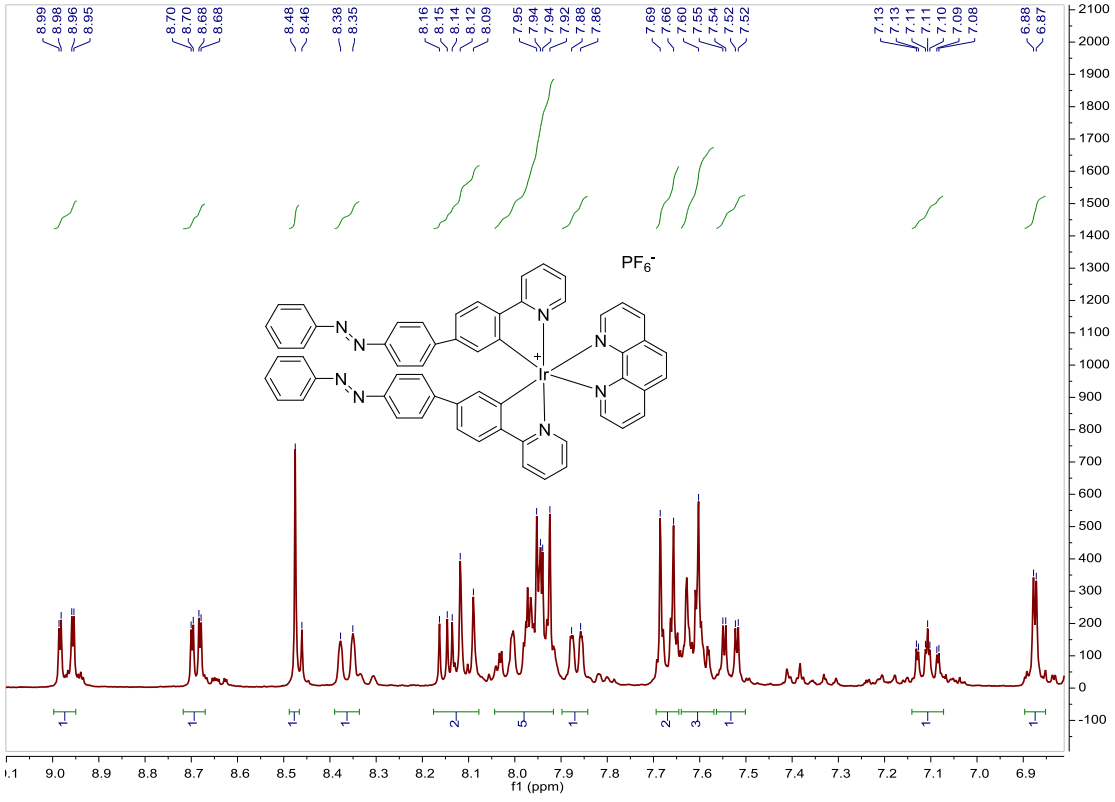

Fig. S137. ^{1}H NMR spectrum of **Dphen** in acetone-*d*$_6$, 300 MHz.

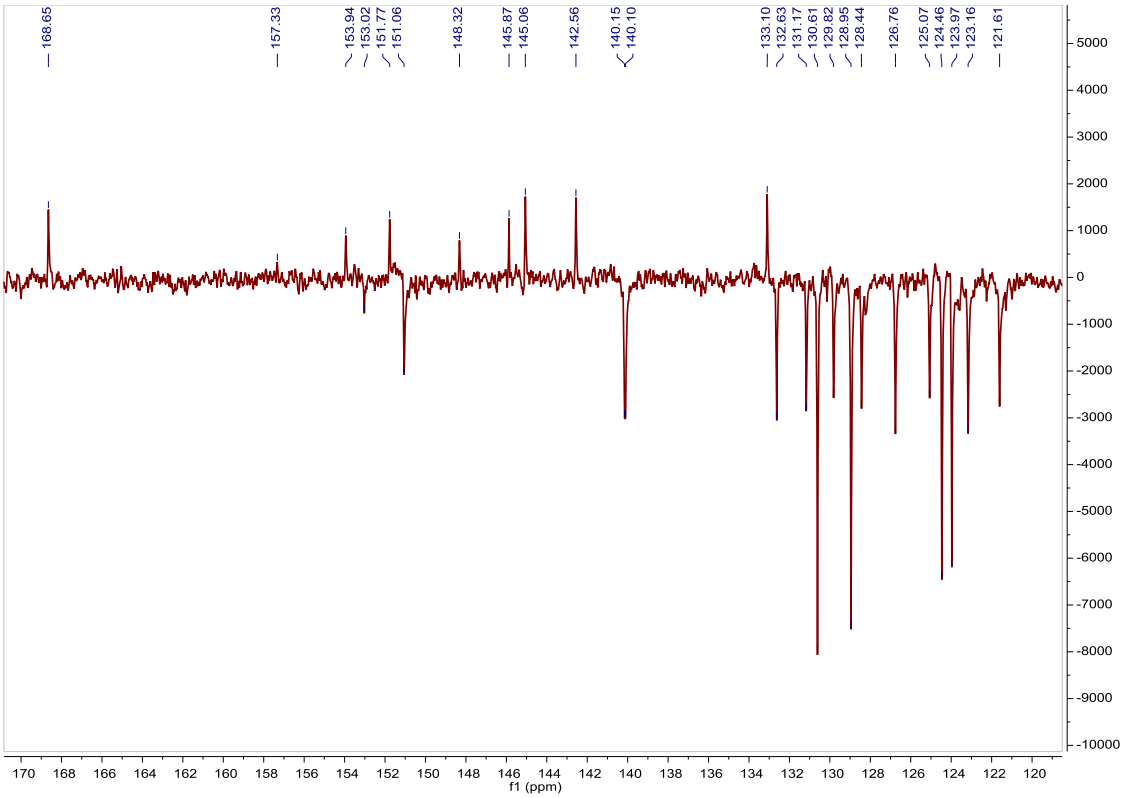

Fig. S138. ^{13}C APT NMR spectrum of **Dphen** in acetone-d_6, 75 MHz.

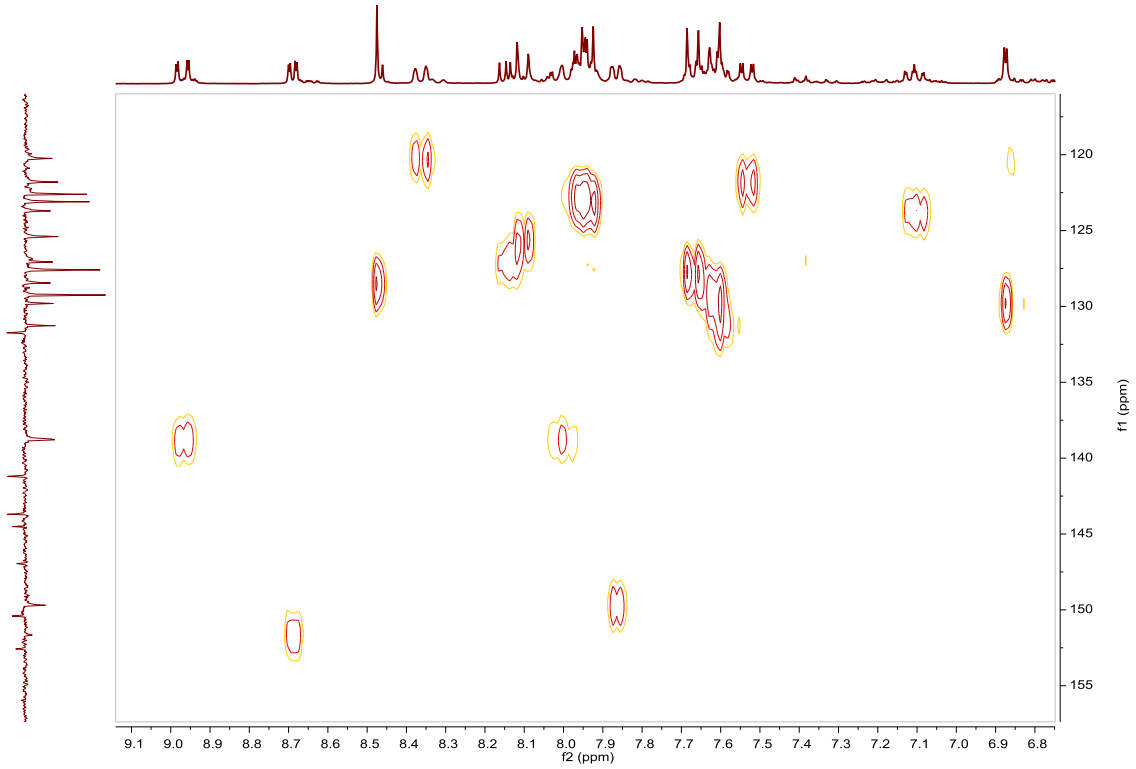

Fig. S139. HSQC NMR spectrum of **Dphen** in acetone-d_6.

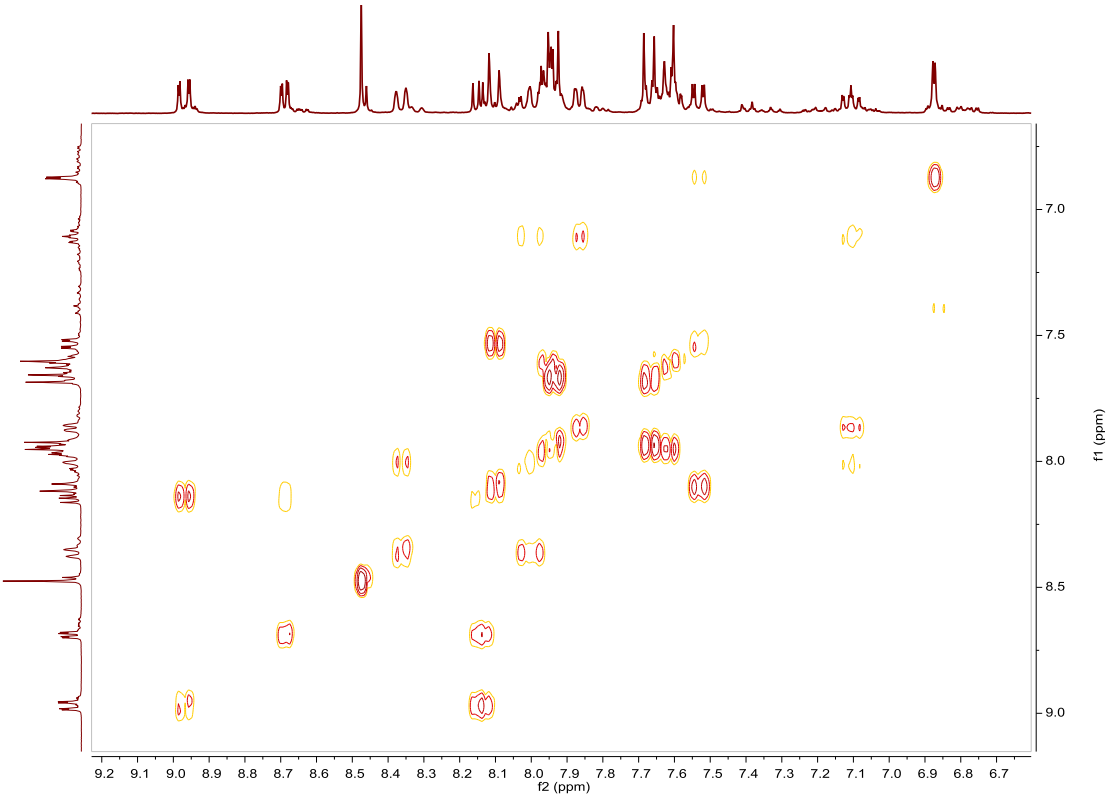

Fig. S140. COSY NMR spectrum of **Dphen** in acetone-d_6.

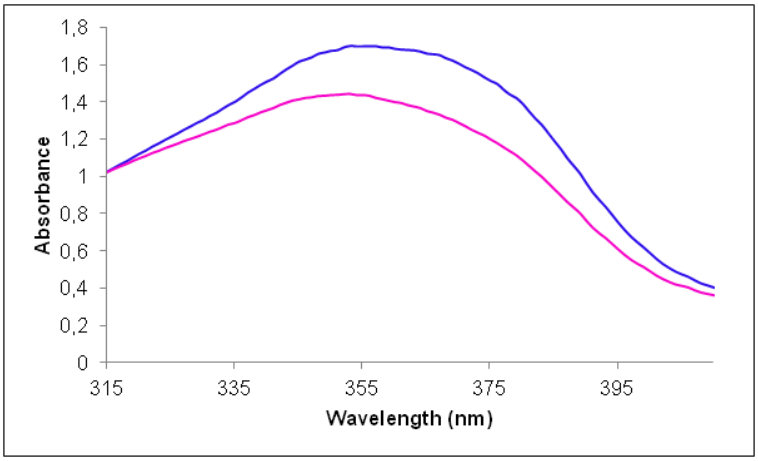

Fig. S141. UV/Vis spectra of **Dphen** in CH_3CN. Before (blue line) and after (pink line) irradiation at 362nm, $2.47 \cdot 10^{-5}$M.

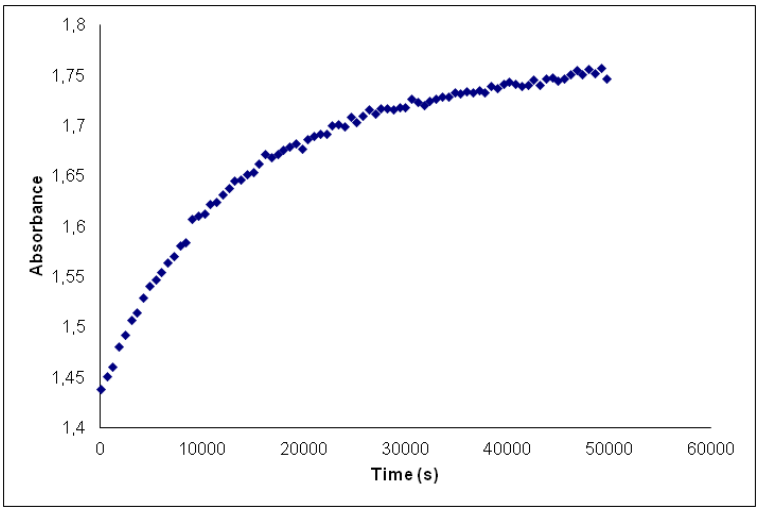

Fig. S142. Cis to trans thermal isomerization kinetics of **Dphen**. Absorption change of the band 355nm at 328 K in CH_3CN after irradiation at 362 nm. ($2.47 \cdot 10^{-5}$M).

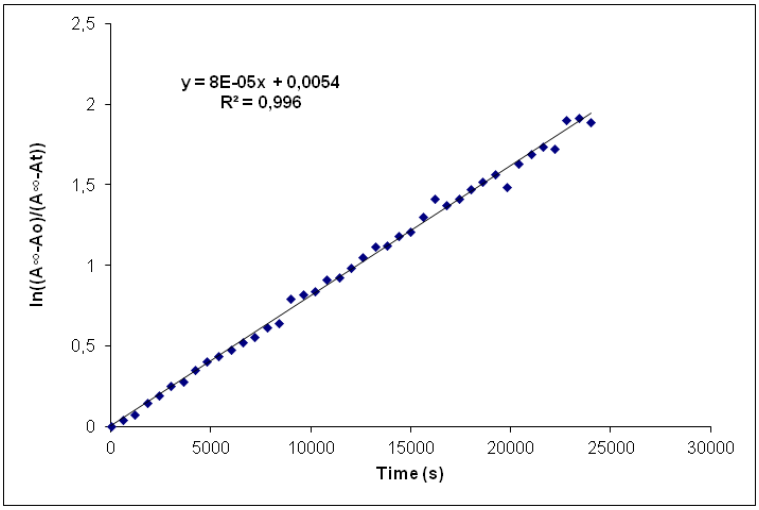

Fig. S143. Cis to trans thermal isomerization kinetics of **Dphen**. First-order plot. k (s^{-1}) = $8.0 \cdot 10^{-5}$. Half-life (min) = 144.

Compound Abipy-dibr, $[Ir(ppy)_2(bipy\text{-}dibr)]PF_6$. Synthesis and characterization.

SYNTHESIS

Under a N_2 atmosphere, $[Ir(ppy)_2Cl]_2$ (0.100 g, 0.093 mmol) were added over a suspension of 4,4'-dibromo-2,2'-bipyridine (0.060 g, 0.186 mmol) in 8 mL CH_2Cl_2–MeOH 2/1. The reaction mixture was refluxed, under N_2, for 15 h. To the resulting solution, 0.035 g of KPF_6 were added and the solution was stirred for an 1 h. The solvent was evaporated and the reaction mixture was filtrated through a celite path in CH_2Cl_2. The product was obtained after purified by column chromatography (silica gel, CH_2Cl_2 as eluent) as an orange solid. Yield 81%.

Elemental Analysis: calculated for ($C_{32}H_{22}Br_2IrN_4PF_6$): C, 40.06; H, 2.31; N, 5.84. Found: C, 39.61; H, 2.61; N, 5.55.

Exact Mass: ESI-MS $[C_{32}H_{22}Br_2IrN_4]^+$: calculated: m/z= 812.9840, found: m/z= 812.9817.

^{1}H NMR (500 MHz, acetone-d_6): δ 9.23 (s, 1H), 8.26 (d, J = 8.1 Hz, 1H), 8.03–7.95 (m, 3H), 7.91 (d, J = 7.5 Hz, 1H), 7.18 (t, J = 6.3 Hz, 1H), 7.06 (t, J = 7.3 Hz, 1H), 6.93 (t, J = 7.0 Hz, 1H), 6.34 (d, J = 7.1 Hz, 1H).

^{13}C NMR (126 MHz, acetone-d_6): δ 167.63 (C_{quat}), 156.45 (C_{quat}), 151.40 (CH), 149.66 (CH), 149.57 (C_{quat}), 144.08 (C_{quat}), 138.88 (CH), 135.88 (C_{quat}), 132.30 (CH), 131.60 (CH), 130.49 (CH), 128.93 (CH), 125.05 (CH), 123.75 (CH), 122.77 (CH), 120.03 (CH).

UV/Vis (CH_3CN), λ, nm (ε, 10^4 M^{-1} cm^{-1}): 253 (4.7), 312 (1.9), 377 (0.75).

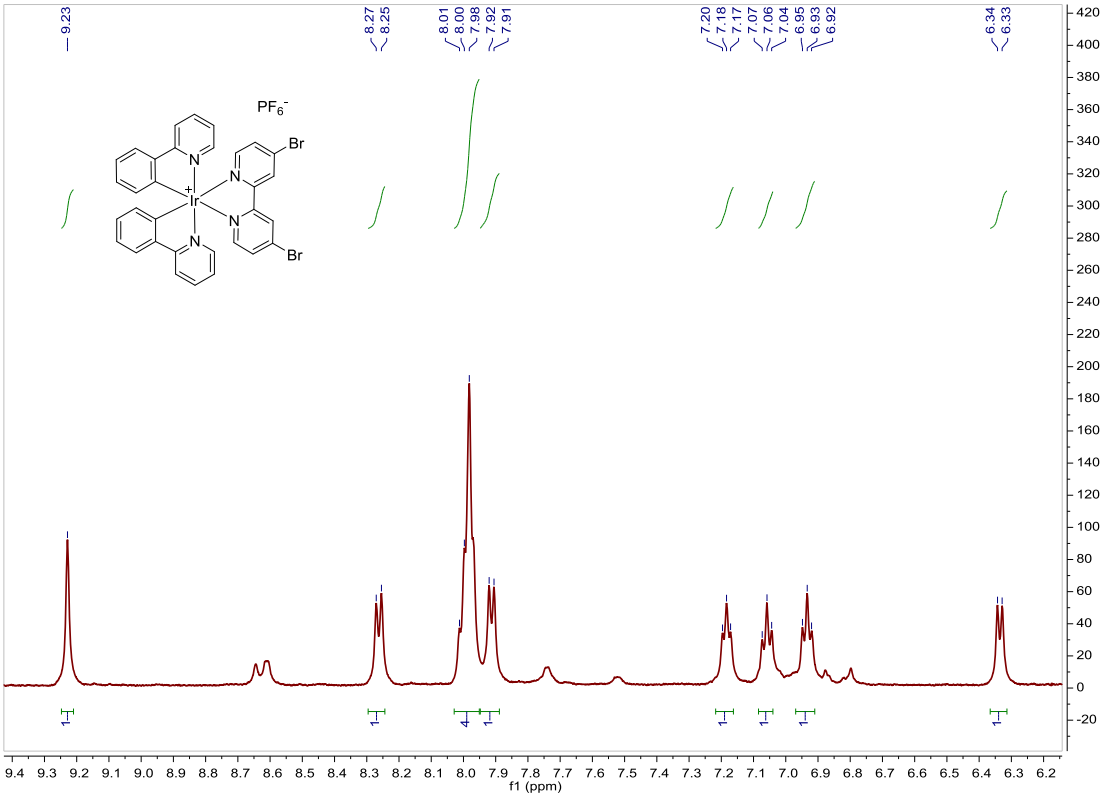

Fig. S144. ^{1}H NMR spectrum of **Abipy-dibr** in acetone-d_6, 500 MHz.

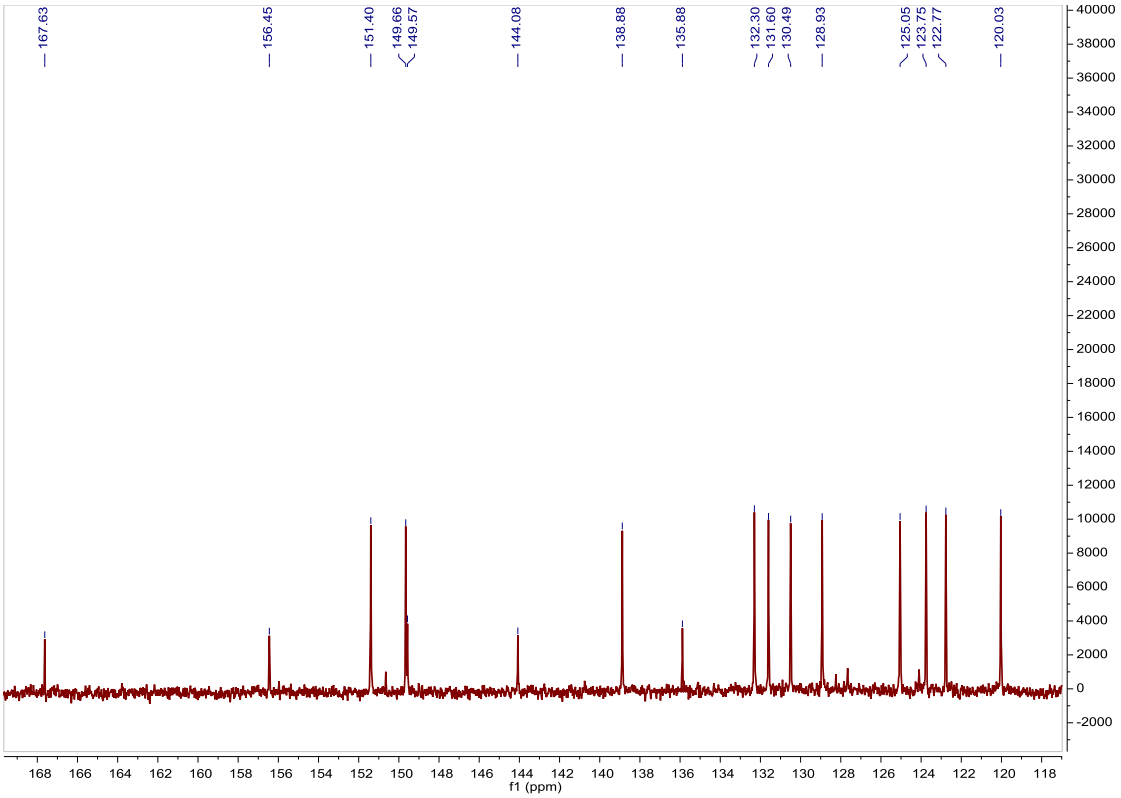

Fig. S145. ^{13}C NMR spectrum of **Abipy-dibr** in acetone-d_6, 126 MHz.

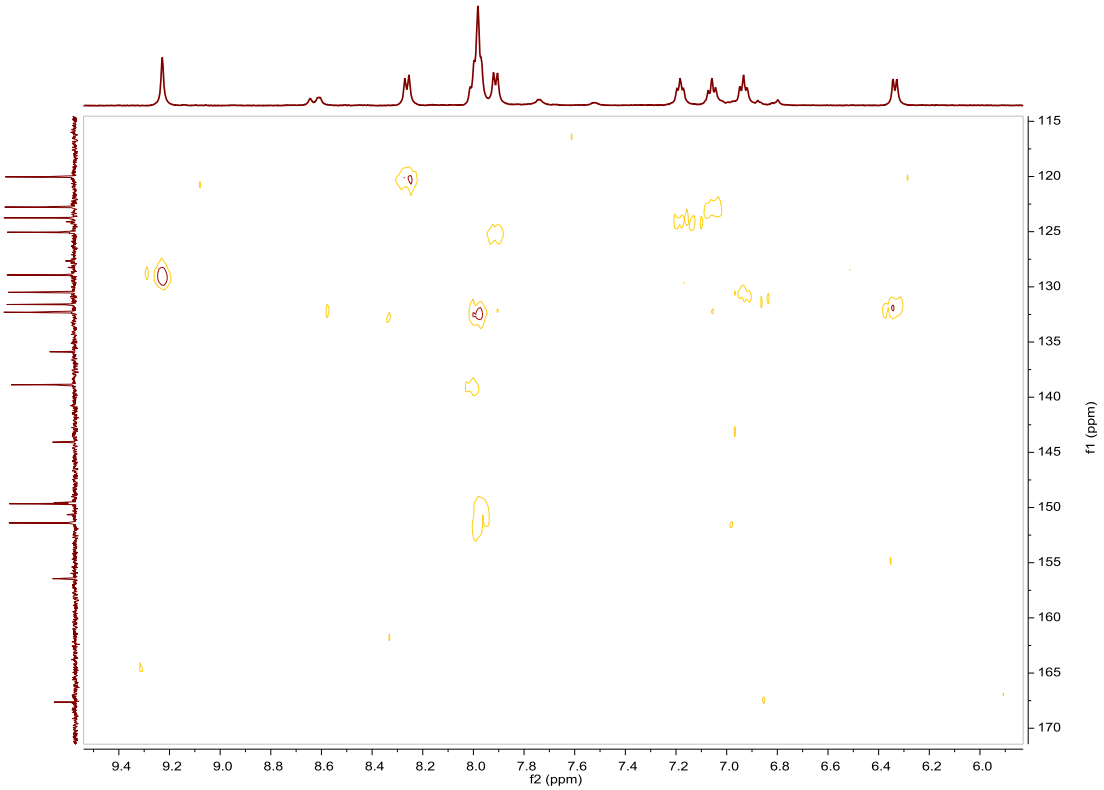

Fig. S146. HSQC NMR spectrum of **Abipy-dibr** in acetone-d_6.

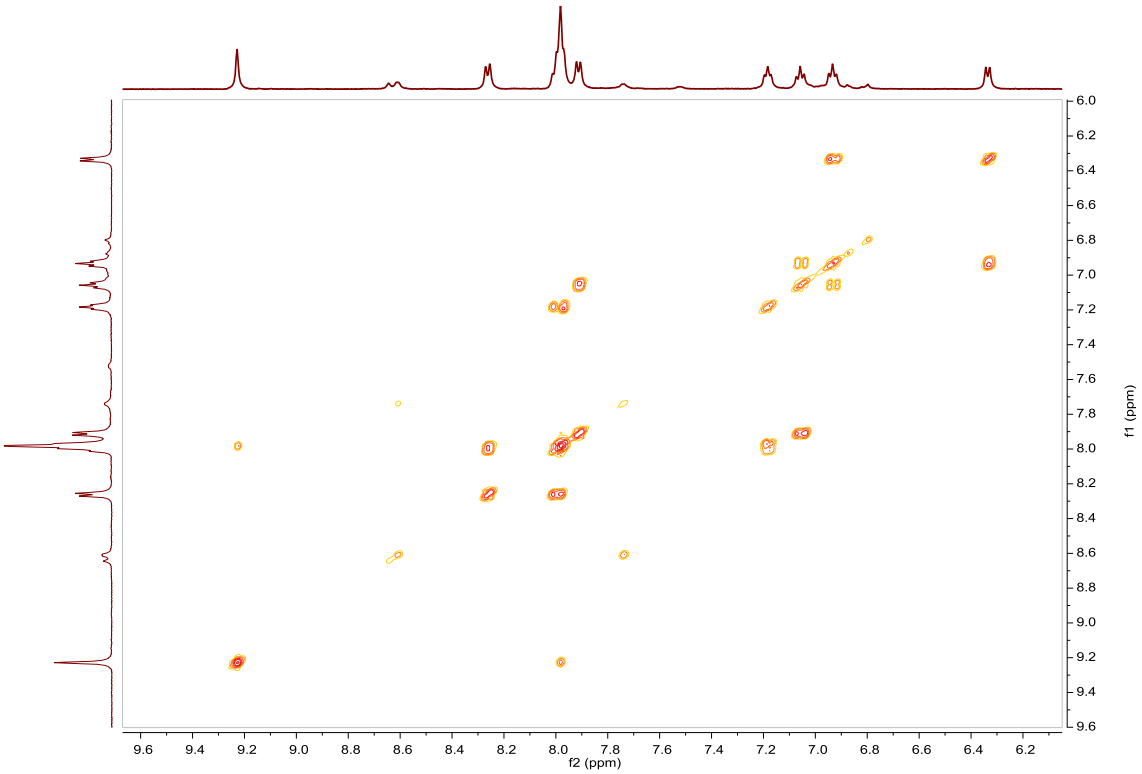

Fig. S147. COSY NMR spectrum of **Abipy-dibr** in acetone-d_6.

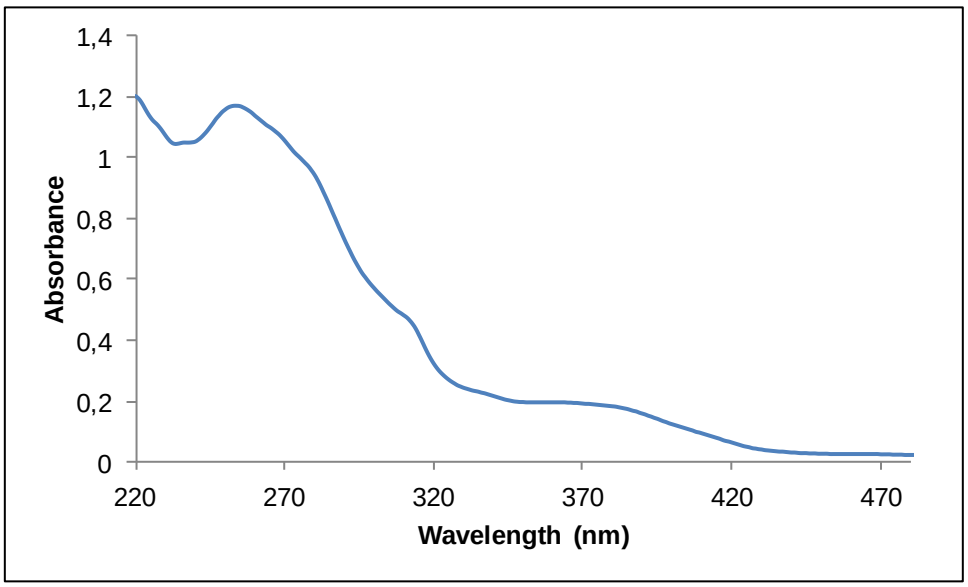

Fig. S148. UV/Vis spectra of **Abipy-dibr** in CH_3CN, $2.46 \cdot 10^{-5}$M.

Compound Bbipy-dibr, [Ir(Fppy)$_2$(bipy-dibr)]PF$_6$. Synthesis and characterization.

SYNTHESIS

Under a N_2 atmosphere, $[Ir(Fppy)_2Cl]_2$ (0.100 g, 0.082 mmol) were added over a suspension of 4,4'-dibromo-2,2'-bipyridine (0.052 g, 0.164 mmol) in 8 mL CH_2Cl_2–MeOH 2/1. The reaction mixture was refluxed, under N_2, for 15 h. To the resulting yellow solution, 0.05 g of KPF_6 were added and the solution was stirred for an 1 h. The solvent was evaporated and the reaction mixture was filtrated through a celite path in CH_2Cl_2. The product was obtained after purified by column chromatography (silica gel, CH_2Cl_2 as eluent) as a yellow solid. Yield 59%.

Elemental Analysis: calculated for ($C_{32}H_{18}Br_2F_4IrN_4PF_6$): C, 37.26; H, 1.76; N, 5.43. Found: C, 37.38; H, 1.99; N, 5.05.

Exact Mass: ESI-MS $[C_{32}H_{18}Br_2F_4IrN_4]^+$: calculated: m/z= 884.9464, found: m/z= 884.9450.

^{1}H NMR (500 MHz, acetone-d_6): δ 9.26 (s, 1H), 8.41 (d, *J* = 10 Hz, 1H), 8.10 (m, 2H), 8.06 (d, J = 5 Hz, 1H), 8.00 (d, *J* = 5 Hz, 1H), 7.27 (t, *J* = 5 Hz, 1H), 6.79 (t, *J* = 10 Hz, 1H), 5.79 (d, *J* = 5 Hz, 1H).

^{13}C NMR (126 MHz, acetone-d_6): 163.72 (d, *J* = 6.3 Hz, C_{quat}), 163.61 (dd, *J* = 12.6 Hz, J = 255.3 Hz, C_{quat}),161.44 (dd, *J* = 12.6, J = 260.3, C_{quat}), 156.19 (s, C_{quat}), 153.60 (d, *J* = 6.3, C_{quat}), 151.80 (s, CH), 150.19 (s, CH), 140.01 (s, CH), 136.60 (s, C_{quat}), 132.62 (s, CH), 129.23 (s, CH), 127.99 (s, C_{quat}), 124.31 (s, CH), 123.79 (d, *J* = 18.9 Hz, CH), 113.80 (d, *J* = 16.3 Hz, CH), 99.03 (pst, *J* = 27.7 Hz, CH).

UV/Vis (CH_3CN), λ, nm (ε, 10^4 M^{-1} cm^{-1}): 242 (5.7), 298 (2.5), 310 (2.3), 361 (0.76).

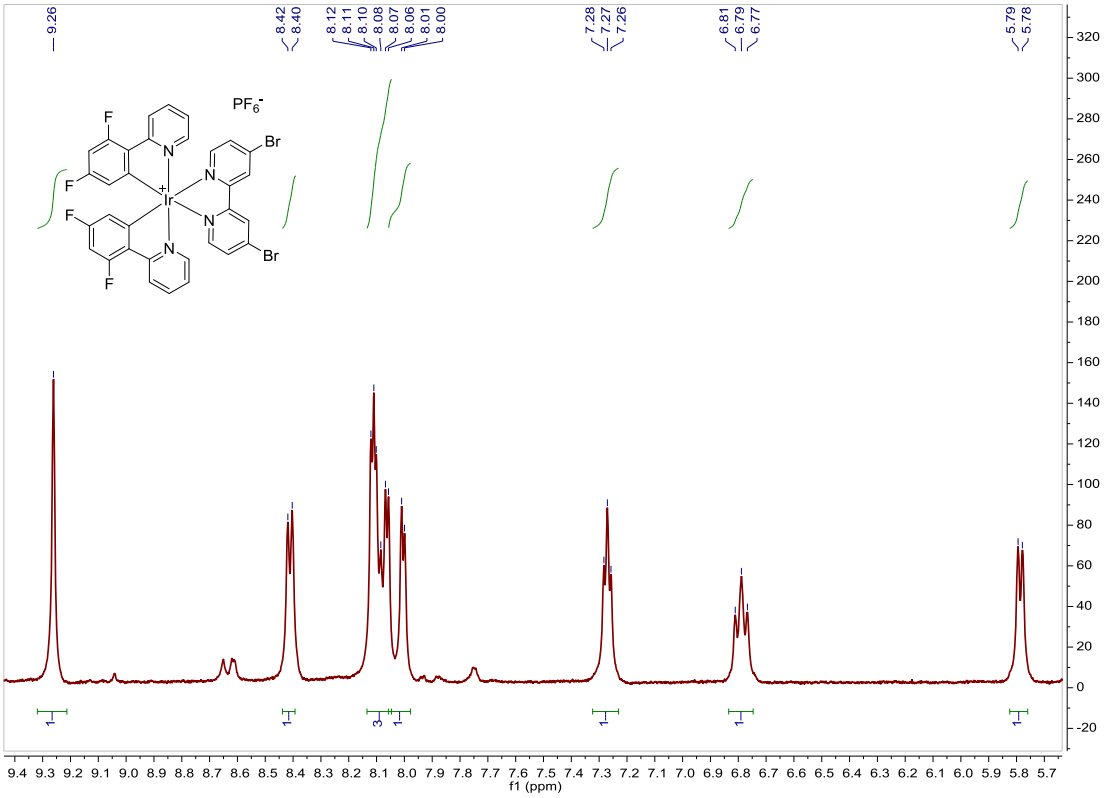

Fig. S149. ^{1}H NMR spectrum of **Bbipy-dibr** in acetone-d_6, 500 MHz.

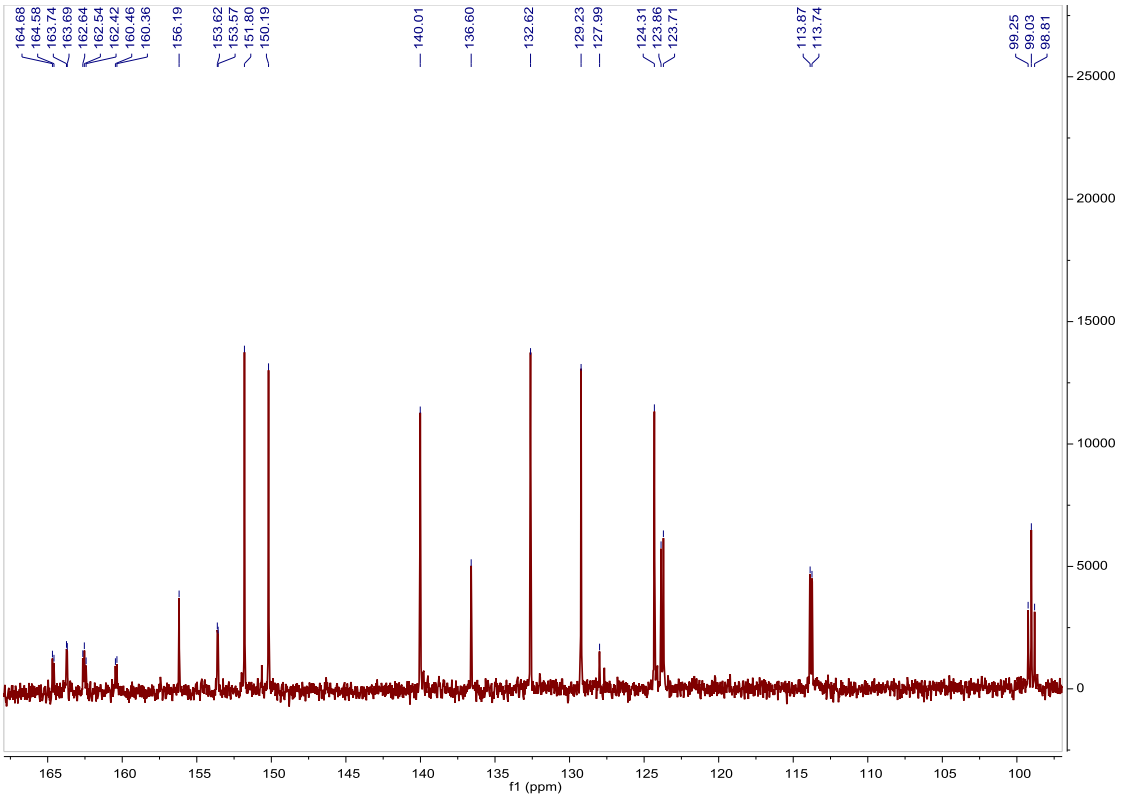

Fig. S150. ^{13}C NMR spectrum of **Bbipy-dibr** in acetone-d_6, 126 MHz.

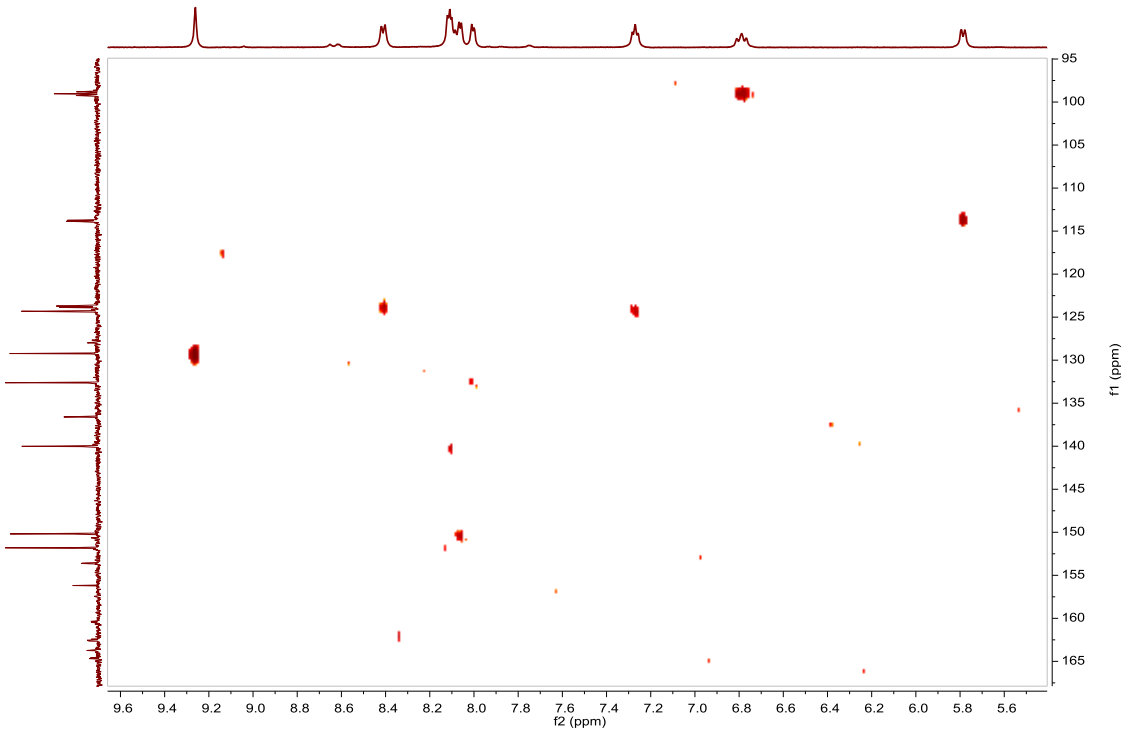

Fig. S151. HSQC NMR spectrum of **Bbipy-dibr** in acetone-d_6.

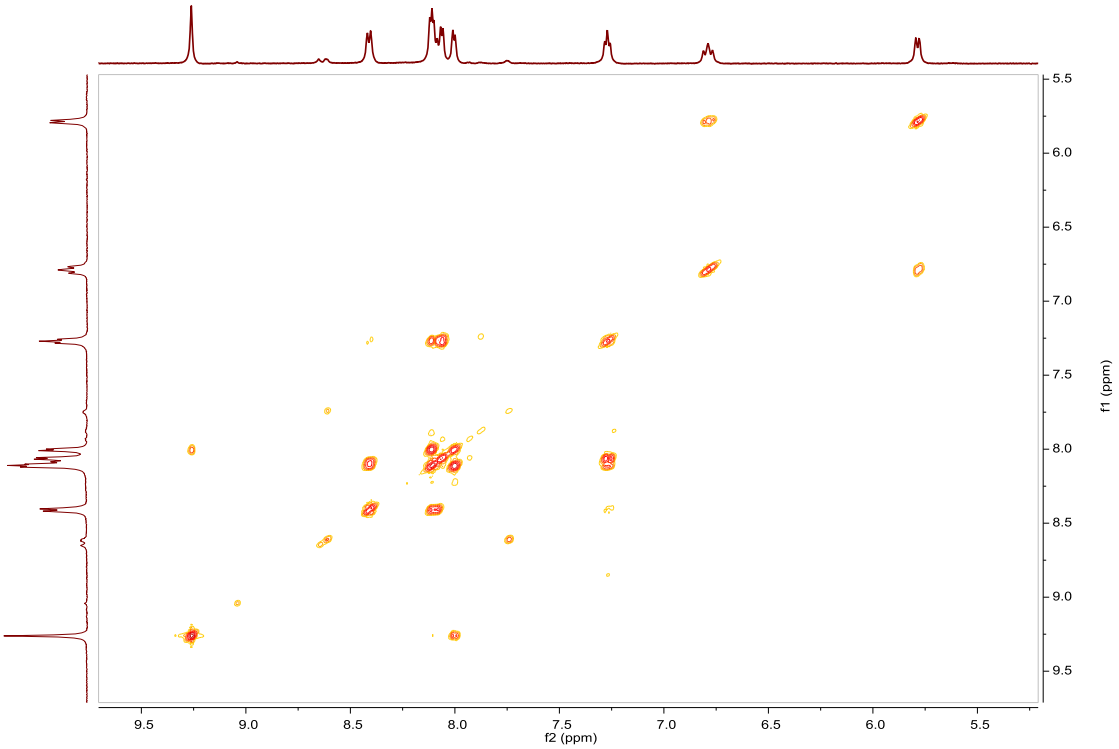

Fig. S152. COSY NMR spectrum of **Bbipy-dibr** in acetone-d_6.

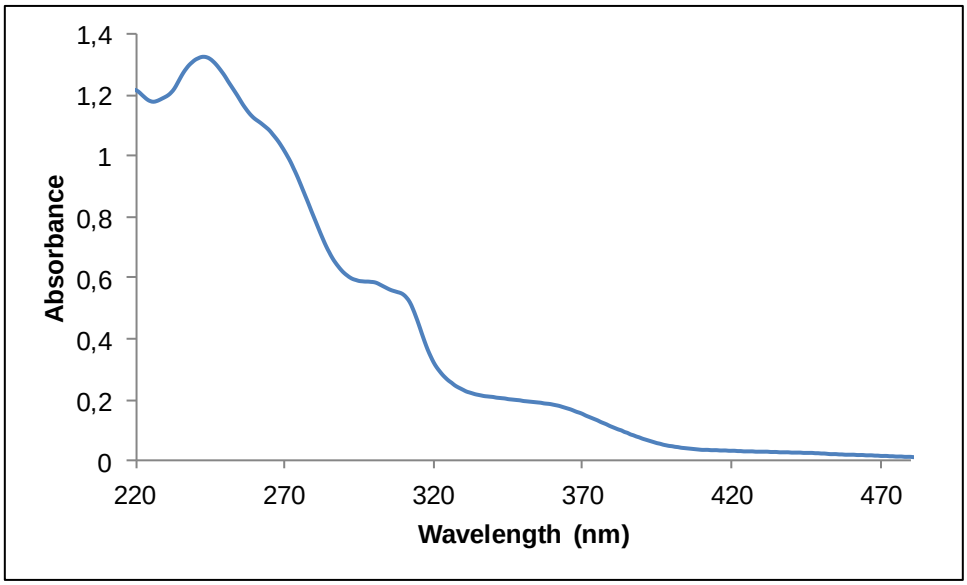

Fig. S153. UV/Vis spectra of **Bbipy-dibr** in CH_3CN, $2.34 \cdot 10^{-5}$M.

Compound Cbipy-dibr, [Ir(Brppy)$_2$(bipy-dibr)]PF$_6$. Synthesis and characterization.

SYNTHESIS

Under a N_2 atmosphere, $[Ir(Brppy)_2Cl]_2$ (0.100 g, 0.072 mmol) were added over a suspension of 4,4'-dibromo-2,2'-bipyridine (0.045 g, 0.144 mmol) in 8 mL CH_2Cl_2–MeOH 2/1. The reaction mixture was refluxed, under N_2, for 15 h. To the resulting orange solution, 0.05 g of KPF_6 were added and the solution was stirred for an 1 h. The solvent was evaporated and the desired compound was obtained after filtration through a celite path in CH_2Cl_2 as a brown solid. Yield 87%.

Elemental Analysis: calculated for ($C_{32}H_{20}Br_4IrN_4PF_6$): C, 34.40; H, 1.80; N, 5.01. Found: C, 33.96; H, 1.84; N, 4.93.

Exact Mass: ESI-MS $[C_{32}H_{20}Br_4IrN_4]^+$: calculated: m/z= 968.8051, found: m/z= 968.8026.

^{1}H NMR (500 MHz, acetone-*d*$_6$): δ 9.25 (d, J = 1.7 Hz, 1H), 8.32 (d, J = 8.1 Hz, 1H), 8.04 (m, 4H), 7.90 (d, J = 8.35 Hz, 1H), 7.27 (m, 2H), 6.39 (d, J = 2.0 Hz, 1H).

^{13}C NMR (126 MHz, acetone-*d*$_6$): δ 166.34 (C_{quat}), 156.32 (C_{quat}), 151.68 (CH), 151.58 (C_{quat}), 149.92 (CH), 143.41 (C_{quat}), 139.44 (CH), 136.34 (C_{quat}), 133.77 (CH), 132.52 (CH), 129.11 (CH), 126.87 (CH), 126.08 (CH), 124.95 (C_{quat}), 124.46 (CH), 120.65 (CH).

UV/Vis (CH_3CN), λ, nm (ε, 10^4 M^{-1} cm^{-1}): 254 (6.1), 267 (6.2), 299 (4.0), 391 (0.61).

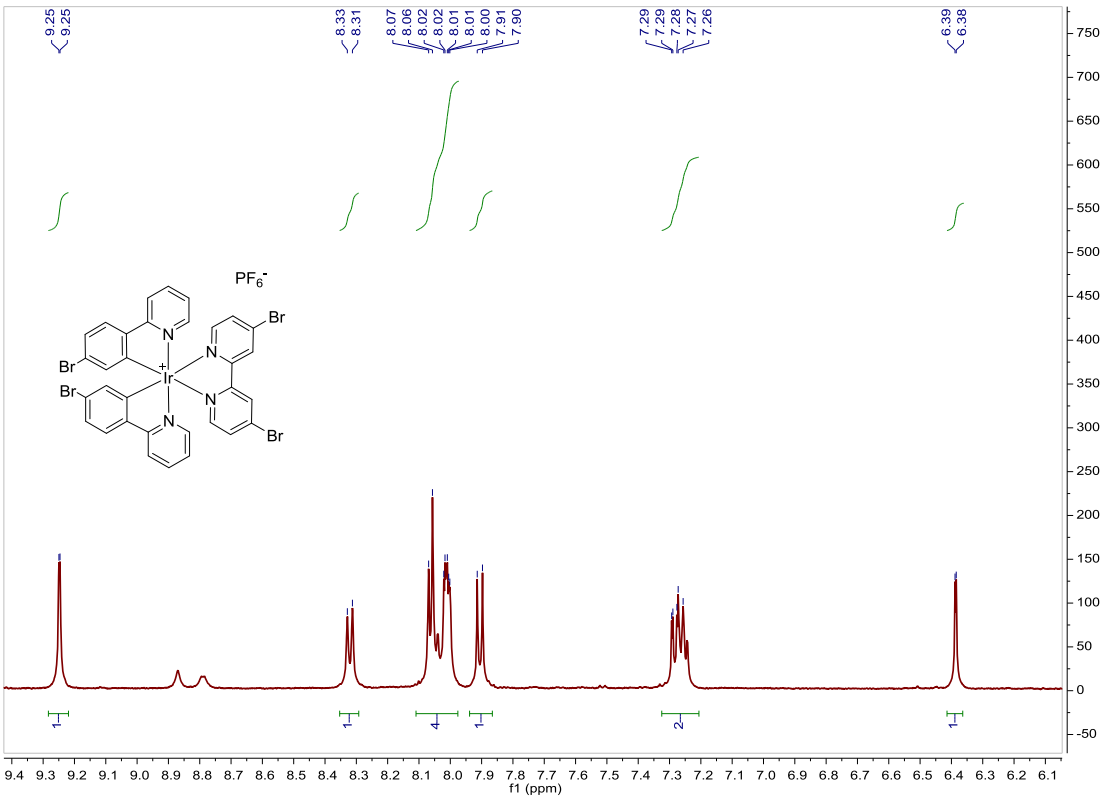

Fig. S154. ^{1}H NMR spectrum of **Cbipy-dibr** in acetone-*d*$_6$, 500 MHz.

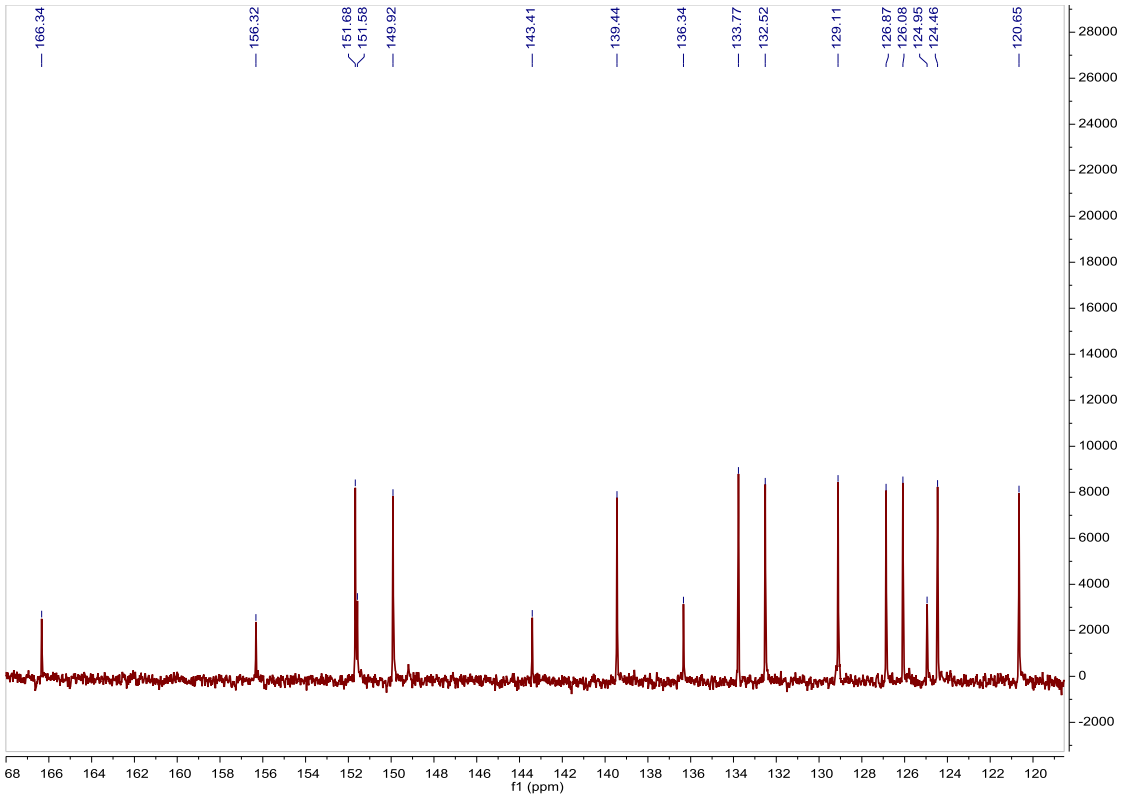

Fig. S155. ^{13}C NMR spectrum of **Cbipy-dibr** in acetone-d_6, 126 MHz.

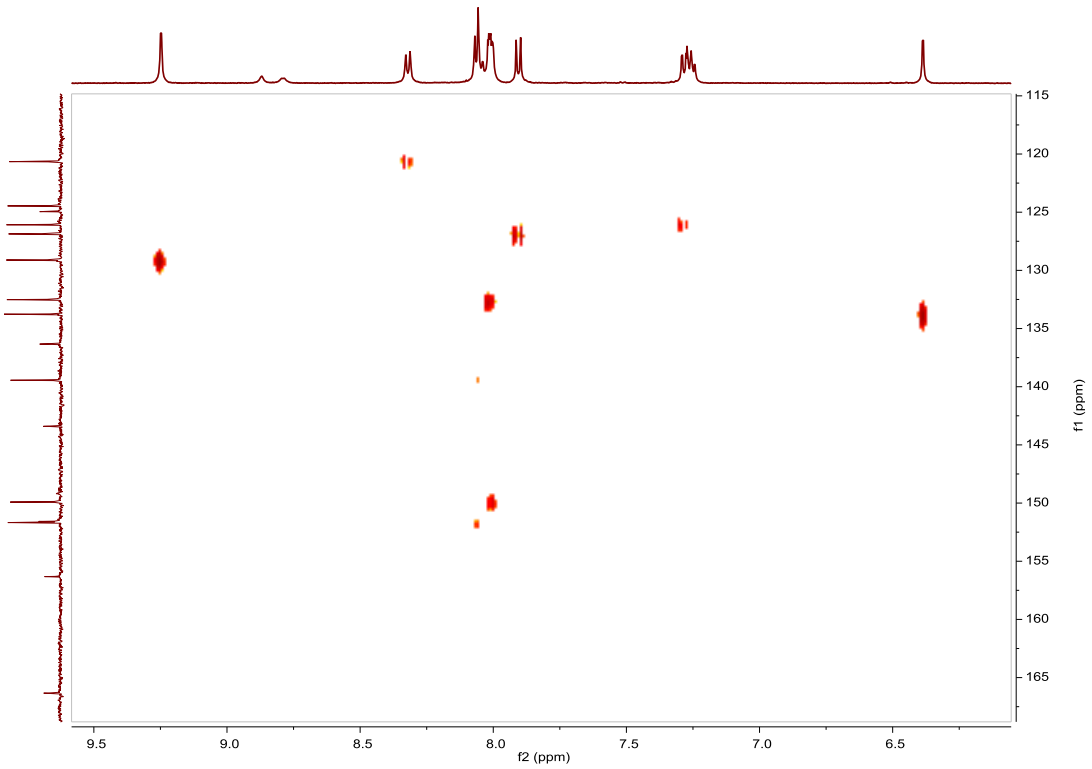

Fig. S156. HSQC NMR spectrum of **Cbipy-dibr** in acetone-d_6.

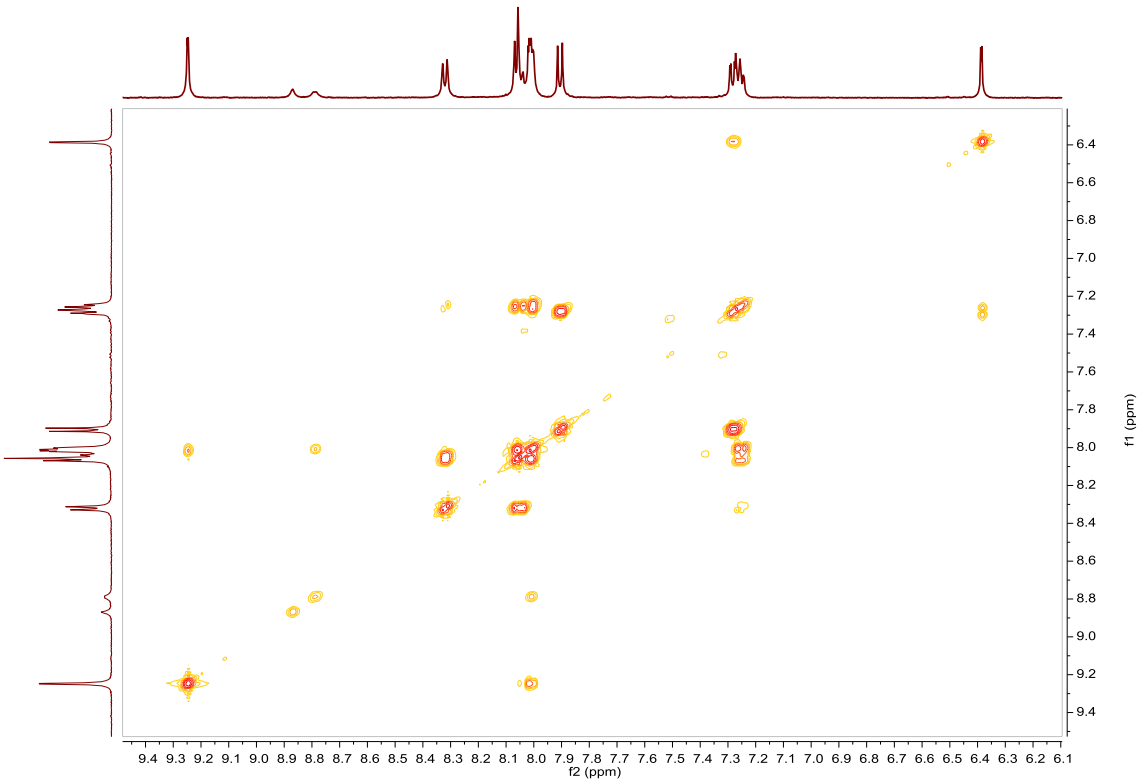

Fig. S157. COSY NMR spectrum of **Cbipy-dibr** in acetone-d_6.

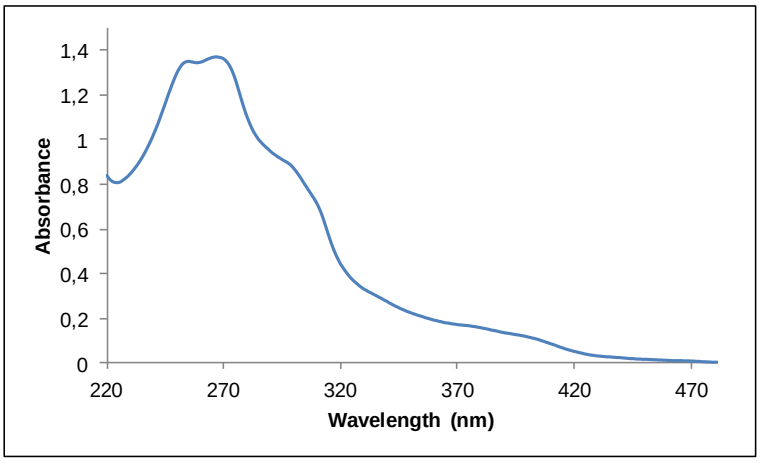

Fig. S158. UV/Vis spectra of **Cbipy-dibr** in CH_3CN, $2.20 \cdot 10^{-5}$M.

Compound A1, $[Ir(ppy)_2(1)]PF_6$. Synthesis, characterization and photoisomerization studies.

SYNTHESIS

Under a N_2 atmosphere, $[Ir(ppy)_2Cl]_2$ (0.058 g, 0.054 mmol) were added over a suspension of **L1** (0.040 g, 0.109 mmol) in 4 ml CH_2Cl_2–MeOH 2/1. The reaction mixture was refluxed, under N_2, for 15 h. After solvent evaporation the product was purified by column chromatography (silica gel, CH_2Cl_2). When the unreacted $[Ir(ppy)_2Cl]_2$ eluted, 0.05 g of KPF_6 were added on top of the column and the polarity of the eluent was gradually increased to 100% acetone to elute $[Ir(ppy)_2(\mathbf{L1})]PF_6$ together with the excess of KPF_6. The desired compound, purified by filtration through a celite path in CH_2Cl_2, was obtained as a dark red solid. Yield 85%.

Elemental Analysis: calculated for ($C_{44}H_{32}IrN_8PF_6$): C, 52.33; H, 3.19; N, 11.09. Found: C, 52.14; H, 3.09; N, 10.71.

Exact Mass: ESI-MS $[C_{44}H_{32}IrN_8]^+$: calculated: m/z= 865.2379, found: m/z= 865.2408.

^{1}H NMR (300 MHz, acetone-d_6): δ 9.39 (d, J = 1.5 Hz, 1H), 8.37 (d, J = 5.8 Hz, 1H), 8.30 (d, J = 8.0 Hz, 1H), 8.13–8.04 (m, 4H), 7.99 (t, J = 8.9 Hz, 2H), 7.73 (m, 3H), 7.22 (pst, J = 6.4 Hz, 1H), 7.10 (pst, J = 7.2 Hz, 1H), 6.99 (pst, J = 7.6 Hz, 1H), 6.43 (d, J = 7.4 Hz, 1H).

^{13}C APT NMR (75 MHz, acetone-d_6): δ 168.96 (C_{quat}), 160.13 (C_{quat}), 159.28 (C_{quat}), 153.77 (CH), 153.72 (C_{quat}), 151.39 (C_{quat}), 150.91 (CH), 145.41 (C_{quat}), 140.17 (CH), 135.16 (CH), 132.95 (CH), 131.80 (CH), 131.08 (2CH), 126.34 (CH), 125.08 (CH), 125.01 (2CH), 124.07 (CH), 121.85 (CH), 121.35 (CH), 119.96 (CH).

UV/Vis (CH_3CN), λ, nm (ε, 10^4 M^{-1} cm^{-1}): 327 (5.3), 404 (1.7), 513 (0.26).

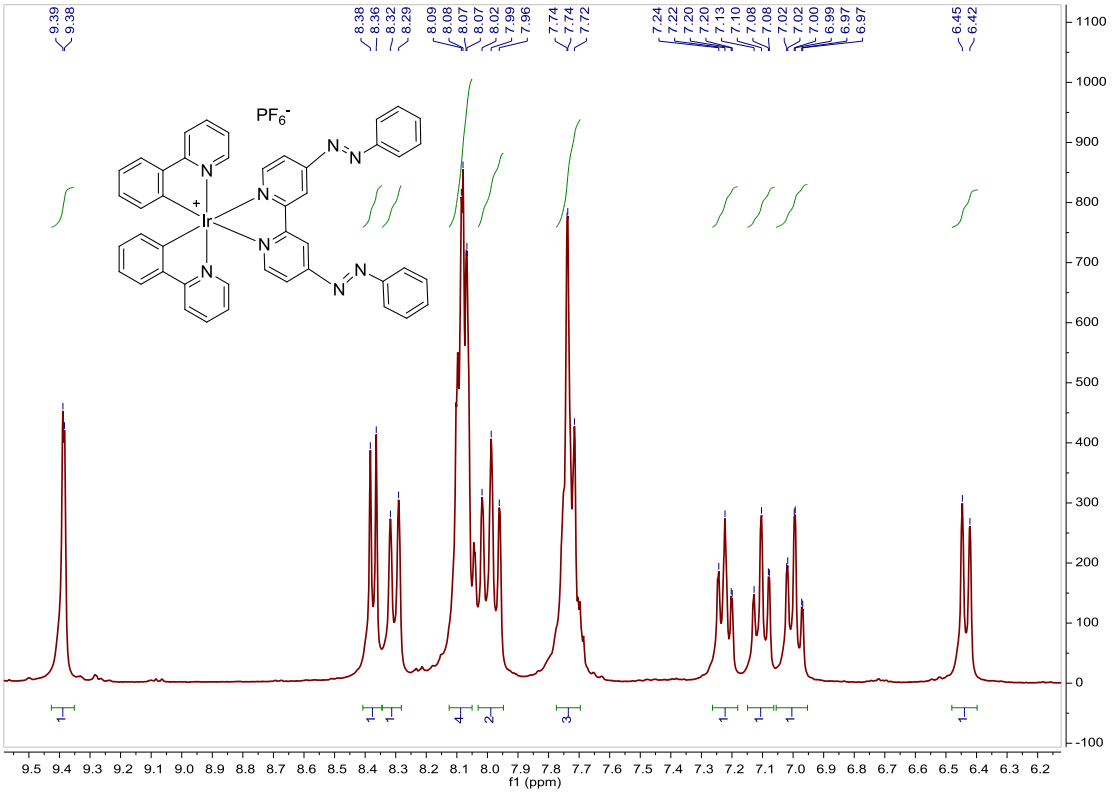

Fig. S159. ^{1}H NMR spectrum of **A1** in acetone-d_6, 300 MHz.

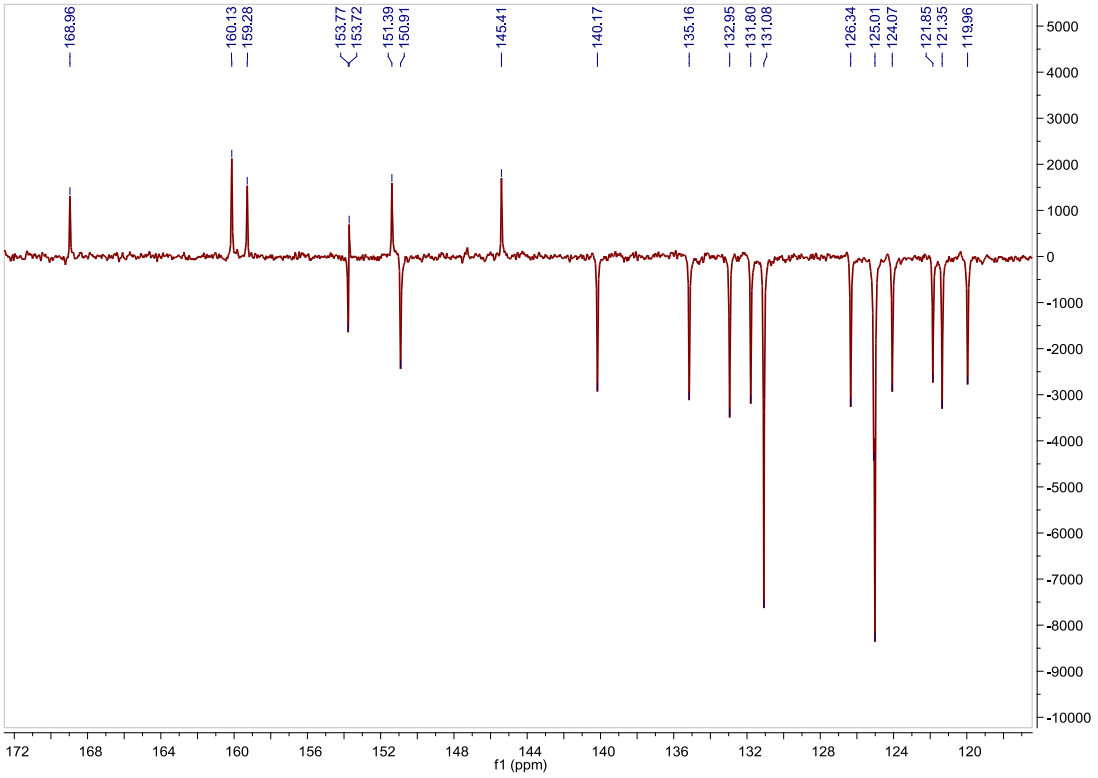

Fig. S160. ^{13}C APT NMR spectrum of **A1** in acetone-d_6, 75 MHz.

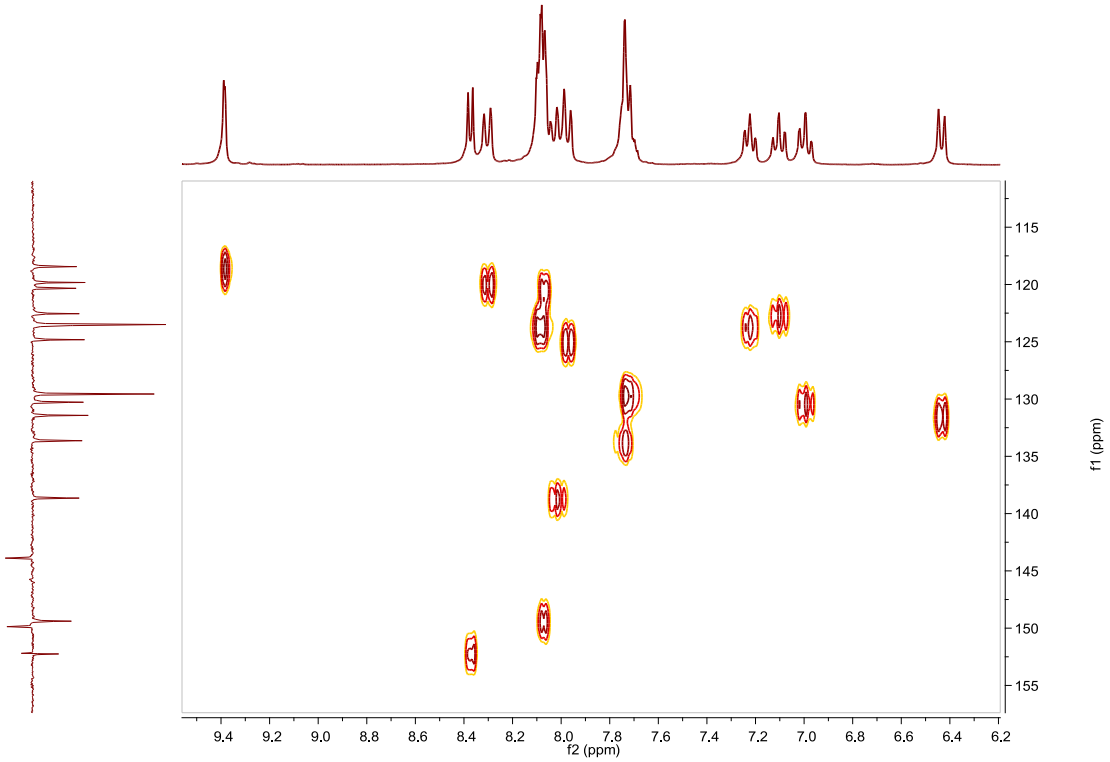

Fig. S161. HSQC NMR spectrum of **A1** in acetone-d_6.

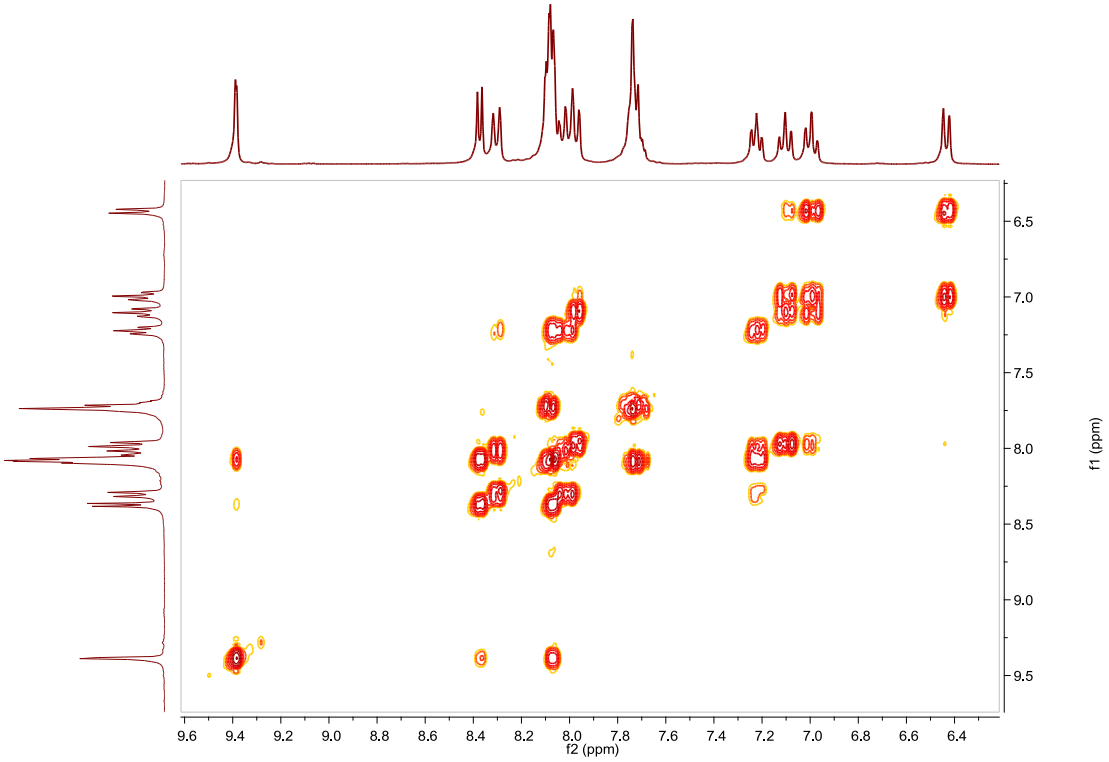

Fig. S162. COSY NMR spectrum of **A1** in acetone-d_6.

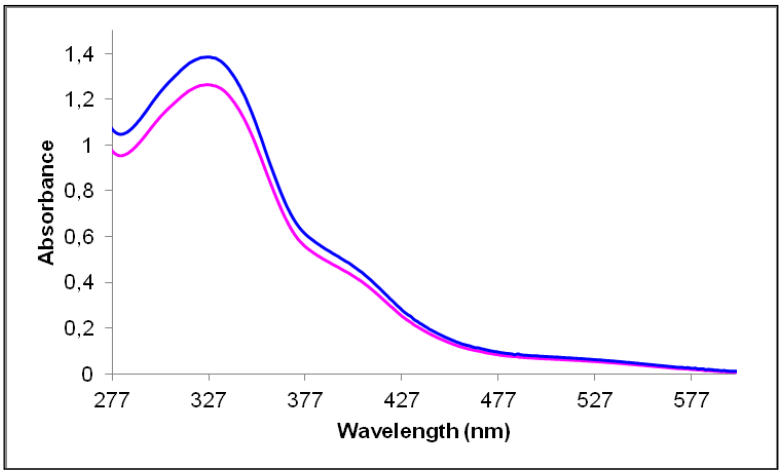

Fig. S163. UV/Vis spectra of **A1** in CH_3CN. Before (blue line) and after (pink line) irradiation at 348nm, $2.62 \cdot 10^{-5}$ M.

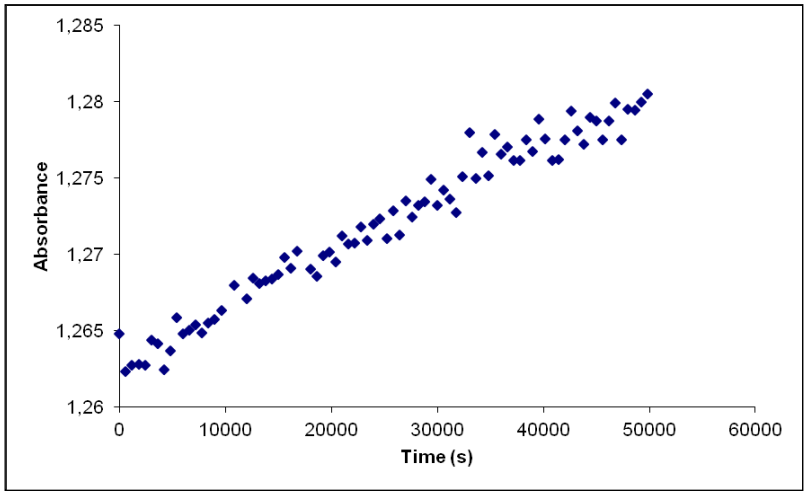

Fig. S164. Cis to trans thermal isomerization kinetics of **A1**. Absorption change of the band 327nm at 328 K in CH_3CN after irradiation at 348 nm. ($2.62 \cdot 10^{-5}$ M).

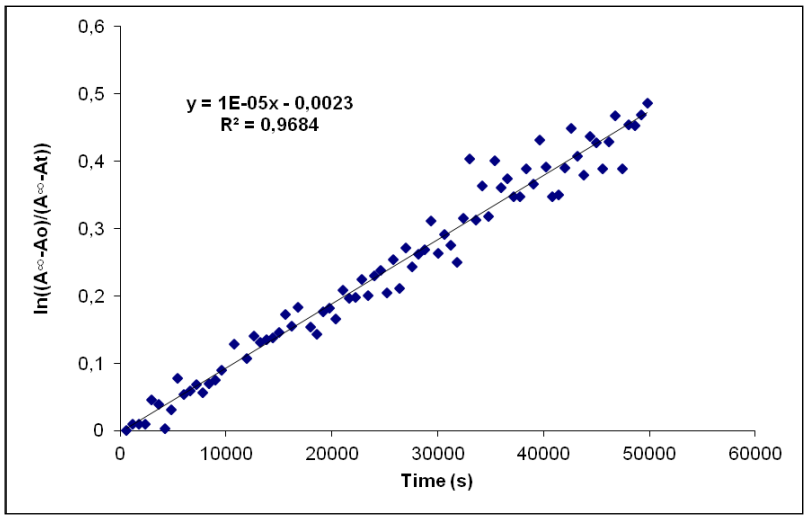

Fig. S165. Cis to trans thermal isomerization kinetics of **A1**. First-order plot. k (s^{-1}) = $1.0 \cdot 10^{-5}$. Half-life (min) = 1155.

Compound B1, $[Ir(Fppy)_2(1)]PF_6$. Synthesis, characterization and photoisomerization studies.

SYNTHESIS

Under a N_2 atmosphere, $[Ir(Fppy)_2Cl]_2$ (0.100 g, 0.082 mmol) were added over a suspension of **L1** (0.06 g, 0.164 mmol) in 8 ml CH_2Cl_2–MeOH 2/1. The reaction mixture was refluxed, under N_2, for 15 h. After solvent evaporation, the insoluble portion in CH_2Cl_2 was removed and the product was purified by column chromatography (silica gel, CH_2Cl_2). When the unreacted $[Ir(Fppy)_2Cl]_2$ eluted, 0.05 g of KPF_6 were added on top of the column and the polarity of the eluent was gradually increased to 100% acetone to elute $[Ir(Fppy)_2(\mathbf{L1})PF_6$ together with the excess of KPF_6. The desired compound, purified by filtration through a celite path in CH_2Cl_2, was obtained as a dark red solid. Yield 88%.

Elemental Analysis: calculated for ($C_{44}H_{28}F_4IrN_8PF_6 \cdot CH_2Cl_2$): C, 46.32; H, 2.59; N, 9.60. Found: C, 46.19; H, 2.72; N, 9.46.

Exact Mass: ESI-MS $[C_{44}H_{28}F_4IrN_8]^+$: calculated: m/z= 937.2002, found: m/z= 937.2034.

^{1}H NMR (300 MHz, acetone-d_6): δ 9.43 (d, J = 1.8 Hz, 1H), 8.51 (d, J = 5.9 Hz, 1H), 8.47 (d, J = 8.4 Hz, 1H), 8.17 (d, J = 5.9 Hz, 1H), 8.10 (m, 4H), 7.74 (m, 3H), 7.31 (ddd, J = 1.3 Hz, J = 5.9 Hz, J = 7.3 Hz, 1H), 6.84 (ddd, J = 2.4 Hz, J = 9.4 Hz, J = 12.6 Hz, 1H), 5.89 (dd, J = 2.4 Hz, J = 8.6 Hz, 1H).

^{13}C APT NMR (75 MHz, acetone-d_6): δ 165.08 (d, J = 6.7 Hz, C_{quat}), 164.95 (dd, J = 12.4 Hz, J = 253.5 Hz, C_{quat}), 162.78 (dd, J = 12.5 Hz, J = 258.3 Hz, C_{quat}), 160.54 (s, C_{quat}), 159.11 (s, C_{quat}), 155.44 (d, J = 6.5 Hz, C_{quat}), 154.22 (s, CH), 153.71 (s, C_{quat}), 151.46 (s, CH), 141.27 (s, CH), 135.29 (s, CH), 131.10 (s, 2CH), 129.29 (s, C_{quat}), 125.62 (s, CH), 125.08 (d, J = 19.2 Hz, CH), 125.06 (s, 2CH), 122.05 (s, CH), 120.31 (s, CH), 115.15 (d, J = 19.6 Hz, CH), 100.30 (t, J = 26.9 Hz, CH).

UV/Vis (CH_3CN), λ, nm (ε, 10^4 M^{-1} cm^{-1}): 328 (4.5), 479 (0.31).

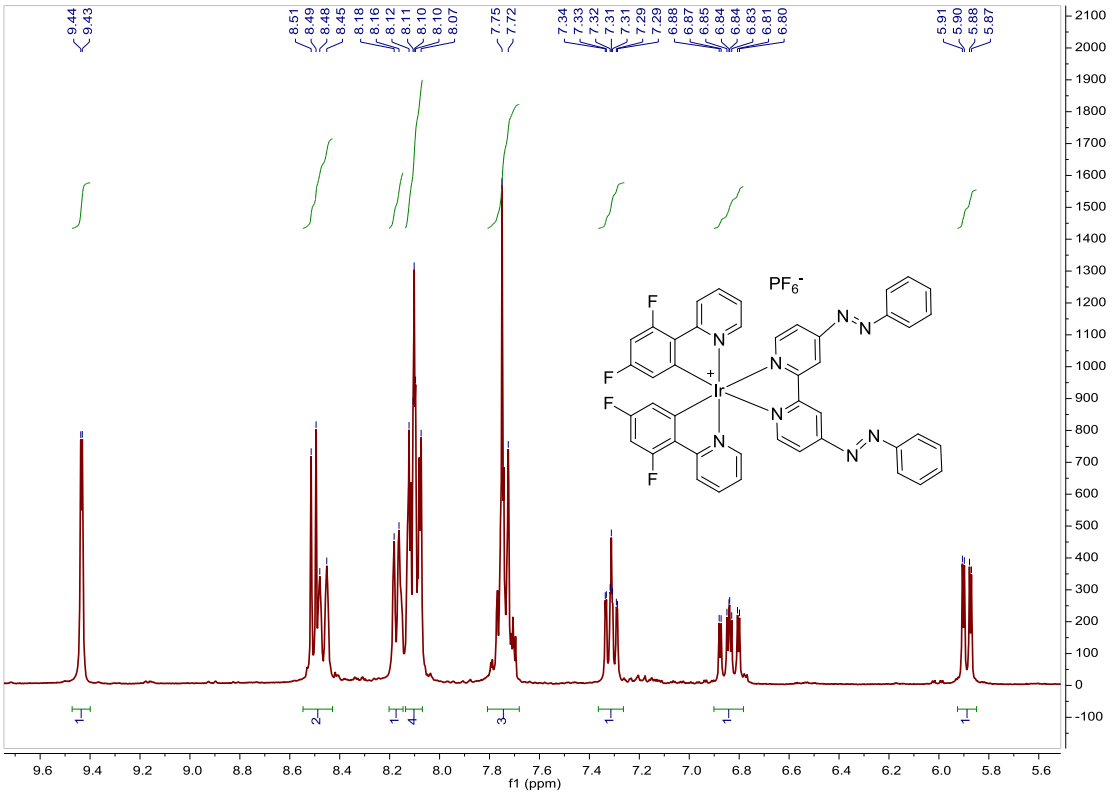

Fig. S166. ^{1}H NMR spectrum of **B1** in acetone-d_6, 300 MHz.

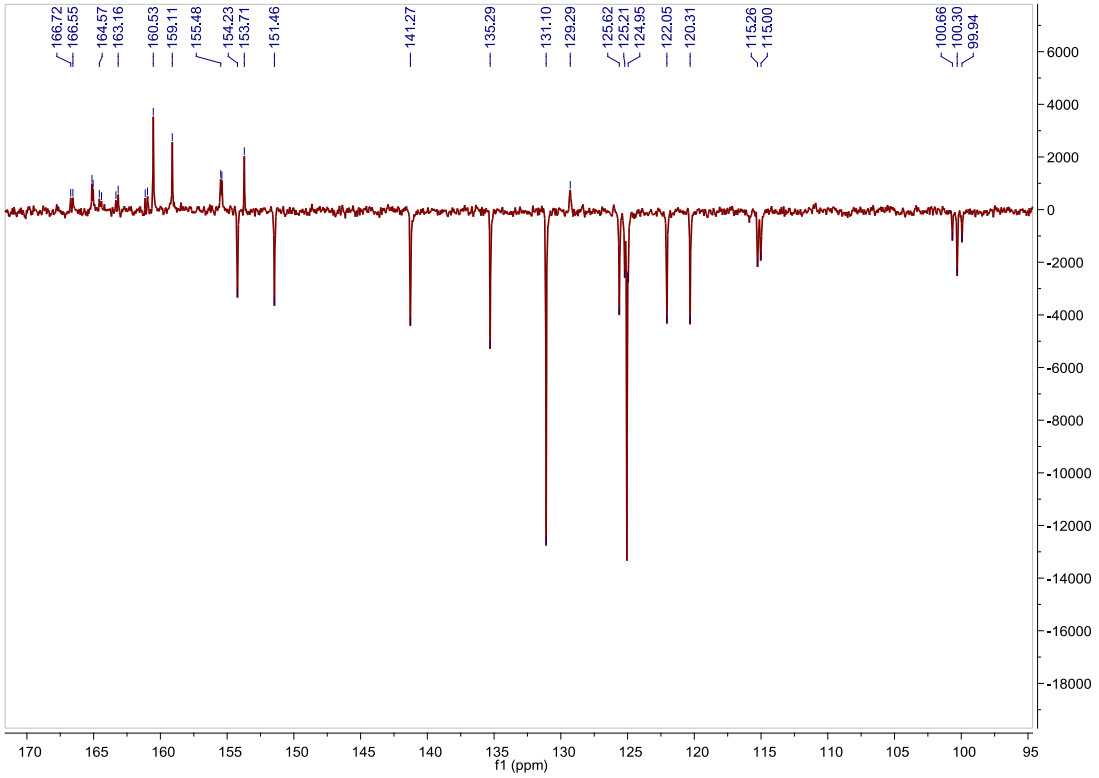

Fig. S167. ^{13}C APT NMR spectrum of **B1** in acetone-d_6, 75 MHz.

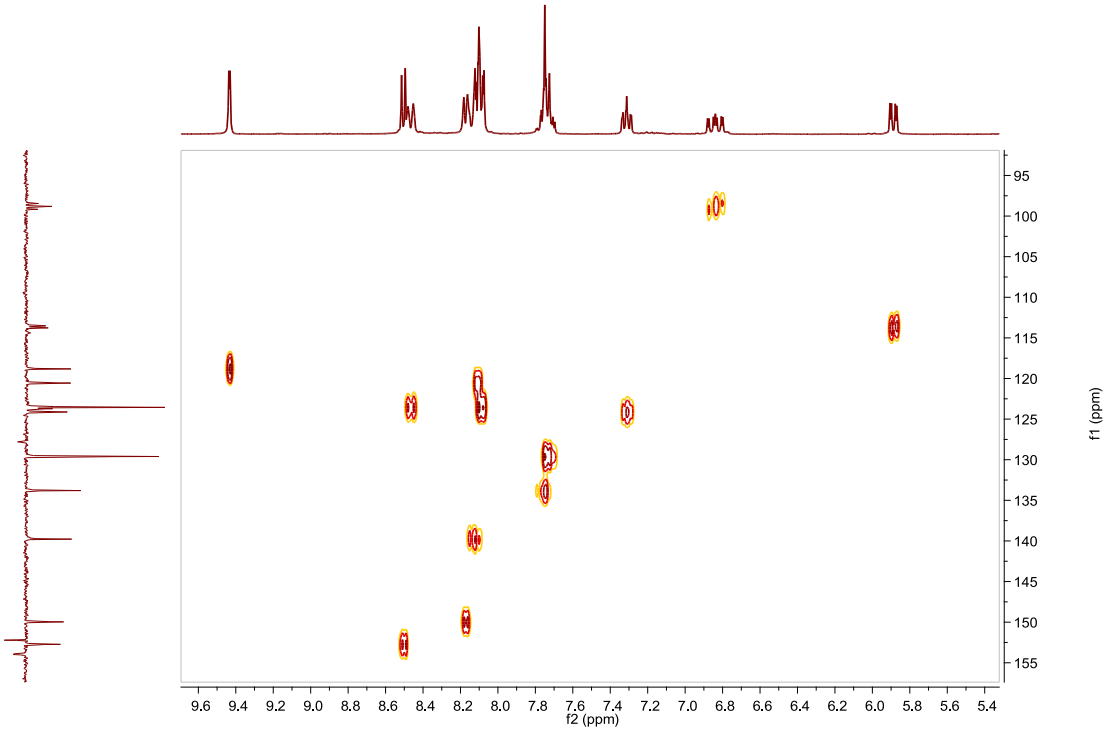

Fig. S168. HSQC NMR spectrum of **B1** in acetone-d_6.

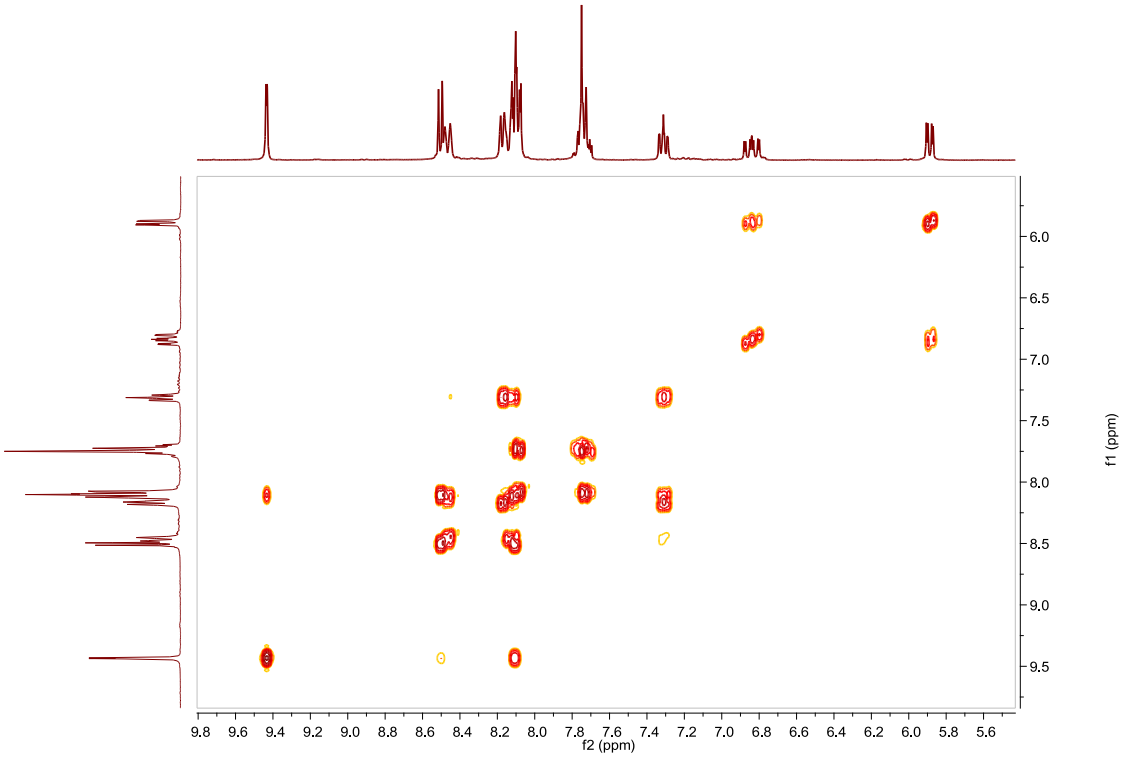

Fig. S169. COSY NMR spectrum of **B1** in acetone-d_6.

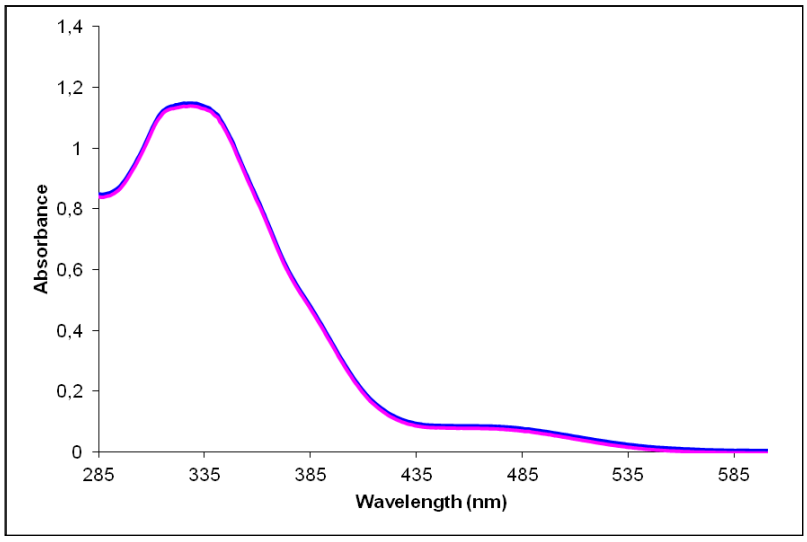

Fig. S170. UV/Vis spectra of **B1** in CH_3CN. Before (blue line) and after (pink line) irradiation at 326nm, $2.55 \cdot 10^{-5}$ M.

Cis to trans thermal isomerization kinetics. Due to the small degree of photoisomerization, it has been not possible to calculate k.

Compound C1, $[Ir(Brppy)_2(1)]PF_6$. Synthesis, characterization and photoisomerization studies.

SYNTHESIS

Under a N_2 atmosphere, $[Ir(Brppy)_2Cl]_2$ (0.200 g, 0.144 mmol) were added over a suspension of **L1** (0.105 g, 0.288 mmol) in 16 ml CH_2Cl_2–MeOH 2/1. The reaction mixture was refluxed, under N_2, for 15 h. After solvent evaporation the product was purified by column chromatography (silica gel, CH_2Cl_2). When the unreacted $[Ir(Brppy)_2Cl]_2$ eluted, 0.1 g of KPF_6 were added on top of the column and the polarity of the eluent was gradually increased to 100% acetone to elute $[Ir(Brppy)_2(\mathbf{L1})]PF_6$ together with the excess of KPF_6. The desired compound was precipitated with ether after filtration through a celite path in CH_2Cl_2 and it was obtained as a dark red solid. Yield 61%.

Elemental Analysis: calculated for ($C_{44}H_{30}Br_2IrN_8PF_6$): C, 45.26; H, 2.59; N, 9.60. Found: C, 45.22; H, 2.51; N, 9.47.

Exact Mass: ESI-MS $[C_{44}H_{30}Br_2IrN_8]^+$: calculated: m/z= 1021.0589, found: m/z= 1021.0573.

^{1}H NMR (300 MHz, acetone-d_6): δ 9.41 (d, J = 1.6 Hz, 1H), 8.45 (d, J = 5.8 Hz, 1H), 8.35 (d, J = 8.0 Hz, 1H), 8.14–8.03 (m, 5H), 7.96 (d, J = 8.4 Hz, 1H), 7.73 (brd, J = 7.0 Hz, 3H), 7.33 (dd, J = 1.8 Hz, J = 8.3 Hz, 1H), 7.28 (d, J = 6.1 Hz, 1H), 6.49 (d, J = 1.9 Hz, 1H).

^{13}C APT NMR (75 MHz, acetone-d_6): δ 167.67 (C_{quat}), 160.38 (C_{quat}), 159.20 (C_{quat}), 154.07 (CH), 153.72 (C_{quat}), 153.43 (C_{quat}), 151.17 (CH), 144.74 (C_{quat}), 140.72 (CH), 135.24 (CH), 135.12 (CH), 131.10 (2CH), 128.17 (CH), 127.38 (CH), 126.30 (C_{quat}), 125.79 (CH), 125.06 (2CH), 122.04 (CH), 121.95 (CH), 120.14 (CH).

UV/Vis (CH_3CN), λ, nm (ε, 10^4 M^{-1} cm^{-1}): 325 (5.3), 392 (2.0), 481 (0.32).

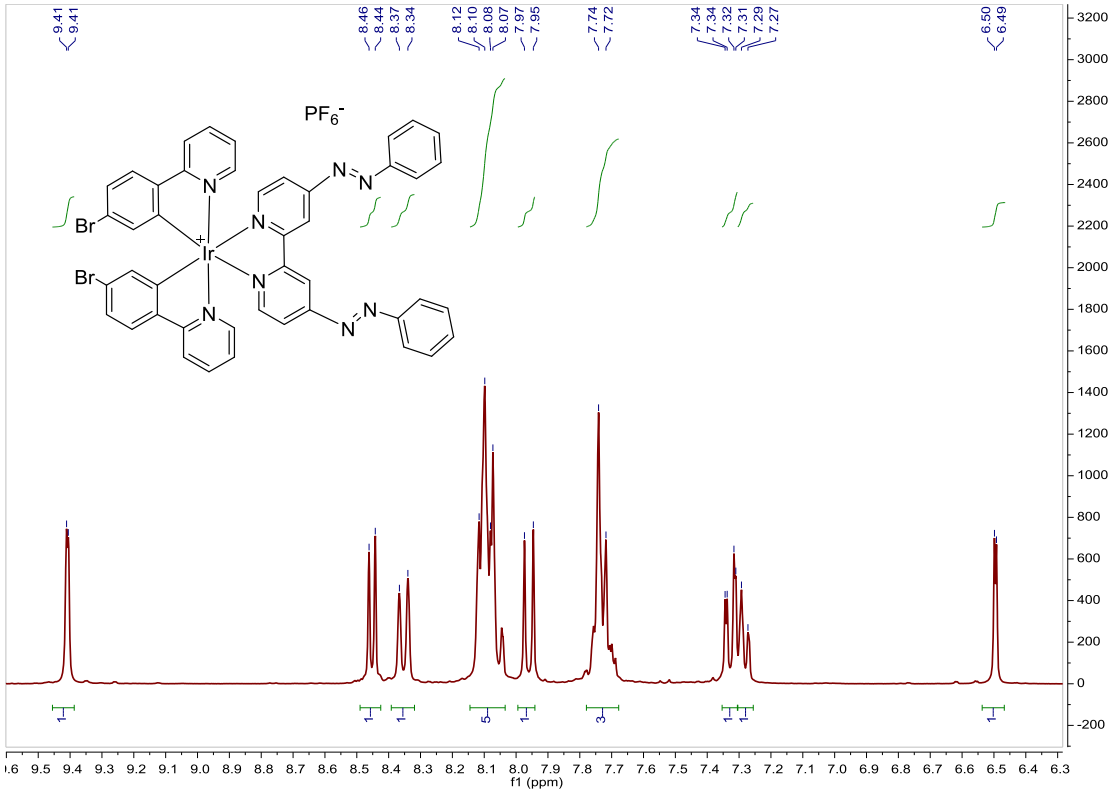

Fig. S171. ^{1}H NMR spectrum of **C1** in acetone-d_6, 300 MHz.

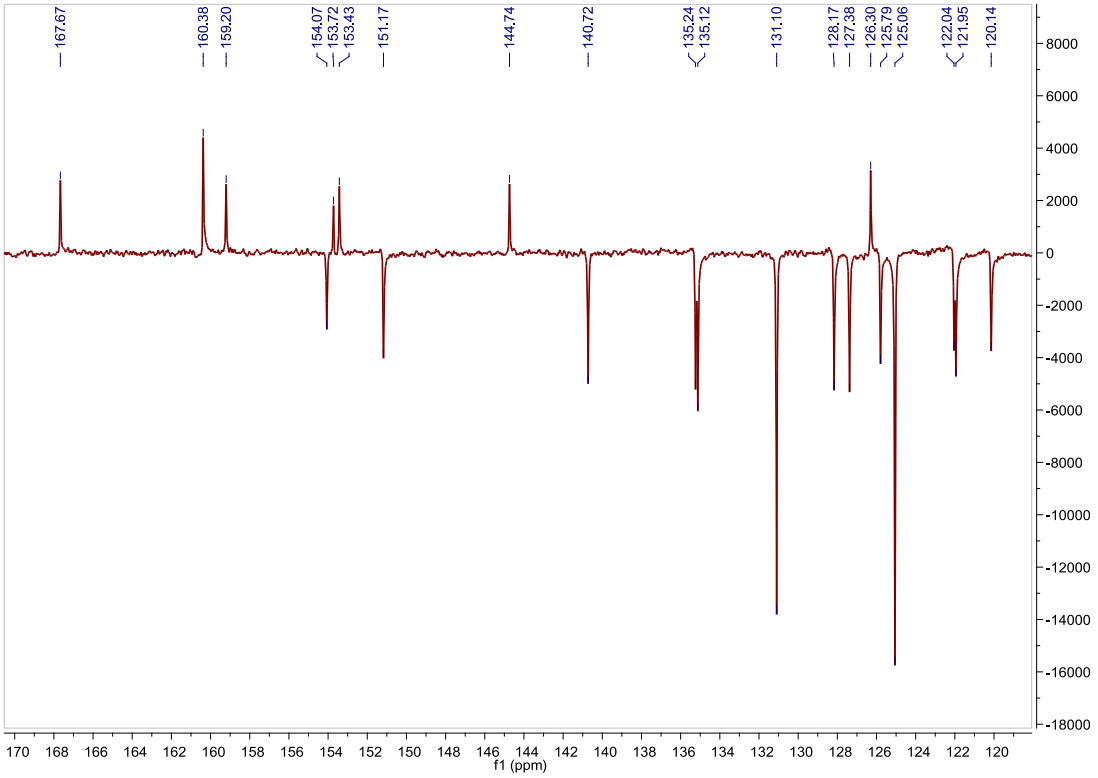

Fig. S172. ^{13}C APT NMR spectrum of **C1** in acetone-d_6, 75 MHz.

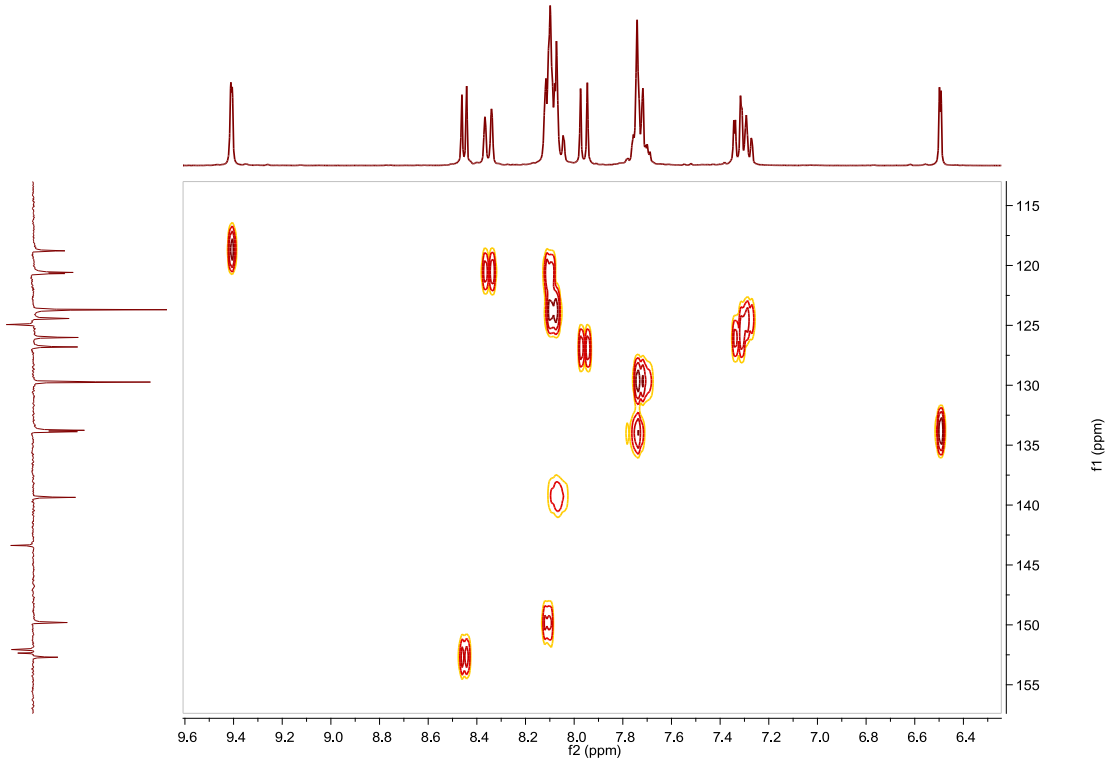

Fig. S173. HSQC NMR spectrum of **C1** in acetone-d_6.

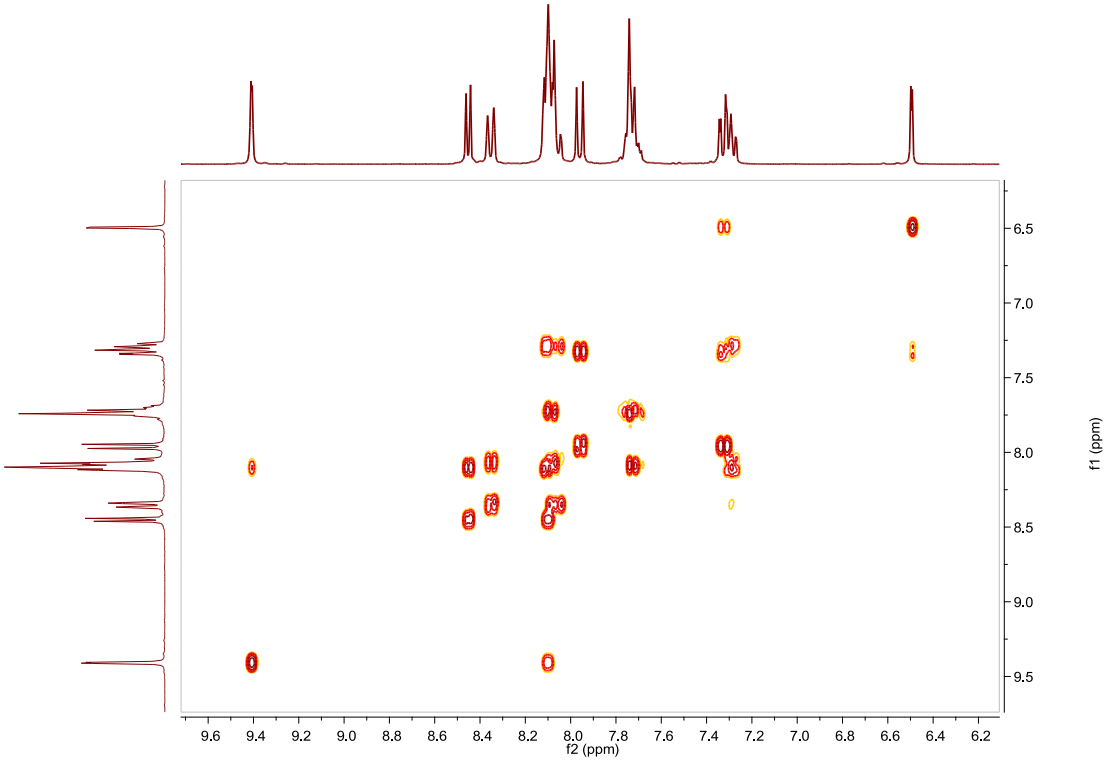

Fig. S174. COSY NMR spectrum of **C1** in acetone-d_6.

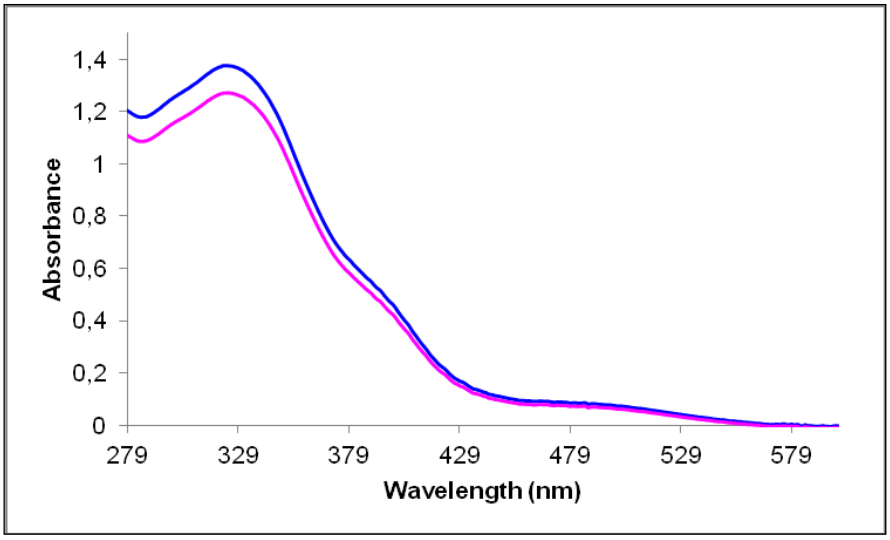

Fig. S175. UV/Vis spectra of **C1** in CH_3CN. Before (blue line) and after (pink line) irradiation at 341nm, $2.60 \cdot 10^{-5}$ M.

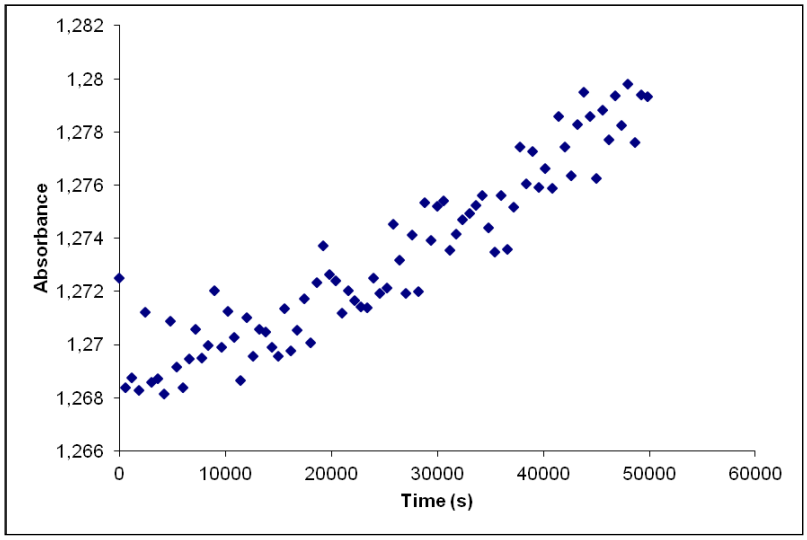

Fig. S176. Cis to trans thermal isomerization kinetics of **C1**. Absorption change of the band 325nm at 328 K in CH_3CN after irradiation at 341 nm. ($2.60 \cdot 10^{-5}$ M).

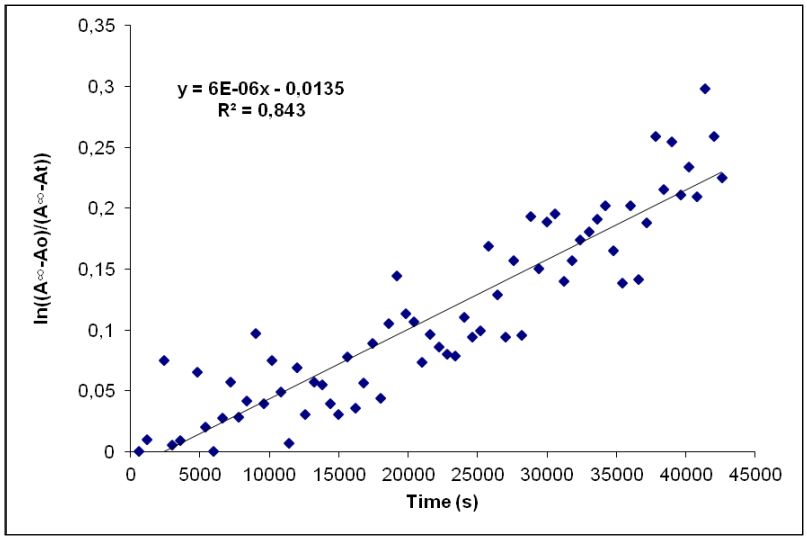

Fig. S177. Cis to trans thermal isomerization kinetics of **C1**. First-order plot. k (s^{-1}) = $6.0 \cdot 10^{-6}$. Half-life (min) = 1925.

Compound D1, [Ir(azoppy)$_2$(1)]PF$_6$. Synthesis, characterization and photoisomerization studies.

SYNTHESIS

Under a N_2 atmosphere, **C1** (0.150 g, 0.128 mmol) and [4-(phenylazo)phenyl]boronic acid **9** (0.07 g, 0.311 mmol) were dissolved in 5 ml of THF. Na_2CO_3 (1 M (aq), 2.5 mL) and $Pd(PPh_3)_4$ (0.0148 g, 0.0128mmol) were added and the solution was degassed by bubbling N_2 for 15 min. The reaction mixture was refluxed (80 °C) for 15 h. The resulting mixture was cooled down to room temperature and the product was extracted with CH_2Cl_2. The organic phase was dried with $MgSO_4$, filtered off and the solvent was evaporated. The residue was purified by column chromatography (silica gel, CH_2Cl_2). To the fraction containing the eluted complex, 0.05 g of KPF_6 were added and the resulting solution was filtered through a celite path. The title compound was obtained as a brown solid. Yield 34%.

Elemental Analysis: calculated for ($C_{68}H_{48}IrN_{12}PF_6 \cdot CH_3COCH_3$): C, 59.70; H, 3.81; N, 11.77. Found: C, 59.87; H, 4.04; N, 11.76.

Exact Mass: ESI-MS $[C_{68}H_{48}IrN_{12}]^+$: calculated: m/z= 1225.3754, found: m/z= 1225.3784.

^{1}H NMR (300 MHz, DMSO-*d*$_6$): δ 9.50 (s, 1H), 8.44 (d, J = 8.2 Hz, 1H), 8.28 (d, J = 5.9 Hz, 1H), 8.18–7.97 (m, 6H), 7.95–7.86 (m, 4H), 7.78–7.69 (m, 3H), 7.61 (brt, J = 6.7 Hz, 5H), 7.51 (d, J = 7.1 Hz, 1H), 7.30 (t, J = 6.4 Hz, 1H), 6.57 (s, 1H).

^{13}C APT NMR (75 MHz, DMSO-*d*$_6$): δ 166.14 (C_{quat}), 158.35 (C_{quat}), 157.42 (C_{quat}), 152.25 (CH), 151.96 (C_{quat}), 151.89 (C_{quat}), 151.05 (C_{quat}), 150.61 (C_{quat}), 149.81 (CH), 144.18 (C_{quat}), 142.96 (C_{quat}), 140.25 (C_{quat}), 139.14 (CH), 133.86 (CH), 131.60 (CH), 129.88 (2CH), 129.49 (2CH), 128.81 (CH), 127.42 (2CH), 125.71 (CH), 124.34 (CH), 123.46 (2CH), 123.19 (2CH), 122.54 (2CH), 122.06 (CH), 121.75 (CH), 120.59 (CH), 119.18 (CH).

UV/Vis (CH_3CN), λ, nm (ε, 10^4 M^{-1} cm^{-1}): 349 (9.3), 425 (2.4).

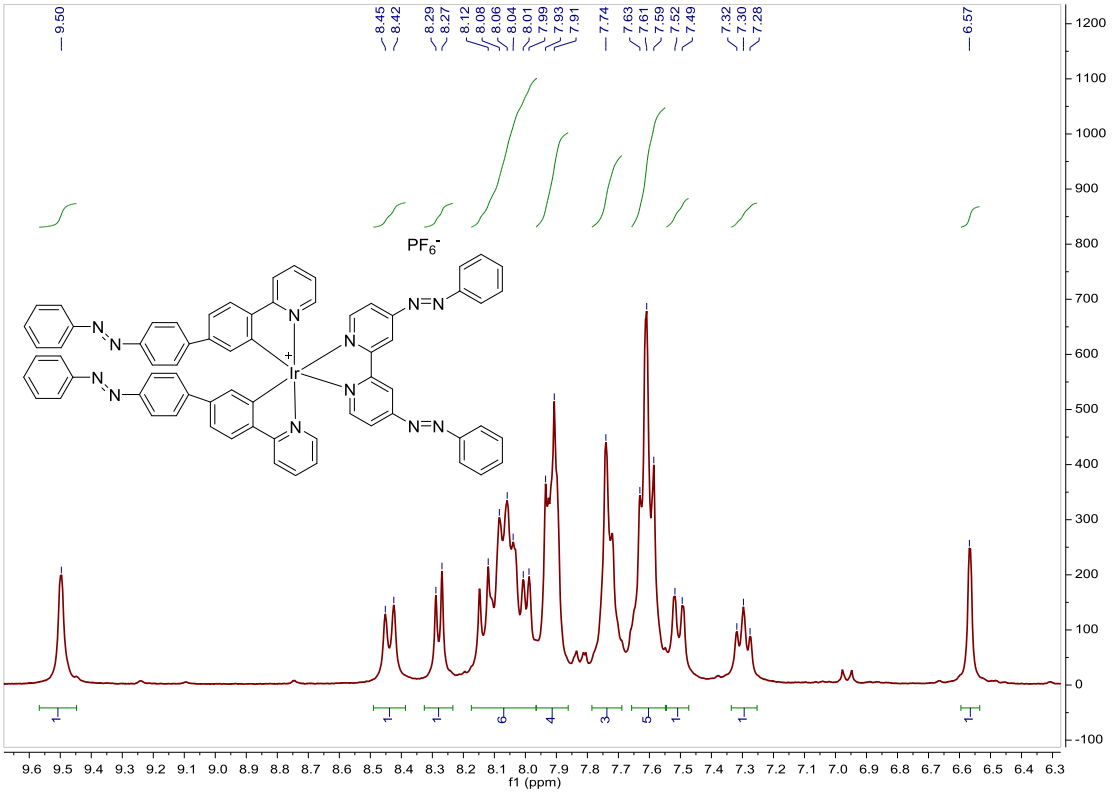

Fig. S178. ^{1}H NMR spectrum of **D1** in DMSO-*d*$_6$, 300 MHz.

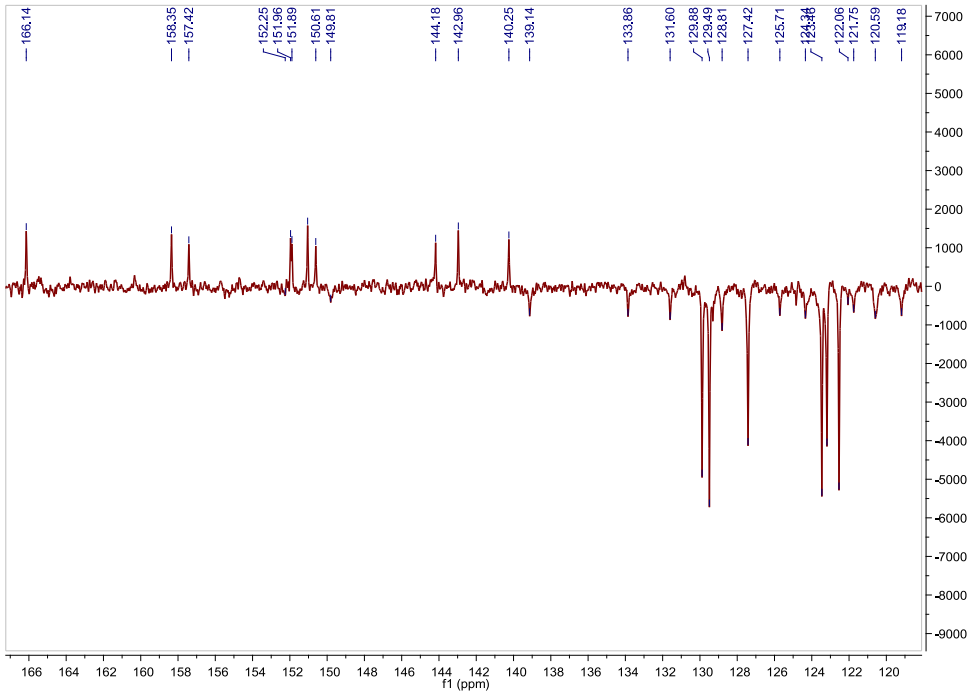

Fig. S179. ^{13}C APT NMR spectrum of **D1** in DMSO-d_6, 75 MHz.

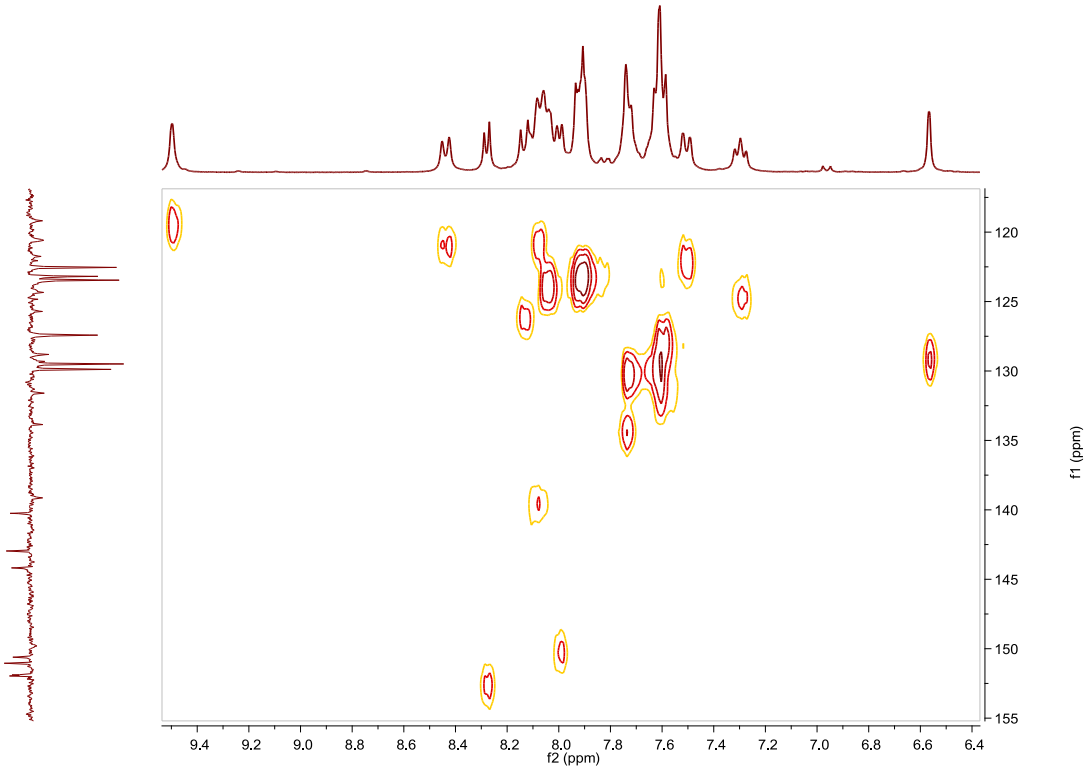

Fig. S180. HSQC NMR spectrum of **D1** in DMSO-d_6.

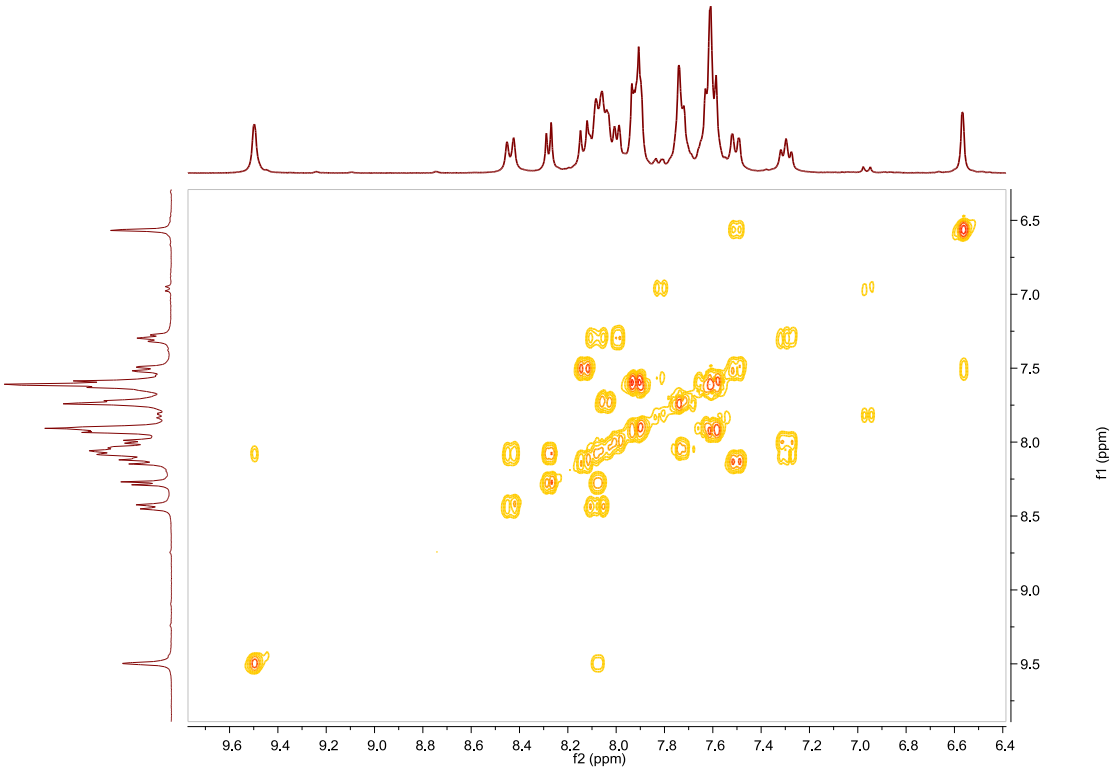

Fig. S181. COSY NMR spectrum of **D1** in DMSO-d_6.

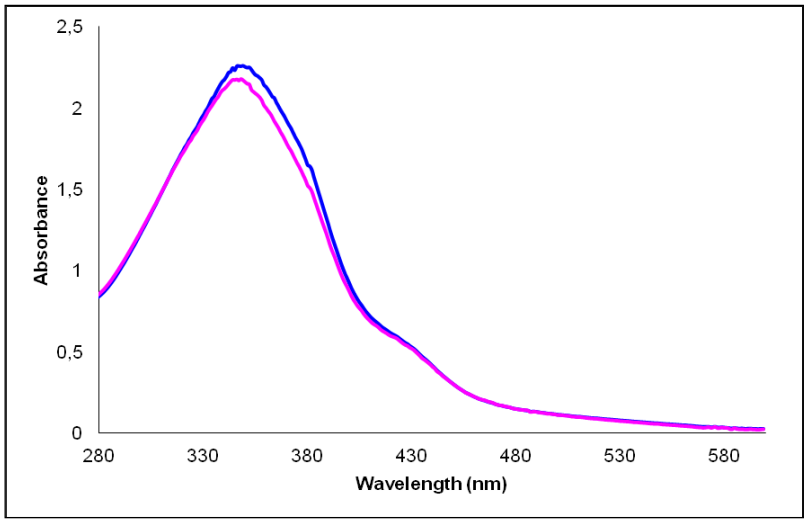

Fig. S182. UV/Vis spectra of **D1** in CH_3CN. Before (blue line) and after (pink line) irradiation at 364nm, $2.44 \cdot 10^{-5}$ M.

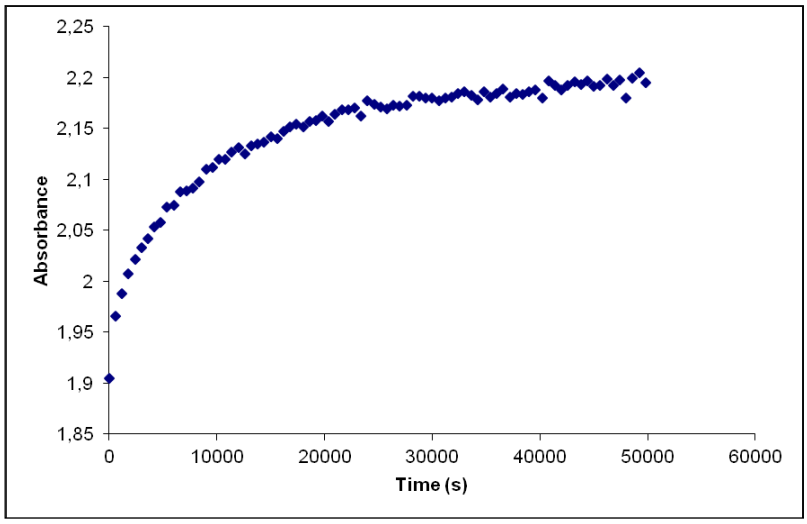

Fig. S183. Cis to trans thermal isomerization kinetics of **D1**. Absorption change of the band 349nm at 328 K in CH_3CN after irradiation at 364 nm. ($2.44 \cdot 10^{-5}$ M).

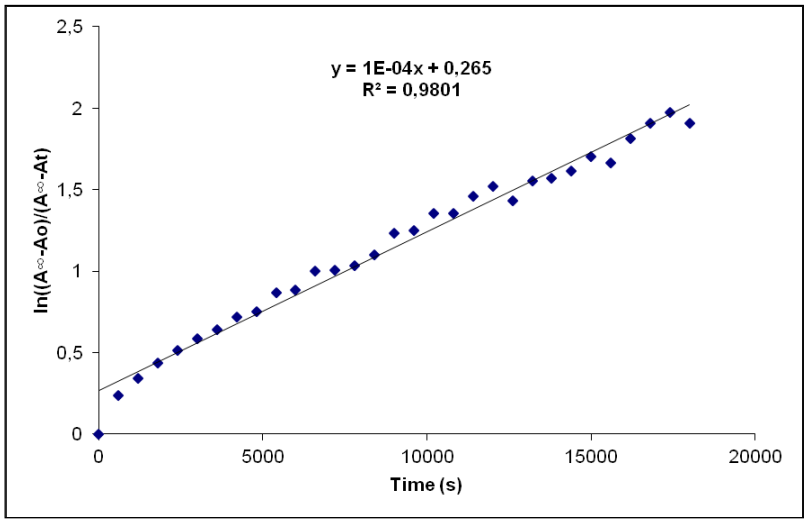

Fig. S184. Cis to trans thermal isomerization kinetics of **D1**. First-order plot. k (s^{-1}) = $1.0 \cdot 10^{-4}$. Half-life (min) = 115.

Compound A2, $[Ir(ppy)_2(2)_2]PF_6$. Synthesis, characterization and photoisomerization studies.

SYNTHESIS

Under a N_2 atmosphere, $[Ir(ppy)_2Cl]_2$ (0.100 g, 0.093 mmol) were dissolved in 8 ml of acetone and AgOTf (0.111 g, 0.432 mmol) were added. The mixture was heated to 56 °C for 2 h and after cooled down to room temperature, AgCl was removed by centrifugation. The resulting solution was added over a 1 h refluxed suspension of **L2** (0.068 g, 0.373 mmol) in 4 ml of acetone and 105 µl of NEt_3. The reaction mixture was refluxed, under N_2, for 15 h. After solvent evaporation the product was purified by column chromatography (silica gel, CH_2Cl_2). When the unreacted $[Ir(ppy)_2Cl]_2$ eluted, 0.05 g of KPF_6 were added on top of the column and the polarity of the eluent was gradually increased to 100% acetone to elute $[Ir(ppy)_2$(**L2**)$]PF_6$ together with the excess of KPF_6. The desired compound was precipitated with ether after filtration through a celite path in CH_2Cl_2 and it was obtained as an orange solid. Yield 50%.

Elemental Analysis: calculated for ($C_{44}H_{34}IrN_8PF_6$): C, 52.22; H, 3.39; N, 11.07. Found: C, 52.4; H, 2.95; N, 11.33.

Exact Mass: ESI-MS $[C_{44}H_{34}IrN_8]^+$: calculated: m/z= 867.2512, found: m/z= 867.2520.

^{1}H NMR (300 MHz, acetone-d_6): δ 9.11 (d, J = 5.3 Hz, 1H), 9.07 (brd, J = 6.8 Hz, 2H), 8.20 (d, J = 7.6 Hz, 1H), 8.12 (ddd, J = 1.4 Hz, J = 7.4 Hz, J = 8.7 Hz, 1H), 7.99 (brdd, J = 1.4 Hz, J = 8.1 Hz, 2H), 7.86 (brd, J = 6.7 Hz, 2H), 7.75 (m, 1H), 7.68 (m, 3H), 7.59 (ddd, J = 1.5 Hz, J = 5.9 Hz, J = 7.4 Hz, 1H), 6.97 (m, 2H), 6.51 (m, 1H).

^{13}C APT NMR (75 MHz, acetone-d_6): δ 169.33 (C_{quat}), 159.03 (C_{quat}), 155.47 (2CH), 153.76 (C_{quat}), 150.88 (CH), 149.03 (C_{quat}), 145.58 (C_{quat}), 140.42 (CH), 134.85 (CH), 133.40 (CH), 131.72 (CH), 130.97 (2CH), 125.81 (CH), 125.18 (CH), 124.80 (2CH), 124.05 (CH), 121.18 (CH), 120.10 (2CH).

UV/Vis (CH_3CN), λ, nm (ε, 10^4 M^{-1} cm^{-1}): 312 (4.7), 460 (0.37).

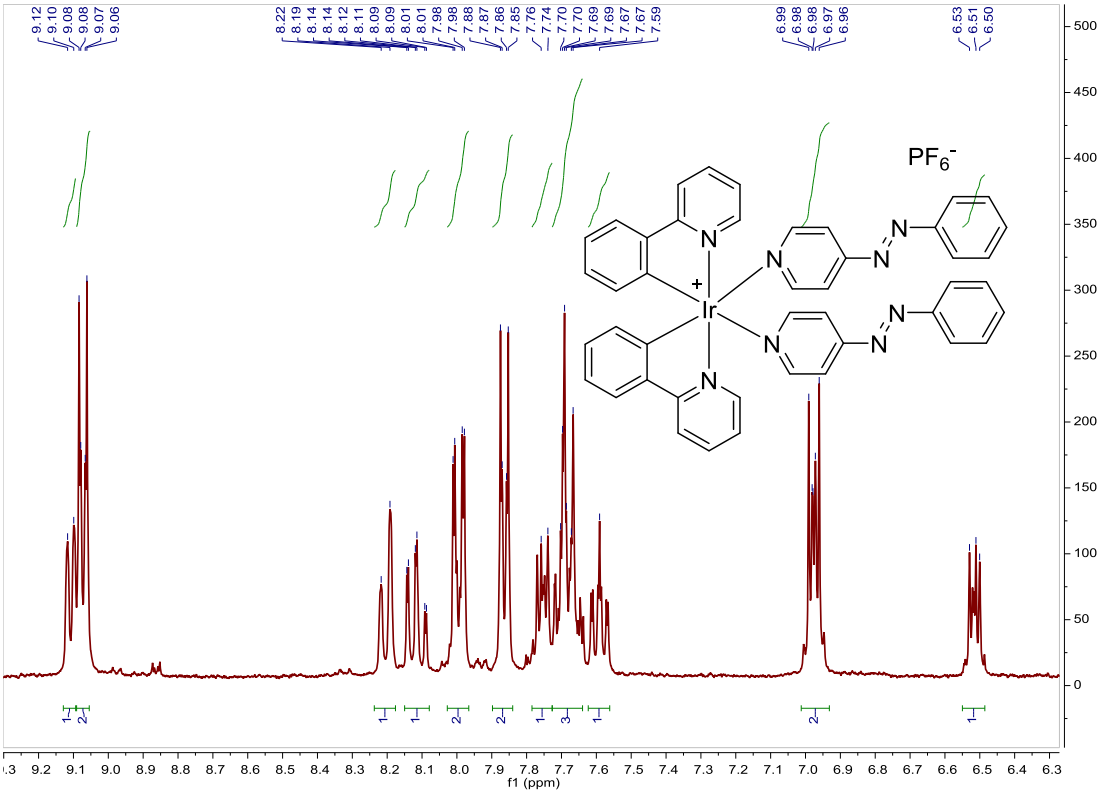

Fig. S185. ^{1}H NMR spectrum of **A2** in acetone-d_6, 300 MHz.

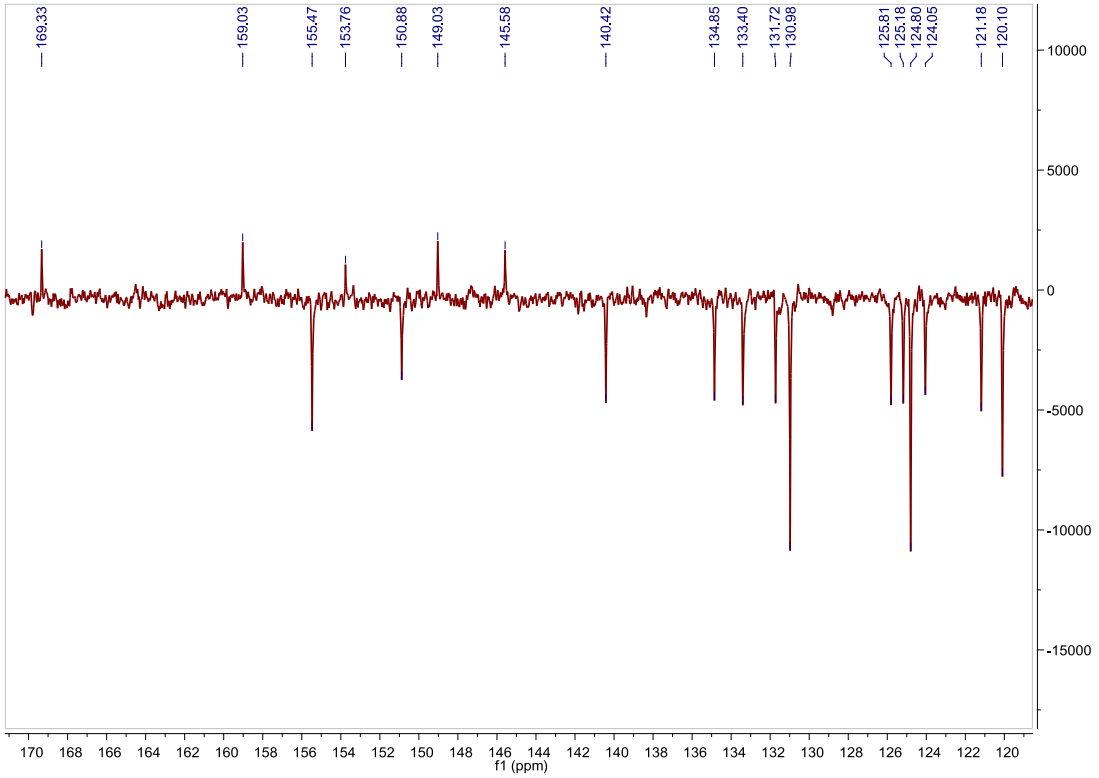

Fig. S186. ^{13}C APT NMR spectrum of **A2** in acetone-d_6, 75 MHz.

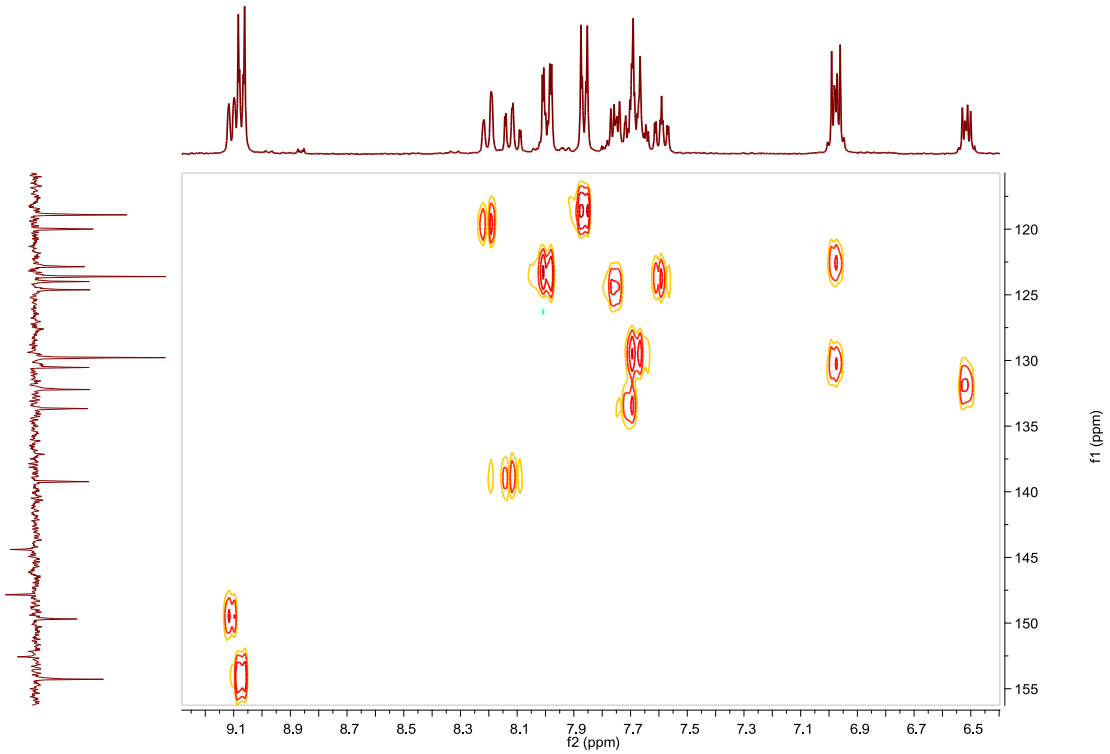

Fig. S187. HSQC NMR spectrum of **A2** in acetone-d_6.

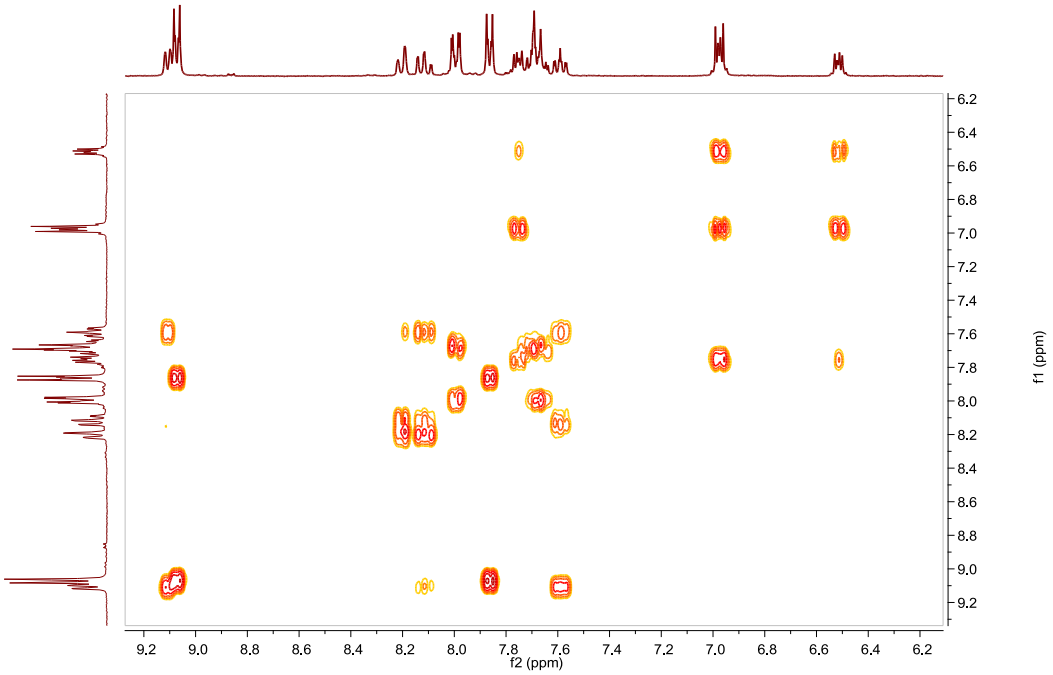

Fig. S188. COSY NMR spectrum of **A2** in acetone-d_6.

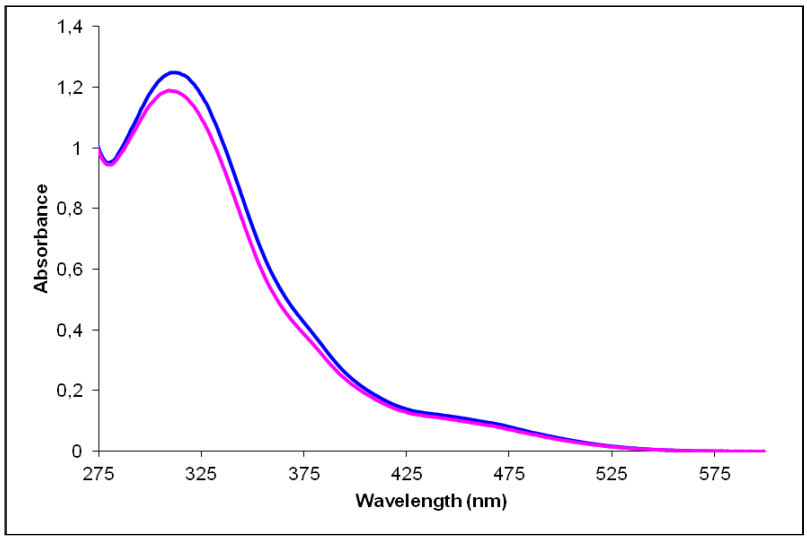

Fig. S189. UV/Vis spectra of **A2** in CH_3CN. Before (blue line) and after (pink line) irradiation at 327nm, $2.65 \cdot 10^{-5}$ M.

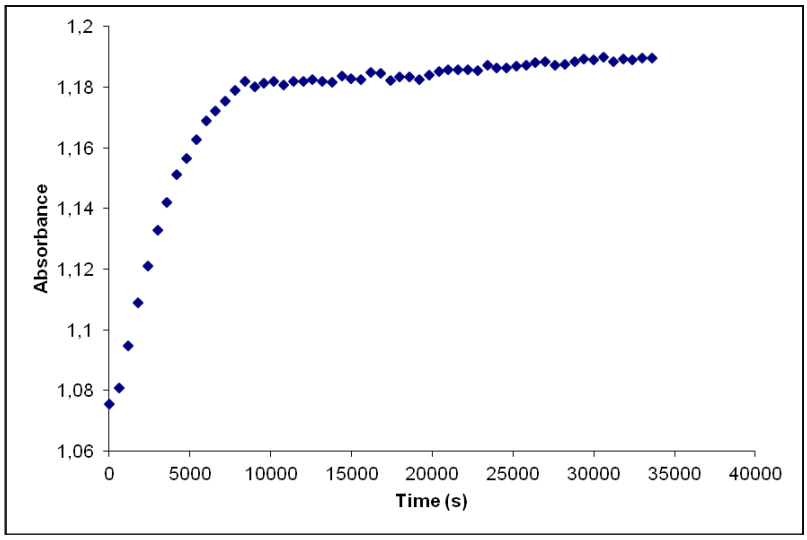

Fig. S190. Cis to trans thermal isomerization kinetics of **A2**. Absorption change of the band 312nm at 328 K in CH_3CN after irradiation at 327 nm. ($2.65 \cdot 10^{-5}$ M).

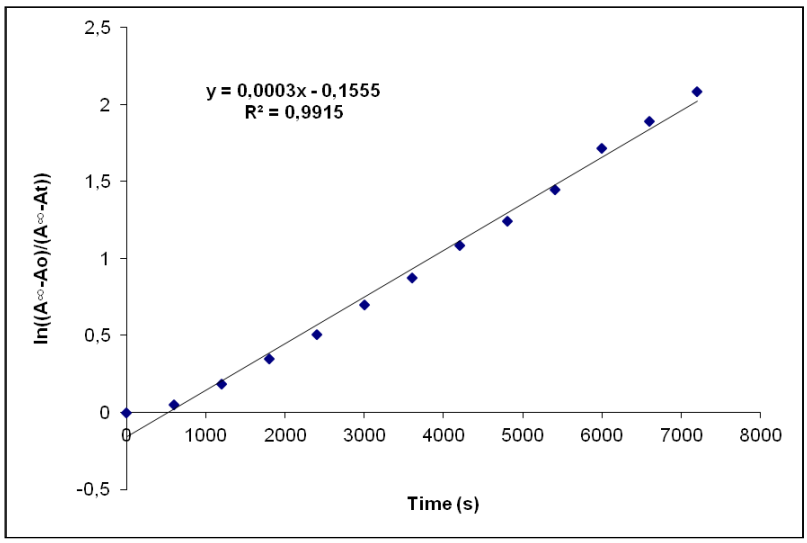

Fig. S191. Cis to trans thermal isomerization kinetics of **A2**. First-order plot. k (s^{-1}) = $3.0 \cdot 10^{-4}$. Half-life (min) = 38.

Compound B2', [Ir(Fppy)$_2$(2)]. Synthesis and characterization.

SYNTHESIS

Under a N_2 atmosphere, $[Ir(Fppy)_2Cl]_2$ (0.100 g, 0.082 mmol) were added over a suspension of **L2** (0.03 g, 0.164 mmol) in 8 ml CH_2Cl_2/MeOH 2/1. The reaction mixture was refluxed, under N_2, for 15 h. After solvent evaporation the product was purified by column chromatography (silica gel, 100% CH_2Cl_2 to 100% acetone). The product was obtained as an orange solid. Yield 87%.

Elemental Analysis: calculated for ($C_{33}H_{20}F_4IrN_5 \cdot CH_2Cl_2$): C, 48.63; H, 2.64; N, 8.34. Found: C, 48.97 ; H, 2.87 ; N, 8.21 .

Exact Mass: ESI-MS $[C_{33}H_{20}F_4IrN_5+H]^+$: calculated: m/z=756.1362 , found: m/z=756.1362.

^{1}H NMR (300 MHz, $CDCl_3$): δ 9.84 (dd, J = 1.0 Hz, J = 5.8 Hz, 1H), 8.24 (d, J = 8.5 Hz, 1H), 8.07 (d, J = 8.3 Hz, 1H), 8.00 (d, J = 5.7 Hz, 1H), 7.83 (dd, J = 1.6 Hz, J = 7.4 Hz, 2H), 7.75–7.62 (m, 2H), 7.56 (m, 2H), 7.50–7.38 (m, 4H), 7.17 (t, J = 6.3 Hz, 1H), 6.98 (ddd, J = 1.0 Hz, J = 5.8 Hz, J = 7.4 Hz, 1H), 6.34 (ddd, J = 2.4 Hz, J = 9.1 Hz, J = 11.8 Hz, 1H), 6.25 (ddd, J = 2.3 Hz, J = 9.3 Hz, J = 12.4 Hz, 1H), 5.73 (dd, J = 2.4 Hz, J = 8.6 Hz, 1H), 5.52 (dd, J = 2.4 Hz, J = 8.7 Hz, 1H).

^{13}C APT NMR (75 MHz, $CDCl_3$): δ 165.17 (d, J = 7.6 Hz, C_{quat}), 164.51 (d, J = 6.1 Hz, C_{quat}), 163.61 (dd, J = 12.9 Hz, J = 256.9 Hz, C_{quat}), 162.77 (dd, J = 12.6 Hz, J = 258.4 Hz, C_{quat}), 161.02 (dd, J = 12.9 Hz, J = 260.7 Hz, C_{quat}), 160.76 (dd, J = 12.9 Hz, J = 259.9 Hz, C_{quat}), 156.97 (s, 2C_{quat}), 154.13 (d, J = 6.8 Hz, C_{quat}), 152.26 (s, C_{quat}), 151.12 (d, J = 6.8 Hz, C_{quat}), 150.93 (s, CH), 148.86 (s, CH), 138.06 (s, CH), 137.69 (s, CH), 133.19 (s, CH), 129.37 (s, 3CH), 127.92 (s, C_{quat}), 127.79 (s, C_{quat}), 123.64 (s, 2CH), 123.36 (d, J = 20.5 Hz, CH), 122.51 (s, CH), 122.47 (d, J = 19.8 Hz, CH), 122.05 (s, CH), 118.15 (s, 2CH), 114.07 (d, J = 17.5 Hz, CH), 113.53 (d, J = 17.5 Hz, CH), 97.90 (t, J = 27.0 Hz, 2CH).

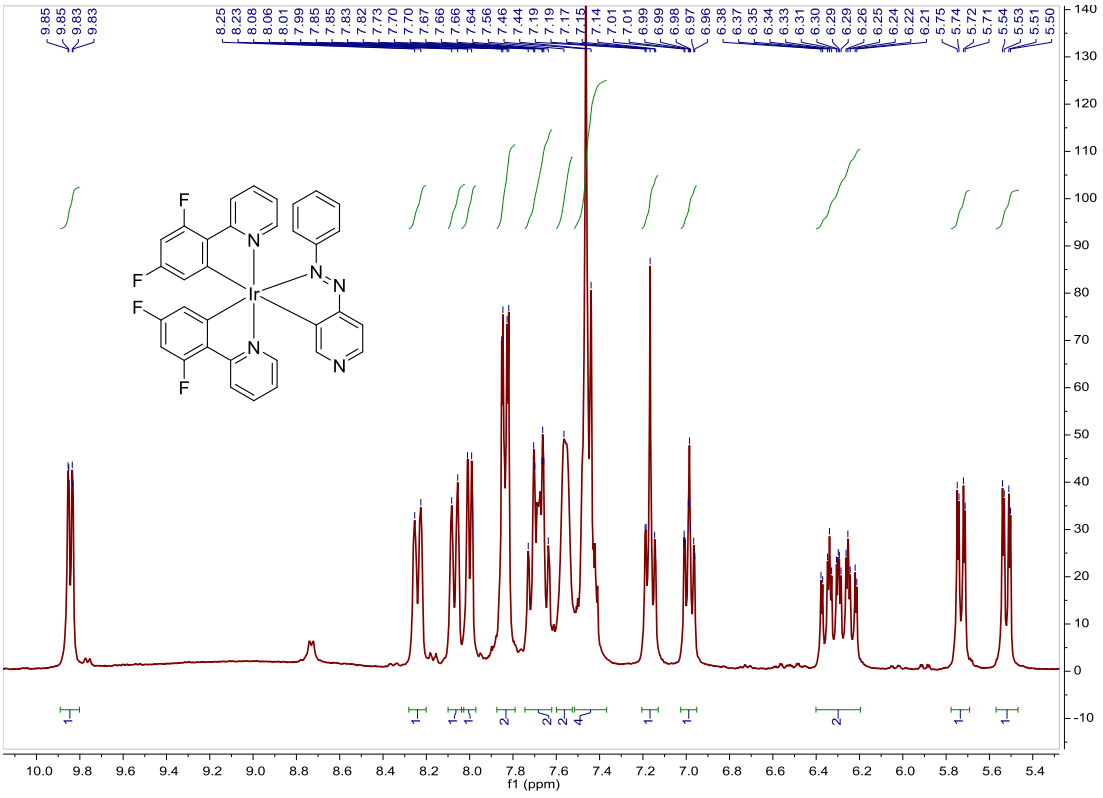

Fig. S192. ^{1}H NMR spectrum of **B2'** in $CDCl_3$, 300 MHz.

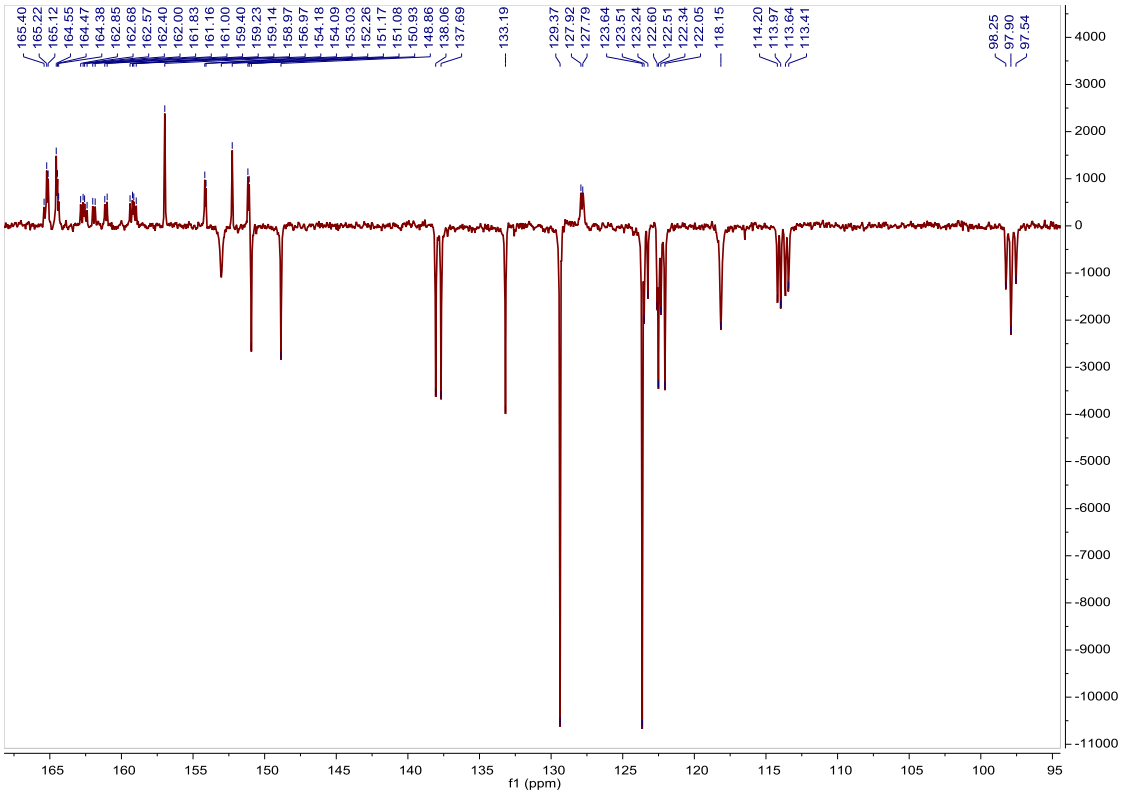

Fig. S193. ^{13}C APT NMR spectrum of **B2'** in $CDCl_3$, 75 MHz.

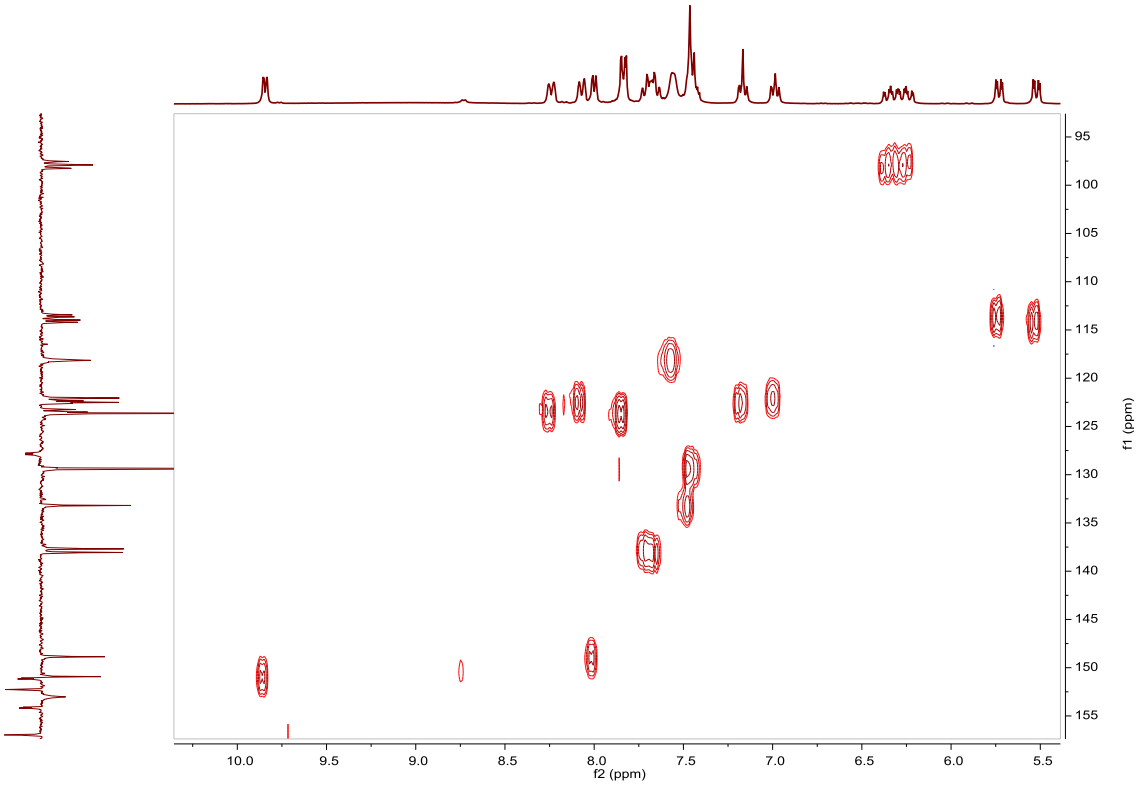

Fig. S194. HSQC NMR spectrum of **B2'** in $CDCl_3$.

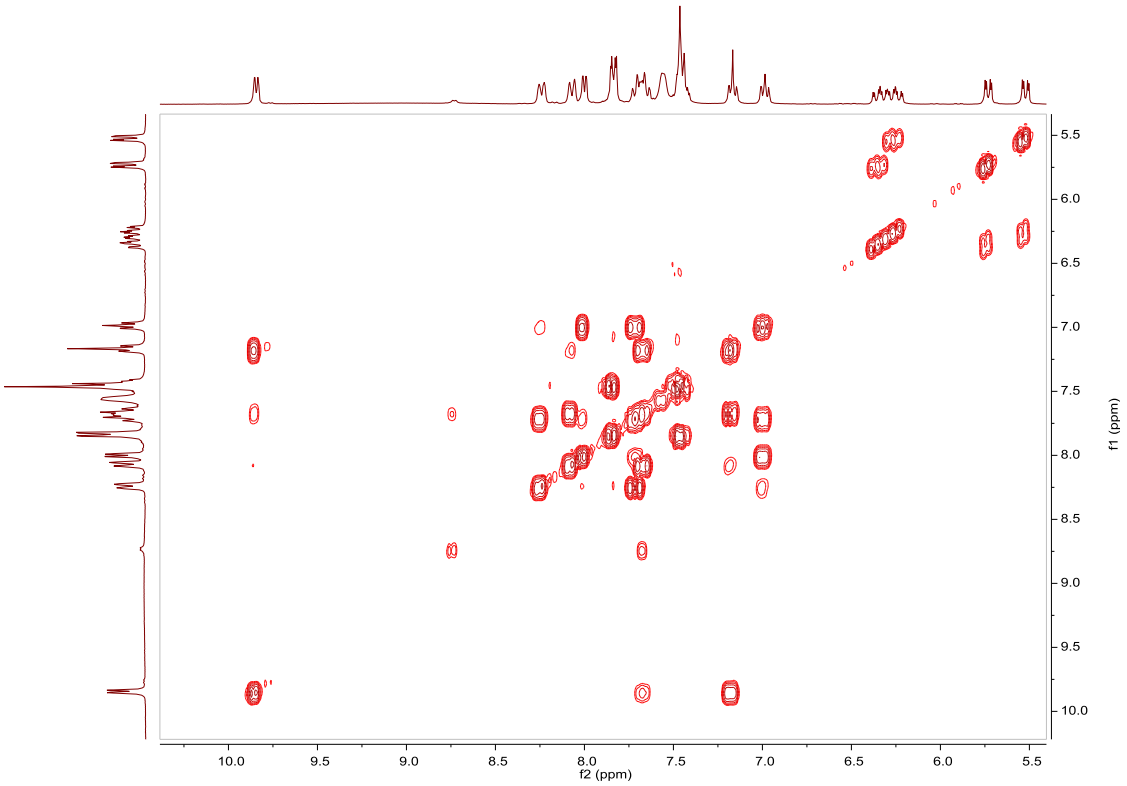

Fig. S195. COSY NMR spectrum of **B2'** in $CDCl_3$.

Compound B2, $[Ir(Fppy)_2(2)_2]PF_6$. Synthesis, characterization and photoisomerization studies.

SYNTHESIS

Under a N_2 atmosphere, $[Ir(Fppy)_2Cl]_2$ (0.150 g, 0.1234 mmol) were dissolved in 11 ml of acetone and AgOTf (0.111 g, 0.432 mmol) were added. The mixture was heated to 56 °C for 2 h and after cooled down to room temperature, AgCl was removed by centrifugation. The resulting solution was added over a 1 h refluxed suspension of **L2** (0.100 g, 0.4936 mmol) in 5 ml of acetone and 140 µl of NEt_3. The reaction mixture was refluxed, under N_2, for 15 h. After solvent evaporation the product was purified by column chromatography (silica gel, CH_2Cl_2). When the unreacted $[Ir(Fppy)_2Cl]_2$ eluted, 0.075 g of KPF_6 were added on top of the column and the polarity of the eluent was gradually increased to 100% acetone to elute $[Ir(Fppy)_2(\mathbf{L2})]PF_6$ together with the excess of KPF_6. The desired compound was precipitated with ether after filtration through a celite path in CH_2Cl_2 and it was obtained as an orange solid. Yield 48%.

Elemental Analysis: calculated for ($C_{44}H_{30}F_4IrN_8PF_6 \cdot CH_3COCH_3$): C, 49.43; H, 3.18; N, 9.81. Found: C, 49.71; H, 3.02; N, 10.16.

Exact Mass: ESI-MS $[C_{44}H_{30}F_4IrN_8]^+$: calculated: m/z= 939.2159, found: m/z= 939.2178.

^{1}H NMR (300 MHz, acetone-d_6): δ 9.22 (d, J = 5.5 Hz, 1H), 9.09 (brd, J = 6.7 Hz, 2H), 8.36 (d, J = 8.4 Hz, 1H), 8.22 (t, J = 7.8 Hz, 1H), 8.00 (brdd, J = 1.6 Hz, J = 8.3 Hz, 2H), 7.91 (brd, J = 6.7 Hz, 2H), 7.68 (m, 4H), 6.71 (ddd, J = 2.3 Hz, J = 9.3 Hz, J = 12.6 Hz, 1H), 6.01 (dd, J = 2.3 Hz, J = 8.5 Hz, 1H).

^{13}C APT NMR (75 MHz, acetone-d_6): δ 165.32 (d, J = 7.1 Hz, C_{quat}), 164.57 (dd, J = 12.4 Hz, J = 254.2 Hz, C_{quat}), 162.06 (dd, J = 13.6 Hz, J = 257.5 Hz, C_{quat}), 159.31 (s, C_{quat}), 155.55 (s, 2CH), 153.76 (s, C_{quat}), 153.31 (d, J = 6.6 Hz, C_{quat}), 151.67 (s, CH), 141.53 (s, CH), 134.93 (s, CH), 130.98 (s, 2CH), 129.41 (s, C_{quat}), 125.80 (s, CH), 124.90 (d, J = 20.5 Hz, CH), 124.85 (s, 2CH), 120.49 (s, 2CH), 115.82 (d, J = 18.0 Hz, CH), 100.32 (t, J = 27.1 Hz, CH).

UV/Vis (CH_3CN), λ, nm (ε, 10^4 M^{-1} cm^{-1}): 318 (4.8), 433 (0.37).

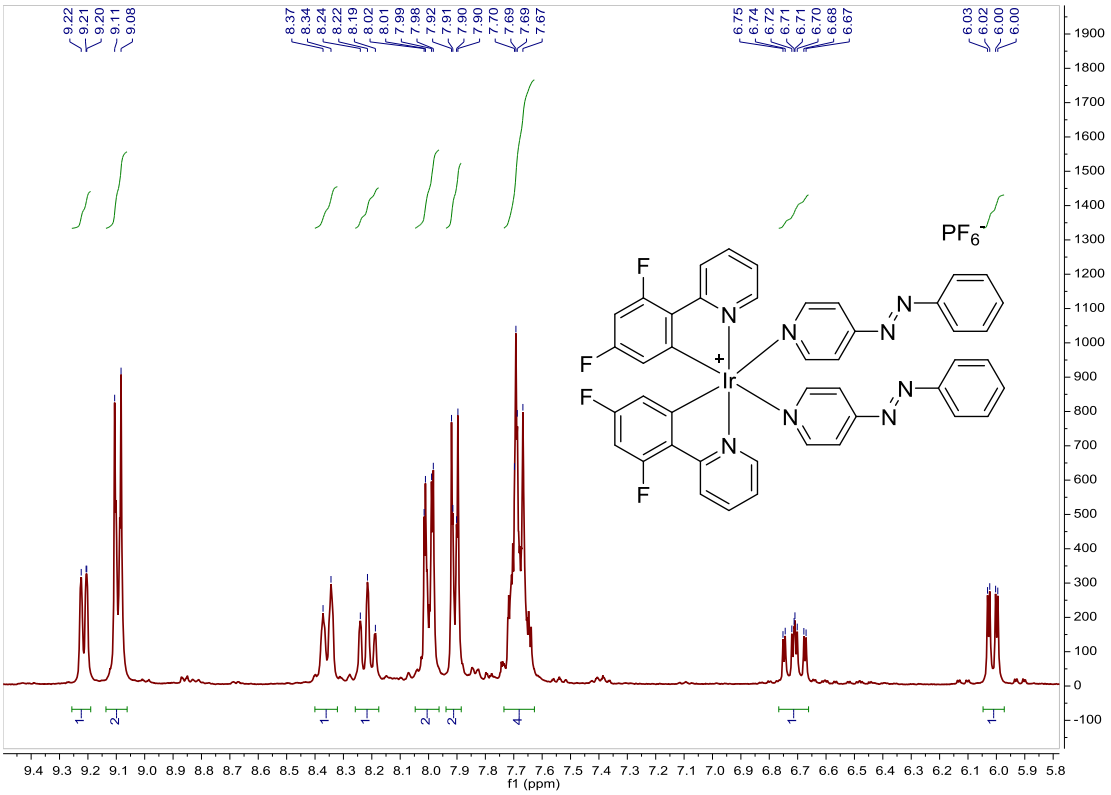

Fig. S196. ^{1}H NMR spectrum of **B2** in acetone-d_6, 300 MHz.

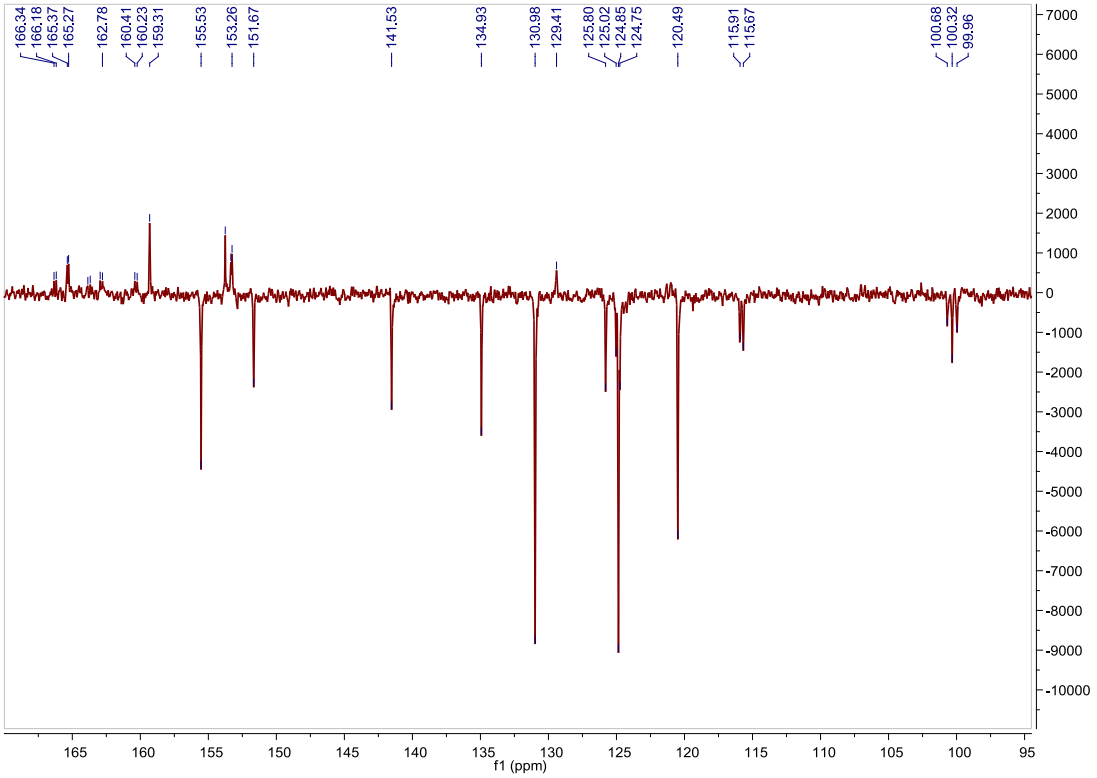

Fig. S197. ^{13}C APT NMR spectrum of **B2** in acetone-d_6, 75 MHz.

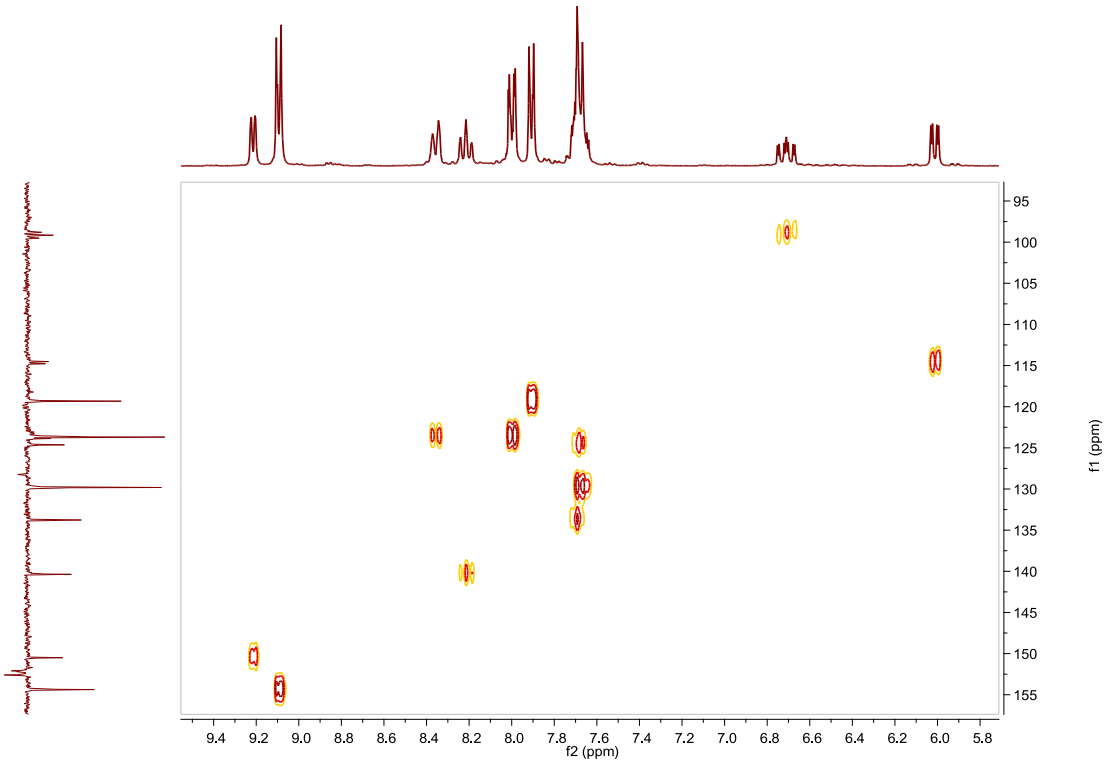

Fig. S198. HSQC NMR spectrum of **B2** in acetone-d_6.

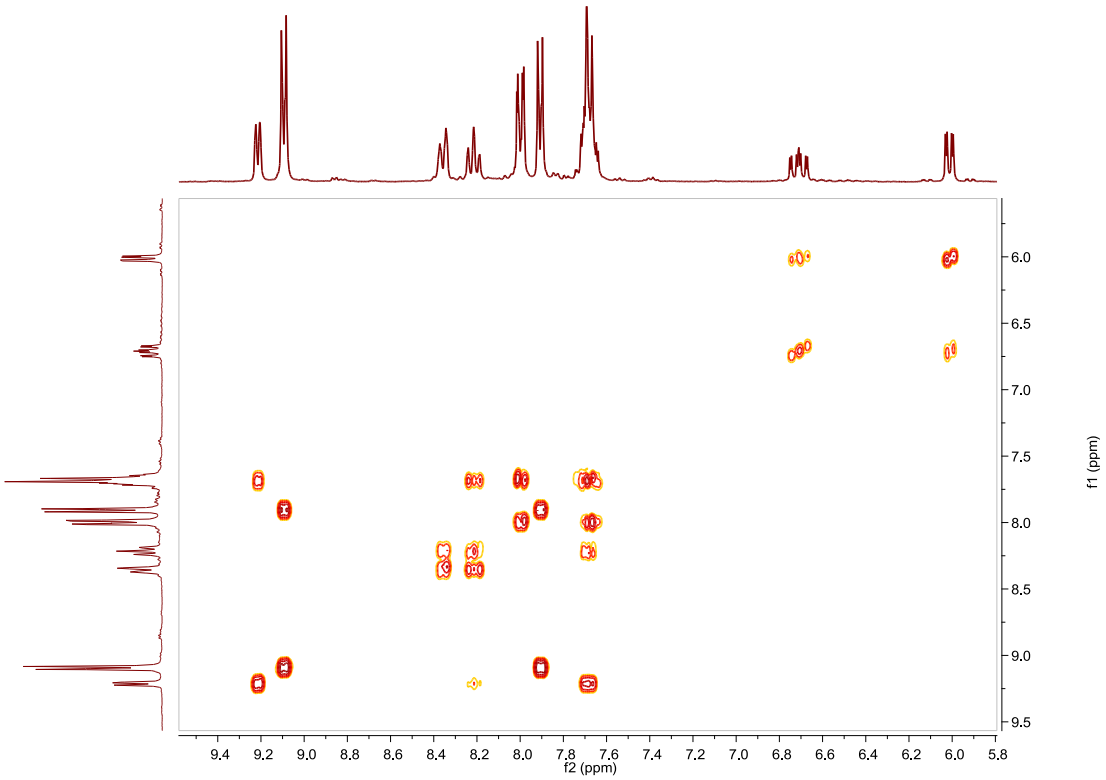

Fig. S199. COSY NMR spectrum of **B2** in acetone-d_6.

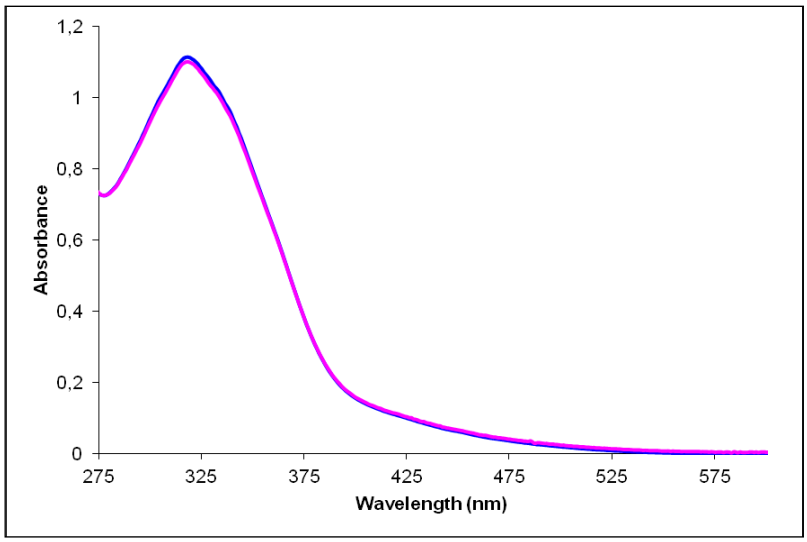

Fig. S200. UV/Vis spectra of **B2** in CH_3CN. Before (blue line) and after (pink line) irradiation at 328nm, $2.32 \cdot 10^{-5}$ M.

Cis to trans thermal isomerization kinetics. Due to the small degree of photoisomerization, it has been not possible to calculate k.

Compound C2, $[Ir(Brppy)_2(2)_2]PF_6$. Synthesis, characterization and photoisomerization studies.

SYNTHESIS

Under a N_2 atmosphere, $[Ir(Brppy)_2Cl]_2$ (0.100 g, 0.072 mmol) were dissolved in 8 ml of acetone and AgOTf (0.085 g, 0.334 mmol) were added. The mixture was heated to 56 °C for 2 h and after cooled down to room temperature, AgCl was removed by centrifugation. The resulting solution was added over a 1 h refluxed suspension of **L2** (0.053 g, 0.288 mmol) in 4 ml of acetone and 80 µl of NEt_3. The reaction mixture was refluxed, under N_2, for 15 h. After solvent evaporation the product was purified by column chromatography (silica gel, CH_2Cl_2). When the unreacted $[Ir(Brppy)_2Cl]_2$ eluted, 0.05 g of KPF_6 were added on top of the column and the polarity of the eluent was gradually increased to 100% acetone to elute $[Ir(Brppy)_2(\mathbf{L2})]PF_6$ together with the excess of KPF_6. The desired compound was precipitated with ether after filtration through a celite path in CH_2Cl_2 and it was obtained as a dark orange solid. Yield 48%.

Elemental Analysis: calculated for ($C_{44}H_{32}Br_2IrN_8PF_6$): C, 45.18; H, 2.76; N, 9.58. Found: C, 45.13; H, 2.68; N, 9.35.

Exact Mass: ESI-MS $[C_{44}H_{32}Br_2IrN_8]^+$: calculated: m/z= 1023.0746, found: m/z= 1023.0744.

^{1}H NMR (300 MHz, acetone-d_6): δ 9.14 (d, J = 5.8 Hz, 1H), 9.09 (brd, J = 6.7 Hz, 2H), 8.25 (d, J = 8.2 Hz, 1H), 8.17 (ddd, J = 1.4 Hz, J = 7.4 Hz, J = 8.7 Hz, 1H), 8.00 (brdd, J = 1.4 Hz, J = 7.9 Hz, 2H), 7.89 (brd, J = 6.7 Hz, 2H), 7.75 (d, J = 8.4 Hz, 1H), 7.72–7.63 (m, 4H), 7.20 (dd, J = 1.9 Hz, J = 8.3 Hz, 1H), 6.59 (d, J = 1.9 Hz, 1H).

^{13}C APT NMR (75 MHz, acetone-d_6): δ 168.01 ($2C_{quat}$), 159.22 (C_{quat}), 155.57 (2CH), 153.75 (C_{quat}), 151.25 (CH), 151.12 (C_{quat}), 144.86 (C_{quat}), 140.97 (CH), 135.54 (CH), 134.92 (CH), 130.98 (2CH), 127.58 (CH), 127.38 (CH), 125.93 (CH), 124.85 (2CH), 121.76 (CH), 120.37 (2CH).

UV/Vis (CH_3CN), λ, nm (ε, 10^4 M^{-1} cm^{-1}): 315 (5.2), 446 (0.43).

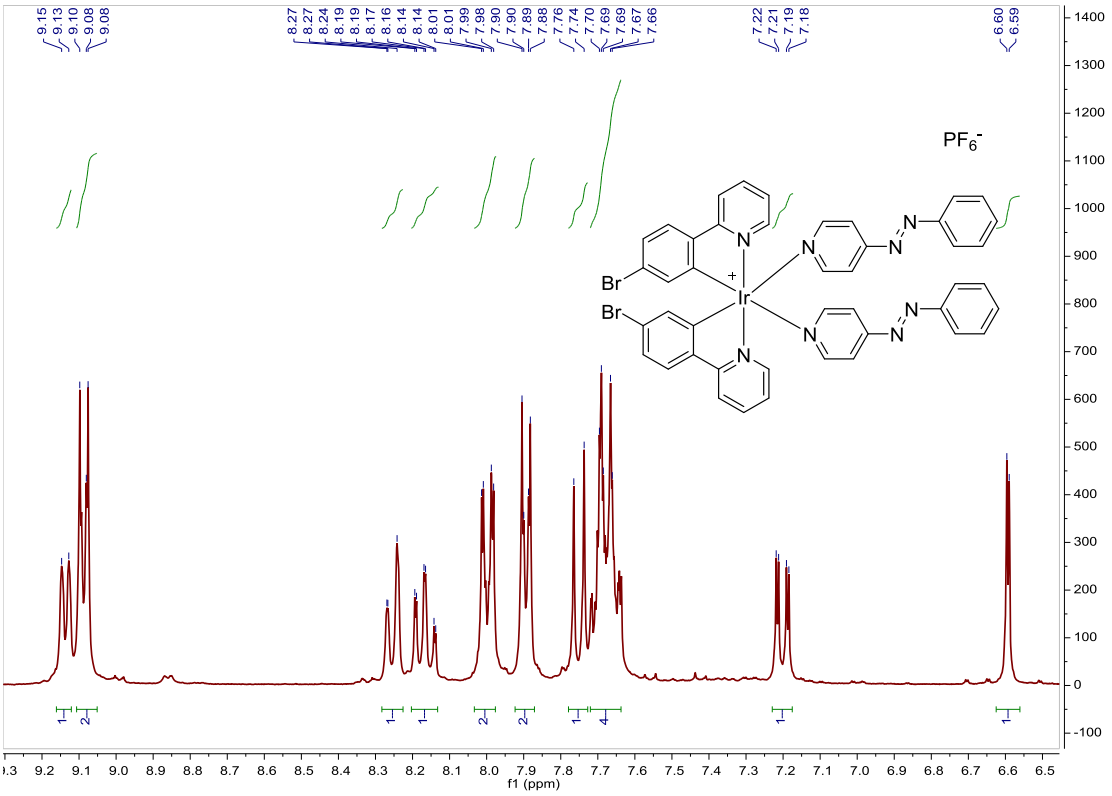

Fig. S201. ^{1}H NMR spectrum of **C2** in acetone-d_6, 300 MHz.

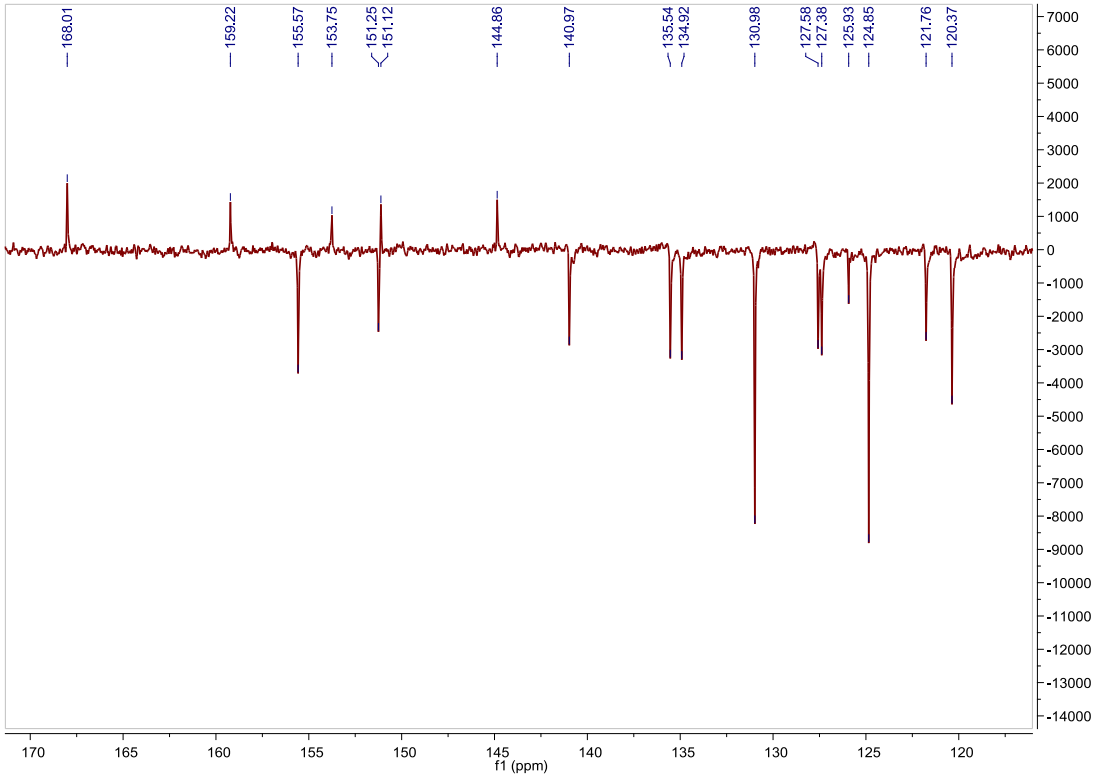

Fig. S202. ^{13}C APT NMR spectrum of **C2** in acetone-d_6, 75 MHz.

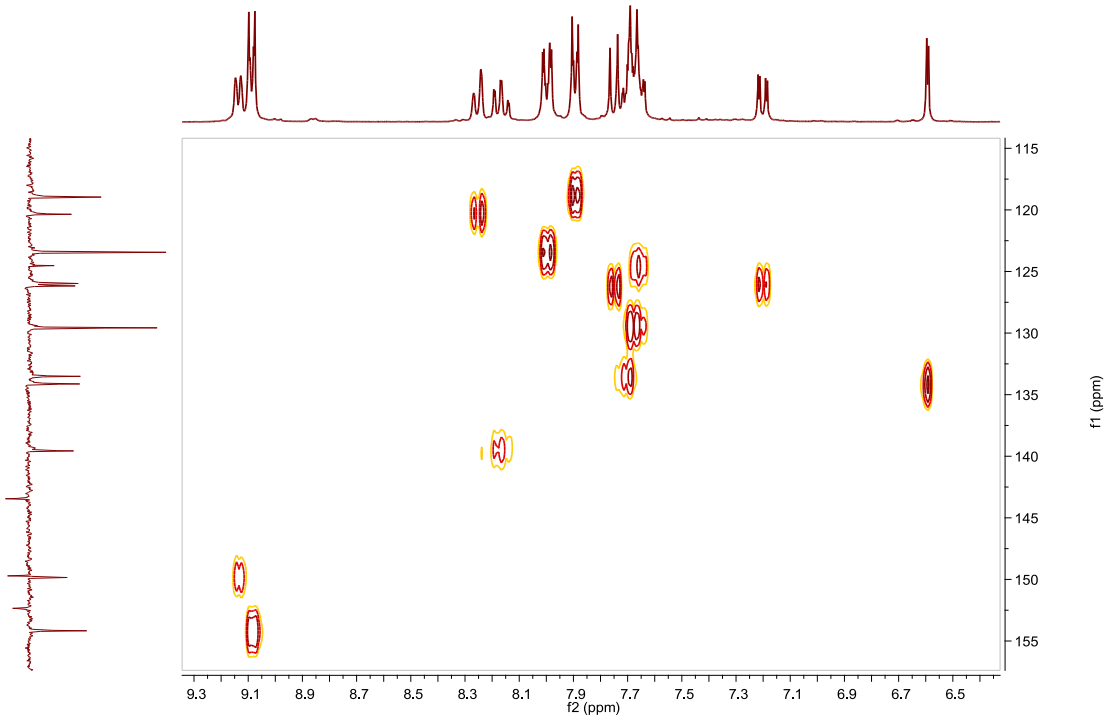

Fig. S203. HSQC NMR spectrum of **C2** in acetone-d_6.

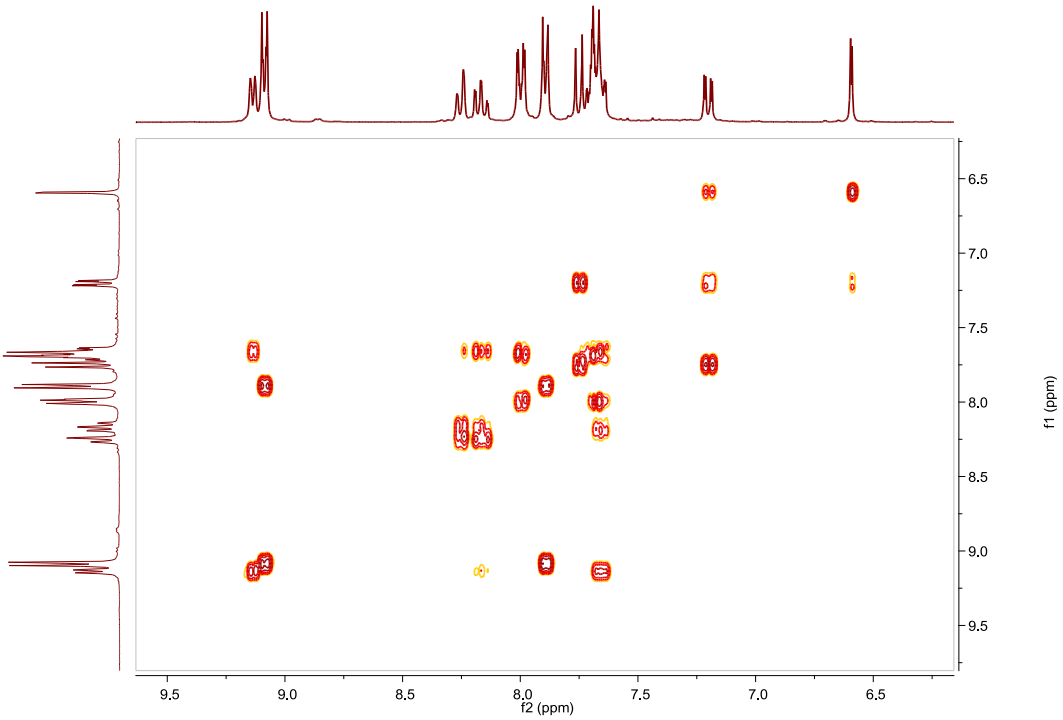

Fig. S204. COSY NMR spectrum of **C2** in acetone-d_6.

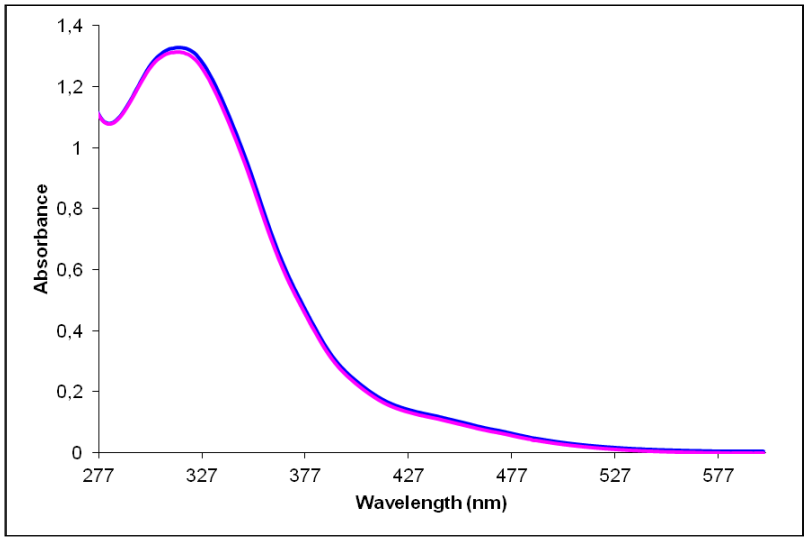

Fig. S205. UV/Vis spectra of **C2** in CH_3CN. Before (blue line) and after (pink line) irradiation at 344nm, $2.54 \cdot 10^{-5}$ M.

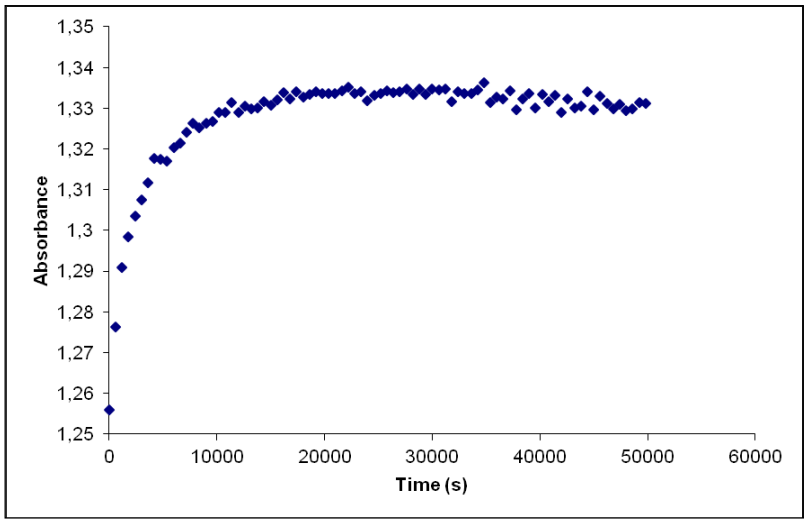

Fig. S206. Cis to trans thermal isomerization kinetics of **C2**. Absorption change of the band 315nm at 328 K in CH_3CN after irradiation at 344 nm. ($2.54 \cdot 10^{-5}$ M).

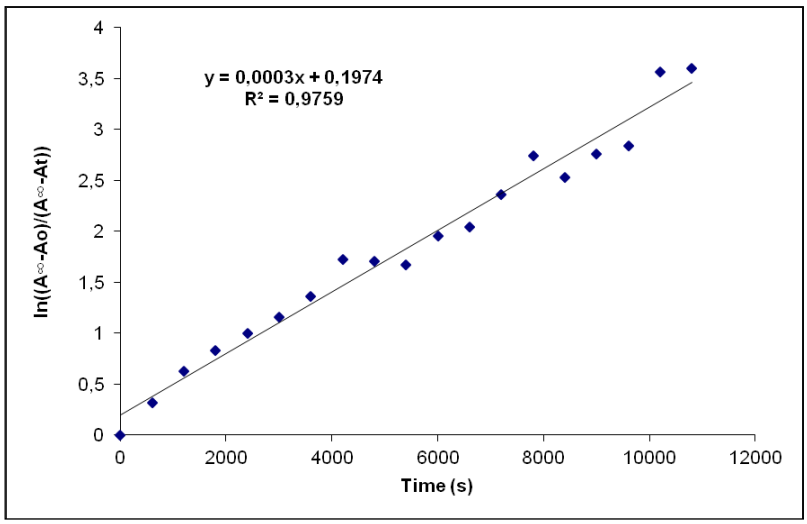

Fig. S207. Cis to trans thermal isomerization kinetics of **C2**. First-order plot. k (s^{-1}) = $3.0 \cdot 10^{-4}$. Half-life (min) = 38.

Compound D2, [Ir(azoppy)$_2$(2)$_2$]PF$_6$. Synthesis, characterization and photoisomerization studies.

SYNTHESIS

Under a N_2 atmosphere, **C2** (0.120 g, 0.103 mmol) and [4-(phenylazo)phenyl]boronic acid pinacol ester **11** (0.077 g, 0.250 mmol) were dissolved in 4 ml of THF. Na_2CO_3 (1M (aq), 2 mL) and $Pd(PPh_3)_4$ (0.012 g, 0.010 mmol) were added and the solution was degassed by bubbling N_2 for 15 min. The reaction mixture was refluxed (80 °C) for 15 h. The resulting mixture was cooled down to room temperature and the product was extracted with CH_2Cl_2. The organic phase was dried with $MgSO_4$, filtered off and the solvent was evaporated. The residue was purified by column chromatography (silica gel, CH_2Cl_2). To the fraction containing the eluted complex, 0.05 g of KPF_6 were added and the resulting solution was filtered through a celite path. The title compound was obtained as a dark red solid. Yield 14%.

Elemental Analys: calculated for ($C_{68}H_{50}IrN_{12}PF_6$): C, 59.51; H, 3.67; N, 12.25. Found: C, 59.81; H, 3.40; N, 11.67.

Exact Mass: ESI-MS $[C_{68}H_{50}IrN_{12}]^+$: calculated: m/z= 1227.3911, found: m/z= 1227.3932.

^{1}H NMR (300 MHz, acetone-d_6): δ 9.28–9.20 (m, 2H), 8.28 (d, J = 7.8 Hz, 1H), 8.17 (t, J = 8.1 Hz, 1H), 8.03–7.83 (m, 9H), 7.71–7.56 (m, 10H), 7.34 (dd, J = 1.6 Hz, J = 8.2 Hz, 1H), 6.89 (d, J = 1.7 Hz, 1H).

^{13}C APT NMR (75 MHz, acetone-d_6): δ 168.80 (C_{quat}), 159.08 (C_{quat}), 155.67 (CH), 153.95 (C_{quat}), 153.76 (C_{quat}), 153.03 (C_{quat}), 151.24 (CH), 149.69 (C_{quat}), 145.82(C_{quat}), 144.94 (C_{quat}), 142.62 (C_{quat}), 140.63 (CH), 134.86 (CH), 132.64 (CH), 131.47 (CH), 130.98 (2CH), 130.89 (CH), 130.62 (2CH), 129.03 (2CH), 126.33 (CH), 125.53 (CH), 124.82 (2CH), 124.71 (CH), 124.45 (2CH), 124.00 (2CH), 123.37 (CH), 121.61 (CH), 120.26 (CH).

UV/Vis (CH_3CN), λ, nm (ε, 10^4 M^{-1} cm^{-1}): 347 (9.0), 427 (1.8).

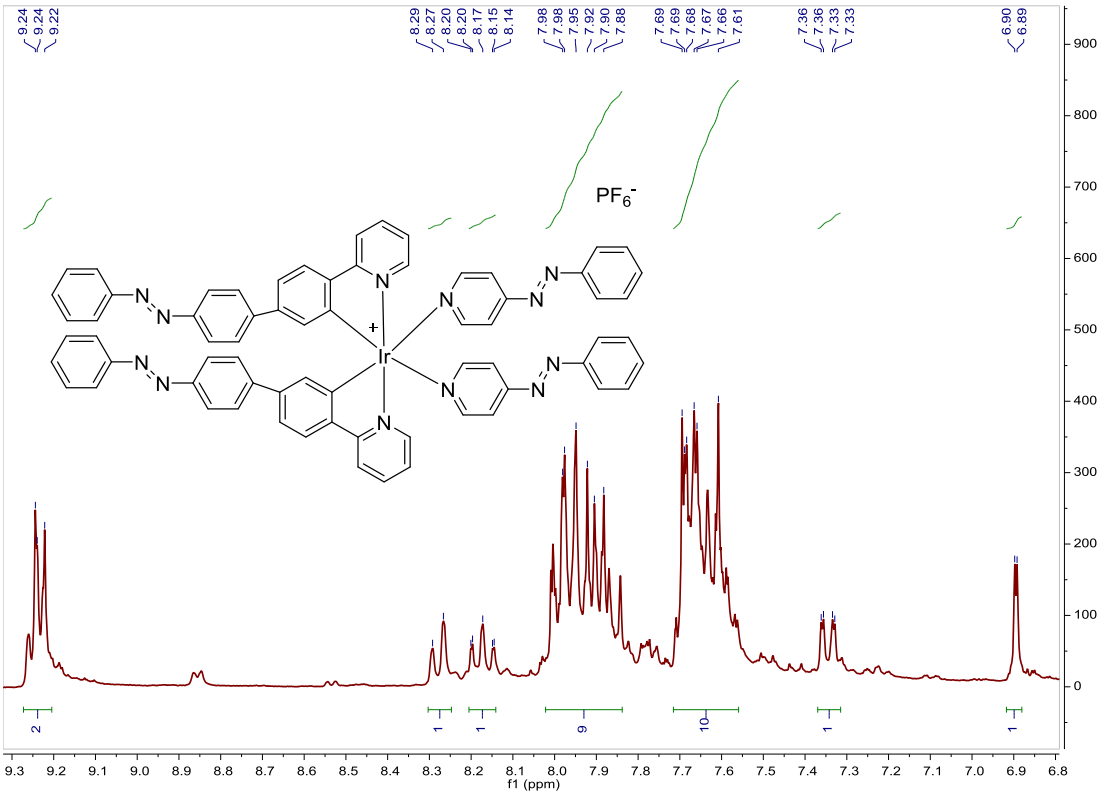

Fig. S208. ^{1}H NMR spectrum of **D2** in acetone-d_6, 300 MHz.

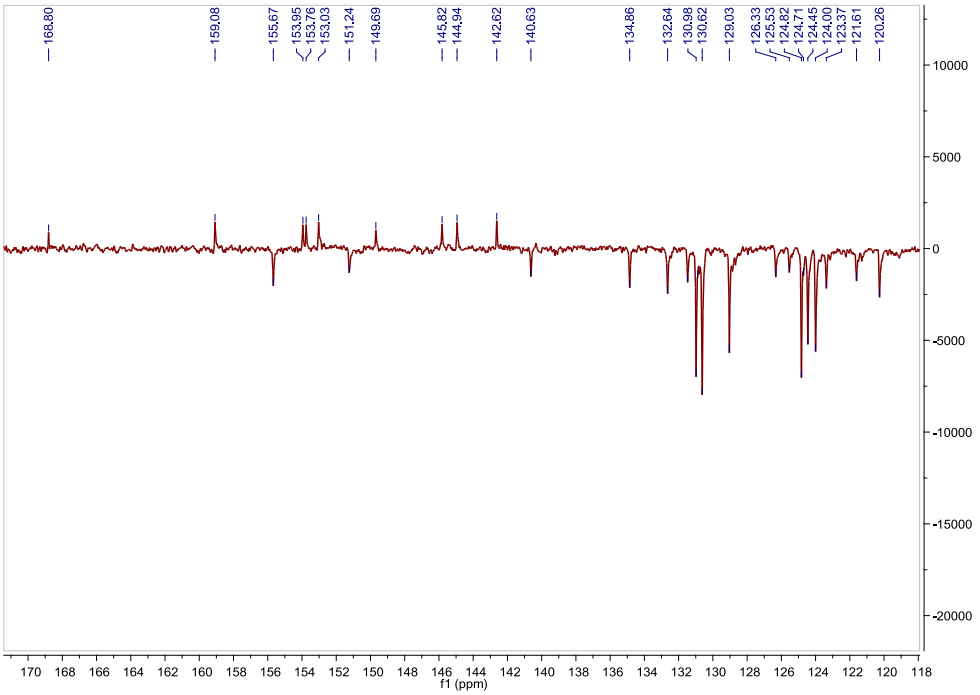

Fig. S209. ^{13}C APT NMR spectrum of **D2** in acetone-d_6, 75 MHz.

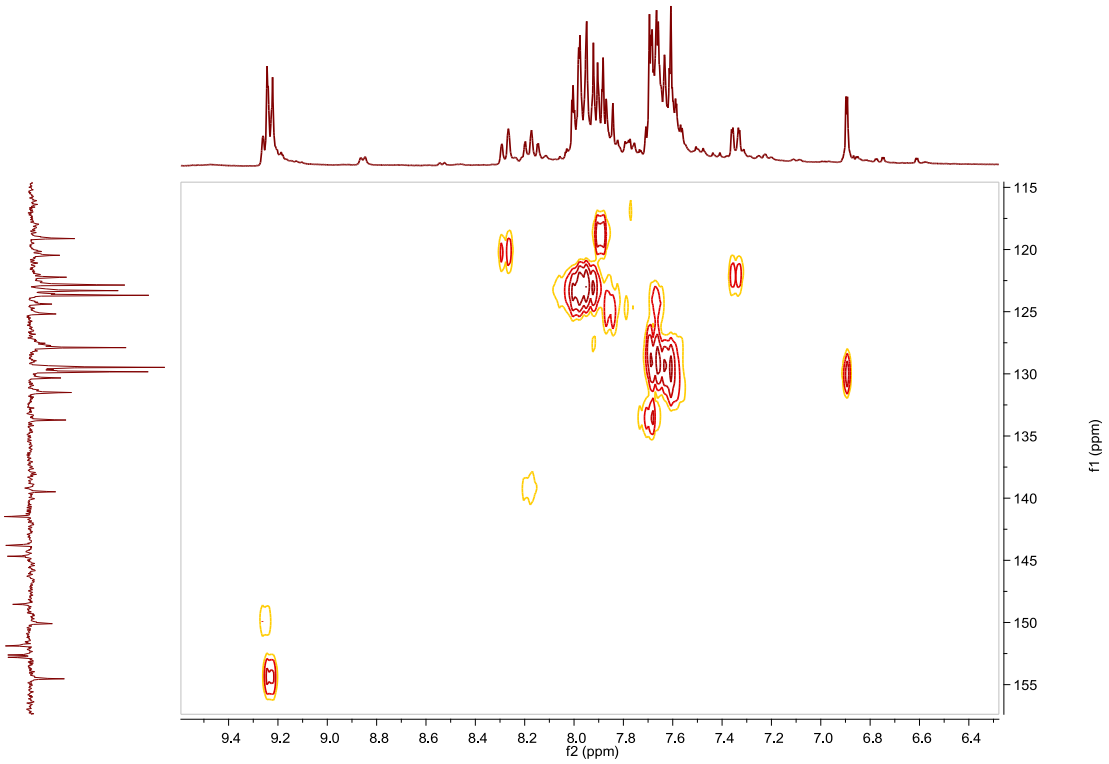

Fig. S210. HSQC NMR spectrum of **D2** in acetone-d_6.

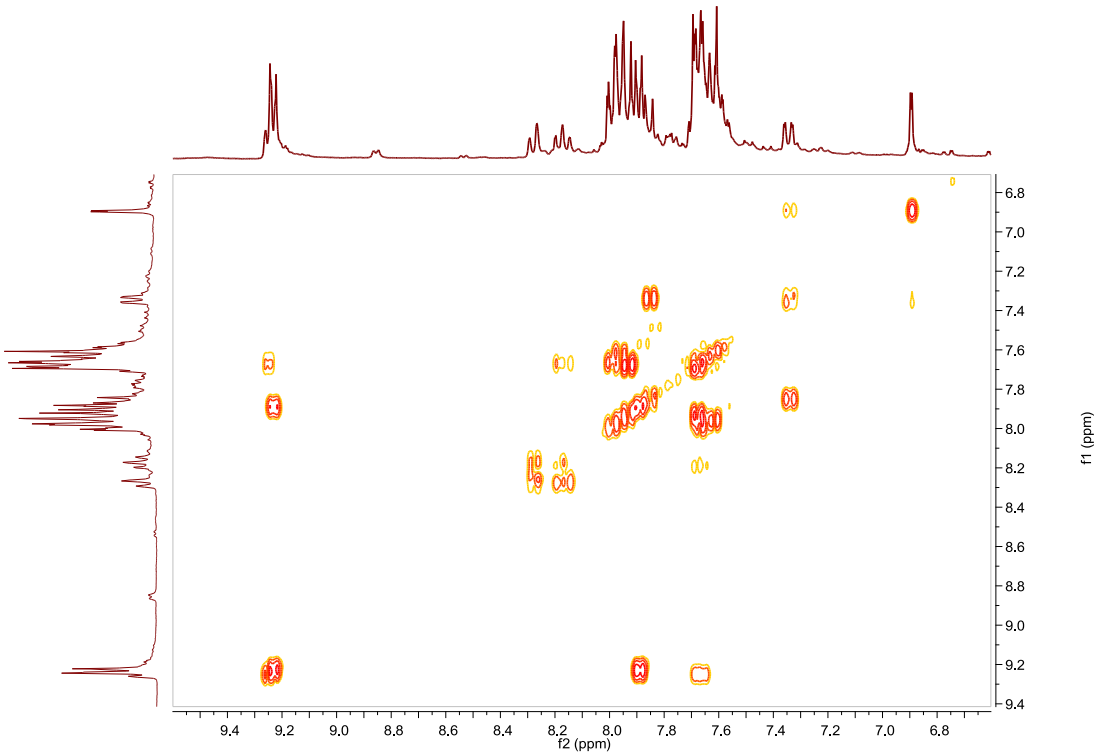

Fig. S211. COSY NMR spectrum of **D2** in acetone-d_6.

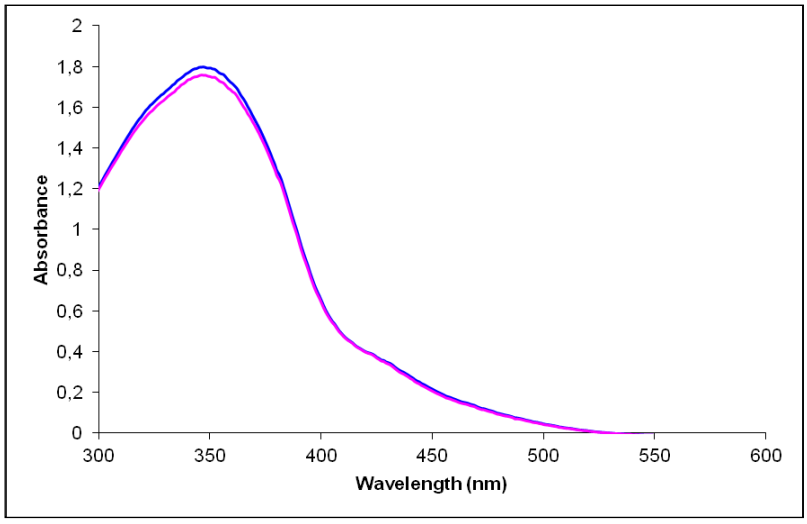

Fig. S212. UV/Vis spectra of **D2** in CH_3CN. Before (blue line) and after (pink line) irradiation at 350nm, $2.00 \cdot 10^{-5}$ M.

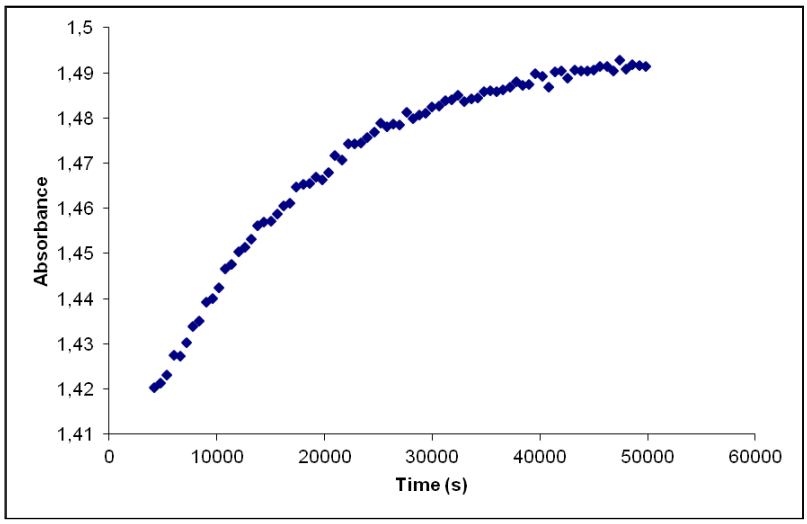

Fig. S213. Cis to trans thermal isomerization kinetics of **D2**. Absorption change of the band 347nm at 328 K in CH_3CN after irradiation at 350 nm. ($2.00 \cdot 10^{-5}$ M).

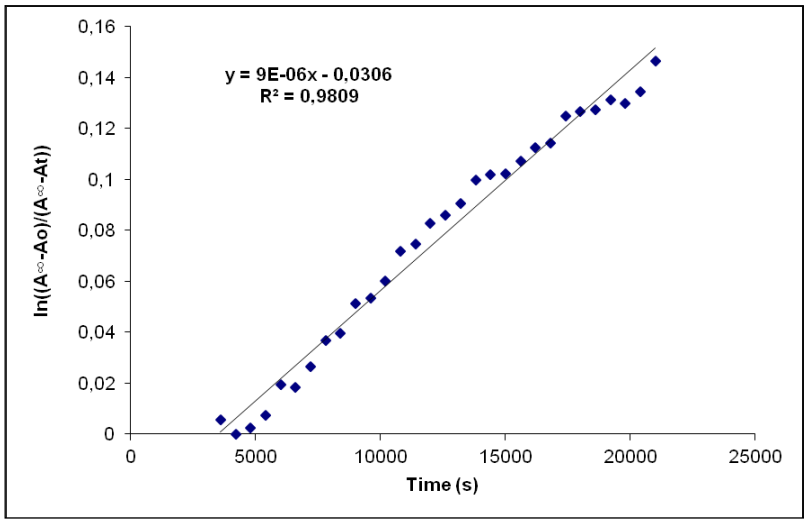

Fig. S214. Cis to trans thermal isomerization kinetics of **D2**. First-order plot. k (s^{-1}) = $9.0 \cdot 10^{-6}$. Half-life (min) = 1284.

Compound A3, [Ir(ppy)$_2$(3)]PF$_6$. Synthesis, characterization and photoisomerization studies.

SYNTHESIS

Under a N_2 atmosphere, $[Ir(ppy)_2Cl]_2$ (0.100 g, 0.093 mmol) were added over a suspension of **L3** (0.096 g, 0.186 mmol) in 8 ml CH_2Cl_2–MeOH 2/1. The reaction mixture was refluxed, under N_2, for 15 h. After solvent evaporation the product was purified by column chromatography (silica gel, CH_2Cl_2). When the unreacted $[Ir(ppy)_2Cl]_2$ eluted, 0.05 g of KPF_6 were added on top of the column and the polarity of the eluent was gradually increased to 100% acetone to elute [Ir(ppy)$_2$(**L3**)]PF_6 together with the excess of KPF_6. The desired compound was precipitated with ether after filtration through a celite path in CH_2Cl_2 and it was obtained as an orange solid. Yield 95%.

Elemental Analysis: calculated for ($C_{56}H_{40}IrN_8PF_6$) C, 57.88; H, 3.47; N, 9.64. Found: C, 58.02; H, 3.43; N, 9.41.

Exact Mass: ESI-MS $[C_{56}H_{40}IrN_8]^+$: calculated: m/z= 1017.3005, found: m/z= 1017.3030.

^{1}H NMR (300 MHz, acetone-*d*$_6$): δ 9.52 (d, J = 1.4 Hz, 1H), 8.35–8.22 (m, 4H), 8.16 (m, 3H), 8.07–7.96 (m, 5H), 7.70–7.62 (m, 3H), 7.24 (ddd, J = 1.3 Hz, J = 6.0 Hz, J = 7.2 Hz, 1H), 7.11 (ddd, J = 1.2 Hz, J = 7.4 Hz, J = 8.5 Hz, 1H), 7.00 (ddd, J = 1.3 Hz, J = 7.4 Hz, J = 8.7 Hz, 1H), 6.45 (dd, J = 0.9 Hz, J = 7.5 Hz, 1H).

^{13}C APT NMR (75 MHz, acetone-*d*$_6$): δ 169.25 (C_{quat}), 158.06 (C_{quat}), 154.86 (C_{quat}), 153.88 (C_{quat}), 152.24 (CH), 151.98 (C_{quat}), 151.30 (C_{quat}), 150.66 (CH), 145.44 (C_{quat}), 140.15 (CH), 139.54 (C_{quat}), 133.23 (CH), 132.97 (CH), 131.76 (CH), 130.74 (2CH), 130.15 (2CH), 127.42 (CH), 126.33 (CH), 125.00 (CH), 124.85 (2CH), 124.22 (2CH), 124.13 (CH), 123.88 (CH), 121.32 (CH).

UV/Vis (CH_3CN), λ, nm (ε, 10^4 M^{-1} cm^{-1}): 338 (7.2), 467 (0.44).

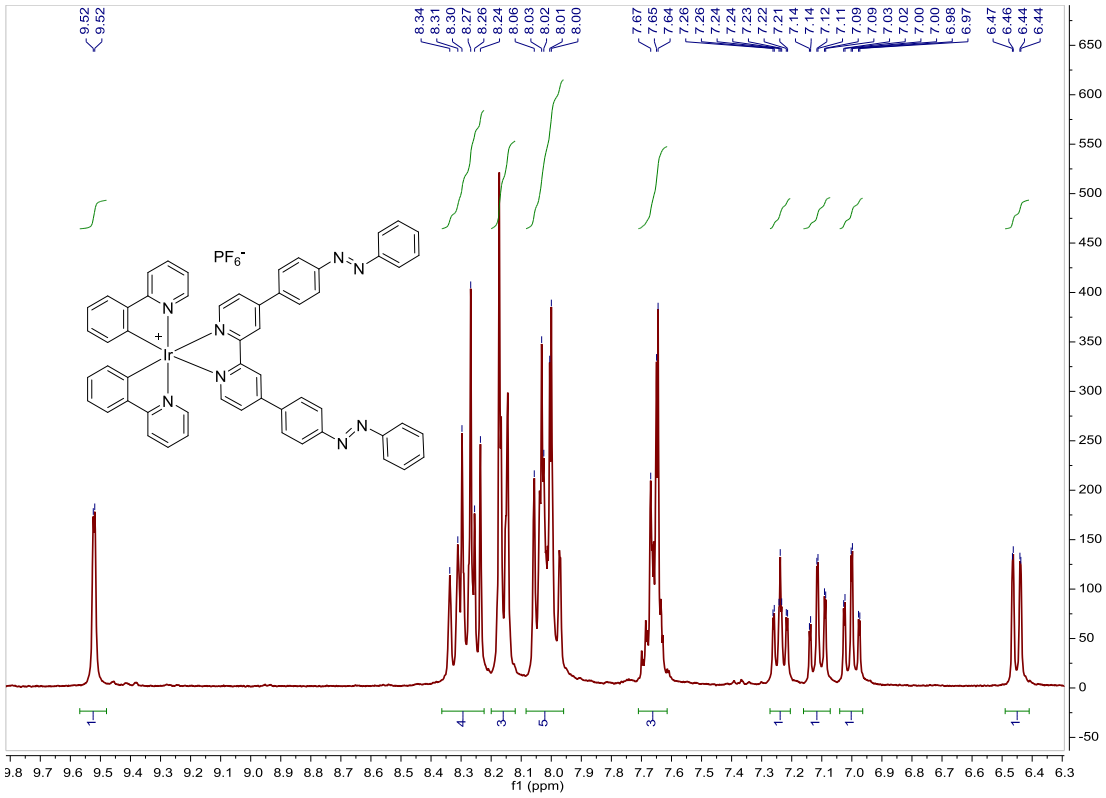

Fig. S215. ^{1}H NMR spectrum of **A3** in acetone-*d*$_6$, 300 MHz.

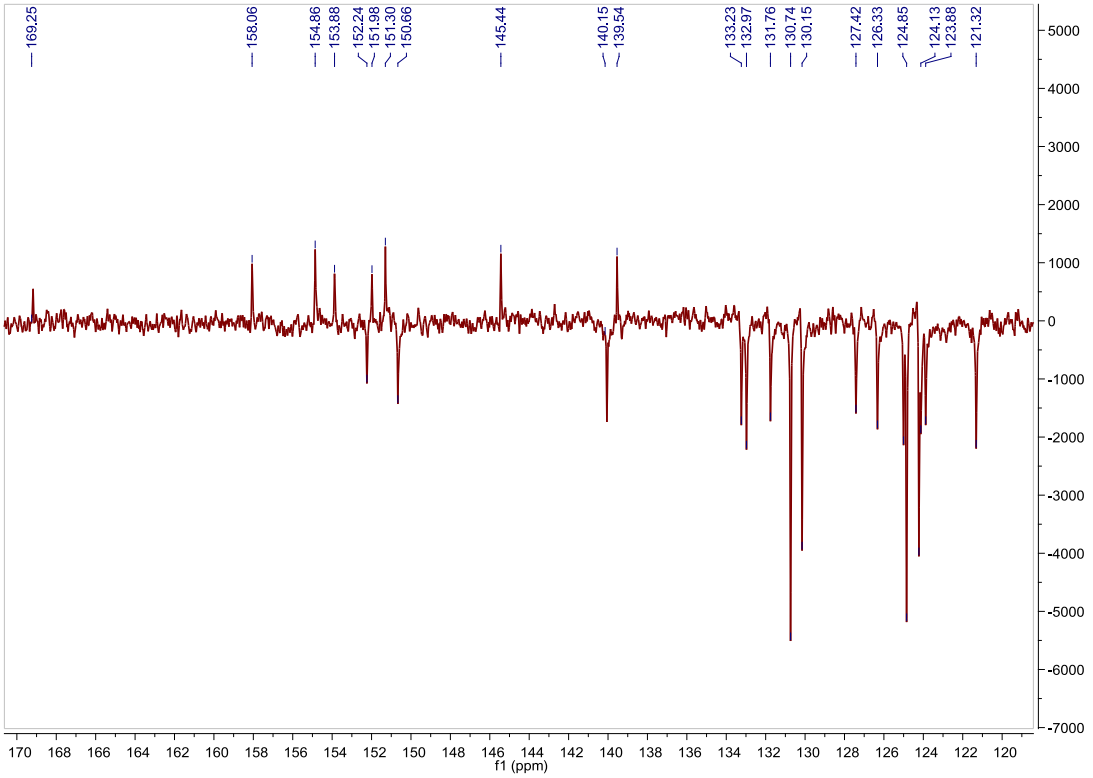

Fig. S216. ^{13}C APT NMR spectrum of **A3** in acetone-d_6, 75 MHz.

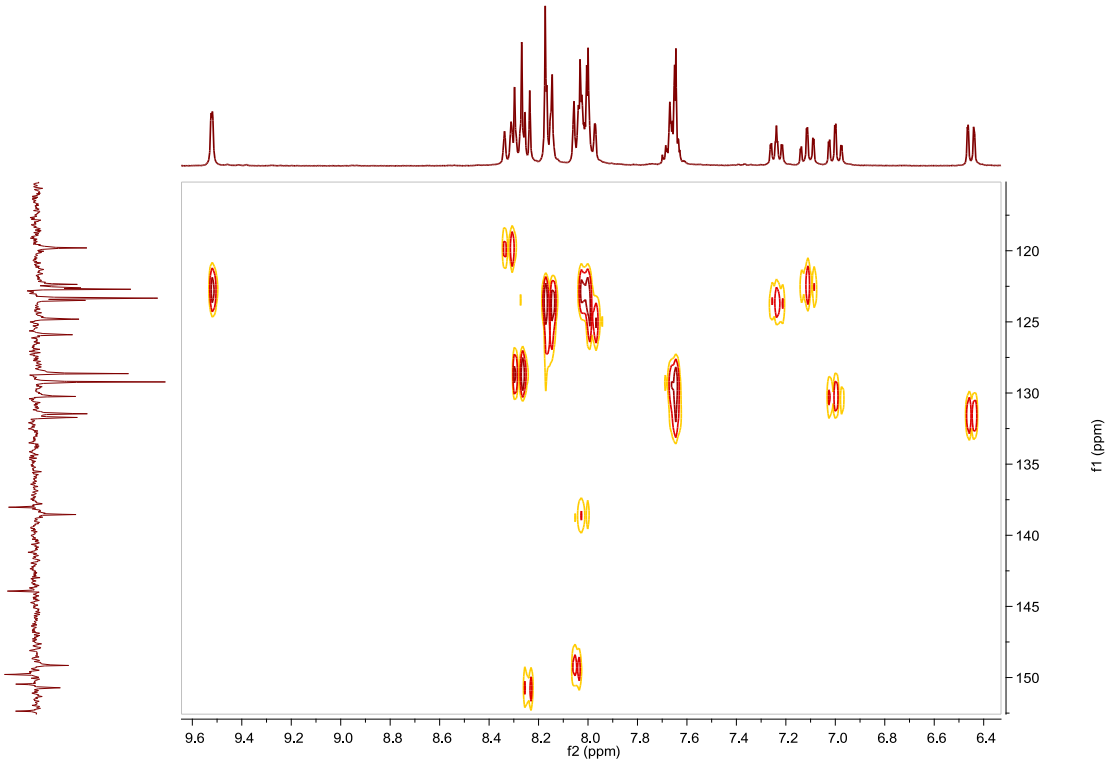

Fig. S217. HSQC NMR spectrum of **A3** in acetone-d_6.

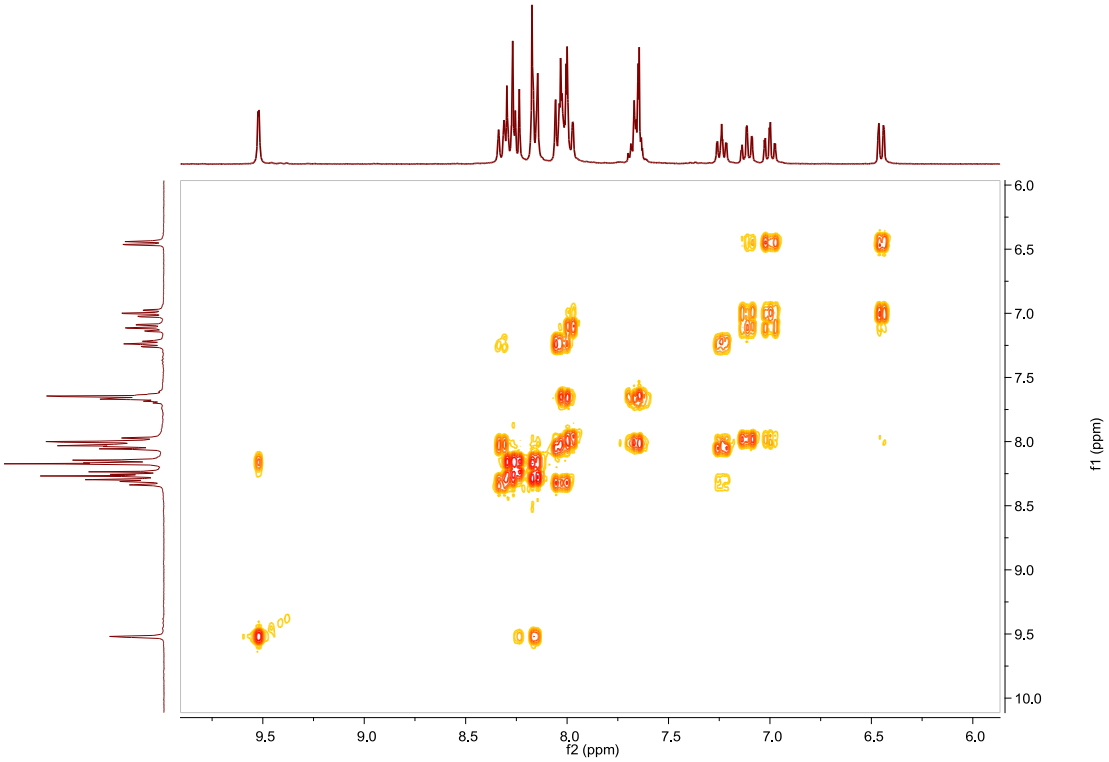

Fig. S218. COSY NMR spectrum of **A3** in acetone-d_6.

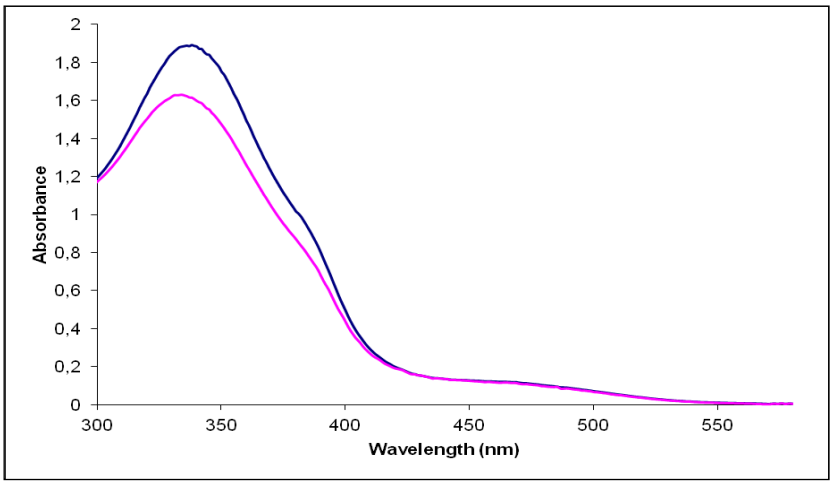

Fig. S219. UV/Vis spectra of **A3** in CH_3CN. Before (blue line) and after (pink line) irradiation at 345nm, $2.64 \cdot 10^{-5}$ M.

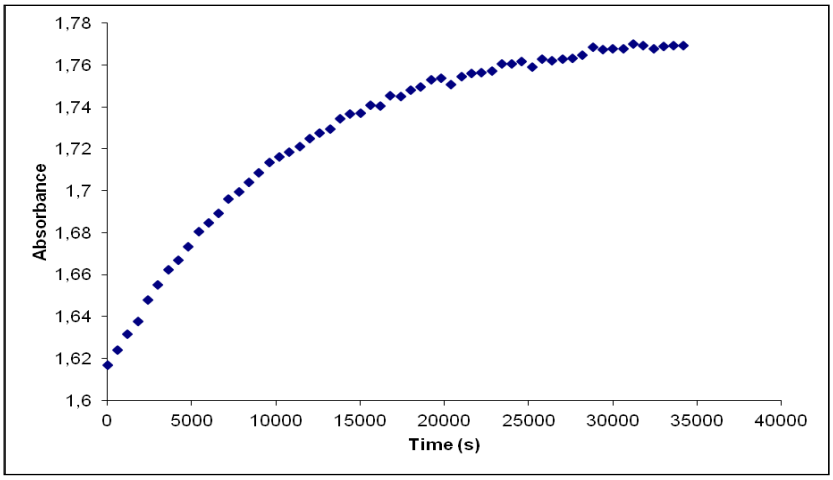

Fig. S220. Cis to trans thermal isomerization kinetics of **A3**. Absorption change of the band 338nm at 328 K in CH_3CN after irradiation at 345 nm. ($2.64 \cdot 10^{-5}$ M).

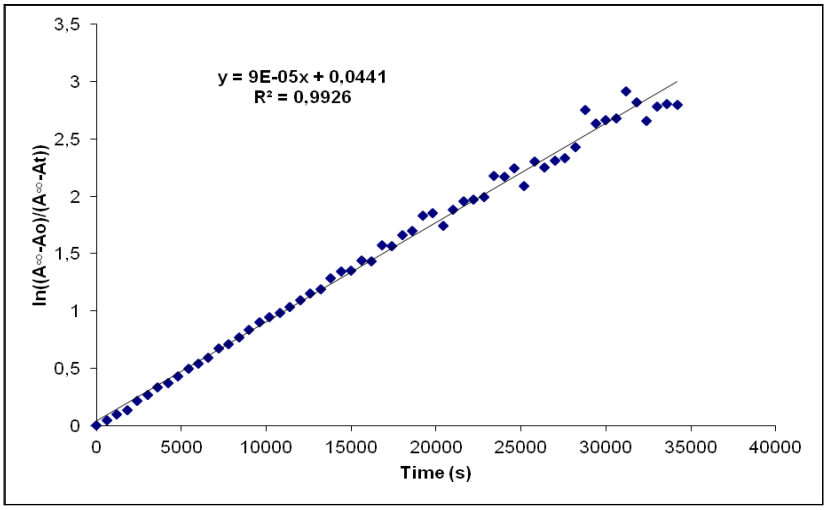

Fig. S221. Cis to trans thermal isomerization kinetics of **A3**. First-order plot. k (s^{-1}) = $9.0 \cdot 10^{-5}$. Half-life (s) = 128.

Compound B3, $[Ir(Fppy)_2(3)]PF_6$. Synthesis, characterization and photoisomerization studies.

SYNTHESIS

Under a N_2 atmosphere, $[Ir(Fppy)_2Cl]_2$ (0.100 g, 0.082 mmol) were added over a suspension of **L3** (0.085 g, 0.164 mmol) in 8 ml CH_2Cl_2–MeOH 2/1. The reaction mixture was refluxed, under N_2, for 15 h. After solvent evaporation the product was purified by column chromatography (silica gel, CH_2Cl_2). When the unreacted $[Ir(Fppy)_2Cl]_2$ eluted, 0.05 g of KPF_6 were added on top of the column and the polarity of the eluent was gradually increased to 100% acetone to elute $[Ir(Fppy)_2$(**L3**)$]PF_6$ together with the excess of KPF_6. The desired compound, purified by filtration through a celite path in CH_2Cl_2, was obtained as an orange solid. Yield 34%.

Elemental Analysis: calculated for ($C_{56}H_{36}F_4IrN_8PF_6{\cdot}CH_3COCH_3$): C, 54.84; H, 3.28; N, 8.67. Found: C, 55.24; H, 3.60; N, 8.28.

Exact Mass: ESI-MS $[C_{56}H_{36}F_4IrN_8]^+$: calculated: m/z= 1089.2628, found: m/z= 1089.2665.

^{1}H NMR (300 MHz, acetone-*d*$_6$): δ 9.54 (s, 1H), 8.48 (brd, *J* = 9.5 Hz, 1H), 8.35 (d, *J* = 5.8 Hz, 1H), 8.27 (brd, *J* = 8.8 Hz, 2H), 8.23–8.09 (m, 5H), 8.05–7.98 (m, 2H), 7.71–7.62 (m, 3H), 7.33 (ddd, J = 1.4 Hz, *J* = 5.8 Hz, J = 7.8 Hz, 1H), 6.84 (ddd, J = 2.3 Hz, J = 9.3 Hz, J = 12.8 Hz, 1H), 5.90 (dd, *J* = 2.3 Hz, J = 8.5 Hz, 1H).

^{13}C APT NMR (75 MHz, acetone-*d*$_6$): δ 165.22 (d, *J* = 6.8 Hz, C_{quat}), 164.96 (dd, J = 12.8 Hz, J = 255.9 Hz, C_{quat}), 162.76 (dd, J = 12.8 Hz, J = 260.47 Hz, C_{quat}), 157.80 (s, C_{quat}), 156.08 (d, *J* = 6.8 Hz, C_{quat}), 154.93 (s, C_{quat}), 153.86 (s, C_{quat}), 152.55 (s, CH), 151.88 (s, C_{quat}), 151.18 (s, CH), 141.18 (s, CH), 139.33 (s, C_{quat}), 133.25 (s, CH), 130.73 (s, 2CH), 130.19 (s, 2CH), 129.30 (s, C_{quat}), 127.73 (s, CH), 125.57 (s, CH), 125.18 (s, CH), 124.85 (s, 2CH), 124.42 (s, CH), 124.22 (s, 2CH), 115.08 (d, *J* = 17.4 Hz, CH), 100.13 (t, *J* = 26.4 Hz, CH).

UV/Vis (CH_3CN), λ, nm (ε, 10^4 M^{-1} cm^{-1}): 343 (7.3), 443 (0.47).

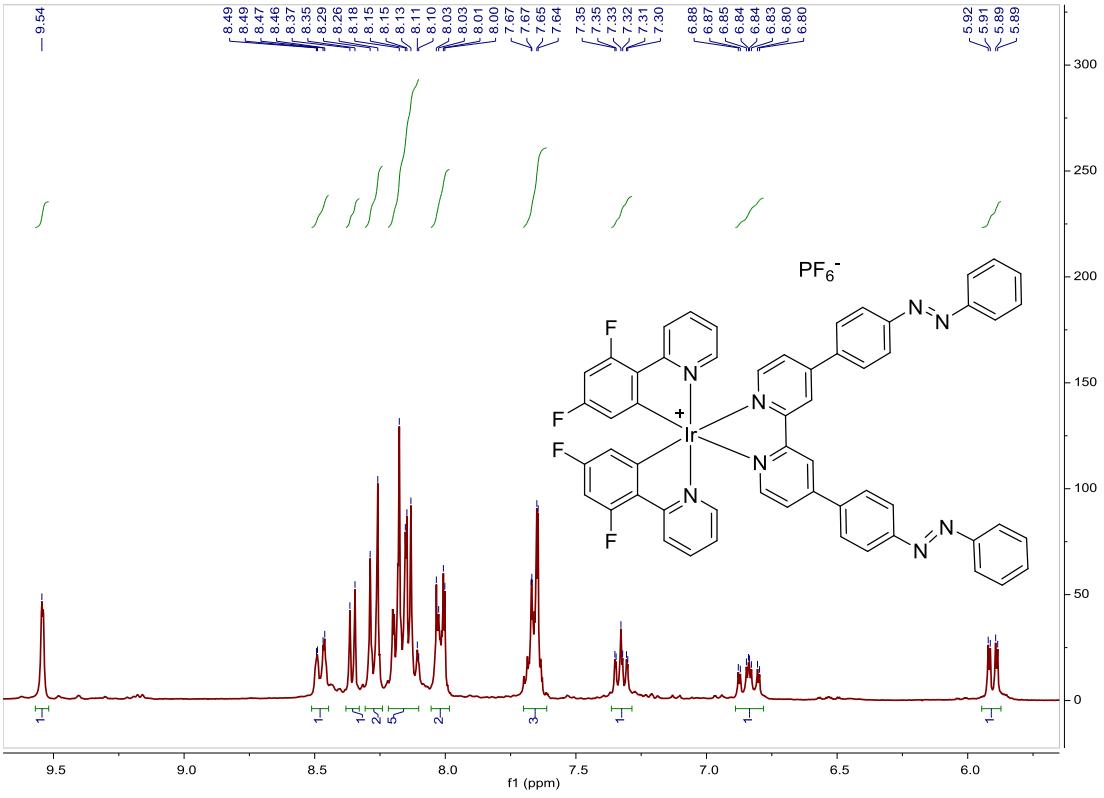

Fig. S222. ^{1}H NMR spectrum of **B3** in acetone-*d*$_6$, 300 MHz.

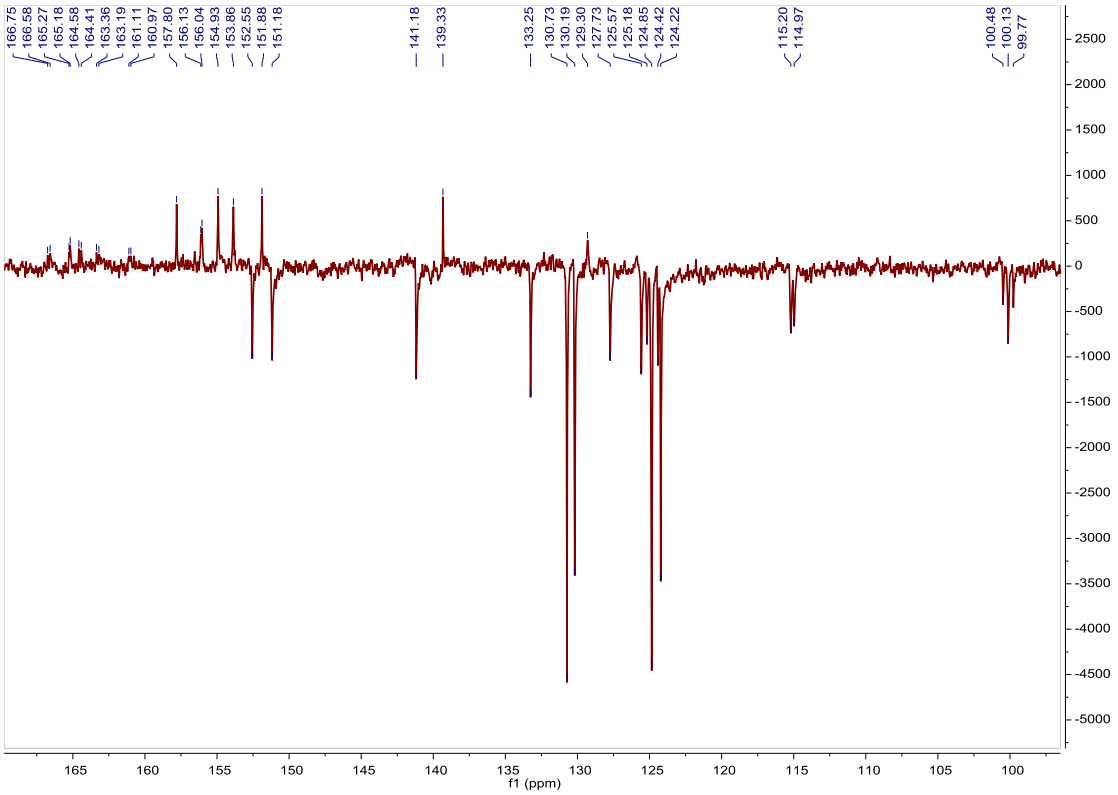

Fig. S223. ^{13}C APT NMR spectrum of **B3** in acetone-d_6, 75 MHz.

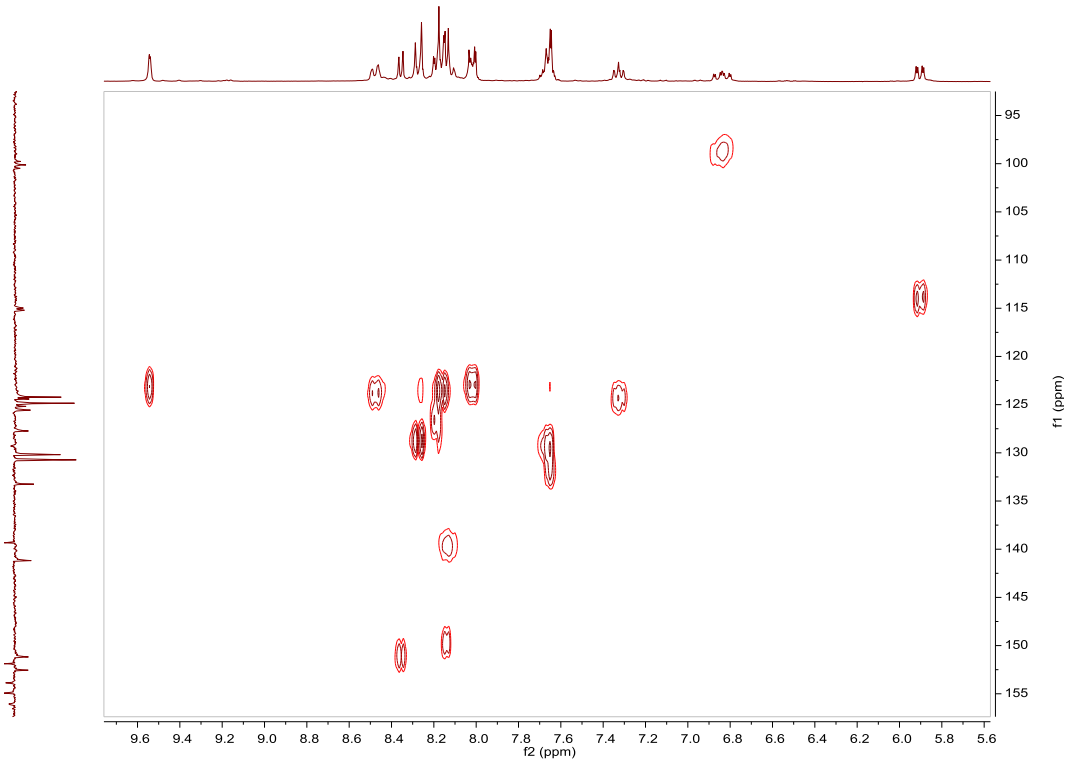

Fig. S224. HSQC NMR spectrum of **B3** in acetone-d_6.

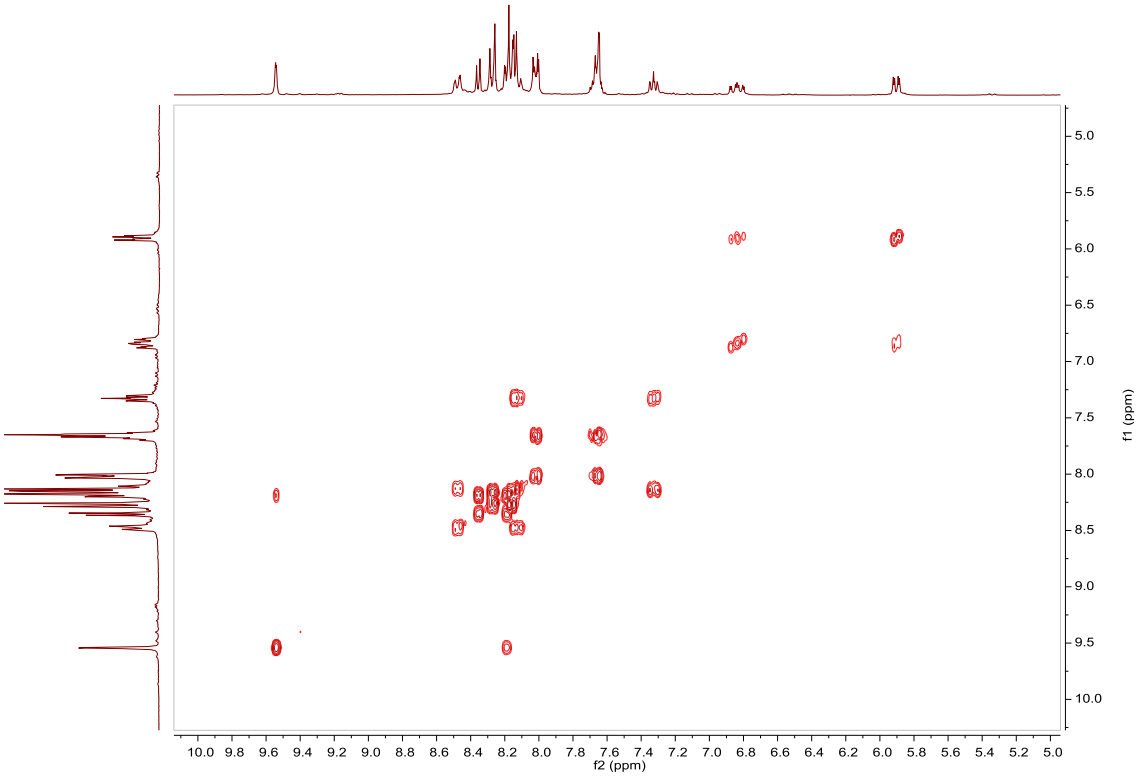

Fig. S225. COSY NMR spectrum of **B3** in acetone-d_6.

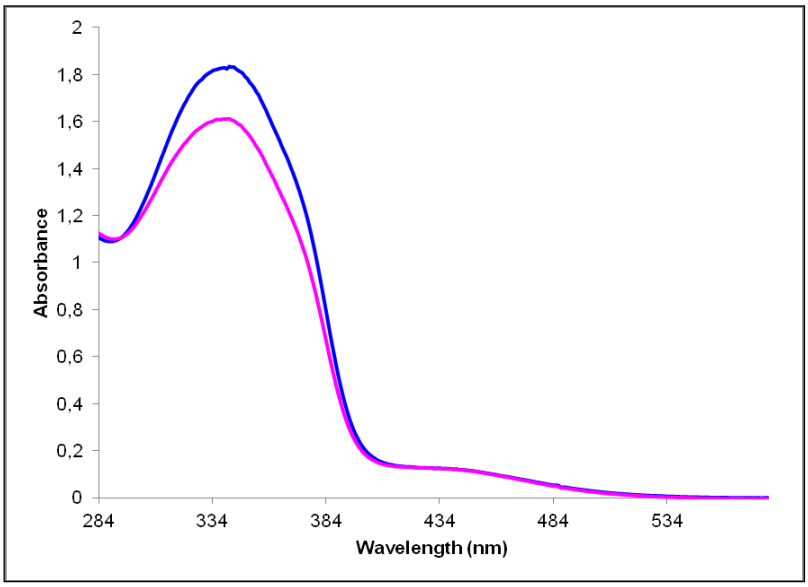

Fig. S226. UV/Vis spectra of **B3** in CH_3CN. Before (blue line) and after (pink line) irradiation at 354nm, $2.52 \cdot 10^{-5}$ M.

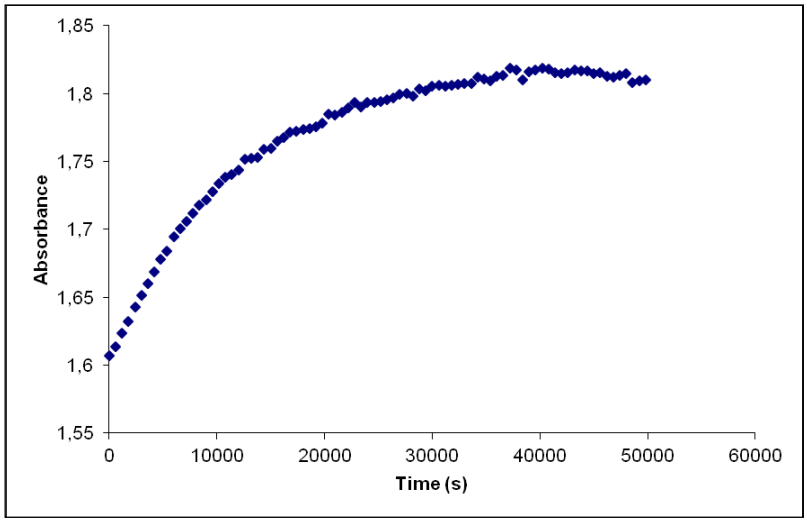

Fig. S227. Cis to trans thermal isomerization kinetics of **B3**. Absorption change of the band 343nm at 328 K in CH_3CN after irradiation at 354 nm. ($2.52 \cdot 10^{-5}$ M).

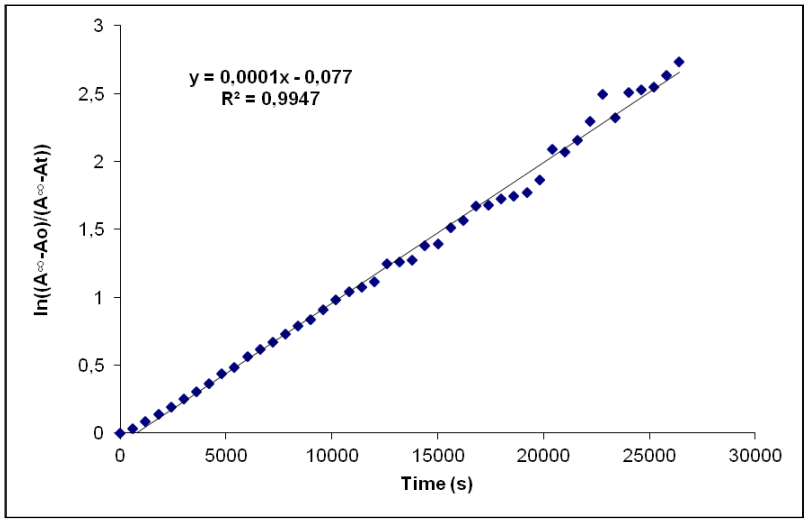

Fig. S228. Cis to trans thermal isomerization kinetics of **B3**. First-order plot. k (s^{-1}) = $1.0 \cdot 10^{-4}$. Half-life (min) = 115.

Compound C3, [Ir(Brppy)$_2$(3)]PF$_6$. Synthesis, characterization and photoisomerization studies.

SYNTHESIS

Under a N_2 atmosphere, $[Ir(Brppy)_2Cl]_2$ (0.100 g, 0.072 mmol) were added over a suspension of **L3** (0.075 g, 0.144 mmol) in 8 ml CH_2Cl_2–MeOH 2/1. The reaction mixture was refluxed, under N_2, for 15h. After solvent evaporation the product was purified by column chromatography (silica gel, CH_2Cl_2). When the unreacted $[Ir(Brppy)_2Cl]_2$ eluted, 0.05 g of KPF_6 were added on top of the column and the polarity of the eluent was gradually increased to 100% acetone to elute $[Ir(Brppy)_2(\mathbf{L3})]PF_6$ together with the excess of KPF_6. The desired compound, purified by filtration through a celite path in CH_2Cl_2, was obtained as an orange solid. Yield 34%.

Elemental Analysis: calculated for ($C_{56}H_{38}Br_2IrN_8PF_6{\cdot}CH_2Cl_2$): C, 48.73; H, 2.87; N, 7.98. Found: C, 48.94; H, 2.90; N, 8.12.

Exact Mass: ESI-MS $[C_{56}H_{38}Br_2IrN_8]^+$: calculated: m/z= 1173.1215, found: m/z= 1173.1235.

^{1}H NMR (300 MHz, acetone-*d*$_6$): δ 9.54 (d, J = 1.6 Hz, 1H), 8.38 (dd, J = 1.2 Hz, J = 8.5 Hz, 1H), 8.32 (d, J = 5.8 Hz, 1H), 8.27 (brd, J = 8.8 Hz, 2H), 8.18 (m, 3H), 8.09 (m, 2H), 8.02 (m, 2H), 7.98 (d, J = 8.4 Hz, 1H), 7.66 (m, 3H), 7.33 (m, 2H), 6.51 (d, J = 2.0 Hz, 1H).

^{13}C APT NMR (75 MHz, acetone-*d*$_6$): δ 167.88 (C_{quat}), 157.94 (C_{quat}), 154.93 (C_{quat}), 154.02 (C_{quat}), 153.88 (C_{quat}), 152.48 (CH), 151.68 (C_{quat}), 150.90 (CH), 144.76 (C_{quat}), 140.64 (CH), 139.43 (C_{quat}), 135.14 (CH), 133.26 (CH), 130.74 (2CH), 130.17 (2CH), 128.16 (CH), 127.66 (CH), 127.20 (CH), 126.31 (C_{quat}), 125.72 (CH), 124.86 (2CH), 124.30 (CH), 124.24 (2CH), 121.94 (CH).

UV/Vis (CH_3CN), λ, nm (ε, 10^4 M^{-1} cm^{-1}): 336 (6.6), 449 (0.24).

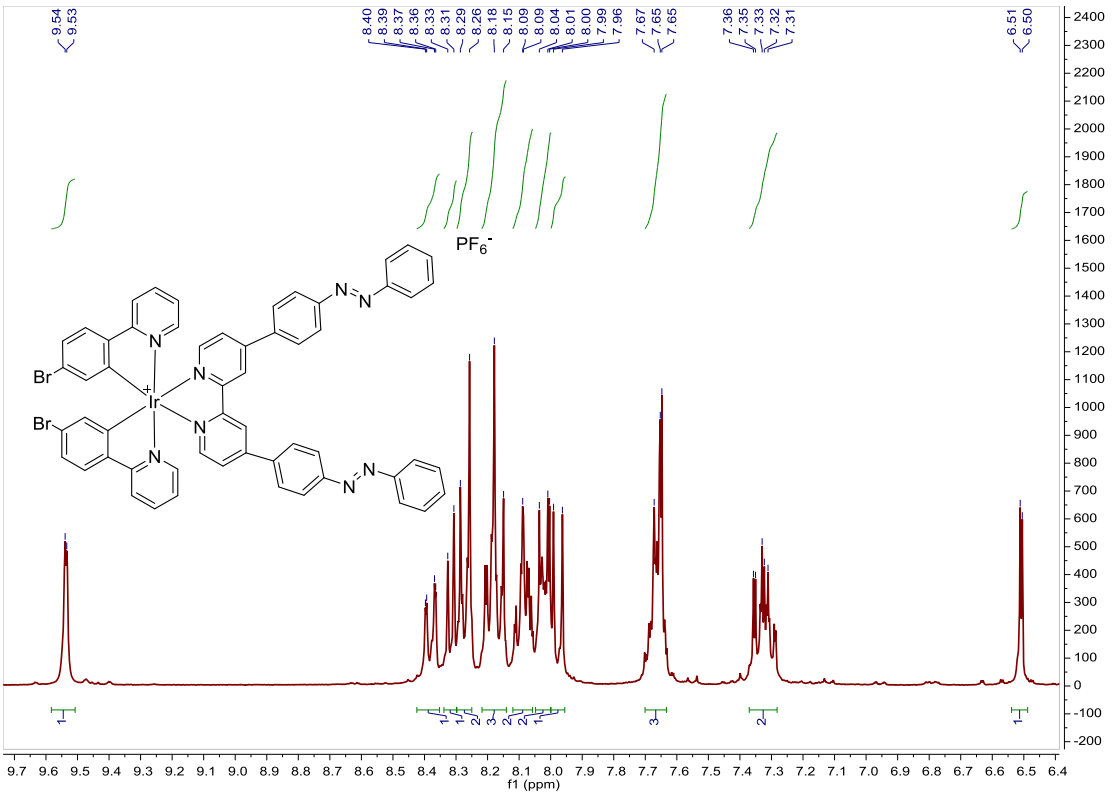

Fig. S229. ^{1}H NMR spectrum of **C3** in acetone-*d*$_6$, 300 MHz.

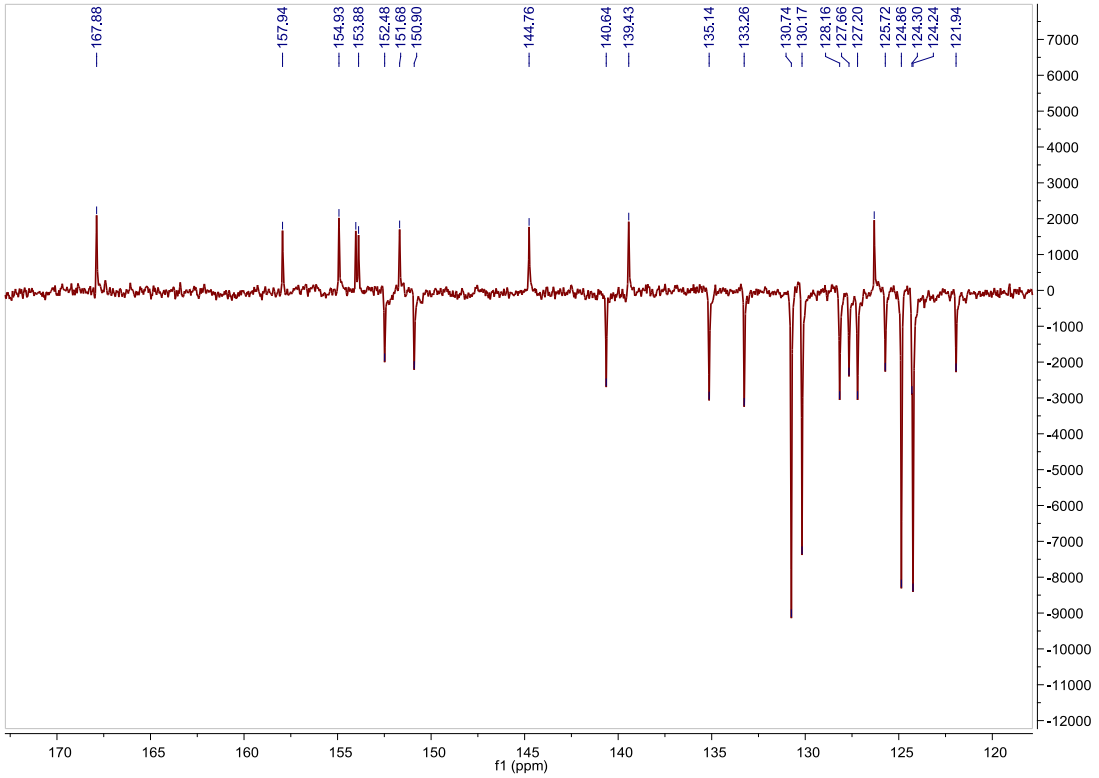

Fig. S230. ^{13}C APT NMR spectrum of **C3** in acetone-d_6, 75 MHz.

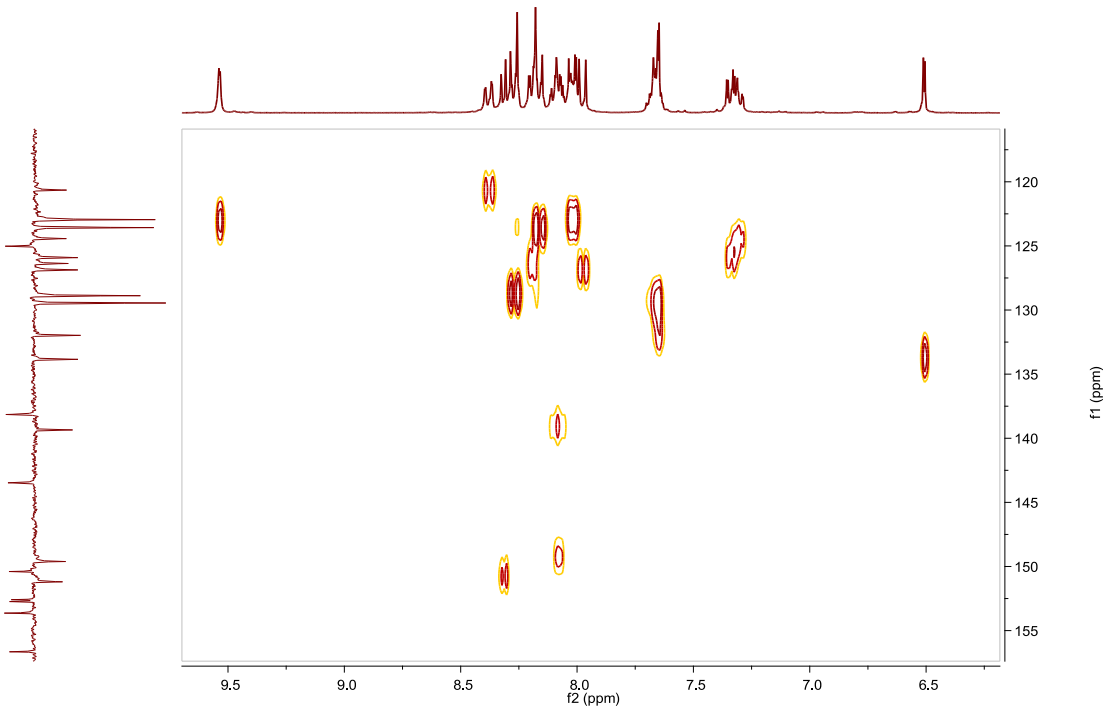

Fig. S231. HSQC NMR spectrum of **C3** in acetone-d_6.

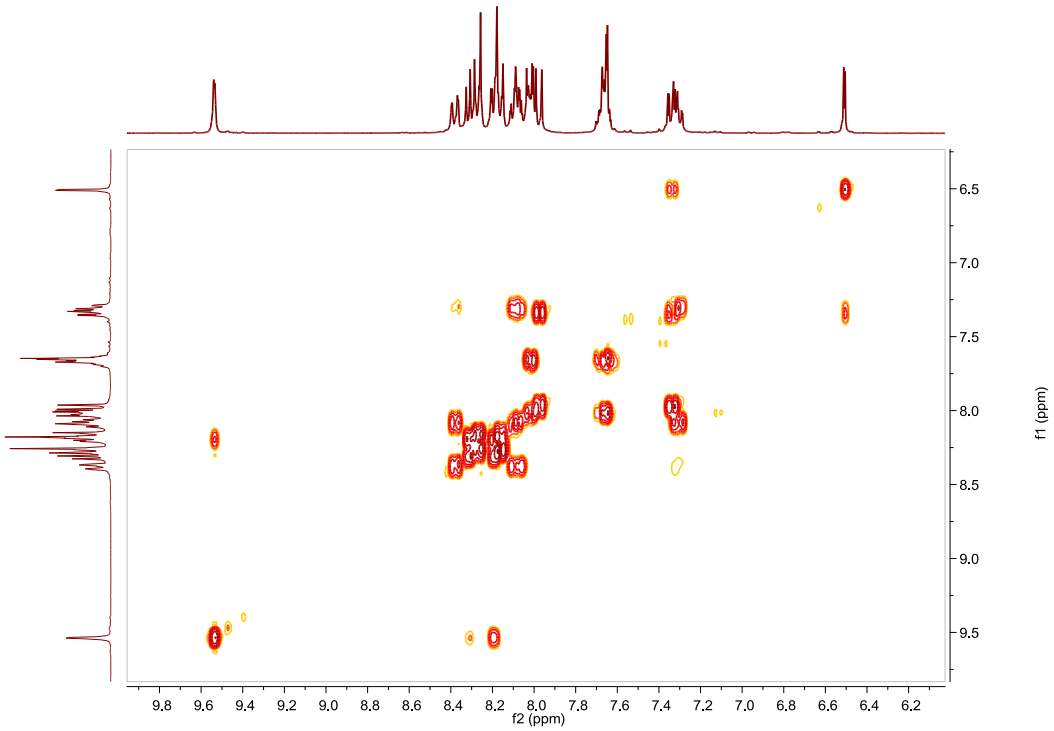

Fig. S232. COSY NMR spectrum of **C3** in acetone-d_6.

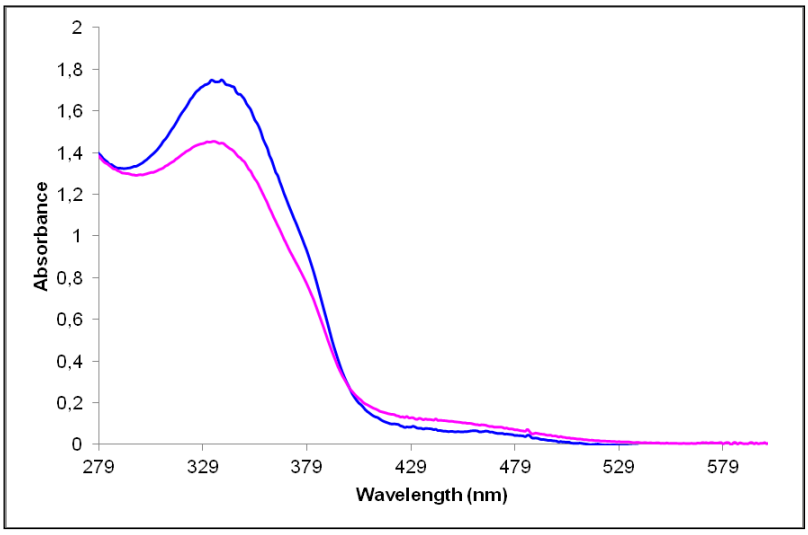

Fig. S233. UV/Vis spectra of **C3** in CH_3CN. Before (blue line) and after (pink line) irradiation at 355nm, $2.62 \cdot 10^{-5}$ M.

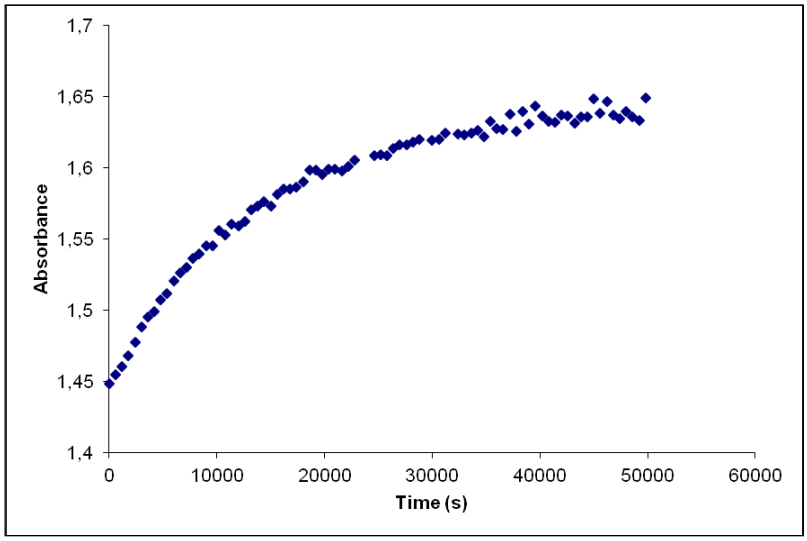

Fig. S234. Cis to trans thermal isomerization kinetics of **C3**. Absorption change of the band 336nm at 328 K in CH_3CN after irradiation at 355 nm. ($2.62 \cdot 10^{-5}$ M).

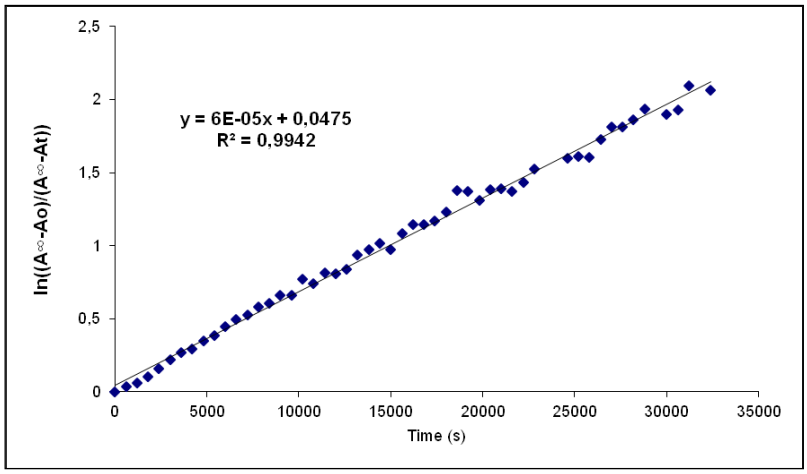

Fig. S235. Cis to trans thermal isomerization kinetics of **C3**. First-order plot. k (s^{-1}) = $6.0 \cdot 10^{-5}$. Half-life (s) = 192.

Compound D3, [Ir(azoppy)$_2$(3)]PF$_6$. Synthesis, characterization and photoisomerization studies.

SYNTHESIS

Under a N_2 atmosphere, **C3** (0.150 g, 0.114 mmol) and [4-(phenylazo)phenyl]boronic acid pinacol ester **11** (0.085 g, 0.276 mmol) were dissolved in 5 ml of THF. Na_2CO_3 (1 M (aq), 2.5 mL) and $Pd(PPh_3)_4$ (0.013 g, 0.011 mmol) were added and the solution was degassed by bubbling N_2 for 15min. The reaction mixture was refluxed (80 °C) for 15 h. The resulting mixture was cooled down to room temperature and the product was extracted with CH_2Cl_2. The organic phase was dried with $MgSO_4$, filtered off and the solvent was evaporated. The residue was purified by column chromatography (silica gel, CH_2Cl_2). To the fraction containing the eluted complex, 0.05 g of KPF_6 were added and the resulting solution was filtered through a celite path. The title compound was obtained as an orange solid. Yield 24%.

Elemental Analysis: calculated for ($C_{80}H_{56}IrN_{12}PF_6 \cdot H_2O$): C, 62.37; H, 3.79; N, 10.91. Found: C, 62.18; H, 3.62; N, 10.34.

Exact Mass: ESI-MS $[C_{80}H_{56}IrN_{12}]^+$: calculated: m/z= 1377.4380, found: m/z= 1377.4351.

^{1}H NMR (300 MHz, acetone-*d*$_6$): δ 9.58 (s, 1H), 8.45 (t, J = 5.8 Hz, 2H), 8.29 (d, J = 8.5 Hz, 2H), 8.24–8.09 (m, 7H), 8.04–7.99 (m, 2H), 7.98–7.92 (m, 4H), 7.71 (m, 7H), 7.55 (dd, J = 1.8 Hz, J = 8.1 Hz, 1H), 7.34 (t, J = 6.8 Hz, 1H), 6.83 (d, J = 1.7 Hz, 1H).

^{13}C APT NMR (75 MHz, acetone-*d*$_6$): δ 168.69 (C_{quat}), 158.11 (C_{quat}), 154.89 (C_{quat}), 153.95 (C_{quat}), 153.88 (C_{quat}), 153.03 (C_{quat}), 152.61 (CH), 152.54 (C_{quat}), 151.41 (C_{quat}), 151.00 (CH), 145.70 (C_{quat}), 145.01 (C_{quat}), 142.67 (C_{quat}), 140.30 (CH), 139.57 (C_{quat}), 133.26 (CH), 132.65 (CH), 131.01 (CH), 130.74 (2CH), 130.62 (2CH), 130.14 (2CH), 129.98 (CH), 128.95 (2CH), 127.57 (CH), 126.87 (CH), 125.31 (CH), 124.86 (2CH), 124.49 (2CH), 124.23 (2CH), 123.98 (2CH), 123.17 (CH), 121.79 (CH).

UV/Vis (CH_3CN), λ, nm (ε, 10^4 M^{-1} cm^{-1}): 350 (12.7), 435 (1.7).

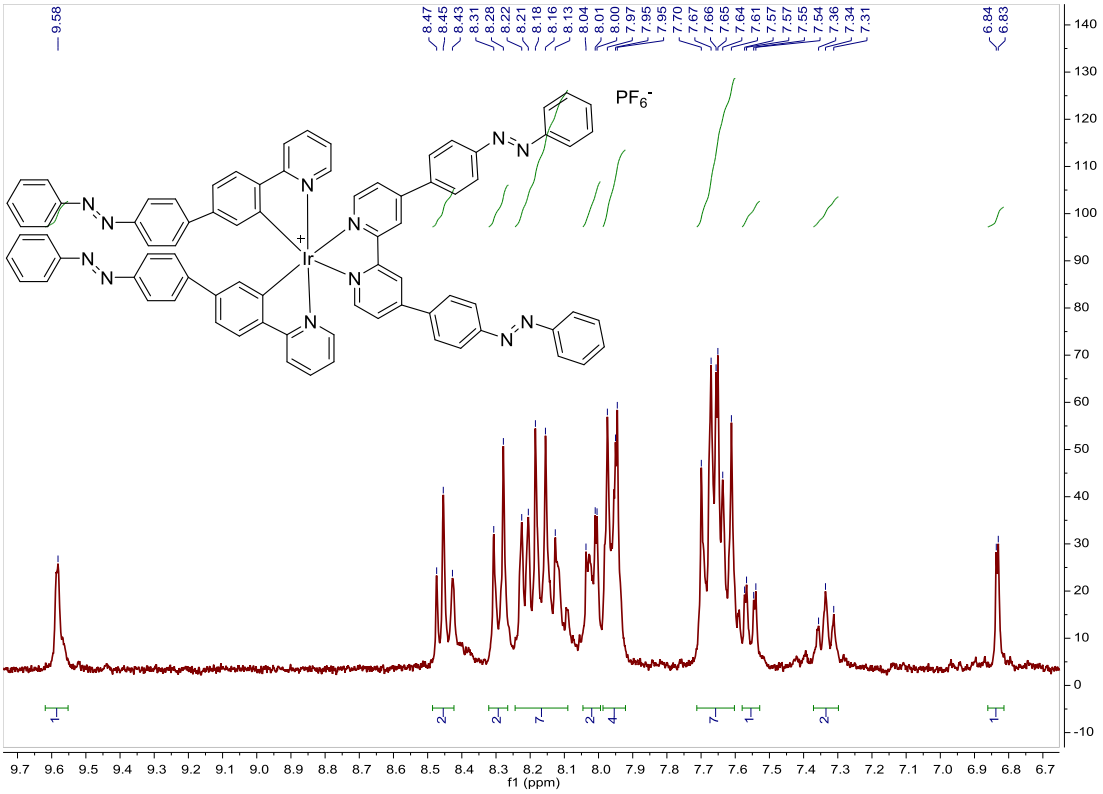

Fig. S236. ^{1}H NMR spectrum of **D3** in acetone-*d*$_6$, 300 MHz.

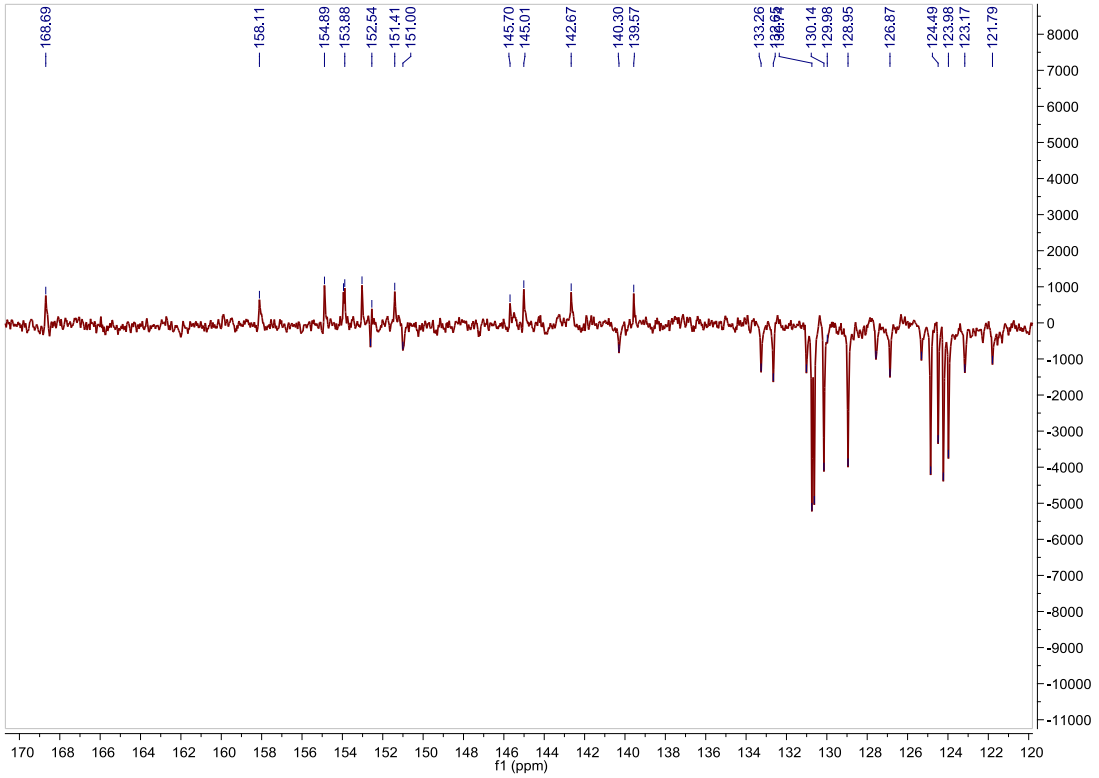

Fig. S237. ^{13}C APT NMR spectrum of **D3** in acetone-d_6, 75 MHz.

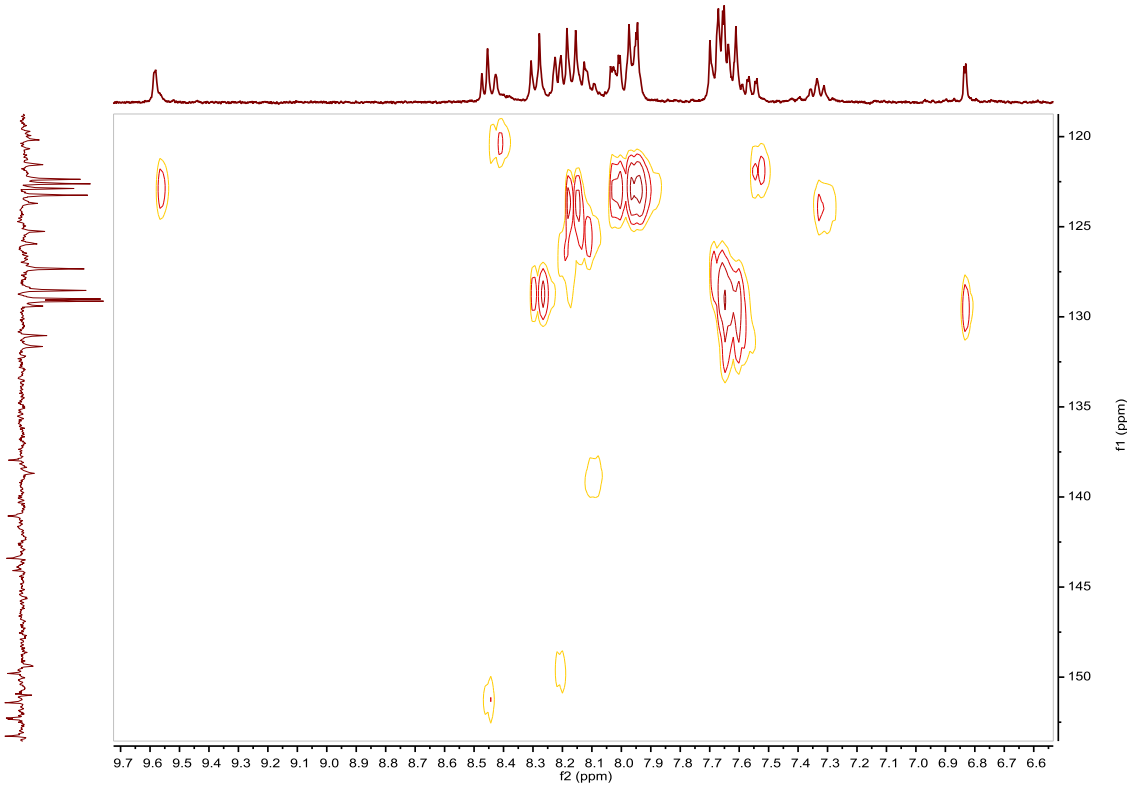

Fig. S238. HSQC NMR spectrum of **D3** in acetone-d_6.

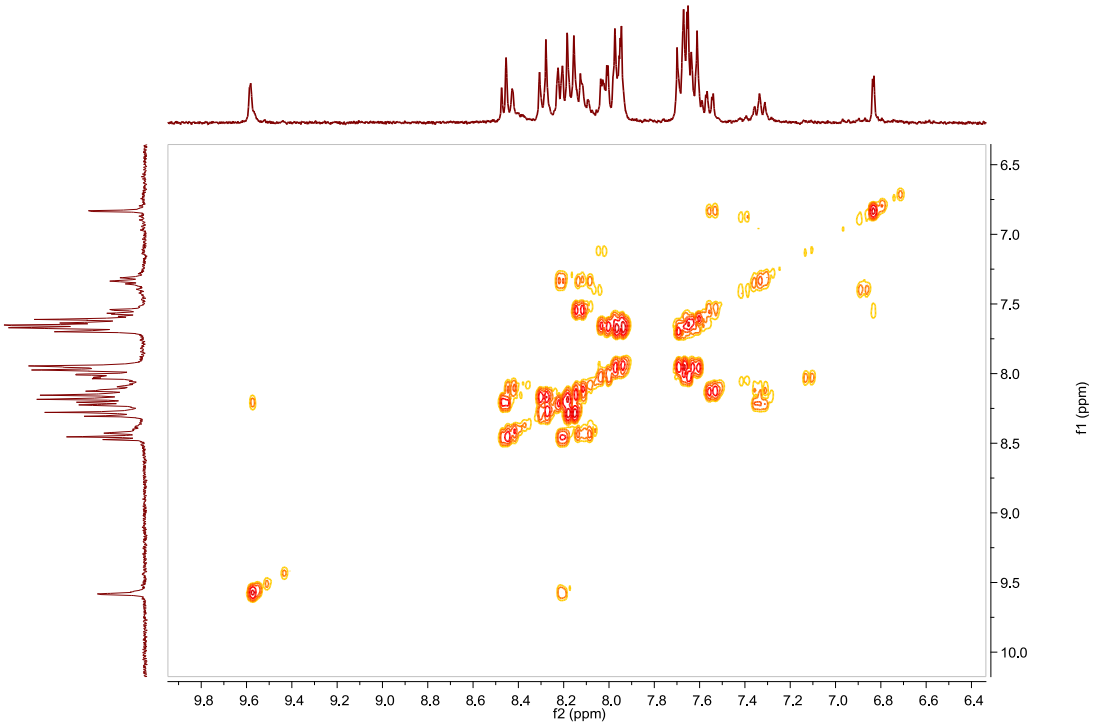

Fig. S239. COSY NMR spectrum of **D3** in acetone-d_6.

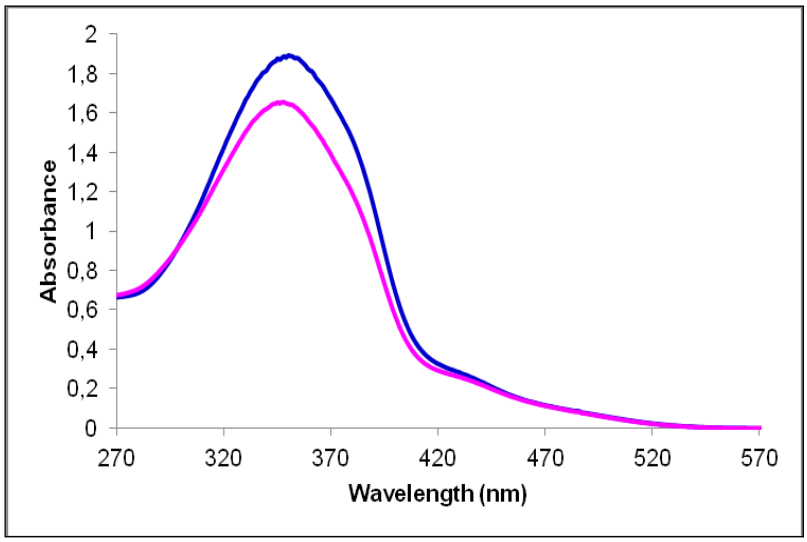

Fig. S240. UV/Vis spectra of **D3** in CH_3CN. Before (blue line) and after (pink line) irradiation at 355nm, $1.5 \cdot 10^{-5}$ M.

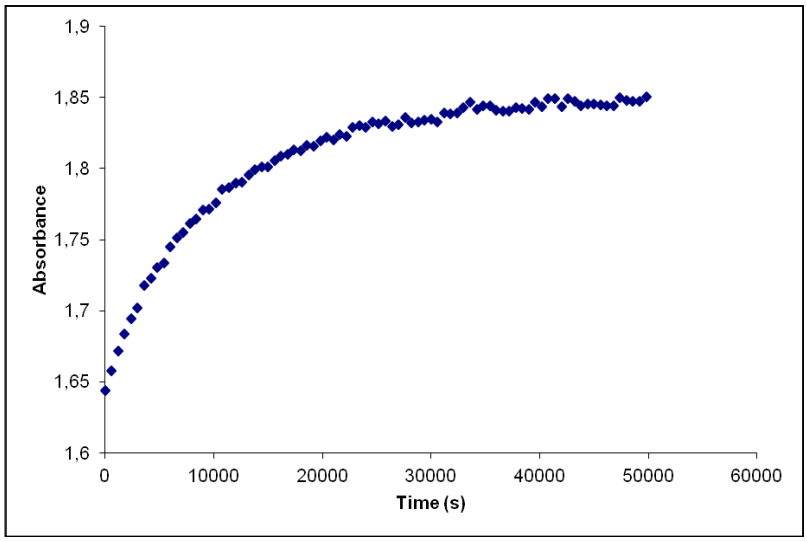

Fig. S241. Cis to trans thermal isomerization kinetics of **D3**. Absorption change of the band 350nm at 328 K in CH_3CN after irradiation at 355 nm. ($1.5 \cdot 10^{-5}$ M).

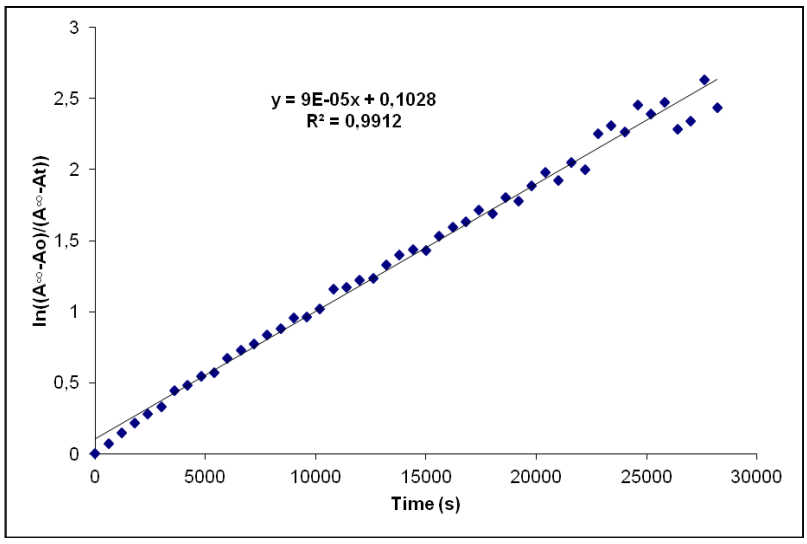

Fig. S242. Cis to trans thermal isomerization kinetics of **D3**. First-order plot. k (s^{-1}) = $9.0 \cdot 10^{-5}$. Half-life (min) = 128.

Compound A4, $[Ir(ppy)_2(4)]PF_6$. Synthesis, characterization and photoisomerization studies.

SYNTHESIS

Under a N_2 atmosphere, $[Ir(ppy)_2Cl]_2$ (0.100 g, 0.093 mmol) were added over a suspension of **L4** (0.077 g, 0.186 mmol) in 8 ml CH_2Cl_2–MeOH 2/1. The reaction mixture was refluxed, under N_2, for 15 h. After solvent evaporation the product was purified by column chromatography (silica gel, CH_2Cl_2). When the unreacted $[Ir(ppy)_2Cl]_2$ eluted, 0.05 g of KPF_6 were added on top of the column and the polarity of the eluent was gradually increased to 100% acetone to elute $[Ir(ppy)_2(\mathbf{L4})]PF_6$ together with the excess of KPF_6. The desired compound, purified by filtration through a celite path in CH_2Cl_2, was obtained as a red solid. Yield 86%.

Elemental Analysis: calculated for ($C_{44}H_{31}BrIrN_6PF_6$): C, 49.82; H, 2.95; N, 7.92. Found: C, 49.71; H, 3.10; N, 7.58.

Exact Mass: ESI-MS $[C_{44}H_{31}BrIrN_6]^+$: calculated: m/z= 915.1423, found: m/z= 915.1398.

^{1}H NMR (300 MHz, acetone-d_6): δ 9.36 (s, 2H), 8.26 (brd, J = 8.5 Hz, 4H), 8.19 (d, J = 5.8 Hz, 1H), 8.12 (brd, J = 8.5 Hz, 3H), 8.06–7.91 (m, 10H), 7.63 (m, 3H), 7.22 (ddd, J = 1.4 Hz, J = 5.8 Hz, J = 7.6 Hz, 2H), 7.07 (ddd, J = 1.0 Hz, J = 7.3 Hz, J = 12.8 Hz, 2H), 6.96 (ddd, J = 1.2 Hz, J = 7.3 Hz, J = 12.6 Hz, 2H), 6.41 (dd, J = 3.6 Hz, J = 7.4 Hz, 2H).

^{13}C APT NMR (75 MHz, acetone-d_6): δ 168.98 (C_{quat}), 168.94 (C_{quat}), 158.78 (C_{quat}), 156.97 (C_{quat}), 154.86 (C_{quat}), 153.88 (C_{quat}), 152.48 (CH), 152.30 (CH), 151.56 (C_{quat}), 151.31 (C_{quat}), 151.25 (C_{quat}), 150.87 (CH), 150.72 (CH), 145.42 (C_{quat}), 145.40 (C_{quat}), 140.12 (2CH), 139.28 (C_{quat}), 137.13 (C_{quat}), 133.22 (CH), 133.15 (CH), 132.93 (2CH), 131.76 (2CH), 130.74 (2CH), 130.13 (2CH), 129.88 (CH), 127.66 (CH), 126.31 (2CH), 125.07 (2CH), 124.84 (2CH), 124.25 (3CH), 123.95 (2CH), 121.30 (2CH).

UV/Vis (CH_3CN), λ, nm (ε, 10^4 M^{-1} cm^{-1}): 333 (4.4), 465 (0.30).

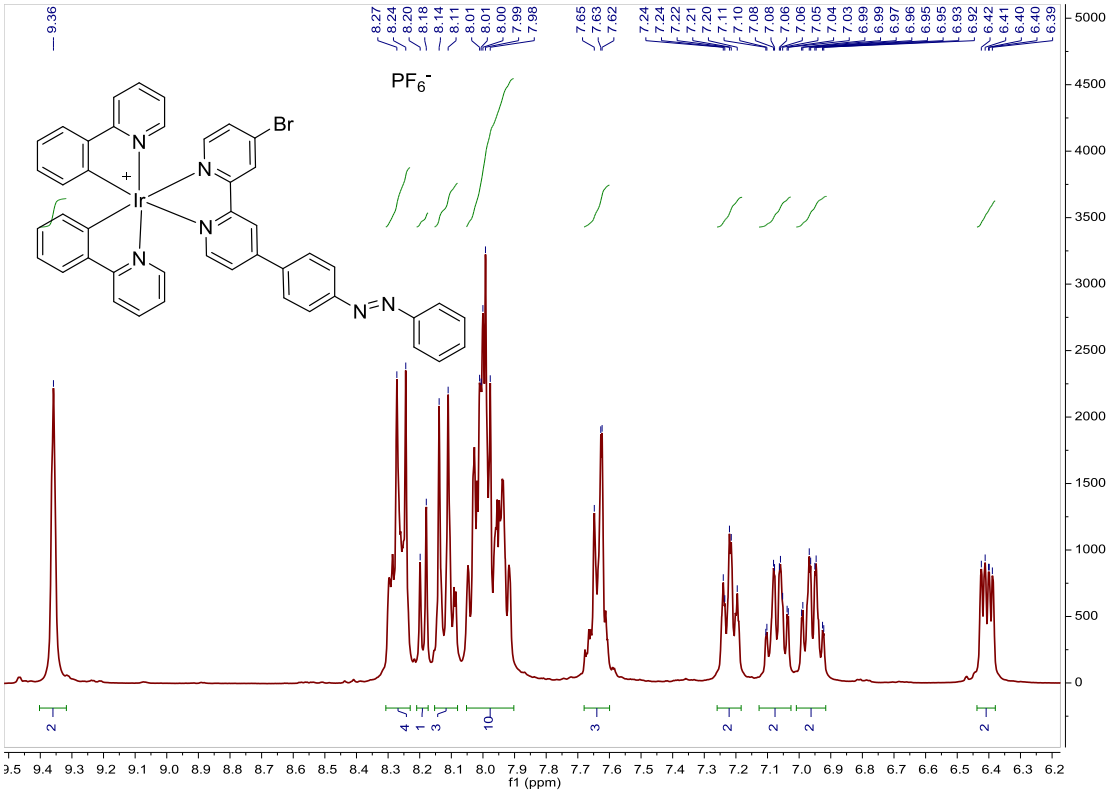

Fig. S243. ^{1}H NMR spectrum of **A4** in acetone-d_6, 300 MHz.

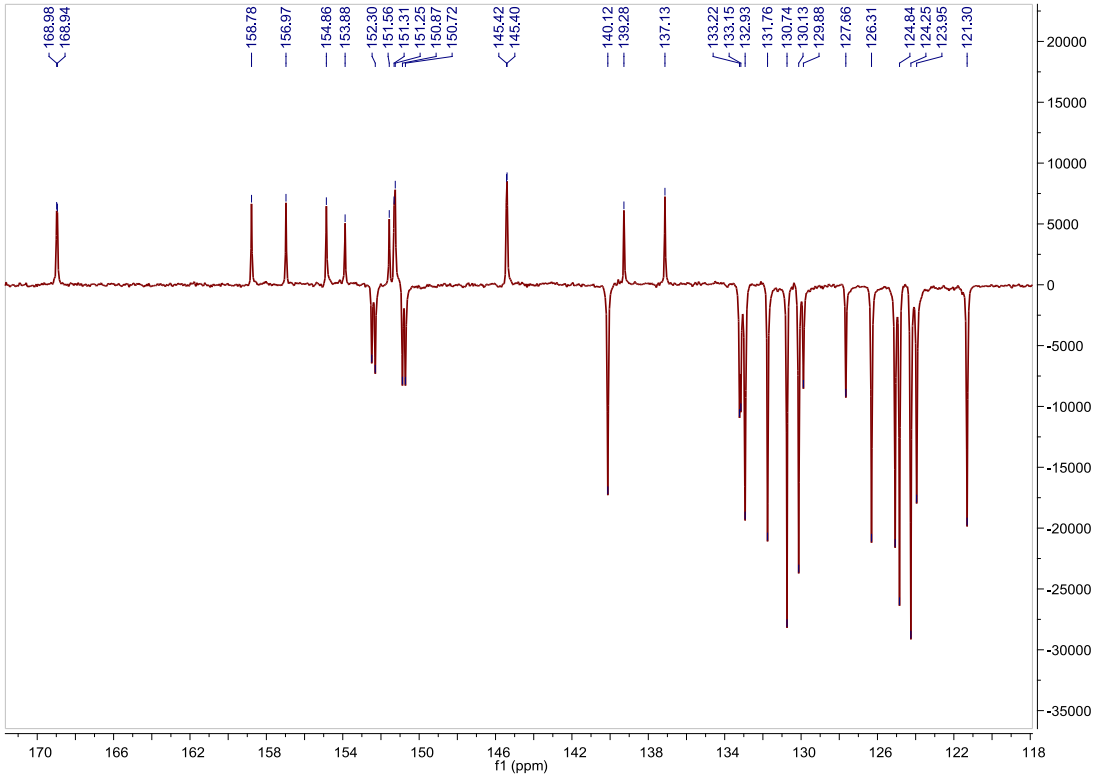

Fig. S244. ^{13}C APT NMR spectrum of **A4** in acetone-d_6, 75 MHz.

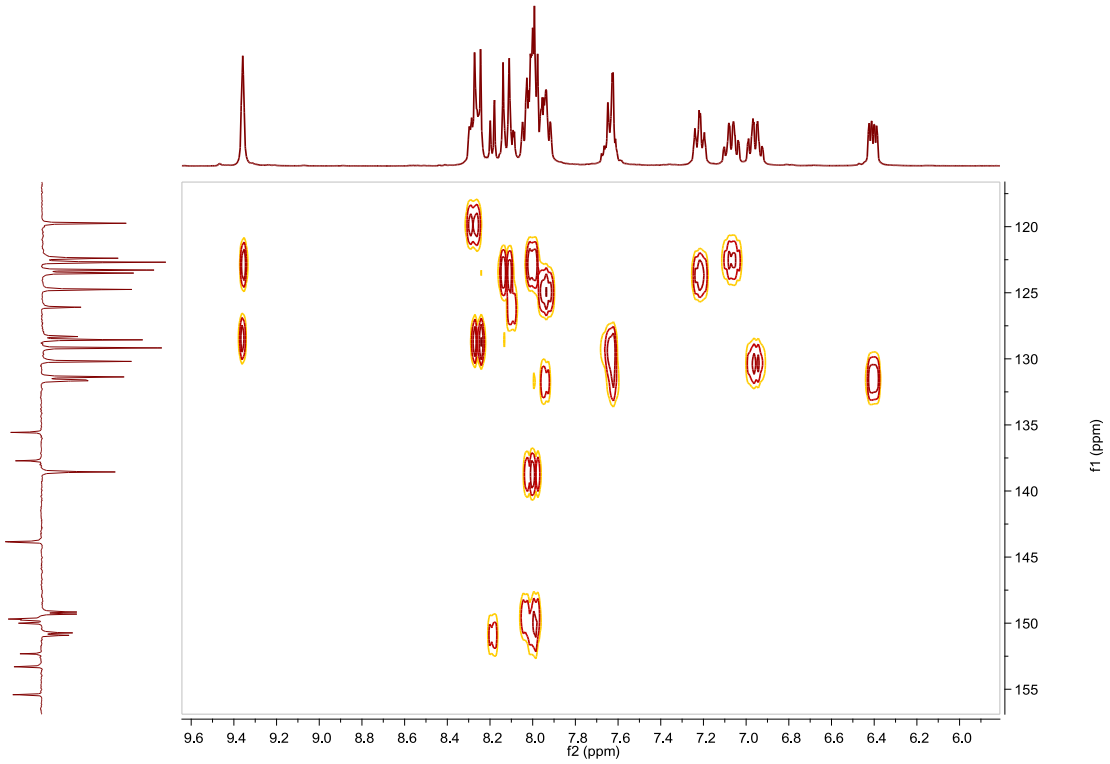

Fig. S245. HSQC NMR spectrum of **A4** in acetone-d_6.

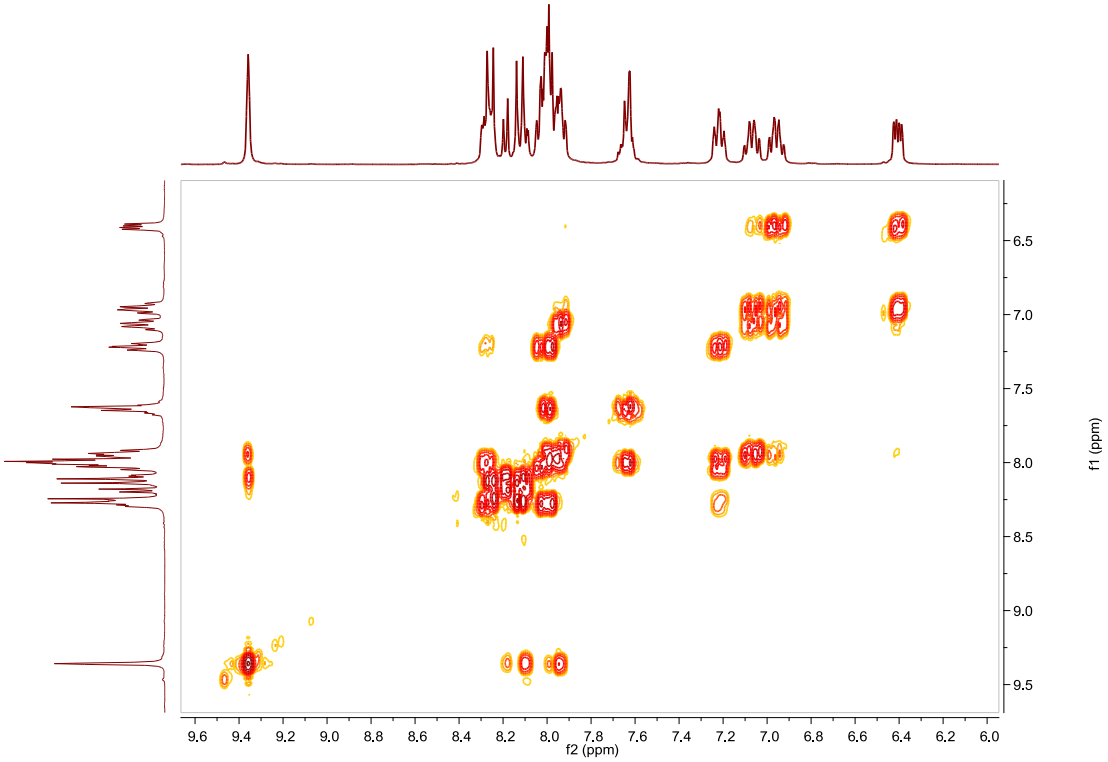

Fig. S246. COSY NMR spectrum of **A4** in acetone-d_6.

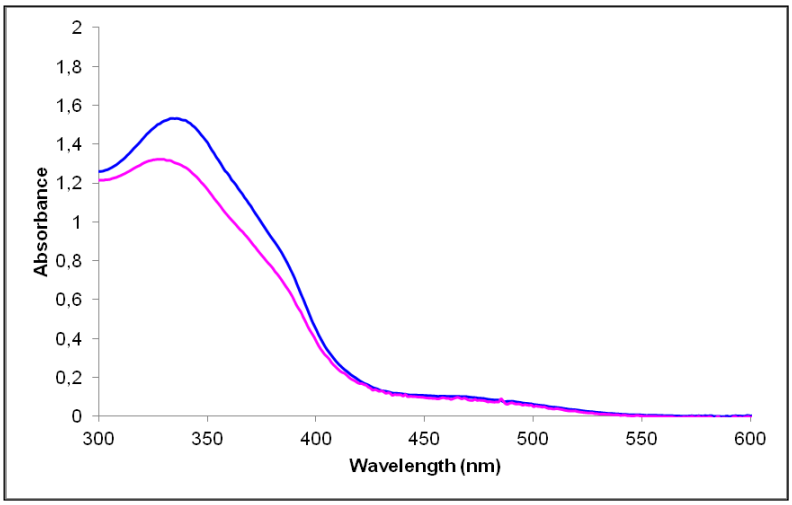

Fig. S247. UV/Vis spectra of **A4** in CH_3CN. Before (blue line) and after (pink line) irradiation at 343nm, $3.45 \cdot 10^{-5}$ M.

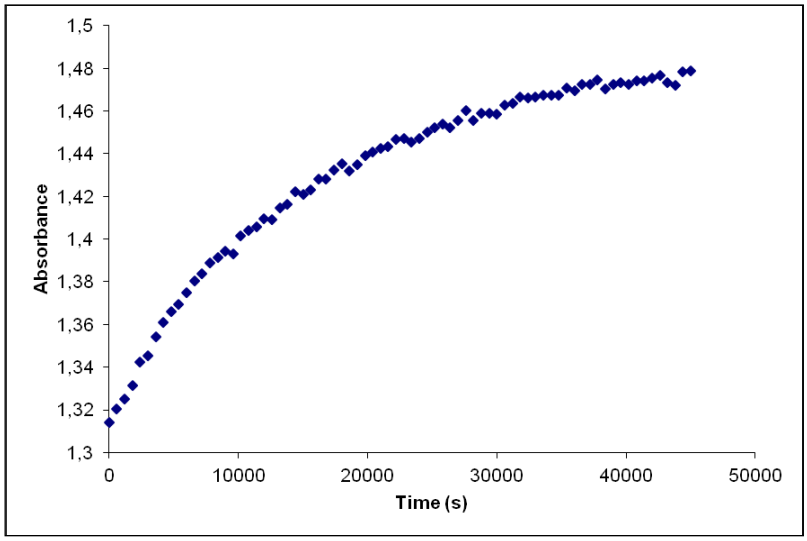

Fig. S248. Cis to trans thermal isomerization kinetics of **A4**. Absorption change of the band 333nm at 328 K in CH_3CN after irradiation at 343 nm. ($3.45 \cdot 10^{-5}$ M).

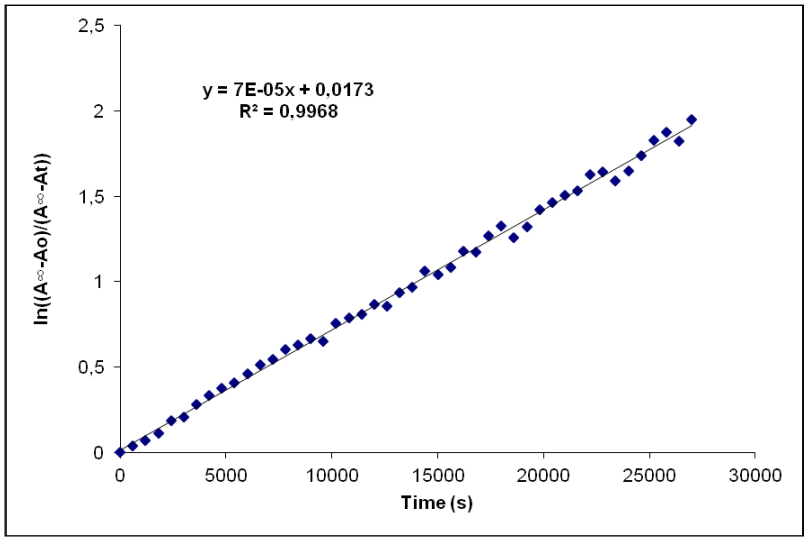

Fig. S249. Cis to trans thermal isomerization kinetics of **A4**. First-order plot. k (s^{-1}) = $7.0 \cdot 10^{-5}$. Half-life (min) = 165.

Compound B4, $[Ir(Fppy)_2(4)]PF_6$. Synthesis, characterization and photoisomerization studies.

SYNTHESIS

Under a N_2 atmosphere, $[Ir(Fppy)_2Cl]_2$ (0.100 g, 0.082 mmol) were added over a suspension of **L4** (0.068 g, 0.164 mmol) in 8 ml CH_2Cl_2–MeOH 2/1. The reaction mixture was refluxed, under N_2, for 15 h. After solvent evaporation the product was purified by column chromatography (silica gel, CH_2Cl_2). When the unreacted $[Ir(Fppy)_2Cl]_2$ eluted, 0.05 g of KPF_6 were added on top of the column and the polarity of the eluent was gradually increased to 100% acetone to elute $[Ir(Fppy)_2(\mathbf{L4})]PF_6$ together with the excess of KPF_6. The desired compound was precipitated with ether after filtration through a celite path in CH_2Cl_2 and it was obtained as an orange solid. Yield 87%.

Elemental Analysis: calculated for $(C_{44}H_{27}BrF_4IrN_6PF_6 \cdot CH_3COCH_3)$: C, 47.40; H, 2.79; N, 7.06. Found: C, 47.23; H, 2.88; N, 7.27.

Exact Mass: ESI-MS $[C_{44}H_{27}BrF_4IrN_6]^+$: calculated: m/z= 987.1032, found: m/z= 987.1014.

^{1}H NMR (300 MHz, acetone-d_6): δ 9.43 (brs, 2H), 8.44 (m, 2H), 8.33 (d, J = 5.8 Hz, 1H), 8.28 (brd, J = 8.8 Hz, 2H), 8.20 (dd, J = 1.8 Hz, J = 5.8 Hz, 1H), 8.17–8.07 (m, 7H), 8.01 (m, 3H), 7.65 (m, 3H), 7.31 (m, 2H), 6.82 (m, 2H), 5.87 (t, J = 2.6 Hz, 1H), 5.84 (t, J = 2.6 Hz, 1H).

^{13}C APT NMR (75 MHz, acetone-d_6): δ 165.10 (brs, 2C_{quat}), 165.00 (dd, J = 12.2 Hz, J = 254.5 Hz, 2C_{quat}), 162.82 (dd, J = 12.5 Hz, J = 257.3 Hz, 2C_{quat}), 158.54 (s, C_{quat}), 156.79 (s, C_{quat}), 155.62 (d, J = 6.3 Hz, C_{quat}), 155.36 (d, J = 6.4 Hz, C_{quat}), 154.99 (s, C_{quat}), 153.88 (s, C_{quat}), 152.92 (s, CH), 152.70 (s, CH), 151.85 (s, C_{quat}), 151.41 (s, CH), 151.27 (s, CH), 141.23 (s, 2CH), 139.06 (s, C_{quat}), 137.82 (s, C_{quat}), 133.50 (s, CH), 133.27 (s, CH), 130.74 (s, 2CH), 130.16 (s, 3CH), 129.29 (s, 2C_{quat}), 127.97 (s, CH), 125.59 (s, 2CH), 125.04 (d, J = 22.5 Hz, CH), 124.87 (s, 3CH), 124.72 (d, J = 20.8 Hz, CH), 124.24 (s, 2CH), 115.09 (d, J = 17.7 Hz, 2CH), 100.19 (t, J = 26.9 Hz, 2CH).

UV/Vis (CH_3CN), λ, nm (ε, 10^4 M^{-1} cm^{-1}): 339 (4.3), 440 (0.33).

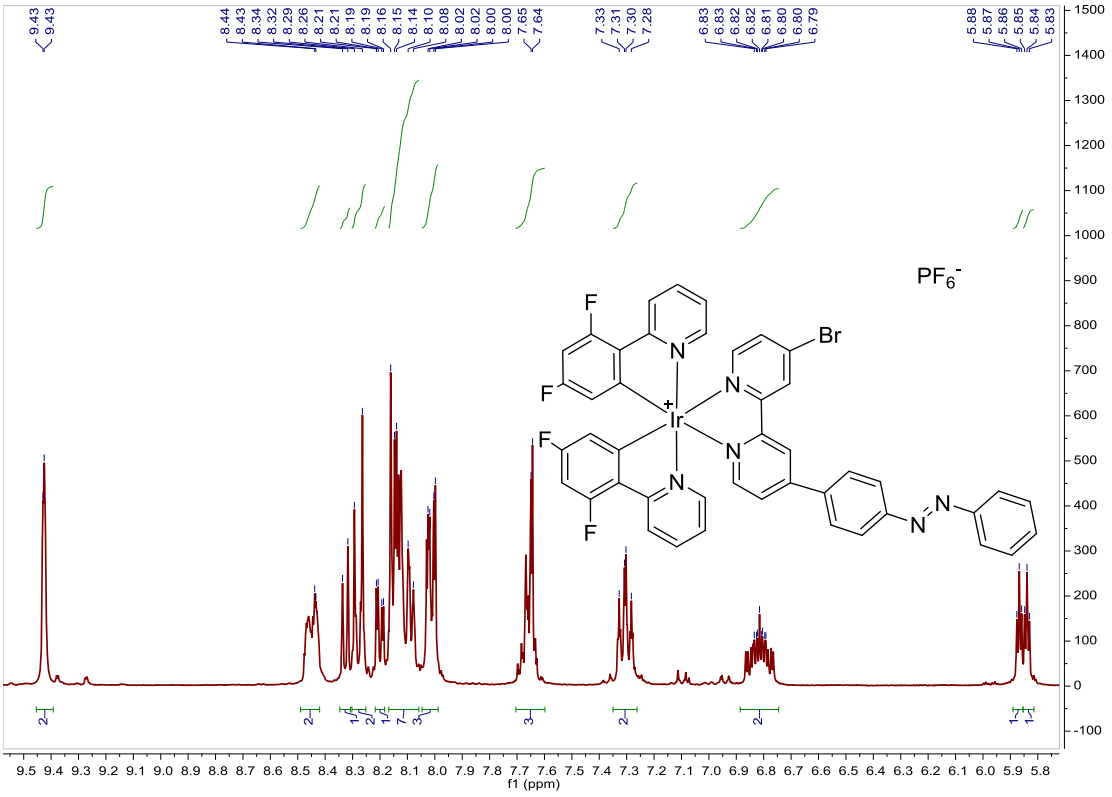

Fig. S250. ^{1}H NMR spectrum of **B4** in acetone-d_6, 300 MHz.

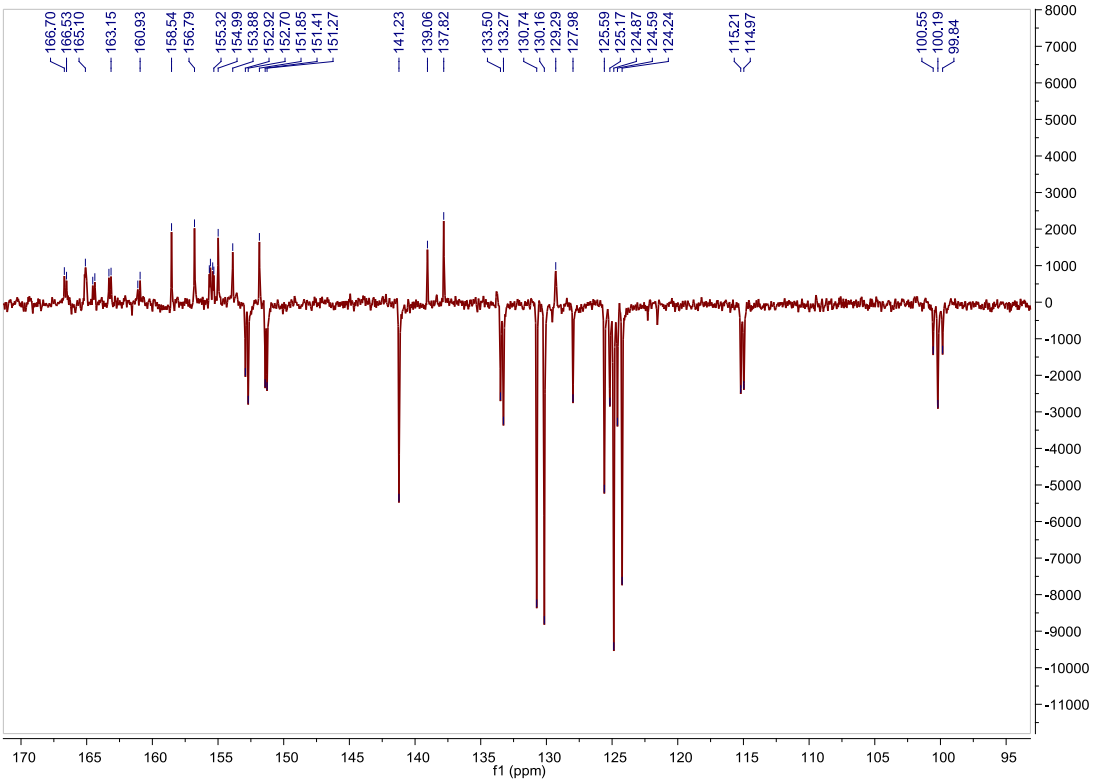

Fig. S251. ^{13}C APT NMR spectrum of **B4** in acetone-d_6, 75 MHz.

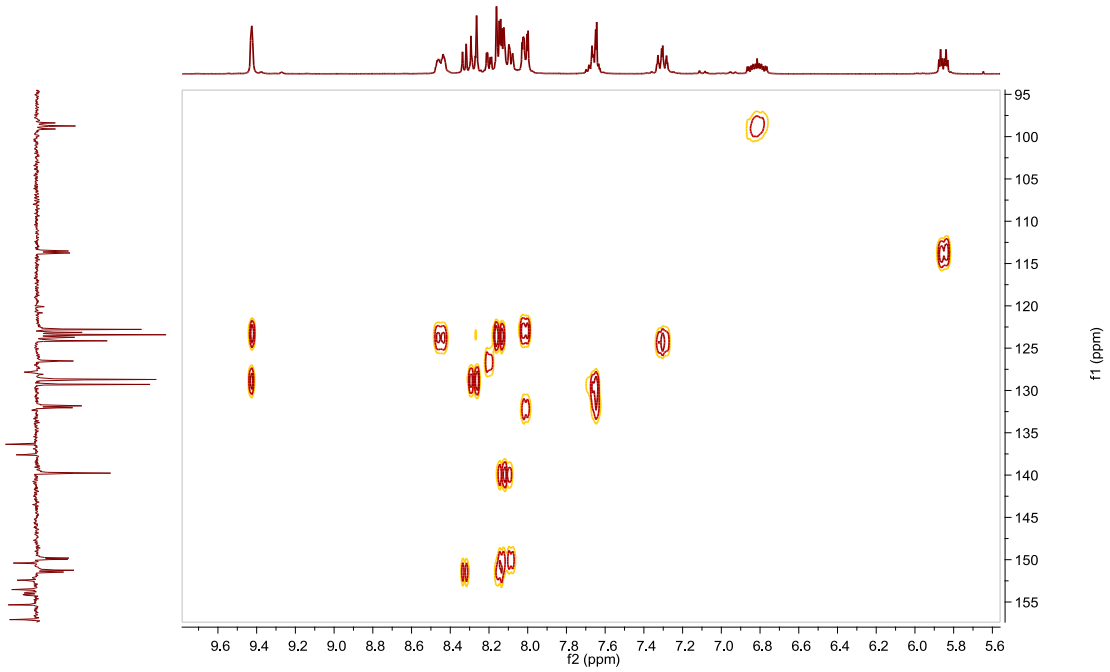

Fig. S252. HSQC NMR spectrum of **B4** in acetone-d_6.

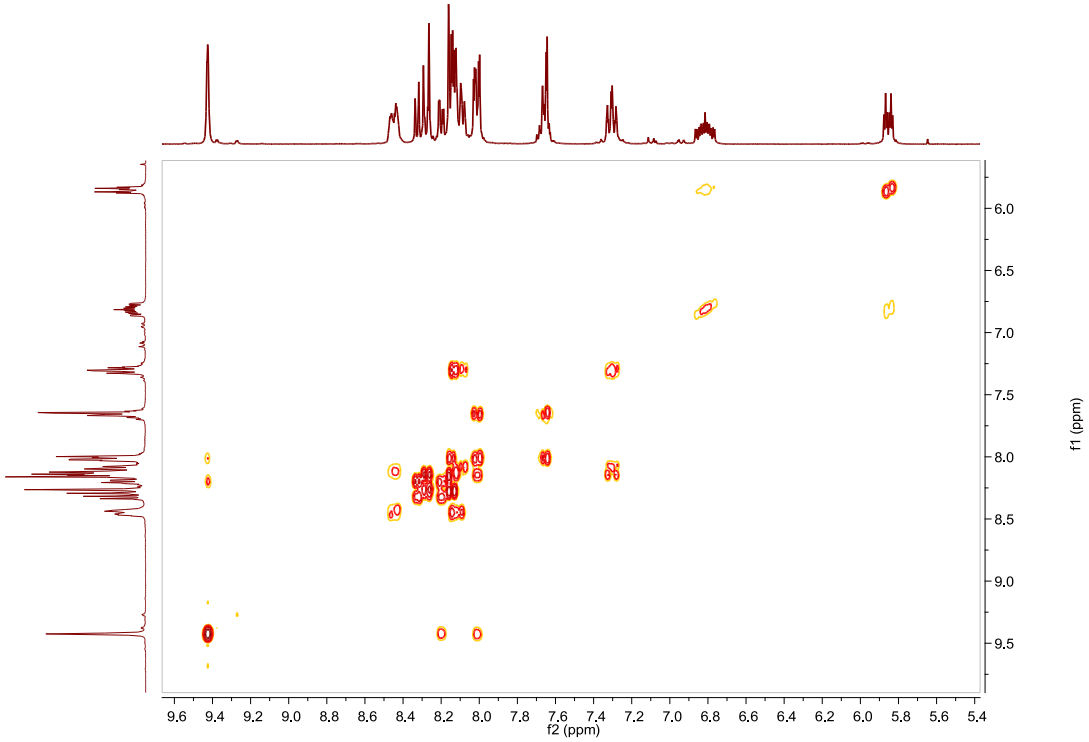

Fig. S253. COSY NMR spectrum of **B4** in acetone-d_6.

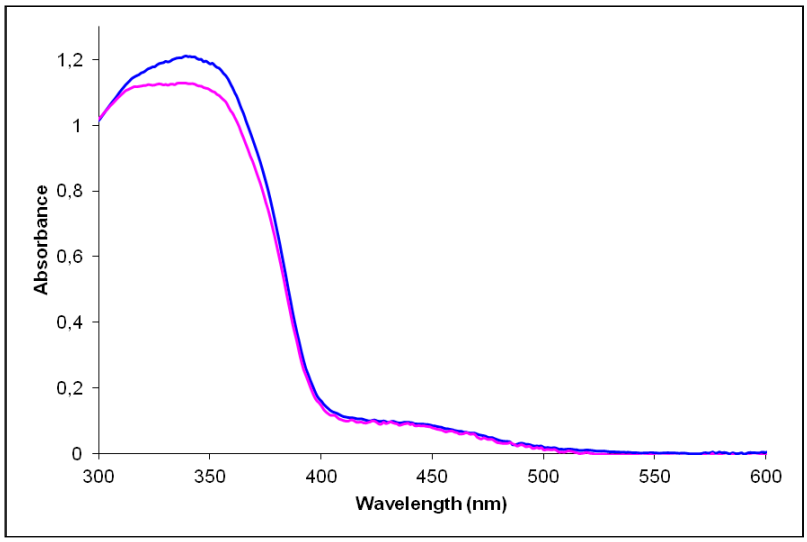

Fig. S254. UV/Vis spectra of **B4** in CH_3CN. Before (blue line) and after (pink line) irradiation at 351nm, $2.82 \cdot 10^{-5}$ M.

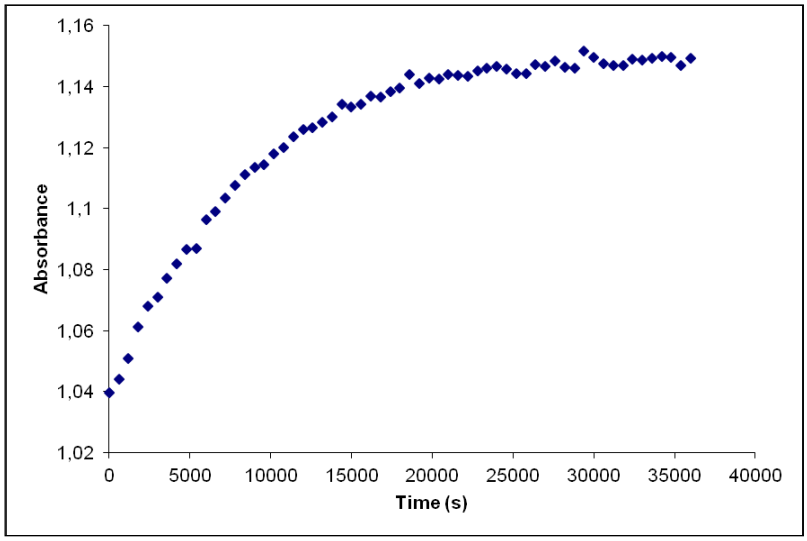

Fig. S255. Cis to trans thermal isomerization kinetics of **B4**. Absorption change of the band 339nm at 328 K in CH_3CN after irradiation at 351 nm. ($2.82 \cdot 10^{-5}$ M).

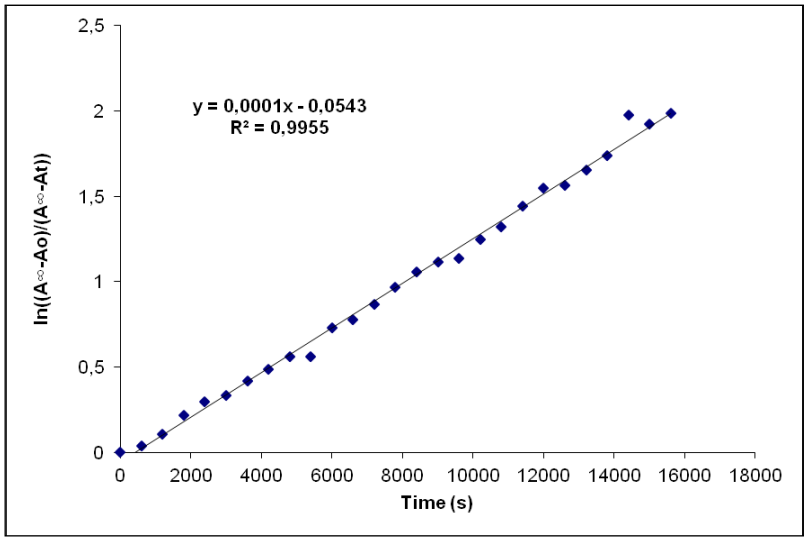

Fig. S256. Cis to trans thermal isomerization kinetics of **B4**. First-order plot. k (s^{-1}) = $1.0 \cdot 10^{-4}$. Half-life (min) = 115.

Compound C4, $[Ir(Brppy)_2(4)]PF_6$. Synthesis, characterization and photoisomerization studies.

SYNTHESIS

Under a N_2 atmosphere, $[Ir(Brppy)_2Cl]_2$ (0.100 g, 0.072 mmol) were added over a suspension of **L4** (0.06 g, 0.144 mmol) in 8 ml CH_2Cl_2–MeOH 2/1. The reaction mixture was refluxed, under N_2, for 15 h. After solvent evaporation the product was purified by column chromatography (silica gel, CH_2Cl_2). When the unreacted $[Ir(Brppy)_2Cl]_2$ eluted, 0.05 g of KPF_6 were added on top of the column and the polarity of the eluent was gradually increased to 100% acetone to elute $[Ir(Brppy)_2(\mathbf{L4})]PF_6$ together with the excess of KPF_6. The desired compound, purified by filtration through a celite path in CH_2Cl_2, was obtained as an orange solid. Yield 98%.

Elemental Analysis: calculated for ($C_{44}H_{29}Br_3IrN_6PF_6$): C, 43.37; H, 2.40; N, 6.90. Found: C, 42.97; H, 2.83; N, 6.79.

Exact Mass: ESI-MS $[C_{44}H_{29}Br_3IrN_6]^+$: calculated: m/z= 1070.9607, found: m/z= 1070.9579.

^{1}H NMR (300 MHz, acetone-d_6): δ 9.40 (d, J = 1.7 Hz, 2H), 8.34 (m, 2H), 8.27 (m, 3H), 8.18 (dd, J = 1.8 Hz, J = 5.9 Hz, 1H), 8.14 (brd, J = 8.7 Hz, 2H), 8.11–8.05 (m, 4H), 8.05–7.98 (m, 4H), 7.95 (dd, J = 5.7 Hz, J = 8.4 Hz, 2H), 7.69–7.62 (m, 3H), 7.35–7.25 (m, 4H), 6.46 (dd, J = 2.0 Hz, J = 3.1 Hz, 2H).

^{13}C APT NMR (75 MHz, acetone-d_6): δ 167.71 (C_{quat}), 167.66 (C_{quat}), 158.66 (C_{quat}), 156.90 (C_{quat}), 154.94 (C_{quat}), 153.88 (C_{quat}), 153.59 (C_{quat}), 153.34 (C_{quat}), 152.77 (CH), 152.55 (CH), 151.64 (C_{quat}), 151.13 (CH), 150.97 (CH), 144.74 (C_{quat}), 144.72 (C_{quat}), 140.67 (2CH), 139.15 (C_{quat}), 137.58 (C_{quat}), 135.10 (CH), 135.07 (CH), 133.38 (CH), 133.25 (CH), 130.74 (2CH), 130.15 (2CH), 130.07 (CH), 128.13 (2CH), 127.87 (CH), 127.26 (2CH), 126.26 (2C_{quat}), 125.76 (2CH), 124.86 (2CH), 124.48 (CH), 124.25 (2CH), 121.90 (2CH).

UV/Vis (CH_3CN), λ, nm (ε, 10^4 M^{-1} cm^{-1}): 336 (4.7), 453 (0.35).

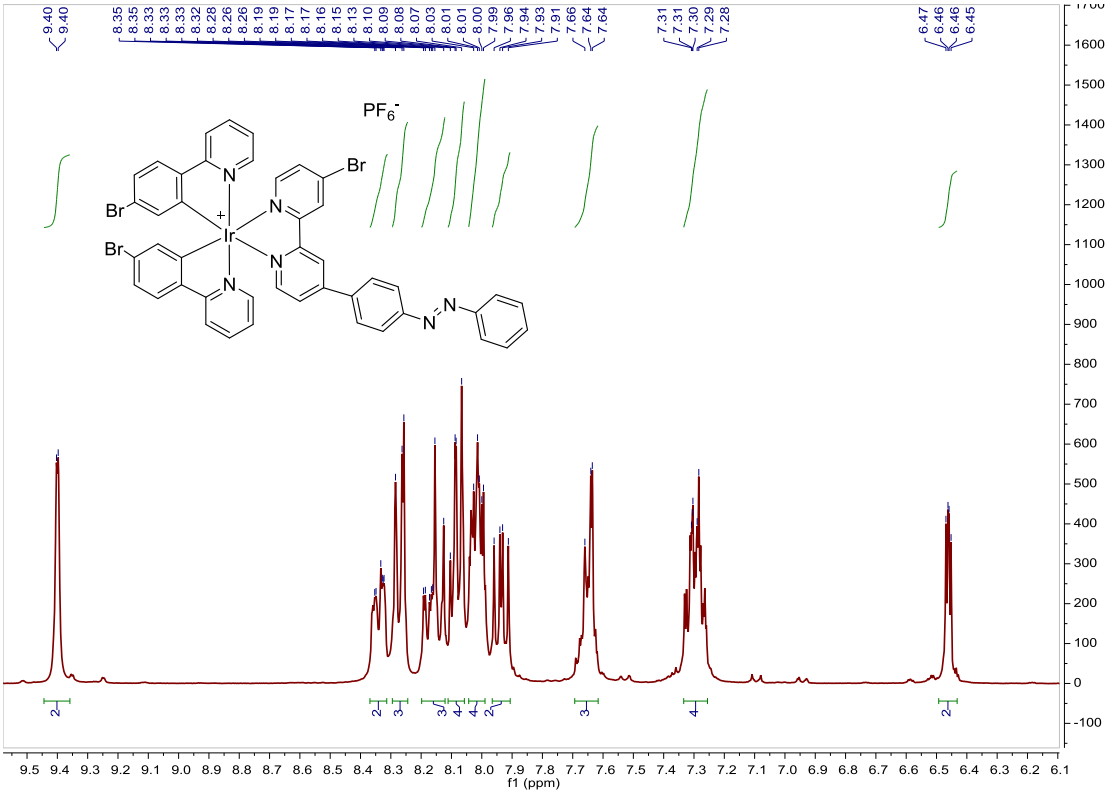

Fig. S257. ^{1}H NMR spectrum of **C4** in acetone-d_6, 300 MHz.

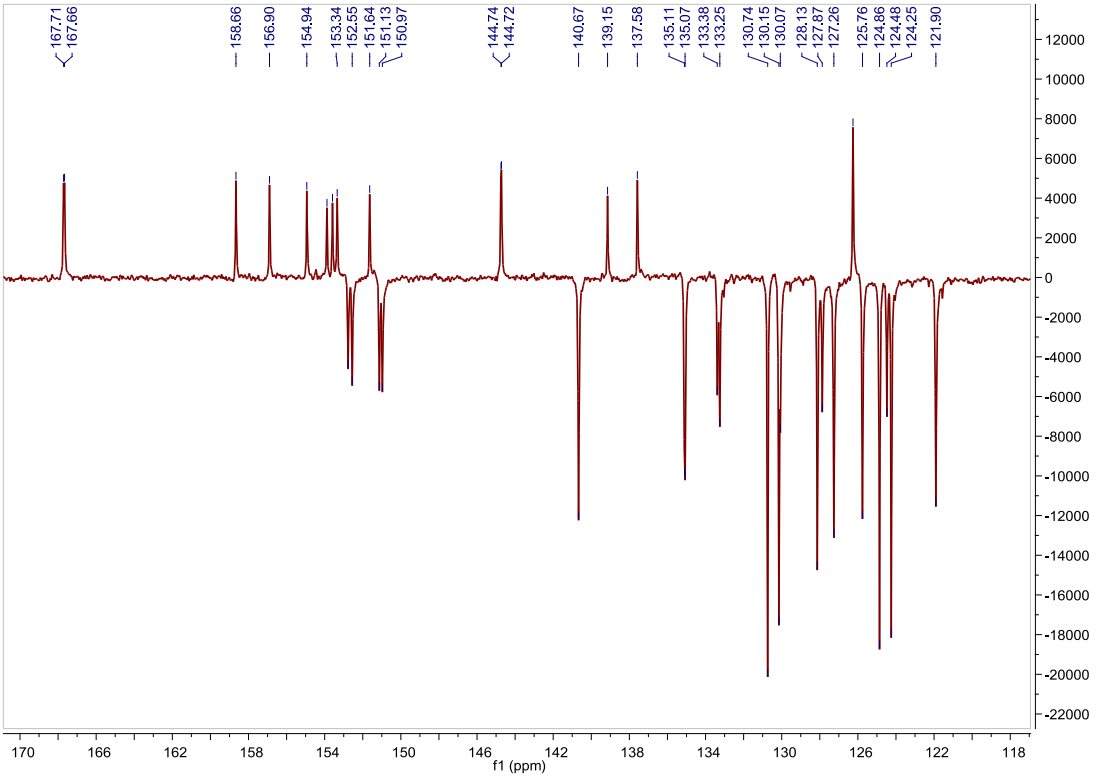

Fig. S258. ^{13}C APT NMR spectrum of **C4** in acetone-d_6, 75 MHz.

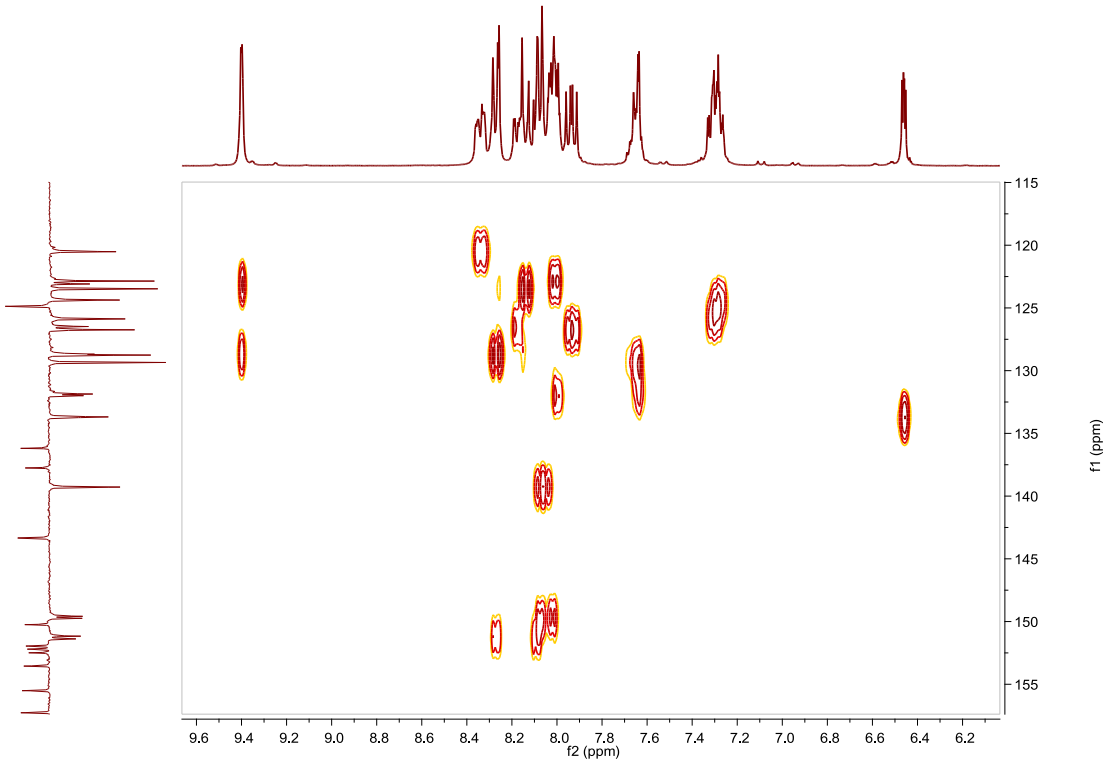

Fig. S259. HSQC NMR spectrum of **C4** in acetone-d_6.

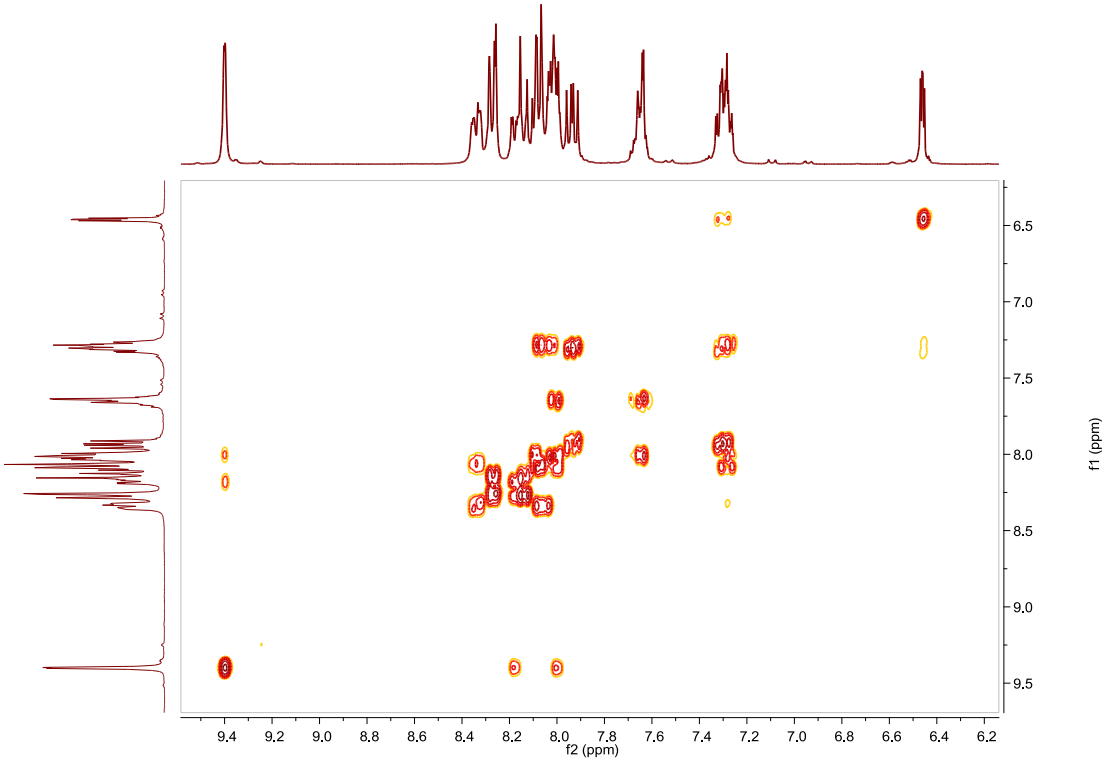

Fig. S260. COSY NMR spectrum of **C4** in acetone-d_6.

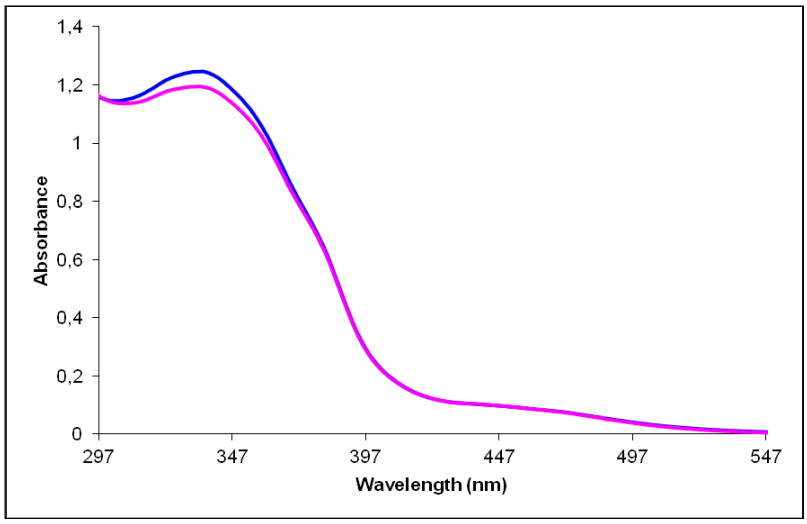

Fig. S261. UV/Vis spectra of **C4** in CH_3CN. Before (blue line) and after (pink line) irradiation at 336nm, $2.61 \cdot 10^{-5}$ M.

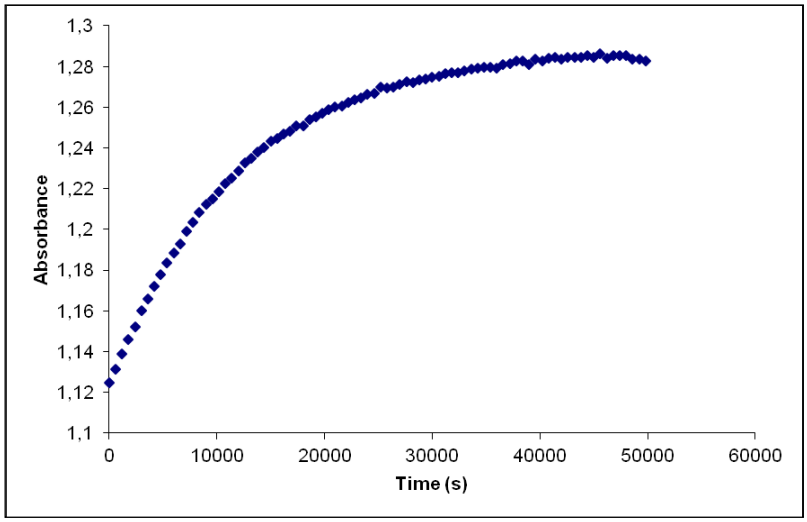

Fig. S262. Cis to trans thermal isomerization kinetics of **C4**. Absorption change of the band 336nm at 328 K in CH_3CN after irradiation at 336 nm. ($2.61 \cdot 10^{-5}$ M).

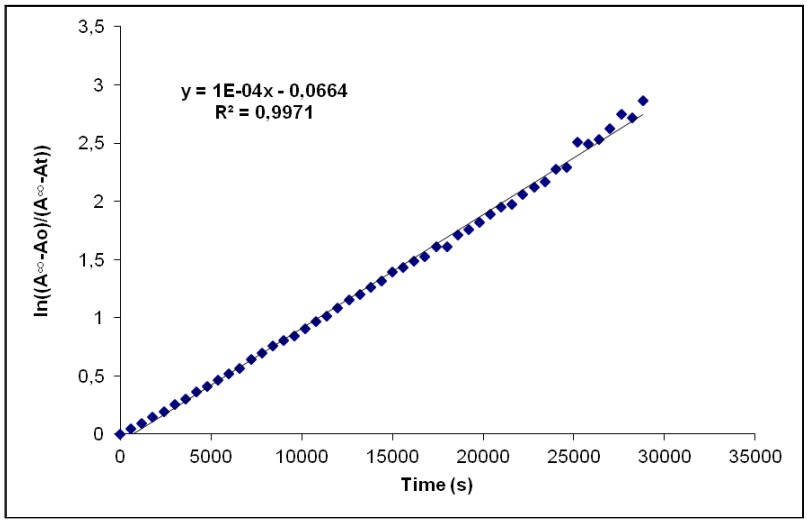

Fig. S263. Cis to trans thermal isomerization kinetics of **C4**. First-order plot. k (s^{-1}) = $1.0 \cdot 10^{-4}$. Half-life (min) = 115.

Compound A5, [Ir(ppy)$_2$(5)]PF$_6$. Synthesis, characterization and photoisomerization studies.

SYNTHESIS

Under a N_2 atmosphere, $[Ir(ppy)_2Cl]_2$ (0.052 g, 0.048 mmol) were added over a suspension of **L5** (0.05 g, 0.097 mmol) in 4 ml CH_2Cl_2–MeOH 2/1. The reaction mixture was refluxed, under N_2, for 15 h. After solvent evaporation the product was purified by column chromatography (silica gel, CH_2Cl_2). When the unreacted $[Ir(ppy)_2Cl]_2$ eluted, 0.025 g of KPF_6 were added on top of the column and the polarity of the eluent was gradually increased to 100% acetone to elute $[Ir(ppy)_2$(**L5**)$]PF_6$ together with the excess of KPF_6. The desired compound, purified by filtration through a celite path in CH_2Cl_2, was obtained as an orange solid. Yield 75%.

Elemental Analysis: calculated for ($C_{56}H_{40}IrN_8PF_6$): C, 57.88; H, 3.47; N, 9.64. Found: C, 57.48; H, 3.61; N, 9.55.

Exact Mass: ESI-MS $[C_{56}H_{40}IrN_8]^+$: calculated: m/z= 1017.3005, found: m/z= 1017.2991.

^{1}H NMR (300 MHz, acetone-*d*$_6$): δ 9.55 (s, 1H), 8.48 (s, 1H), 8.32 (d, J=8.1 Hz, 1H), 8.26 (d, J=5.8 Hz, 1H), 8.14 (m, 3H), 8.01 (m, 6H), 7.85 (pst, J=7.9 Hz, 1H), 7.63 (m, 2H), 7.24 (pst, J=6.0 Hz, 1H), 7.11 (pst, J=7.6 Hz, 1H), 6.99 (pst, J=7.3 Hz, 1H), 6.46 (d, J=7.4 Hz, 1H).

^{13}C APT NMR (75 MHz, acetone-*d*$_6$): δ 173.48 (C_{quat}), 162.42 (C_{quat}), 158.89 (C_{quat}), 158.03 (C_{quat}), 156.55 (CH), 156.29 (C_{quat}), 156.06 (C_{quat}), 154.98 (CH), 149.76 (C_{quat}), 144.35 (CH), 143.00 (C_{quat}), 137.46 (CH), 137.28 (CH), 136.12 (CH), 136.07 (1C, CH), 135.82 (1C, CH), 135.04 (2C, CH), 131.96 (1C, CH), 130.62 (CH), 129.40 (CH), 129.31 (CH), 128.71 (CH), 128.42 (2CH), 128.18 (CH), 128.09 (CH), 125.61 (CH).

UV/Vis (CH_3CN), λ, nm (ε, 10^4 M^{-1} cm^{-1}): 290 (6.5), 381 (1.1), 462 (0.21).

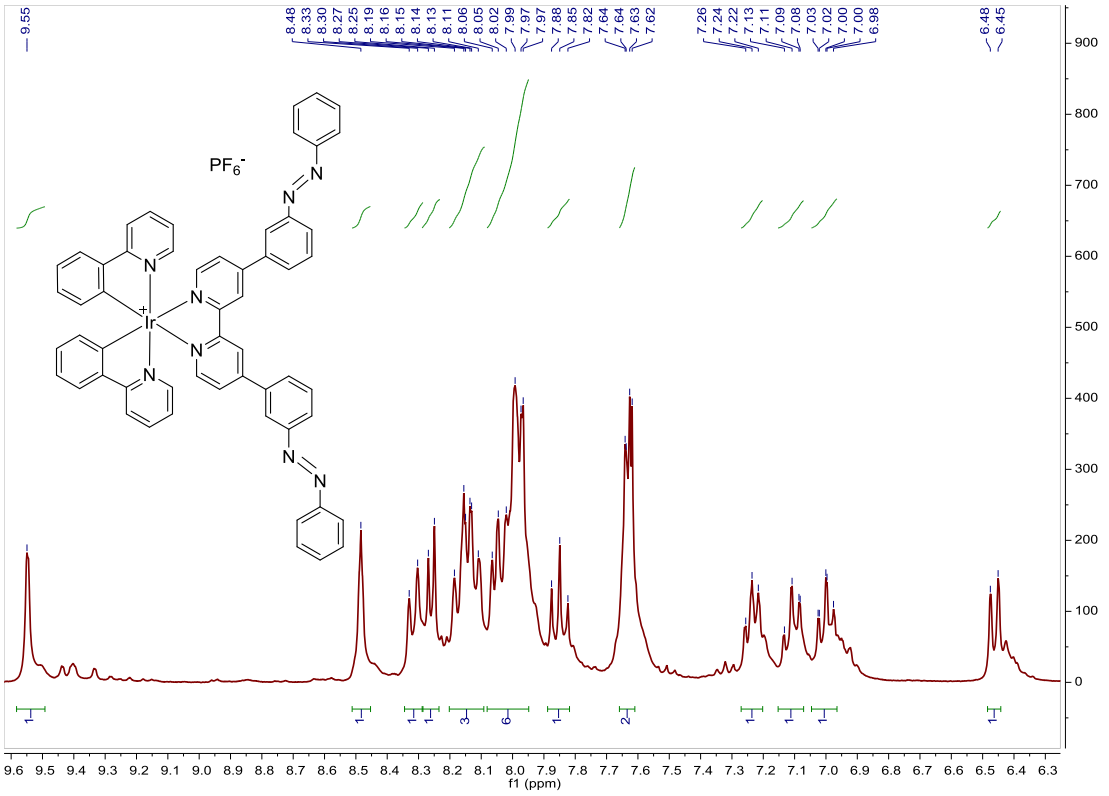

Fig. S264. ^{1}H NMR spectrum of **A5** in acetone-*d*$_6$, 300 MHz.

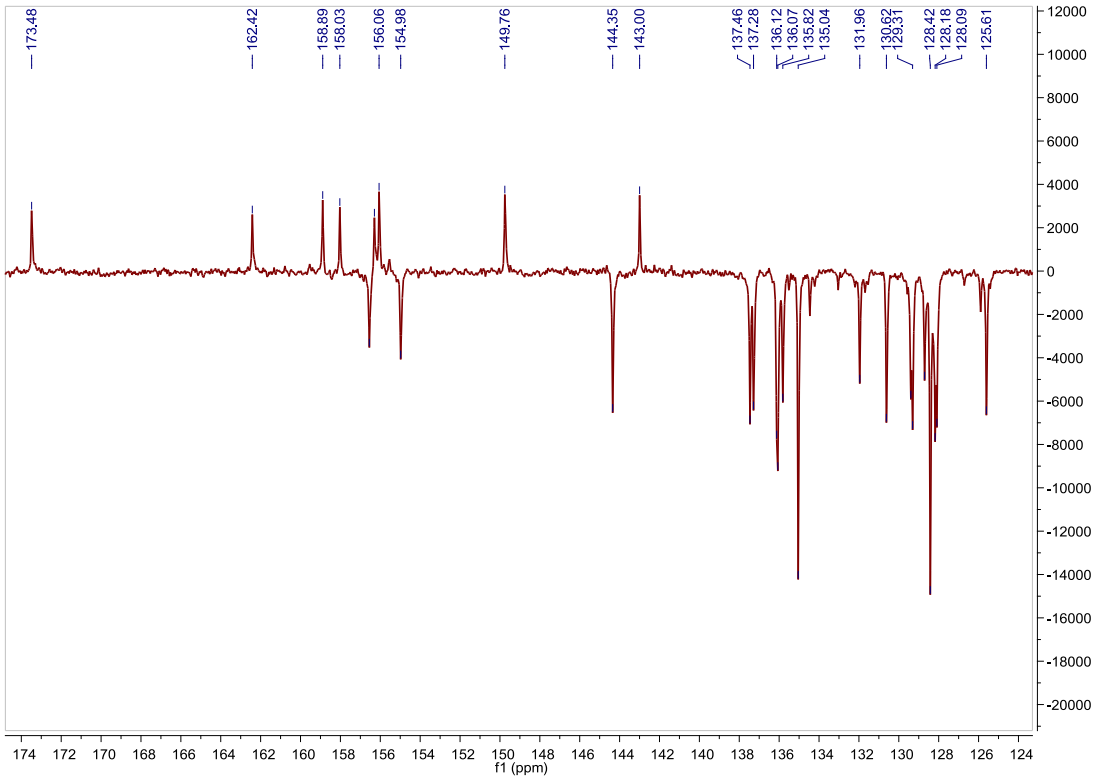

Fig. S265. ^{13}C APT NMR spectrum of **A5** in acetone-d_6, 75 MHz.

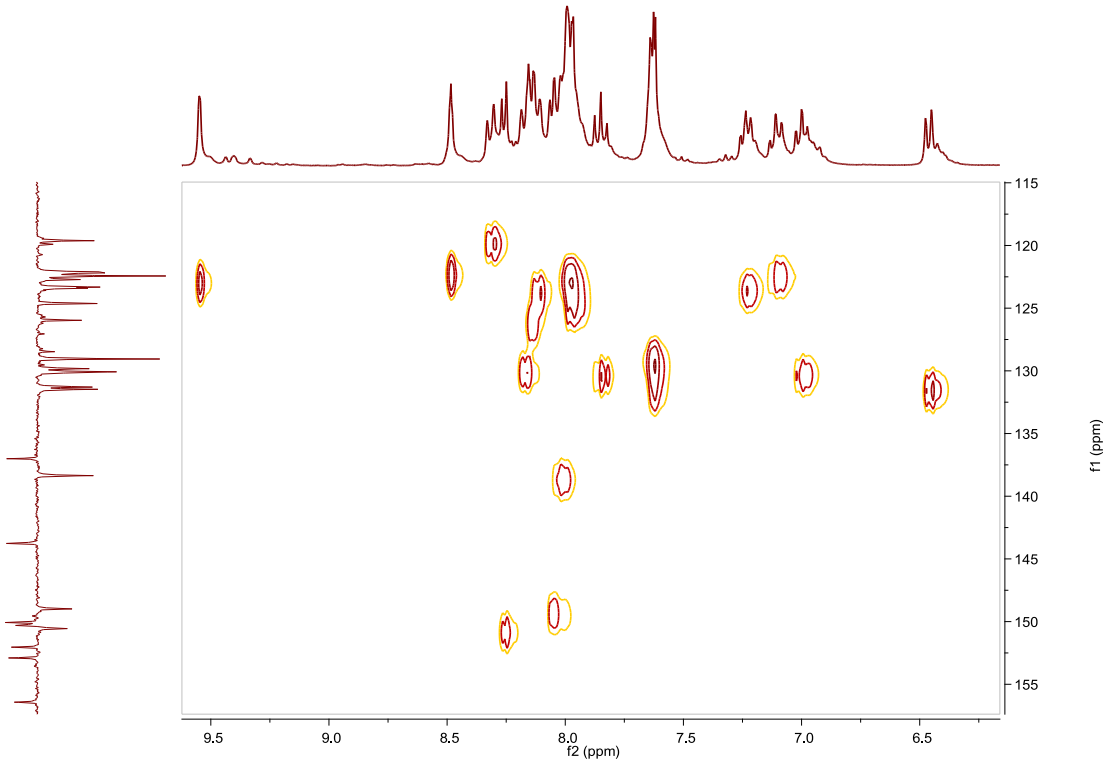

Fig. S266. HSQC NMR spectrum of **A5** in acetone-d_6.

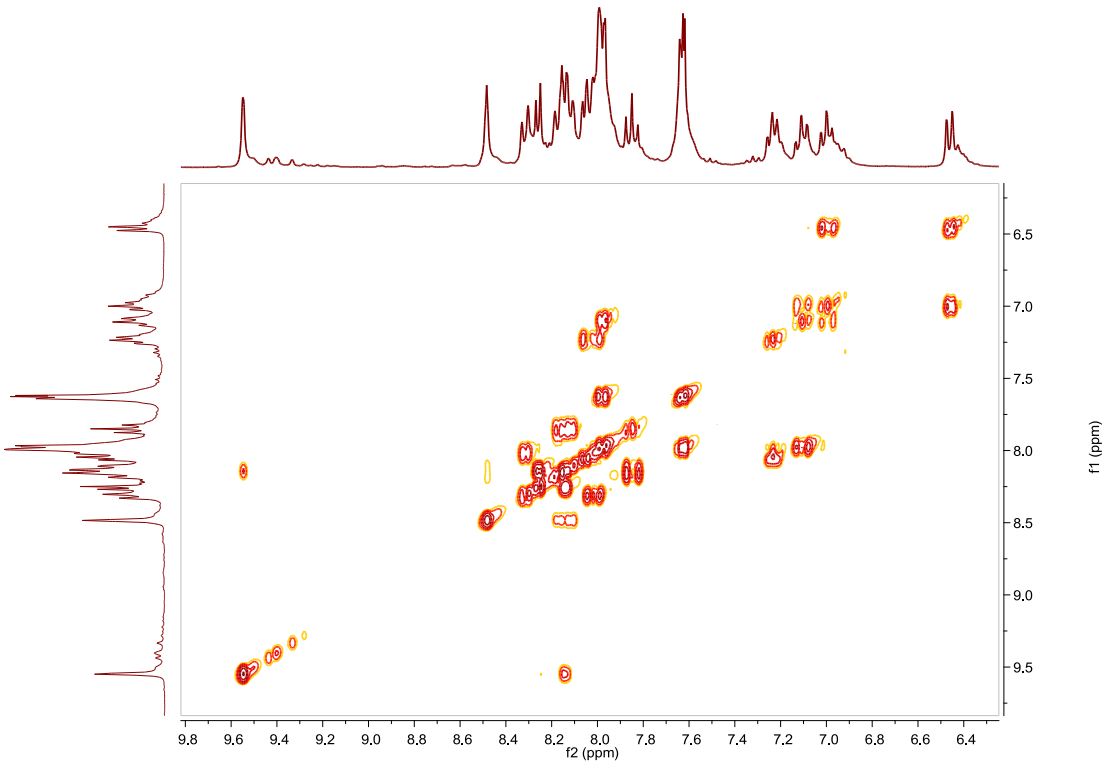

Fig. S267. COSY NMR spectrum of **A5** in acetone-d_6.

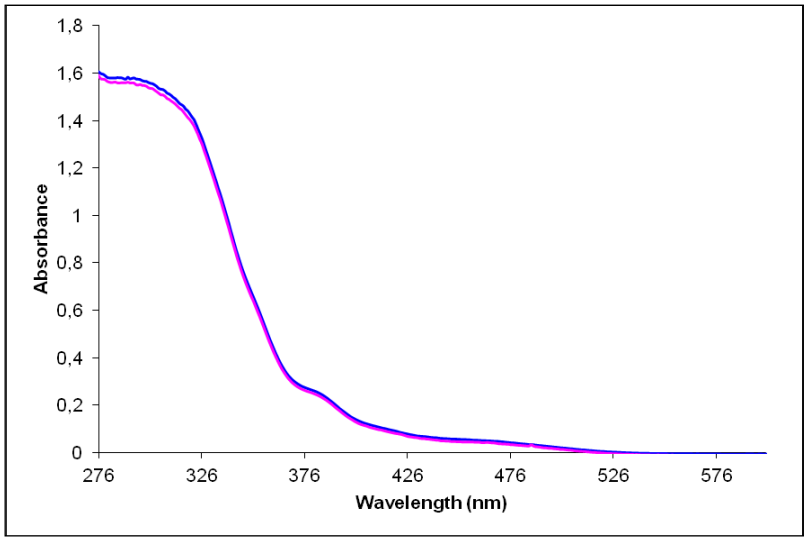

Fig. S268. UV/Vis spectra of **A5** in CH_3CN. Before (blue line) and after (pink line) irradiation at 319nm, $2.44 \cdot 10^{-5}$ M.

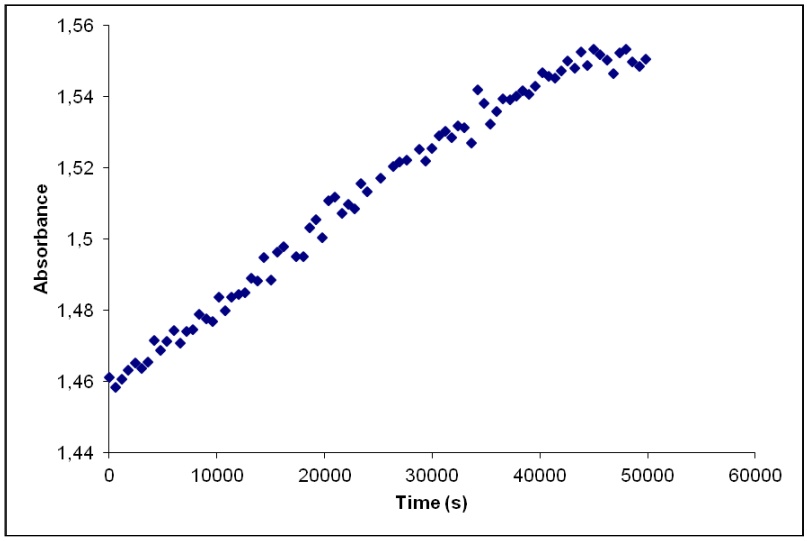

Fig. S269. Cis to trans thermal isomerization kinetics of **A5**. Absorption change of the band 290nm at 328 K in CH_3CN after irradiation at 319 nm. ($2.44 \cdot 10^{-5}$ M).

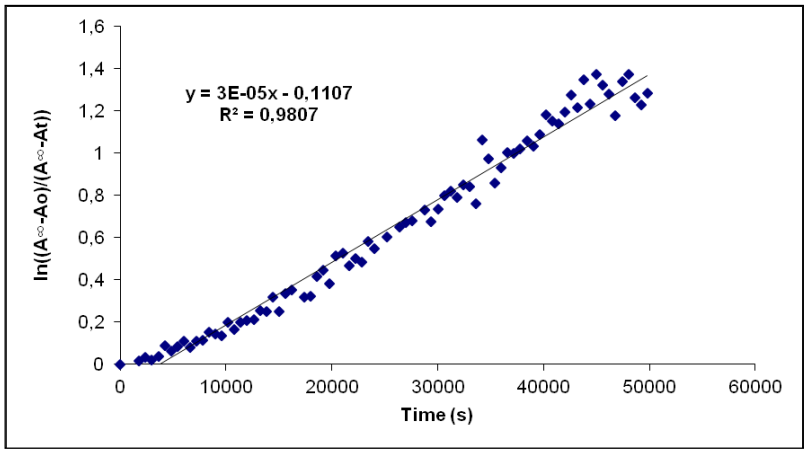

Fig. S270. Cis to trans thermal isomerization kinetics of **A5**. First-order plot. k (s^{-1}) = $3.0 \cdot 10^{-5}$. Half-life (min) = 385.

Compound B5, [Ir(Fppy)$_2$(5)]PF$_6$. Synthesis, characterization and photoisomerization studies.

SYNTHESIS

Under a N_2 atmosphere, $[Ir(Fppy)_2Cl]_2$ (0.100 g, 0.082 mmol) were added over a suspension of **L5** (0.085 g, 0.164 mmol) in 8 ml CH_2Cl_2–MeOH 2/1. The reaction mixture was refluxed, under N_2, for 15 h. After solvent evaporation the product was purified by column chromatography (silica gel, CH_2Cl_2). When the unreacted $[Ir(Fppy)_2Cl]_2$ eluted, 0.05 g of KPF_6 were added on top of the column and the polarity of the eluent was gradually increased to 100% acetone to elute $[Ir(Fppy)_2$(**L5**)$]PF_6$ together with the excess of KPF_6. The desired compound, purified by filtration through a celite path in CH_2Cl_2, was obtained as a red solid. Yield 85%.

Elemental Analysis: calculated for ($C_{56}H_{38}F_4IrN_8PF_6 \cdot CH_3COCH_3$): C, 54.84; H, 3.28; N, 8.67. Found: C, 54.70; H, 3.29; N, 8.34.

Exact Mass: ESI-MS $[C_{56}H_{36}F_4IrN_8]^+$: calculated: m/z= 1089.2628, found: m/z= 1089.2600.

^{1}H NMR (300 MHz, acetone-d_6): δ 9.58 (d, J = 1.4 Hz, 1H), 8.48 (m, 2H), 8.37 (d, J = 5.8 Hz, 1H), 8.16 (m, 5H), 7.99 (d, J = 4.3 Hz, 1H), 7.97 (d, J = 2.1 Hz, 1H), 7.86 (pst, J = 7.9 Hz, 1H), 7.63 (m, 3H), 7.33 (pst, J = 6.6 Hz, 1H), 6.83 (ddd, J = 2.3 Hz, J = 9.4 Hz, J = 12.4 Hz, 1H), 5.92 (dd, J = 2.3 Hz, J = 8.6 Hz, 1H).

^{13}C APT NMR (75 MHz, acetone-d_6): δ 165.25 (d, J = 6.9 Hz, C_{quat}), 164.99 (dd, J = 12.5 Hz, J = 254.7 Hz, C_{quat}), 162.80 (dd, J = 12.91 Hz, J = 257.8 Hz, C_{quat}), 157.88 (s, C_{quat}), 156.18 (d, J = 6.3 Hz, C_{quat}), 154.57 (s, C_{quat}), 153.72 (s, C_{quat}), 152.57 (s, CH), 152.36 (s, C_{quat}), 151.23 (s, CH), 141.19 (s, CH), 138.53 (s, C_{quat}), 133.18 (s, CH), 131.88 (s, CH), 131.56 (s, CH), 130.75 (s, 2CH), 129.34 (s, C_{quat}), 127.98 (s, CH), 125.62 (s, CH), 125.35 (s, CH), 125.06 (d, J = 19.8 Hz, CH), 124.74 (s, CH), 124.14 (s, 2CH), 123.72 (s, CH), 115.13 (d, J = 16.1 Hz, CH), 100.13 (t, J = 27.0 Hz, CH).

UV/Vis (CH_3CN), λ, nm (ε, 10^4 M^{-1} cm^{-1}): 311 (6.1), 436 (0.26).

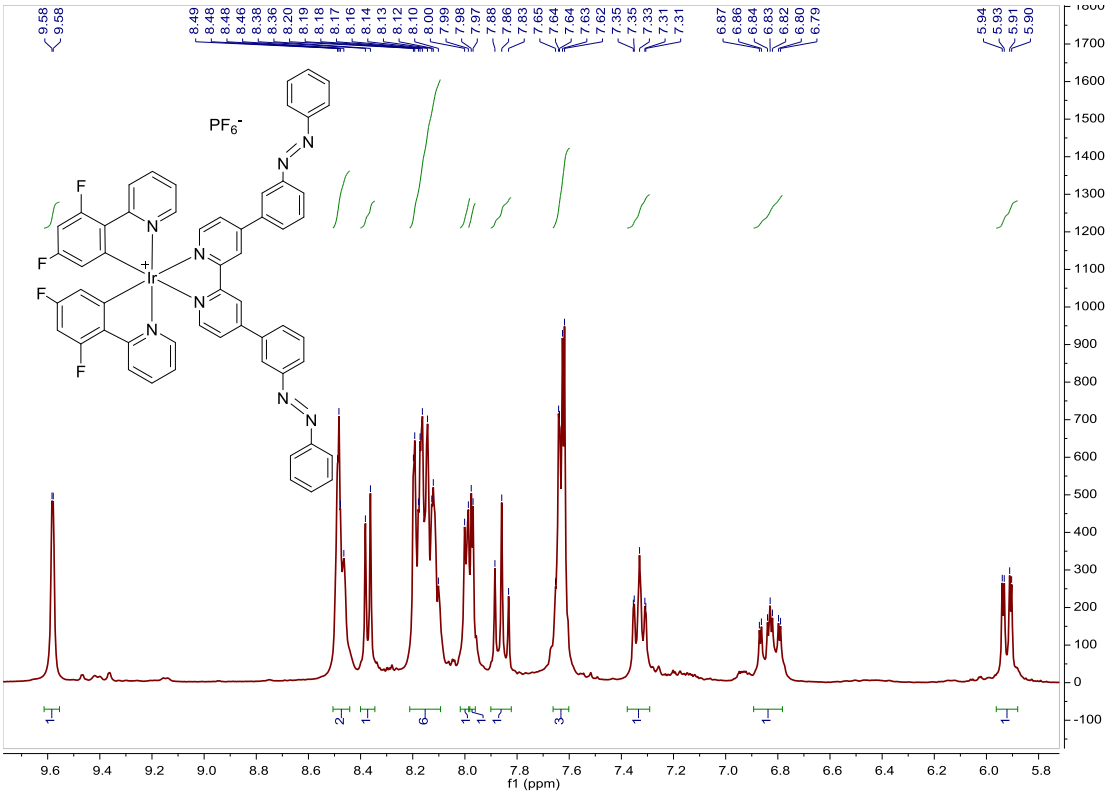

Fig. S271. ^{1}H NMR spectrum of **B5** in acetone-d_6, 300 MHz.

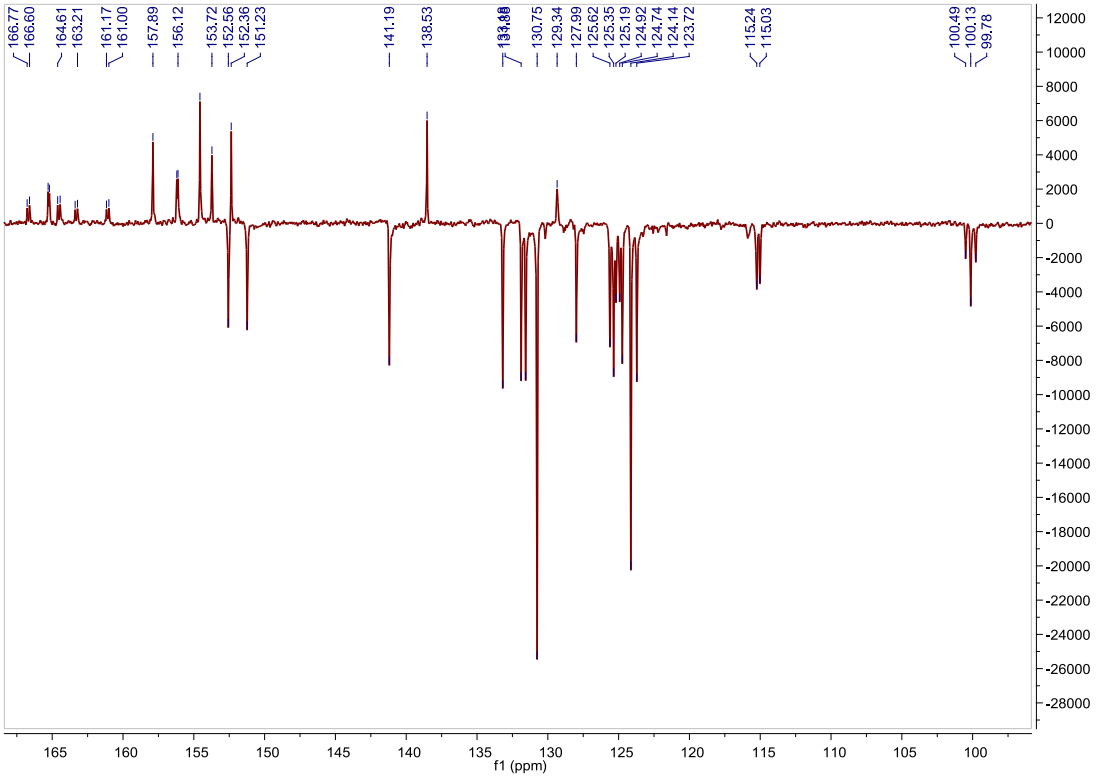

Fig. S272. ^{13}C APT NMR spectrum of **B5** in acetone-d_6, 75 MHz.

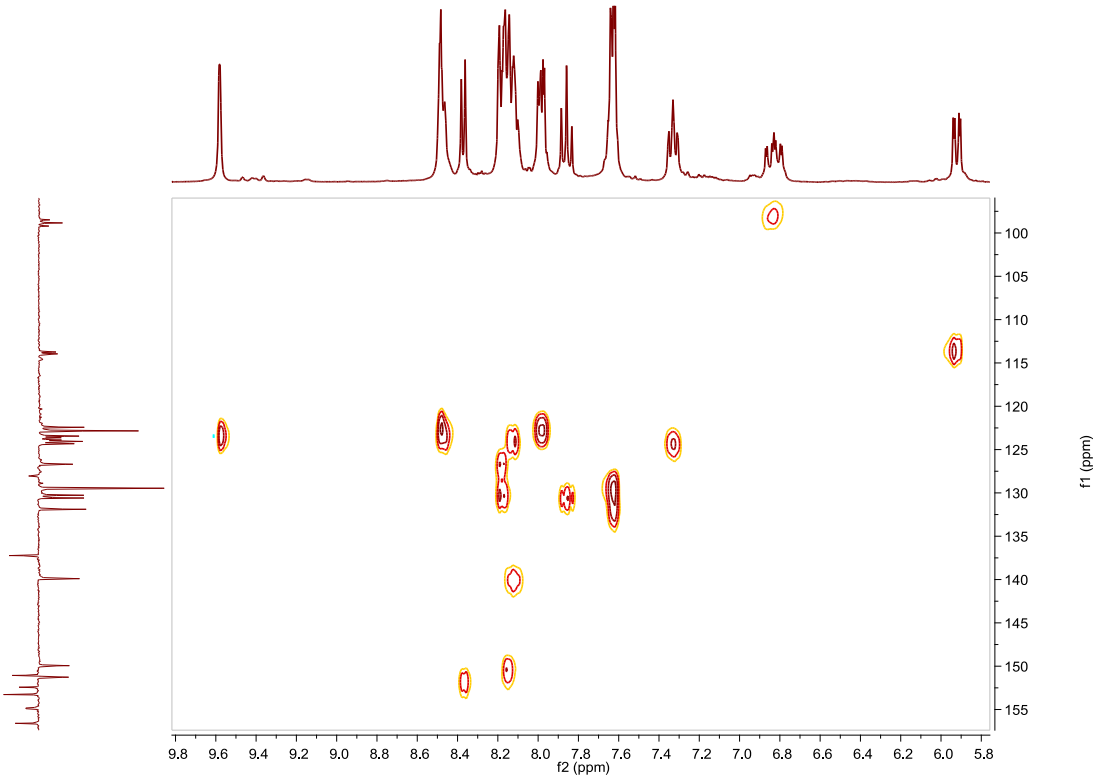

Fig. S273. HSQC NMR spectrum of **B5** in acetone-d_6.

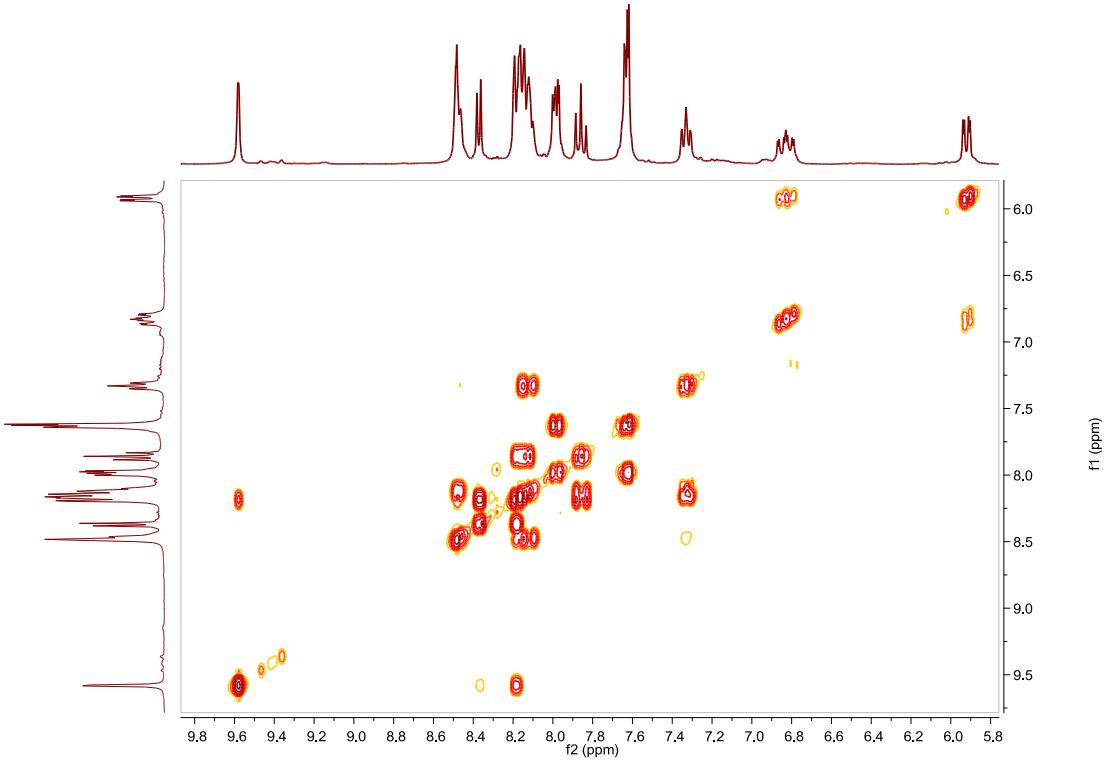

Fig. S274. COSY NMR spectrum of **B5** in acetone-d_6.

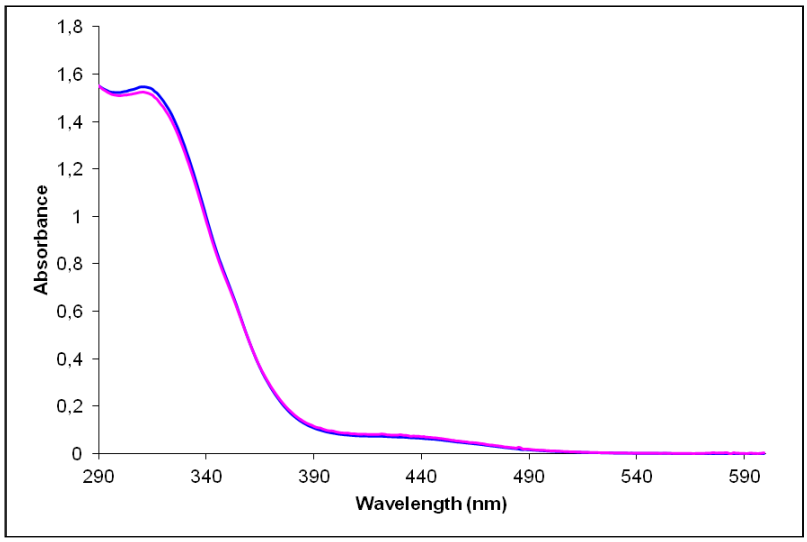

Fig. S275. UV/Vis spectra of **B5** in CH_3CN. Before (blue line) and after (pink line) irradiation at 319nm, $2.52 \cdot 10^{-5}$ M.

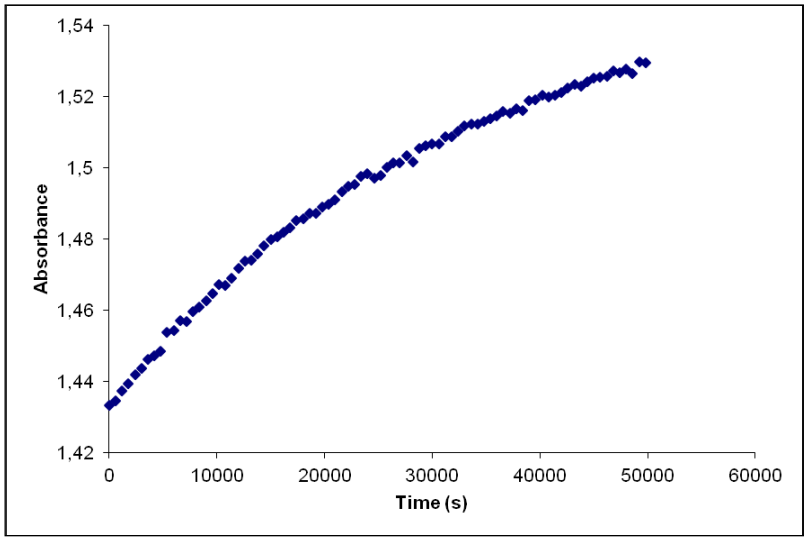

Fig. S276. Cis to trans thermal isomerization kinetics of **B5**. Absorption change of the band 311nm at 328 K in CH_3CN after irradiation at 319 nm. ($2.52 \cdot 10^{-5}$ M).

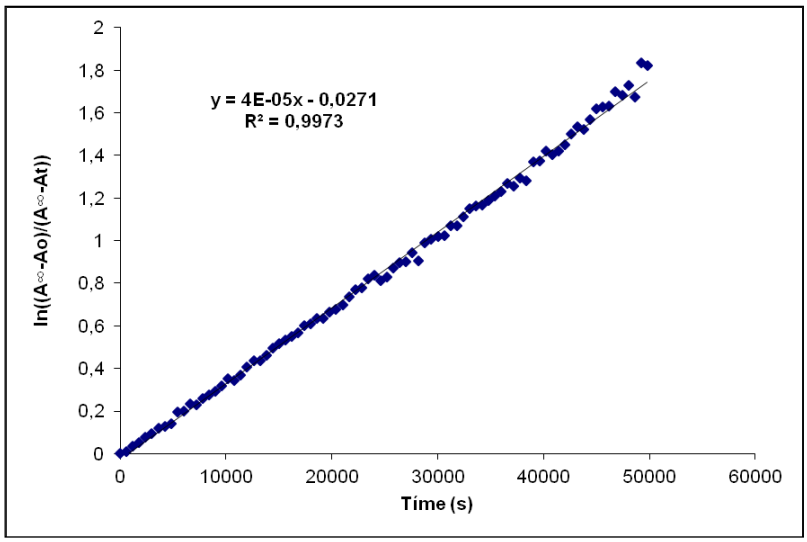

Fig. S277. Cis to trans thermal isomerization kinetics of **B5**. First-order plot. k (s^{-1}) = $4.0 \cdot 10^{-5}$. Half-life (min) = 289.

Compound C5, [Ir(Brppy)$_2$(5)]PF$_6$. Synthesis, characterization and photoisomerization studies.

SYNTHESIS

Under a N_2 atmosphere, [Ir(Brppy)$_2$Cl]$_2$ (0.100 g, 0.072 mmol) were added over a suspension of **L5** (0.074 g, 0.144 mmol) in 8 ml CH_2Cl_2–MeOH 2/1. The reaction mixture was refluxed, under N_2, for 15 h. After solvent evaporation the product was purified by column chromatography (silica gel, CH_2Cl_2). When the unreacted [Ir(Brppy)$_2$Cl]$_2$ eluted, 0.05 g of KPF_6 were added on top of the column and the polarity of the eluent was gradually increased to 100% acetone to elute [Ir(Brppy)$_2$(**L5**)]PF_6 together with the excess of KPF_6. The desired compound, purified by filtration through a celite path in CH_2Cl_2, was obtained as an orange solid. Yield 66%.

Elemental Analysis: calculated for ($C_{56}H_{38}Br_2IrN_8PF_6$): C, 50.96; H, 2.90; N, 8.49. Found: C, 51.12; H, 2.90; N, 8.10.

Exact Mass: ESI-MS $[C_{56}H_{38}Br_2IrN_8]^+$: calculated: m/z= 1173.1215, found: m/z= 1173.1239.

^{1}H NMR (300 MHz, acetone-*d*$_6$): δ 9.58 (d, J = 1.4 Hz, 1H), 8.49 (pst, J = 1.7 Hz, 1H), 8.38 (brd, J = 8.8 Hz, 1H), 8.33 (d, J = 5.8 Hz, 1H), 8.20 (dd, J = 1.8 Hz, J = 5.8 Hz, 1H), 8.16 (brd, J = 5.4 Hz, 1H), 8.09 (m, 3H), 7.98 (m, 3H), 7.86 (t, J = 7.9 Hz, 1H), 7.63 (m, 3H), 7.32 (m, 2H), 6.51 (d, J = 1.9 Hz, 1H).

^{13}C APT NMR (75 MHz, acetone-*d*$_6$): δ 167.89 (C_{quat}), 158.01 (C_{quat}), 154.59 (C_{quat}), 154.05 (C_{quat}), 153.72 (C_{quat}), 152.49 (CH), 152.14 (C_{quat}), 150.92 (CH), 144.77 (C_{quat}), 140.62 (CH), 138.59 (C_{quat}), 135.14 (CH), 133.19 (CH), 131.87 (CH), 131.51 (CH), 130.75 (2CH), 128.16 (CH), 127.89 (CH), 127.20 (CH), 126.31 (C_{quat}), 125.72 (CH), 125.26 (CH), 124.60 (CH), 124.12 (2CH), 123.75 (CH), 121.93 (CH).

UV/Vis (CH_3CN), λ, nm (ε, 10^4 M^{-1} cm^{-1}): 320 (6.4), 377 (1.1), 450 (0.25).

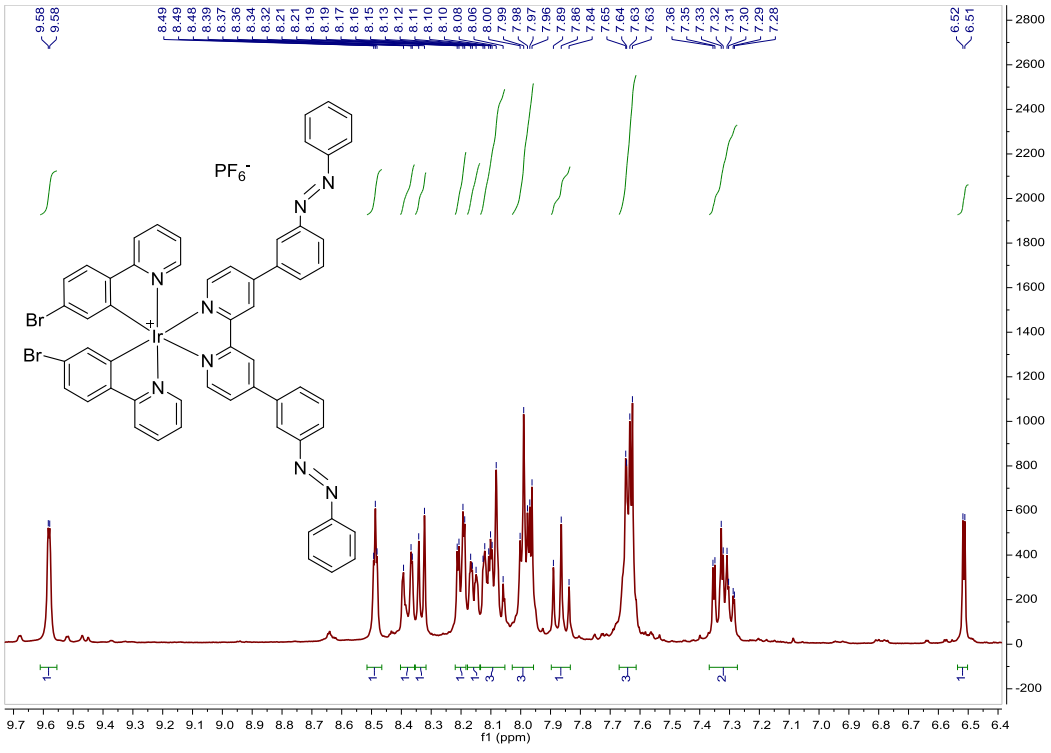

Fig. S278. ^{1}H NMR spectrum of **C5** in acetone-*d*$_6$, 300 MHz.

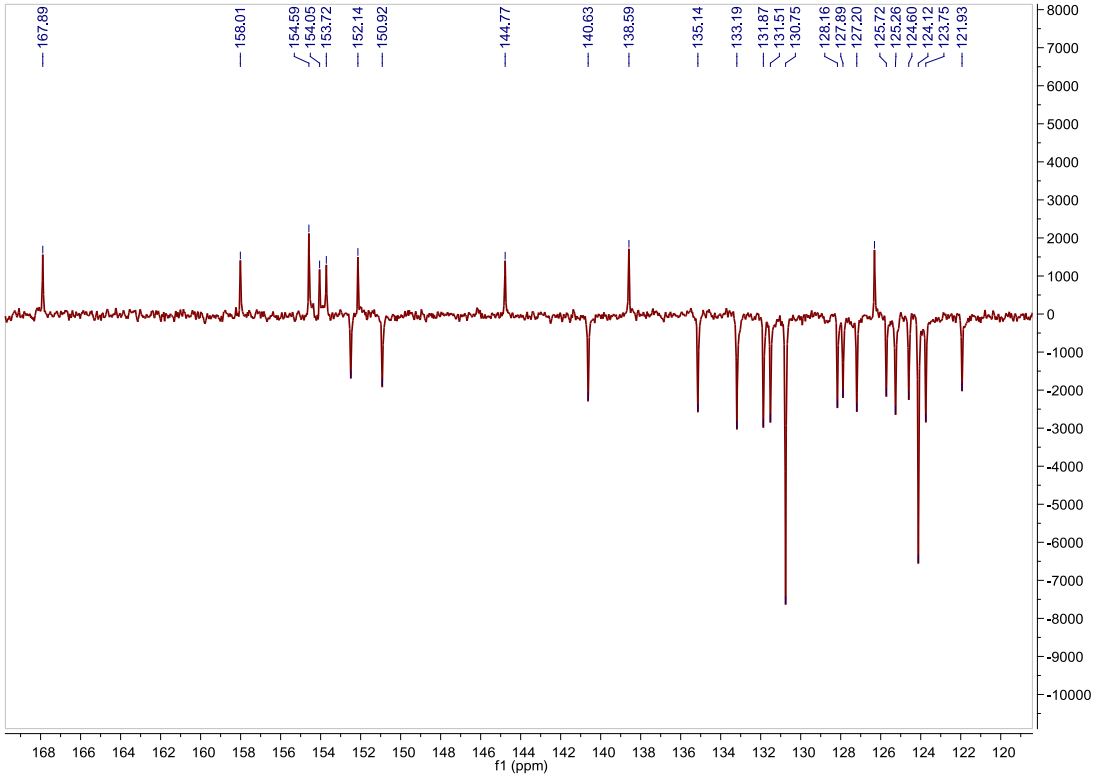

Fig. S279. ^{13}C APT NMR spectrum of **C5** in acetone-d_6, 75 MHz.

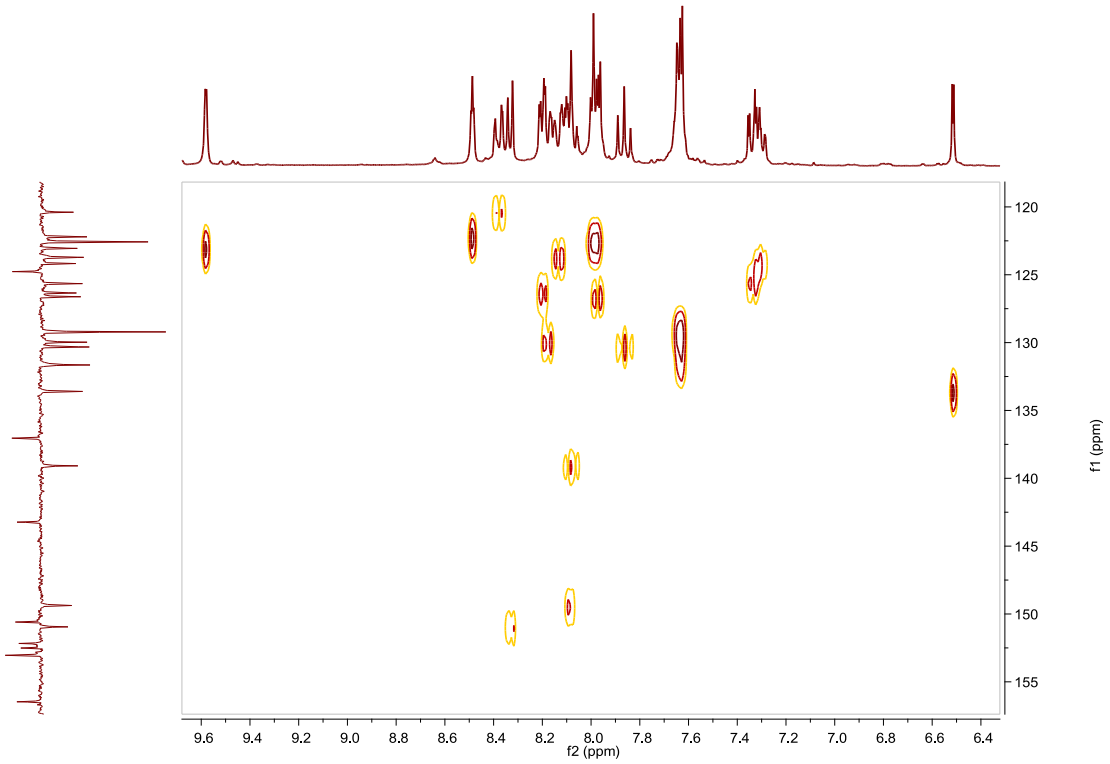

Fig. S280. HSQC NMR spectrum of **C5** in acetone-d_6.

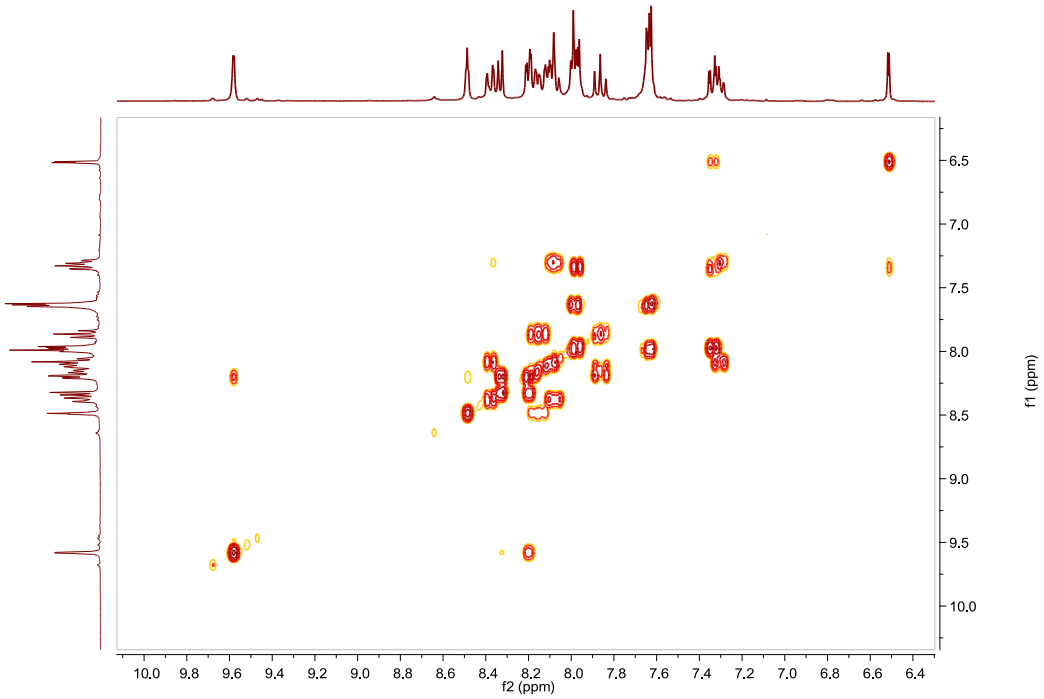

Fig. S281. COSY NMR spectrum of **C5** in acetone-d_6.

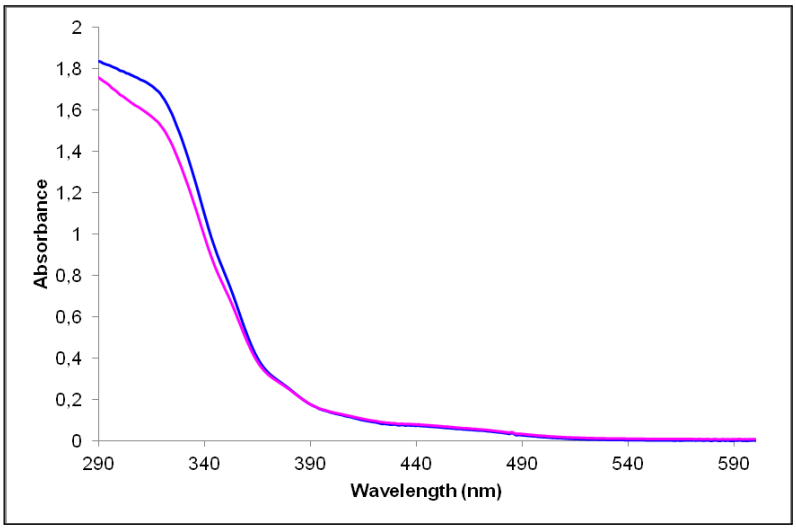

Fig. S282. UV/Vis spectra of **C5** in CH_3CN. Before (blue line) and after (pink line) irradiation at 318nm, $2.59 \cdot 10^{-5}$ M.

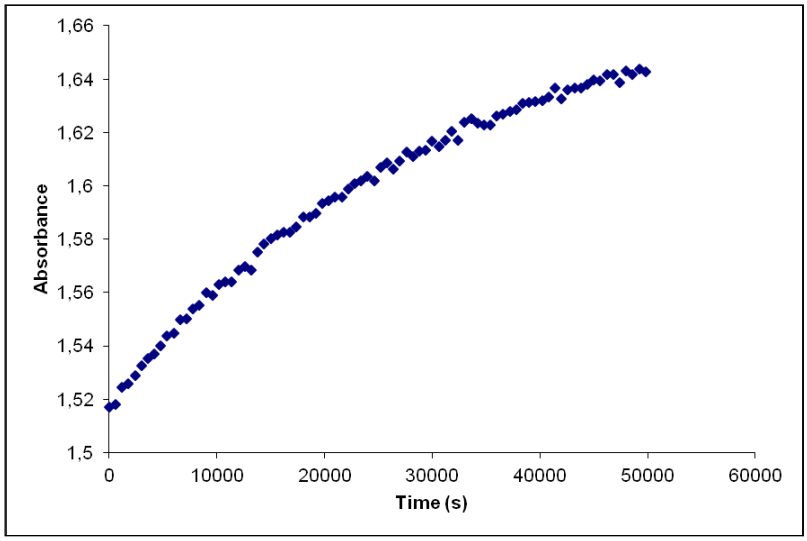

Fig. S283. Cis to trans thermal isomerization kinetics of **C5**. Absorption change of the band 320nm at 328 K in CH_3CN after irradiation at 318 nm. ($2.59 \cdot 10^{-5}$ M).

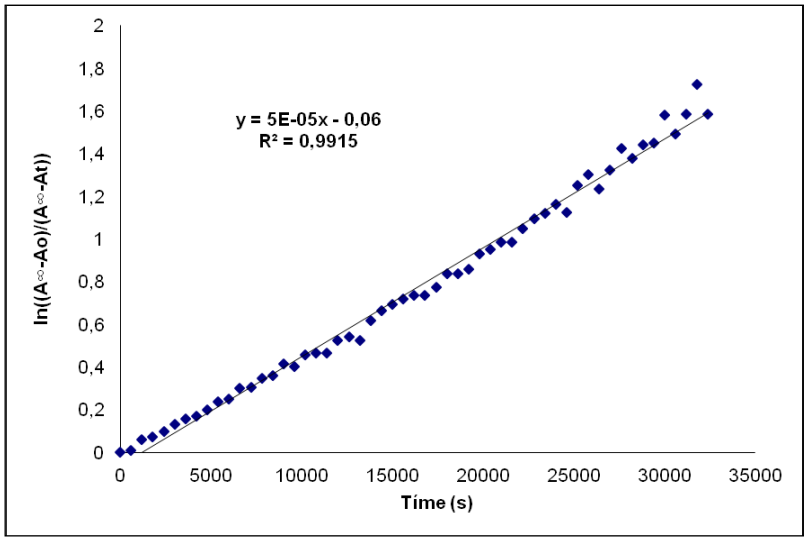

Fig. S284. Cis to trans thermal isomerization kinetics of **C5**. First-order plot. k (s^{-1}) = $5.0 \cdot 10^{-5}$. Half-life (min) = 231.

Compound D5, [Ir(azoppy)$_2$(5)]PF$_6$. Synthesis, characterization and photoisomerization studies.

SYNTHESIS

Under a N_2 atmosphere, **C5** (0.150 g, 0.114 mmol) and [4-(phenylazo)phenyl]boronic acid pinacol ester **11** (0.085 g, 0.277 mmol) were dissolved in 5 ml of THF. Na_2CO_3 (1 M (aq), 2.5 mL) and $Pd(PPh_3)_4$ (0.013 g, 0.0114 mmol) were added and the solution was degassed by bubbling N_2 for 15 min. The reaction mixture was refluxed (80 °C) for 15 h. The resulting mixture was cooled down to room temperature and the product was extracted with CH_2Cl_2. The organic phase was dried with $MgSO_4$, filtered off and the solvent was evaporated. The residue was purified by column chromatography (silica gel, CH_2Cl_2). To the fraction containing the eluted complex, 0.05 g of KPF_6 were added and the resulting solution was filtered through a celite path. The title compound was obtained as a dark orange solid. Yield 26%.

Elemental Analysis: calculated for ($C_{80}H_{56}IrN_{12}PF_6$): C, 63.11; H, 3.71; N, 11.04. Found: C, 62.90; H, 3.80; N, 10.56.

Exact Mass: ESI-MS $[C_{80}H_{56}IrN_{12}]^+$: calculated: m/z= 1377.4380, found: m/z= 1377.4392.

^{1}H NMR (300 MHz, acetone-*d*$_6$): δ 9.56 (d, J = 1.3 Hz, 1H), 8.48 (t, J = 1.6 Hz, 1H), 8.44 (d, J = 5.8 Hz, 1H), 8.36 (d, J = 8.0 Hz, 1H), 8.25–7.80 (m, 13H), 7.71–7.55 (m, 8H), 7.45 (dd, J = 1.8 Hz, J = 8.1 Hz, 1H), 7.32 (ddd, J = 1.2 Hz, J = 5.9 Hz, J = 7.3 Hz, 1H), 6.85 (d, J = 1.6 Hz, 1H).

^{13}C APT NMR (75 MHz, acetone-*d*$_6$): δ 168.64 (C_{quat}), 158.14(C_{quat}), 154.57 (C_{quat}), 153.91 (C_{quat}), 153.72 (C_{quat}), 152.97 (C_{quat}), 152.53 (CH), 151.83 (C_{quat}), 151.31 (C_{quat}), 151.02 (CH), 145.69 (C_{quat}), 144.96 (C_{quat}), 142.63 (C_{quat}), 140.27 (CH), 138.65 (C_{quat}), 133.18 (CH), 132.63 (CH), 131.84 (CH), 131.52 (CH), 131.01 (CH), 130.75 (2CH), 130.61 (2CH), 130.15 (CH), 128.93 (2CH), 127.73 (CH), 126.87 (CH), 125.35 (CH), 125.19 (CH), 124.49 (2CH), 124.14 (2CH), 123.99 (2CH), 123.76 (CH), 123.17 (CH), 121.75 (CH).

UV/Vis (CH_3CN), λ, nm (ε, 10^4 M^{-1} cm^{-1}): 337 (9.9), 430 (1.7).

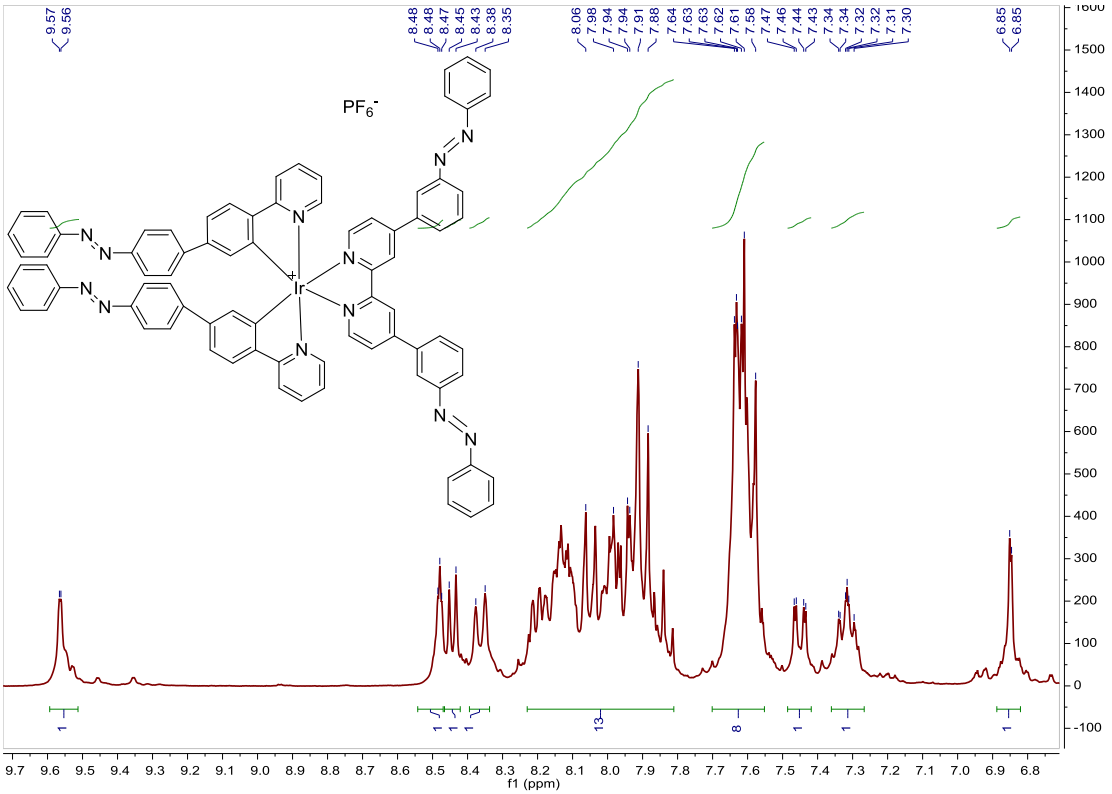

Fig. S285. ^{1}H NMR spectrum of **D5** in acetone-*d*$_6$, 300 MHz.

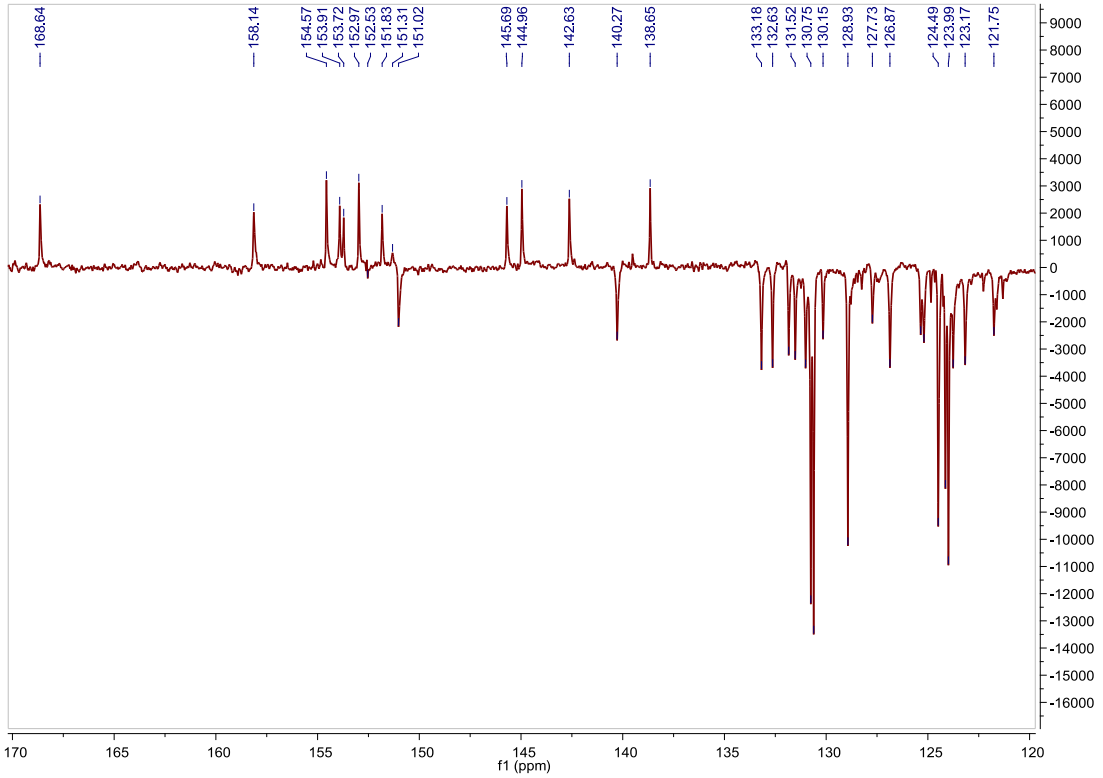

Fig. S286. ^{13}C APT NMR spectrum of **D5** in acetone-d_6, 75 MHz.

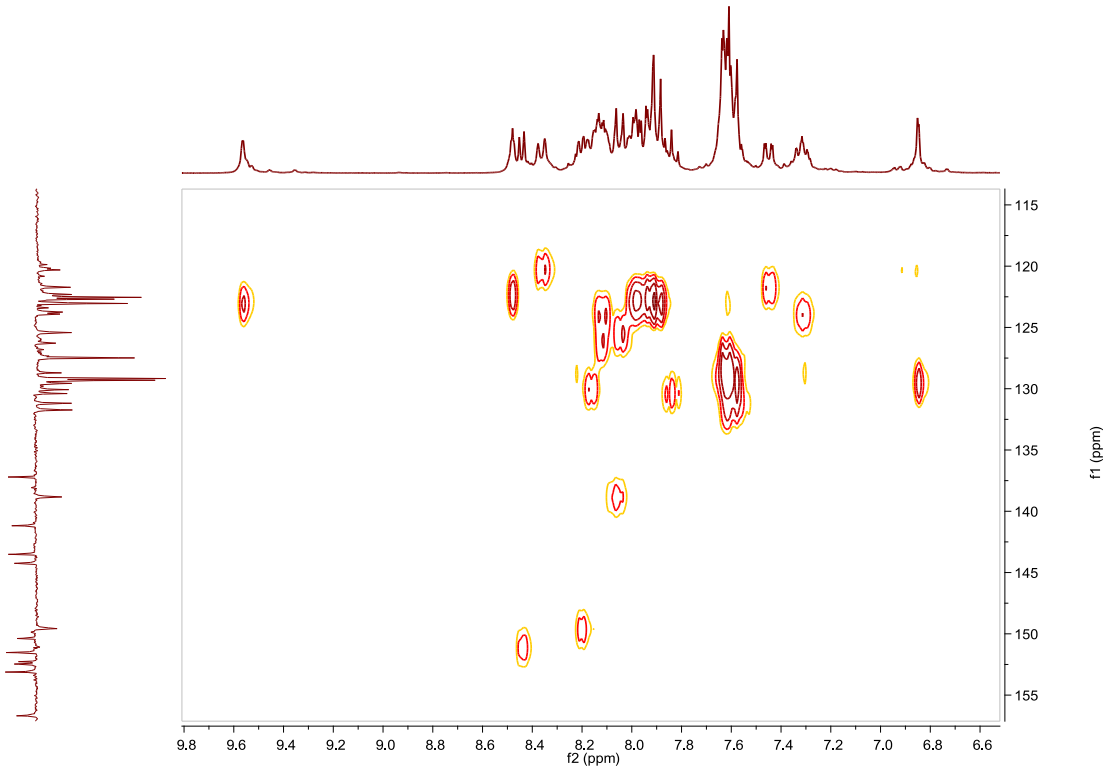

Fig. S287. HSQC NMR spectrum of **D5** in acetone-d_6.

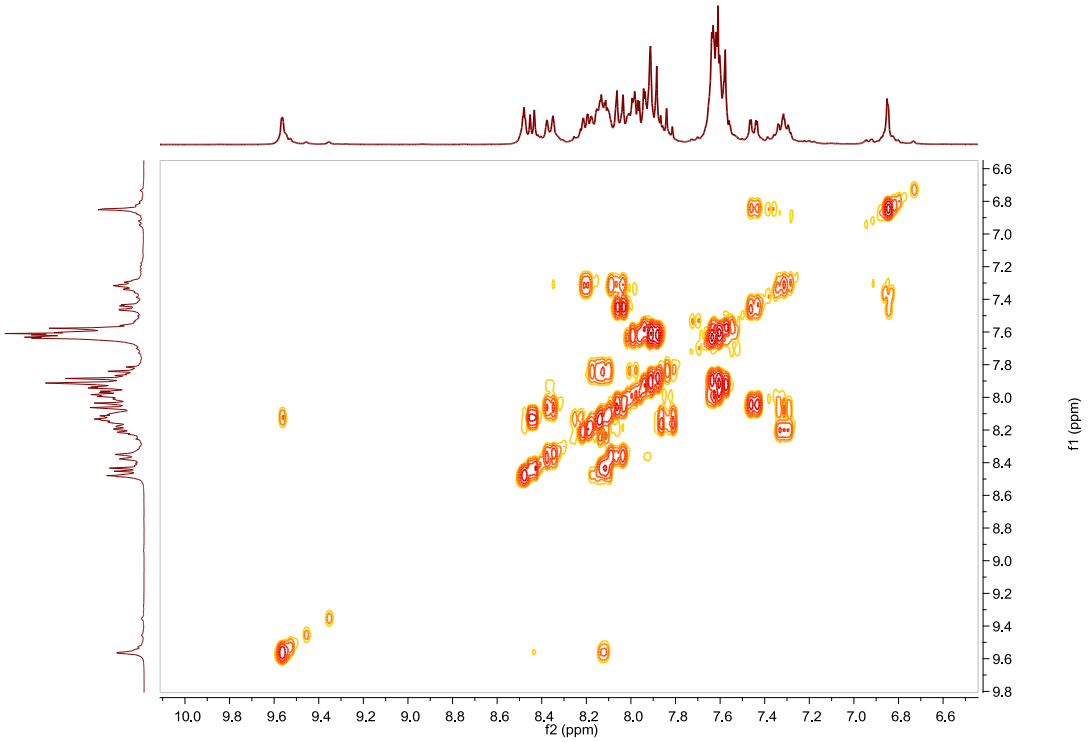

Fig. S288. COSY NMR spectrum of **D5** in acetone-d_6.

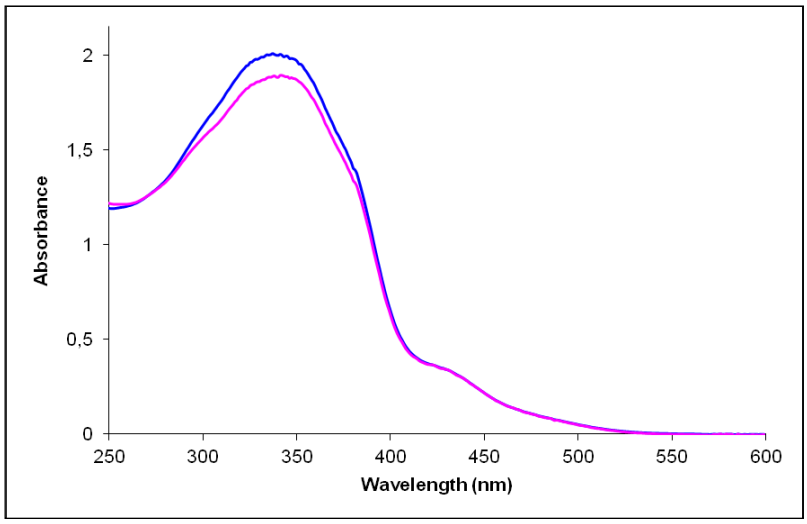

Fig. S289. UV/Vis spectra of **D5** in CH_3CN. Before (blue line) and after (pink line) irradiation at 327nm, $2.03 \cdot 10^{-5}$ M.

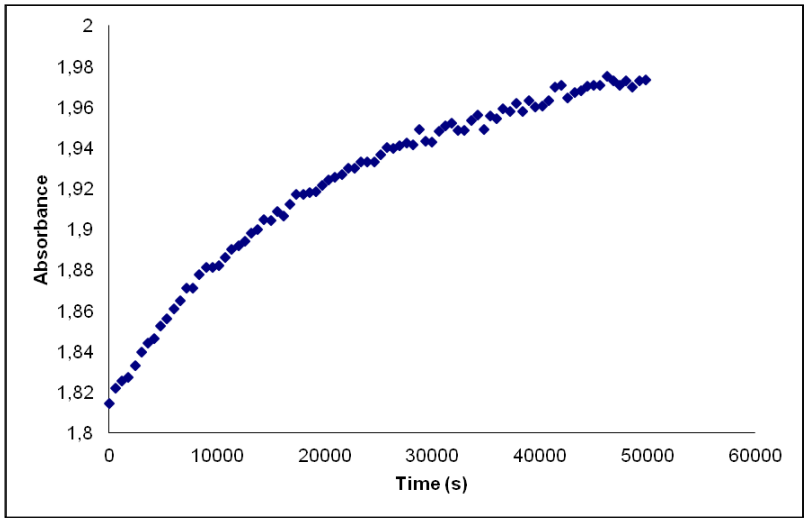

Fig. S290. Cis to trans thermal isomerization kinetics of **D5**. Absorption change of the band 337nm at 328 K in CH_3CN after irradiation at 327 nm. ($2.03 \cdot 10^{-5}$ M).

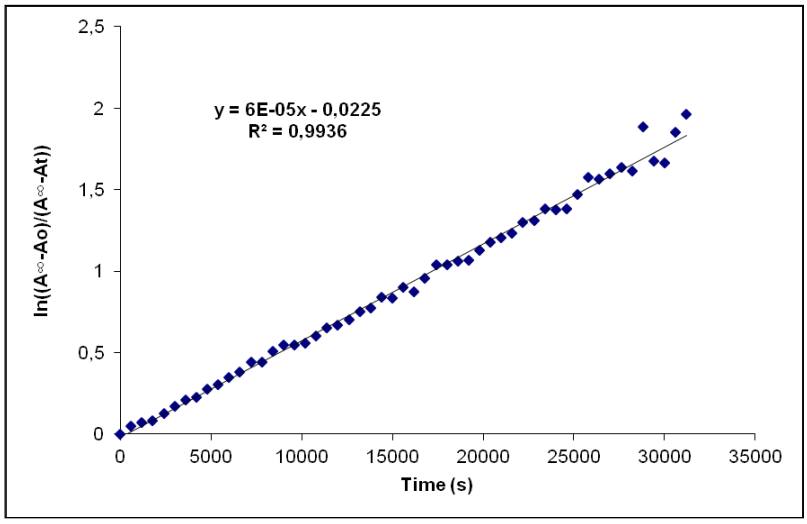

Fig. S291. Cis to trans thermal isomerization kinetics of **D5**. First-order plot. k (s^{-1}) = $6.0 \cdot 10^{-5}$. Half-life (min) = 192.

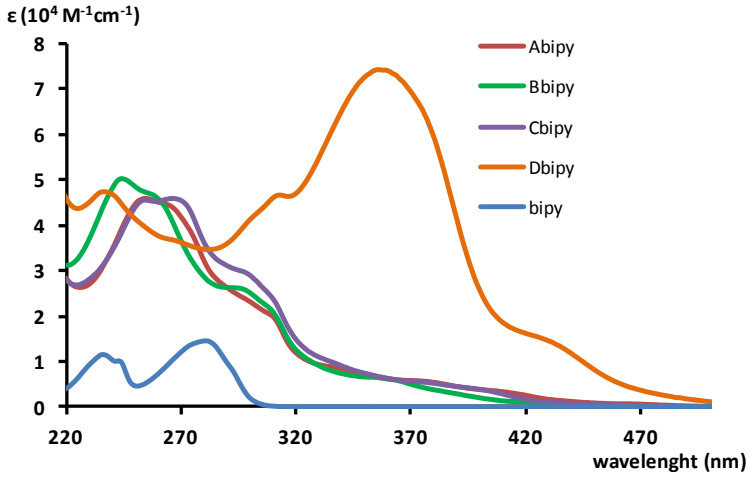

Fig. S292. UV-Vis absorption spectra of model complexes **A**–**D** with 2,2’-bipyridine. The spectra of 2,2’-bipyridine (bipy) is also shown for comparative purposes.

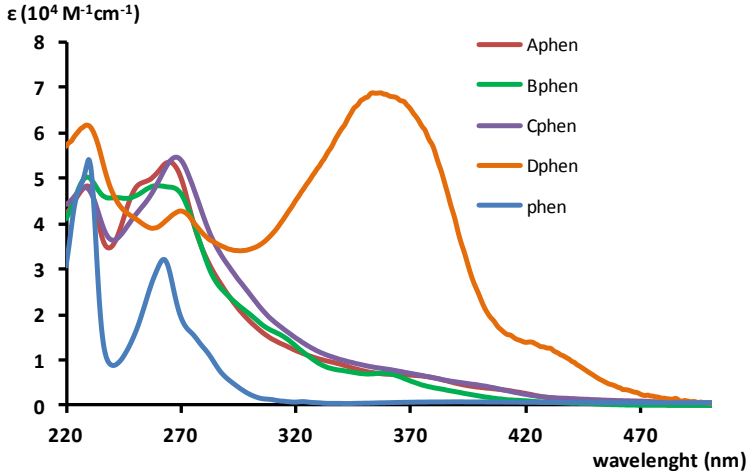

Fig. S293. UV-Vis absorption spectra of model complexes **A**–**D** with 1,10-phenanthroline. The spectra of 1,10-phenanthroline (phen) is also shown for comparative purposes.

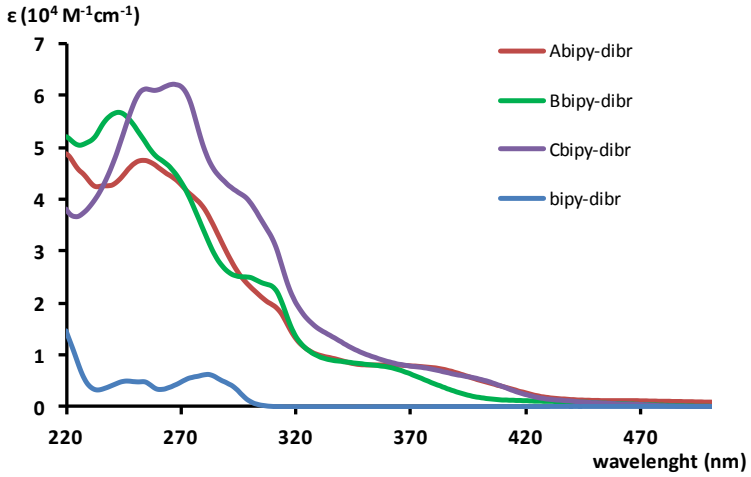

Fig. S294. UV-Vis absorption spectra of model complexes **A**–**C** with 4,4'-dibromo-2,2’-bipyridine. The spectra of 4,4'-dibromo-2,2’-bipyridine (bipy-dibr) is also shown for comparative purposes.

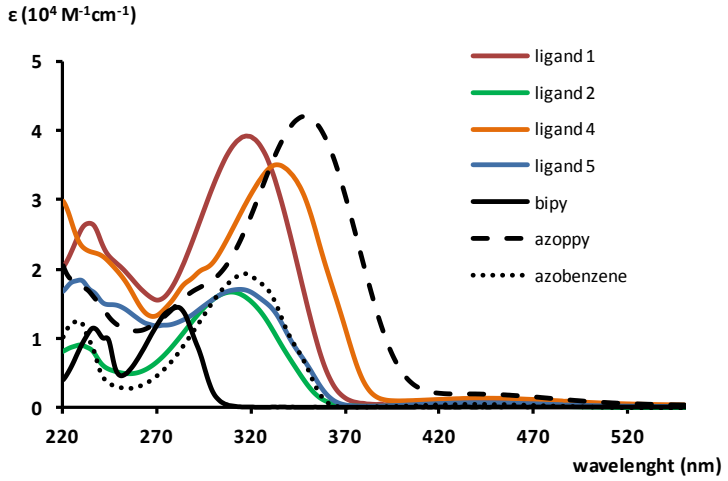

Fig. S295. UV-Vis absorption spectra of ligands **1**, **2, 4** and **5**. The spectra of 2,2'-bipyridine (bipy), 2-phenyl(4-azophenyl)pyridine (azobipy) and azobenzene are also shown for comparative purposes.

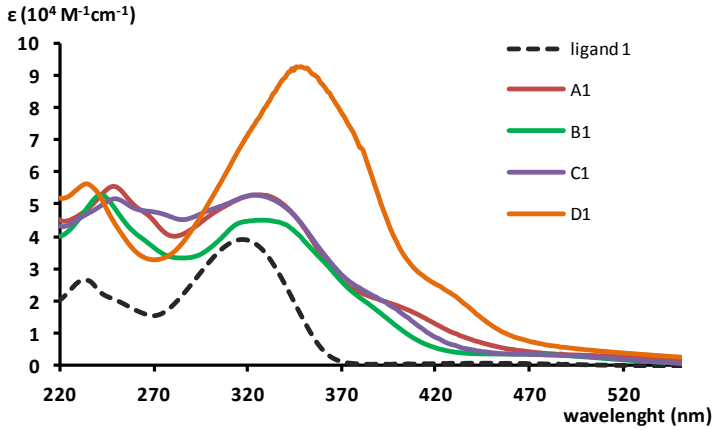

Fig. S296. UV-Vis absorption spectra of complexes **A1**–**D1** and ligand **1**.

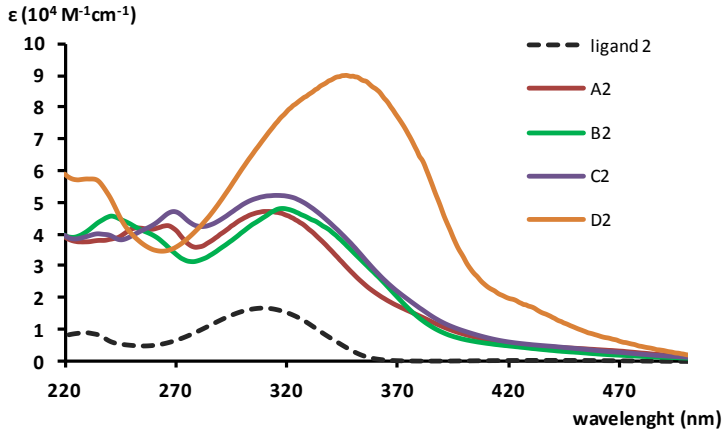

Fig. S297. UV-Vis absorption spectra of complexes **A2**–**D2** and ligand **2**.

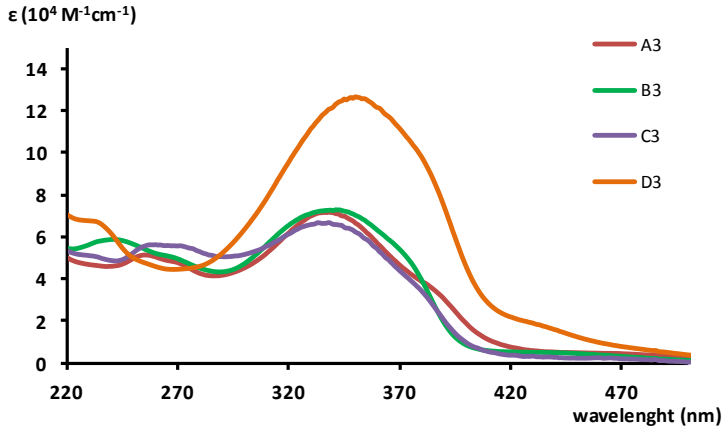

Fig. S298. UV-Vis absorption spectra of complexes **A3**–**D3**.

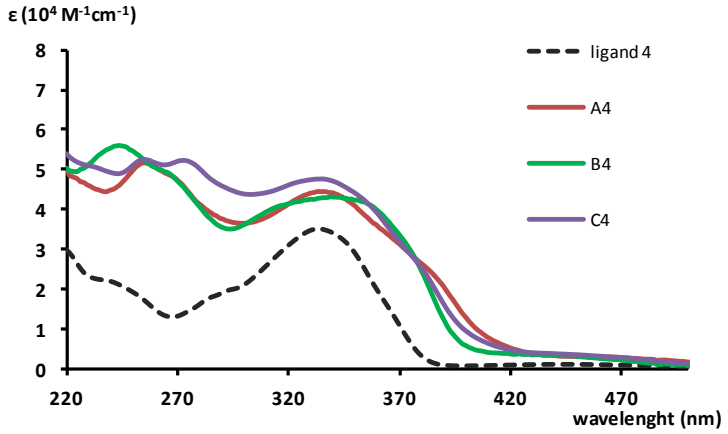

Fig. S299. UV-Vis absorption spectra of complexes **A4**–**C4** and ligand **4**.

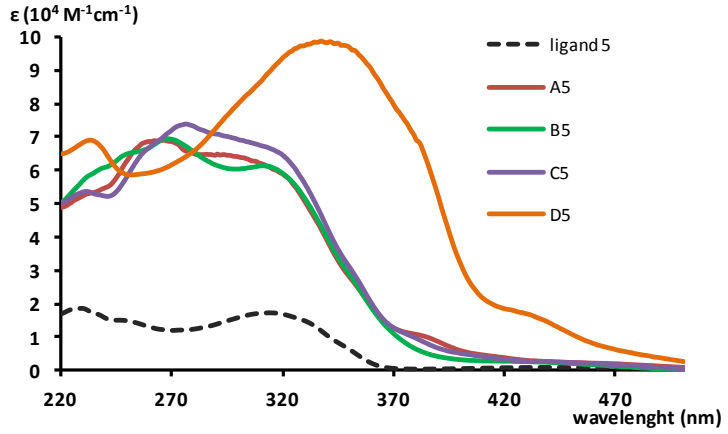

Fig. S300. UV-Vis absorption spectra of complexes **A5**–**D5** and ligand **5**.

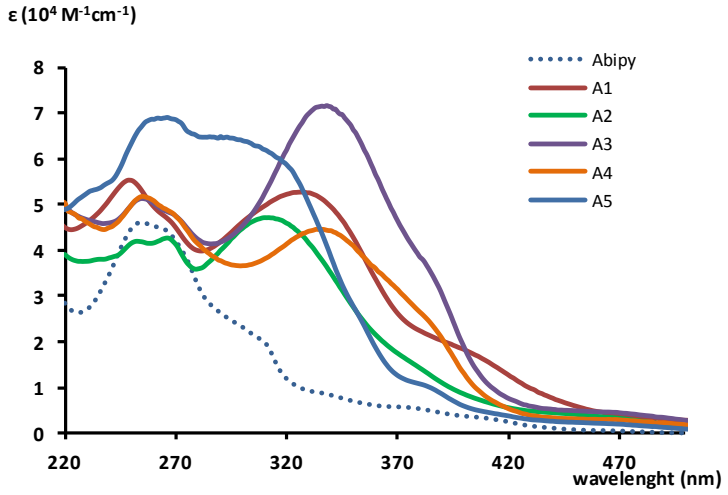

Fig. S301. UV-Vis absorption spectra of complexes **A1**–**A5**. The spectra of compound **Abipy** is also shown for comparative purposes.

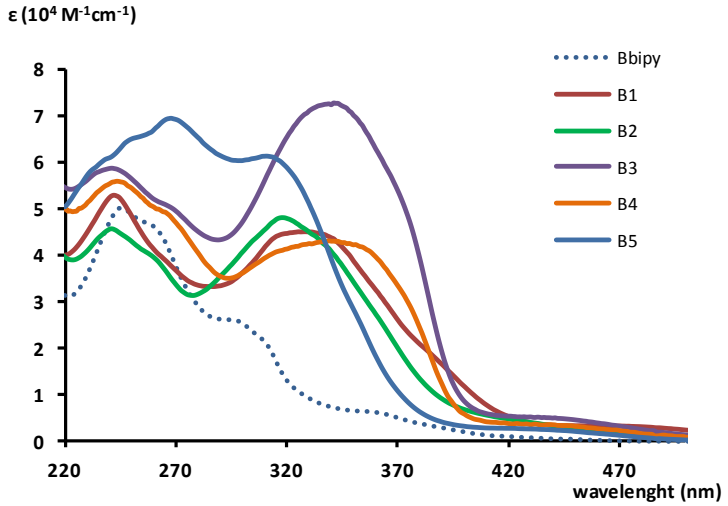

Fig. S302. UV-Vis absorption spectra of complexes **B1**–**B5**. The spectra of compound **Bbipy** is also shown for comparative purposes.

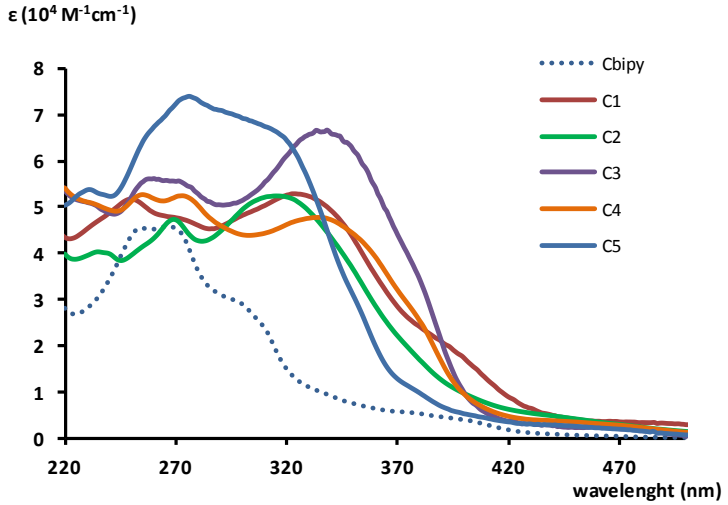

Fig. S303. UV-Vis absorption spectra of complexes **C1**–**C5**. The spectra of compound **Cbipy** is also shown for comparative purposes.

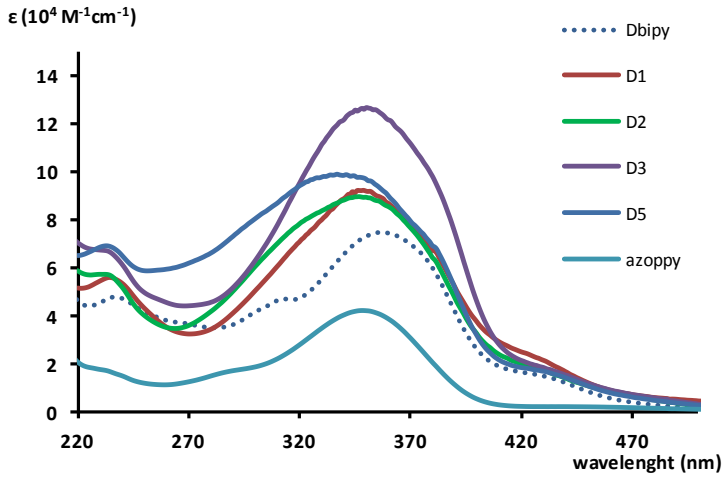

Fig. S304. UV-Vis absorption spectra of complexes **D1**–**D5**. The spectra of compound **Dbipy**, and **azoppy** = ((2-azobenzene)pyridine) are also shown for comparative purposes.

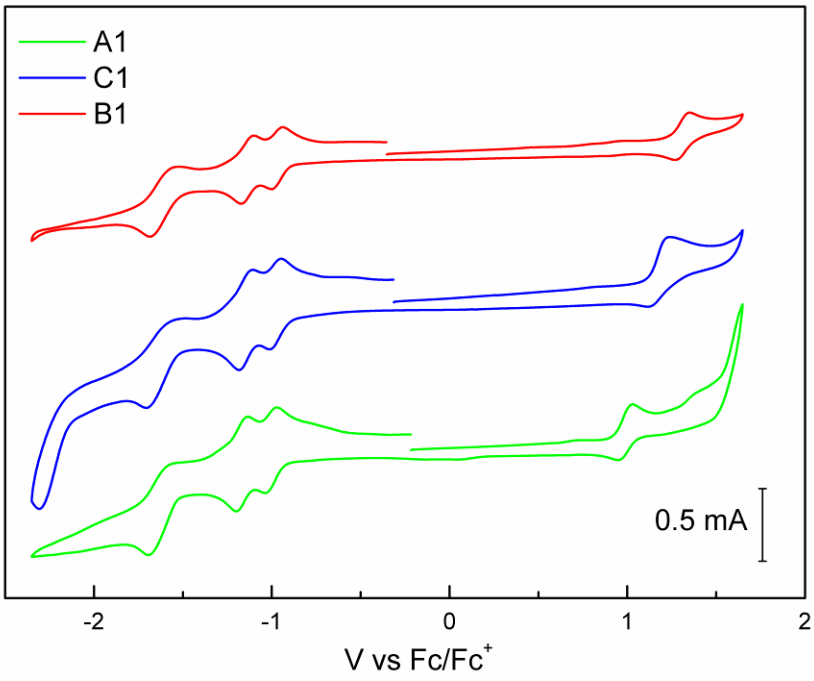

Figure S305. Cyclo-voltammograms (10^{-3} M, dry ACN) of **A1**, **B1** and **C1** containing 0.1 M $TBAPF_6$ as the supporting electrolyte, scan rate of 100 mV s^{-1}.

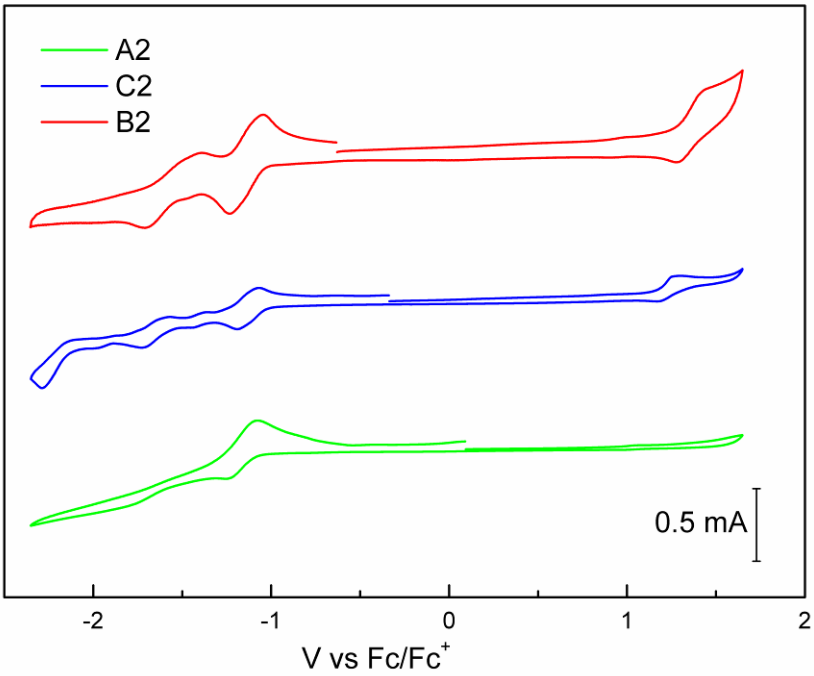

Figure S306. Cyclo-voltammograms (10^{-3} M, dry ACN) of **A2**, **B2** and **C2** containing 0.1 M $TBAPF_6$ as the supporting electrolyte, scan rate of 100 mV s^{-1}.

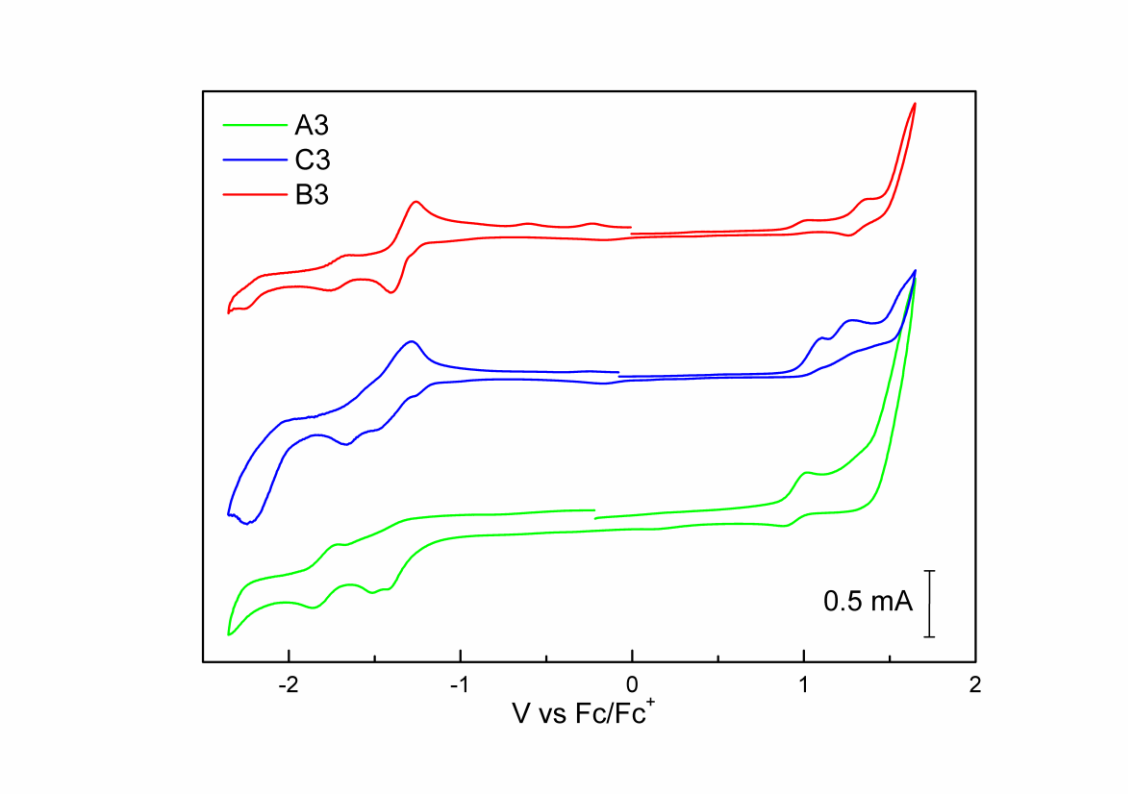

Figure S307. Cyclo-voltammograms (10^{-3} M, dry ACN) of **A3**, **B3** and **C3** containing 0.1 M $TBAPF_6$ as the supporting electrolyte, scan rate of 100 mV s^{-1}.

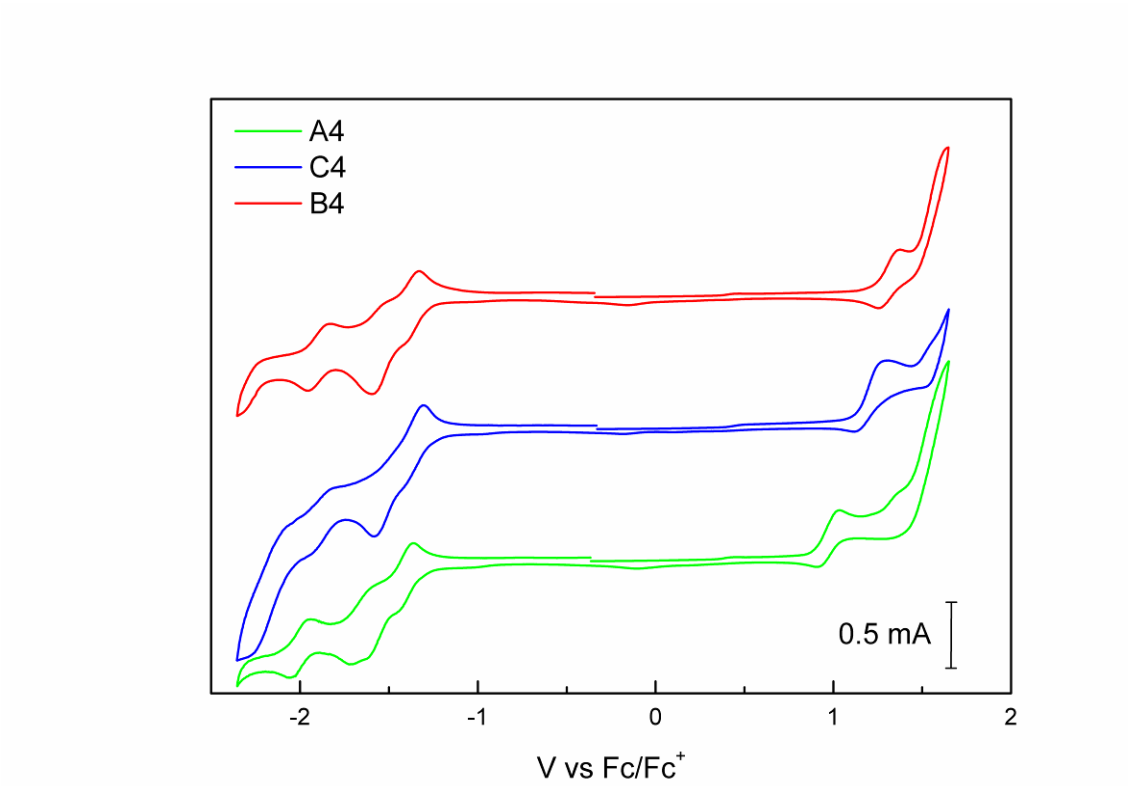

Figure S308. Cyclo-voltammograms (10^{-3} M, dry ACN) of **A4**, **B4** and **C4** containing 0.1 M $TBAPF_6$ as the supporting electrolyte, scan rate of 100 mV s^{-1}.

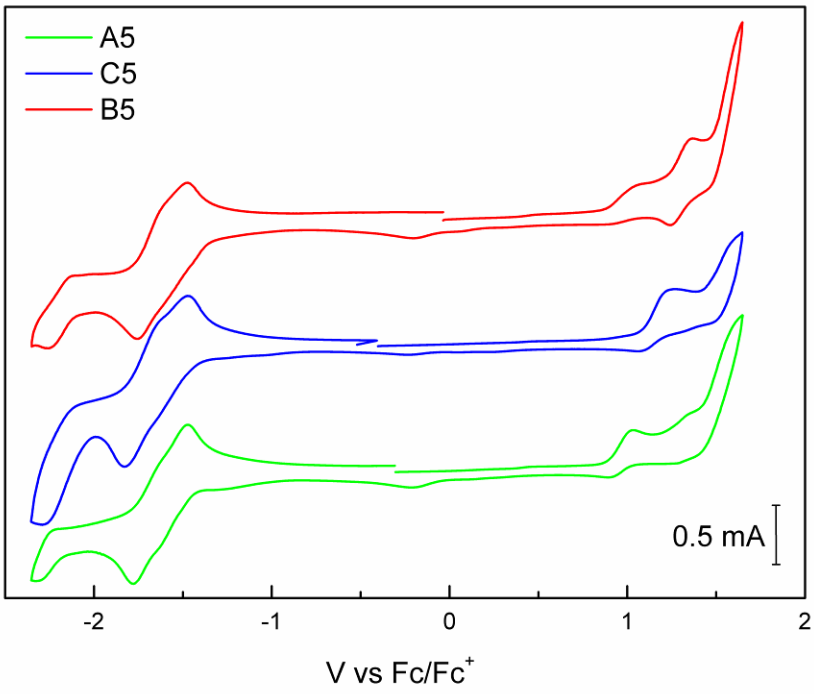

Figure S309. Cyclo-voltammograms (10^{-3} M, dry ACN) of **A5**, **B5** and **C5** containing 0.1 M $TBAPF_6$ as the supporting electrolyte, scan rate of 100 mV s^{-1}.

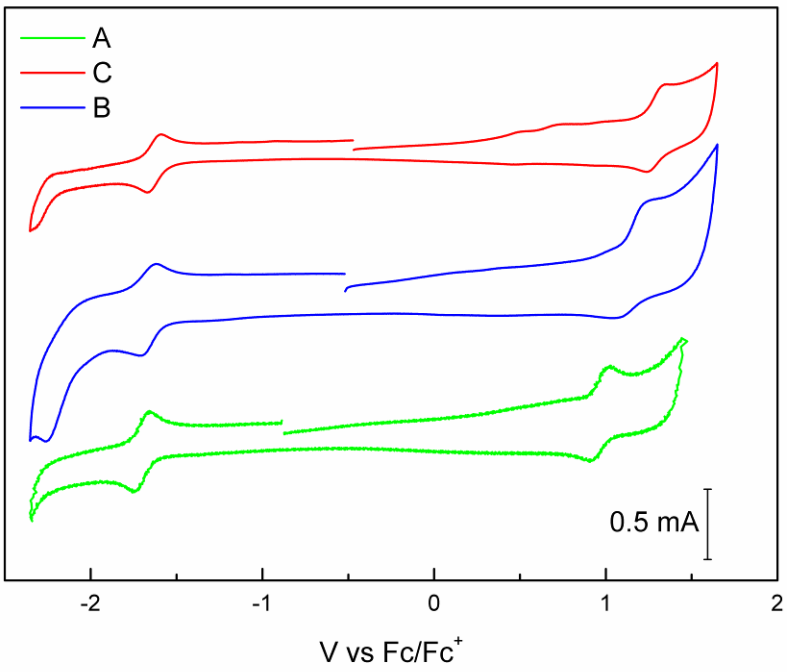

Figure S310. Cyclo-voltammograms (10^{-3} M, dry ACN) of **Abipy**, **Bbipy** and **Cbipy** containing 0.1 M $TBAPF_6$ as the supporting electrolyte, scan rate of 100 mV s^{-1}.

Table S1. Secondary MLCT transitions of complexes A, C computed at TD-CAM-B3LYP(PCM)/6-31+G*&LANL2DZ level of theory. Orbitals in italics and underlined are mainly located on the Ir(bipy) moiety or the azo moiety respectively.

	E [eV]	*f*	*transition*
A1	3.57	0.75	*HOMO-4*→LUMO (49%)
B1	3.66	0.66	*HOMO-4*→LUMO (65%)
C1	3.64	0.92	*HOMO-4*→LUMO (57%)
A2	3.83	1.16	*HOMO-3*→LUMO (30%) *HOMO-2*→LUMO+1 (25%)
B2	3.82	0.59	*HOMO*→LUMO (47%)
A3	3.67	1.12	*HOMO-3*→LUMO (44%) *HOMO-2*→LUMO+1 (38%)
B3	3.73	2.21	*HOMO-1*→LUMO (44%) *HOMO-2*→LUMO+1 (38%)
C3	3.67	1.15	*HOMO-3*→LUMO (48%) *HOMO-2*→LUMO+1 (42%)

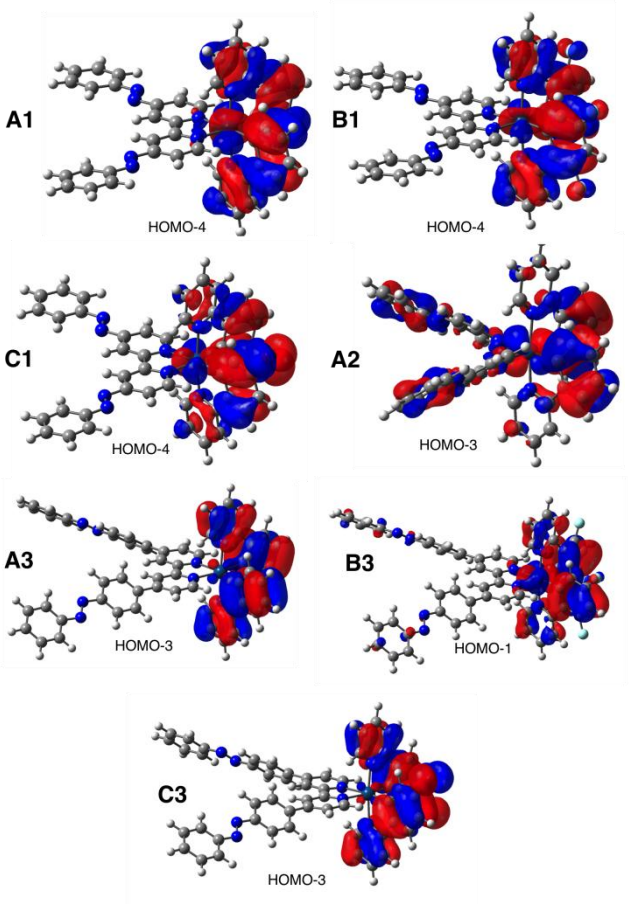

Figure S311. Orbitals AC1–3 involved on the MLCT secondary transitions

Cartesian coordinates and energy in hartrees (optimized at the CAM-B3LYP(PCM)/6-31+G*&LANL2DZ level) of all the stationary points discussed in the main text.

1 (HF= -1175.8277845)

Center Number	Atomic Number	Atomic Type	Coordinates (Angstroms) X	Y	Z
1	6	0	0.501431	0.553514	-0.018730
2	6	0	0.888552	2.816208	-0.017216
3	6	0	1.864904	0.274106	-0.022241
4	6	0	2.268438	2.639853	-0.021902
5	1	0	0.464281	3.816664	-0.015421
6	6	0	2.761529	1.340335	-0.022284
7	1	0	2.213331	-0.748852	-0.026082
8	1	0	2.945631	3.486730	-0.024419
9	6	0	-0.888552	-2.816209	-0.017210
10	6	0	-0.501431	-0.553514	-0.018728
11	6	0	-2.268438	-2.639854	-0.021893
12	1	0	-0.464281	-3.816665	-0.015416
13	6	0	-1.864904	-0.274107	-0.022235
14	6	0	-2.761530	-1.340335	-0.022274
15	1	0	-2.213331	0.748852	-0.026076
16	7	0	0.021142	1.806956	-0.015825
17	7	0	-4.181704	-1.206294	-0.028590
18	7	0	-4.590958	-0.032063	0.030257
19	6	0	-6.000805	0.130633	0.021517
20	6	0	-6.447165	1.450707	0.090004
21	6	0	-6.918412	-0.924487	-0.049735
22	6	0	-7.811422	1.724532	0.087587
23	1	0	-5.714162	2.249435	0.144372
24	6	0	-8.276879	-0.644151	-0.051491
25	1	0	-6.559619	-1.945640	-0.102512
26	6	0	-8.726115	0.677658	0.016844
27	1	0	-8.158291	2.751585	0.140722
28	1	0	-8.994301	-1.457162	-0.106450
29	1	0	-9.791529	0.886825	0.014716
30	1	0	-2.945631	-3.486731	-0.024407
31	7	0	-0.021142	-1.806957	-0.015823
32	7	0	4.181703	1.206294	-0.028604
33	7	0	4.590958	0.032062	0.030236
34	6	0	6.000805	-0.130633	0.021509
35	6	0	6.447166	-1.450707	0.089986
36	6	0	6.918413	0.924489	-0.049722
37	6	0	7.811423	-1.724531	0.087580
38	1	0	5.714162	-2.249437	0.144338
39	6	0	8.276880	0.644153	-0.051467
40	1	0	6.559619	1.945641	-0.102491
41	6	0	8.726116	-0.677656	0.016858
42	1	0	8.158291	-2.751585	0.140707
43	1	0	8.994302	1.457166	-0.106410
44	1	0	9.791530	-0.886822	0.014738

2 (HF= -588.5051537)

Center Number	Atomic Number	Atomic Type	Coordinates (Angstroms) X	Y	Z
1	6	0	3.670945	1.239519	0.170027
2	6	0	4.022545	-0.991615	-0.174518
3	6	0	2.292461	1.083835	0.193231
4	6	0	2.657672	-1.259831	-0.161015
5	1	0	4.736126	-1.798341	-0.318689
6	6	0	1.775141	-0.199936	0.017281
7	1	0	1.637922	1.932421	0.348826
8	1	0	2.283006	-2.269486	-0.289836
9	7	0	4.533334	0.231097	-0.012326
10	7	0	0.387949	-0.524581	0.028683
11	7	0	-0.371375	0.459300	-0.047767
12	6	0	-1.760590	0.169061	-0.019360
13	6	0	-2.602132	1.271591	-0.170074
14	6	0	-2.296421	-1.113124	0.150999
15	6	0	-3.982821	1.099181	-0.156919
16	1	0	-2.160157	2.254768	-0.297410
17	6	0	-3.673694	-1.277256	0.165151
18	1	0	-1.632570	-1.961086	0.271346
19	6	0	-4.518640	-0.174595	0.010802
20	1	0	-4.637259	1.956799	-0.275864
21	1	0	-4.096446	-2.268347	0.298079
22	1	0	-5.595410	-0.313246	0.023411
23	1	0	4.108636	2.224821	0.306384

3 (HF= -1637.695097)

Center Number	Atomic Number	Atomic Type	Coordinates (Angstroms) X	Y	Z
1	7	0	-1.228193	-1.010334	0.855697
2	7	0	4.695871	-0.450141	6.938666
3	7	0	4.911078	-1.435328	7.670613
4	6	0	-1.403687	-1.610852	2.032257
5	1	0	-2.338577	-2.150524	2.161289
6	6	0	-0.475763	-1.570575	3.065114
7	1	0	-0.694422	-2.067150	4.004249
8	6	0	0.713916	-0.862985	2.876381
9	6	0	0.896534	-0.234908	1.643828
10	1	0	1.803133	0.313531	1.422348
11	6	0	-0.090162	-0.330075	0.663773
12	6	0	1.744602	-0.780390	3.939845
13	6	0	2.007013	-1.882185	4.768373
14	1	0	1.464328	-2.809987	4.616647
15	6	0	2.968500	-1.816910	5.763310
16	1	0	3.170903	-2.675763	6.392061
17	6	0	3.690201	-0.633466	5.951927
18	6	0	3.437736	0.468525	5.136193
19	1	0	4.000471	1.382433	5.297889
20	6	0	2.474816	0.395169	4.137786
21	1	0	2.277117	1.266908	3.522441
22	6	0	5.918199	-1.255776	8.657382
23	6	0	6.144260	-2.353607	9.488055
24	1	0	5.556293	-3.253755	9.338116
25	6	0	7.109219	-2.284110	10.488578

26	1	0	7.282817	-3.139548	11.133867
27	6	0	7.848515	-1.116754	10.657564
28	1	0	8.602527	-1.058527	11.436678
29	6	0	7.621667	-0.018352	9.824055
30	1	0	8.200499	0.890612	9.957299
31	6	0	6.660747	-0.081018	8.824951
32	1	0	6.478425	0.765346	8.173284
33	7	0	1.228193	1.010334	-0.855697
34	7	0	-4.695871	0.450141	-6.938666
35	7	0	-4.911078	1.435328	-7.670613
36	6	0	1.403687	1.610852	-2.032257
37	1	0	2.338577	2.150524	-2.161289
38	6	0	0.475763	1.570575	-3.065114
39	1	0	0.694422	2.067150	-4.004249
40	6	0	-0.713916	0.862985	-2.876381
41	6	0	-0.896534	0.234908	-1.643828
42	1	0	-1.803133	-0.313531	-1.422348
43	6	0	0.090162	0.330075	-0.663773
44	6	0	-1.744602	0.780390	-3.939845
45	6	0	-2.007013	1.882185	-4.768373
46	1	0	-1.464328	2.809987	-4.616647
47	6	0	-2.968500	1.816910	-5.763310
48	1	0	-3.170903	2.675763	-6.392061
49	6	0	-3.690201	0.633466	-5.951927
50	6	0	-3.437736	-0.468525	-5.136193
51	1	0	-4.000471	-1.382433	-5.297889
52	6	0	-2.474816	-0.395169	-4.137786
53	1	0	-2.277117	-1.266908	-3.522441
54	6	0	-5.918199	1.255776	-8.657382
55	6	0	-6.144260	2.353607	-9.488055
56	1	0	-5.556293	3.253755	-9.338116
57	6	0	-7.109219	2.284110	-10.488578
58	1	0	-7.282817	3.139548	-11.133867
59	6	0	-7.848515	1.116754	-10.657564
60	1	0	-8.602527	1.058527	-11.436678
61	6	0	-7.621667	0.018352	-9.824055
62	1	0	-8.200499	-0.890612	-9.957299
63	6	0	-6.660747	0.081018	-8.824951
64	1	0	-6.478425	-0.765346	-8.173284

---

4 (HF= -3637.6444873)

Center Number	Atomic Number	Atomic Type	Coordinates (Angstroms) X	Y	Z
1	6	0	3.677285	-0.239252	0.066504
2	6	0	4.139885	-2.450894	0.454794
3	6	0	5.034208	0.071920	-0.035023
4	6	0	5.513381	-2.249281	0.371211
5	1	0	3.750467	-3.446521	0.650036
6	6	0	5.947143	-0.956403	0.120658
7	1	0	5.343769	1.089527	-0.230188
8	1	0	6.205557	-3.072834	0.497827
9	6	0	2.189291	3.039063	-0.462937
10	6	0	2.647184	0.828285	-0.097442
11	6	0	0.817917	2.829258	-0.389711
12	1	0	2.578699	4.036671	-0.649383
13	6	0	1.290691	0.522703	-0.012969
14	6	0	0.342562	1.536498	-0.157500
15	1	0	0.995140	-0.499061	0.188239
16	7	0	3.239737	-1.480874	0.307231
17	7	0	-5.253950	0.519065	0.252629
18	7	0	-5.708125	-0.538226	-0.225421
19	6	0	-7.110038	-0.722667	-0.081630
20	6	0	-7.618971	-1.895465	-0.640104
21	6	0	-7.964035	0.176706	0.567477
22	6	0	-8.979912	-2.174474	-0.556379
23	1	0	-6.936381	-2.577992	-1.136783
24	6	0	-9.319748	-0.107875	0.648416
25	1	0	-7.558579	1.083729	1.000062
26	6	0	-9.831347	-1.281153	0.087748
27	1	0	-9.373424	-3.087238	-0.992645
28	1	0	-9.985928	0.586565	1.151359
29	1	0	-10.893630	-1.495217	0.155890
30	1	0	0.138332	3.662212	-0.532912
31	7	0	3.093488	2.070842	-0.321177
32	6	0	-1.109384	1.248995	-0.063778
33	6	0	-1.637041	0.055628	-0.580133
34	6	0	-1.980447	2.160567	0.540036
35	6	0	-2.991558	-0.221937	-0.499523
36	1	0	-0.979123	-0.655453	-1.069764
37	6	0	-3.339203	1.885830	0.628796
38	1	0	-1.594376	3.081730	0.964543
39	6	0	-3.851619	0.697845	0.109749
40	1	0	-3.391175	-1.141992	-0.908995
41	1	0	-4.016938	2.586667	1.105807
42	35	0	7.797774	-0.590567	-0.011299

A1 (HF=-2237.3793297)

Center Number	Atomic Number	Atomic Type	Coordinates (Angstroms) X	Y	Z
1	77	0	-2.041213	-0.000001	0.000001
2	6	0	-1.423810	-0.111055	-2.975859
3	6	0	-3.048384	1.444463	-2.334141
4	6	0	-1.536672	0.238434	-4.308460
5	1	0	-0.736604	-0.882951	-2.653808
6	6	0	-3.200423	1.838101	-3.665221
7	6	0	-2.444130	1.236244	-4.657154
8	1	0	-0.925935	-0.262885	-5.049980
9	1	0	-3.913076	2.612923	-3.919017
10	1	0	-2.561267	1.539462	-5.692395
11	6	0	-3.478378	-1.410057	-0.060437
12	6	0	-3.790445	-1.988495	1.190642
13	6	0	-4.167068	-1.897625	-1.178341
14	6	0	-4.740600	-3.009668	1.308677
15	6	0	-5.113195	-2.914039	-1.063787
16	1	0	-3.965646	-1.482618	-2.161800
17	6	0	-5.404030	-3.474808	0.181073
18	1	0	-6.140944	-4.267064	0.269935
19	6	0	0.896233	-0.739393	-0.073092
20	6	0	-0.397748	-2.657721	-0.276498
21	6	0	2.063997	-1.485646	-0.133246
22	6	0	0.725596	-3.466576	-0.341280
23	1	0	-1.396571	-3.073923	-0.330855

24	6	0	1.978253	-2.869978	-0.271931
25	1	0	3.039199	-1.023292	-0.075891
26	1	0	0.630425	-4.540885	-0.446479
27	6	0	-0.397749	2.657721	0.276483
28	6	0	0.896233	0.739396	0.073065
29	6	0	0.725595	3.466578	0.341253
30	1	0	-1.396572	3.073922	0.330850
31	6	0	2.063996	1.485650	0.133206
32	6	0	1.978251	2.869982	0.271893
33	1	0	3.039198	1.023298	0.075840
34	6	0	-1.423781	0.111054	2.975854
35	6	0	-3.048360	-1.444465	2.334153
36	6	0	-1.536630	-0.238435	4.308456
37	1	0	-0.736579	0.882950	2.653796
38	6	0	-3.200386	-1.838103	3.665235
39	6	0	-2.444084	-1.236245	4.657160
40	1	0	-0.925886	0.262885	5.049971
41	1	0	-3.913036	-2.612926	3.919038
42	1	0	-2.561211	-1.539462	5.692402
43	6	0	-3.478379	1.410053	0.060452
44	6	0	-4.167059	1.897620	1.178363
45	6	0	-3.790458	1.988492	-1.190623
46	6	0	-5.113188	2.914034	1.063819
47	1	0	-3.965627	1.482613	2.161821
48	6	0	-4.740615	3.009664	-1.308649
49	6	0	-5.404035	3.474803	-0.181038
50	1	0	-6.140951	4.267058	-0.269893
51	7	0	-0.320110	-1.328736	-0.149132
52	7	0	-2.155193	0.472614	-2.012642
53	7	0	-2.155173	-0.472616	2.012645
54	7	0	3.101599	3.741667	0.348980
55	7	0	4.202583	3.159556	0.308114
56	6	0	5.346173	3.989875	0.381746
57	6	0	6.570618	3.320119	0.343465
58	6	0	5.301669	5.386368	0.487045
59	6	0	7.758060	4.041978	0.411068
60	1	0	6.574236	2.237883	0.261521
61	6	0	6.489616	6.098482	0.553508
62	1	0	4.344482	5.893442	0.515183
63	6	0	7.717343	5.429871	0.516082
64	1	0	8.710796	3.523284	0.381867
65	1	0	6.465264	7.180618	0.635080
66	1	0	8.641735	5.996747	0.569181
67	1	0	0.630423	4.540887	0.446452
68	1	0	-4.968709	-3.448400	2.275279
69	1	0	-5.629592	-3.271983	-1.950680
70	1	0	-5.629577	3.271976	1.950717
71	1	0	-4.968734	3.448396	-2.275248
72	7	0	-0.320110	1.328737	0.149117
73	7	0	3.101601	-3.741661	-0.349033
74	7	0	4.202584	-3.159550	-0.308155
75	6	0	5.346176	-3.989870	-0.381760
76	6	0	6.570620	-3.320115	-0.343465
77	6	0	5.301673	-5.386364	-0.487049
78	6	0	7.758063	-4.041975	-0.411044
79	1	0	6.574238	-2.237878	-0.261529
80	6	0	6.489620	-6.098479	-0.553487
81	1	0	4.344486	-5.893438	-0.515198
82	6	0	7.717347	-5.429868	-0.516046
83	1	0	8.710799	-3.523281	-0.381832
84	1	0	6.465269	-7.180616	-0.635051
85	1	0	8.641739	-5.996745	-0.569126

B1 (HF= -2634.2785179)

Center Number	Atomic Number	Atomic Type	Coordinates (Angstroms) X	Y	Z
1	77	0	-1.437376	-0.000101	-0.000040
2	9	0	-4.479281	3.482043	-2.543322
3	9	0	-4.478786	-3.482452	2.543551
4	9	0	-5.144199	3.358245	2.079184
5	9	0	-5.144050	-3.358855	-2.078911
6	7	0	0.276690	1.331447	0.102505
7	7	0	0.276852	-1.331461	-0.102717
8	7	0	3.813518	3.576322	0.177197
9	7	0	3.814000	-3.575838	-0.177953
10	7	0	3.699908	4.809358	0.319473
11	7	0	3.700551	-4.809061	-0.318764
12	7	0	-1.550212	0.414578	-2.023845
13	7	0	-1.549989	-0.414784	2.023776
14	6	0	0.200748	2.668737	0.179703
15	1	0	-0.797976	3.086113	0.222139
16	6	0	0.201084	-2.668756	-0.179928
17	1	0	-0.797587	-3.086266	-0.222265
18	6	0	1.316576	3.483610	0.209810
19	1	0	1.212557	4.558850	0.272592
20	6	0	1.317018	-3.483483	-0.210183
21	1	0	1.213128	-4.558734	-0.272990
22	6	0	2.572379	2.880825	0.156935
23	6	0	2.572748	-2.880536	-0.157417
24	6	0	2.655191	1.496242	0.070217
25	1	0	3.634321	1.037898	0.024248
26	6	0	2.655378	-1.495935	-0.070754
27	1	0	3.634452	-1.037457	-0.024927
28	6	0	1.488840	0.740189	0.044389
29	6	0	1.488931	-0.740038	-0.044765
30	6	0	4.908555	5.543852	0.342117
31	6	0	4.909335	-5.543323	-0.341704
32	6	0	4.763274	6.922049	0.512893
33	1	0	3.764949	7.335483	0.614429
34	6	0	4.764214	-6.921700	-0.511165
35	1	0	3.765898	-7.335435	-0.611557
36	6	0	5.889243	7.738328	0.550743
37	1	0	5.778644	8.809603	0.683718
38	6	0	5.890330	-7.737771	-0.549206
39	1	0	5.779855	-8.809182	-0.681182
40	6	0	7.155417	7.174449	0.417295
41	1	0	8.036562	7.808002	0.446187
42	6	0	7.156484	-7.173512	-0.417216
43	1	0	8.037741	-7.806902	-0.446242
44	6	0	7.298342	5.793836	0.245739
45	1	0	8.288523	5.361348	0.142114
46	6	0	7.299248	-5.792723	-0.246936
47	1	0	8.289418	-5.359946	-0.144423
48	6	0	6.181343	4.973288	0.207532
49	1	0	6.279539	3.902295	0.075474
50	6	0	6.182109	-4.972378	-0.208580
51	1	0	6.280178	-3.901253	-0.077502
52	6	0	-0.808097	-0.200558	-2.957523

53	1	0	-0.123484	-0.959117	-2.601494
54	6	0	-0.807844	0.200420	2.957385
55	1	0	-0.123304	0.959014	2.601288
56	6	0	-0.906765	0.100106	-4.303280
57	1	0	-0.286952	-0.426237	-5.019336
58	6	0	-0.906385	-0.100228	4.303155
59	1	0	-0.286557	0.426176	5.019154
60	6	0	-1.812056	1.080807	-4.693968
61	1	0	-1.920614	1.347889	-5.739938
62	6	0	-1.811584	-1.080978	4.693930
63	1	0	-1.920065	-1.348030	5.739916
64	6	0	-2.583099	1.718164	-3.734043
65	1	0	-3.291934	2.479352	-4.023386
66	6	0	-2.582649	-1.718414	3.734075
67	1	0	-3.291412	-2.479642	4.023491
68	6	0	-2.445251	1.373839	-2.386814
69	6	0	-2.444918	-1.374117	2.386828
70	6	0	-3.190404	1.940732	-1.256462
71	6	0	-3.190121	-1.941084	1.256545
72	6	0	-4.157540	2.943193	-1.340902
73	6	0	-4.157178	-2.943613	1.341091
74	6	0	-4.832249	3.442281	-0.244157
75	1	0	-5.577698	4.221200	-0.345443
76	6	0	-4.831927	-3.442786	0.244409
77	1	0	-5.577299	-4.221770	0.345771
78	6	0	-4.500286	2.891968	0.981587
79	6	0	-4.500104	-2.892480	-0.981377
80	6	0	-3.552487	1.897614	1.138804
81	1	0	-3.355082	1.521788	2.136263
82	6	0	-3.552396	-1.898055	-1.138691
83	1	0	-3.355102	-1.522238	-2.136177
84	6	0	-2.877218	1.404803	0.018956
85	6	0	-2.877085	-1.405156	-0.018909

C1 (HF= -7379.2018165)

Center Number	Atomic Number	Atomic Type	Coordinates (Angstroms) X	Y	Z
1	6	0	2.442645	-1.402178	-0.118287
2	6	0	2.767232	-1.807919	-1.431760
3	6	0	3.729621	-2.792169	-1.672394
4	6	0	4.393961	-3.397910	-0.614713
5	6	0	4.073184	-2.998862	0.678220
6	6	0	3.121497	-2.021319	0.937050
7	6	0	2.022708	-1.128918	-2.498844
8	7	0	1.120614	-0.214029	-2.057580
9	6	0	0.384569	0.480107	-2.940684
10	6	0	0.502817	0.302474	-4.306550
11	6	0	1.420087	-0.634024	-4.776825
12	6	0	2.180893	-1.350158	-3.867418
13	77	0	1.002780	-0.000337	-0.000811
14	6	0	2.443518	1.400711	0.118391
15	6	0	2.766000	1.806721	1.432288
16	6	0	3.728755	2.790288	1.674342
17	6	0	4.395471	3.395075	0.617621
18	6	0	4.076719	2.995852	-0.675785
19	6	0	3.124691	2.018992	-0.935917
20	6	0	2.018975	1.128882	2.498404
21	7	0	1.117818	0.213646	2.055887
22	6	0	0.379805	-0.479849	2.937837
23	6	0	0.494812	-0.300815	4.303847
24	6	0	1.410552	0.636520	4.775322
25	6	0	2.173596	1.351753	3.867043
26	7	0	-0.713741	1.336657	0.022291
27	6	0	-0.638706	2.674654	0.085032
28	6	0	-1.754647	3.486479	0.162671
29	6	0	-3.009524	2.879522	0.177231
30	6	0	-3.091706	1.494137	0.105783
31	6	0	-1.925133	0.741564	0.031191
32	7	0	-4.250506	3.570680	0.262010
33	7	0	-4.134605	4.805672	0.383247
34	6	0	-5.343766	5.534705	0.472702
35	6	0	-5.195957	6.913799	0.632726
36	6	0	-6.322070	7.724445	0.734813
37	6	0	-7.590923	7.154193	0.674760
38	6	0	-7.736437	5.772767	0.512671
39	6	0	-6.619289	4.957764	0.411581
40	6	0	-1.925412	-0.739646	-0.041114
41	7	0	-0.714617	-1.335603	-0.026384
42	6	0	-0.640235	-2.673835	-0.087277
43	6	0	-1.756402	-3.484923	-0.168100
44	6	0	-3.010811	-2.877012	-0.189114
45	6	0	-3.092202	-1.491459	-0.121246
46	7	0	-4.252010	-3.567031	-0.280092
47	7	0	-4.137804	-4.805091	-0.366333
48	6	0	-5.347390	-5.532625	-0.463575
49	6	0	-5.201498	-6.917298	-0.567488
50	6	0	-6.327989	-7.727183	-0.671108
51	6	0	-7.595368	-7.150364	-0.669965
52	6	0	-7.738970	-5.763216	-0.565252
53	6	0	-6.621337	-4.949077	-0.461952
54	1	0	0.359608	3.095119	0.069840
55	1	0	0.357855	-3.094802	-0.068098
56	1	0	-1.651410	4.562522	0.212449
57	1	0	-1.653775	-4.561121	-0.215775
58	1	0	-4.069725	1.031104	0.118929
59	1	0	-4.069721	-1.027616	-0.141072
60	1	0	-4.195608	7.332468	0.676209
61	1	0	-4.202258	-7.340816	-0.566201
62	1	0	-6.209352	8.796397	0.860490
63	1	0	-6.216816	-8.803564	-0.752437
64	1	0	-8.472154	7.783376	0.753558
65	1	0	-8.476893	-7.778893	-0.750813
66	1	0	-8.728758	5.335306	0.466005
67	1	0	-8.730102	-5.320598	-0.565079
68	1	0	-6.719491	3.886136	0.286365
69	1	0	-6.720050	-3.873078	-0.380986
70	1	0	-0.313120	-1.199403	2.521330
71	1	0	-0.309372	1.199309	-2.525271
72	1	0	-0.120629	-0.885970	4.976825
73	1	0	-0.111497	0.887818	-4.980377
74	1	0	1.529214	0.805912	5.840384
75	1	0	1.541751	-0.801819	-5.841810
76	1	0	2.892195	2.082586	4.216637
77	1	0	2.900688	-2.080284	-4.216016
78	1	0	5.142728	4.158948	0.797299
79	1	0	5.141002	-4.162215	-0.793361
80	1	0	2.917202	1.745689	-1.964322
81	1	0	2.912252	-1.748238	1.965168

82	1	0	3.975482	-3.100667	-2.683303
83	35	0	4.974663	-3.822808	2.142744
84	35	0	4.981615	3.818382	-2.138973
85	1	0	3.972914	3.099009	2.685608

A2 (HF= -2238.5601268)

Center Number	Atomic Number	Atomic Type	Coordinates (Angstroms) X	Y	Z
1	77	0	-0.000002	1.409036	-0.000056
2	7	0	1.602689	-0.157489	0.000481
3	7	0	4.679110	-3.020401	-0.274156
4	7	0	5.708618	-2.808872	0.395509
5	7	0	0.332289	1.514079	-2.046652
6	6	0	2.767661	0.048568	0.644410
7	1	0	2.849051	0.974419	1.200844
8	6	0	3.823022	-0.842981	0.607764
9	1	0	4.737174	-0.630209	1.146765
10	6	0	3.683042	-2.012276	-0.140835
11	6	0	2.490348	-2.226060	-0.822666
12	1	0	2.350417	-3.119459	-1.420269
13	6	0	1.482627	-1.279267	-0.725294
14	1	0	0.544700	-1.424359	-1.247133
15	6	0	6.726081	-3.787970	0.293921
16	6	0	7.876496	-3.528136	1.041050
17	1	0	7.921874	-2.620793	1.634875
18	6	0	8.938662	-4.426411	1.014766
19	1	0	9.833570	-4.225470	1.594788
20	6	0	8.846776	-5.581775	0.243055
21	1	0	9.673045	-6.285670	0.220182
22	6	0	7.693118	-5.840435	-0.503810
23	1	0	7.627856	-6.743388	-1.102797
24	6	0	6.630546	-4.949523	-0.483670
25	1	0	5.731594	-5.139967	-1.057858
26	6	0	-0.285901	0.758296	-2.968461
27	1	0	-1.018802	0.052975	-2.599248
28	6	0	-0.018032	0.861120	-4.320862
29	1	0	-0.546940	0.228374	-5.023686
30	6	0	0.934601	1.787100	-4.738077
31	1	0	1.173196	1.899501	-5.790560
32	6	0	1.578200	2.565028	-3.790079
33	1	0	2.323928	3.288348	-4.095618
34	6	0	1.268760	2.418788	-2.436734
35	6	0	1.876782	3.176521	-1.337500
36	6	0	2.857684	4.155873	-1.530419
37	1	0	3.217917	4.393853	-2.526541
38	6	0	3.382904	4.837597	-0.440454
39	1	0	4.143928	5.597626	-0.587857
40	6	0	2.920263	4.537494	0.841430
41	1	0	3.322506	5.069999	1.699250
42	6	0	1.943441	3.561454	1.029948
43	1	0	1.602301	3.355698	2.040764
44	6	0	1.402092	2.851797	-0.048555
45	7	0	-1.602174	-0.158035	-0.001878
46	7	0	-4.677630	-3.022179	0.270754
47	7	0	-5.707625	-2.809971	-0.397943
48	7	0	-0.331889	1.511944	2.046633
49	6	0	-2.767632	0.048602	-0.644740
50	1	0	-2.849728	0.975306	-1.199652
51	6	0	-3.822744	-0.843260	-0.608630
52	1	0	-4.737316	-0.629971	-1.146714
53	6	0	-3.681971	-2.013545	0.138271
54	6	0	-2.488794	-2.227934	0.819061
55	1	0	-2.348245	-3.122108	1.415358
56	6	0	-1.481403	-1.280721	0.722372
57	1	0	-0.543130	-1.426263	1.243461
58	6	0	-6.725862	-3.788125	-0.295008
59	6	0	-7.876841	-3.527427	-1.040968
60	1	0	-7.922059	-2.620155	-1.634913
61	6	0	-8.939737	-4.424799	-1.013440
62	1	0	-9.835070	-4.223201	-1.592578
63	6	0	-8.848028	-5.580119	-0.241644
64	1	0	-9.674873	-6.283306	-0.217795
65	6	0	-7.693822	-5.839630	0.504078
66	1	0	-7.628703	-6.742545	1.103139
67	6	0	-6.630519	-4.949619	0.482698
68	1	0	-5.731120	-5.140750	1.055956
69	6	0	0.287304	0.755885	2.967533
70	1	0	1.020871	0.051710	2.597414
71	6	0	0.019678	0.857166	4.320095
72	1	0	0.549382	0.224269	5.022184
73	6	0	-0.933713	1.781874	4.738421
74	1	0	-1.172107	1.893085	5.791077
75	6	0	-1.578229	2.560176	3.791342
76	1	0	-2.324447	3.282607	4.097782
77	6	0	-1.269017	2.415508	2.437773
78	6	0	-1.877734	3.173950	1.339387
79	6	0	-2.859179	4.152539	1.533437
80	1	0	-3.219464	4.389256	2.529841
81	6	0	-3.384821	4.835191	0.444255
82	1	0	-4.146251	5.594641	0.592540
83	6	0	-2.922020	4.536830	-0.837979
84	1	0	-3.324571	5.070098	-1.695180
85	6	0	-1.944636	3.561576	-1.027633
86	1	0	-1.603387	3.357203	-2.038692
87	6	0	-1.402891	2.850968	0.050049

B2 (HF=- 2635.4585829)

Center Number	Atomic Number	Atomic Type	Coordinates (Angstroms) X	Y	Z
1	6	0	1.397348	2.511428	-0.023021
2	6	0	1.896257	2.830779	-1.310004
3	6	0	2.868040	3.825820	-1.421334
4	6	0	3.369496	4.522854	-0.339353
5	6	0	2.852194	4.186407	0.898897
6	6	0	1.888350	3.211311	1.081683
7	6	0	1.321267	2.067226	-2.422987
8	7	0	0.374787	1.167237	-2.037119
9	6	0	-0.229693	0.399184	-2.956439
10	6	0	0.059335	0.479698	-4.306122
11	6	0	1.020430	1.395452	-4.718707
12	6	0	1.653040	2.189573	-3.774489
13	77	0	0.000000	1.067073	-0.000001

14	7	0	1.595916	-0.493075	0.025785
15	6	0	2.753306	-0.287943	0.684613
16	6	0	3.810226	-1.177298	0.655773
17	6	0	3.680915	-2.343722	-0.099190
18	6	0	2.495088	-2.558240	-0.792678
19	6	0	1.485138	-1.613678	-0.704289
20	7	0	4.680132	-3.349209	-0.225735
21	7	0	5.713812	-3.122535	0.432735
22	6	0	6.735668	-4.096931	0.337266
23	6	0	7.888232	-3.822597	1.076034
24	6	0	8.955028	-4.715405	1.054399
25	6	0	8.865801	-5.879241	0.295166
26	6	0	7.710300	-6.152071	-0.443865
27	6	0	6.642917	-5.267007	-0.428020
28	7	0	-1.595900	-0.493090	-0.025816
29	6	0	-2.753279	-0.287973	-0.684667
30	6	0	-3.810190	-1.177340	-0.655846
31	6	0	-3.680879	-2.343762	0.099121
32	6	0	-2.495061	-2.558269	0.792626
33	6	0	-1.485121	-1.613693	0.704258
34	7	0	-4.680082	-3.349267	0.225639
35	7	0	-5.713803	-3.122544	-0.432749
36	6	0	-6.735662	-4.096937	-0.337267
37	6	0	-7.888279	-3.822543	-1.075931
38	6	0	-8.955080	-4.715345	-1.054278
39	6	0	-8.865805	-5.879233	-0.295130
40	6	0	-7.710252	-6.152122	0.443796
41	6	0	-6.642863	-5.267065	0.427932
42	7	0	-0.374793	1.167199	2.037119
43	6	0	0.229682	0.399129	2.956427
44	6	0	-0.059350	0.479620	4.306111
45	6	0	-1.020446	1.395366	4.718709
46	6	0	-1.653054	2.189503	3.774503
47	6	0	-1.321276	2.067180	2.423000
48	6	0	-1.896268	2.830748	1.310028
49	6	0	-2.868057	3.825781	1.421374
50	6	0	-3.369517	4.522828	0.339402
51	6	0	-2.852215	4.186401	-0.898853
52	6	0	-1.888365	3.211314	-1.081653
53	6	0	-1.397357	2.511418	0.023041
54	1	0	-2.828105	0.633955	-1.248279
55	1	0	-4.717630	-0.965000	-1.206166
56	1	0	-2.362241	-3.450420	1.393600
57	1	0	-0.553615	-1.760142	1.236534
58	1	0	-7.931503	-2.908453	-1.659471
59	1	0	-9.851660	-4.503444	-1.627747
60	1	0	-9.695801	-6.578831	-0.275786
61	1	0	-7.647534	-7.061441	1.033326
62	1	0	-5.742545	-5.468160	0.996325
63	1	0	0.969844	-0.298592	2.587984
64	1	0	0.460246	-0.162731	5.007014
65	1	0	-1.278723	1.491812	5.768034
66	1	0	-2.404025	2.902645	4.079411
67	9	0	-3.370737	4.156817	2.636508
68	1	0	-4.123542	5.290333	0.462015
69	9	0	-3.317798	4.853374	-1.982286
70	1	0	-1.533214	3.015675	-2.087302
71	1	0	2.828134	0.633988	1.248219
72	1	0	4.717676	-0.964945	1.206072
73	1	0	2.362270	-3.450390	-1.393654
74	1	0	0.553624	-1.760136	-1.236549
75	1	0	7.931420	-2.908547	1.659638
76	1	0	9.851567	-4.503552	1.627949
77	1	0	9.695793	-6.578845	0.275835
78	1	0	7.647619	-7.061349	-1.033462
79	1	0	5.742640	-5.468056	-0.996494
80	1	0	-0.969856	-0.298542	-2.588005
81	1	0	-0.460264	-0.162639	-5.007034
82	1	0	1.278703	1.491917	-5.768031
83	1	0	2.404008	2.902722	-4.079388
84	9	0	3.370716	4.156878	-2.636464
85	1	0	4.123515	5.290366	-0.461954
86	9	0	3.317774	4.853367	1.982340
87	1	0	1.533200	3.015656	2.087330

C2 (HF= -7380.3822089)

Center Number	Atomic Number	Atomic Type	Coordinates (Angstroms) X	Y	Z
1	6	0	-1.393489	2.075058	0.129795
2	6	0	-1.793795	2.400849	1.442799
3	6	0	-2.755684	3.384511	1.686473
4	6	0	-3.339916	4.072110	0.631183
5	6	0	-2.938561	3.756722	-0.661957
6	6	0	-1.983554	2.782249	-0.922644
7	6	0	-1.128728	1.639951	2.506345
8	7	0	-0.216210	0.735221	2.063427
9	6	0	0.451454	-0.021938	2.948950
10	6	0	0.257156	0.080110	4.314111
11	6	0	-0.670635	1.005570	4.783834
12	6	0	-1.364649	1.785588	3.873437
13	77	0	-0.000001	0.630629	0.000010
14	7	0	-1.597610	-0.928911	0.091406
15	6	0	-2.800253	-0.722399	-0.479064
16	6	0	-3.853984	-1.609788	-0.369348
17	6	0	-3.670989	-2.774317	0.377017
18	6	0	-2.433919	-2.995212	0.972178
19	6	0	-1.433484	-2.050365	0.809993
20	7	0	-4.658798	-3.779984	0.569717
21	7	0	-5.795089	-3.456641	0.172893
22	6	0	-6.807983	-4.432738	0.331930
23	6	0	-8.078620	-4.045319	-0.097672
24	6	0	-9.147342	-4.929449	0.011690
25	6	0	-8.942129	-6.197501	0.549108
26	6	0	-7.668386	-6.583495	0.978338
27	6	0	-6.598243	-5.707790	0.873488
28	7	0	1.597595	-0.928923	-0.091378
29	6	0	2.800279	-0.722367	0.478987
30	6	0	3.854002	-1.609765	0.369265
31	6	0	3.670952	-2.774353	-0.376993
32	6	0	2.433840	-2.995291	-0.972053
33	6	0	1.433419	-2.050430	-0.809872
34	7	0	4.658745	-3.780038	-0.569686
35	7	0	5.795060	-3.456673	-0.172946
36	6	0	6.807939	-4.432789	-0.331966
37	6	0	8.078600	-4.045347	0.097543
38	6	0	9.147311	-4.929493	-0.011810
39	6	0	8.942061	-6.197582	-0.549126
40	6	0	7.668293	-6.583599	-0.978261

41	6	0	6.598162	-5.707879	-0.873419
42	7	0	0.216195	0.735205	-2.063407
43	6	0	-0.451513	-0.021925	-2.948921
44	6	0	-0.257220	0.080108	-4.314084
45	6	0	0.670610	1.005524	-4.783818
46	6	0	1.364663	1.785517	-3.873430
47	6	0	1.128746	1.639897	-2.506335
48	6	0	1.793839	2.400784	-1.442797
49	6	0	2.755753	3.384420	-1.686482
50	6	0	3.339996	4.072022	-0.631200
51	6	0	2.938626	3.756667	0.661943
52	6	0	1.983593	2.782221	0.922642
53	6	0	1.393517	2.075027	-0.129789
54	1	0	2.915120	0.199017	1.036669
55	1	0	4.798923	-1.398936	0.853357
56	1	0	2.255570	-3.890220	-1.556971
57	1	0	0.464171	-2.197878	-1.269588
58	1	0	8.210974	-3.051401	0.512905
59	1	0	10.135680	-4.629807	0.321341
60	1	0	9.773246	-6.890663	-0.635657
61	1	0	7.515267	-7.573896	-1.395682
62	1	0	5.606767	-5.996056	-1.202375
63	1	0	-1.163894	-0.726302	-2.540021
64	1	0	-0.823568	-0.553183	-4.986505
65	1	0	0.851330	1.116711	-5.847790
66	1	0	2.091891	2.508928	-4.220391
67	1	0	3.063531	3.629687	-2.697776
68	1	0	4.087421	4.835339	-0.812597
69	35	0	3.725710	4.694265	2.123410
70	1	0	1.704870	2.580205	1.950951
71	1	0	-2.915049	0.198936	-1.036835
72	1	0	-4.798869	-1.398998	-0.853528
73	1	0	-2.255692	-3.890095	1.557179
74	1	0	-0.464270	-2.197779	1.269790
75	1	0	-8.210965	-3.051402	-0.513113
76	1	0	-10.135692	-4.629781	-0.321534
77	1	0	-9.773323	-6.890570	0.635647
78	1	0	-7.515388	-7.573762	1.395839
79	1	0	-5.606868	-5.995949	1.202515
80	1	0	1.163800	-0.726355	2.540060
81	1	0	0.823468	-0.553206	4.986539
82	1	0	-0.851360	1.116768	5.847804
83	1	0	-2.091853	2.509027	4.220390
84	1	0	-3.063454	3.629800	2.697764
85	1	0	-4.087322	4.835448	0.812570
86	35	0	-3.725628	4.694314	-2.123438
87	1	0	-1.704840	2.580209	-1.950952

A3 (HF=- 2699.2390597)

Center Number	Atomic Number	Atomic Type	Coordinates (Angstroms) X	Y	Z
1	77	0	-3.415494	0.051526	0.017476
2	7	0	-1.758176	-1.358138	-0.104803
3	7	0	-1.630081	1.296447	0.135370
4	7	0	5.022588	-6.451140	-0.576100
5	7	0	5.691903	5.586050	0.490750
6	7	0	6.037133	-6.173747	0.091723
7	7	0	5.789800	6.669641	-0.116284
8	7	0	-3.507982	0.486252	-2.004840
9	7	0	-3.547608	-0.369666	2.039708
10	6	0	-1.892739	-2.685471	-0.211958
11	1	0	-2.909460	-3.058366	-0.251335
12	6	0	-1.636137	2.631731	0.226110
13	1	0	-2.612021	3.100702	0.273548
14	6	0	-0.810554	-3.545544	-0.268616
15	1	0	-0.986767	-4.612571	-0.337053
16	6	0	-0.475939	3.384386	0.271556
17	1	0	-0.548541	4.461327	0.367753
18	6	0	0.483999	-3.024637	-0.212913
19	6	0	0.762138	2.740428	0.222721
20	6	0	0.611286	-1.639017	-0.093743
21	1	0	1.598286	-1.197529	-0.067326
22	6	0	0.755462	1.347508	0.120837
23	1	0	1.695941	0.817057	0.055008
24	6	0	-0.517000	-0.829673	-0.040310
25	6	0	-0.445552	0.650075	0.076504
26	6	0	1.676078	-3.900666	-0.284200
27	6	0	2.033698	3.497850	0.276788
28	6	0	1.677326	-5.030243	-1.108276
29	1	0	0.809298	-5.263149	-1.716426
30	6	0	2.148497	4.742583	-0.360974
31	1	0	1.306931	5.144835	-0.916038
32	6	0	2.798866	-5.846395	-1.180710
33	1	0	2.809276	-6.718539	-1.826364
34	6	0	3.333461	5.458658	-0.318242
35	1	0	3.418642	6.414496	-0.821028
36	6	0	3.933591	-5.549779	-0.426851
37	6	0	4.431338	4.939100	0.376113
38	6	0	3.942864	-4.425196	0.405286
39	1	0	4.822055	-4.201621	0.997442
40	6	0	4.326306	3.706359	1.018843
41	1	0	5.183139	3.321345	1.562144
42	6	0	2.823779	-3.611411	0.469741
43	1	0	2.833485	-2.752271	1.133103
44	6	0	3.138261	2.988610	0.966210
45	1	0	3.066531	2.039797	1.487886
46	6	0	-2.802548	-0.148878	-2.954762
47	1	0	-2.150913	-0.943702	-2.615268
48	6	0	-2.788563	0.201610	2.988818
49	1	0	-2.066830	0.933035	2.648440
50	6	0	-2.898367	0.177916	-4.294461
51	1	0	-2.310040	-0.365295	-5.024534
52	6	0	-2.916003	-0.110515	4.329387
53	1	0	-2.281631	0.379188	5.058759
54	6	0	-3.760074	1.207855	-4.665196
55	1	0	-3.862810	1.494449	-5.706693
56	6	0	-3.869282	-1.055548	4.701998
57	1	0	-3.999592	-1.327771	5.744274
58	6	0	-4.488945	1.863512	-3.687018
59	1	0	-5.165307	2.664728	-3.957733
60	6	0	-4.654498	-1.644163	3.724748
61	1	0	-5.403359	-2.377506	3.997059
62	6	0	-4.355715	1.490968	-2.347787
63	6	0	-4.485515	-1.290074	2.384537
64	6	0	-5.071664	2.092893	-1.216847
65	6	0	-5.254823	-1.824273	1.254614
66	6	0	-5.974832	3.153168	-1.357481
67	1	0	-6.184588	3.579559	-2.333746

68	6	0	-6.253240	-2.795027	1.397327
69	1	0	-6.499633	-3.200177	2.374098
70	6	0	-6.614677	3.673523	-0.240419
71	1	0	-7.315026	4.496219	-0.346867
72	6	0	-6.941899	-3.252409	0.281754
73	1	0	-7.716828	-4.005048	0.389838
74	6	0	-6.347465	3.128468	1.016752
75	6	0	-6.627163	-2.734856	-0.976019
76	6	0	-5.448613	2.072717	1.153596
77	1	0	-5.264749	1.670992	2.146009
78	6	0	-5.632467	-1.769147	-1.115121
79	1	0	-5.413632	-1.386781	-2.108105
80	6	0	-4.784409	1.528675	0.046725
81	6	0	-4.917746	-1.290066	-0.009763
82	6	0	7.130166	-7.069715	-0.051623
83	6	0	7.045052	7.325120	-0.003280
84	6	0	7.116739	-8.210046	-0.864152
85	1	0	6.227155	-8.452479	-1.433432
86	6	0	7.159498	8.522995	-0.709965
87	1	0	6.309756	8.873754	-1.287247
88	6	0	8.245735	-9.014592	-0.927454
89	1	0	8.240735	-9.900088	-1.555761
90	6	0	8.348313	9.245966	-0.668448
91	1	0	8.435669	10.176876	-1.219753
92	6	0	9.387225	-8.691843	-0.187951
93	1	0	10.265755	-9.327350	-0.244107
94	6	0	9.421082	8.771466	0.081761
95	1	0	10.349859	9.332662	0.117621
96	6	0	9.397704	-7.557624	0.619661
97	1	0	10.282311	-7.304283	1.195374
98	6	0	9.303896	7.572584	0.790886
99	1	0	10.141840	7.206174	1.376106
100	6	0	8.268571	-6.746471	0.687970
101	1	0	8.253564	-5.857458	1.310701
102	6	0	8.121929	6.846269	0.752852
103	1	0	8.021482	5.916420	1.300135
104	1	0	-7.163014	-3.086996	-1.853685
105	1	0	-6.845550	3.529689	1.895597

B3 (HF= -3096.1382408)

Center Number	Atomic Number	Atomic Type	Coordinates (Angstroms) X	Y	Z
1	6	0	8.472294	6.890749	0.775305
2	6	0	7.391384	7.363629	0.021158
3	6	0	7.495703	8.565143	-0.680922
4	6	0	8.678484	9.297765	-0.636793
5	6	0	9.755244	8.829258	0.111460
6	6	0	9.648170	7.626718	0.815998
7	7	0	6.141555	6.698465	-0.094020
8	7	0	6.052652	5.611344	0.508048
9	6	0	4.796750	4.955541	0.391162
10	6	0	3.694616	5.470720	-0.299658
11	6	0	2.514639	4.746705	-0.344510
12	6	0	2.409586	3.498193	0.287457
13	6	0	3.518439	2.992906	0.972854
14	6	0	4.701335	3.718898	1.027849
15	6	0	1.143183	2.732900	0.231746
16	6	0	-0.098913	3.368684	0.284291
17	6	0	-1.254344	2.609500	0.236512
18	7	0	-1.239879	1.274385	0.139913
19	6	0	-0.050863	0.635413	0.077730
20	6	0	1.145134	1.340158	0.124504
21	77	0	-3.008924	0.020995	0.014966
22	6	0	-4.505757	-1.322800	-0.025836
23	6	0	-4.838849	-1.868013	1.240827
24	6	0	-5.846969	-2.830422	1.310413
25	6	0	-6.544284	-3.281597	0.207078
26	6	0	-6.191775	-2.724168	-1.009765
27	6	0	-5.203600	-1.767738	-1.152148
28	6	0	-0.114243	-0.843459	-0.045435
29	7	0	-1.353352	-1.377518	-0.115320
30	6	0	-1.481552	-2.705147	-0.230182
31	6	0	-0.395218	-3.559364	-0.288387
32	6	0	0.896798	-3.032994	-0.226555
33	6	0	1.017239	-1.647184	-0.100294
34	6	0	2.093002	-3.902773	-0.298920
35	6	0	2.100475	-5.030069	-1.126076
36	6	0	3.226353	-5.840036	-1.199839
37	6	0	4.358822	-5.539493	-0.444167
38	6	0	4.361583	-4.417368	0.391300
39	6	0	3.238384	-3.609454	0.456943
40	7	0	5.452843	-6.434610	-0.595147
41	7	0	6.465630	-6.152622	0.073395
42	6	0	7.563880	-7.041822	-0.071340
43	6	0	7.557160	-8.180885	-0.885747
44	6	0	8.690935	-8.978539	-0.950407
45	6	0	9.830510	-8.650142	-0.210419
46	6	0	9.834285	-7.517241	0.599099
47	6	0	8.700334	-6.712975	0.668800
48	6	0	-4.069098	-1.352230	2.379217
49	7	0	-3.136372	-0.424011	2.030805
50	6	0	-2.368772	0.144639	2.973176
51	6	0	-2.477487	-0.174737	4.313877
52	6	0	-3.420672	-1.125035	4.689727
53	6	0	-4.218302	-1.714194	3.720726
54	7	0	-3.100782	0.477772	-2.000738
55	6	0	-2.380238	-0.147696	-2.944319
56	6	0	-2.462856	0.182329	-4.284295
57	6	0	-3.327713	1.205265	-4.658040
58	6	0	-4.075228	1.854656	-3.687619
59	6	0	-3.955028	1.479462	-2.346858
60	6	0	-4.677796	2.056117	-1.206886
61	6	0	-5.601847	3.099699	-1.273795
62	6	0	-6.256047	3.607436	-0.168625
63	6	0	-5.948453	3.022121	1.047331
64	6	0	-5.043527	1.986250	1.187100
65	6	0	-4.388376	1.484665	0.058889
66	1	0	-2.495201	-3.084941	-0.275050
67	1	0	-2.231708	3.074373	0.287203
68	1	0	-0.566884	-4.626630	-0.362854
69	1	0	-0.178841	4.444588	0.385177
70	1	0	2.001878	-1.200880	-0.069549
71	1	0	2.088699	0.815654	0.056045
72	1	0	1.234330	-5.265865	-1.735765
73	1	0	1.669806	5.145755	-0.896880
74	1	0	3.241903	-6.710254	-1.847945
75	1	0	3.772566	6.429538	-0.797864

76	1	0	5.239036	-4.191026	0.984949
77	1	0	5.561464	3.337356	1.568345
78	1	0	3.243198	-2.752290	1.122875
79	1	0	3.454090	2.041077	1.489960
80	1	0	-1.726900	-0.938803	-2.600441
81	1	0	-1.654867	0.881150	2.628316
82	1	0	-1.861969	-0.354055	-5.009013
83	1	0	-1.836090	0.314097	5.037512
84	1	0	-3.422718	1.496274	-5.698948
85	1	0	-3.538211	-1.405616	5.731204
86	1	0	-4.752131	2.649086	-3.963753
87	1	0	-4.956717	-2.451148	3.998655
88	9	0	-5.899700	3.672846	-2.466720
89	9	0	-6.188908	-3.376180	2.504355
90	1	0	-6.967967	4.418703	-0.256253
91	1	0	-7.321726	-4.030078	0.296765
92	1	0	-4.862874	1.584858	2.177843
93	1	0	-4.992723	-1.383279	-2.143608
94	1	0	6.668995	-8.427700	-1.455362
95	1	0	6.642940	8.911060	-1.256661
96	1	0	8.691225	-9.863027	-1.580142
97	1	0	8.758036	10.231498	-1.184482
98	1	0	10.712827	-9.280277	-0.267676
99	1	0	10.679315	9.398030	0.149404
100	1	0	10.717399	-7.259592	1.175186
101	1	0	10.489219	7.265080	1.399721
102	1	0	8.680023	-5.825102	1.292996
103	1	0	8.379612	5.958025	1.319050
104	9	0	-6.856929	-3.143937	-2.113722
105	9	0	-6.573295	3.495902	2.152968

C3 (HF= -7841.0615953)

Center Number	Atomic Number	Atomic Type	Coordinates (Angstroms) X	Y	Z
1	77	0	2.527844	-0.011269	-0.020678
2	35	0	6.395406	3.740289	-2.462108
3	35	0	6.624406	-3.505846	2.428680
4	7	0	0.856197	-1.397741	0.069064
5	7	0	0.767455	1.262492	-0.109076
6	7	0	-5.983733	-6.431296	0.152410
7	7	0	-6.484481	5.683941	-0.027593
8	7	0	-6.958741	-6.141782	-0.567086
9	7	0	-6.518225	6.772989	0.576669
10	7	0	2.625362	0.378528	2.011210
11	7	0	2.655876	-0.391731	-2.051806
12	6	0	0.971516	-2.730011	0.128263
13	1	0	1.981570	-3.119810	0.170062
14	6	0	0.793952	2.599786	-0.160024
15	1	0	1.775220	3.055685	-0.218254
16	6	0	-0.122791	-3.576141	0.132462
17	1	0	0.038214	-4.647293	0.162766
18	6	0	-0.353961	3.371779	-0.150453
19	1	0	-0.264931	4.449654	-0.216888
20	6	0	-1.408980	-3.036053	0.067529
21	6	0	-1.601101	2.747665	-0.078186
22	6	0	-1.516120	-1.645001	0.004024
23	1	0	-2.496139	-1.188928	-0.032580
24	6	0	-1.615755	1.351993	-0.024202
25	1	0	-2.561964	0.834814	0.062716
26	6	0	-0.377081	-0.849793	0.009261
27	6	0	-0.426671	0.633880	-0.044782
28	6	0	-2.611921	-3.899801	0.069486
29	6	0	-2.859095	3.528412	-0.054178
30	6	0	-2.648893	-5.059322	0.849859
31	1	0	-1.802683	-5.323152	1.475820
32	6	0	-2.919895	4.755827	0.623441
33	1	0	-2.046217	5.126718	1.149896
34	6	0	-3.778925	-5.866784	0.855702
35	1	0	-3.817801	-6.761928	1.467878
36	6	0	-4.091662	5.493424	0.658168
37	1	0	-4.134808	6.434873	1.192323
38	6	0	-4.884744	-5.533138	0.074893
39	6	0	-5.231336	5.013247	0.004036
40	6	0	-4.858606	-4.377326	-0.712878
41	1	0	-5.716278	-4.123712	-1.324269
42	6	0	-5.181233	3.796896	-0.675449
43	1	0	-6.071153	3.441528	-1.184701
44	6	0	-3.732249	-3.570855	-0.708918
45	1	0	-3.714003	-2.686556	-1.338262
46	6	0	-4.005137	3.058158	-0.702436
47	1	0	-3.976964	2.123153	-1.252487
48	6	0	1.908375	-0.264774	2.946733
49	1	0	1.244037	-1.041485	2.590668
50	6	0	1.902417	0.206330	-2.988647
51	1	0	1.187810	0.937641	-2.633597
52	6	0	2.009238	0.032766	4.293110
53	1	0	1.411418	-0.515791	5.011284
54	6	0	2.028145	-0.080063	-4.335358
55	1	0	1.398977	0.430682	-5.054647
56	6	0	2.887551	1.039520	4.686178
57	1	0	2.994184	1.302055	5.733495
58	6	0	2.972138	-1.025919	-4.727382
59	1	0	3.100374	-1.277487	-5.774970
60	6	0	3.629008	1.703320	3.722537
61	1	0	4.318989	2.486570	4.010851
62	6	0	3.751537	-1.642613	-3.762342
63	1	0	4.493273	-2.377419	-4.049790
64	6	0	3.489851	1.360554	2.377104
65	6	0	3.584339	-1.313987	-2.416579
66	6	0	4.218359	1.972325	1.259307
67	6	0	4.347334	-1.879175	-1.297264
68	6	0	5.142603	3.008275	1.419567
69	1	0	5.366037	3.413509	2.401201
70	6	0	5.337075	-2.852985	-1.455849
71	1	0	5.588343	-3.242331	-2.437206
72	6	0	5.796707	3.542108	0.317608
73	1	0	6.514130	4.345912	0.433502
74	6	0	6.021623	-3.344181	-0.352558
75	1	0	6.790078	-4.099544	-0.467113
76	6	0	5.504718	3.019038	-0.937521
77	6	0	5.693015	-2.842273	0.902172
78	6	0	4.589791	1.989895	-1.116214
79	1	0	4.401296	1.619140	-2.117420
80	6	0	4.712688	-1.874910	1.079291
81	1	0	4.498108	-1.518004	2.080279
82	6	0	3.920494	1.442513	-0.015985
83	6	0	4.012244	-1.371128	-0.022337
84	6	0	-8.061501	-7.034331	-0.493320

85	6	0	-7.766640	7.450088	0.554403
86	6	0	-8.107818	-8.166952	0.328723
87	1	0	-7.261544	-8.404639	0.962425
88	6	0	-7.792224	8.676548	1.219694
89	1	0	-6.885190	9.031020	1.699256
90	6	0	-9.239969	-8.969473	0.319438
91	1	0	-9.281338	-9.848675	0.955179
92	6	0	-8.966493	9.422861	1.260729
93	1	0	-8.984445	10.376635	1.778540
94	6	0	-10.325450	-8.652464	-0.502262
95	1	0	-11.206887	-9.286417	-0.502761
96	6	0	-10.114521	8.941469	0.636959
97	1	0	-11.032770	9.520030	0.667182
98	6	0	-10.276869	-7.525500	-1.318580
99	1	0	-11.118064	-7.276528	-1.957754
100	6	0	-10.087222	7.712619	-0.028734
101	1	0	-10.984423	7.340153	-0.513690
102	6	0	-9.144644	-6.715700	-1.313468
103	1	0	-9.084370	-5.831971	-1.940956
104	6	0	-8.919621	6.963778	-0.073997
105	1	0	-8.889002	6.009801	-0.587026

A4 (HF= -4698.8768485)

Center Number	Atomic Number	Atomic Type	Coordinates (Angstroms) X	Y	Z
1	77	0	2.563727	-0.446593	0.060923
2	6	0	2.243186	-0.353017	-2.961840
3	6	0	2.789967	-2.442047	-2.063186
4	6	0	2.225983	-0.850555	-4.251352
5	1	0	2.039852	0.690722	-2.759470
6	6	0	2.784126	-2.996929	-3.344551
7	6	0	2.501677	-2.202545	-4.443243
8	1	0	2.001947	-0.190013	-5.080609
9	1	0	3.003702	-4.049088	-3.476346
10	1	0	2.498048	-2.631132	-5.440056
11	6	0	4.525136	0.009637	0.052870
12	6	0	5.028948	0.471765	1.289808
13	6	0	5.422240	-0.045027	-1.021420
14	6	0	6.364091	0.866596	1.434672
15	6	0	6.751755	0.346999	-0.879781
16	1	0	5.083965	-0.397832	-1.991514
17	6	0	7.228357	0.805313	0.349648
18	1	0	8.264062	1.111617	0.459595
19	6	0	0.449082	1.687355	-0.342175
20	6	0	2.558133	2.637393	-0.529480
21	6	0	-0.153284	2.926208	-0.539140
22	6	0	2.033362	3.902656	-0.736521
23	1	0	3.629057	2.472813	-0.516087
24	6	0	0.653011	4.036676	-0.738271
25	1	0	-1.228559	3.034782	-0.534153
26	1	0	2.691157	4.748941	-0.888510
27	6	0	-0.245041	-1.828035	0.325192
28	6	0	-0.330232	0.442213	-0.120485
29	6	0	-1.624840	-1.933086	0.308091
30	1	0	0.381971	-2.690372	0.519026
31	6	0	-1.718330	0.404139	-0.155784
32	6	0	-2.397984	-0.796808	0.062245
33	1	0	-2.282742	1.300147	-0.377038
34	6	0	1.827292	0.086930	2.962505
35	6	0	4.055437	0.507313	2.387696
36	6	0	2.038050	0.461815	4.276169
37	1	0	0.855415	-0.247554	2.622600
38	6	0	4.322708	0.898767	3.701207
39	6	0	3.313998	0.877552	4.649953
40	1	0	1.218674	0.426309	4.984379
41	1	0	5.321026	1.215757	3.976284
42	1	0	3.519333	1.179810	5.671661
43	6	0	3.051382	-2.377867	0.354859
44	6	0	3.329339	-3.026371	1.564914
45	6	0	3.081056	-3.164140	-0.819069
46	6	0	3.613731	-4.389616	1.610739
47	1	0	3.324246	-2.464514	2.494732
48	6	0	3.366484	-4.533892	-0.775627
49	6	0	3.633273	-5.149670	0.439980
50	1	0	3.854878	-6.211826	0.476169
51	7	0	1.792607	1.556625	-0.339848
52	7	0	2.516268	-1.121981	-1.895309
53	7	0	2.804079	0.107579	2.041040
54	7	0	-8.084000	-1.141176	-0.068654
55	7	0	-8.750352	-0.197227	0.397382
56	6	0	-10.160968	-0.354769	0.341197
57	6	0	-10.902138	0.712408	0.850444
58	6	0	-10.810762	-1.481967	-0.176388
59	6	0	-12.293143	0.660577	0.844321
60	1	0	-10.374841	1.574400	1.246995
61	6	0	-12.197796	-1.527455	-0.178868
62	1	0	-10.225500	-2.305588	-0.567951
63	6	0	-12.941787	-0.458988	0.329850
64	1	0	-12.867966	1.491713	1.240481
65	1	0	-12.706762	-2.399340	-0.578393
66	1	0	-14.026585	-0.503753	0.323807
67	1	0	-2.083386	-2.894582	0.506708
68	1	0	6.738384	1.224189	2.389009
69	1	0	7.423031	0.294544	-1.733015
70	1	0	3.823537	-4.864434	2.565676
71	1	0	3.382472	-5.128071	-1.684217
72	7	0	0.395210	-0.671442	0.119050
73	6	0	-3.877225	-0.858095	0.033596
74	6	0	-4.646133	0.201085	0.539608
75	6	0	-4.531690	-1.975854	-0.492970
76	6	0	-6.030141	0.147070	0.525926
77	1	0	-4.155822	1.066948	0.973202
78	6	0	-5.919351	-2.032056	-0.515009
79	1	0	-3.958638	-2.797988	-0.909240
80	6	0	-6.673452	-0.976146	-0.004694
81	1	0	-6.617959	0.962890	0.929028
82	1	0	-6.432868	-2.892972	-0.930555
83	35	0	-0.132625	5.729181	-1.007220

B4 (HF= -5095.77266)

Center Number	Atomic Number	Atomic Type	Coordinates (Angstroms) X	Y	Z

1	6	0	10.470346	-0.381795	0.444719
2	6	0	11.132047	-0.962915	-0.641727
3	6	0	12.521197	-0.990295	-0.655497
4	6	0	13.250829	-0.447562	0.405030
5	6	0	12.587603	0.131951	1.485546
6	6	0	11.196279	0.174833	1.500793
7	7	0	9.056129	-0.279749	0.542994
8	7	0	8.410524	-1.007492	-0.235394
9	6	0	6.997970	-0.864628	-0.161161
10	6	0	6.252084	-1.906375	-0.709994
11	6	0	4.864311	-1.867797	-0.669215
12	6	0	4.200856	-0.772697	-0.103194
13	6	0	4.966868	0.283301	0.419767
14	6	0	6.351432	0.242308	0.398417
15	6	0	2.722622	-0.716678	-0.070187
16	6	0	1.939327	-1.867806	0.055808
17	6	0	0.560758	-1.758442	0.074899
18	7	0	-0.080359	-0.588852	-0.027341
19	6	0	0.654851	0.539237	-0.155514
20	6	0	2.039524	0.500673	-0.173735
21	77	0	-2.220107	-0.316795	0.062251
22	6	0	-4.150510	0.224048	0.260694
23	6	0	-4.524074	0.558882	1.585850
24	6	0	-5.784582	1.124103	1.804347
25	6	0	-6.694739	1.374572	0.800026
26	6	0	-6.298685	1.010572	-0.475634
27	6	0	-5.074138	0.446358	-0.768730
28	6	0	-0.115359	1.806879	-0.255040
29	7	0	-1.450033	1.707102	-0.084038
30	6	0	-2.196079	2.818439	-0.131911
31	6	0	-1.666555	4.074389	-0.372888
32	6	0	-0.297679	4.170111	-0.585880
33	6	0	0.492276	3.033274	-0.516693
34	6	0	-3.507784	0.311061	2.620239
35	7	0	-2.323907	-0.133266	2.121630
36	6	0	-1.315539	-0.427296	2.955570
37	6	0	-1.416970	-0.299123	4.327857
38	6	0	-2.622418	0.149531	4.859585
39	6	0	-3.672711	0.450029	4.003154
40	35	0	0.484747	5.839315	-0.968031
41	7	0	-2.324879	-0.620330	-1.987567
42	6	0	-2.167679	0.352941	-2.902069
43	6	0	-2.220359	0.113278	-4.262317
44	6	0	-2.437395	-1.195903	-4.692233
45	6	0	-2.619602	-2.199391	-3.752148
46	6	0	-2.580272	-1.896000	-2.387649
47	6	0	-2.796550	-2.830625	-1.272537
48	6	0	-3.067243	-4.194906	-1.392502
49	6	0	-3.237670	-5.039449	-0.314441
50	6	0	-3.115811	-4.456612	0.935032
51	6	0	-2.858723	-3.116804	1.137231
52	6	0	-2.696654	-2.272581	0.030820
53	1	0	-0.060194	-2.640273	0.182667
54	1	0	2.384689	-2.851423	0.162778
55	1	0	2.600003	1.421641	-0.281020
56	1	0	-1.992026	1.350154	-2.517690
57	1	0	-2.098352	0.933400	-4.961255
58	1	0	-2.467341	-1.431754	-5.751981
59	1	0	-2.795367	-3.217322	-4.067939
60	9	0	-3.182980	-4.768176	-2.610569
61	1	0	-3.462785	-6.092558	-0.444240
62	9	0	-3.265900	-5.255644	2.016499
63	1	0	-2.792331	-2.744724	2.154634
64	1	0	-0.402904	-0.782114	2.493034
65	1	0	-0.570613	-0.549089	4.959002
66	1	0	-2.745047	0.257660	5.932569
67	1	0	-4.621540	0.784862	4.398270
68	9	0	-6.170706	1.465875	3.053814
69	1	0	-7.657298	1.835113	0.998702
70	9	0	-7.170521	1.232018	-1.481544
71	1	0	-4.846670	0.178869	-1.796478
72	1	0	-3.259755	2.686570	0.025250
73	1	0	-2.310887	4.945812	-0.397379
74	1	0	1.561126	3.103307	-0.669290
75	1	0	4.300295	-2.684950	-1.106890
76	1	0	6.767540	-2.746136	-1.166087
77	1	0	6.935498	1.060917	0.804246
78	1	0	10.558673	-1.380672	-1.462664
79	1	0	13.152325	0.557460	2.309823
80	1	0	10.659821	0.628715	2.328636
81	1	0	4.473395	1.141392	0.866887
82	1	0	13.040466	-1.435421	-1.500349
83	1	0	14.337624	-0.471372	0.383841

C4 (HF= -9840.6990776)

Center Number	Atomic Number	Atomic Type	Coordinates (Angstroms) X	Y	Z
1	6	0	-10.930095	-0.602282	0.075892
2	6	0	-11.515931	-1.464238	1.011048
3	6	0	-12.899006	-1.555157	1.080309
4	6	0	-13.701976	-0.794819	0.225204
5	6	0	-13.116817	0.061786	-0.703543
6	6	0	-11.730204	0.158756	-0.777441
7	7	0	-9.530046	-0.425516	-0.085663
8	7	0	-8.809765	-1.120753	0.656052
9	6	0	-7.410516	-0.931793	0.490356
10	6	0	-6.594984	-1.752695	1.268222
11	6	0	-5.212480	-1.652437	1.179280
12	6	0	-4.625314	-0.719998	0.318632
13	6	0	-5.455641	0.105533	-0.454868
14	6	0	-6.834696	0.003088	-0.376466
15	6	0	-3.152261	-0.605339	0.224503
16	6	0	-2.323458	-1.725684	0.309256
17	6	0	-0.951627	-1.567627	0.218880
18	7	0	-0.371005	-0.374487	0.045204
19	6	0	-1.151463	0.724610	-0.041196
20	6	0	-2.534106	0.635035	0.048165
21	77	0	1.776773	-0.034816	-0.018128
22	6	0	3.711448	0.493977	-0.192304
23	6	0	4.183431	0.581846	-1.520917
24	6	0	5.497690	0.964605	-1.802168
25	6	0	6.376518	1.268024	-0.771256
26	6	0	5.911454	1.181671	0.536465
27	6	0	4.609498	0.802092	0.835429
28	6	0	-0.438048	2.013451	-0.228070
29	7	0	0.910724	1.954515	-0.211257
30	6	0	1.619486	3.078376	-0.370191

31	6	0	1.029141	4.318162	-0.552002
32	6	0	-0.356306	4.377682	-0.574518
33	6	0	-1.103908	3.220911	-0.412633
34	6	0	3.199342	0.250135	-2.558427
35	7	0	1.971332	-0.080077	-2.080094
36	6	0	0.987870	-0.410905	-2.932542
37	6	0	1.169682	-0.431475	-4.302888
38	6	0	2.421333	-0.093376	-4.811107
39	6	0	3.437190	0.247989	-3.933281
40	35	0	-1.227696	6.029348	-0.827093
41	7	0	1.779552	-0.101430	2.051689
42	6	0	1.458527	0.930313	2.849031
43	6	0	1.476983	0.835615	4.228151
44	6	0	1.840592	-0.378758	4.804780
45	6	0	2.170698	-1.444581	3.983854
46	6	0	2.137191	-1.293109	2.597201
47	6	0	2.467749	-2.332591	1.615349
48	6	0	2.847662	-3.630369	1.968155
49	6	0	3.144174	-4.566118	0.986624
50	6	0	3.050158	-4.175345	-0.344727
51	6	0	2.676099	-2.890204	-0.714387
52	6	0	2.373028	-1.935808	0.262914
53	1	0	-0.283791	-2.419039	0.276210
54	1	0	-2.733178	-2.722007	0.425476
55	1	0	-3.140365	1.529926	0.009637
56	1	0	1.186017	1.853043	2.353109
57	1	0	1.212248	1.696872	4.829985
58	1	0	1.867377	-0.492244	5.883445
59	1	0	2.456908	-2.395552	4.415461
60	1	0	2.918375	-3.930834	3.008589
61	1	0	3.439121	-5.574389	1.252137
62	35	0	3.450791	-5.449925	-1.705547
63	1	0	2.622010	-2.639195	-1.767562
64	1	0	0.035297	-0.669535	-2.488521
65	1	0	0.345951	-0.707449	-4.950473
66	1	0	2.603231	-0.097977	-5.880693
67	1	0	4.417172	0.511093	-4.311539
68	1	0	5.855545	1.032584	-2.824421
69	1	0	7.397014	1.565578	-0.981754
70	35	0	7.104918	1.596393	1.964822
71	1	0	4.300738	0.749425	1.873270
72	1	0	2.697627	2.973452	-0.346597
73	1	0	1.642445	5.201792	-0.674270
74	1	0	-2.183428	3.267808	-0.437941
75	1	0	-4.591369	-2.287181	1.802860
76	1	0	-7.057024	-2.465650	1.943311
77	1	0	-7.470319	0.636599	-0.983266
78	1	0	-10.885183	-2.049212	1.669964
79	1	0	-13.737542	0.653761	-1.368689
80	1	0	-11.251391	0.820306	-1.492586
81	1	0	-5.017599	0.820132	-1.144582
82	1	0	-13.358879	-2.221381	1.803850
83	1	0	-14.783139	-0.872880	0.286980

GAUSSIAN 09 (FULL REFERENCE): Gaussian 09, Revision D.01, Frisch, M. J.; Trucks, G. W.; Schlegel, H. B.; Scuseria, G. E.; Robb, M. A.; Cheeseman, J. R.; Scalmani, G.; Barone, V.; Mennucci, B.; Petersson, G. A.; Nakatsuji, H.; Caricato M.; Li, X.; Hratchian, H. P.; Izmaylov, A. F.; Bloino, J.; Zheng, G.; Sonnenberg, J. L.; Hada, M.; Ehara, M.; Toyota, K.; Fukuda, R.; Hasegawa, J.; Ishida, M.; Nakajima, T.; Honda, Y.; Kitao, O.; Nakai, H.; Vreven, T.; Montgomery, J. A.; Peralta, J. E., Jr.; Ogliaro, F.; Bearpark, M.; Heyd, J. J.; Brothers, E.; Kudin, K. N.; Staroverov, V. N.; Keith, T.; Kobayashi, R.; Normand, J.; Raghavachari, K.; Rendell, A.; Burant, J. C.; Iyengar, S. S.; Tomasi, J.; Cossi, M.; Rega, N.; Millam, J. M.; Klene, M.; Knox, J. E.; Cross, J. B.; Bakken, V.; Adamo, C.; Jaramillo, J.; Gomperts, R.; Stratmann, R. E.; Yazyev, O.; Austin, A. J.; Cammi, R.; Pomelli, C.; Ochterski, J. W.; Martin, R. L.; Morokuma, K.; Zakrzewski, V. G.; Voth, G. A.; Salvador, P.; Dannenberg, J. J.; Dapprich, S.; Daniels, A. D.; Farkas, O.; Foresman, J. B.; Ortiz, J. V.; Cioslowski, J.; Fox, D. J., Gaussian, Inc., Wallingford CT, **2013**.

Compound [Ru(p-Cym)(4,4'-dinitro-2,2'-bipyridine)(Cl)]Cl. Synthesis and characterization.

SYNTHESIS

Under a N_2 atmosphere, $Ru_2(p\text{-}Cym)_2Cl_4$ (0.1 g, 0.16 mmol) and 4,4'-dinitro-2,2'-bipyridine (0.08 g, 0.326 mmol) were dissolved in 10 mL of CH_2Cl_2. The reaction mixture was refluxed for 15 h. It was cooled to room temperature and the brown solid was filtered. Yield 63%.

Elemental Analysis: calculated for ($C_{20}H_{20}Cl_2N_4O_4Ru{\cdot}2CH_2Cl_2$): C, 36.59; H, 3.35; N, 7.76. Found: C, 36.39; H, 3.19; N, 8.24.

Exact Mass: ESI-MS $[C_{20}H_{20}ClN_4O_4Ru]^+$: calculated: m/z= 517.0217, found: m/z= 517.0228.

^{1}H NMR (300 MHz, THF-d_8): δ 9.20 (d, J = 2.3 Hz, 2H, (bipy)), 9.11 (d, J = 4.8 Hz, 2H, (bipy)), 8.25 (dd, J = 2.2 Hz, J = 5.3 Hz, 2H, (bipy)), 7.11 (s, 2H, (p-Cym)), 7.10 (s, 2H, (p-Cym)), 2.87 (m, 1H, (11)), 2.31 (s, 3H, (13)), 1.25 (d, J = 6.9 Hz, 6H, (12)).

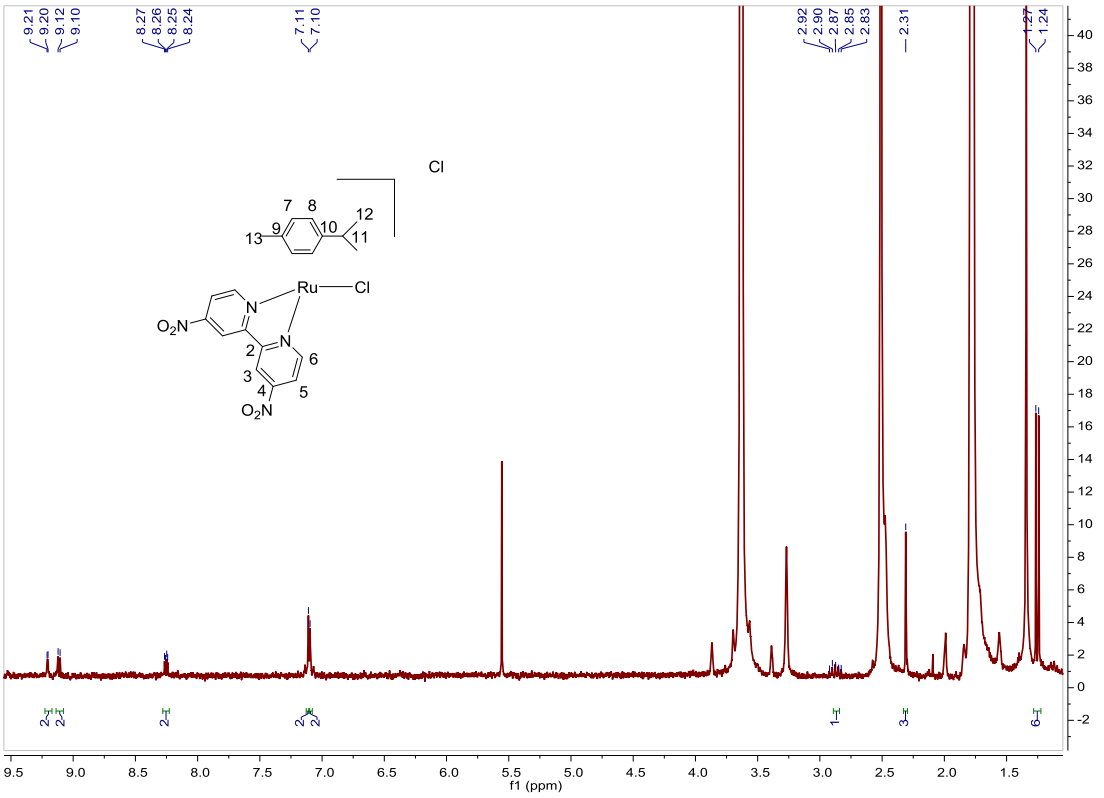

Fig. S312. ^{1}H NMR spectrum of **[Ru(p-Cym)(4,4'-dinitro-2,2'-bipyridine)(Cl)]Cl** in THF-d_8, 300 MHz.

Compound [Ru(p-Cym)(4,4'-bis(diethylphosphonate)-2,2'-bipyridine)(Cl)]Cl. Synthesis and characterization.

SYNTHESIS

Under a N_2 atmosphere, $Ru_2(p\text{-}Cym)_2Cl_4$ (0.043 g, 0.070 mmol) and 4,4'-bis(diethylphosphonate)-2,2'-bipyridine (0.060 g, 0.140 mmol) were dissolved in 4 mL of CH_2Cl_2. The reaction mixture was refluxed for 15 h. It was cooled to room temperature, the solvent was evaporated and the desired compound was obtained as a dark green solid. Yield 92%.

Elemental Analysis: calculated for ($C_{28}H_{40}Cl_2N_2O_6P_2Ru \cdot CH_2Cl_2$): C, 42.50; H, 5.17; N, 3.42. Found: C, 42.31; H, 5.46; N, 3.25.

Exact Mass: ESI-MS $[C_{28}H_{40}ClN_2O_6P_2Ru]^+$: calculated: m/z= 699.1094, found: m/z= 699.1103.

^{1}H NMR (300 MHz, $CDCl_3$): δ 10.33 (brdd, J = 4.1 Hz, J = 5.2 Hz, 2H, (6)), 8.46 (d, J = 13.4 Hz, 2H, (3)), 8.09 (ddd, J = 0.9 Hz, J = 5.5 Hz, J = 12.3 Hz, 2H, (5)), 6.56 (d, J = 6.1 Hz, 2H, (8)), 6.40 (d, J = 6.1 Hz, 2H, (7)), 4.36–4.12 (m, 8H, (14)), 2.77 (sep, J = 6.9 Hz, 1H, (11)), 2.33 (s, 3H, (13)), 1.39 (brdd, J = 7.2 Hz, J = 14.7 Hz, 12H, (15)), 1.06 (d, J = 6.9 Hz, 6H, (12)).

^{13}C NMR (75 MHz, $CDCl_3$): δ 157.46 (d, J = 12.7 Hz, 2CH, (6)), 153.39 (d, J = 13.5 Hz, $2C_{quat}$, (bipy)), 141.05 (d, J = 187.5 Hz, $2C_{quat}$, (bipy)), 129.10 (d, J = 7.5 Hz, 2CH, (5)), 124.23 (d, J = 10.5 Hz, 2CH, (3)), 105.57 (s, C_{quat}, (p-Cym)), 105.09 (s, C_{quat}, (p-Cym)), 87.64 (s, 2CH, (8)), 84.74 (s, 2CH, (7)), 63.27 (s, $4CH_2$, (14)), 30.68 (s, CH, (11)), 21.78 (s, $2CH_3$, (12)), 18.69 (s, CH_3, (13)), 15.96 (s, $4CH_3$, (15)).

^{31}P NMR (162 MHz, $CDCl_3$): δ 11.26 (s, 2P).

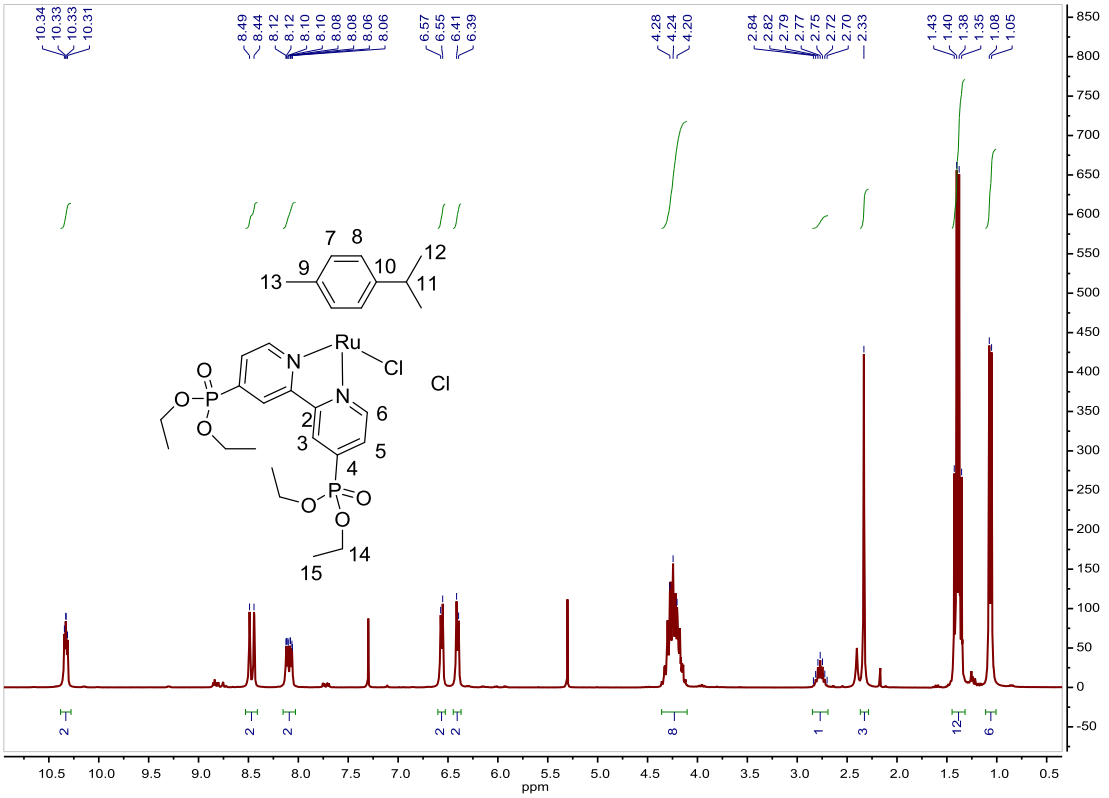

Fig. S313. ^{1}H NMR spectrum of **[Ru(p-Cym)(4,4'-bis(diethylphosphonate)-2,2'-bipyridine)(Cl)]Cl** in $CDCl_3$, 300 MHz.

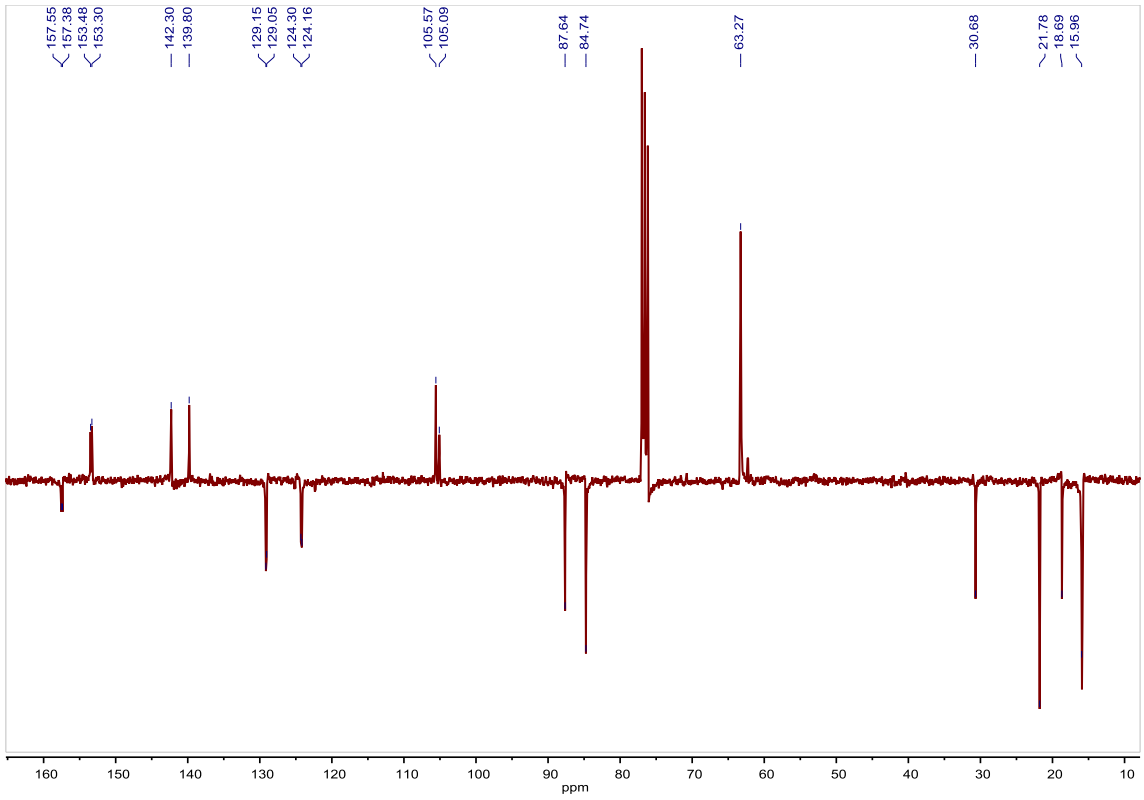

Fig. S314. ^{13}C NMR spectrum of **[Ru(p-Cym)(4,4'-bis(diethylphosphonate)-2,2'-bipyridine)(Cl)]Cl** in $CDCl_3$, 75 MHz.

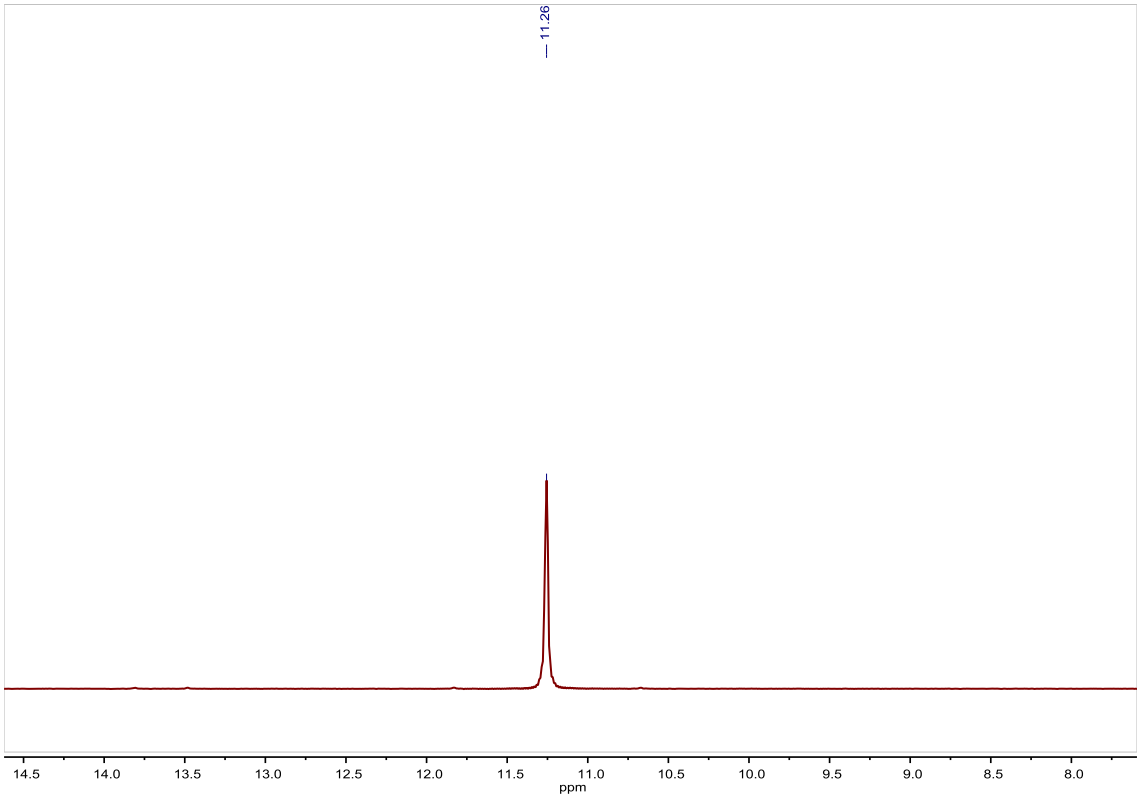

Fig. S315. ^{31}P NMR spectrum of **[Ru(p-Cym)(4,4'-bis(diethylphosphonate)-2,2'-bipyridine)(Cl)]Cl** in $CDCl_3$, 162 MHz.

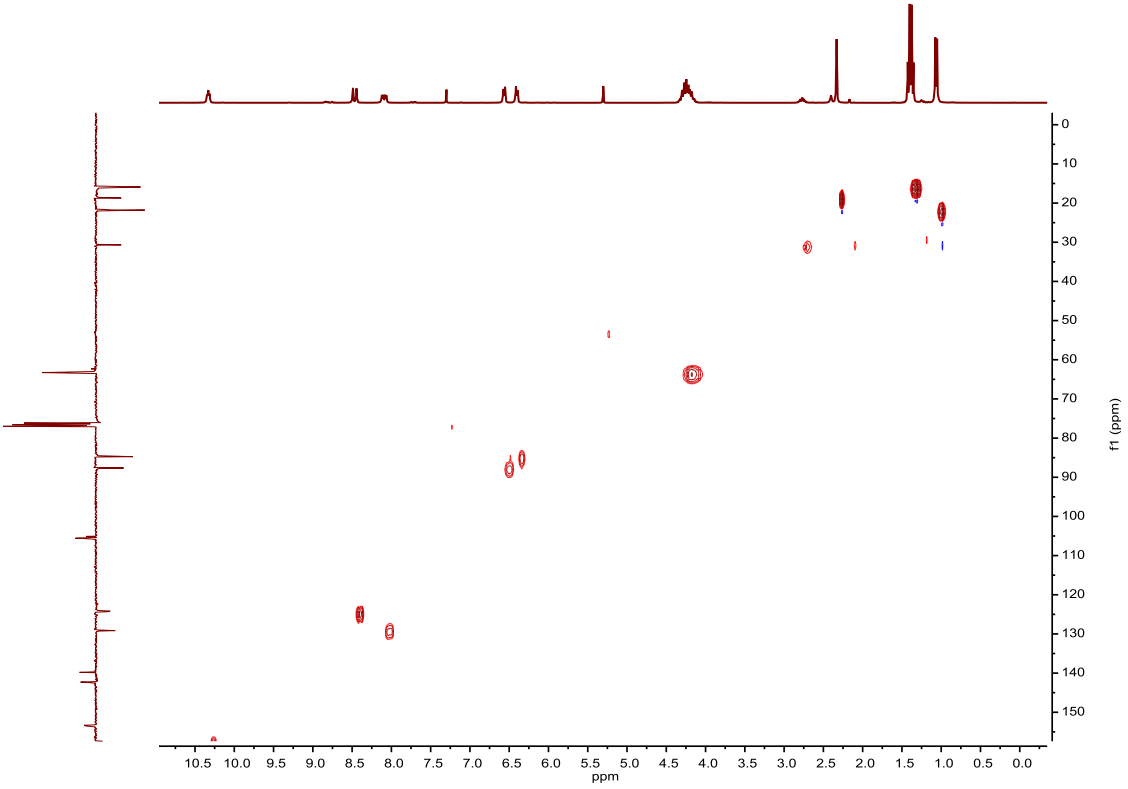

Fig. S316. HSQC NMR spectrum of **[Ru(p-Cym)(4,4'-bis(diethylphosphonate)-2,2'-bipyridine)(Cl)]Cl** in $CDCl_3$.

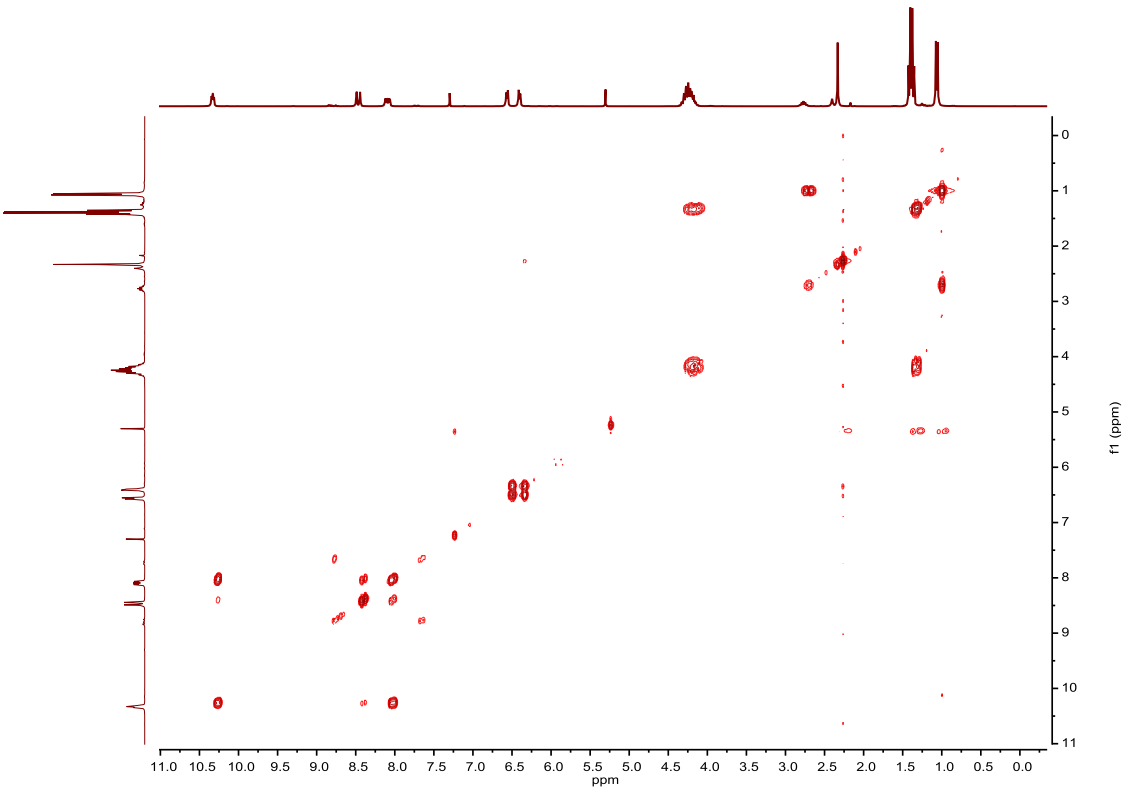

Fig. S317. COSY NMR spectrum of **[Ru(p-Cym)(4,4'-bis(diethylphosphonate)-2,2'-bipyridine)(Cl)]Cl** in $CDCl_3$.

Compound [Ru(p-Cym)(4,4'-dicarboxy-2,2'-bipyridine)(Cl)]Cl. Synthesis and characterization.

SYNTHESIS

Under a N_2 atmosphere, $[Ru(p\text{-}Cym)Cl_2]_2$ (0.188 g, 0.31 mmol) and 4,4'-dicarboxy-2,2'-bipyridine (0.15 g, 0.61 mmol) were dissolved in 10 mL of ethanol. The reaction mixture was refluxed for 15 h. It was cooled to room temperature and the orange solid that precipitated was filtered off. Yield 71%. The spectroscopic data are coincident with those described in the literature.[39]

^{1}H NMR (300 MHz, MeOD): δ 9.73 (d, J = 5.1 Hz, 2H, (6)), 9.00 (s, 2H, (3)), 8.25 (d, J = 4.6 Hz, 2H, (5)), 6.25 (d, J = 5.7 Hz, 2H, (8)), 6.01 (d, J = 5.8 Hz, 2H, (7)), 2.72 (sep, J = 6.8 Hz, 1H, (11)), 2.30 (s, 3H, (13)), 1.10 (d, J = 6.8 Hz, 6H, (12)).

^{13}C APT NMR (75 MHz, MeOD): δ 157.98 (2CH, (6)), 156.61 ($2C_{quat}$, (bipy)), 143.16 ($2C_{quat}$, (bipy)), 128.13 (2CH, (5)), 124.59 (2CH, (3)), 107.32 (C_{quat}, (p-Cym)), 106.17 (C_{quat}, (p-Cym)), 88.64 (2CH, (8)), 86.36 (2CH, (7)), 32.37 (CH, (11)), 22.34 ($2CH_3$, (12)), 18.97 (CH_3, (13)).

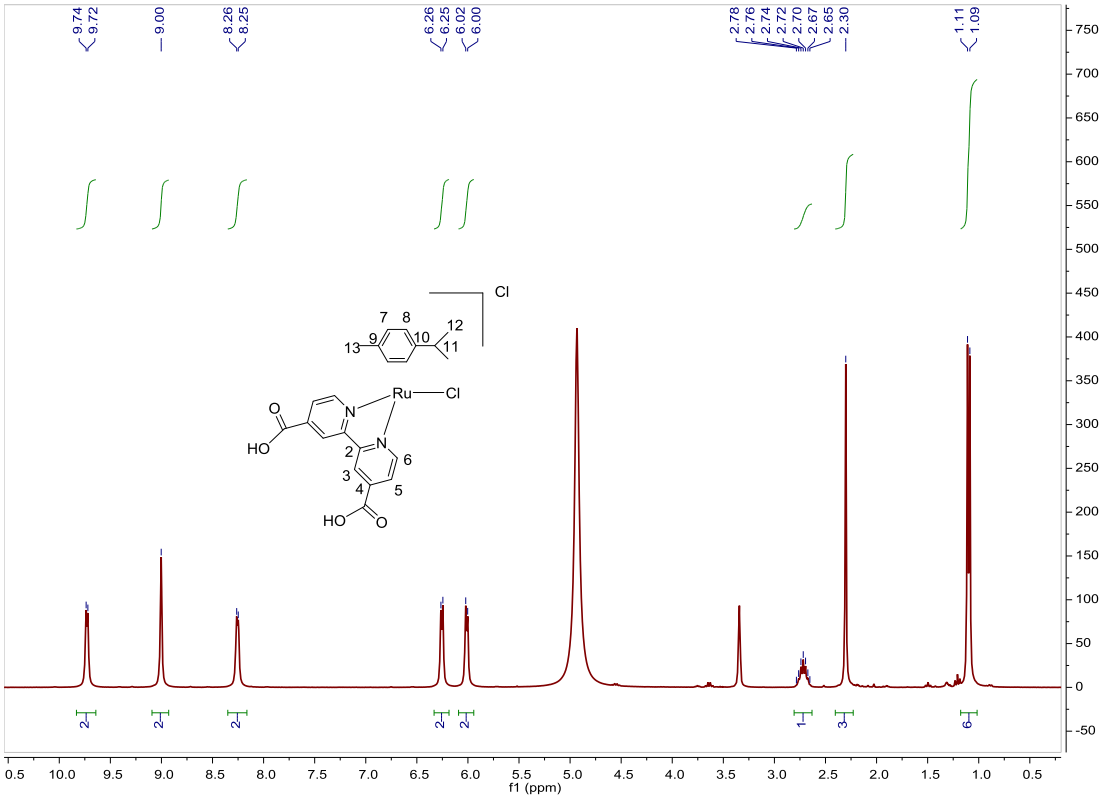

Fig. S318. ^{1}H NMR spectrum of **[Ru(p-Cym)(4,4'-dicarboxy-2,2'-bipyridine)(Cl)]Cl** in MeOD-d_4, 300 MHz.

[39] A. Kopecky, G. Liu, A. Agushi, A. G. Agrios, E. Galoppini, *Tetrahedron*, **2014**, *70*, 6271–6275.

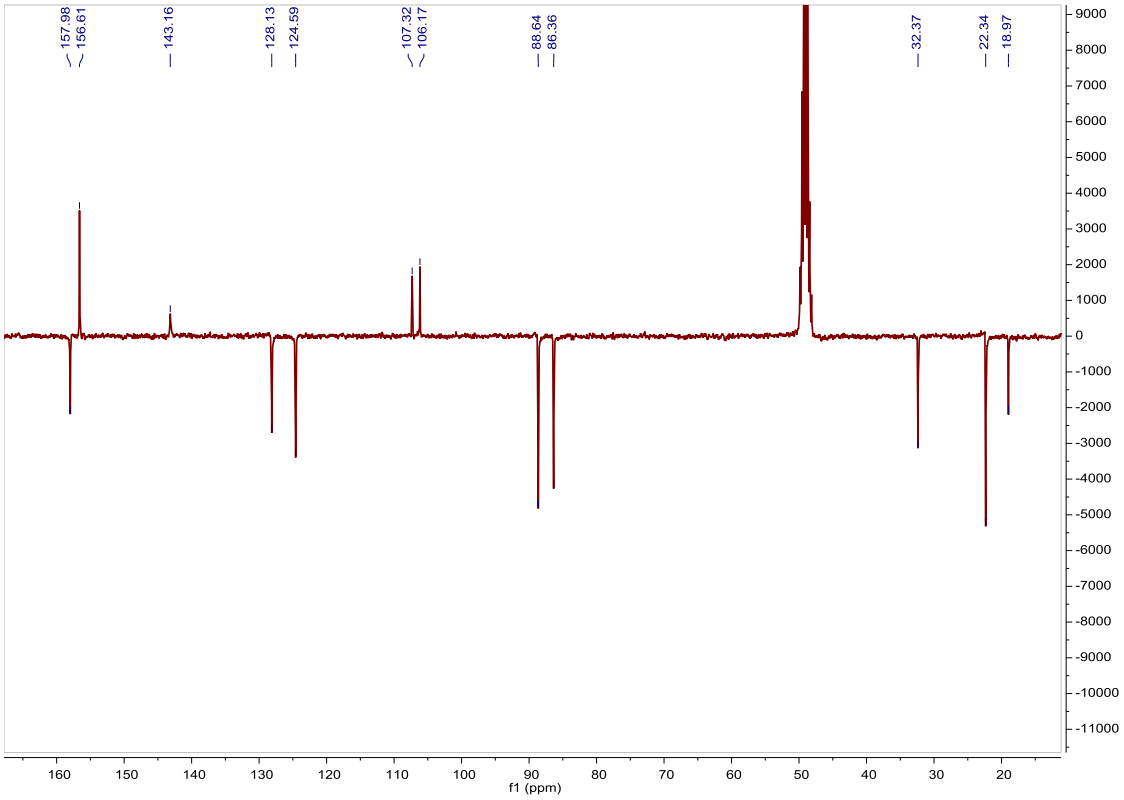

Fig. S319. ^{13}C NMR spectrum of **[Ru(p-Cym)(4,4'-dicarboxy-2,2'-bipyridine)(Cl)]Cl** in MeOD-d_4, 75 MHz.

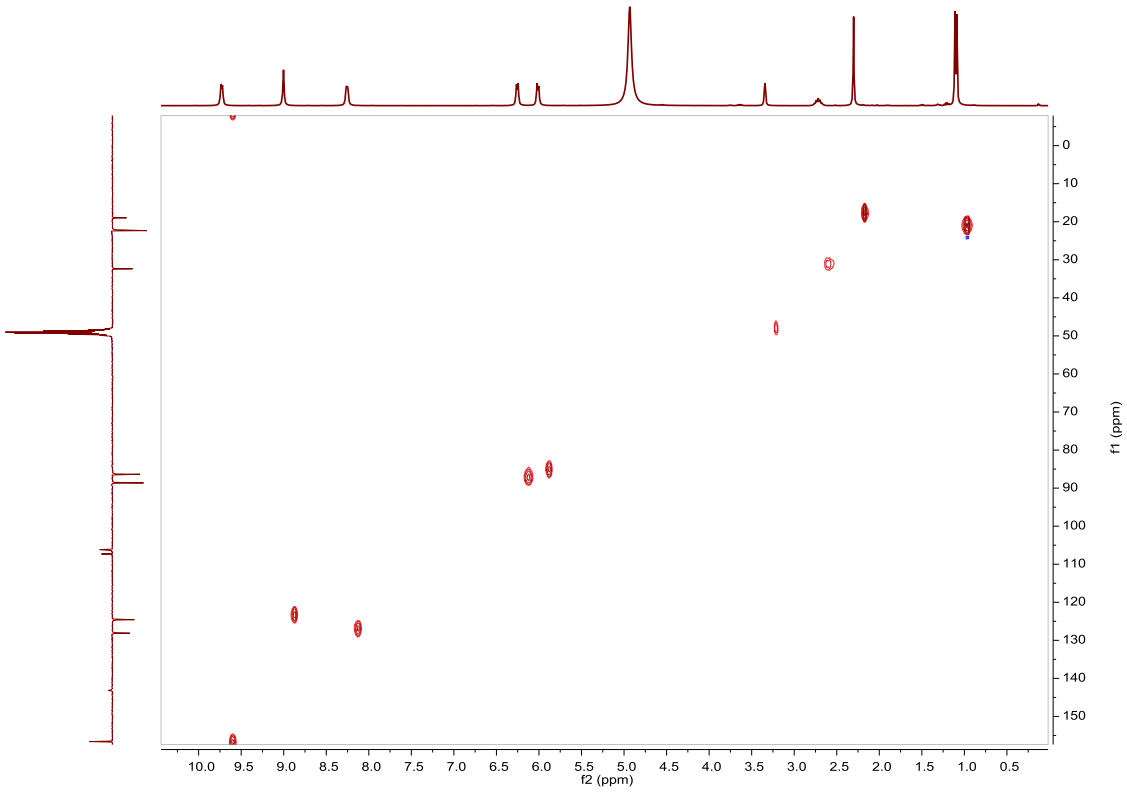

Fig. S320. HSQC NMR spectrum of **[Ru(p-Cym)(4,4'-dicarboxy-2,2'-bipyridine)(Cl)]Cl** in MeOD-d_4.

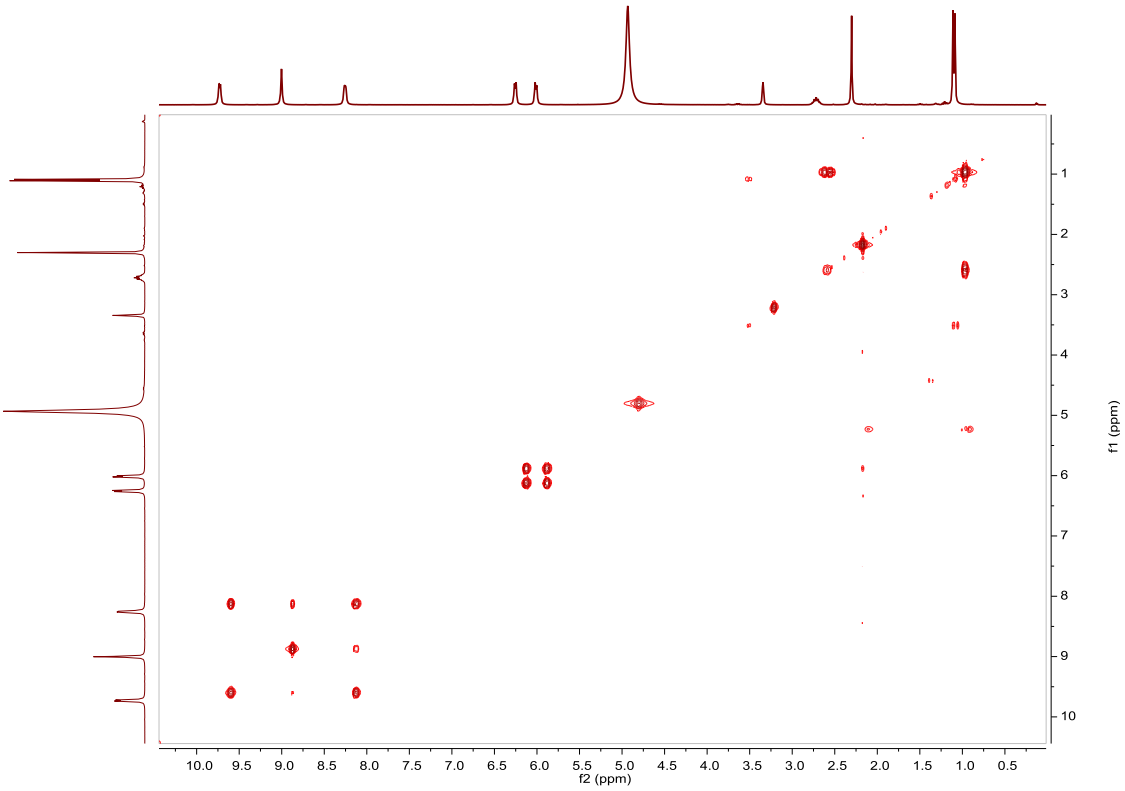

Fig. S321. COSY NMR spectrum of **[Ru(p-Cym)(4,4'-dicarboxy-2,2'-bipyridine)(Cl)]Cl** in MeOD-d_4.

Compound [Ru(p-Cym)(4,4'-bis(ethynyl)-2,2'-bipyridine)(Cl)]Cl. Synthesis and characterization.

SYNTHESIS

Under a N_2 atmosphere, $Ru_2(p\text{-}Cym)_2Cl_4$ (0.130 g, 0.214 mmol) and 4,4'-bis(ethynyl)-2,2'-bipyridine (0.087 g, 0.428 mmol) were dissolved in 10 mL of acetone. The reaction mixture was refluxed for 15 h. It was cooled to room temperature, the solvent was evaporated and the desired compound was obtained as a light brown solid. Yield 77%.

Elemental Analysis: calculated for ($C_{24}H_{22}Cl_2N_2Ru$): C, 56.48; H, 4.34; N, 5.49. Found: C, 56.44; H, 4.88; N, 5.74.

Exact Mass: ESI-MS $[C_{24}H_{22}ClN_2Ru]^+$: calculated: m/z= 475.0515, found: m/z= 475.0517.

^{1}H NMR (300 MHz, MeOD-d_4): δ 9.47 (d, J = 5.9 Hz, 2H, (6)), 8.69 (d, J = 1.8 Hz, 2H, (3)), 7.82 (dd, J = 1.7 Hz, J = 5.9 Hz, 2H, (5)), 6.16 (d, J = 6.4 Hz, 2H, (8)), 5.91 (d, J = 6.4 Hz, 2H, (7)), 4.47 (s, 2H, (15)), 2.70 (sep, J = 6.9 Hz, 1H, (11)), 2.29 (s, 3H, (13)), 1.10 (d, J = 6.9 Hz, 6H, (12)).

^{13}C NMR (75 MHz, MeOD-d_4): δ 156.79 (2CH, (6)), 156.03 ($2C_{quat}$, (bipy)), 135.84 ($2C_{quat}$, (bipy)), 130.97 (2CH, (5)), 127.64 (2CH, (3)), 106.86 (C_{quat}, (p-Cym)), 105.94 (C_{quat}, (p-Cym)), 89.63 (2CH, (15)), 88.31 (2CH, (8)), 85.92 (2CH, (7)), 80.15 (C_{quat}, (14)), 32.38 (CH, (11)), 22.32 ($2CH_3$, (12)), 18.92 (CH_3, (13)).

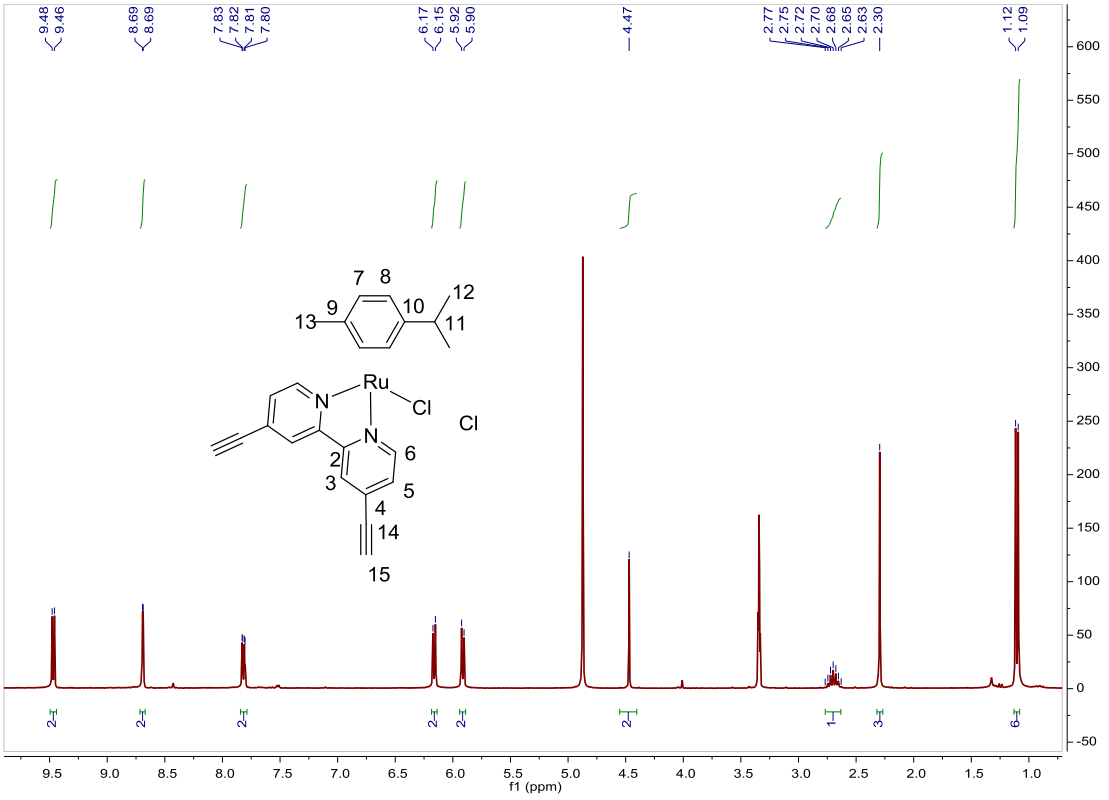

Fig. S322. ^{1}H NMR spectrum of **[Ru(p-Cym)(4,4'-bis(ethynyl)-2,2'-bipyridine)(Cl)]Cl** in MeOD-d_4, 300 MHz.

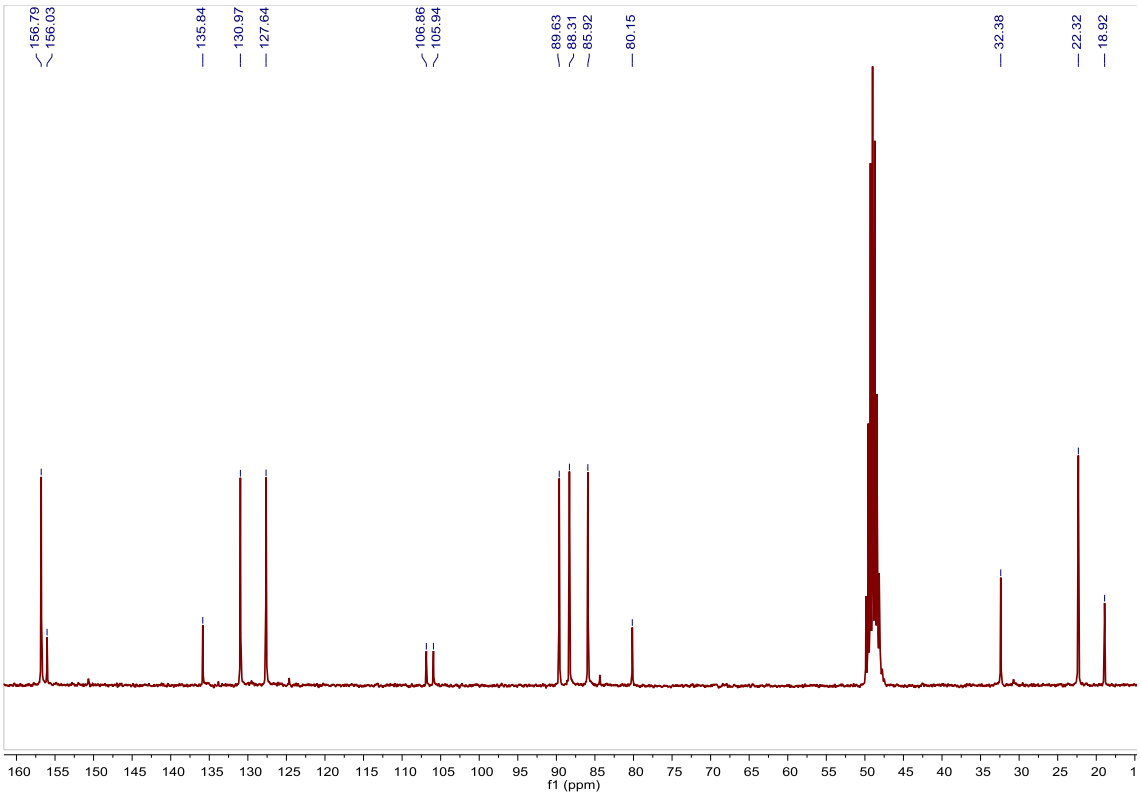

Fig. S323. ^{13}C NMR spectrum of **[Ru(p-Cym)(4,4'-bis(ethynyl)-2,2'-bipyridine)(Cl)]Cl** in MeOD-d_4, 75 MHz.

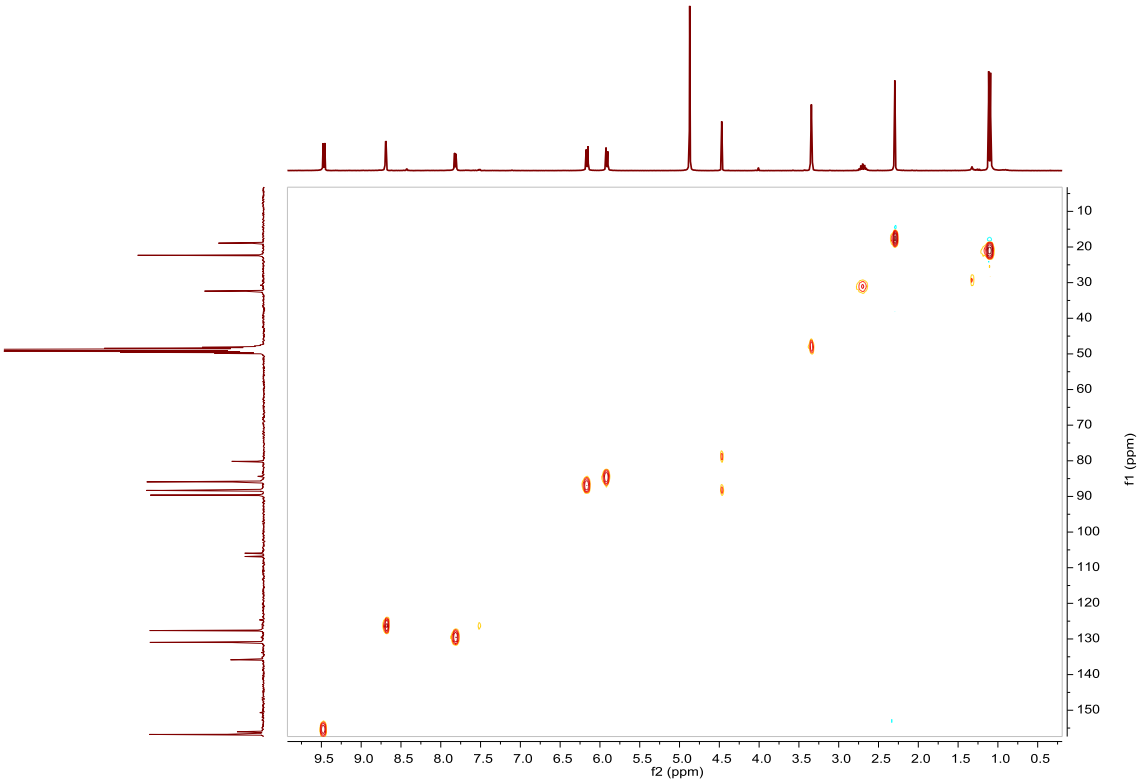

Fig. S324. HSQC NMR spectrum of **[Ru(p-Cym)(4,4'-bis(ethynyl)-2,2'-bipyridine)(Cl)]Cl** in MeOD-d_4.

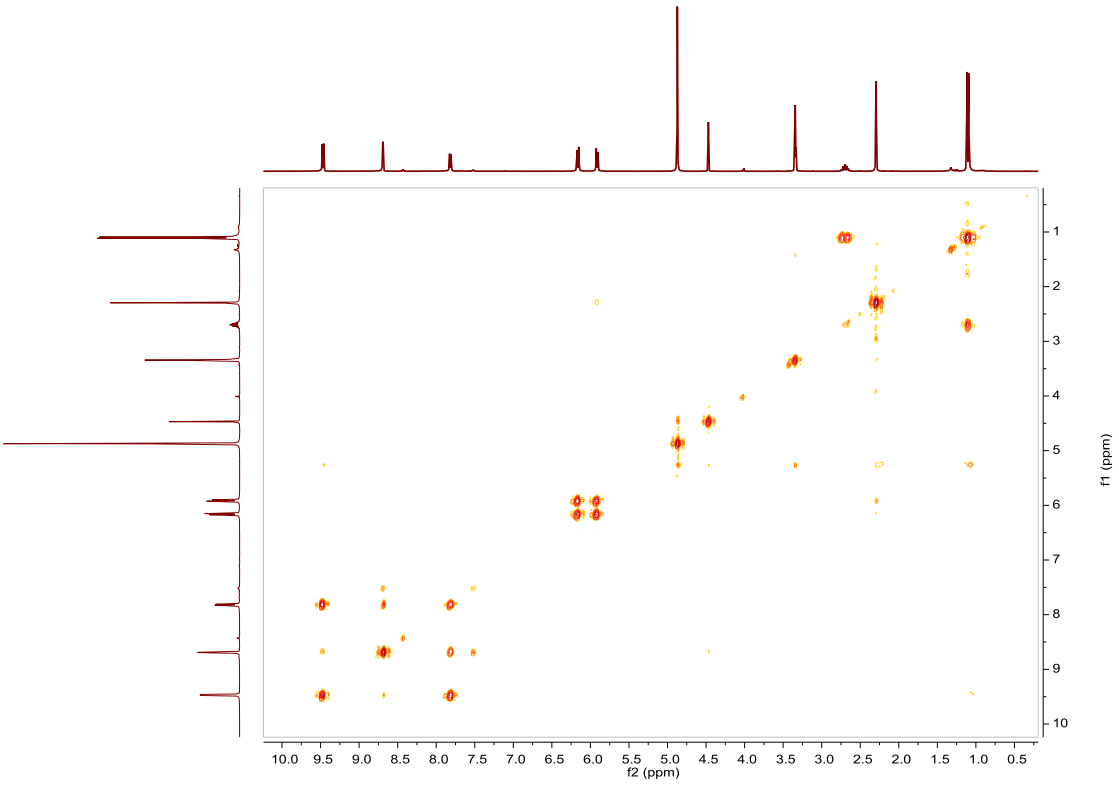

Fig. S325. COSY NMR spectrum of **[Ru(p-Cym)(4,4'-bis(ethynyl)-2,2'-bipyridine)(Cl)]Cl** in MeOD-d_4.

Compound [Ru(p-Cym)(4,4'-dibromo-2,2'-bipyridine)(Cl)]Cl. Synthesis and characterization.

SYNTHESIS

Under a N_2 atmosphere, $Ru_2(p\text{-}Cym)_2Cl_4$ (0.1 g, 0.16 mmol) and 4,4'-dibromo-2,2'-bipyridine (0.10 g, 0.32 mmol) were dissolved in 10 mL of acetone. The reaction mixture was refluxed for 15 h. It was cooled to room temperature and the yellow solid that precipitated was filtered off. Yield 85%.

Elemental Analysis: calculated for ($C_{20}H_{20}Br_2Cl_2N_2Ru$): C, 38.73; H, 3.25; N, 4.52. Found: C, 38.25; H, 3.41; N, 4.52.

Exact Mass: ESI-MS $[C_{20}H_{20}Br_2ClN_2Ru]^+$: calculated: m/z= 584.8705, found: m/z= 584.8706.

^{1}H NMR (300 MHz, MeOD-d_4): δ 9.33 (d, J = 6.1 Hz, 2H, (6)), 8.91 (d, J = 2.1 Hz, 2H, (3)), 8.05 (dd, J = 2.1 Hz, J = 6.1 Hz, 2H, (5)), 6.16 (d, J = 6.4 Hz, 2H, (8)), 5.91 (d, J = 6.4 Hz, 2H, (7)), 2.72 (sep, J = 6.9 Hz, 1H, (11)), 2.29 (s, 3H, (13)), 1.12 (d, J = 6.9 Hz, 6H, (12)).

^{13}C APT NMR (75 MHz, MeOD-d_4): δ 157.14 (2CH, (6)), 156.19 ($2C_{quat}$, (bipy)), 138.12 ($2C_{quat}$, (bipy)), 132.52 (2CH, (5)), 129.08 (2CH, (3)), 106.95 (C_{quat}, (p-Cym)), 105.70 (C_{quat}, (p-Cym)), 88.02 (2CH, (8)), 85.72 (2CH, (7)), 32.39 (CH, (11)), 22.36 ($2CH_3$, (12)), 18.91 (CH_3, (13)).

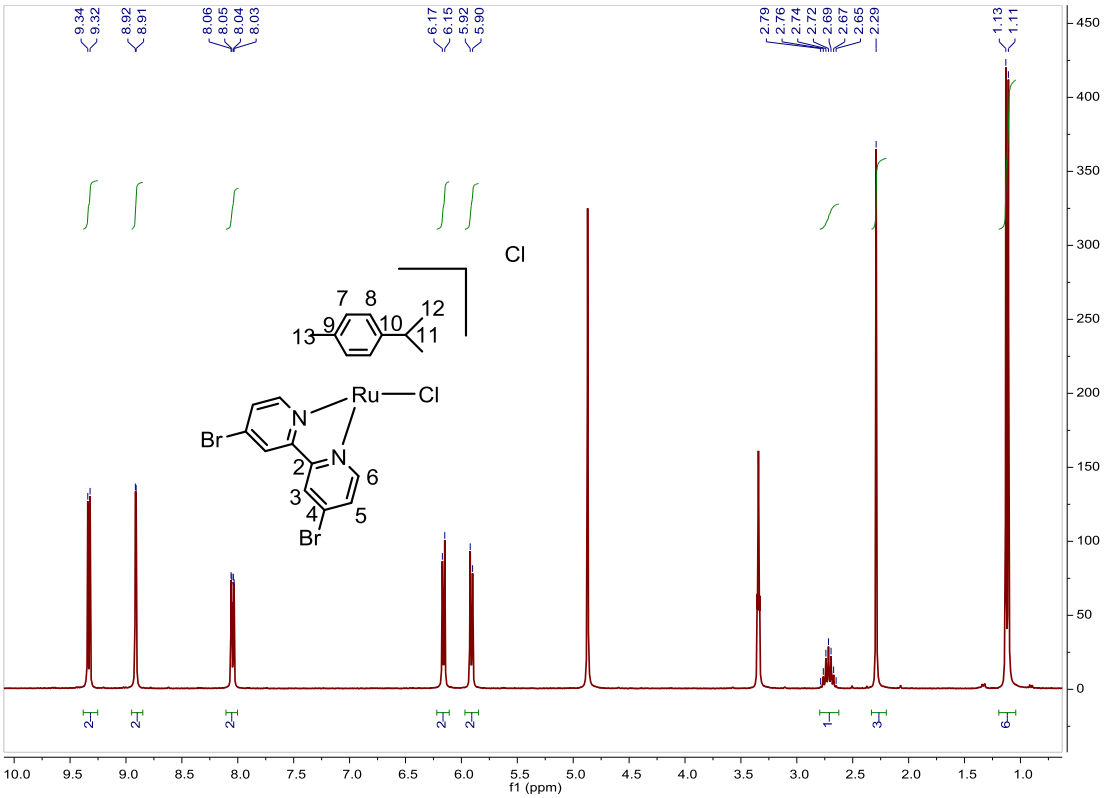

Fig. S326. ^{1}H NMR spectrum of **[Ru(p-Cym)(4,4'-dibromo-2,2'-bipyridine)(Cl)]Cl** in MeOD-d_4, 300 MHz.

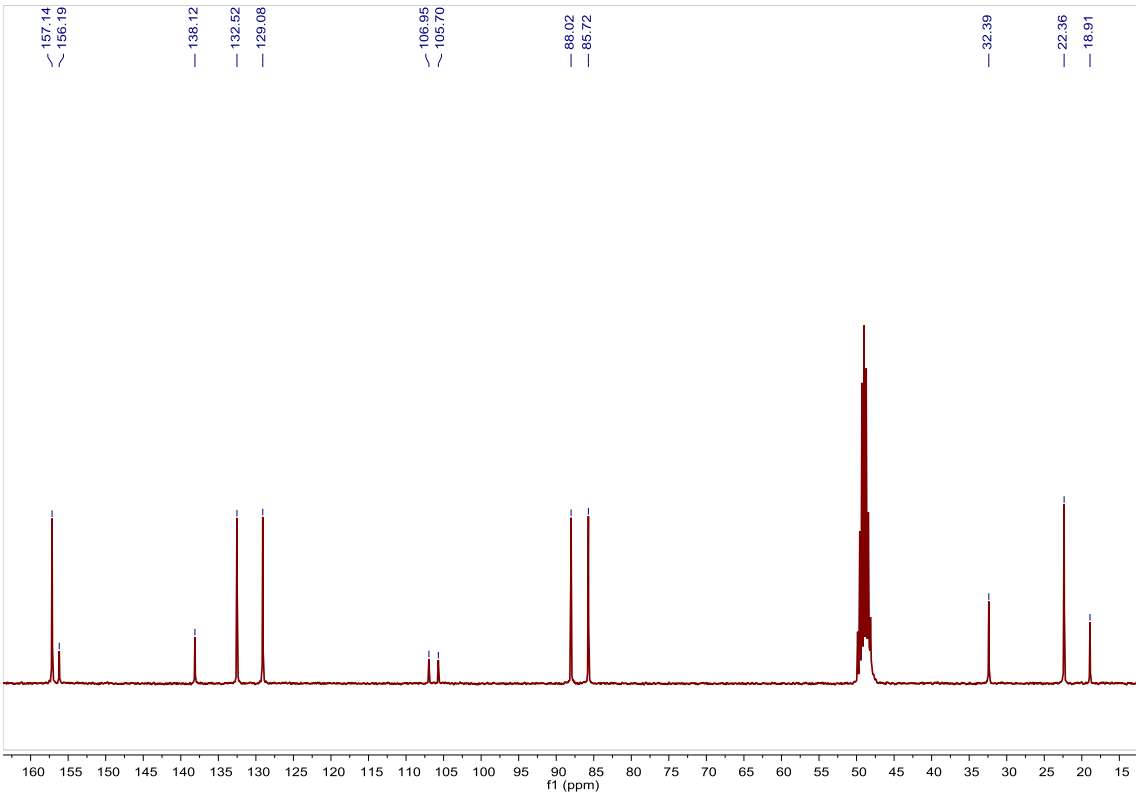

Fig. S327. ^{13}C NMR spectrum of **[Ru(p-Cym)(4,4'-dibromo-2,2'-bipyridine)(Cl)]Cl** in MeOD-d_4, 75 MHz.

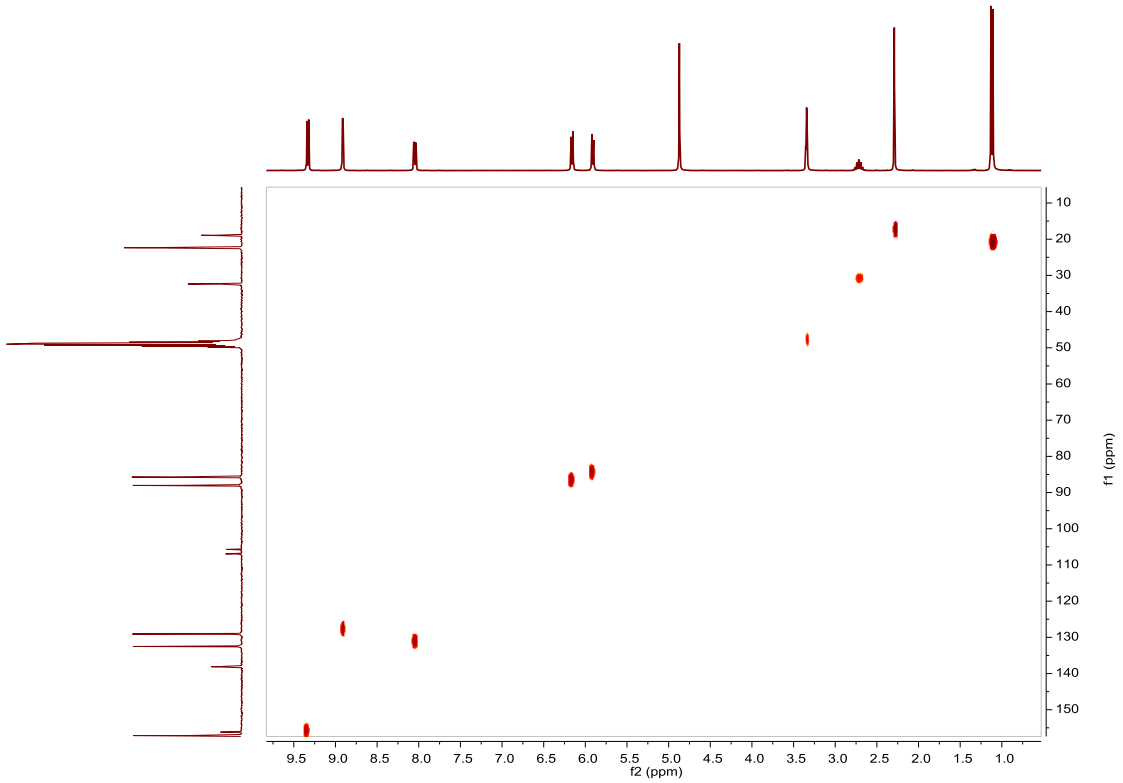

Fig. S328. HSQC NMR spectrum of **[Ru(p-Cym)(4,4'-dibromo-2,2'-bipyridine)(Cl)]Cl** in MeOD-d_4.

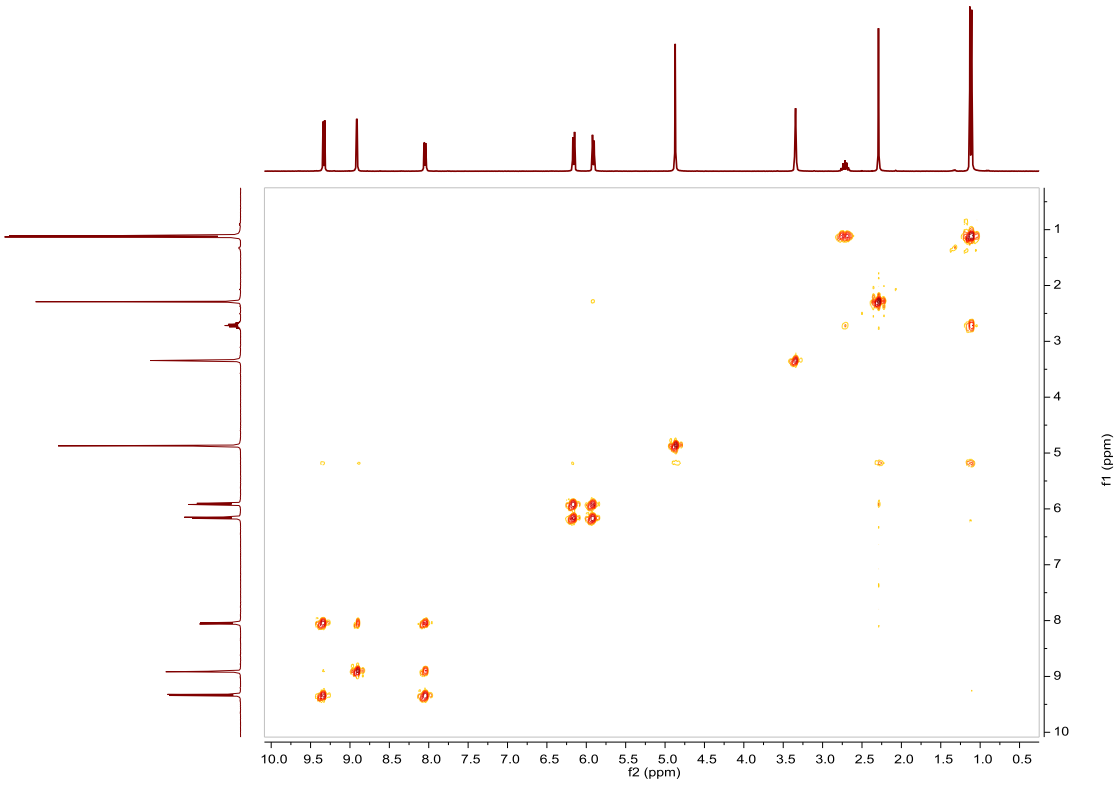

Fig. S329. COSY NMR spectrum of **[Ru(p-Cym)(4,4'-dibromo-2,2'-bipyridine)(Cl)]Cl** in MeOD-d_4.

Compound [Ru(p-Cym)(2,2'-bipyridine)(Cl)]Cl. Synthesis and characterization.

SYNTHESIS

Under a N_2 atmosphere, $Ru_2(p\text{-}Cym)_2Cl_4$ (0.350 g, 0.57 mmol) and 2,2'-bipyridine (0.178 g, 1.14 mmol) were dissolved in 20 mL of acetone. The reaction mixture was refluxed for 15 h. It was cooled to room temperature and the yellow solid that precipitated was filtered off. Yield 93%. The spectroscopic data are coincident with those described in the literature.[40]

^{1}H NMR (300 MHz, MeOD-d_4): δ 9.51 (d, J = 5.0 Hz, 2H), 8.54 (d, J = 8.1 Hz, 2H), 8.27 (ddd, J = 1.4 Hz, J = 7.9 Hz, J = 9.2 Hz, 2H), 7.80 (ddd, J = 1.3 Hz, J = 5.7 Hz, J = 7.3 Hz, 2H), 6.15 (d, J = 6.3 Hz, 2H, (p-Cym)), 5.90 (d, J = 6.3 Hz, 2H, (p-Cym)), 2.67 (sep, J = 6.9 Hz, 1H, (11)), 2.31 (s, 3H, (13)), 1.07 (d, J = 6.9 Hz, 6H, (12)).

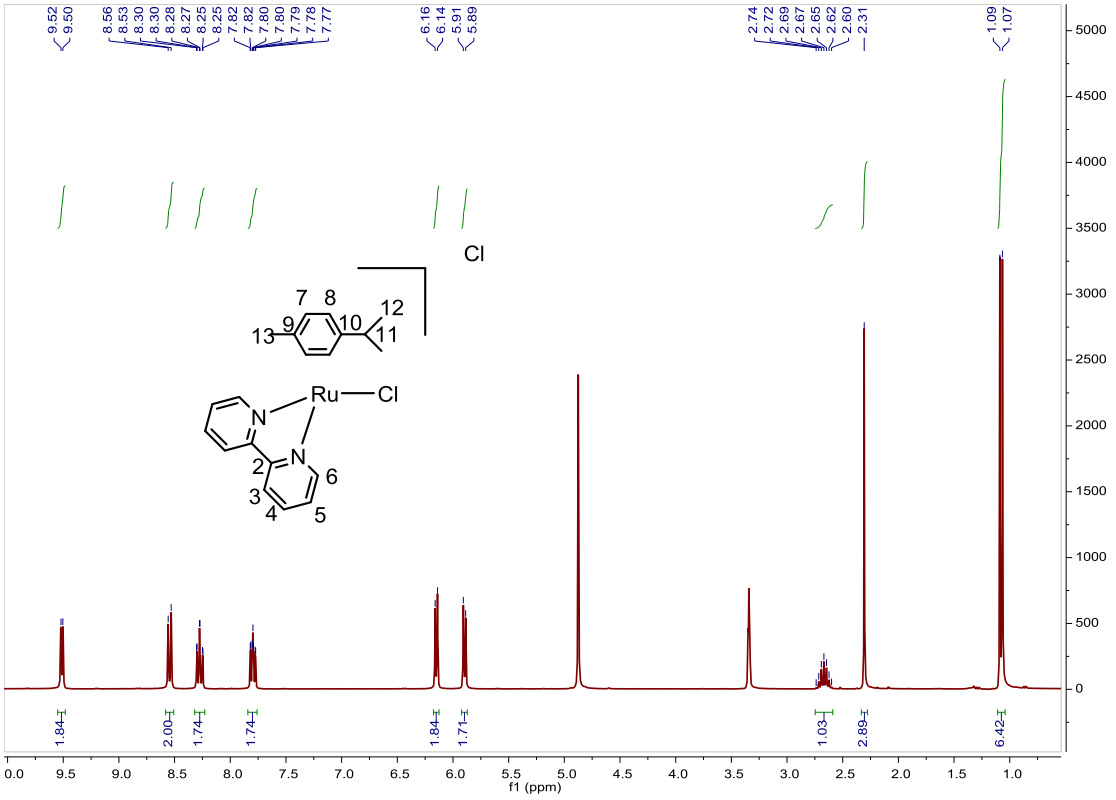

Fig. S330. ^{1}H NMR spectrum of **[Ru(p-Cym)(2,2'-bipyridine)(Cl)]Cl** in MeOD-d_4, 300 MHz.

[40] R. R. Dykeman, K. L. Luska, M. E. Thibault, M. D. Jones, M. Schlaf, M. Khanfar, N. J. Taylor, J. F. Britten and L. Harrington, *J. Mol. Catal. A: Chemical*, **2007**, *277*, 233–251.

Compound [Ru(p-Cym)(4,4'-dimethyl-2,2'-bipyridine)Cl]Cl. Synthesis and characterization.

SYNTHESIS

Under a N_2 atmosphere, $[Ru(p\text{-}Cym)Cl_2]_2$ (0.1 g, 0.16 mmol) and 4,4'-dimethyl-2,2'-bipyridine (0.06 g, 0.326 mmol) were dissolved in 10 mL of acetone. The reaction mixture was refluxed for 15 h. It was cooled to room temperature and the yellow solid that precipitated was filtered off. Yield 78%. The spectroscopic data are coincident with those described in the literature.[41]

^{1}H NMR (300 MHz, MeOD-*d*$_4$): δ 9.31 (d, J = 5.8 Hz, 2H, (6)), 8.39 (s, 2H, (3)), 7.71 (d, J = 5.7 Hz, 2H, (5)), 6.10 (d, J = 6.1 Hz, 2H, (8)), 5.85 (d, J = 6.3 Hz, 2H, (7)), 2.64 (s, 7H, (11+14)), 2.29 (s, 3H, (13)), 1.06 (d, J = 6.9 Hz, 6H, (12)).

^{13}C APT NMR (75 MHz, MeOD-*d*$_4$): δ 154.66 (2CH, (6)), 154.62 ($2C_{quat}$, (bipy)), 152.76 ($2C_{quat}$, (bipy)), 128.25 (2CH, (5)), 124.19 (2CH, (3)), 104.13 (C_{quat}, (p-Cym)), 104.03 (C_{quat}, (p-Cym)), 86.85 (2CH, (8)), 83.83 (2CH, (7)), 30.99 (CH, (11)), 20.95 ($2CH_3$, (12)), 19.91 ($2CH_3$, (14)), 17.85 (CH_3, (13)).

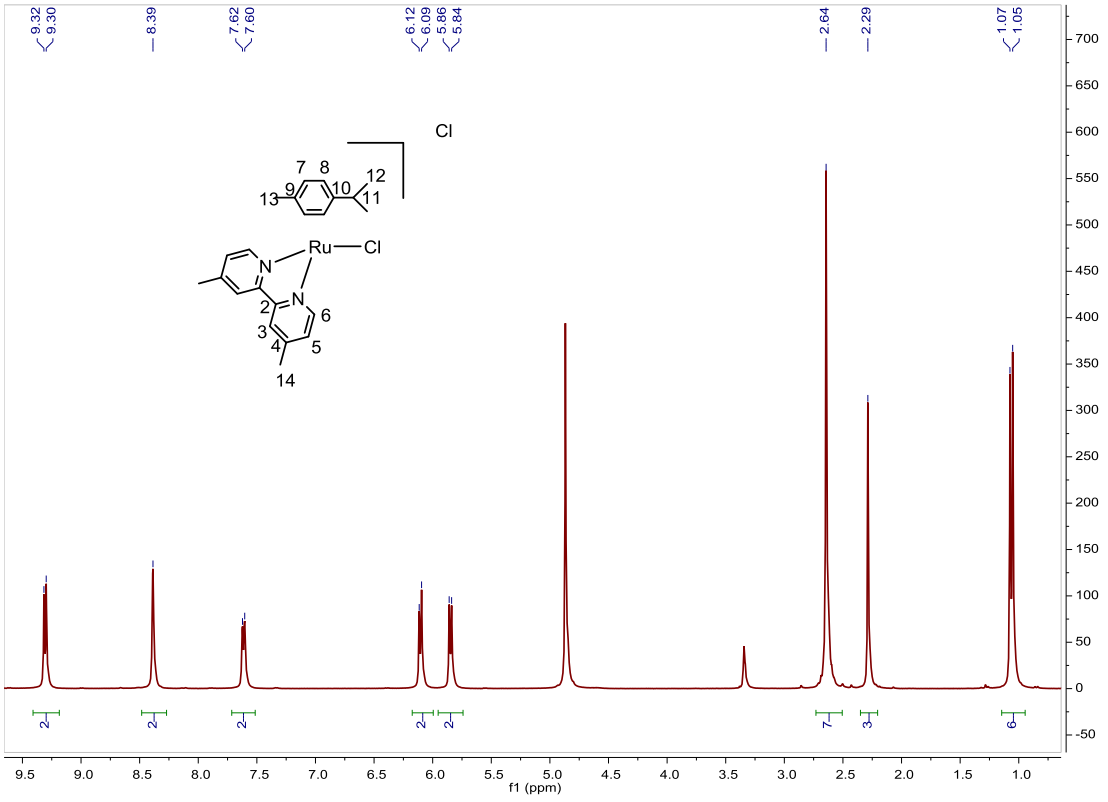

Fig S331. ^{1}H NMR spectrum of **[Ru(p-Cym)(4,4'-dimethyl-2,2'-bipyridine)Cl]Cl** in MeOD-*d*$_4$, 300 MHz.

[41] C. E. Welby, G. K. Armitage, H. Bartley, A. Wilkinson, A. Sinopoli, B. S. Uppal, C. R. Rice, P. I. P. Elliott, *Chem. Eur. J.* **2014**, *20*, 8467–8476.

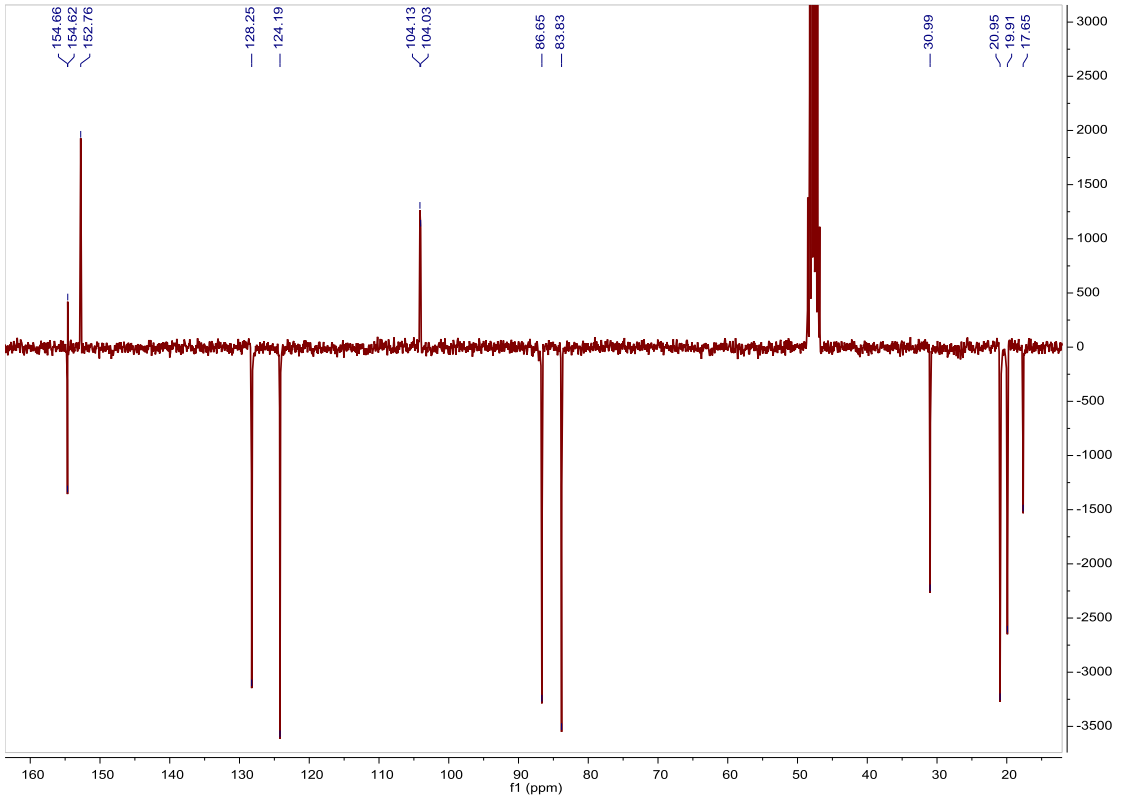

Fig S332. ^{13}C APT NMR spectrum of **[Ru(p-Cym)(4,4'-dimethyl-2,2'-bipyridine)Cl]Cl** in MeOD-d_4, 75 MHz.

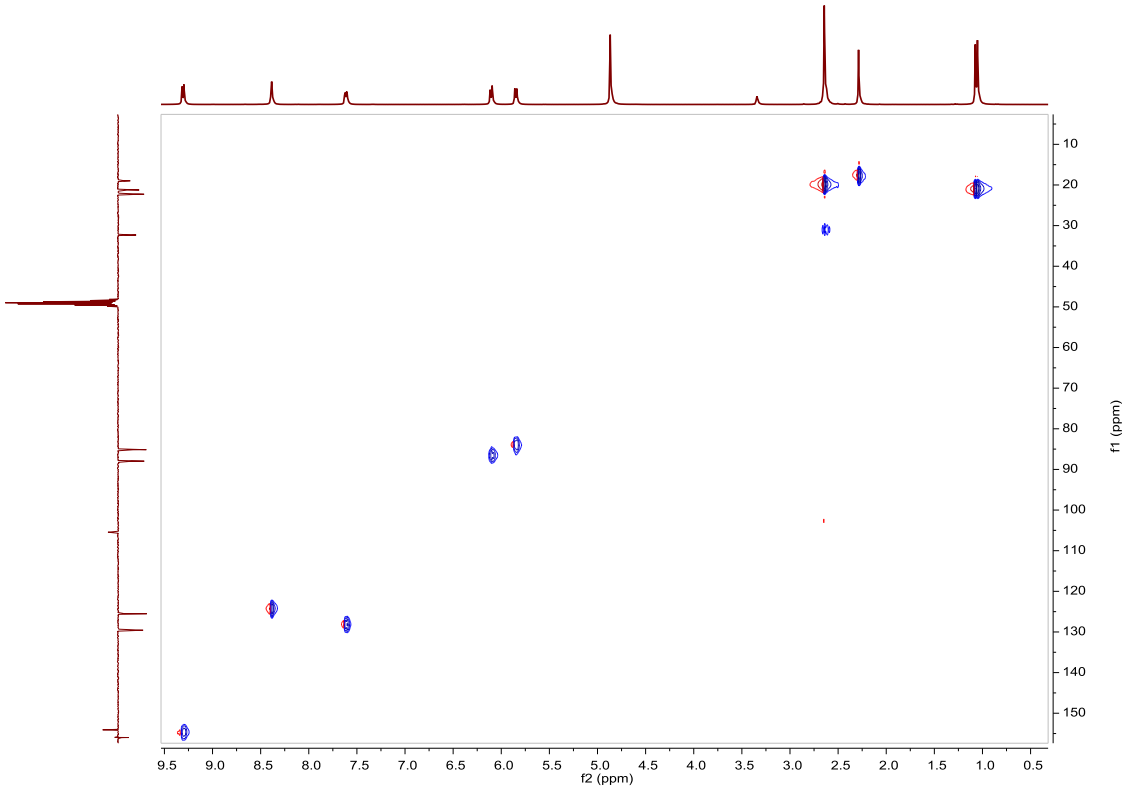

Fig S333. HSQC NMR spectrum of **[Ru(p-Cym)(4,4'-dimethyl-2,2'-bipyridine)Cl]Cl** in MeOD-d_4.

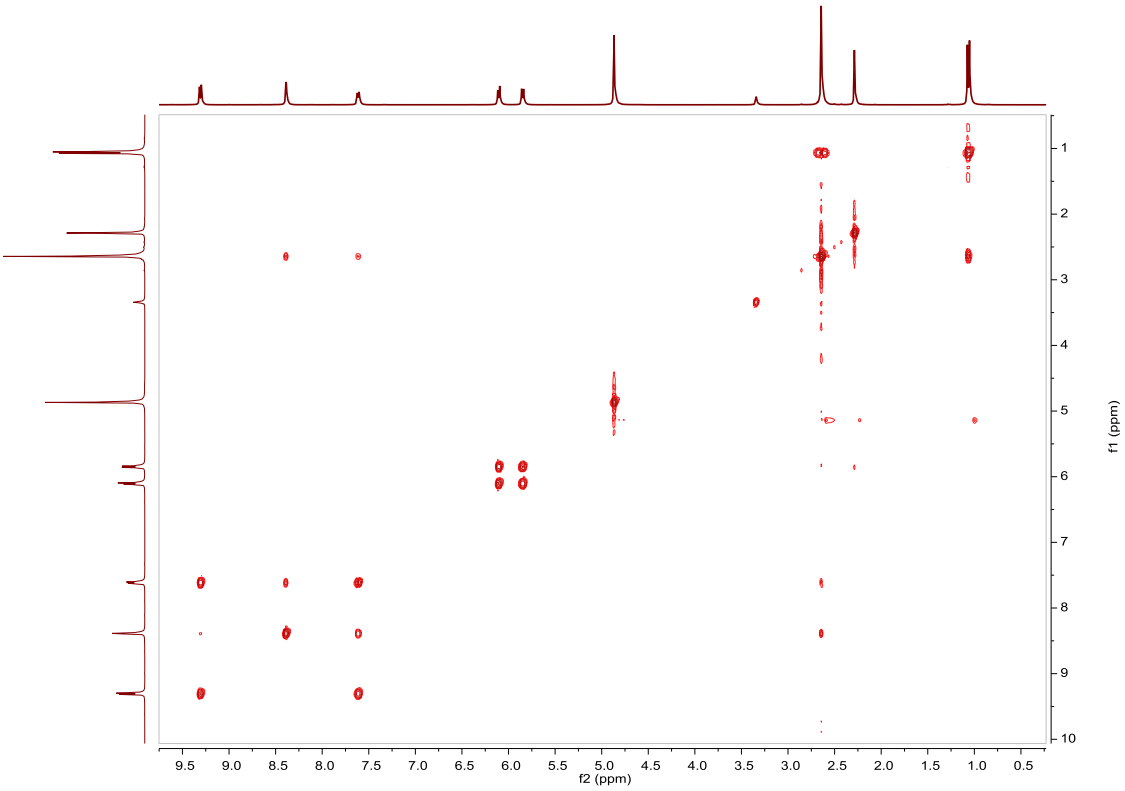

Fig S334. COSY NMR spectrum of **[Ru(p-Cym)(4,4'-dimethyl-2,2'-bipyridine)Cl]Cl** in MeOD-d_4, 300 MHz.

Compound [Ru(p-Cym)(4,4'-diazido-2,2'-bipyridine)(Cl)]Cl. Synthesis and characterization.

SYNTHESIS

Under a N_2 atmosphere, $Ru_2(p\text{-}Cym)_2Cl_4$ (0.1 g, 0.16 mmol) and 4,4'-diazido-2,2'-bipyridine (0.077 g, 0.32 mmol) were dissolved in 10 mL of acetone. The reaction mixture was refluxed for 15 h. It was cooled to room temperature and the solvent was evaporated. The product was purified by column chromatography (alumina, 100% CH_2Cl_2 to 1/100 MeOH/CH_2Cl_2). After reducing the volume of solvent of the collected fraction, the product was precipitated with ether, and obtained as a yellow solid. Yield 53%.

Elemental Analysis: calculated for ($C_{20}H_{20}Cl_2N_8Ru \cdot CH_2Cl_2$): C, 40.08; H, 3.52; N, 17.81. Found: C, 40.26; H, 3.30; N, 17.73.

Exact Mass: ESI-MS $[C_{20}H_{20}ClN_8Ru]^+$: calculated: m/z= 503.0575, found: m/z= 503.0571.

^{1}H NMR (300 MHz, MeOD-*d*$_4$): δ 9.33 (d, J = 6.3 Hz, 2H, (6)), 8.28 (d, J = 2.2 Hz, 2H, (3)), 7.48 (dd, J = 2.4 Hz, J = 6.3 Hz, 2H, (5)), 6.11 (d, J = 6.1 Hz, 2H, (8)), 5.85 (d, J = 6.1 Hz, 2H, (7)), 2.68 (sep, J = 6.9 Hz, 1H, (11)), 2.30 (s, 3H, (13)), 1.10 (d, J = 6.9 Hz, 6H, (12)).

^{13}C APT NMR (75 MHz, MeOD-*d*$_4$): δ 157.26 (2CH, (6)), 157.08 ($2C_{quat}$, (bipy)), 154.83 ($2C_{quat}$, (bipy)), 119.14 (2CH, (5)), 115.85 (2CH, (3)), 105.78 (Cquat, (p-Cym)), 105.50 (Cquat, (p-Cym)), 87.84 (2CH, (8)), 85.12 (2CH, (7)), 32.35 (CH, (11)), 22.34 ($2CH_3$, (12)), 18.97 (CH_3, (13)).

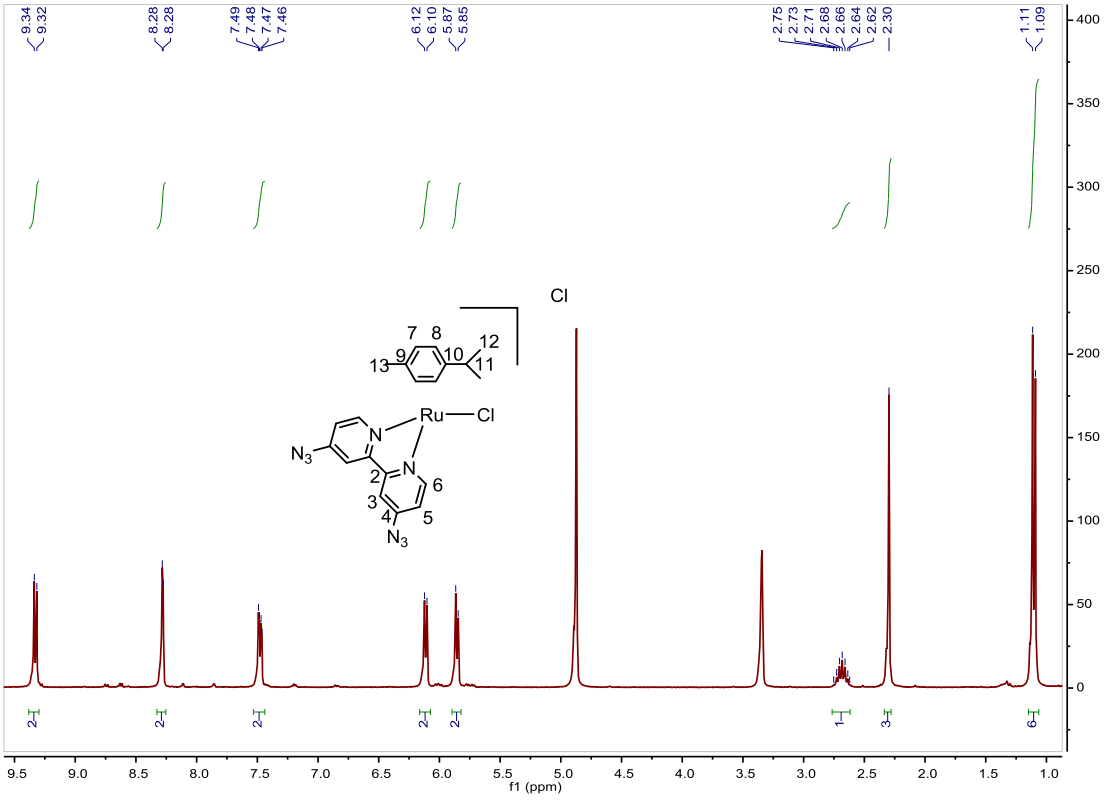

Fig. S335. ^{1}H NMR spectrum of **[Ru(p-Cym)(4,4'-diazido-2,2'-bipyridine)(Cl)]Cl** in MeOD-*d*$_4$, 300 MHz.

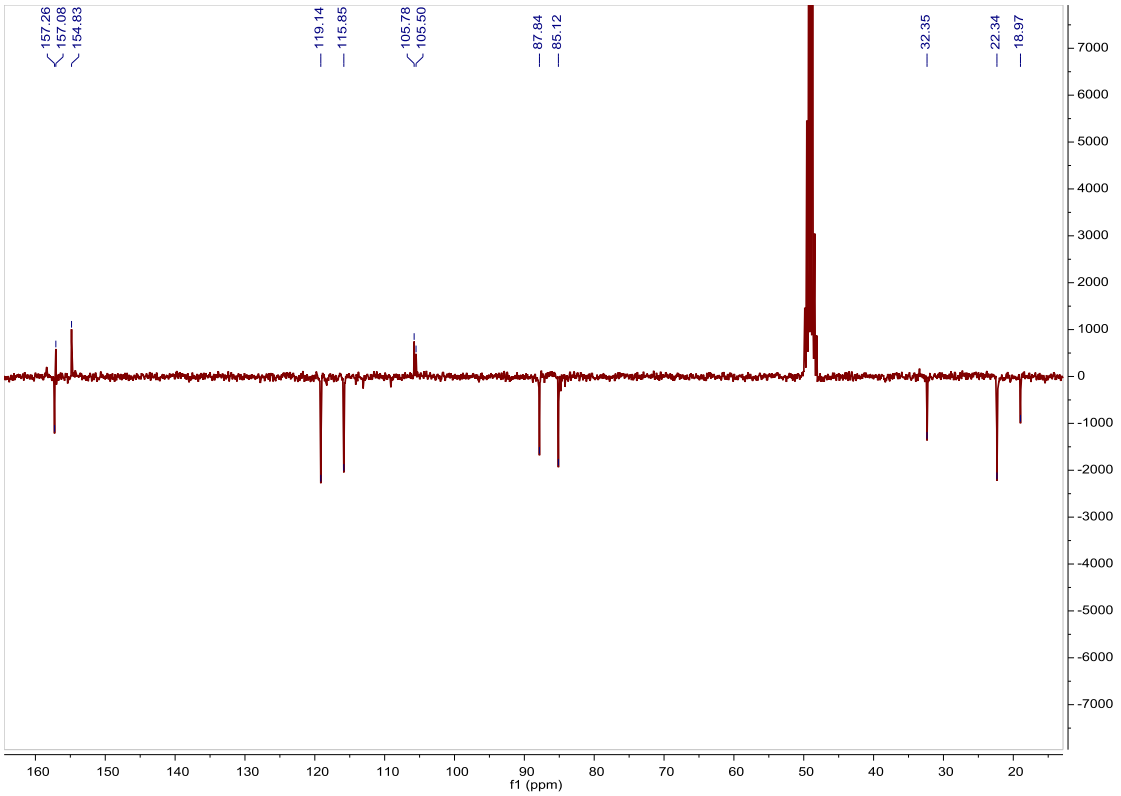

Fig. S336. ^{13}C APT NMR spectrum of **[Ru(p-Cym)(4,4'-diazido-2,2'-bipyridine)(Cl)]Cl** in MeOD-d_4, 75 MHz.

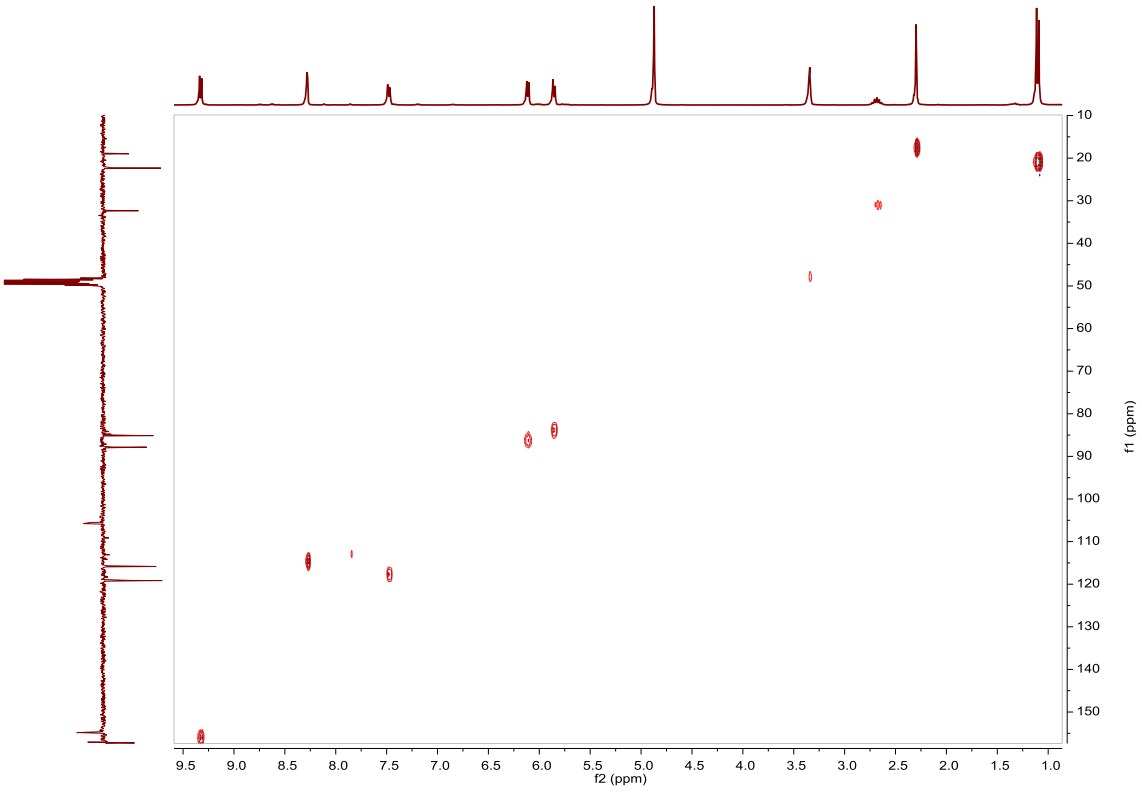

Fig. S337. HSQC NMR spectrum of **[Ru(p-Cym)(4,4'-diazido-2,2'-bipyridine)(Cl)]Cl** in MeOD-d_4.

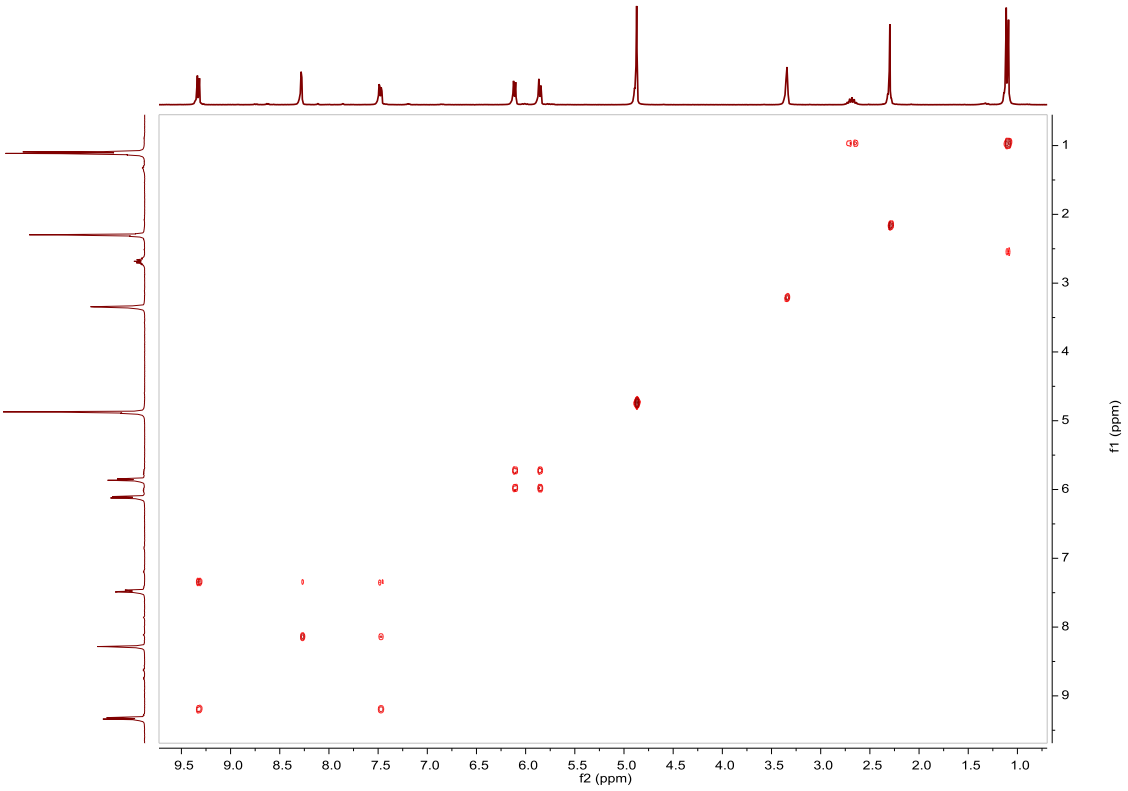

Fig. S338. COSY NMR spectrum of **[Ru(p-Cym)(4,4'-diazido-2,2'-bipyridine)(Cl)]Cl** in MeOD-d_4.

Compound [Ru(p-Cym)(4,4'-diamino-2,2'-bipyridine)(Cl)]Cl. Synthesis and characterization.

SYNTHESIS

Under a N_2 atmosphere, $Ru_2(p\text{-}Cym)_2Cl_4$ (0.1 g, 0.16 mmol) and 4,4'-diamino-2,2'-bipyridine (0.06 g, 0.326 mmol) were dissolved in 10 mL of acetone. The reaction mixture was refluxed for 15 h. It was cooled to room temperature and the brown solid that precipitated was filtered. Yield 60%.

Elemental Analysis: calculated for ($C_{20}H_{24}Cl_2N_4Ru$): C, 48.78; H, 4.91; N, 11.38. Found: C, 48.17; H, 4.88; N, 11.46.

Exact Mass: ESI-MS $[C_{20}H_{24}ClN_4Ru]^+$: calculated: m/z= 451.0765, found: m/z= 451.0768.

^{1}H NMR (300 MHz, MeOD-d_4): δ 8.70 (d, J = 6.6 Hz, 2H, (6)), 7.22 (d, J = 2.5 Hz, 2H, (3)), 6.77 (dd, J = 2.5 Hz, J = 6.6 Hz, 2H, (5)), 5.90 (d, J = 6.4 Hz, 2H, (8)), 5.63 (d J = 6.1 Hz, 2H, (7)), 2.61 (sep, J = 6.9 Hz, 1H, (11)), 2.26 (s, 3H, (13)), 1.08 (d, J = 6.9 Hz, 6H, (12)).

^{13}C APT NMR (75 MHz, MeOD-d_4): δ 158.16 ($2C_{quat}$, (bipy)), 156.61 ($2C_{quat}$, (bipy)), 155.09 (2CH, (6)), 112.55 (2CH, (5)), 107.61 (2CH, (3)), 104.12 (C_{quat}, (p-Cym)), 102.91 (C_{quat}, (p-Cym)), 87.07 (2CH, (8)), 83.93 (2CH, (7)), 32.24 (CH, (11)), 22.28 ($2CH_3$, (12)), 19.02 (CH_3, (13)).

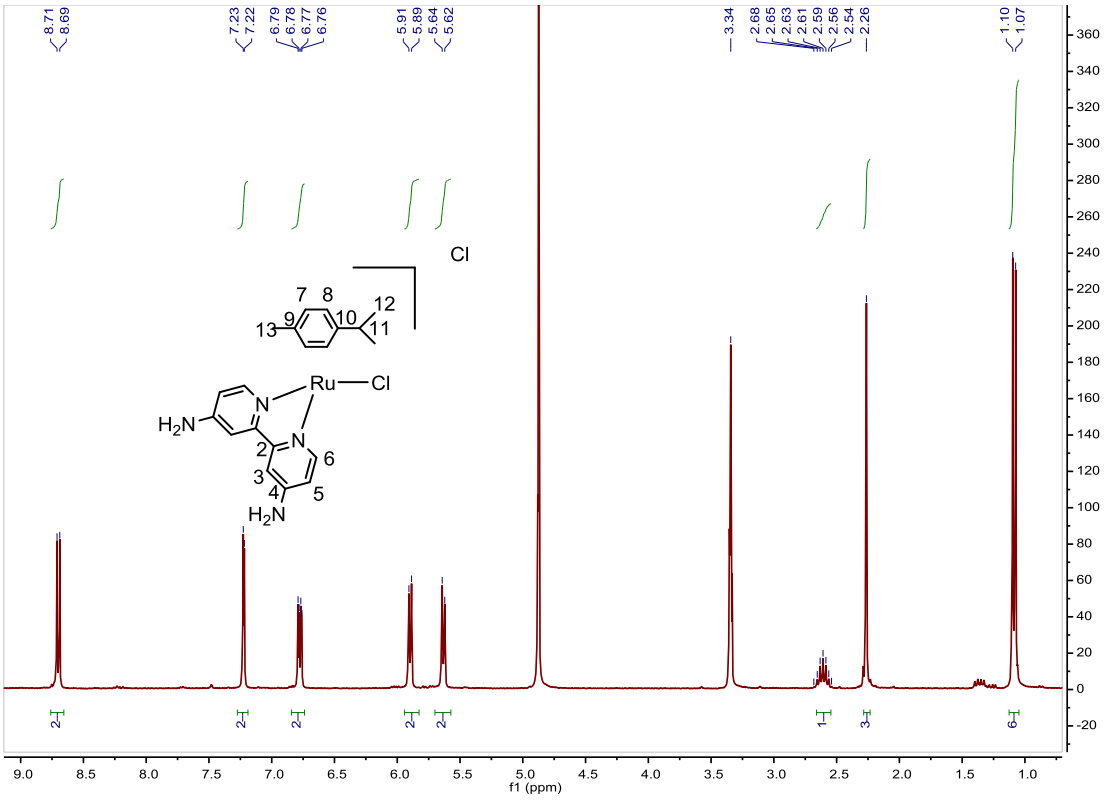

Fig. S339. ^{1}H NMR spectrum of **[Ru(p-Cym)(4,4'-diamino-2,2'-bipyridine)(Cl)]Cl** in MeOD-d_4, 300 MHz.

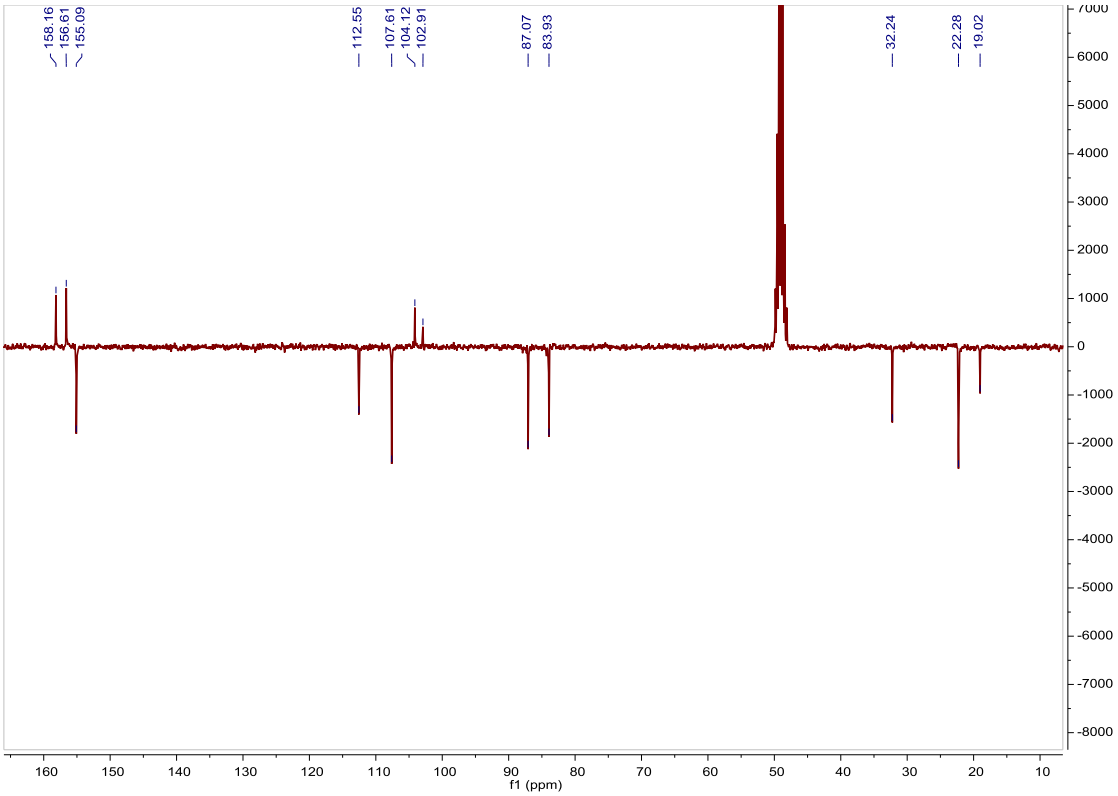

Fig. S340. ^{13}C APT NMR spectrum of **[Ru(p-Cym)(4,4'-diamino-2,2'-bipyridine)(Cl)]Cl** in MeOD-d_4, 75 MHz.

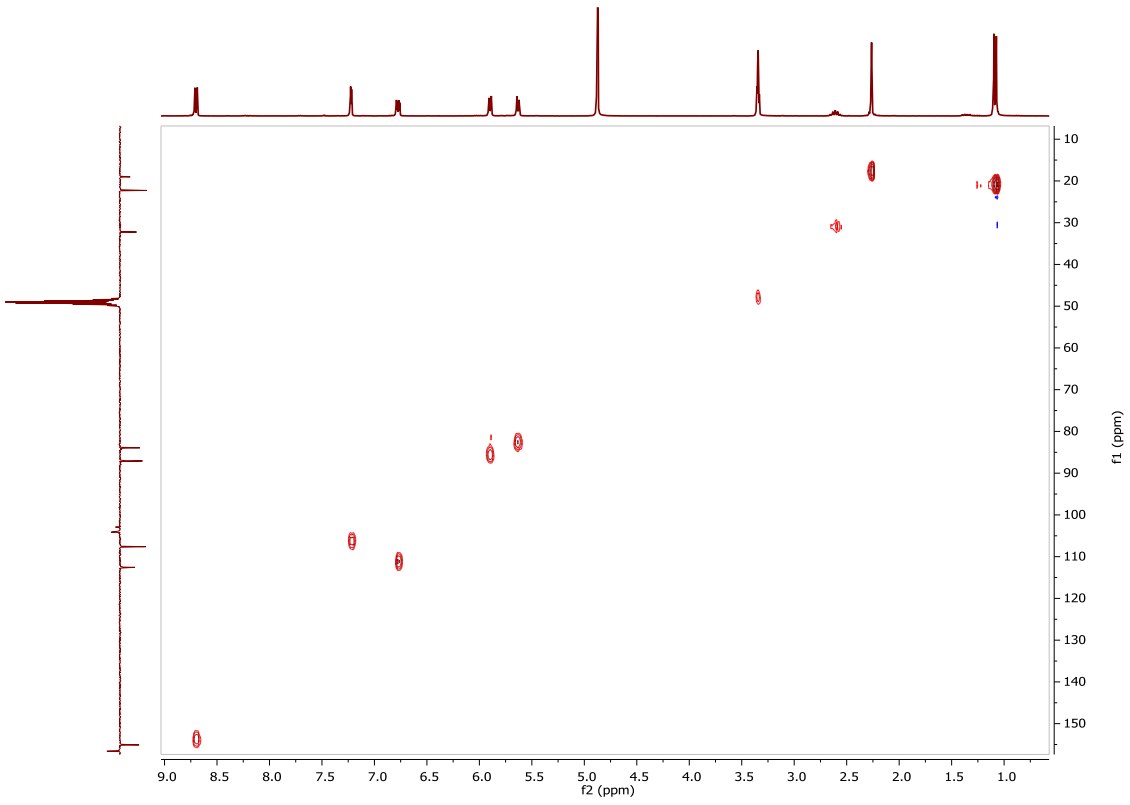

Fig. S341. HSQC NMR spectrum of **[Ru(p-Cym)(4,4'-diamino-2,2'-bipyridine)(Cl)]Cl** in MeOD-d_4.

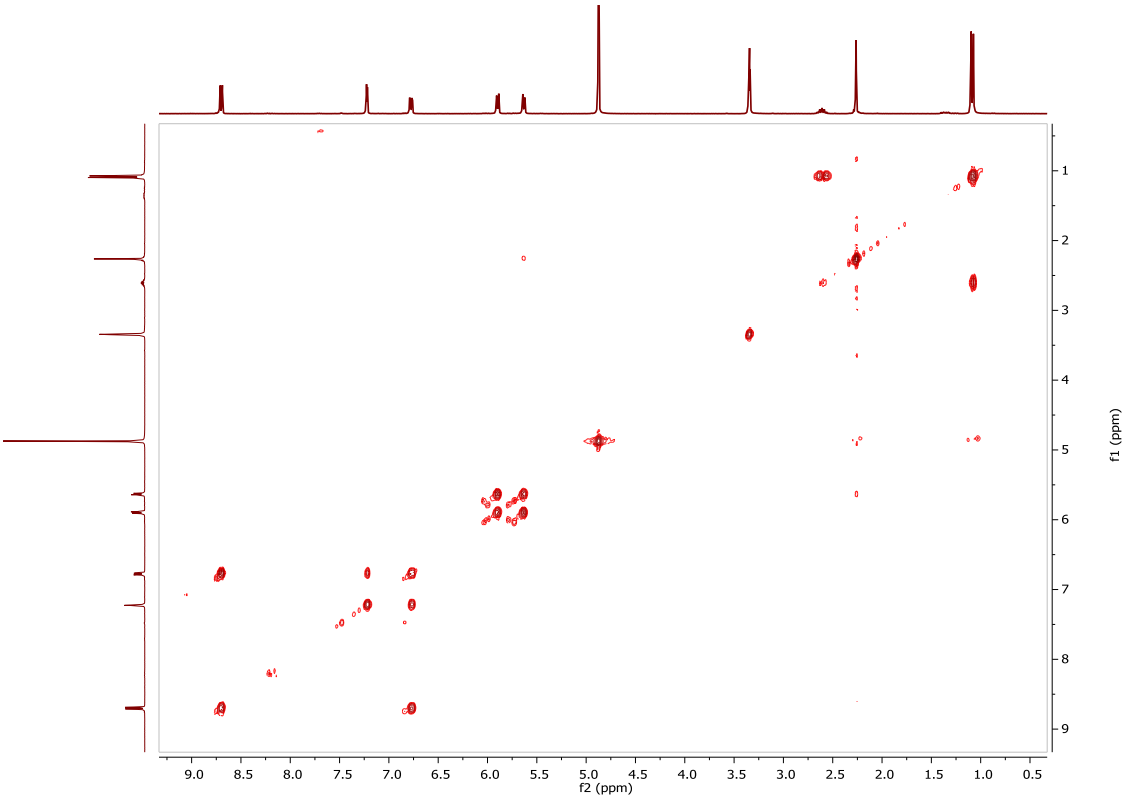

Fig. S342. COSY NMR spectrum of **[Ru(p-Cym)(4,4'-diamino-2,2'-bipyridine)(Cl)]Cl** in MeOD-d_4.

Compound [Ru(p-Cym)(4-bromo-4'-azido-2,2'-bipyridine)(Cl)]Cl. Synthesis and characterization.

SYNTHESIS

Under a N_2 atmosphere, $Ru_2(p\text{-}Cym)_2Cl_4$ (0.1 g, 0.16 mmol) and 4-bromo-4'-azido-2,2'-bipyridine (0.084 g, 0.30 mmol) were dissolved in 10 mL of acetone. The reaction mixture was refluxed for 15 h. It was cooled to room temperature, the solvent was evaporated and the desired compound was obtained after precipitated with CH_2Cl_2/Et_2O as a dark red solid. Yield 49%.

Elemental Analysis: calculated for ($C_{20}H_{20}BrCl_2N_5Ru$): C, 41.25; H, 3.46; N, 12.03. Found: C, 40.76; H, 3.63; N, 11.81.

Exact Mass: ESI-MS $[C_{20}H_{20}BrClN_5Ru]^+$: calculated: m/z= 545.9632, found: m/z= 545.9642.

^{1}H NMR (300 MHz, MeOD-*d*$_4$): δ 9.33 (d, J = 2.4 Hz, 1H, (6)), 9.31 (d, J = 2.2 Hz, 1H, (6')), 8.93 (d, J = 2.1 Hz, 1H, (3)), 8.30 (d, J = 2.5 Hz, 1H, (3')), 8.02 (dd, J = 2.1 Hz, J 6.1 Hz, 1H, (5)), 7.49 (dd, J = 2.4 Hz, J = 6.3 Hz, 1H, (5')), 6.14 (d, J = 4.3 Hz, 1H, (8)), 6.12 (d, J = 4.2 Hz, 1H, (8')), 5.88 (d, J = 4.1 Hz, 1H, (7)), 5.86 (d, J = 4.1 Hz, 1H, (7')), 2.70 (sep, J = 6.9 Hz, 1H, (11)), 2.30 (s, 3H, (13)), 1.12 (d, J = 1.9 Hz, 3H, (12)), 1.10 (d, J = 1.9 Hz, 3H, (12')).

^{13}C NMR (75 MHz, MeOD-*d*$_4$): δ 157.40 (CH, (6)), 157.03 (CH, (6')), 156.82 (Cquat, (bipy)), 156.38 (Cquat, (bipy)), 154.89 (Cquat, (bipy)), 138.04 (Cquat, (bipy)), 132.27 (CH, (5)), 128.76 (CH, (3)), 119.37 (CH, (5')), 116.16 (CH, (3')), 106.35 (Cquat, (p-Cym)), 105.59 (Cquat, (p-Cym)), 88.03 (CH, (8)), 87.83 (CH, (8')), 85.51 (CH, (7)), 85.31 (CH, (7')), 32.35 (CH, (11)), 22.36 (CH_3, (13)), 18.96 (CH_3, (12)), 15.43 (CH_3, (12')).

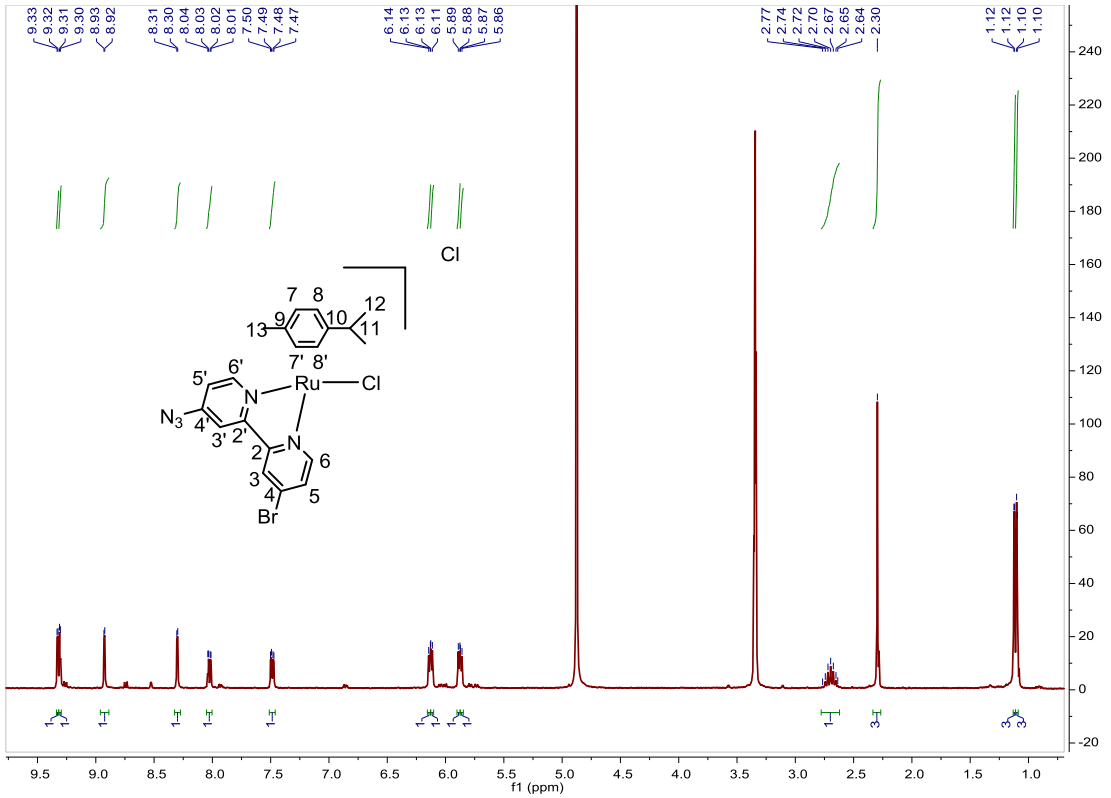

Fig. S343. ^{1}H NMR spectrum of **[Ru(p-Cym)(4-bromo-4'-azido-2,2'-bipyridine)(Cl)]Cl** in MeOD-*d*$_4$, 300 MHz.

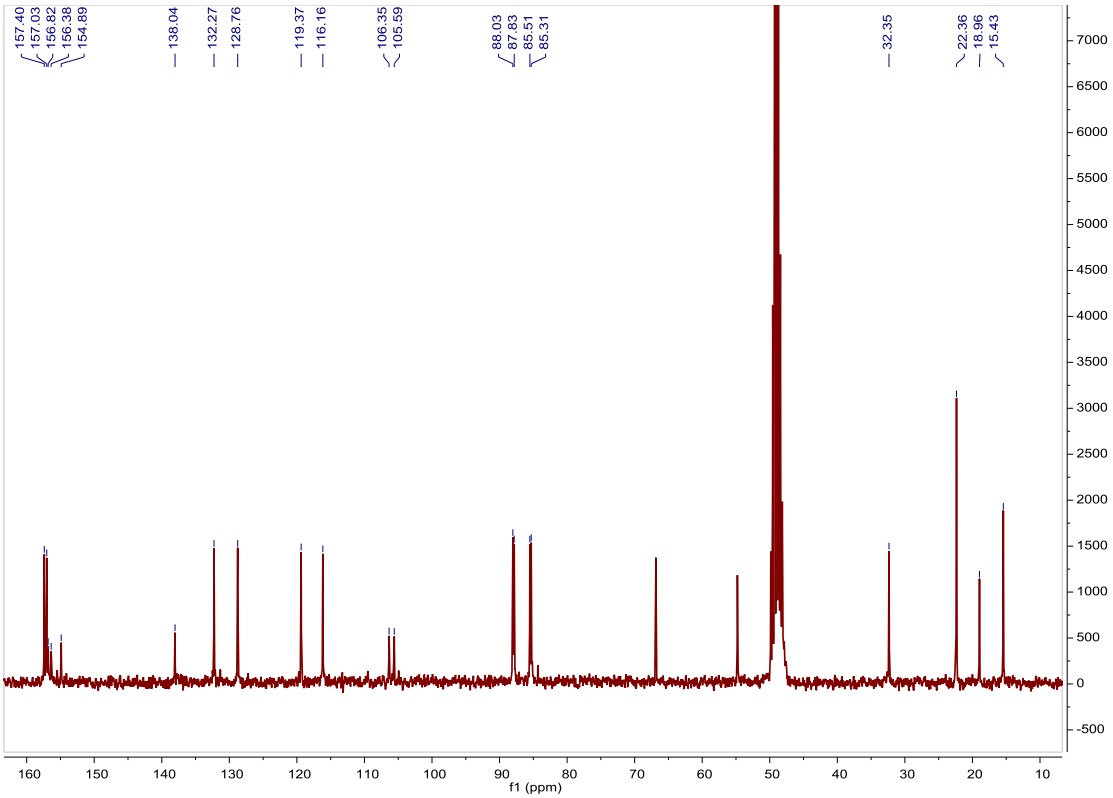

Fig. S344. ^{13}C NMR spectrum of **[Ru(p-Cym)(4-bromo-4'-azido-2,2'-bipyridine)(Cl)]Cl** in MeOD-d_4, 75 MHz.

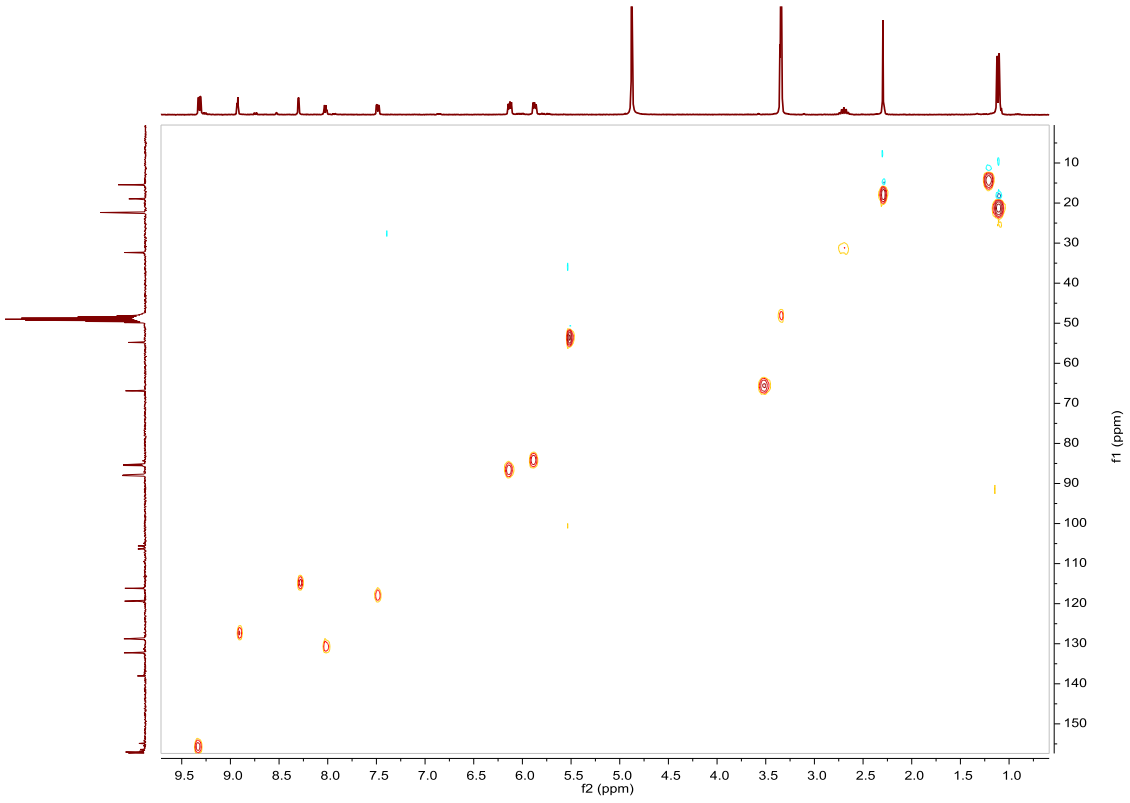

Fig. S345. HSQC NMR spectrum of **[Ru(p-Cym)(4-bromo-4'-azido-2,2'-bipyridine)(Cl)]Cl** in MeOD-d_4.

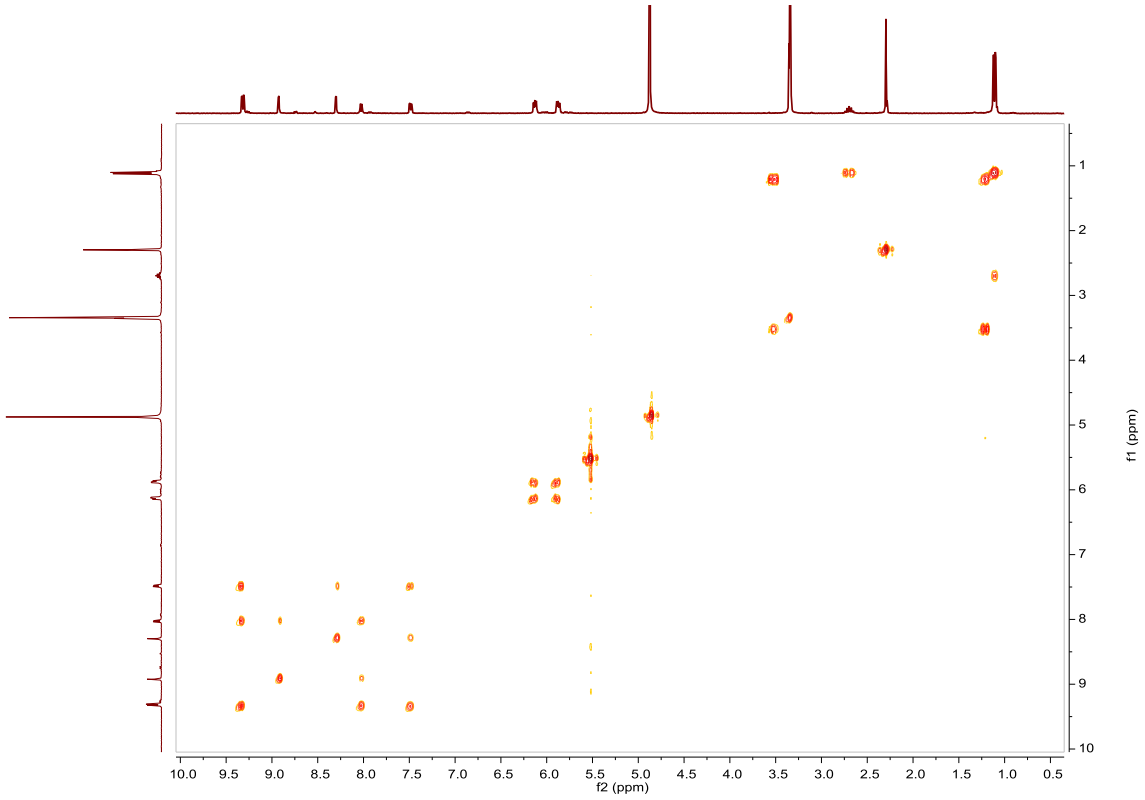

Fig. S346. COSY NMR spectrum of **[Ru(p-Cym)(4-bromo-4'-azido-2,2'-bipyridine)(Cl)]Cl** in MeOD-d_4.

Compound [Ru(p-Cym)(2,2'-bis(4-phenylazopyridine)(Cl)]Cl. Synthesis, characterization and photoisomerization studies.

SYNTHESIS

Under a N_2 atmosphere, $Ru_2(p\text{-}Cym)_2Cl_4$ (0.1 g, 0.16 mmol) and 2,2'-bis(4-phenylazopyridine) (0.119 g, 0.326 mmol) were dissolved in 10 mL of acetone. The reaction mixture was refluxed for 15 h. It was cooled to room temperature and the solid was filtered. The desired compound was obtained after precipitated with CH_2Cl_2/Et_2O as a dark red solid. Yield 73%.

Elemental Analysis: calculated for ($C_{32}H_{30}Cl_2N_6Ru{\cdot}CH_2Cl_2$): C, 52.46; H, 4.27; N, 11.12. Found: C, 52.33; H, 4.30; N, 11.09.

Exact Mass: ESI-MS $[C_{32}H_{30}ClN_6Ru]^+$: calculated: m/z= 635.1264, found: m/z= 635.1282.

^{1}H NMR (300 MHz, MeOD-d_4): δ 9.69 (d, J = 6.1 Hz, 2H, (6)), 8.98 (s, 2H, (3)), 8.19–8.04 (m, 6H, (5+15)), 7.77–7.61 (m, 6H, (16+17)), 6.24 (d, J = 6.2 Hz, 2H, (8)), 6.00 (d, J = 6.2 Hz, 2H, (7)), 2.75 (sep, J = 6.8 Hz, 1H, (11)), 2.34 (s, 3H, (13)), 1.13 (d, J = 6.9 Hz, 6H, (12)).

^{13}C APT NMR (75 MHz, MeOD-d_4): δ 160.37 ($2C_{quat}$, (bipy)), 158.42 (2CH, (6)), 157.91 ($2C_{quat}$, (bipy)), 153.73 ($2C_{quat}$, (bipy), 135.13 (2CH, (17)), 130.76 (4CH, (16)), 125.16 (4CH, (15)), 120.49 (2CH, (5)), 118.74 (2CH, (3)), 107.02 (C_{quat}, (p-Cym)), 106.04(C_{quat}, (p-Cym)), 88.47 (2CH, (8)), 86.13 (2CH, (7)), 32.34 (CH, (11)), 22.38 ($2CH_3$, (12)), 19.02 (CH_3, (13)).

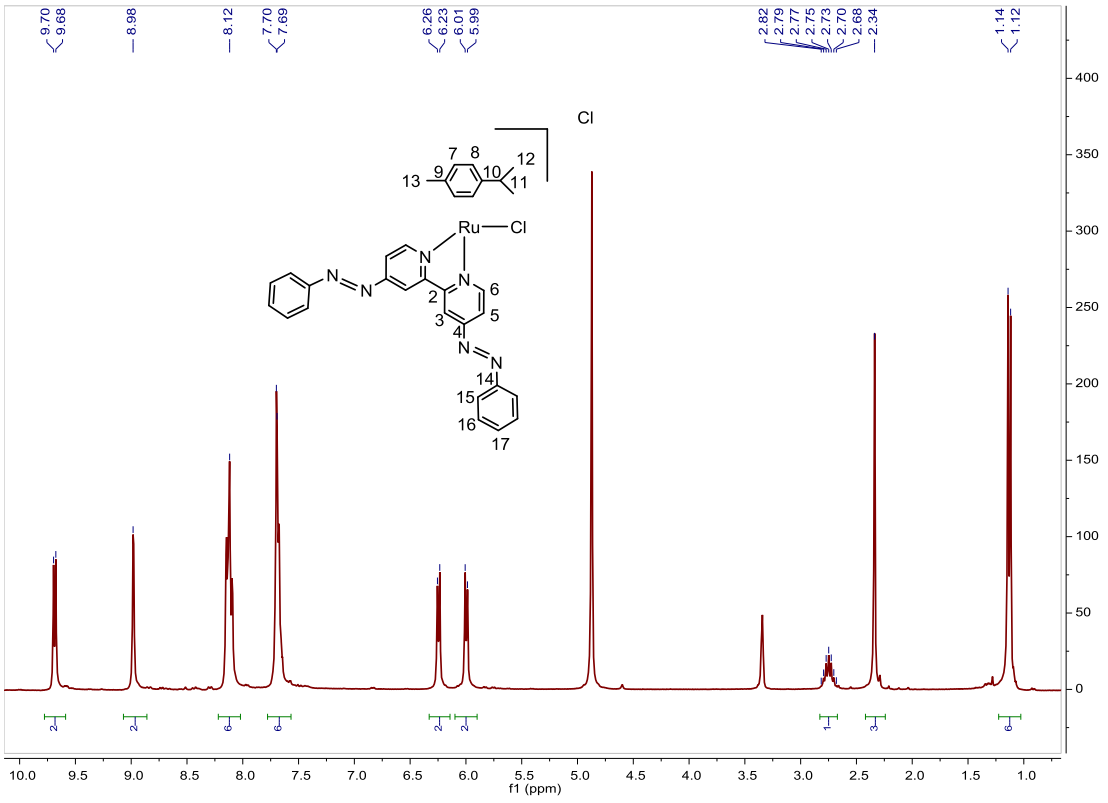

Fig. S347. ^{1}H NMR spectrum of **[Ru(p-Cym)(2,2'-bis(4-phenylazopyridine)(Cl)]Cl** in MeOD-d_4, 300 MHz.

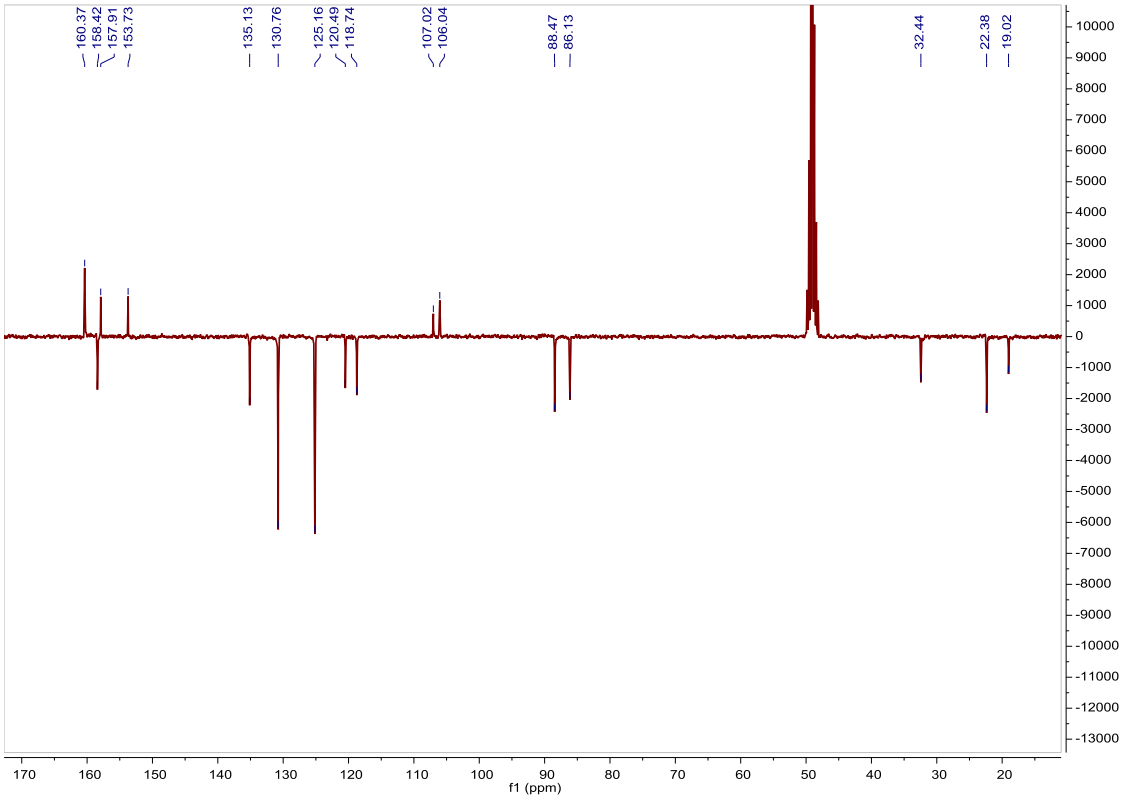

Fig. S348. ^{13}C APT NMR spectrum of **[Ru(p-Cym)(2,2'-bis(4-phenylazopyridine)(Cl)]Cl** in MeOD-d_4, 75 MHz.

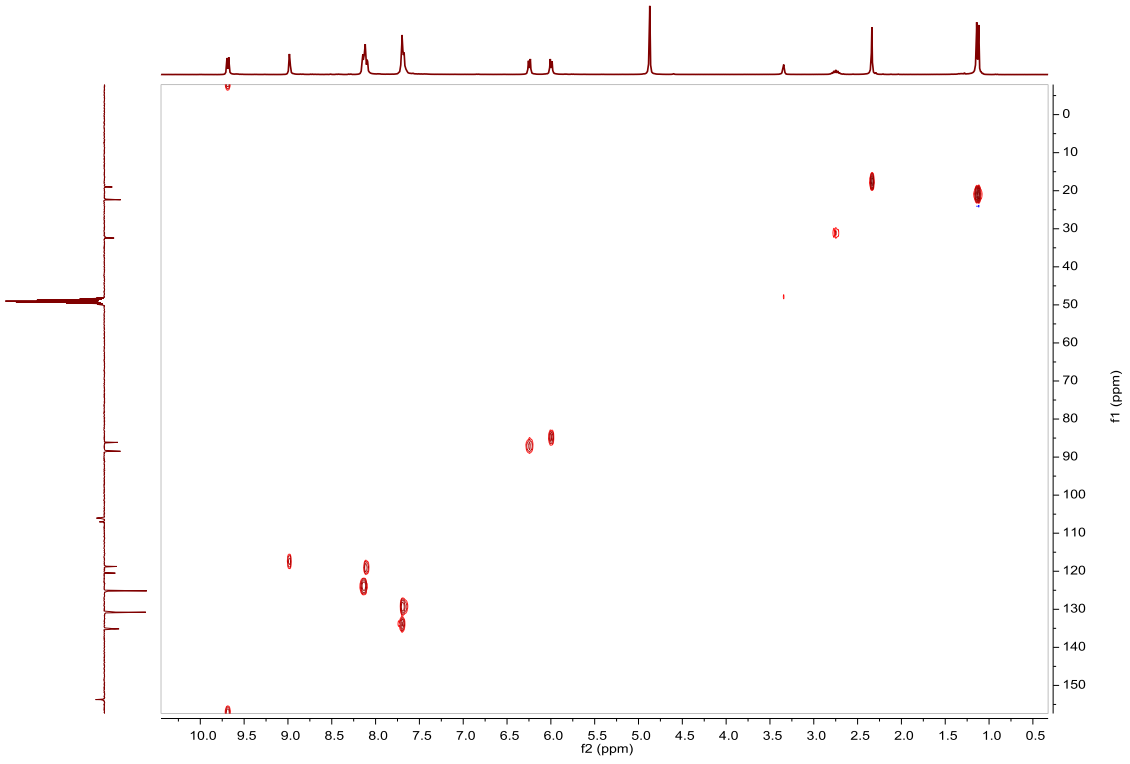

Fig. S349. HSQC NMR spectrum of **[Ru(p-Cym)(2,2'-bis(4-phenylazopyridine)(Cl)]Cl** in MeOD-d_4.

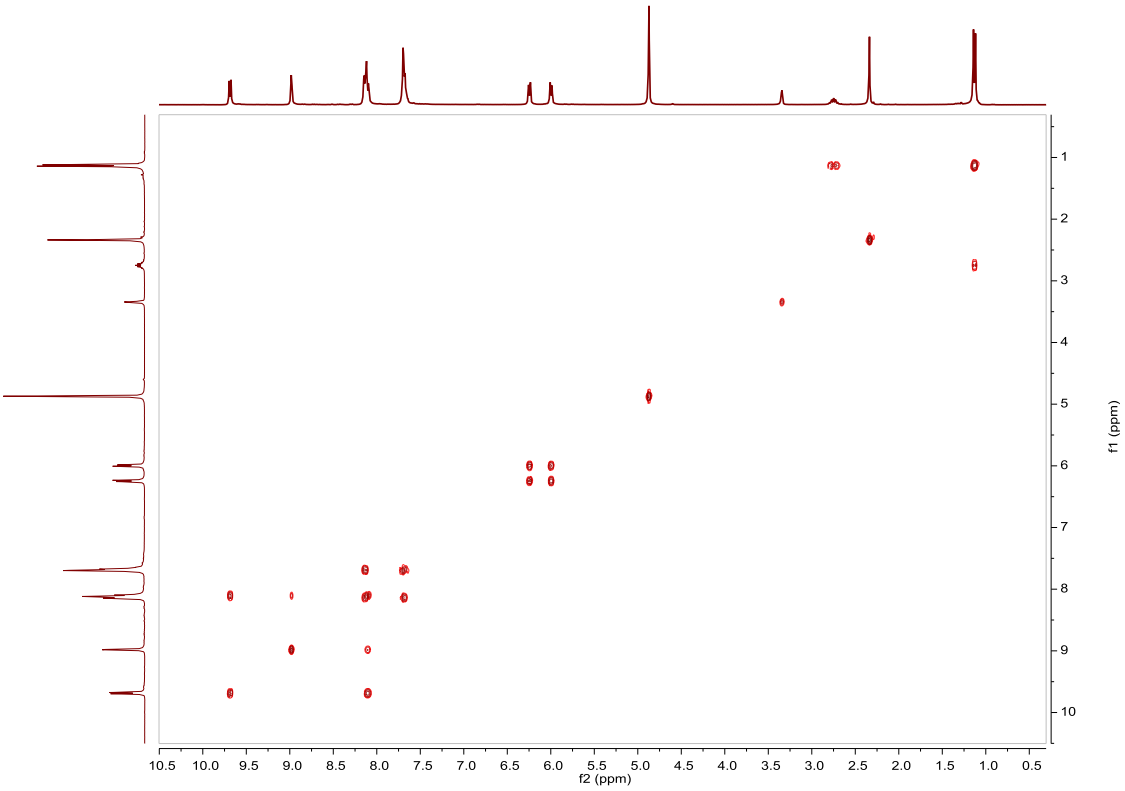

Fig. S350. COSY NMR spectrum of **[Ru(p-Cym)(2,2'-bis(4-phenylazopyridine)(Cl)]Cl** in MeOD-d_4.

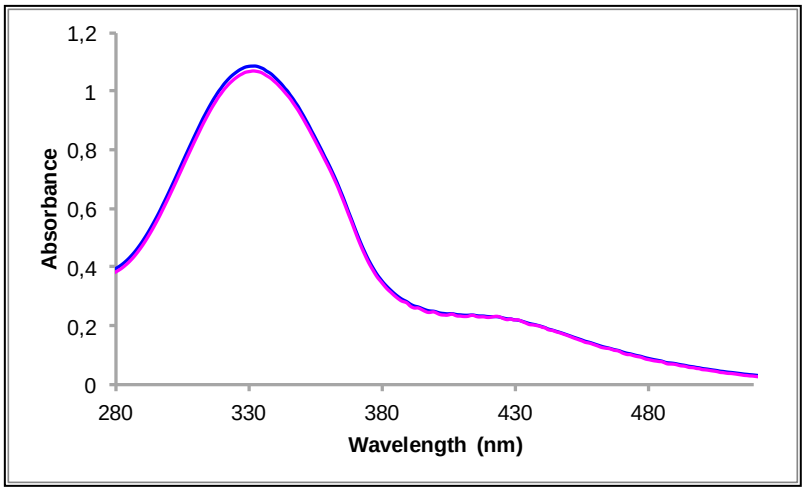

Fig. S351. UV/Vis spectra of **[Ru(p-Cym)(2,2'-bis(4-phenylazopyridine)(Cl)]Cl** in CH_3CN. Before (blue line) and after (pink line) irradiation at 316nm, $2.62 \cdot 10^{-5}$ M.

Cis to trans thermal isomerization kinetics. Due to the small degree of photoisomerization, it has been not possible to calculate k.

Compound [Ru(p-Cym)(4-phenylazopyridine)(Cl)$_2$]. Synthesis, characterization and photoisomerization studies.

SYNTHESIS

Under a N_2 atmosphere, Ru_2(p-Cym)$_2Cl_4$ (0.2 g, 0.32 mmol) and (4-phenylazopyridine) (0.117 g, 0.64 mmol) were dissolved in 20 mL of acetone. The reaction mixture was refluxed for 15 h. It was cooled to room temperature, the solvent was evaporated and the product was obtained as an orange solid. Yield 71%.

Elemental Analysis: calculated for ($C_{21}H_{23}Cl_2N_3Ru$): C, 51.54; H, 4.74; N, 8.59. Found: C, 51.51; H, 4.71; N, 8.55.

Exact Mass: ESI-MS $[C_{21}H_{23}ClN_3Ru]^+$ (M-Cl): calculated: m/z= 454.0619, found: m/z= 454.0618.

^{1}H NMR (300 MHz, $CDCl_3$): δ 9.26 (d, J = 6.9 Hz, 2H, (azopy)), 8.06–7.96 (m, 2H, (15+19)), 7.75 (d, J = 6.7 Hz, 2H, (azopy)), 7.64–7.55 (m, 3H, (16+17+18)), 5.52 (d, J = 5.7 Hz, 2H, (8)), 5.30 (d, J = 5.8 Hz, 2H, (7)), 3.06 (sep, J = 6.9 Hz, 1H, (11)), 2.17 (s, 3H, (13)), 1.37 (d, J = 6.9 Hz, 6H, (12)).

^{13}C APT NMR (75 MHz, $CDCl_3$): δ 157.12 (C_{quat}, (azopy)), 155.93 (2CH, (azopy)), 151.76 (C_{quat}, (azopy)), 132.78 (CH, (17)), 128.92 (2CH, (16+18)), 123.35 (2CH, (15+19)), 116.50 (2CH, (azopy)), 103.26 (C_{quat}, (p-Cym)), 96.88 (C_{quat}, (p-Cym), 82.58 (2CH, (8)), 81.88 (2CH, (7)), 30.24 (CH, (11)), 21.86 ($2CH_3$, (12)), 17.83 (CH_3, (13)).

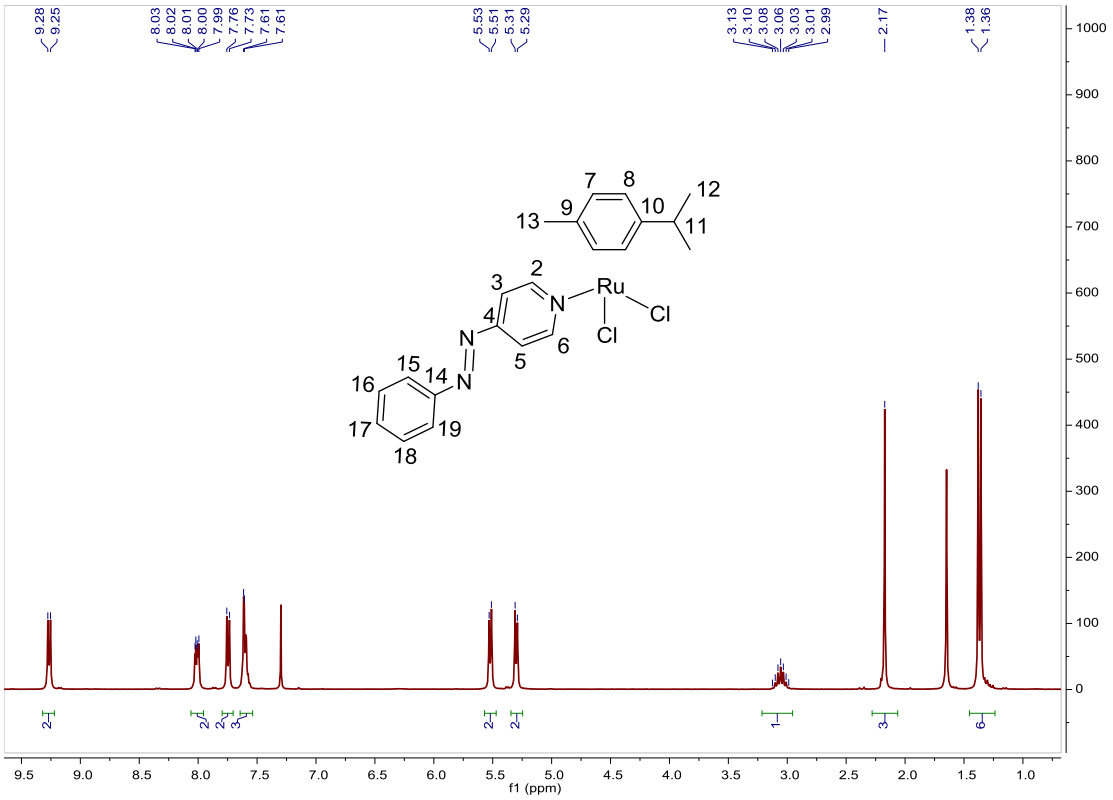

Fig. S352. ^{1}H NMR spectrum of **[Ru(p-Cym)(4-phenylazopyridine)(Cl)$_2$]** in $CDCl_3$, 300 MHz.

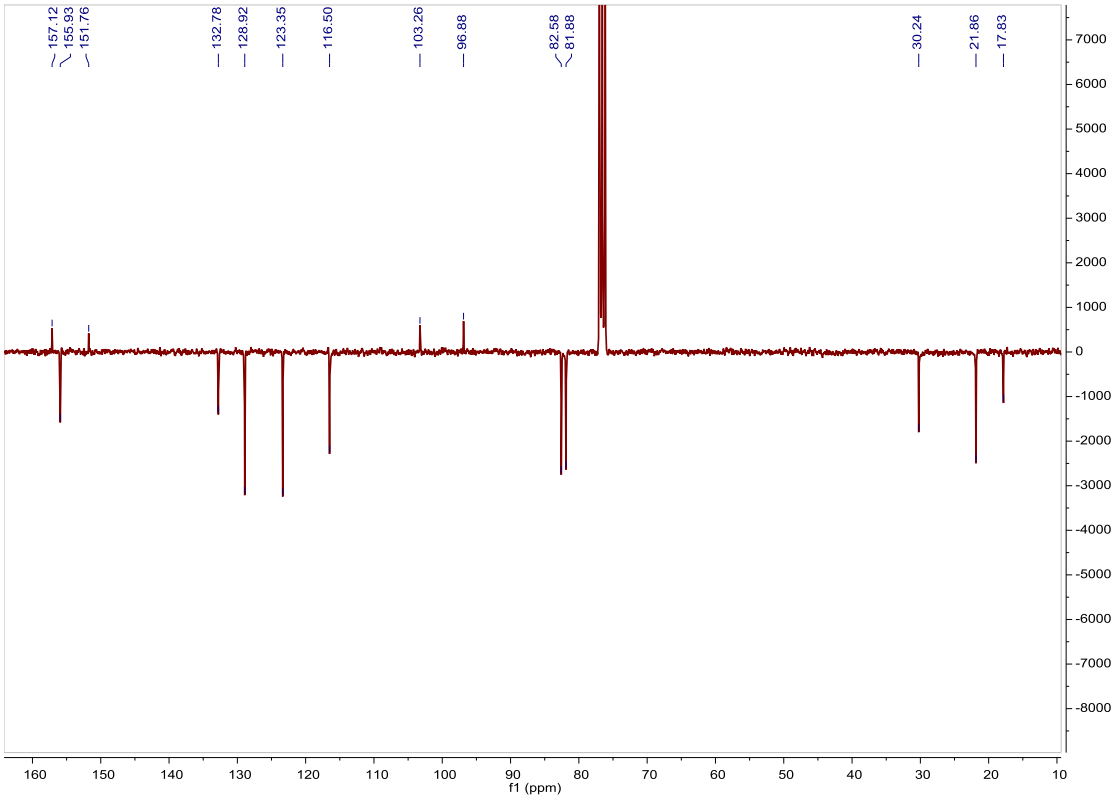

Fig. S353. ^{13}C APT NMR spectrum of **[Ru(p-Cym)(4-phenylazopyridine)(Cl)$_2$]** in $CDCl_3$, 75 MHz.

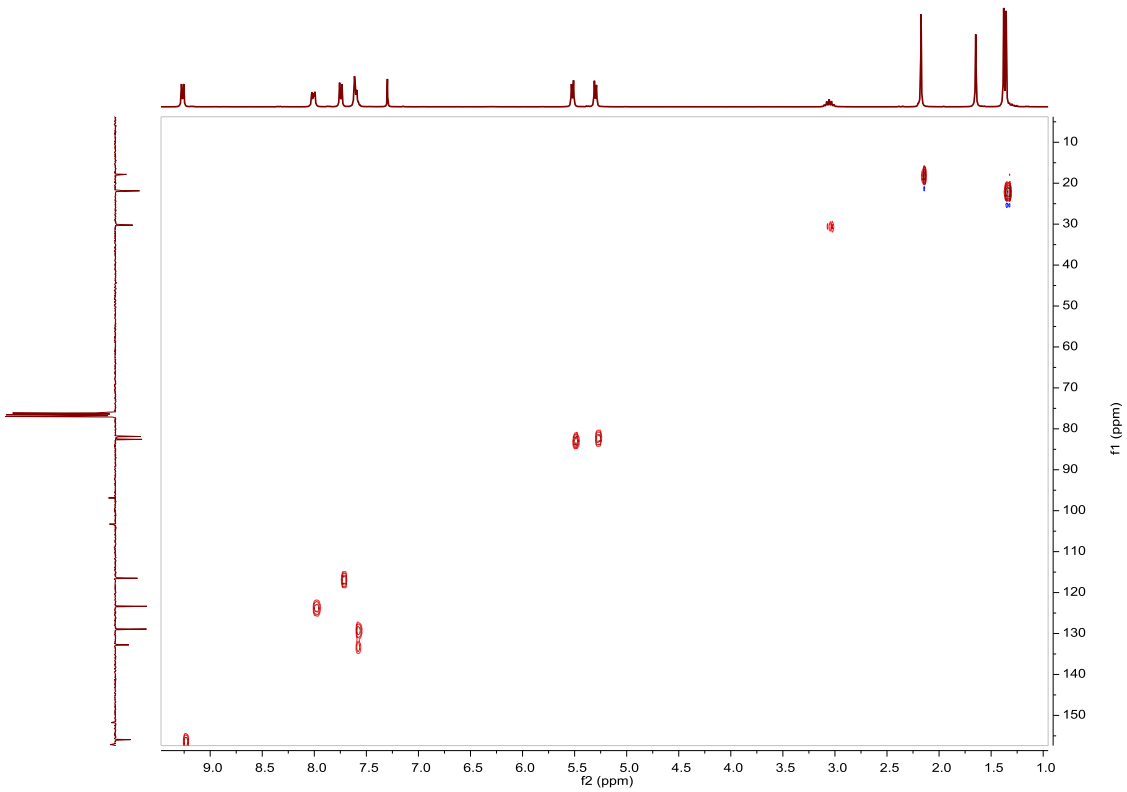

Fig. S354. HSQC NMR spectrum of **[Ru(p-Cym)(4-phenylazopyridine)(Cl)$_2$]** in $CDCl_3$.

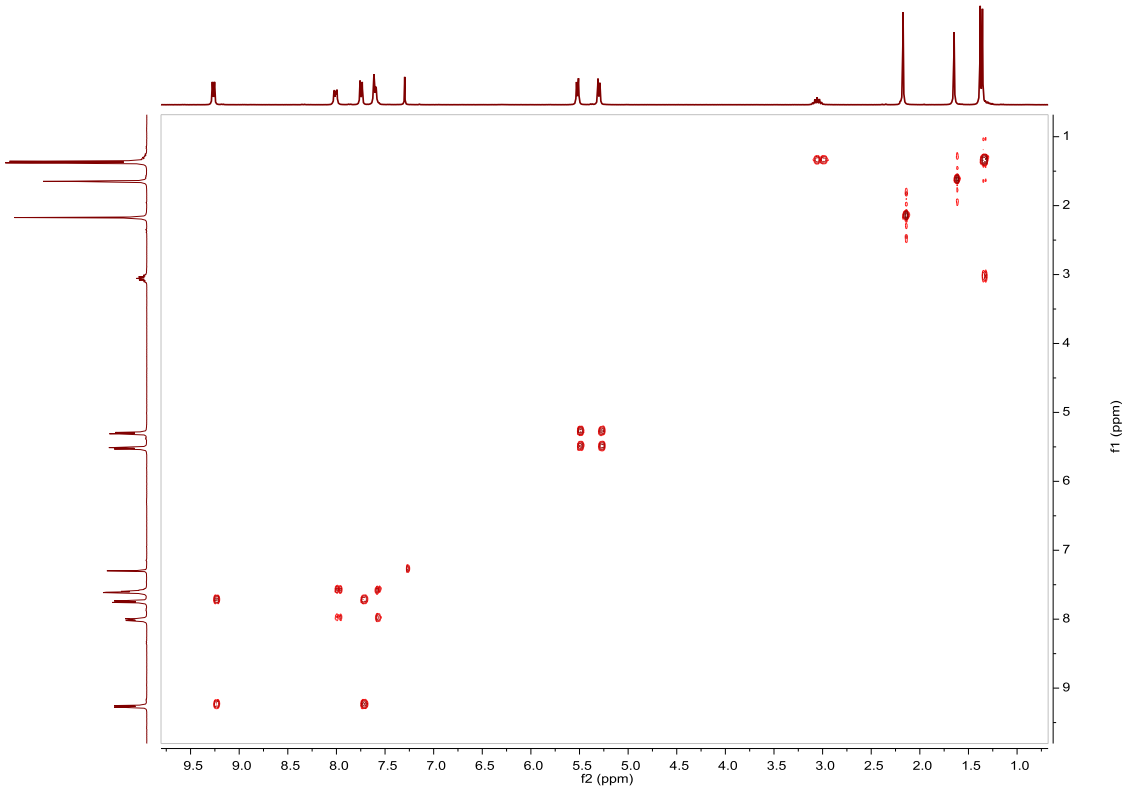

Fig. S355. COSY NMR spectrum of **[Ru(p-Cym)(4-phenylazopyridine)(Cl)$_2$]** in $CDCl_3$.

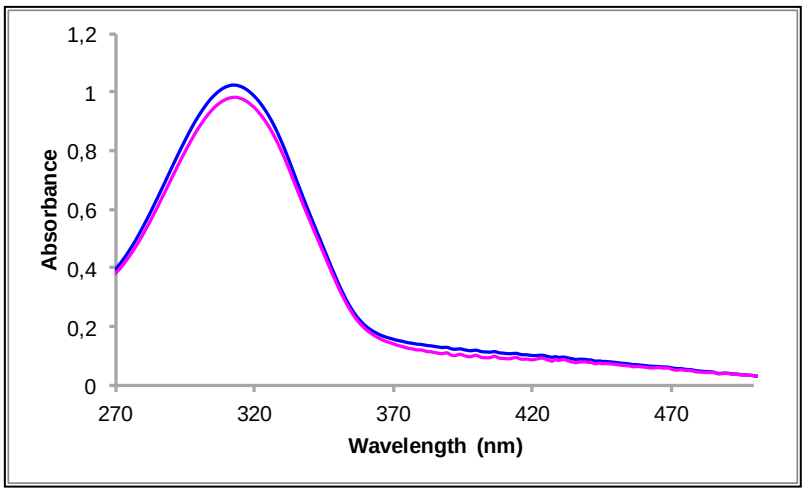

Fig. S356. UV/Vis spectra of **[Ru(p-Cym)(4-phenylazopyridine)(Cl)$_2$]** in ACN. Before (blue line) and after (pink line) irradiation at 311nm, $5.50 \cdot 10^{-5}$M.

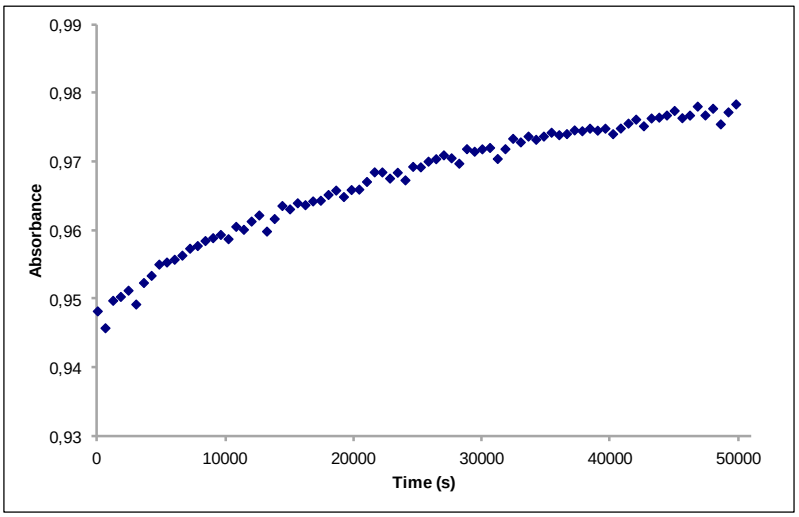

Fig. S357. Cis to trans thermal isomerization kinetics of **[Ru(p-Cym)(4-phenylazopyridine)(Cl)$_2$]**. Absorption change of the band 312nm at 338 K in ACN after irradiation at 311 nm. ($5.50 \cdot 10^{-5}$M).

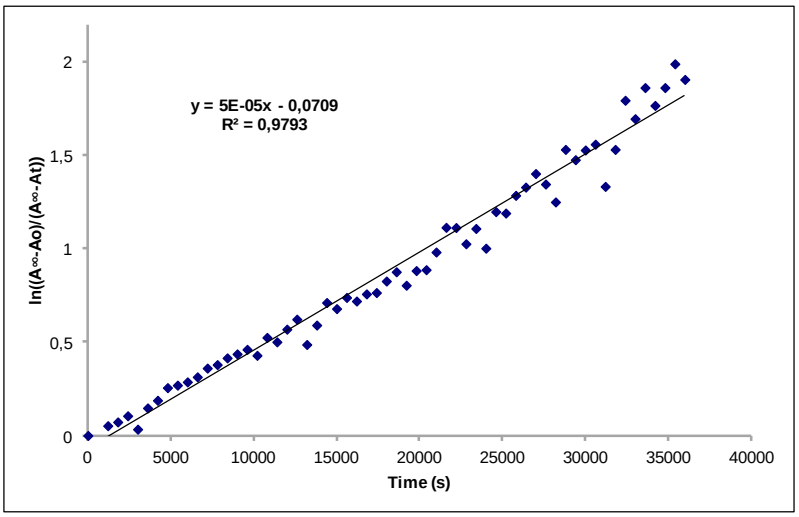

Fig. S358. Cis to trans thermal isomerization kinetics of **[Ru(p-Cym)(4-phenylazopyridine)(Cl)$_2$]**. First-order plot. k (s^{-1}) = $5.0 \cdot 10^{-5}$. Half-life (min) = 231.

Compound [Ru(p-Cym)(4-phenylazopyridine)$_2$(Cl)]PF$_6$. Synthesis, characterization and photoisomerization studies.

SYNTHESIS[42]

Under a N_2 atmosphere, [Ru(p-Cym)(4-phenylazopyridine)(Cl_2)] (0.319 g, 0.65 mmol) and AgPF6 (0.160 g, 0.63 mmol) were dissolved in 20 mL of acetone and 20 mL of methanol. The mixture was stirred for 1 h, AgCl was removed by filtration and 4-phenylazopyridine (0.119 g, 0.65 mmol) were added. The reaction mixture was stirred for 15 h and the solvent was evaporated. The product was obtained as a red solid after precipitation with acetone/ether. Yield 55%.

Elemental Analysis: calculated for ($C_{32}H_{32}ClN_6RuPF_6$): C, 49.14; H, 4.12; N, 10.75. Found: C, 49.23; H, 4.01; N, 10.59.

Exact Mass: ESI-MS $[C_{21}H_{23}ClN_3Ru]^+$ (M-L-PF_6): calculated: m/z= 454.0619, found: m/z= 454.0618.

^{1}H NMR (300 MHz, $CDCl_3$): δ 9.27 (d, J = 6.9 Hz, 4H, (azopy)), 7.97 (dd, J = 1.6 Hz, J = 7.5 Hz, 4H, (15+19)), 7.87 (d, J = 6.9 Hz, 4H, (azopy)), 7.57 (brd, J = 7.3 Hz, 6H, (16+17+18)), 6.03 (d, J = 6.1 Hz, 2H, (8)), 5.78 (d, J = 6.1 Hz, 2H, (7)), 2.67 (sep, J = 6.9 Hz, 1H, (11)), 1.86 (s, 3H, (13)), 1.23 (d, J = 6.9 Hz, 6H, (12)).

^{13}C APT NMR (75 MHz, $CDCl_3$): δ 157.66 (2C_{quat}, (azopy)), 155.29 (4CH, (azopy)), 151.74 (2C_{quat}, (azopy)), 133.09 (2CH, (17)), 128.94 (4CH, (16)), 123.47 (4CH, (15)), 118.22 (4CH, (azopy)), 102.59 (C_{quat}, (p-Cym)), 101.80 (C_{quat}, (p-Cym)), 88.49 (2CH, (8)), 81.77 (2CH, (7)), 30.45 (CH, (11)), 21.84 ($2CH_3$, (12)), 17.39 (CH_3, (13)).

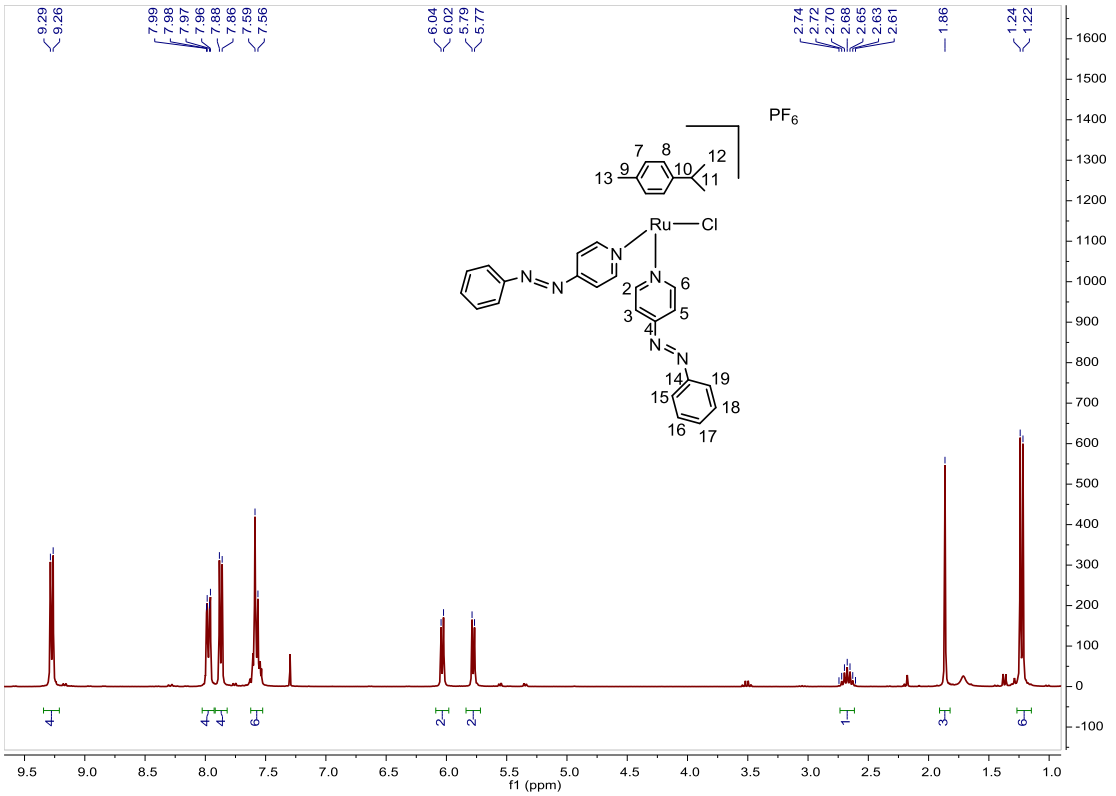

Fig. S359. ^{1}H NMR spectrum of **[Ru(p-Cym)(4-phenylazopyridine)$_2$(Cl)]PF$_6$** in $CDCl_3$, 300 MHz.

[42] S. J. Dickson, M. J. Paterson, C. E. Willans, K. M. Anderson and J. W. Steed, *Chem. Eur. J.*, **2008**, *14*, 7296–7305.

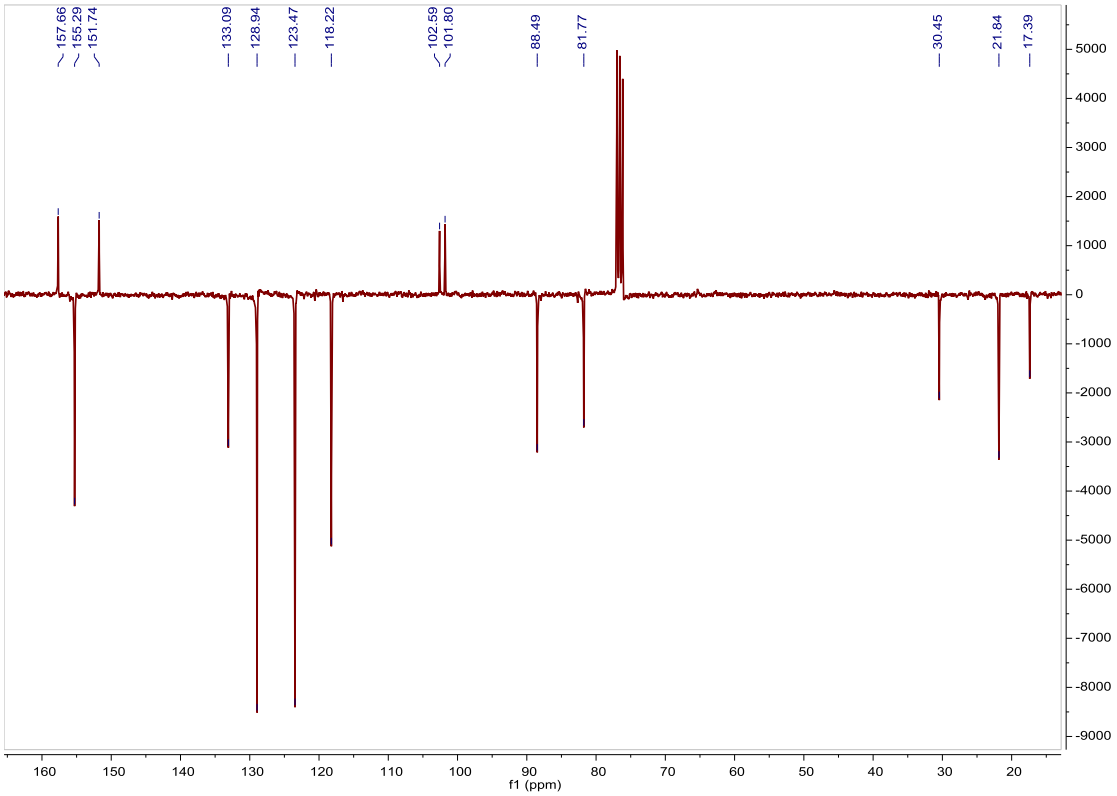

Fig. S360. ^{13}C APT NMR spectrum of **[Ru(p-Cym)(4-phenylazopyridine)$_2$(Cl)]PF$_6$** in $CDCl_3$, 75 MHz.

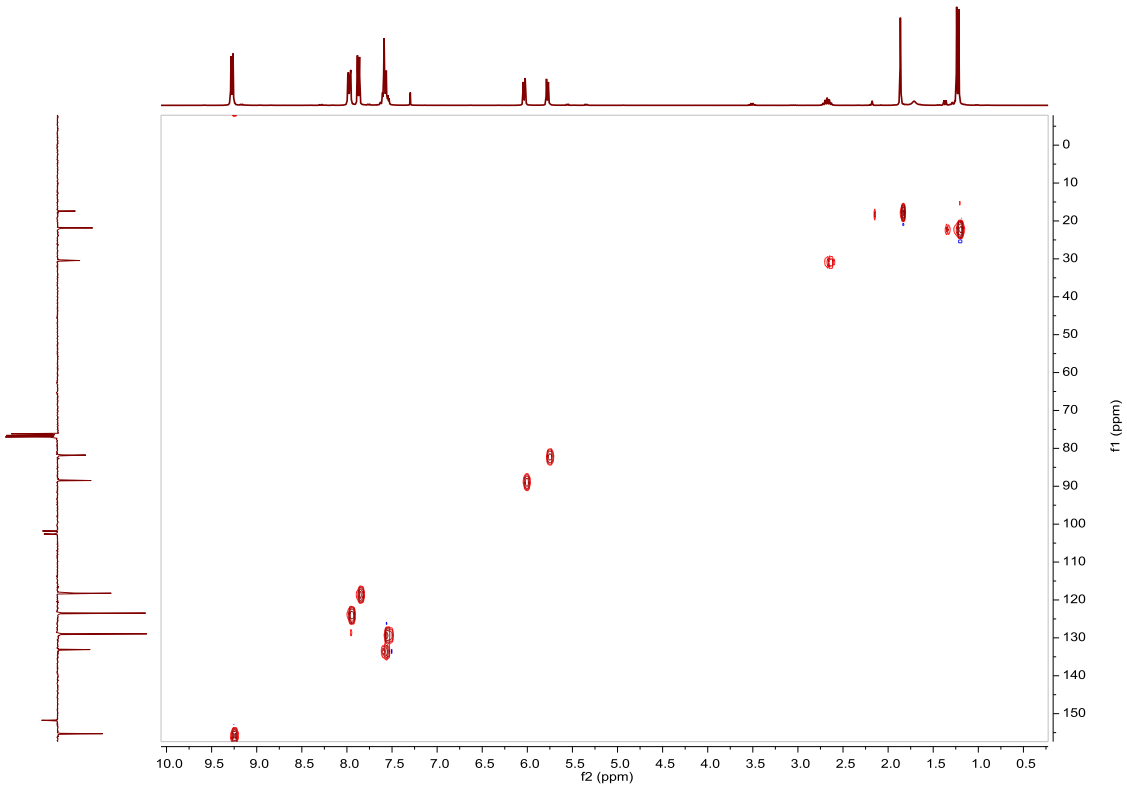

Fig. S361. HSQC NMR spectrum of **[Ru(p-Cym)(4-phenylazopyridine)$_2$(Cl)]PF$_6$** in $CDCl_3$.

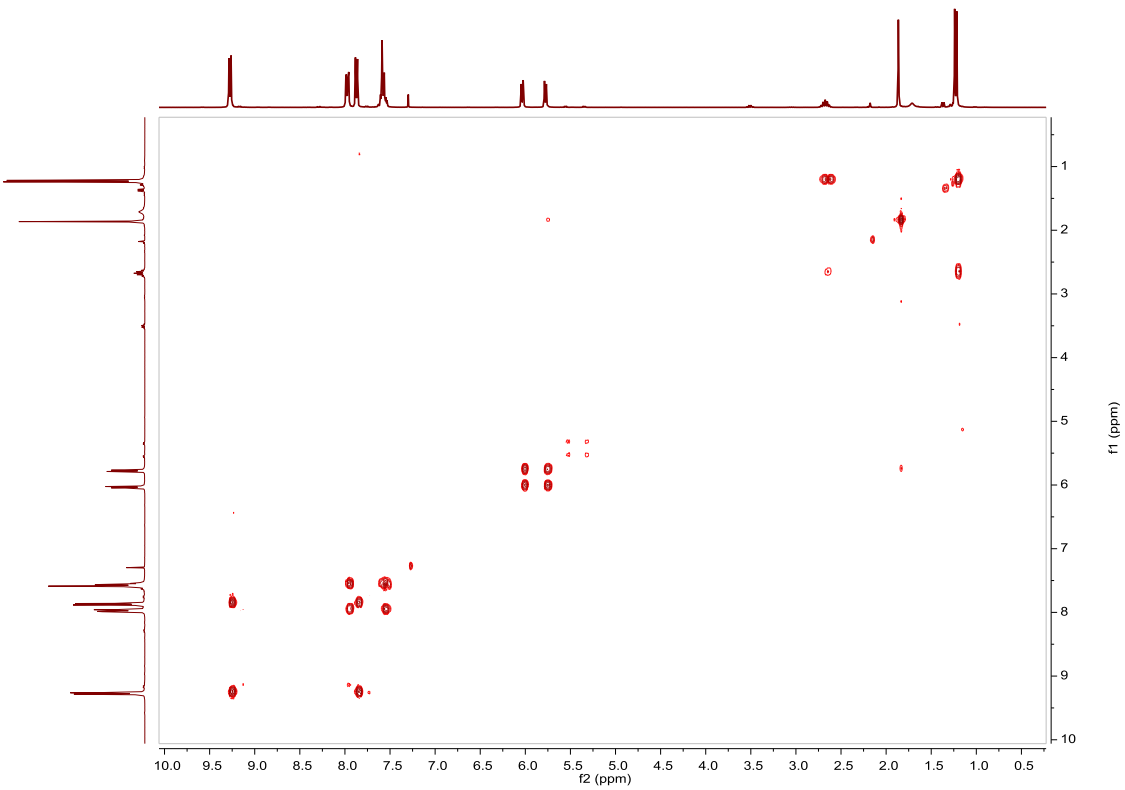

Fig. S362. COSY NMR spectrum of **[Ru(p-Cym)(4-phenylazopyridine)$_2$(Cl)]PF$_6$** in $CDCl_3$.

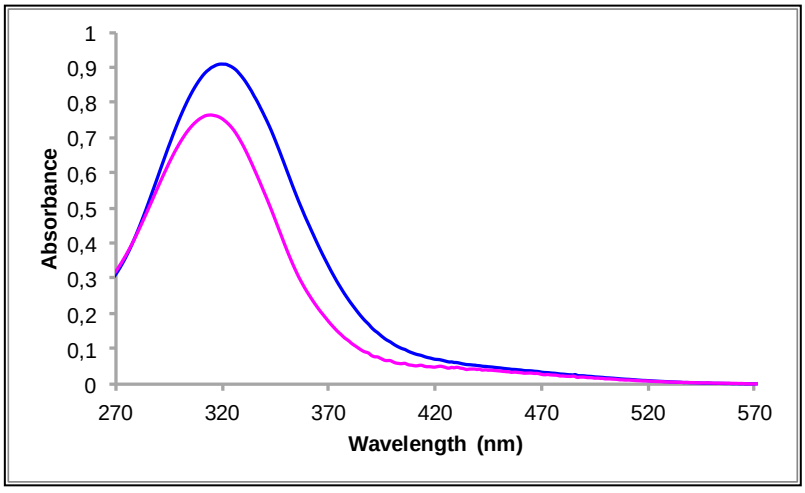

Fig. S363. UV/Vis spectra of **[Ru(p-Cym)(4-phenylazopyridine)$_2$(Cl)]PF$_6$** in ACN. Before (blue line) and after (pink line) irradiation at 347nm, $2.50 \cdot 10^{-5}$M.

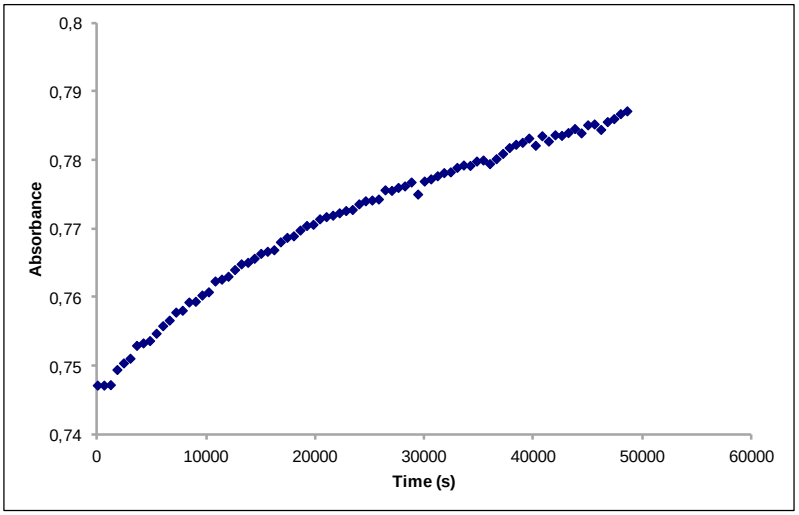

Fig. S364. Cis to trans thermal isomerization kinetics of **[Ru(p-Cym)(4-phenylazopyridine)$_2$(Cl)]PF$_6$**. Absorption change of the band 320nm at 338 K in ACN after irradiation at 347 nm. ($2.50\cdot10^{-5}$M).

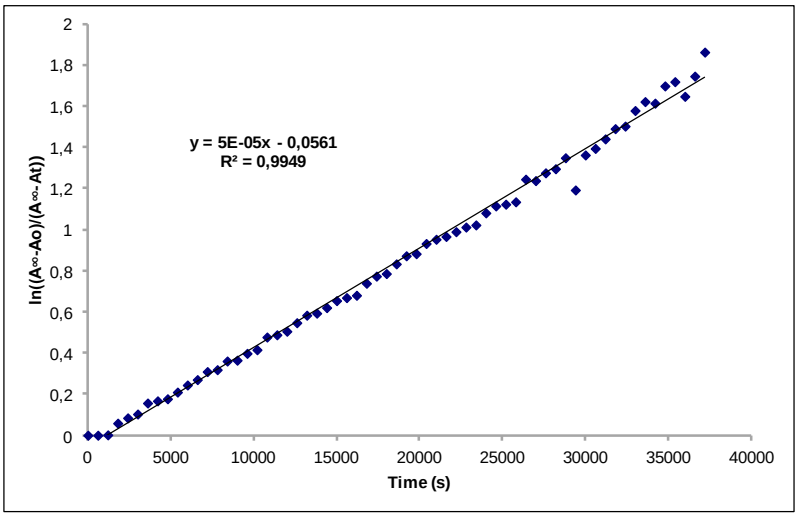

Fig. S365. Cis to trans thermal isomerization kinetics of **[Ru(p-Cym)(4-phenylazopyridine)$_2$(Cl)]PF$_6$**. First-order plot. k (s^{-1}) = $5.0\cdot10^{-5}$. Half-life (min) = 231.

Compound [Ru(p-Cym)(pyridine)$_1$(Cl)$_2$]. Synthesis and characterization.

SYNTHESIS

Under a N_2 atmosphere, Ru_2(p-Cym)$_2Cl_4$ (0.2 g, 0.32 mmol) and pyridine (53 µL, 0.65 mmol) were dissolved in 20 mL of acetone. The reaction mixture was refluxed for 15 h. It was cooled to room temperature, the solvent was evaporated and the product was obtained as an orange solid. Yield 89%. The spectroscopic data are coincident with those described in the literature.[43]

^{1}H NMR (300 MHz, CDCl$_3$): δ 9.09 (brdd, J = 1.5 Hz, J = 6.5 Hz, 2H, (2+6)), 7.78 (tt, J = 1.5 Hz, J = 7.6 Hz, 1H, (4)), 7.35 (t, J = 6.5 Hz, 2H, (3+5)), 5.48 (d, J = 5.9 Hz, 2H, (8)), 5.26 (d, J = 5.9 Hz, 2H, (7)), 3.04 (sep, J = 6.9 Hz, 1H, (11)), 2.14 (s, 3H, (13)), 1.35 (d, J = 6.9 Hz, 6H, (12)).

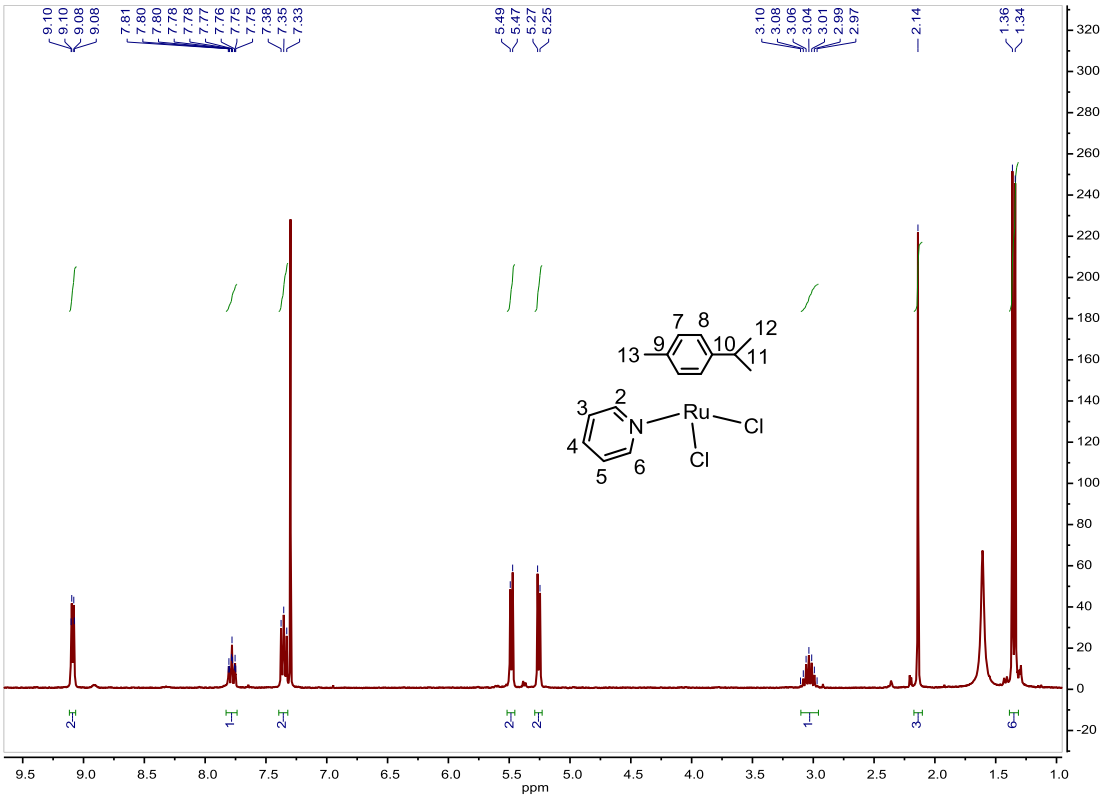

Fig. S366. ^{1}H NMR spectrum of **[Ru(p-Cym)(pyridine)$_1$(Cl)$_2$]** in $CDCl_3$, 300 MHz.

[43] C. A. Vock, C. Scolaro, A. D. Phillips, R. Scopelliti, G. Sava and P. J. Dyson, *J. Med. Chem.*, **2006**, *49*, 5552–5561.

Compound [Ru(p-Cym)(pyridine)$_2$(Cl)]PF$_6$. Synthesis and characterization.

SYNTHESIS[42]

Under a N_2 atmosphere, [Ru(p-Cym)(pyridine)(Cl_2)] (0.218 g, 0.566 mmol) and AgPF6 (0.142 g, 0.566 mmol) were dissolved in 15 mL of acetone and 15 mL of methanol. The mixture was stirred for 1 h, AgCl was removed by filtration and pyridine (0.05 mL, 0.623 mmol) were added. The reaction mixture was stirred for 4 h and the solvent was evaporated. The product was obtained as a yellow solid after precipitation with CH_2Cl_2/ether. Yield 45%.

Elemental Analysis: calculated for ($C_{20}H_{24}ClN_2RuPF_6 \cdot CH_2Cl_2$): C, 38.28; H, 3.98; N, 4.25. Found: C, 38.14; H, 4.00; N, 4.21.

Exact Mass: ESI-MS $[C_{15}H_{19}ClNRu]^+$ (M-L-PF_6): calculated: m/z= 350.0250, found: m/z= 350.0243.

^{1}H NMR (300 MHz, $CDCl_3$): δ 9.09 (brdd, J = 1.6 Hz, J = 6.6 Hz, 4H, (2+6)), 7.87 (tt, J = 1.5 Hz, J = 7.6 Hz, 2H, (4)), 7.54–7.47 (m, 4H, (3+5)), 5.94 (d, J = 6.1 Hz, 2H, (8)), 5.66 (d, J = 6.1 Hz, 2H, (7)), 2.59 (sep, J = 6.9 Hz, 1H, (11)), 1.76 (s, 3H, (13)), 1.19 (d, J = 6.9 Hz, 6H, (12)).

^{13}C NMR (75 MHz, $CDCl_3$): δ 154.14 (4CH, (2+6)), 139.03 (2CH, (4)), 126.23 (4CH, (3+5)), 102.72 (C_{quat}, (p-Cym)), 101.96 (C_{quat}, (p-Cym)), 88.71 (2CH, (8)), 81.97 (2CH, (7)), 30.83 (CH, (11)), 22.25 ($2CH_3$, (12)), 17.68 (CH_3, (13)).

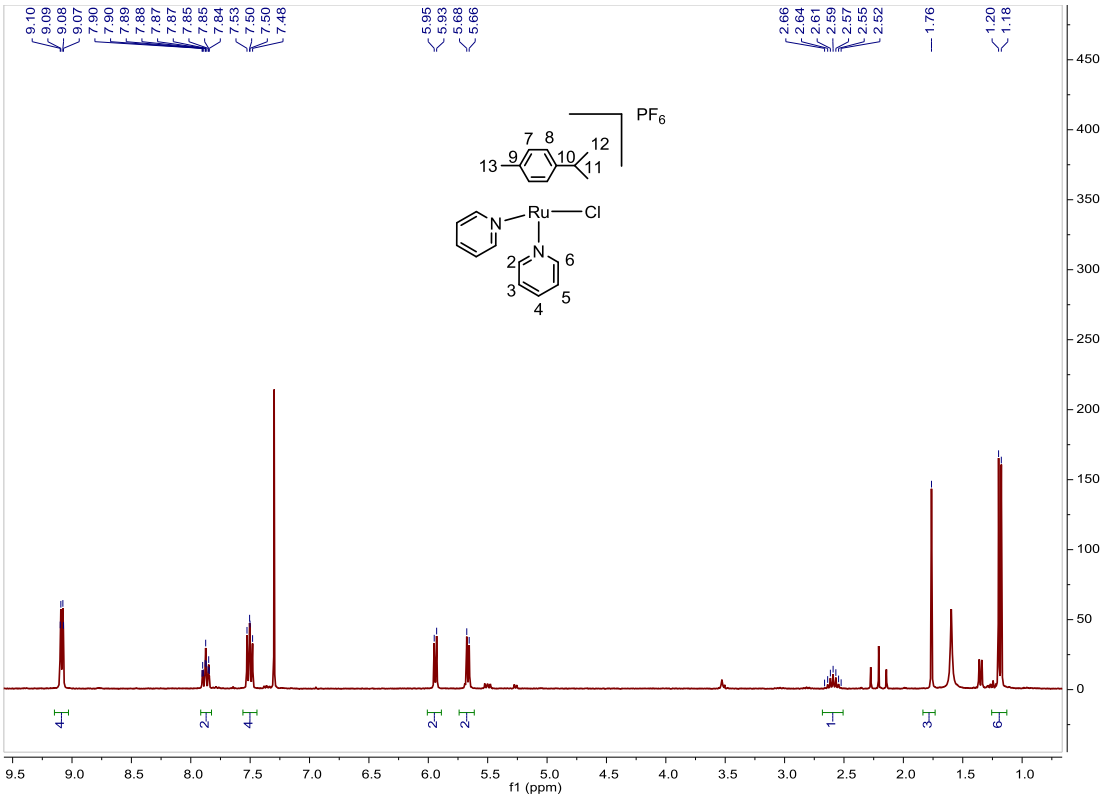

Fig. S367. ^{1}H NMR spectrum of **[Ru(p-Cym)(pyridine)$_2$(Cl)]PF$_6$** in $CDCl_3$, 300 MHz.

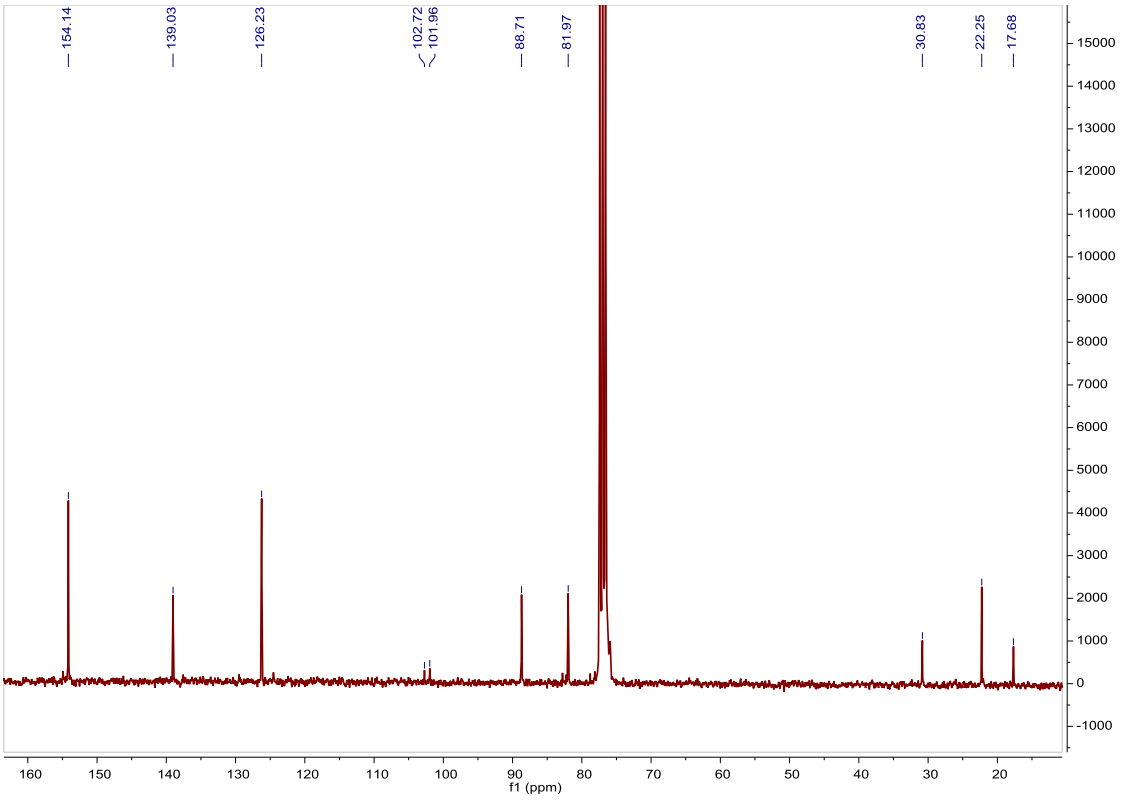

Fig. S368. ^{13}C NMR spectrum of **[Ru(p-Cym)(pyridine)$_2$(Cl)]PF$_6$** in $CDCl_3$, 75 MHz.

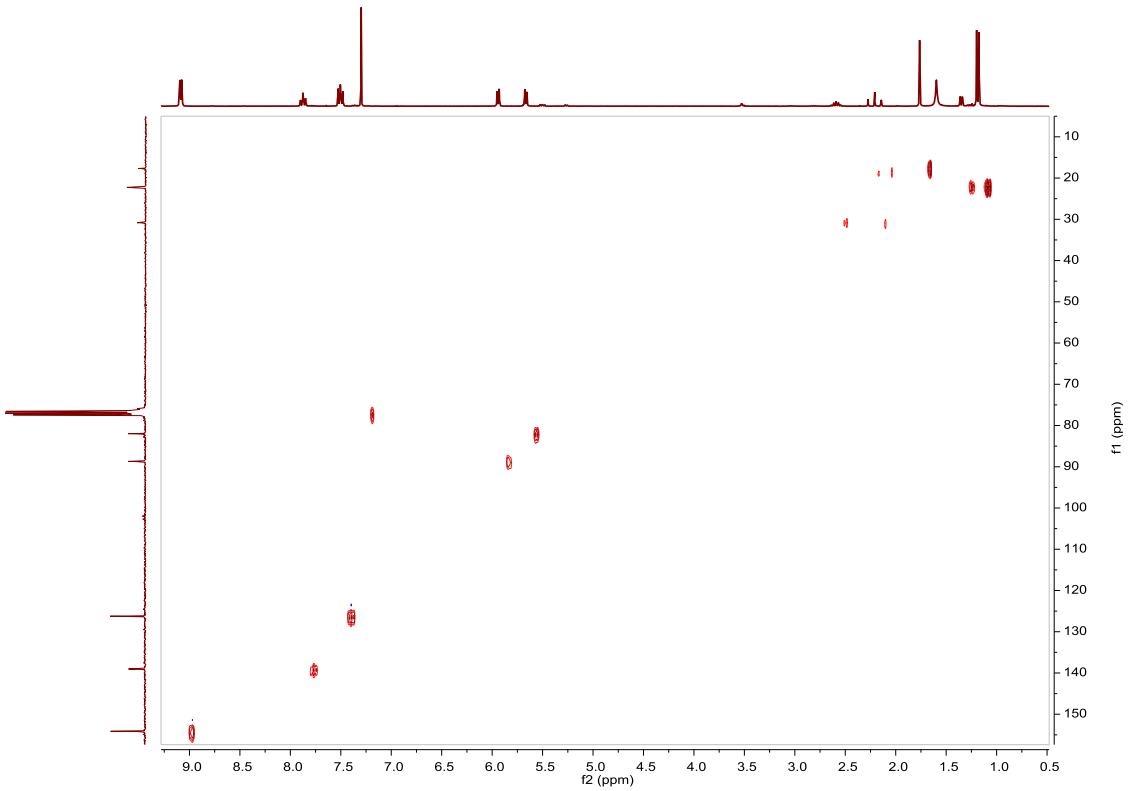

Fig. S369. HSQC NMR spectrum of **[Ru(p-Cym)(pyridine)$_2$(Cl)]PF$_6$** in $CDCl_3$.

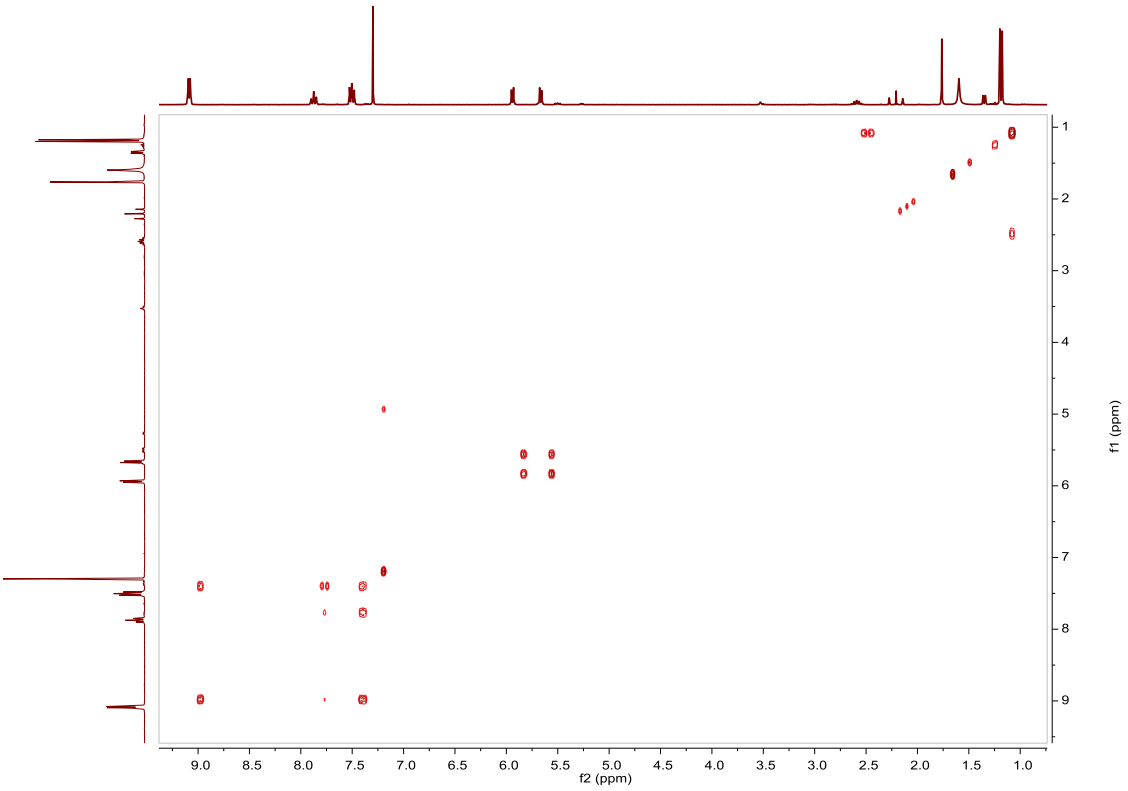

Fig. S370. COSY NMR spectrum of **[Ru(p-Cym)(pyridine)$_2$(Cl)]PF$_6$** in $CDCl_3$.

Compound [Ru(p-Cym)(4,4'-bis(*p*-azobenzene)-2,2'-bipyridine)(Cl)]Cl. Synthesis, characterization and photoisomerization studies.

SYNTHESIS

Under a N_2 atmosphere, $Ru_2(p\text{-}Cym)_2Cl_4$ (0.100 g, 0.163 mmol) and 4,4'-bis(*p*-azobenzene)-2,2'-bipyridine (0.168 g, 0.326 mmol) were dissolved in 10 mL of acetone. The reaction mixture was refluxed for 15 h. It was cooled to room temperature and the dark red solid was filtered. Yield 70%.

Elemental Analysis: calculated for ($C_{44}H_{38}Cl_2N_6Ru$): C, 64.23; H, 4.66; N, 10.21. Found: C, 63.79; H, 4.70; N, 10.13.

Exact Mass: ESI-MS $[C_{44}H_{38}ClN_6Ru]^+$: calculated: m/z= 787.1890, found: m/z= 787.1917.

^{1}H NMR (300 MHz, $CDCl_3$): δ 9.88 (brd, J = 5.5 Hz, 2H, (bipy)), 8.62 (s, 2H, (bipy)), 8.00 (m, 10H, (bipy)), 7.91 (brd, J = 7.9 Hz, 4H, (bipy)), 7.58–7.45 (m, 6H, (bipy)), 6.29 (d, J = 5.6 Hz, 2H, (8)), 6.16 (d, J = 5.4 Hz, 2H, (7)), 2.72 (sep, J = 6.8 Hz, 1H, (11)), 2.28 (s, 3H, (13)), 1.06 (d, J = 6.8 Hz, 6H, (12)).

^{13}C APT NMR (75 MHz, $CDCl_3$): δ 156.48 (2CH, (bipy)), 154.32 ($2C_{quat}$, (bipy)), 153.08 ($2C_{quat}$, (bipy)), 151.98 ($2C_{quat}$, (bipy)), 149.70 ($2C_{quat}$, (bipy)), 136.44 ($2C_{quat}$, (bipy)), 131.20(2CH, (bipy)), 128.70 (4CH, (bipy)), 128.11 (4CH, (bipy)), 125.02 (2CH, (bipy)), 123.35 (4CH, (bipy)), 122.66 (4CH, (bipy)), 120.27 (2CH, (bipy)), 104.46 (C_{quat}, (p-Cym)), 103.47 (C_{quat}, (p-Cym)), 86.87 (2CH, (8)), 84.38 (2CH, (7)), 30.66 (CH, (11)), 21.79 ($2CH_3$, (12)) 18.59 (CH_3, (13)).

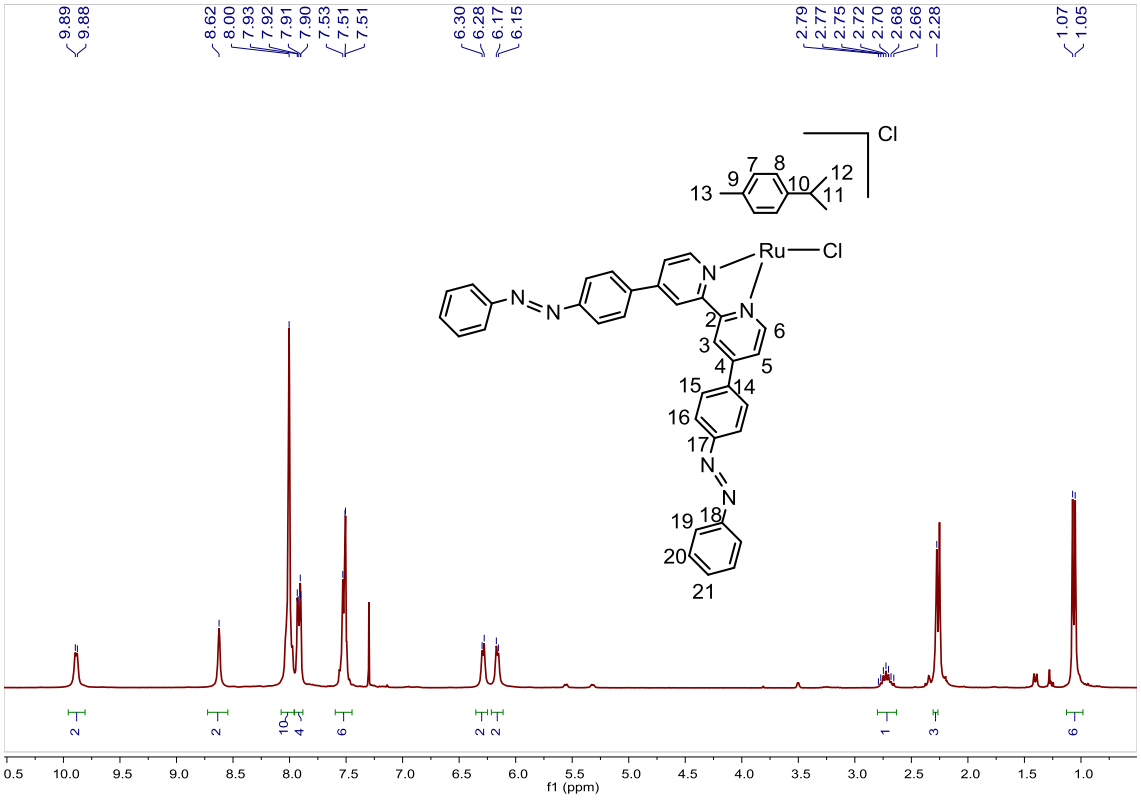

Fig. S371. ^{1}H NMR spectrum of **[Ru(p-Cym)(4,4'-bis(*p*-azobenzene)-2,2'-bipyridine)(Cl)]Cl** in $CDCl_3$, 300 MHz.

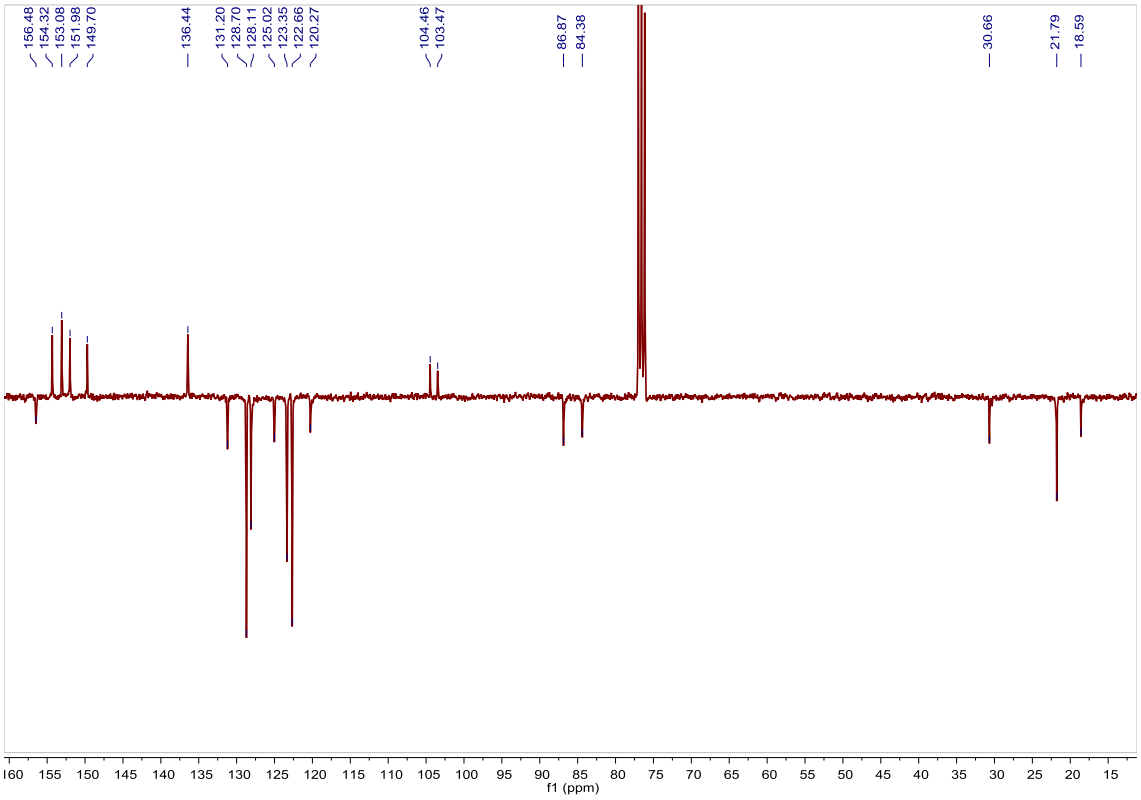

Fig. S372. ^{13}C APT NMR spectrum of **[Ru(p-Cym)(4,4'-bis(*p*-azobenzene)-2,2'-bipyridine)(Cl)]Cl** in $CDCl_3$, 75 MHz.

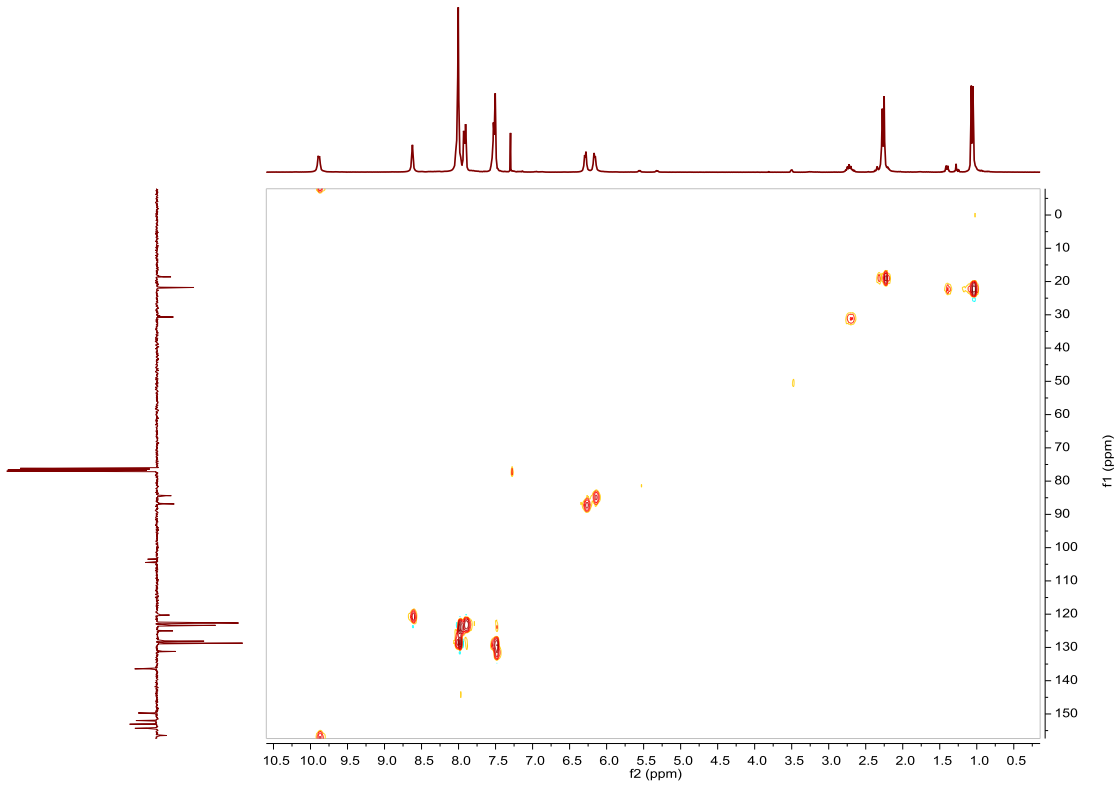

Fig. S373. HSQC spectrum of **[Ru(p-Cym)(4,4'-bis(*p*-azobenzene)-2,2'-bipyridine)(Cl)]Cl** in $CDCl_3$.

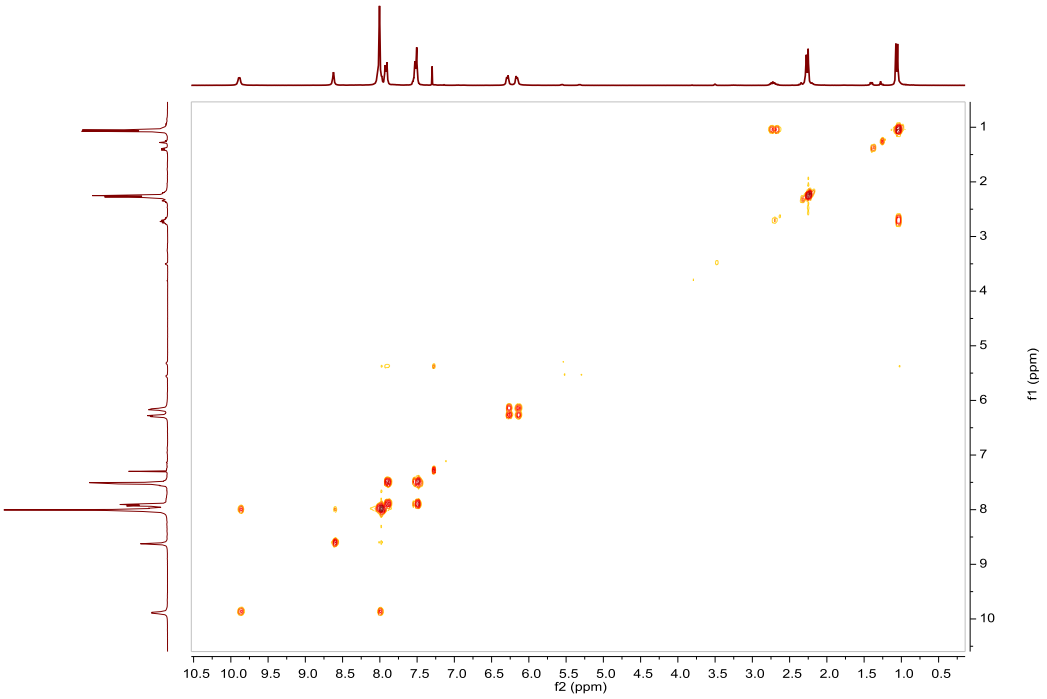

Fig. S374. COSY spectrum of **[Ru(p-Cym)(4,4'-bis(*p*-azobenzene)-2,2'-bipyridine)(Cl)]Cl** in $CDCl_3$.

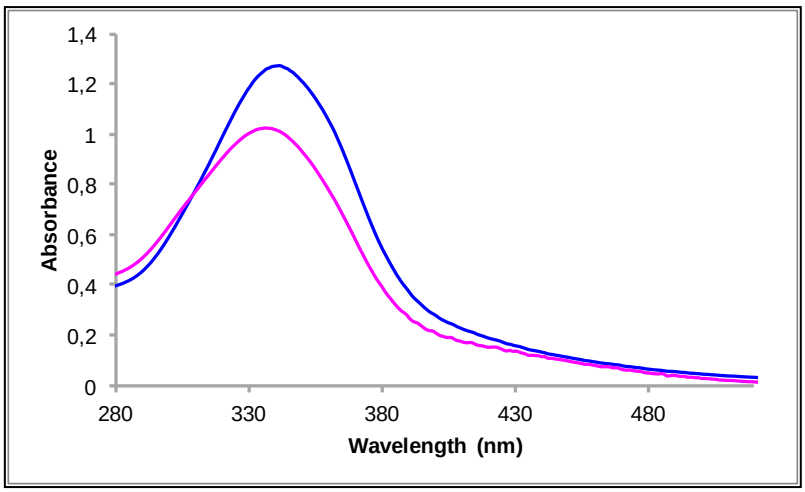

Fig. S375. UV/Vis spectra of **[Ru(p-Cym)(4,4'-bis(*p*-azobenzene)-2,2'-bipyridine)(Cl)]Cl** in ACN. Before (blue line) and after (pink line) irradiation at 350nm, $2.54 \cdot 10^{-5}$M.

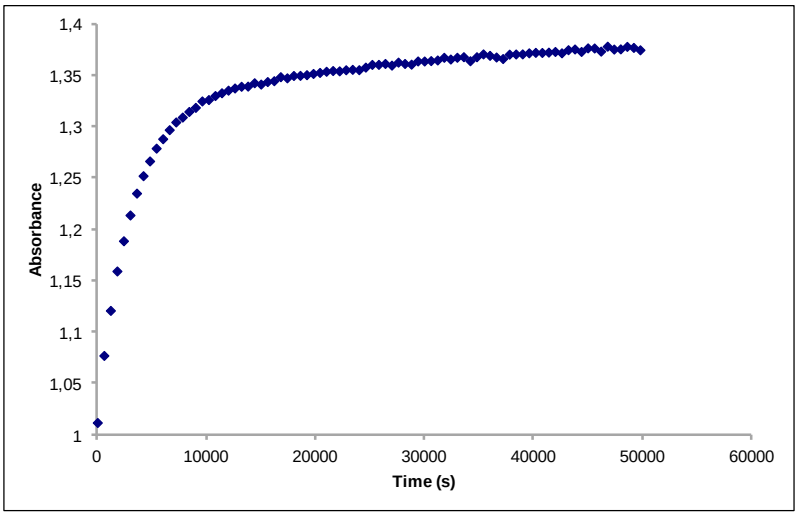

Fig. S376. Cis to trans thermal isomerization kinetics of **[Ru(p-Cym)(4,4'-bis(*p*-azobenzene)-2,2'-bipyridine)(Cl)]Cl**. Absorption change of the band 341nm at 338 K in ACN after irradiation at 350 nm. ($2.54 \cdot 10^{-5}$M).

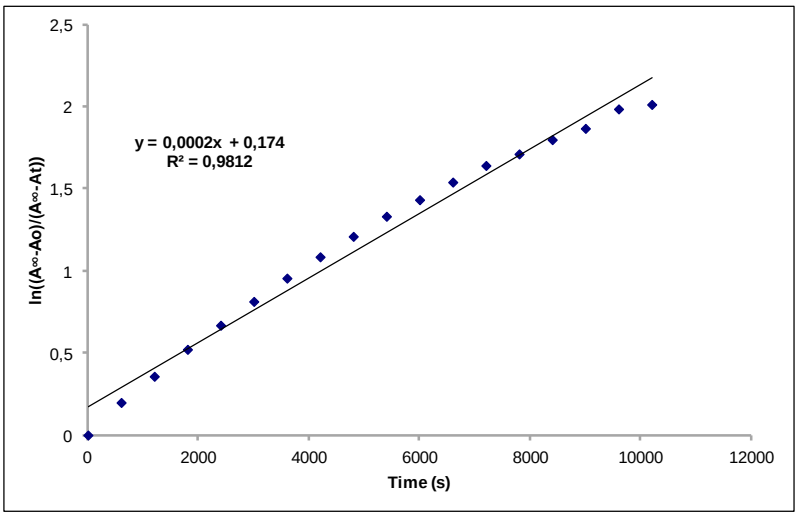

Fig. S377. Cis to trans thermal isomerization kinetics of **[Ru(p-Cym)(4,4'-bis(*p*-azobenzene)-2,2'-bipyridine)(Cl)]Cl**. First-order plot. k (s^{-1}) = $2.0 \cdot 10^{-4}$. Half-life (min) = 58.

Compound [Ru(p-Cym)(4-(*p*-azobenzene)-4'-bromo-2,2'-bipyridine)(Cl)]Cl. Synthesis, characterization and photoisomerization studies.

SYNTHESIS

Under a N_2 atmosphere, $Ru_2(p\text{-}Cym)_2Cl_4$ (0.100 g, 0.163 mmol) and 4-(*p*-azobenzene)-4'-bromo-2,2'-bipyridine (0.135 g, 0.326 mmol) were dissolved in 10 mL of acetone. The reaction mixture was refluxed for 15 h. It was cooled to room temperature and the solid was filtered. The desired compound was obtained after precipitated with CH_2Cl_2/Et_2O as an orange solid Yield 65%.

Elemental Analysis: calculated for ($C_{32}H_{29}BrCl_2N_4Ru{\cdot}CH_2Cl_2$): C, 49.15; H, 3.87; N, 6.95. Found: C, 49.04; H, 3.80; N, 6.77.

Exact Mass: ESI-MS $[C_{32}H_{29}BrClN_4Ru]^+$: calculated: m/z= 685.0308, found: m/z= 685.0334.

^{1}H NMR (300 MHz, MeOD *d_4*): δ 9.39 (d, J = 6.0 Hz, 1H, (bipy)), 9.20 (d, J = 6.1 Hz, 1H, (bipy)), 8.92 (brd, J = 1.8 Hz, 1H, (bipy)), 8.76 (brd, J = 1.5 Hz, 1H, (bipy)), 8.12–7.94 (m, 5H, (bipy)), 7.93–7.80 (m, 3H, (bipy)), 7.52–7.40 (m, 3H, (bipy)), 6.04 (m, 2H, (8+8')), 5.80 (m, 2H, (7+7')), 2.59 (sep, J = 6.9 Hz, 1H, (11)), 2.17 (s, 3H, (13)), 0.99 (d, J = 6.8 Hz, 6H, (12)).

^{13}C APT NMR (75 MHz, MeOD *d_4*): δ 157.24 (C_{quat}, (bipy)), 157.11 (CH, (bipy)), 156.98 (CH, (bipy)), 155.79 (C_{quat}, (bipy)), 155.11 (C_{quat}, (bipy)), 153.96 (C_{quat}, (bipy)), 152.07 (C_{quat}, (bipy)), 138.53 (C_{quat}, (bipy)), 138.05 (C_{quat}, (bipy)), 132.97 (CH, (bipy)), 132.11 (CH, (bipy)), 130.41 (2CH, (bipy)), 129.85 (2CH, (bipy)), 128.83 (CH, (bipy)), 126.43 (CH, (bipy)), 124.77 (2CH, (bipy)), 124.08 (2CH, (bipy)), 122.93 (CH, (bipy)), 106.64 (Cquat, (p-Cym)), 105.62 (Cquat, (p-Cym)), 88.21 (CH, (8 or 8')), 88.00 (CH, (8 or 8')), 85.87 (CH, (7 or 7')), 85.68 (CH, (7 or 7')), 32.41 (CH, (11)), 22.37 ($2CH_3$, (12)), 18.97 (CH_3, (13)).

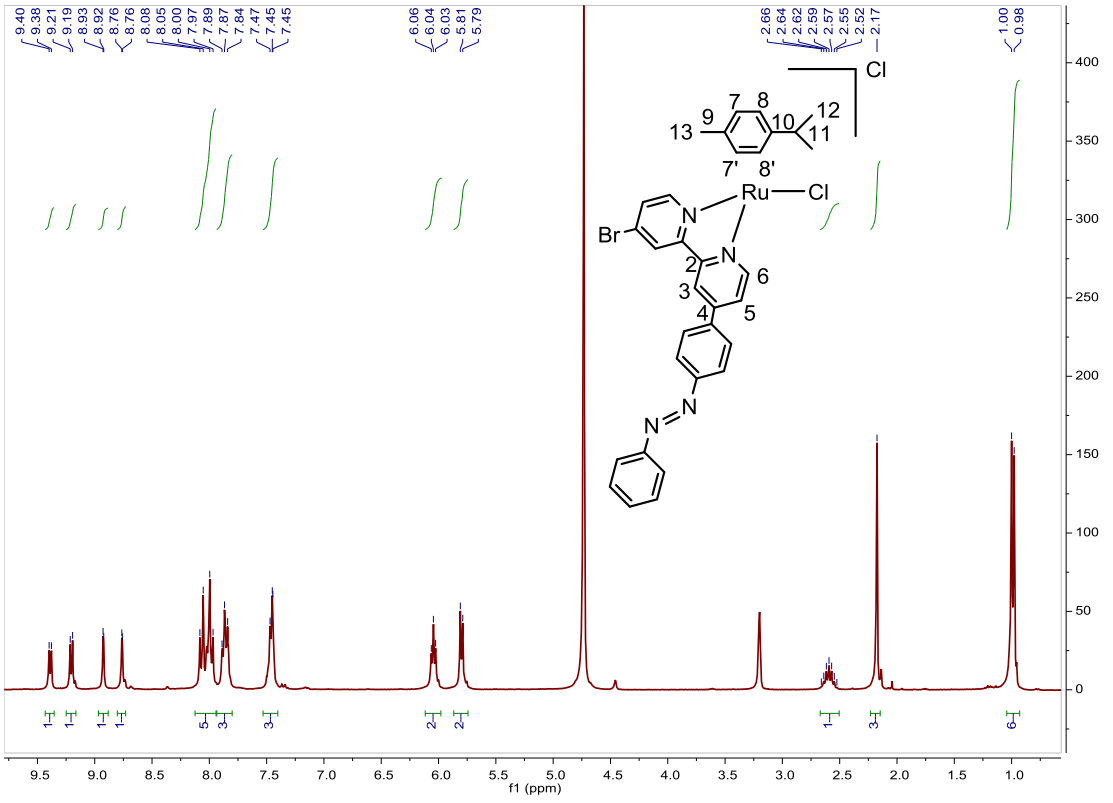

Fig. S378. ^{1}H NMR spectrum of **[Ru(p-Cym)(4-(*p*-azobenzene)-4'-bromo-2,2'-bipyridine)(Cl)]Cl** in MeOD-*d_4*, 300 MHz.

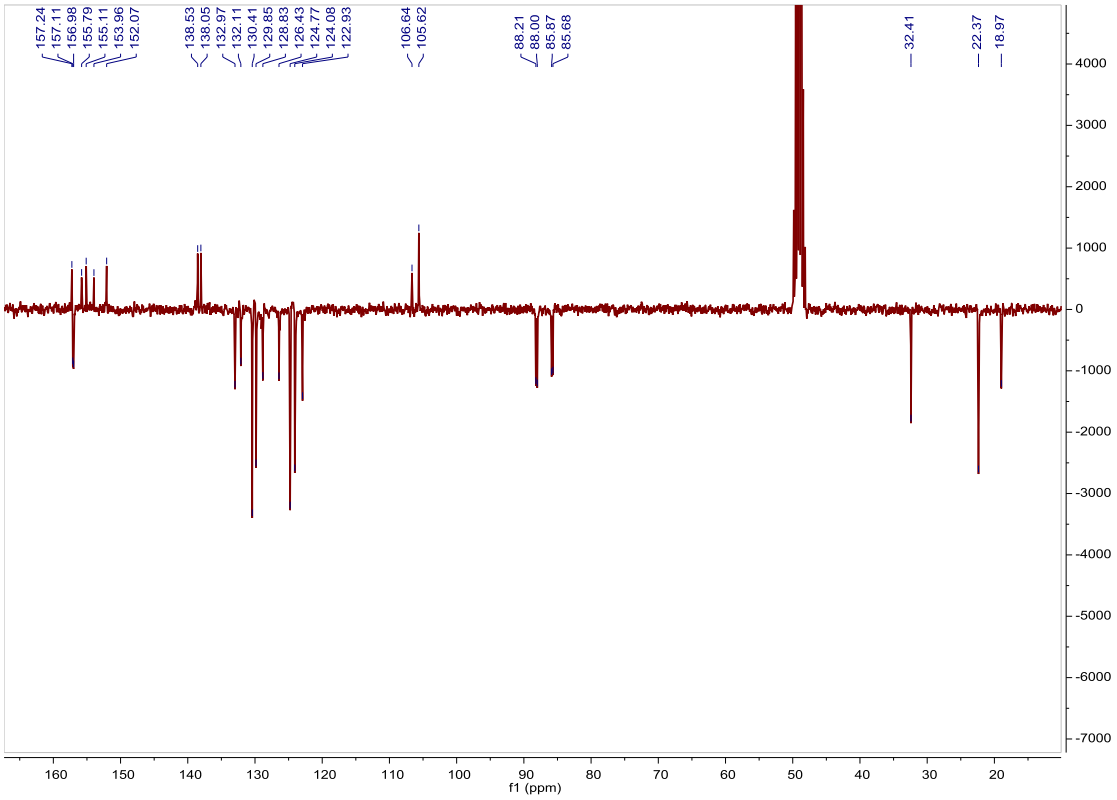

Fig. S379. ^{13}C APT NMR spectrum of **[Ru(p-Cym)(4-(*p*-azobenzene)-4'-bromo-2,2'-bipyridine)(Cl)]Cl** in MeOD-d_4, 75 MHz.

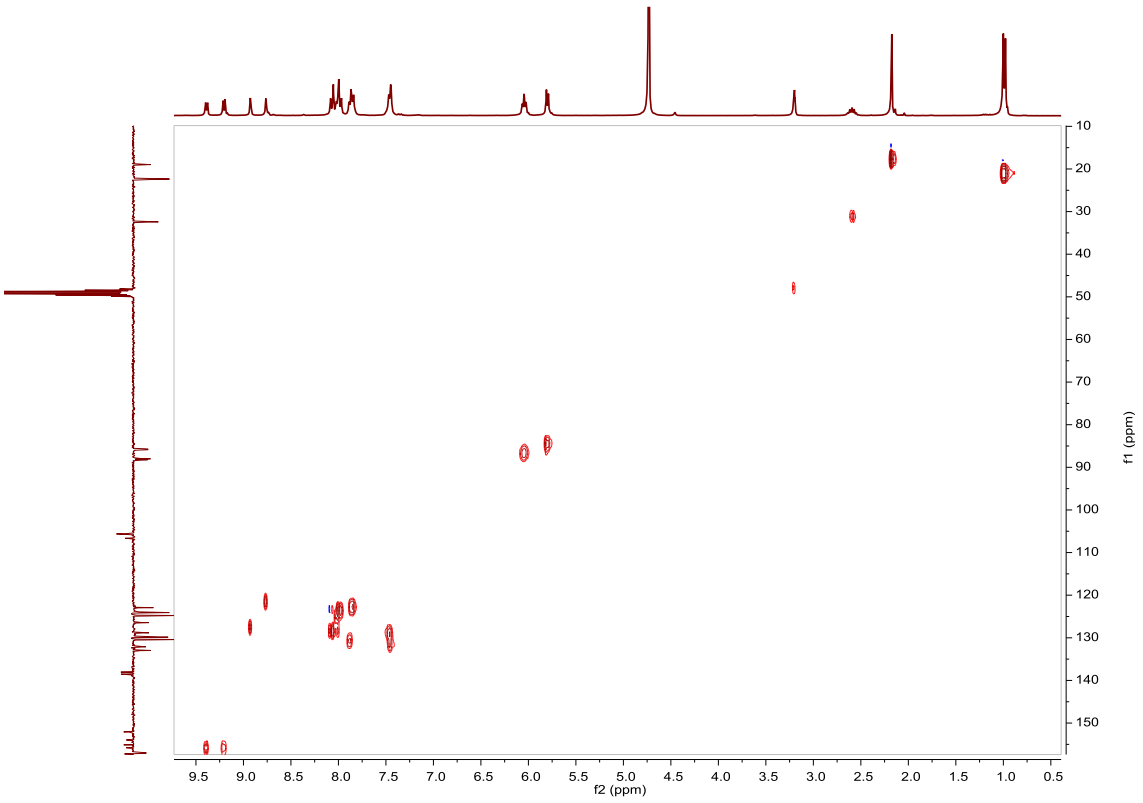

Fig. S380. HSQC NMR spectrum of **[Ru(p-Cym)(4-(*p*-azobenzene)-4'-bromo-2,2'-bipyridine)(Cl)]Cl** in MeOD-d_4.

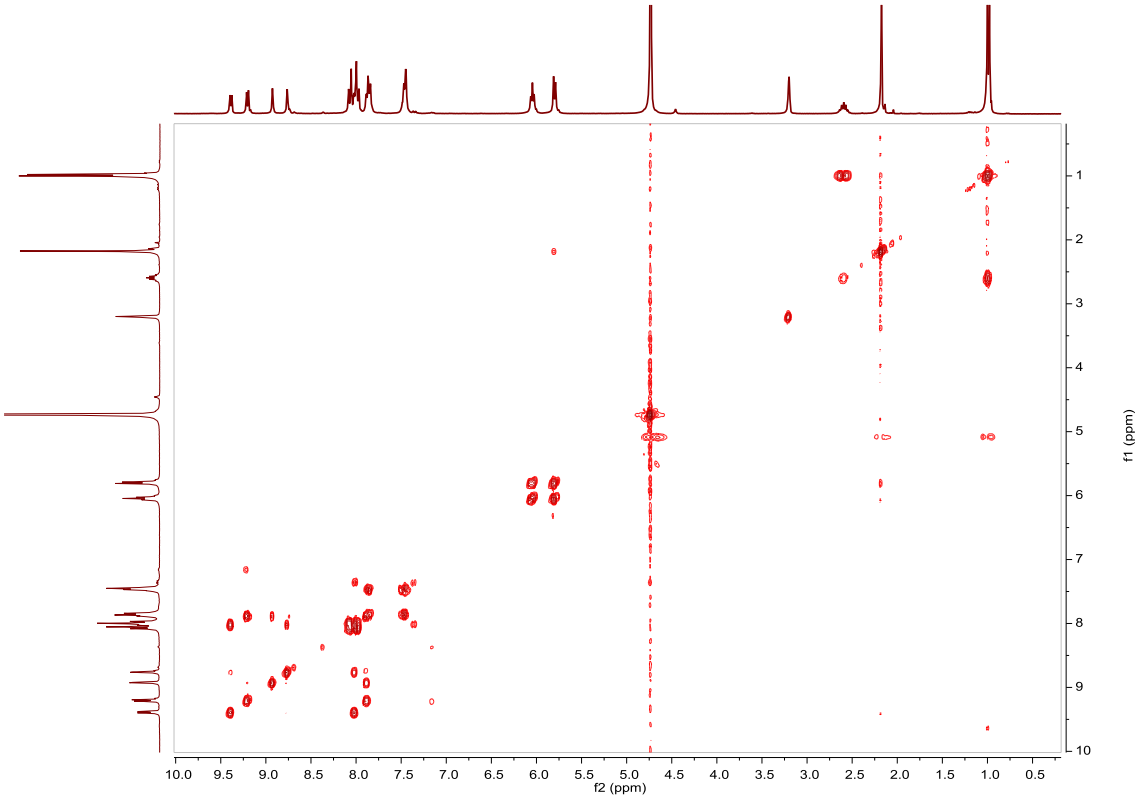

Fig. S381. COSY NMR spectrum of **[Ru(p-Cym)(4-(*p*-azobenzene)-4'-bromo-2,2'-bipyridine)(Cl)]Cl** in MeOD-d_4.

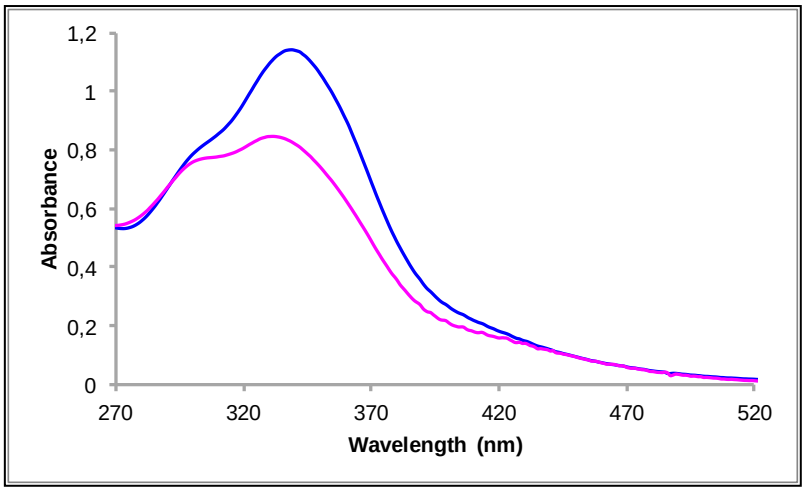

Fig. S382. UV/Vis spectra of **[Ru(p-Cym)(4-(*p*-azobenzene)-4'-bromo-2,2'-bipyridine)(Cl)]Cl** in ACN. Before (blue line) and after (pink line) irradiation at 344nm, $3.09 \cdot 10^{-5}$M.

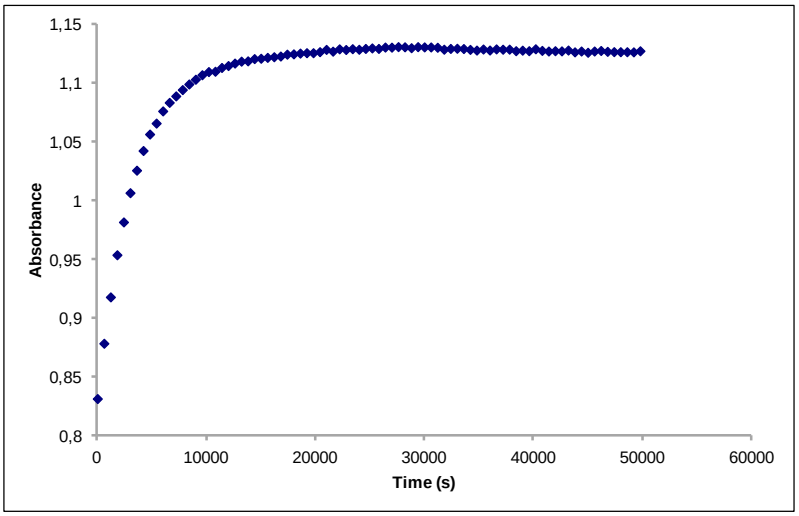

Fig. S383. Cis to trans thermal isomerization kinetics of **[Ru(p-Cym)(4-(*p*-azobenzene)-4'-bromo-2,2'-bipyridine)(Cl)]Cl**. Absorption change of the band 338nm at 338 K in ACN after irradiation at 344 nm. ($3.09 \cdot 10^{-5}$M).

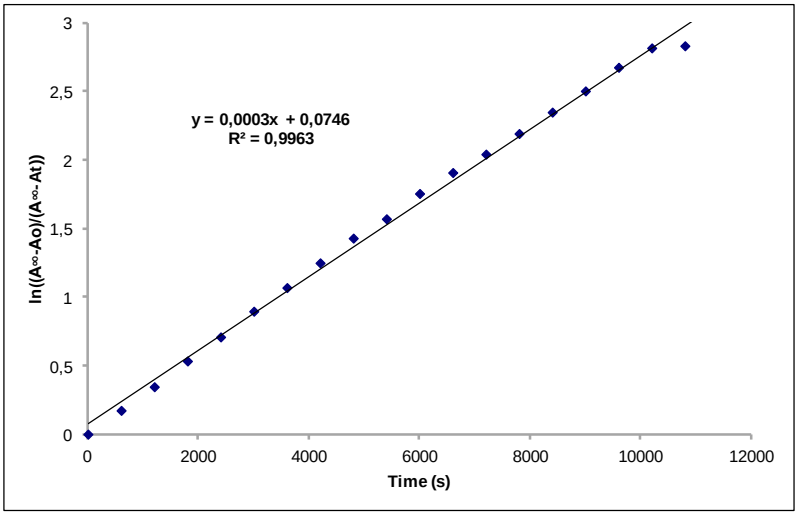

Fig. S384. Cis to trans thermal isomerization kinetics of **[Ru(p-Cym)(4-(*p*-azobenzene)-4'-bromo-2,2'-bipyridine)(Cl)]Cl**. First-order plot. k (s^{-1}) = $3.0 \cdot 10^{-4}$. Half-life (min) = 38.

Compound [Ru(p-Cym)(4,4'-bis(*m*-azobenzene)-2,2'-bipyridine)(Cl)]Cl. Synthesis, characterization and photoisomerization studies.

SYNTHESIS

Under a N_2 atmosphere, $Ru_2(p\text{-}Cym)_2Cl_4$ (0.100 g, 0.163 mmol) and 4,4'-bis(*m*-azobenzene)-2,2'-bipyridine (0.168 g, 0.326 mmol) were dissolved in 10 mL of acetone. The reaction mixture was refluxed for 15 h and ,4'-bis(*m*-azobenzene)-2,2'-bipyridine (0.168 g, 0.326 mmol) were added. It was refluxed for another 15 h. It was cooled to room temperature and the solid was filtered. The desired compound was obtained after precipitated with CH_2Cl_2/Et_2O as a brown solid. Yield 54%.

Elemental Analysis: calculated for ($C_{44}H_{38}Cl_2N_6Ru{\cdot}CH_2Cl_2$): C, 59.54; H, 4.44; N, 9.26. Found: C, 58.94; H, 4.43; N, 9.03.

Exact Mass: ESI-MS $[C_{44}H_{38}ClN_6Ru]^+$: calculated: m/z= 787.1890, found: m/z= 787.1920.

^{1}H NMR (300 MHz, $CDCl_3$): δ 9.98 (s, 2H, (bipy)), 8.51 (s, 2H, (bipy)), 8.26 (s, 2H, (bipy)), 8.13–7.86 (m, 10H, (bipy)), 7.71 (t, J = 7.2 Hz, 2H, (bipy)), 7.55–7.45 (m, 6H, (bipy)), 6.38 (s, 2H, (7 or 8)), 6.23 (s, 2H, (7 or 8)), 2.79 (m, 1H, (11)), 2.32 (s, 3H, (13)), 1.12 (d, J = 6.4 Hz, 6H, (12)).

^{13}C APT NMR (75 MHz, $CDCl_3$): δ 156.88 (2CH, (bipy)), 154.36 ($2C_{quat}$, (bipy)), 152.64 ($2C_{quat}$, (bipy)), 151.84 ($2C_{quat}$, (bipy)), 150.30 ($2C_{quat}$, (bipy)), 135.76 ($2C_{quat}$, (bipy)), 131.19 (2CH, (bipy)), 130.10 (2CH, (bipy)), 129.50 (2CH, (bipy)), 128.75 (4CH, (bipy)), 125.47 (2CH, (bipy)), 124.69 (2CH, (bipy)), 122.61 (4CH, (bipy)), 121.02 (2CH, (bipy)), 120.24 (2CH, (bipy)), 104.47 (Cquat, (p-Cym)), 103.84 (Cquat, (p-Cym)), 87.18 (2CH, (7 or 8)), 84.50 (2CH, (7 or 8)), 30.76 (CH, (11)), 21.86 ($2CH_3$, (12)), 18.72 (CH_3, (13)).

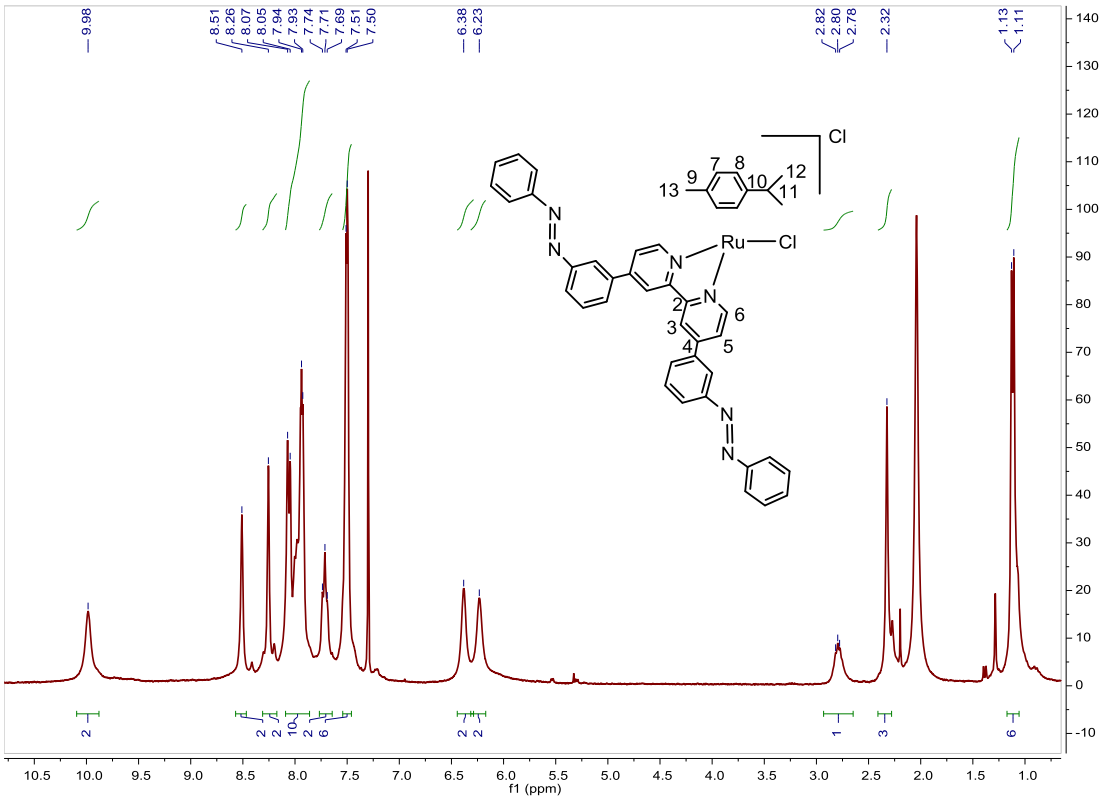

Fig. S385. ^{1}H NMR spectrum of **[Ru(p-Cym)(4,4'-bis(*m*-azobenzene)-2,2'-bipyridine)(Cl)]Cl** in $CDCl_3$, 300 MHz.

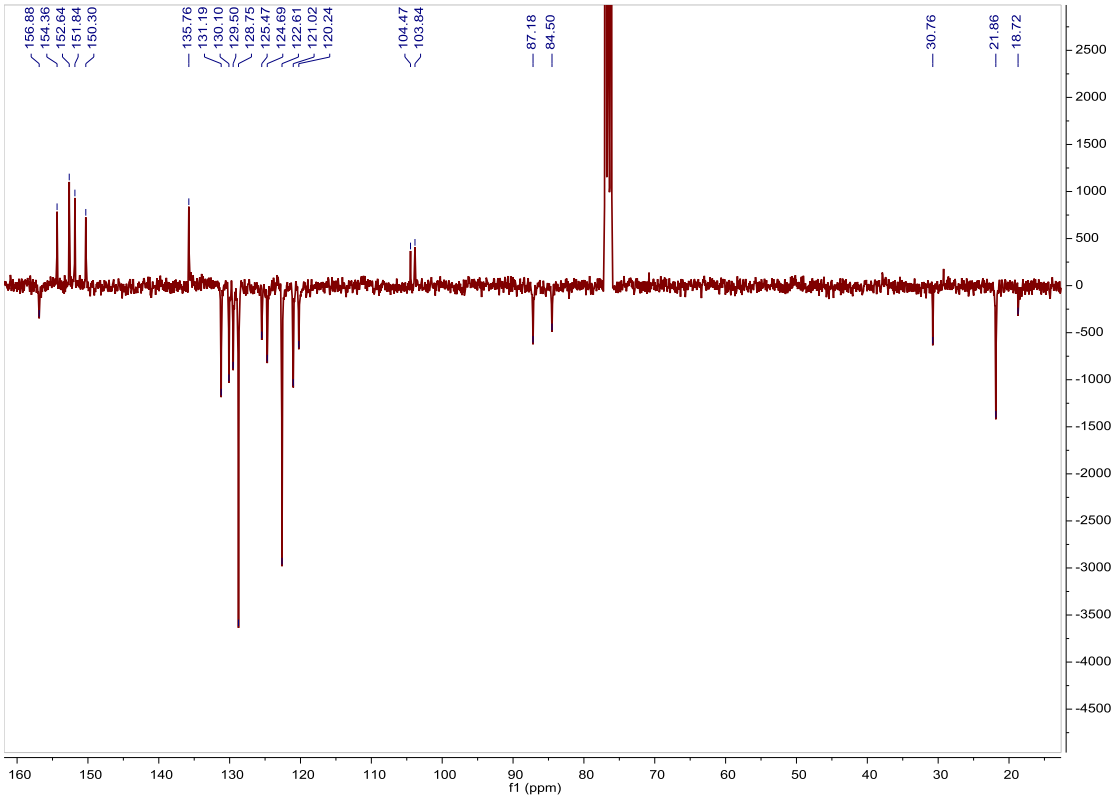

Fig. S386. ^{13}C APT NMR spectrum of **[Ru(p-Cym)(4,4'-bis(*m*-azobenzene)-2,2'-bipyridine)(Cl)]Cl** in $CDCl_3$, 75 MHz.

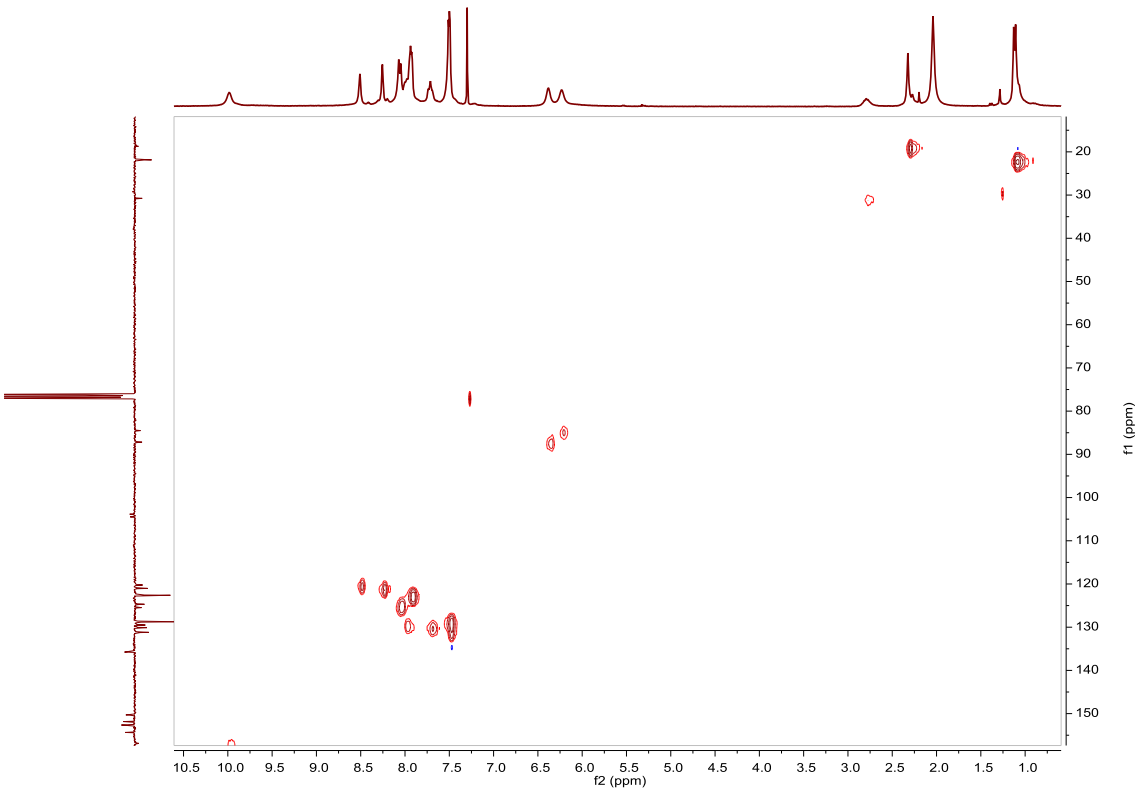

Fig. S387. HSQC NMR spectrum of **[Ru(p-Cym)(4,4'-bis(*m*-azobenzene)-2,2'-bipyridine)(Cl)]Cl** in $CDCl_3$.

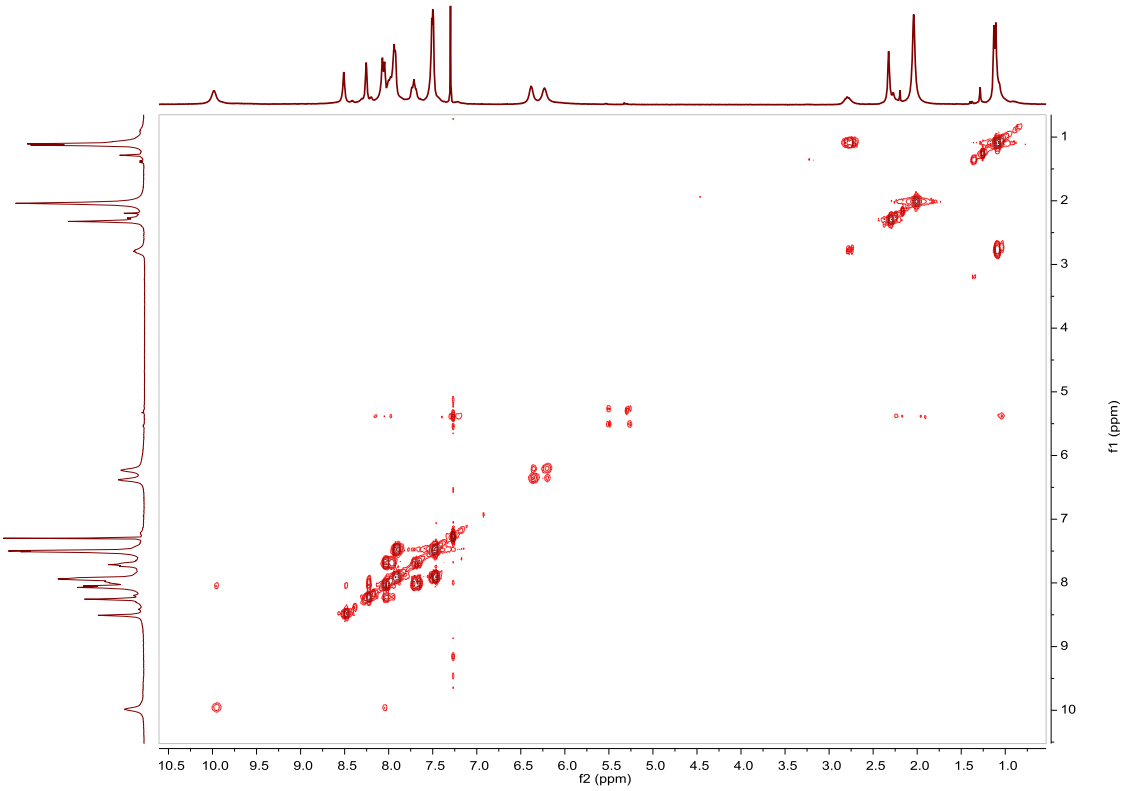

Fig. S388. COSY NMR spectrum of **[Ru(p-Cym)(4,4'-bis(*m*-azobenzene)-2,2'-bipyridine)(Cl)]Cl** in $CDCl_3$.

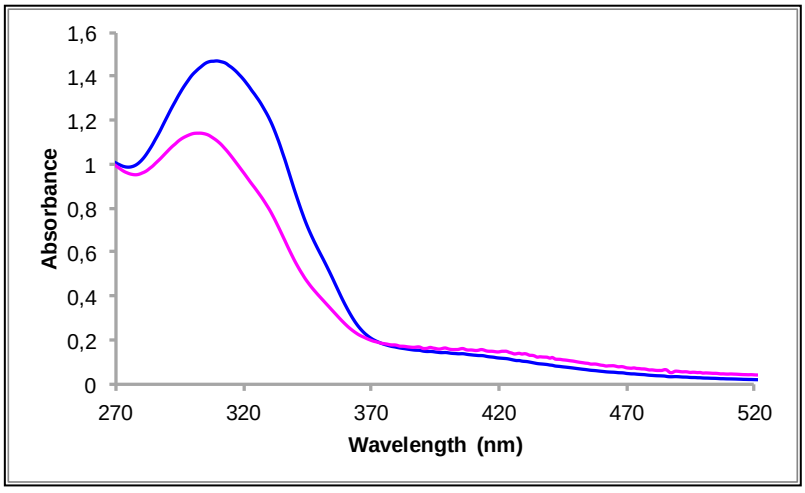

Fig. S389. UV/Vis spectra of **[Ru(p-Cym)(4,4'-bis(*m*-azobenzene)-2,2'-bipyridine)(Cl)]Cl** in ACN. Before (blue line) and after (pink line) irradiation at 322nm, $2.61 \cdot 10^{-5}$M.

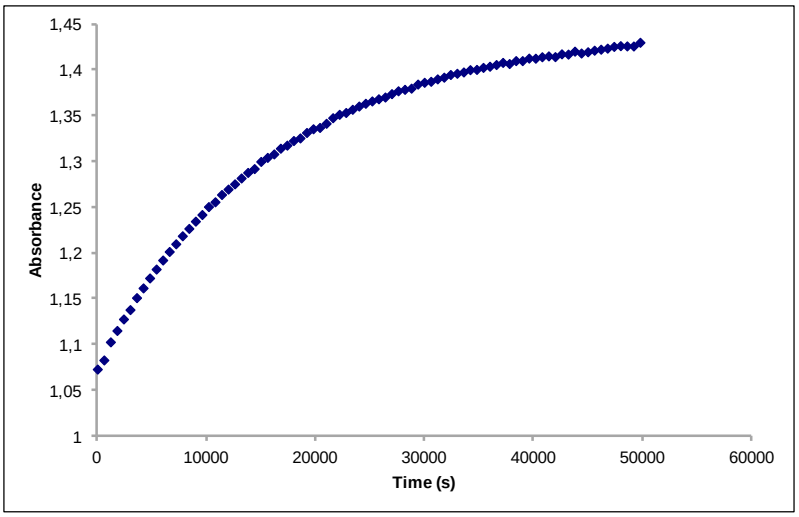

Fig. S390. Cis to trans thermal isomerization kinetics of **[Ru(p-Cym)(4,4'-bis(*m*-azobenzene)-2,2'-bipyridine)(Cl)]Cl**. Absorption change of the band 309nm at 338 K in ACN after irradiation at 322 nm. ($2.61 \cdot 10^{-5}$M).

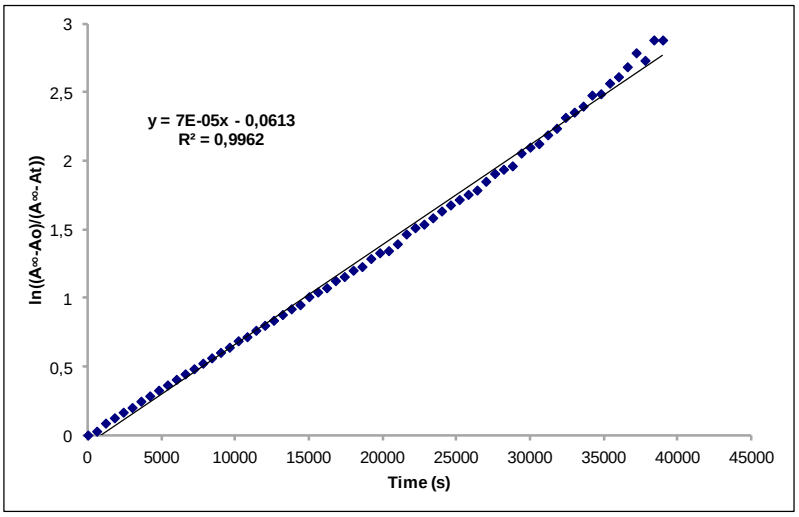

Fig. S391. Cis to trans thermal isomerization kinetics of **[Ru(p-Cym)(4,4'-bis(*m*-azobenzene)-2,2'-bipyridine)(Cl)]Cl**. First-order plot. k (s^{-1}) = $7.0 \cdot 10^{-5}$. Half-life (min) = 165.

Compound [Ru(p-Cym)(tris(*m*-phenylazobenzene)phosphine)(Cl)$_2$]. Synthesis, characterization and photoisomerization studies.

SYNTHESIS

Under a N_2 atmosphere, $Ru_2(p\text{-}Cym)_2Cl_4$ (0.100 g, 0.163 mmol) and tris(*m*-phenylazobenzene)phosphine (0.206 g, 0.359 mmol) were dissolved in 27 mL of hexane. The reaction mixture was refluxed for 15 h. It was cooled to room temperature and the solvent was evaporated. The desired compound was obtained after precipitation with CH_2Cl_2/ether as a red solid. Yield 90%.

Elemental Analysis: calculated for ($C_{46}H_{41}Cl_2N_6PRu$): C, 62.73; H, 4.69; N, 9.54. Found: C, 62.72; H, 4.96; N, 9.28.

Exact Mass: ESI-MS [M-2Cl+H]: calculated: m/z= 811.2252, found: m/z= 811.2248.

^{1}H NMR (300 MHz, $CDCl_3$): δ 8.48 (d, J = 11.0 Hz, 3H, (6)), 8.11 (t, J = 8.7 Hz, 3H, (2)), 7.90 (d, J = 7.0 Hz, 3H, (4)), 7.79 (m, 6H, (15)), 7.48 (ddd, J = 2.5 Hz, J = 7.7 Hz, J = 10.2 Hz, 3H, (3)), 7.38 (m, 9H, (16+17)), 5.27 (d, J = 6.1 Hz, 2H, (8)), 5.09 (d, J = 5.6 Hz, 2H, (7)), 2.81 (sep, J = 6.9 Hz, 1H, (11)), 1.88 (s, 3H, (13)), 1.04 (d, J = 6.9 Hz, 6H, (12)).

^{13}C APT NMR (75 MHz, $CDCl_3$): δ 151.94 (s, C_{quat}), 151.57 (d, J = 9.7 Hz, C_{quat}), 136.70 (d, J = 9.7 Hz, 3CH, (2)), 134.33 (d, J = 45.0 Hz, C_{quat}), 130.89 (s, 3CH, (17)), 128.98 (s, 3CH, (3)), 128.85 (d, J = 4.5 Hz, 3CH, (6)), 128.59 (s, 6CH, (16)), 123.44 (s, 3CH, (4)), 122.57(s, 6CH, (15)), 110.91 (s, C_{quat}), 96.54 (s, C_{quat}), 88.63 (s, 2CH, (7)), 87.07 (d, J = 5.2 Hz, 2CH, (8)), 29.87 (s, CH, (11)), 21.54 (s, $2CH_3$, (12)), 17.42 (s, CH_3, (13)).

^{31}P NMR (202 MHz, $CDCl_3$): δ 28.18 (s, 1P).

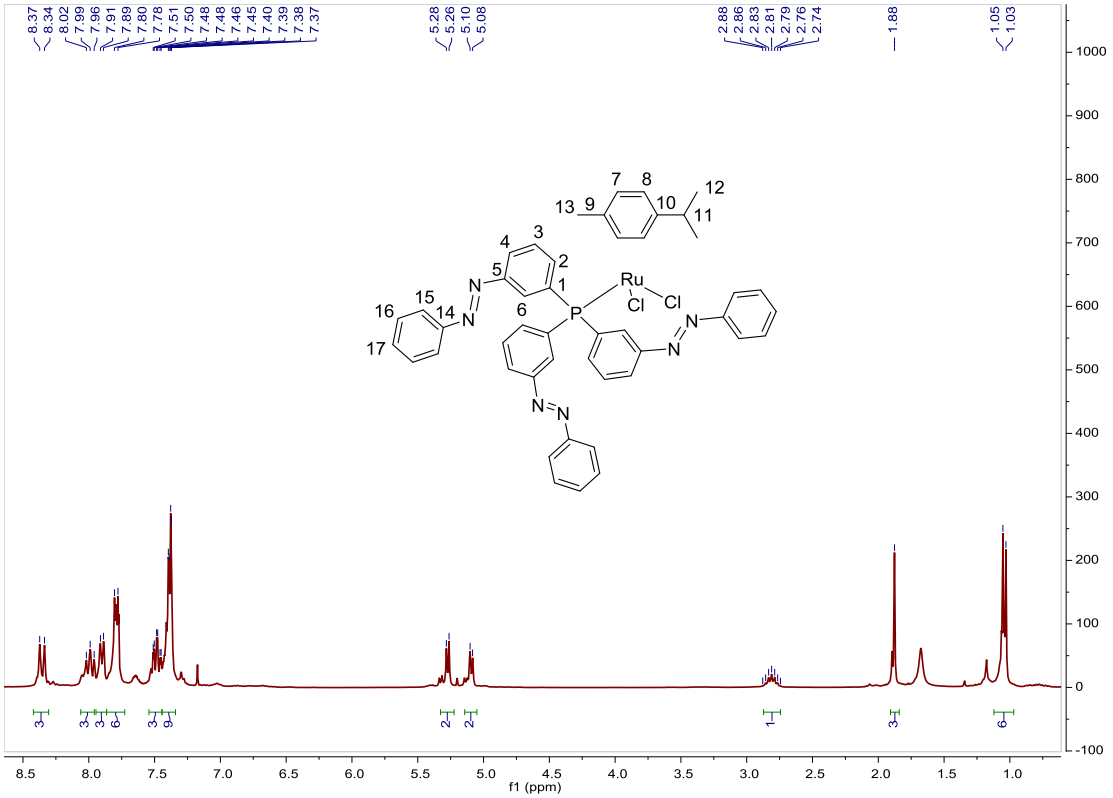

Fig. S392. ^{1}H NMR spectrum of **[Ru(p-Cym)(tris(*m*-phenylazobenzene)phosphine)(Cl)$_2$]** in $CDCl_3$, 300 MHz.

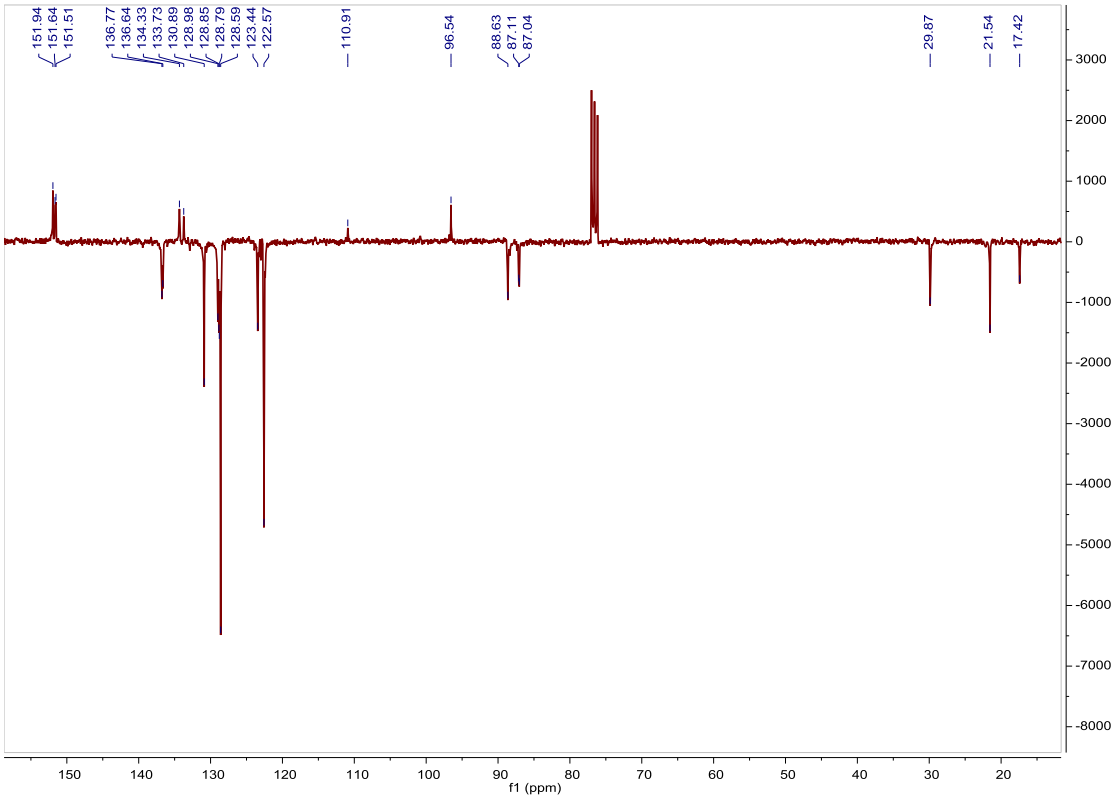

Fig. S393. ^{13}C APT NMR spectrum of **[Ru(p-Cym)(tris(*m*-phenylazobenzene)phosphine)(Cl)$_2$]** in $CDCl_3$, 75 MHz.

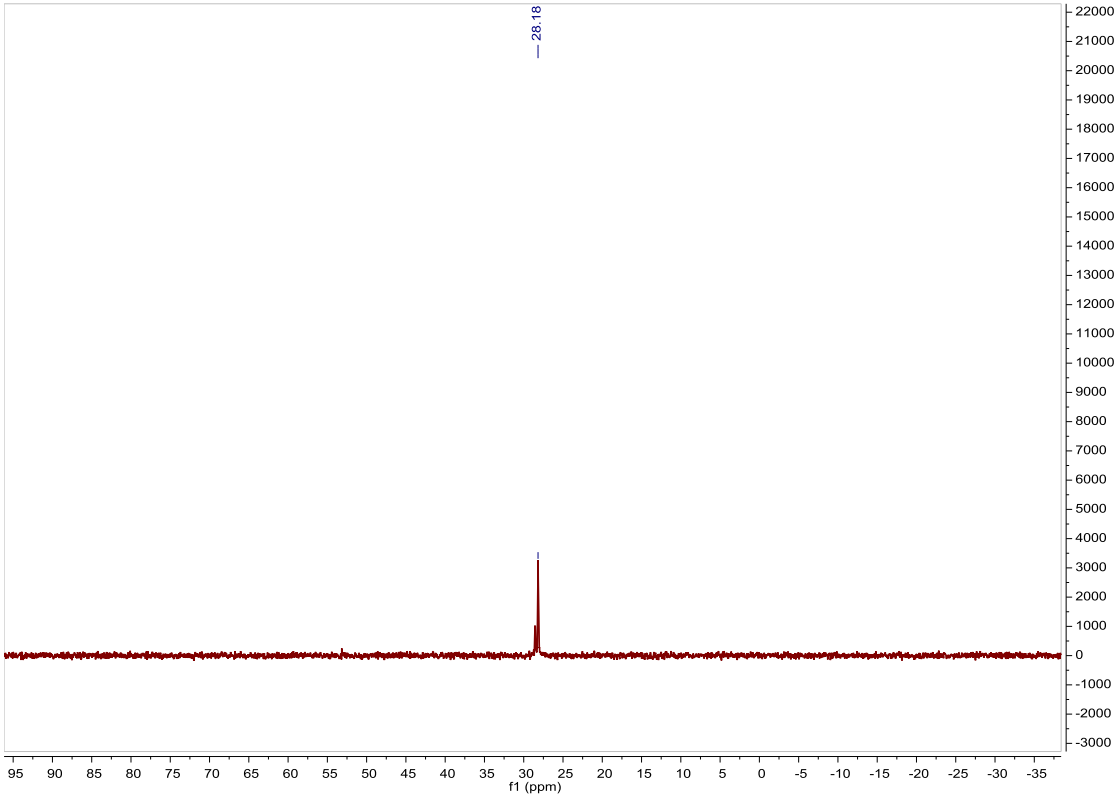

Fig. S394. ^{31}P NMR spectrum of **[Ru(p-Cym)(tris(*m*-phenylazobenzene)phosphine)(Cl)$_2$]** in $CDCl_3$, 202 MHz.

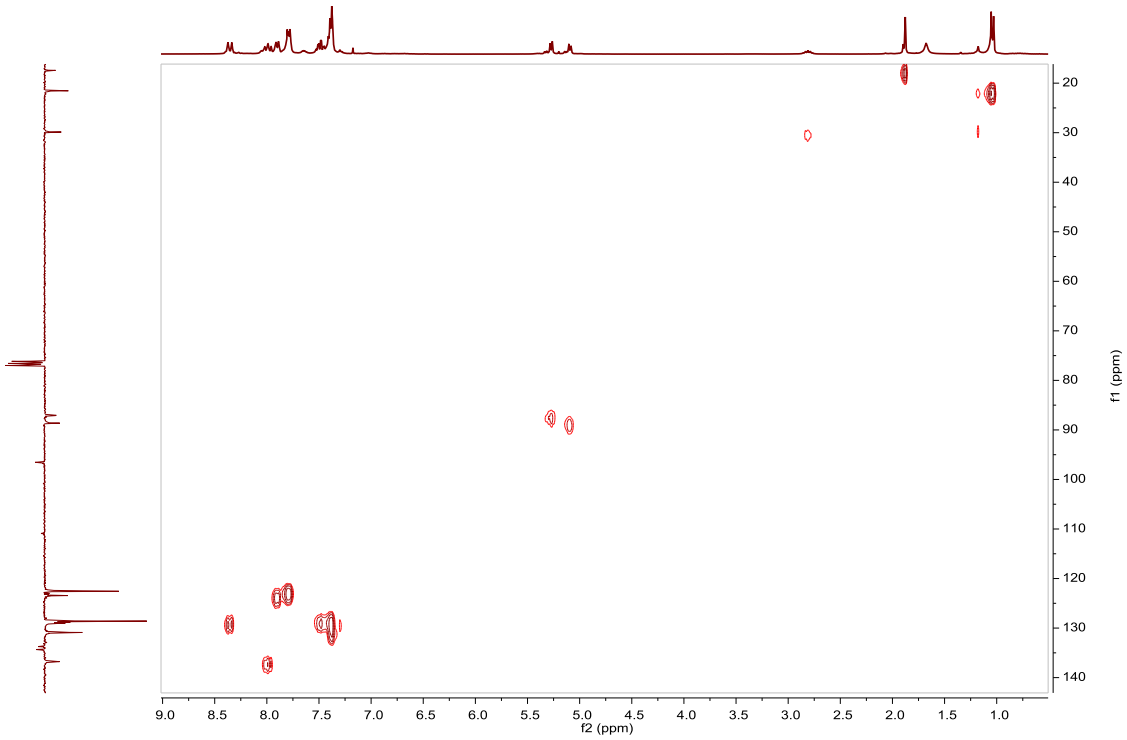

Fig. S395. HSQC NMR spectrum of **[Ru(p-Cym)(tris(*m*-phenylazobenzene)phosphine)(Cl)$_2$]** in $CDCl_3$.

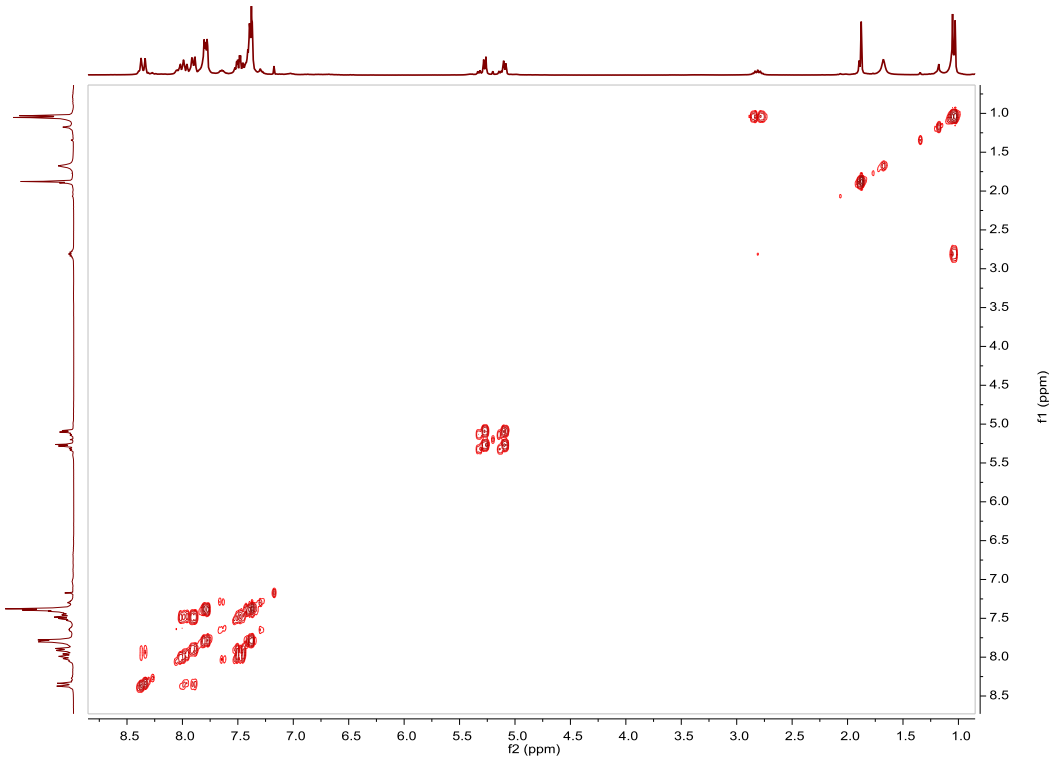

Fig. S396. COSY NMR spectrum of **[Ru(p-Cym)(tris(*m*-phenylazobenzene)phosphine)(Cl)$_2$]** in $CDCl_3$.

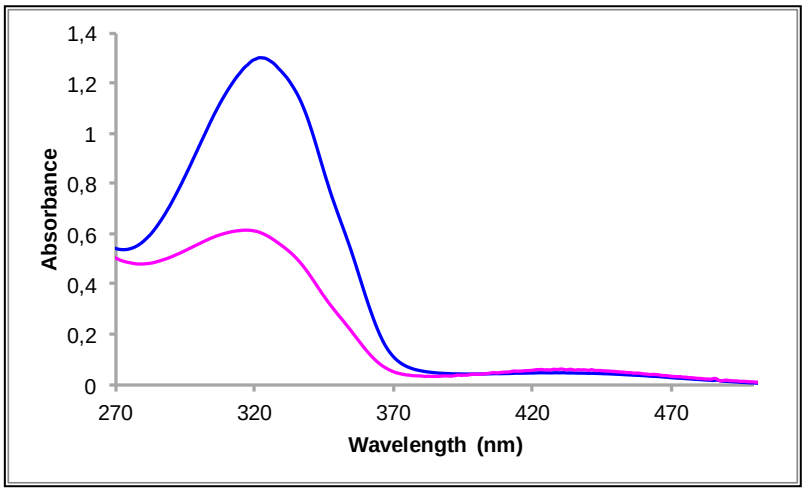

Fig. S397. UV/Vis spectra of **[Ru(p-Cym)(tris(*m*-phenylazobenzene)phosphine)(Cl)$_2$]** in ACN. Before (blue line) and after (pink line) irradiation at 324nm, 2.32·10^{-5}M.

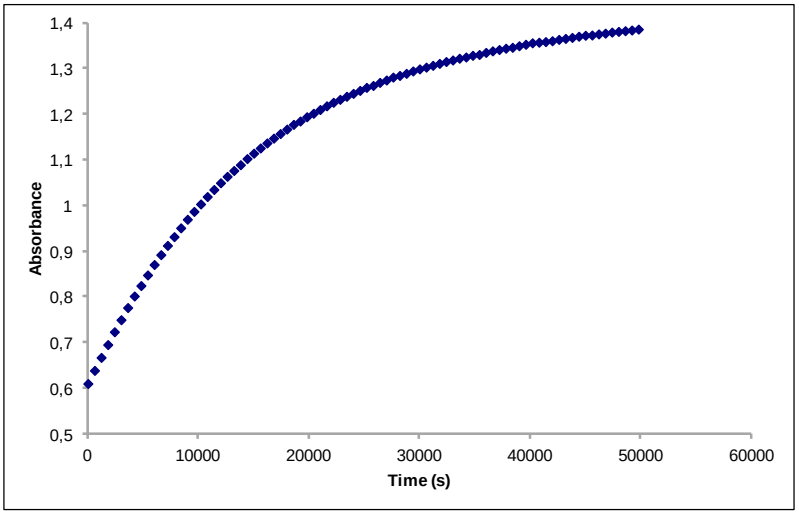

Fig. S398. Cis to trans thermal isomerization kinetics of **[Ru(p-Cym)(tris(*m*-phenylazobenzene)phosphine)(Cl)$_2$]**. Absorption change of the band 321nm at 338 K in ACN after irradiation at 324 nm. (2.32·10^{-5}M).

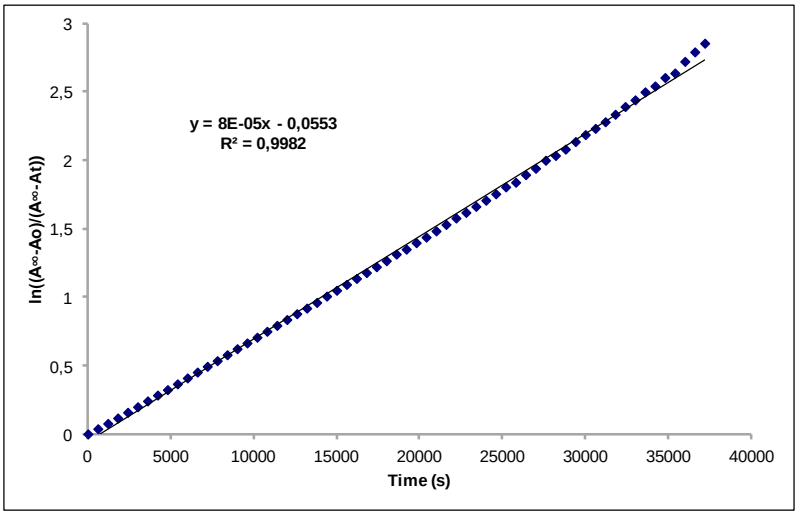

Fig. S399. Cis to trans thermal isomerization kinetics of **[Ru(p-Cym)(tris(*m*-phenylazobenzene)phosphine)(Cl)$_2$]**. First-order plot. k (s^{-1}) = $8.0 \cdot 10^{-5}$. Half-life (min) = 144.

Compound [Ru(p-Cym)(tris(*p*-phenylazobenzene)phosphine)(Cl)$_2$]. Synthesis, characterization and photoisomerization studies.

SYNTHESIS

Under a N_2 atmosphere, Ru_2(p-Cym)$_2Cl_4$ (0.11 g, 0.17 mmol) and tris(*p*-phenylazobenzene)phosphine (0.2 g, 0.348 mmol) were dissolved in 15 mL of hexane. The reaction mixture was refluxed for 15 h. It was cooled to room temperature and the red solid was filtered. Yield 95%.

Elemental Analysis: calculated for ($C_{46}H_{41}Cl_2N_6PRu$): C, 62.73; H, 4.69; N, 9.54. Found: C, 62.93; H, 4.90; N, 9.36.

Exact Mass: ESI-MS [M-2Cl+H]: calculated: m/z= 811.2252, found: m/z= 811.2229.

^{1}H NMR (300 MHz, $CDCl_3$): δ 7.97 (t, J = 8.5 Hz, 6H, (azo)), 7.82 (m, 12H, (azo)), 7.42 (m, 9H, (azo)), 5.21 (d, J = 6.1 Hz, 2H, (8)), 4.98 (d, J = 5.6 Hz, 2H, (7)), 2.83 (sep, J = 6.9 Hz, 1H, (11)), 1.85 (s, 3H, (13)), 1.06 (d, J = 6.9 Hz, 6H, (12)).

^{13}C APT NMR (75 MHz, $CDCl_3$): δ 153.58 (s, 3C_{quat}, (azo)), 152.76 (s, 3C_{quat}, (azo)), 136.22 (d, J = 45 Hz, 3Cquat, (azo)), 135.47 (d, J = 9.7 Hz, 6CH, (azo)), 131.78 (s, 3CH (azo)), 129.33 (s, 6CH, (azo)), 123.27 (s, 6CH, (azo)), 122.47 (d, J = 10.5 Hz, 6CH, (azo)), 112.07 (s, C_{quat}, (p-Cym)), 96.65 (s, C_{quat}, (p-Cym)), 89.37 (brd, J = 2.2 Hz, 2CH, (7)), 87.60 (d, J = 5.2 Hz, 2CH, (8)), 30.63 (s, CH, (11)), 22.10 (s, 2CH_3, (12)), 18.13 (s, CH_3, (13)).

^{31}P NMR (202 MHz, $CDCl_3$): δ 25.79 (s, 1P).

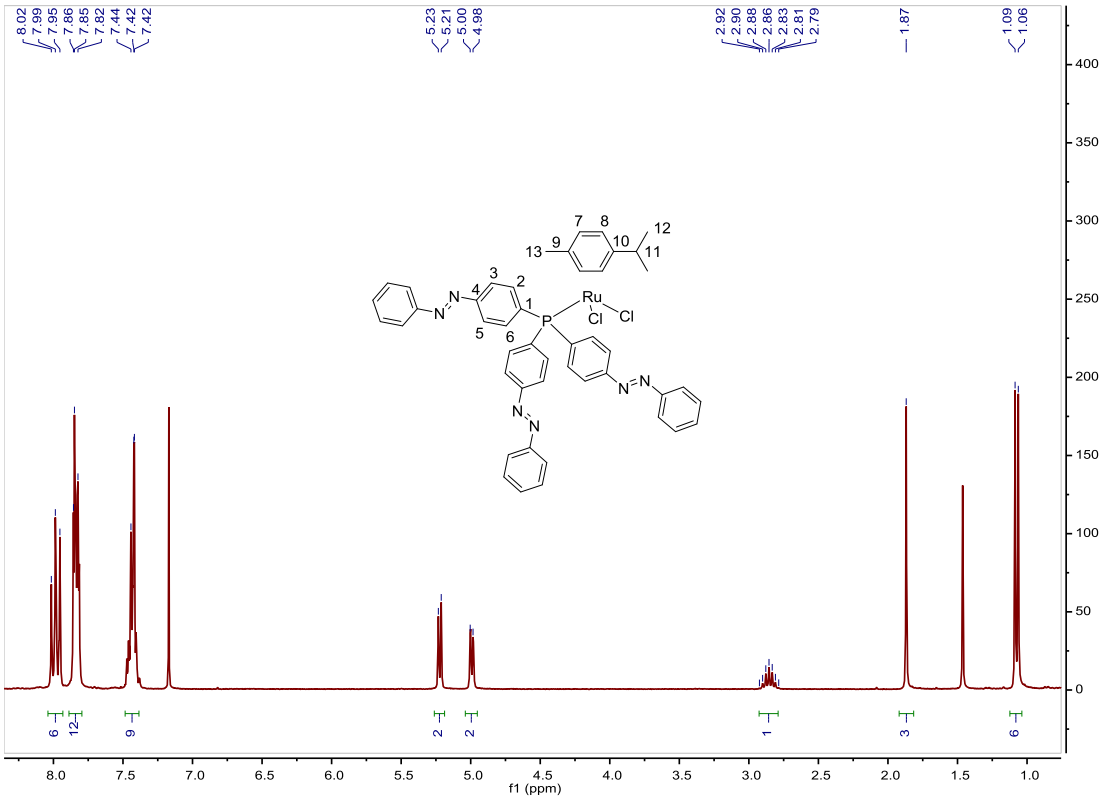

Fig. S400. ^{1}H NMR spectrum of **[Ru(p-Cym)(tris(*p*-phenylazobenzene)phosphine)(Cl)$_2$]** in $CDCl_3$, 300 MHz.

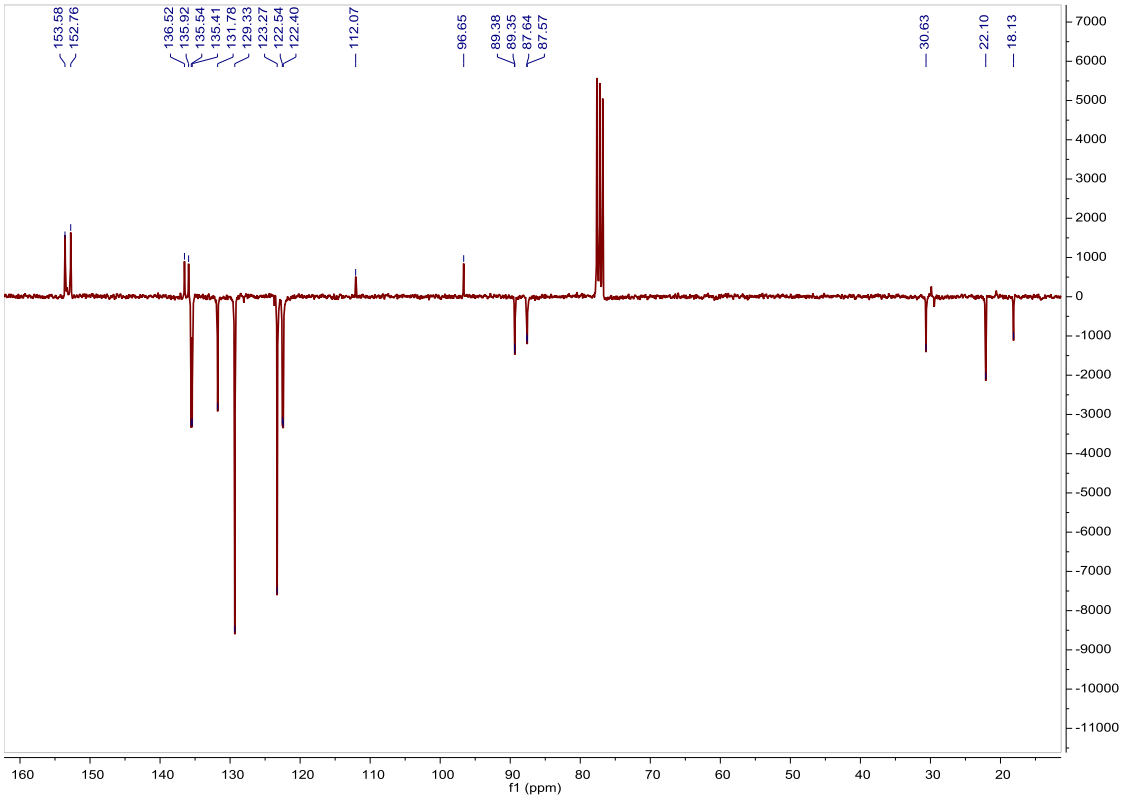

Fig. S401. ^{13}C APT NMR spectrum of **[Ru(p-Cym)(tris(*p*-phenylazobenzene)phosphine)(Cl)$_2$]** in $CDCl_3$, 75 MHz.

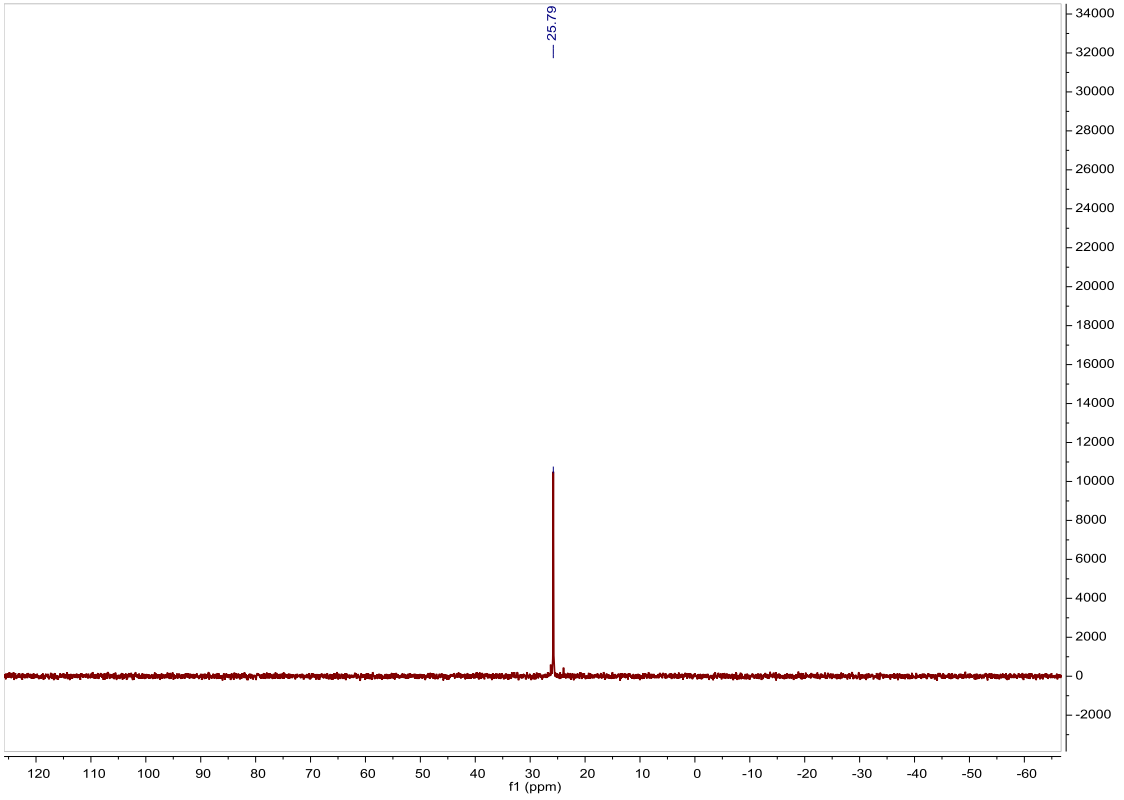

Fig. S402. ^{31}P NMR spectrum of **[Ru(p-Cym)(tris(*p*-phenylazobenzene)phosphine)(Cl)$_2$]** in $CDCl_3$, 202 MHz.

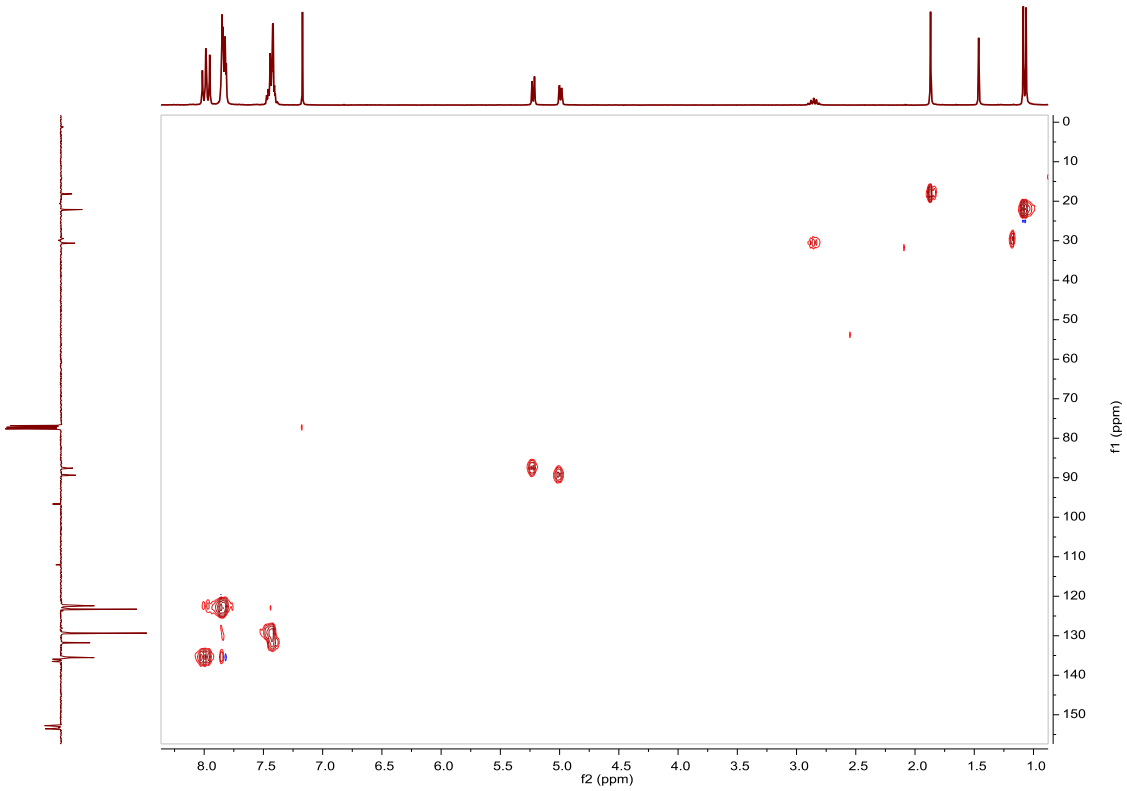

Fig. S403. HSQC NMR spectrum of **[Ru(p-Cym)(tris(*p*-phenylazobenzene)phosphine)(Cl)$_2$]** in $CDCl_3$.

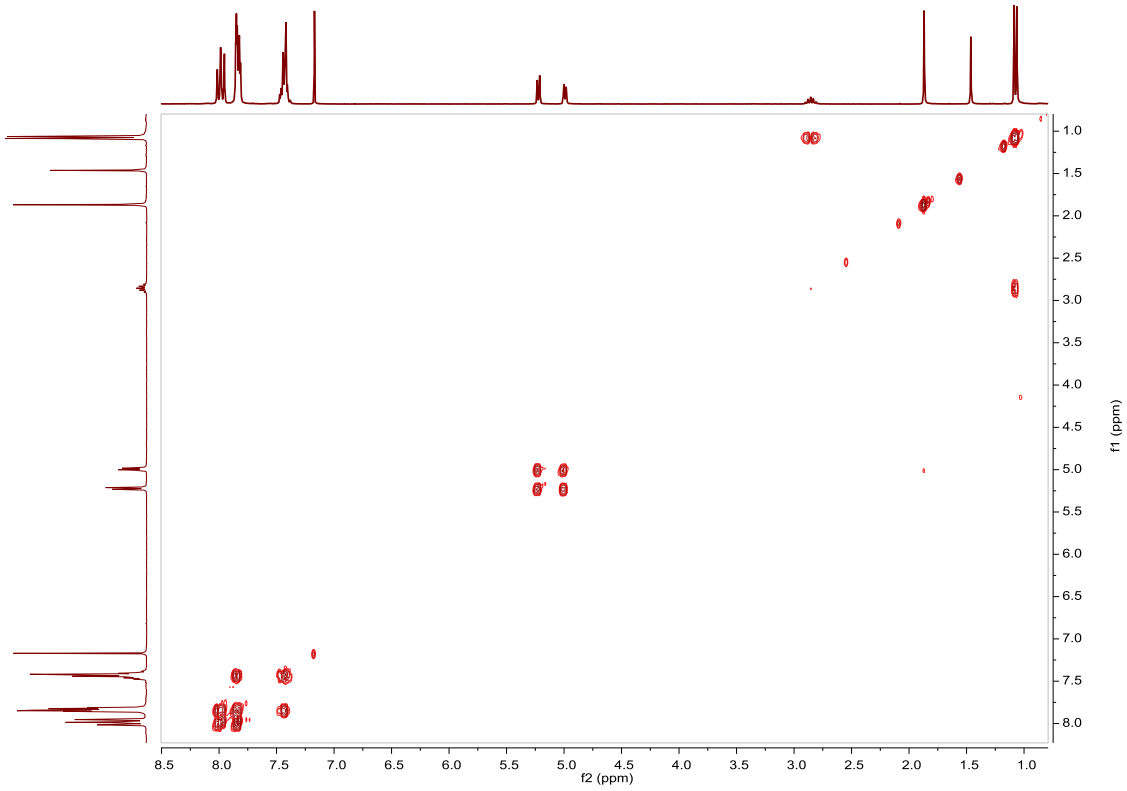

Fig. S404. COSY NMR spectrum of **[Ru(p-Cym)(tris(*p*-phenylazobenzene)phosphine)(Cl)$_2$]** in $CDCl_3$.

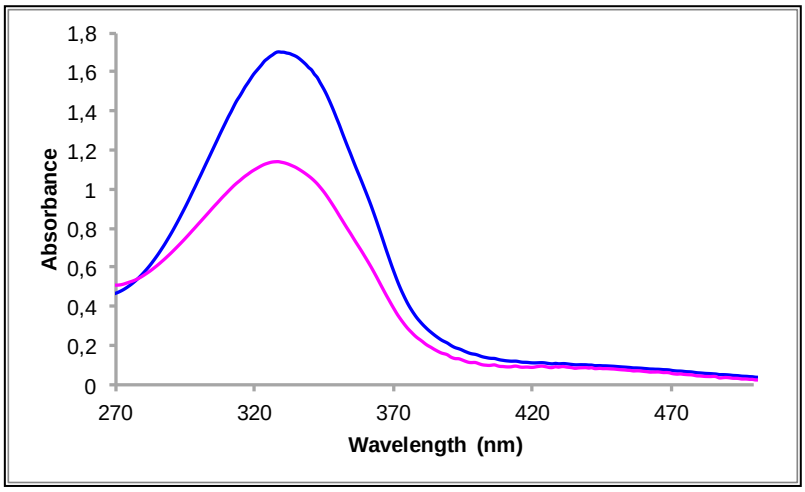

Fig. S405. UV/Vis spectra of **[Ru(p-Cym)(tris(*p*-phenylazobenzene)phosphine)(Cl)$_2$]** in ACN. Before (blue line) and after (pink line) irradiation at 334nm, 2.46·10^{-5}M.

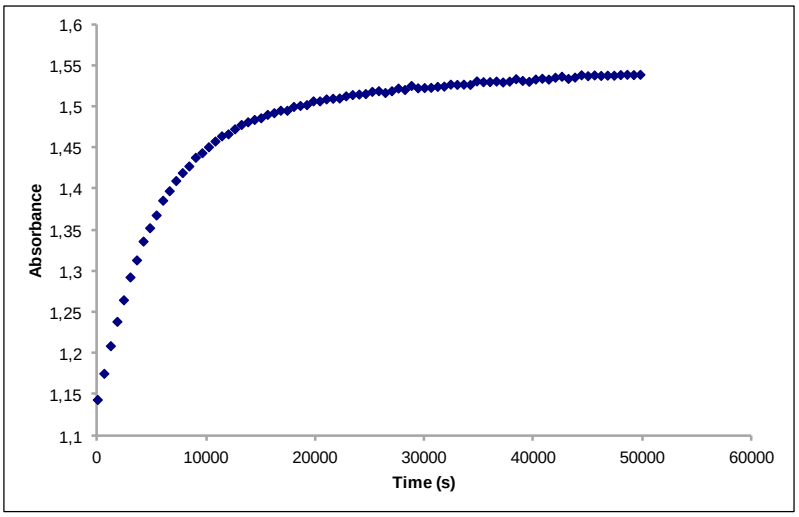

Fig. S406. Cis to trans thermal isomerization kinetics of **[Ru(p-Cym)(tris(*p*-phenylazobenzene)phosphine)(Cl)$_2$]**. Absorption change of the band 328nm at 338 K in ACN after irradiation at 334 nm. (2.46·10^{-5}M).

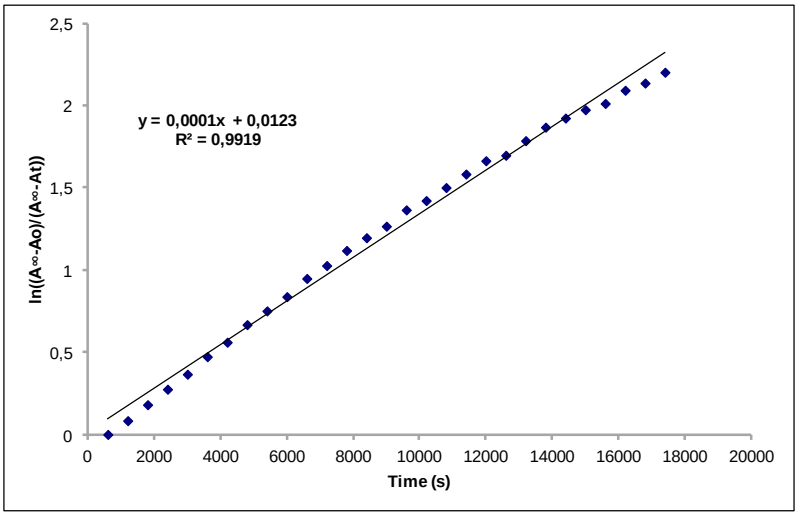

Fig. S407. Cis to trans thermal isomerization kinetics of **[Ru(p-Cym)(tris(*p*-phenylazobenzene)phosphine)(Cl)$_2$]**. First-order plot. k (s^{-1}) = $1.0 \cdot 10^{-4}$. Half-life (min) = 115.

Compound [Ru(p-Cym)(PPh_3)($Cl)_2$]. Synthesis and characterization.

SYNTHESIS

Under a N_2 atmosphere, Ru_2(p-Cym)$_2Cl_4$ (0.200 g, 0.326 mmol) and triphenylphosphine (0.171 g, 0.653 mmol) were dissolved in 15 mL of hexane. The reaction mixture was refluxed for 15 h. It was cooled to room temperature and the product was obtained as an orange solid after filtrating and washing with ether. Yield 77%. The spectroscopic data are coincident with those described in the literature.[44]

^{1}H NMR (500 MHz, $CDCl_3$): δ 7.85 (t, J = 8.7 Hz, 6H, (2+6)), 7.44–7.34 (m, 9H, (3+4+5)), 5.22 (d, J = 5.9 Hz, 2H, (8)), 5.01 (d, J = 5.9 Hz, 2H, (7)), 2.87 (sep, J = 6.9 Hz, 1H, (11)), 1.89 (s, 3H, (13)), 1.13 (d, J = 6.9 Hz, 6H, (12)).

^{31}P NMR (202 MHz, $CDCl_3$): δ 25.40 (s, 1P).

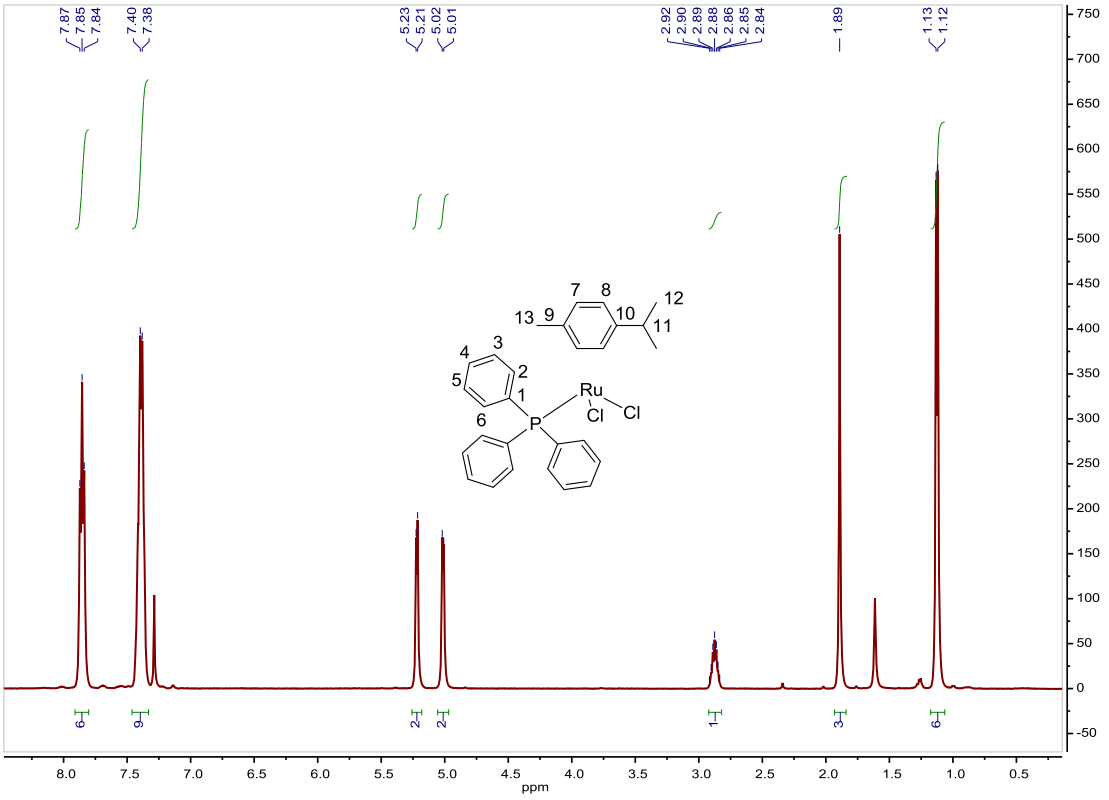

Fig. S408. ^{1}H NMR spectrum of **[Ru(p-Cym)(PPh_3)($Cl)_2$]** in $CDCl_3$, 500 MHz.

[44] E. Hodson and S. J. Simpson, *Polyhedron*, **2004**, *23*, 2695–2707.

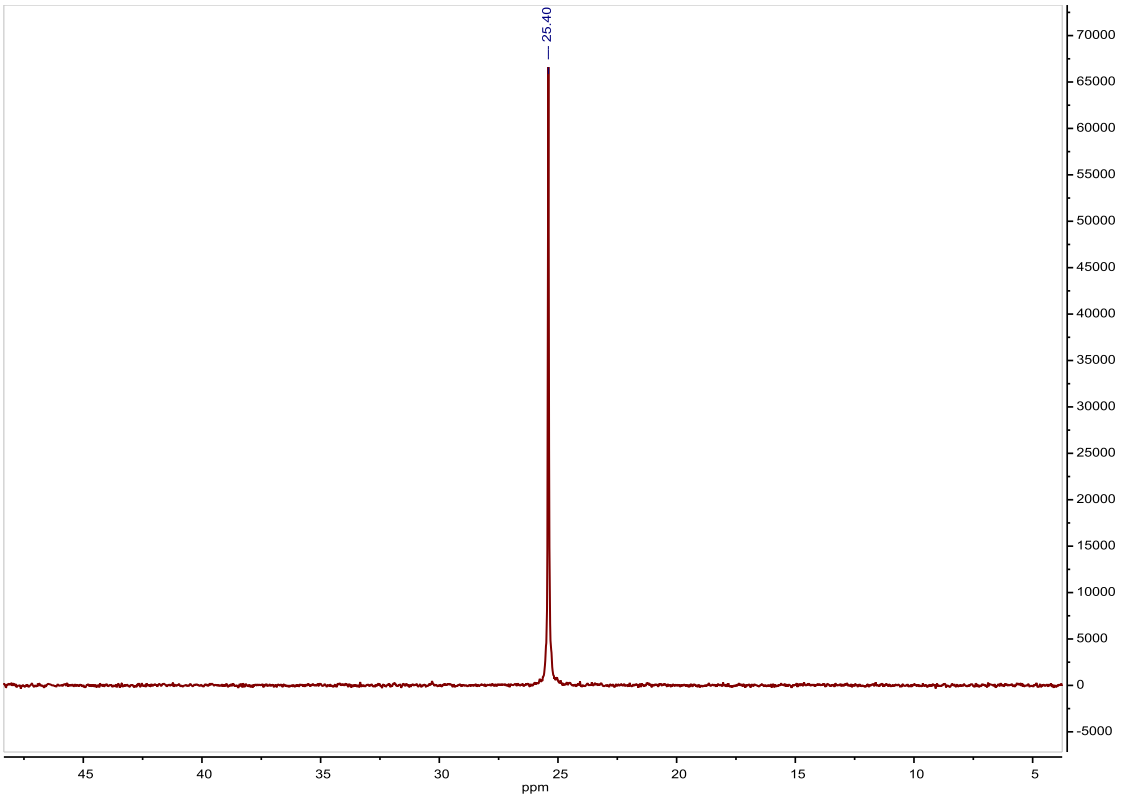

Fig. S409. ^{31}P NMR spectrum of **[Ru(p-Cym)(PPh_3)$(Cl)_2$]** in $CDCl_3$, 202 MHz.

H_3NBD_3. Synthesis and characterization.

SYNTHESIS[45]

Under a N_2 atmosphere, $NaBD_4$ (0.5 g, 11.95 mmol) and $(NH_4)_2CO_3$ (1.14 g, 11.95 mmol) were stirred in freshly distilled THF (13 mL). The reaction mixture was heated at 40 °C for 7 h and stirred at room temperature overnight. The reaction mixture was filtered through a celite path, using THF to wash the celite. The product was obtained as a white solid after sublimation at 40 °C–80 °C under vacuum. Yield 61%. The spectroscopic data are coincident with those described in the literature.

^{1}H NMR (400 MHz, THF-d_8): δ 2.11 (t, J = 41.1 Hz, NH_3).

^{11}B NMR (128 MHz, THF-d_8): δ -24.39 (s, BD_3).

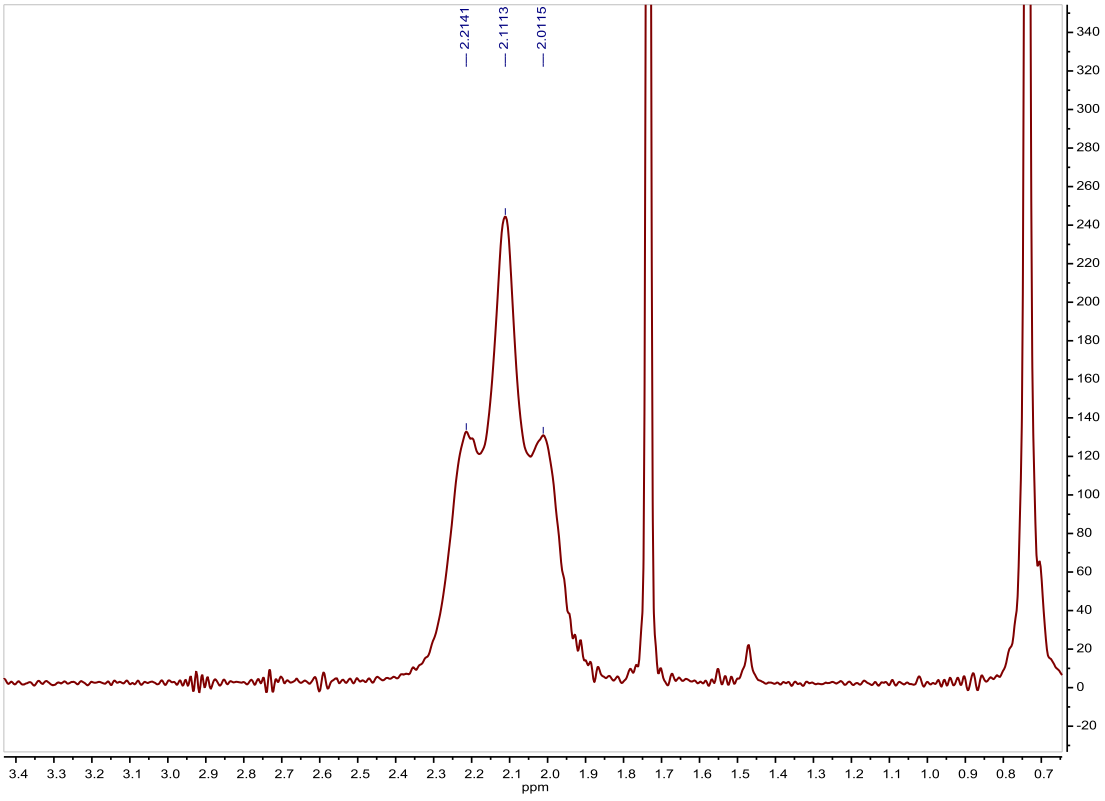

Fig. S410. ^{1}H NMR spectrum of **H_3NBD_3** in THF-d_8, 400 MHz.

[45] X. Yang, T. Fox and H. Berke, *Chem. Commun.*, **2011**, *47*, 2053–2055.

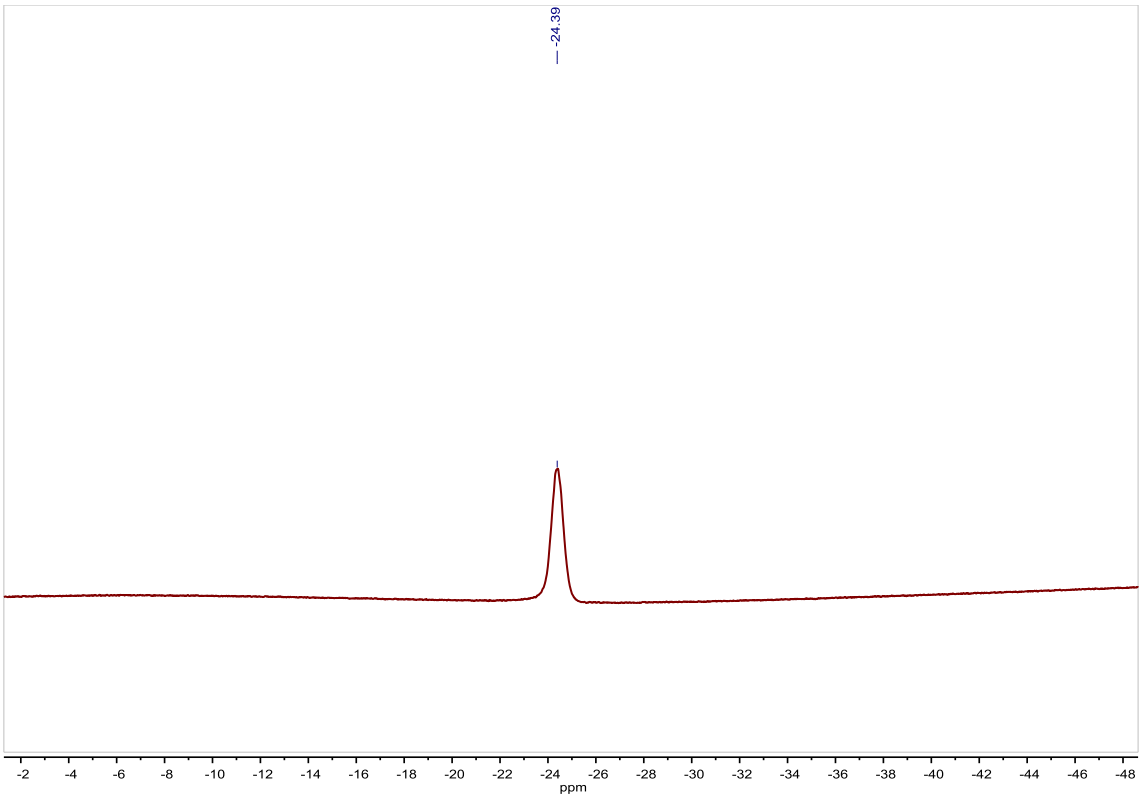

Fig. S411. ^{11}B NMR spectrum of **H_3NBD_3** in THF-d_8, 128 MHz.

Table S2. Crystal data and details of refinement for ligand **3**.

Empirical formula	$C_{34}H_{24}N_6$
Formula weight	516.61
Temperature (K)	293(2)
Wavelength (Å)	1.54184
Crystal system	Monoclinic
Space group	P21/c
Unit cell dimensions (Å / °)	a = 5.3183(4), α = 90.00 b = 9.7998(5), β = 92.498(6) c = 24.1834(15), γ = 90.00
Volume ($Å^3$)	1259.20(14)
Z	2
Calculated Density (Mg/m^3)	1.362
Absorption coefficient (mm^{-1})	0.653
F(000)	540
Theta range (°) for data collection	3.66 - 74.02
Index ranges	-6<=h<=4, -11<=k<=11, -29<=l<=29
Reflections collected	5514
Data [I>2σ(I)]	2469
Parameters	181
Restraints	0
Goodness-of-fit on F^2	1.099
Final R indices [I>2σ(I)]	R1 = 0.0475, wR2 = 0.1270
R indices (all data)	R1 = 0.0542, wR2 = 0.1311
Largest diff. peak and hole ($e/Å^3$)	0.270, -0.191

Table S3. Crystal data and details of refinement for **Aphen**.

Empirical formula	$C_{34}H_{24}F_6IrN_4P$
Formula weight	825.74
Temperature (K)	100(2)
Wavelength (Å)	0.71073
Crystal system	Triclinic
Space group	P-1
Unit cell dimensions (Å / °)	a = 15.0969(2), α = 90.00 b = 23.0030(4), β = 94.974(2) c = 18.9451(3), γ = 90.00
Volume ($Å^3$)	6554.36(18)
Z	8
Calculated Density (Mg/m^3)	1.674
Absorption coefficient (mm^{-1})	4.187
F(000)	3216
Theta range (°) for data collection	1.62 - 28.38
Index ranges	-20<=h<=19, -30<=k<=28, -25<=l<=23
Reflections collected	22666
Data [I>2σ(I)]	7459
Parameters	415
Restraints	0
Goodness-of-fit on F^2	1.063
Final R indices [I>2σ(I)]	R1 = 0.0179, wR2 = 0.0402
R indices (all data)	R1 = 0.0231, wR2 = 0.0420
Largest diff. peak and hole ($e/Å^3$)	0.913, -0.458

Table S4. Crystal data and details of refinement for **Cphen**.

Empirical formula	$C_{34}H_{22}Br_2F_6IrN_4P$
Formula weight	983.95
Temperature (K)	293(2)
Wavelength (Å)	1.54184
Crystal system	Triclinic
Space group	P-1
Unit cell dimensions (Å / °)	a = 10.42190(10), α = 90.021(2) b = 16.6122(3), β = 90.0170(10) c = 50.6413(10), γ = 92.7320(10)
Volume ($Å^3$)	8757.6(2)
Z	1
Calculated Density (Mg/m^3)	1.480
Absorption coefficient (mm^{-1})	4.957
F(000)	3728
Theta range (°) for data collection	1.72 - 28.28
Index ranges	-13<=h<=10, -22<=k<=22, -66<=l<=58
Reflections collected	68576
Data [I>2σ(I)]	38643
Parameters	1484
Restraints	147
Goodness-of-fit on F^2	1.103
Final R indices [I>2σ(I)]	R1 = 0.1102, wR2 = 0.2705
R indices (all data)	R1 = 0.1684, wR2 = 0.3073
Largest diff. peak and hole ($e/Å^3$)	1.836, -3.057

Table S5. Crystal data and details of refinement for **BbipyBr**.

Empirical formula	$C_{32}H_{18}Br_2F_{10}IrN_4P$
Formula weight	1031.51
Temperature (K)	293(2)
Wavelength (Å)	1.54184
Crystal system	Monoclinic
Space group	P21/n
Unit cell dimensions (Å / °)	a = 9.7933(3), α = 90.00 b = 22.1886(8), β = 98.771(4) c = 14.7348(6), γ = 90.00
Volume ($Å^3$)	3164.4(2)
Z	13
Calculated Density (Mg/m^3)	2.165
Absorption coefficient (mm^{-1})	12.443
F(000)	1960
Theta range (°) for data collection	3.63 - 74.05
Index ranges	-12<=h<=12, -19<=k<=27, -18<=l<=18
Reflections collected	23312
Data [I>2σ(I)]	6366
Parameters	451
Restraints	0
Goodness-of-fit on F^2	1.154
Final R indices [I>2σ(I)]	R1 = 0.0463, wR2 = 0.1012
R indices (all data)	R1 = 0.0569, wR2 = 0.1065
Largest diff. peak and hole ($e/Å^3$)	1.441, -1.318

Table S6. Crystal data and details of refinement for **CbipyBr**.

Empirical formula	$C_{32}H_{20}Br_4F_6IrN_4P$
Formula weight	1117.34
Temperature (K)	293(2)
Wavelength (Å)	1.54184
Crystal system	Monoclinic
Space group	C c
Unit cell dimensions (Å / °)	a = 12.9278(3), α = 90.00 b = 28.0093(5), β = 95.485(2) c = 11.2643(3), γ = 90.00
Volume ($Å^3$)	4060.11(16)
Z	17
Calculated Density (Mg/m^3)	1.828
Absorption coefficient (mm^{-1})	11.827
F(000)	2104
Theta range (°) for data collection	3.16 - 74.13
Index ranges	-16<=h<=13, -34<=k<=30, -13<=l<=14
Reflections collected	16221
Data [I>2σ(I)]	7096
Parameters	433
Restraints	473
Goodness-of-fit on F^2	1.066
Final R indices [I>2σ(I)]	R1 = 0.0590, wR2 = 0.1663
R indices (all data)	R1 = 0.0760, wR2 = 0.1832
Largest diff. peak and hole ($e/Å^3$)	2.560, -2.811

Table S7. Crystal data and details of refinement for **B1**.

Empirical formula	$C_{44}H_{28}F_{10}IrN_8P$
Formula weight	1081.9388
Temperature (K)	100(2)
Wavelength (Å)	0.71073
Crystal system	Monoclinic
Space group	P21/c
Unit cell dimensions (Å / °)	a = 22.4848(6), α = 90.00
	b = 9.4724(2), β = 94.080(3)
	c = 20.0655(7), γ = 90.00
Volume ($Å^3$)	4262.8(2)
Z	4
Calculated Density (Mg/m^3)	1.818
Absorption coefficient (mm^{-1})	3.385
F(000)	2288
Theta range (°) for data collection	1.82 - 26.50
Index ranges	-28<=h<=28, -9<=k<=11, -18<=l<=25
Reflections collected	31975
Data [I>2σ(I)]	8825
Parameters	604
Restraints	0
Goodness-of-fit on F^2	1.113
Final R indices [I>2σ(I)]	R1 = 0.0339, wR2 = 0.0668
R indices (all data)	R1 = 0.0423, wR2 = 0.0697
Largest diff. peak and hole ($e/Å^3$)	0.832, -2.571

Table S8. Crystal data and details of refinement for **A2**.

Empirical formula	$C_{44}H_{34}F_6IrN_8P$
Formula weight	1011.99
Temperature (K)	100(2)
Wavelength (Å)	0.71073
Crystal system	Monoclinic
Space group	C2/c
Unit cell dimensions (Å / °)	a = 17.1660(2), α = 90.00 b = 21.8245(2), β = 93.1940(10) c = 20.9858(4), γ = 90.00
Volume ($Å^3$)	7849.89(19)
Z	8
Calculated Density (Mg/m^3)	1.713
Absorption coefficient (mm^{-1})	3.516
F(000)	4000
Theta range (°) for data collection	1.76 - 26.5
Index ranges	-21<=h<=21, -27<=k<=27, -25<=l<=26
Reflections collected	24093
Data [I>2σ(I)]	8143
Parameters	597
Restraints	80
Goodness-of-fit on F^2	1.087
Final R indices [I>2σ(I)]	R1 = 0.0285, wR2 = 0.0649
R indices (all data)	R1 = 0.0359, wR2 = 0.0686
Largest diff. peak and hole ($e/Å^3$)	1.579, -1.316

Table S9. Crystal data and details of refinement for **C3**.

Empirical formula	$C_{56}H_{38}Br_2F_6IrN_8P$
Formula weight	1319.96
Temperature (K)	100(2)
Wavelength (Å)	1.54184
Crystal system	Triclinic
Space group	P-1
Unit cell dimensions (Å / °)	a = 15.2882(3), α = 85.8675(15) b = 19.3171(3), β = 83.4417(17) c = 20.0260(4), γ = 81.9153(15)
Volume ($Å^3$)	5807.62(19)
Z	4
Calculated Density (Mg/m^3)	1.505
Absorption coefficient (mm^{-1})	6.995
F(000)	2573
Theta range (°) for data collection	2.94 - 74.04
Index ranges	-18<=h<=19, -23<=k<=24, 0<=l<=24
Reflections collected	22937
Data [I>2σ(I)]	22937
Parameters	1481
Restraints	909
Goodness-of-fit on F^2	0.869
Final R indices [I>2σ(I)]	R1 = 0.0552, wR2 = 0.1696
R indices (all data)	R1 = 0.0707, wR2 = 0.1831
Largest diff. peak and hole ($e/Å^3$)	1.998, -1.121

Table S10. Crystal data and details of refinement for **A4**.

Empirical formula	$C_{44}H_{31}BrF_6IrN_6P$
Formula weight	1060.8592
Temperature (K)	100(2)
Wavelength (Å)	0.71073
Crystal system	Monoclinic
Space group	C 2/c
Unit cell dimensions (Å / °)	a = 28.2267(12), α = 90.00 b = 13.2492(3), β = 104.771(4) c = 26.6858(9), γ = 90.00
Volume ($Å^3$)	9650.2(6)
Z	8
Calculated Density (Mg/m^3)	1.460
Absorption coefficient (mm^{-1})	3.686
F(000)	4144
Theta range (°) for data collection	1.58 - 28.29
Index ranges	-37<=h<=35, 0<=k<=17, 0<=l<=35
Reflections collected	10944
Data [I>2σ(I)]	10944
Parameters	575
Restraints	450
Goodness-of-fit on F^2	1.033
Final R indices [I>2σ(I)]	R1 = 0.0790, wR2 = 0.1843
R indices (all data)	R1 = 0.1348, wR2 = 0.2031
Largest diff. peak and hole ($e/Å^3$)	3.385, -1.517

Table S11. Crystal data and details of refinement for [Ru(*p*-Cym)(**17**)Cl]Cl.

Empirical formula	$C_{24}H_{22}Cl_2N_2Ru$
Formula weight	510.4240
Temperature (K)	100(10)
Wavelength (Å)	0.71073
Crystal system	Triclinic
Space group	P -1
Unit cell dimensions (Å / °)	a = 6.9529(2), α = 92.790(6)
	b = 11.5712(7), β = 99.326(4)
	c = 16.8700(13), γ = 96.309(4)
Volume ($Å^3$)	1328.15(14)
Z	2
Calculated Density (Mg/m^3)	1.436
Absorption coefficient (mm^{-1})	0.822
F(000)	580
Theta range (°) for data collection	1.775 - 28.315
Index ranges	-6<=h<=9, -14<=k<=14, -21<=l<=21
Reflections collected	9376
Data [I>2σ(I)]	9376
Parameters	357
Restraints	24
Goodness-of-fit on F^2	1
Final R indices [I>2σ(I)]	R1 = 0.0767, wR2 = 0.1942
R indices (all data)	R1 = 0.1093, wR2 = 0.2107
Largest diff. peak and hole ($e/Å^3$)	1.555, -1.218

Table S12. Crystal data and details of refinement for [Ru(*p*-Cym)(**21**)Cl]Cl.

Empirical formula	$C_{20}H_{20}Cl_2N_8Ru$
Formula weight	544.4060
Temperature (K)	100(10)
Wavelength (Å)	1.54184
Crystal system	Triclinic
Space group	P -1
Unit cell dimensions (Å / °)	a = 9.4232(7), α = 98.121(6) b = 10.4405(5), β = 99.958(7) c = 14.3166(12), γ = 116.027(7)
Volume ($Å^3$)	1208.50(15)
Z	2
Calculated Density (Mg/m^3)	1.496
Absorption coefficient (mm^{-1})	7.419
F(000)	548
Theta range (°) for data collection	3.233 - 68.994
Index ranges	-6<=h<=11, -12<=k<=12, -17<=l<=17
Reflections collected	7871
Data [I>2σ(I)]	4398
Parameters	310
Restraints	66
Goodness-of-fit on F^2	1.139
Final R indices [I>2σ(I)]	R1 = 0.0799, wR2 = 0.2203
R indices (all data)	R1 = 0.0935, wR2 = 0.2324
Largest diff. peak and hole ($e/Å^3$)	2.462, -1.486

Table S13. Crystal data and details of refinement for [Ru(*p*-Cym)(**22**)Cl]Cl.

Empirical formula	$C_{20}H_{20}BrCl_2N_5Ru$
Formula weight	582.2890
Temperature (K)	100.01(10)
Wavelength (Å)	1.54184
Crystal system	Triclinic
Space group	P -1
Unit cell dimensions (Å / °)	a = 10.6051(8), α = 93.576(7)
	b = 10.7857(9), β = 102.190(7)
	c = 16.5095(15), γ = 107.715(7)
Volume ($Å^3$)	1742.0(3)
Z	2
Calculated Density (Mg/m^3)	1.793
Absorption coefficient (mm^{-1})	12.961
F(000)	924
Theta range (°) for data collection	2.764 - 69.99
Index ranges	-13<=h<=13, -7<=k<=13, -18<=l<=20
Reflections collected	12176
Data [I>2σ(I)]	6553
Parameters	484
Restraints	107
Goodness-of-fit on F^2	1.023
Final R indices [I>2σ(I)]	R1 = 0.0659, wR2 = 0.1708
R indices (all data)	R1 = 0.0782, wR2 = 0.1847
Largest diff. peak and hole ($e/Å^3$)	1.629, -1.492

Table S14. Crystal data and details of refinement for [Ru(*p*-Cym)(**2**)$_2$Cl]PF_6.

Empirical formula	$C_{32}H_{32}ClN_6RuPF_6$
Formula weight	782.1342
Temperature (K)	100.00(10)
Wavelength (Å)	0.71073
Crystal system	Monoclinic
Space group	P 21/c
Unit cell dimensions (Å / °)	a = 10.60258(11), α = 90 b = 12.35957(11), β = 92.8039(9) c = 26.4031(3), γ = 90
Volume (Å^3)	3455.81(6)
Z	4
Calculated Density (Mg/m^3)	1.503
Absorption coefficient (mm^{-1})	0.641
F(000)	1584
Theta range (°) for data collection	1.82 - 28.268
Index ranges	-13<=h<=14, -16<=k<=16, -34<=l<=34
Reflections collected	28098
Data [*I*>2σ(*I*)]	7880
Parameters	547
Restraints	204
Goodness-of-fit on F^2	1.063
Final R indices [*I*>2σ(*I*)]	R1 = 0.0379, wR2 = 0.0891
R indices (all data)	R1 = 0.0504, wR2 = 0.0967
Largest diff. peak and hole (e/Å^3)	0.404, -0.391

eman ta zabal zazu

Universidad del País Vasco

Euskal Herriko Unibertsitatea

ikerbasque

Basque Foundation for Science

Supporting Information

Azobenzene-appended iridium(III) and ruthenium(II) complexes. Screening of applications.

PhD Thesis

Ainara Telleria Echaniz

2016

TABLE OF CONTENTS

Chapter 4

Chapter 5

General experimental conditions and instrumentation

All solvents were dried and purified by known procedures and freshly distilled under nitrogen from appropriate drying agents prior to use. All manipulations and reactions involving air and/or moisture-sensitive organometallic compounds were performed under an atmosphere of dry nitrogen using standard Schlenk techniques.

NMR spectra were recorded on a Bruker Avance DPX 300 or 400 MHz and Bruker Avance 500 spectrometers.

EA of the complexes were performed on a microanalizer Leco CHNS-932.

Electrospray ionization Mass Spectrometry (ESI-MS) experiments were carried out on a ultra high performance liquid chromatograph (UPLC) coupled to a high resolution quadrupole-time of flight mass spectrometer (QTOF).

UV-Vis and photoisomerization studies

UV−vis absorption measurements were performed with an Agilent 8453 diode-array spectrophotometer utilizing 10 mm cell-path quartz cuvettes (110 QS).

Measurements of thermal *cis* to *trans* isomerization rates were performed using 10-40 μM solutions of ACN or EtOH. To maximize the initial population of Z derivatives on the PSS, it was followed the procedure described by Monkowius:[1] Using a Shimadzu RF-540 fluorimeter, a 3 mL portion of each sample was irradiated at the corresponding λ_{max} (associated with its π–π* transition band) for 30 min. The λ of the maximum observed after subtracting the first and last spectra of the series was considered as the optimal light wavelength to promote the *Z*–*E* photoisomerization (λ_{opt}). Fresh samples were irradiated at (λ_{opt}) for 30 min, and then placed in a UV−vis spectrophotometer. Their absorbance spectral changes were measured as a function of time for 14 hours. Temperature was controlled with a HP 89090A Peltier temperature control accessory.

Cyclic voltammetry

All electrochemical measurements were carried out in a sealed glass cell under N_2 atmosphere on 10^{-3} M solutions of in anhydrous ACN (containing 0.1 M $TBAPF_6$ as the supporting electrolyte) at a scan rate of 100 mVs^{-1}. The working electrode was a glassy–carbon rod (5 mm diameter) and a Pt wire encapsulated on a porous glass tube was used as counter electrode. The potentials were controlled using a Metrohm Ag/AgCl reference electrode. On the other hand ferrocene/ferrocenium couple (+0.352 V vs Ag/AgCl) was used as the internal standard (10^{-3} M) and all potentials are related to it. The measurements were performed using a Bio-Logic VMP3 potentiostat-galvanostat.

[1] M. Kaiser, S. P. Leitner, C. Hirtenlehner, M. List, A. Gerisch and U. Monkowius, *Dalton Trans.*, **2013**, *42*, 14749–14756.

Computational details

All the calculations were performed with the GAUSSIAN09 suite of programs.[2] Optimization and TDDFT simulation of the absorption processes were carried by using the coulombic-attenuating method developed by Handy et al.[3] named CAM-B3LYP with the standard 6-31+G* and the Hay-Wadt core effective potential (ECP) LANL2DZ[4] basis sets. Solvent effects were estimated using the polarizable continuum model (PCM) within the self-consistent reaction field (SCRF) approach.[5] This method was successfully optimized for vertical excitations and excited estates[6] and was previously proven to give reliable results on the calculation of iridium complexes.[7]

X-ray crystallography

Intensity data were collected on an Agilent Technologies Super-Nova diffractometer, wich was equipped with monochromated Cu kα radiation (λ= 1.54184 Å) and Atlas CCD detector or with monochromated Mo kα radiation (λ= 0.71073 Å) and Eos CCD detector. Data frames were processed (united cell determination, analytical absorption correction with face indexing, intensity data integration and correction for Lorentz and polarization effects) using the Crysalis software package.[8] The structure was solved using Olex2[9] and refined by full-matrix least-squares with SHELXL-97.[10] Final geometrical calculations were carried out with Mercury[11]. and PLATON[12] as integrated in WinGX. [13]

Procedure for the solvolytic dehydrogenation of AB adducts

Catalytic reactions were carried out in a glass reactor connected to an electronic pressure transducer (Man on the moon). 0.69 mmol of the substrate and 0.0034 mmol of the precatalyst were stirred in 0.375 mL of freshly distilled THF for 5–10 min (until no further gas evolution was detected). Addition of 1.125 mL of distilled water to this mixture was considered initial reaction time.

For catalytic reaction under irradiation, the reactor used was made of quartz, and it was immersed in a water bath during the catalytic process. The irradiation lamp used was a an immersion lamp (125 W, 365 nm) thermostated by an external quartz cooling jacket, which temperature was set to 10 °C.

---

[2] Gaussian09, Revision A.02, M. J. Frisch et al., Gaussian Inc., Wallingford CT, **2009**.
[3] T. Yanai, D. P. Tew and N. C. Handy, *Chem. Phys. Lett.*, **2004**, *393*, 51–57.
[4] P. J. May and W. R. Wadt, *J. Chem. Phys.*, **1985**, *82*, 299–303.
[5] R. Cammi, B. Mennucci and J. Tomasi, *J. Phys. Chem. A*, **2000**, *104*, 5631–5637.
[6] A. Charaf-Eddin, A. Planchat, B. Mennucci, C. Adamo and D. Jacquemin, *J. Chem. Theor. Comput.*, **2013**, *9*, 2749–2760.
[7] J. Pérez-Miqueo, A. Telleria, M. Muñoz-Olasagasti, A. Altube, E. García-Lecina, A. de Cózar, Z. Freixa, *Dalton Trans.*, **2015**, *44*, 2075–2091.
[8] CrysAlisPro, Agilent Technologies,Version 1.171.37.31 (release 14-01-2014 CrysAlis171 .NET)(compiled Jan 14 2014,18:38:05).
[9] O. V. Dolomanov, L. J. Bourhis, R. J. Gildea, J. A. K. Howard and H. Puschmann, OLEX2: A complete structure solution, refinement and analysis program, *J. Appl. Cryst.,* **2009**, *42*, 339–341.
[10] G. M. Sheldrick, *Acta Cryst. A64,* **2008**, 112.
[11] C. F. Macrae, *J. Appl. Cryst.*, **2008**, *41*, 466.
[12] A. L. Spek (2010) PLATON, A Multipurpose Crystallographic Tool, Utrecht University, Utrecht, The Netherlands; A. L. Spek, *J. Appl. Cryst.*, **2003**, *36*, 7.
[13] L. J. Farrugia, *J. Appl. Cryst.*, **1999**, *32*, 837.

Immediately, the reactor containing 0.69 mmol of the substrate and 0.0034 mmol of the precatalyst in 0.375 mL of freshly distilled THF the precatalyst was immersed in the bath and stirred for 10 min. The the irradiation lamp was immersed, and immediate addition of 1.125 mL of distilled water to this mixture was considered initial reaction time.

For catalytic experiments where irradiation and no irradiation periods were combined, the lamp was immersed in the water bath only when was it switched on, at not irradiation periods the lamp was pulled out, otherwise the reaction temperature would decrease, due to the external cooling of the lamp.

Synthesis and characterization

Ligand 1 (2,2'-bis(4-phenylazopyridine). Synthesis, characterization and photoisomerization studies.

SYNTHESIS

Under a N_2 atmosphere, 4,4'-diamino-2,2'-bipyridine (0.500 g, 2.68 mmol) were dissolved in 4 mL of NaOH (2 g/4 ml H_2O) and 2 ml of pyridine. The mixture was heated to 80 °C for 45 min and nitrosobenzene (0.750 g, 7 mmol) were added. The reaction mixture was heated to 80 °C for another 15 h. The resulting mixture was cooled down to room temperature. The solid was filtrated, washed with CH_2Cl_2 and H_2O. The product was obtained as an orange solid. Yield 56%.

Elemental Analysis: calculated for ($C_{22}H_{16}N_6$): C, 72.51; H, 4.43; N, 23.06. Found: C, 72.12; H, 3.97; N, 23.04.

Exact Mass: ESI-MS $[C_{22}H_{16}N_6+H]^+$: calculated: m/z= 365.1515, found: m/z= 365.1515.

^{1}H NMR (300 MHz, $CDCl_3$): δ 8.96 (d, J = 5.2 Hz, 1H), 8.92 (d, J = 1.4 Hz, 1H), 8.07 (brd, J = 4.0 Hz, 1H), 8.05 (d, J = 2.2 Hz, 1H), 7.81 (dd, J = 1.9 Hz, J = 5.2 Hz, 1H), 7.60 (m, 3H).

^{13}C APT NMR (75 MHz, $CDCl_3$): δ 158.52 (C_{quat}), 157.74 (C_{quat}), 152.46 (C_{quat}), 150.76 (CH), 132.34 (CH), 129.26 (2CH), 123.48 (2CH), 116.44 (CH), 114.18 (CH).

UV/Vis (CH_3CN), λ, nm (ε, 10^4 M^{-1} cm^{-1}): 317 (3.9), 430 (0.08).

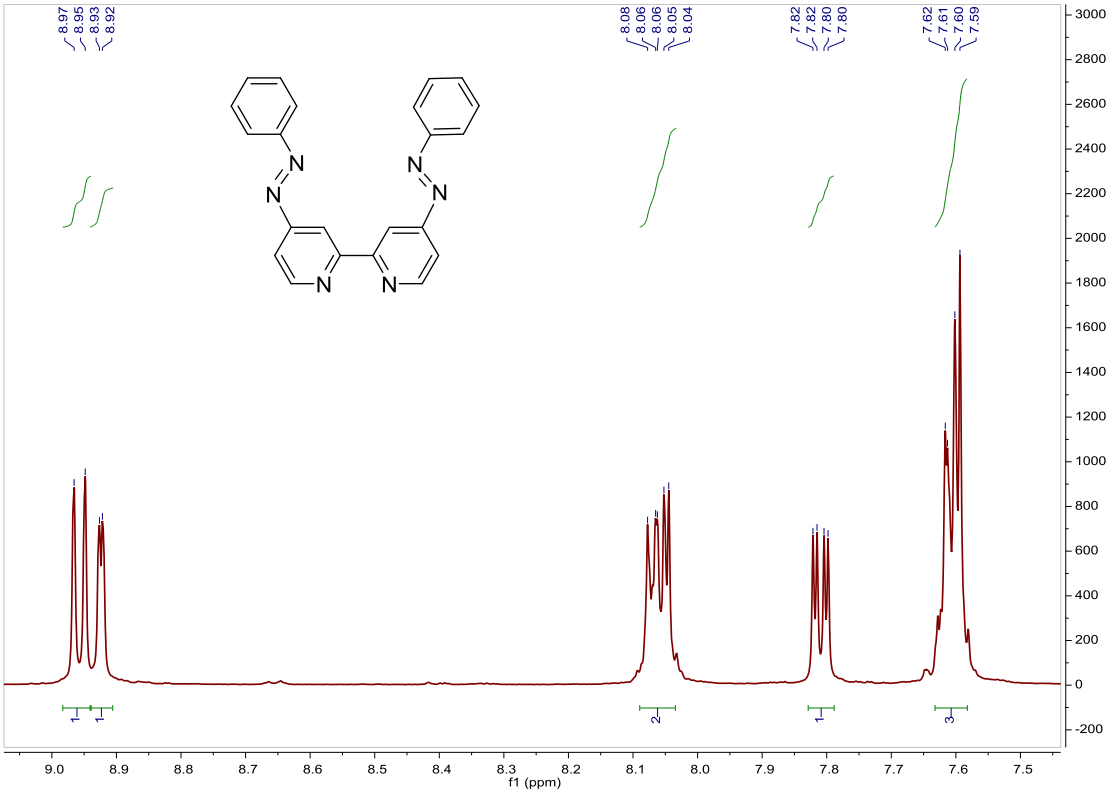

Fig. S1. ^{1}H NMR spectrum of **Ligand 1** in $CDCl_3$, 300 MHz.

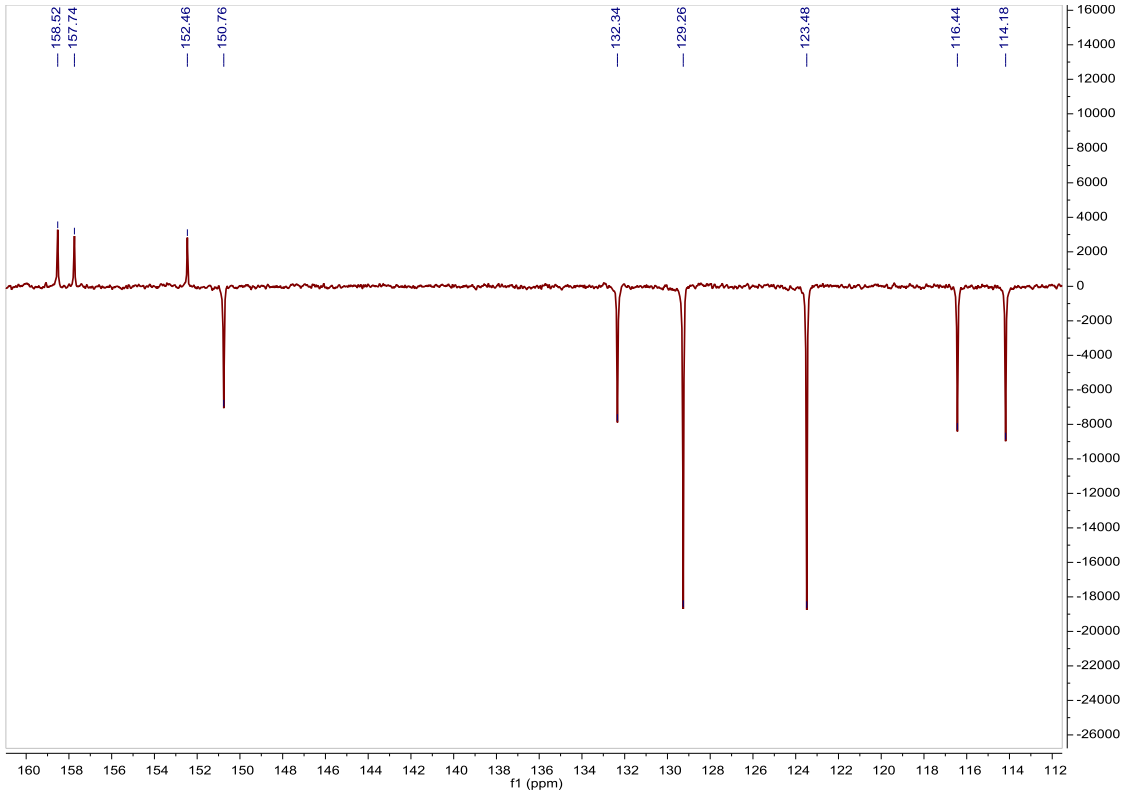

Fig. S2. ^{13}C APT NMR spectrum of **Ligand 1** in $CDCl_3$, 75 MHz.

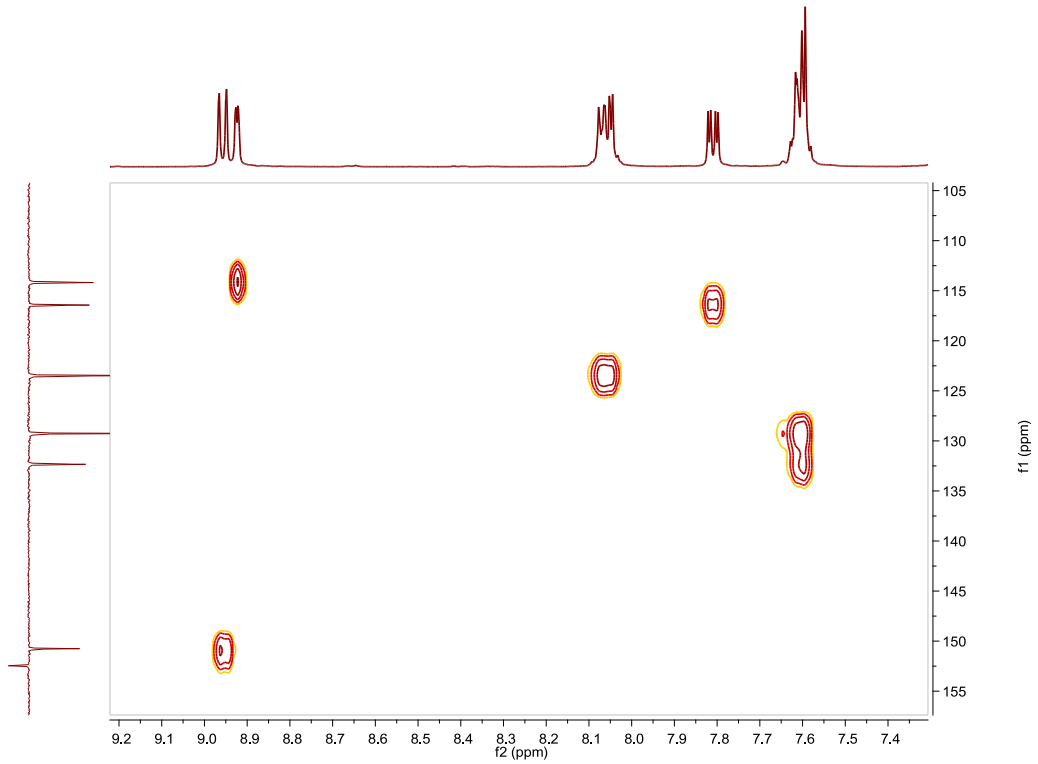

Fig. S3. HSQC NMR spectrum of **Ligand 1** in $CDCl_3$.

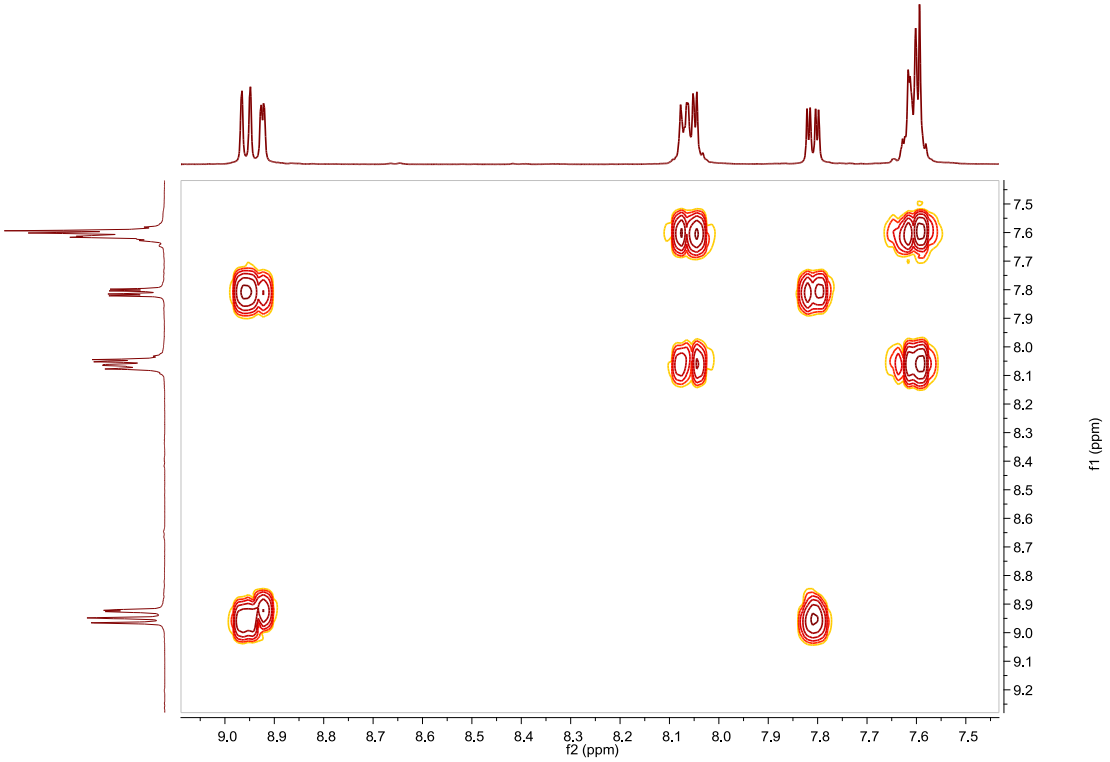

Fig. S4. COSY NMR spectrum of **Ligand 1** in $CDCl_3$.

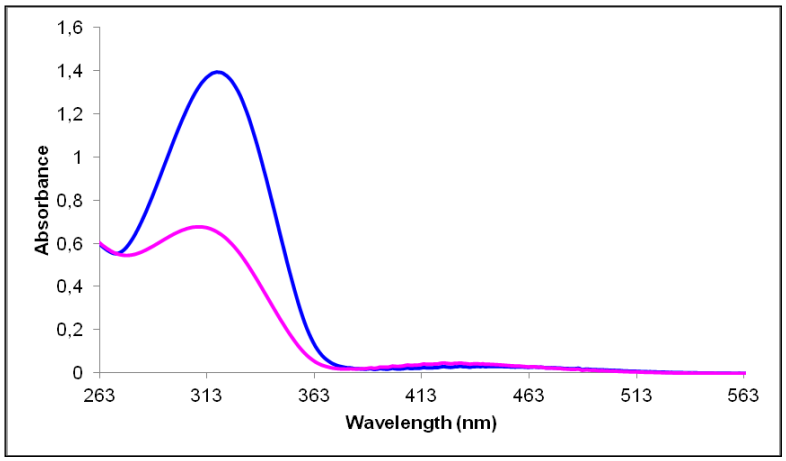

Fig. S5. UV/Vis spectra of **Ligand 1** in CH_3CN. Before (blue line) and after (pink line) irradiation at 325nm, $3.56 \cdot 10^{-5}$ M.

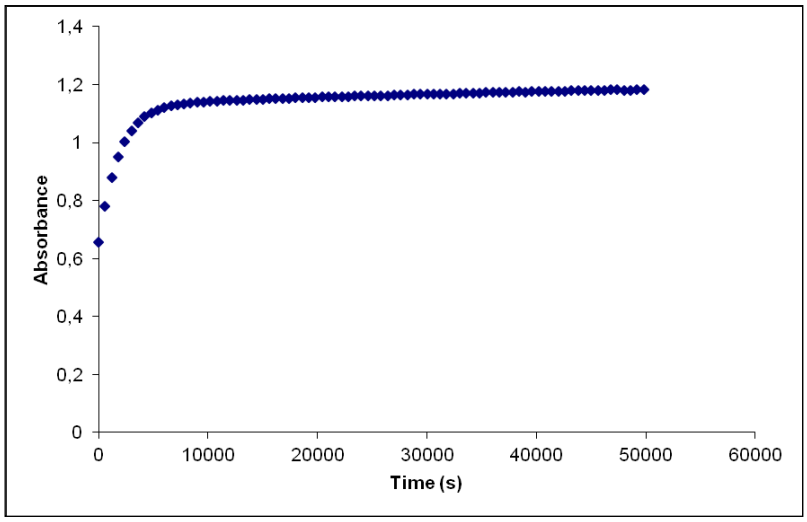

Fig. S6. Cis to trans thermal isomerization kinetics of **Ligand 1**. Absorption change of the band 317nm at 328 K in CH_3CN after irradiation at 325 nm. ($3.56 \cdot 10^{-5}$ M).

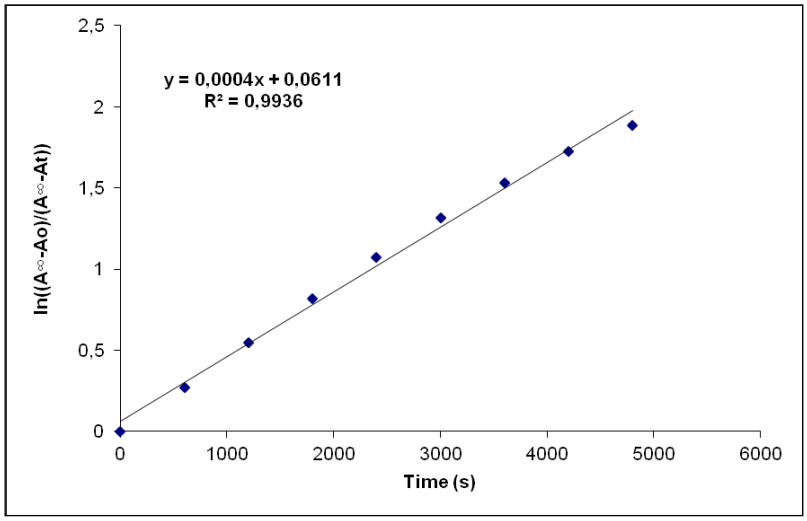

Fig. S7. Cis to trans thermal isomerization kinetics of **Ligand 1**. First-order plot. k (s^{-1}) = $4.0 \cdot 10^{-4}$. Half-life (min) = 29.

Ligand 2, 4-phenylazopyridine. Synthesis, characterization and photoisomerization studies.

SYNTHESIS[14]

Under a N_2 atmosphere, 4-aminopyridine (2.22 g, 23.6 mmol) were dissolved in 10 mL of NaOH (6.5 g/12 ml H_2O) and 7 ml of pyridine. The mixture was heated to 80 °C and nitrosobenzene (3.00 g, 28.0 mmol) were added. The reaction mixture was heated to 80 °C for another 1.5 h. The resulting mixture was cooled down to room temperature and the product was extracted with CH_2Cl_2. To remove the pyridine, the product was dissolved in hexane at 80 °C and cooled down with an ice bath. The product was filtered and was obtained as an orange solid. Yield 88%. The spectroscopic data are coincident with those described in the literature.

^{1}H NMR (300 MHz, $CDCl_3$): δ 8.86 (brd, J = 6.2 Hz, 2H), 8.01 (m, 2H), 7.77 (brd, J = 6.2 Hz, 2H), 7.59 (m, 3H).

UV/Vis (CH_3CN), λ, nm (ε, 10^4 M^{-1} cm^{-1}): 309 (1.6), 435 (0.03).

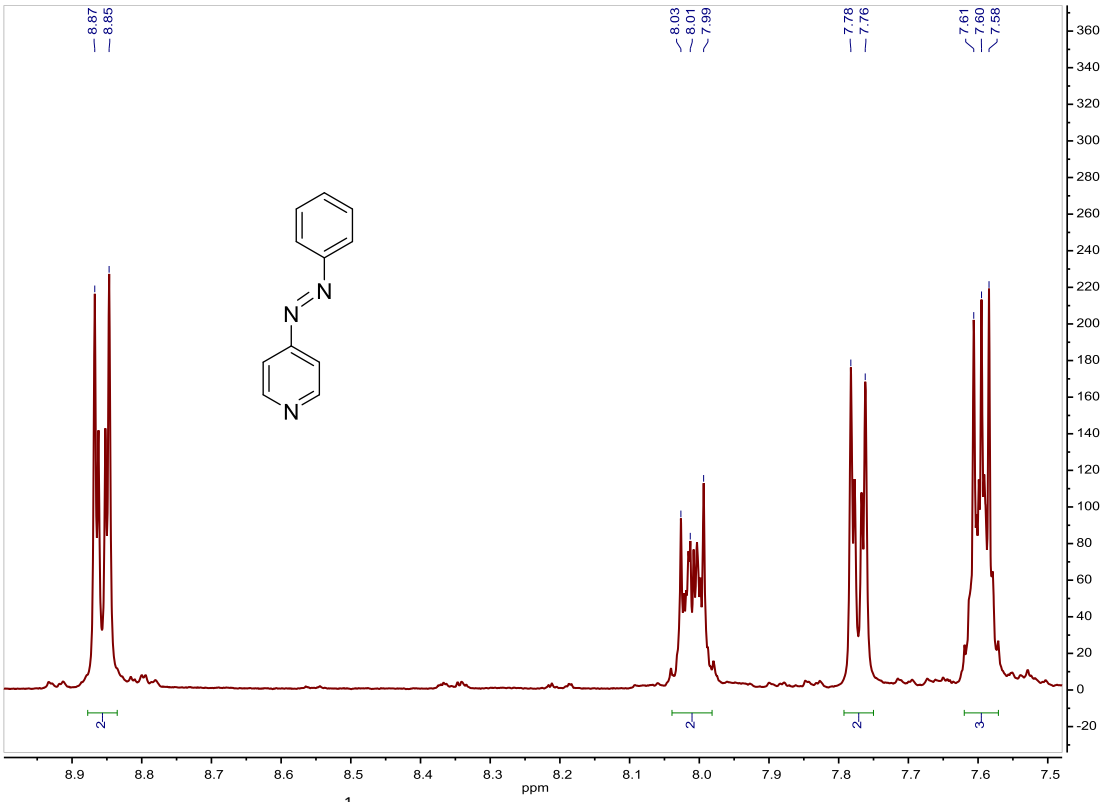

Fig. S8. ^{1}H NMR spectrum of **Ligand 2** in $CDCl_3$, 300 MHz.

[14] Busby, M.; Matousek, P.; Towrie, M.; Vlcek Jr., A., *Inorg. Chim. Acta*, **2007**, *360*, 885–896.

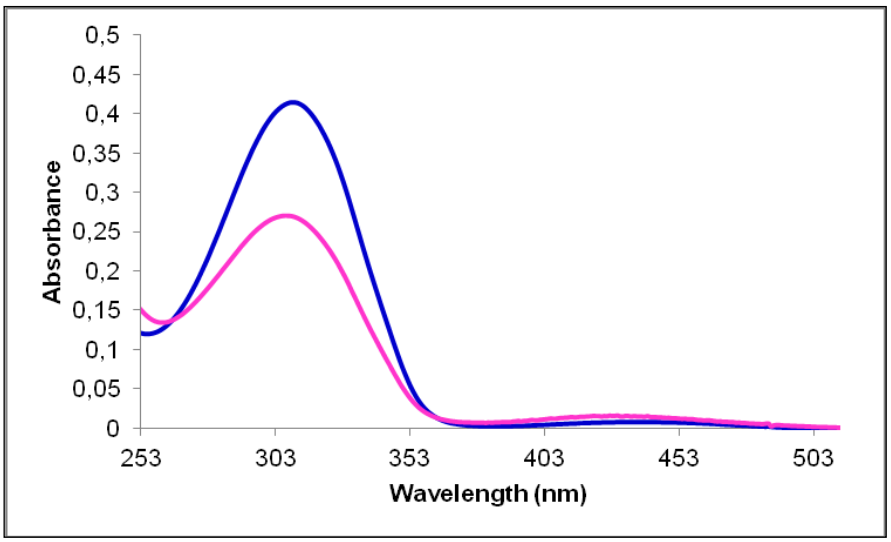

Fig. S9. UV/Vis spectra of **Ligand 2** in CH_3CN. Before (blue line) and after (pink line) irradiation at 312nm, $2.50 \cdot 10^{-5}$ M.

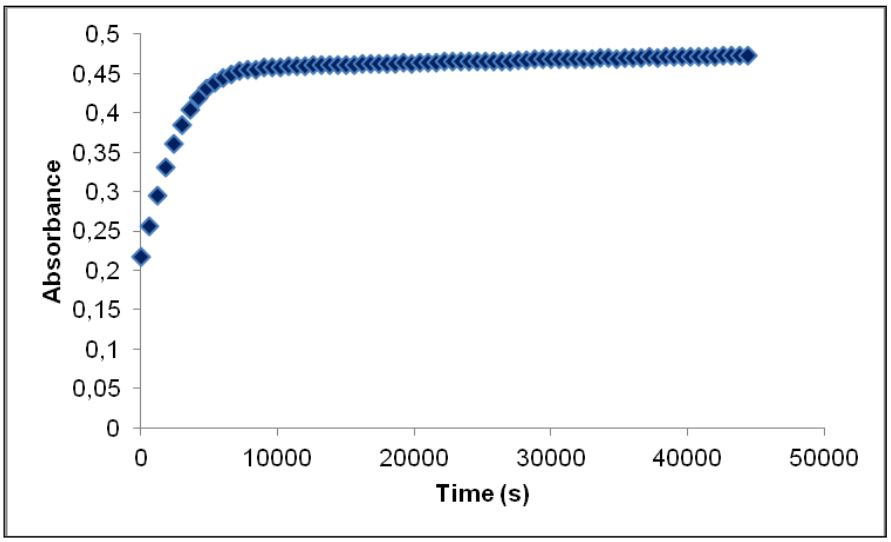

Fig. S10. Cis to trans thermal isomerization kinetics of **Ligand 2**. Absorption change of the band 309nm at 328 K in CH_3CN after irradiation at 312 nm. ($2.50 \cdot 10^{-5}$ M).

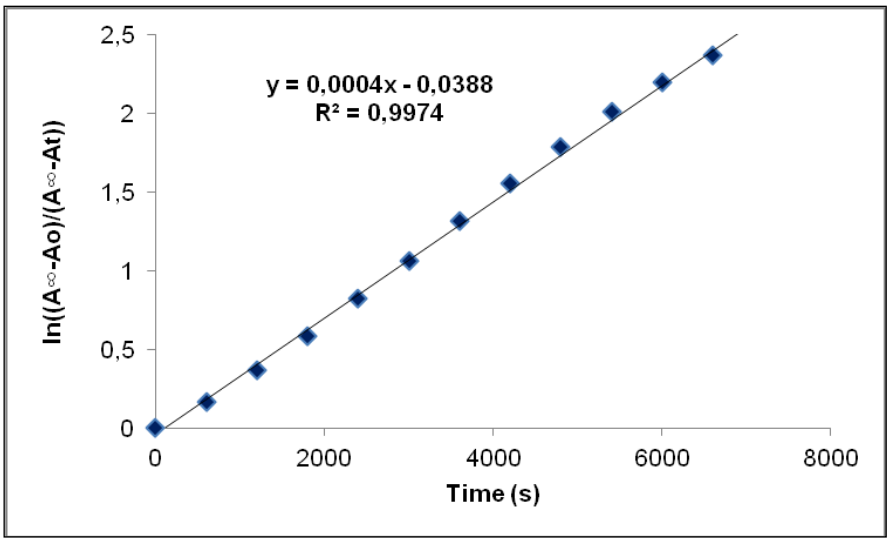

Fig. S11. Cis to trans thermal isomerization kinetics of **Ligand 2**. First-order plot. k (s^{-1}) = $4.0 \cdot 10^{-4}$. Half-life (min) = 29.

Ligand 3, 4,4'-bis(*p*-azobenzene)-2,2'-bipyridine. Synthesis and characterization.

SYNTHESIS.

Under a N_2 atmosphere, 4-4'-dibromo-2,2'-bipyridine (0.6 g, 1.91 mmol) and 4-(phenylazo)phenyl]boronic acid **9** (1.43 g, 6.33 mmol) were dissolved in 35 mL of toluene. K_2CO_3 (16 mL, 2 M,in H_2O) and $Pd(PPh_3)_4$ (0.12 g, 0.104 mmol) were added and the mixture was degassed by N_2 bubbling for 15 min. The reaction mixture was heated to 115 °C for 72 h. The resulting mixture was cooled down to room temperature. The solid was filtrated and washed with CH_2Cl_2 and acetone. The product was obtained as an orange solid. Quantitative yield.

Elemental Analysis: calculated for ($C_{34}H_{24}N_6 \cdot CH_2Cl_2$): C, 69.89; H, 4.36; N, 13.97. Found: C, 70.03; H, 4.45; N, 14.25.

Exact Mass: ESI-MS $[C_{34}H_{24}N_6+H]^+$: calculated: m/z= 517.2141, found: m/z= 517.2147.

Ligand 4, 4-(*p*-azobenzene)-4'-bromo-2,2'-bipyridine. Synthesis, characterization and photoisomerization studies.

SYNTHESIS.

Under a N_2 atmosphere, 4-4'-dibromo-2,2'-bipyridine (1.00 g, 3.18 mmol) and [4-(phenylazo)phenyl]boronic acid pinacol ester **11** (0.98 g, 3.18 mmol) were dissolved in 60 mL of toluene. K_2CO_3 (27 mL, 2 M in H_2O) and $Pd(PPh_3)_4$ (0.184 g, 0.159 mmol) were added and the mixture was degassed by N_2 bubbling for 15 min. The reaction mixture was heated to 115 °C for 15 h. The resulting mixture was cooled down to room temperature and the orange solid (ligand **3**) was removed by filtration. The product was extracted from the filtrated with CH_2Cl_2. The organic phase was dried with $MgSO_4$ and the solvent was evaporated. The product was purified by column chromatography (silica gel, 100% CH_2Cl_2 to 100% acetone), and it was obtained as an orange solid. Yield 38%.

Elemental Analysis: calculated for ($C_{22}H_{15}BrN_4$): C, 63.63; H, 3.64; N, 13.49. Found: C, 63.42; H, 3.62; N, 13.23.

Exact Mass: ESI-MS $[C_{22}H_{15}BrN_4+H]^+$: calculated: m/z= 415.0558, found: m/z= 415.0566.

^{1}H NMR (300 MHz, $CDCl_3$): δ 8.80 (d, J = 5.1 Hz, 1H), 8.75 (dd, J = 1.7 Hz, J = 8.8 Hz, 2H), 8.56 (d, J = 5.2 Hz, 1H), 8.09 (d, J = 8.5 Hz, 2H), 8.00 (dd, J = 1.8 Hz, J = 8.3 Hz, 2H), 7.96 (d, J = 8.4 Hz, 2H), 7.66 (dd, J = 1.8 Hz, J = 5.0 Hz, 1H), 7.56 (m, 4H).

^{13}C APT NMR (75 MHz, $CDCl_3$): δ 157.25 (C_{quat}), 155.44 (C_{quat}), 152.90 (C_{quat}), 152.66 (C_{quat}), 149.84 (2CH), 148.49 (C_{quat}), 140.35 (C_{quat}), 134.03 (C_{quat}), 131.32 (CH), 129.14 (2CH), 127.95 (2CH), 127.06 (CH), 124.74 (CH), 123.56 (2CH), 122.99 (2CH), 122.07 (CH), 119.24 (CH).

UV/Vis (CH_3CN), λ, nm (ε, 10^4 M^{-1} cm^{-1}): 334 (3.5), 443 (0.13).

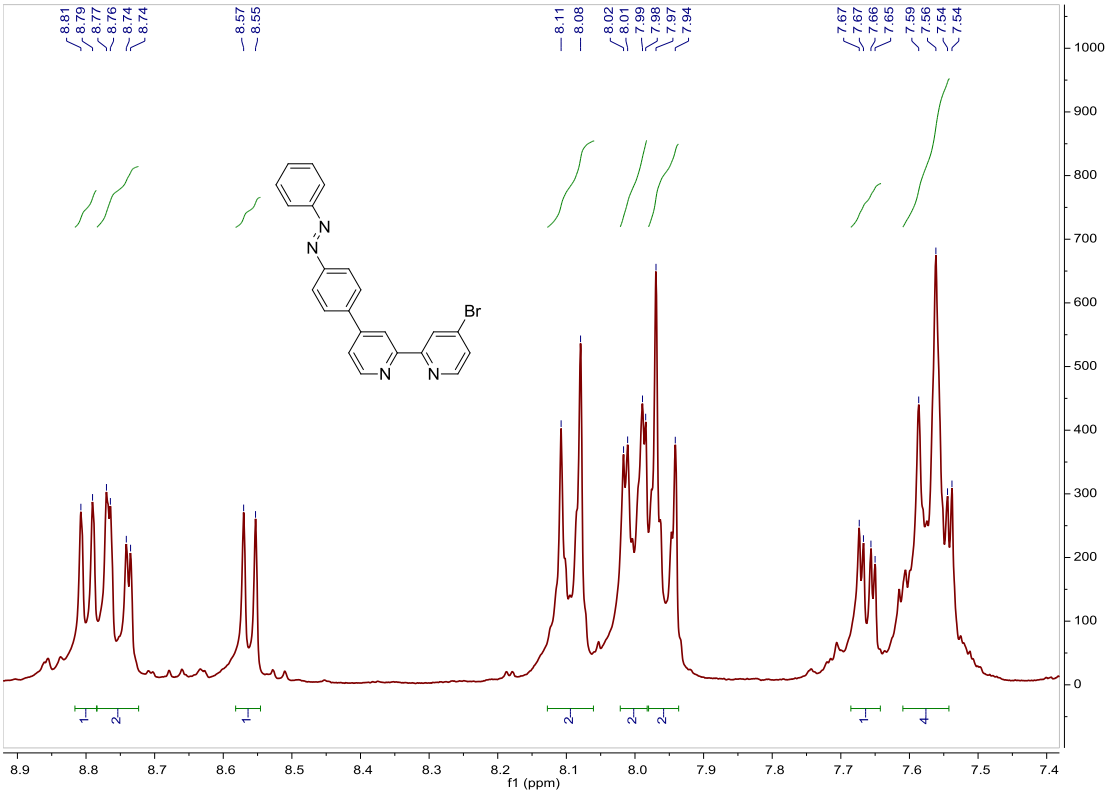

Fig. S12. ^{1}H NMR spectrum of **Ligand 4** in $CDCl_3$, 300 MHz.

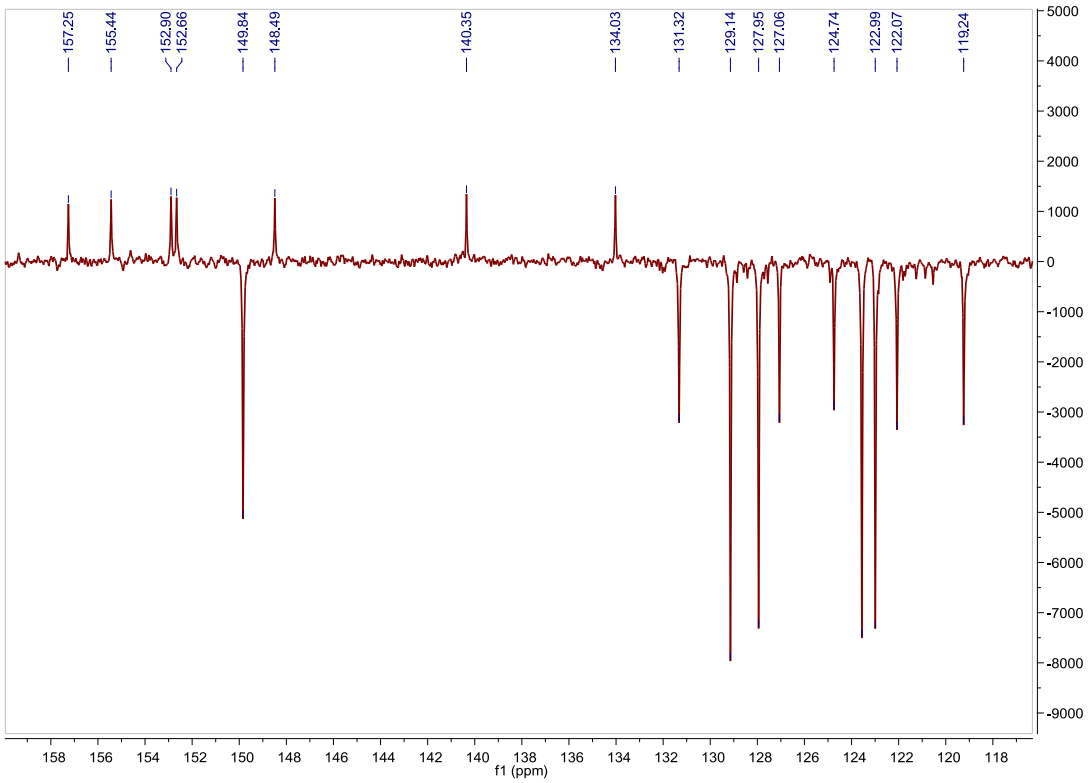

Fig. S13. ^{13}C APT NMR spectrum of **Ligand 4** in $CDCl_3$, 75 MHz.

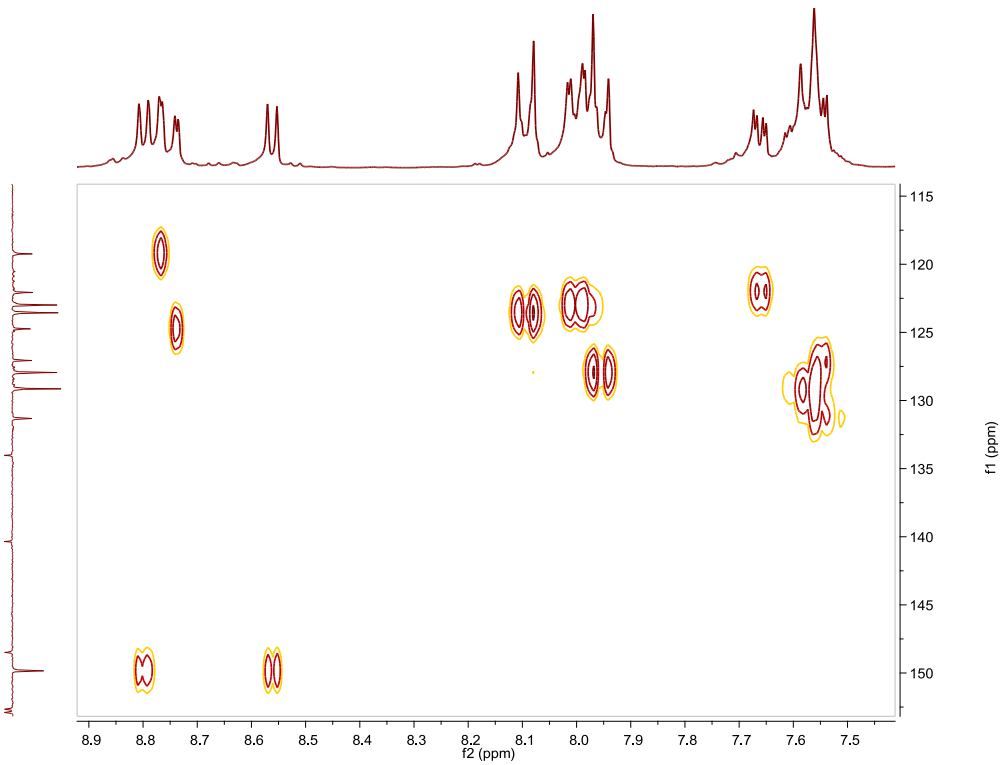

Fig. S14. HSQC NMR spectrum of **Ligand 4** in $CDCl_3$.

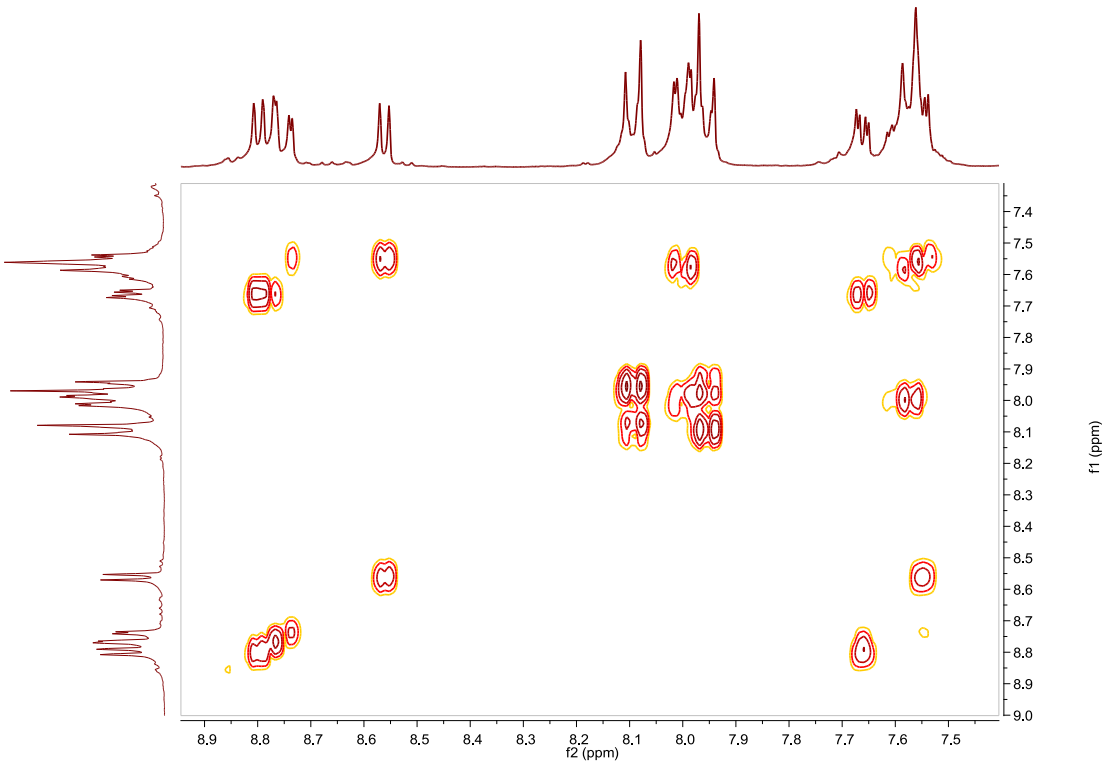

Fig. S15. COSY NMR spectrum of **Ligand 4** in $CDCl_3$.

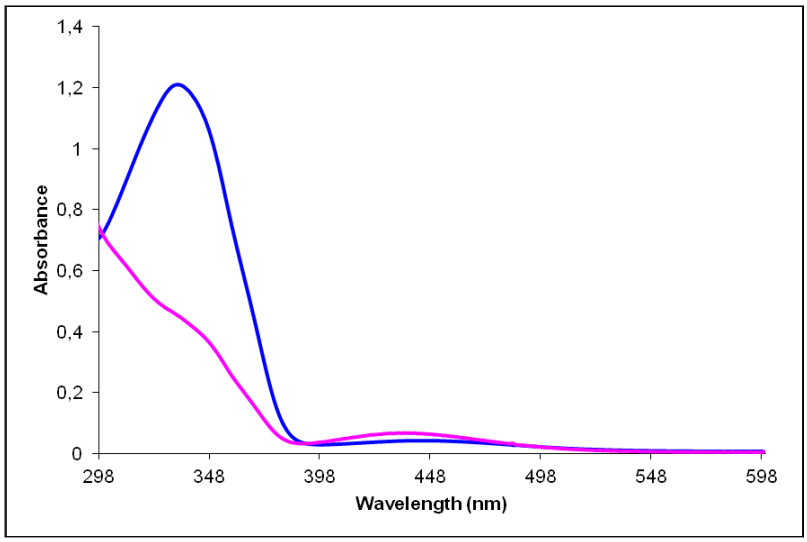

Fig. S16. UV/Vis spectra of **Ligand 4** in CH_3CN. Before (blue line) and after (pink line) irradiation at 337nm, $3.46 \cdot 10^{-5}$ M.

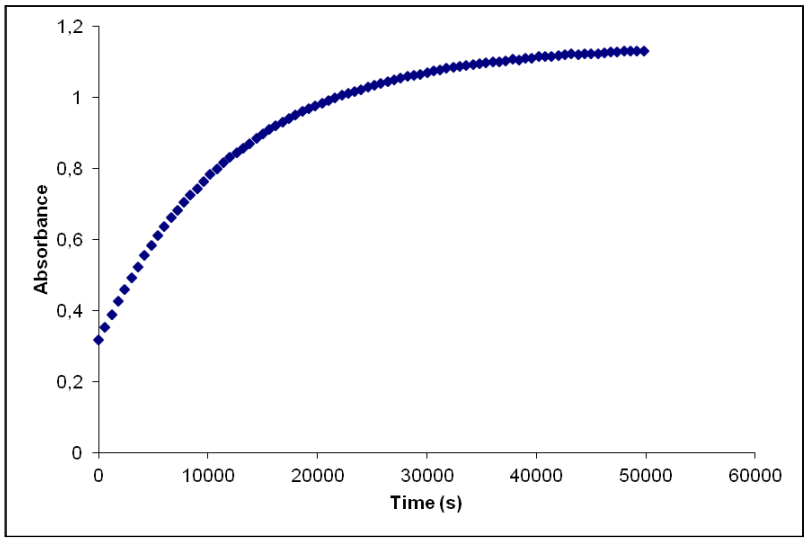

Fig. S17. Cis to trans thermal isomerization kinetics of **Ligand 4**. Absorption change of the band 334nm at 328 K in CH_3CN after irradiation at 337 nm. ($3.46 \cdot 10^{-5}$ M).

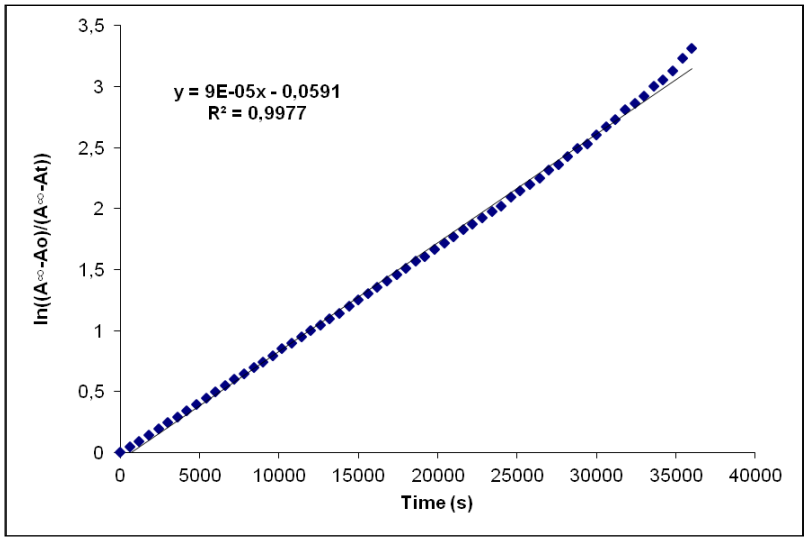

Fig. S18. Cis to trans thermal isomerization kinetics of **Ligand 4**. First-order plot. k (s^{-1}) = $9.0 \cdot 10^{-5}$. Half-life (min) = 128.

Ligand 5, 4,4'-bis(*m*-azobenzene)-2,2'-bipyridine. Synthesis, characterization and photoisomerization studies.

SYNTHESIS

Under a N_2 atmosphere, 4-4'-dibromo-2,2'-bipyridine (0.436 g, 1.39 mmol) and [3-(phenylazo)phenyl]boronic acid **9** (0.785 g, 3.47 mmol) were dissolved in 26 mL of toluene. K_2CO_3 (12 mL, 2 M in H_2O) and $Pd(PPh_3)_4$ (0.08 g, 0.07 mmol) were added and the mixture was degassed by N_2 bubbling for 15 min. The reaction mixture was heated to 115 °C for 15 h. The resulting mixture was cooled down to room temperature and the product was extracted with CH_2Cl_2. The organic phase was dried with $MgSO_4$ and the solvent was evaporated. The product was obtained as an orange solid. Yield 71%.

Elemental Analysis: calculated for ($C_{34}H_{24}N_6 \cdot H_2O$): C, 76.39; H, 4.90; N, 15.72. Found: C, 75.92; H, 4.42; N, 15.28.

Exact Mass: ESI-MS $[C_{34}H_{24}N_6+H]^+$: calculated: m/z= 517.2141, found: m/z= 517.2146.

^{1}H NMR (300 MHz, $CDCl_3$): δ 8.89 (d, J=1.2 Hz, 1H), 8.85 (d, J=5.1 Hz, 1H), 8.39 (pst, J=1.7 Hz, 1H), 8.06 (dpst, J=7.9 Hz, J=1.0 Hz, 1H), 8.02 (brdd, J=8.2 Hz, J=1.8 Hz, 2H), 7.96 (dpst, J=8.1 Hz, J=1.1 Hz, 1H), 7.71 (m, 2H), 7.57 (m, 3H).

^{13}C APT NMR (75 MHz, $CDCl_3$): δ 156.71 (C_{quat}), 153.19 (C_{quat}), 152.58 (C_{quat}), 149.80 (CH), 148.68 (C_{quat}), 139.38 (C_{quat}), 131.29 (CH), 129.82 (CH), 129.53 (CH), 129.15 (2CH), 123.25 (CH), 122.98 (2CH), 121.84 (CH), 121.77 (CH), 119.32 (CH).

UV/Vis (CH_3CN), λ, nm: 314 , 435. (The low solubility of these ligand in CH_3CN was too small for an accurate determination of the corresponding extinction coefficients).

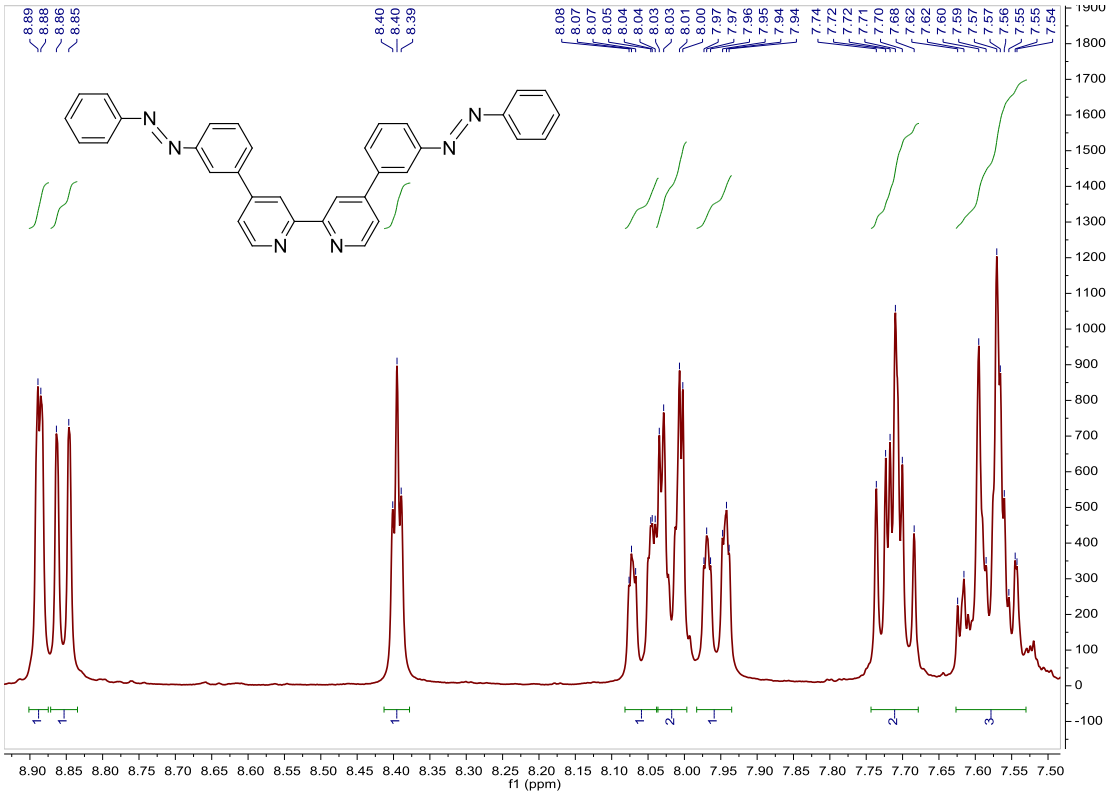

Fig. S19. ^{1}H NMR spectrum of **Ligand 5** in $CDCl_3$, 300 MHz.

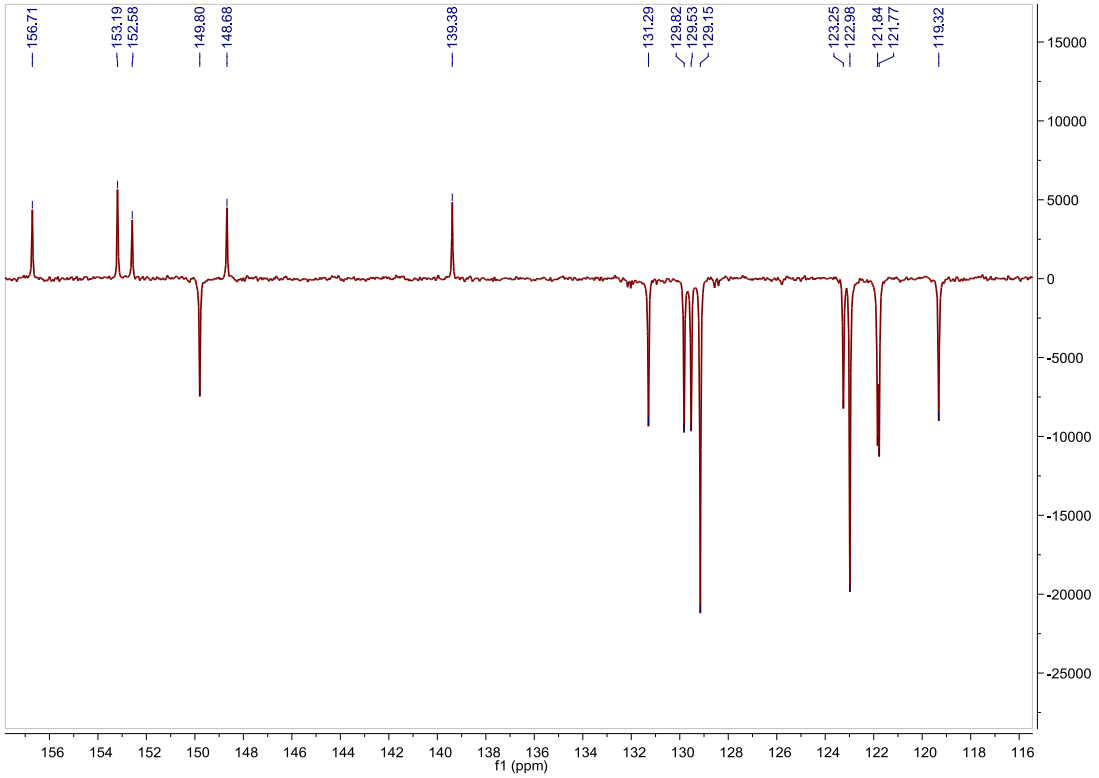

Fig. S20. ^{13}C APT NMR spectrum of **Ligand 5** in $CDCl_3$, 75 MHz.

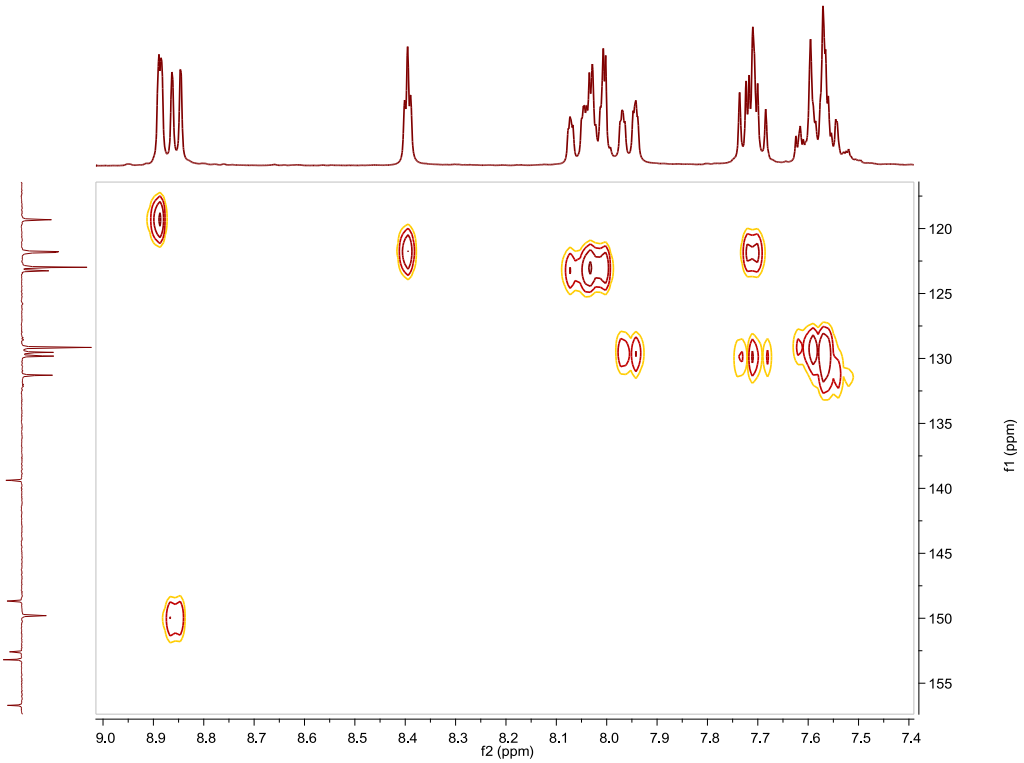

Fig. S21. HSQC NMR spectrum of **Ligand 5** in $CDCl_3$.

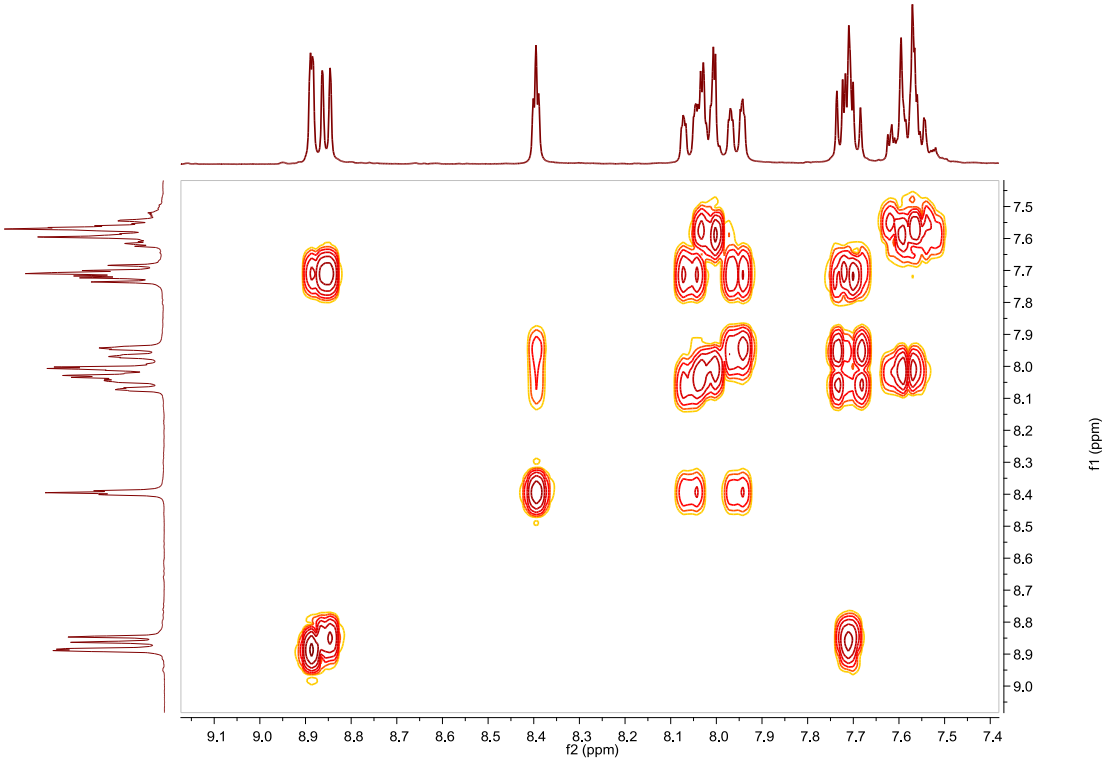

Fig. S22. COSY NMR spectrum of **Ligand 5** in $CDCl_3$.

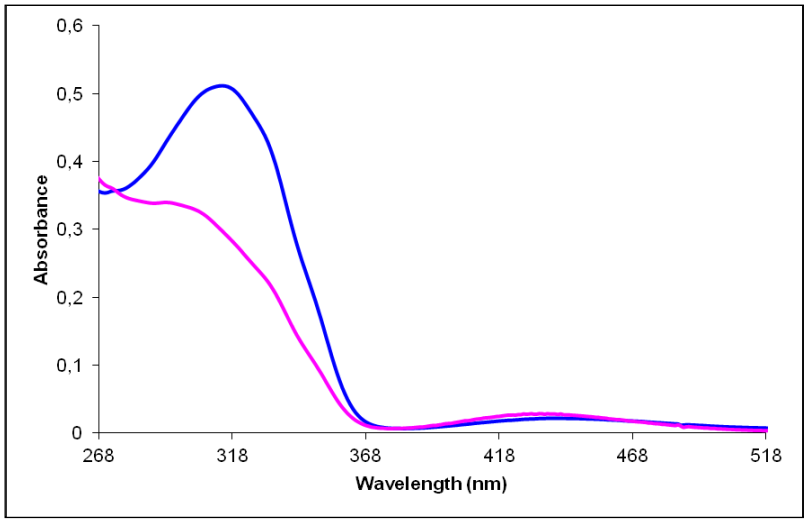

Fig. S23. UV/Vis spectra of **Ligand 5** in CH_3CN. Before (blue line) and after (pink line) irradiation at 320nm, $3.00 \cdot 10^{-5}$ M.

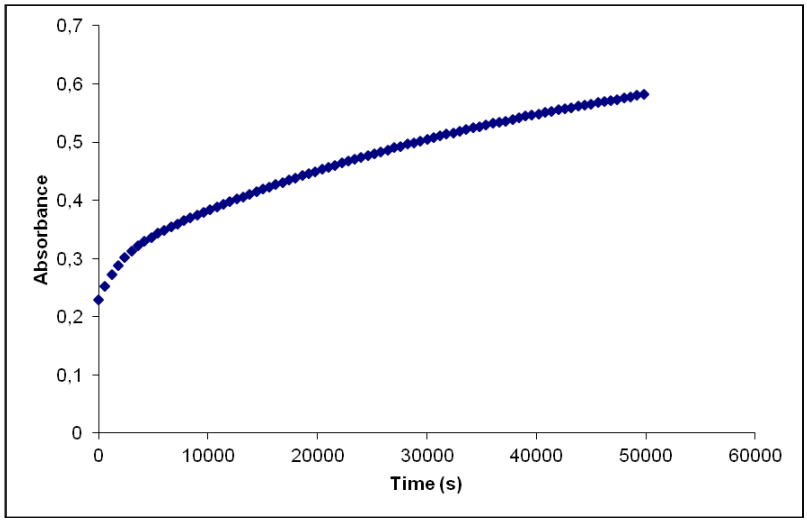

Fig. S24. Cis to trans thermal isomerization kinetics of **Ligand 5**. Absorption change of the band 314nm at 328 K in CH_3CN after irradiation at 320 nm. ($3.00 \cdot 10^{-5}$ M).

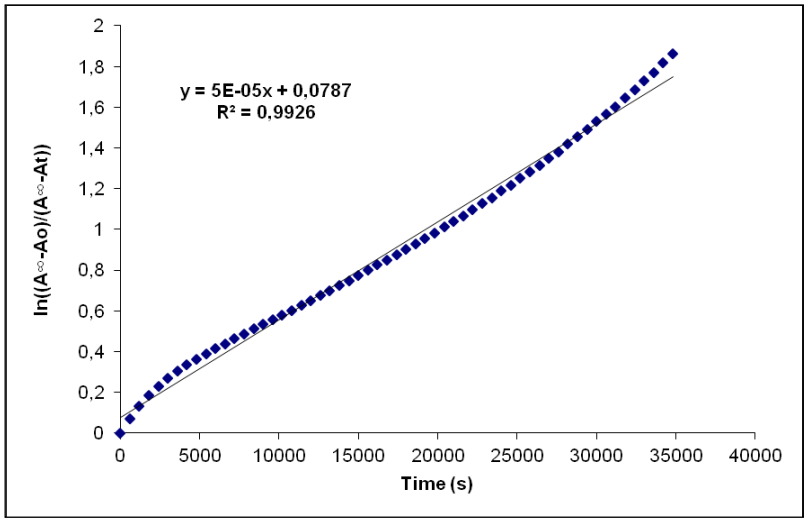

Fig. S25. Cis to trans thermal isomerization kinetics of **Ligand 5**. First-order plot. k (s^{-1}) = $5.0 \cdot 10^{-5}$. Half-life (min) = 231.

2,2'-bipyridine-*N*,*N*'-dioxide, 6. Synthesis and characterization.

SYNTHESIS[15]

2,2'-bipyridine (20.0 g, 128.2 mmol) were dissolved in glacial acetic acid (140 mL) and 30% H_2O_2 (50 mL) was added. The reaction mixture was refluxed at 80 °C for 16 h. After cooling to room temperature acetone (400 mL) was added and the product was precipitated as a white solid. The product was obtained by filtration and concentrating the mother liquor. Yield 97%. The spectroscopic data are coincident with those described in the literature.

^{1}H NMR (300 MHz, D_2O): δ 8.46–8.40 (m, 2H), 7.85–7.77 (m, 2H), 7.76–7.68 (m, 4H).

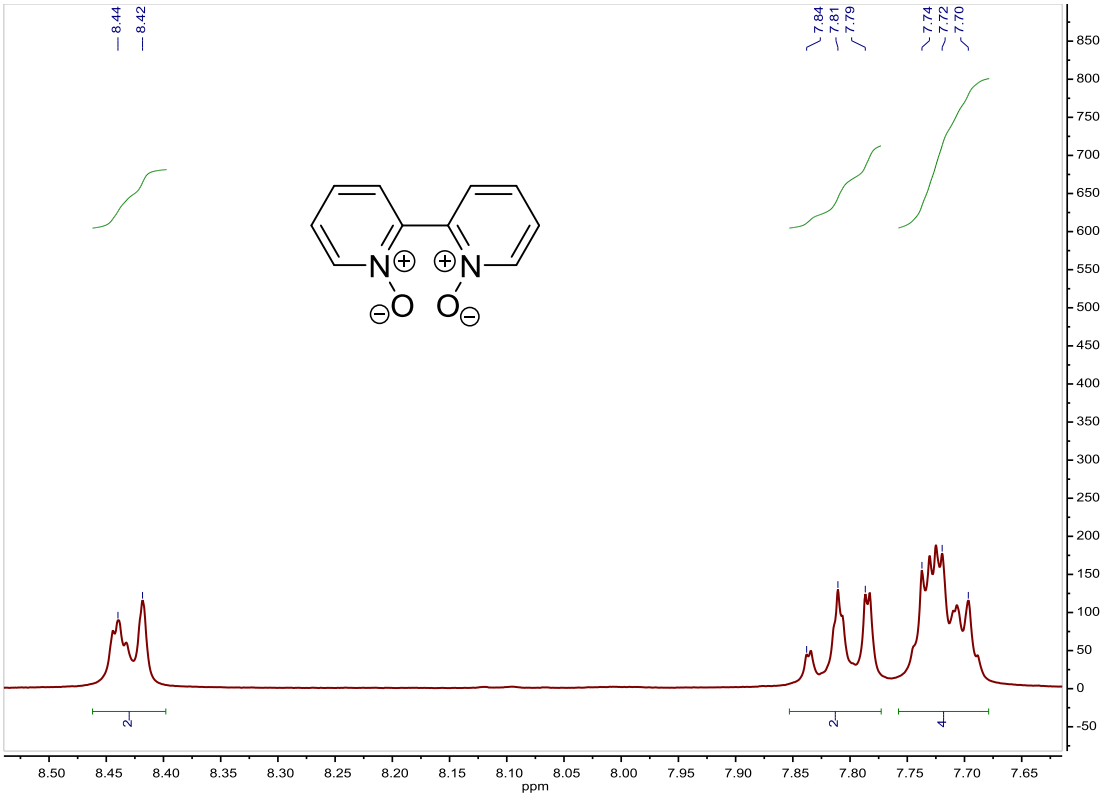

Fig. S26. ^{1}H NMR spectrum of 2,2'-bipyridine-*N*,*N*'-dioxide **6** in D_2O, 300 MHz.

[15] D. Zhang, J. P. Telo, C. Liao, S. E. Hightower and E. L. Clennan, *J. Phys. Chem. A*, **2007**, 13567–13574.

4,4'-dinitro-2,2'-bipyridine-N,N'-dioxide, 7. Synthesis and characterization.

SYNTHESIS[15]

A solution of 2,2'-bipyridine (20.0 g, 106.4 mmol) in 64 mL of sulfuric acid were cooled to 0 °C and fuming HNO_3 (34 mL) was added dropwise. The mixture was heated at 77 °C for 2 days. After cooling to room temperature the solution was poured into a mixture of ice and liquid N_2 (200 mL). The mixture was stirred until all the red fumes were liberated. The yellow solid was filtered off. Yield 53%. The spectroscopic data are coincident with those described in the literature.

^{1}H NMR (300 MHz, DMSO-d_6): δ 8.70 (d, J = 3.3 Hz, 2H), 8.60 (d, J = 7.2 Hz, 2H), 8.38 (dd, J = 3.3 Hz, J = 7.2 Hz, 2H).

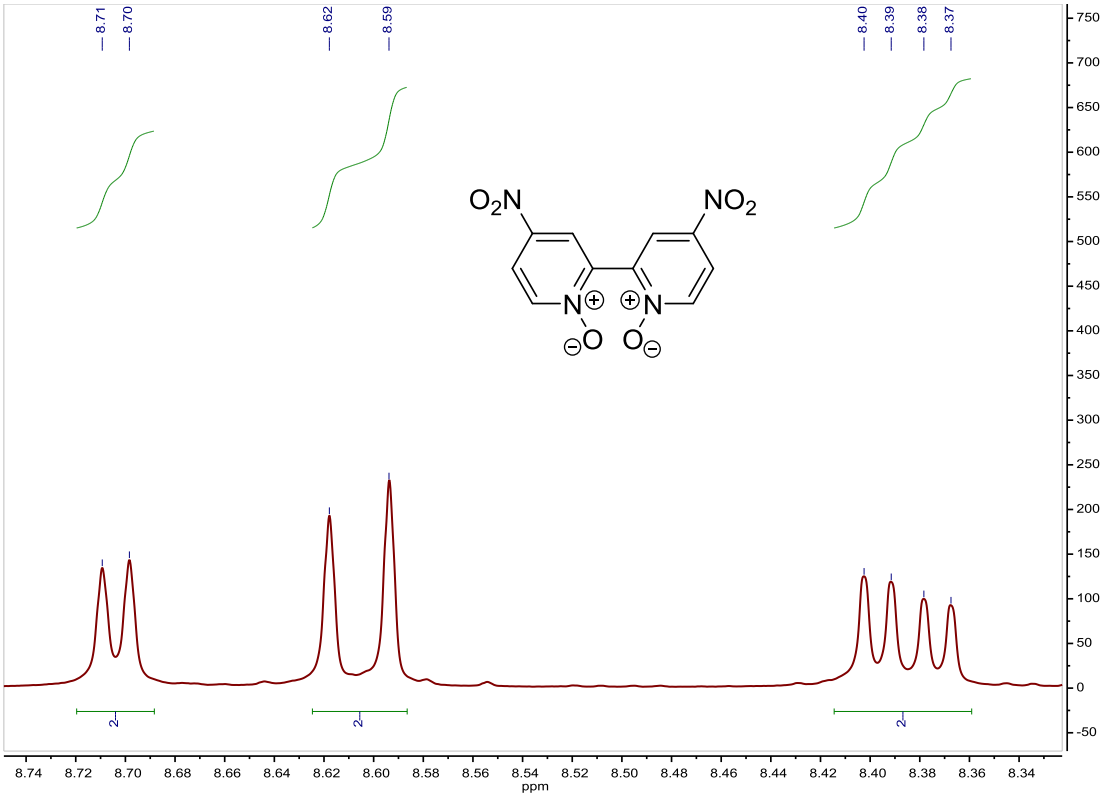

Fig. S27. ^{1}H NMR spectrum of 4,4'-dinitro-2,2'-bipyridine-N,N'-dioxide **7** in DMSO-d_6, 300 MHz.

4,4'-diamino-2,2'-bipyridine, 8. Synthesis and characterization.

SYNTHESIS[16]

4,4'-dinitro-2,2'-bipyridine-N,N'-dioxide **7** (4.0 g, 14.4 mmol) were dissolved in EtOH (133 mL) and 10% palladium on carbon (0.96 g, 9.03 mmol) were added. A solution of hydrazine monohydrate (5.4 mL, 112 mmol) in EtOH (27 mL) was added dropwise and the mixture was refluxed at 80 °C for 16 h. The mixture was filtered hot and washed with cold diethyl ether. The solvent of the filtrate was evaporated and the product was obtained as a brown solid. Yield 65%. The spectroscopic data are coincident with those described in the literature.

^{1}H NMR (300 MHz, DMSO-d_6): δ 8.04 (d, J = 5.5 Hz, 2H), 7.55 (d, J = 2.2 Hz, 2H), 6.46 (dd, J = 2.3 Hz, J = 5.5 Hz, 2H).

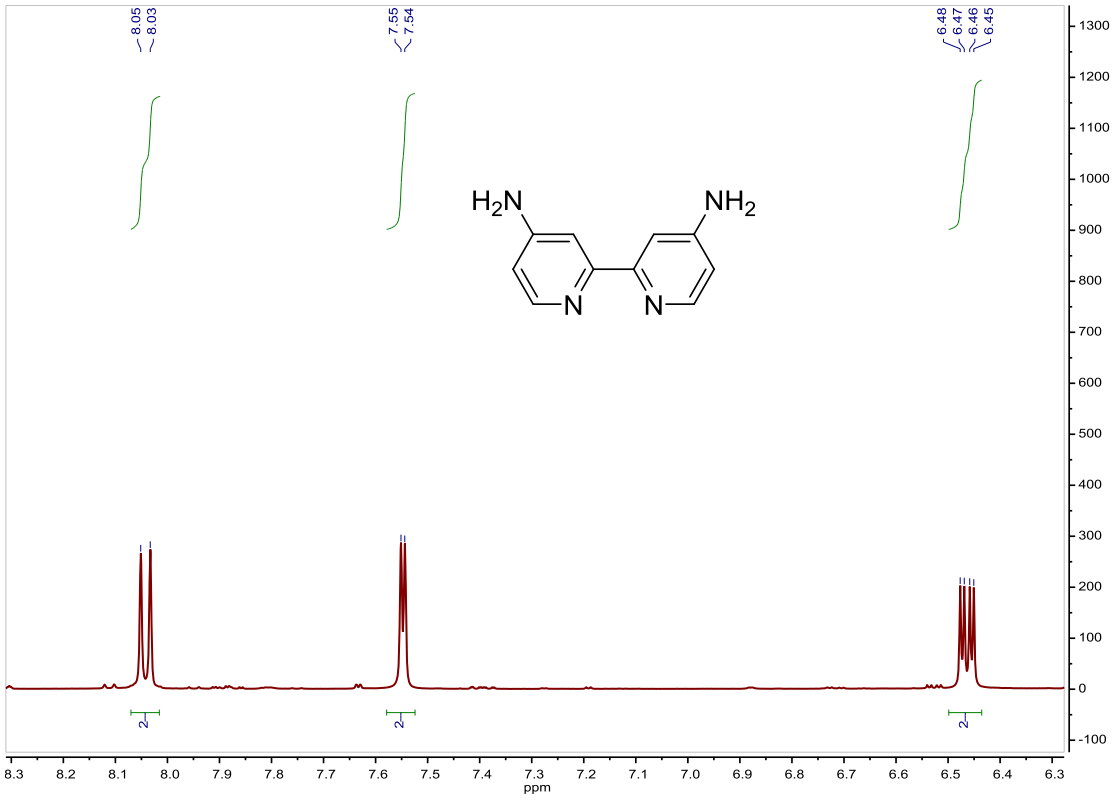

Fig. S28. ^{1}H NMR spectrum of 4,4'-diamino-2,2'-bipyridine **8** in DMSO-d_6, 300 MHz.

[16] O. Maury, J-P. Guégan, T. Renouard, A. Hilton, P. Dupau, N. Sandon, L. Toupet and H. Le Bozec, *New J. Chem.*, **2001**, *25*, 1553–1566.

[4-(phenylazo)phenyl]boronic acid 9. Synthesis and characterization.

SYNTHESIS[17]

The starting 4-iodoazobenzene (1.5 g, 4.87 mmol) was azeotropically dried with toluene under a N_2 atmosphere and dissolved in 40 mL of freshly distilled THF. The solution was cooled to -100 °C, *n*-BuLi 1.6 M in hexanes (3.5 mL, 5.6 mmol) were added and it was stirred for 30 min. The mixture was added to a solution of trimethyl borate (0.6 mL, 5.38 mmol) in 5 mL of freshly distilled THF at -100 °C. The reaction temperature was gradually raised up to room temperature and it was stirred overnight. A mixture of H_2SO_4/H_2O 1/10 (55 mL) was added at 0 °C. The organic layer was separated and the aqueous layer was extracted with Et_2O. An aqueous NaOH solution was added to the combined organic solution and the aqueous layer was washed with Et_2O. A mixture of H_2SO_4/H_2O 1/10 (100 mL) was added to the aqueous layer and an orange product precipitated. The product was purified by column chromatography (silica gel, CH_2Cl_2) and was obtained as an orange solid. Yield 20%. The spectroscopic data are coincident with those described in the literature.[18]

Elemental Analysis: calculated for ($C_{12}H_{11}BN_2O_2$): C, 63.76; H, 4.91; N, 12.39. Found: C, 64.61; H, 4.81; N, 12.30.

^{1}H NMR (300 MHz, $CDCl_3$): δ 8.27 (d, J = 8.1 Hz, 2H, (2 or 3)), 7.91 (d, J = 8.3 Hz, 2H, (2 or 3)), 7.88 (d, J = 9.1 Hz, 2H, (6)), 7.50–7.39 (m, 3H, (7+8)).

^{13}C APT NMR (75 MHz, $CDCl_3$): δ 154.85 (C_{quat}), 152.23 (C_{quat}), 136.14 (2CH, (2 or 3)), 130.96 (CH, (8)), 128.68 (2CH, (7)), 122.66 (2CH, (6)), 121.79 (2CH, (2 or 3)), (carbon bearing boron substituent not observed).

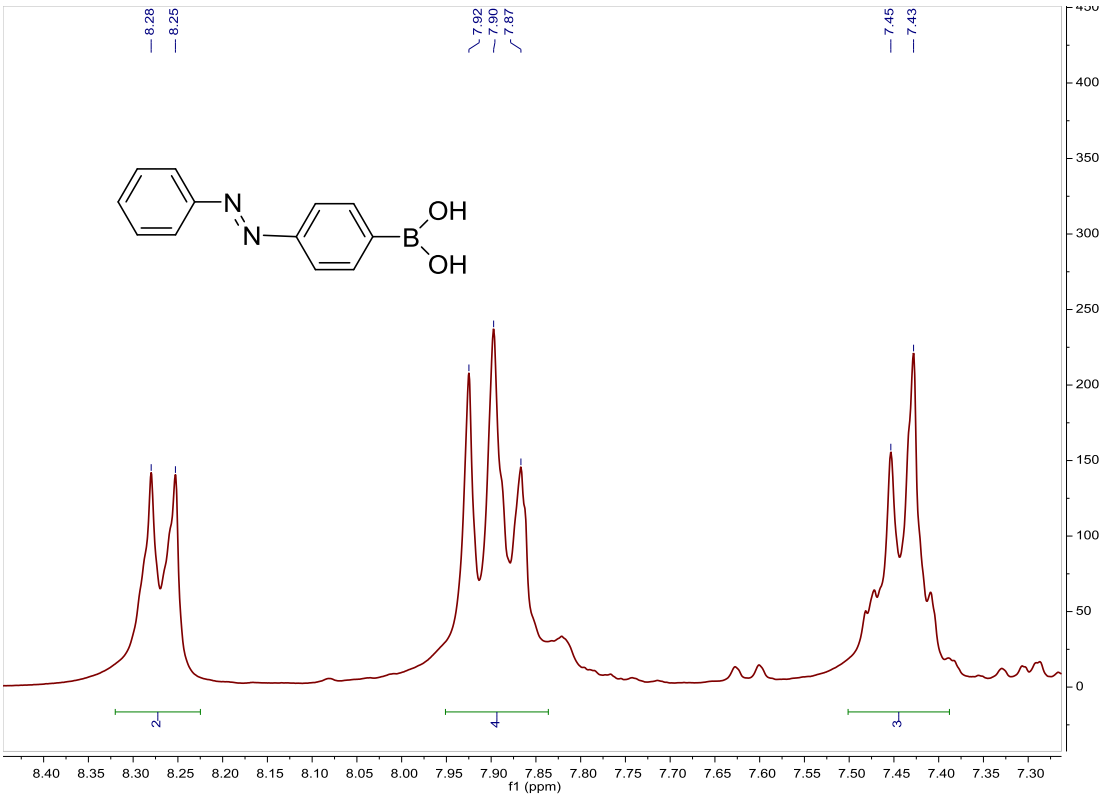

Fig. S29. ^{1}H NMR spectrum of [4-(phenylazo)phenyl]boronic acid **9** in $CDCl_3$, 300 MHz.

[17] N. Kano, J. Yoshino and T. Kawashima, *Org. Lett.*, **2005**, *7*, 3909–3911.

[18] K. Owashi, K. Ueno, T. Satomi, G. Chen and H. Otsuka, *Trans. Mater. Res. Soc. Japan,* **2007**, *32*, 777–780.

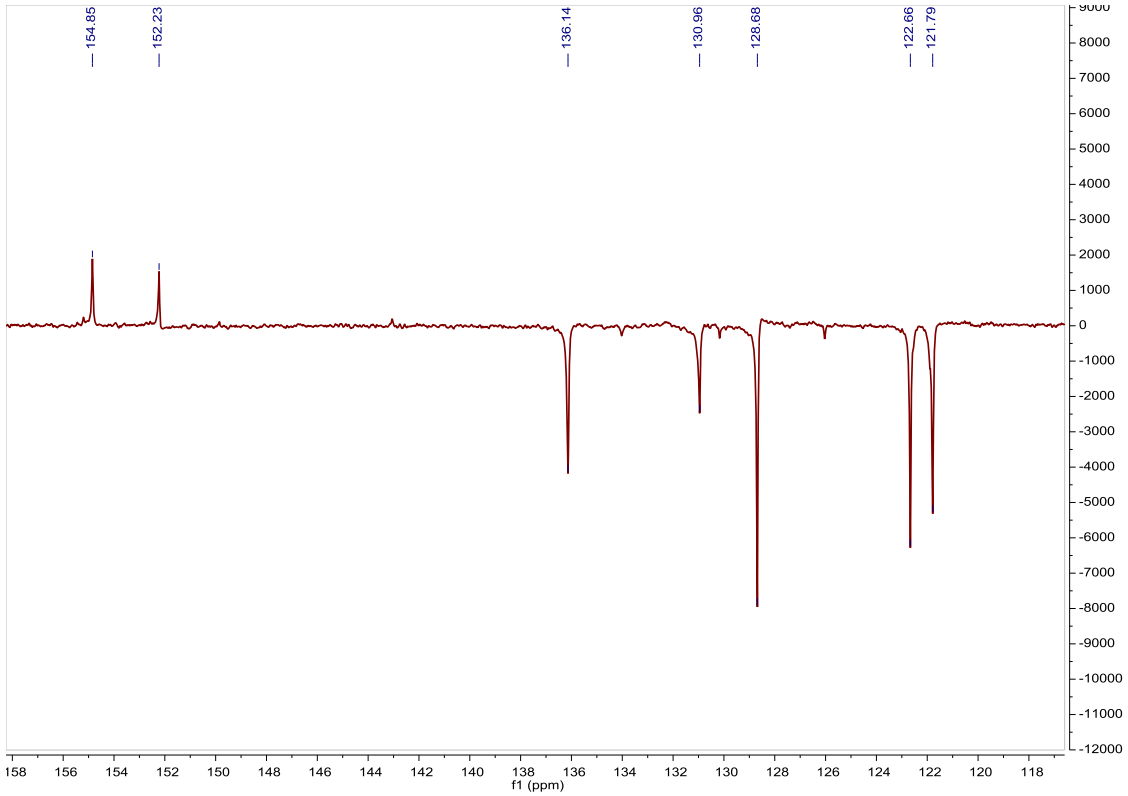

Fig. S30. ^{13}C APT NMR spectrum of [4-(phenylazo)phenyl]boronic acid **9** in $CDCl_3$, 75 MHz.

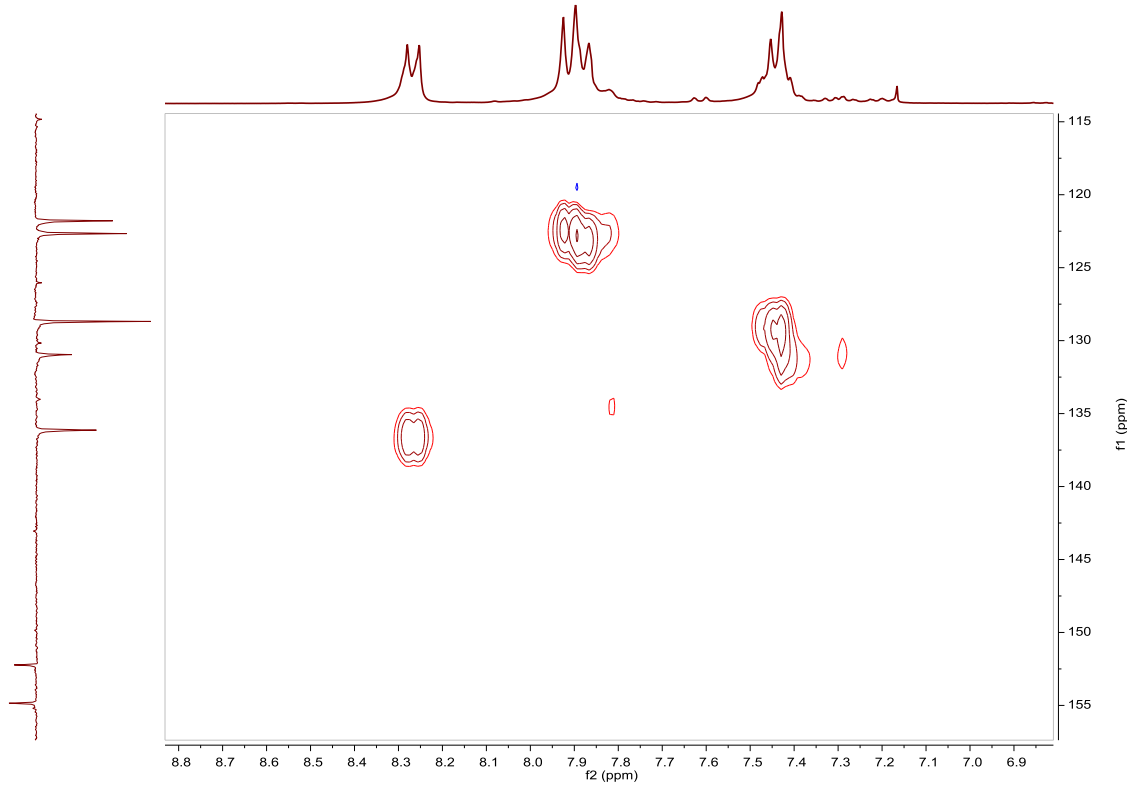

Fig. S31. HSQC spectrum of [4-(phenylazo)phenyl]boronic acid **9** in $CDCl_3$.

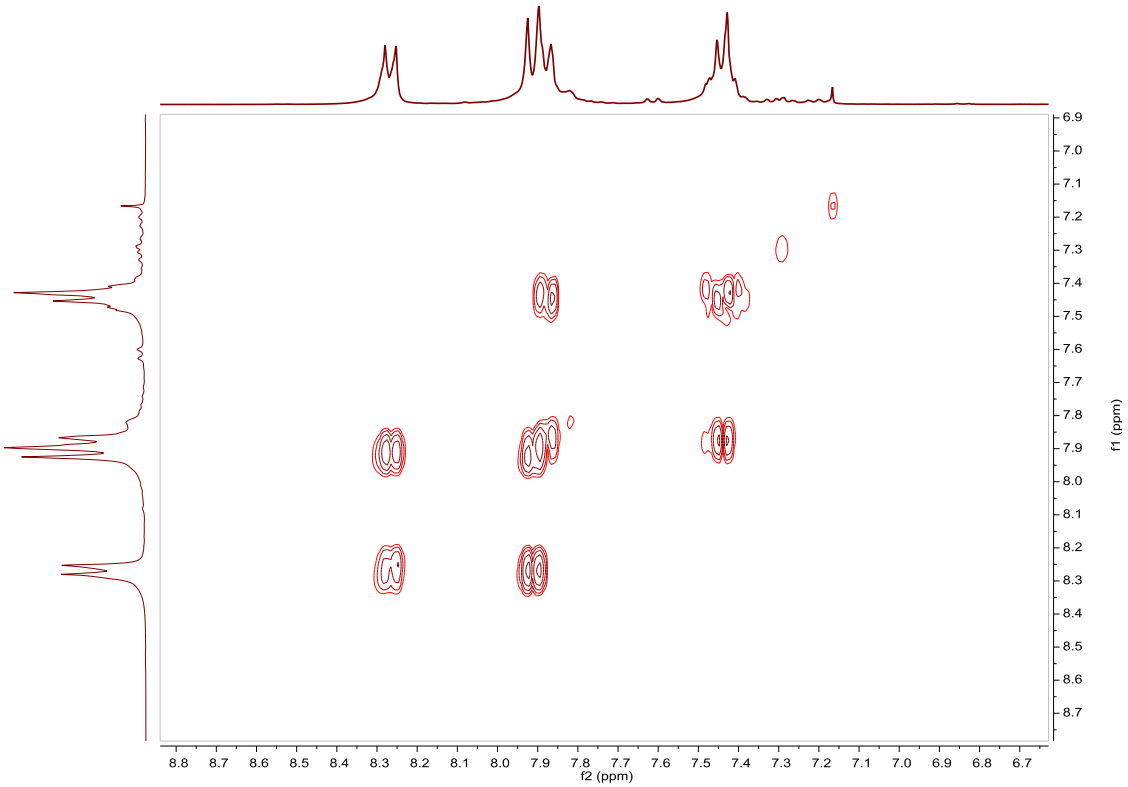

Fig. S32. COSY spectrum of [4-(phenylazo)phenyl]boronic acid **9** in $CDCl_3$.

[3-(phenylazo)phenyl]boronic acid 10. Synthesis and characterization.

SYNTHESIS[17]

The starting 3-iodoazobenzene (3.0 g, 9.74 mmol) was azeotropically dried with toluene under a N_2 atmosphere and dissolved in 80 mL of freshly distilled THF. The solution was cooled to -100 °C, *n*-BuLi 1.6 M in hexanes (7.0 mL, 11.2 mmol) were added and it was stirred for 30 min. The mixture was added to a solution of trimethyl borate (1.20 mL, 10.76 mmol) in 10 mL of freshly distilled THF at -100 °C. The reaction temperature was gradually raised up to room temperature and it was stirred overnight. A mixture of H_2SO_4/H_2O 1/10 (110 mL) was added at 0 °C. The organic layer was separated and the aqueous layer was extracted with Et_2O. An aqueous NaOH solution was added to the combined organic solution and the aqueous layer was washed with Et_2O. A mixture of H_2SO_4/H_2O 1/10 (200 mL) was added to the aqueous layer and a brown product precipitated. The product was filtrated and was obtained as a brown solid. Yield 61%. The spectroscopic data are coincident with those described in the literature.[18]

^{1}H NMR (300 MHz, $CDCl_3$): δ 8.31 (s, 1H), 8.09–8.04 (m, 1H), 7.97 (brd, J = 1.8 Hz, J = 8.3 Hz, 2H), 7.95–7.90 (m, 1H), 7.65–7.50 (m, 4H).

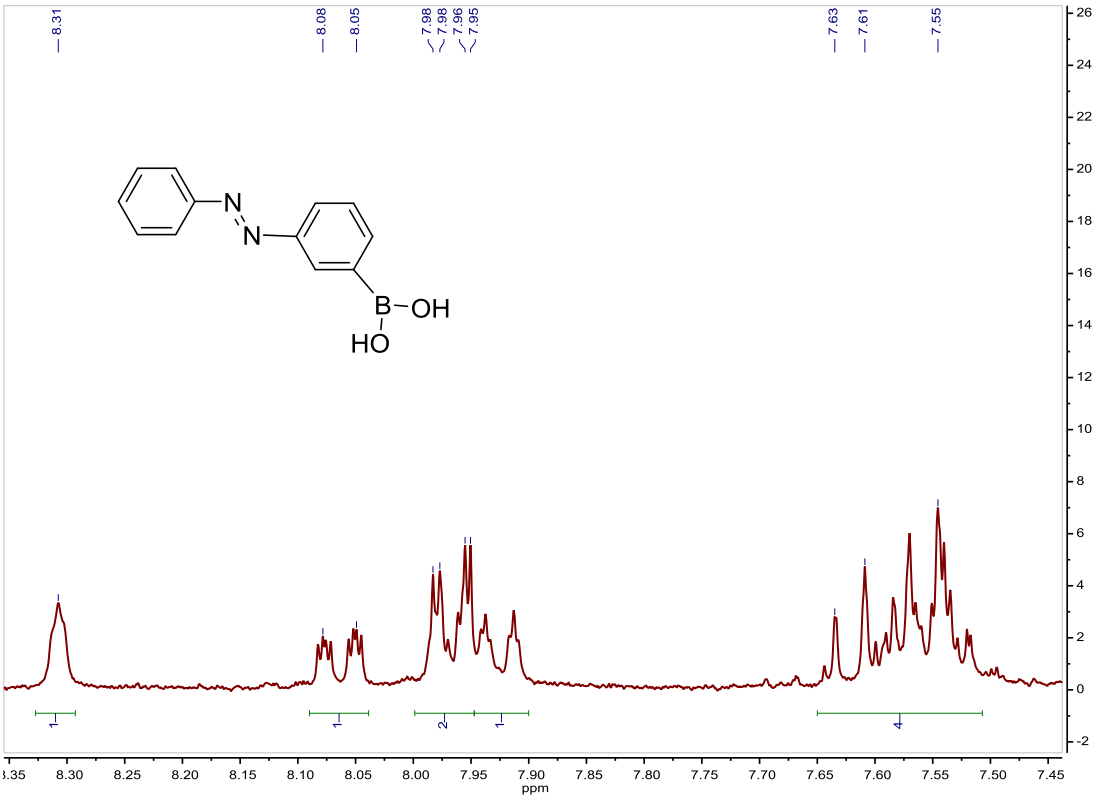

Fig. S33. ^{1}H NMR spectrum of [3-(phenylazo)phenyl]boronic acid **10** in $CDCl_3$, 300 MHz.

[4-(phenylazo)phenyl]boronic acid pinacol ester 11. Synthesis and characterization.

SYNTHESIS[19]

Nitrosobenzene (2.49 g, 23.25 mmol) were dissolved in glacial acetic acid (84 mL) to give a green solution. (4,4,5,5-Tetramethyl-1,3,2-dioxaborolan-2-yl)aniline (3.5 g, 15.98 mmol) were added and the mixture was refluxed at 118 °C for 3.5 h. After cooling to room temperature, H_2O (100 mL) were added and the solution was neutralized with $NaHCO_3$. The product was extracted with CH_2Cl_2 and purified by column chromatography (silica gel, CH_2Cl_2). It was obtained as an orange solid. Yield 82%. The spectroscopic data are coincident with those described in the literature.

^{1}H NMR (300 MHz, $CDCl_3$): δ 8.03–7.91 (m, 6H), 7.60–7.50 (m, 3H).

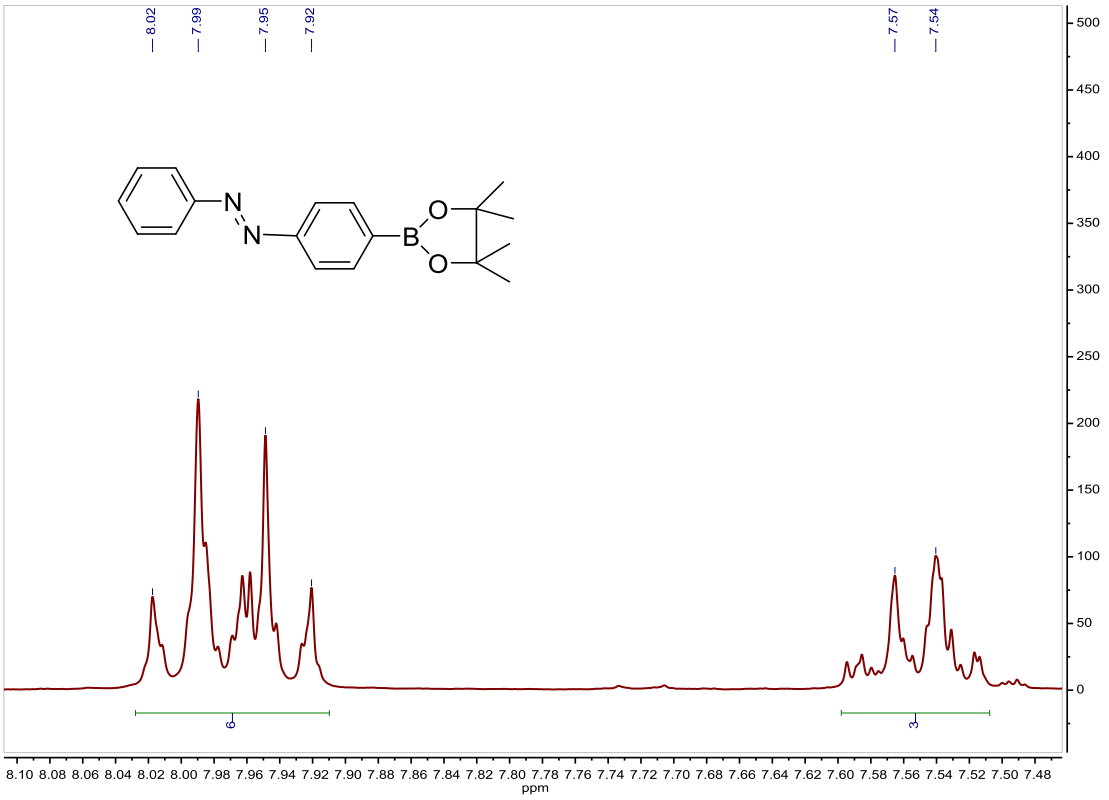

Fig. S34. ^{1}H NMR spectrum of [4-(phenylazo)phenyl]boronic acid pinacol ester **11** in $CDCl_3$, 300 MHz.

[19] J. H. Harvey, B. K. Butler and D. Trauner, *Tetrahedron Lett.*, **2007**, *48*, 1661–1664.

Ligand 12, tris(*m*-azobenzene)phosphane. Synthesis, characterization and photoisomerization studies.

SYNTHESIS[20]

The starting 3-iodoazobenzene (3.0 g, 9.74 mmol) was azeotropically dried with toluene under a N_2 atmosphere and dissolved in 60 mL of freshly distilled THF. The solution was cooled to -110 °C, *n*-BuLi 1.6 M in hexanes (6.0 mL, 9.6 mmol) were added and it was stirred for 30 min. PCl_3 (285 µL, 3.28 mmol) were added, the reaction temperature was gradually raised up to room temperature and it was stirred overnight. The solvent was evaporated and the product was purified by column chromatography (silica gel, CH_2Cl_2/Hexane 1/1). The product was obtained as an orange solid. Yield 14%. The spectroscopic data are coincident with those described in the literature.

^{1}H NMR (500 MHz, $CDCl_3$): δ 7.86–8.13 (m, 12H), 7.45–7.60 (m, 15H).

^{31}P NMR (202.5 MHz, $CDCl_3$): δ -3.74.

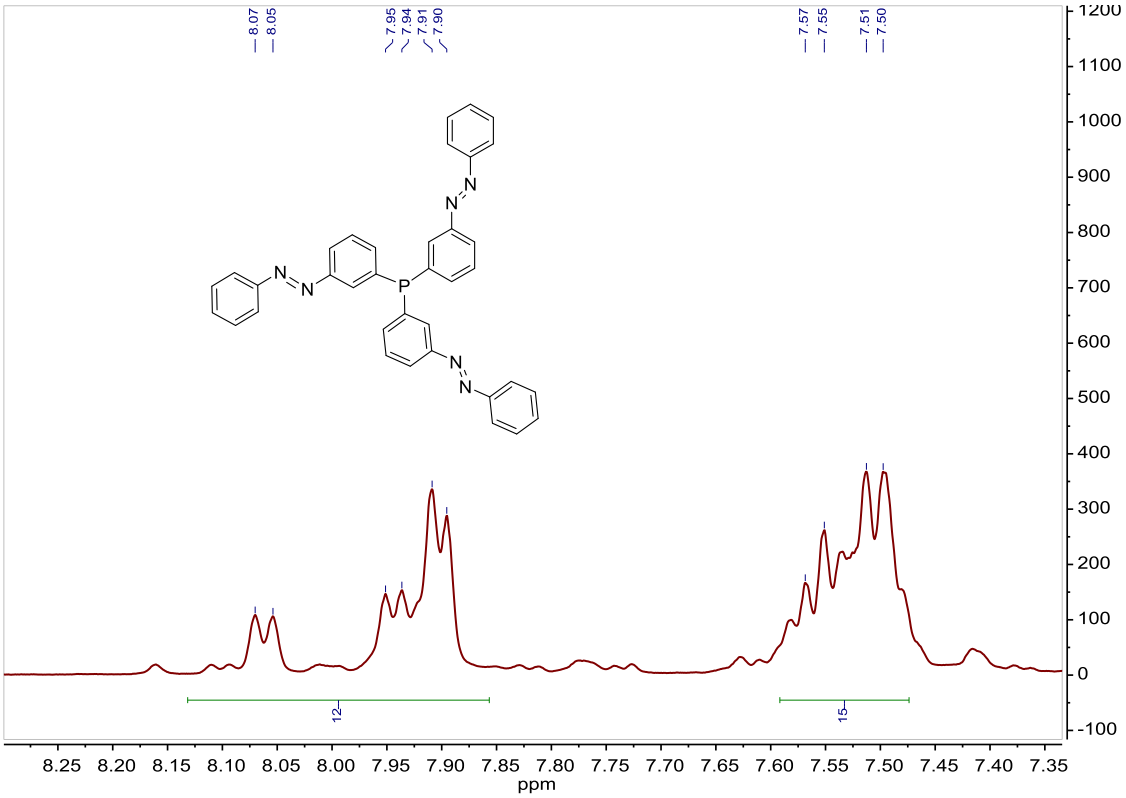

Fig. S35. ^{1}H NMR spectrum of tris(*m*-azobenzene)phosphane **Ligand 12**, in $CDCl_3$, 500 MHz.

[20] M. D. Segarra-Maset, P. W. N. M. van Leeuwen, and Z. Freixa, *Eur. J. Inorg. Chem.*, **2010**, 2075–2078.

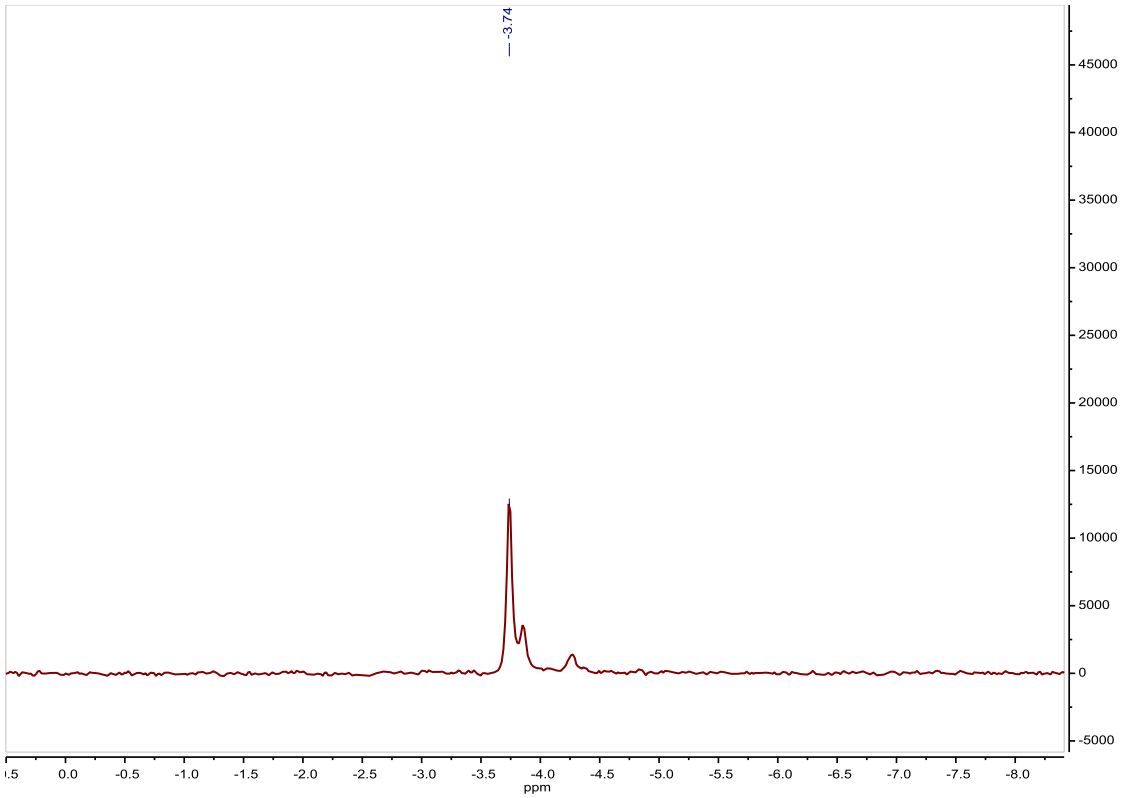

Fig. S36. ^{31}P NMR spectrum of tris(*m*-azobenzene)phosphane **Ligand 12**, in $CDCl_3$, 202.5 MHz.

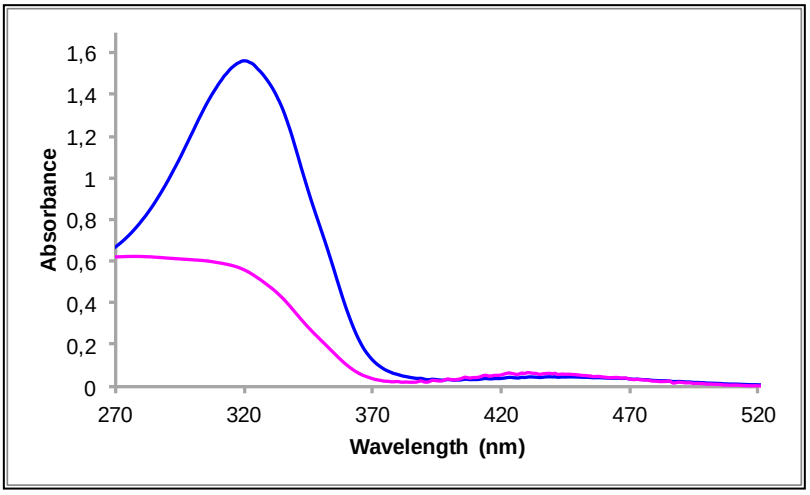

Fig. S37. UV/Vis spectra of tris(*m*-azobenzene)phosphane **Ligand 12** in ACN. Before (blue line) and after (pink line) irradiation at 323 nm, $2.57 \cdot 10^{-5}$M.

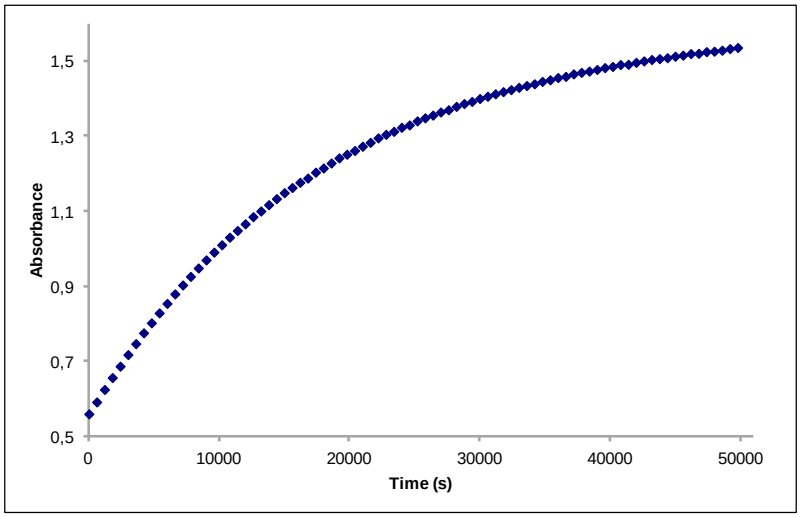

Fig. S38. Cis to trans thermal isomerization kinetics of tris(*m*-azobenzene)phosphane **Ligand 12**. Absorption change of the band 320 nm at 338 K in ACN after irradiation at 323 nm. ($2.57 \cdot 10^{-5}$M).

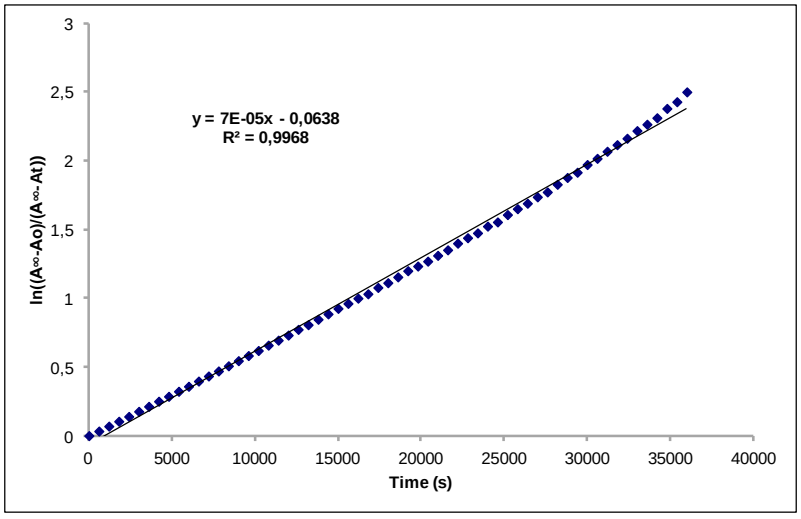

Fig. S39. Cis to trans thermal isomerization kinetics of tris(*m*-azobenzene)phosphane **Ligand 12**. First-order plot. k (s^{-1}) = $7.0 \cdot 10^{-5}$. Half-life (min) = 165.

Ligand 13, tris(*p*-azobenzene)phosphane. Synthesis, characterization and photoisomerization studies.

SYNTHESIS[20]

The starting 4-iodoazobenzene (1.5 g, 4.87 mmol) was azeotropically dried with toluene under a N_2 atmosphere and dissolved in 30 mL of freshly distilled THF. The solution was cooled to -80 °C, *n*-BuLi 1.6 M in hexanes (4.5 mL, 7.3 mmol) were added and it was stirred for 30 min. PCl_3 (142 µL, 1.63 mmol) were added, the reaction temperature was gradually raised up to room temperature and it was stirred overnight. The solvent was evaporated, the residue was washed with EtOH and the product was obtained as an orange solid. Yield 10%.

Elemental Analysis: calculated for ($C_{36}H_{27}N_6P$·EtOH): C, 73.53; H, 5.36; N, 13.54. Found: C, 73.88; H, 4.98; N, 13.85.

Exact Mass: ESI-MS $[C_{36}H_{27}N_6P + H]^+$: calculated: m/z= 575.2113, found: m/z= 575.2123.

^{1}H NMR (300 MHz, $CDCl_3$): δ 7.88–7.79 (m, 12H), 7.49–7.38 (m, 15H).

^{13}C APT NMR (75 MHz, $CDCl_3$): δ 152.51 (s, $3C_{quat}$), 152.22 (s, $3C_{quat}$), 139.42 (d, J = 12.7 Hz, $3C_{quat}$), 134.09 (d, J = 20.2 Hz, 6CH), 130.86 (s, 3CH), 128.68 (s, 6CH), 122.54 (s, 6CH), 122.50 (d, J = 6.0 Hz, 6CH).

^{31}P NMR (202.5 MHz, $CDCl_3$): δ -3.69 (s, 1P).

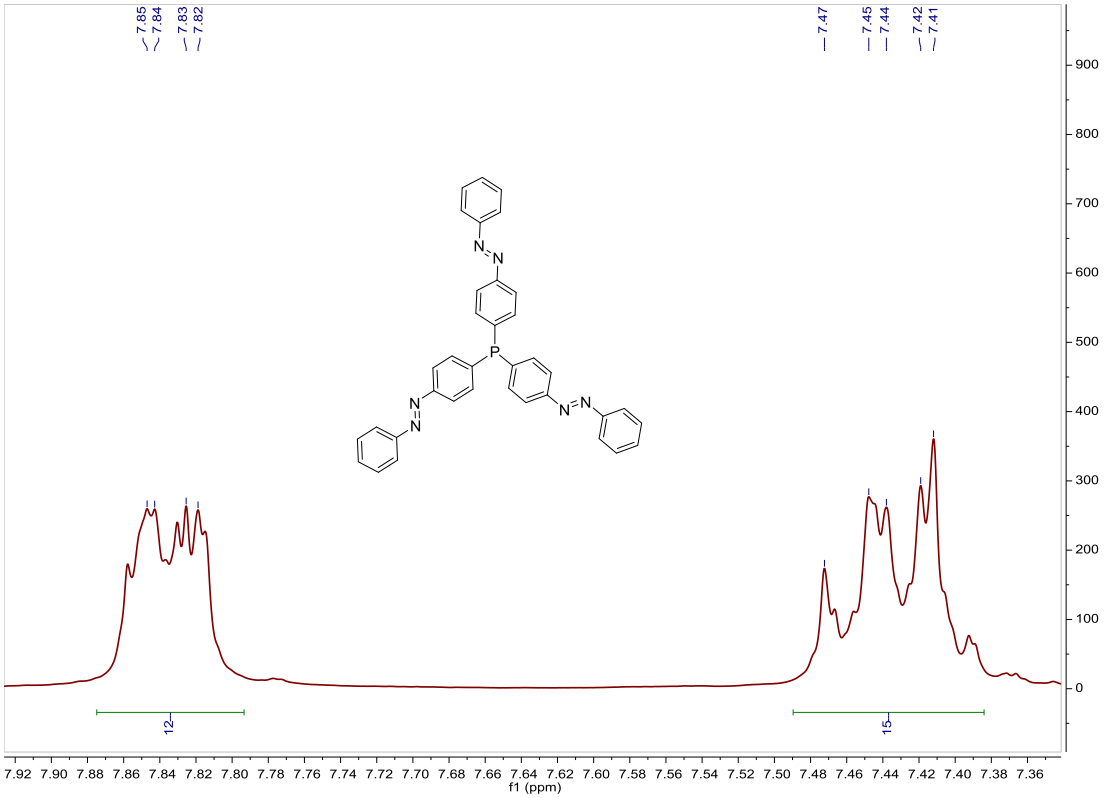

Fig. S40. ^{1}H NMR spectrum of tris(*p*-azobenzene)phosphane **Ligand 13** in $CDCl_3$, 300 MHz.

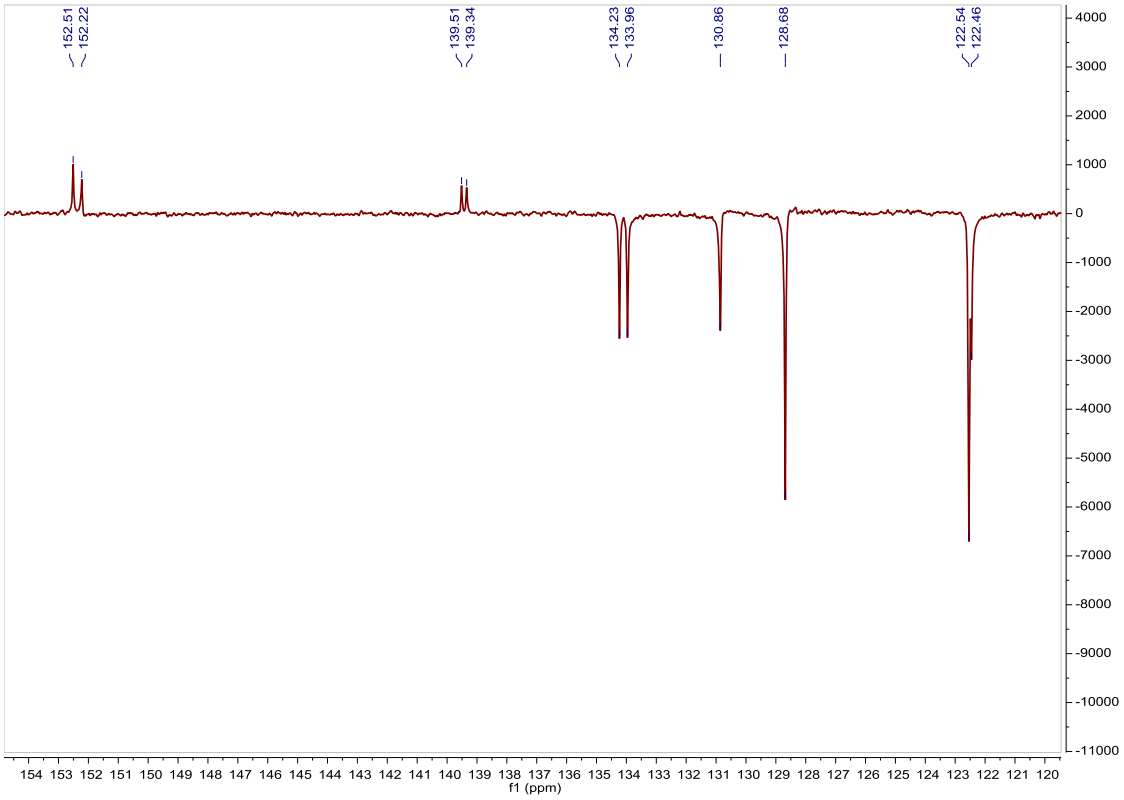

Fig. S41. ^{13}C APT NMR spectrum of tris(*p*-azobenzene)phosphane **Ligand 13** in $CDCl_3$, 75 MHz.

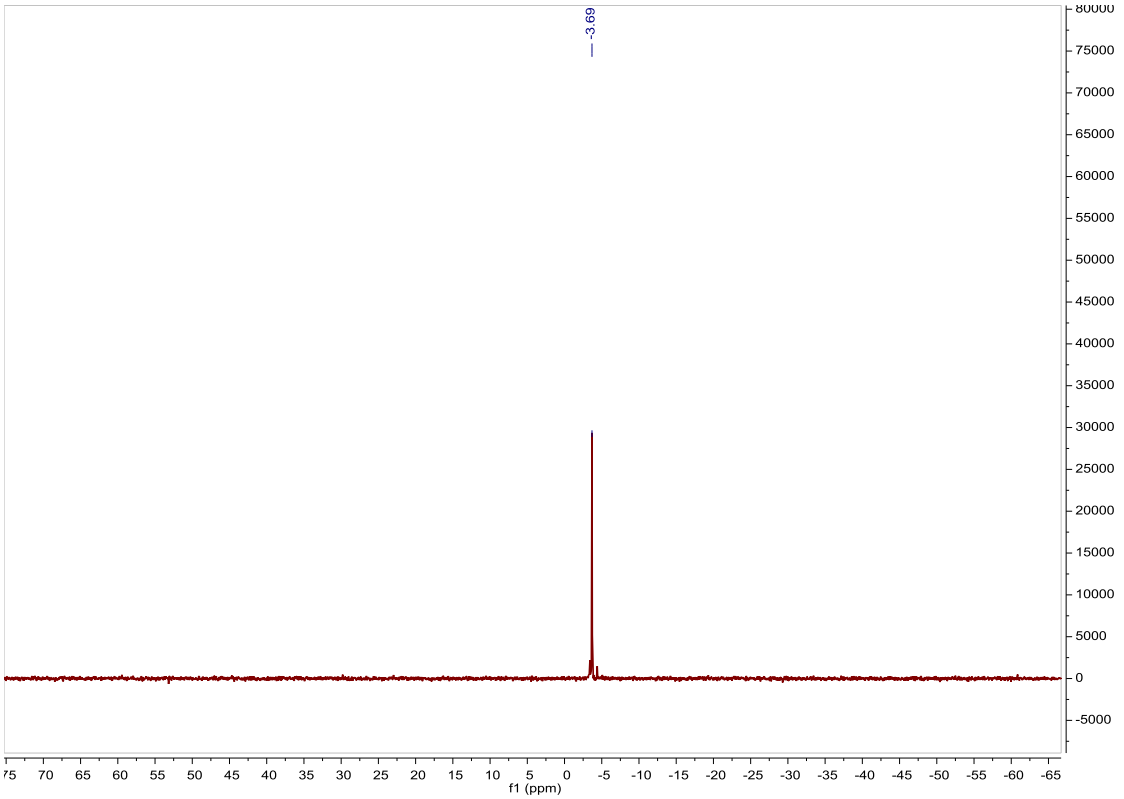

Fig. S42. ^{31}P NMR spectrum of tris(*p*-azobenzene)phosphane **Ligand 13** in $CDCl_3$, 202.5 MHz.

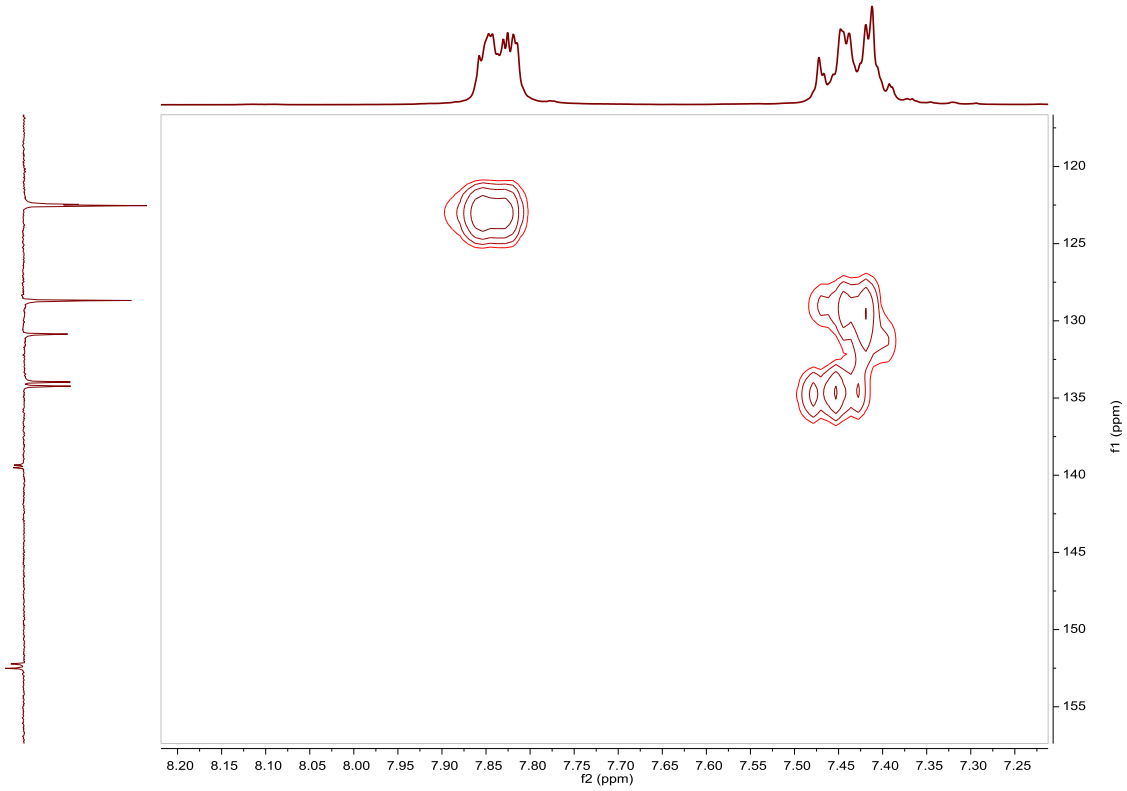

Fig. S43. HSQC NMR spectrum of tris(*p*-azobenzene)phosphane **Ligand 13** in $CDCl_3$.

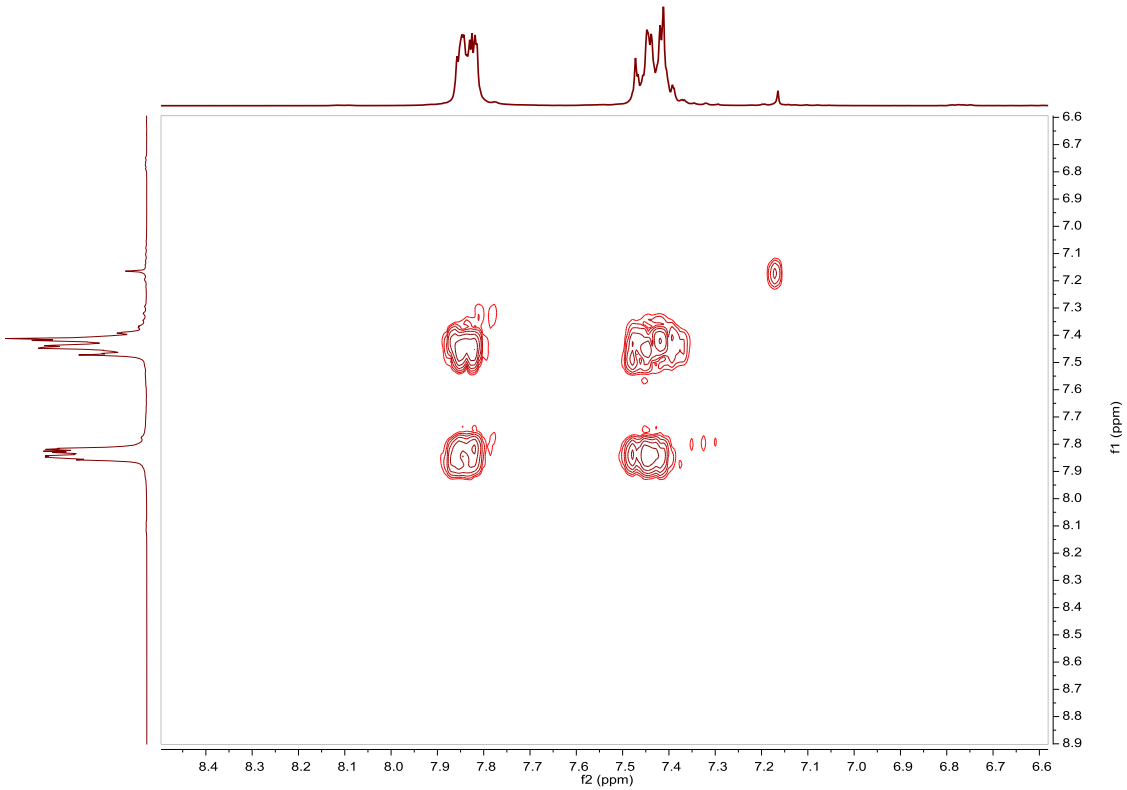

Fig. S44. COSY NMR spectrum of tris(*p*-azobenzene)phosphane **Ligand 13** in $CDCl_3$.

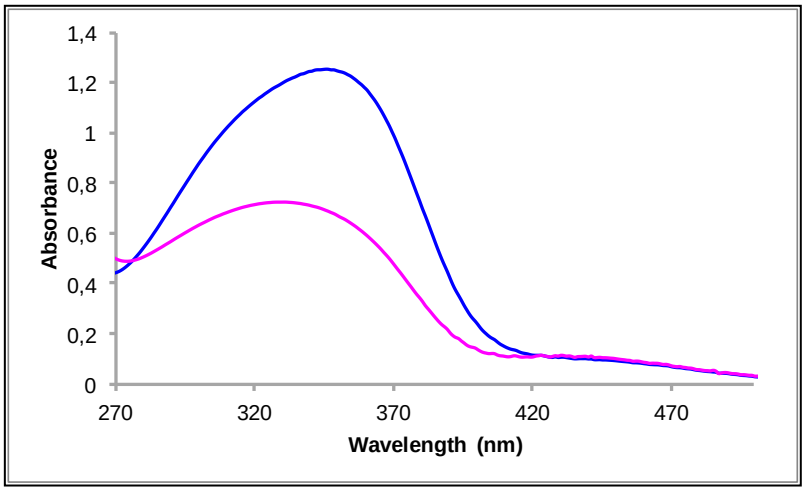

Fig. S45. UV/Vis spectra of tris(*p*-azobenzene)phosphane **Ligand 13** in ACN. Before (blue line) and after (pink line) irradiation at 354nm, $2.72 \cdot 10^{-5}$M.

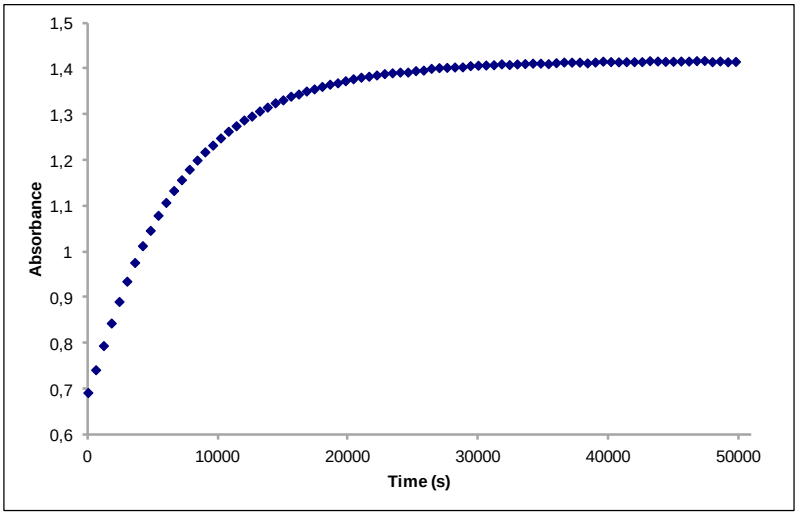

Fig. S46. Cis to trans thermal isomerization kinetics of tris(*p*-azobenzene)phosphane **Ligand 13**. Absorption change of the band 345nm at 338 K in ACN after irradiation at 354 nm. ($2.72 \cdot 10^{-5}$M).

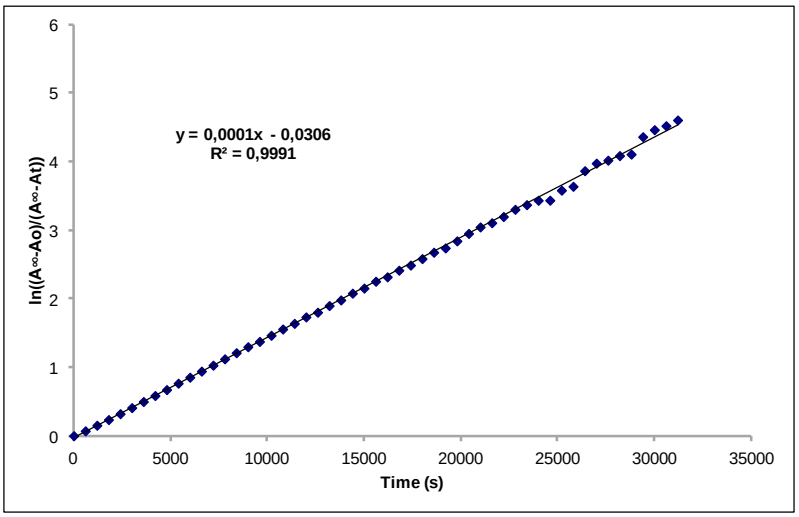

Fig. S47. Cis to trans thermal isomerization kinetics of tris(*p*-azobenzene)phosphane **Ligand 13**. First-order plot. k (s^{-1}) = $1.0 \cdot 10^{-4}$. Half-life (min) = 115.

Ligand 14, 4,4'-dinitro-2,2'-bipyridine. Synthesis and characterization.

SYNTHESIS[21]

4,4'-dinitro-2,2'-bipyridine-N-oxide (1,40 g, 5.03 mmol) were dissolved in freshly distilled CH_2Cl_2. To the solution PCl_3 (16 mL, 183.42 mmol) were added dropwise and the mixture was refluxed for 14 h. After cooling to room temperature, the white solid was removed by filtration and the solution was poured into ice/water (200 mL). An aqueous solution of NaOH was added until pH = 8 and the product was extracted with CH_2Cl_2. The product was redissolved in CH_2Cl_2 and obtained as a yellow solid. Yield 50%. The spectroscopic data are coincident with those described in the literature.

^{1}H NMR (300 MHz, $CDCl_3$): δ 9.24 (d, J = 1.7 Hz, 2H), 9.07 (d, J = 5.3 Hz, 2H), 8.16 (dd, J = 2.2 Hz, J = 5.3 Hz, 2H).

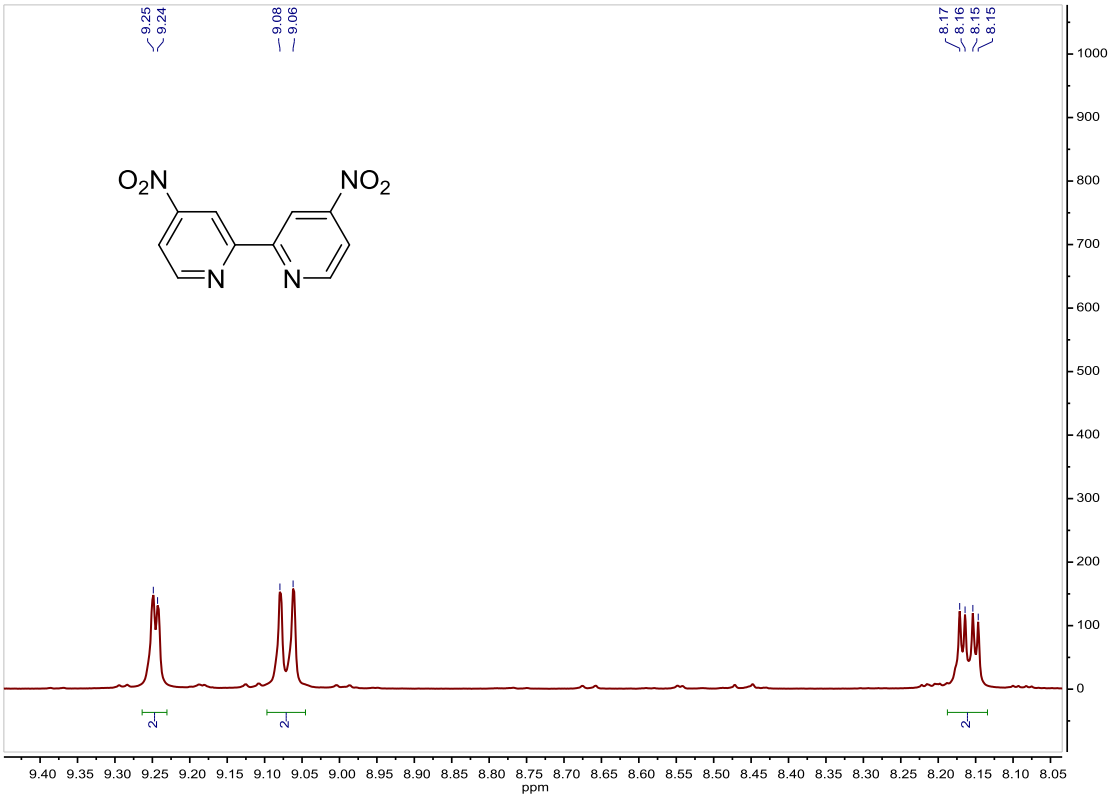

Fig. S48. ^{1}H NMR spectrum of **Ligand 14** in $CDCl_3$, 300 MHz.

[21] H. Arzoumanian and R. Bakhtchadjian, *Transition Metal Chemistry*, **2006**, *31*, 681–689.

Ligand 15, 4,4'-bis(diethylphosphonate)-2,2'-bipyridine. Synthesis and characterization.

SYNTHESIS[22]

4,4'-dibromo-2,2'-bipyridine (0.5 g, 1.6 mmol) was dissolved in 5 ml of freshly distilled toluene and stirred under nitrogen for 20 min. Diethyl phosphite (0.56 ml, 4.35 mmol) and distilled $N(Et)_3$ (0.61 ml) were added and the mixture was stirred for 10 min. The catalyst, $Pd(PPh_3)_4$ (0.18 g, 0.16 mmol), was added and the mixture was heated at 90 °C for 4 h. After cooling to room temperature ether was added and the precipitated was removed by filtration. The product was purified by column chromatography (silica gel, 100% CH_2Cl_2 to 100% acetone) to yield (60%) of the diethylphosphonate bipyridine. The spectroscopic data are coincident with those described in the literature.

^{1}H NMR (300 MHz, $CDCl_3$): δ 8.88 (t, J = 5.5 Hz, 1H), 8.81 (d, J = 14.2 Hz, 1H), 7.76 (ddd, J = 1.4 Hz, J = 4.8 Hz, J = 13.0 Hz, 1H), 4.24 (m, 4H), 1.40 (t, J = 7.0 Hz, 6H).

UV/Vis (EtOH), λ, nm (ε, 10^4 M^{-1} cm^{-1}): 240 (1.2), 292 (1.45).

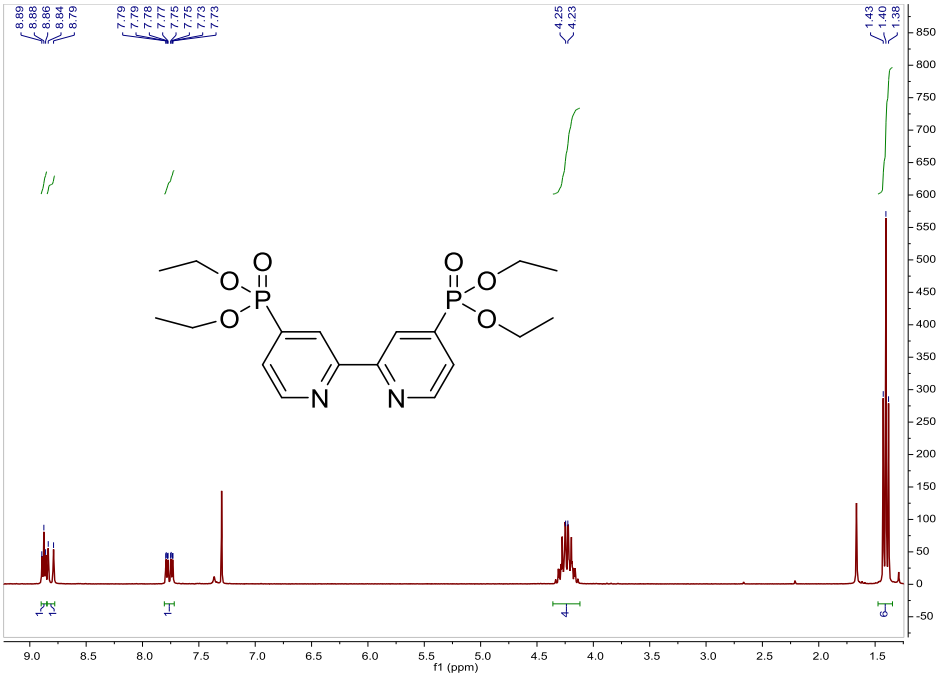

Fig. S49. ^{1}H NMR spectrum of **Ligand 15** in $CDCl_3$, 300 MHz.

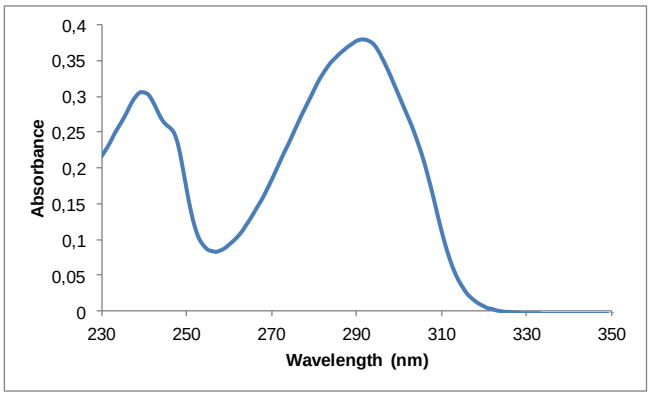

Fig. S50. UV/Vis spectra of **Ligand 15** in EtOH, $2.62 \cdot 10^{-5}$M.

[22] M. Montalti, S. Wadhwa, W. Y. Kim, R. A. Kipp and R. H. Schmehl, *Inorg. Chem.*, **2000**, *39*, 76–84.

Ligand 16, 4,4'-bis(carboxy)-2,2'-bipyridine. Synthesis and characterization.

SYNTHESIS[23]

4,4'-dimethyl-2,2'-bipyridine (0.74 g, 4 mmol) was added slowly and with a vigorous stirring to a solution of $Na_2Cr_2O_7 \cdot 2H_2O$ (5.52 g, 18.5 mmol) in 25 ml concentrated sulfuric acid. After 30 min stirring, the mixture was poured into 200 ml of cold water and the precipitated was filtered. The obtained solid was dissolved in 10% NaOH aqueous solution and 10% HCl aqueous solution was added to reach pH = 2. The precipitated was filtered to yield (100%) of the desired compound as a white solid. The spectroscopic data are coincident with those described in the literature.

^{1}H NMR (300 MHz, DMSO-d_6): δ 8.93 (d, J = 5.0 Hz, 1H), 8.86 (s, 1H), 7.93 (dd, J = 1.5 Hz, J = 5.0 Hz, 1H).

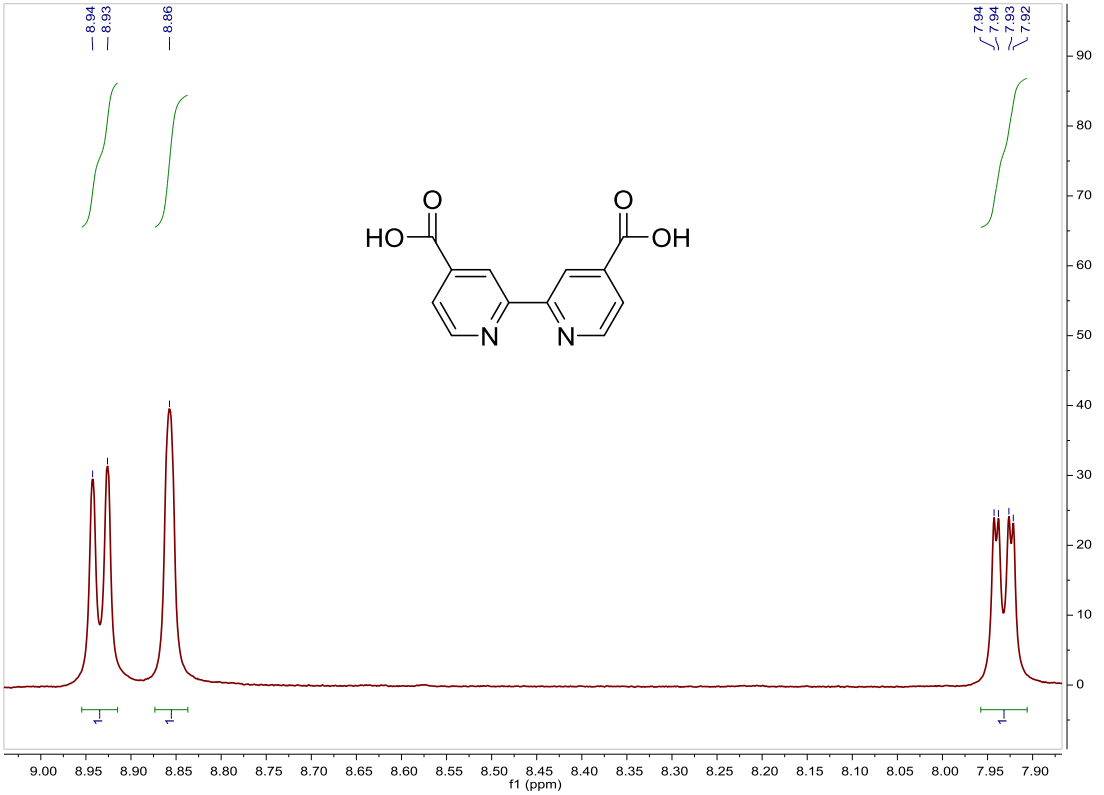

Fig. S51. ^{1}H NMR spectrum of **Ligand 16** in DMSO-d_6, 300 MHz.

[23] K. F. Lin, J. S. Ni, C. H. Tseng, C. Y. Hung and K. Y. Liu, *Mater. Chem. Phys.*, **2013**, *142*, 420–427.

Ligand 17, 4,4'-bis(ethynyl)-2,2'-bipyridine. Synthesis and characterization.

SYNTHESIS[24,25]

4,4'-dibromo-2,2'-bipyridine (1.00 g, 3.18 mmol), CuI (0.02 g, 0.11 mmol) and $Pd(PPh_3)_4$ (0.04 g, 0.06 mmol) were dissolved in freshly distilled NEt_3 (20 mL). (trimethylsilyl)acetylene (1 mL, 7.08 mmol) were added and the mixture was refluxed for 3.5 h. The solvent was evaporated and 4,4'-bis(trimethylsilyl)ethynyl)-2,2'-bipyridine was obtained after purification by column chromatography (alumina, CH_2Cl_2). The product was dissolved in MeOH (50 mL) and K_2CO_3 (1.14 g, 8.26 mmol) were added, the mixture was stirred overnight. The solvent was evaporated and the residue was partitioned between ethyl acetate and water. The ethyl acetate was evaporated and the product was obtained after purification by column chromatography (alumina, CH_2Cl_2) as a white solid. Yield: 77%. The spectroscopic data are coincident with those described in the literature.

^{1}H NMR (500 MHz, $CDCl_3$): δ 8.69 (d, J = 4.9 Hz, 2H), 8.52 (s, 2H), 7.41 (d, J = 5.0 Hz, 2H), 3.35 (s, 2H).

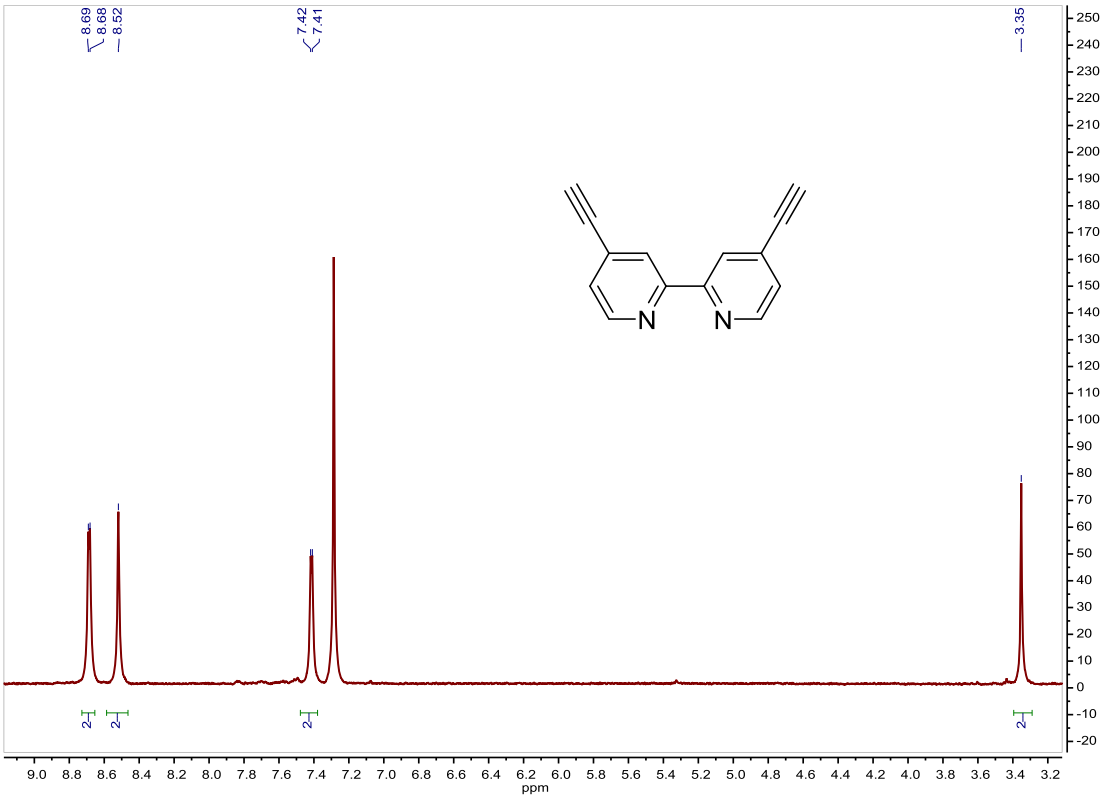

Fig. S52. ^{1}H NMR spectrum of **Ligand 17** in $CDCl_3$, 500 MHz.

[24] P. V. James, K. Yoosaf, J. Kumar, K. G. Thomas, A. Listorti, G. Accorsi and N. Armaroli, *Photochem. Photobiol. Sci.*, **2009**, *8*, 1432–1440.

[25] T. R. Kelly, Y.–J. Lee and R. J. Mears, *J. Org. Chem.*, **1997**, *62*, 2774–2781.

Ligand 21, 4,4'-diazido-2,2'-bipyridine. Synthesis and characterization.

SYNTHESIS[26]

4,4'-dibromo-2,2'-bipyridine (2.00 g, 6.37 mmol) and NaN_3 (2.46 g, 37.8 mmol) were dissolved in DMF (70 mL). The mixture was refluxed for 2 days. After cooling to room temperature, H_2O was added and the product was extracted with Et_2O. It was purified by column chromatography (silica, CH_2Cl_2) and it was obtained as a white solid. Yield: 35%. The spectroscopic data are coincident with those described in the literature.

^{1}H NMR (500 MHz, $CDCl_3$): δ 8.61 (d, J = 5.2 Hz, 2H), 8.19 (s, 2H), 7.41 (dd, J = 2.1 Hz, J = 5.2 Hz, 2H).

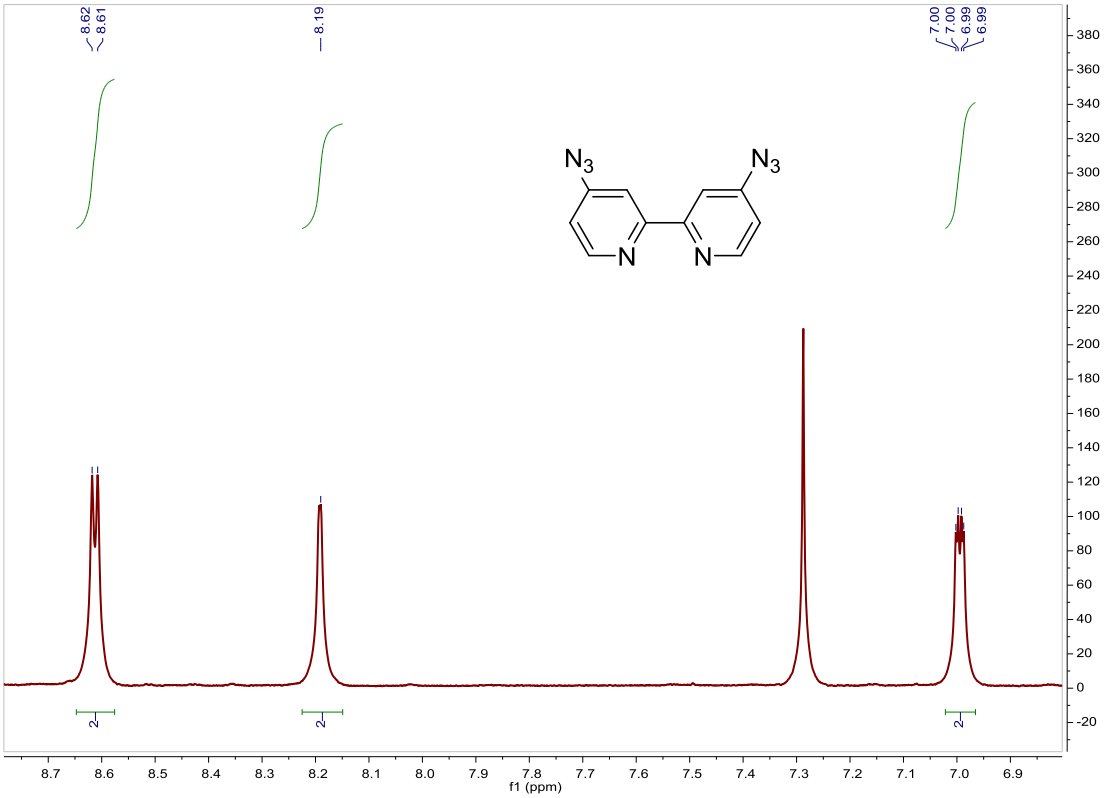

Fig. S53. ^{1}H NMR spectrum of **Ligand 21** in $CDCl_3$, 500 MHz.

[26] P. Fabbrizzi, B. Cecconi and S. Cicchi, *Synlett*, **2011**, *2*, 223–226.

Ligand 22, 4-bromo-4'-azido-2,2'-bipyridine. Synthesis and characterization.

SYNTHESIS[26]

4,4'-dibromo-2,2'-bipyridine (2.00 g, 6.37 mmol) and NaN_3 (2.46 g, 37.8 mmol) were dissolved in DMF (70 mL). The mixture was refluxed for 2 days. After cooling to room temperature, H_2O was added and the product was extracted with Et_2O. It was purified by column chromatography (silica, CH_2Cl_2) and it was obtained as a white solid. Yield: 13%. The spectroscopic data are coincident with those described in the literature.

^{1}H NMR (500 MHz, $CDCl_3$): δ 8.66 (d, J = 1.6 Hz, 1H), 8.61 (d, J = 5.4 Hz, 1H), 8.51 (d, J = 5.1 Hz, 1H), 8.16 (d, J = 2.3 Hz, 1H), 7.53 (dd, J = 2.0 Hz, J = 5.2 Hz, 1H), 6.99 (dd, J = 2.3 Hz, J = 5.4 Hz, 1H).

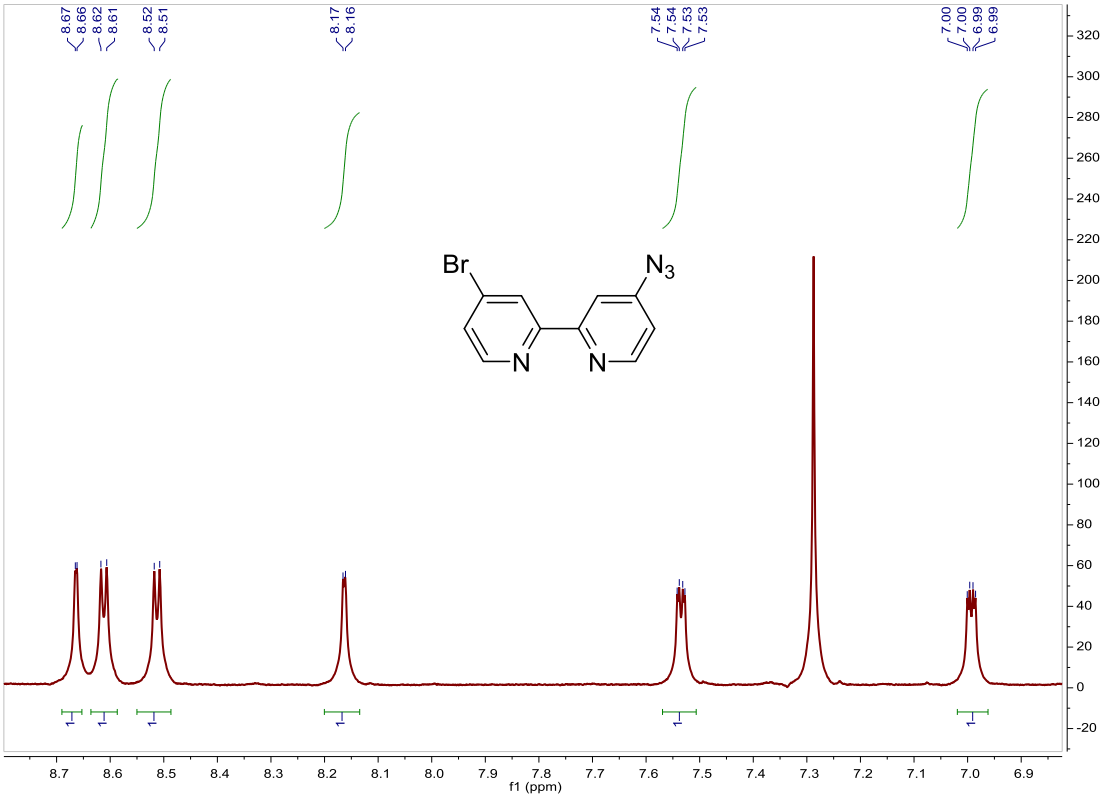

Fig. S54. ^{1}H NMR spectrum of **Ligand 22** in $CDCl_3$, 500 MHz.

[Ir(ppy)$_2$Cl]$_2$. Synthesis and characterization.

SYNTHESIS[27]

Under a N_2 atmosphere, $IrCl_3 \cdot 3H_2O$ (1.00 g, 2.84 mmol) and 2-phenylpyridine (0.81 mL, 5.67 mmol) were dissolved in 30 mL of ethoxyethanol/water 2/1. The reaction mixture was refluxed at 120 °C, under N_2, for 15 h. After cooling to room temperature, the product was filtered and washed with water, hexane and diethyl-ether. The product was obtained as a yellow solid. Yield 88%. The spectroscopic data are coincident with those described in the literature.[28]

^{1}H NMR (300 MHz, $CDCl_3$): δ 9.28 (d, J = 5.8 Hz, 1H), 7.90 (d, J = 8.1 Hz, 1H), 7.77 (ddd, J = 1.6 Hz, J = 7.4 Hz, J = 8.9 Hz, 1H), 7.52 (dd, J = 1.2 Hz, J = 7.8 Hz, 1H), 6.84–6.73 (m, 2H), 6.59 (ddd, J = 1.3 Hz, J = 7.7 Hz, J = 8.8 Hz, 1H), 5.97 (dd, J = 0.8 Hz, J = 7.7 Hz, 1H).

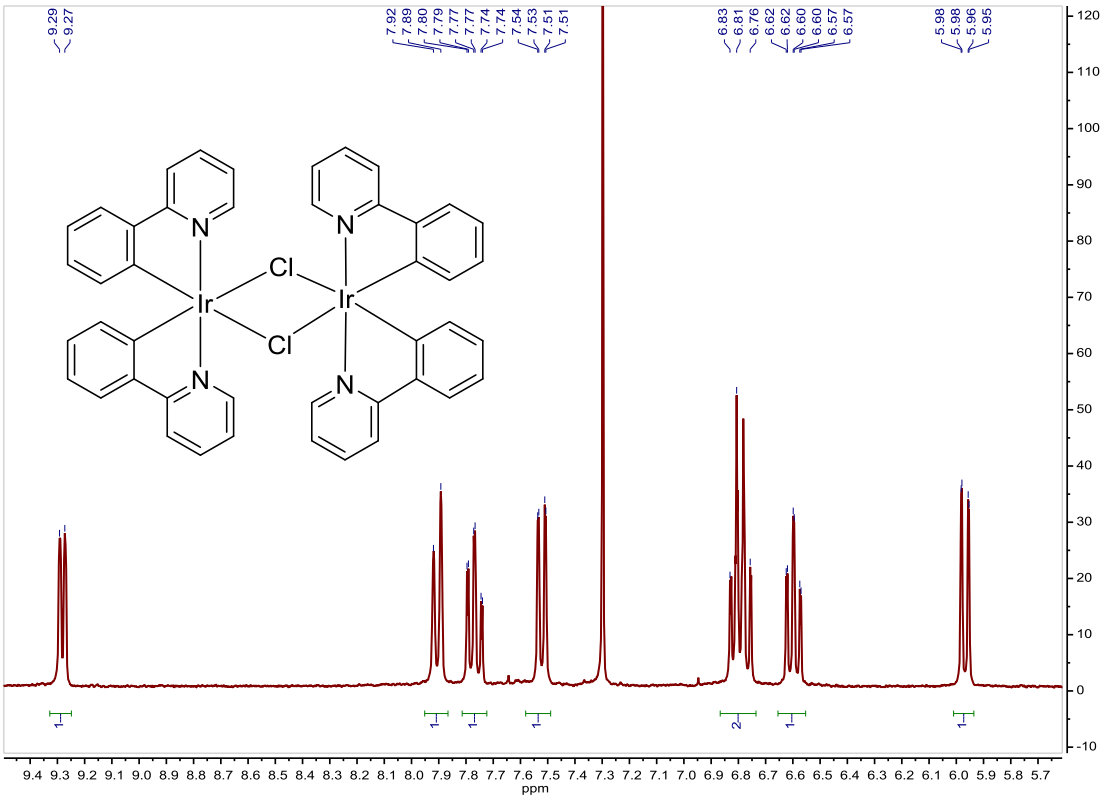

Fig. S55. ^{1}H NMR spectrum of **[Ir(ppy)$_2$Cl]$_2$** in $CDCl_3$, 300 MHz.

[27] S. Sprouse, K. A. King, P. J. Spellane and R. J. Watts, *J. Am. Chem. Soc.*, **1984**, *106*, 6647–6653.

[28] A. A. Rachford, R. Ziessel, T. Bura, P. Retailleau and F. N. Castellano, *Inorg. Chem.*, **2010**, *49*, 3730–3736.

[Ir(Fppy)$_2$Cl]$_2$. Synthesis and characterization.

SYNTHESIS[27]

Under a N_2 atmosphere, $IrCl_3 \cdot 3H_2O$ (2.31 g, 6.56 mmol) and 2-(2,4-difluorophenyl)pyridine (2.0 mL, 13.12 mmol) were dissolved in 60 mL of ethoxyethanol/water 2/1. The reaction mixture was refluxed at 120 °C, under N_2, for 15 h. After cooling to room temperature, the product was filtered and washed with water, hexane and diethyl-ether. The product was obtained as a yellow solid. Yield 73%. The spectroscopic data are coincident with those described in the literature.[29]

^{1}H NMR (300 MHz, $CDCl_3$): δ 9.16 (d, J = 5.8 Hz, 1H), 8.34 (d, J = 8.4 Hz, 1H), 7.86 (t, J = 8.1 Hz, 1H), 6.91–6.82 (m, 1H), 6.37 (ddd, J = 2.3 Hz, J = 9.1 Hz, J = 11.5 Hz, 1H), 5.32 (dd, J = 2.4 Hz, J = 9.1 Hz, 1H).

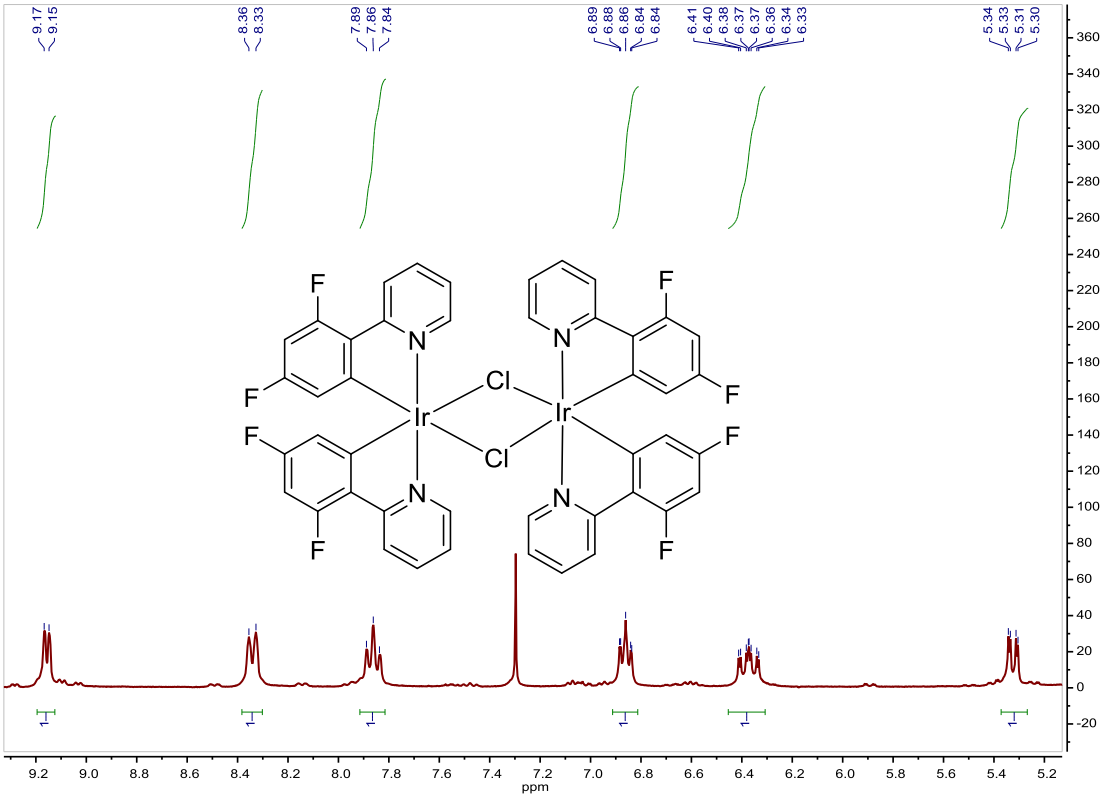

Fig. S56. ^{1}H NMR spectrum of **[Ir(Fppy)$_2$Cl]$_2$** in $CDCl_3$, 300 MHz.

[29] F. Dumur, M. Lepeltier, H. Z. Siboni, D. Gigmes and H. Aziz, *Synthetic Metals*, **2014**, *198*, 131–136.

2-(4-bromophenyl)-4,4,5,5-tetramethyl-[1,3,2]dioxaborolane. Synthesis and characterization.

SYNTHESIS[30]

Under a N_2 atmosphere, to a solution of aryl iodide (8.0 g, 28.3 mmol), CuI (0.54 g, 2.83 mmol) and NaH (1.02 g, 42.5 mmol) in freshly distilled THF (110 mL), pinacolborane (6.6 mL, 42.43 mmol) were added and the reaction mixture was stirred for 15 h at room temperature. A saturated NH_4Cl (140 mL) solution was added and the product was extracted with ethyl acetate. The organic phase was dried over $MgSO_4$ and the solvent was evaporated. The product was purified by column chromatography (silica, 100% hexane to 100% ethyl acetate) and it was obtained as a yellow liquid. Yield 82%. The spectroscopic data are coincident with those described in the literature.

^{1}H NMR (300 MHz, $CDCl_3$): δ 7.70 (brd, J = 8.2 Hz, 2H), 7.54 (brd, J = 8.3 Hz, 2H), 1.37 (s, 12H).

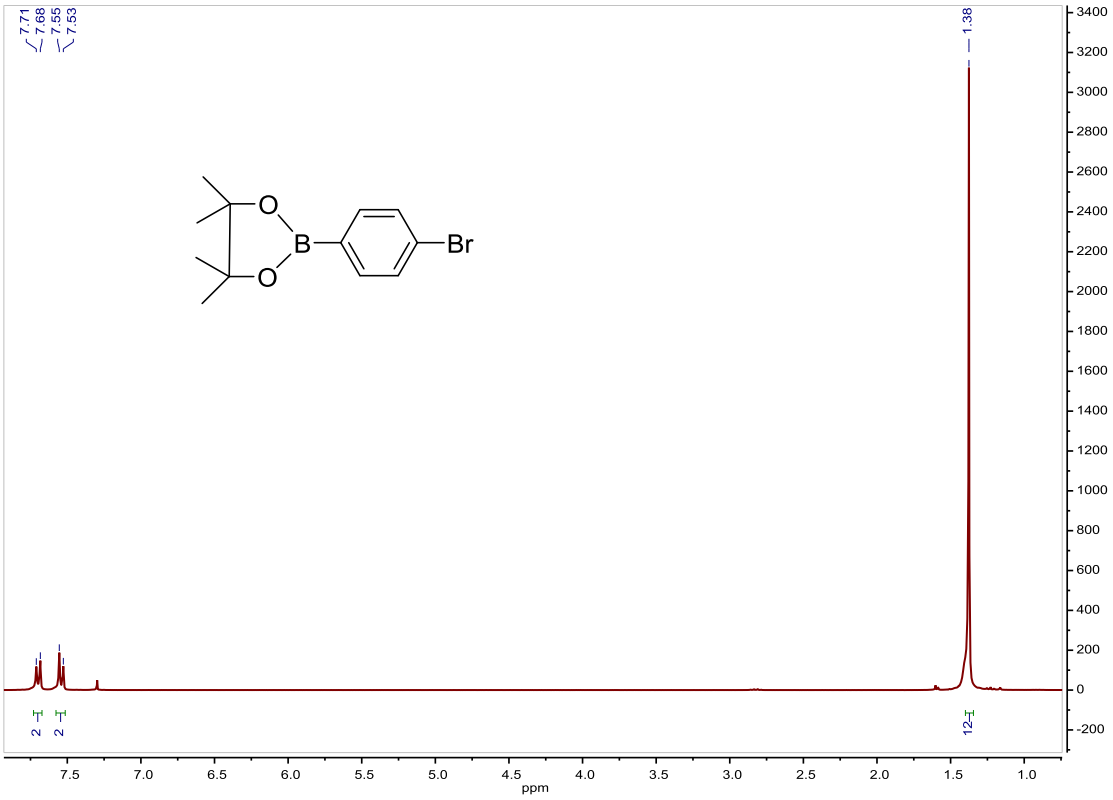

Fig. S57. ^{1}H NMR spectrum of **2-(4-bromophenyl)-4,4,5,5-tetramethyl-[1,3,2]dioxaborolane** in $CDCl_3$, 300 MHz.

[30] W. Zhu and D. Ma, *Org. Lett.*, **2006**, *8*, 261–263.

2-(4-bromophenyl)pyridine. Synthesis and characterization.

SYNTHESIS[31]

Under a N_2 atmosphere, a solution of 2-bromopyridine (2.22 mL, 23.3 mmol) and $Pd(PPh_3)_4$ (0.61 g, 0.53 mmol) in DME (66 mL) was added to a solution of 2-(4-bromophenyl)-4,4,5,5-tetramethyl-[1,3,2]dioxaborolane (6.6 g, 23.3 mmol) in EtOH (66 mL). Na_2CO_3 (2M, 36 mL) was added and the reaction mixture was heated to 95 °C for 15 h. After cooling to room temperature, the solid was removed by filtration and the solvent was evaporated. The impurities that were not soluble in EtOAc and hexane were also removed. The product was obtained as a yellow solid. Yield 36%. The spectroscopic data are coincident with those described in the literature.[32]

^{1}H NMR (300 MHz, $CDCl_3$): δ 8.70 (ddd, J = 1.0 Hz, J = 1.8 Hz, J = 4.8 Hz, 1H), 7.89 (brd, J = 8.7 Hz, 2H), 7.80–7.68 (m, 2H), 7.62 (brd, J = 8.7 Hz, 2H), 7.30–7.23 (m, 1H).

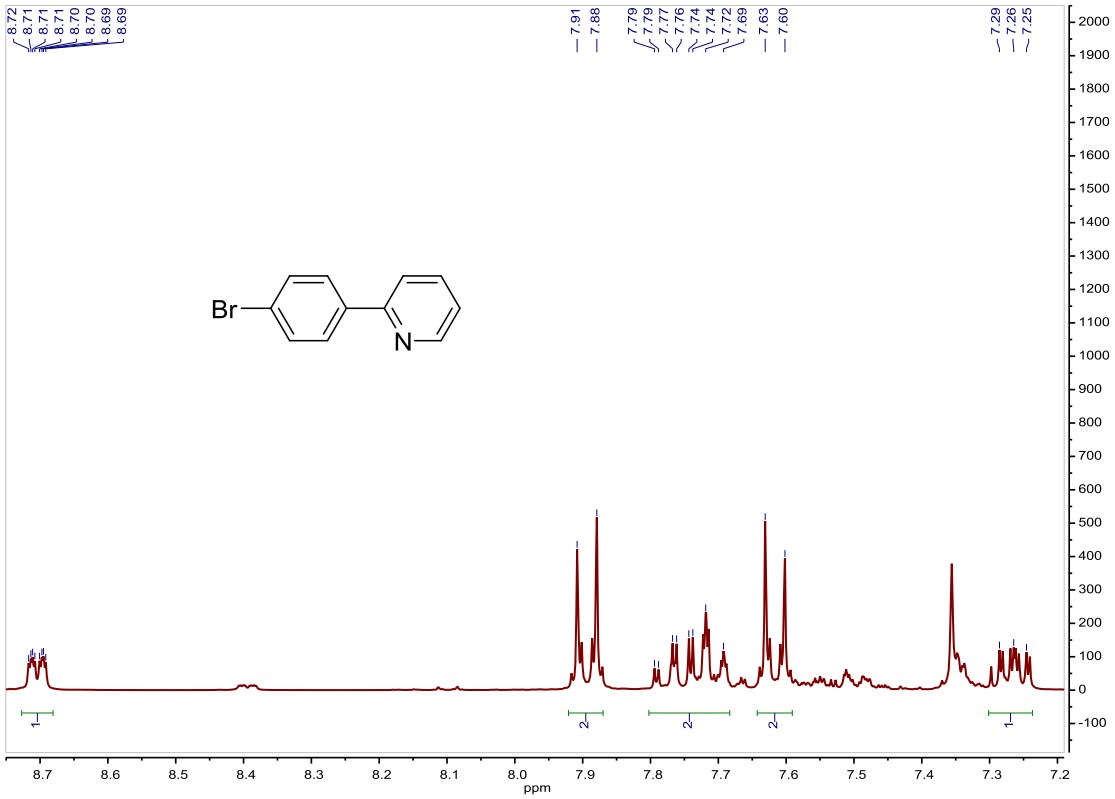

Fig. S58. ^{1}H NMR spectrum of **2-(4-bromophenyl)pyridine** in $CDCl_3$, 300 MHz.

[31] H.-Y. Yang, J.-M. Son and W.-J. Joo, US Patent, 2010/0133992.

[32] A. J. Sandee, C. K. Williams, N. R. Evans, J. E. Davies, C. E. Boothby, A. Köhler, R. H. Friend and A. B. Holmes, *J. Am. Chem. Soc.*, **2004**, *126*, 7041–7048.

[Ir(Brppy)$_2$Cl]$_2$. Synthesis and characterization.

SYNTHESIS[27]

Under a N_2 atmosphere, $IrCl_3 \cdot 3H_2O$ (1.50 g, 4.26 mmol) and 2-(4-bromophenyl)pyridine (2.0 g, 8.53 mmol) were dissolved in 45 mL of ethoxyethanol/water 2/1. The reaction mixture was refluxed at 120 °C, under N_2, for 15 h. After cooling to room temperature, the product was filtered and washed with water, hexane and diethyl-ether. The product was obtained as a yellow solid. Yield 92%. The spectroscopic data are coincident with those described in the literature.[32]

^{1}H NMR (300 MHz, $CDCl_3$): δ 9.14 (d, J = 5.8 Hz, 1H), 7.90 (d, J = 7.4 Hz, 1H), 7.83 (ddd, J = 1.5 Hz, J = 7.2 Hz, J = 8.7 Hz, 1H), 7.41 (d, J = 8.3 Hz, 1H), 7.00 (dd, J = 1.9 Hz, J = 8.2 Hz, 1H), 6.86 (ddd, J = 1.6 Hz, J = 5.9 Hz, J = 7.3 Hz, 1H), 5.98 (d, J = 1.9 Hz, 1H).

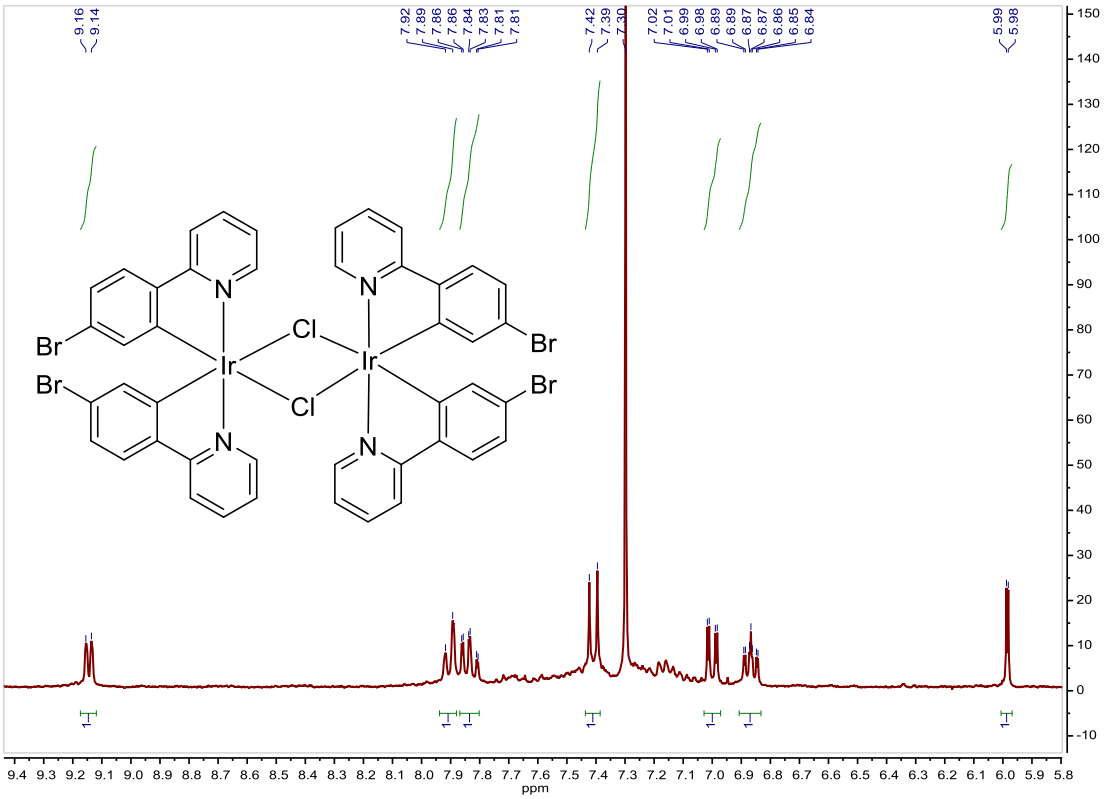

Fig. S59. ^{1}H NMR spectrum of **[Ir(Brppy)$_2$Cl]$_2$** in $CDCl_3$, 300 MHz.

Compound A15, [Ir(ppy)$_2$(4,4'-bis(diethylphosphonate)-2,2'-bipyridine)]PF$_6$. Synthesis and characterization.

SYNTHESIS

Under a N_2 atmosphere, $[Ir(ppy)_2Cl]_2$ (0.100 g, 0.093 mmol) were added over a suspension of 4,4'-bis(diethylphosphonate)-2,2'-bipyridine (0.08 g, 0.186 mmol) in 8 ml CH_2Cl_2–MeOH 2/1. The reaction mixture was refluxed, under N_2, for 15 h. After solvent evaporation the product was purified by column chromatography (silica gel, CH_2Cl_2). When the unreacted $[Ir(ppy)_2Cl]_2$ eluted, 0.05 g of KPF_6 were added on top of the column and the polarity of the eluent was gradually increased to 100% acetone to elute $[Ir(ppy)_2$(4,4'-bis(diethylphosphonate)-2,2'-bipyridine)]PF_6 together with the excess of KPF_6. The desired compound was precipitated with ether after filtration through a celite path in CH_2Cl_2 and it was obtained as a red solid. Yield 40%.

Elemental Analysis: calculated for ($C_{40}H_{42}IrN_4O_6P_3F_6$): C, 44.74; H, 3.94; N, 5.22. Found: C, 44.44; H, 4.06; N, 5.21.

Exact Mass: ESI-MS $[C_{40}H_{42}IrN_4O_6P_2]^+$: calculated: m/z= 929.2209, found: m/z= 929.2216.

^{1}H NMR (300 MHz, acetone-*d*$_6$): δ 9.01 (d, J = 13.7 Hz, 1H), 8.16 (t, J = 4.8 Hz, 1H), 8.09 (d, J = 8.1 Hz, 1H), 7.89–7.70 (m, 4H), 6.98 (ddd, J = 1.3 Hz, J = 5.9 Hz, J = 7.3 Hz, 1H), 6.90 (ddd, J = 1.3 Hz, J = 7.4 Hz, J = 8.6 Hz, 1H), 6.79 (ddd, J = 1.4 Hz, J = 7.4 Hz, J = 8.8 Hz, 1H), 6.19 (d, J = 7.4 Hz, 1H), 4.19 –3.95 (m, 4H), 1.18 (dt, J = 6.7 Hz, J = 6.8 Hz, 6H).

^{13}C APT NMR (75 MHz, acetone-*d*$_6$): δ 167.16 (s, C_{quat}), 155.94 (d, J = 13.6 Hz, C_{quat}), 150.95 (d, J = 13.9 Hz, CH), 149.50 (s, CH), 149.42 (s, C_{quat}), 143.82 (s, C_{quat}), 141.35 (d, J = 187.5 Hz, C_{quat}), 138.72 (s, CH), 131.33 (s, CH), 130.27 (s, CH), 130.13 (d, J = 8.6 Hz, CH), 126.83 (d, J = 9.8 Hz, CH), 124.83 (s, CH), 123.55 (s, CH), 122.63 (s, CH), 119.85 (s, CH), 63.00 (d, J = 5.7 Hz, $2CH_2$), 15.60 (d, J = 5.8 Hz, $2CH_3$).

^{31}P NMR (162 MHz, acetone-*d*$_6$): δ 11.29 (s, 1P), -144.07(sep, J = 707.8 Hz, 1P).

UV/Vis (EtOH), λ, nm (ε, 10^4 M^{-1} cm^{-1}): 250 (5.1), 290 (4.1), 378 (1.0).

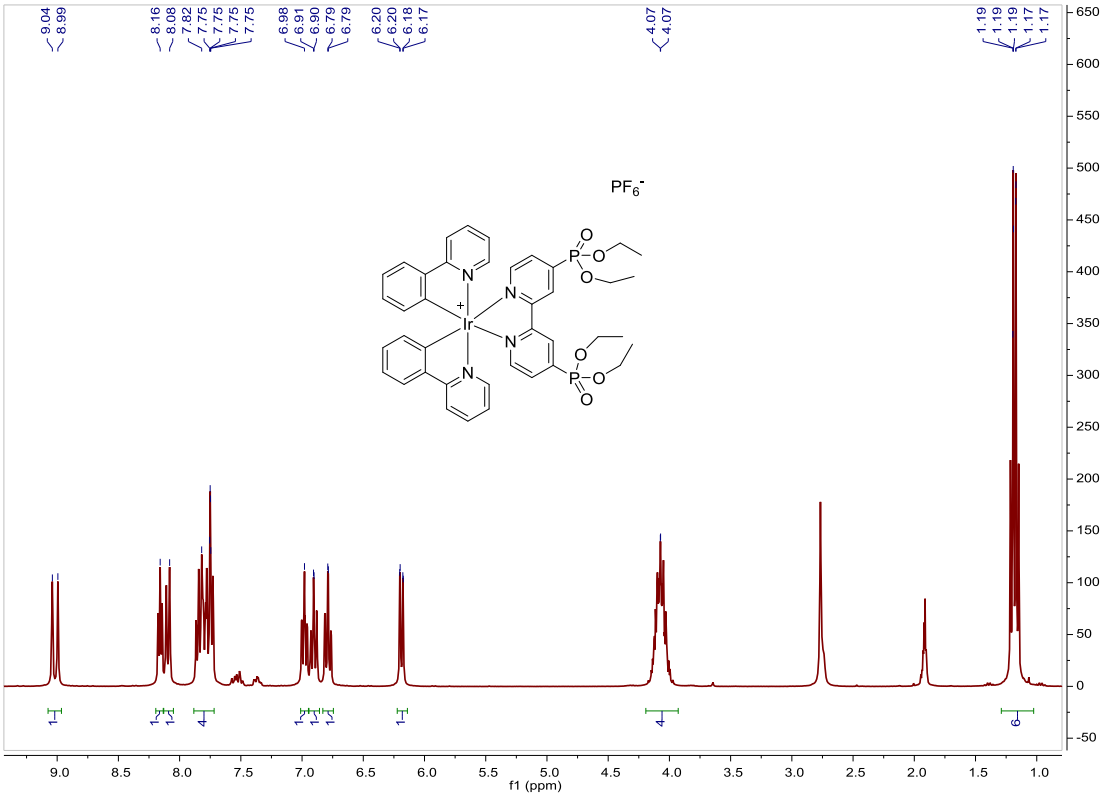

Fig. S60. ^{1}H NMR spectrum of **A15** in acetone-*d*$_6$, 300 MHz.

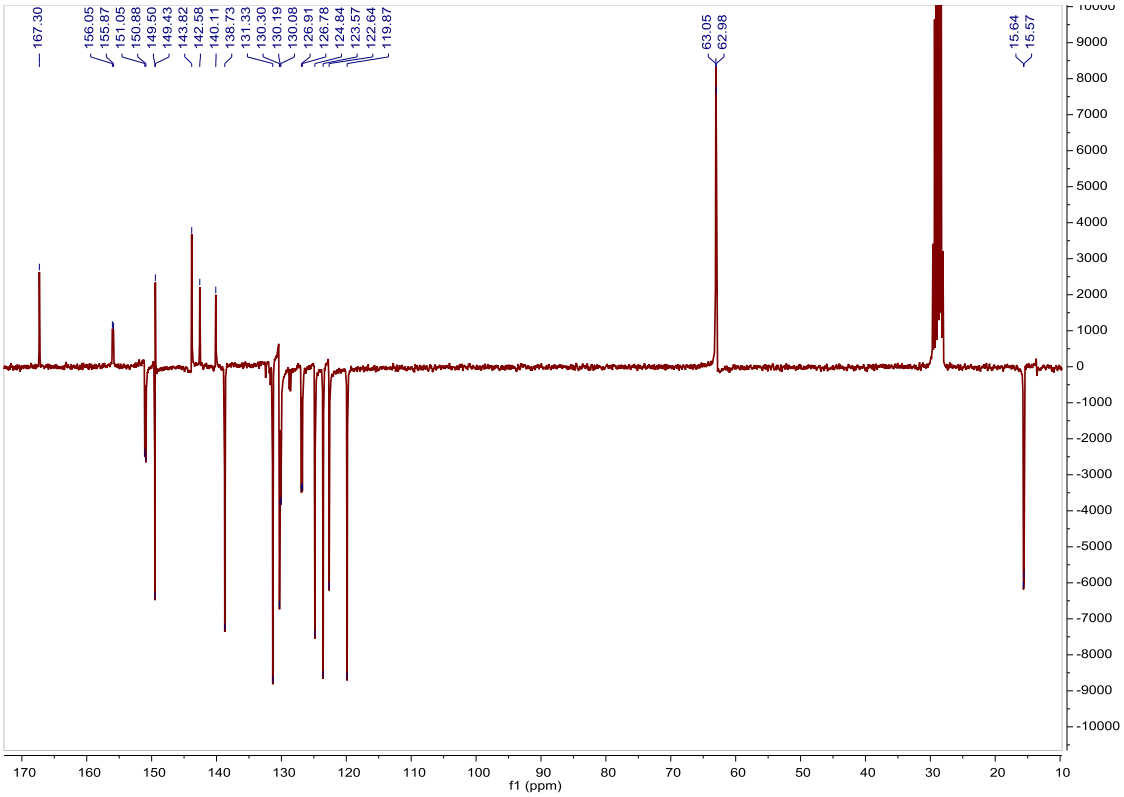

Fig. S61. ^{13}C APT NMR spectrum of **A15** in acetone-d_6, 75 MHz.

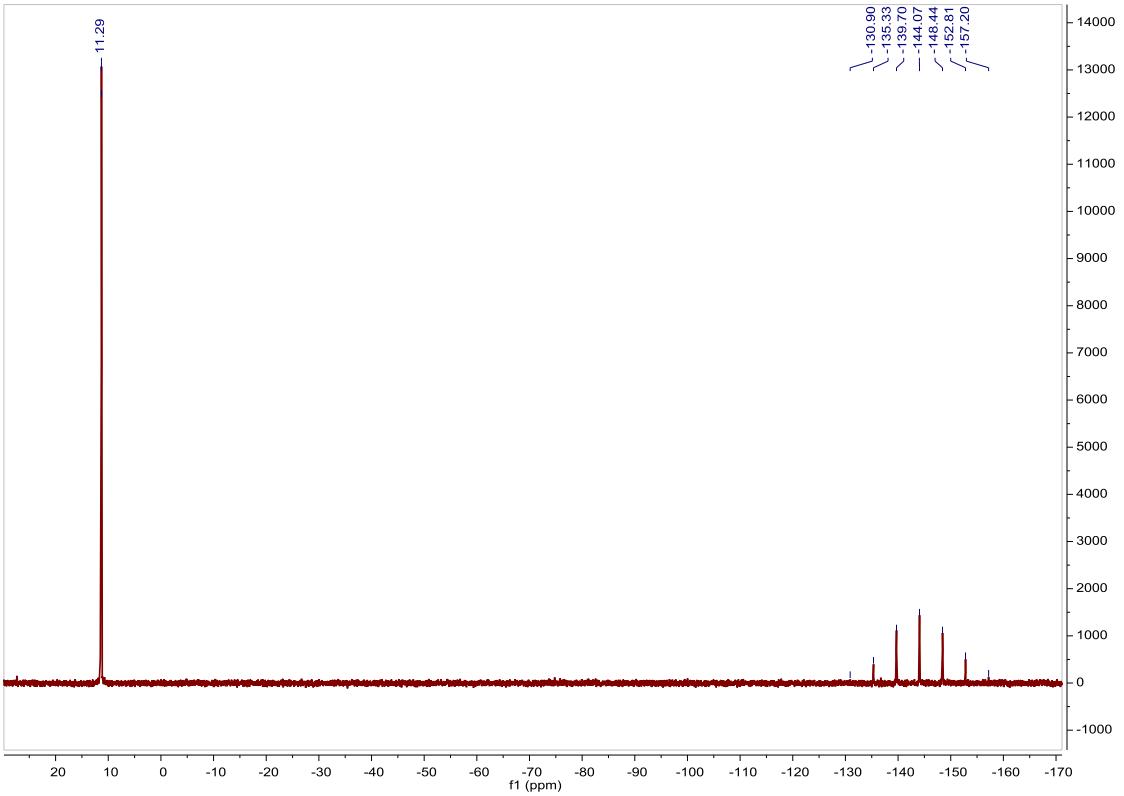

Fig. S62. ^{31}P NMR spectrum of **A15** in acetone-d_6, 162 MHz.

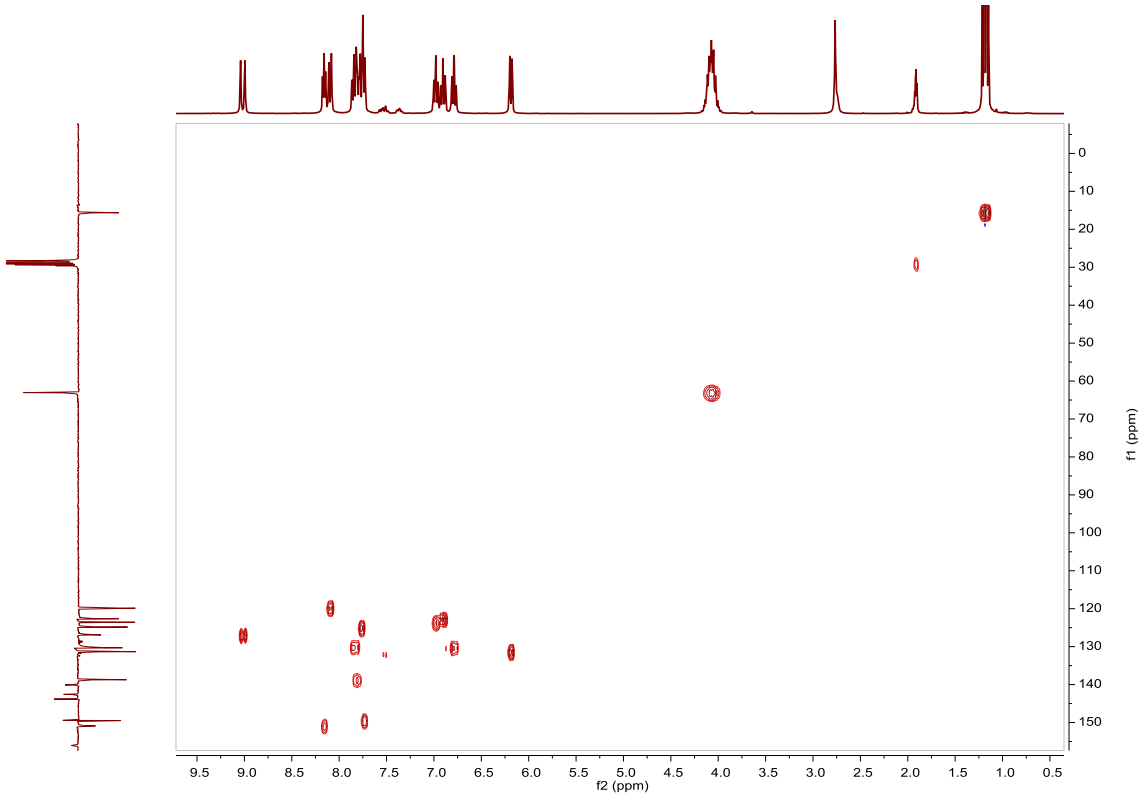

Fig. S63. HSQC NMR spectrum of **A15** in acetone-d_6.

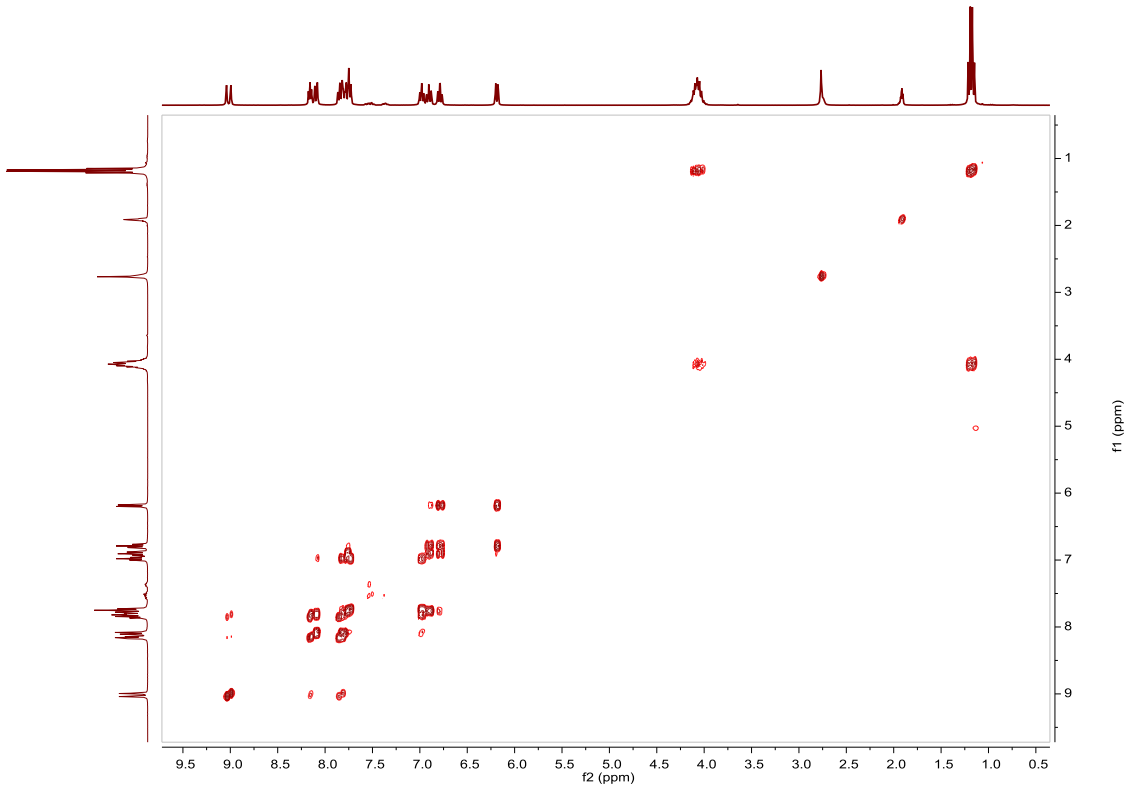

Fig. S64. COSY NMR spectrum of **A15** in acetone-d_6.

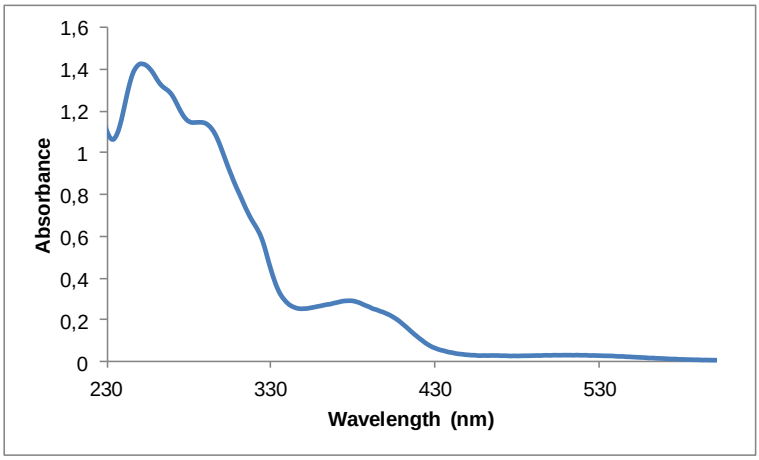

Fig. S65. UV/Vis spectra of **A15** in EtOH, $2.79 \cdot 10^{-5}$M.

Compound B15, [Ir(ppy-F_2)$_2$(4,4'-bis(diethylphosphonate)-2,2'-bipyridine)]PF_6. Synthesis and characterization.

SYNTHESIS

Under a N_2 atmosphere, [Ir(ppy-F_2)$_2$Cl]$_2$ (0.100 g, 0.082 mmol) were added over a suspension of 4,4'-bis(diethylphosphonate)-2,2'-bipyridine (0.07 g, 0.164 mmol) in 8 ml CH_2Cl_2–MeOH 2/1. The reaction mixture was refluxed, under N_2, for 15 h. After solvent evaporation the product was purified by column chromatography (silica gel, CH_2Cl_2). When the unreacted [Ir(ppy-F_2)$_2$Cl]$_2$ eluted, 0.05 g of KPF_6 were added on top of the column and the polarity of the eluent was gradually increased to 100% acetone to elute [Ir(ppy-F_2)$_2$(4,4'-bis(diethylphosphonate)-2,2'-bipyridine)]PF_6 together with the excess of KPF_6. The desired compound was precipitated with ether after filtration through a celite path in CH_2Cl_2 and it was obtained as a yellow solid. Yield 40%.

Elemental Analysis: calculated for ($C_{40}H_{38}F_4IrN_4O_6P_3F_6$): C, 41.93; H, 3.34; N, 4.89. Found: C, 41.97; H, 3.38; N, 5.13.

Exact Mass: ESI-MS $[C_{40}H_{38}F_4IrN_4O_6P_2]^+$: calculated: m/z= 1001.1832, found: m/z= 1001.1854.

^{1}H NMR (300 MHz, acetone-d_6): δ 9.04 (d, J = 13.8 Hz, 1H), 8.33–8.19 (m, 2H), 7.92 (t, J = 7.6 Hz, 1H), 7.87 (dd, J = 1.4 Hz, J = 5.5 Hz, 1H), 7.83 (dd, J = 1.4 Hz, J = 5.7 Hz, 1H), 7.06 (ddd, J = 1.4 Hz, J = 5.8 Hz, J = 7.4 Hz, 1H), 6.64 (ddd, J = 2.4 Hz, J = 9.3 Hz, J = 12.7 Hz, 1H), 5.63 (dd, J = 2.3 Hz, J = 8.5 Hz, 1H), 4.17–3.97 (m, 4H), 1.18 (dt, J = 6.5 Hz, J = 6.2 Hz, 6H).

^{13}C APT NMR (75 MHz, acetone-d_6): δ 163.20 (dd, J = 12.5 Hz, J = 254.0 Hz, C_{quat}), 163.14 (d, J = 7.0 Hz, C_{quat}), 161.03 (dd, J = 12.8 Hz, J = 258.4 Hz, C_{quat}), 155.46 (d, J = 13.6 Hz, C_{quat}), 153.19 (d, J = 6.6 Hz, C_{quat}), 151.12 (d, J = 12.7 Hz, CH), 149.79 (s, CH), 141.78 (d, J = 184.1 Hz, C_{quat}), 139.54 (s, CH), 130.20 (d, J = 8.4 Hz, CH), 127.47 (s, C_{quat}), 126.82 (d, J = 10.4 Hz, CH), 123.82 (s, CH), 123.30 (d, J = 19.9 Hz, CH), 113.29 (d, J = 20.1 Hz, CH), 98.61 (t, J = 27.1 Hz, CH), 62.75 (d, J = 5.0 Hz, $2CH_2$), 15.33 (d, J = 5.8 Hz, $2CH_3$).

^{31}P NMR (162 MHz, acetone-d_6): δ 10.99 (s, 1P), -144.08 (sep, J = 707.8 Hz, 1P).

UV/Vis (EtOH), λ, nm (ε, 10^4 M^{-1} cm^{-1}): 244 (6.0), 312 (3.4), 358 (1.1).

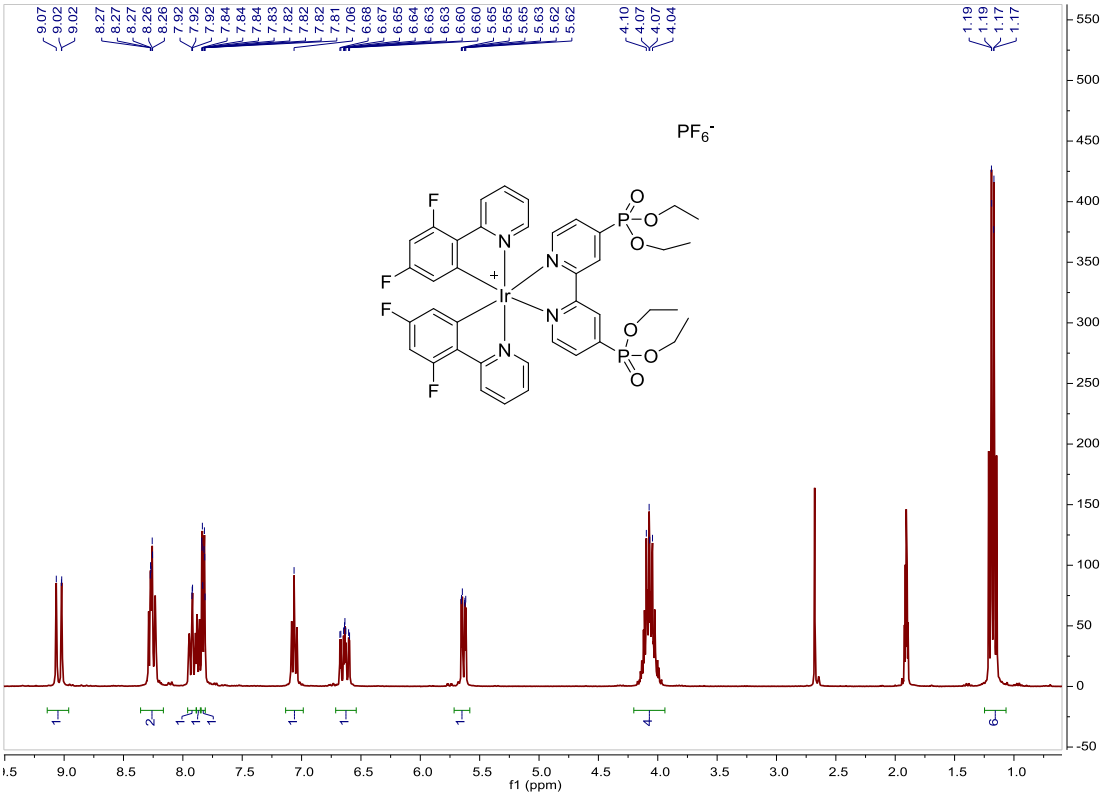

Fig. S66. ^{1}H NMR spectrum of **B15** in acetone-d_6, 300 MHz.

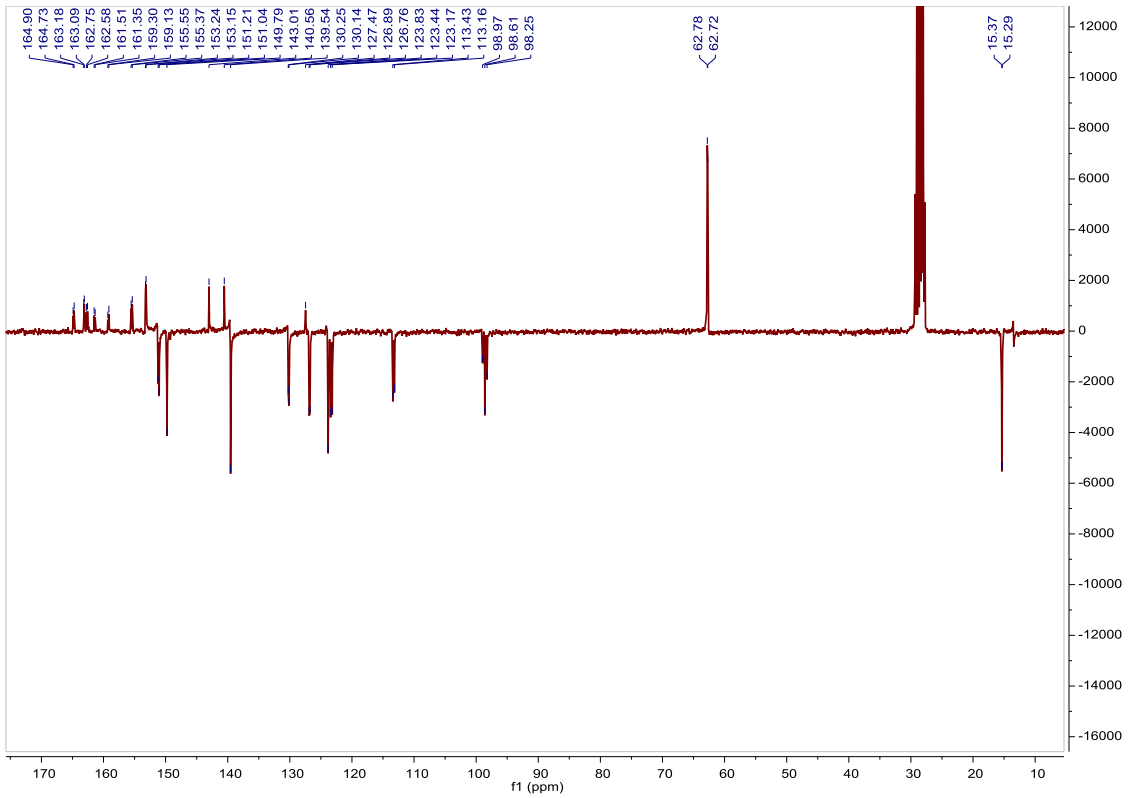

Fig. S67. ^{13}C APT NMR spectrum of **B15** in acetone-d_6, 75 MHz.

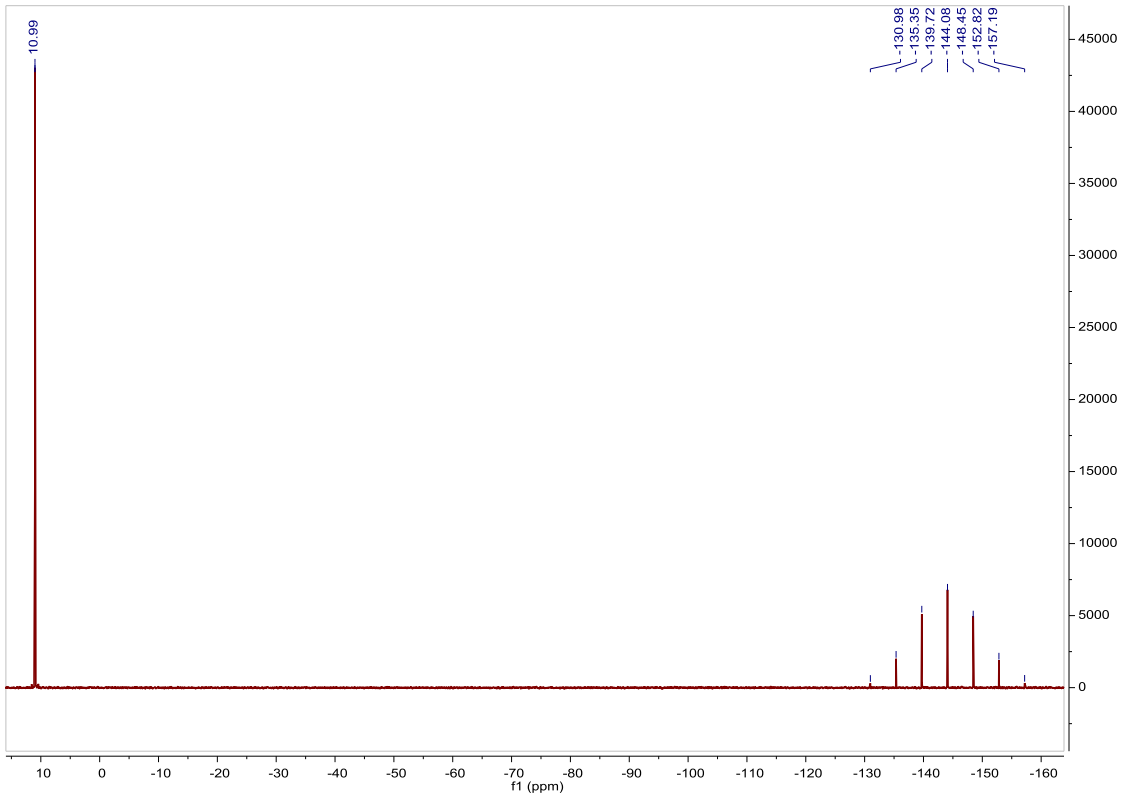

Fig. S68. ^{31}P NMR spectrum of **B15** in acetone-d_6, 162 MHz.

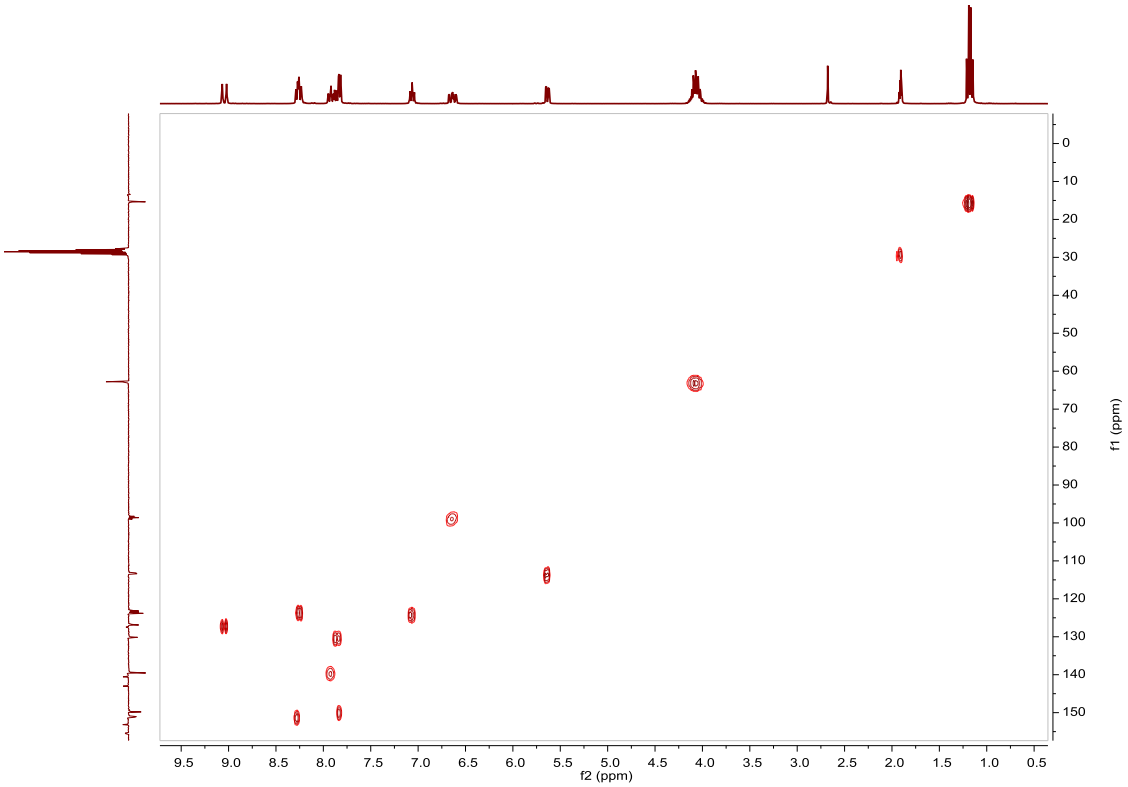

Fig. S69. HSQC NMR spectrum of **B15** in acetone-d_6.

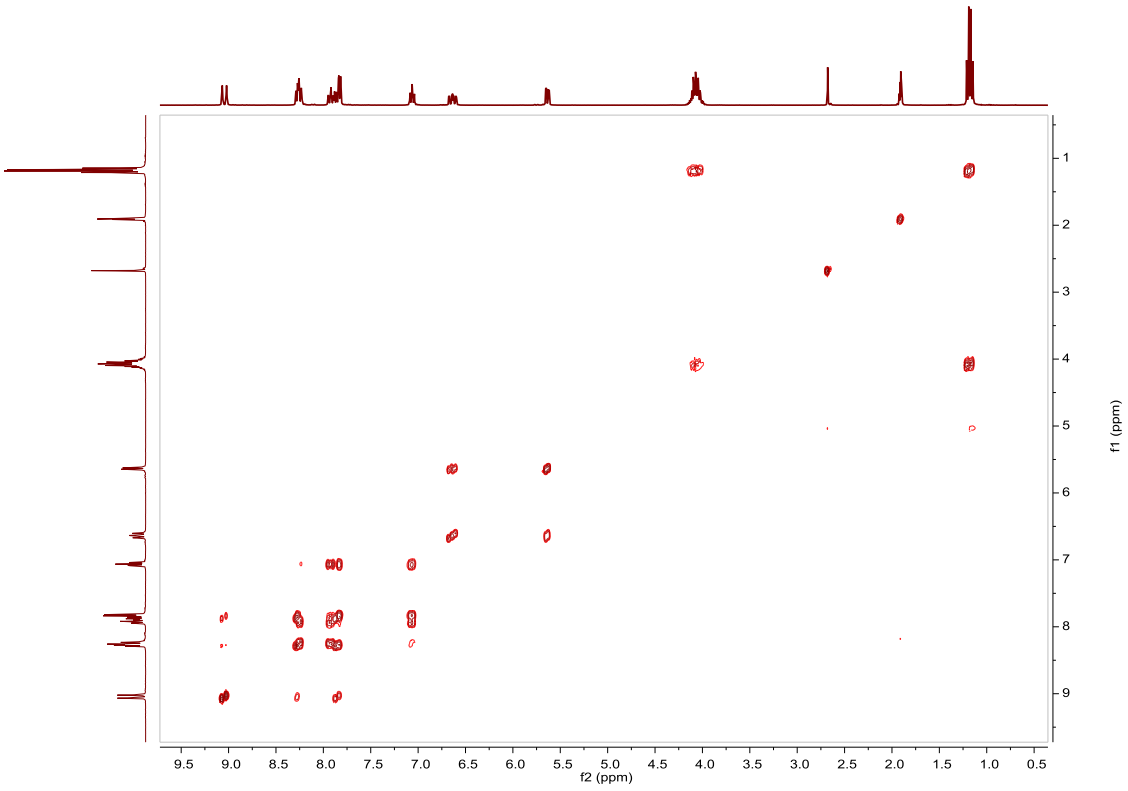

Fig. S70. COSY NMR spectrum of **B15** in acetone-d_6.

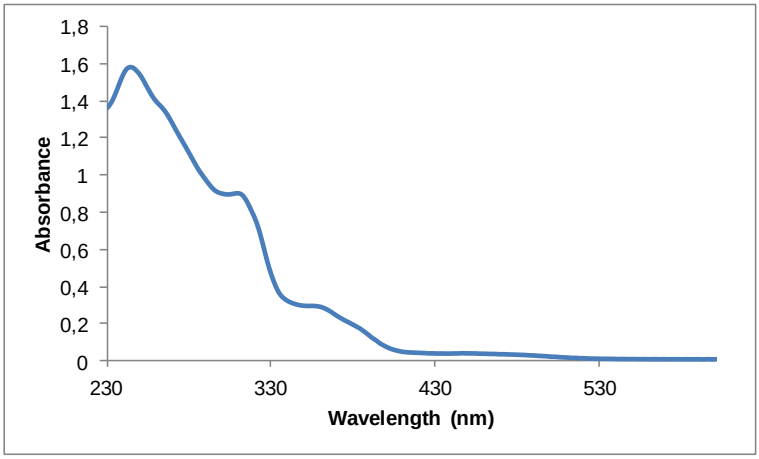

Fig. S71. UV/Vis spectra of **B15** in EtOH, $2.62 \cdot 10^{-5}$M.

Compound C15, [Ir(ppy-Br)$_2$(4,4'-bis(diethylphosphonate)-2,2'-bipyridine)]PF$_6$. Synthesis and characterization.

SYNTHESIS

Under a N_2 atmosphere, $[Ir(ppy\text{-}Br)_2Cl]_2$ (0.200 g, 0.144 mmol) were added over a suspension of 4,4'-bis(diethylphosphonate)-2,2'-bipyridine (0.123 g, 0.288 mmol) in 16 ml CH_2Cl_2–MeOH 2/1. The reaction mixture was refluxed, under N_2, for 15 h. After solvent evaporation the product was purified by column chromatography (silica gel, CH_2Cl_2). When the unreacted $[Ir(ppy\text{-}Br)_2Cl]_2$ eluted, 0.05 g of KPF_6 were added on top of the column and the polarity of the eluent was gradually increased to 100% acetone to elute $[Ir(ppy\text{-}Br)_2$(4,4'-bis(diethylphosphonate)-2,2'-bipyridine)$]PF_6$ together with the excess of KPF_6. The desired compound was precipitated with ether after filtration through a celite path in CH_2Cl_2 and it was obtained as a red solid. Yield 68%.

Elemental Analysis: calculated for ($C_{40}H_{40}Br_2IrN_4O_6P_3F_6{\cdot}CH_2Cl_2$): C, 37.40; H, 3.22; N, 4.26. Found: C, 37.05; H, 3.24; N, 4.41.

Exact Mass: ESI-MS $[C_{40}H_{40}Br_2IrN_4O_6P_2]^+$: calculated: m/z= 1085.0419, found: m/z= 1085.0454.

^{1}H NMR (300 MHz, acetone-d_6): δ 9.20 (d, J = 13.6 Hz, 1H), 8.40 (t, J = 4.9 Hz, 1H), 8.32 (d, J = 7.9 Hz, 1H), 8.05 (brd, J = 6.2 Hz, 1H), 8.03–7.99 (m, 1H), 7.94 (brd, J = 5.1 Hz, 1H), 7.92 (d, J = 8.5 Hz, 1H), 7.30 (dd, J = 2.0 Hz, J = 8.3 Hz, 1H), 7.21 (ddd, J = 1.4 Hz, J = 5.8 Hz, J = 7.3 Hz, 1H), 6.41 (d, J = 1.9 Hz, 1H), 4.41–4.10 (m, 4H), 1.35 (dt, J = 6.6 Hz, J = 7.1 Hz, 6H).

^{13}C APT NMR (75 MHz, acetone-d_6): δ 165.79 (s, C_{quat}), 155.61 (d, J = 14.74 Hz, C_{quat}), 151.21 (s, C_{quat}), 151.03 (d, J = 12.6 Hz, CH), 149.52 (s, CH), 142.91 (s, C_{quat}), 141.58 (d, J = 184.3 Hz, C_{quat}), 139.03 (s, CH), 133.28 (s, CH), 130.13 (d, J = 8.4 Hz, CH), 126.76 (d, J = 10.4 Hz, CH), 126.43 (s, CH), 125.71 (s, CH), 124.54 (s, C_{quat}), 124.01 (s, CH), 120.23 (s, CH), 62.77 (d, J = 4.0 Hz, $2CH_2$), 15.38 (d, J = 5.8 Hz, $2CH_3$).

^{31}P NMR (162 MHz, acetone-d_6): δ 11.10 (s, 1P), -144.07 (sep, J = 707.7 Hz, 1P).

UV/Vis (EtOH), λ, nm (ε, 10^4 M^{-1} cm^{-1}): 252 (3.7), 272 (3.8), 376 (0.7).

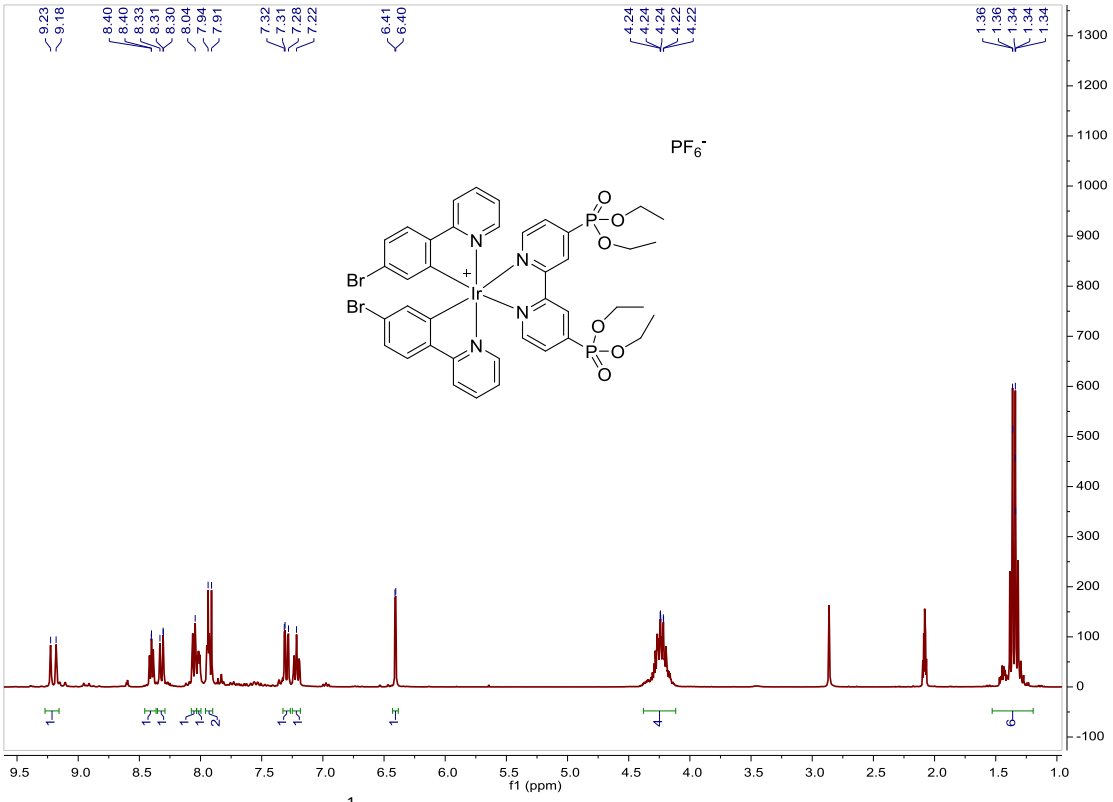

Fig. S72. ^{1}H NMR spectrum of **C15** in acetone-d_6, 300 MHz.

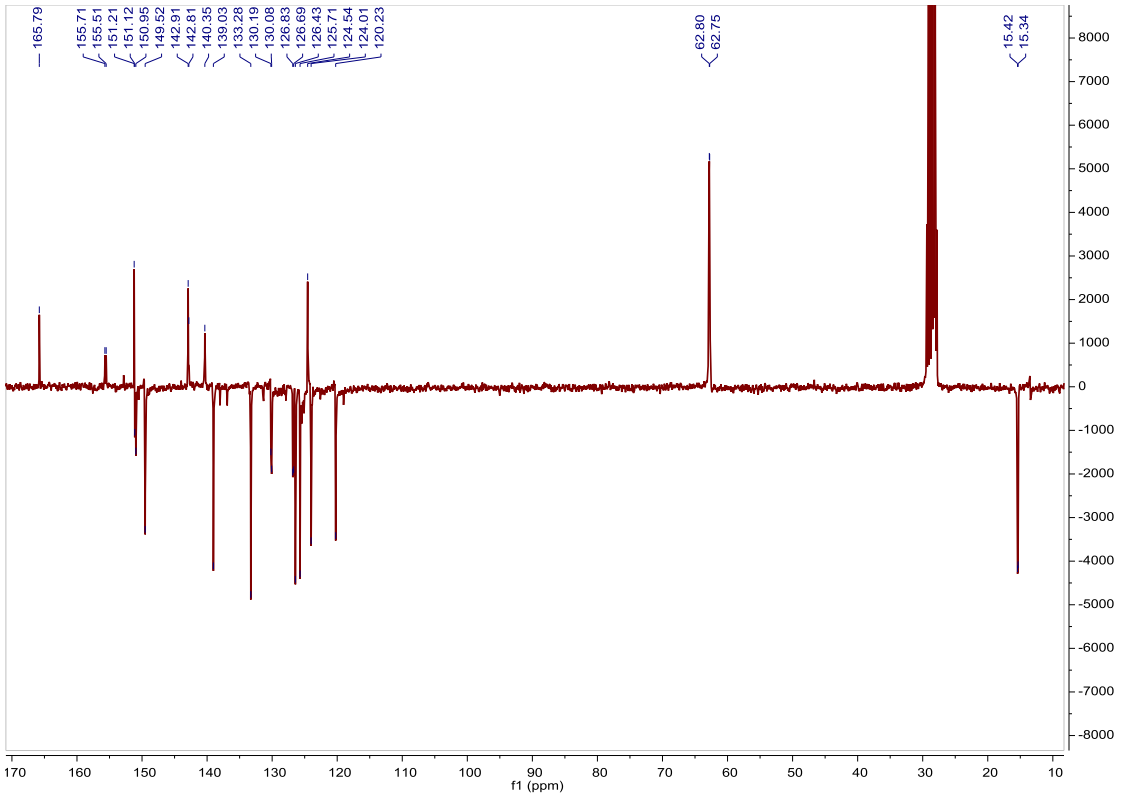

Fig. S73. ^{13}C APT NMR spectrum of **C15** in acetone-d_6, 75 MHz.

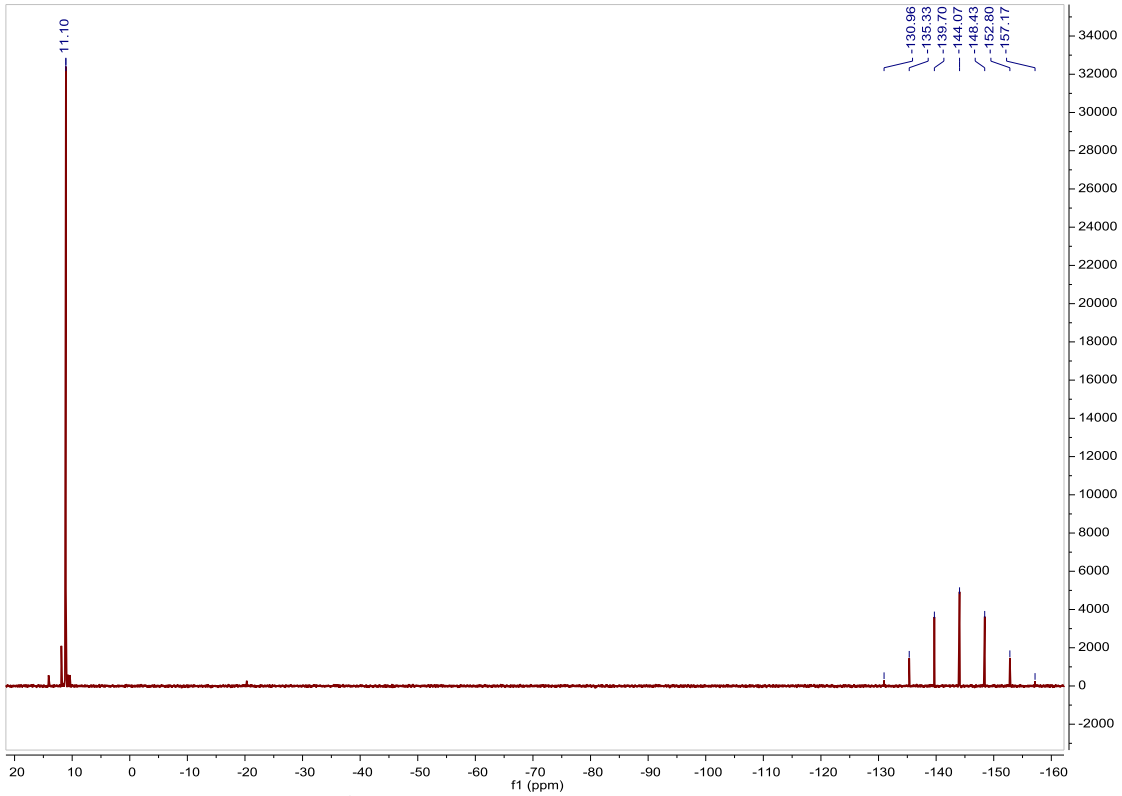

Fig. S74. ^{31}P NMR spectrum of **C15** in acetone-d_6, 162 MHz.

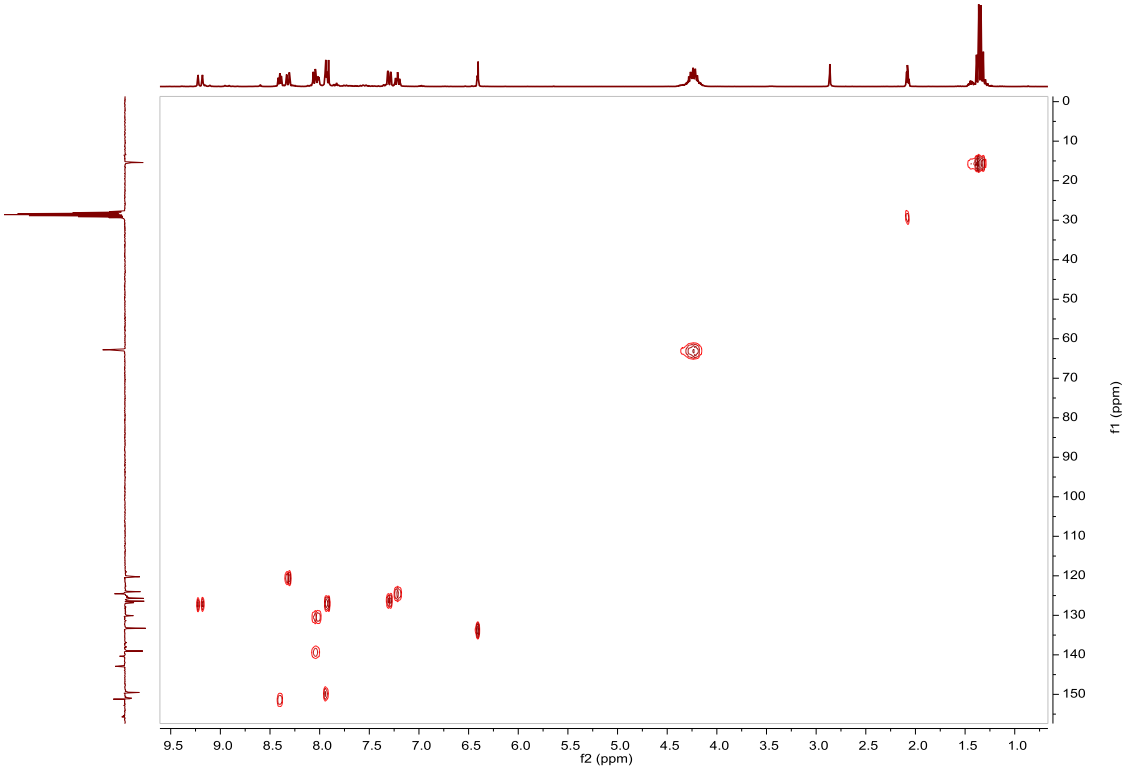

Fig. S75. HSQC NMR spectrum of **C15** in acetone-d_6.

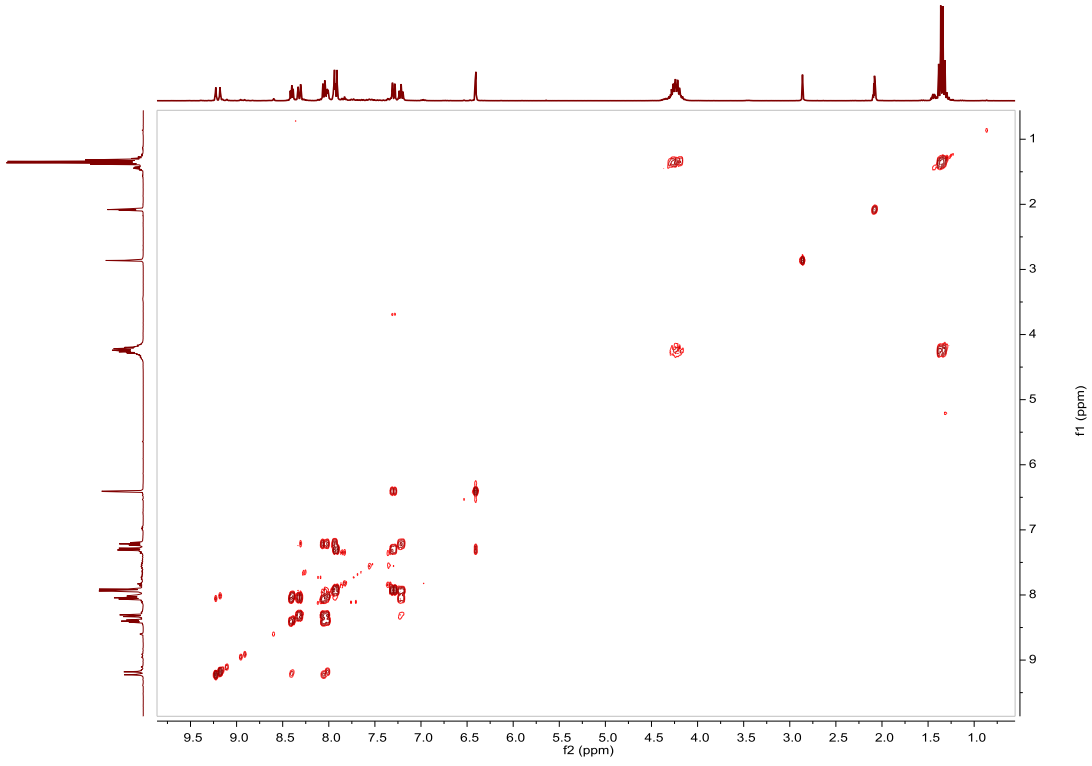

Fig. S76. COSY NMR spectrum of **C15** in acetone-d_6.

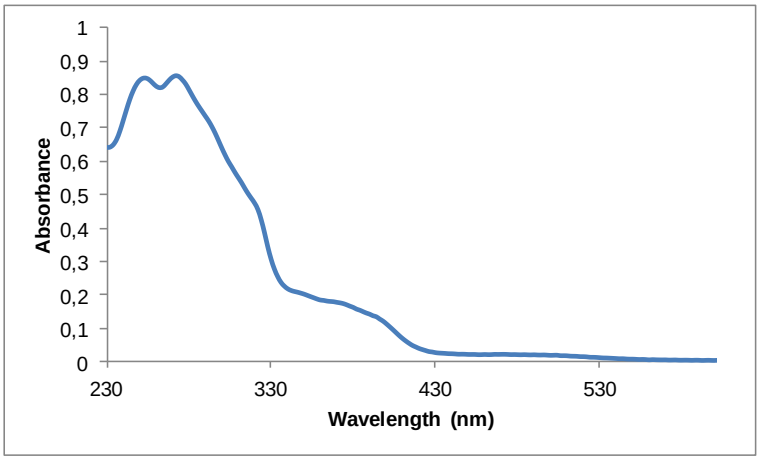

Fig. S77. UV/Vis spectra of **C15** in EtOH, $2.27 \cdot 10^{-5}$M.

Compound D15, [Ir((5-azobenzyl-2-pyridyl)phenyl)2(4,4'-bis(diethylphosphonate)-2,2'-bipyridine)]PF_6. Synthesis, characterization and photoisomerization studies.

SYNTHESIS

Under a N_2 atmosphere, $[Ir((5\text{-azobenzyl-2-pyridyl})phenyl)_2Cl]_2$ (0.03 g, 0.017 mmol) were added over a suspension of 4,4'-bis(diethylphosphonate)-2,2'-bipyridine (0.014 g, 0.033 mmol) in 3 ml CH_2Cl_2–MeOH 2/1. The reaction mixture was refluxed, under N_2, for 15 h. After solvent evaporation the product was purified by column chromatography (silica gel, $CH_2Cl_2/CH_3(CO)CH_3$ 1/9). 0.007 g of KPF_6 were added on top of the column to elute $[Ir((5\text{-azobenzyl-2-pyridyl})phenyl)_2(4,4'\text{-bis(diethylphosphonate)-2,2'-bipyridine})]PF_6$ together with the excess of KPF_6. The desired compound was precipitated with hexane after filtration through a celite path in CH_2Cl_2 and it was obtained as an orange solid. Yield 33%.

Elemental Analysis: calculated for ($C_{64}H_{58}IrN_8O_6P_3F_6 \cdot 2CH_2Cl_2$): C, 49.42; H, 3.90; N, 6.99. Found: C, 48.72 ; H, 3.66 ; N, 6.97.

Exact Mass: ESI-MS $[C_{64}H_{58}IrN_8O_6P_2]^+$: calculated: m/z= 1289.3584, found: m/z= 1289.3606.

^{1}H NMR (300 MHz, acetone-d_6): δ 9.09 (d, J = 13.6 Hz, 1H), 8.39 (t, J = 5.0 Hz, 1H), 8.20 (brd, J = 7.6 Hz, 1H), 7.96–7.85 (m, 4H), 7.83–7.73 (m, 4H), 7.53–7.42 (m, 5H), 7.33 (dd, J = 1.8 Hz, J = 8.1 Hz, 1H), 7.09 (ddd, J = 1.3 Hz, J = 5.8 Hz, J = 7.3 Hz, 1H), 6.58 (d, J = 1.7 Hz, 1H), 4.21–4.01 (m, 4H), 1.26–1.14 (m, 6H).

^{13}C APT NMR (75 MHz, acetone-d_6): δ 166.85 (C_{quat}), 152.45 (C_{quat}), 151.51 (C_{quat}), 151.28 (CH), 149.99 (C_{quat}), 149.85 (CH), 144.02 (C_{quat}), 143.40 (C_{quat}), 142.71 (C_{quat}), 141.19 (C_{quat}), 140.24 (C_{quat}), 138.91 (CH), 131.14 (CH), 130.16 (CH), 129.39 (CH), 129.12 (2CH), 127.43 (2CH), 126.93 (CH), 125.35 (CH), 123.80 (CH), 122.96 (2CH), 122.47(2CH), 121.88 (CH), 120.29 (CH), 62.99 (d, J = 5.6 Hz, $2CH_2$), 15.59 (d, J = 5.8 Hz, $2CH_3$).

^{31}P NMR (202 MHz, acetone-d_6): δ 12.28 (s, 1P), -143.03 (sep, J = 705.0 Hz, 1P).

UV/Vis (EtOH), λ, nm (ε, 10^4 M^{-1} cm^{-1}): 365 (7.0), 420 (1.9).

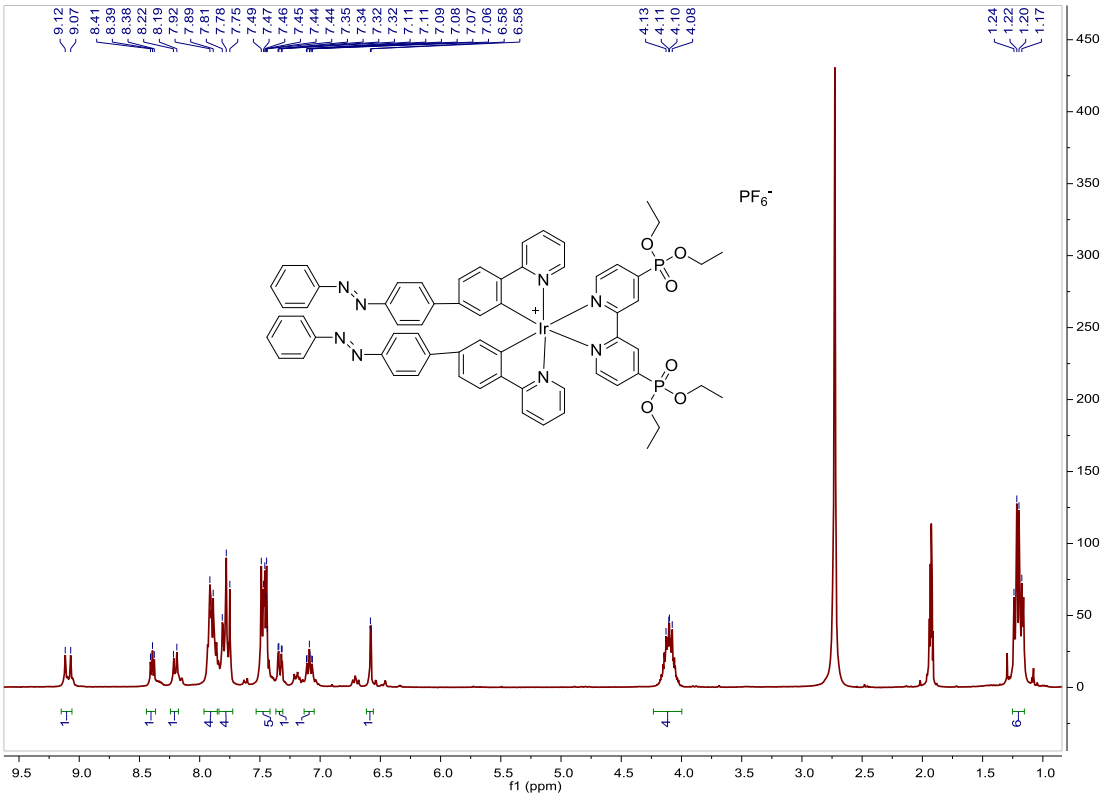

Fig. S78. ^{1}H NMR spectrum of **D15** in acetone-d_6, 300 MHz.

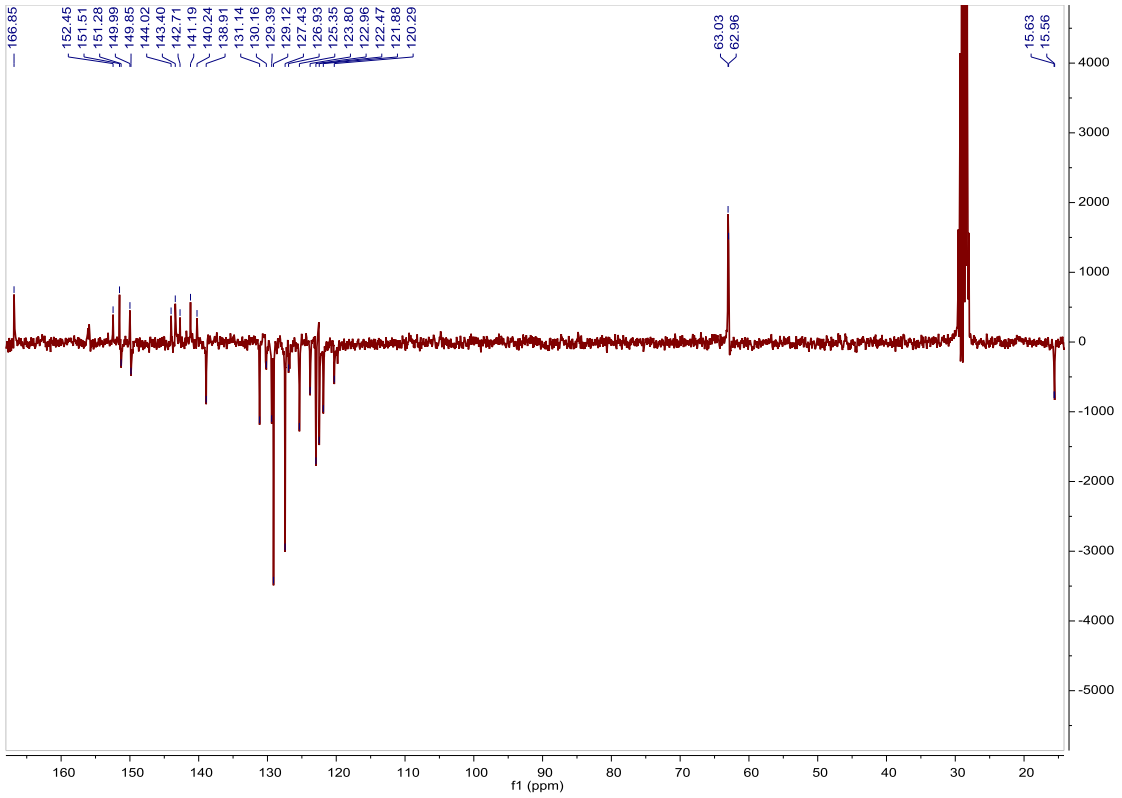

Fig. S79. ^{13}C APT NMR spectrum of **D15** in acetone-d_6, 75 MHz.

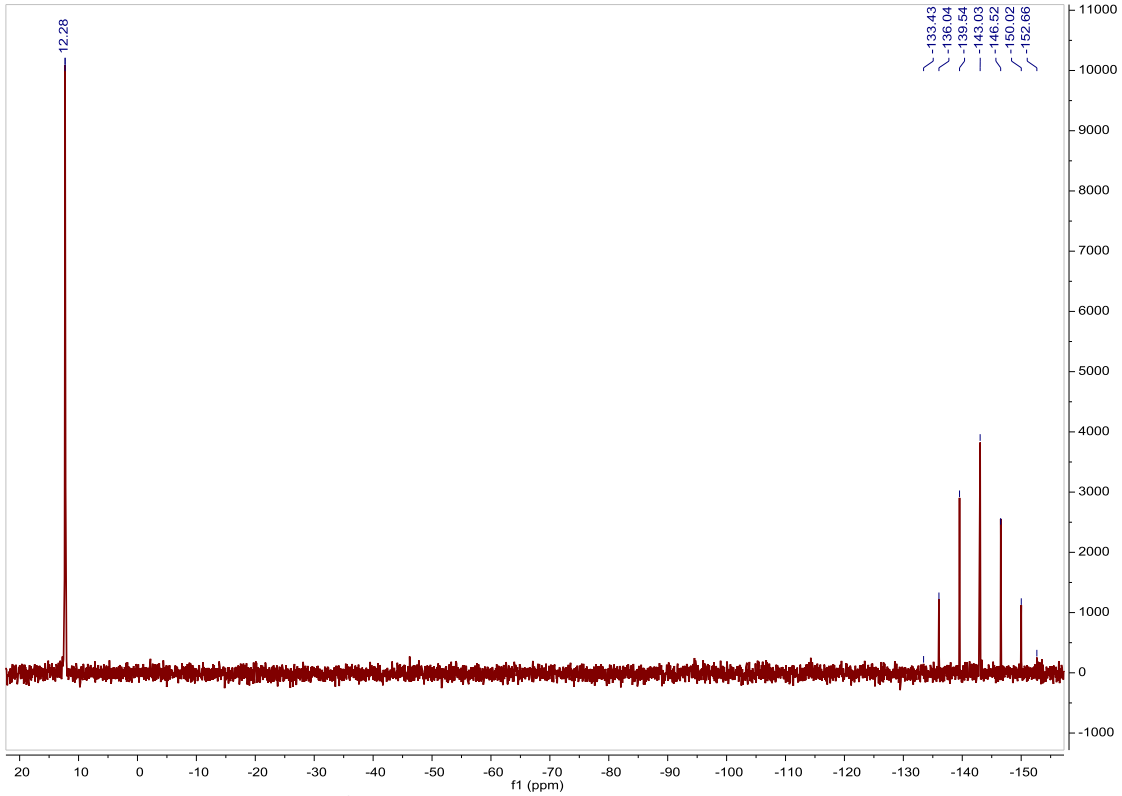

Fig. S80. ^{31}P NMR spectrum of **D15** in acetone-d_6, 162 MHz.

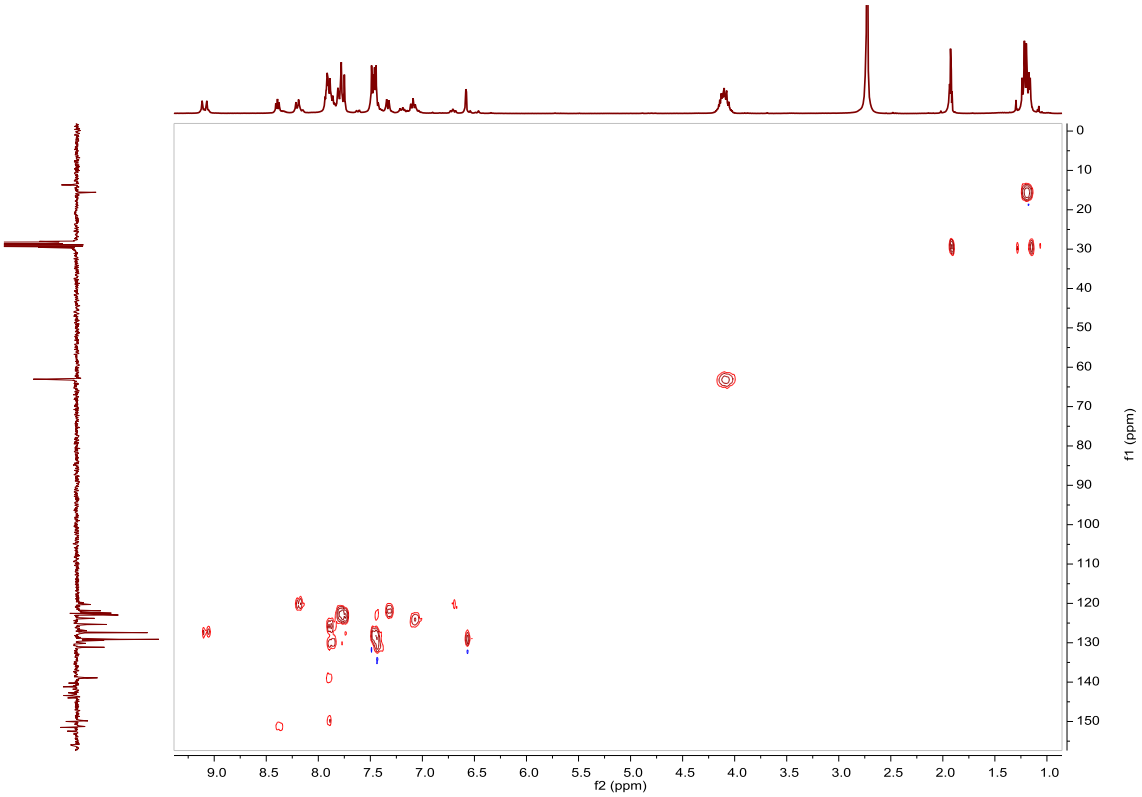

Fig. S81. HSQC NMR spectrum of **D15** in acetone-d_6.

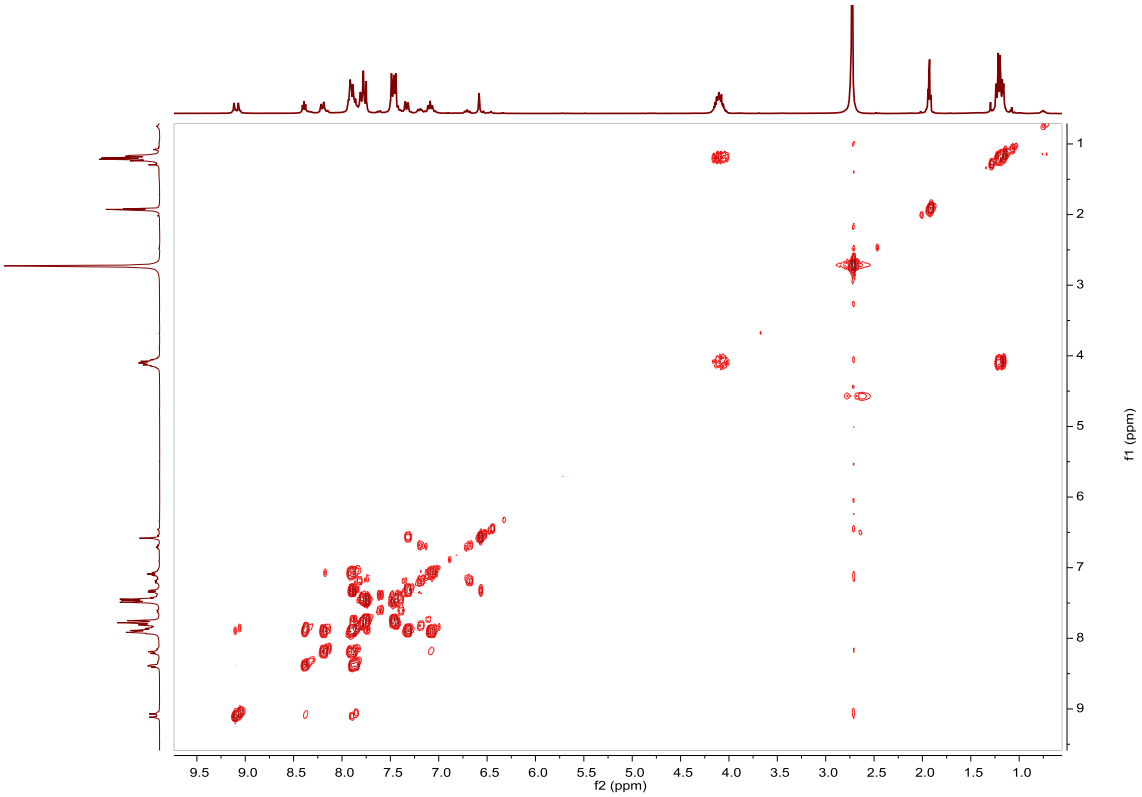

Fig. S82. COSY NMR spectrum of **D15** in acetone-d_6.

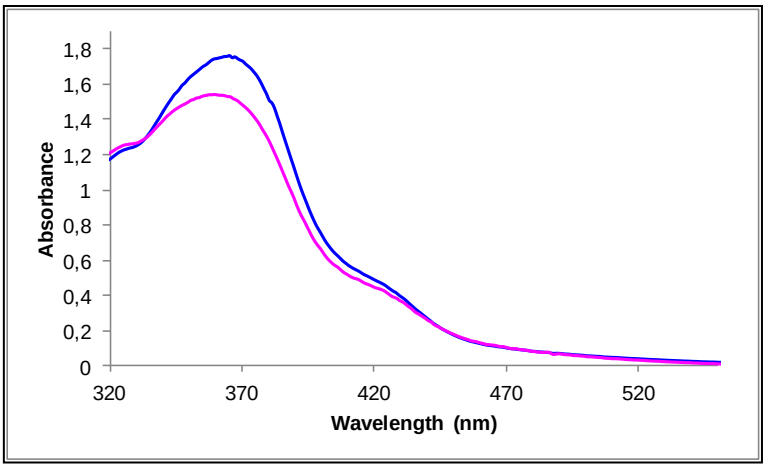

Fig. S83. UV/Vis spectra of **D15** in EtOH. Before (blue line) and after (pink line) irradiation at 377nm, $2.51 \cdot 10^{-5}$M.

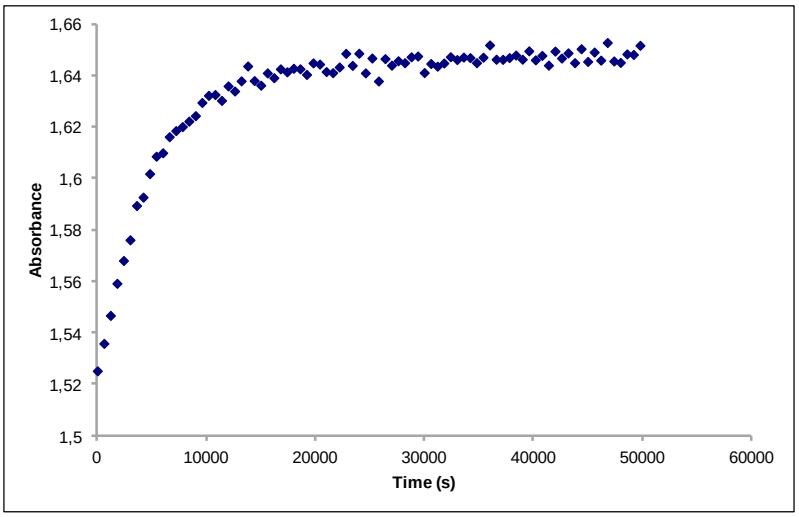

Fig. S84. Cis to trans thermal isomerization kinetics of **D15**. Absorption change of the band 365nm at 328 K in EtOH after irradiation at 377 nm. ($2.51 \cdot 10^{-5}$M).

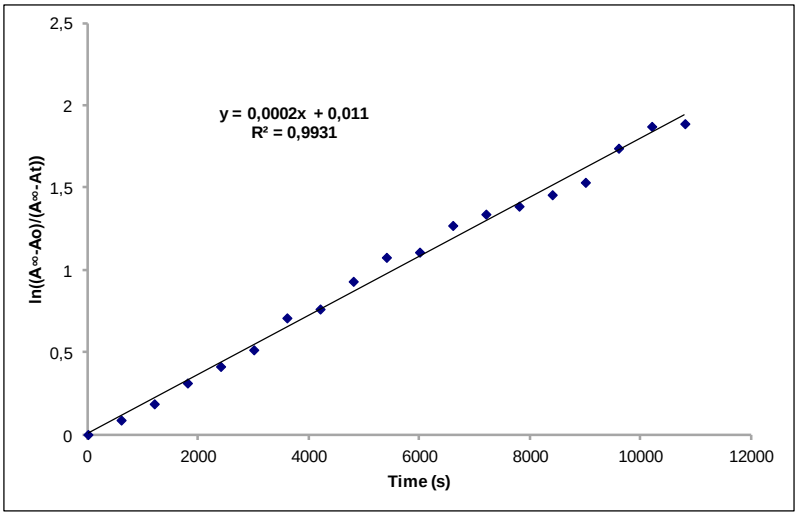

Fig. S85. Cis to trans thermal isomerization kinetics of **D15**. First-order plot. k (s^{-1}) = $2.0 \cdot 10^{-4}$. Half-life (min) = 58.

Compound A16, [Ir(ppy)$_2$(4,4'-bis(carboxy)-2,2'-bipyridine)]PF$_6$. Synthesis and characterization.

SYNTHESIS

Under a N_2 atmosphere, $[Ir(ppy)_2Cl]_2$ (0.100 g, 0.093 mmol) were dissolved in 6 ml of acetone and $Ag(CF_3SO_3)$ (0.096 g, 0.372 mmol) were added. The mixture was heated to 56 °C for 2 h and after cooled down to room temperature, AgCl was removed by centrifugation. The resulting solution was added over a 1 h refluxed suspension of 4,4'-bis(carboxy)-2,2'-bipyridine (0.057 g, 0.232 mmol) in 3 ml of acetone and 102 µl of $N(Et)_3$. The reaction mixture was refluxed, under N_2, for 15 h. After solvent evaporation the product was purified by column chromatography (silica gel, CH_2Cl_2). When the unreacted $[Ir(ppy)_2Cl]_2$ eluted, 0.05 g of KPF_6 were added on top of the column and the polarity of the eluent was gradually increased to 100% methanol to elute $[Ir(ppy)_2(4,4'\text{-bis(carboxy)-2,2'-bipyridine})]PF_6$ together with the excess of KPF_6. The desired compound washed with acetone was obtained as an orange solid. Yield 72%. The spectroscopic data are coincident with those described in the literature.[33]

Exact Mass: ESI-MS $[C_{34}H_{24}IrN_4O_4]^+$: calculated: m/z= 745.1427, found: m/z= 745.1447.

^{1}H NMR (300 MHz, DMSO-*d*$_6$): δ 8.90 (s, 1H), 8.26 (d, J = 7.9 Hz, 1H), 7.97–7.78 (m, 4H), 7.63 (d, J = 4.7 Hz, 1H), 7.16 (t, J = 5.9 Hz, 1H), 7.03 (t, J = 6.9 Hz, 1H), 6.91 (t, J = 7.0 Hz, 1H), 6.21 (d, J = 7.3 Hz, 1H).

UV/Vis (EtOH), λ, nm (ε, 10^4 M^{-1} cm^{-1}): 254 (4.2), 268 (3.9), 320 (1.8), 380 (0.8).

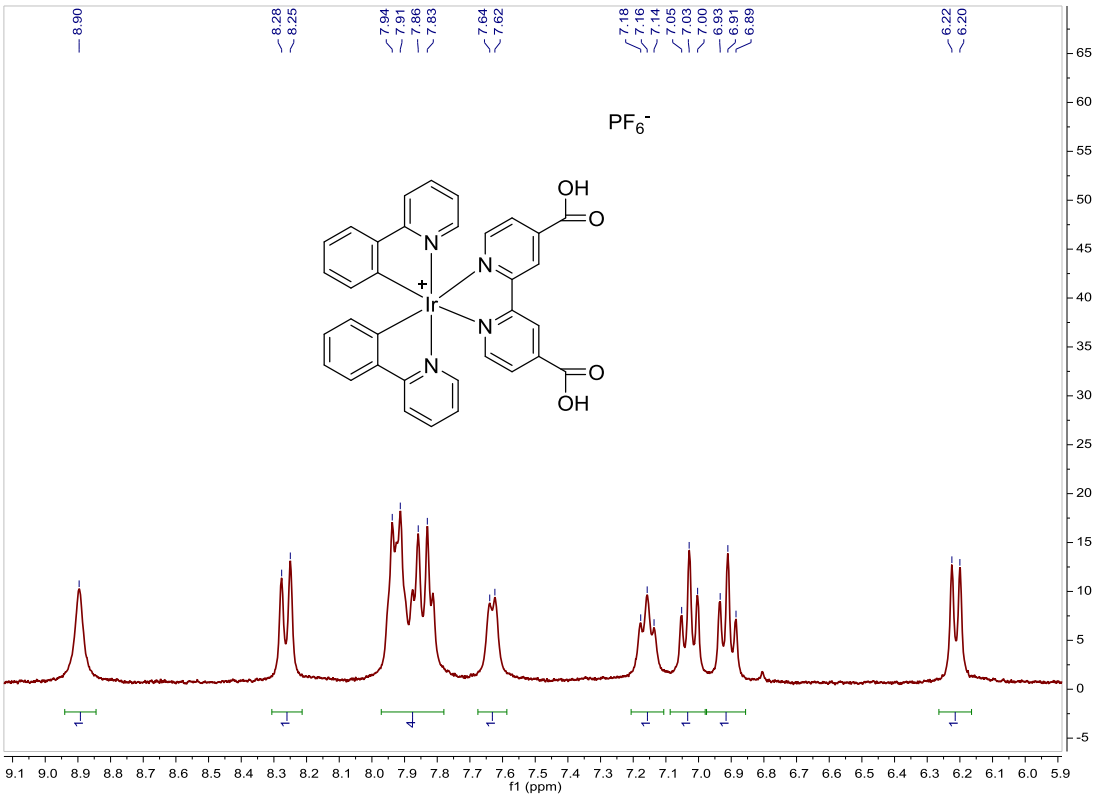

Fig. S86. ^{1}H NMR spectrum of **A16** in DMSO-*d*$_6$, 300 MHz.

[33] Z. Ning, Q. Zhang, W. Wu and H. Tian, *J. Organomet. Chem.*, **2009**, *694*, 2705–2711.

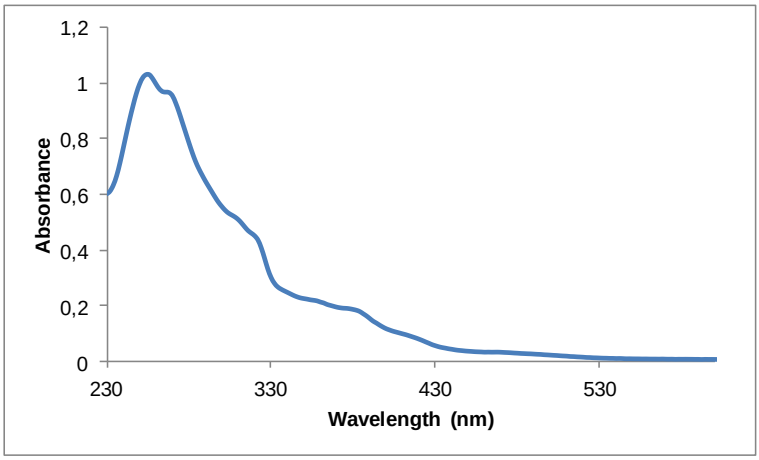

Fig. S87. UV/Vis spectra of **A16** in EtOH, $2.47 \cdot 10^{-5}$M.

Compound B16, [Ir(ppy-F_2)$_2$(4,4'-bis(carboxy)-2,2'-bipyridine)]PF_6. Synthesis and characterization.

SYNTHESIS

Under a N_2 atmosphere, $[Ir(ppy\text{-}F_2)_2Cl]_2$ (0.100 g, 0.082 mmol) were dissolved in 6 ml of acetone and $Ag(CF_3SO_3)$ (0.084 g, 0.328 mmol) were added. The mixture was heated to 56 °C for 2 h and after cooled down to room temperature, AgCl was removed by centrifugation. The resulting solution was added over a 1 h refluxed suspension of 4,4'-bis(carboxy)-2,2'-bipyridine (0.05 g, 0.206 mmol) in 3 ml of acetone and 90 µl of $N(Et)_3$. The reaction mixture was refluxed, under N_2, for 15 h. After solvent evaporation the product was purified by column chromatography (silica gel, CH_2Cl_2). When the unreacted $[Ir(ppy\text{-}F_2)_2Cl]_2$ eluted, 0.05 g of KPF_6 were added on top of the column and the polarity of the eluent was gradually increased to 100% methanol to elute $[Ir(ppy\text{-}F_2)_2$(4,4'-bis(carboxy)-2,2'-bipyridine)]PF_6 together with the excess of KPF_6. The desired compound washed with acetone was obtained as a yellow solid. Yield 52%. The spectroscopic data are coincident with those described in the literature.[34]

Exact Mass: ESI-MS $[C_{34}H_{20}F_4IrN_4O_4]^+$: calculated: m/z= 817.1050 , found: m/z= 817.1060 .

^{1}H NMR (300 MHz, DMSO-d_6): δ 8.88 (s, 1H), 8.30 (d, J = 8.4 Hz, 1H), 8.03 (t, J = 7.3 Hz, 1H), 7.88 (brd, J = 6.4 Hz, 2H), 7.71 (s, 1H), 7.24 (t, J = 6.3 Hz, 1H), 6.97 (ddd, J = 1.9 Hz, J = 2.3 Hz, J = 11.8 Hz, 1H), 5.64 (d, J = 6.7 Hz, 1H).

UV/Vis (EtOH), λ, nm (ε, 10^4 M^{-1} cm^{-1}): 248 (3.6), 262 (3.4), 306 (1.8), 362 (0.6).

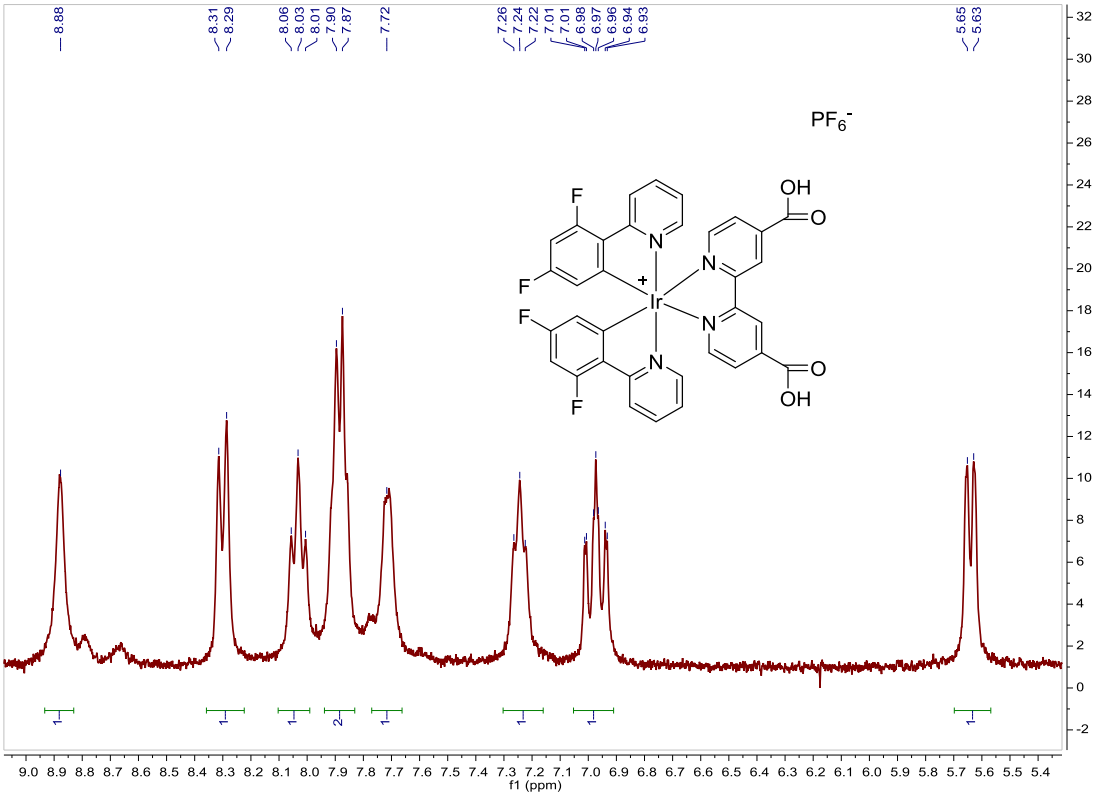

Fig. S88. ^{1}H NMR spectrum of **B16** in DMSO-d_6, 300 MHz.

[34] W. Jiang, Y. Gao, Y. Sun, F. Ding, Y. Xu, Z. Bian, F. Li, J. Bian and C. Huang, *Inorg. Chem.*, **2010,** *49*, 3252–3260.

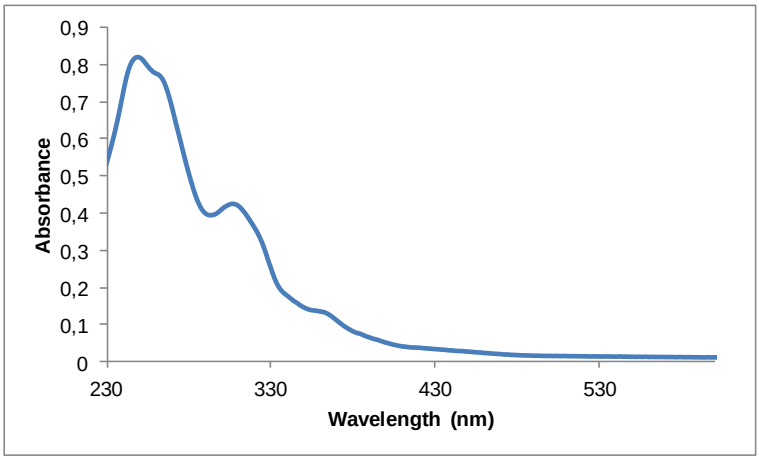

Fig. S89. UV/Vis spectra of **B16** in EtOH, $2.29 \cdot 10^{-5}$M.

Compound C16, [Ir(ppy-Br)$_2$(4,4'-bis(carboxy)-2,2'-bipyridine)]PF$_6$. Synthesis and characterization.

SYNTHESIS

Under a N_2 atmosphere, $[Ir(ppy\text{-}Br)_2Cl]_2$ (0.150 g, 0.108 mmol) were dissolved in 8 ml of acetone and $Ag(CF_3SO_3)$ (0.111 g, 0.432 mmol) were added. The mixture was heated to 56 °C for 2 h and after cooled down to room temperature, AgCl was removed by centrifugation. The resulting solution was added over a 1 h refluxed suspension of 4,4'-bis(carboxy)-2,2'-bipyridine (0.066 g, 0.270 mmol) in 4 ml of acetone and 119 µl of $N(Et)_3$. The reaction mixture was refluxed, under N_2, for 15 h. After solvent evaporation the product was purified by column chromatography (silica gel, CH_2Cl_2). When the unreacted $[Ir(ppy\text{-}Br)_2Cl]_2$ eluted, 0.05 g of KPF_6 were added on top of the column and the polarity of the eluent was gradually increased to 100% methanol to elute $[Ir(ppy\text{-}Br)_2(4,4'\text{-bis(carboxy)-2,2'-bipyridine)}]PF_6$ together with the excess of KPF_6. The desired compound washed with acetone and ether was obtained as a yellow solid. Yield 41%.

Elemental Analysis: calculated for $(C_{34}H_{22}Br_2IrN_4O_4PF_6{\cdot}CH_3COCH_3)$: C, 40.19; H, 2.55; N, 5.07. Found: C, 39.99; H, 2.62; N, 5.47.

Exact Mass: ESI-MS $[C_{34}H_{22}Br_2IrN_4O_4]^+$: calculated: m/z= 900.9637 , found: m/z= 900.9625.

^{1}H NMR (300 MHz, DMSO-d_6): δ 8.80 (s, 1H), 8.23 (d, J = 8.2 Hz, 1H), 7.93–7.78 (m, 3H), 7.74 (d, J = 5.4 Hz, 1H), 7.57 (d, J = 5.5 Hz, 1H), 7.21–7.06 (m, 2H), 6.09 (s, 1H).

UV/Vis (EtOH), λ, nm (ε, 10^4 M^{-1} cm^{-1}): 254 (2.4), 270 (2.5), 310 (1.5).

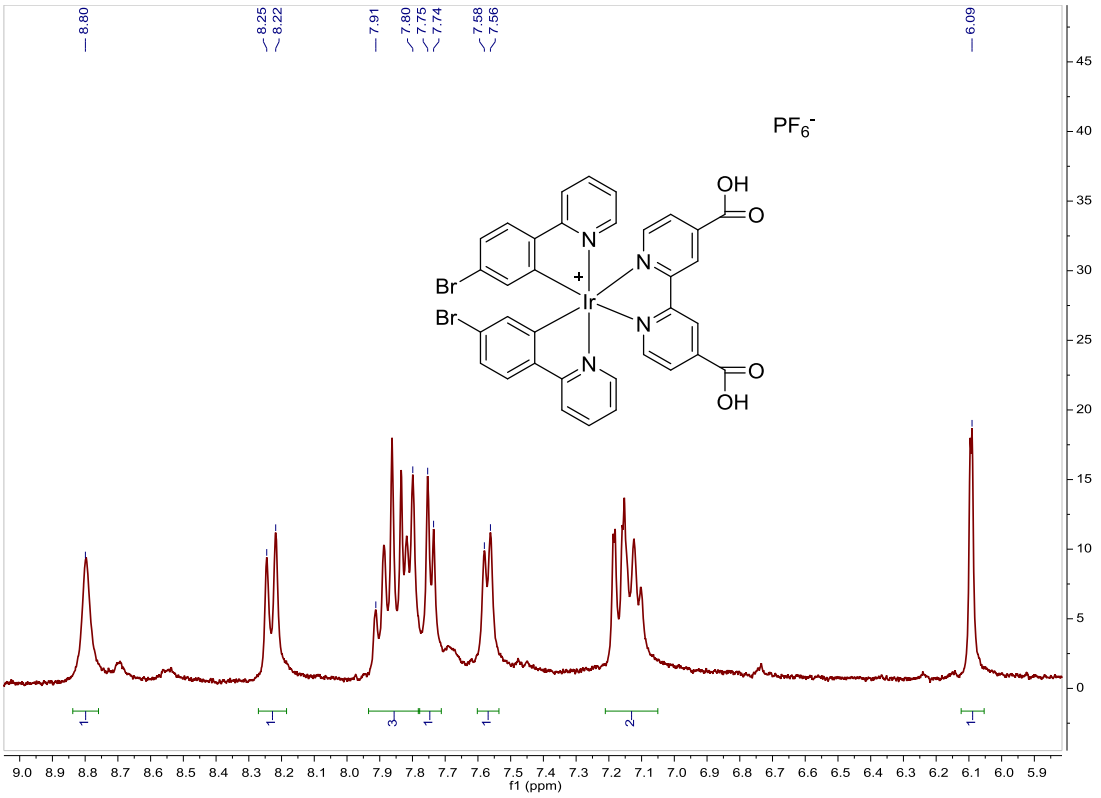

Fig. S90. ^{1}H NMR spectrum of **C16** in DMSO-d_6, 300 MHz.

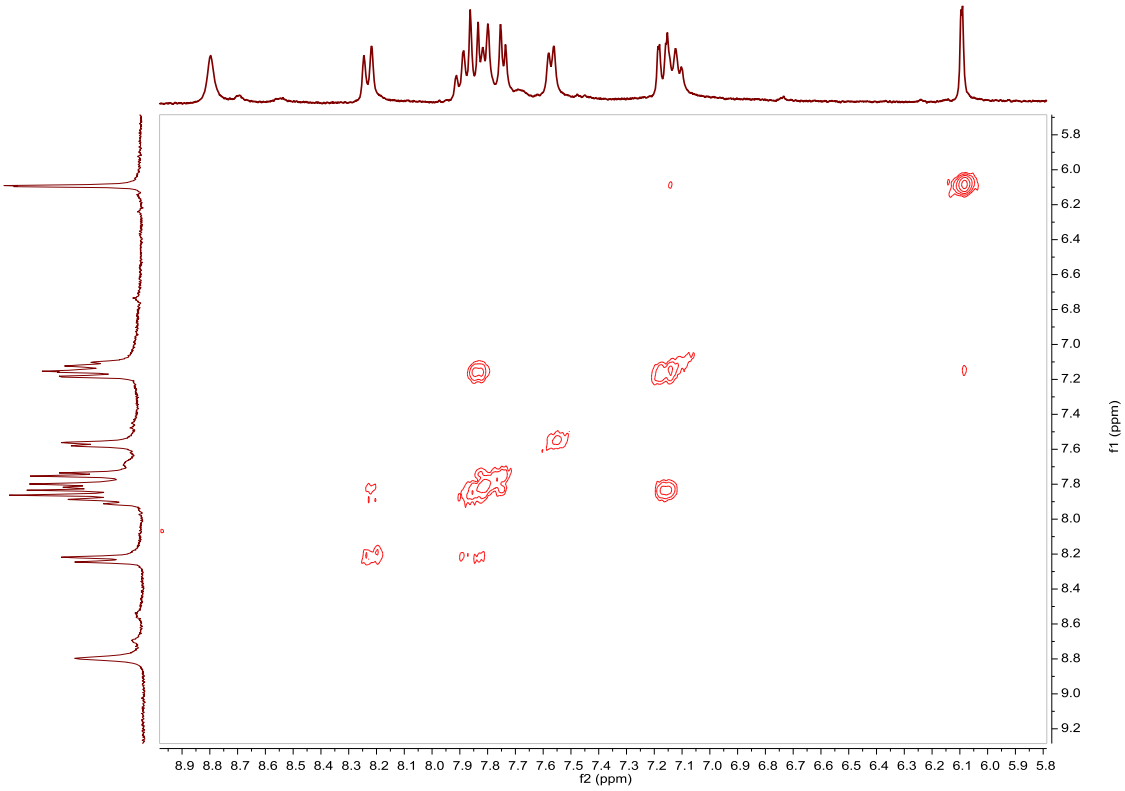

Fig. S91. COSY NMR spectrum of **C16** in DMSO-d_6.

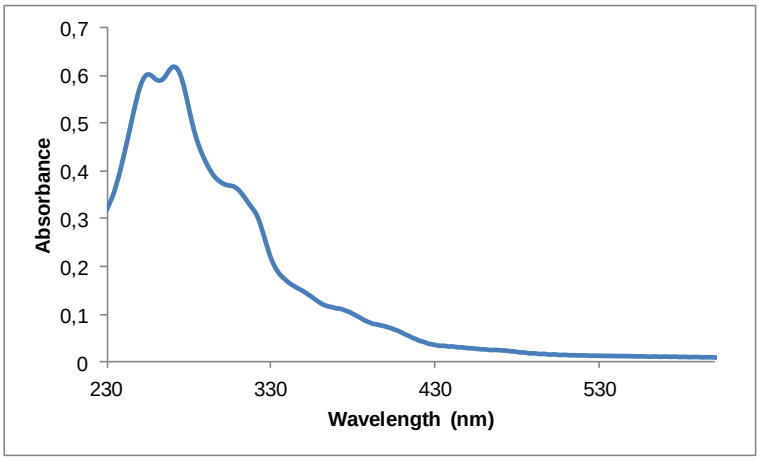

Fig. S92. UV/Vis spectra of **C16** in EtOH, $2.48 \cdot 10^{-5}$M.

Compound D16, [Ir((5-azobenzyl-2-pyridyl)phenyl)$_2$(4,4'-bis(carboxy)-2,2'-bipyridine)] PF_6. Synthesis, characterization and photoisomerization studies.

SYNTHESIS

Under a N_2 atmosphere, [Ir((5-azobenzyl-2-pyridyl)phenyl)$_2$Cl]$_2$ (0.100 g, 0.056 mmol) were dissolved in 4 ml of acetone and Ag(CF_3SO_3) (0.057 g, 0.224 mmol) were added. The mixture was heated to 56 °C for 2 h and after cooled down to room temperature, AgCl was removed by centrifugation. The resulting solution was added over a 1 h refluxed suspension of 4,4'-bis(carboxy)-2,2'-bipyridine (0.034 g, 0.141 mmol) in 2 ml of acetone. The reaction mixture was refluxed, under N_2, for 15 h. After solvent evaporation the solid that was not soluble in MeOH was removed, NH_4PF_6 (0.02 g, 0.123 mmol) were added and the solution was stirred during 1 h. The desired compound was obtained after precipitation with hexane as an orange solid. Yield 63%.

Exact Mass: ESI-MS $[C_{58}H_{40}IrN_8O_4]^+$: calculated: m/z= 1105.2802 , found: m/z= 1105.2839.

^{1}H NMR (300 MHz, DMSO-d_6): δ 9.32 (s, 1H), 8.41 (d, J = 7.6 Hz, 1H), 8.24 (d, J = 5.5 Hz, 1H), 8.19–8.00 (m, 3H), 7.91 (d, J = 7.6 Hz, 3H), 7.83 (d, J = 5.4 Hz, 1H), 7.72–7.53 (m, 5H), 7.49 (d, J = 6.4 Hz, 1H), 7.24 (t, J = 6.7 Hz, 2H), 6.50 (s, 1H).

UV/Vis (EtOH), λ, nm (ε, 10^4 M^{-1} cm^{-1}): 360 (4.3), 425 (1.1).

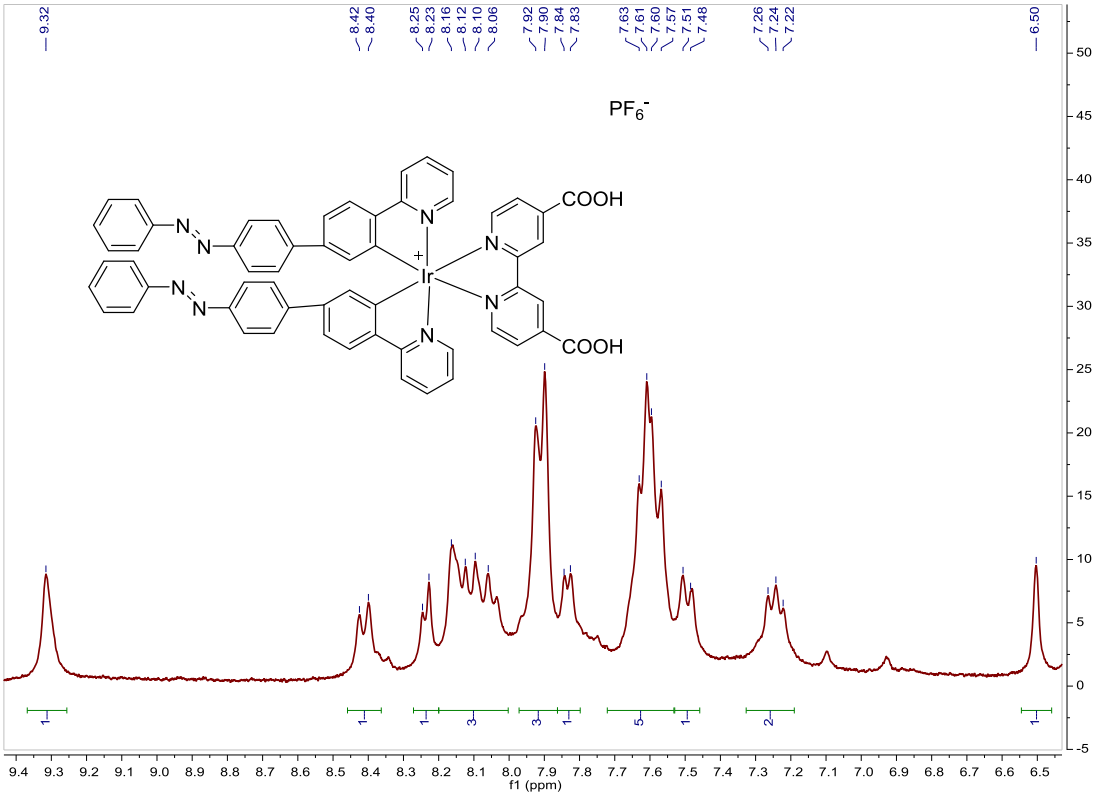

Fig. S93. ^{1}H NMR spectrum of **D16** in DMSO-d_6, 300 MHz.

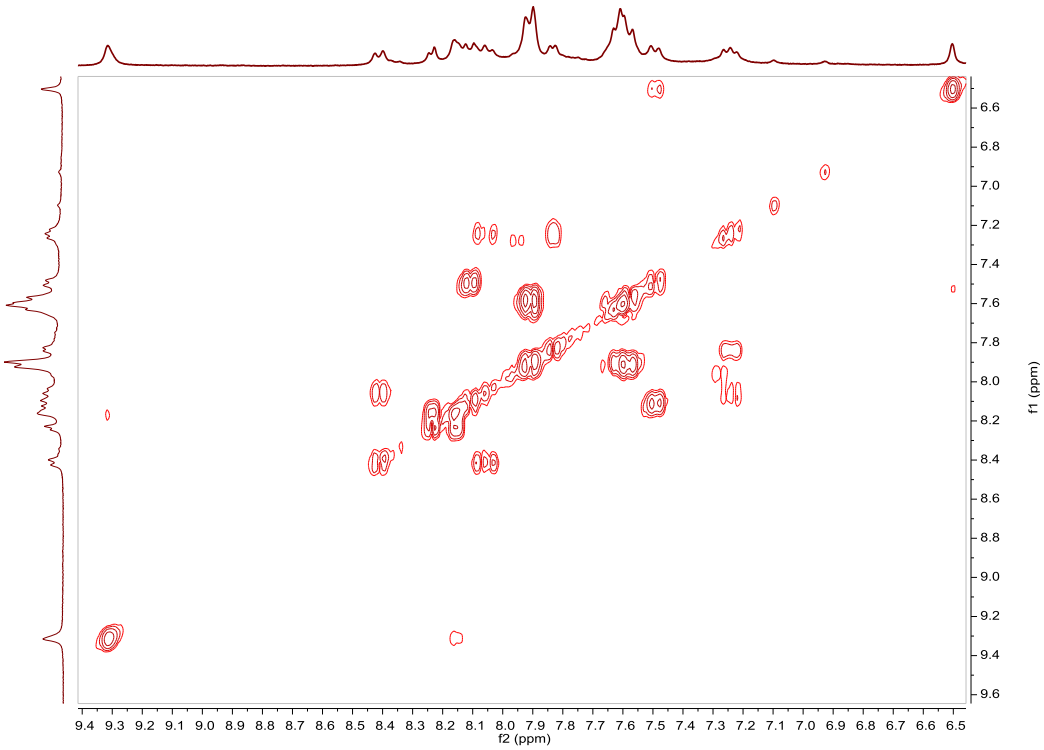

Fig. S94. COSY NMR spectrum of **D16** in DMSO-d_6.

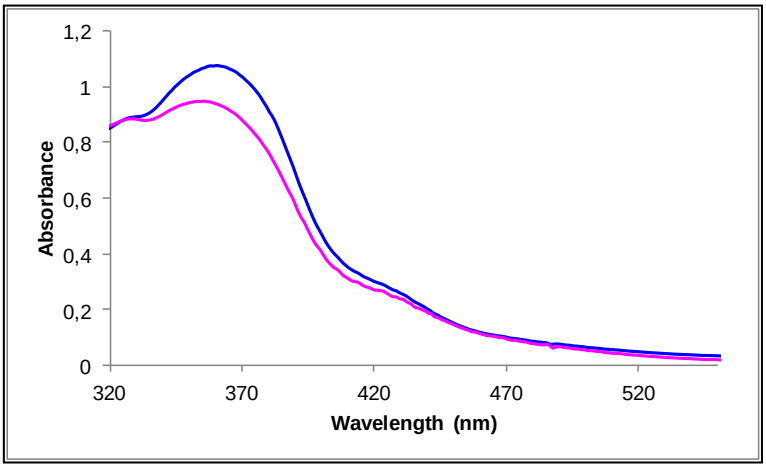

Fig. S95. UV/Vis spectra of **D16** in EtOH. Before (blue line) and after (pink line) irradiation at 374nm, $2.49 \cdot 10^{-5}$M.

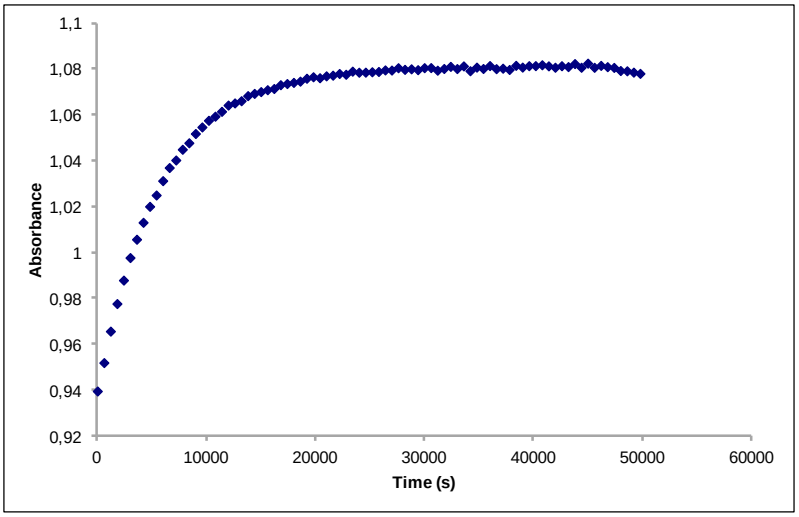

Fig. S96. Cis to trans thermal isomerization kinetics of **D16**. Absorption change of the band 360nm at 328 K in EtOH after irradiation at 374 nm. ($2.49 \cdot 10^{-5}$M).

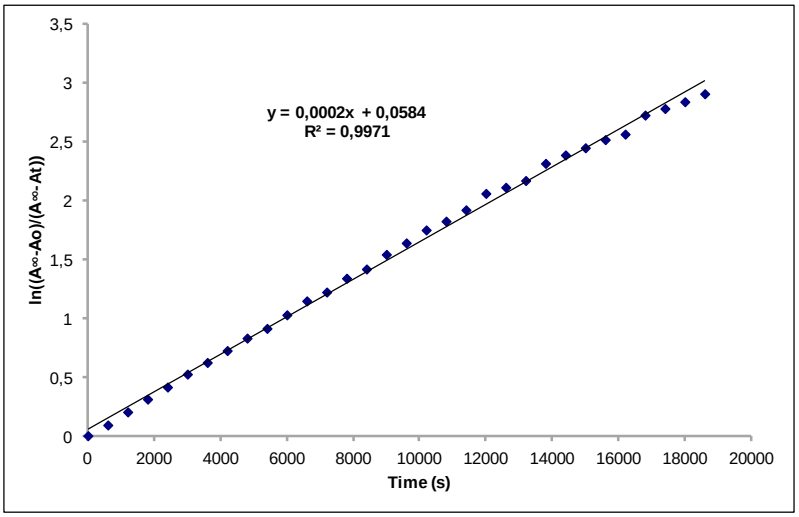

Fig. S97. Cis to trans thermal isomerization kinetics of **D16**. First-order plot. k (s^{-1}) = $2.0 \cdot 10^{-4}$. Half-life (min) = 58.

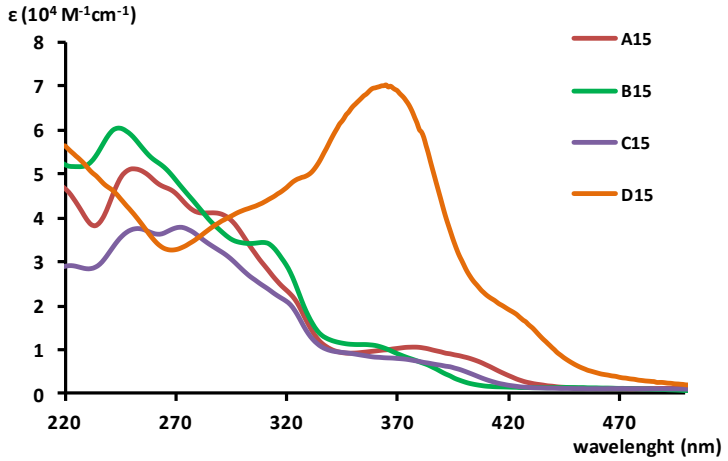

Fig. S98. UV-Vis absorption spectra of complexes **A**–**D** with 4,4'-bis(diethylphosphonate)-2,2'-bipyridine.

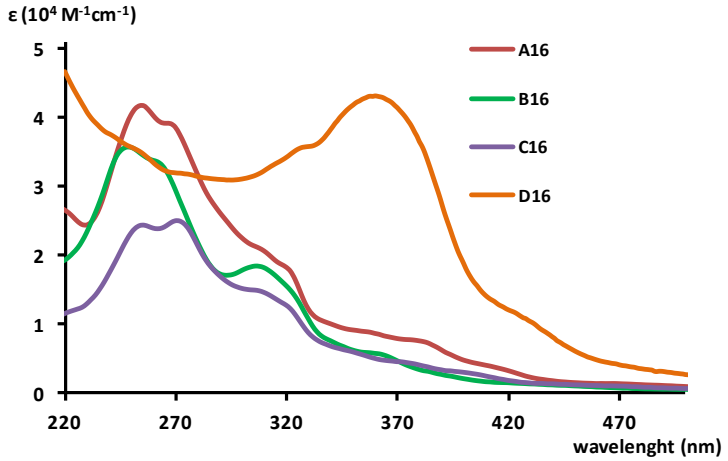

Fig. S99. UV-Vis absorption spectra of complexes **A**–**D** with 4,4'-bis(carboxy)-2,2'-bipyridine.

Compound Abipy, $[Ir(ppy)_2(bipy)]PF_6$. Synthesis and characterization.

SYNTHESIS

Under a N_2 atmosphere, $[Ir(ppy)_2Cl]_2$ (0.200 g, 0.186 mmol) were added over a suspension of 2,2'-bipyridine (0.058 g, 0.371 mmol) in 15 mL CH_2Cl_2–MeOH 2/1. The reaction mixture was refluxed, under N_2, for 15 h. To the resulting orange solution, 0.07 g of KPF_6 were added and the solution was stirred for an 1 h. The solvent was evaporated and the desired compound was obtained after filtration through a celite path in CH_2Cl_2 as a yellow solid. Yield 97%. The spectroscopic data are coincident with those described in the literature.[35]

^{1}H NMR (500 MHz, CD_2Cl_2): δ 8.56 (d, J = 8.1 Hz, 1H), 8.15 (t, J = 7.7 Hz, 1H), 8.05 (d, J = 4.5 Hz, 1H), 7.99 (d, J = 8.1 Hz, 1H), 7.81 (t, J =7.4 Hz, 1H), 7.77 (d, J = 7.7 Hz, 1H), 7.52 (d, J = 5.5 Hz, 1H), 7.49 (t, J = 5.9 Hz, 1H), 7.11 (t, J = 7.3 Hz, 1H), 7.02 (t, J =6.0 Hz, 1H), 6.97 (t, J = 7.4 Hz, 1H), 6.34 (d, J = 7.6 Hz, 1H).

^{13}C NMR (126 MHz, CD_2Cl_2): δ 168.16 (C_{quat}), 156.10 (C_{quat}) , 151.12 (CH), 150.26 (C_{quat}) , 148.89 (CH), 144.06 (C_{quat}), 139.84 (CH), 138.60 (CH), 132.02 (CH), 131.11 (CH), 128.67(CH), 125.30 (CH), 125.03 (CH), 123.69 (CH), 123.12 (CH), 120.25 (CH).

UV/Vis (CH_3CN), λ, nm (ε, 10^4 M^{-1} cm^{-1}): 254 (4.6), 265 (4.4), 309 (2.0), 376 (0.57).

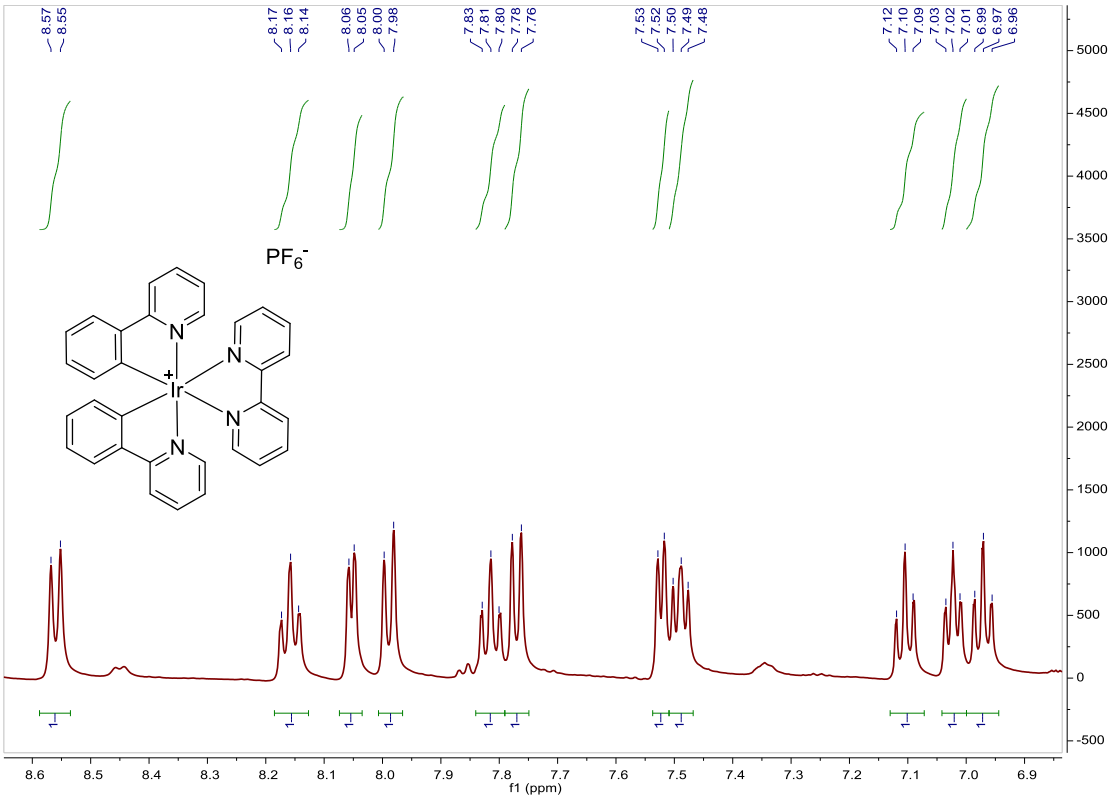

Fig. S100. ^{1}H NMR spectrum of **Abipy** in CD_2Cl_2, 500 MHz.

[35] R. D. Costa, E. Ortí, H. J. Bolink, S. Graber, S. Schaffner, M. Neuburger, C. E. Housecroft and E. C. Constable, *Adv. Funct. Mater.*, **2009**, *19*, 3456–3463.

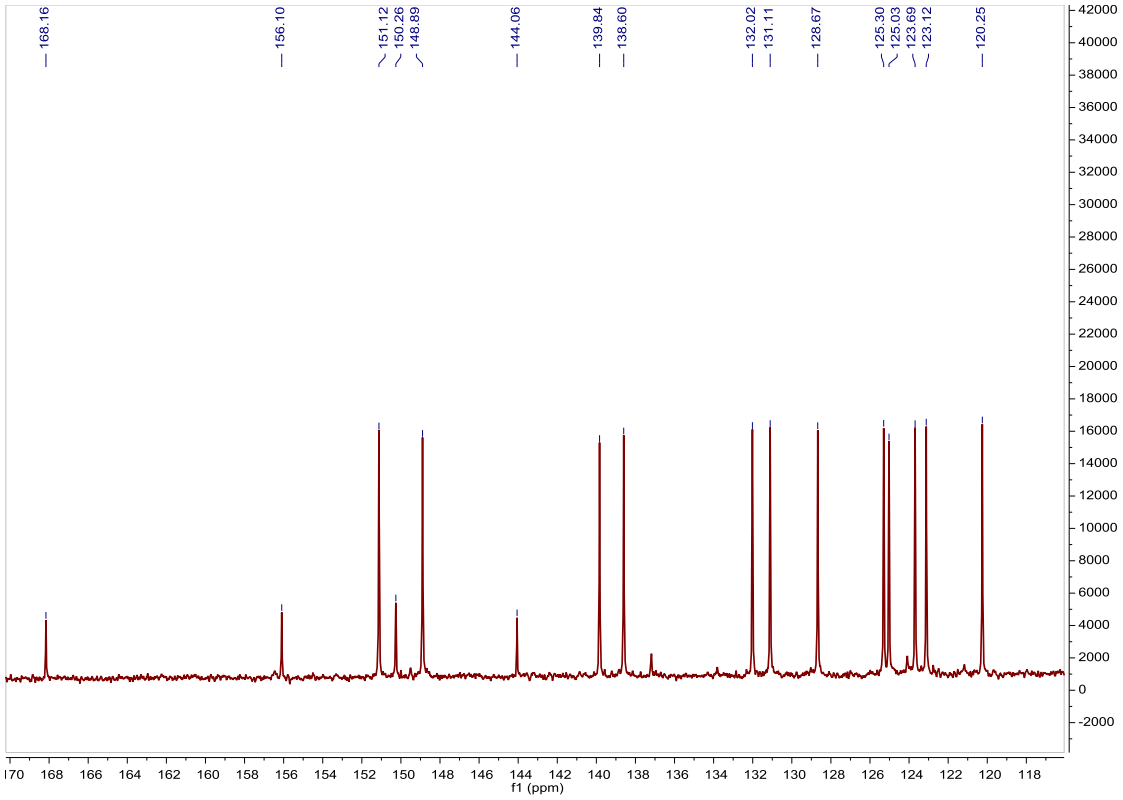

Fig. S101. ^{13}C NMR spectrum of **Abipy** in CD_2Cl_2, 126 MHz.

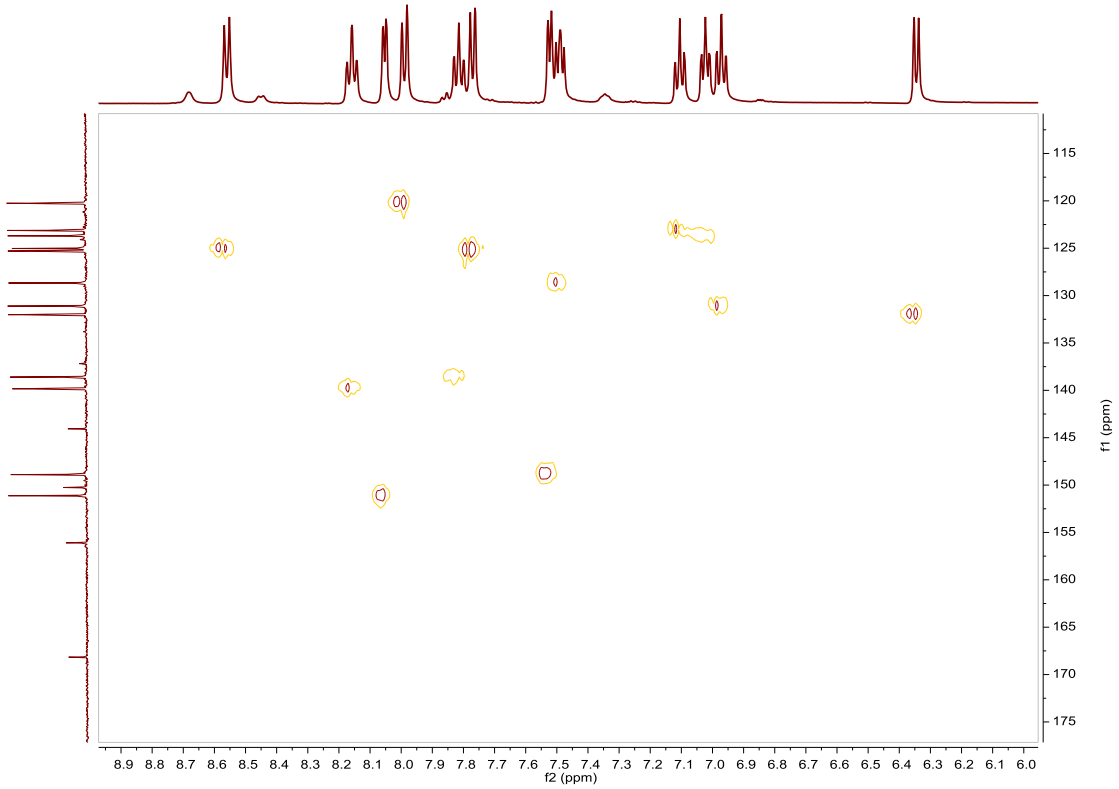

Fig. S102. HSQC NMR spectrum of **Abipy** in CD_2Cl_2.

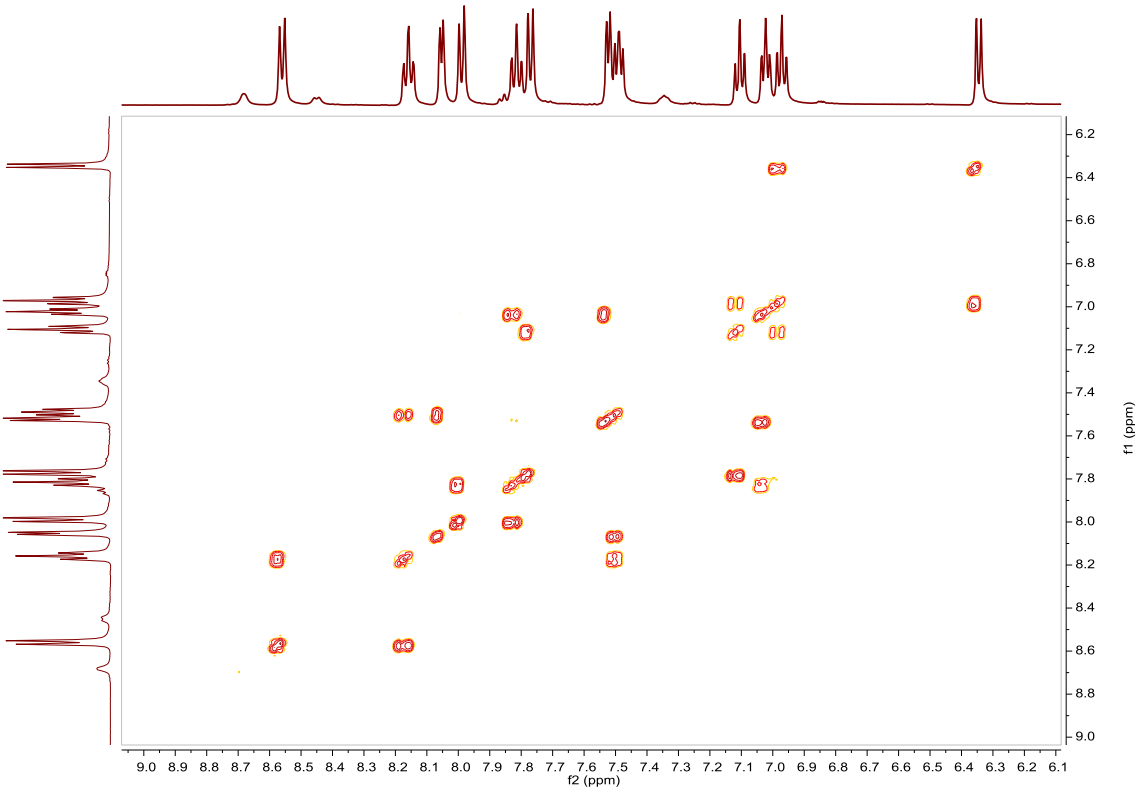

Fig. S103. COSY NMR spectrum of **Abipy** in CD_2Cl_2.

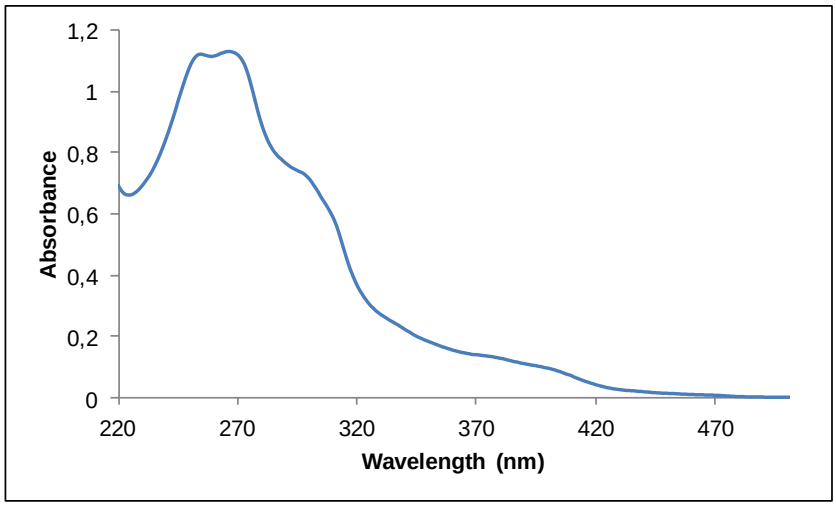

Fig. S104. UV/Vis spectra of **Abipy** in CH_3CN, $2.45 \cdot 10^{-5}$M.

Compound Bbipy, $[Ir(Fppy)_2(bipy)]PF_6$. Synthesis and characterization.

SYNTHESIS

Under a N_2 atmosphere, $[Ir(Fppy)_2Cl]_2$ (0.231 g, 0.190 mmol) were added over a suspension of 2,2'-bipyridine (0.059 g, 0.38 mmol) in 15 mL CH_2Cl_2–MeOH 2/1. The reaction mixture was refluxed, under N_2, for 15 h. To the resulting orange solution, 0.07 g of KPF_6 were added and the solution was stirred for an 1 h. The solvent was evaporated and the desired compound was obtained after filtration through a celite path in CH_2Cl_2 as a yellow solid. Yield 84%. The spectroscopic data are coincident with those described in the literature.[36]

^{1}H NMR (400 MHz, CD_2Cl_2): δ 9.08 (d, J = 8.2 Hz, 1H), 8.37 (d, J = 8.4 Hz, 1H), 8.28 (t, J = 7.1 Hz, 1H), 8.03 (d, J = 5.2 Hz, 1H), 7.89 (t, J = 7.8 Hz, 1H), 7.55 (m, 2H), 7.10 (t, J = 7.1 Hz, 1H), 6.65 (ddd, J = 2.3 Hz, J = 9.2 Hz, J = 11.8 Hz, 1H), 5.80 (dd, J = 2.3 Hz, J = 8.4 Hz, 1H).

^{13}C NMR (100 MHz, CD_2Cl_2): δ 164.24 (d, J = 6.9 Hz, C_{quat}), 163.74 (dd, J = 12.3 Hz, J = 256.3 Hz, C_{quat}), 161.53 (dd, J = 12.6 Hz, J = 259.4 Hz, C_{quat}), 155.67 (s, C_{quat}), 153.77 (d, J = 6.5 Hz, C_{quat}), 150.24 (s, CH), 148.65 (s, CH), 140.43 (s, CH), 139.20 (s, CH), 128.48 (s, CH), 127.68 (s, C_{quat}), 126.19 (s, CH), 123.86 (d, J = 20.1 Hz, CH), 123.68 (s, CH), 113.96 (dd, J = 2.0 Hz, J = 17.6 Hz, CH), 99.06 (t, J = 26.7 Hz, CH).

UV/Vis (CH_3CN), λ, nm (ε, 10^4 M^{-1} cm^{-1}): 245 (5.0), 261 (4.6), 296 (2.6), 359 (0.64).

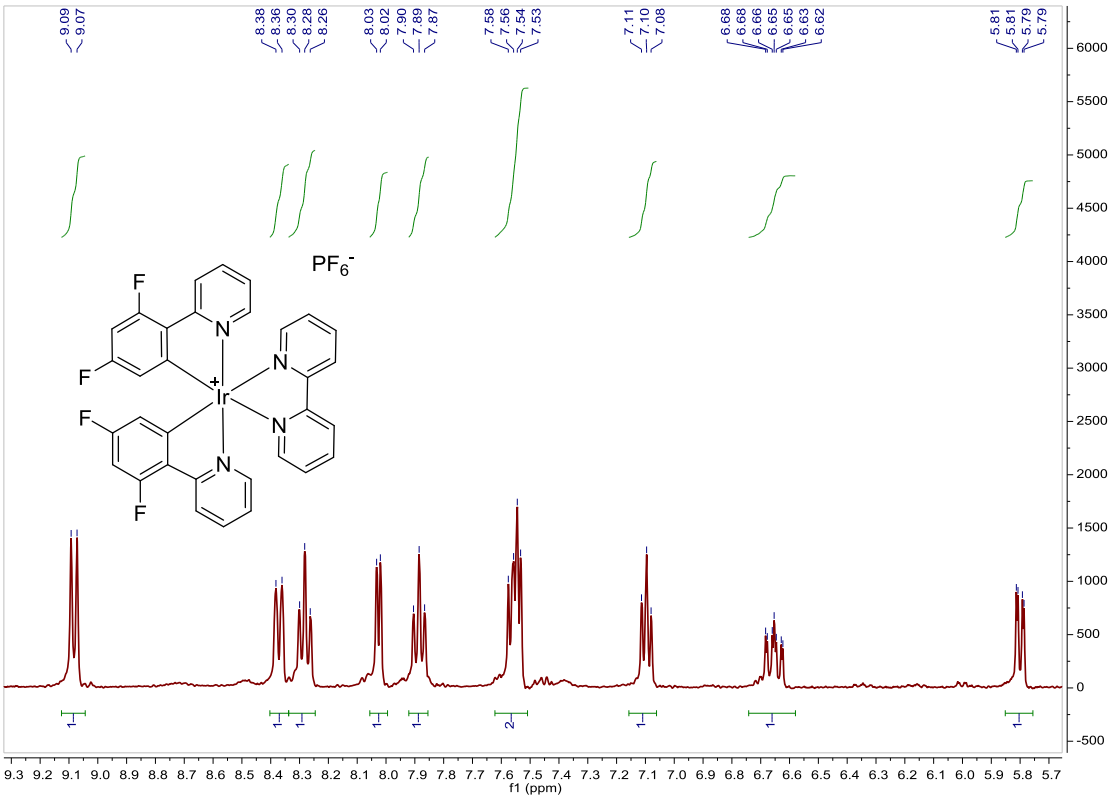

Fig. S105. ^{1}H NMR spectrum of **Bbipy** in CD_2Cl_2, 400 MHz.

[36] F. Lafolet, S. Welter, Z. Popovic and L. De Cola, *J. Mater. Chem.*, **2005**, *15*, 2820–2828.

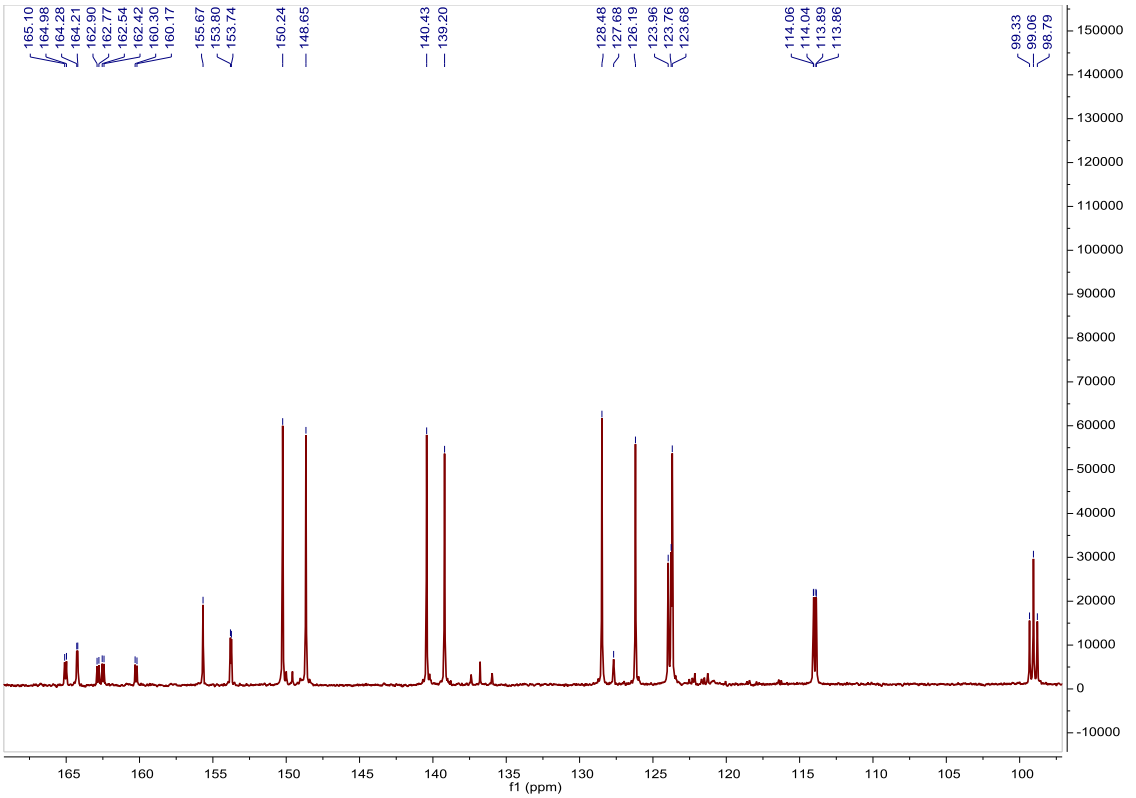

Fig. S106. ^{13}C NMR spectrum of **Bbipy** in CD_2Cl_2, 100 MHz.

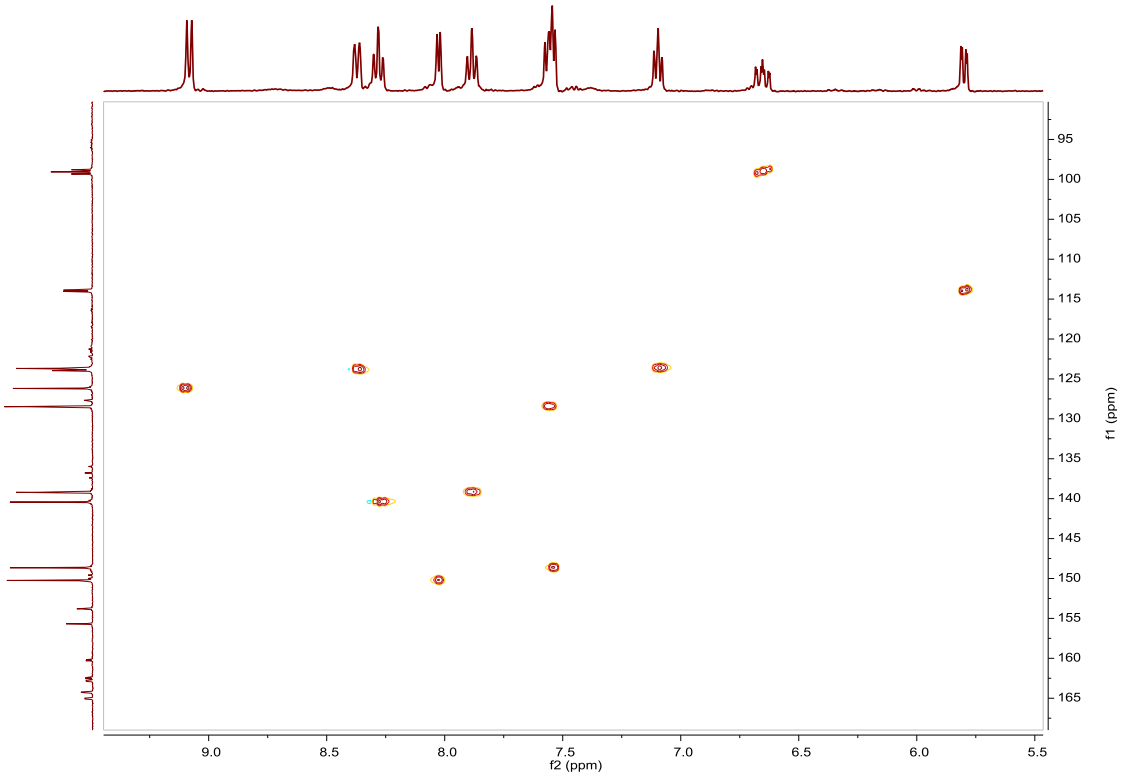

Fig. S107. HSQC NMR spectrum of **Bbipy** in CD_2Cl_2.

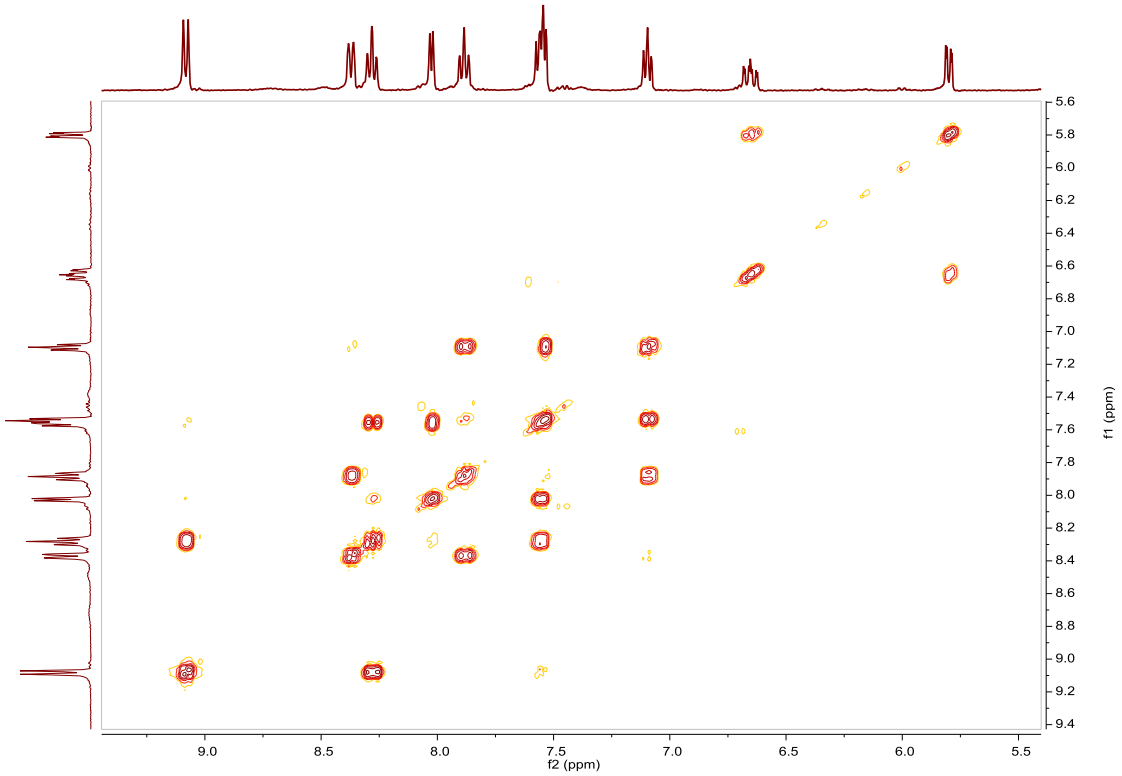

Fig. S108. COSY NMR spectrum of **Bbipy** in CD_2Cl_2.

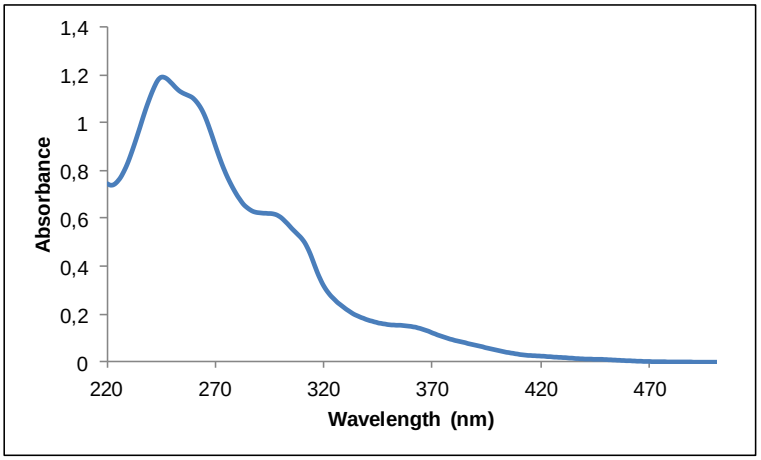

Fig. S109. UV/Vis spectra of **Bbipy** in CH_3CN, $2.37 \cdot 10^{-5}$M.

Compound Cbipy, $[Ir(Brppy)_2(bipy)]PF_6$. Synthesis and characterization.

SYNTHESIS

Under a N_2 atmosphere, $[Ir(Brppy)_2Cl]_2$ (0.200 g, 0.144 mmol) were added over a suspension of 2,2'-bipyridine (0.045 g, 0.288 mmol) in 16 mL CH_2Cl_2–MeOH 2/1. The reaction mixture was refluxed, under N_2, for 15 h. After solvent evaporation the product was purified by column chromatography (silica gel, CH_2Cl_2). When the unreacted $[Ir(ppy\text{-}Br)_2Cl]_2$ eluted, 0.10 g of KPF_6 were added on top of the column and the polarity of the eluent was gradually increased to 100% acetone to elute $[Ir(Brppy)_2(bipy)]PF_6$ together with the excess of KPF_6. The desired compound was precipitated with ether after filtration through a celite path in CH_2Cl_2 and it was obtained as a yellow solid. Yield 46%.

Elemental Analysis: calculated for ($C_{32}H_{22}Br_2IrN_4PF_6$): C, 40.06; H, 2.31; N, 5.84. Found: C, 40.11; H, 2.45; N, 5.37.

Exact Mass: ESI-MS $[C_{32}H_{22}Br_2IrN_4]^+$: calculated: m/z= 812.9840, found: m/z= 812.9813.

^{1}H NMR (300 MHz, acetone-d_6): δ 8.89 (d, J = 8.2 Hz, 1H), 8.35 (ddd, J = 1.6 Hz, J = 7.9 Hz, J = 9.4 Hz, 1H), 8.32 (d, J = 8.0 Hz, 1H), 8.20 (d, J = 5.4 Hz, 1H), 8.04 (ddd, J = 1.5 Hz, J = 7.5 Hz, J = 9.0 Hz, 1H), 7.90 (m, 2H), 7.77 (ddd, J = 1.2 Hz, J = 7.0 Hz, J = 7.6 Hz, 1H), 7.27 (m, 2H), 6.44 (d, J = 1.9 Hz, 1H).

^{13}C APT NMR (75 MHz, acetone-d_6): δ 167.76 (C_{quat}), 157.25 (C_{quat}), 153.80 (C_{quat}), 152.19 (CH), 150.79 (CH), 144.69 (C_{quat}), 141.31 (CH), 140.54 (CH), 135.08 (CH), 130.14 (CH), 128.08 (CH), 127.12 (CH), 126.34 (CH), 126.21 (C_{quat}), 125.63 (CH), 121.84 (CH).

UV/Vis (CH_3CN), λ, nm (ε, 10^4 M^{-1} cm^{-1}): 255 (4.5), 267 (4.6), 295 (3.0), 378 (0.53), 402 (0.37).

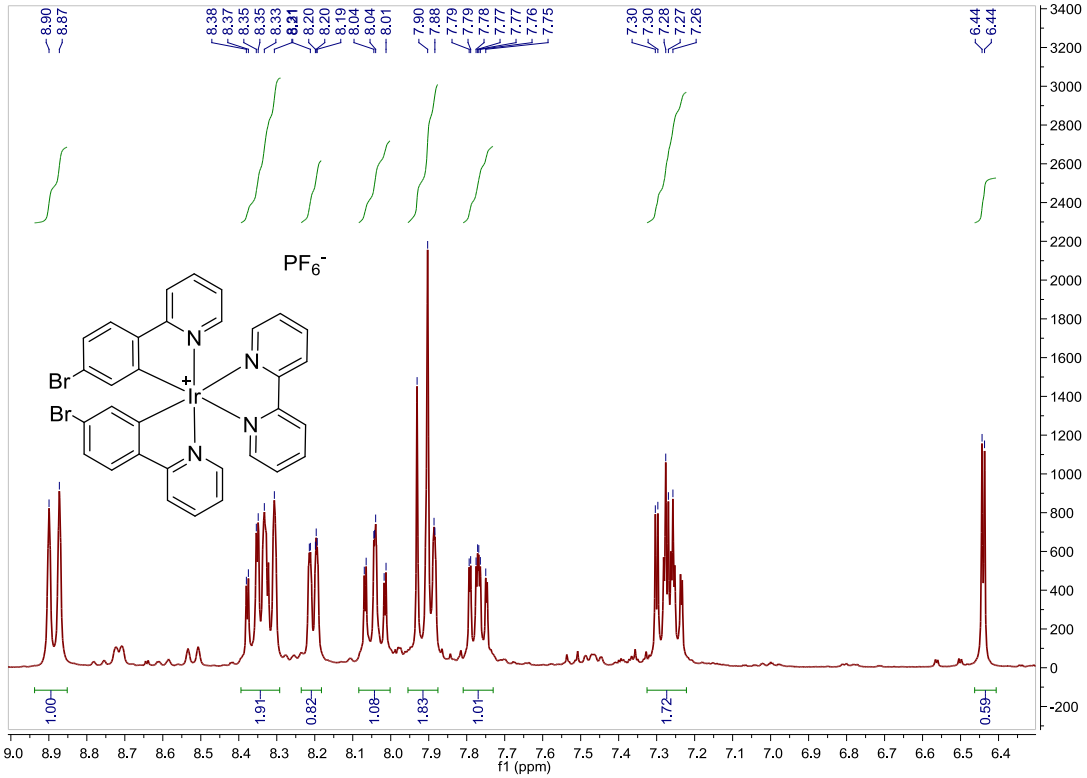

Fig. S110. ^{1}H NMR spectrum of **Cbipy** in acetone-d_6, 300 MHz.

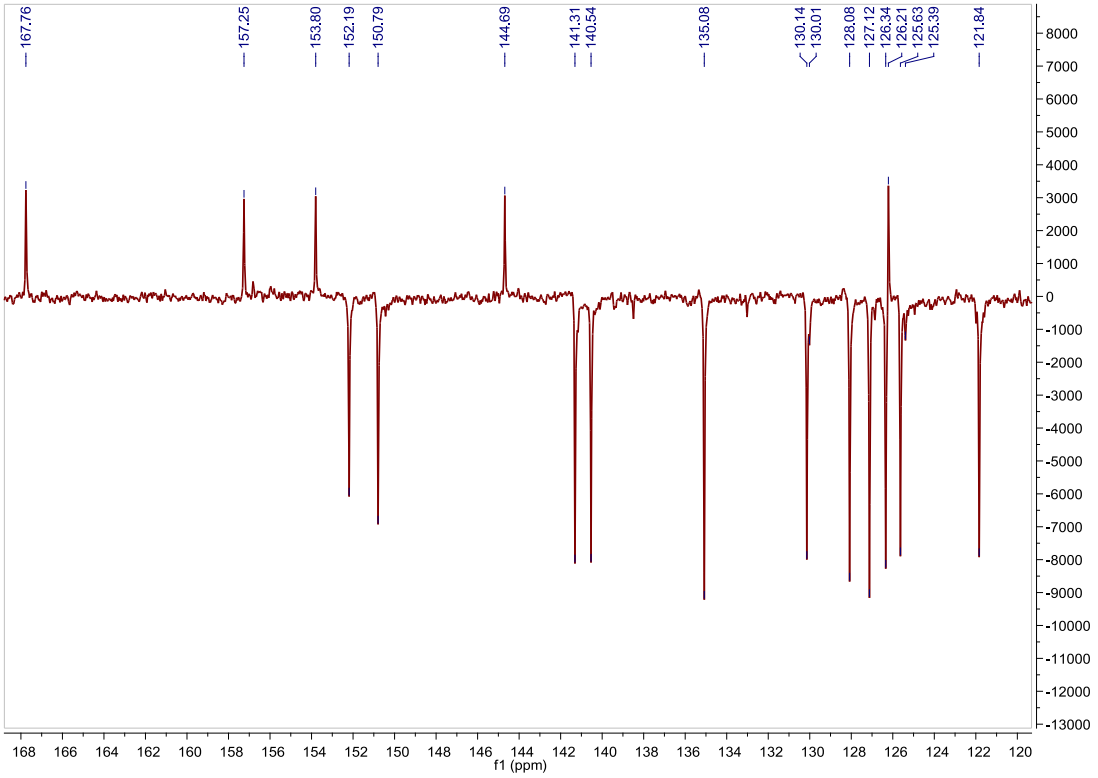

Fig. S111. ^{13}C APT NMR spectrum of **Cbipy** in acetone-d_6, 75 MHz.

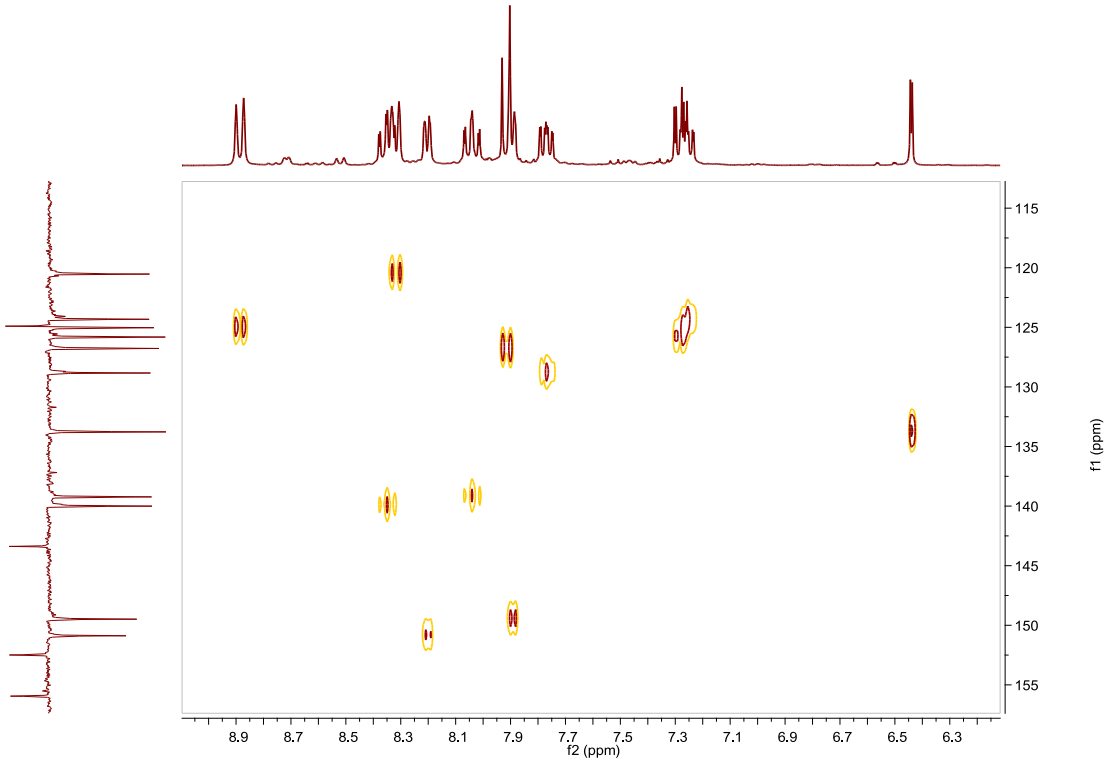

Fig. S112. HSQC NMR spectrum of **Cbipy** in acetone-d_6.

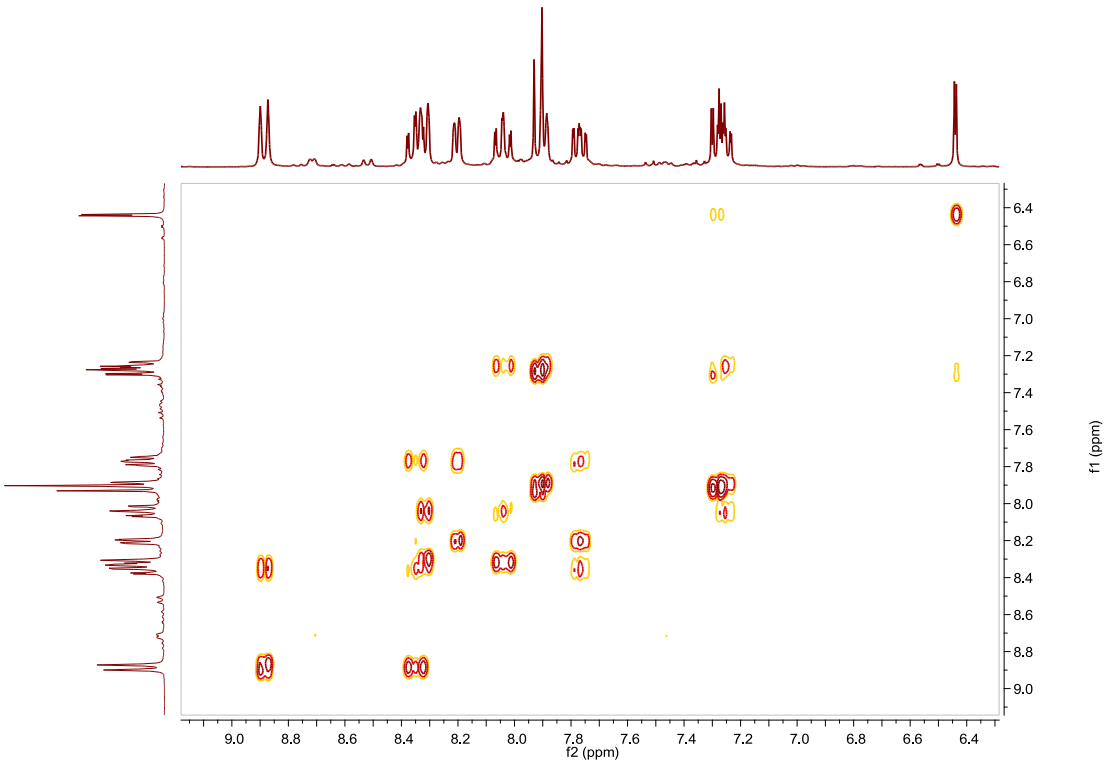

Fig. S113. COSY NMR spectrum of **Cbipy** in acetone-d_6.

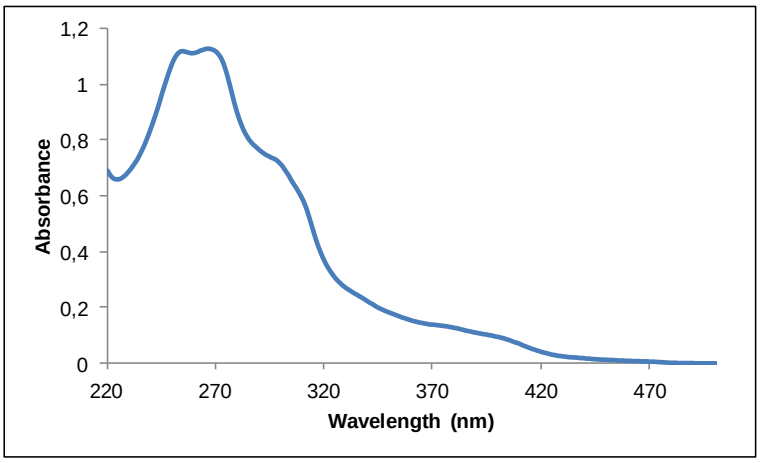

Fig. S114. UV/Vis spectra of **Cbipy** in CH_3CN, $2.46 \cdot 10^{-5}$M.

Compound Dbipy, [Ir(azoppy)$_2$(bipy)]PF$_6$. Synthesis, characterization and photoisomerization studies.

SYNTHESIS

Under a N_2 atmosphere, **C-bipy** (0.065 g, 0.068 mmol) and [4-(phenylazo)phenyl]boronic acid **6** (0.036 g, 0.160 mmol) were dissolved in 4 mL of THF. Na_2CO_3 (1M (aq), 2 mL) and $Pd(PPh_3)_4$ (0.0079 g, 0.0068 mmol) were added and the solution was degassed by bubbling N_2 for 15 min. The reaction mixture was refluxed (80 °C) for 15 h. The resulting mixture was cooled down to room temperature and the product was extracted with CH_2Cl_2. The organic phase was dried with $MgSO_4$, filtered off and the solvent was evaporated. The residue was purified by column chromatography (silica gel, CH_2Cl_2). To the fraction containing the eluted complex, 0.05 g of KPF_6 were added and the resulting solution was filtered through a celite path. The title compound was obtained as an orange solid. Yield 10%.

Elemental Analysis: calculated for ($C_{56}H_{40}IrN_8PF_6 \cdot CH_3COCH_3$): C, 57.88; H, 3.47; N, 9.64. Found: C, 58.03; H, 3.68; N, 9.09.

Exact Mass: ESI-MS $[C_{56}H_{40}IrN_8]^+$: calculated: m/z= 1017.3005, found: m/z= 1017.3036.

^{1}H NMR (300 MHz, acetone-d_6): δ 8.93 (d, J = 7.9 Hz, 1H), 8.42–8.33 (m, 3H), 8.11–8.01 (m, 3H), 7.98–7.89 (m, 4H), 7.79 (ddd, J = 1.1 Hz, J = 5.4 Hz, J = 7.4 Hz, 1H), 7.68–7.57 (m, 5H), 7.50 (dd, J = 1.9 Hz, J = 8.1 Hz, 1H), 7.28 (ddd, J = 1.3 Hz, J = 5.9 Hz, J = 7.3 Hz, 1H), 6.76 (d, J = 1.7 Hz, 1H).

^{13}C APT NMR (75 MHz, acetone-d_6): δ 168.60 (C_{quat}), 157.43 (C_{quat}), 153.94 (C_{quat}), 153.00 (C_{quat}), 152.35 (CH), 152.28 (C_{quat}), 150.88 (CH), 145.61 (C_{quat}), 144.99 (C_{quat}), 142.59 (C_{quat}), 141.00 (CH), 140.20 (CH), 132.63 (CH), 130.97 (CH), 130.61 (2CH), 130.03 (CH), 128.93 (2CH), 126.79 (CH), 126.20 (CH), 125.21 (CH), 124.45 (2CH), 123.97 (2CH), 123.09 (CH), 121.70 (CH).

UV/Vis (CH_3CN), λ, nm (ε, 10^4 M^{-1} cm^{-1}): 355 (7.4).

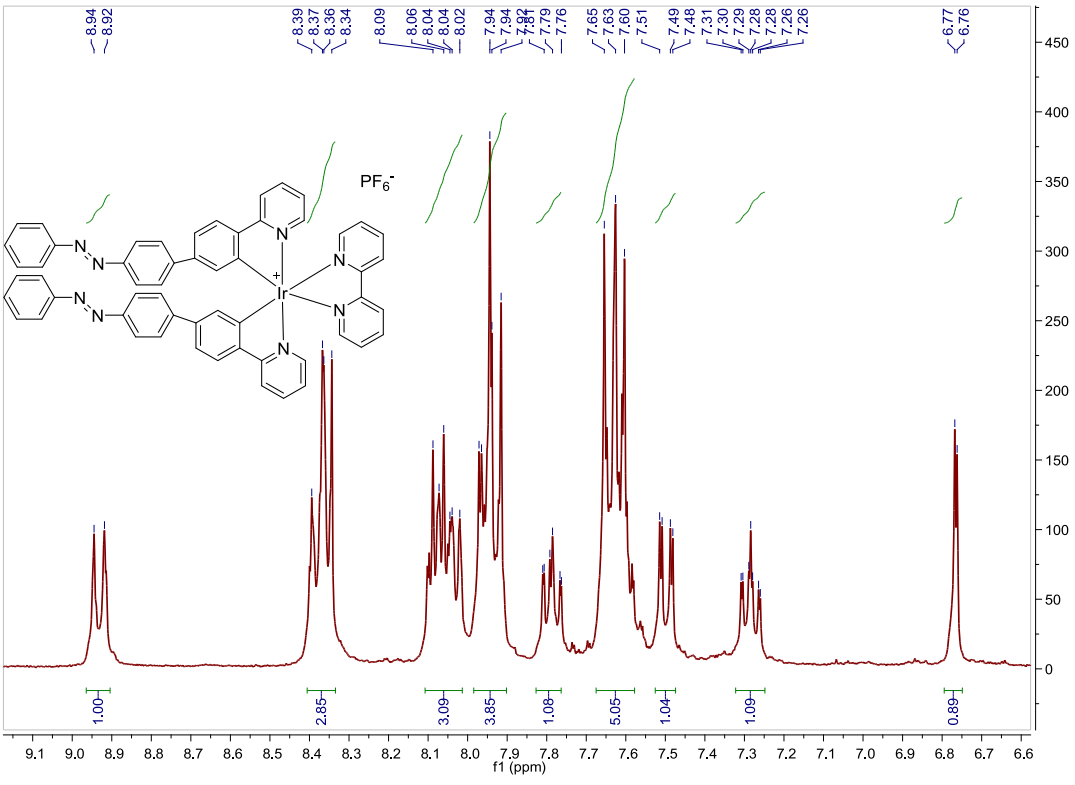

Fig. S115. ^{1}H NMR spectrum of **Dbipy** in acetone-d_6, 300 MHz.

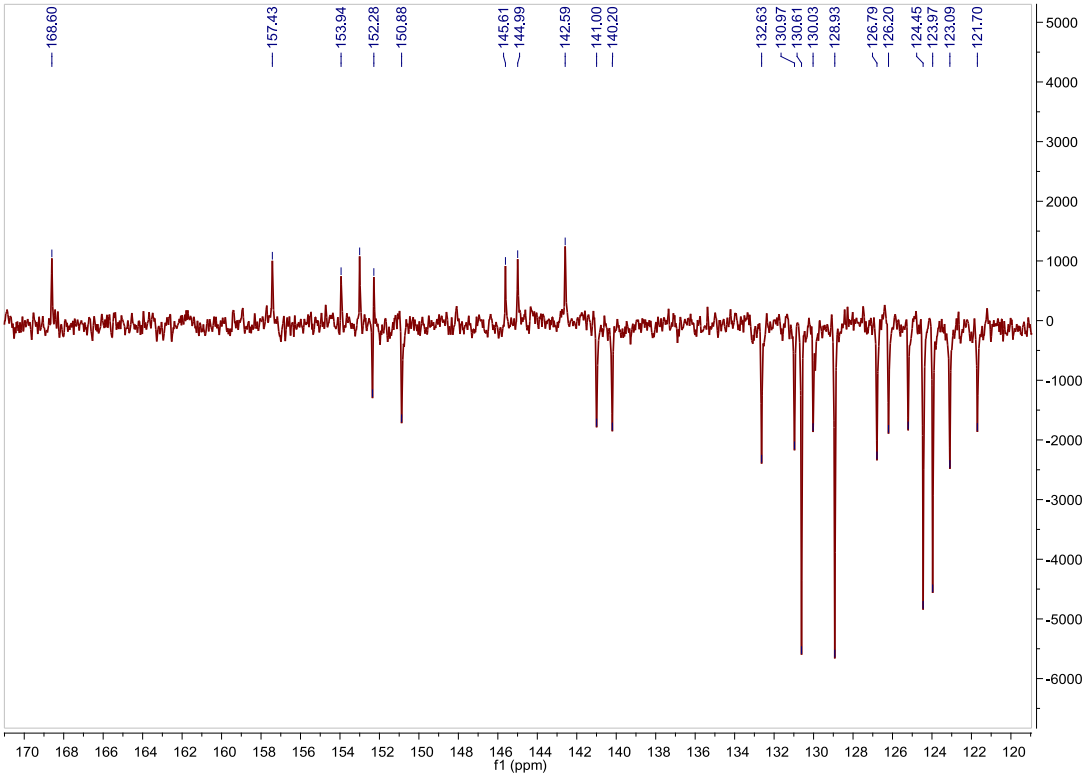

Fig. S116. ^{13}C APT NMR spectrum of **Dbipy** in acetone-d_6, 75 MHz.

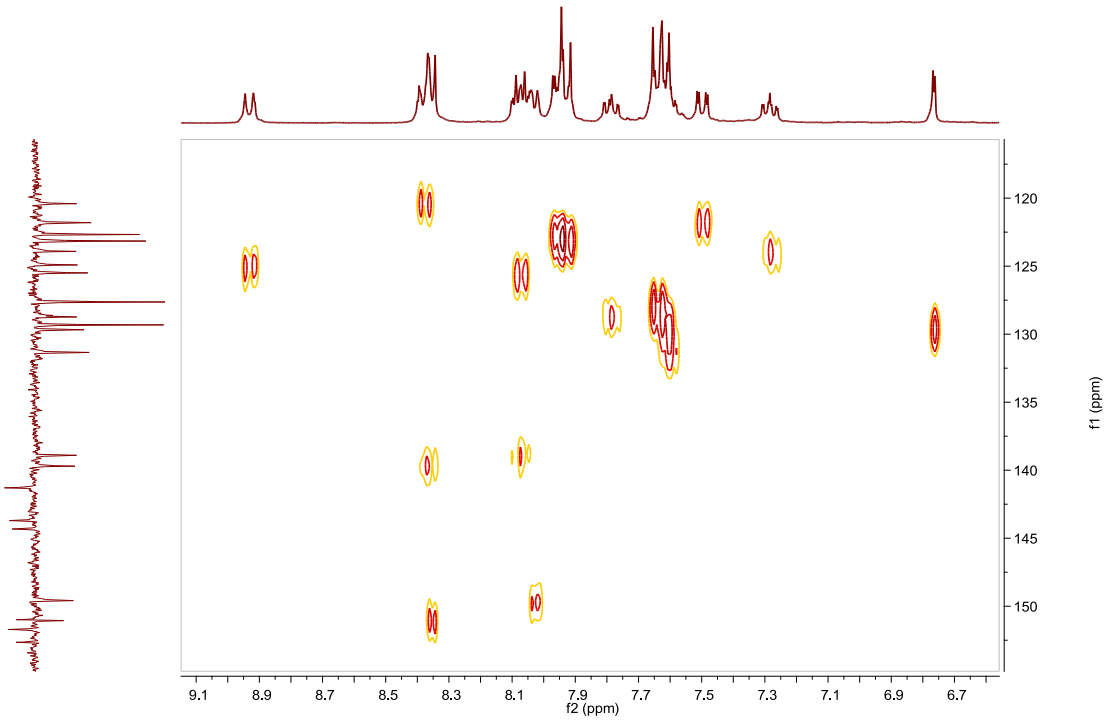

Fig. S117. HSQC NMR spectrum of **Dbipy** in acetone-d_6.

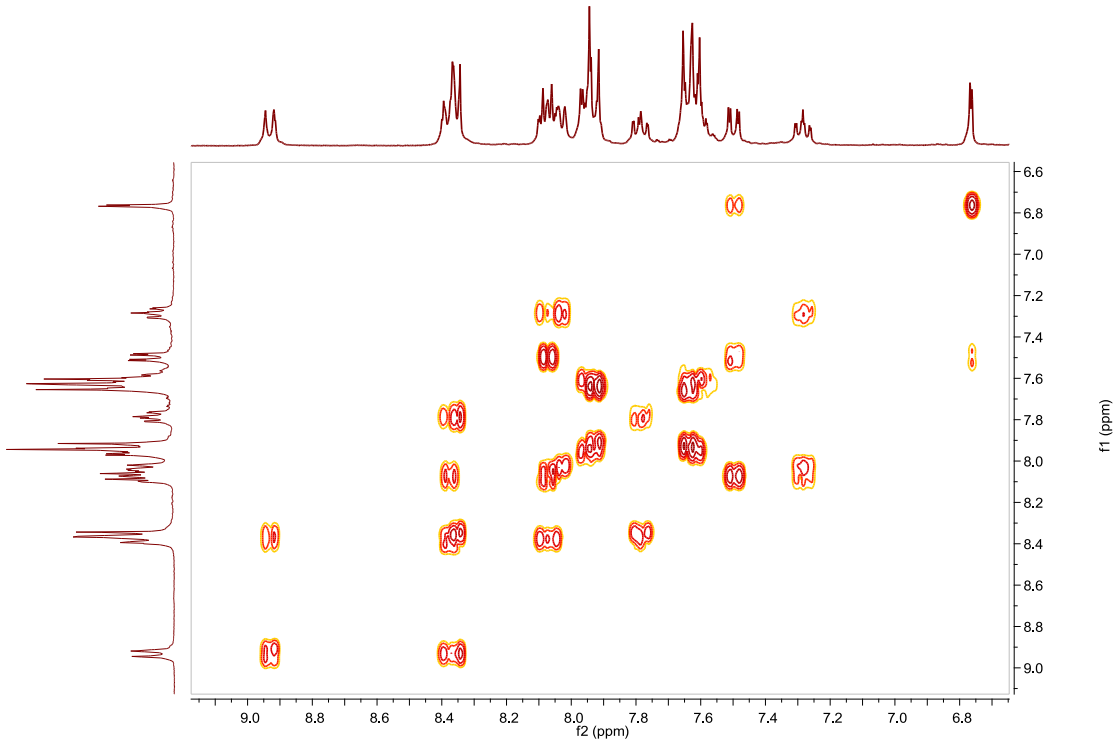

Fig. S118. COSY NMR spectrum of **Dbipy** in acetone-d_6.

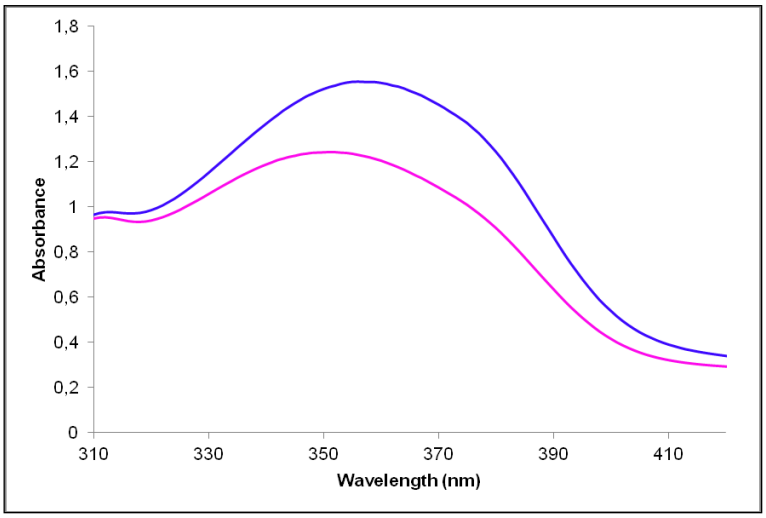

Fig. S119. UV/Vis spectra of **Dbipy** in CH_3CN. Before (blue line) and after (pink line) irradiation at 373nm, $2.09 \cdot 10^{-5}$M.

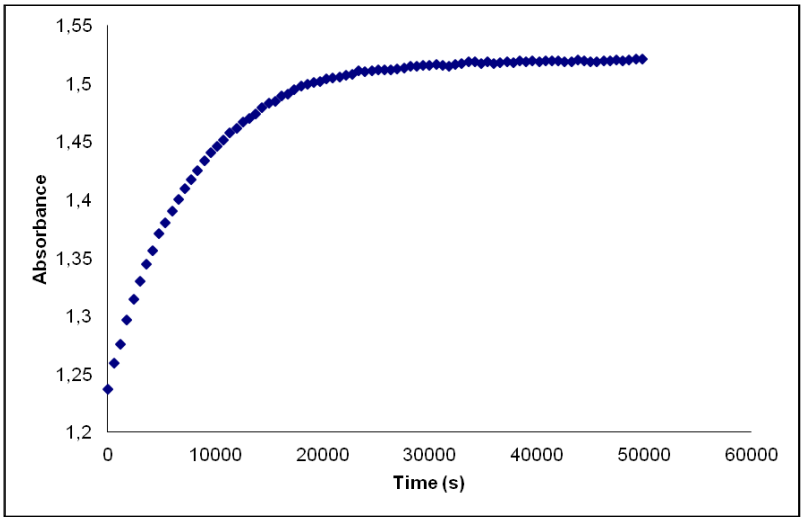

Fig. S120. Cis to trans thermal isomerization kinetics of **Dbipy**. Absorption change of the band 355nm at 328 K in CH_3CN after irradiation at 373 nm. ($2.09 \cdot 10^{-5}$M).

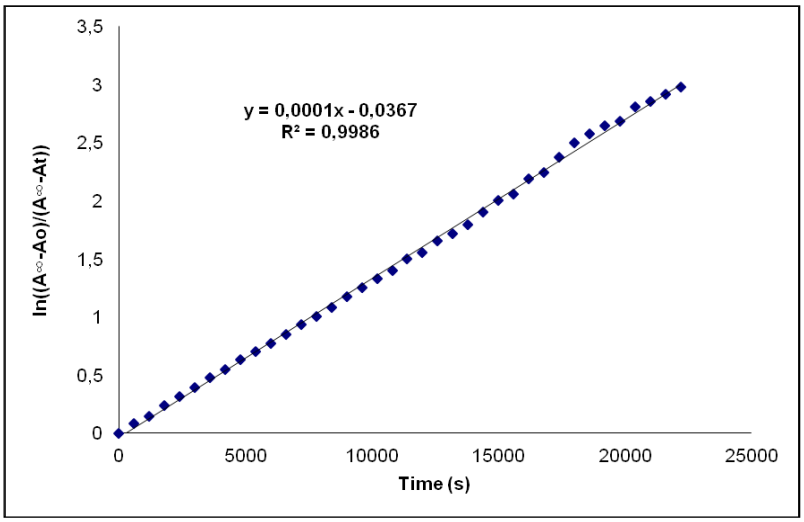

Fig. S121. Cis to trans thermal isomerization kinetics of **Dbipy**. First-order plot. k (s^{-1}) = $1.0 \cdot 10^{-4}$. Half-life (min) = 115.

Compound Aphen, $[Ir(ppy)_2(phen)]PF_6$. Synthesis and characterization.

SYNTHESIS

Under a N_2 atmosphere, $[Ir(ppy)_2Cl]_2$ (0.200 g, 0.186 mmol) were added over a suspension of 1,10-phenanthroline (0.140 g, 0.777 mmol) in 15 mL CH_2Cl_2–MeOH 2/1. The reaction mixture was refluxed, under N_2, for 15 h. To the resulting orange solution, 0.07 g of KPF_6 were added and the it was stirred for an 1 h. The solvent was evaporated and the desired compound was obtained after filtration through a celite path in CH_2Cl_2 as a yellow solid. Yield 57%. The spectroscopic data are coincident with those described in the literature.[37]

^{1}H NMR (500 MHz, DMSO-d_6): δ 8.91 (dd, , J = 1.1 Hz, J = 8.3 Hz, 1H), 8.40 (s, 1H), 8.27 (d, J = 8.2 Hz, 1H), 8.22 (dd, J = 1.0 Hz, J = 5.1 Hz, 1H), 8.06 (dd, J = 5.1 Hz, J = 8.2 Hz, 1H), 7.96 (d, J = 7.6 Hz, 1H), 7.88 (t, J = 8.1 Hz, 1H), 7.47 (d, J = 5.6 Hz, 1H), 7.07 (t, J = 7.3 Hz, 1H), 6.99 (t, J = 6.2 Hz, 1H), 6.96 (t, J = 6.6 Hz, 1H), 6.31 (d, J = 7.4 Hz, 1H).

^{13}C NMR (126 MHz, DMSO-d_6): δ 167.40 (C_{quat}), 151.18 (CH), 150.37 (C_{quat}), 149.64 (CH), 146.64 (C_{quat}), 144.59 (C_{quat}), 139.36 (CH), 139.23 (CH), 131.80 (CH), 131.69 (C_{quat}), 130.74 (CH), 128.89 (CH), 127.67 (CH), 125.59 (CH), 124.39 (CH), 122.91 (CH), 120.50 (CH).

UV/Vis (CH_3CN), λ, nm (ε, 10^4 M^{-1} cm^{-1}): 229 (4.8), 253 (4.9), 265 (5.3), 376 (0.64).

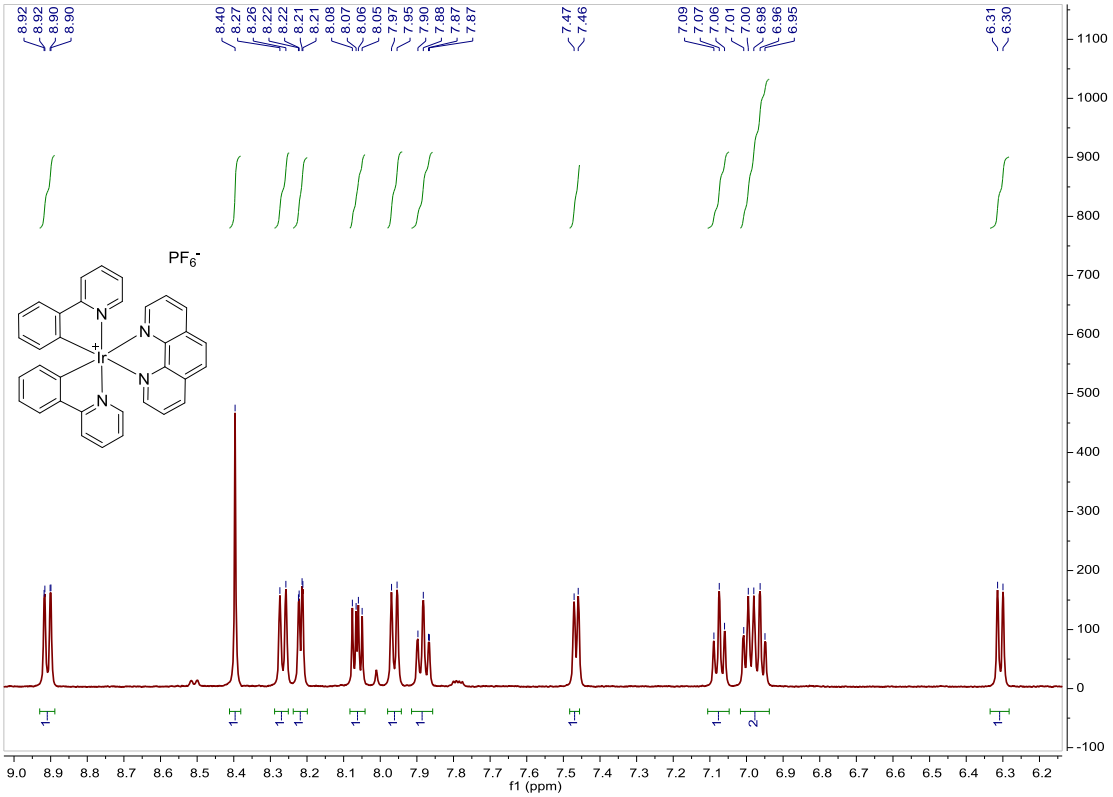

Fig. S122. ^{1}H NMR spectrum of **Aphen** in DMSO-d_6, 500 MHz.

[37] J. I. Kim, I. Shin, H. Kim and J. Lee, *J. Am. Chem. Soc.*, **2005**, *127*, 1614–1615.

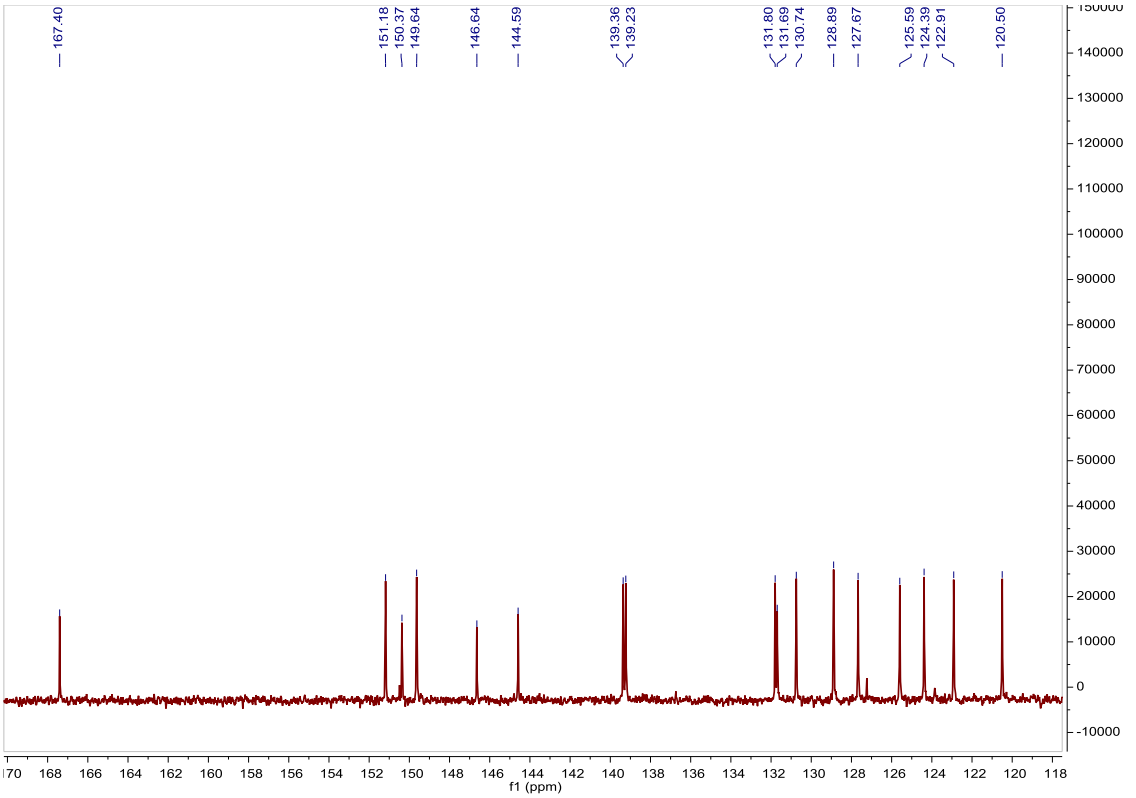

Fig. S123. ^{13}C NMR spectrum of **Aphen** in DMSO-d_6, 126 MHz.

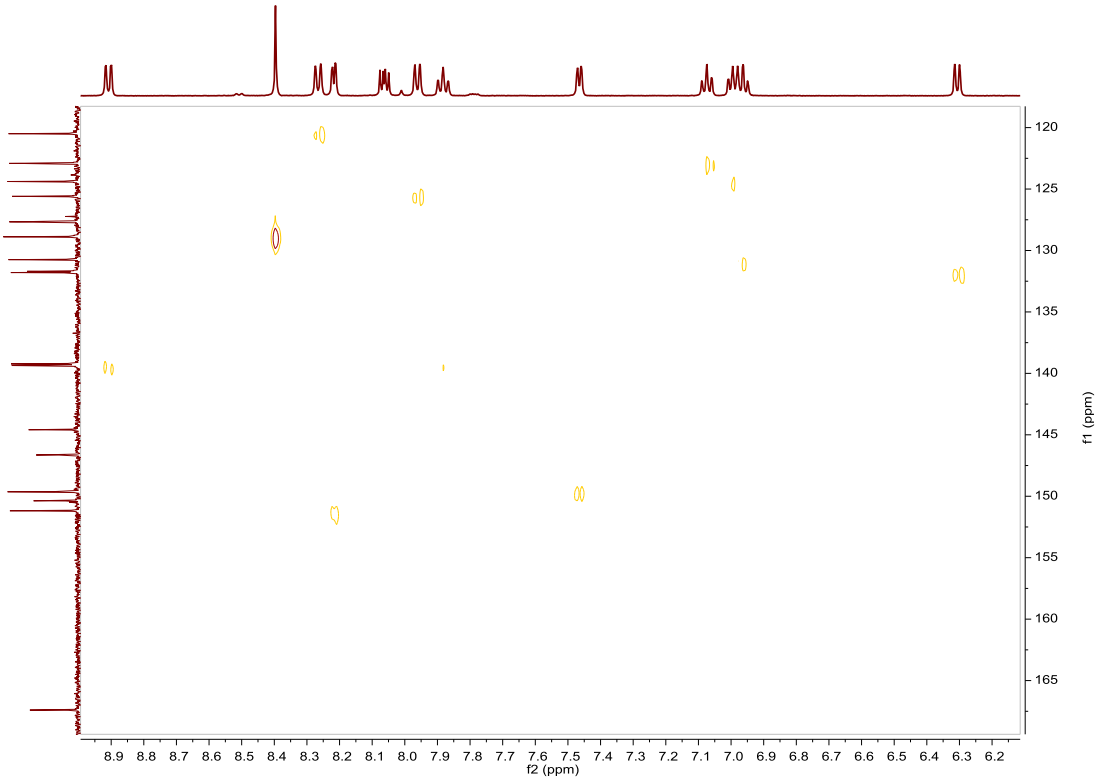

Fig. S124. HSQC NMR spectrum of **Aphen** in DMSO-d_6.

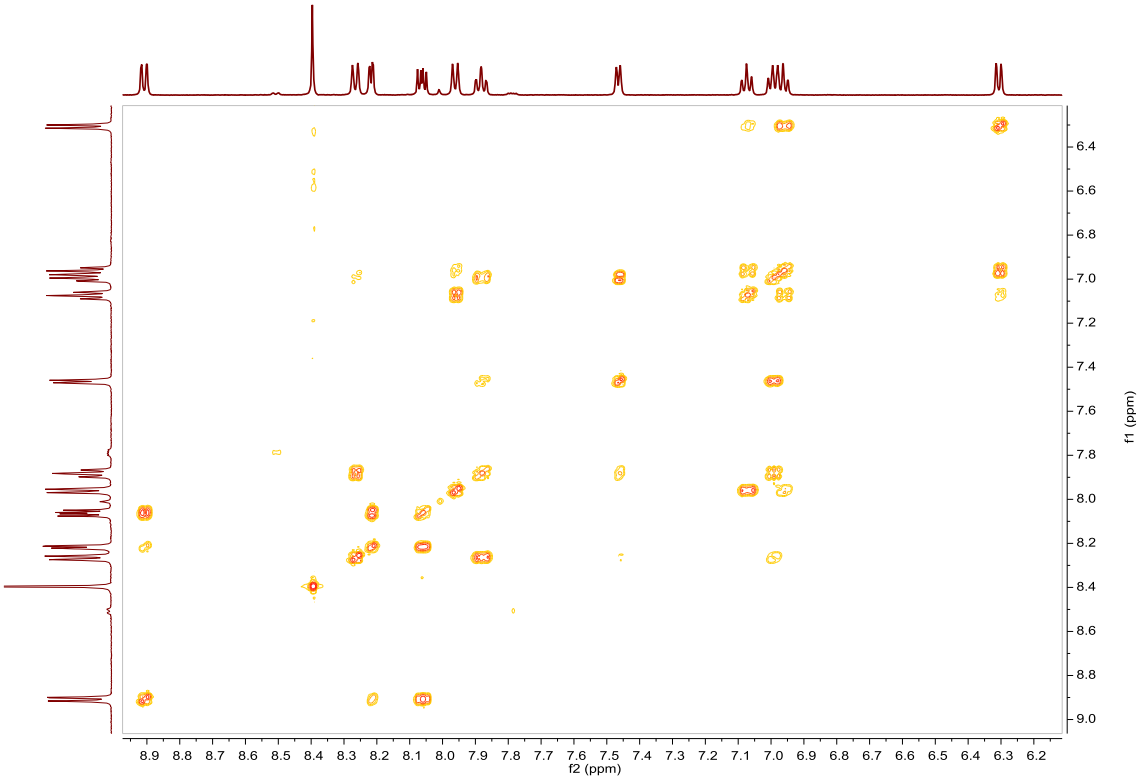

Fig. S125. COSY NMR spectrum of **Aphen** in DMSO-d_6.

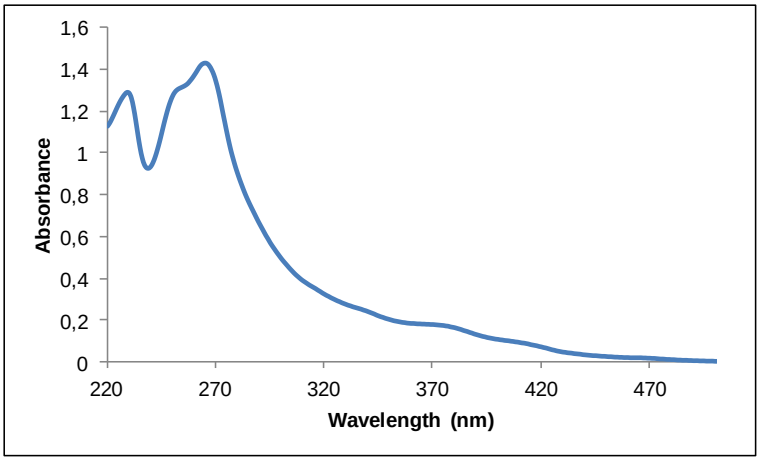

Fig. S126. UV/Vis spectra of **Aphen** in CH_3CN, $2.67 \cdot 10^{-5}$M.

Compound Bphen, [Ir(Fppy)$_2$(phen)]PF$_6$. Synthesis and characterization.

SYNTHESIS

Under a N_2 atmosphere, $[Ir(Fppy)_2Cl]_2$ (0.231 g, 0.190 mmol) were added over a suspension of 1,10-phenanthroline (0.057 g, 0.32 mmol) in 15 mL CH_2Cl_2–MeOH 2/1. The reaction mixture was refluxed, under N_2, for 15 h. To the resulting yellow solution, 0.07 g of KPF_6 were added and the it was stirred for an 1 h. The solvent was evaporated and the desired compound was obtained after filtration through a celite path in CH_2Cl_2 as a yellow solid. Yield 90%. The spectroscopic data are coincident with those described in the literature.[38]

^{1}H NMR (500 MHz, DMSO-*d*$_6$): δ 8.94 (dd, J = 1.1 Hz, *J* = 8.2 Hz, 1H), 8.41 (s, 1H), 8.29 (t, *J* = 10.5 Hz, 2H), 8.06 (dd, J = 5.1 Hz, *J* = 8.2 Hz, 1H), 7.96 (t, *J* = 8.05 Hz, 1H), 7.52 (d, *J* = 5.1 Hz, 1H), 7.06 (t, *J* = 6.15 Hz, 1H), 7.01 (t, J = 10.5 Hz, 1H), 5.71 (dd, J = 2.2 Hz, *J* = 8.3 Hz, 1H).

^{13}C NMR (126 MHz, DMSO-*d*$_6$): δ 162.78 (dd, *J* = 12.5 Hz, J = 252.5 Hz, C_{quat}), 162.77 (d, *J* = 7.5 Hz, C_{quat}), 160.68 (dd, J = 12.5 Hz, J = 257.5 Hz, C_{quat}), 153.90 (d, J = 6.25 Hz, C_{quat}), 151.21 (s, CH), 149.80 (s, CH), 145.73 (s, C_{quat}), 139.91 (s, CH), 139.32 (s, CH), 131.25 (s, C_{quat}), 128.40 (s, CH), 127.83 (s, C_{quat}), 127.44 (s, CH), 124.45 (s, CH), 123.27 (d, J = 20.0 Hz, CH), 113.42 (d, J = 16.25 Hz, CH), 99.11 (t, J = 26.25 Hz, CH).

UV/Vis (CH_3CN), λ, nm (ε, 10^4 M^{-1} cm^{-1}): 230 (5.0), 264 (4.8), 310 (1.6), 359 (0.71).

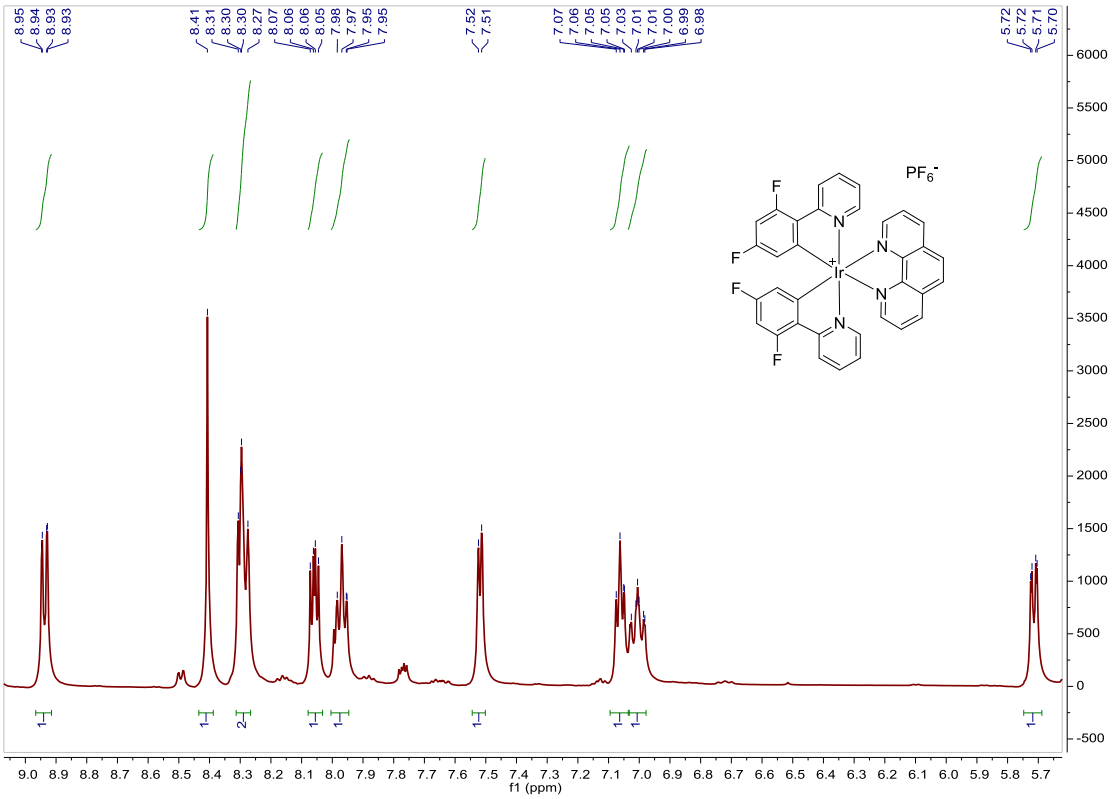

Fig. S127. ^{1}H NMR spectrum of **Bphen** in DMSO-*d*$_6$, 500 MHz.

[38] Y. You, S. Lee, T. Kim, K. Ohkubo, W. Chae, S. Fukuzumi, G. Jhon, W. Nam, S. J. Lippard, *J. Am. Chem. Soc.*, **2011**, *133*, 18328–18342.

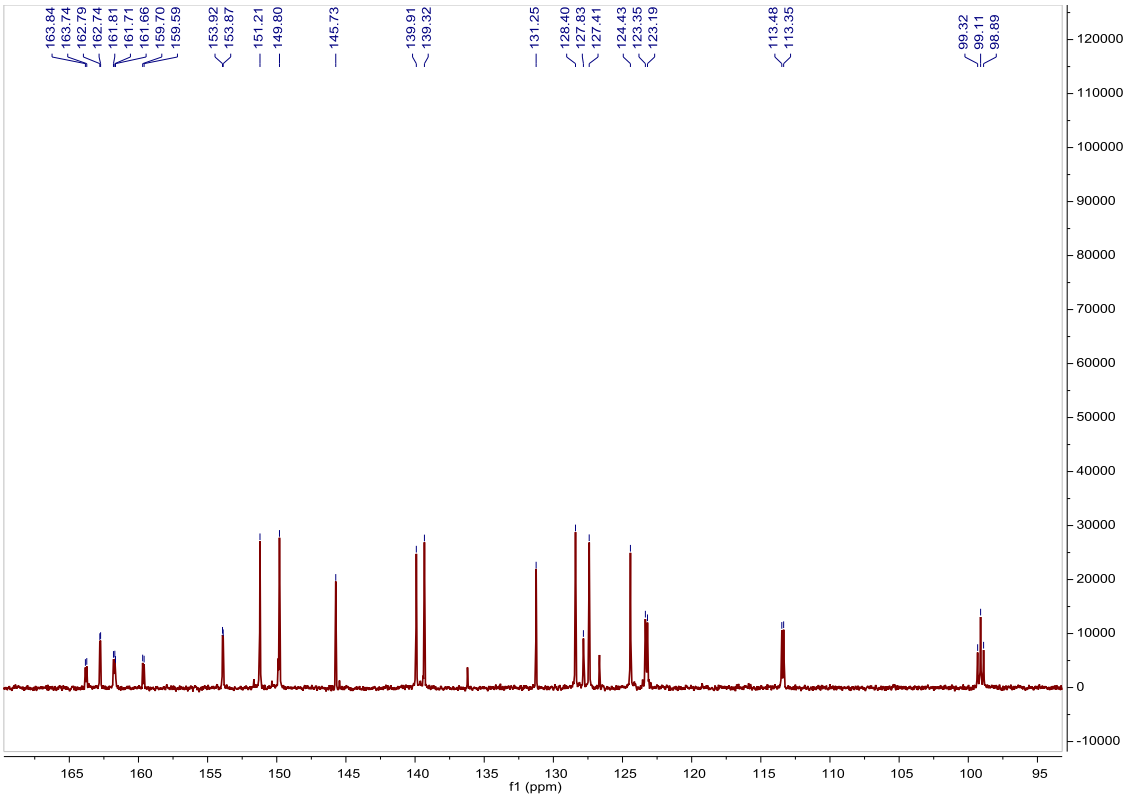

Fig. S128. ^{13}C NMR spectrum of **Bphen** in DMSO-d_6, 126 MHz.

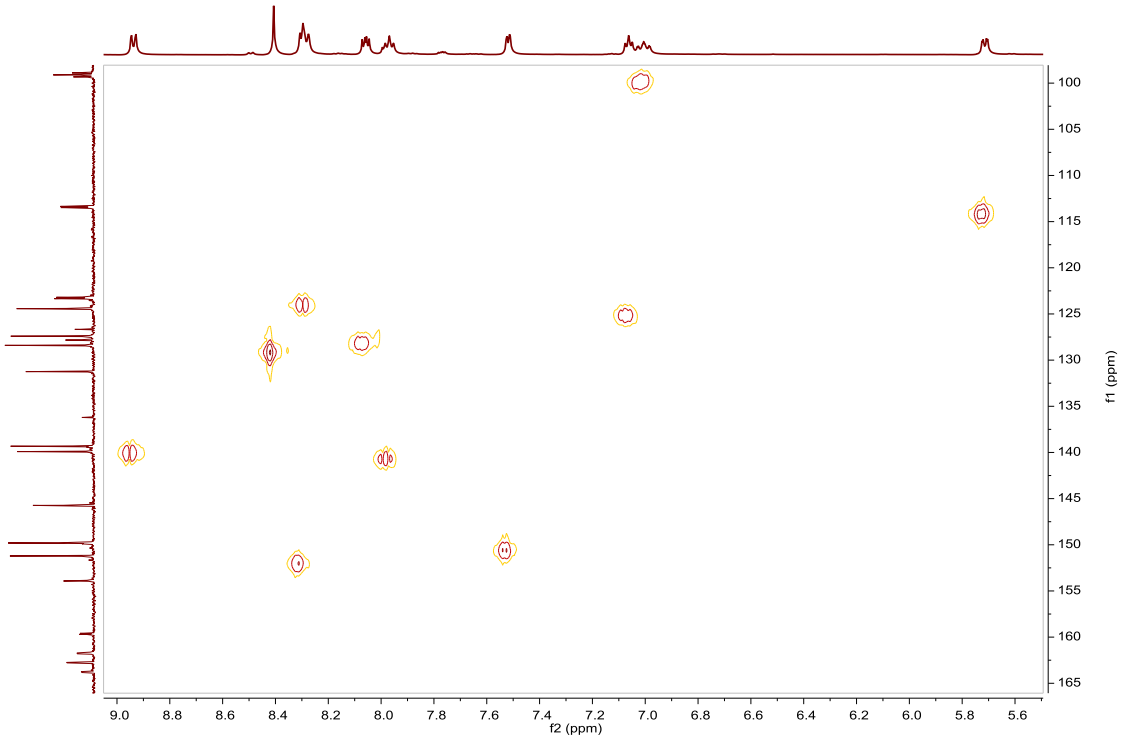

Fig. S129. HSQC NMR spectrum of **Bphen** in DMSO-d_6.

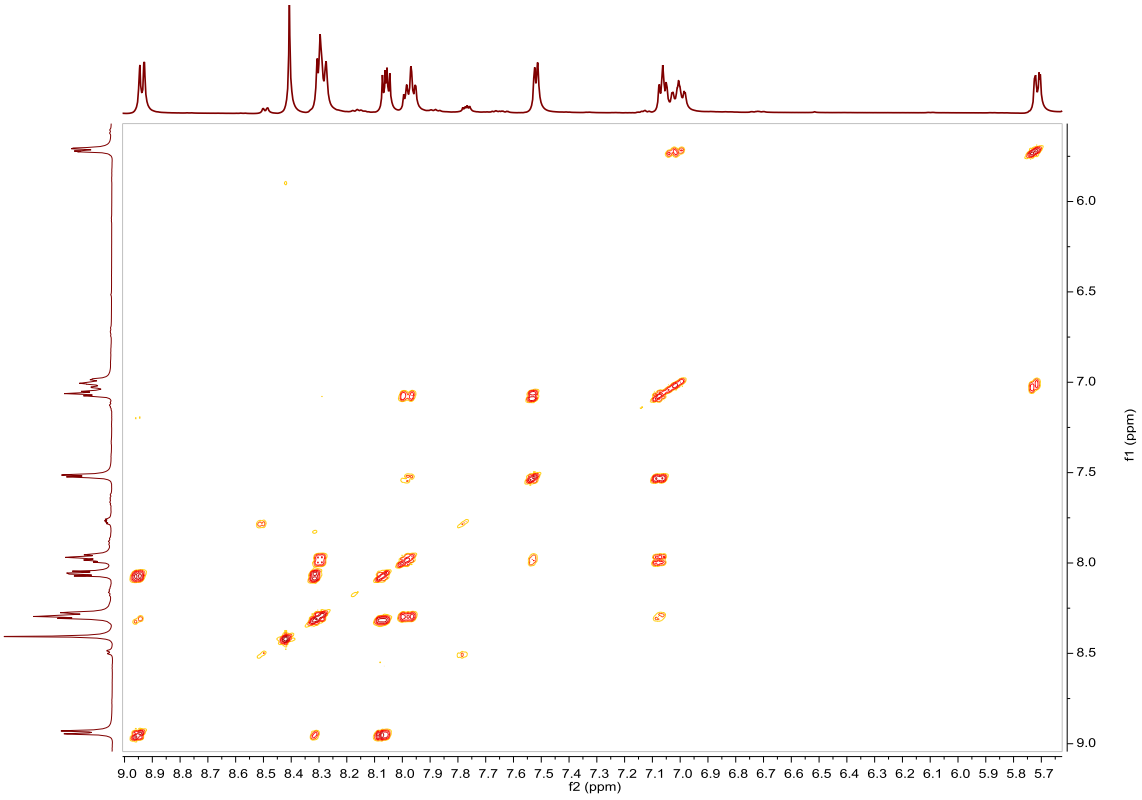

Fig. S130. COSY NMR spectrum of **Bphen** in DMSO-d_6.

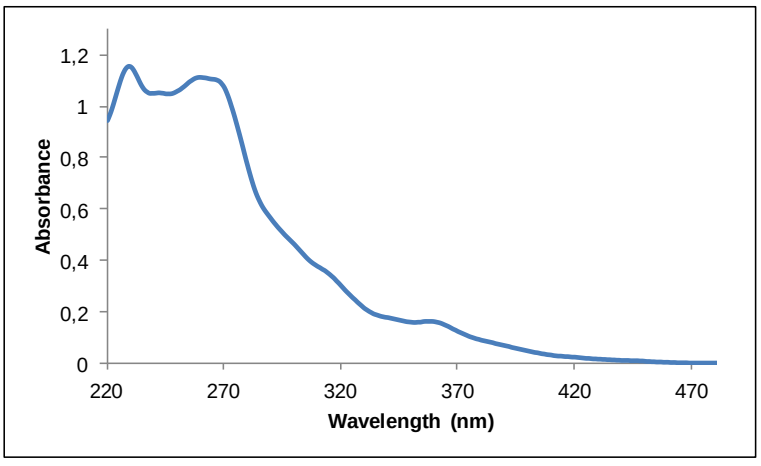

Fig. S131. UV/Vis spectra of **Bphen** in CH_3CN, $2.31 \cdot 10^{-5}$M.

Compound Cphen, $[Ir(Brppy)_2(phen)]PF_6$. Synthesis and characterization.

SYNTHESIS

Under a N_2 atmosphere, $[Ir(Brppy)_2Cl]_2$ (0.100 g, 0.072 mmol) were added over a suspension of 1,10-phenanthroline (0.026 g, 0.144 mmol) in 8 mL CH_2Cl_2–MeOH 2/1. The reaction mixture was refluxed, under N_2, for 15 h. After solvent evaporation the product was purified by column chromatography (silica gel, CH_2Cl_2). When the unreacted $[Ir(ppy\text{-}Br)_2Cl]_2$ eluted, 0.05 g of KPF_6 were added on top of the column and the polarity of the eluent was gradually increased to 100% acetone to elute $[Ir(Brppy)_2(phen)]PF_6$ together with the excess of KPF_6. The desired compound, purified by filtration through a celite path in CH_2Cl_2, was obtained as a yellow solid. Yield 63%.

Elemental Analysis: calculated for $(C_{34}H_{22}Br_2IrN_4PF_6{\cdot}2CH_3COCH_3)$: C, 43.69; H, 3.12; N, 5.09. Found: C, 43.89; H, 3.42; N, 5.01.

Exact Mass: ESI-MS $[C_{34}H_{22}Br_2IrN_4]^+$: calculated: m/z= 836.9840, found: m/z= 836.9802.

^{1}H NMR (300 MHz, acetone-d_6): δ 8.96 (dd, J = 1.4 Hz, J = 8.3 Hz, 1H), 8.56 (dd, J = 1.4 Hz, J = 5.0 Hz, 1H), 8.45 (s, 1H), 8.31 (d, J = 7.9 Hz, 1H), 8.13 (dd, J = 5.1 Hz, J = 8.3 Hz, 1H), 7.97 (ddd, J = 1.5 Hz, J = 7.5 Hz, J = 9.0 Hz, 1H), 7.95 (d, J = 8.4 Hz, 1H), 7.73 (d, J = 5.8 Hz, 1H), 7.33 (dd, J = 2.0 Hz, J = 8.3 Hz, 1H), 7.07 (ddd, J = 1.4 Hz, J = 5.8 Hz, J = 7.3 Hz, 1H), 6.54 (d, J = 1.9 Hz, 1H).

^{13}C APT NMR (75 MHz, acetone-d_6): δ 167.83 (C_{quat}), 153.26 (C_{quat}), 152.92 (CH), 150.95 (CH), 148.10 (C_{quat}), 144.94 (C_{quat}), 140.44 (2CH), 135.27 (CH), 133.14 (C_{quat}), 129.85 (CH), 128.63 (CH), 128.05 (CH), 127.20 (CH), 126.18 (C_{quat}), 125.47 (CH), 121.76 (CH).

UV/Vis (CH_3CN), λ, nm (ε, 10^4 M^{-1} cm^{-1}): 228 (4.8), 268 (5.5), 356 (0.81), 395 (0.46).

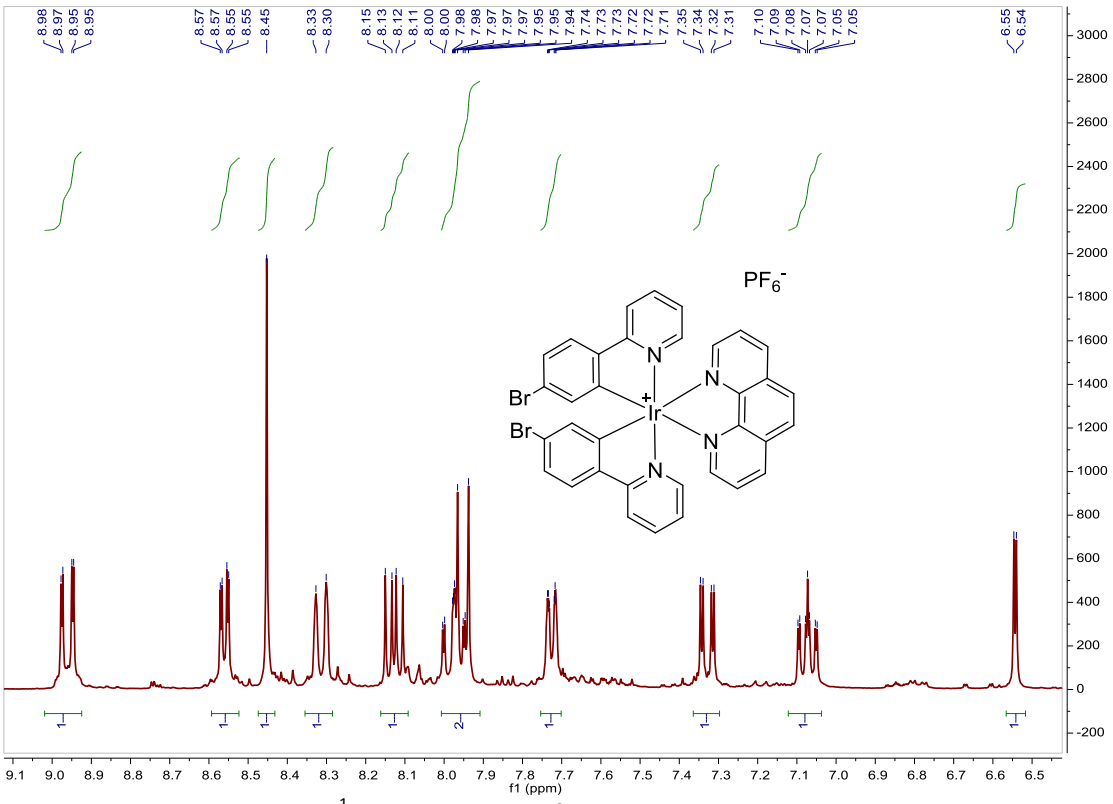

Fig. S132. ^{1}H NMR spectrum of **Cphen** in acetone-d_6, 300 MHz.

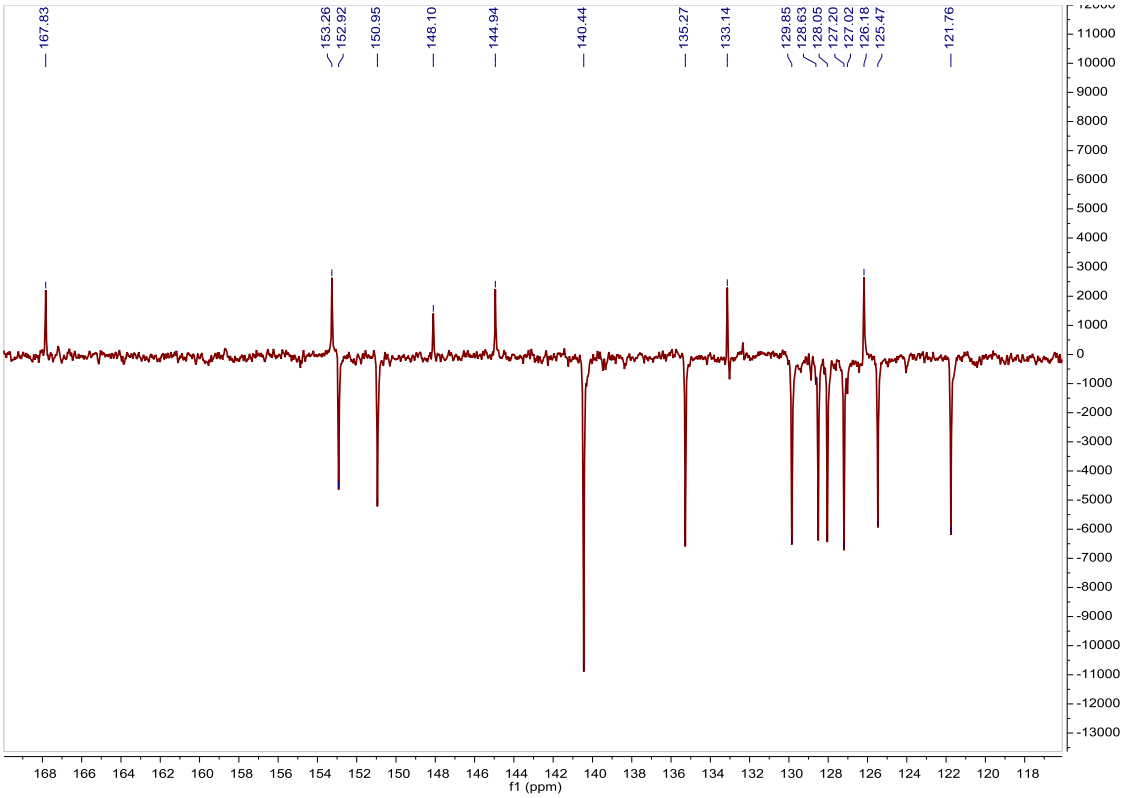

Fig. S133. ^{13}C APT NMR spectrum of **Cphen** in acetone-d_6, 75 MHz.

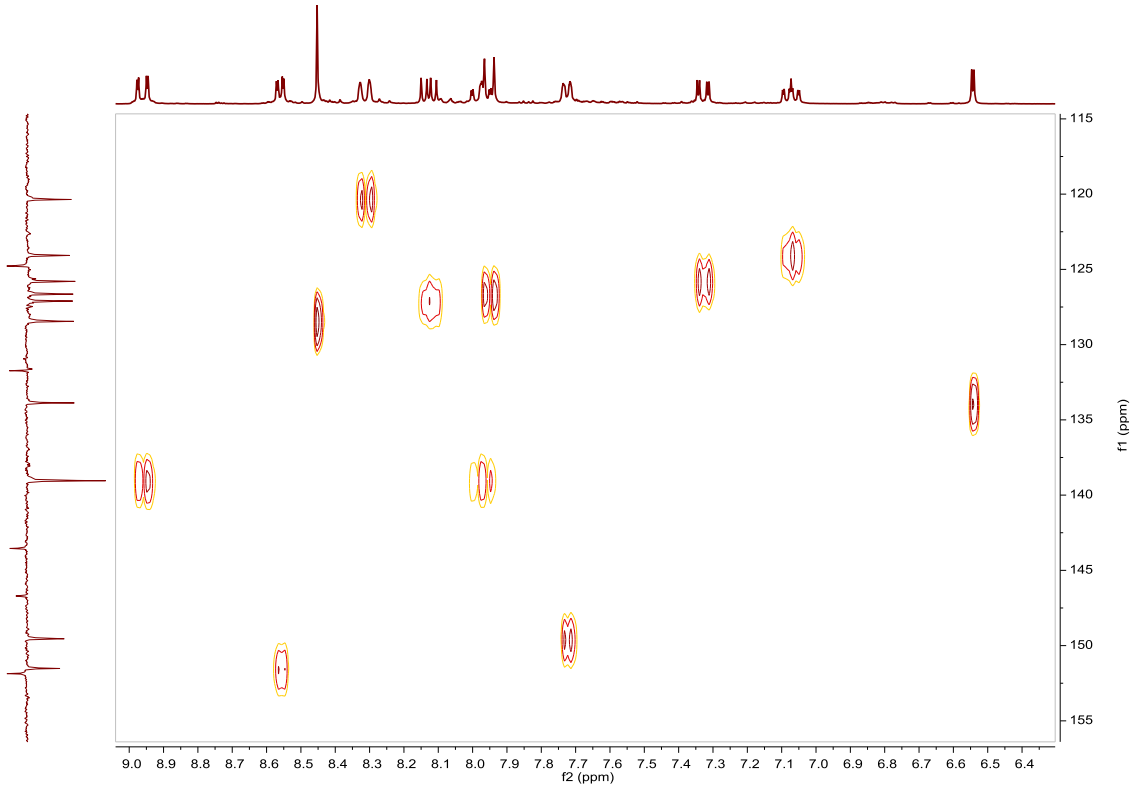

Fig. S134. HSQC NMR spectrum of **Cphen** in acetone-d_6.

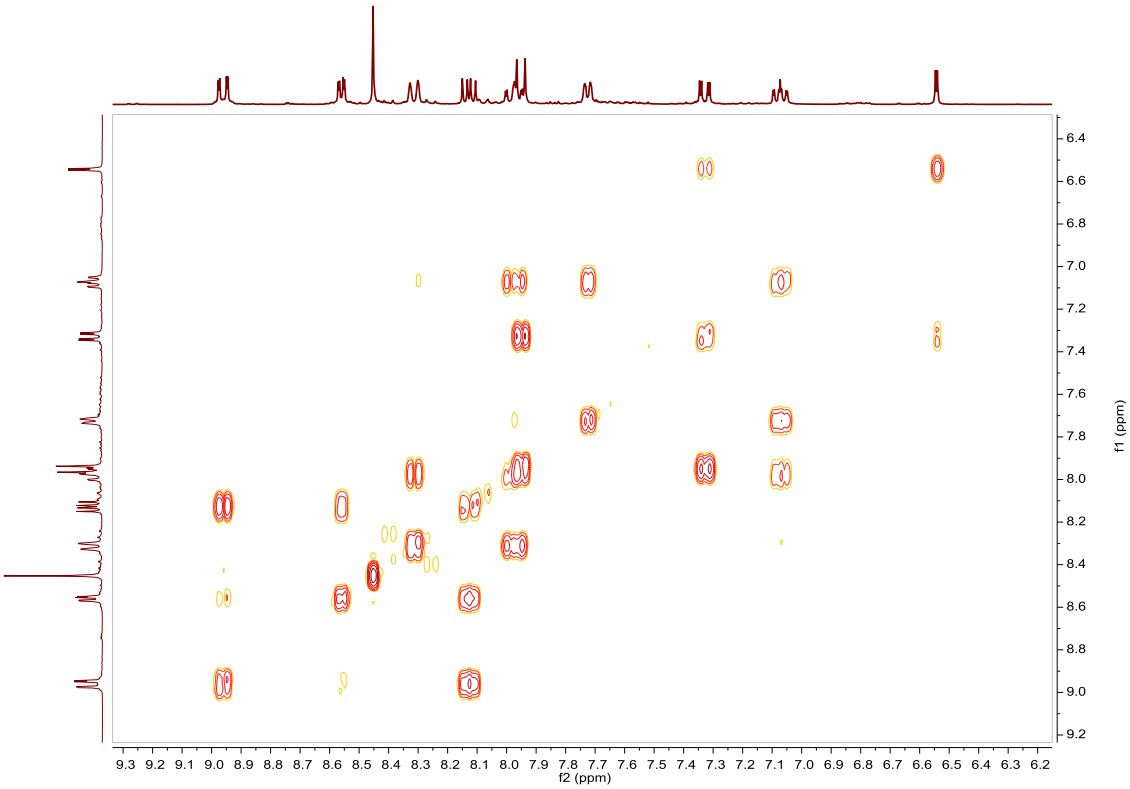

Fig. S135. COSY NMR spectrum of **Cphen** in acetone-d_6.

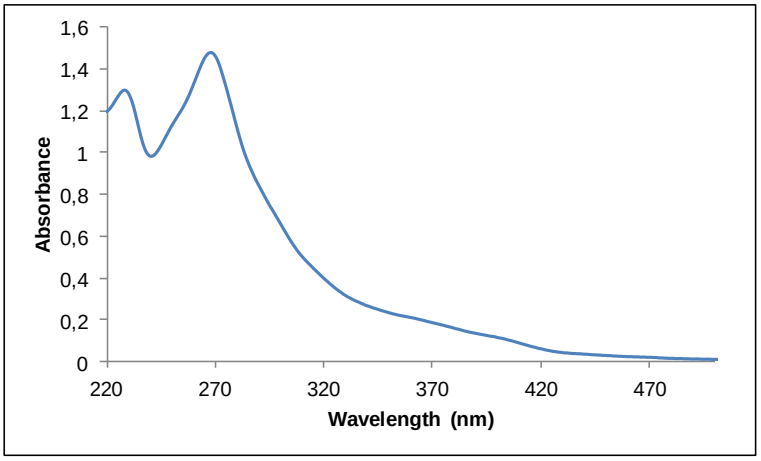

Fig. S136. UV/Vis spectra of **Cphen** in CH_3CN, $2.70 \cdot 10^{-5}$M.

Compound Dphen, [Ir(azoppy)$_2$(phen)]PF$_6$. Synthesis, characterization and photoisomerization studies.

SYNTHESIS

Under a N_2 atmosphere, **Cphen** (0.1 g, 0.102 mmol) and [4-(phenylazo)phenyl]boronic acid **6** (0.056 g, 0.247 mmol) were dissolved in 4 mL of THF. Na_2CO_3 (1M (aq), 2 mL) and $Pd(PPh_3)_4$ (0.012 g, 0.010 mmol) were added and the solution was degassed by bubbling N_2 for 15 min. The reaction mixture was refluxed (80 °C) for 15 h. The resulting mixture was cooled down to room temperature and the product was extracted with CH_2Cl_2. The organic phase was dried with $MgSO_4$, filtered off and the solvent was evaporated. The residue was purified by column chromatography (silica gel, CH_2Cl_2). To the fraction containing the eluted complex, 0.05 g of KPF_6 were added and the resulting solution was filtered through a celite path. The title compound was obtained as an orange solid. Yield 50%.

Elemental Analysis: calculated for ($C_{58}H_{40}IrN_8PF_6$): C, 58.73; H, 3.40; N, 9.45. Found: C, 58.69; H, 3.07; N, 9.35.

Exact Mass: ESI-MS $[C_{58}H_{40}IrN_8]^+$: calculated: m/z= 1041.3005, found: m/z= 1041.3031.

^{1}H NMR (300 MHz, acetone-*d*$_6$): δ 8.97 (dd, J = 1.4 Hz, J = 8.3 Hz, 1H), 8.69 (dd, J = 1.4 Hz, J = 5.0 Hz, 1H), 8.47 (s, 1H), 8.36 (d, J = 8.0 Hz, 1H), 8.17–8.08 (m, 2H), 8.04–7.91 (m, 5H), 7.87 (d, J = 5.8 Hz, 1H), 7.67 (brd, J = 8.6 Hz, 2H), 7.64–7.57 (m, 3H), 7.53 (dd, J = 1.9 Hz, J = 8.1 Hz, 1H), 7.11 (ddd, J = 1.3 Hz, J = 5.9 Hz, J = 7.3 Hz, 1H), 6.87 (d, J = 1.8 Hz, 1H).

^{13}C APT NMR (75 MHz, acetone-*d*$_6$): δ 168.65 (C_{quat}), 157.33 (C_{quat}), 153.94 (C_{quat}), 153.02 (CH), 151.77 (C_{quat}), 151.06 (CH), 148.32 (C_{quat}), 145.87 (C_{quat}), 145.06 (C_{quat}), 142.56 (C_{quat}), 140.15 (CH), 140.10 (CH), 133.10 (C_{quat}), 132.63 (CH), 131.17 (CH), 130.61 (2CH), 129.82 (CH), 128.95 (2CH), 128.44 (CH), 126.76 (CH), 125.07 (CH), 124.46 (2CH), 123.97 (2CH), 123.16 (CH), 121.61 (CH).

UV/Vis (CH_3CN), λ, nm (ε, 10^4 M^{-1} cm^{-1}): 355 (6.9).

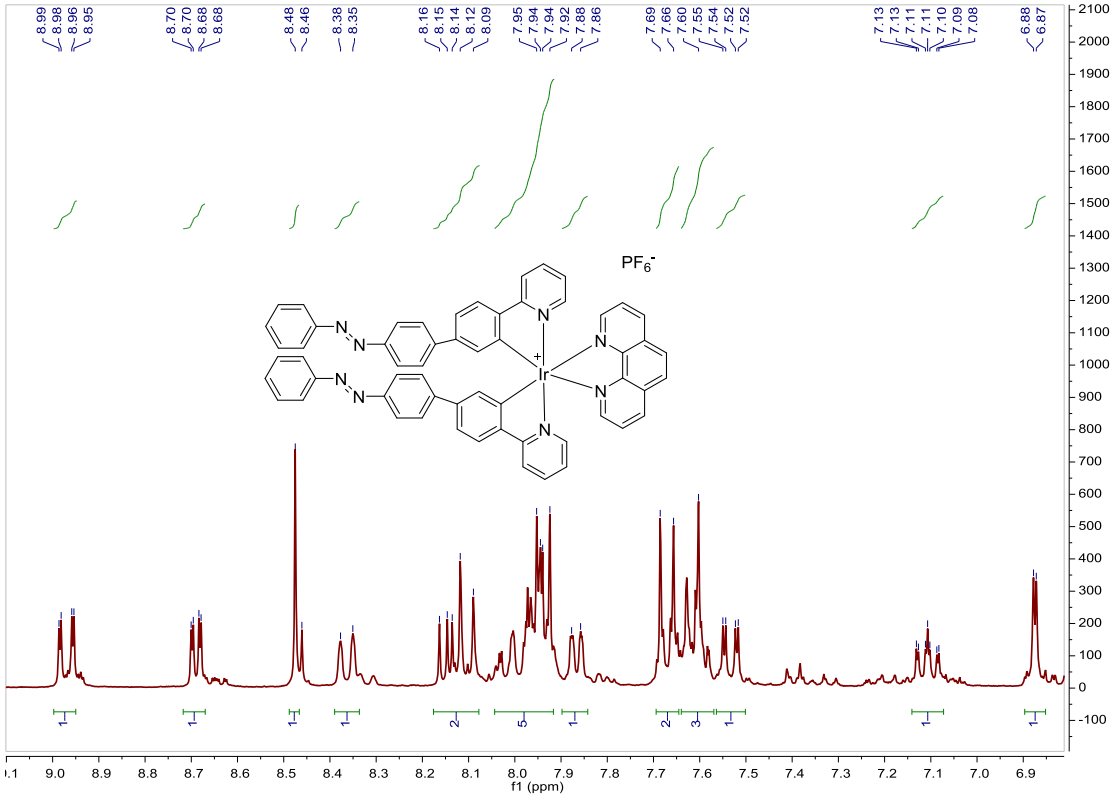

Fig. S137. ^{1}H NMR spectrum of **Dphen** in acetone-*d*$_6$, 300 MHz.

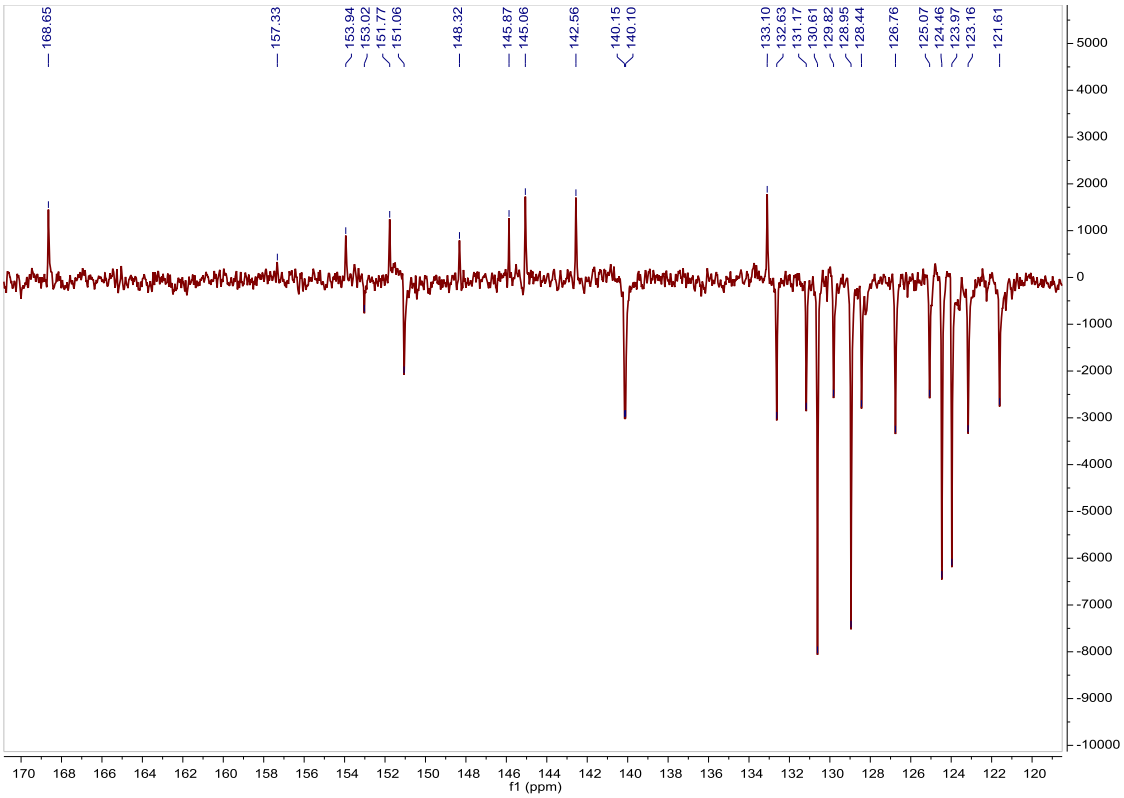

Fig. S138. ^{13}C APT NMR spectrum of **Dphen** in acetone-d_6, 75 MHz.

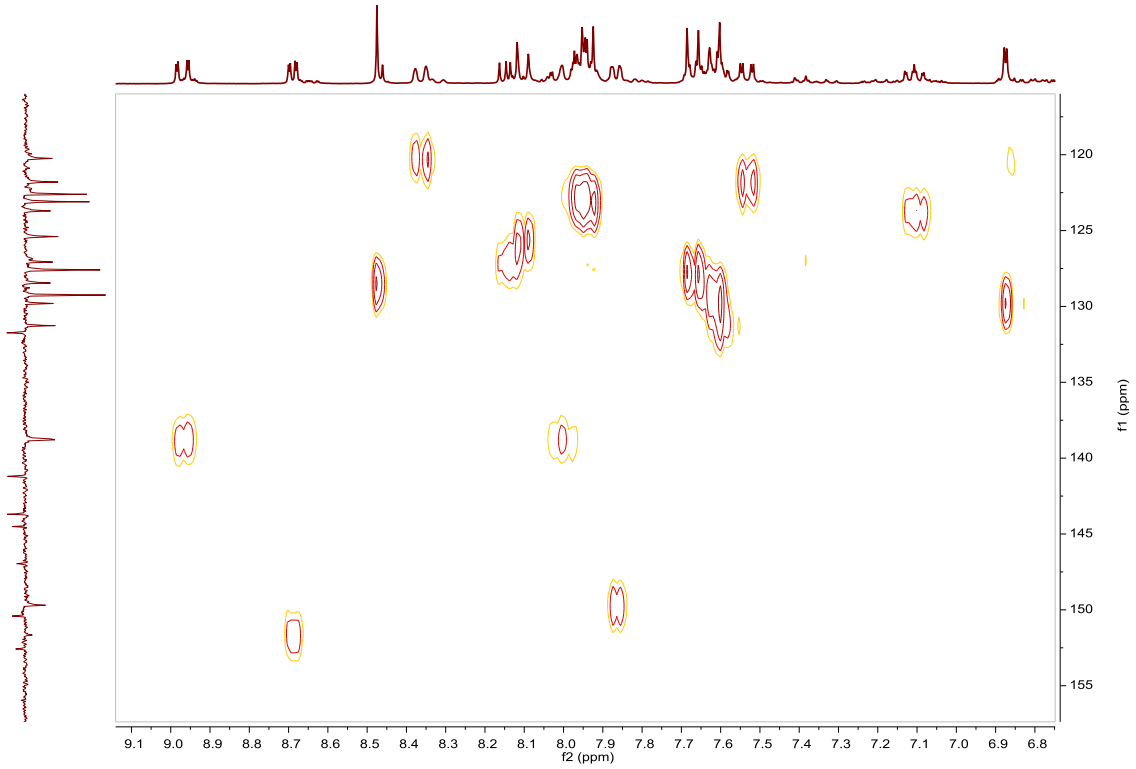

Fig. S139. HSQC NMR spectrum of **Dphen** in acetone-d_6.

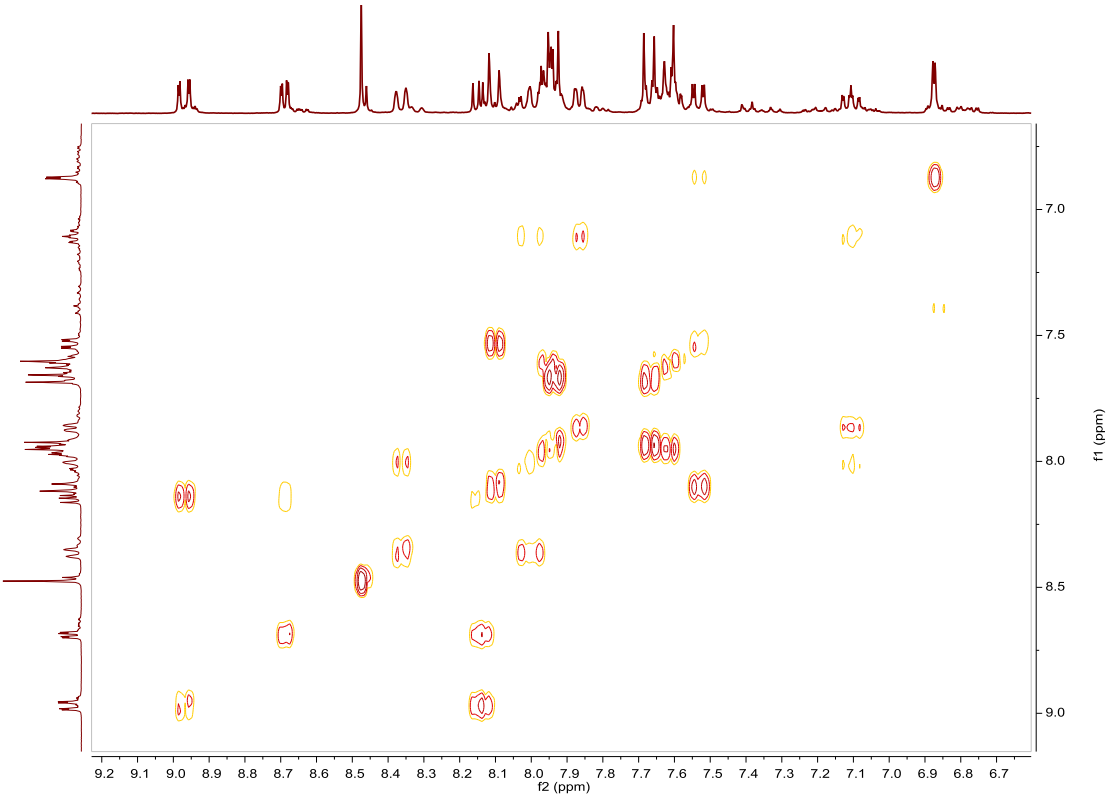

Fig. S140. COSY NMR spectrum of **Dphen** in acetone-d_6.

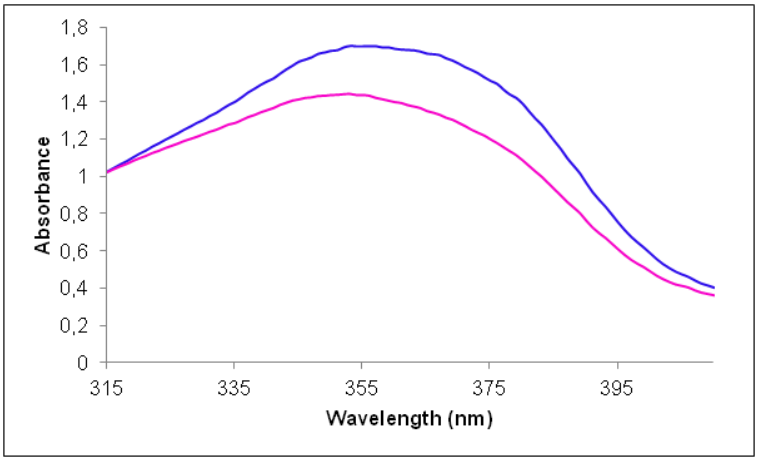

Fig. S141. UV/Vis spectra of **Dphen** in CH_3CN. Before (blue line) and after (pink line) irradiation at 362nm, $2.47 \cdot 10^{-5}$M.

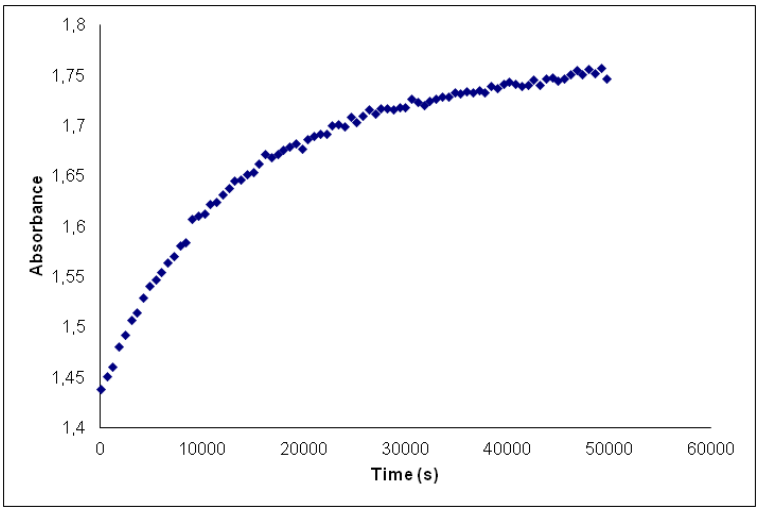

Fig. S142. Cis to trans thermal isomerization kinetics of **Dphen**. Absorption change of the band 355nm at 328 K in CH_3CN after irradiation at 362 nm. ($2.47 \cdot 10^{-5}$M).

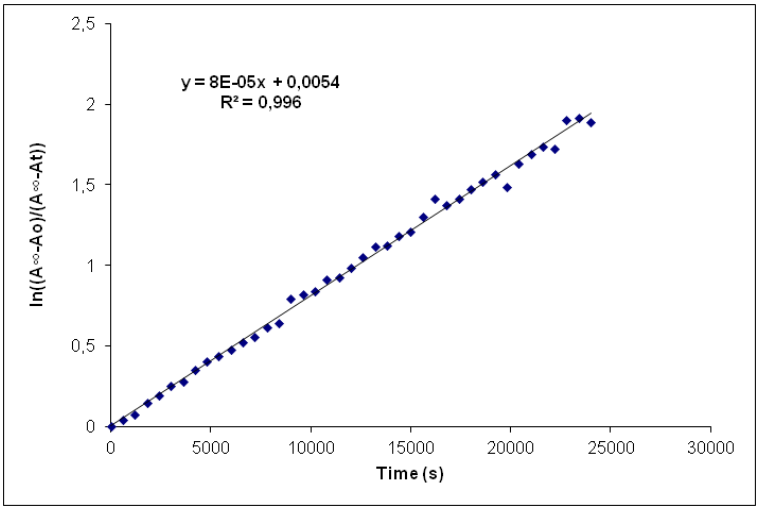

Fig. S143. Cis to trans thermal isomerization kinetics of **Dphen**. First-order plot. k (s^{-1}) = $8.0 \cdot 10^{-5}$. Half-life (min) = 144.

Compound Abipy-dibr, $[Ir(ppy)_2(bipy\text{-}dibr)]PF_6$. Synthesis and characterization.

SYNTHESIS

Under a N_2 atmosphere, $[Ir(ppy)_2Cl]_2$ (0.100 g, 0.093 mmol) were added over a suspension of 4,4'-dibromo-2,2'-bipyridine (0.060 g, 0.186 mmol) in 8 mL CH_2Cl_2–MeOH 2/1. The reaction mixture was refluxed, under N_2, for 15 h. To the resulting solution, 0.035 g of KPF_6 were added and the solution was stirred for an 1 h. The solvent was evaporated and the reaction mixture was filtrated through a celite path in CH_2Cl_2. The product was obtained after purified by column chromatography (silica gel, CH_2Cl_2 as eluent) as an orange solid. Yield 81%.

Elemental Analysis: calculated for ($C_{32}H_{22}Br_2IrN_4PF_6$): C, 40.06; H, 2.31; N, 5.84. Found: C, 39.61; H, 2.61; N, 5.55.

Exact Mass: ESI-MS $[C_{32}H_{22}Br_2IrN_4]^+$: calculated: m/z= 812.9840, found: m/z= 812.9817.

^{1}H NMR (500 MHz, acetone-d_6): δ 9.23 (s, 1H), 8.26 (d, J = 8.1 Hz, 1H), 8.03–7.95 (m, 3H), 7.91 (d, J = 7.5 Hz, 1H), 7.18 (t, J = 6.3 Hz, 1H), 7.06 (t, J = 7.3 Hz, 1H), 6.93 (t, J = 7.0 Hz, 1H), 6.34 (d, J = 7.1 Hz, 1H).

^{13}C NMR (126 MHz, acetone-d_6): δ 167.63 (C_{quat}), 156.45 (C_{quat}), 151.40 (CH), 149.66 (CH), 149.57 (C_{quat}), 144.08 (C_{quat}), 138.88 (CH), 135.88 (C_{quat}), 132.30 (CH), 131.60 (CH), 130.49 (CH), 128.93 (CH), 125.05 (CH), 123.75 (CH), 122.77 (CH), 120.03 (CH).

UV/Vis (CH_3CN), λ, nm (ε, 10^4 M^{-1} cm^{-1}): 253 (4.7), 312 (1.9), 377 (0.75).

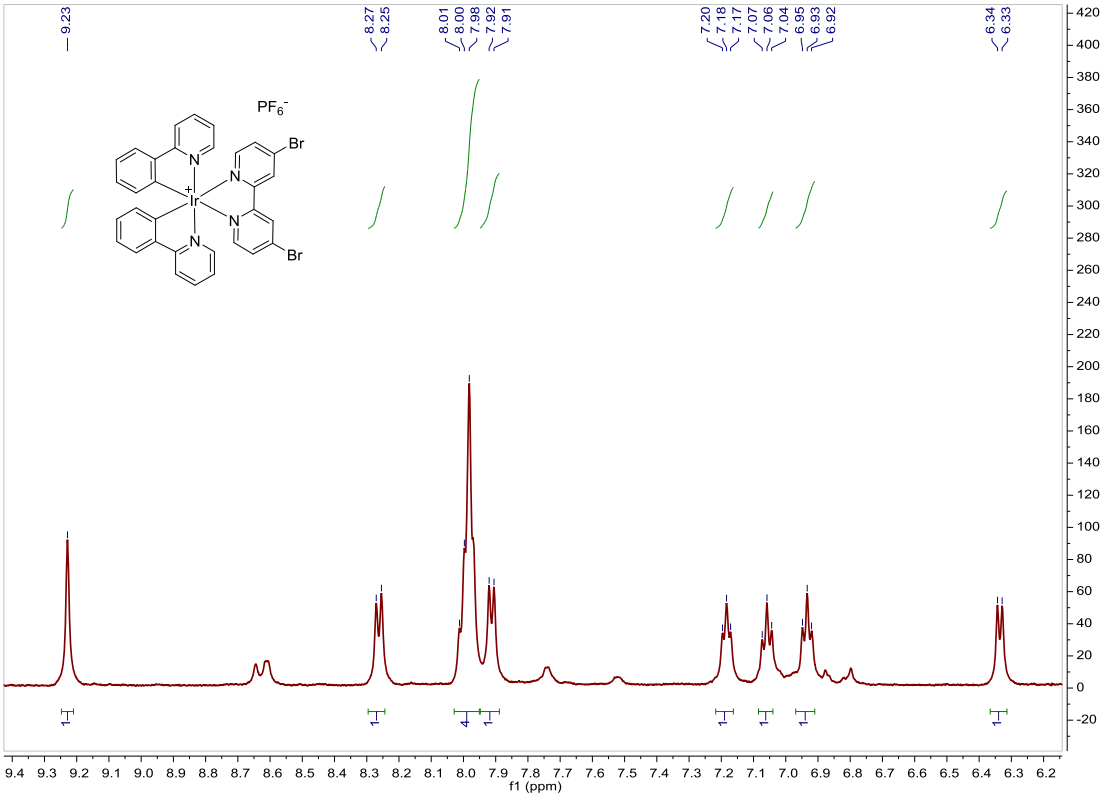

Fig. S144. ^{1}H NMR spectrum of **Abipy-dibr** in acetone-d_6, 500 MHz.

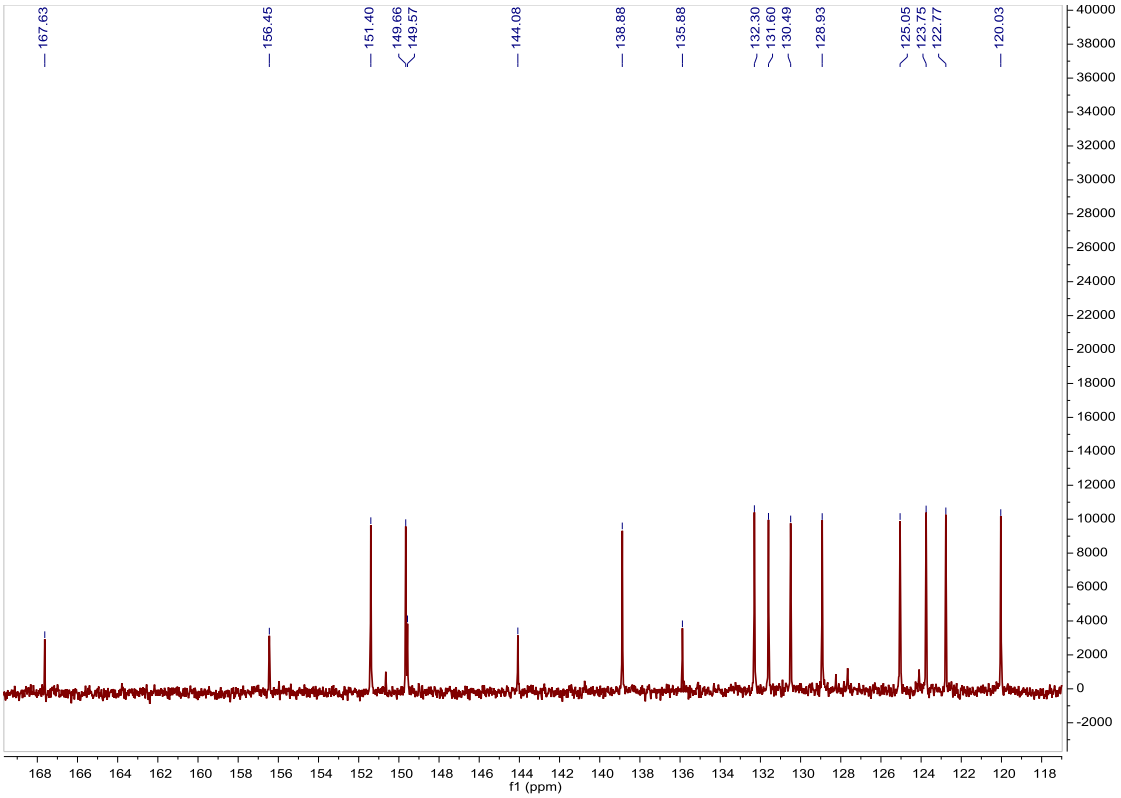

Fig. S145. ^{13}C NMR spectrum of **Abipy-dibr** in acetone-d_6, 126 MHz.

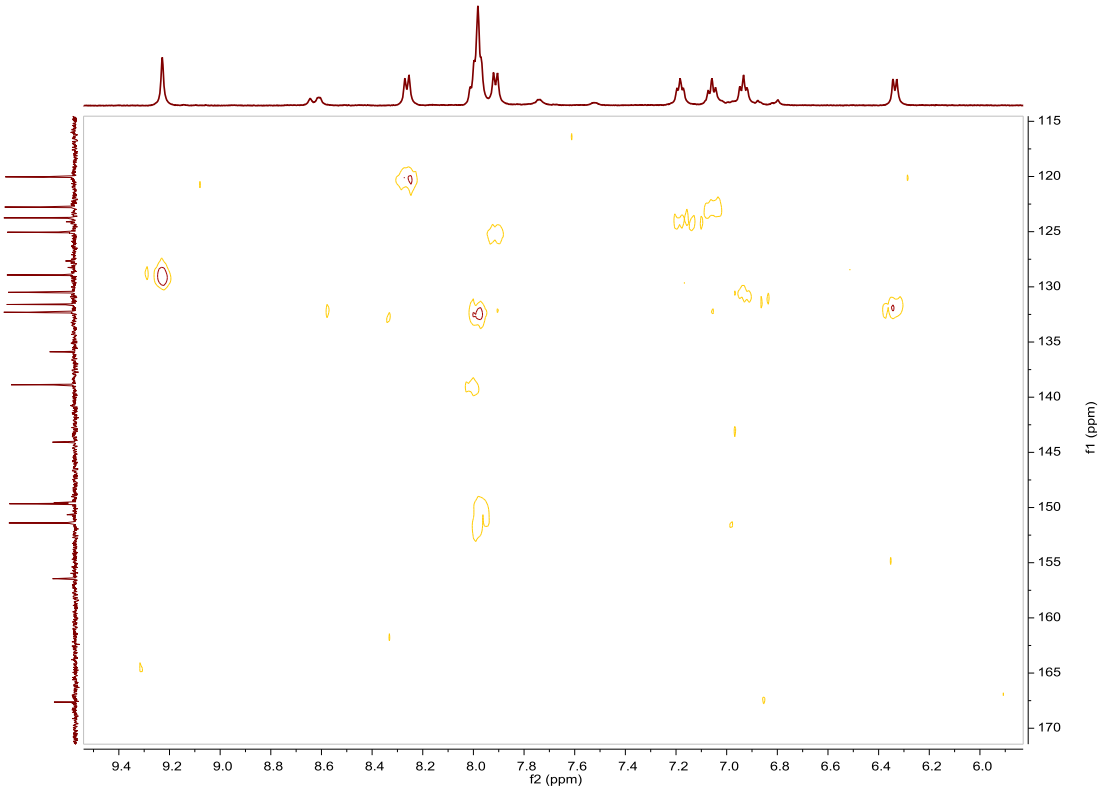

Fig. S146. HSQC NMR spectrum of **Abipy-dibr** in acetone-d_6.

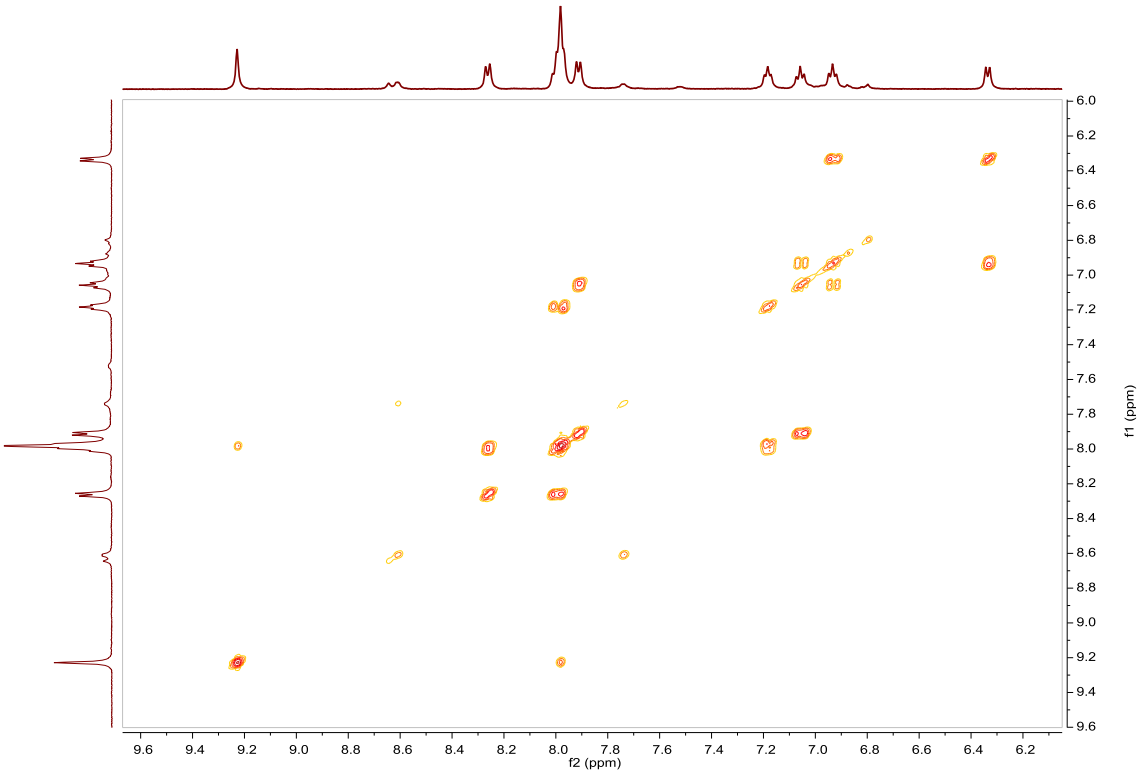

Fig. S147. COSY NMR spectrum of **Abipy-dibr** in acetone-d_6.

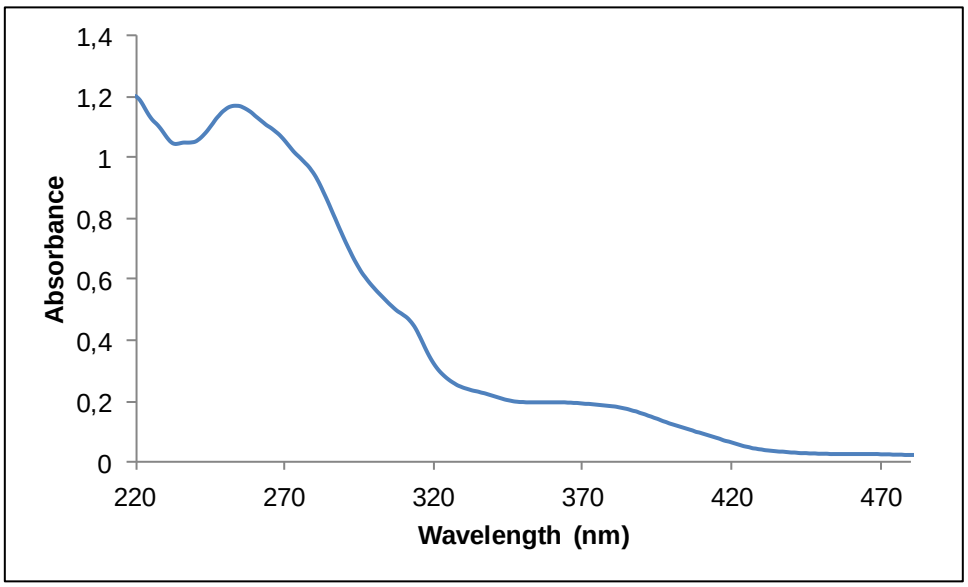

Fig. S148. UV/Vis spectra of **Abipy-dibr** in CH_3CN, $2.46 \cdot 10^{-5}$M.

Compound Bbipy-dibr, [Ir(Fppy)$_2$(bipy-dibr)]PF$_6$. Synthesis and characterization.

SYNTHESIS

Under a N_2 atmosphere, $[Ir(Fppy)_2Cl]_2$ (0.100 g, 0.082 mmol) were added over a suspension of 4,4'-dibromo-2,2'-bipyridine (0.052 g, 0.164 mmol) in 8 mL CH_2Cl_2–MeOH 2/1. The reaction mixture was refluxed, under N_2, for 15 h. To the resulting yellow solution, 0.05 g of KPF_6 were added and the solution was stirred for an 1 h. The solvent was evaporated and the reaction mixture was filtrated through a celite path in CH_2Cl_2. The product was obtained after purified by column chromatography (silica gel, CH_2Cl_2 as eluent) as a yellow solid. Yield 59%.

Elemental Analysis: calculated for ($C_{32}H_{18}Br_2F_4IrN_4PF_6$): C, 37.26; H, 1.76; N, 5.43. Found: C, 37.38; H, 1.99; N, 5.05.

Exact Mass: ESI-MS $[C_{32}H_{18}Br_2F_4IrN_4]^+$: calculated: m/z= 884.9464, found: m/z= 884.9450.

^{1}H NMR (500 MHz, acetone-d_6): δ 9.26 (s, 1H), 8.41 (d, *J* = 10 Hz, 1H), 8.10 (m, 2H), 8.06 (d, J = 5 Hz, 1H), 8.00 (d, *J* = 5 Hz, 1H), 7.27 (t, *J* = 5 Hz, 1H), 6.79 (t, *J* = 10 Hz, 1H), 5.79 (d, *J* = 5 Hz, 1H).

^{13}C NMR (126 MHz, acetone-d_6): 163.72 (d, *J* = 6.3 Hz, C_{quat}), 163.61 (dd, *J* = 12.6 Hz, J = 255.3 Hz, C_{quat}),161.44 (dd, *J* = 12.6, J = 260.3, C_{quat}), 156.19 (s, C_{quat}), 153.60 (d, *J* = 6.3, C_{quat}), 151.80 (s, CH), 150.19 (s, CH), 140.01 (s, CH), 136.60 (s, C_{quat}), 132.62 (s, CH), 129.23 (s, CH), 127.99 (s, C_{quat}), 124.31 (s, CH), 123.79 (d, *J* = 18.9 Hz, CH), 113.80 (d, *J* = 16.3 Hz, CH), 99.03 (pst, *J* = 27.7 Hz, CH).

UV/Vis (CH_3CN), λ, nm (ε, 10^4 M^{-1} cm^{-1}): 242 (5.7), 298 (2.5), 310 (2.3), 361 (0.76).

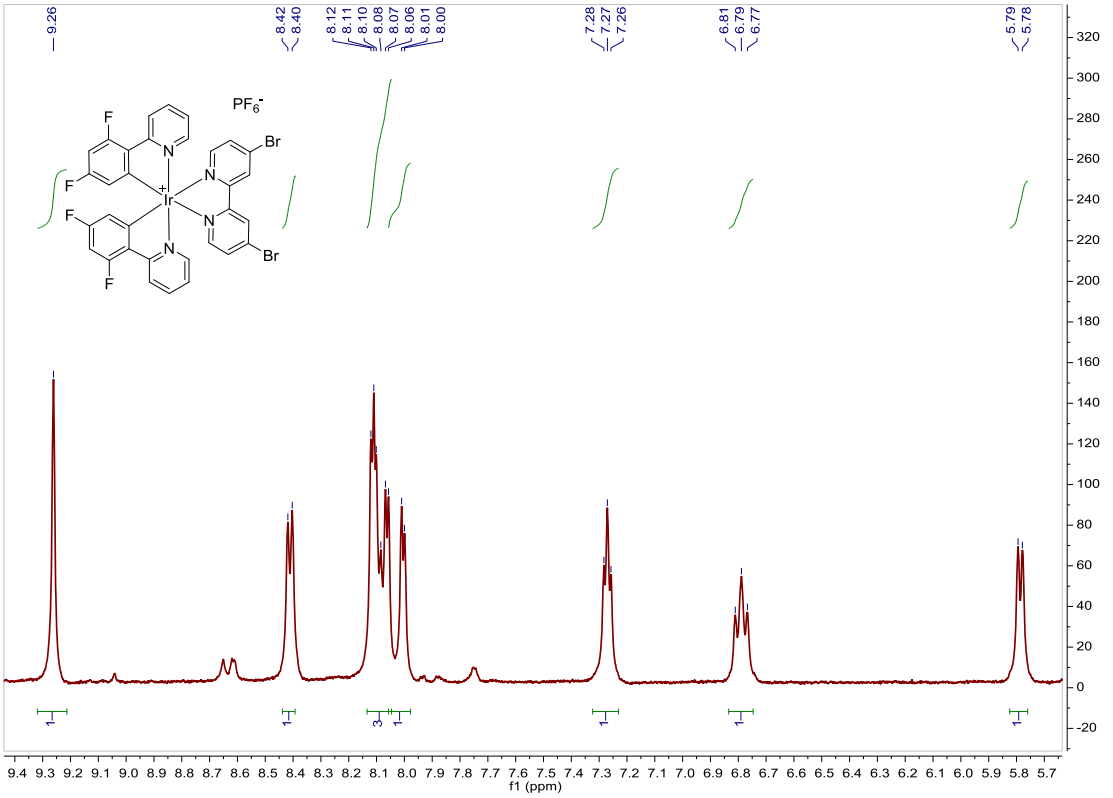

Fig. S149. ^{1}H NMR spectrum of **Bbipy-dibr** in acetone-d_6, 500 MHz.

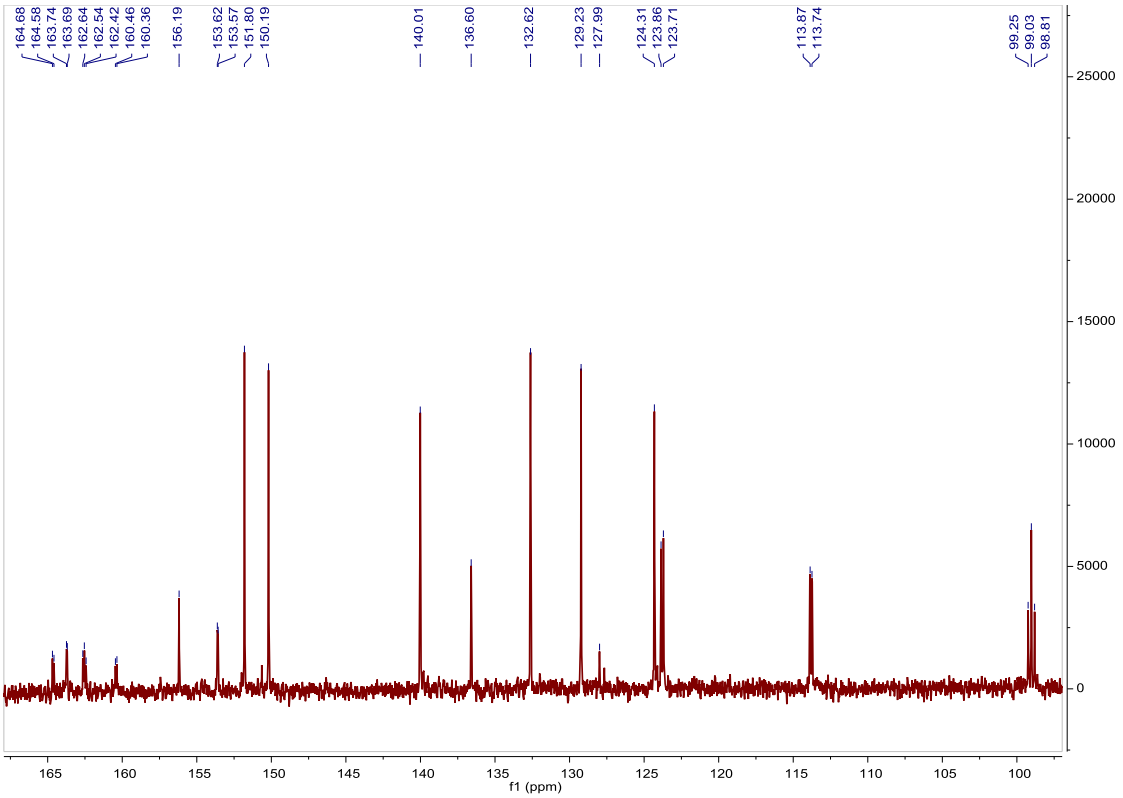

Fig. S150. ^{13}C NMR spectrum of **Bbipy-dibr** in acetone-d_6, 126 MHz.

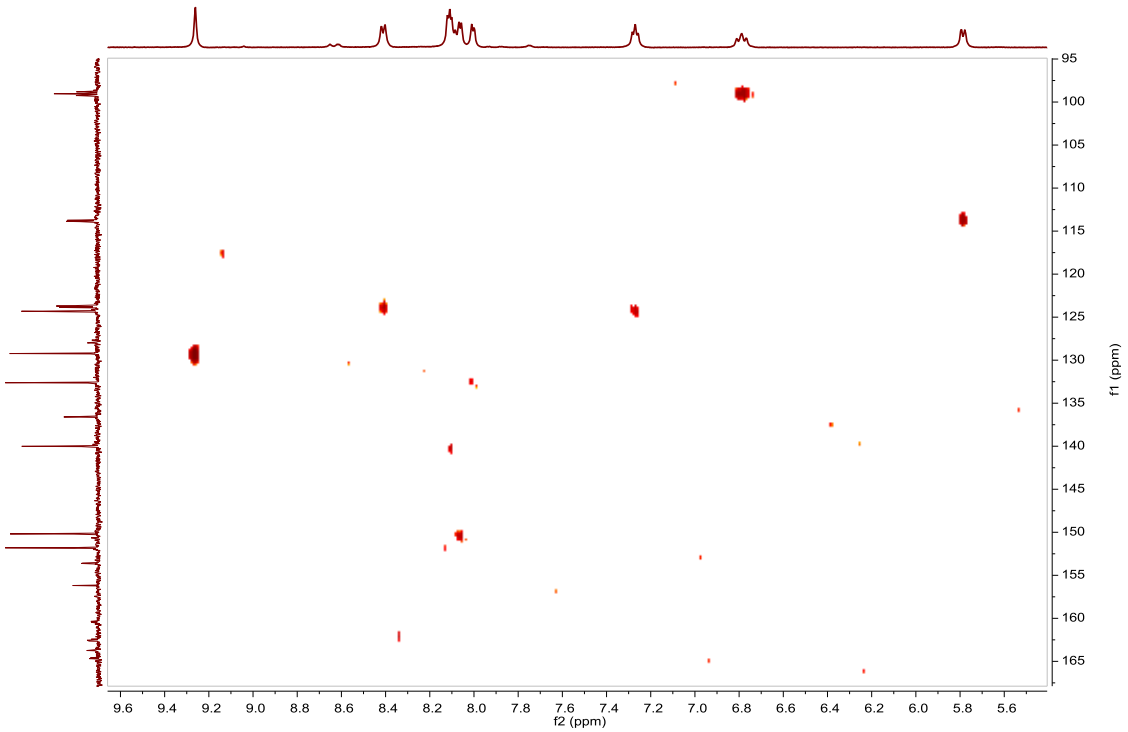

Fig. S151. HSQC NMR spectrum of **Bbipy-dibr** in acetone-d_6.

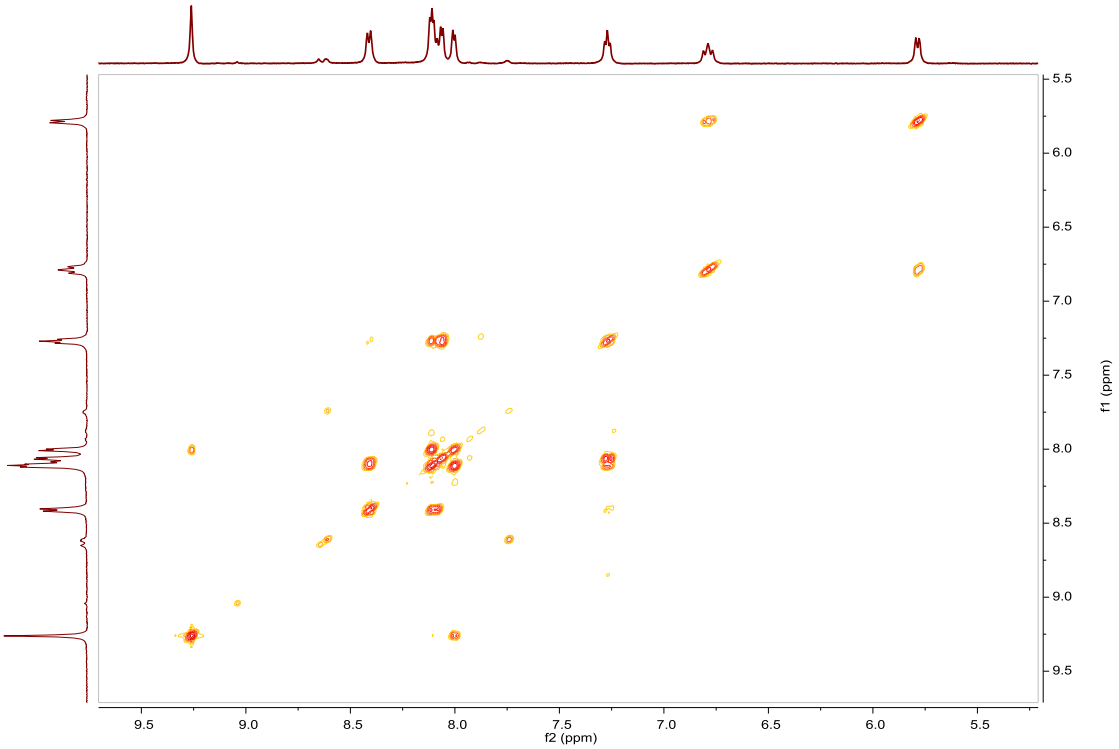

Fig. S152. COSY NMR spectrum of **Bbipy-dibr** in acetone-d_6.

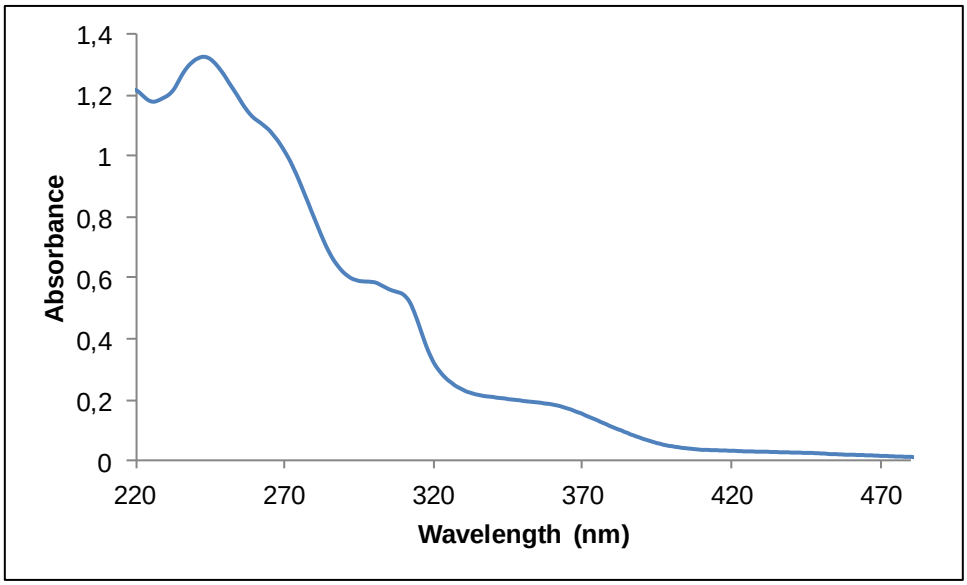

Fig. S153. UV/Vis spectra of **Bbipy-dibr** in CH_3CN, $2.34 \cdot 10^{-5}$M.

Compound Cbipy-dibr, [Ir(Brppy)$_2$(bipy-dibr)]PF$_6$. Synthesis and characterization.

SYNTHESIS

Under a N_2 atmosphere, $[Ir(Brppy)_2Cl]_2$ (0.100 g, 0.072 mmol) were added over a suspension of 4,4'-dibromo-2,2'-bipyridine (0.045 g, 0.144 mmol) in 8 mL CH_2Cl_2–MeOH 2/1. The reaction mixture was refluxed, under N_2, for 15 h. To the resulting orange solution, 0.05 g of KPF_6 were added and the solution was stirred for an 1 h. The solvent was evaporated and the desired compound was obtained after filtration through a celite path in CH_2Cl_2 as a brown solid. Yield 87%.

Elemental Analysis: calculated for ($C_{32}H_{20}Br_4IrN_4PF_6$): C, 34.40; H, 1.80; N, 5.01. Found: C, 33.96; H, 1.84; N, 4.93.

Exact Mass: ESI-MS $[C_{32}H_{20}Br_4IrN_4]^+$: calculated: m/z= 968.8051, found: m/z= 968.8026.

^{1}H NMR (500 MHz, acetone-*d*$_6$): δ 9.25 (d, J = 1.7 Hz, 1H), 8.32 (d, J = 8.1 Hz, 1H), 8.04 (m, 4H), 7.90 (d, J = 8.35 Hz, 1H), 7.27 (m, 2H), 6.39 (d, J = 2.0 Hz, 1H).

^{13}C NMR (126 MHz, acetone-*d*$_6$): δ 166.34 (C_{quat}), 156.32 (C_{quat}), 151.68 (CH), 151.58 (C_{quat}), 149.92 (CH), 143.41 (C_{quat}), 139.44 (CH), 136.34 (C_{quat}), 133.77 (CH), 132.52 (CH), 129.11 (CH), 126.87 (CH), 126.08 (CH), 124.95 (C_{quat}), 124.46 (CH), 120.65 (CH).

UV/Vis (CH_3CN), λ, nm (ε, 10^4 M^{-1} cm^{-1}): 254 (6.1), 267 (6.2), 299 (4.0), 391 (0.61).

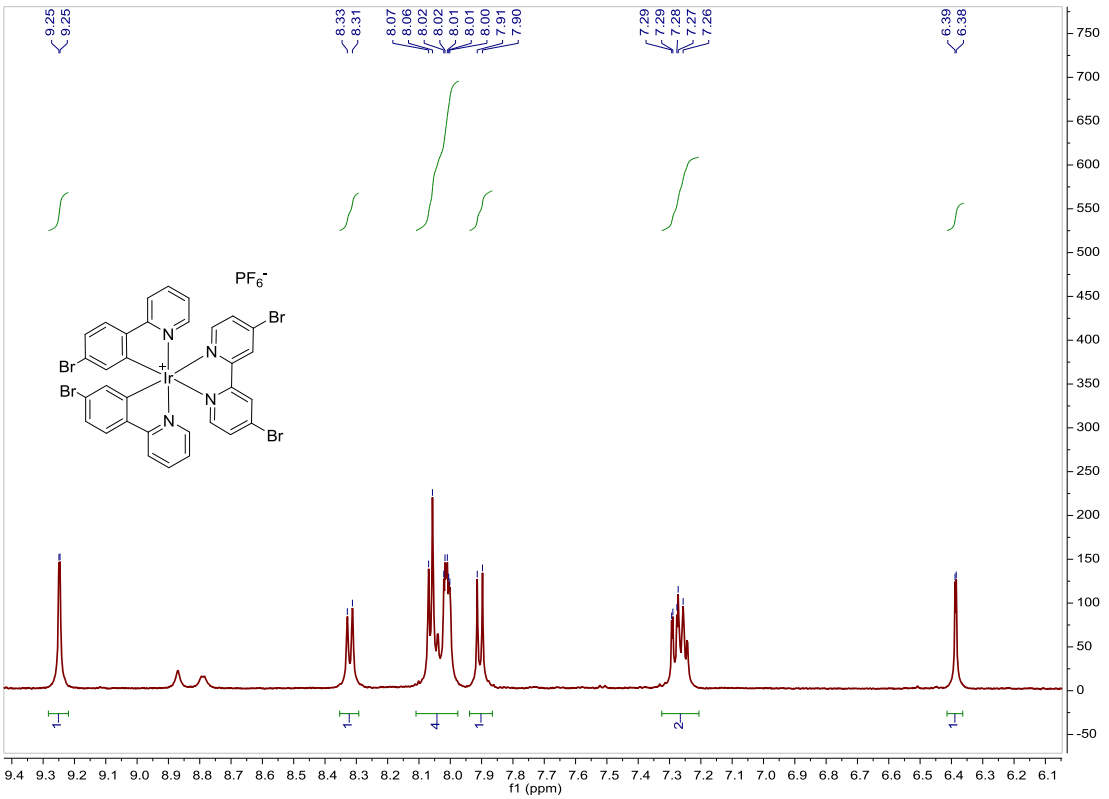

Fig. S154. ^{1}H NMR spectrum of **Cbipy-dibr** in acetone-*d*$_6$, 500 MHz.

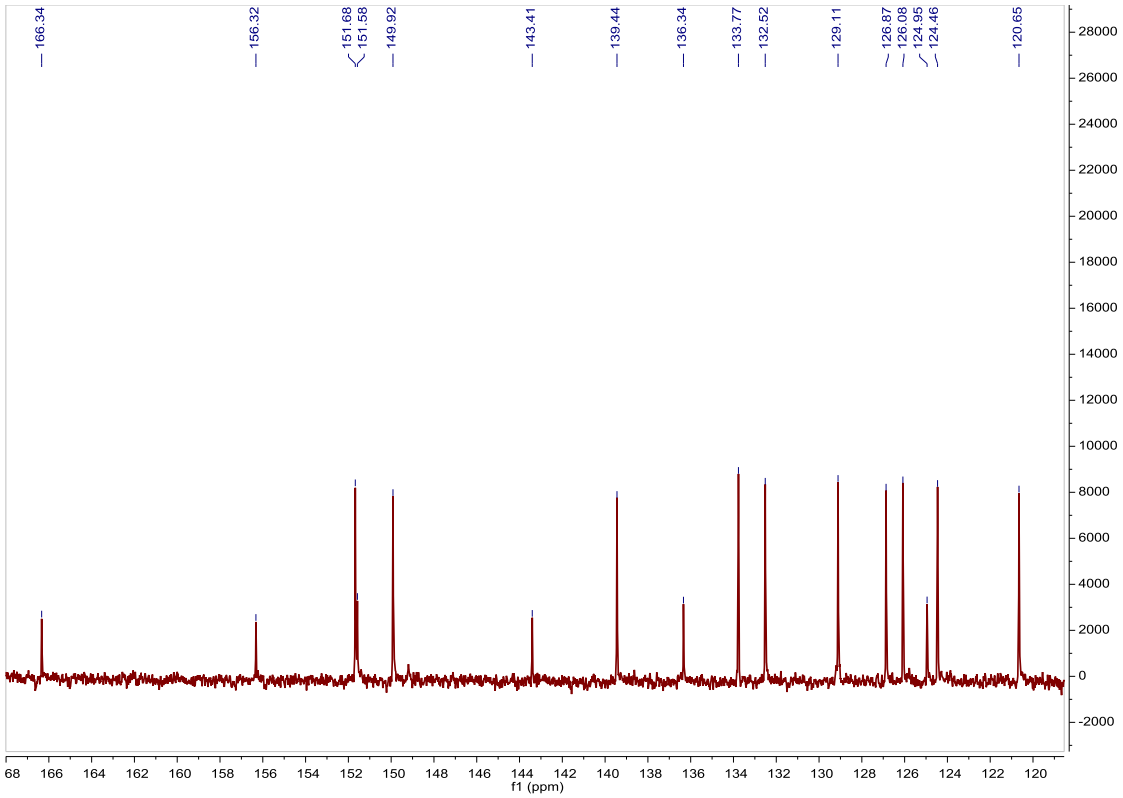

Fig. S155. ^{13}C NMR spectrum of **Cbipy-dibr** in acetone-d_6, 126 MHz.

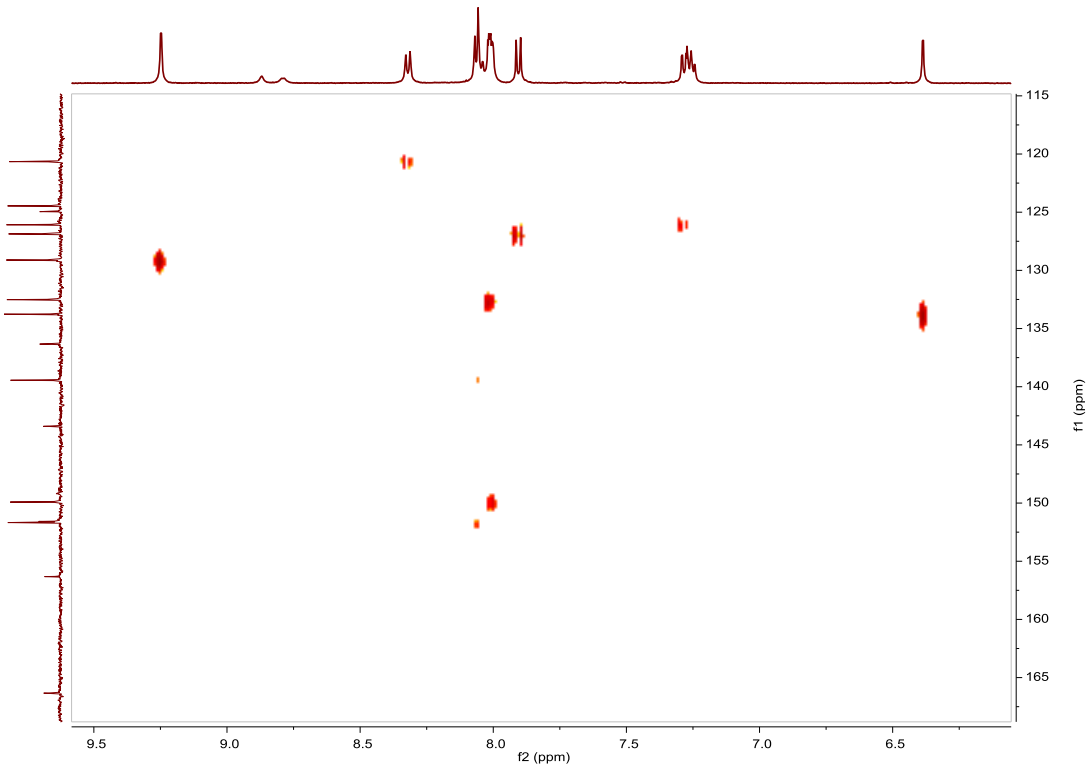

Fig. S156. HSQC NMR spectrum of **Cbipy-dibr** in acetone-d_6.

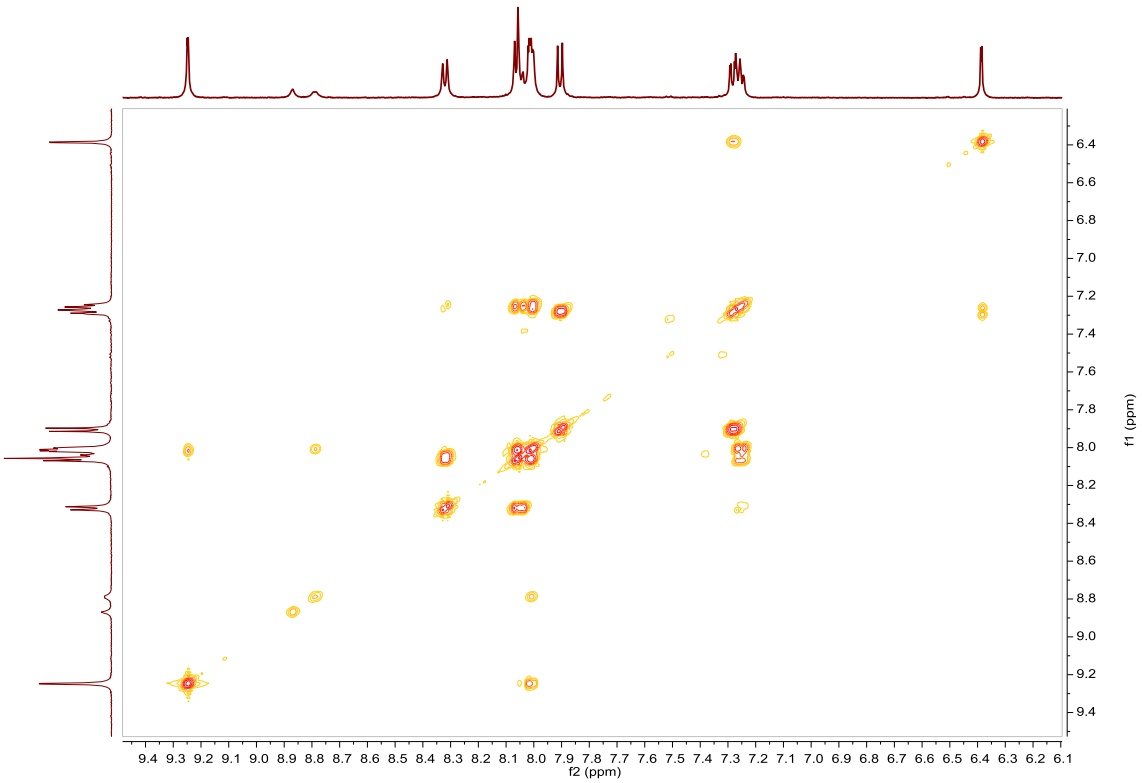

Fig. S157. COSY NMR spectrum of **Cbipy-dibr** in acetone-d_6.

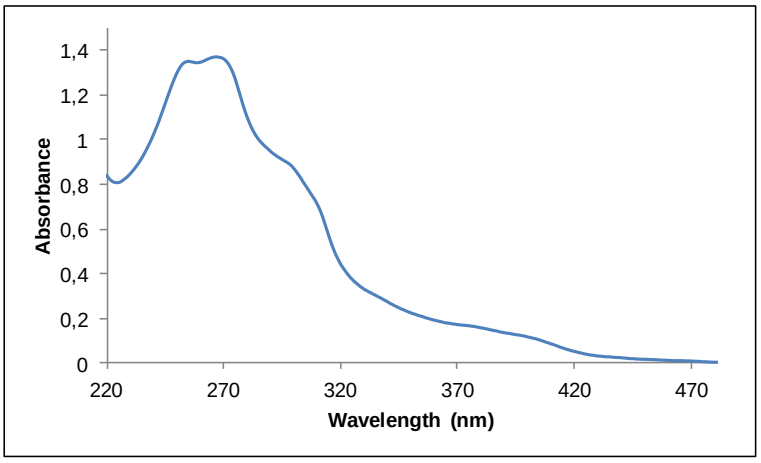

Fig. S158. UV/Vis spectra of **Cbipy-dibr** in CH_3CN, $2.20 \cdot 10^{-5}$M.

Compound A1, $[Ir(ppy)_2(1)]PF_6$. Synthesis, characterization and photoisomerization studies.

SYNTHESIS

Under a N_2 atmosphere, $[Ir(ppy)_2Cl]_2$ (0.058 g, 0.054 mmol) were added over a suspension of **L1** (0.040 g, 0.109 mmol) in 4 ml CH_2Cl_2–MeOH 2/1. The reaction mixture was refluxed, under N_2, for 15 h. After solvent evaporation the product was purified by column chromatography (silica gel, CH_2Cl_2). When the unreacted $[Ir(ppy)_2Cl]_2$ eluted, 0.05 g of KPF_6 were added on top of the column and the polarity of the eluent was gradually increased to 100% acetone to elute $[Ir(ppy)_2(\mathbf{L1})]PF_6$ together with the excess of KPF_6. The desired compound, purified by filtration through a celite path in CH_2Cl_2, was obtained as a dark red solid. Yield 85%.

Elemental Analysis: calculated for ($C_{44}H_{32}IrN_8PF_6$): C, 52.33; H, 3.19; N, 11.09. Found: C, 52.14; H, 3.09; N, 10.71.

Exact Mass: ESI-MS $[C_{44}H_{32}IrN_8]^+$: calculated: m/z= 865.2379, found: m/z= 865.2408.

^{1}H NMR (300 MHz, acetone-d_6): δ 9.39 (d, J = 1.5 Hz, 1H), 8.37 (d, J = 5.8 Hz, 1H), 8.30 (d, J = 8.0 Hz, 1H), 8.13–8.04 (m, 4H), 7.99 (t, J = 8.9 Hz, 2H), 7.73 (m, 3H), 7.22 (pst, J = 6.4 Hz, 1H), 7.10 (pst, J = 7.2 Hz, 1H), 6.99 (pst, J = 7.6 Hz, 1H), 6.43 (d, J = 7.4 Hz, 1H).

^{13}C APT NMR (75 MHz, acetone-d_6): δ 168.96 (C_{quat}), 160.13 (C_{quat}), 159.28 (C_{quat}), 153.77 (CH), 153.72 (C_{quat}), 151.39 (C_{quat}), 150.91 (CH), 145.41 (C_{quat}), 140.17 (CH), 135.16 (CH), 132.95 (CH), 131.80 (CH), 131.08 (2CH), 126.34 (CH), 125.08 (CH), 125.01 (2CH), 124.07 (CH), 121.85 (CH), 121.35 (CH), 119.96 (CH).

UV/Vis (CH_3CN), λ, nm (ε, 10^4 M^{-1} cm^{-1}): 327 (5.3), 404 (1.7), 513 (0.26).

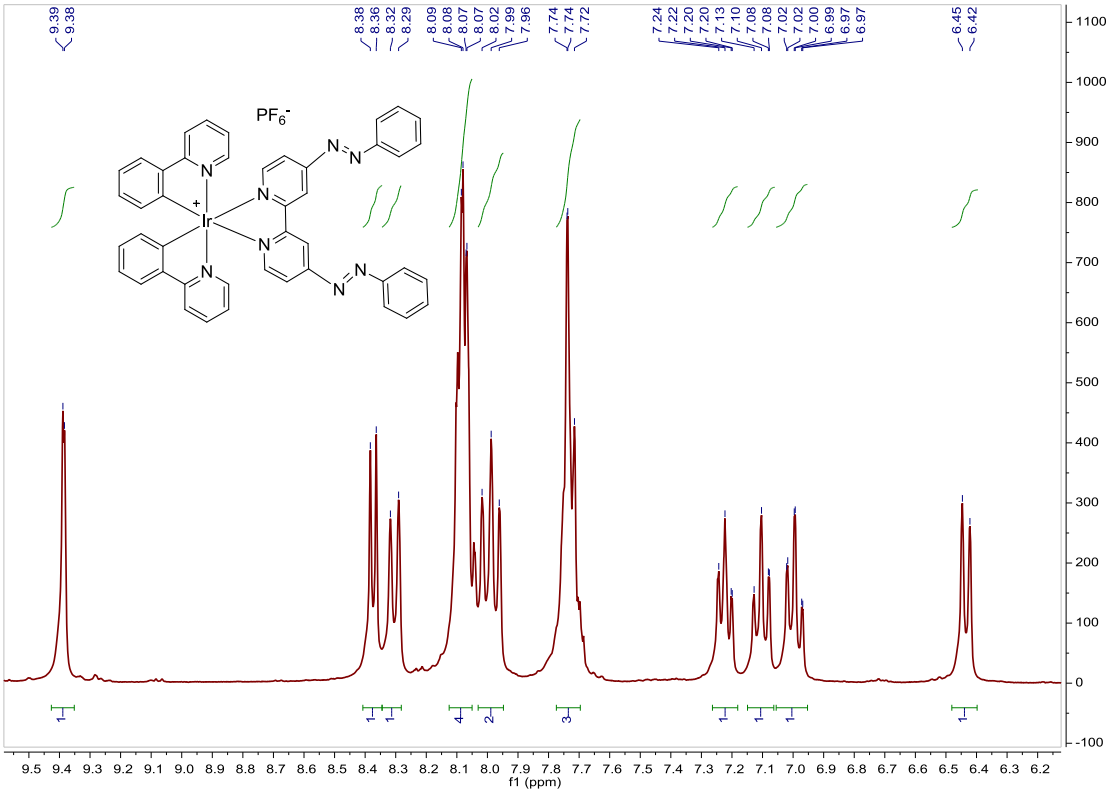

Fig. S159. ^{1}H NMR spectrum of **A1** in acetone-d_6, 300 MHz.

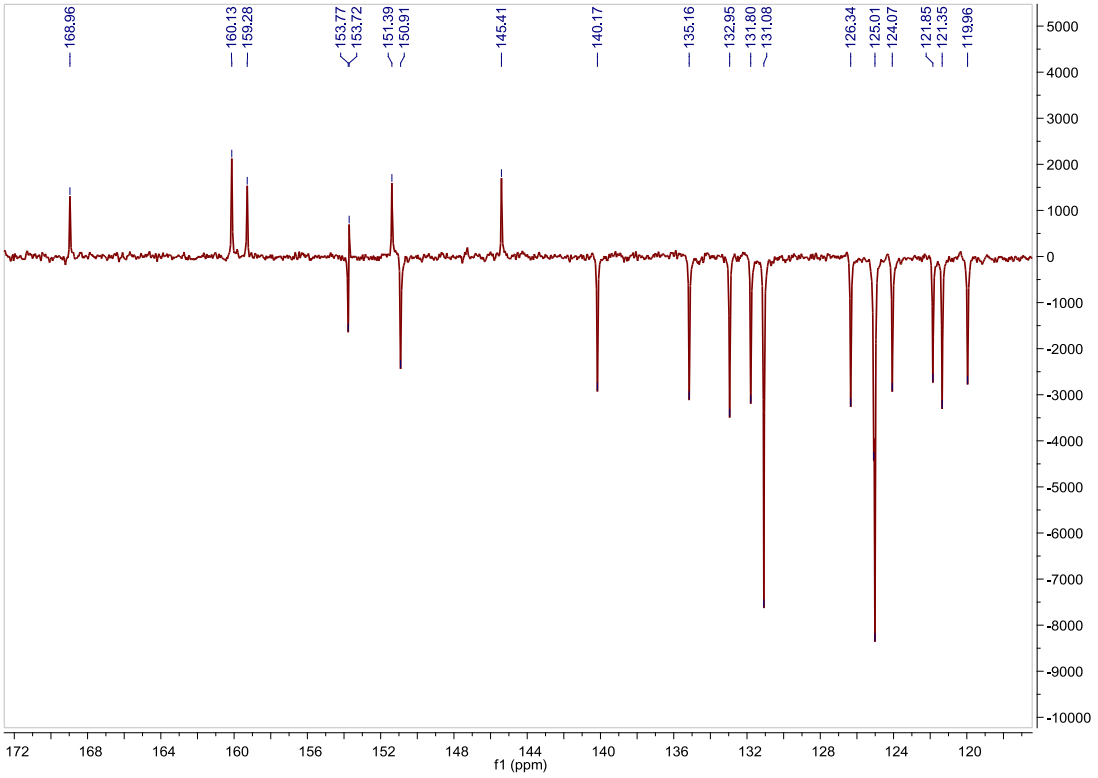

Fig. S160. ^{13}C APT NMR spectrum of **A1** in acetone-d_6, 75 MHz.

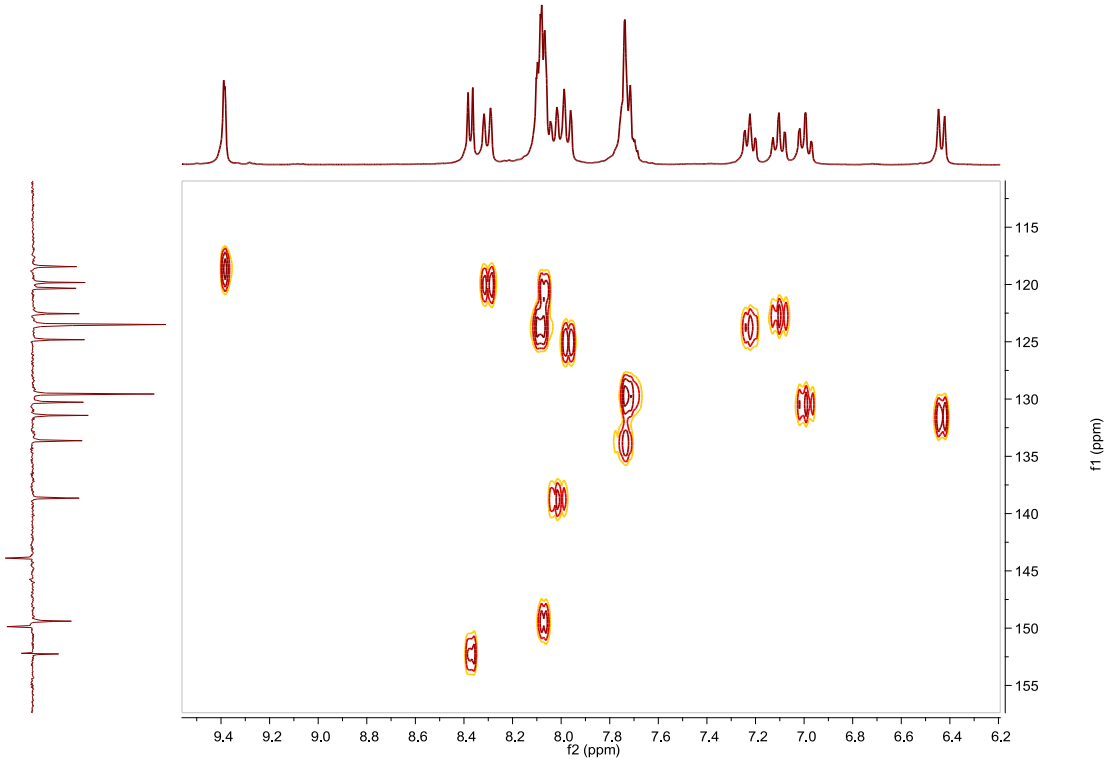

Fig. S161. HSQC NMR spectrum of **A1** in acetone-d_6.

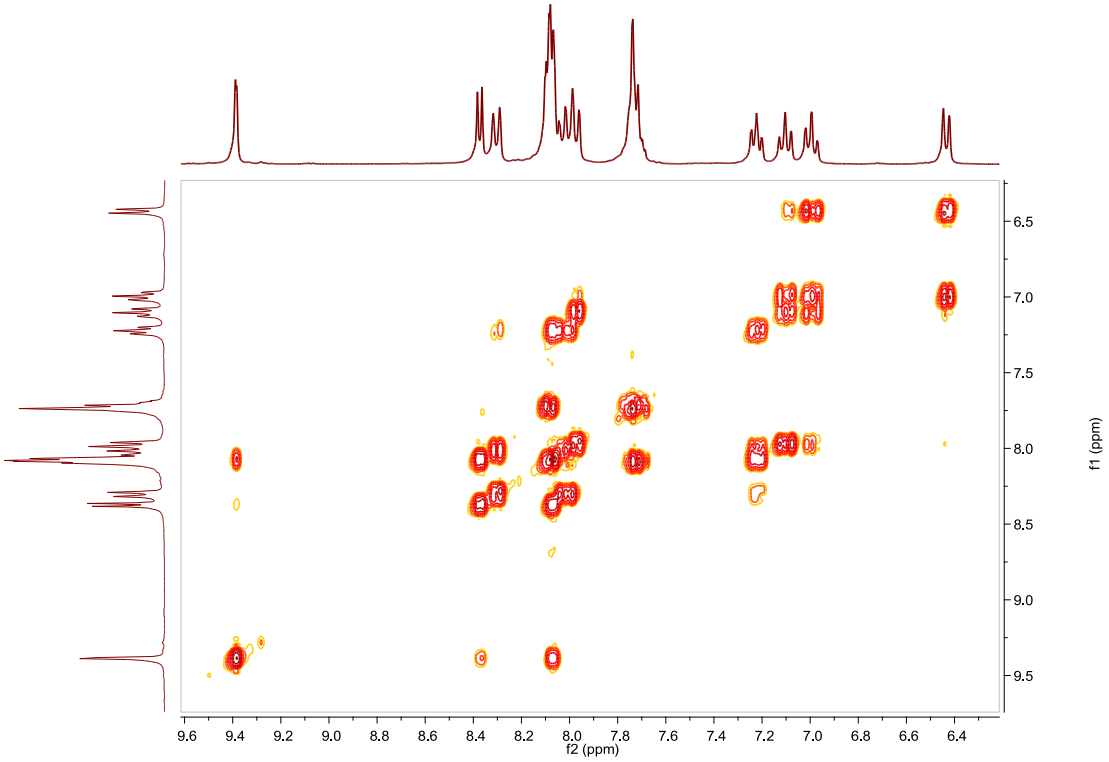

Fig. S162. COSY NMR spectrum of **A1** in acetone-d_6.

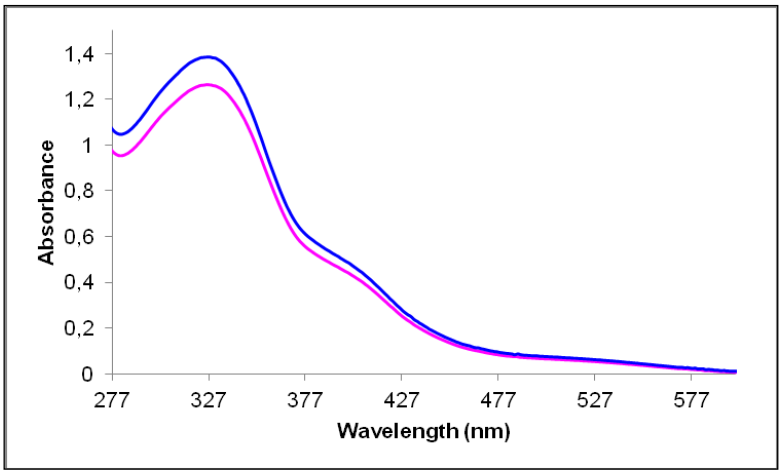

Fig. S163. UV/Vis spectra of **A1** in CH_3CN. Before (blue line) and after (pink line) irradiation at 348nm, $2.62 \cdot 10^{-5}$ M.

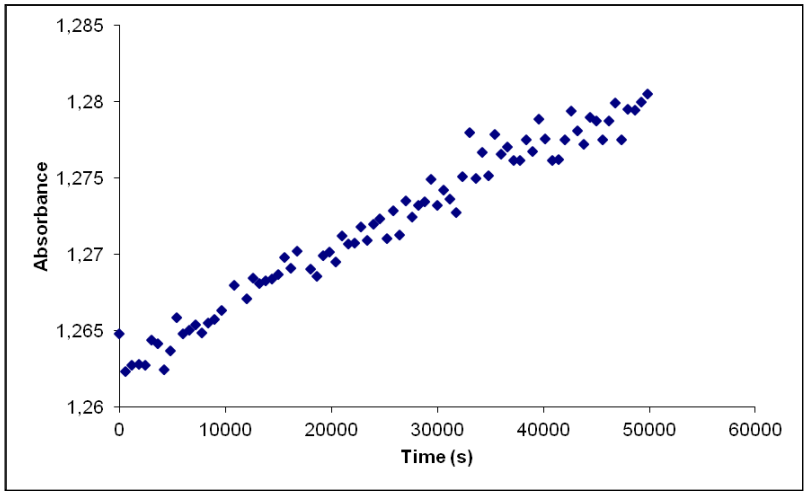

Fig. S164. Cis to trans thermal isomerization kinetics of **A1**. Absorption change of the band 327nm at 328 K in CH_3CN after irradiation at 348 nm. ($2.62 \cdot 10^{-5}$ M).

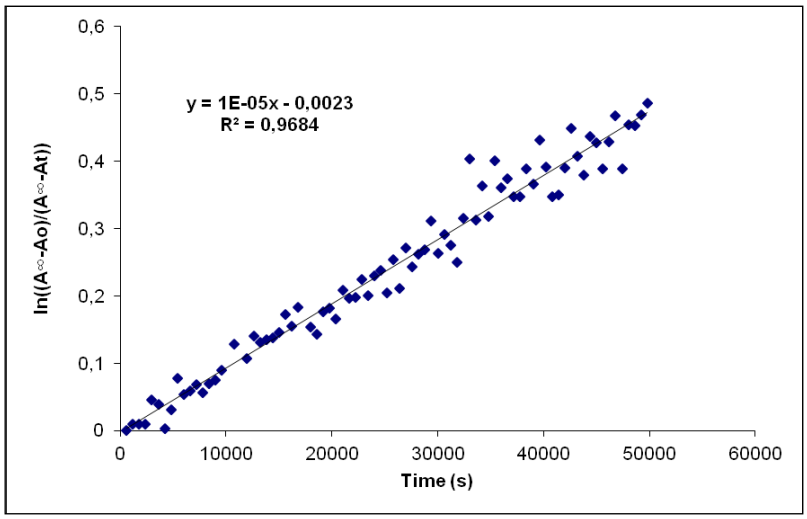

Fig. S165. Cis to trans thermal isomerization kinetics of **A1**. First-order plot. k (s^{-1}) = $1.0 \cdot 10^{-5}$. Half-life (min) = 1155.

Compound B1, $[Ir(Fppy)_2(1)]PF_6$. Synthesis, characterization and photoisomerization studies.

SYNTHESIS

Under a N_2 atmosphere, $[Ir(Fppy)_2Cl]_2$ (0.100 g, 0.082 mmol) were added over a suspension of **L1** (0.06 g, 0.164 mmol) in 8 ml CH_2Cl_2–MeOH 2/1. The reaction mixture was refluxed, under N_2, for 15 h. After solvent evaporation, the insoluble portion in CH_2Cl_2 was removed and the product was purified by column chromatography (silica gel, CH_2Cl_2). When the unreacted $[Ir(Fppy)_2Cl]_2$ eluted, 0.05 g of KPF_6 were added on top of the column and the polarity of the eluent was gradually increased to 100% acetone to elute $[Ir(Fppy)_2(\mathbf{L1})PF_6$ together with the excess of KPF_6. The desired compound, purified by filtration through a celite path in CH_2Cl_2, was obtained as a dark red solid. Yield 88%.

Elemental Analysis: calculated for ($C_{44}H_{28}F_4IrN_8PF_6 \cdot CH_2Cl_2$): C, 46.32; H, 2.59; N, 9.60. Found: C, 46.19; H, 2.72; N, 9.46.

Exact Mass: ESI-MS $[C_{44}H_{28}F_4IrN_8]^+$: calculated: m/z= 937.2002, found: m/z= 937.2034.

^{1}H NMR (300 MHz, acetone-d_6): δ 9.43 (d, J = 1.8 Hz, 1H), 8.51 (d, J = 5.9 Hz, 1H), 8.47 (d, J = 8.4 Hz, 1H), 8.17 (d, J = 5.9 Hz, 1H), 8.10 (m, 4H), 7.74 (m, 3H), 7.31 (ddd, J = 1.3 Hz, J = 5.9 Hz, J = 7.3 Hz, 1H), 6.84 (ddd, J = 2.4 Hz, J = 9.4 Hz, J = 12.6 Hz, 1H), 5.89 (dd, J = 2.4 Hz, J = 8.6 Hz, 1H).

^{13}C APT NMR (75 MHz, acetone-d_6): δ 165.08 (d, J = 6.7 Hz, C_{quat}), 164.95 (dd, J = 12.4 Hz, J = 253.5 Hz, C_{quat}), 162.78 (dd, J = 12.5 Hz, J = 258.3 Hz, C_{quat}), 160.54 (s, C_{quat}), 159.11 (s, C_{quat}), 155.44 (d, J = 6.5 Hz, C_{quat}), 154.22 (s, CH), 153.71 (s, C_{quat}), 151.46 (s, CH), 141.27 (s, CH), 135.29 (s, CH), 131.10 (s, 2CH), 129.29 (s, C_{quat}), 125.62 (s, CH), 125.08 (d, J = 19.2 Hz, CH), 125.06 (s, 2CH), 122.05 (s, CH), 120.31 (s, CH), 115.15 (d, J = 19.6 Hz, CH), 100.30 (t, J = 26.9 Hz, CH).

UV/Vis (CH_3CN), λ, nm (ε, 10^4 M^{-1} cm^{-1}): 328 (4.5), 479 (0.31).

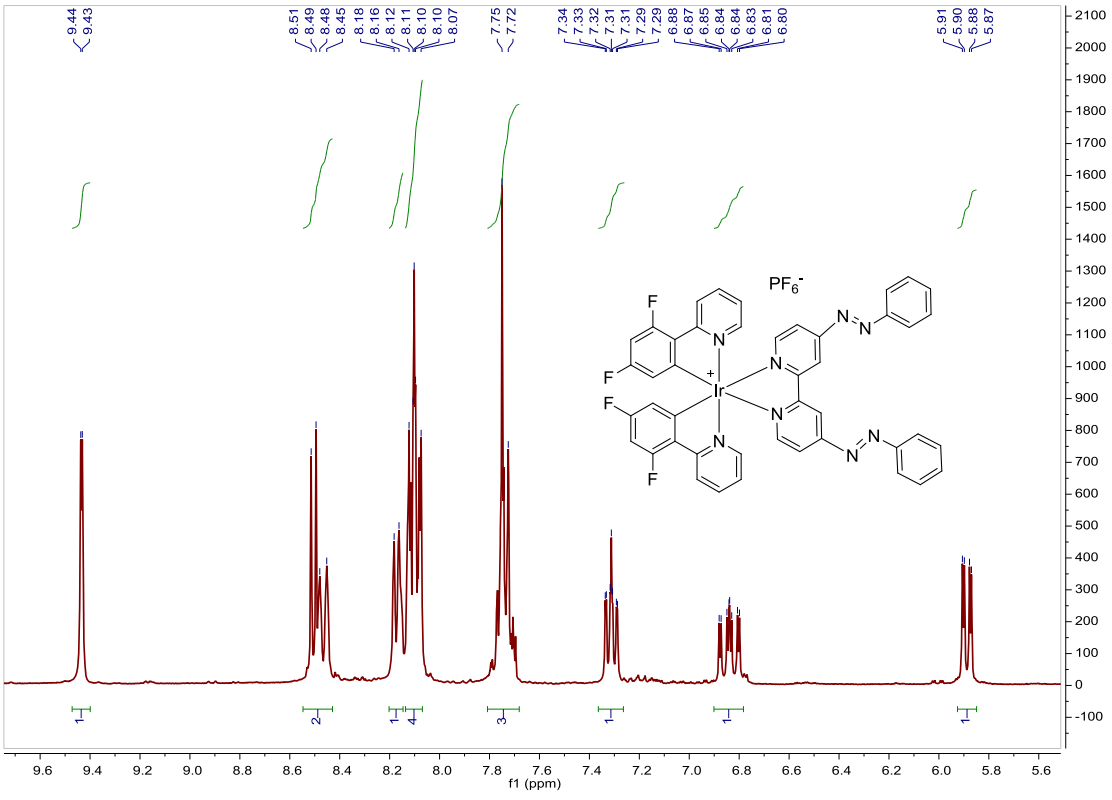

Fig. S166. ^{1}H NMR spectrum of **B1** in acetone-d_6, 300 MHz.

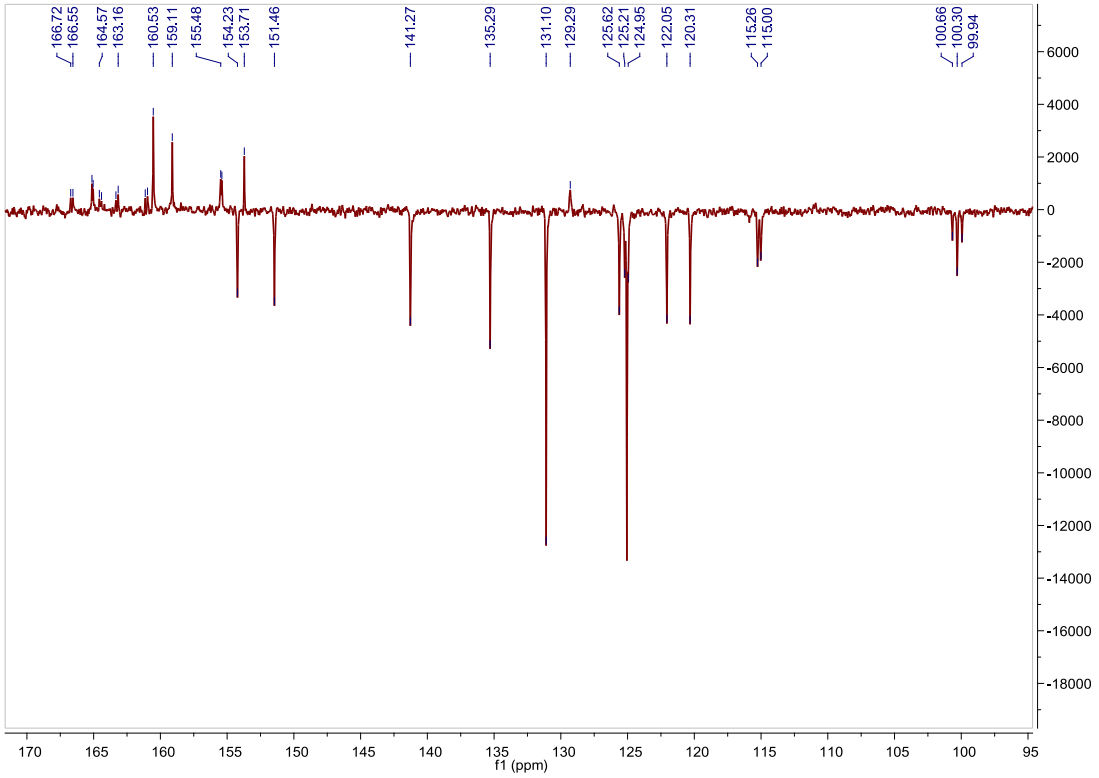

Fig. S167. ^{13}C APT NMR spectrum of **B1** in acetone-d_6, 75 MHz.

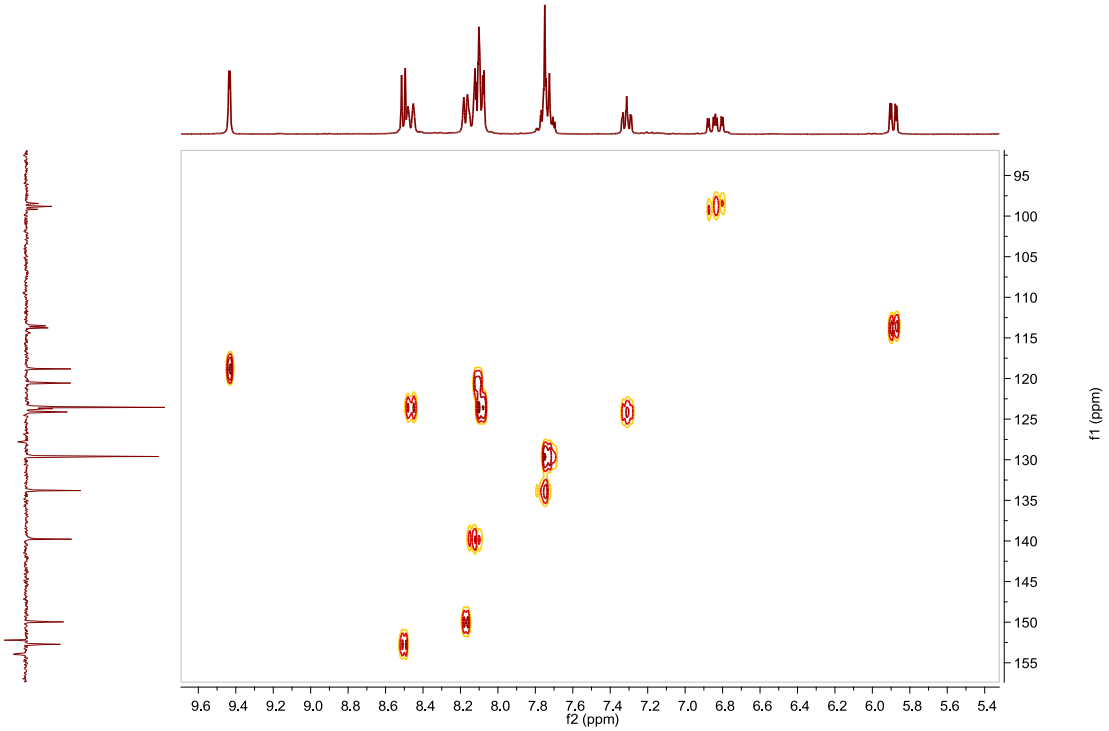

Fig. S168. HSQC NMR spectrum of **B1** in acetone-d_6.

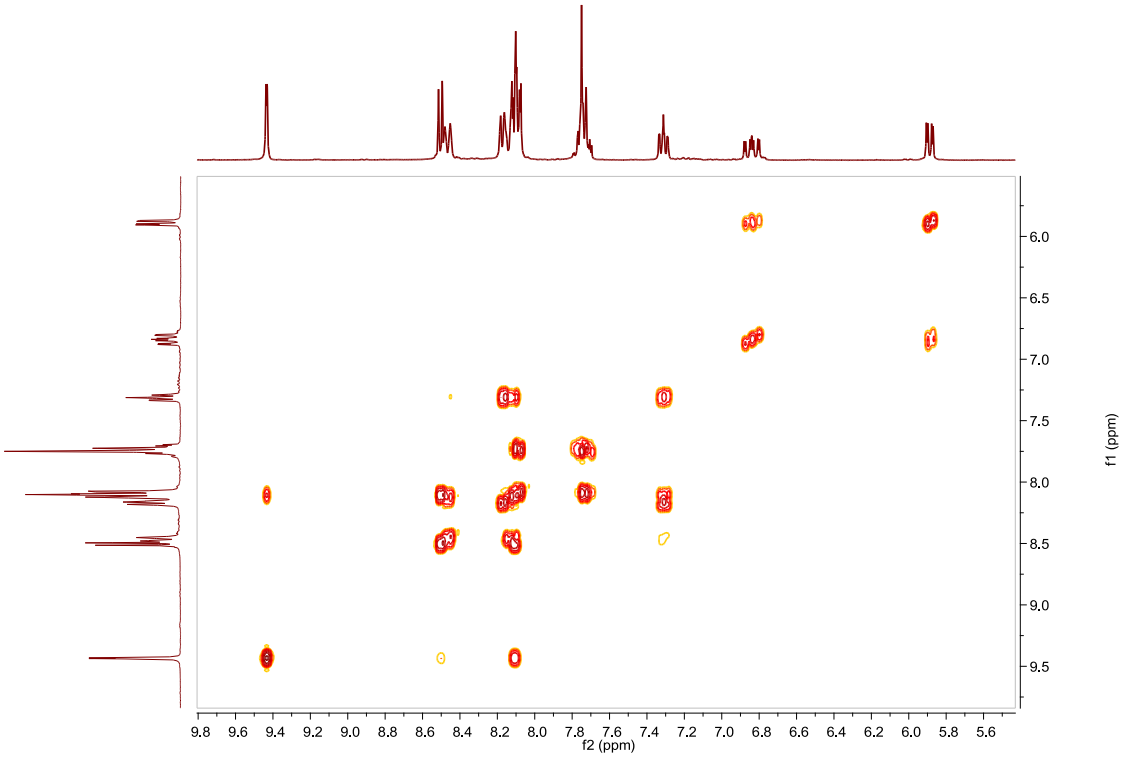

Fig. S169. COSY NMR spectrum of **B1** in acetone-d_6.

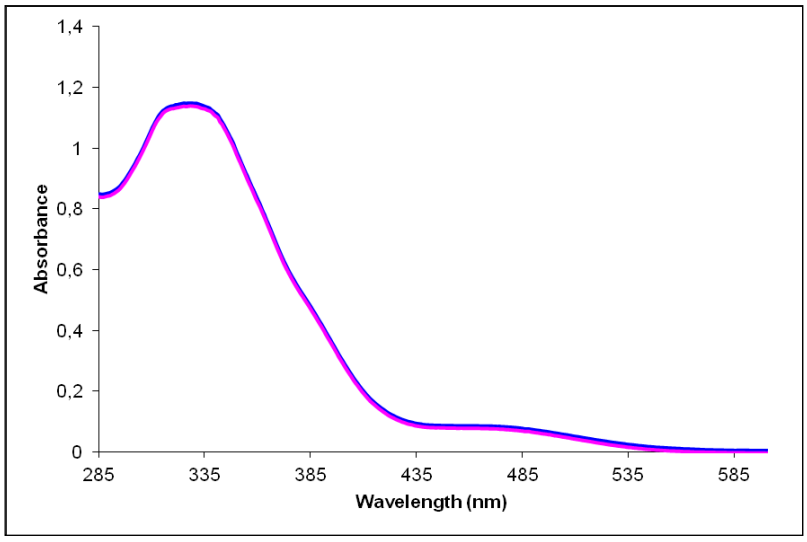

Fig. S170. UV/Vis spectra of **B1** in CH_3CN. Before (blue line) and after (pink line) irradiation at 326nm, $2.55 \cdot 10^{-5}$ M.

Cis to trans thermal isomerization kinetics. Due to the small degree of photoisomerization, it has been not possible to calculate k.

Compound C1, $[Ir(Brppy)_2(1)]PF_6$. Synthesis, characterization and photoisomerization studies.

SYNTHESIS

Under a N_2 atmosphere, $[Ir(Brppy)_2Cl]_2$ (0.200 g, 0.144 mmol) were added over a suspension of **L1** (0.105 g, 0.288 mmol) in 16 ml CH_2Cl_2–MeOH 2/1. The reaction mixture was refluxed, under N_2, for 15 h. After solvent evaporation the product was purified by column chromatography (silica gel, CH_2Cl_2). When the unreacted $[Ir(Brppy)_2Cl]_2$ eluted, 0.1 g of KPF_6 were added on top of the column and the polarity of the eluent was gradually increased to 100% acetone to elute $[Ir(Brppy)_2(\mathbf{L1})]PF_6$ together with the excess of KPF_6. The desired compound was precipitated with ether after filtration through a celite path in CH_2Cl_2 and it was obtained as a dark red solid. Yield 61%.

Elemental Analysis: calculated for ($C_{44}H_{30}Br_2IrN_8PF_6$): C, 45.26; H, 2.59; N, 9.60. Found: C, 45.22; H, 2.51; N, 9.47.

Exact Mass: ESI-MS $[C_{44}H_{30}Br_2IrN_8]^+$: calculated: m/z= 1021.0589, found: m/z= 1021.0573.

^{1}H NMR (300 MHz, acetone-d_6): δ 9.41 (d, J = 1.6 Hz, 1H), 8.45 (d, J = 5.8 Hz, 1H), 8.35 (d, J = 8.0 Hz, 1H), 8.14–8.03 (m, 5H), 7.96 (d, J = 8.4 Hz, 1H), 7.73 (brd, J = 7.0 Hz, 3H), 7.33 (dd, J = 1.8 Hz, J = 8.3 Hz, 1H), 7.28 (d, J = 6.1 Hz, 1H), 6.49 (d, J = 1.9 Hz, 1H).

^{13}C APT NMR (75 MHz, acetone-d_6): δ 167.67 (C_{quat}), 160.38 (C_{quat}), 159.20 (C_{quat}), 154.07 (CH), 153.72 (C_{quat}), 153.43 (C_{quat}), 151.17 (CH), 144.74 (C_{quat}), 140.72 (CH), 135.24 (CH), 135.12 (CH), 131.10 (2CH), 128.17 (CH), 127.38 (CH), 126.30 (C_{quat}), 125.79 (CH), 125.06 (2CH), 122.04 (CH), 121.95 (CH), 120.14 (CH).

UV/Vis (CH_3CN), λ, nm (ε, 10^4 M^{-1} cm^{-1}): 325 (5.3), 392 (2.0), 481 (0.32).

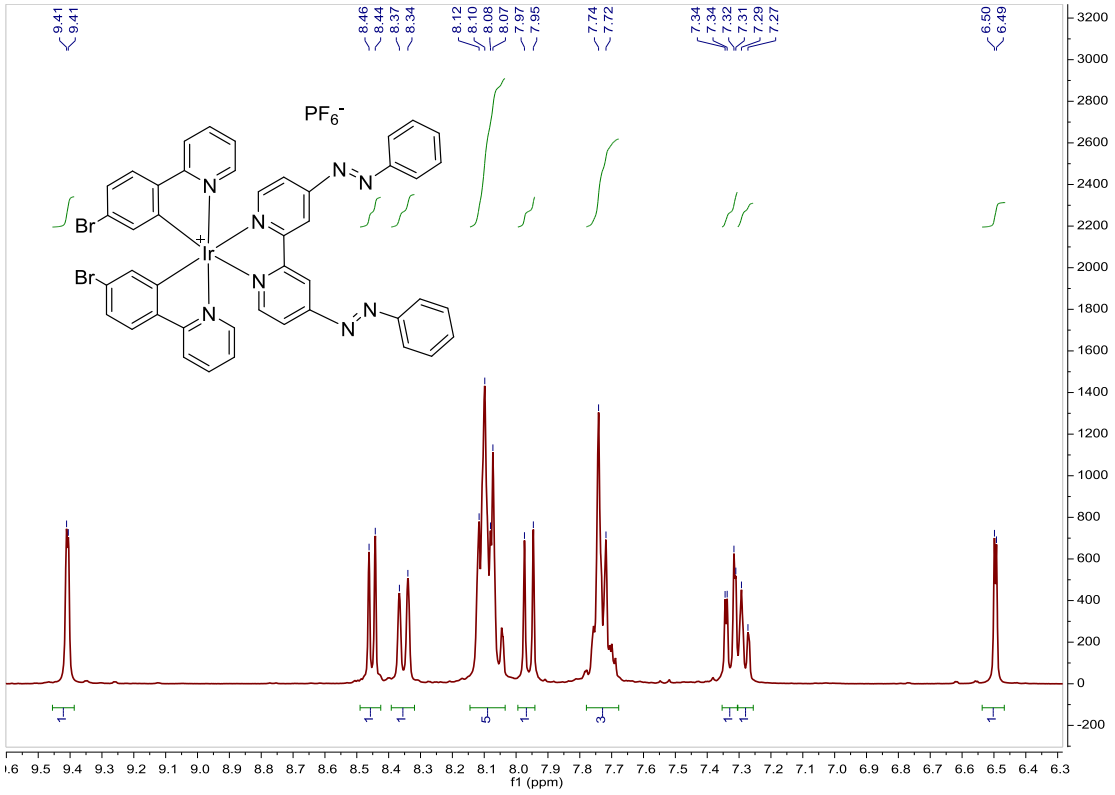

Fig. S171. ^{1}H NMR spectrum of **C1** in acetone-d_6, 300 MHz.

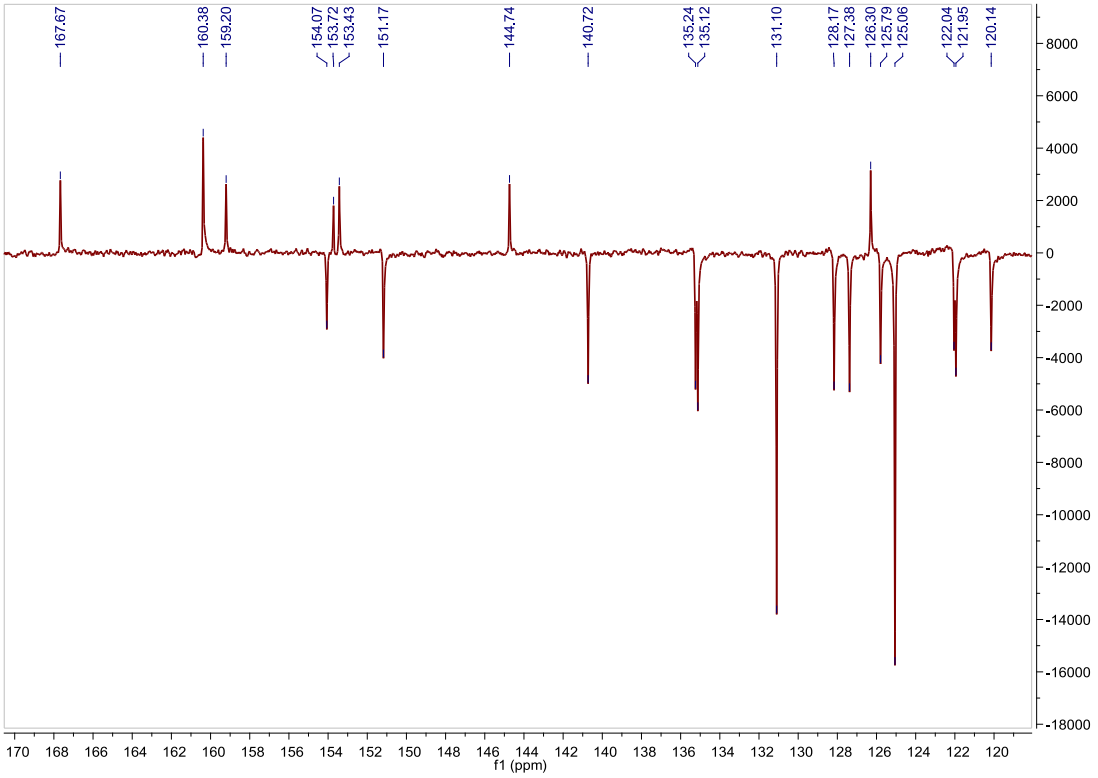

Fig. S172. ^{13}C APT NMR spectrum of **C1** in acetone-d_6, 75 MHz.

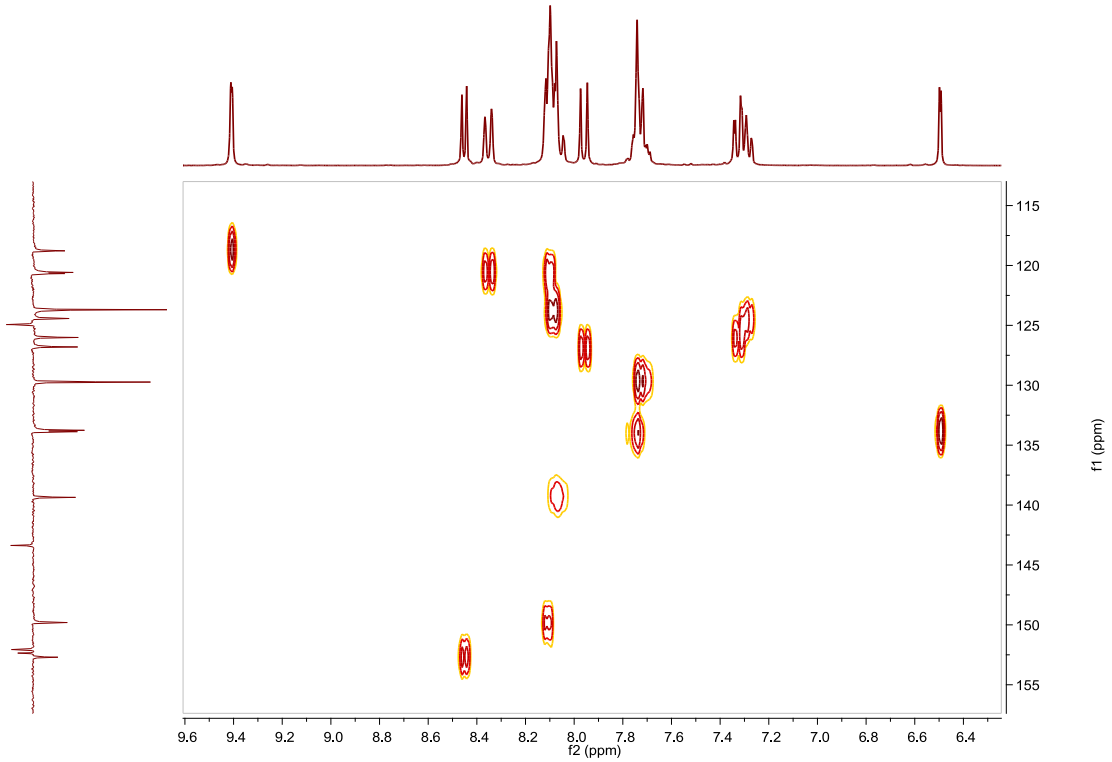

Fig. S173. HSQC NMR spectrum of **C1** in acetone-d_6.

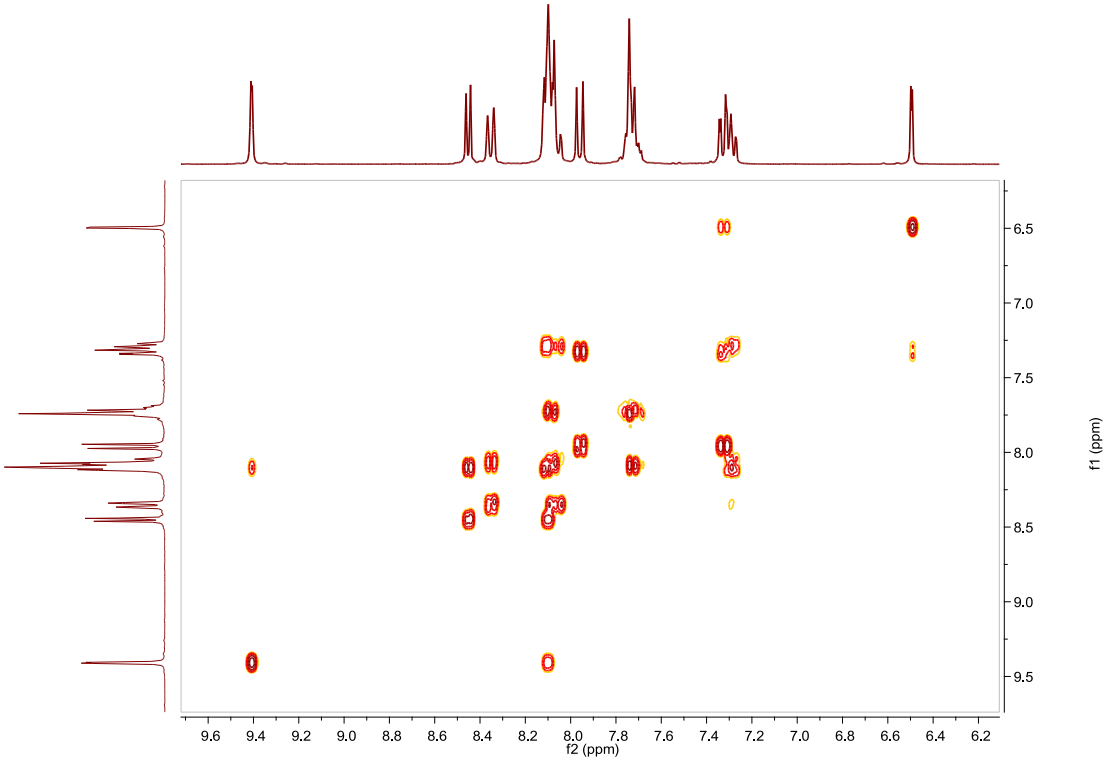

Fig. S174. COSY NMR spectrum of **C1** in acetone-d_6.

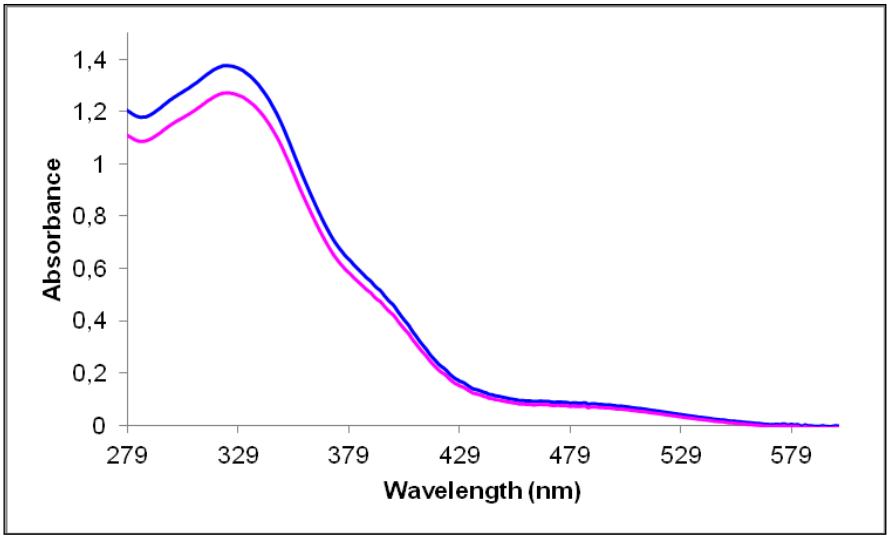

Fig. S175. UV/Vis spectra of **C1** in CH_3CN. Before (blue line) and after (pink line) irradiation at 341nm, $2.60 \cdot 10^{-5}$ M.

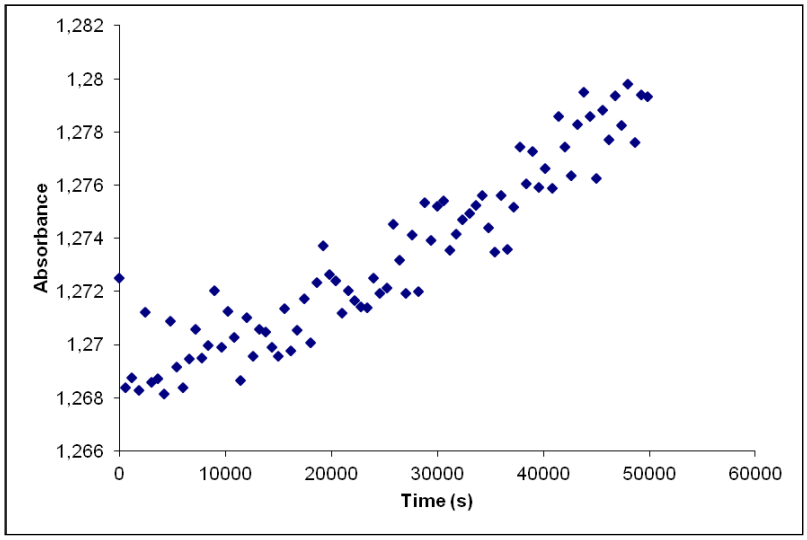

Fig. S176. Cis to trans thermal isomerization kinetics of **C1**. Absorption change of the band 325nm at 328 K in CH_3CN after irradiation at 341 nm. ($2.60 \cdot 10^{-5}$ M).

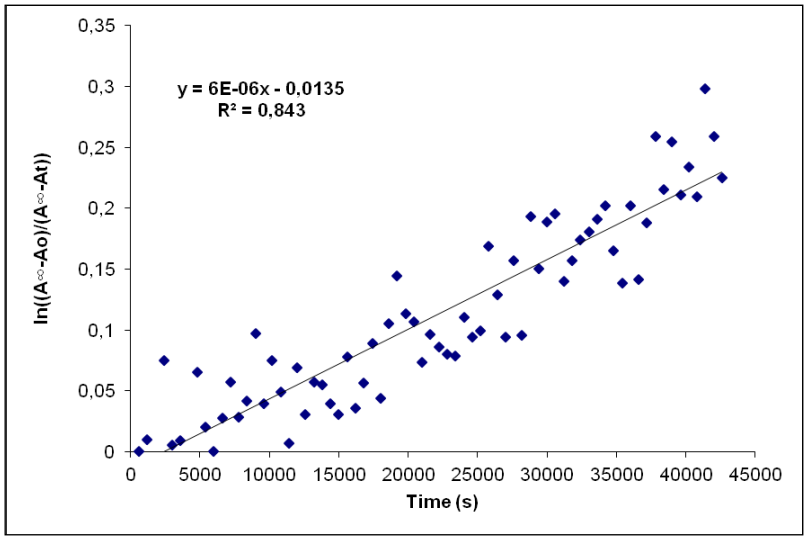

Fig. S177. Cis to trans thermal isomerization kinetics of **C1**. First-order plot. k (s^{-1}) = $6.0 \cdot 10^{-6}$. Half-life (min) = 1925.

Compound D1, [Ir(azoppy)$_2$(1)]PF$_6$. Synthesis, characterization and photoisomerization studies.

SYNTHESIS

Under a N_2 atmosphere, **C1** (0.150 g, 0.128 mmol) and [4-(phenylazo)phenyl]boronic acid **9** (0.07 g, 0.311 mmol) were dissolved in 5 ml of THF. Na_2CO_3 (1 M (aq), 2.5 mL) and $Pd(PPh_3)_4$ (0.0148 g, 0.0128mmol) were added and the solution was degassed by bubbling N_2 for 15 min. The reaction mixture was refluxed (80 °C) for 15 h. The resulting mixture was cooled down to room temperature and the product was extracted with CH_2Cl_2. The organic phase was dried with $MgSO_4$, filtered off and the solvent was evaporated. The residue was purified by column chromatography (silica gel, CH_2Cl_2). To the fraction containing the eluted complex, 0.05 g of KPF_6 were added and the resulting solution was filtered through a celite path. The title compound was obtained as a brown solid. Yield 34%.

Elemental Analysis: calculated for ($C_{68}H_{48}IrN_{12}PF_6 \cdot CH_3COCH_3$): C, 59.70; H, 3.81; N, 11.77. Found: C, 59.87; H, 4.04; N, 11.76.

Exact Mass: ESI-MS $[C_{68}H_{48}IrN_{12}]^+$: calculated: m/z= 1225.3754, found: m/z= 1225.3784.

^{1}H NMR (300 MHz, DMSO-*d*$_6$): δ 9.50 (s, 1H), 8.44 (d, J = 8.2 Hz, 1H), 8.28 (d, J = 5.9 Hz, 1H), 8.18–7.97 (m, 6H), 7.95–7.86 (m, 4H), 7.78–7.69 (m, 3H), 7.61 (brt, J = 6.7 Hz, 5H), 7.51 (d, J = 7.1 Hz, 1H), 7.30 (t, J = 6.4 Hz, 1H), 6.57 (s, 1H).

^{13}C APT NMR (75 MHz, DMSO-*d*$_6$): δ 166.14 (C_{quat}), 158.35 (C_{quat}), 157.42 (C_{quat}), 152.25 (CH), 151.96 (C_{quat}), 151.89 (C_{quat}), 151.05 (C_{quat}), 150.61 (C_{quat}), 149.81 (CH), 144.18 (C_{quat}), 142.96 (C_{quat}), 140.25 (C_{quat}), 139.14 (CH), 133.86 (CH), 131.60 (CH), 129.88 (2CH), 129.49 (2CH), 128.81 (CH), 127.42 (2CH), 125.71 (CH), 124.34 (CH), 123.46 (2CH), 123.19 (2CH), 122.54 (2CH), 122.06 (CH), 121.75 (CH), 120.59 (CH), 119.18 (CH).

UV/Vis (CH_3CN), λ, nm (ε, 10^4 M^{-1} cm^{-1}): 349 (9.3), 425 (2.4).

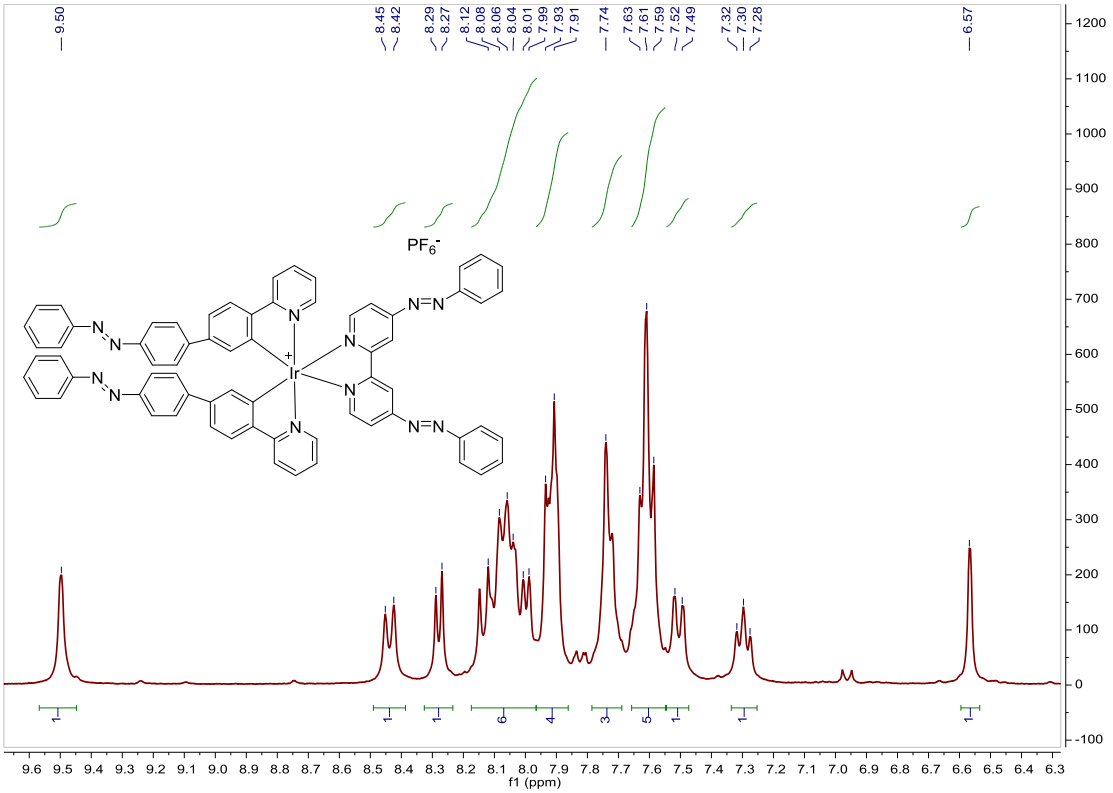

Fig. S178. ^{1}H NMR spectrum of **D1** in DMSO-*d*$_6$, 300 MHz.

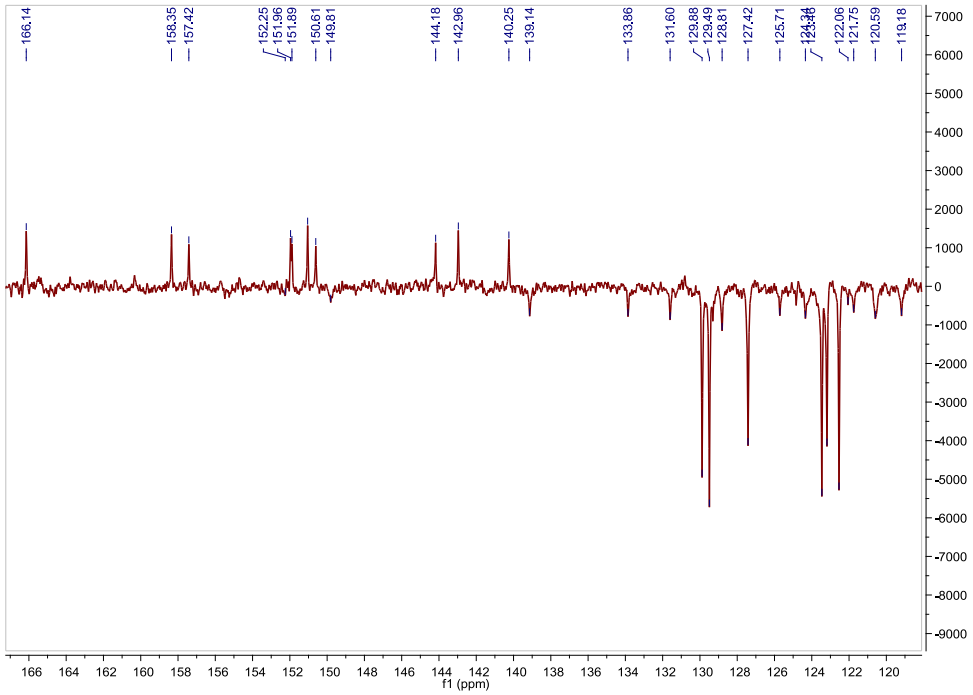

Fig. S179. ^{13}C APT NMR spectrum of **D1** in DMSO-d_6, 75 MHz.

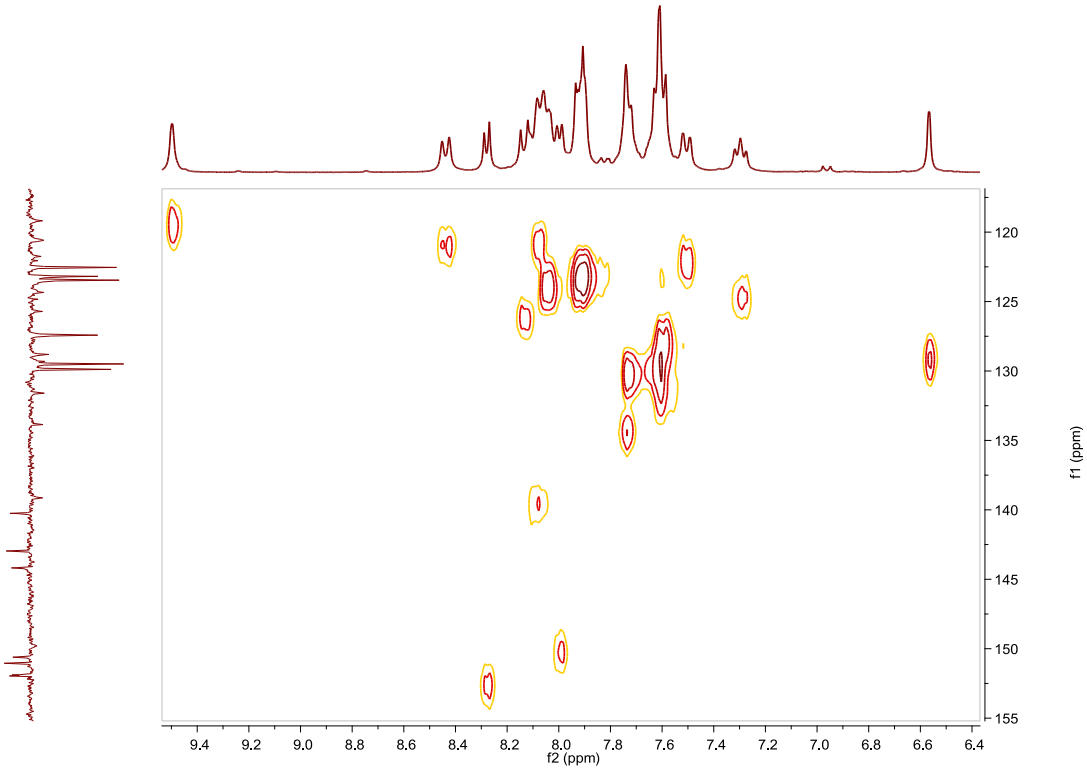

Fig. S180. HSQC NMR spectrum of **D1** in DMSO-d_6.

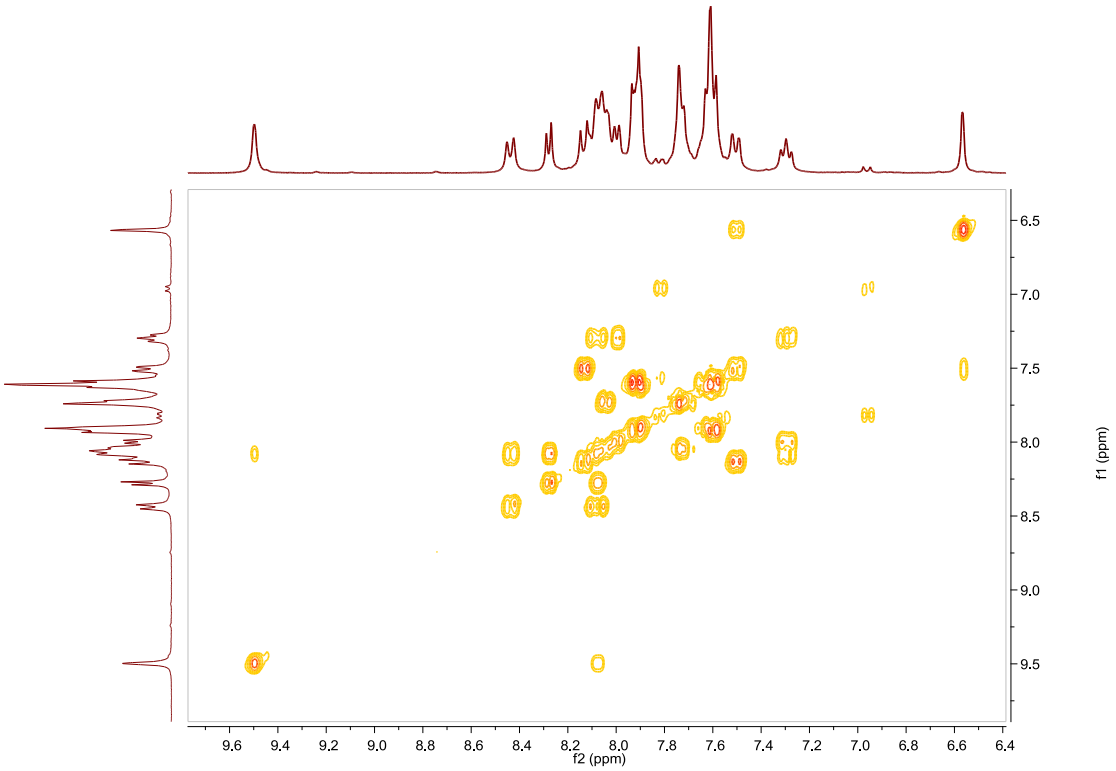

Fig. S181. COSY NMR spectrum of **D1** in DMSO-d_6.

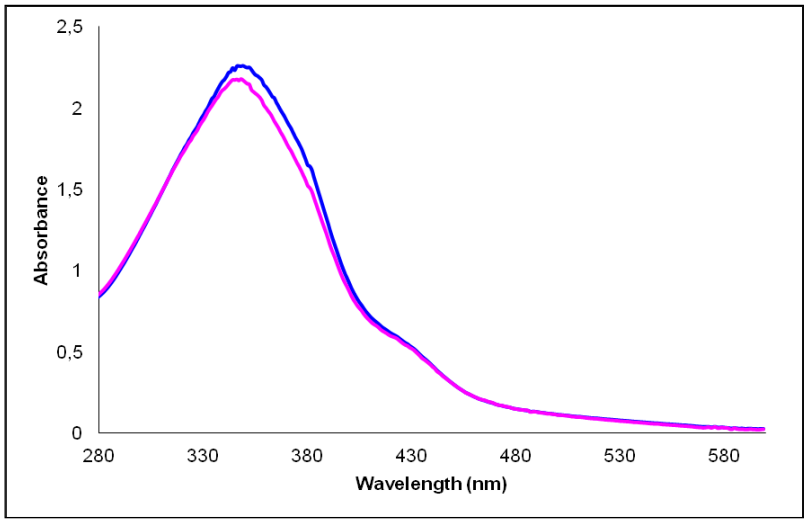

Fig. S182. UV/Vis spectra of **D1** in CH_3CN. Before (blue line) and after (pink line) irradiation at 364nm, $2.44 \cdot 10^{-5}$ M.

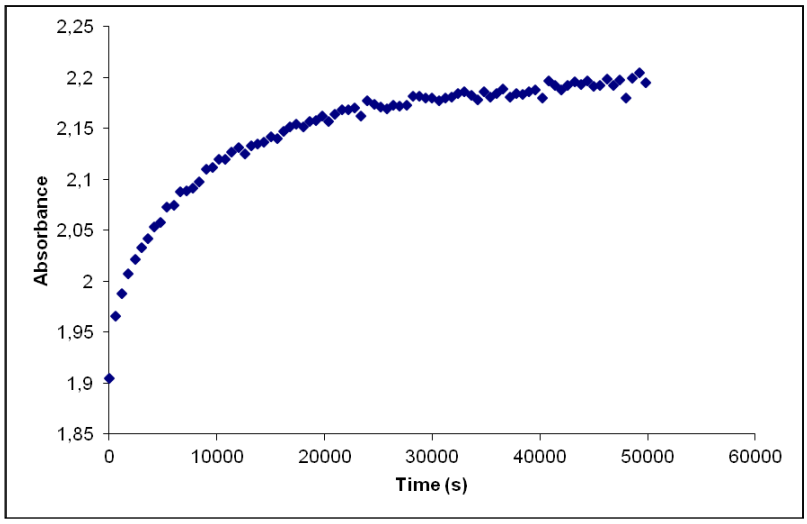

Fig. S183. Cis to trans thermal isomerization kinetics of **D1**. Absorption change of the band 349nm at 328 K in CH_3CN after irradiation at 364 nm. ($2.44 \cdot 10^{-5}$ M).

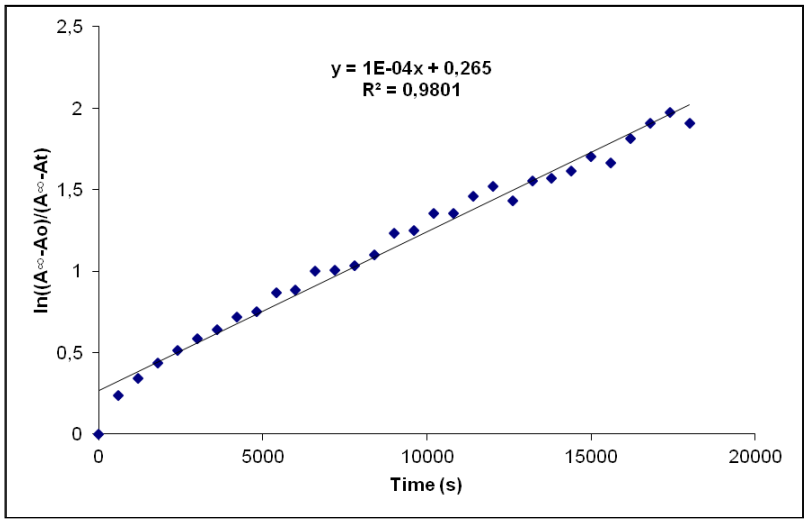

Fig. S184. Cis to trans thermal isomerization kinetics of **D1**. First-order plot. k (s^{-1}) = $1.0 \cdot 10^{-4}$. Half-life (min) = 115.

Compound A2, $[Ir(ppy)_2(2)_2]PF_6$. Synthesis, characterization and photoisomerization studies.

SYNTHESIS

Under a N_2 atmosphere, $[Ir(ppy)_2Cl]_2$ (0.100 g, 0.093 mmol) were dissolved in 8 ml of acetone and AgOTf (0.111 g, 0.432 mmol) were added. The mixture was heated to 56 °C for 2 h and after cooled down to room temperature, AgCl was removed by centrifugation. The resulting solution was added over a 1 h refluxed suspension of **L2** (0.068 g, 0.373 mmol) in 4 ml of acetone and 105 µl of NEt_3. The reaction mixture was refluxed, under N_2, for 15 h. After solvent evaporation the product was purified by column chromatography (silica gel, CH_2Cl_2). When the unreacted $[Ir(ppy)_2Cl]_2$ eluted, 0.05 g of KPF_6 were added on top of the column and the polarity of the eluent was gradually increased to 100% acetone to elute $[Ir(ppy)_2$(**L2**)$]PF_6$ together with the excess of KPF_6. The desired compound was precipitated with ether after filtration through a celite path in CH_2Cl_2 and it was obtained as an orange solid. Yield 50%.

Elemental Analysis: calculated for ($C_{44}H_{34}IrN_8PF_6$): C, 52.22; H, 3.39; N, 11.07. Found: C, 52.4; H, 2.95; N, 11.33.

Exact Mass: ESI-MS $[C_{44}H_{34}IrN_8]^+$: calculated: m/z= 867.2512, found: m/z= 867.2520.

^{1}H NMR (300 MHz, acetone-d_6): δ 9.11 (d, J = 5.3 Hz, 1H), 9.07 (brd, J = 6.8 Hz, 2H), 8.20 (d, J = 7.6 Hz, 1H), 8.12 (ddd, J = 1.4 Hz, J = 7.4 Hz, J = 8.7 Hz, 1H), 7.99 (brdd, J = 1.4 Hz, J = 8.1 Hz, 2H), 7.86 (brd, J = 6.7 Hz, 2H), 7.75 (m, 1H), 7.68 (m, 3H), 7.59 (ddd, J = 1.5 Hz, J = 5.9 Hz, J = 7.4 Hz, 1H), 6.97 (m, 2H), 6.51 (m, 1H).

^{13}C APT NMR (75 MHz, acetone-d_6): δ 169.33 (C_{quat}), 159.03 (C_{quat}), 155.47 (2CH), 153.76 (C_{quat}), 150.88 (CH), 149.03 (C_{quat}), 145.58 (C_{quat}), 140.42 (CH), 134.85 (CH), 133.40 (CH), 131.72 (CH), 130.97 (2CH), 125.81 (CH), 125.18 (CH), 124.80 (2CH), 124.05 (CH), 121.18 (CH), 120.10 (2CH).

UV/Vis (CH_3CN), λ, nm (ε, 10^4 M^{-1} cm^{-1}): 312 (4.7), 460 (0.37).

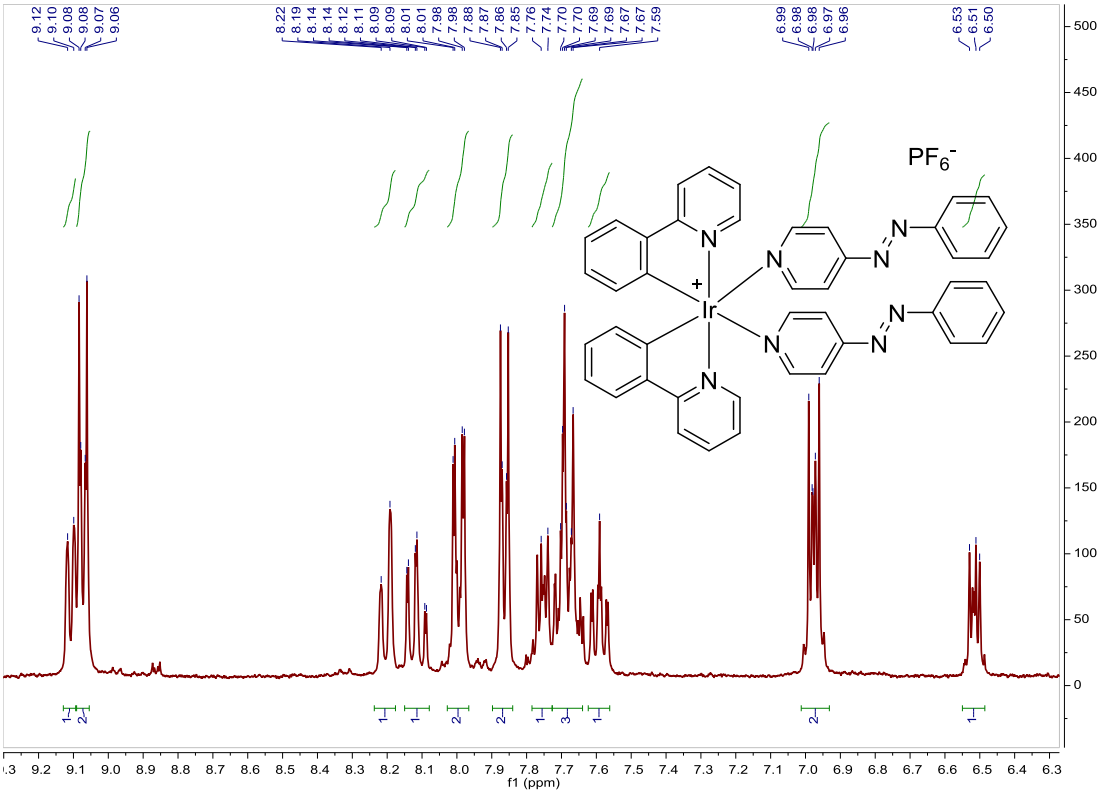

Fig. S185. ^{1}H NMR spectrum of **A2** in acetone-d_6, 300 MHz.

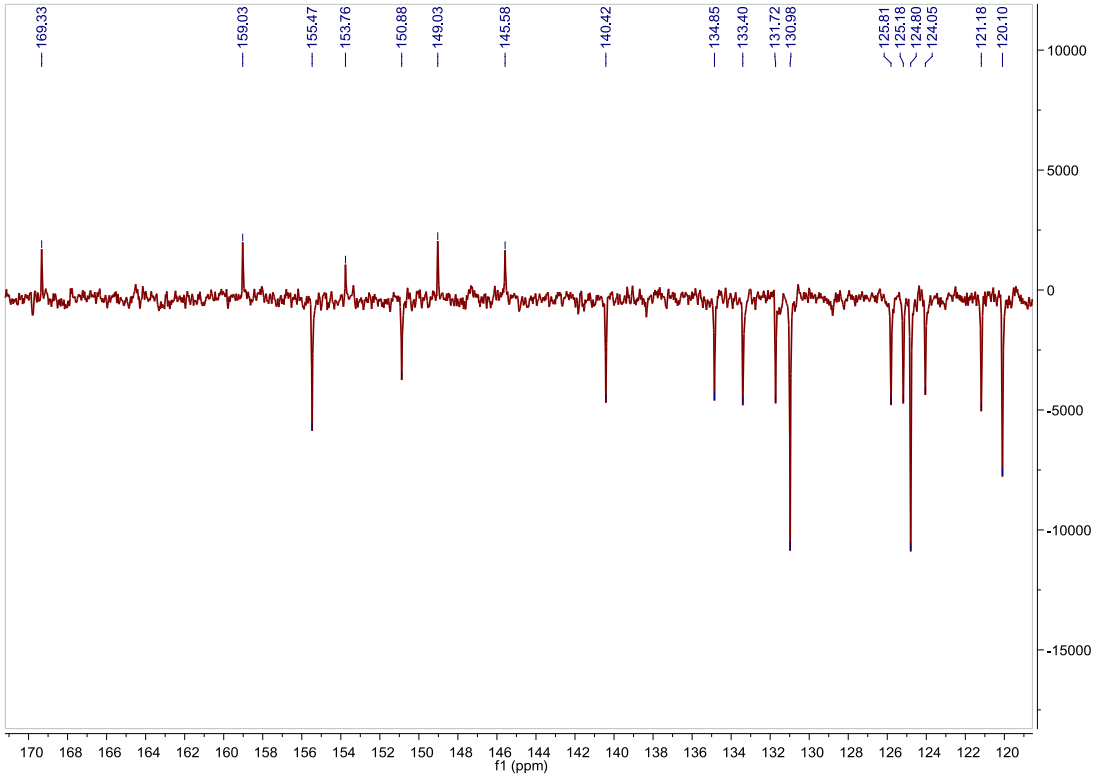

Fig. S186. ^{13}C APT NMR spectrum of **A2** in acetone-d_6, 75 MHz.

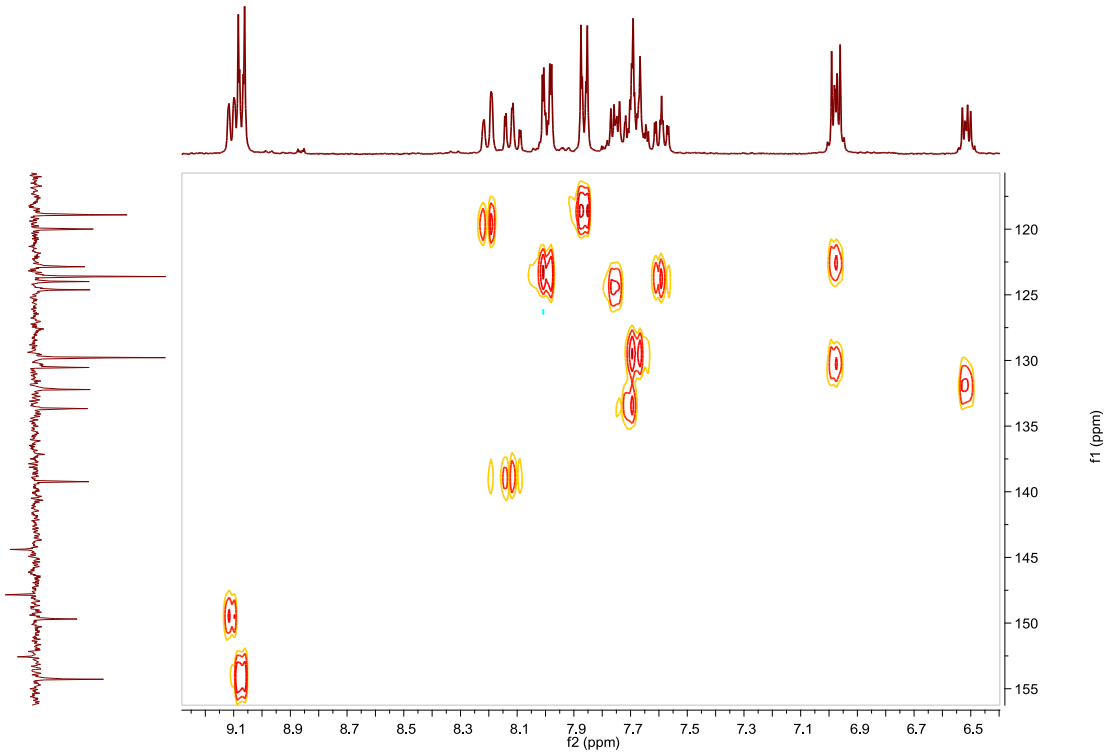

Fig. S187. HSQC NMR spectrum of **A2** in acetone-d_6.

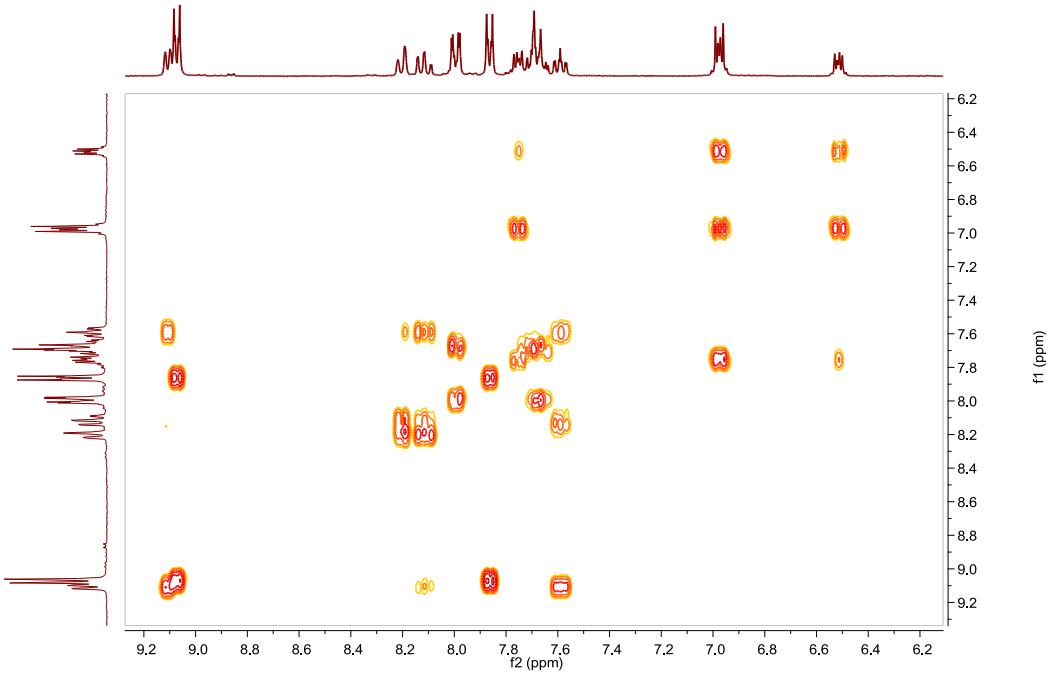

Fig. S188. COSY NMR spectrum of **A2** in acetone-d_6.

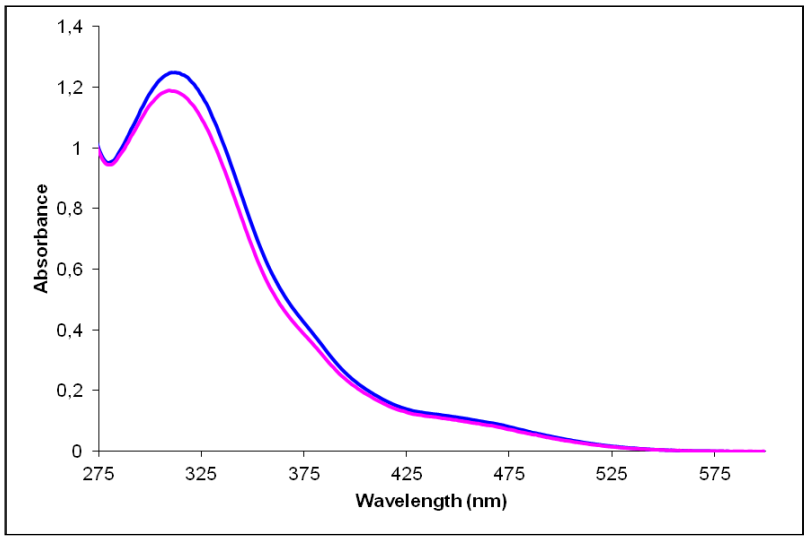

Fig. S189. UV/Vis spectra of **A2** in CH_3CN. Before (blue line) and after (pink line) irradiation at 327nm, $2.65 \cdot 10^{-5}$ M.

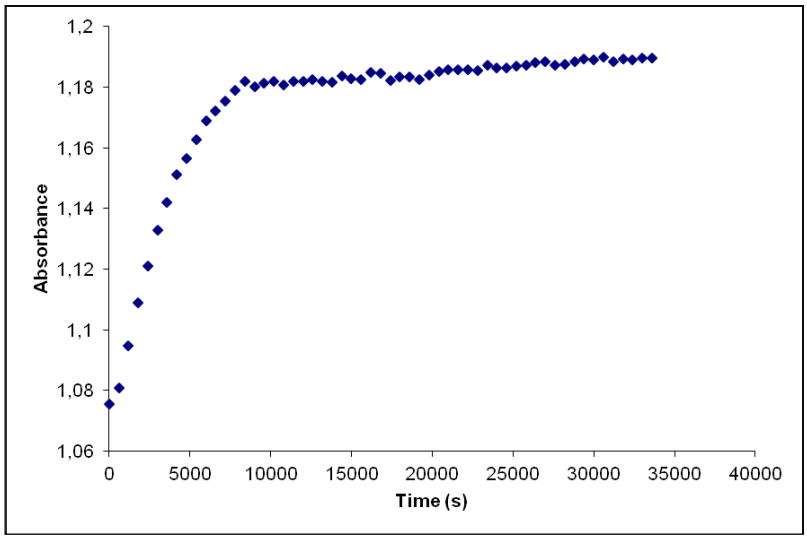

Fig. S190. Cis to trans thermal isomerization kinetics of **A2**. Absorption change of the band 312nm at 328 K in CH_3CN after irradiation at 327 nm. ($2.65 \cdot 10^{-5}$ M).

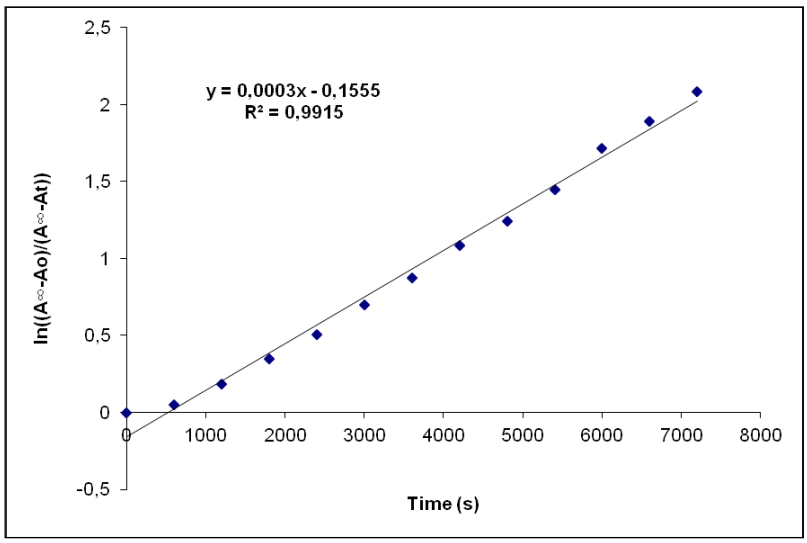

Fig. S191. Cis to trans thermal isomerization kinetics of **A2**. First-order plot. k (s^{-1}) = $3.0 \cdot 10^{-4}$. Half-life (min) = 38.

Compound B2', [Ir(Fppy)$_2$(2)]. Synthesis and characterization.

SYNTHESIS

Under a N_2 atmosphere, $[Ir(Fppy)_2Cl]_2$ (0.100 g, 0.082 mmol) were added over a suspension of **L2** (0.03 g, 0.164 mmol) in 8 ml CH_2Cl_2/MeOH 2/1. The reaction mixture was refluxed, under N_2, for 15 h. After solvent evaporation the product was purified by column chromatography (silica gel, 100% CH_2Cl_2 to 100% acetone). The product was obtained as an orange solid. Yield 87%.

Elemental Analysis: calculated for ($C_{33}H_{20}F_4IrN_5 \cdot CH_2Cl_2$): C, 48.63; H, 2.64; N, 8.34. Found: C, 48.97 ; H, 2.87 ; N, 8.21 .

Exact Mass: ESI-MS $[C_{33}H_{20}F_4IrN_5+H]^+$: calculated: m/z=756.1362 , found: m/z=756.1362.

^{1}H NMR (300 MHz, $CDCl_3$): δ 9.84 (dd, J = 1.0 Hz, J = 5.8 Hz, 1H), 8.24 (d, J = 8.5 Hz, 1H), 8.07 (d, J = 8.3 Hz, 1H), 8.00 (d, J = 5.7 Hz, 1H), 7.83 (dd, J = 1.6 Hz, J = 7.4 Hz, 2H), 7.75–7.62 (m, 2H), 7.56 (m, 2H), 7.50–7.38 (m, 4H), 7.17 (t, J = 6.3 Hz, 1H), 6.98 (ddd, J = 1.0 Hz, J = 5.8 Hz, J = 7.4 Hz, 1H), 6.34 (ddd, J = 2.4 Hz, J = 9.1 Hz, J = 11.8 Hz, 1H), 6.25 (ddd, J = 2.3 Hz, J = 9.3 Hz, J = 12.4 Hz, 1H), 5.73 (dd, J = 2.4 Hz, J = 8.6 Hz, 1H), 5.52 (dd, J = 2.4 Hz, J = 8.7 Hz, 1H).

^{13}C APT NMR (75 MHz, $CDCl_3$): δ 165.17 (d, J = 7.6 Hz, C_{quat}), 164.51 (d, J = 6.1 Hz, C_{quat}), 163.61 (dd, J = 12.9 Hz, J = 256.9 Hz, C_{quat}), 162.77 (dd, J = 12.6 Hz, J = 258.4 Hz, C_{quat}), 161.02 (dd, J = 12.9 Hz, J = 260.7 Hz, C_{quat}), 160.76 (dd, J = 12.9 Hz, J = 259.9 Hz, C_{quat}), 156.97 (s, 2C_{quat}), 154.13 (d, J = 6.8 Hz, C_{quat}), 152.26 (s, C_{quat}), 151.12 (d, J = 6.8 Hz, C_{quat}), 150.93 (s, CH), 148.86 (s, CH), 138.06 (s, CH), 137.69 (s, CH), 133.19 (s, CH), 129.37 (s, 3CH), 127.92 (s, C_{quat}), 127.79 (s, C_{quat}), 123.64 (s, 2CH), 123.36 (d, J = 20.5 Hz, CH), 122.51 (s, CH), 122.47 (d, J = 19.8 Hz, CH), 122.05 (s, CH), 118.15 (s, 2CH), 114.07 (d, J = 17.5 Hz, CH), 113.53 (d, J = 17.5 Hz, CH), 97.90 (t, J = 27.0 Hz, 2CH).

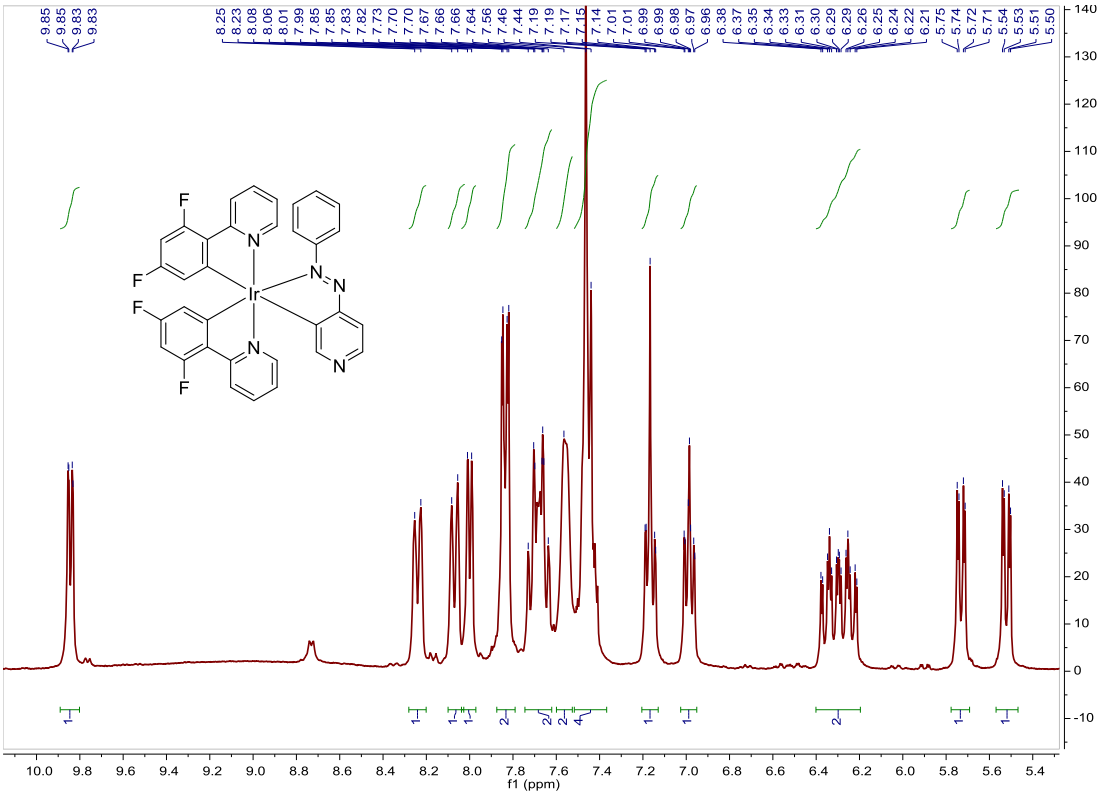

Fig. S192. ^{1}H NMR spectrum of **B2'** in $CDCl_3$, 300 MHz.

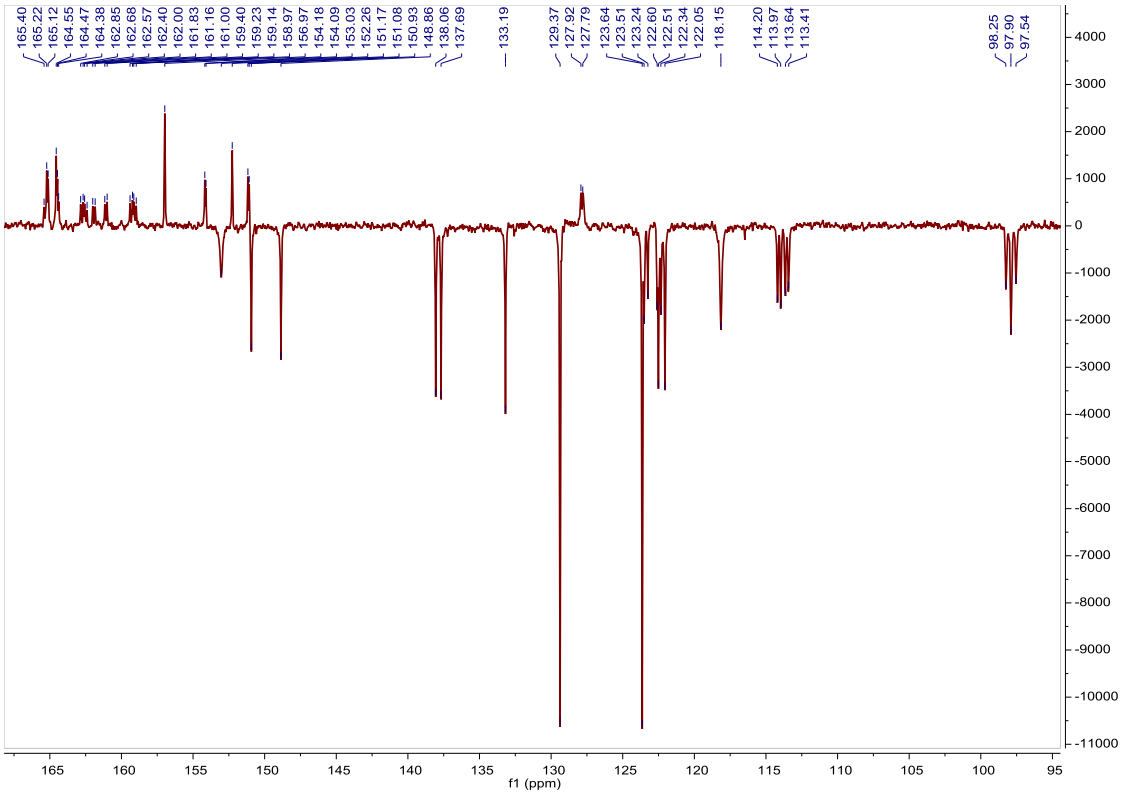

Fig. S193. ^{13}C APT NMR spectrum of **B2'** in $CDCl_3$, 75 MHz.

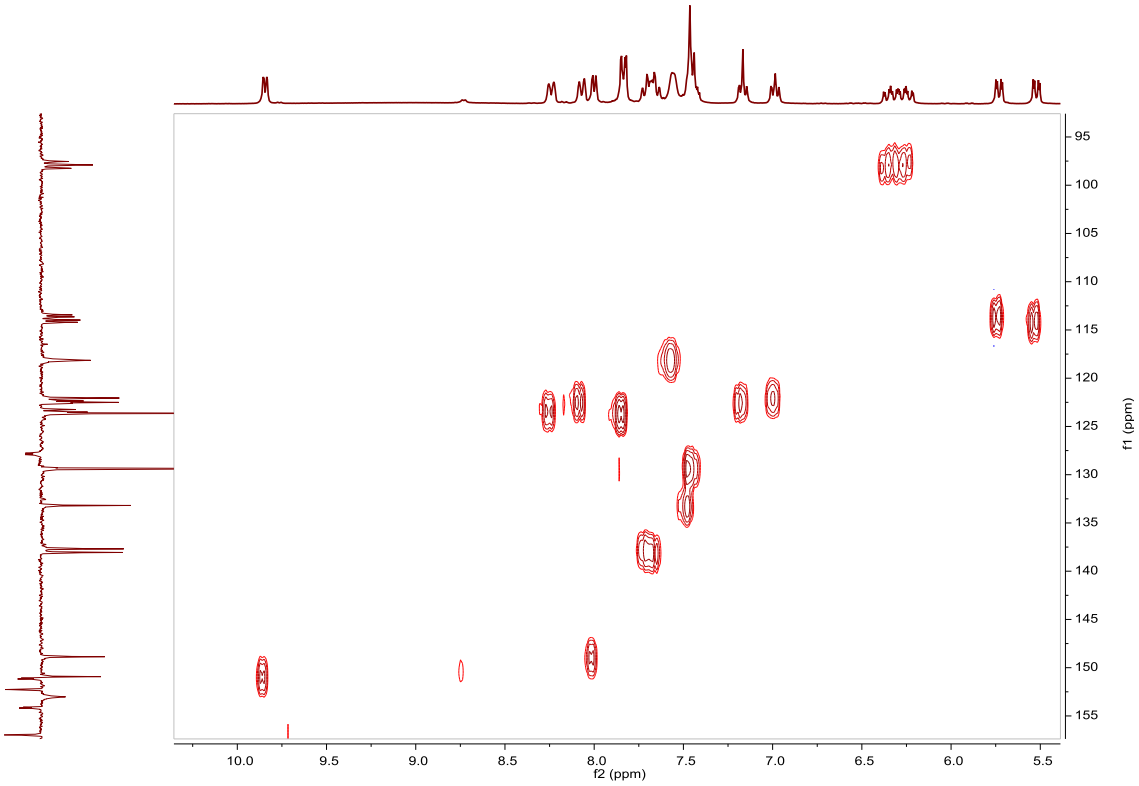

Fig. S194. HSQC NMR spectrum of **B2'** in $CDCl_3$.

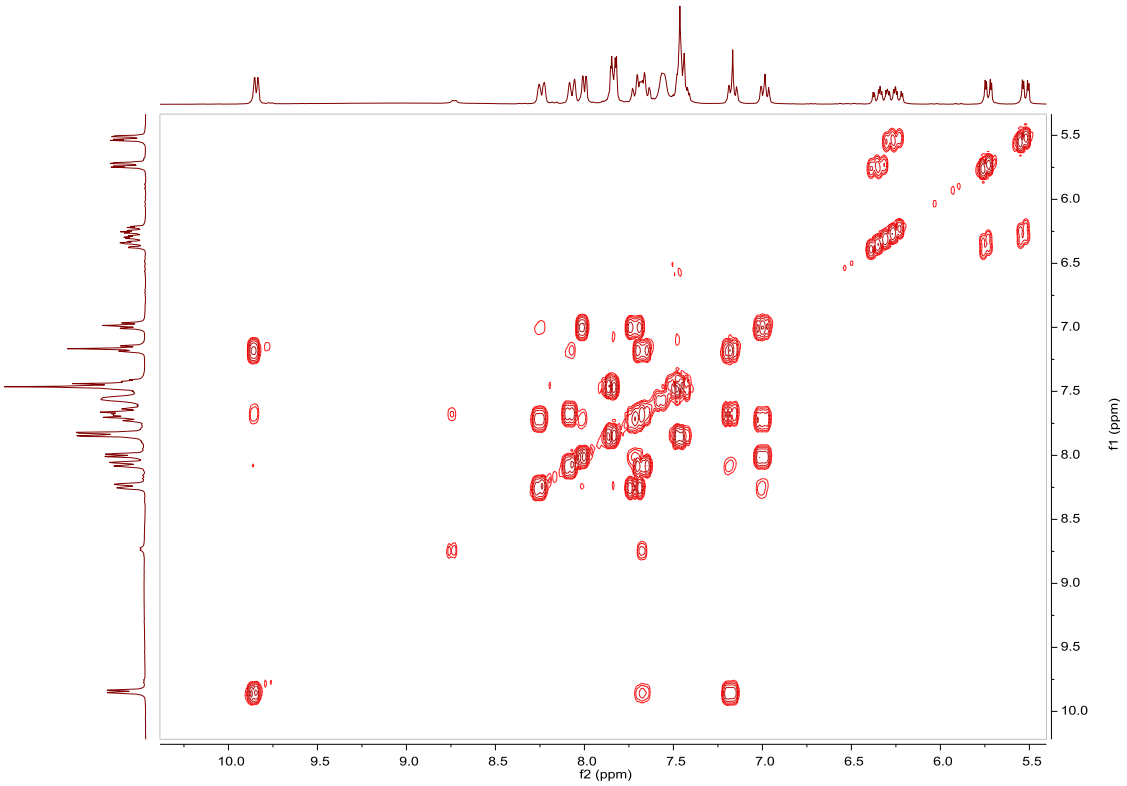

Fig. S195. COSY NMR spectrum of **B2'** in $CDCl_3$.

Compound B2, $[Ir(Fppy)_2(2)_2]PF_6$. Synthesis, characterization and photoisomerization studies.

SYNTHESIS

Under a N_2 atmosphere, $[Ir(Fppy)_2Cl]_2$ (0.150 g, 0.1234 mmol) were dissolved in 11 ml of acetone and AgOTf (0.111 g, 0.432 mmol) were added. The mixture was heated to 56 °C for 2 h and after cooled down to room temperature, AgCl was removed by centrifugation. The resulting solution was added over a 1 h refluxed suspension of **L2** (0.100 g, 0.4936 mmol) in 5 ml of acetone and 140 µl of NEt_3. The reaction mixture was refluxed, under N_2, for 15 h. After solvent evaporation the product was purified by column chromatography (silica gel, CH_2Cl_2). When the unreacted $[Ir(Fppy)_2Cl]_2$ eluted, 0.075 g of KPF_6 were added on top of the column and the polarity of the eluent was gradually increased to 100% acetone to elute $[Ir(Fppy)_2(\mathbf{L2})]PF_6$ together with the excess of KPF_6. The desired compound was precipitated with ether after filtration through a celite path in CH_2Cl_2 and it was obtained as an orange solid. Yield 48%.

Elemental Analysis: calculated for ($C_{44}H_{30}F_4IrN_8PF_6 \cdot CH_3COCH_3$): C, 49.43; H, 3.18; N, 9.81. Found: C, 49.71; H, 3.02; N, 10.16.

Exact Mass: ESI-MS $[C_{44}H_{30}F_4IrN_8]^+$: calculated: m/z= 939.2159, found: m/z= 939.2178.

^{1}H NMR (300 MHz, acetone-d_6): δ 9.22 (d, J = 5.5 Hz, 1H), 9.09 (brd, J = 6.7 Hz, 2H), 8.36 (d, J = 8.4 Hz, 1H), 8.22 (t, J = 7.8 Hz, 1H), 8.00 (brdd, J = 1.6 Hz, J = 8.3 Hz, 2H), 7.91 (brd, J = 6.7 Hz, 2H), 7.68 (m, 4H), 6.71 (ddd, J = 2.3 Hz, J = 9.3 Hz, J = 12.6 Hz, 1H), 6.01 (dd, J = 2.3 Hz, J = 8.5 Hz, 1H).

^{13}C APT NMR (75 MHz, acetone-d_6): δ 165.32 (d, J = 7.1 Hz, C_{quat}), 164.57 (dd, J = 12.4 Hz, J = 254.2 Hz, C_{quat}), 162.06 (dd, J = 13.6 Hz, J = 257.5 Hz, C_{quat}), 159.31 (s, C_{quat}), 155.55 (s, 2CH), 153.76 (s, C_{quat}), 153.31 (d, J = 6.6 Hz, C_{quat}), 151.67 (s, CH), 141.53 (s, CH), 134.93 (s, CH), 130.98 (s, 2CH), 129.41 (s, C_{quat}), 125.80 (s, CH), 124.90 (d, J = 20.5 Hz, CH), 124.85 (s, 2CH), 120.49 (s, 2CH), 115.82 (d, J = 18.0 Hz, CH), 100.32 (t, J = 27.1 Hz, CH).

UV/Vis (CH_3CN), λ, nm (ε, 10^4 M^{-1} cm^{-1}): 318 (4.8), 433 (0.37).

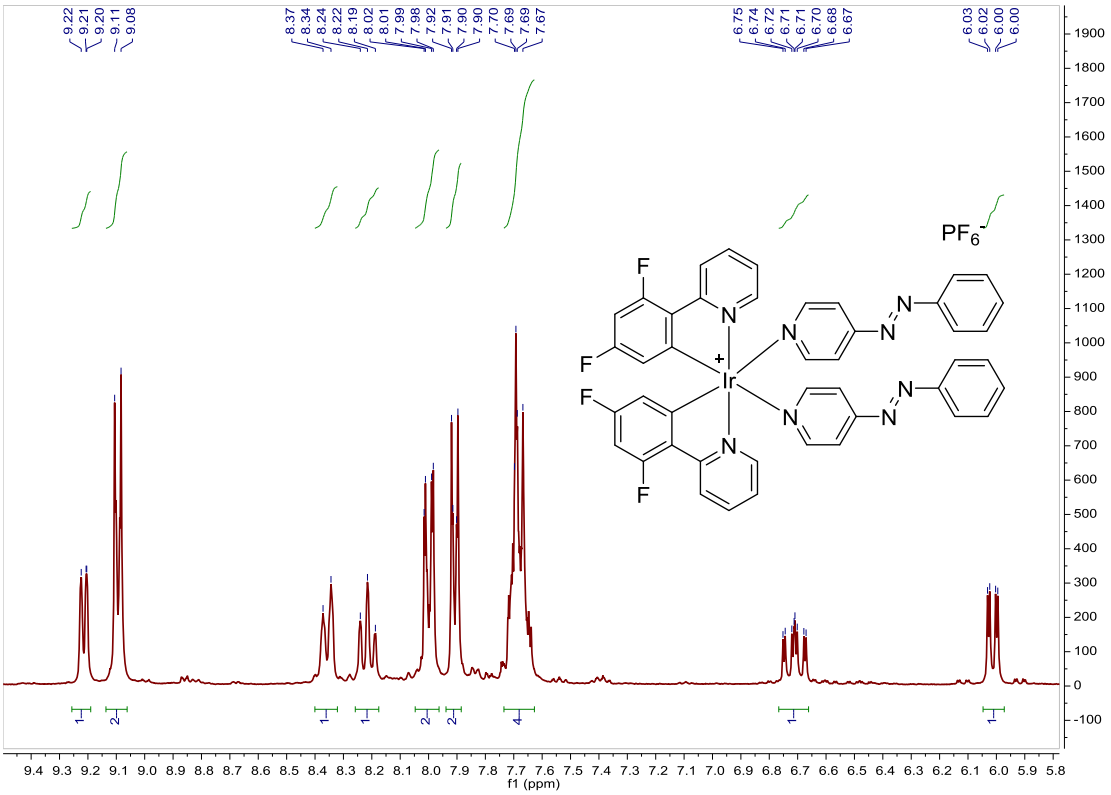

Fig. S196. ^{1}H NMR spectrum of **B2** in acetone-d_6, 300 MHz.

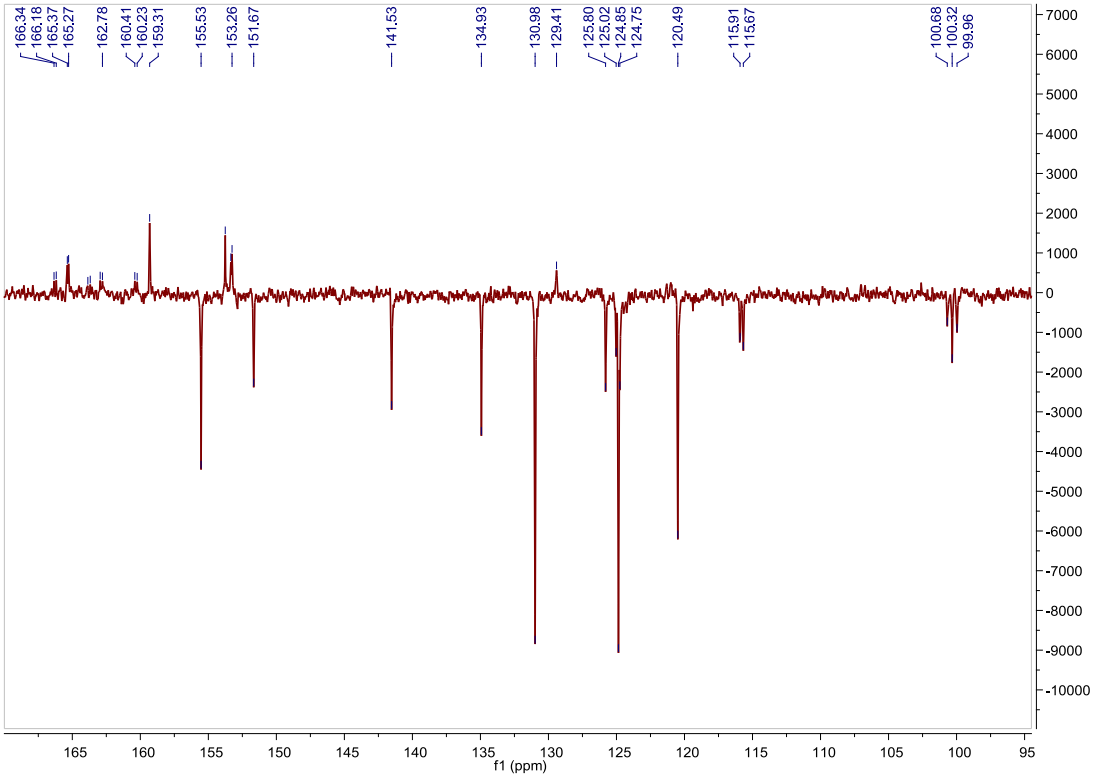

Fig. S197. ^{13}C APT NMR spectrum of **B2** in acetone-d_6, 75 MHz.

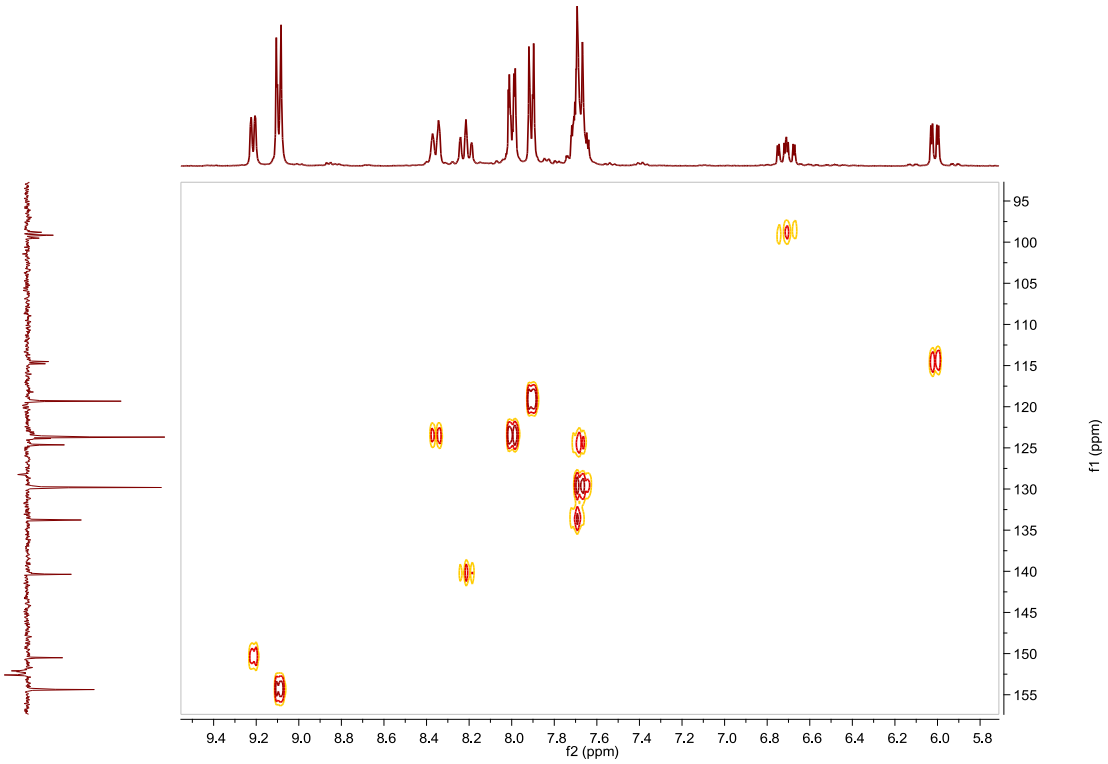

Fig. S198. HSQC NMR spectrum of **B2** in acetone-d_6.

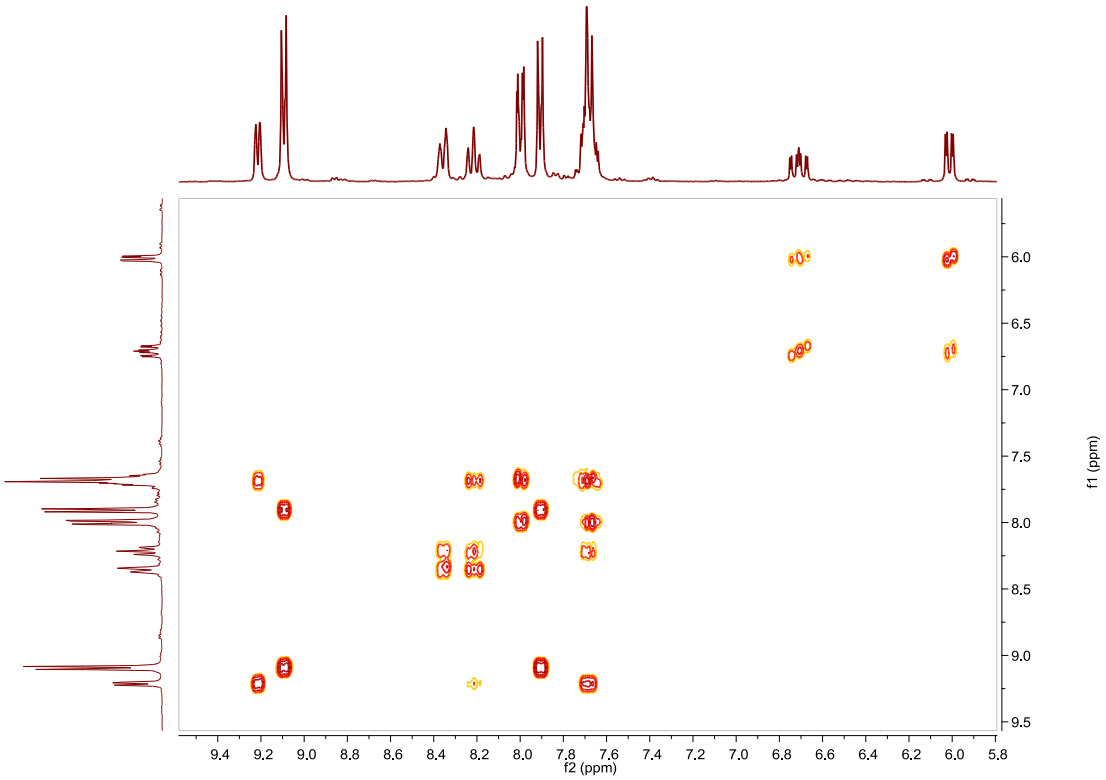

Fig. S199. COSY NMR spectrum of **B2** in acetone-d_6.

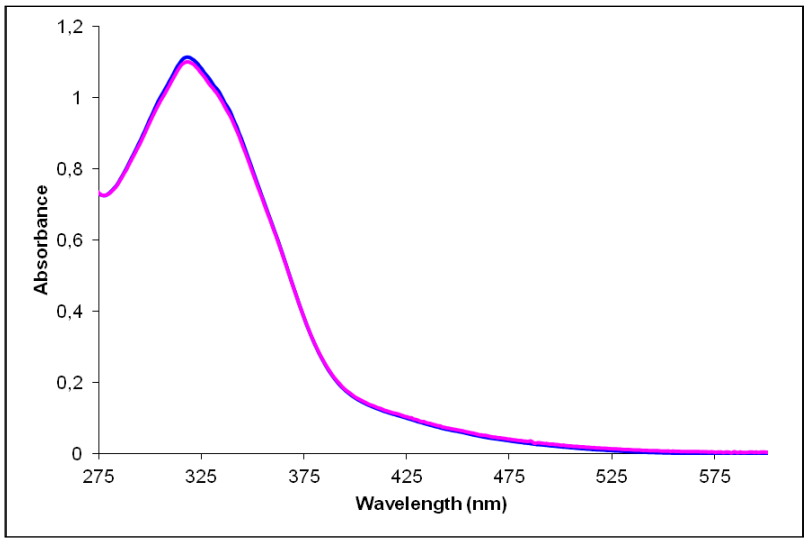

Fig. S200. UV/Vis spectra of **B2** in CH_3CN. Before (blue line) and after (pink line) irradiation at 328nm, $2.32 \cdot 10^{-5}$ M.

Cis to trans thermal isomerization kinetics. Due to the small degree of photoisomerization, it has been not possible to calculate k.

Compound C2, $[Ir(Brppy)_2(2)_2]PF_6$. Synthesis, characterization and photoisomerization studies.

SYNTHESIS

Under a N_2 atmosphere, $[Ir(Brppy)_2Cl]_2$ (0.100 g, 0.072 mmol) were dissolved in 8 ml of acetone and AgOTf (0.085 g, 0.334 mmol) were added. The mixture was heated to 56 °C for 2 h and after cooled down to room temperature, AgCl was removed by centrifugation. The resulting solution was added over a 1 h refluxed suspension of **L2** (0.053 g, 0.288 mmol) in 4 ml of acetone and 80 µl of NEt_3. The reaction mixture was refluxed, under N_2, for 15 h. After solvent evaporation the product was purified by column chromatography (silica gel, CH_2Cl_2). When the unreacted $[Ir(Brppy)_2Cl]_2$ eluted, 0.05 g of KPF_6 were added on top of the column and the polarity of the eluent was gradually increased to 100% acetone to elute $[Ir(Brppy)_2(\mathbf{L2})]PF_6$ together with the excess of KPF_6. The desired compound was precipitated with ether after filtration through a celite path in CH_2Cl_2 and it was obtained as a dark orange solid. Yield 48%.

Elemental Analysis: calculated for ($C_{44}H_{32}Br_2IrN_8PF_6$): C, 45.18; H, 2.76; N, 9.58. Found: C, 45.13; H, 2.68; N, 9.35.

Exact Mass: ESI-MS $[C_{44}H_{32}Br_2IrN_8]^+$: calculated: m/z= 1023.0746, found: m/z= 1023.0744.

^{1}H NMR (300 MHz, acetone-d_6): δ 9.14 (d, J = 5.8 Hz, 1H), 9.09 (brd, J = 6.7 Hz, 2H), 8.25 (d, J = 8.2 Hz, 1H), 8.17 (ddd, J = 1.4 Hz, J = 7.4 Hz, J = 8.7 Hz, 1H), 8.00 (brdd, J = 1.4 Hz, J = 7.9 Hz, 2H), 7.89 (brd, J = 6.7 Hz, 2H), 7.75 (d, J = 8.4 Hz, 1H), 7.72–7.63 (m, 4H), 7.20 (dd, J = 1.9 Hz, J = 8.3 Hz, 1H), 6.59 (d, J = 1.9 Hz, 1H).

^{13}C APT NMR (75 MHz, acetone-d_6): δ 168.01 ($2C_{quat}$), 159.22 (C_{quat}), 155.57 (2CH), 153.75 (C_{quat}), 151.25 (CH), 151.12 (C_{quat}), 144.86 (C_{quat}), 140.97 (CH), 135.54 (CH), 134.92 (CH), 130.98 (2CH), 127.58 (CH), 127.38 (CH), 125.93 (CH), 124.85 (2CH), 121.76 (CH), 120.37 (2CH).

UV/Vis (CH_3CN), λ, nm (ε, 10^4 M^{-1} cm^{-1}): 315 (5.2), 446 (0.43).

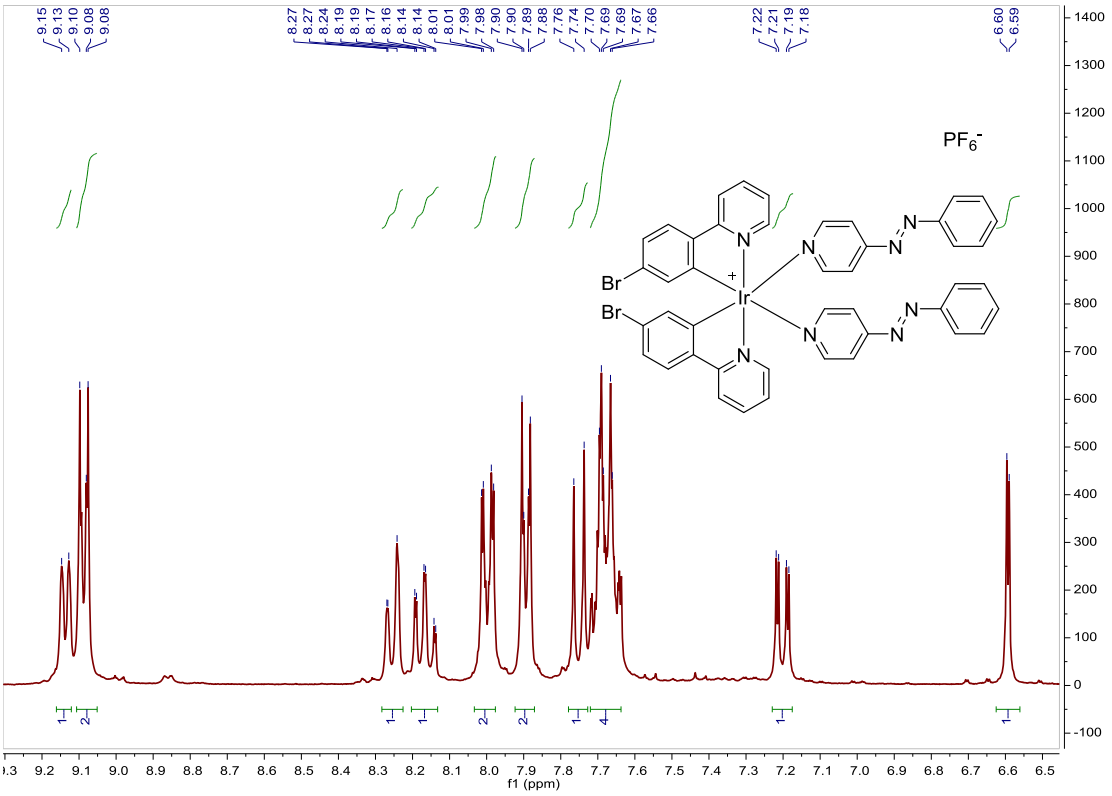

Fig. S201. ^{1}H NMR spectrum of **C2** in acetone-d_6, 300 MHz.

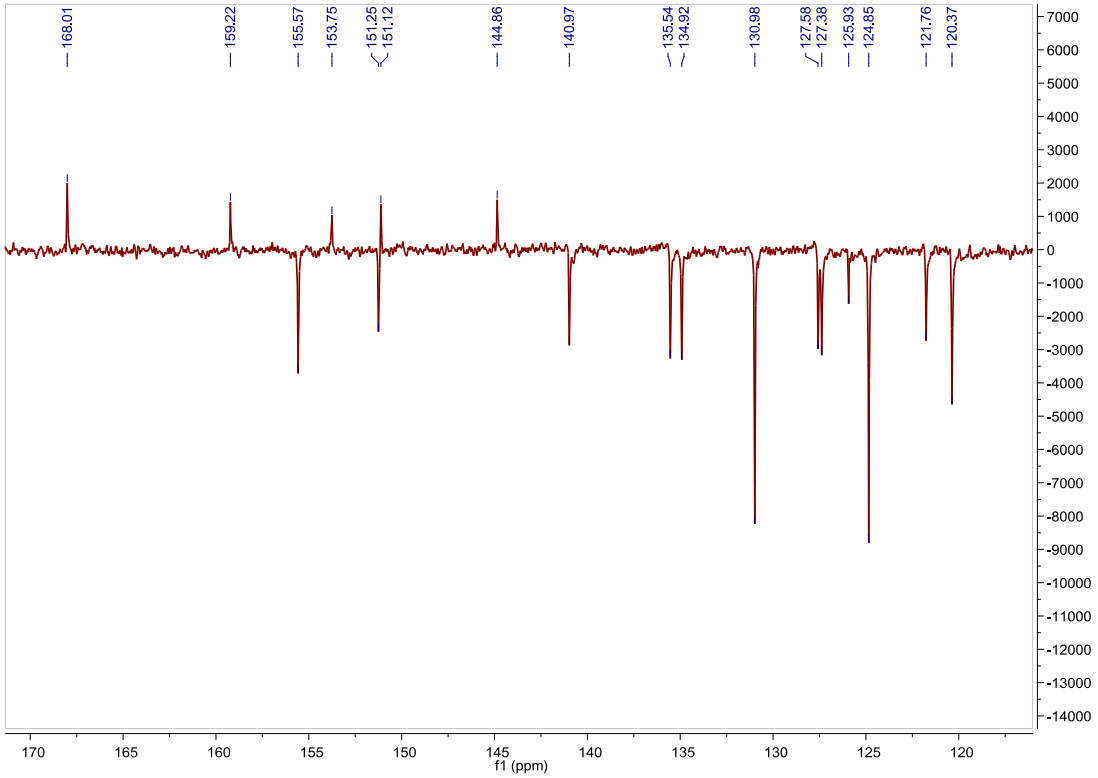

Fig. S202. ^{13}C APT NMR spectrum of **C2** in acetone-d_6, 75 MHz.

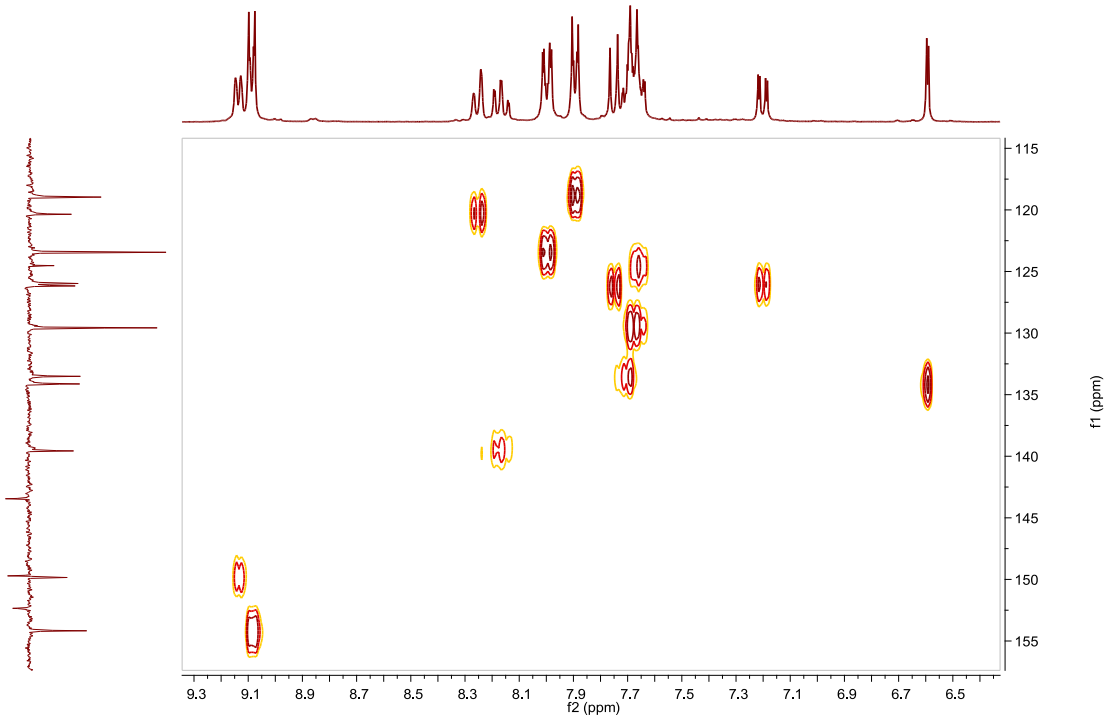

Fig. S203. HSQC NMR spectrum of **C2** in acetone-d_6.

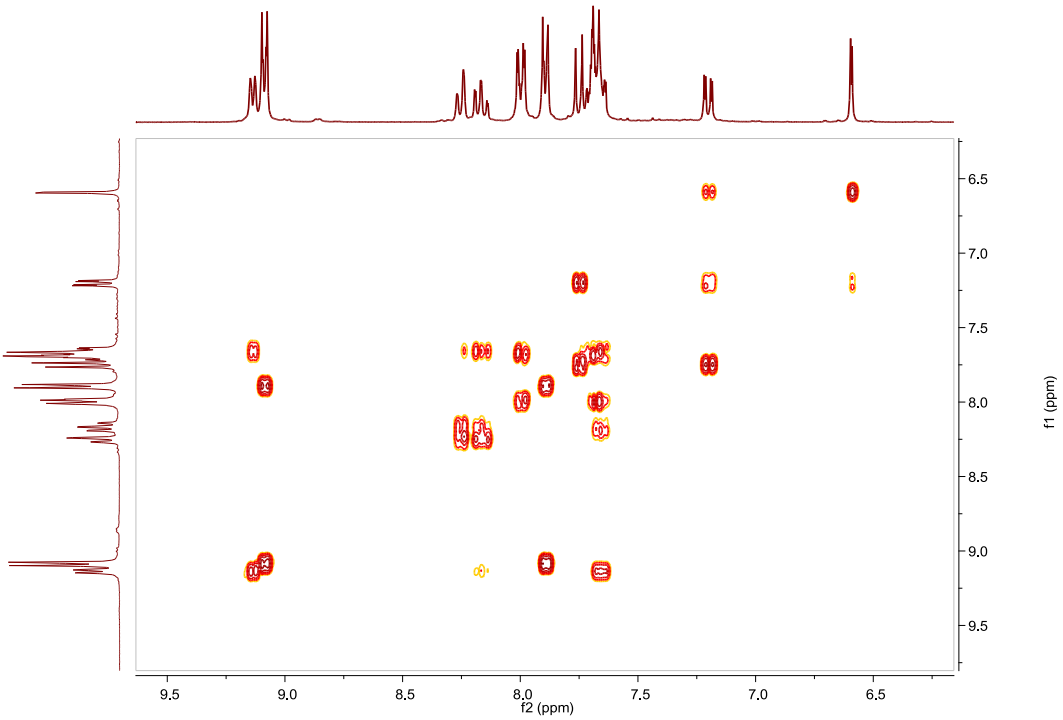

Fig. S204. COSY NMR spectrum of **C2** in acetone-d_6.

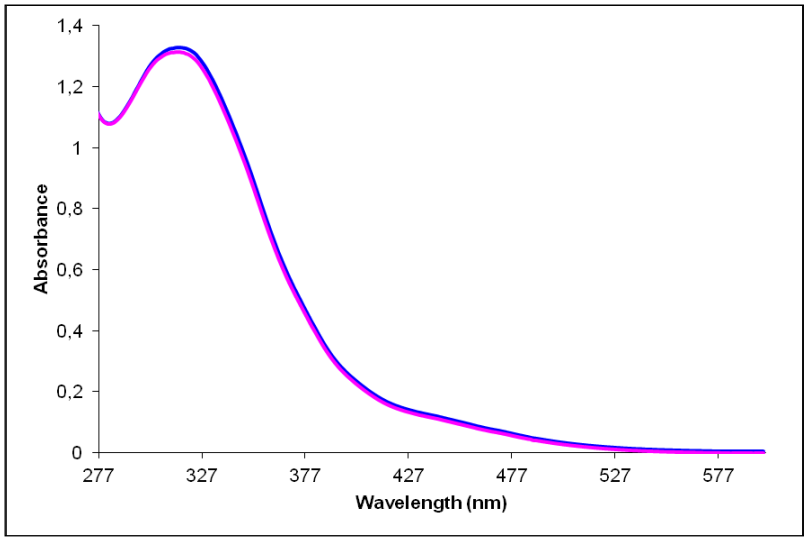

Fig. S205. UV/Vis spectra of **C2** in CH_3CN. Before (blue line) and after (pink line) irradiation at 344nm, $2.54 \cdot 10^{-5}$ M.

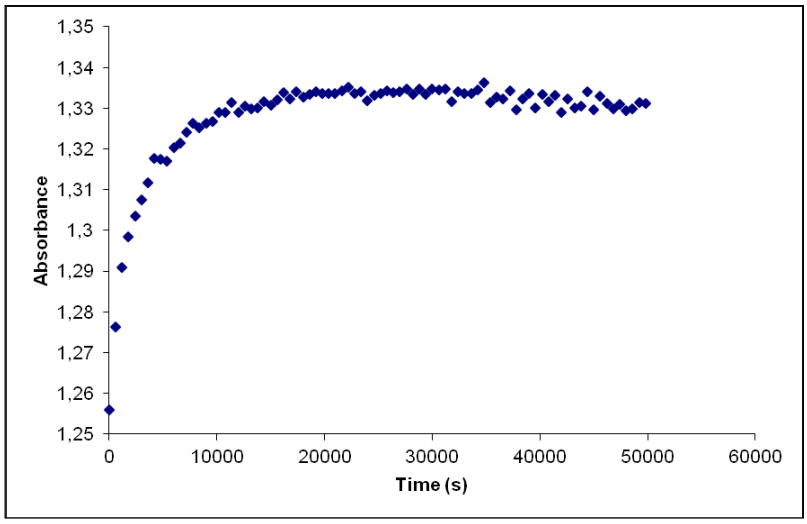

Fig. S206. Cis to trans thermal isomerization kinetics of **C2**. Absorption change of the band 315nm at 328 K in CH_3CN after irradiation at 344 nm. ($2.54 \cdot 10^{-5}$ M).

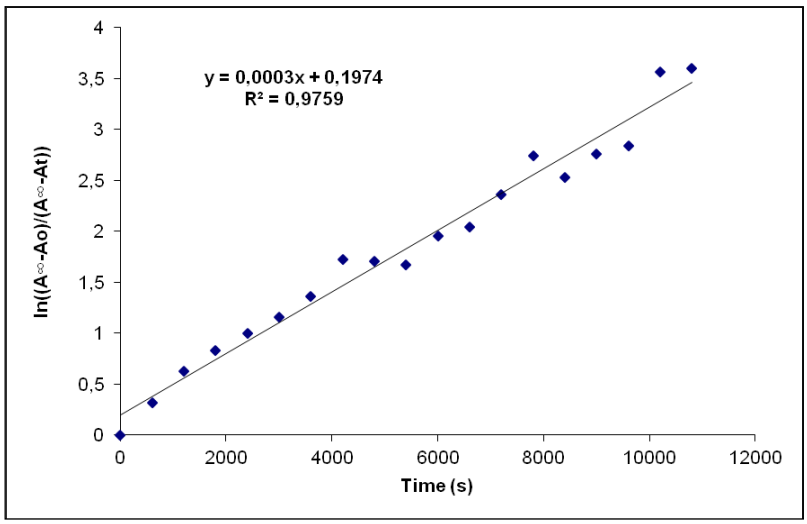

Fig. S207. Cis to trans thermal isomerization kinetics of **C2**. First-order plot. k (s^{-1}) = $3.0 \cdot 10^{-4}$. Half-life (min) = 38.

Compound D2, [Ir(azoppy)$_2$(2)$_2$]PF$_6$. Synthesis, characterization and photoisomerization studies.

SYNTHESIS

Under a N_2 atmosphere, **C2** (0.120 g, 0.103 mmol) and [4-(phenylazo)phenyl]boronic acid pinacol ester **11** (0.077 g, 0.250 mmol) were dissolved in 4 ml of THF. Na_2CO_3 (1M (aq), 2 mL) and $Pd(PPh_3)_4$ (0.012 g, 0.010 mmol) were added and the solution was degassed by bubbling N_2 for 15 min. The reaction mixture was refluxed (80 °C) for 15 h. The resulting mixture was cooled down to room temperature and the product was extracted with CH_2Cl_2. The organic phase was dried with $MgSO_4$, filtered off and the solvent was evaporated. The residue was purified by column chromatography (silica gel, CH_2Cl_2). To the fraction containing the eluted complex, 0.05 g of KPF_6 were added and the resulting solution was filtered through a celite path. The title compound was obtained as a dark red solid. Yield 14%.

Elemental Analys: calculated for ($C_{68}H_{50}IrN_{12}PF_6$): C, 59.51; H, 3.67; N, 12.25. Found: C, 59.81; H, 3.40; N, 11.67.

Exact Mass: ESI-MS $[C_{68}H_{50}IrN_{12}]^+$: calculated: m/z= 1227.3911, found: m/z= 1227.3932.

^{1}H NMR (300 MHz, acetone-d_6): δ 9.28–9.20 (m, 2H), 8.28 (d, J = 7.8 Hz, 1H), 8.17 (t, J = 8.1 Hz, 1H), 8.03–7.83 (m, 9H), 7.71–7.56 (m, 10H), 7.34 (dd, J = 1.6 Hz, J = 8.2 Hz, 1H), 6.89 (d, J = 1.7 Hz, 1H).

^{13}C APT NMR (75 MHz, acetone-d_6): δ 168.80 (C_{quat}), 159.08 (C_{quat}), 155.67 (CH), 153.95 (C_{quat}), 153.76 (C_{quat}), 153.03 (C_{quat}), 151.24 (CH), 149.69 (C_{quat}), 145.82(C_{quat}), 144.94 (C_{quat}), 142.62 (C_{quat}), 140.63 (CH), 134.86 (CH), 132.64 (CH), 131.47 (CH), 130.98 (2CH), 130.89 (CH), 130.62 (2CH), 129.03 (2CH), 126.33 (CH), 125.53 (CH), 124.82 (2CH), 124.71 (CH), 124.45 (2CH), 124.00 (2CH), 123.37 (CH), 121.61 (CH), 120.26 (CH).

UV/Vis (CH_3CN), λ, nm (ε, 10^4 M^{-1} cm^{-1}): 347 (9.0), 427 (1.8).

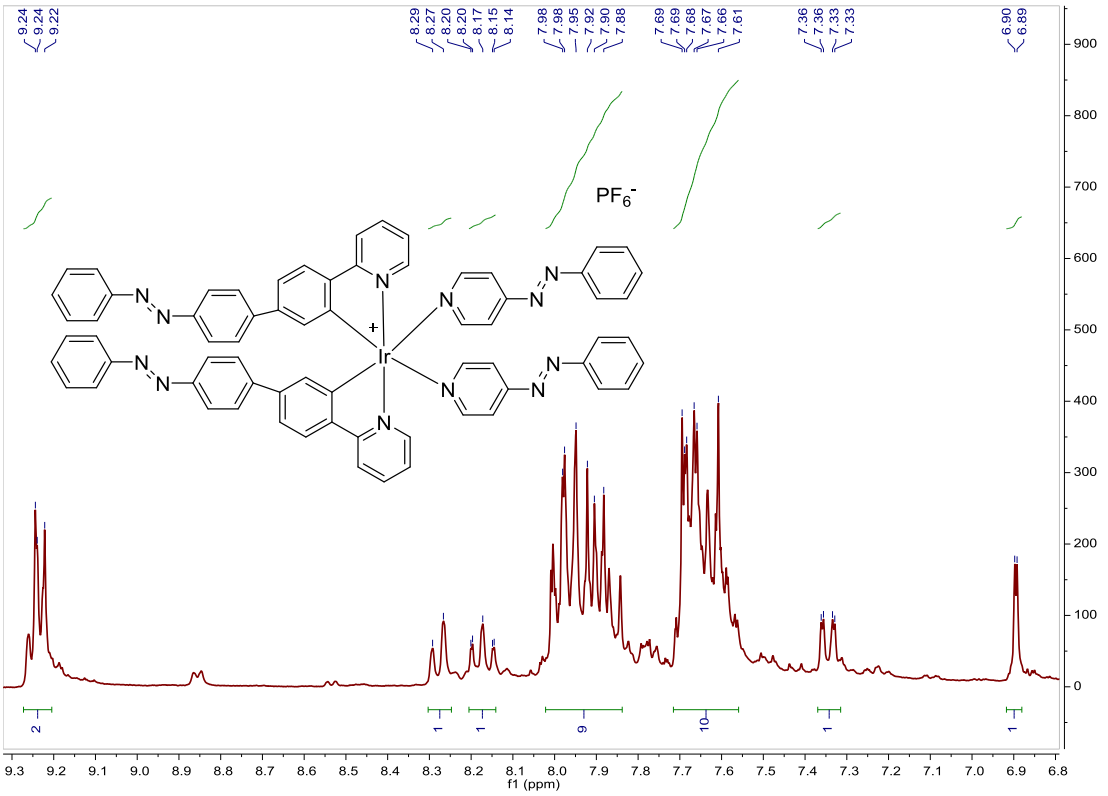

Fig. S208. ^{1}H NMR spectrum of **D2** in acetone-d_6, 300 MHz.

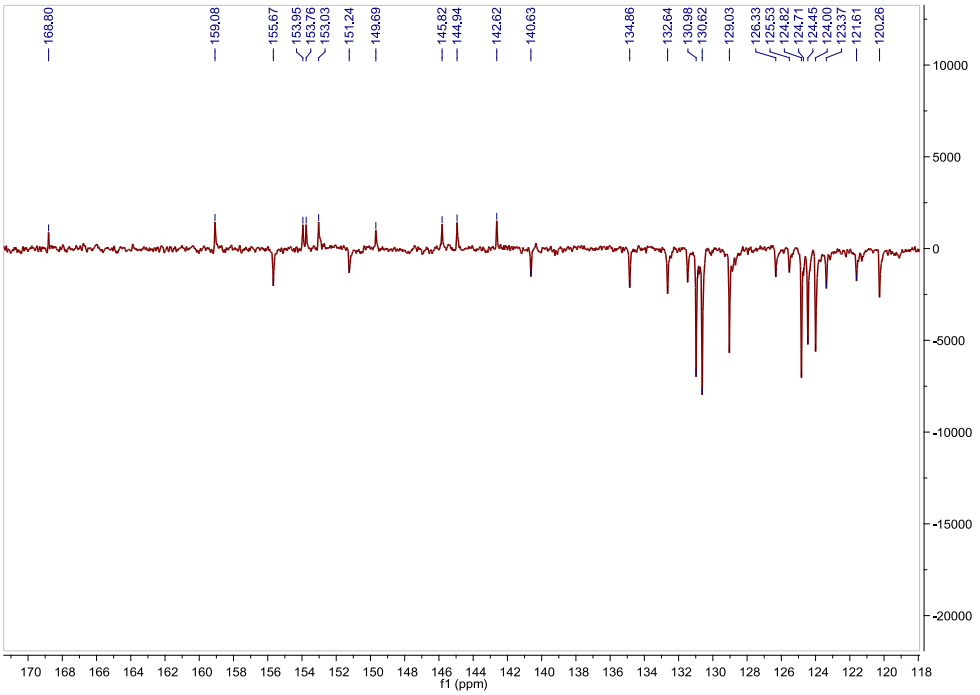

Fig. S209. ^{13}C APT NMR spectrum of **D2** in acetone-d_6, 75 MHz.

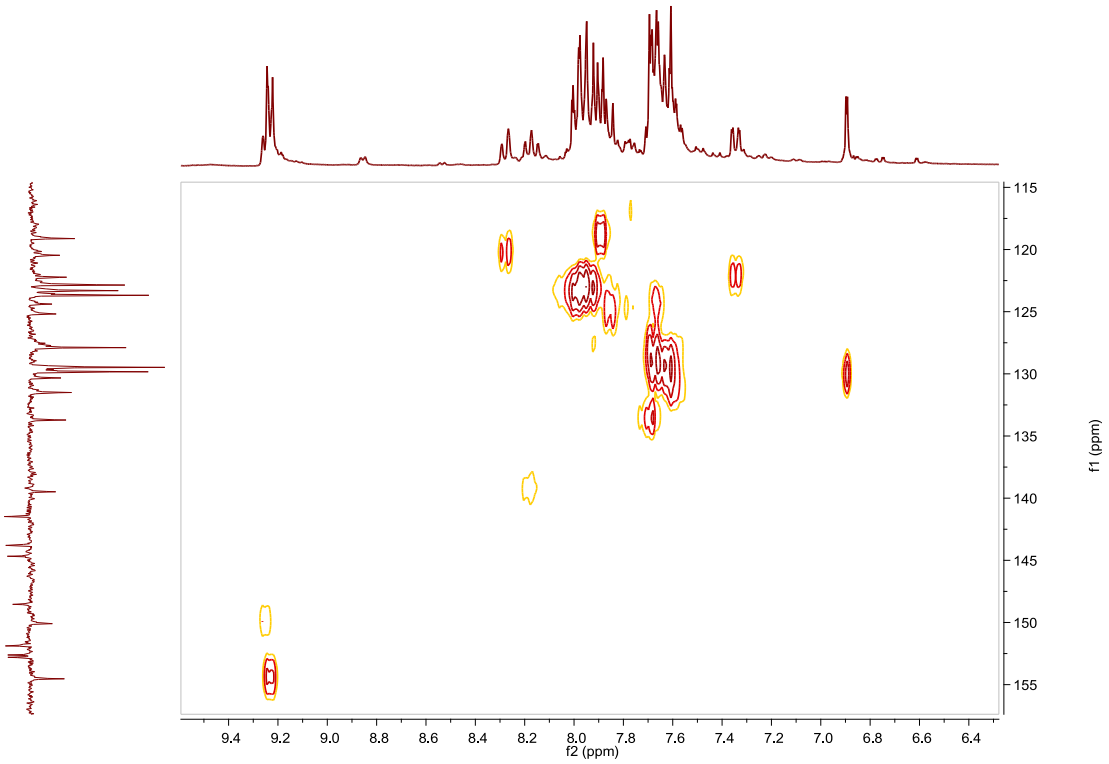

Fig. S210. HSQC NMR spectrum of **D2** in acetone-d_6.

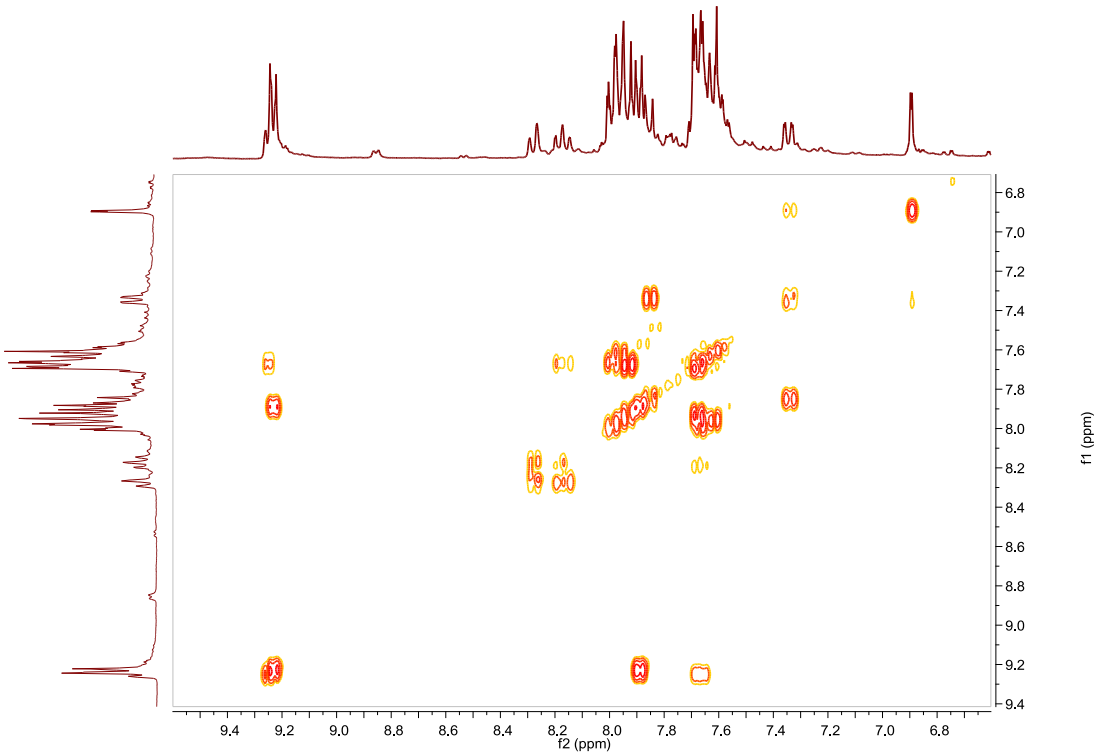

Fig. S211. COSY NMR spectrum of **D2** in acetone-d_6.

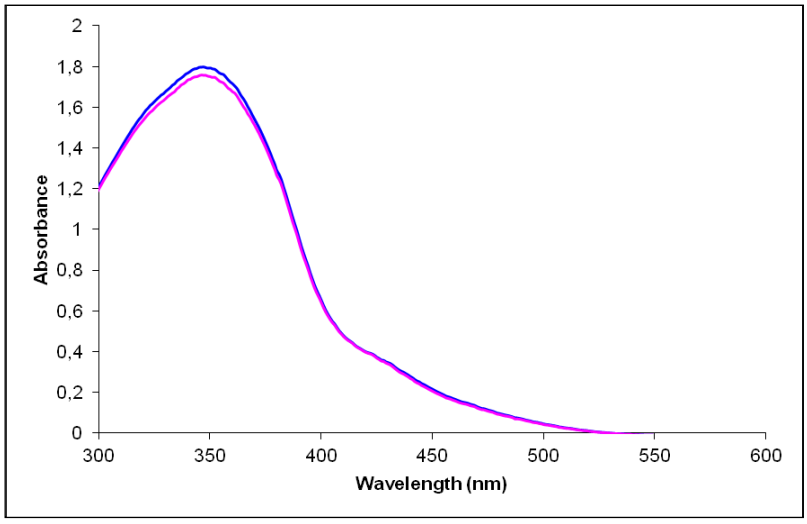

Fig. S212. UV/Vis spectra of **D2** in CH_3CN. Before (blue line) and after (pink line) irradiation at 350nm, $2.00 \cdot 10^{-5}$ M.

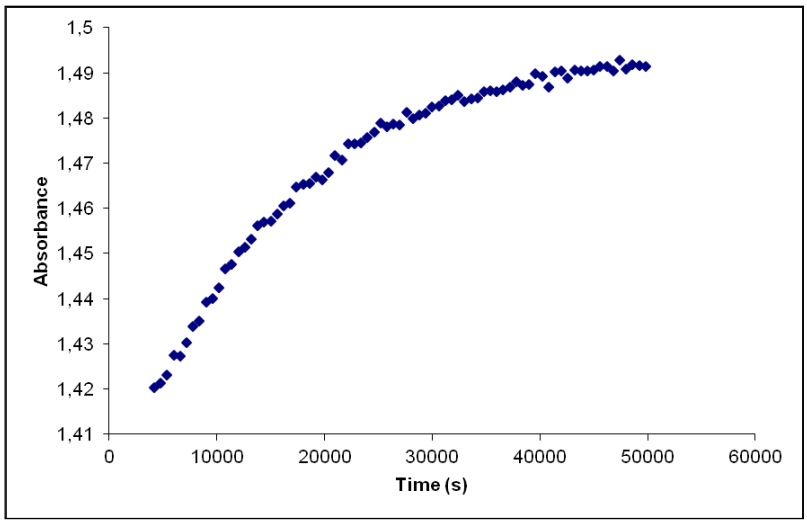

Fig. S213. Cis to trans thermal isomerization kinetics of **D2**. Absorption change of the band 347nm at 328 K in CH_3CN after irradiation at 350 nm. ($2.00 \cdot 10^{-5}$ M).

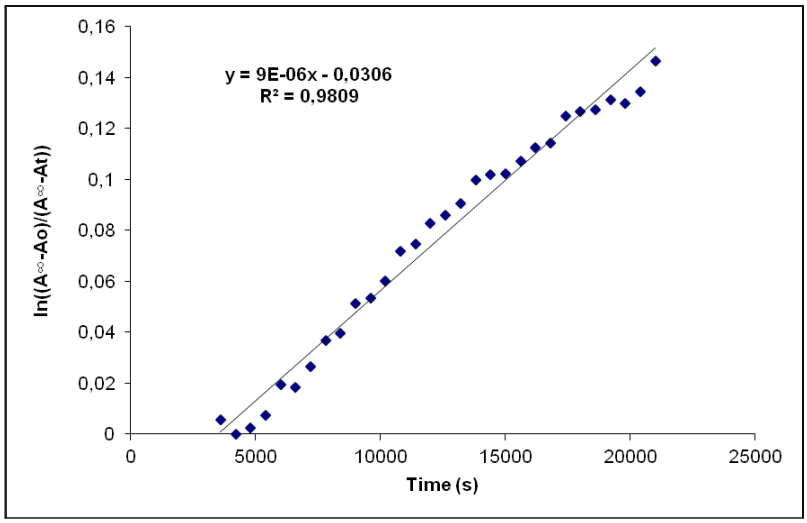

Fig. S214. Cis to trans thermal isomerization kinetics of **D2**. First-order plot. k (s^{-1}) = $9.0 \cdot 10^{-6}$. Half-life (min) = 1284.

Compound A3, [Ir(ppy)$_2$(3)]PF$_6$. Synthesis, characterization and photoisomerization studies.

SYNTHESIS

Under a N_2 atmosphere, $[Ir(ppy)_2Cl]_2$ (0.100 g, 0.093 mmol) were added over a suspension of **L3** (0.096 g, 0.186 mmol) in 8 ml CH_2Cl_2–MeOH 2/1. The reaction mixture was refluxed, under N_2, for 15 h. After solvent evaporation the product was purified by column chromatography (silica gel, CH_2Cl_2). When the unreacted $[Ir(ppy)_2Cl]_2$ eluted, 0.05 g of KPF_6 were added on top of the column and the polarity of the eluent was gradually increased to 100% acetone to elute [Ir(ppy)$_2$(**L3**)]PF_6 together with the excess of KPF_6. The desired compound was precipitated with ether after filtration through a celite path in CH_2Cl_2 and it was obtained as an orange solid. Yield 95%.

Elemental Analysis: calculated for ($C_{56}H_{40}IrN_8PF_6$) C, 57.88; H, 3.47; N, 9.64. Found: C, 58.02; H, 3.43; N, 9.41.

Exact Mass: ESI-MS $[C_{56}H_{40}IrN_8]^+$: calculated: m/z= 1017.3005, found: m/z= 1017.3030.

^{1}H NMR (300 MHz, acetone-*d*$_6$): δ 9.52 (d, J = 1.4 Hz, 1H), 8.35–8.22 (m, 4H), 8.16 (m, 3H), 8.07–7.96 (m, 5H), 7.70–7.62 (m, 3H), 7.24 (ddd, J = 1.3 Hz, J = 6.0 Hz, J = 7.2 Hz, 1H), 7.11 (ddd, J = 1.2 Hz, J = 7.4 Hz, J = 8.5 Hz, 1H), 7.00 (ddd, J = 1.3 Hz, J = 7.4 Hz, J = 8.7 Hz, 1H), 6.45 (dd, J = 0.9 Hz, J = 7.5 Hz, 1H).

^{13}C APT NMR (75 MHz, acetone-*d*$_6$): δ 169.25 (C_{quat}), 158.06 (C_{quat}), 154.86 (C_{quat}), 153.88 (C_{quat}), 152.24 (CH), 151.98 (C_{quat}), 151.30 (C_{quat}), 150.66 (CH), 145.44 (C_{quat}), 140.15 (CH), 139.54 (C_{quat}), 133.23 (CH), 132.97 (CH), 131.76 (CH), 130.74 (2CH), 130.15 (2CH), 127.42 (CH), 126.33 (CH), 125.00 (CH), 124.85 (2CH), 124.22 (2CH), 124.13 (CH), 123.88 (CH), 121.32 (CH).

UV/Vis (CH_3CN), λ, nm (ε, 10^4 M^{-1} cm^{-1}): 338 (7.2), 467 (0.44).

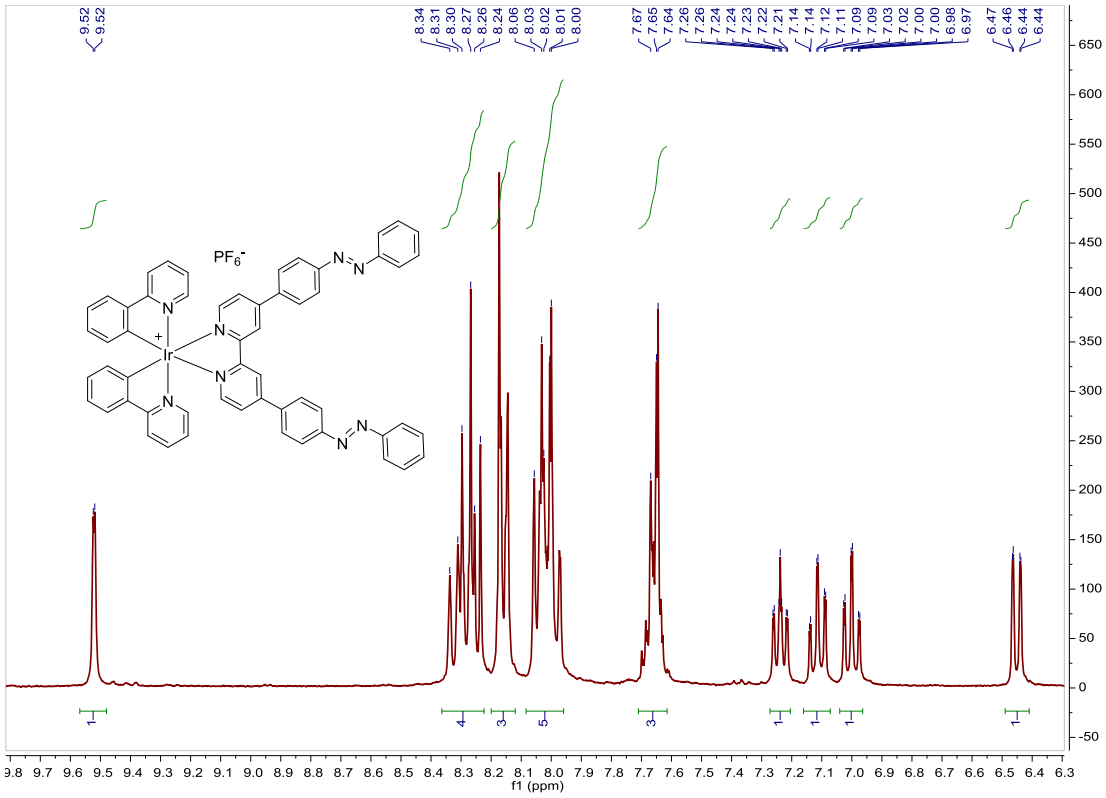

Fig. S215. ^{1}H NMR spectrum of **A3** in acetone-*d*$_6$, 300 MHz.

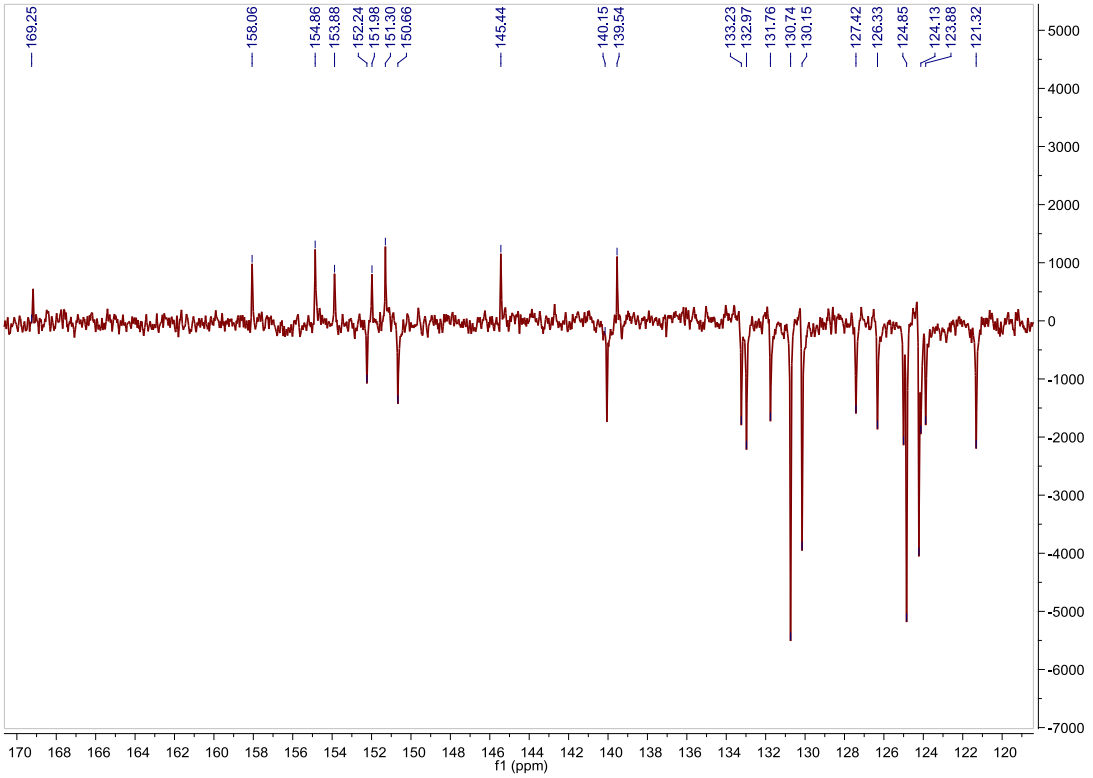

Fig. S216. ^{13}C APT NMR spectrum of **A3** in acetone-d_6, 75 MHz.

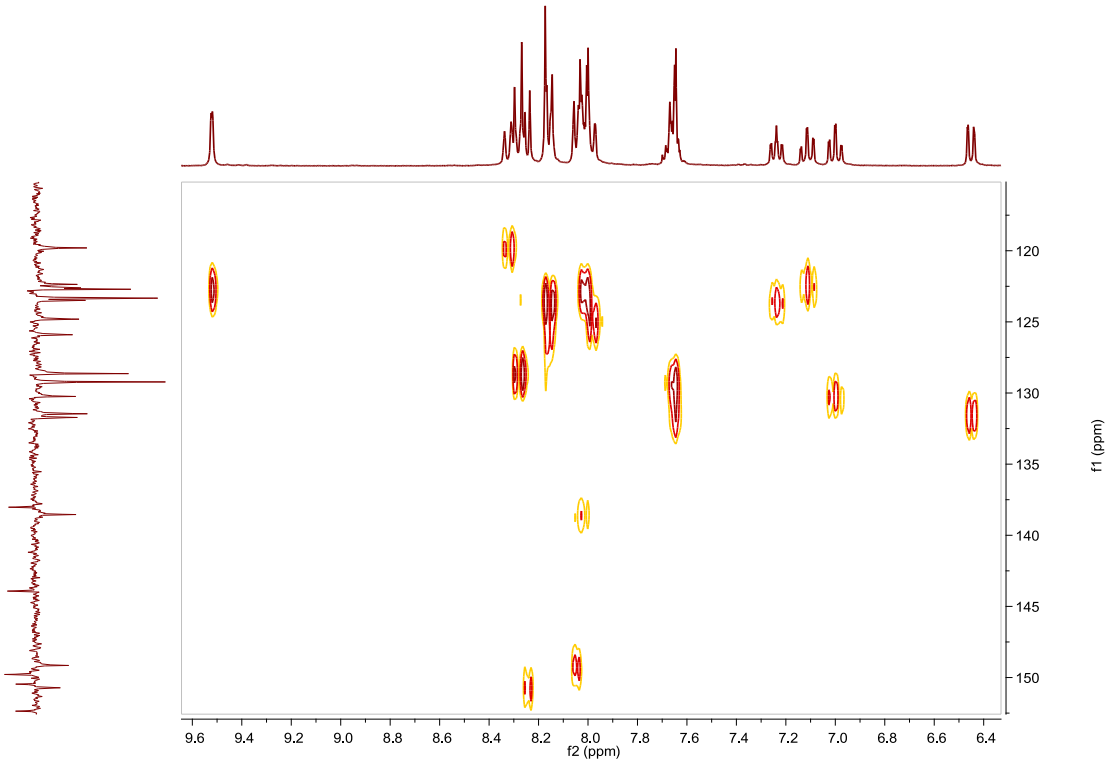

Fig. S217. HSQC NMR spectrum of **A3** in acetone-d_6.

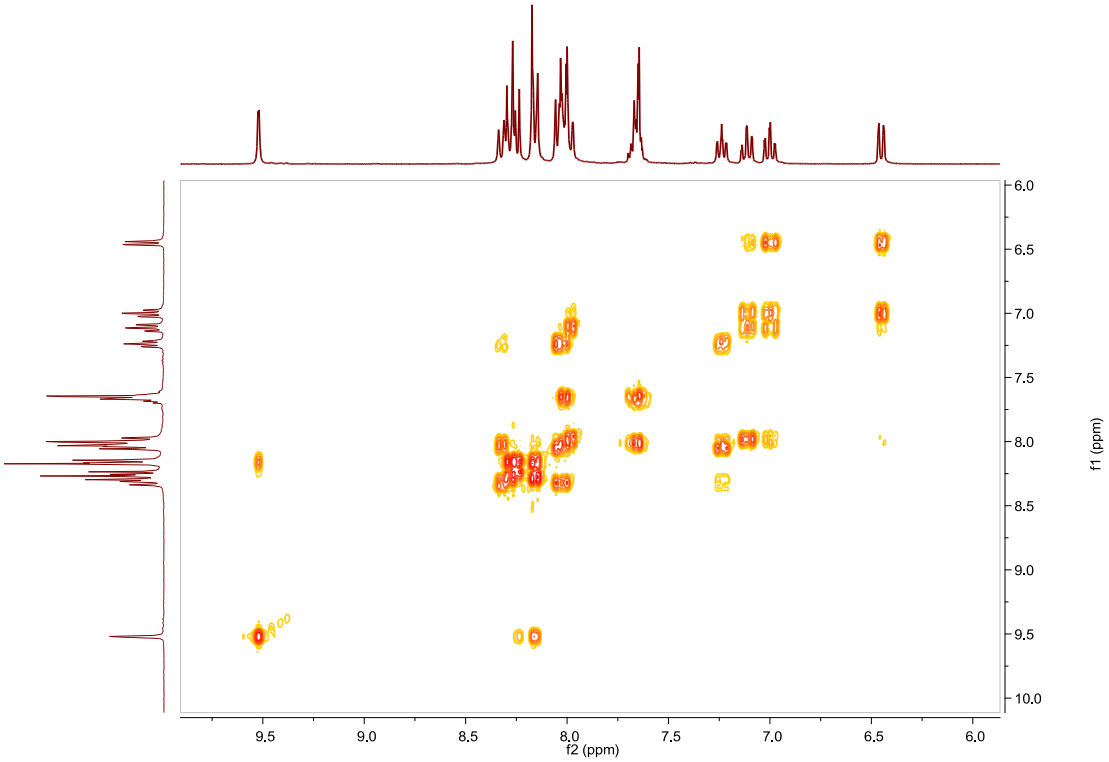

Fig. S218. COSY NMR spectrum of **A3** in acetone-d_6.

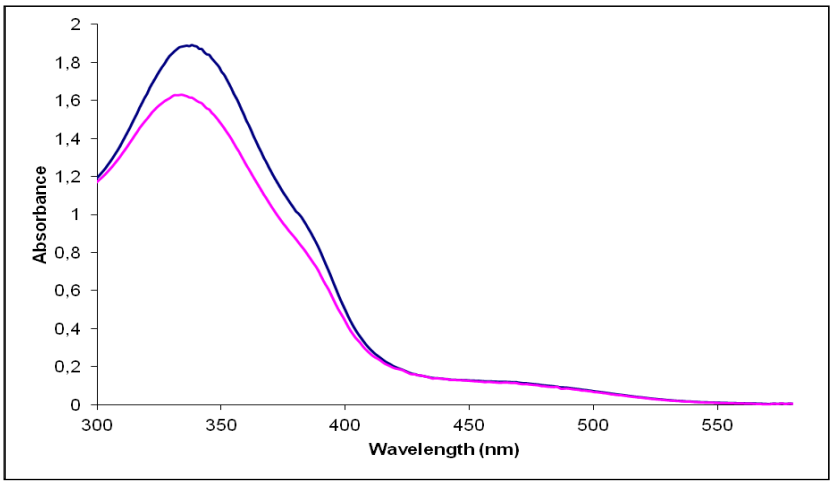

Fig. S219. UV/Vis spectra of **A3** in CH_3CN. Before (blue line) and after (pink line) irradiation at 345nm, $2.64 \cdot 10^{-5}$ M.

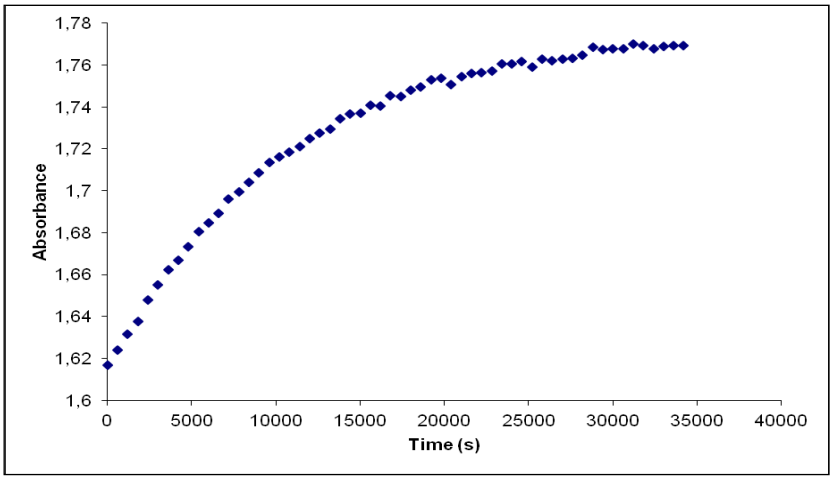

Fig. S220. Cis to trans thermal isomerization kinetics of **A3**. Absorption change of the band 338nm at 328 K in CH_3CN after irradiation at 345 nm. ($2.64 \cdot 10^{-5}$ M).

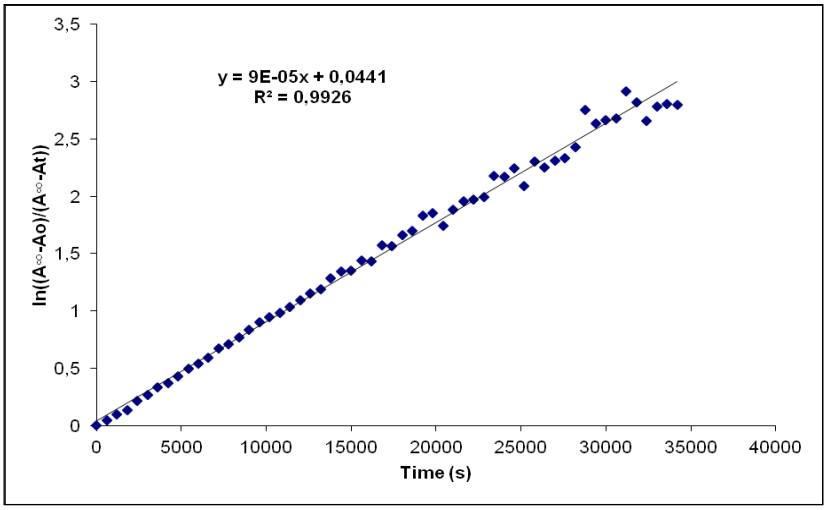

Fig. S221. Cis to trans thermal isomerization kinetics of **A3**. First-order plot. k (s^{-1}) = $9.0 \cdot 10^{-5}$. Half-life (s) = 128.

Compound B3, $[Ir(Fppy)_2(3)]PF_6$. Synthesis, characterization and photoisomerization studies.

SYNTHESIS

Under a N_2 atmosphere, $[Ir(Fppy)_2Cl]_2$ (0.100 g, 0.082 mmol) were added over a suspension of **L3** (0.085 g, 0.164 mmol) in 8 ml CH_2Cl_2–MeOH 2/1. The reaction mixture was refluxed, under N_2, for 15 h. After solvent evaporation the product was purified by column chromatography (silica gel, CH_2Cl_2). When the unreacted $[Ir(Fppy)_2Cl]_2$ eluted, 0.05 g of KPF_6 were added on top of the column and the polarity of the eluent was gradually increased to 100% acetone to elute $[Ir(Fppy)_2$(**L3**)$]PF_6$ together with the excess of KPF_6. The desired compound, purified by filtration through a celite path in CH_2Cl_2, was obtained as an orange solid. Yield 34%.

Elemental Analysis: calculated for ($C_{56}H_{36}F_4IrN_8PF_6{\cdot}CH_3COCH_3$): C, 54.84; H, 3.28; N, 8.67. Found: C, 55.24; H, 3.60; N, 8.28.

Exact Mass: ESI-MS $[C_{56}H_{36}F_4IrN_8]^+$: calculated: m/z= 1089.2628, found: m/z= 1089.2665.

^{1}H NMR (300 MHz, acetone-*d*$_6$): δ 9.54 (s, 1H), 8.48 (brd, *J* = 9.5 Hz, 1H), 8.35 (d, *J* = 5.8 Hz, 1H), 8.27 (brd, *J* = 8.8 Hz, 2H), 8.23–8.09 (m, 5H), 8.05–7.98 (m, 2H), 7.71–7.62 (m, 3H), 7.33 (ddd, J = 1.4 Hz, *J* = 5.8 Hz, J = 7.8 Hz, 1H), 6.84 (ddd, J = 2.3 Hz, J = 9.3 Hz, J = 12.8 Hz, 1H), 5.90 (dd, *J* = 2.3 Hz, J = 8.5 Hz, 1H).

^{13}C APT NMR (75 MHz, acetone-*d*$_6$): δ 165.22 (d, *J* = 6.8 Hz, C_{quat}), 164.96 (dd, J = 12.8 Hz, J = 255.9 Hz, C_{quat}), 162.76 (dd, J = 12.8 Hz, J = 260.47 Hz, C_{quat}), 157.80 (s, C_{quat}), 156.08 (d, *J* = 6.8 Hz, C_{quat}), 154.93 (s, C_{quat}), 153.86 (s, C_{quat}), 152.55 (s, CH), 151.88 (s, C_{quat}), 151.18 (s, CH), 141.18 (s, CH), 139.33 (s, C_{quat}), 133.25 (s, CH), 130.73 (s, 2CH), 130.19 (s, 2CH), 129.30 (s, C_{quat}), 127.73 (s, CH), 125.57 (s, CH), 125.18 (s, CH), 124.85 (s, 2CH), 124.42 (s, CH), 124.22 (s, 2CH), 115.08 (d, *J* = 17.4 Hz, CH), 100.13 (t, *J* = 26.4 Hz, CH).

UV/Vis (CH_3CN), λ, nm (ε, 10^4 M^{-1} cm^{-1}): 343 (7.3), 443 (0.47).

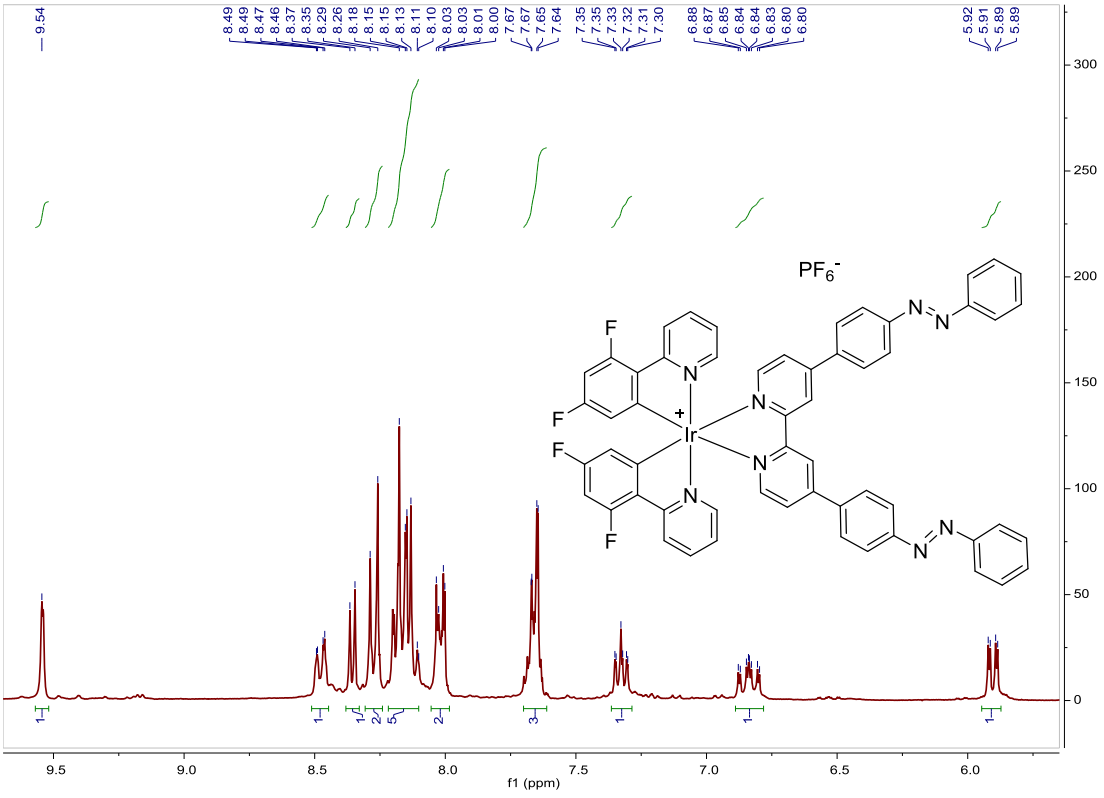

Fig. S222. ^{1}H NMR spectrum of **B3** in acetone-*d*$_6$, 300 MHz.

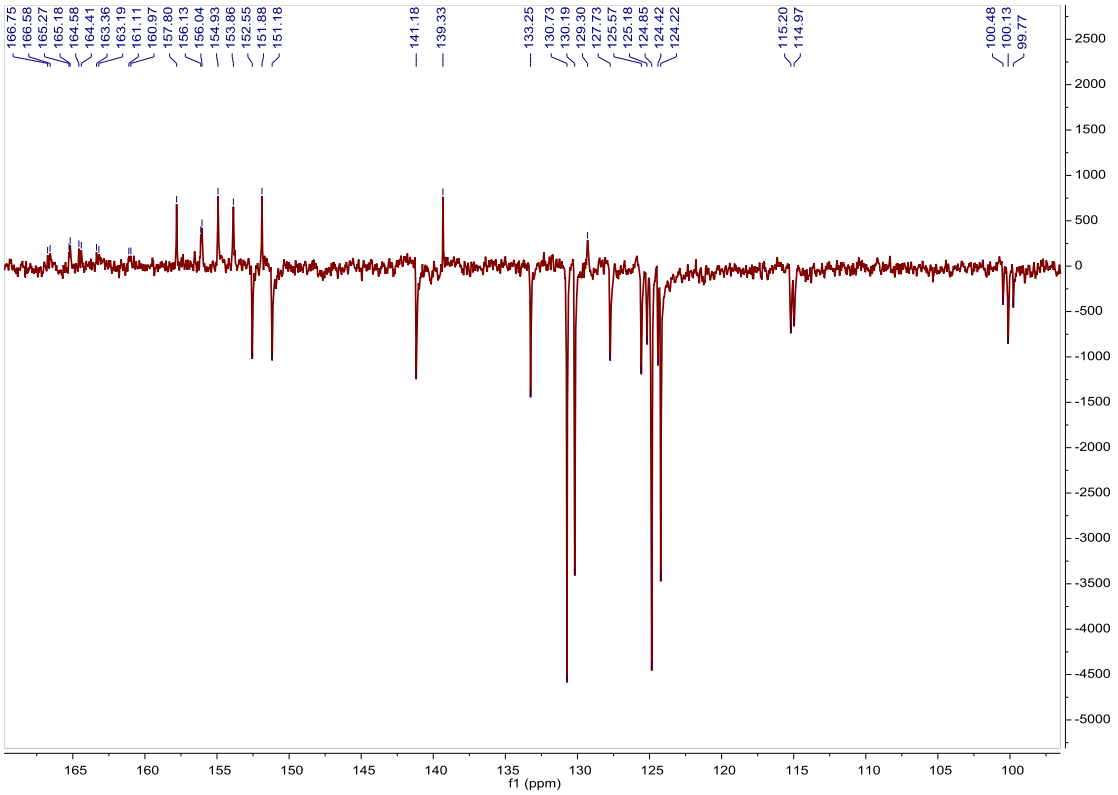

Fig. S223. ^{13}C APT NMR spectrum of **B3** in acetone-d_6, 75 MHz.

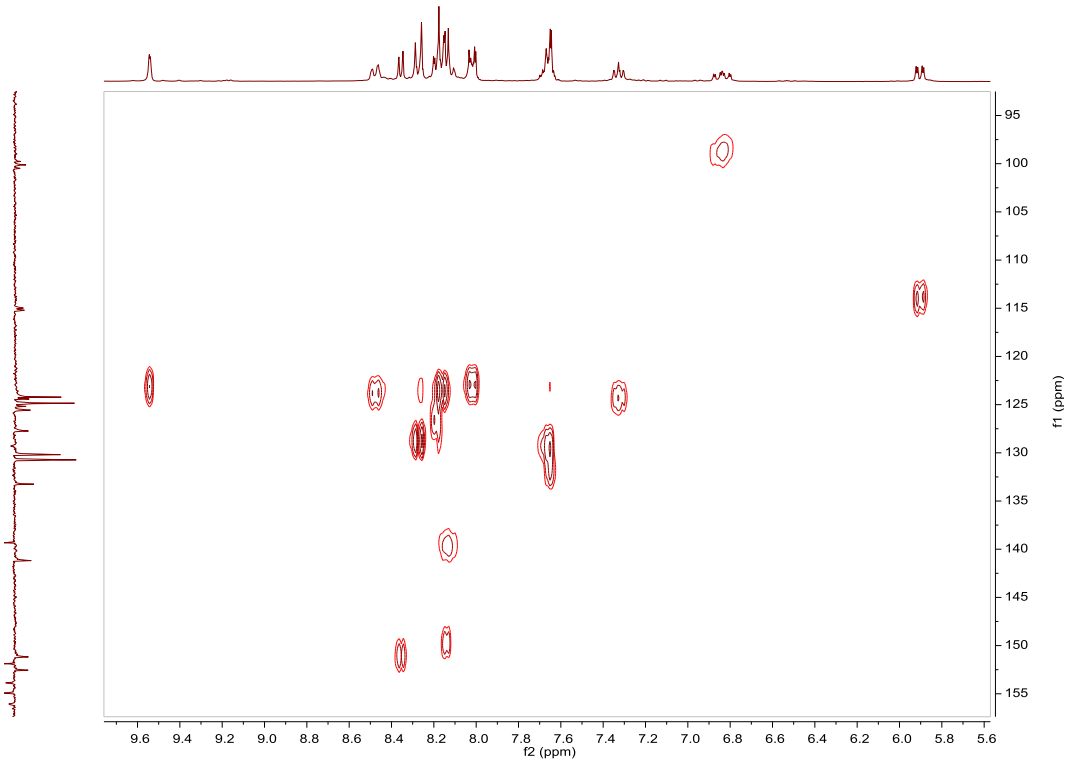

Fig. S224. HSQC NMR spectrum of **B3** in acetone-d_6.

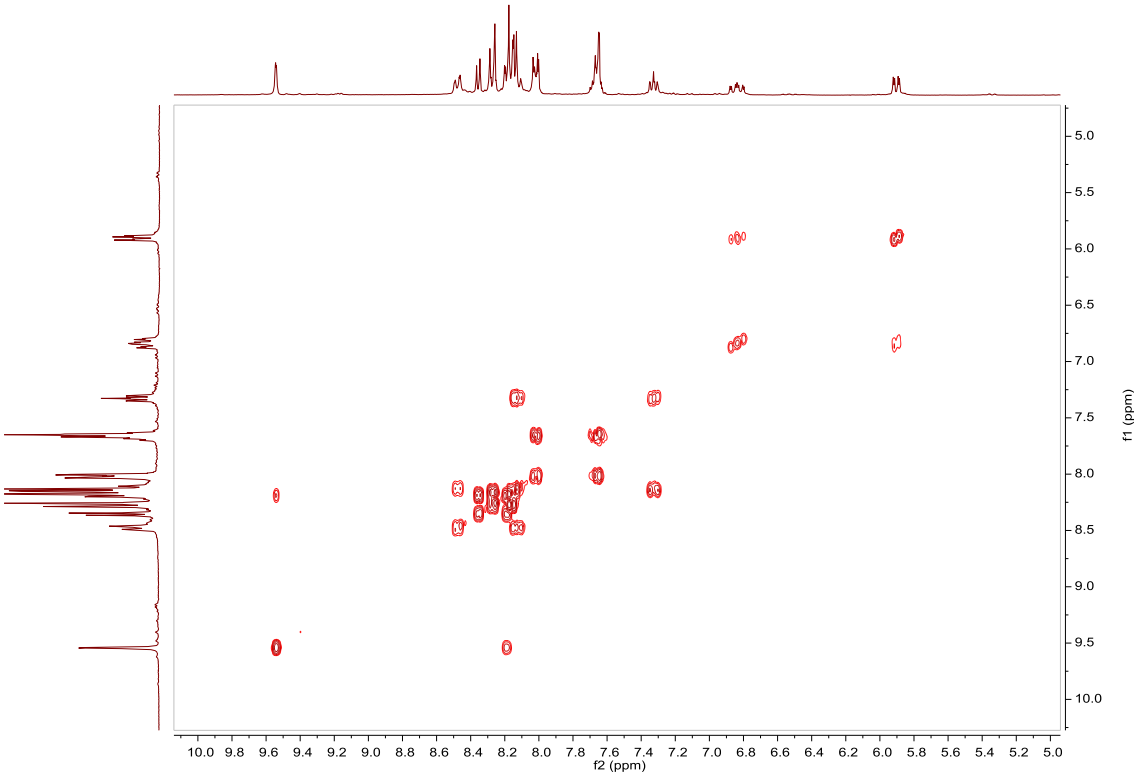

Fig. S225. COSY NMR spectrum of **B3** in acetone-d_6.

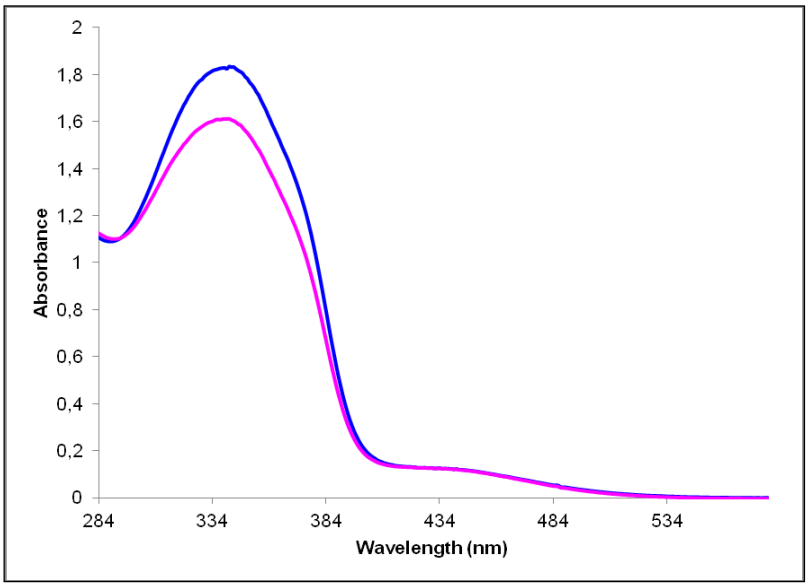

Fig. S226. UV/Vis spectra of **B3** in CH_3CN. Before (blue line) and after (pink line) irradiation at 354nm, $2.52 \cdot 10^{-5}$ M.

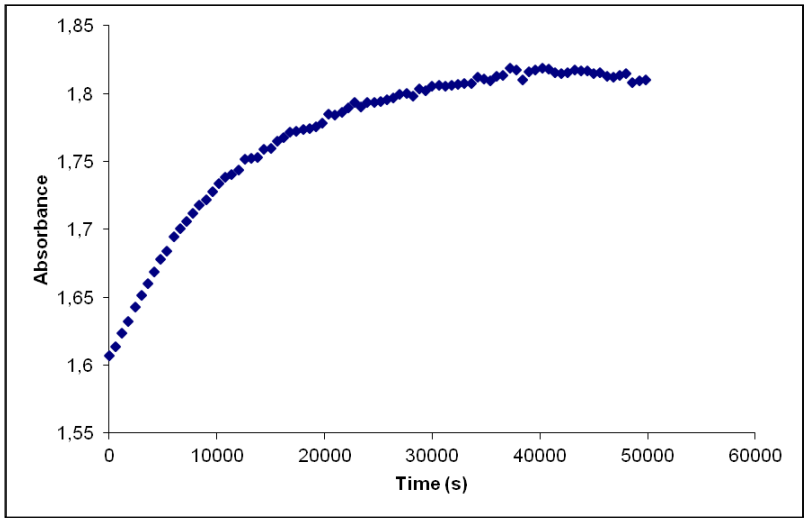

Fig. S227. Cis to trans thermal isomerization kinetics of **B3**. Absorption change of the band 343nm at 328 K in CH_3CN after irradiation at 354 nm. ($2.52 \cdot 10^{-5}$ M).

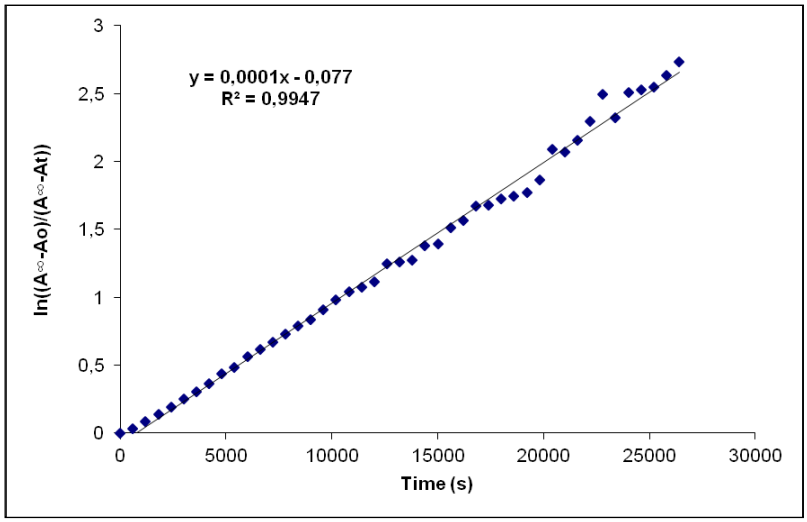

Fig. S228. Cis to trans thermal isomerization kinetics of **B3**. First-order plot. k (s^{-1}) = $1.0 \cdot 10^{-4}$. Half-life (min) = 115.

Compound C3, [Ir(Brppy)$_2$(3)]PF$_6$. Synthesis, characterization and photoisomerization studies.

SYNTHESIS

Under a N_2 atmosphere, $[Ir(Brppy)_2Cl]_2$ (0.100 g, 0.072 mmol) were added over a suspension of **L3** (0.075 g, 0.144 mmol) in 8 ml CH_2Cl_2–MeOH 2/1. The reaction mixture was refluxed, under N_2, for 15h. After solvent evaporation the product was purified by column chromatography (silica gel, CH_2Cl_2). When the unreacted $[Ir(Brppy)_2Cl]_2$ eluted, 0.05 g of KPF_6 were added on top of the column and the polarity of the eluent was gradually increased to 100% acetone to elute $[Ir(Brppy)_2(\mathbf{L3})]PF_6$ together with the excess of KPF_6. The desired compound, purified by filtration through a celite path in CH_2Cl_2, was obtained as an orange solid. Yield 34%.

Elemental Analysis: calculated for ($C_{56}H_{38}Br_2IrN_8PF_6{\cdot}CH_2Cl_2$): C, 48.73; H, 2.87; N, 7.98. Found: C, 48.94; H, 2.90; N, 8.12.

Exact Mass: ESI-MS $[C_{56}H_{38}Br_2IrN_8]^+$: calculated: m/z= 1173.1215, found: m/z= 1173.1235.

^{1}H NMR (300 MHz, acetone-*d*$_6$): δ 9.54 (d, J = 1.6 Hz, 1H), 8.38 (dd, J = 1.2 Hz, J = 8.5 Hz, 1H), 8.32 (d, J = 5.8 Hz, 1H), 8.27 (brd, J = 8.8 Hz, 2H), 8.18 (m, 3H), 8.09 (m, 2H), 8.02 (m, 2H), 7.98 (d, J = 8.4 Hz, 1H), 7.66 (m, 3H), 7.33 (m, 2H), 6.51 (d, J = 2.0 Hz, 1H).

^{13}C APT NMR (75 MHz, acetone-*d*$_6$): δ 167.88 (C_{quat}), 157.94 (C_{quat}), 154.93 (C_{quat}), 154.02 (C_{quat}), 153.88 (C_{quat}), 152.48 (CH), 151.68 (C_{quat}), 150.90 (CH), 144.76 (C_{quat}), 140.64 (CH), 139.43 (C_{quat}), 135.14 (CH), 133.26 (CH), 130.74 (2CH), 130.17 (2CH), 128.16 (CH), 127.66 (CH), 127.20 (CH), 126.31 (C_{quat}), 125.72 (CH), 124.86 (2CH), 124.30 (CH), 124.24 (2CH), 121.94 (CH).

UV/Vis (CH_3CN), λ, nm (ε, 10^4 M^{-1} cm^{-1}): 336 (6.6), 449 (0.24).

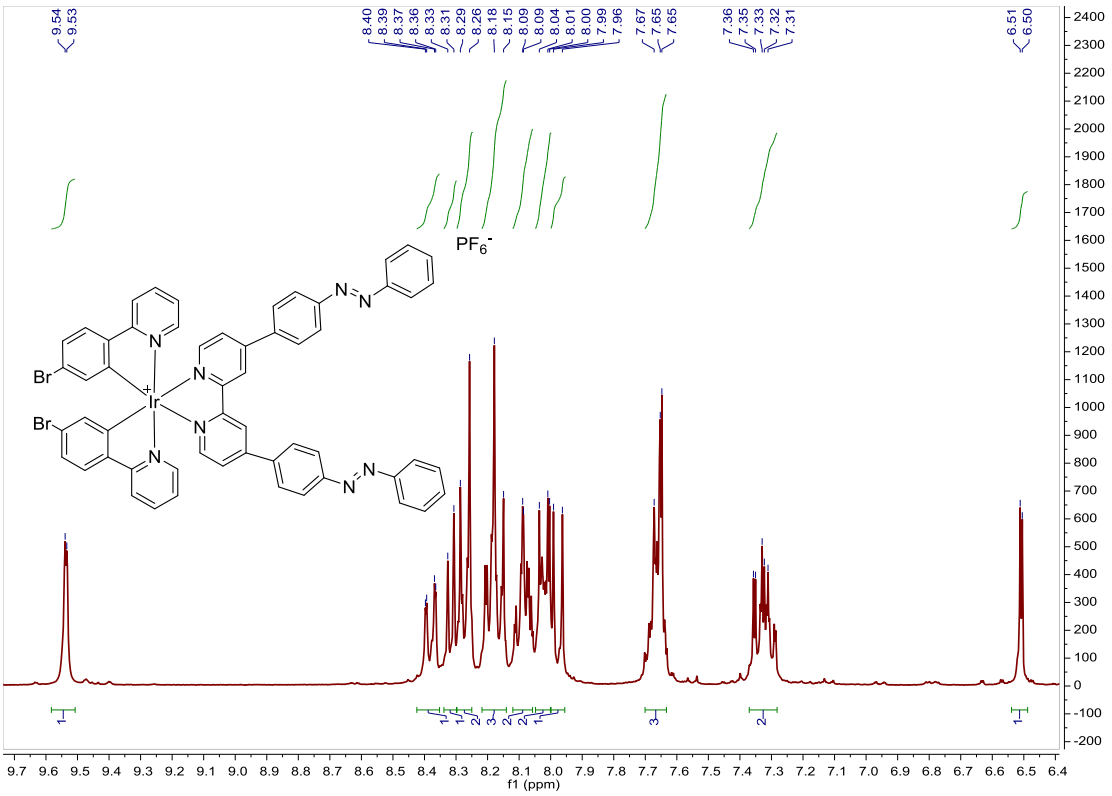

Fig. S229. ^{1}H NMR spectrum of **C3** in acetone-*d*$_6$, 300 MHz.

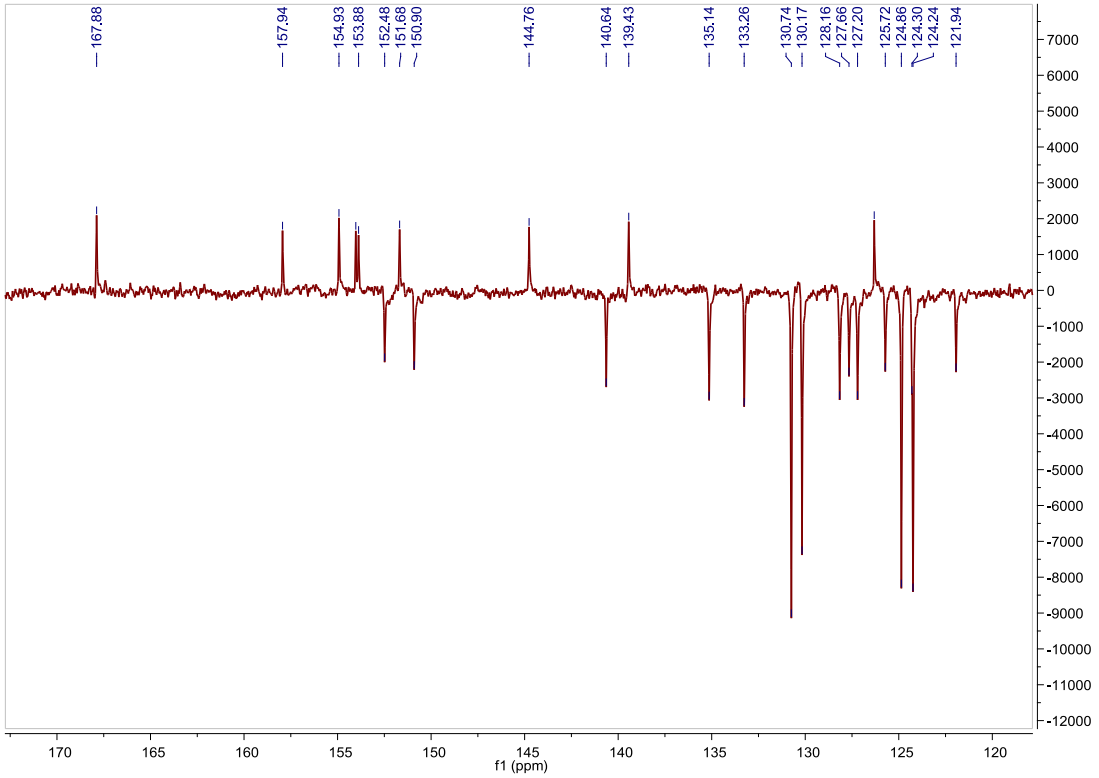

Fig. S230. ^{13}C APT NMR spectrum of **C3** in acetone-d_6, 75 MHz.

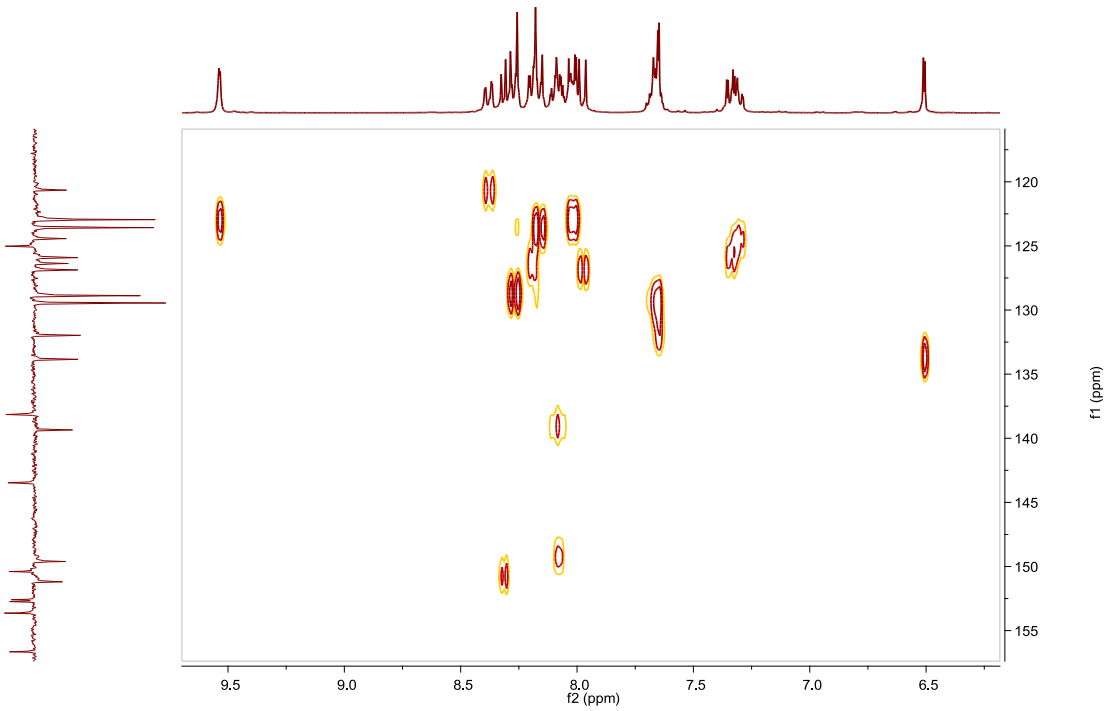

Fig. S231. HSQC NMR spectrum of **C3** in acetone-d_6.

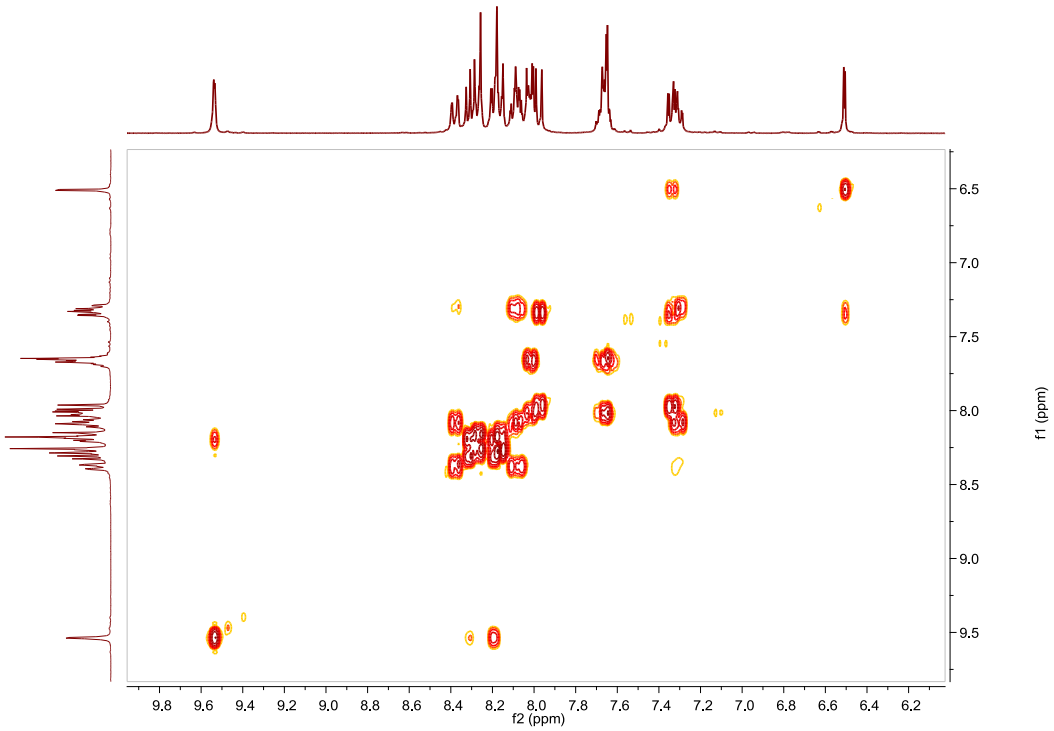

Fig. S232. COSY NMR spectrum of **C3** in acetone-d_6.

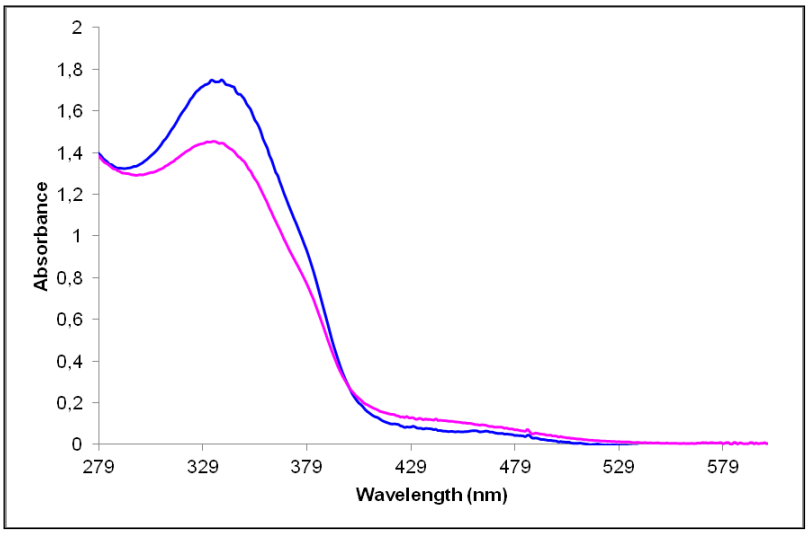

Fig. S233. UV/Vis spectra of **C3** in CH_3CN. Before (blue line) and after (pink line) irradiation at 355nm, $2.62 \cdot 10^{-5}$ M.

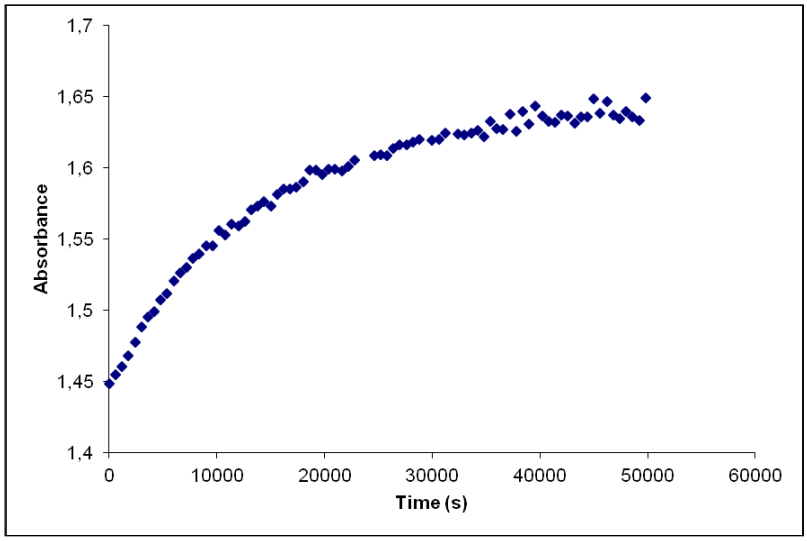

Fig. S234. Cis to trans thermal isomerization kinetics of **C3**. Absorption change of the band 336nm at 328 K in CH_3CN after irradiation at 355 nm. ($2.62 \cdot 10^{-5}$ M).

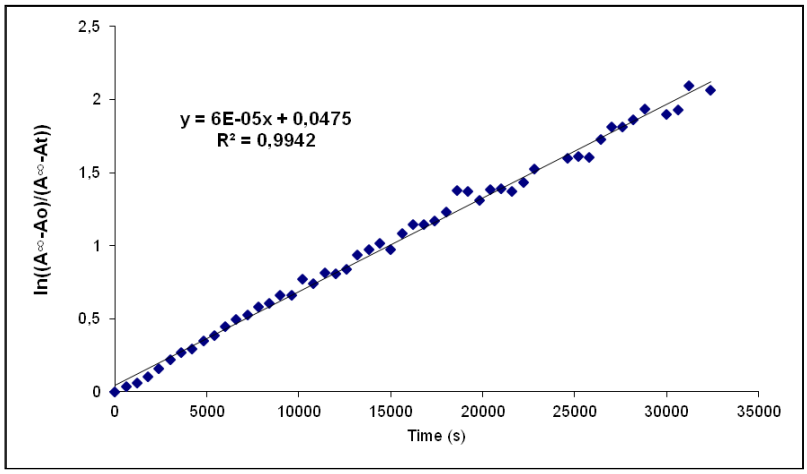

Fig. S235. Cis to trans thermal isomerization kinetics of **C3**. First-order plot. k (s^{-1}) = $6.0 \cdot 10^{-5}$. Half-life (s) = 192.

Compound D3, [Ir(azoppy)$_2$(3)]PF$_6$. Synthesis, characterization and photoisomerization studies.

SYNTHESIS

Under a N_2 atmosphere, **C3** (0.150 g, 0.114 mmol) and [4-(phenylazo)phenyl]boronic acid pinacol ester **11** (0.085 g, 0.276 mmol) were dissolved in 5 ml of THF. Na_2CO_3 (1 M (aq), 2.5 mL) and $Pd(PPh_3)_4$ (0.013 g, 0.011 mmol) were added and the solution was degassed by bubbling N_2 for 15min. The reaction mixture was refluxed (80 °C) for 15 h. The resulting mixture was cooled down to room temperature and the product was extracted with CH_2Cl_2. The organic phase was dried with $MgSO_4$, filtered off and the solvent was evaporated. The residue was purified by column chromatography (silica gel, CH_2Cl_2). To the fraction containing the eluted complex, 0.05 g of KPF_6 were added and the resulting solution was filtered through a celite path. The title compound was obtained as an orange solid. Yield 24%.

Elemental Analysis: calculated for ($C_{80}H_{56}IrN_{12}PF_6 \cdot H_2O$): C, 62.37; H, 3.79; N, 10.91. Found: C, 62.18; H, 3.62; N, 10.34.

Exact Mass: ESI-MS $[C_{80}H_{56}IrN_{12}]^+$: calculated: m/z= 1377.4380, found: m/z= 1377.4351.

^{1}H NMR (300 MHz, acetone-*d*$_6$): δ 9.58 (s, 1H), 8.45 (t, J = 5.8 Hz, 2H), 8.29 (d, J = 8.5 Hz, 2H), 8.24–8.09 (m, 7H), 8.04–7.99 (m, 2H), 7.98–7.92 (m, 4H), 7.71 (m, 7H), 7.55 (dd, J = 1.8 Hz, J = 8.1 Hz, 1H), 7.34 (t, J = 6.8 Hz, 1H), 6.83 (d, J = 1.7 Hz, 1H).

^{13}C APT NMR (75 MHz, acetone-*d*$_6$): δ 168.69 (C_{quat}), 158.11 (C_{quat}), 154.89 (C_{quat}), 153.95 (C_{quat}), 153.88 (C_{quat}), 153.03 (C_{quat}), 152.61 (CH), 152.54 (C_{quat}), 151.41 (C_{quat}), 151.00 (CH), 145.70 (C_{quat}), 145.01 (C_{quat}), 142.67 (C_{quat}), 140.30 (CH), 139.57 (C_{quat}), 133.26 (CH), 132.65 (CH), 131.01 (CH), 130.74 (2CH), 130.62 (2CH), 130.14 (2CH), 129.98 (CH), 128.95 (2CH), 127.57 (CH), 126.87 (CH), 125.31 (CH), 124.86 (2CH), 124.49 (2CH), 124.23 (2CH), 123.98 (2CH), 123.17 (CH), 121.79 (CH).

UV/Vis (CH_3CN), λ, nm (ε, 10^4 M^{-1} cm^{-1}): 350 (12.7), 435 (1.7).

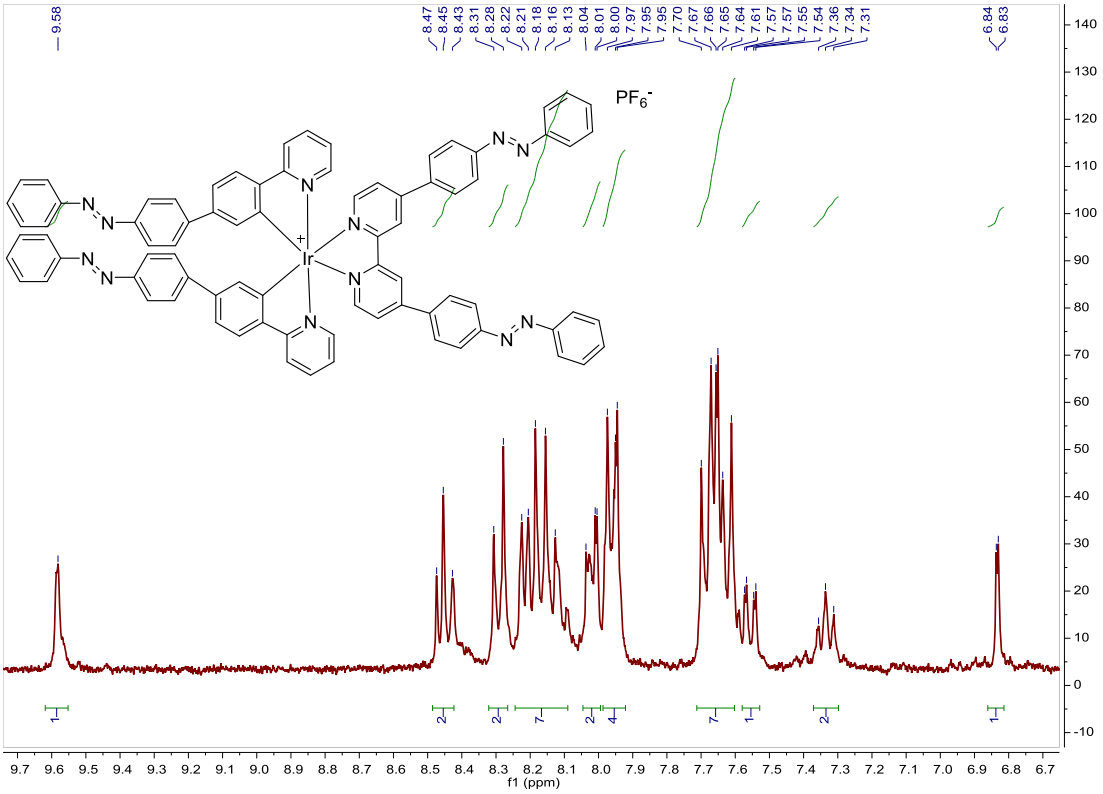

Fig. S236. ^{1}H NMR spectrum of **D3** in acetone-*d*$_6$, 300 MHz.

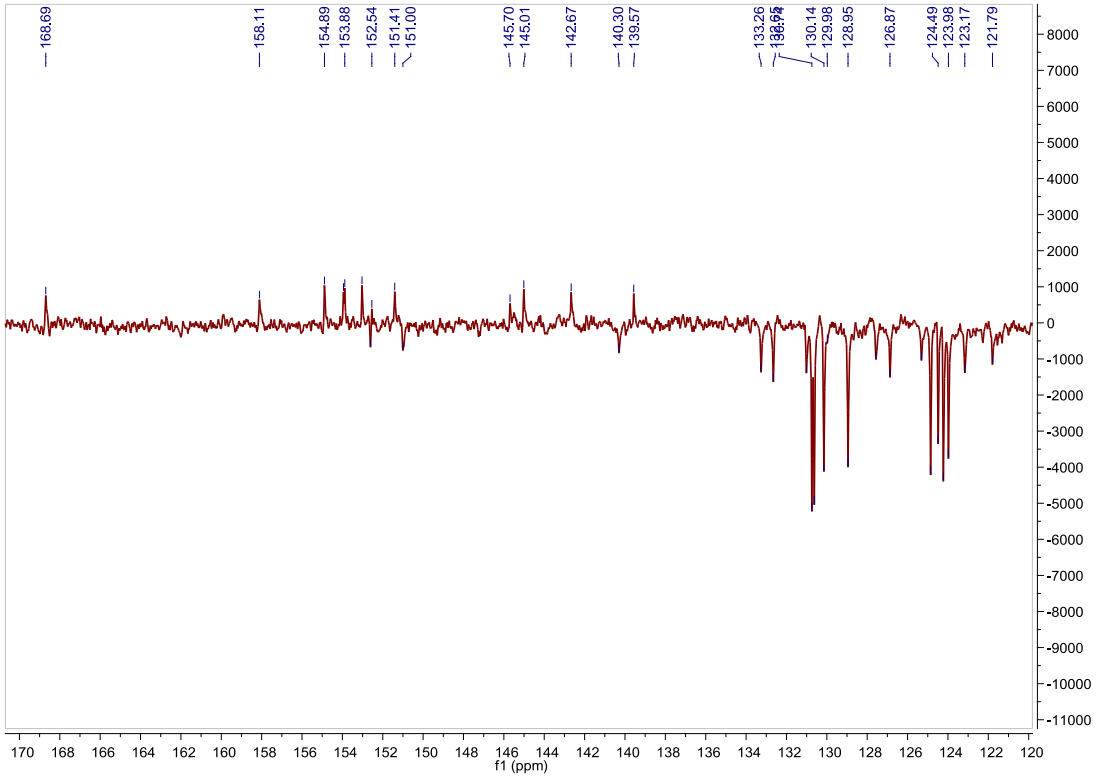

Fig. S237. ^{13}C APT NMR spectrum of **D3** in acetone-d_6, 75 MHz.

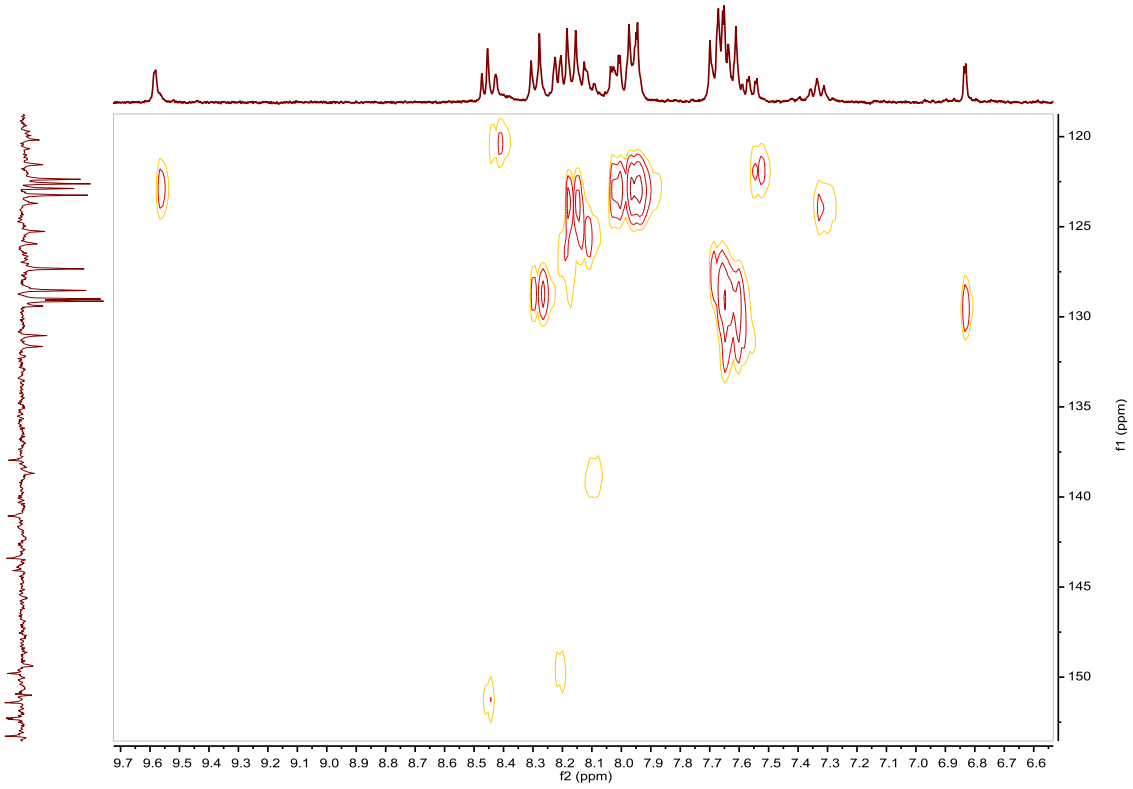

Fig. S238. HSQC NMR spectrum of **D3** in acetone-d_6.

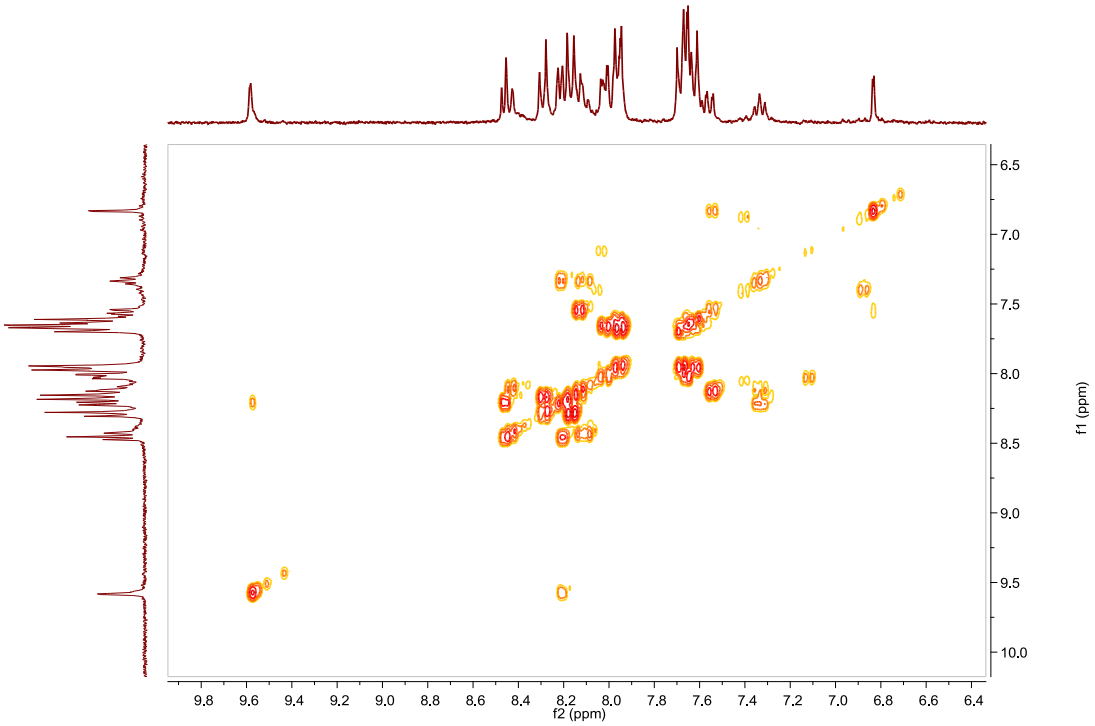

Fig. S239. COSY NMR spectrum of **D3** in acetone-d_6.

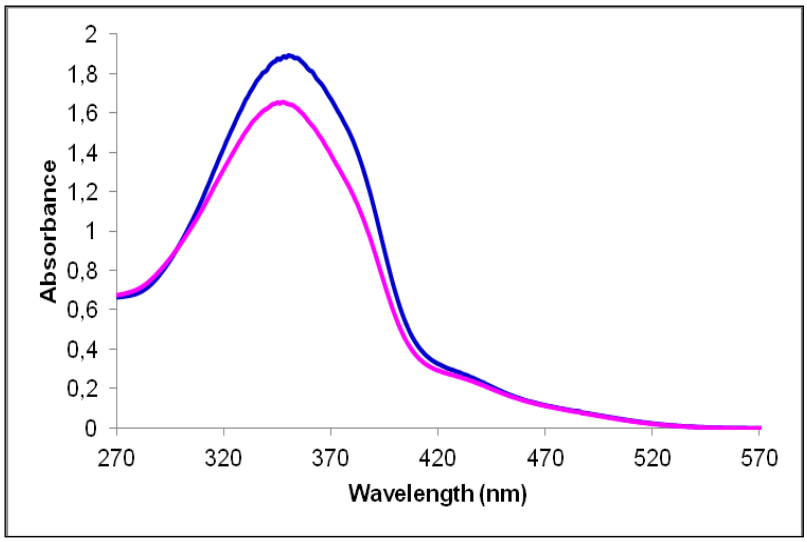

Fig. S240. UV/Vis spectra of **D3** in CH_3CN. Before (blue line) and after (pink line) irradiation at 355nm, $1.5 \cdot 10^{-5}$ M.

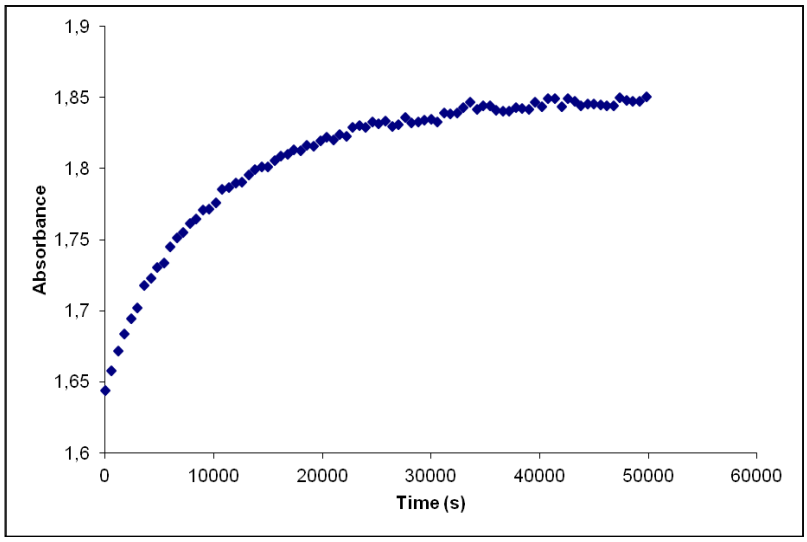

Fig. S241. Cis to trans thermal isomerization kinetics of **D3**. Absorption change of the band 350nm at 328 K in CH_3CN after irradiation at 355 nm. ($1.5 \cdot 10^{-5}$ M).

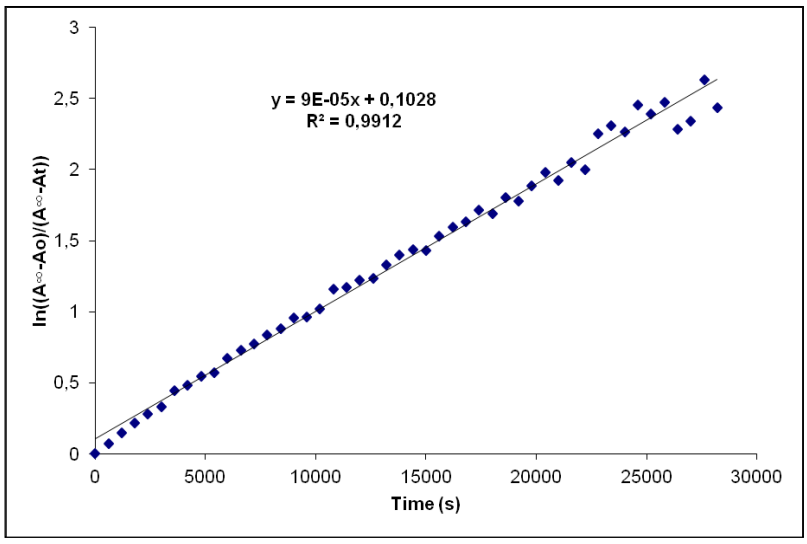

Fig. S242. Cis to trans thermal isomerization kinetics of **D3**. First-order plot. k (s^{-1}) = $9.0 \cdot 10^{-5}$. Half-life (min) = 128.

Compound A4, $[Ir(ppy)_2(4)]PF_6$. Synthesis, characterization and photoisomerization studies.

SYNTHESIS

Under a N_2 atmosphere, $[Ir(ppy)_2Cl]_2$ (0.100 g, 0.093 mmol) were added over a suspension of **L4** (0.077 g, 0.186 mmol) in 8 ml CH_2Cl_2–MeOH 2/1. The reaction mixture was refluxed, under N_2, for 15 h. After solvent evaporation the product was purified by column chromatography (silica gel, CH_2Cl_2). When the unreacted $[Ir(ppy)_2Cl]_2$ eluted, 0.05 g of KPF_6 were added on top of the column and the polarity of the eluent was gradually increased to 100% acetone to elute $[Ir(ppy)_2(\mathbf{L4})]PF_6$ together with the excess of KPF_6. The desired compound, purified by filtration through a celite path in CH_2Cl_2, was obtained as a red solid. Yield 86%.

Elemental Analysis: calculated for ($C_{44}H_{31}BrIrN_6PF_6$): C, 49.82; H, 2.95; N, 7.92. Found: C, 49.71; H, 3.10; N, 7.58.

Exact Mass: ESI-MS $[C_{44}H_{31}BrIrN_6]^+$: calculated: m/z= 915.1423, found: m/z= 915.1398.

^{1}H NMR (300 MHz, acetone-d_6): δ 9.36 (s, 2H), 8.26 (brd, J = 8.5 Hz, 4H), 8.19 (d, J = 5.8 Hz, 1H), 8.12 (brd, J = 8.5 Hz, 3H), 8.06–7.91 (m, 10H), 7.63 (m, 3H), 7.22 (ddd, J = 1.4 Hz, J = 5.8 Hz, J = 7.6 Hz, 2H), 7.07 (ddd, J = 1.0 Hz, J = 7.3 Hz, J = 12.8 Hz, 2H), 6.96 (ddd, J = 1.2 Hz, J = 7.3 Hz, J = 12.6 Hz, 2H), 6.41 (dd, J = 3.6 Hz, J = 7.4 Hz, 2H).

^{13}C APT NMR (75 MHz, acetone-d_6): δ 168.98 (C_{quat}), 168.94 (C_{quat}), 158.78 (C_{quat}), 156.97 (C_{quat}), 154.86 (C_{quat}), 153.88 (C_{quat}), 152.48 (CH), 152.30 (CH), 151.56 (C_{quat}), 151.31 (C_{quat}), 151.25 (C_{quat}), 150.87 (CH), 150.72 (CH), 145.42 (C_{quat}), 145.40 (C_{quat}), 140.12 (2CH), 139.28 (C_{quat}), 137.13 (C_{quat}), 133.22 (CH), 133.15 (CH), 132.93 (2CH), 131.76 (2CH), 130.74 (2CH), 130.13 (2CH), 129.88 (CH), 127.66 (CH), 126.31 (2CH), 125.07 (2CH), 124.84 (2CH), 124.25 (3CH), 123.95 (2CH), 121.30 (2CH).

UV/Vis (CH_3CN), λ, nm (ε, 10^4 M^{-1} cm^{-1}): 333 (4.4), 465 (0.30).

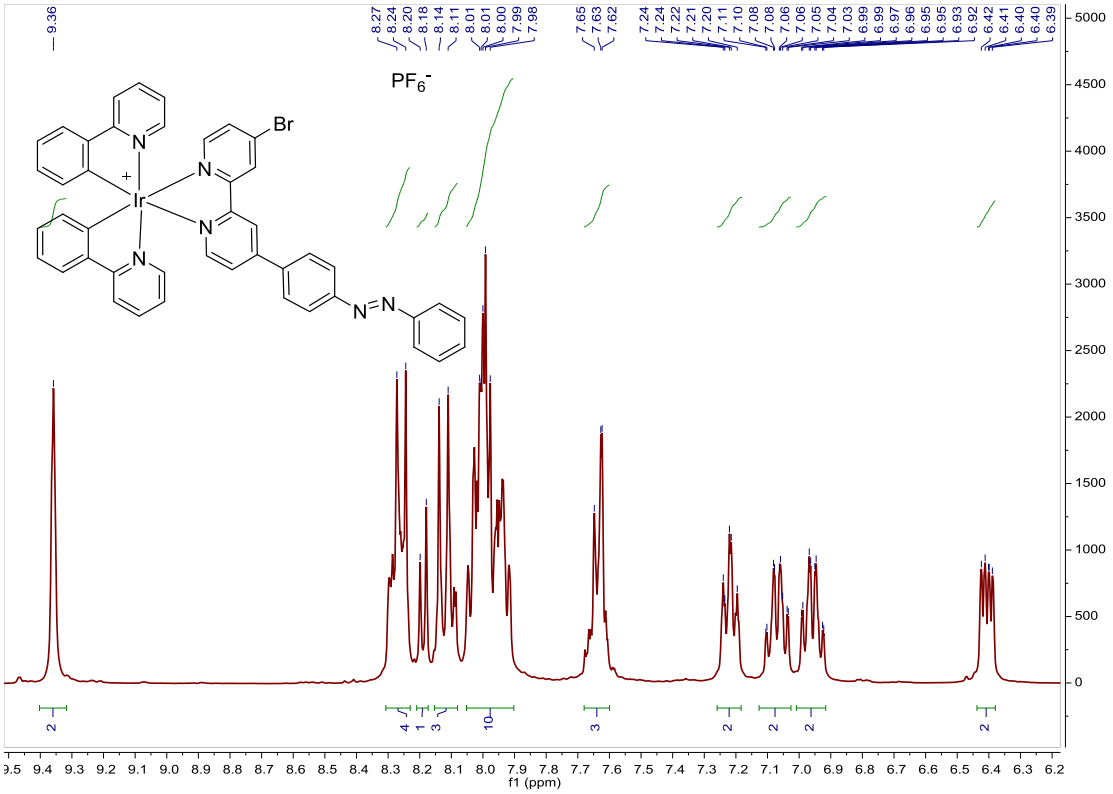

Fig. S243. ^{1}H NMR spectrum of **A4** in acetone-d_6, 300 MHz.

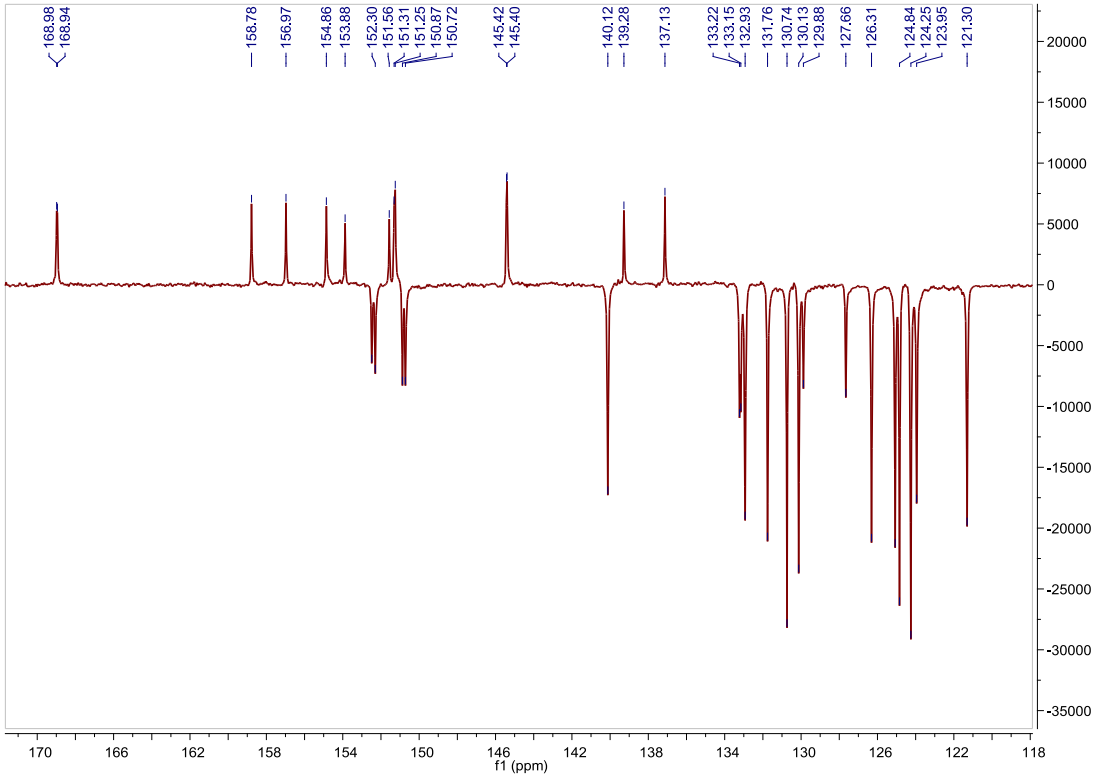

Fig. S244. ^{13}C APT NMR spectrum of **A4** in acetone-d_6, 75 MHz.

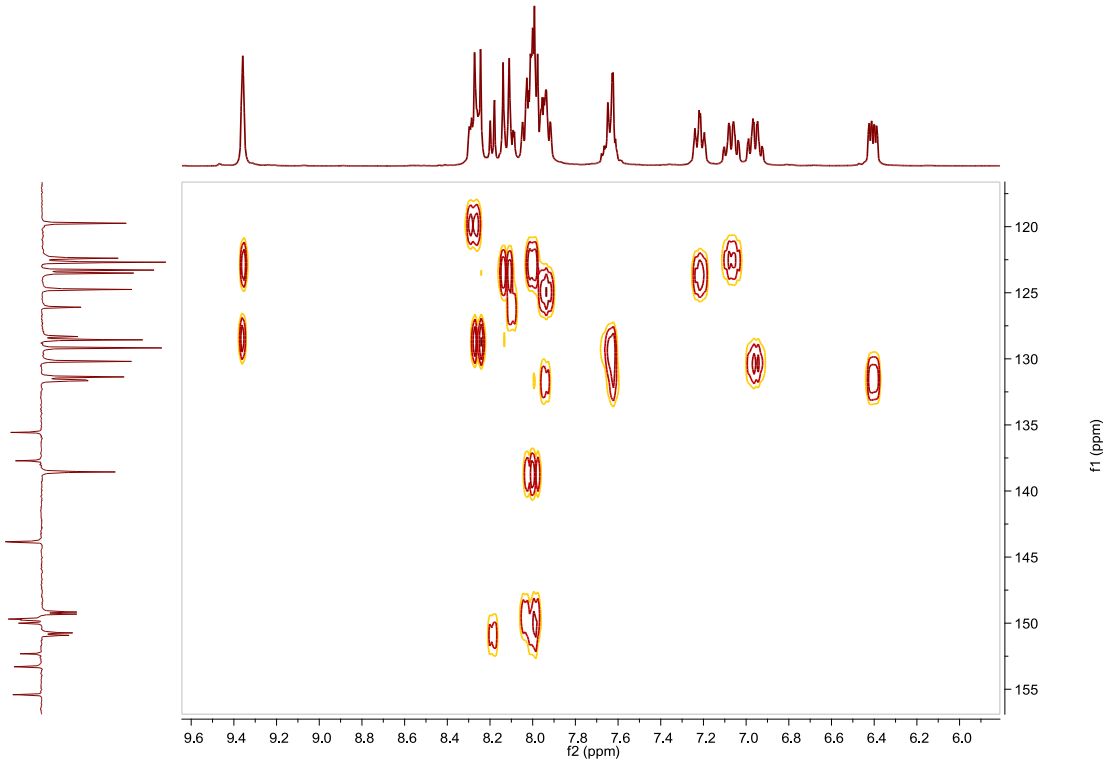

Fig. S245. HSQC NMR spectrum of **A4** in acetone-d_6.

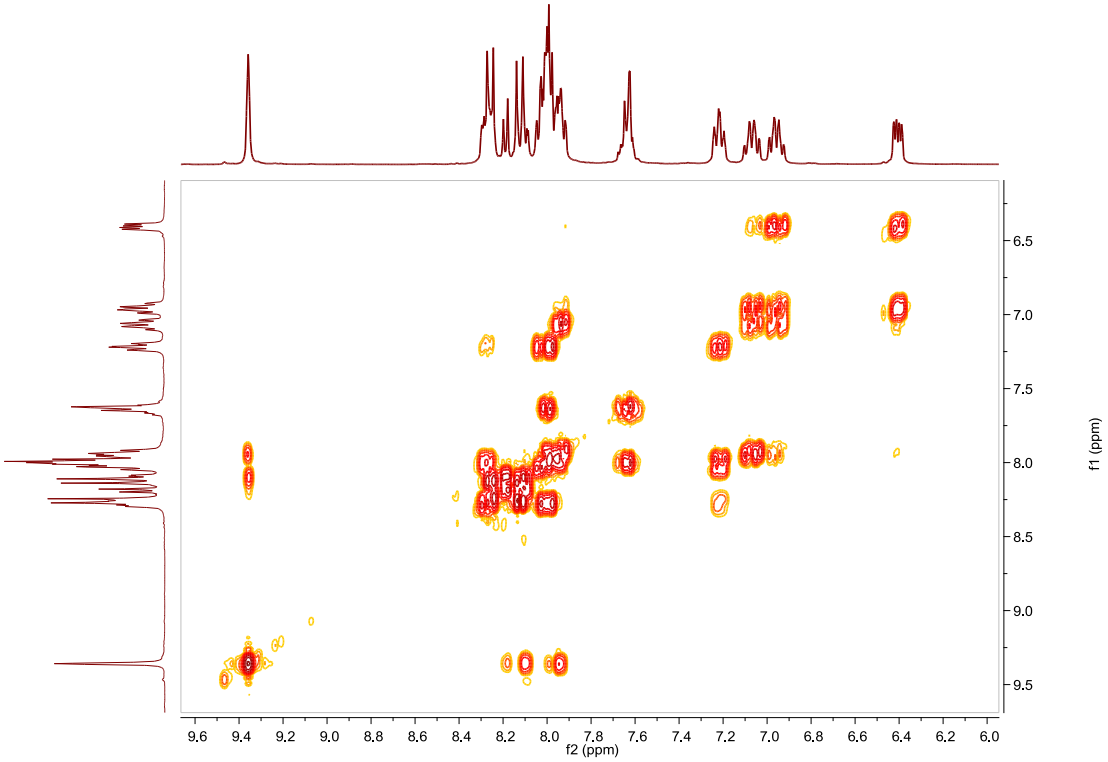

Fig. S246. COSY NMR spectrum of **A4** in acetone-d_6.

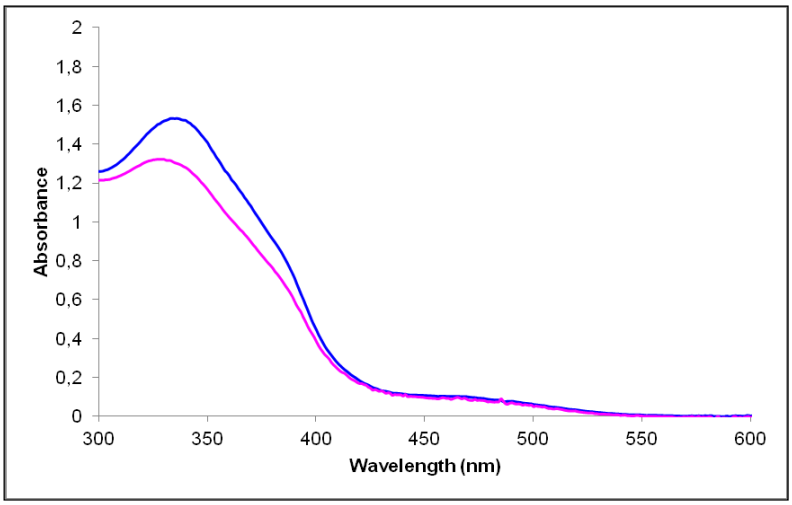

Fig. S247. UV/Vis spectra of **A4** in CH_3CN. Before (blue line) and after (pink line) irradiation at 343nm, $3.45 \cdot 10^{-5}$ M.

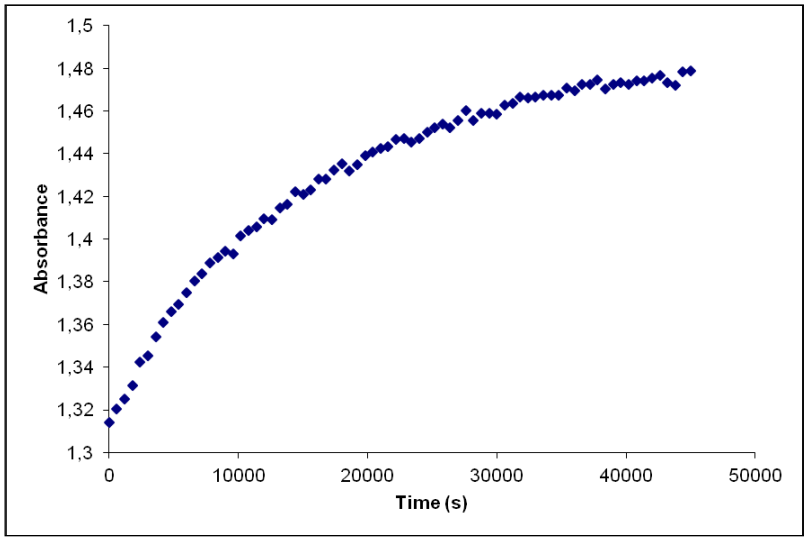

Fig. S248. Cis to trans thermal isomerization kinetics of **A4**. Absorption change of the band 333nm at 328 K in CH_3CN after irradiation at 343 nm. ($3.45 \cdot 10^{-5}$ M).

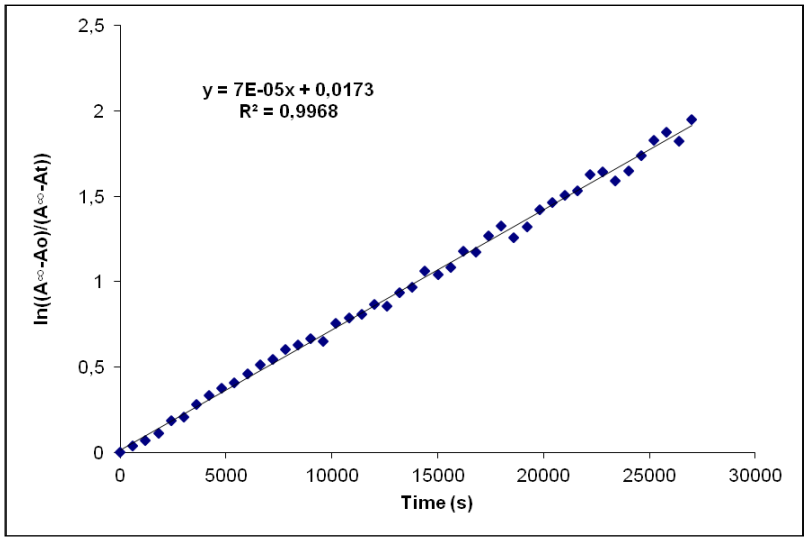

Fig. S249. Cis to trans thermal isomerization kinetics of **A4**. First-order plot. k (s^{-1}) = $7.0 \cdot 10^{-5}$. Half-life (min) = 165.

Compound B4, $[Ir(Fppy)_2(4)]PF_6$. Synthesis, characterization and photoisomerization studies.

SYNTHESIS

Under a N_2 atmosphere, $[Ir(Fppy)_2Cl]_2$ (0.100 g, 0.082 mmol) were added over a suspension of **L4** (0.068 g, 0.164 mmol) in 8 ml CH_2Cl_2–MeOH 2/1. The reaction mixture was refluxed, under N_2, for 15 h. After solvent evaporation the product was purified by column chromatography (silica gel, CH_2Cl_2). When the unreacted $[Ir(Fppy)_2Cl]_2$ eluted, 0.05 g of KPF_6 were added on top of the column and the polarity of the eluent was gradually increased to 100% acetone to elute $[Ir(Fppy)_2(\mathbf{L4})]PF_6$ together with the excess of KPF_6. The desired compound was precipitated with ether after filtration through a celite path in CH_2Cl_2 and it was obtained as an orange solid. Yield 87%.

Elemental Analysis: calculated for $(C_{44}H_{27}BrF_4IrN_6PF_6 \cdot CH_3COCH_3)$: C, 47.40; H, 2.79; N, 7.06. Found: C, 47.23; H, 2.88; N, 7.27.

Exact Mass: ESI-MS $[C_{44}H_{27}BrF_4IrN_6]^+$: calculated: m/z= 987.1032, found: m/z= 987.1014.

^{1}H NMR (300 MHz, acetone-d_6): δ 9.43 (brs, 2H), 8.44 (m, 2H), 8.33 (d, J = 5.8 Hz, 1H), 8.28 (brd, J = 8.8 Hz, 2H), 8.20 (dd, J = 1.8 Hz, J = 5.8 Hz, 1H), 8.17–8.07 (m, 7H), 8.01 (m, 3H), 7.65 (m, 3H), 7.31 (m, 2H), 6.82 (m, 2H), 5.87 (t, J = 2.6 Hz, 1H), 5.84 (t, J = 2.6 Hz, 1H).

^{13}C APT NMR (75 MHz, acetone-d_6): δ 165.10 (brs, 2C_{quat}), 165.00 (dd, J = 12.2 Hz, J = 254.5 Hz, 2C_{quat}), 162.82 (dd, J = 12.5 Hz, J = 257.3 Hz, 2C_{quat}), 158.54 (s, C_{quat}), 156.79 (s, C_{quat}), 155.62 (d, J = 6.3 Hz, C_{quat}), 155.36 (d, J = 6.4 Hz, C_{quat}), 154.99 (s, C_{quat}), 153.88 (s, C_{quat}), 152.92 (s, CH), 152.70 (s, CH), 151.85 (s, C_{quat}), 151.41 (s, CH), 151.27 (s, CH), 141.23 (s, 2CH), 139.06 (s, C_{quat}), 137.82 (s, C_{quat}), 133.50 (s, CH), 133.27 (s, CH), 130.74 (s, 2CH), 130.16 (s, 3CH), 129.29 (s, 2C_{quat}), 127.97 (s, CH), 125.59 (s, 2CH), 125.04 (d, J = 22.5 Hz, CH), 124.87 (s, 3CH), 124.72 (d, J = 20.8 Hz, CH), 124.24 (s, 2CH), 115.09 (d, J = 17.7 Hz, 2CH), 100.19 (t, J = 26.9 Hz, 2CH).

UV/Vis (CH_3CN), λ, nm (ε, 10^4 M^{-1} cm^{-1}): 339 (4.3), 440 (0.33).

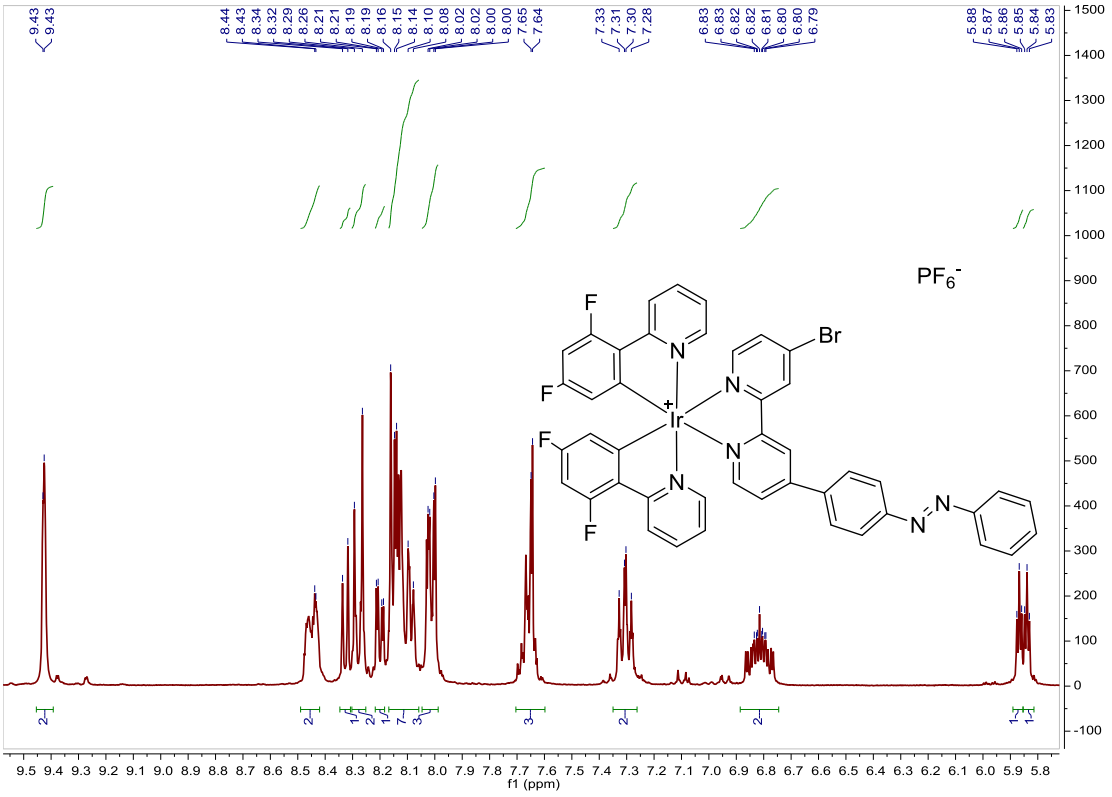

Fig. S250. ^{1}H NMR spectrum of **B4** in acetone-d_6, 300 MHz.

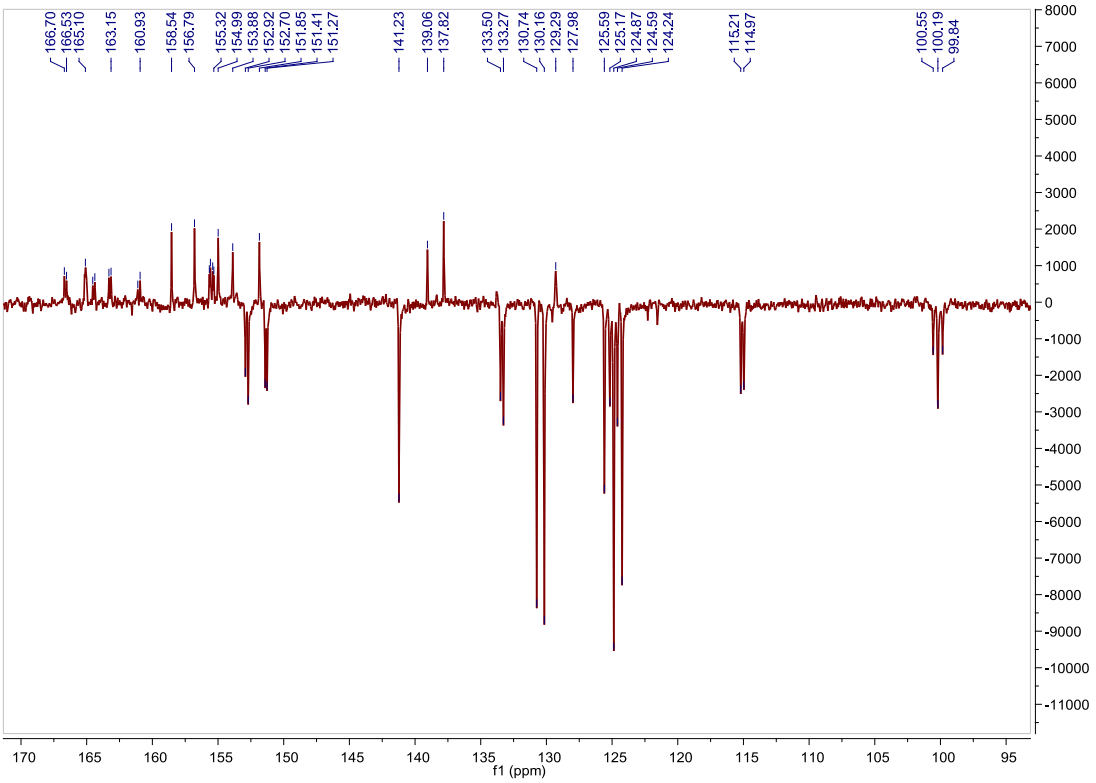

Fig. S251. ^{13}C APT NMR spectrum of **B4** in acetone-d_6, 75 MHz.

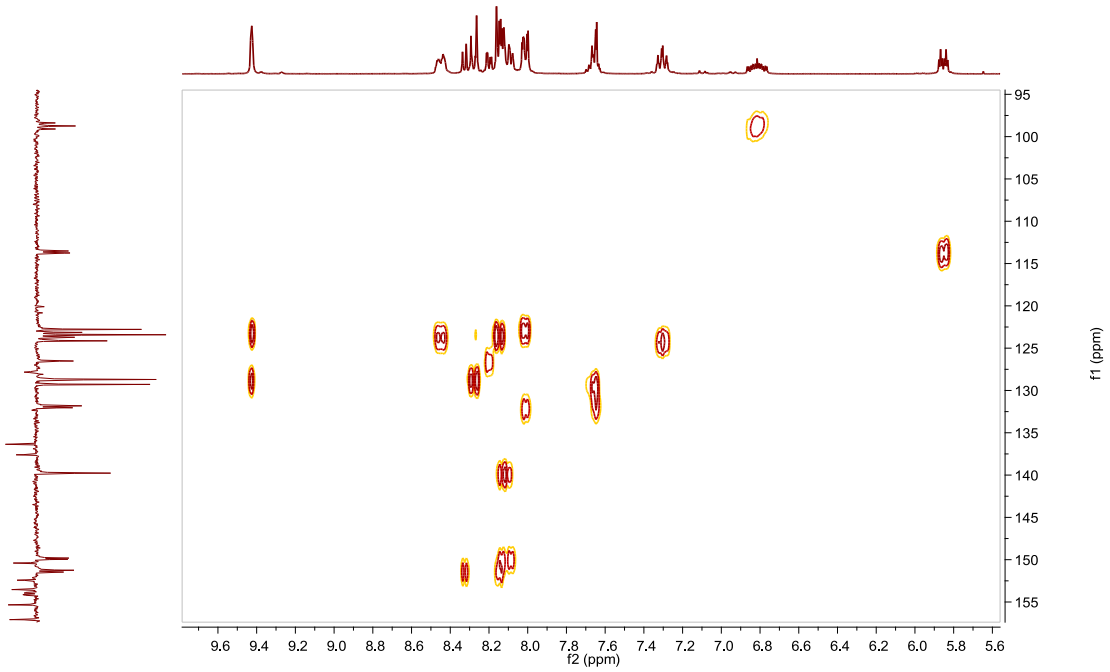

Fig. S252. HSQC NMR spectrum of **B4** in acetone-d_6.

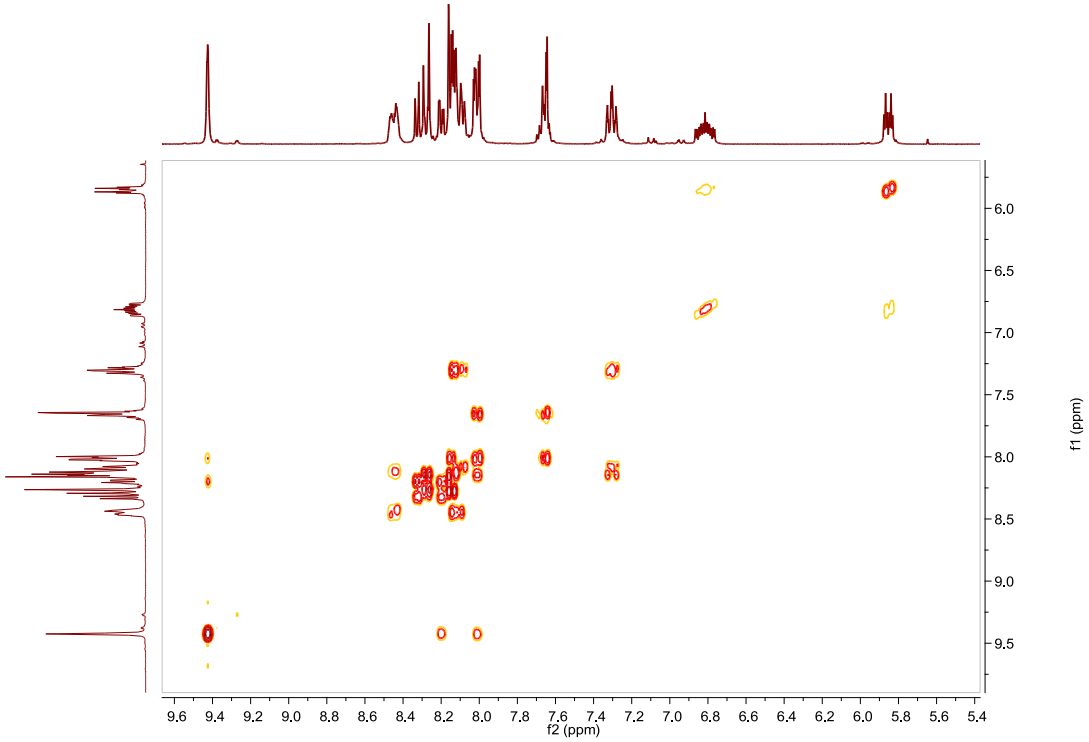

Fig. S253. COSY NMR spectrum of **B4** in acetone-d_6.

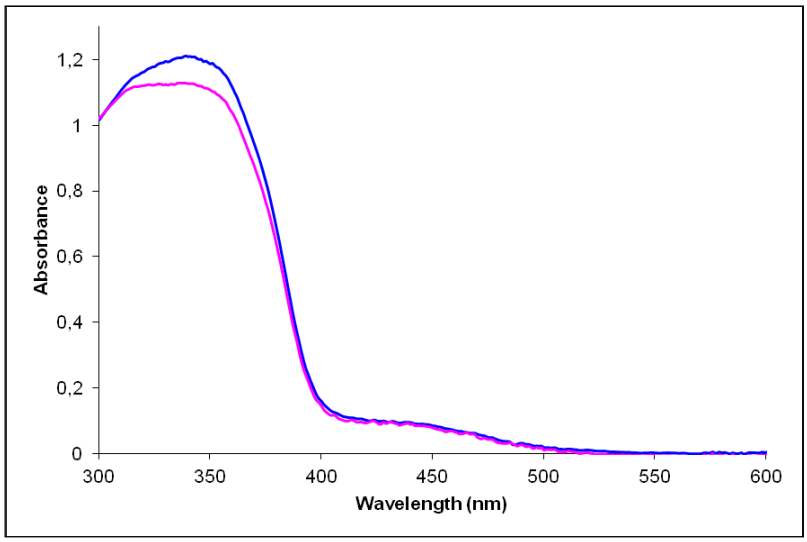

Fig. S254. UV/Vis spectra of **B4** in CH_3CN. Before (blue line) and after (pink line) irradiation at 351nm, $2.82 \cdot 10^{-5}$ M.

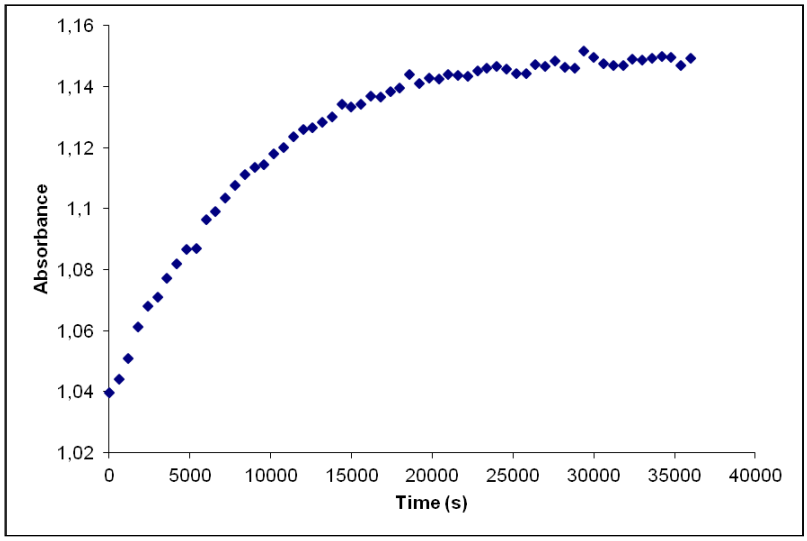

Fig. S255. Cis to trans thermal isomerization kinetics of **B4**. Absorption change of the band 339nm at 328 K in CH_3CN after irradiation at 351 nm. ($2.82 \cdot 10^{-5}$ M).

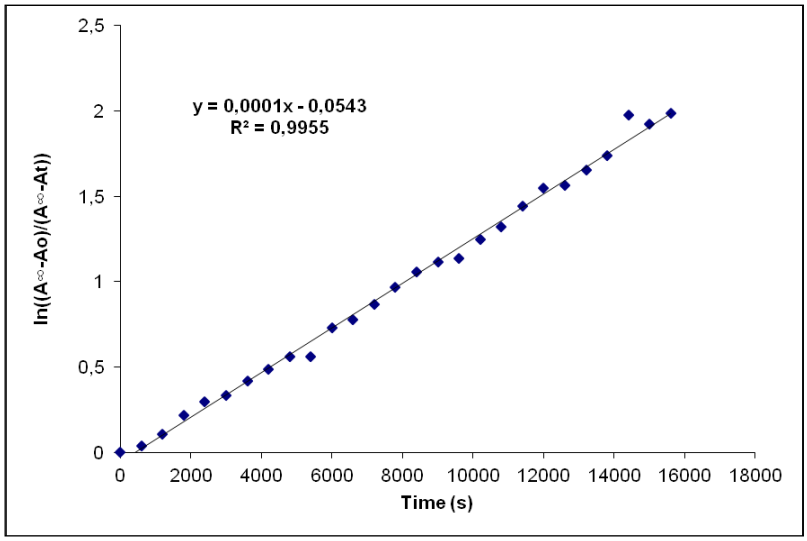

Fig. S256. Cis to trans thermal isomerization kinetics of **B4**. First-order plot. k (s^{-1}) = $1.0 \cdot 10^{-4}$. Half-life (min) = 115.

Compound C4, $[Ir(Brppy)_2(4)]PF_6$. Synthesis, characterization and photoisomerization studies.

SYNTHESIS

Under a N_2 atmosphere, $[Ir(Brppy)_2Cl]_2$ (0.100 g, 0.072 mmol) were added over a suspension of **L4** (0.06 g, 0.144 mmol) in 8 ml CH_2Cl_2–MeOH 2/1. The reaction mixture was refluxed, under N_2, for 15 h. After solvent evaporation the product was purified by column chromatography (silica gel, CH_2Cl_2). When the unreacted $[Ir(Brppy)_2Cl]_2$ eluted, 0.05 g of KPF_6 were added on top of the column and the polarity of the eluent was gradually increased to 100% acetone to elute $[Ir(Brppy)_2(\mathbf{L4})]PF_6$ together with the excess of KPF_6. The desired compound, purified by filtration through a celite path in CH_2Cl_2, was obtained as an orange solid. Yield 98%.

Elemental Analysis: calculated for ($C_{44}H_{29}Br_3IrN_6PF_6$): C, 43.37; H, 2.40; N, 6.90. Found: C, 42.97; H, 2.83; N, 6.79.

Exact Mass: ESI-MS $[C_{44}H_{29}Br_3IrN_6]^+$: calculated: m/z= 1070.9607, found: m/z= 1070.9579.

^{1}H NMR (300 MHz, acetone-d_6): δ 9.40 (d, J = 1.7 Hz, 2H), 8.34 (m, 2H), 8.27 (m, 3H), 8.18 (dd, J = 1.8 Hz, J = 5.9 Hz, 1H), 8.14 (brd, J = 8.7 Hz, 2H), 8.11–8.05 (m, 4H), 8.05–7.98 (m, 4H), 7.95 (dd, J = 5.7 Hz, J = 8.4 Hz, 2H), 7.69–7.62 (m, 3H), 7.35–7.25 (m, 4H), 6.46 (dd, J = 2.0 Hz, J = 3.1 Hz, 2H).

^{13}C APT NMR (75 MHz, acetone-d_6): δ 167.71 (C_{quat}), 167.66 (C_{quat}), 158.66 (C_{quat}), 156.90 (C_{quat}), 154.94 (C_{quat}), 153.88 (C_{quat}), 153.59 (C_{quat}), 153.34 (C_{quat}), 152.77 (CH), 152.55 (CH), 151.64 (C_{quat}), 151.13 (CH), 150.97 (CH), 144.74 (C_{quat}), 144.72 (C_{quat}), 140.67 (2CH), 139.15 (C_{quat}), 137.58 (C_{quat}), 135.10 (CH), 135.07 (CH), 133.38 (CH), 133.25 (CH), 130.74 (2CH), 130.15 (2CH), 130.07 (CH), 128.13 (2CH), 127.87 (CH), 127.26 (2CH), 126.26 (2C_{quat}), 125.76 (2CH), 124.86 (2CH), 124.48 (CH), 124.25 (2CH), 121.90 (2CH).

UV/Vis (CH_3CN), λ, nm (ε, 10^4 M^{-1} cm^{-1}): 336 (4.7), 453 (0.35).

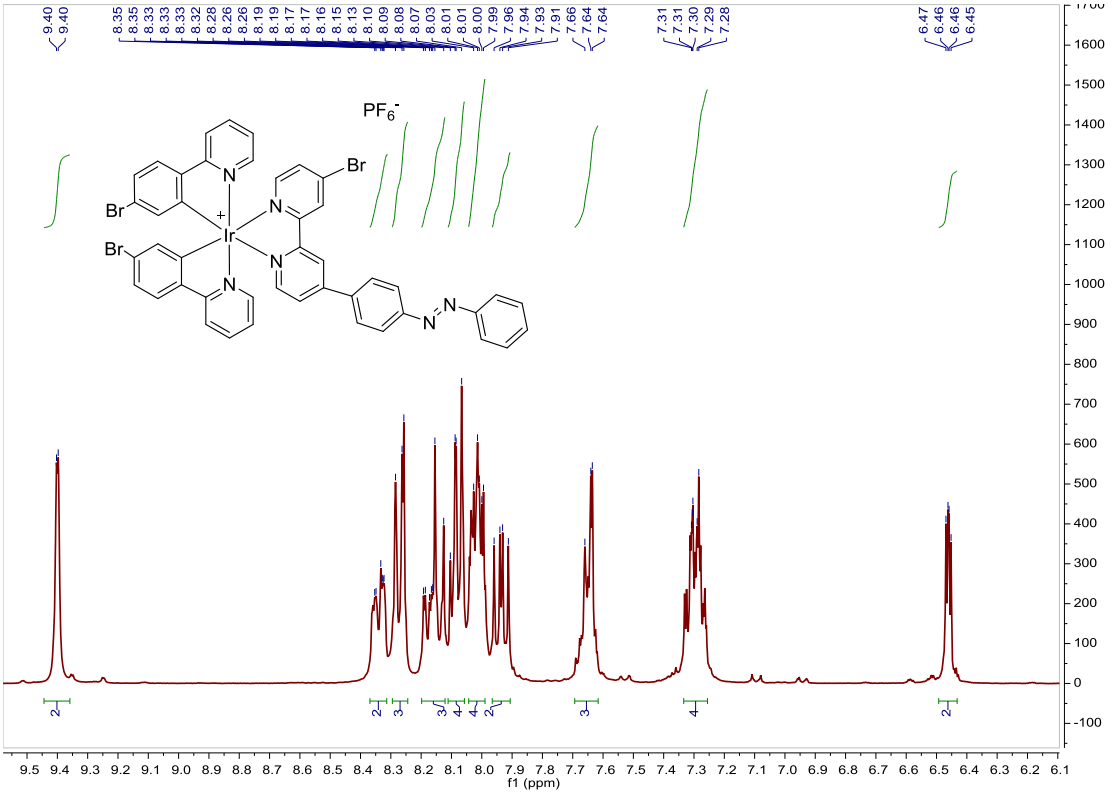

Fig. S257. ^{1}H NMR spectrum of **C4** in acetone-d_6, 300 MHz.

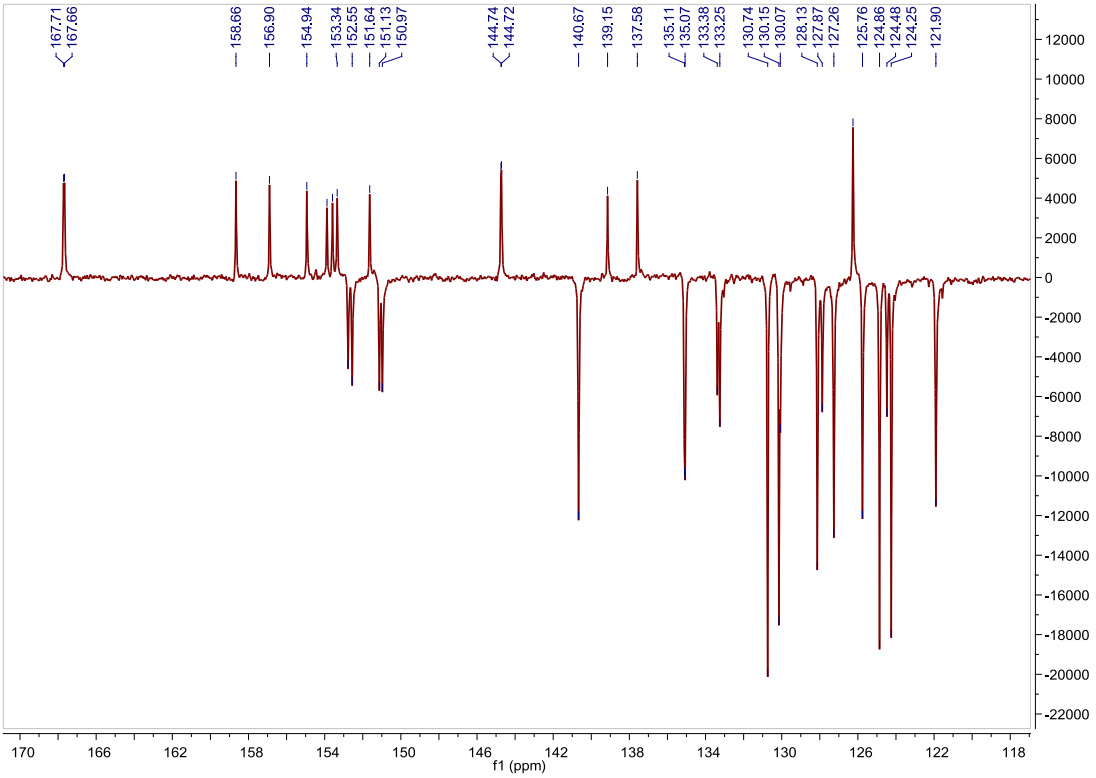

Fig. S258. ^{13}C APT NMR spectrum of **C4** in acetone-d_6, 75 MHz.

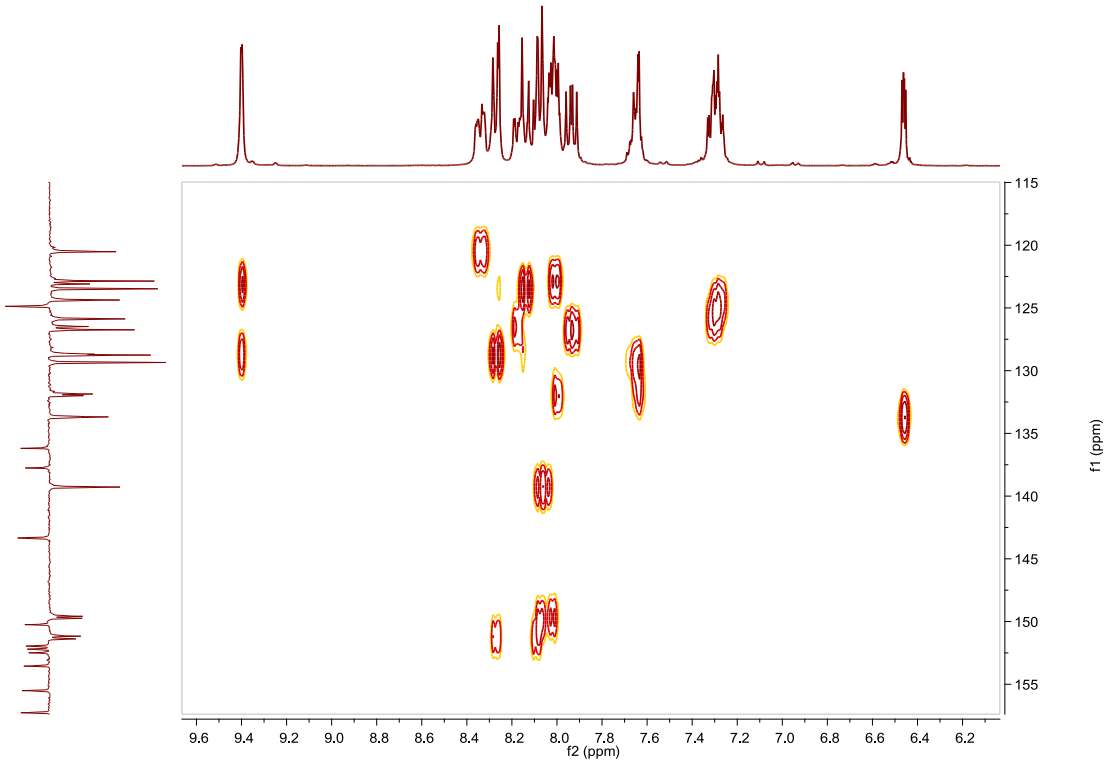

Fig. S259. HSQC NMR spectrum of **C4** in acetone-d_6.

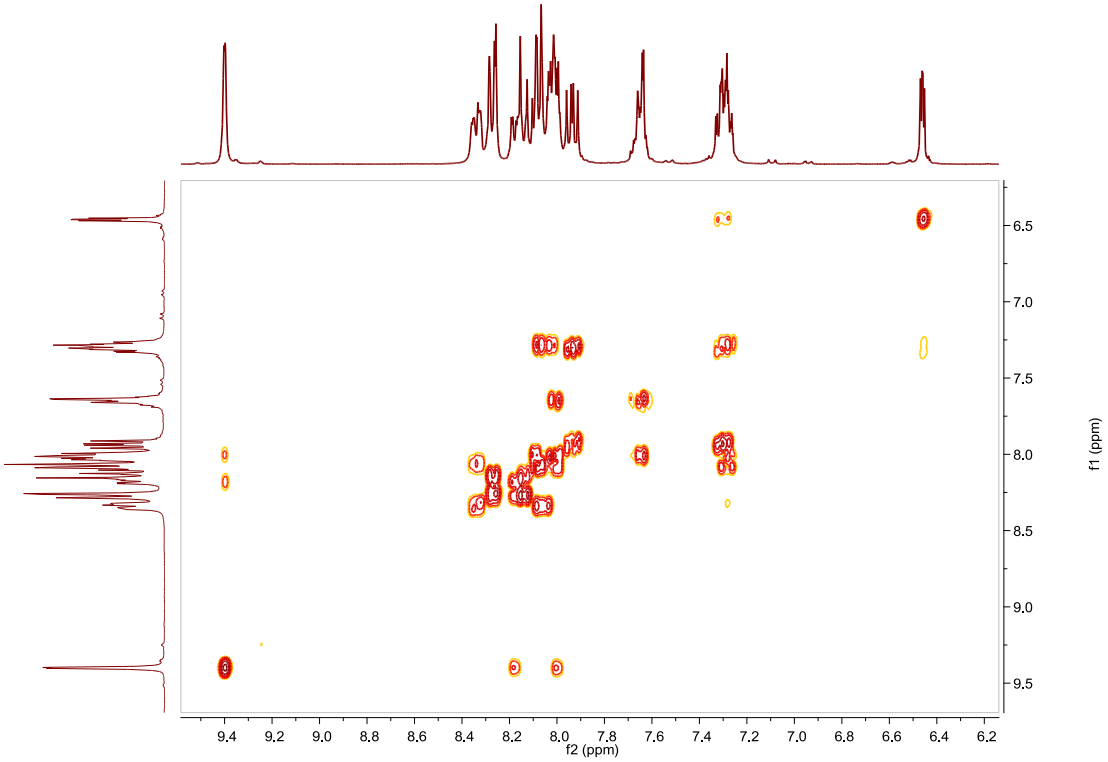

Fig. S260. COSY NMR spectrum of **C4** in acetone-d_6.

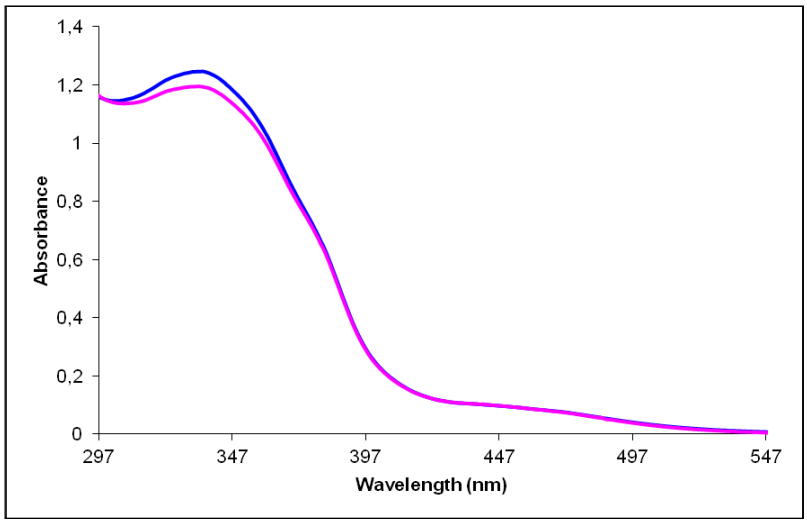

Fig. S261. UV/Vis spectra of **C4** in CH_3CN. Before (blue line) and after (pink line) irradiation at 336nm, $2.61 \cdot 10^{-5}$ M.

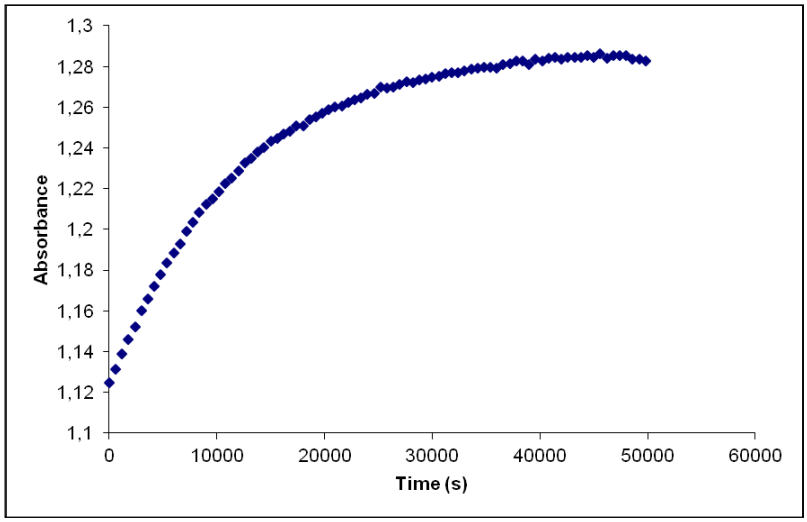

Fig. S262. Cis to trans thermal isomerization kinetics of **C4**. Absorption change of the band 336nm at 328 K in CH_3CN after irradiation at 336 nm. ($2.61 \cdot 10^{-5}$ M).

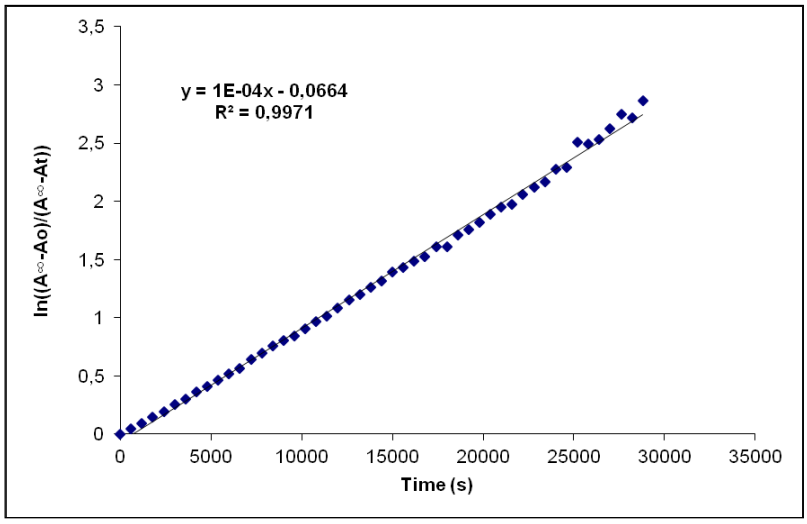

Fig. S263. Cis to trans thermal isomerization kinetics of **C4**. First-order plot. k (s^{-1}) = $1.0 \cdot 10^{-4}$. Half-life (min) = 115.

Compound A5, [Ir(ppy)$_2$(5)]PF$_6$. Synthesis, characterization and photoisomerization studies.

SYNTHESIS

Under a N_2 atmosphere, $[Ir(ppy)_2Cl]_2$ (0.052 g, 0.048 mmol) were added over a suspension of **L5** (0.05 g, 0.097 mmol) in 4 ml CH_2Cl_2–MeOH 2/1. The reaction mixture was refluxed, under N_2, for 15 h. After solvent evaporation the product was purified by column chromatography (silica gel, CH_2Cl_2). When the unreacted $[Ir(ppy)_2Cl]_2$ eluted, 0.025 g of KPF_6 were added on top of the column and the polarity of the eluent was gradually increased to 100% acetone to elute $[Ir(ppy)_2$(**L5**)$]PF_6$ together with the excess of KPF_6. The desired compound, purified by filtration through a celite path in CH_2Cl_2, was obtained as an orange solid. Yield 75%.

Elemental Analysis: calculated for ($C_{56}H_{40}IrN_8PF_6$): C, 57.88; H, 3.47; N, 9.64. Found: C, 57.48; H, 3.61; N, 9.55.

Exact Mass: ESI-MS $[C_{56}H_{40}IrN_8]^+$: calculated: m/z= 1017.3005, found: m/z= 1017.2991.

^{1}H NMR (300 MHz, acetone-*d*$_6$): δ 9.55 (s, 1H), 8.48 (s, 1H), 8.32 (d, J=8.1 Hz, 1H), 8.26 (d, J=5.8 Hz, 1H), 8.14 (m, 3H), 8.01 (m, 6H), 7.85 (pst, J=7.9 Hz, 1H), 7.63 (m, 2H), 7.24 (pst, J=6.0 Hz, 1H), 7.11 (pst, J=7.6 Hz, 1H), 6.99 (pst, J=7.3 Hz, 1H), 6.46 (d, J=7.4 Hz, 1H).

^{13}C APT NMR (75 MHz, acetone-*d*$_6$): δ 173.48 (C_{quat}), 162.42 (C_{quat}), 158.89 (C_{quat}), 158.03 (C_{quat}), 156.55 (CH), 156.29 (C_{quat}), 156.06 (C_{quat}), 154.98 (CH), 149.76 (C_{quat}), 144.35 (CH), 143.00 (C_{quat}), 137.46 (CH), 137.28 (CH), 136.12 (CH), 136.07 (1C, CH), 135.82 (1C, CH), 135.04 (2C, CH), 131.96 (1C, CH), 130.62 (CH), 129.40 (CH), 129.31 (CH), 128.71 (CH), 128.42 (2CH), 128.18 (CH), 128.09 (CH), 125.61 (CH).

UV/Vis (CH_3CN), λ, nm (ε, 10^4 M^{-1} cm^{-1}): 290 (6.5), 381 (1.1), 462 (0.21).

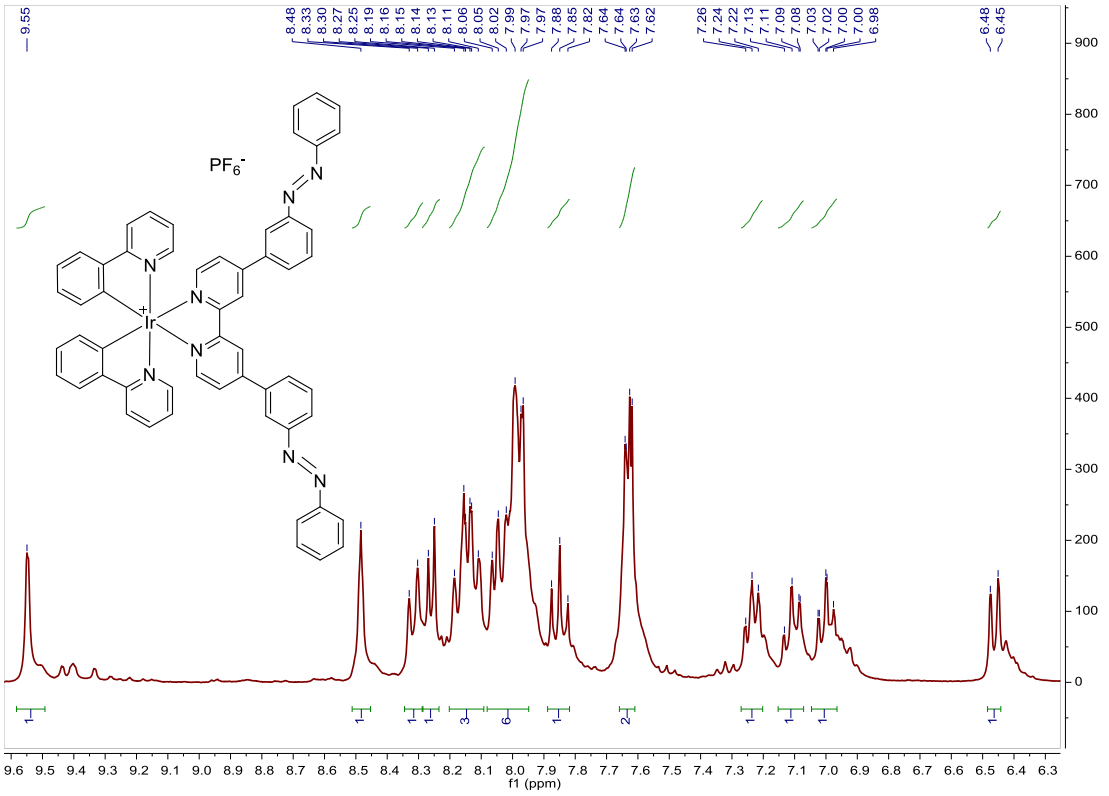

Fig. S264. ^{1}H NMR spectrum of **A5** in acetone-*d*$_6$, 300 MHz.

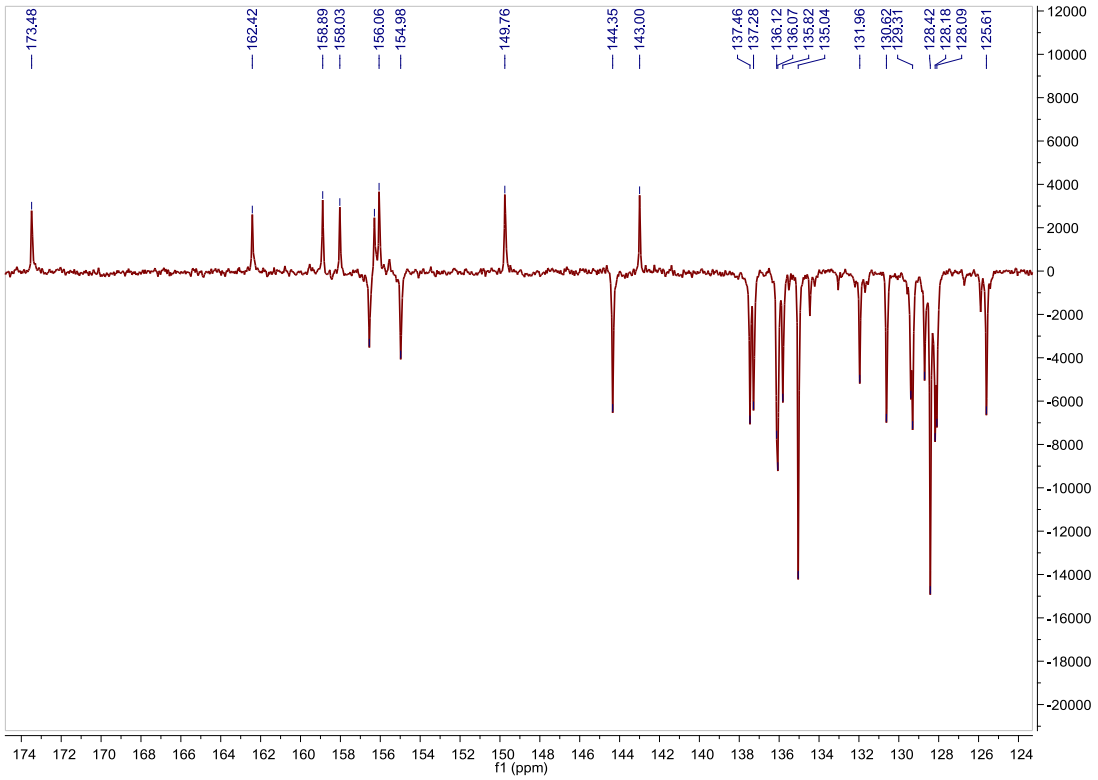

Fig. S265. ^{13}C APT NMR spectrum of **A5** in acetone-d_6, 75 MHz.

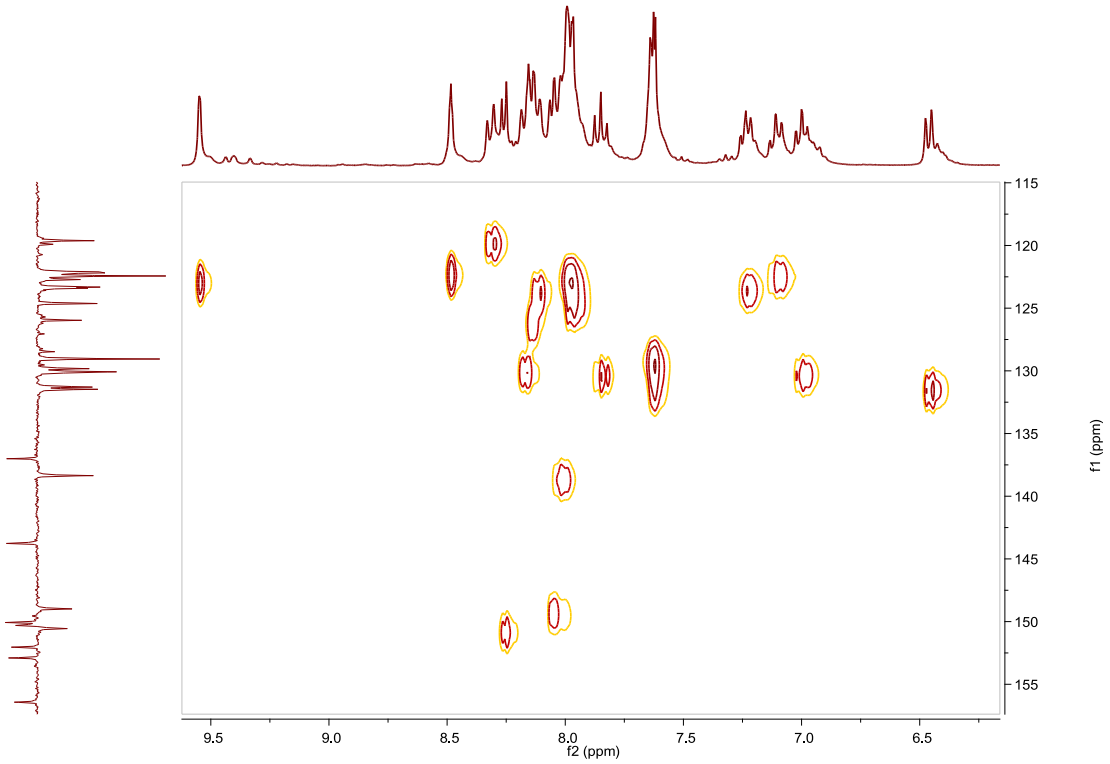

Fig. S266. HSQC NMR spectrum of **A5** in acetone-d_6.

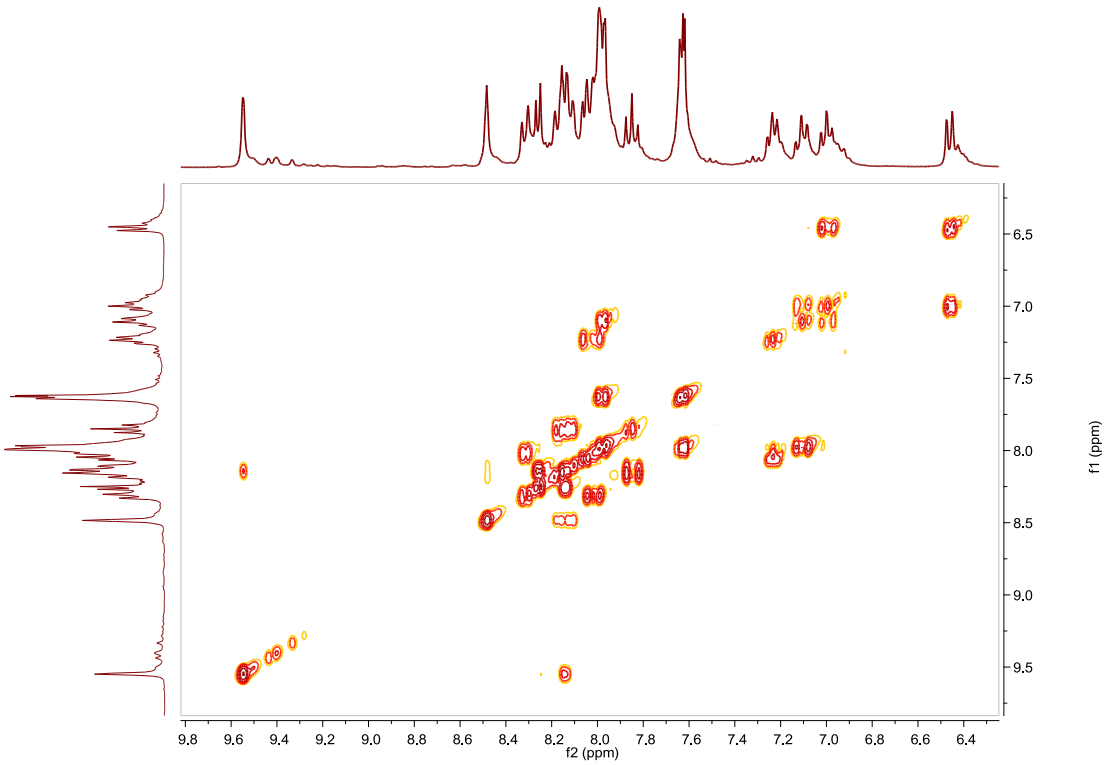

Fig. S267. COSY NMR spectrum of **A5** in acetone-d_6.

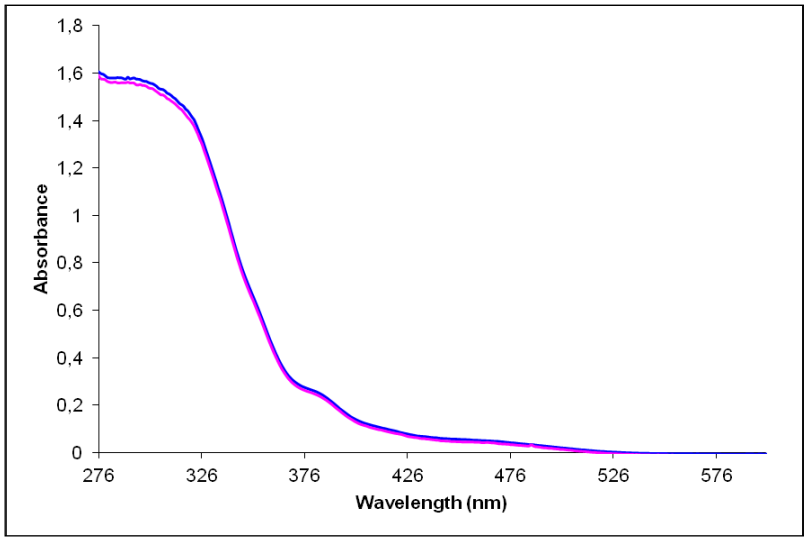

Fig. S268. UV/Vis spectra of **A5** in CH_3CN. Before (blue line) and after (pink line) irradiation at 319nm, $2.44 \cdot 10^{-5}$ M.

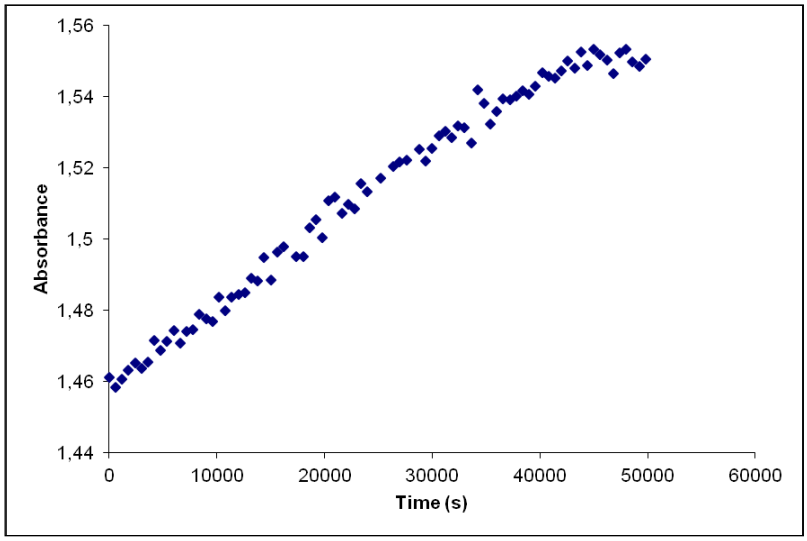

Fig. S269. Cis to trans thermal isomerization kinetics of **A5**. Absorption change of the band 290nm at 328 K in CH_3CN after irradiation at 319 nm. ($2.44 \cdot 10^{-5}$ M).

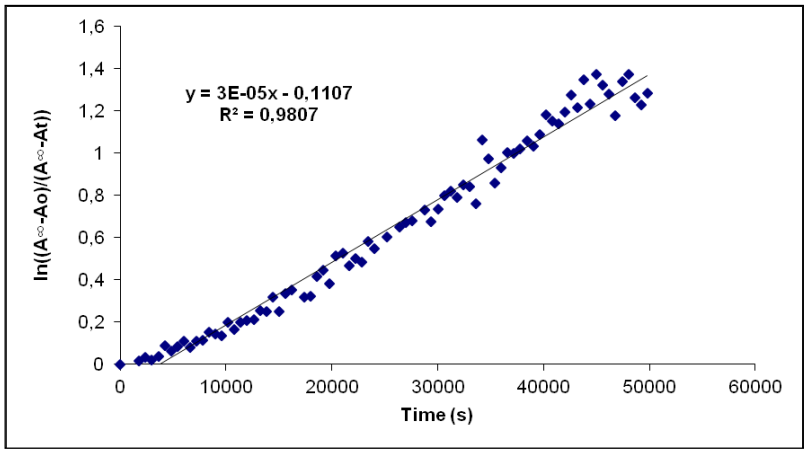

Fig. S270. Cis to trans thermal isomerization kinetics of **A5**. First-order plot. k (s^{-1}) = $3.0 \cdot 10^{-5}$. Half-life (min) = 385.

Compound B5, [Ir(Fppy)$_2$(5)]PF$_6$. Synthesis, characterization and photoisomerization studies.

SYNTHESIS

Under a N_2 atmosphere, $[Ir(Fppy)_2Cl]_2$ (0.100 g, 0.082 mmol) were added over a suspension of **L5** (0.085 g, 0.164 mmol) in 8 ml CH_2Cl_2–MeOH 2/1. The reaction mixture was refluxed, under N_2, for 15 h. After solvent evaporation the product was purified by column chromatography (silica gel, CH_2Cl_2). When the unreacted $[Ir(Fppy)_2Cl]_2$ eluted, 0.05 g of KPF_6 were added on top of the column and the polarity of the eluent was gradually increased to 100% acetone to elute $[Ir(Fppy)_2$(**L5**)$]PF_6$ together with the excess of KPF_6. The desired compound, purified by filtration through a celite path in CH_2Cl_2, was obtained as a red solid. Yield 85%.

Elemental Analysis: calculated for ($C_{56}H_{38}F_4IrN_8PF_6 \cdot CH_3COCH_3$): C, 54.84; H, 3.28; N, 8.67. Found: C, 54.70; H, 3.29; N, 8.34.

Exact Mass: ESI-MS $[C_{56}H_{36}F_4IrN_8]^+$: calculated: m/z= 1089.2628, found: m/z= 1089.2600.

^{1}H NMR (300 MHz, acetone-d_6): δ 9.58 (d, J = 1.4 Hz, 1H), 8.48 (m, 2H), 8.37 (d, J = 5.8 Hz, 1H), 8.16 (m, 5H), 7.99 (d, J = 4.3 Hz, 1H), 7.97 (d, J = 2.1 Hz, 1H), 7.86 (pst, J = 7.9 Hz, 1H), 7.63 (m, 3H), 7.33 (pst, J = 6.6 Hz, 1H), 6.83 (ddd, J = 2.3 Hz, J = 9.4 Hz, J = 12.4 Hz, 1H), 5.92 (dd, J = 2.3 Hz, J = 8.6 Hz, 1H).

^{13}C APT NMR (75 MHz, acetone-d_6): δ 165.25 (d, J = 6.9 Hz, C_{quat}), 164.99 (dd, J = 12.5 Hz, J = 254.7 Hz, C_{quat}), 162.80 (dd, J = 12.91 Hz, J = 257.8 Hz, C_{quat}), 157.88 (s, C_{quat}), 156.18 (d, J = 6.3 Hz, C_{quat}), 154.57 (s, C_{quat}), 153.72 (s, C_{quat}), 152.57 (s, CH), 152.36 (s, C_{quat}), 151.23 (s, CH), 141.19 (s, CH), 138.53 (s, C_{quat}), 133.18 (s, CH), 131.88 (s, CH), 131.56 (s, CH), 130.75 (s, 2CH), 129.34 (s, C_{quat}), 127.98 (s, CH), 125.62 (s, CH), 125.35 (s, CH), 125.06 (d, J = 19.8 Hz, CH), 124.74 (s, CH), 124.14 (s, 2CH), 123.72 (s, CH), 115.13 (d, J = 16.1 Hz, CH), 100.13 (t, J = 27.0 Hz, CH).

UV/Vis (CH_3CN), λ, nm (ε, 10^4 M^{-1} cm^{-1}): 311 (6.1), 436 (0.26).

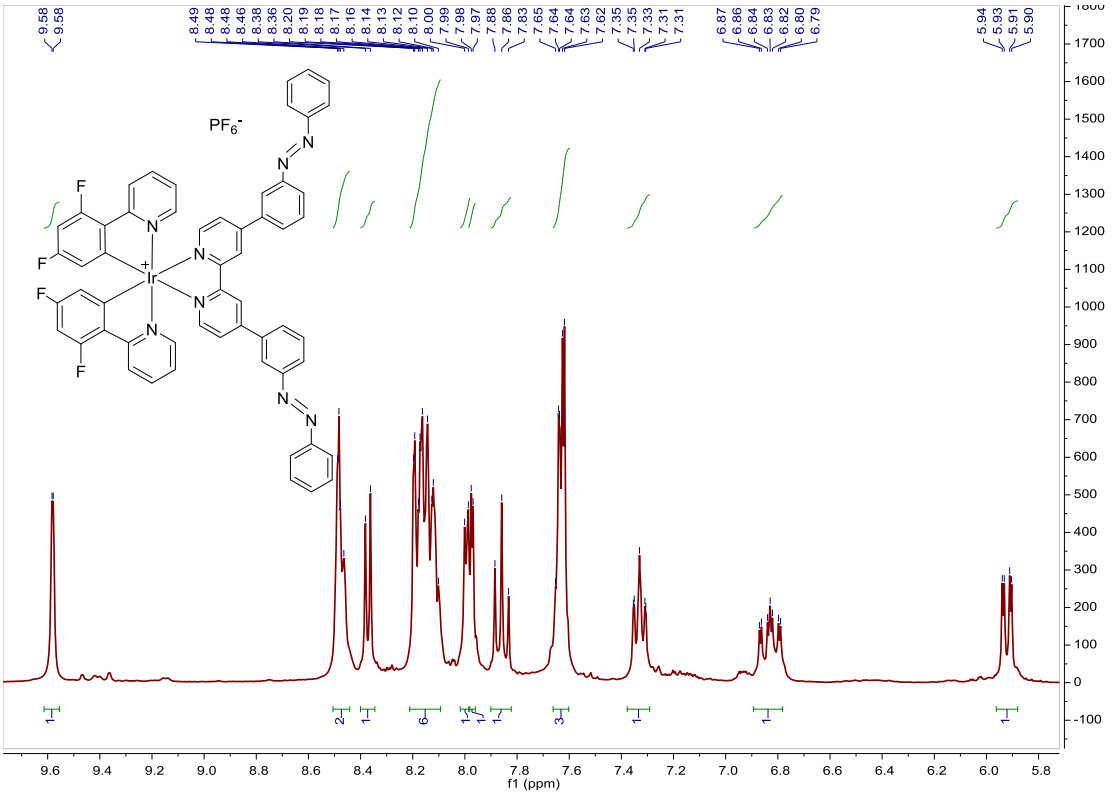

Fig. S271. ^{1}H NMR spectrum of **B5** in acetone-d_6, 300 MHz.

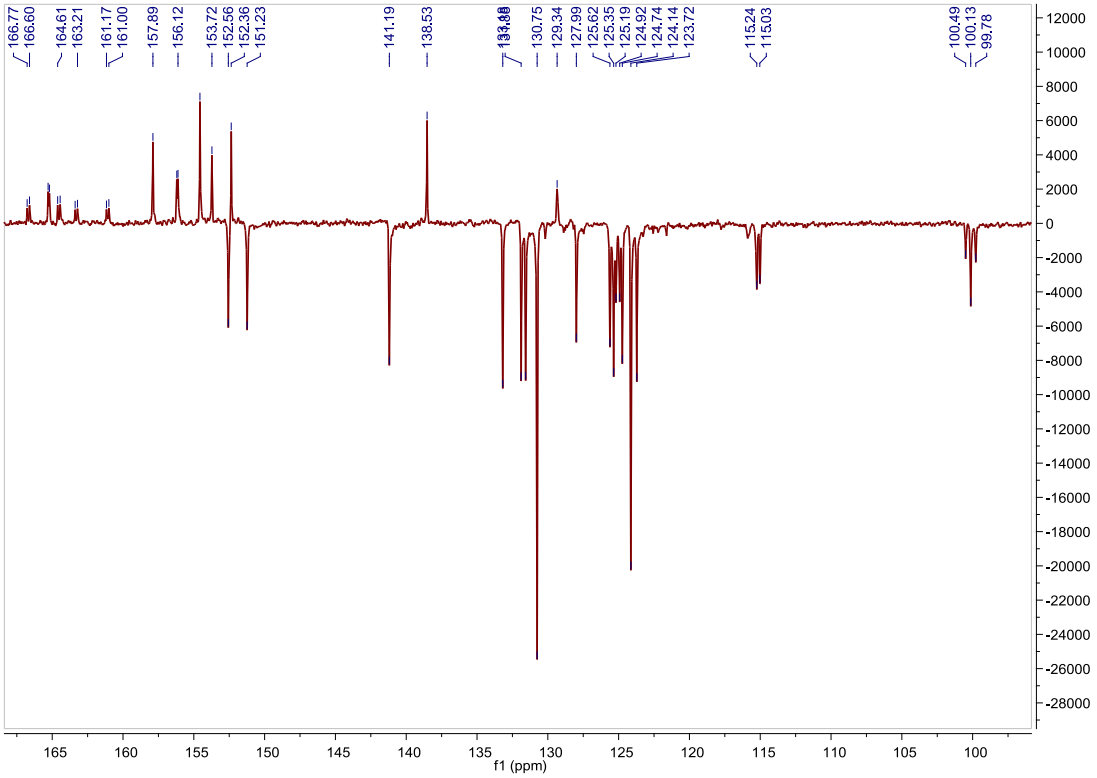

Fig. S272. ^{13}C APT NMR spectrum of **B5** in acetone-d_6, 75 MHz.

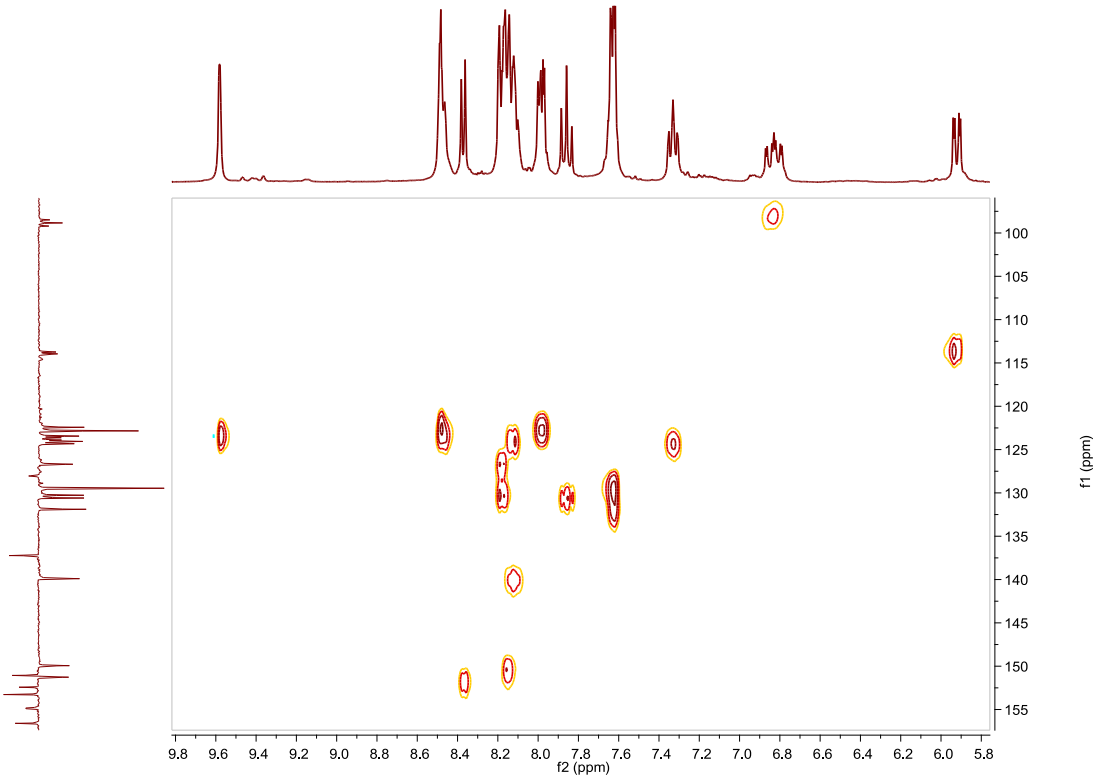

Fig. S273. HSQC NMR spectrum of **B5** in acetone-d_6.

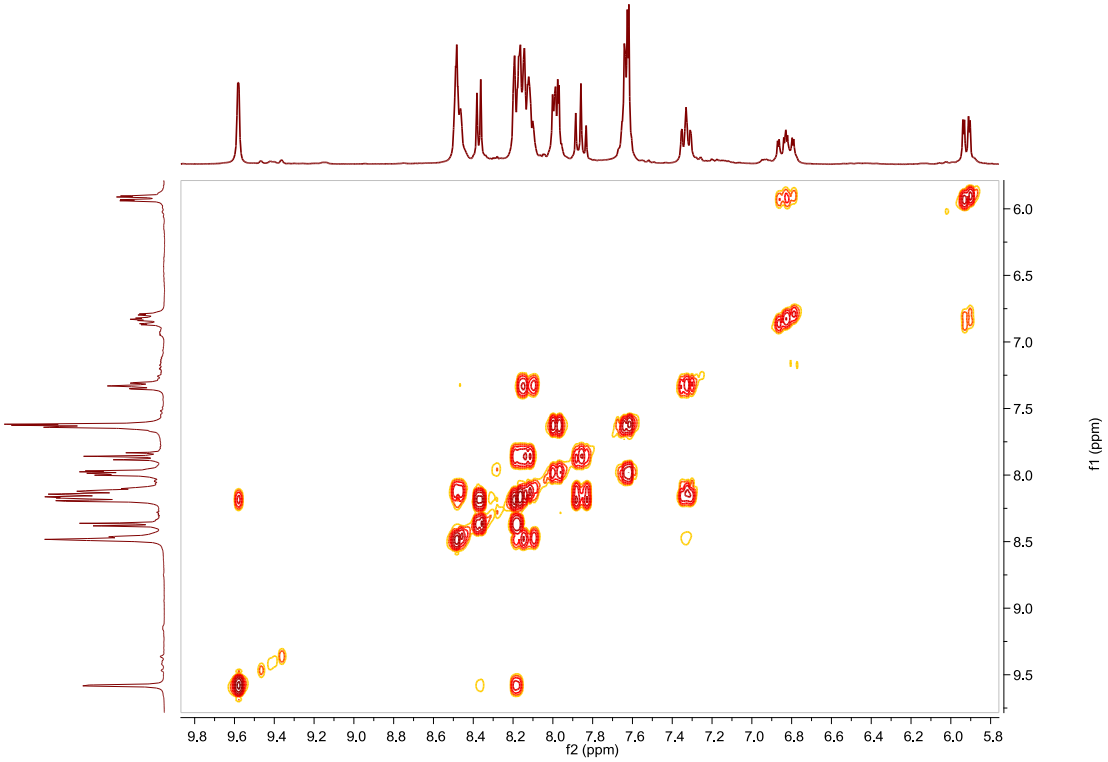

Fig. S274. COSY NMR spectrum of **B5** in acetone-d_6.

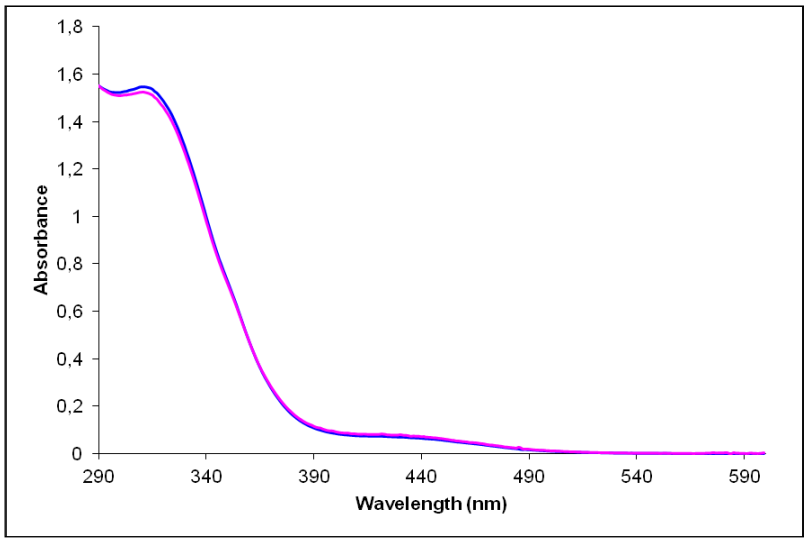

Fig. S275. UV/Vis spectra of **B5** in CH_3CN. Before (blue line) and after (pink line) irradiation at 319nm, $2.52 \cdot 10^{-5}$ M.

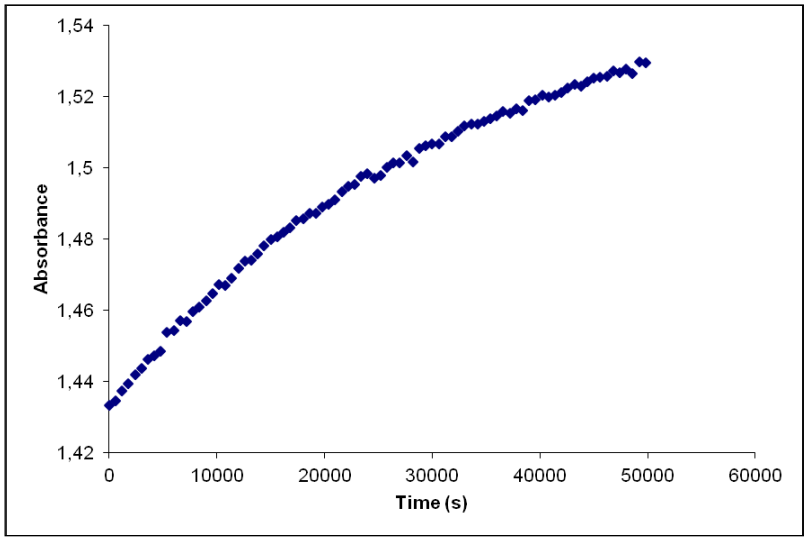

Fig. S276. Cis to trans thermal isomerization kinetics of **B5**. Absorption change of the band 311nm at 328 K in CH_3CN after irradiation at 319 nm. ($2.52 \cdot 10^{-5}$ M).

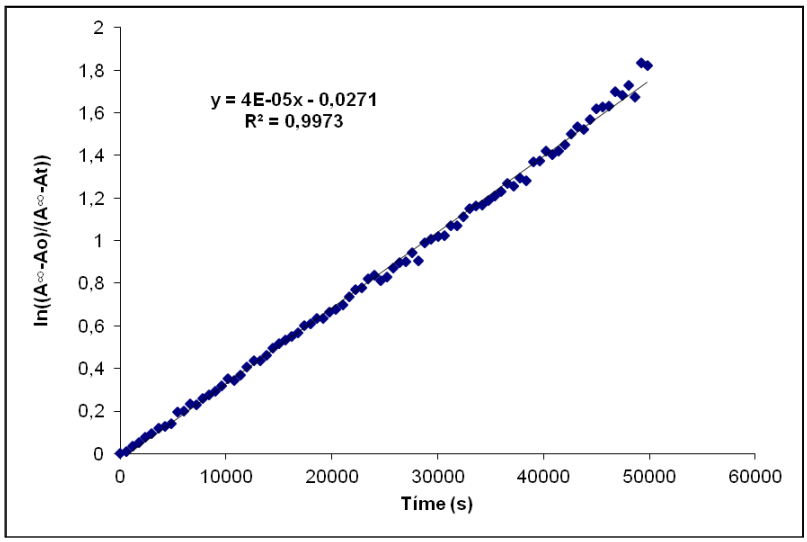

Fig. S277. Cis to trans thermal isomerization kinetics of **B5**. First-order plot. k (s^{-1}) = $4.0 \cdot 10^{-5}$. Half-life (min) = 289.

Compound C5, [Ir(Brppy)$_2$(5)]PF$_6$. Synthesis, characterization and photoisomerization studies.

SYNTHESIS

Under a N_2 atmosphere, [Ir(Brppy)$_2$Cl]$_2$ (0.100 g, 0.072 mmol) were added over a suspension of **L5** (0.074 g, 0.144 mmol) in 8 ml CH_2Cl_2–MeOH 2/1. The reaction mixture was refluxed, under N_2, for 15 h. After solvent evaporation the product was purified by column chromatography (silica gel, CH_2Cl_2). When the unreacted [Ir(Brppy)$_2$Cl]$_2$ eluted, 0.05 g of KPF_6 were added on top of the column and the polarity of the eluent was gradually increased to 100% acetone to elute [Ir(Brppy)$_2$(**L5**)]PF_6 together with the excess of KPF_6. The desired compound, purified by filtration through a celite path in CH_2Cl_2, was obtained as an orange solid. Yield 66%.

Elemental Analysis: calculated for ($C_{56}H_{38}Br_2IrN_8PF_6$): C, 50.96; H, 2.90; N, 8.49. Found: C, 51.12; H, 2.90; N, 8.10.

Exact Mass: ESI-MS $[C_{56}H_{38}Br_2IrN_8]^+$: calculated: m/z= 1173.1215, found: m/z= 1173.1239.

^{1}H NMR (300 MHz, acetone-*d*$_6$): δ 9.58 (d, J = 1.4 Hz, 1H), 8.49 (pst, J = 1.7 Hz, 1H), 8.38 (brd, J = 8.8 Hz, 1H), 8.33 (d, J = 5.8 Hz, 1H), 8.20 (dd, J = 1.8 Hz, J = 5.8 Hz, 1H), 8.16 (brd, J = 5.4 Hz, 1H), 8.09 (m, 3H), 7.98 (m, 3H), 7.86 (t, J = 7.9 Hz, 1H), 7.63 (m, 3H), 7.32 (m, 2H), 6.51 (d, J = 1.9 Hz, 1H).

^{13}C APT NMR (75 MHz, acetone-*d*$_6$): δ 167.89 (C_{quat}), 158.01 (C_{quat}), 154.59 (C_{quat}), 154.05 (C_{quat}), 153.72 (C_{quat}), 152.49 (CH), 152.14 (C_{quat}), 150.92 (CH), 144.77 (C_{quat}), 140.62 (CH), 138.59 (C_{quat}), 135.14 (CH), 133.19 (CH), 131.87 (CH), 131.51 (CH), 130.75 (2CH), 128.16 (CH), 127.89 (CH), 127.20 (CH), 126.31 (C_{quat}), 125.72 (CH), 125.26 (CH), 124.60 (CH), 124.12 (2CH), 123.75 (CH), 121.93 (CH).

UV/Vis (CH_3CN), λ, nm (ε, 10^4 M^{-1} cm^{-1}): 320 (6.4), 377 (1.1), 450 (0.25).

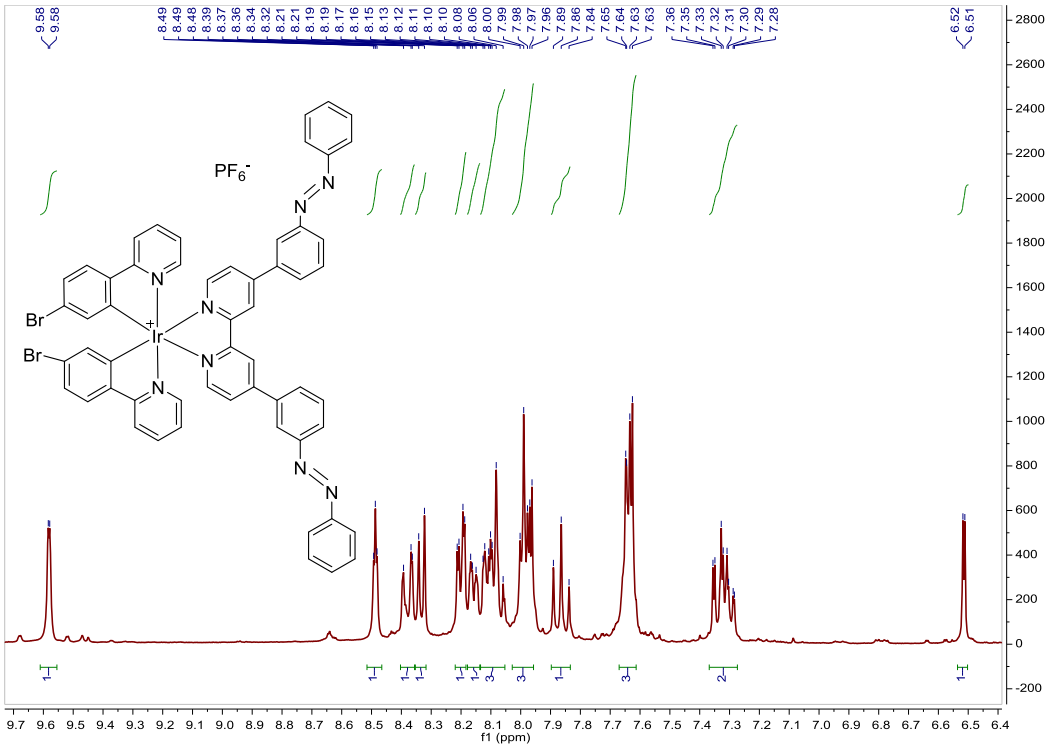

Fig. S278. ^{1}H NMR spectrum of **C5** in acetone-*d*$_6$, 300 MHz.

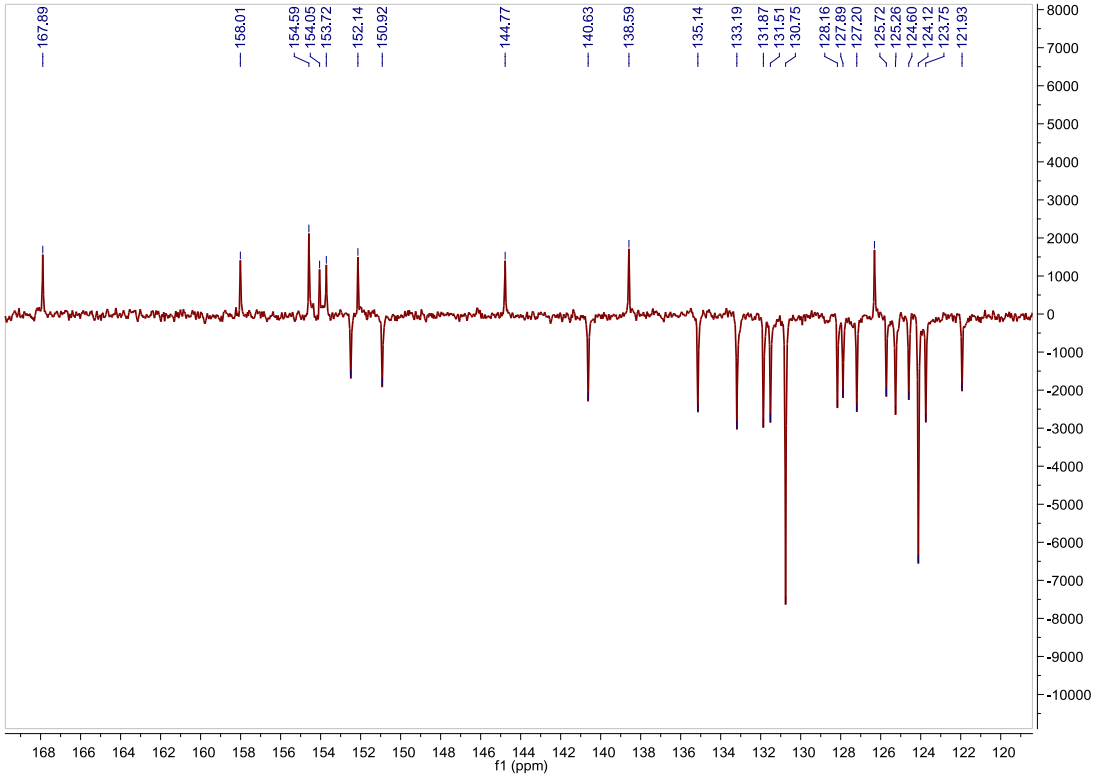

Fig. S279. ^{13}C APT NMR spectrum of **C5** in acetone-d_6, 75 MHz.

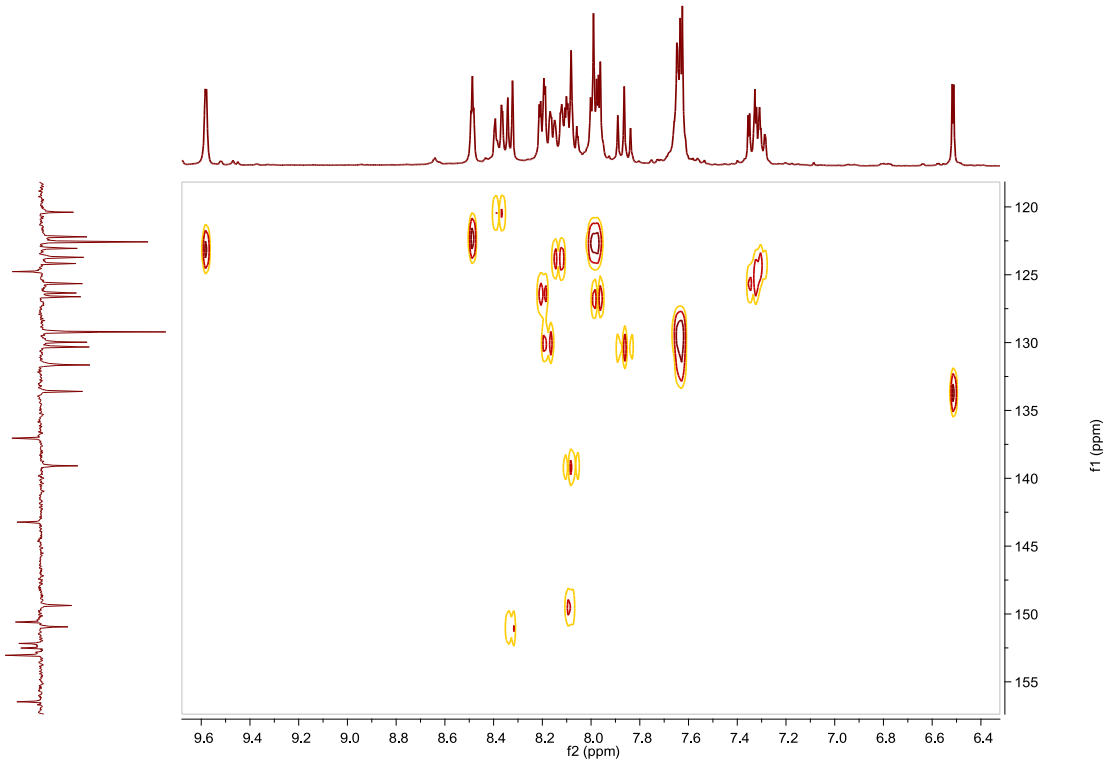

Fig. S280. HSQC NMR spectrum of **C5** in acetone-d_6.

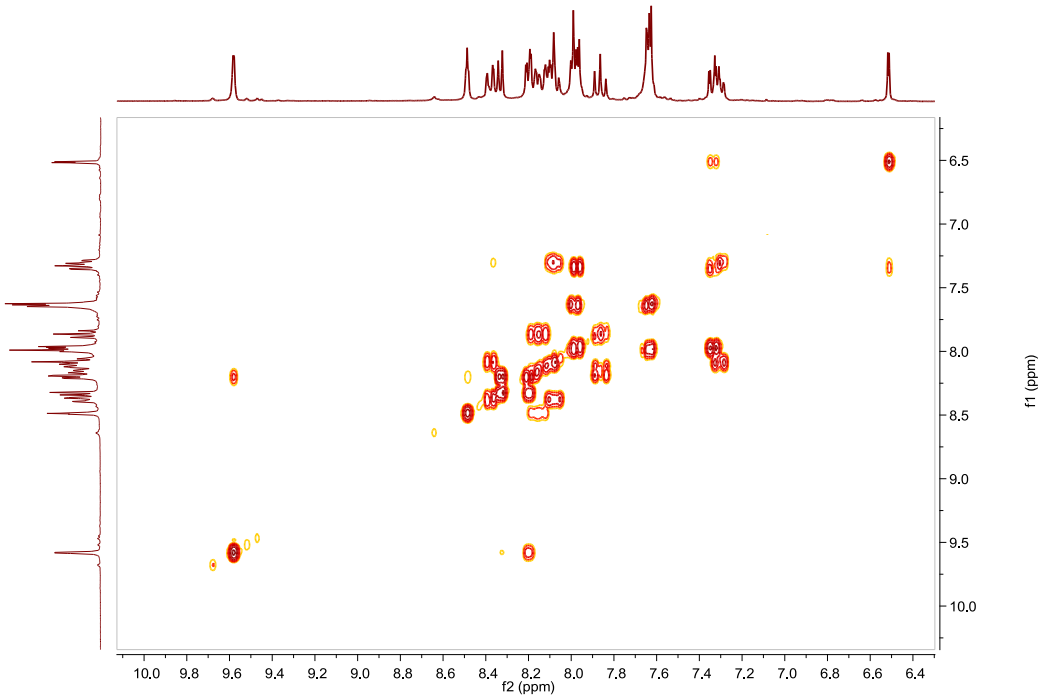

Fig. S281. COSY NMR spectrum of **C5** in acetone-d_6.

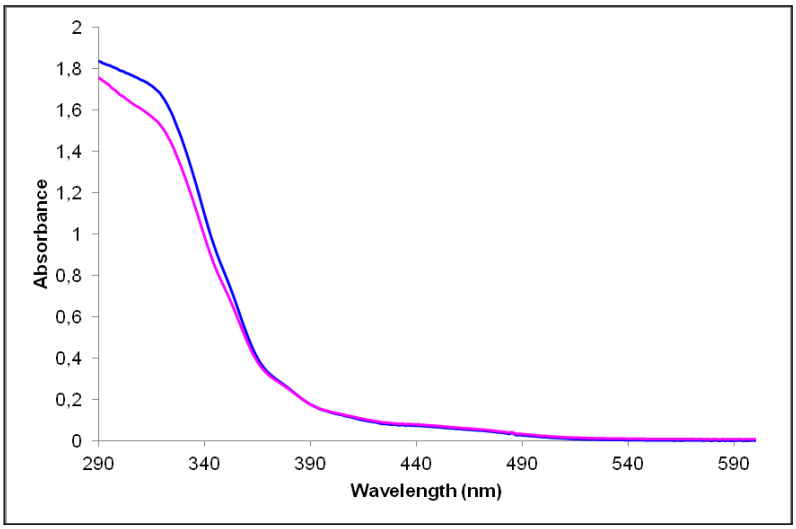

Fig. S282. UV/Vis spectra of **C5** in CH_3CN. Before (blue line) and after (pink line) irradiation at 318nm, $2.59 \cdot 10^{-5}$ M.

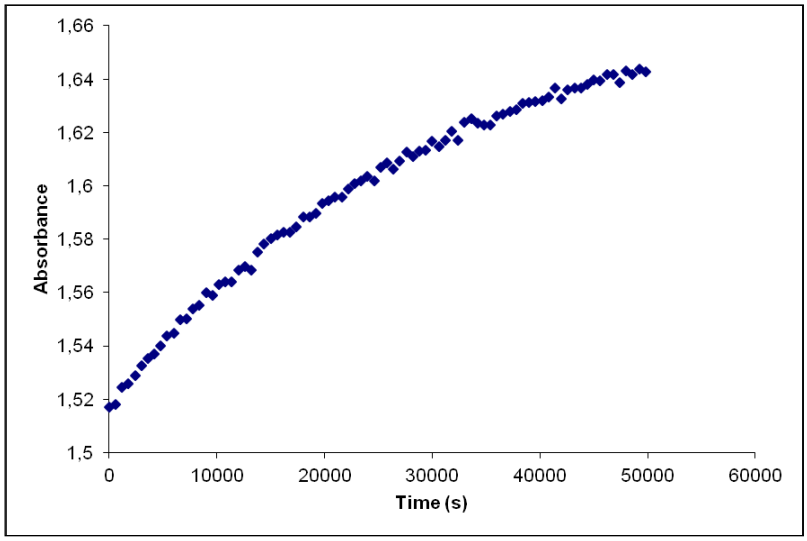

Fig. S283. Cis to trans thermal isomerization kinetics of **C5**. Absorption change of the band 320nm at 328 K in CH_3CN after irradiation at 318 nm. ($2.59 \cdot 10^{-5}$ M).

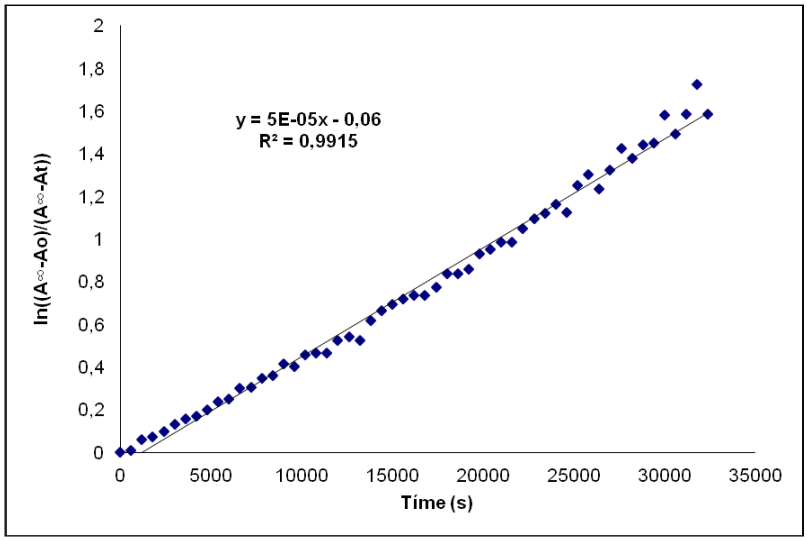

Fig. S284. Cis to trans thermal isomerization kinetics of **C5**. First-order plot. k (s^{-1}) = $5.0 \cdot 10^{-5}$. Half-life (min) = 231.

Compound D5, [Ir(azoppy)$_2$(5)]PF$_6$. Synthesis, characterization and photoisomerization studies.

SYNTHESIS

Under a N_2 atmosphere, **C5** (0.150 g, 0.114 mmol) and [4-(phenylazo)phenyl]boronic acid pinacol ester **11** (0.085 g, 0.277 mmol) were dissolved in 5 ml of THF. Na_2CO_3 (1 M (aq), 2.5 mL) and $Pd(PPh_3)_4$ (0.013 g, 0.0114 mmol) were added and the solution was degassed by bubbling N_2 for 15 min. The reaction mixture was refluxed (80 °C) for 15 h. The resulting mixture was cooled down to room temperature and the product was extracted with CH_2Cl_2. The organic phase was dried with $MgSO_4$, filtered off and the solvent was evaporated. The residue was purified by column chromatography (silica gel, CH_2Cl_2). To the fraction containing the eluted complex, 0.05 g of KPF_6 were added and the resulting solution was filtered through a celite path. The title compound was obtained as a dark orange solid. Yield 26%.

Elemental Analysis: calculated for ($C_{80}H_{56}IrN_{12}PF_6$): C, 63.11; H, 3.71; N, 11.04. Found: C, 62.90; H, 3.80; N, 10.56.

Exact Mass: ESI-MS $[C_{80}H_{56}IrN_{12}]^+$: calculated: m/z= 1377.4380, found: m/z= 1377.4392.

^{1}H NMR (300 MHz, acetone-*d*$_6$): δ 9.56 (d, J = 1.3 Hz, 1H), 8.48 (t, J = 1.6 Hz, 1H), 8.44 (d, J = 5.8 Hz, 1H), 8.36 (d, J = 8.0 Hz, 1H), 8.25–7.80 (m, 13H), 7.71–7.55 (m, 8H), 7.45 (dd, J = 1.8 Hz, J = 8.1 Hz, 1H), 7.32 (ddd, J = 1.2 Hz, J = 5.9 Hz, J = 7.3 Hz, 1H), 6.85 (d, J = 1.6 Hz, 1H).

^{13}C APT NMR (75 MHz, acetone-*d*$_6$): δ 168.64 (C_{quat}), 158.14(C_{quat}), 154.57 (C_{quat}), 153.91 (C_{quat}), 153.72 (C_{quat}), 152.97 (C_{quat}), 152.53 (CH), 151.83 (C_{quat}), 151.31 (C_{quat}), 151.02 (CH), 145.69 (C_{quat}), 144.96 (C_{quat}), 142.63 (C_{quat}), 140.27 (CH), 138.65 (C_{quat}), 133.18 (CH), 132.63 (CH), 131.84 (CH), 131.52 (CH), 131.01 (CH), 130.75 (2CH), 130.61 (2CH), 130.15 (CH), 128.93 (2CH), 127.73 (CH), 126.87 (CH), 125.35 (CH), 125.19 (CH), 124.49 (2CH), 124.14 (2CH), 123.99 (2CH), 123.76 (CH), 123.17 (CH), 121.75 (CH).

UV/Vis (CH_3CN), λ, nm (ε, 10^4 M^{-1} cm^{-1}): 337 (9.9), 430 (1.7).

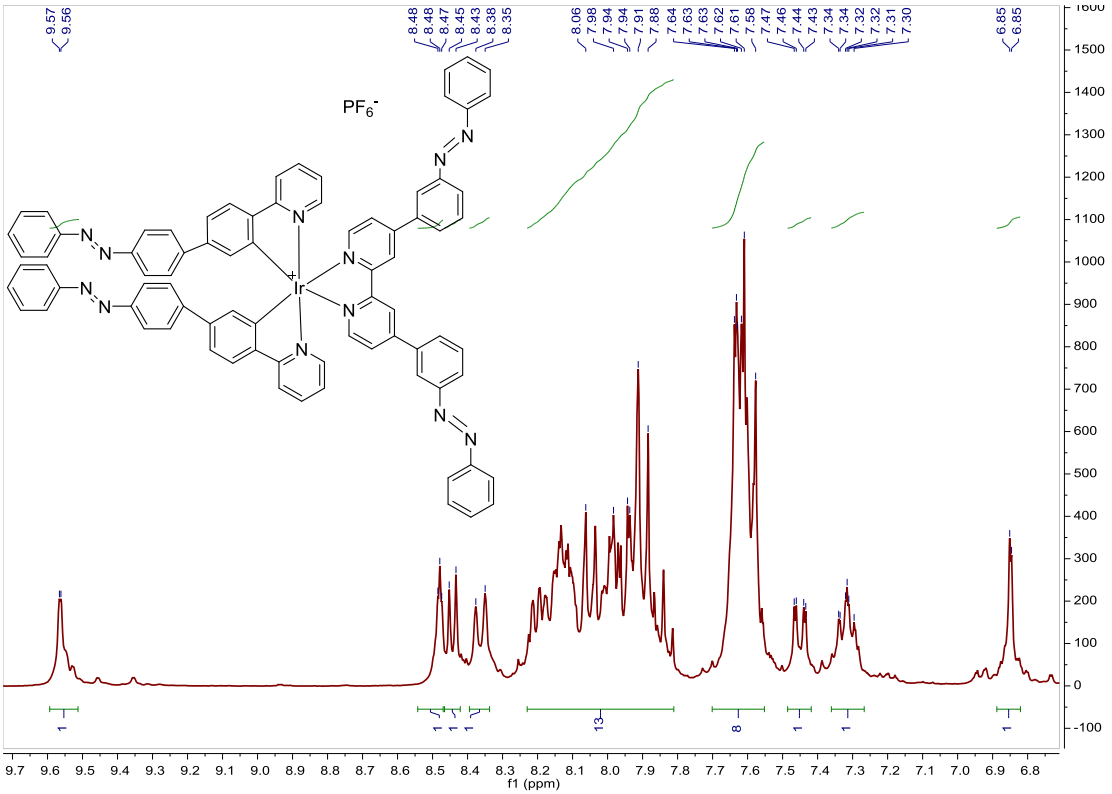

Fig. S285. ^{1}H NMR spectrum of **D5** in acetone-*d*$_6$, 300 MHz.

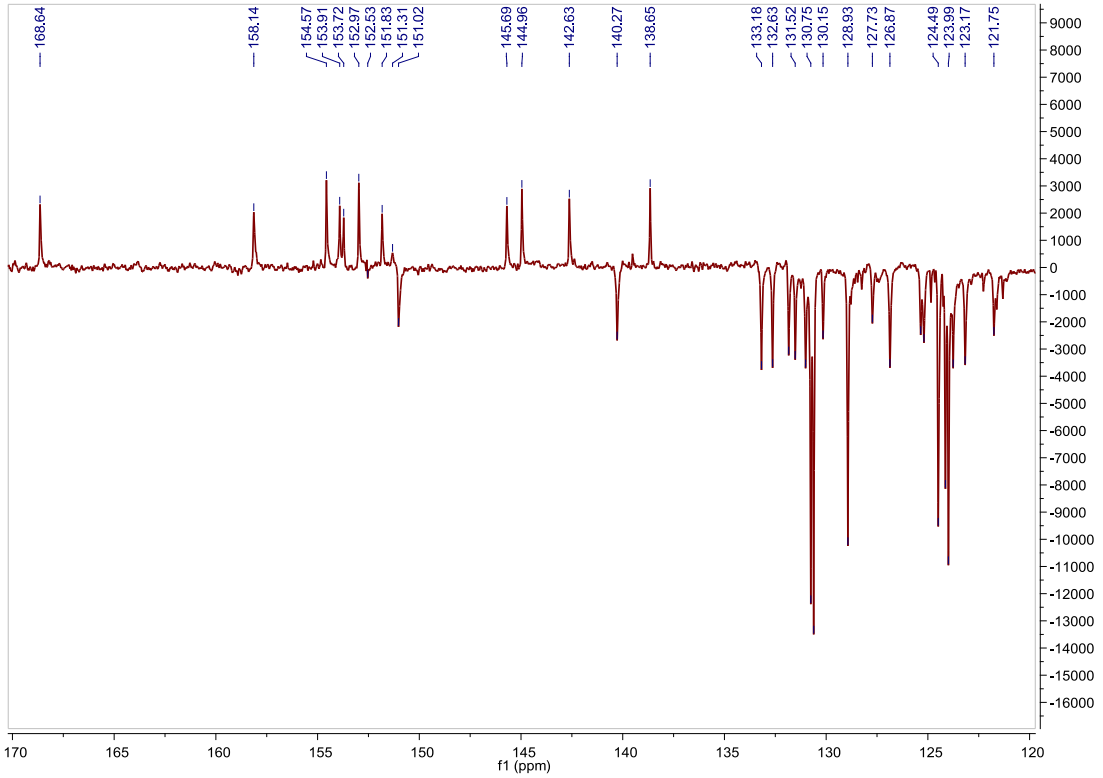

Fig. S286. ^{13}C APT NMR spectrum of **D5** in acetone-d_6, 75 MHz.

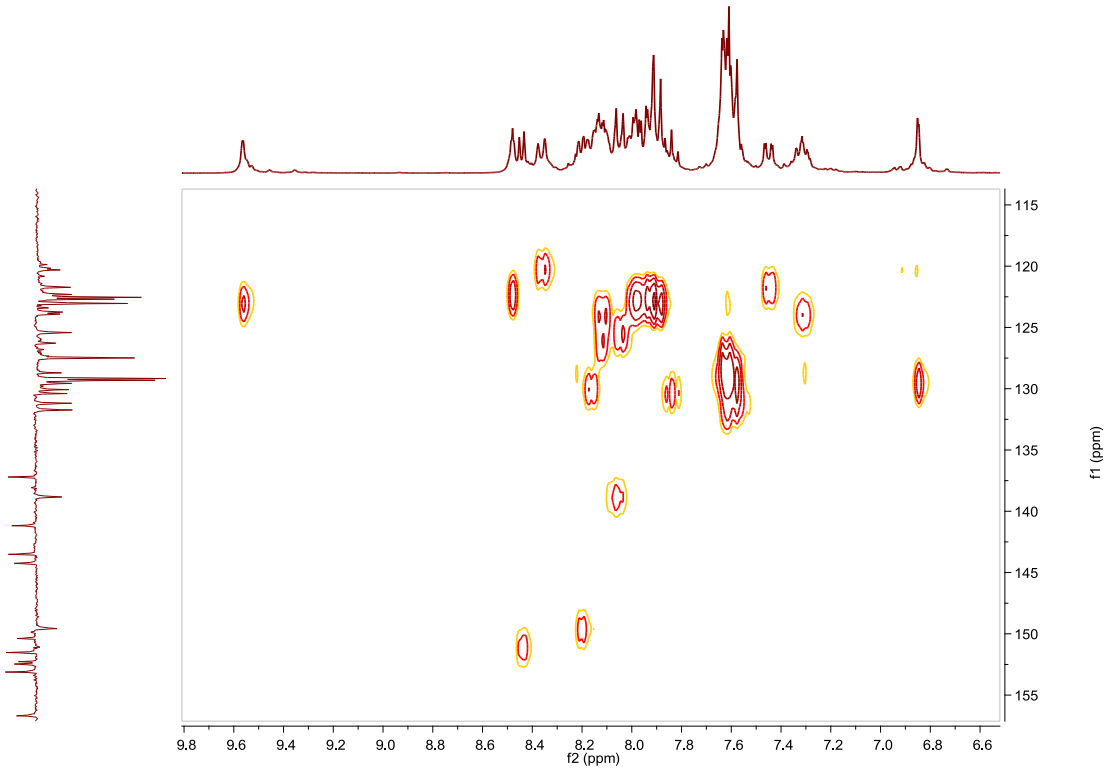

Fig. S287. HSQC NMR spectrum of **D5** in acetone-d_6.

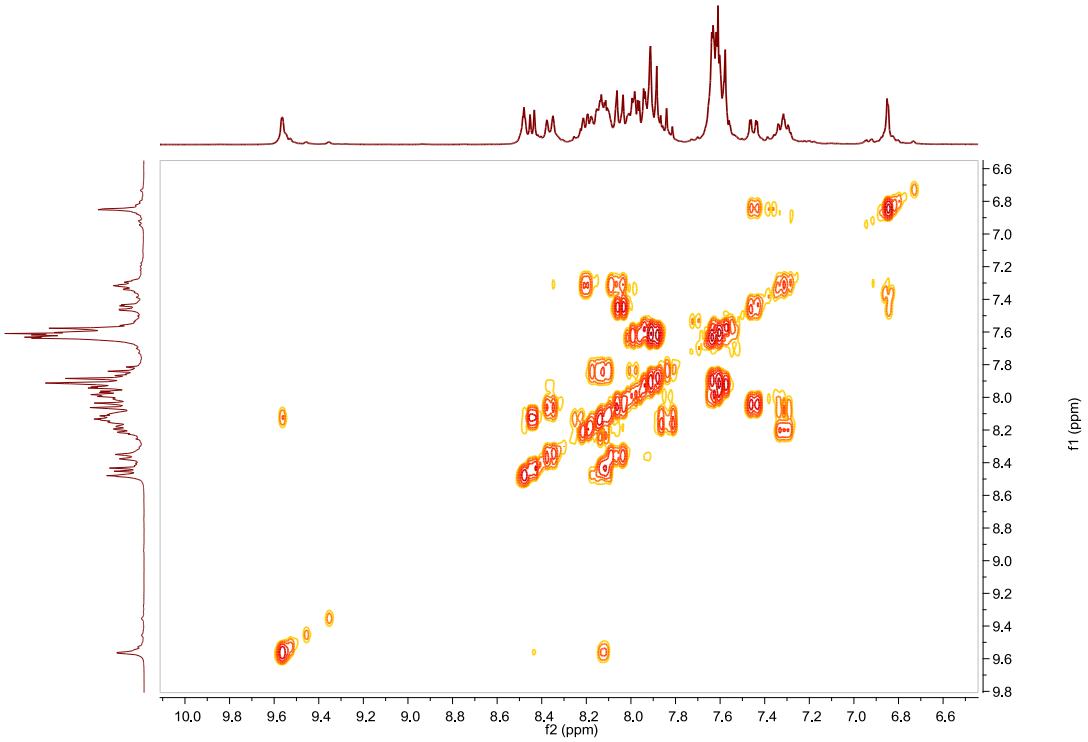

Fig. S288. COSY NMR spectrum of **D5** in acetone-d_6.

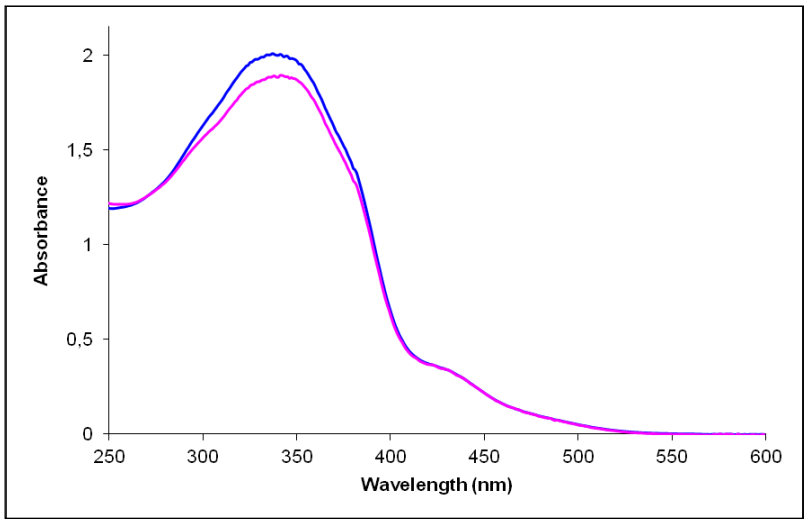

Fig. S289. UV/Vis spectra of **D5** in CH_3CN. Before (blue line) and after (pink line) irradiation at 327nm, $2.03 \cdot 10^{-5}$ M.

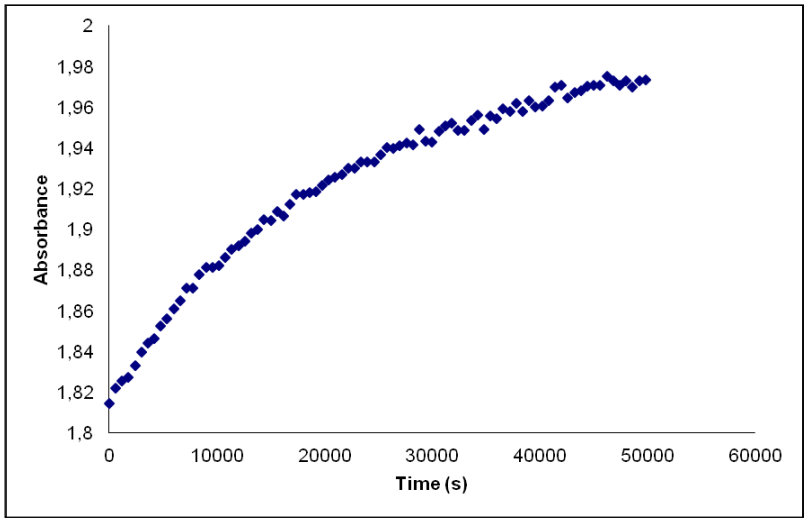

Fig. S290. Cis to trans thermal isomerization kinetics of **D5**. Absorption change of the band 337nm at 328 K in CH_3CN after irradiation at 327 nm. ($2.03 \cdot 10^{-5}$ M).

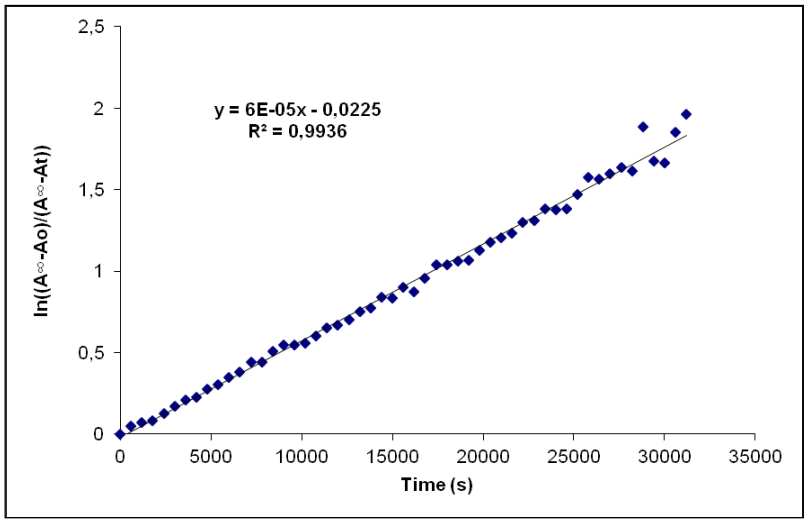

Fig. S291. Cis to trans thermal isomerization kinetics of **D5**. First-order plot. k (s^{-1}) = $6.0 \cdot 10^{-5}$. Half-life (min) = 192.

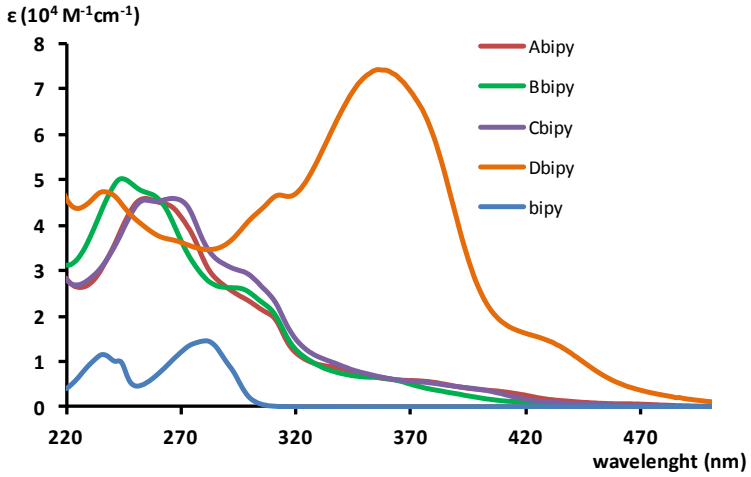

Fig. S292. UV-Vis absorption spectra of model complexes **A**–**D** with 2,2’-bipyridine. The spectra of 2,2’-bipyridine (bipy) is also shown for comparative purposes.

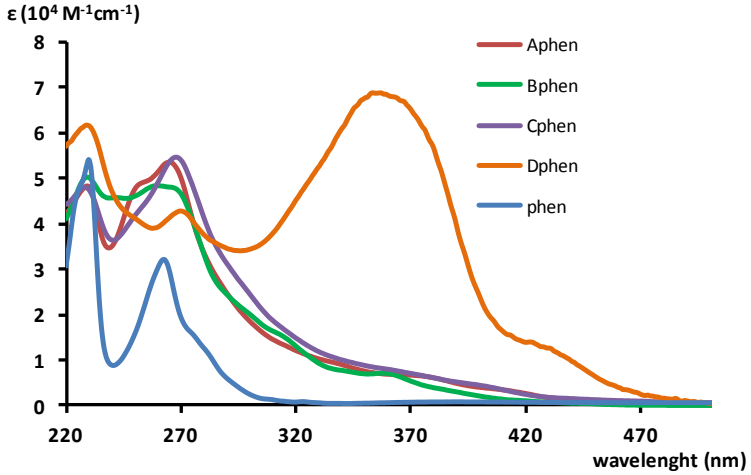

Fig. S293. UV-Vis absorption spectra of model complexes **A**–**D** with 1,10-phenanthroline. The spectra of 1,10-phenanthroline (phen) is also shown for comparative purposes.

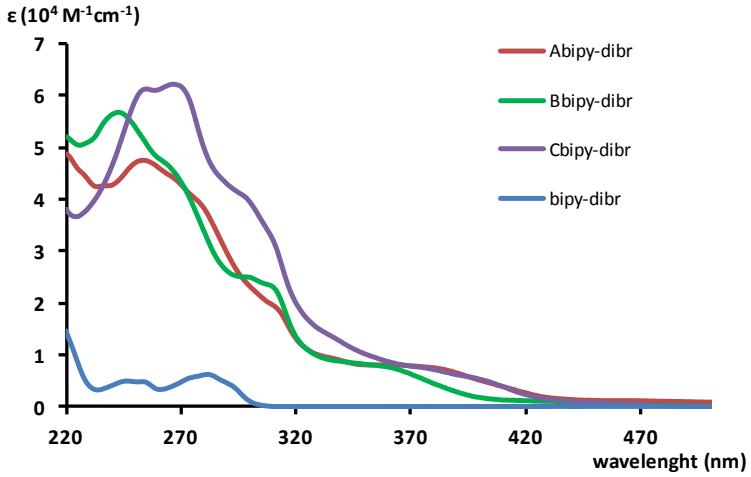

Fig. S294. UV-Vis absorption spectra of model complexes **A**–**C** with 4,4'-dibromo-2,2’-bipyridine. The spectra of 4,4'-dibromo-2,2’-bipyridine (bipy-dibr) is also shown for comparative purposes.

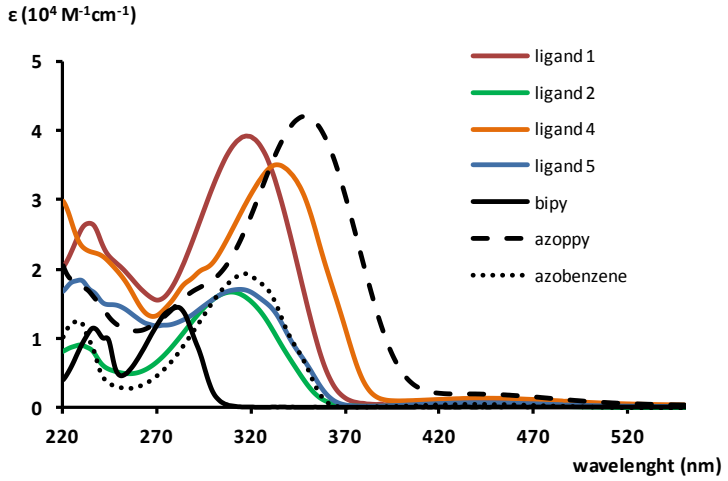

Fig. S295. UV-Vis absorption spectra of ligands **1**, **2, 4** and **5**. The spectra of 2,2'-bipyridine (bipy), 2-phenyl(4-azophenyl)pyridine (azobipy) and azobenzene are also shown for comparative purposes.

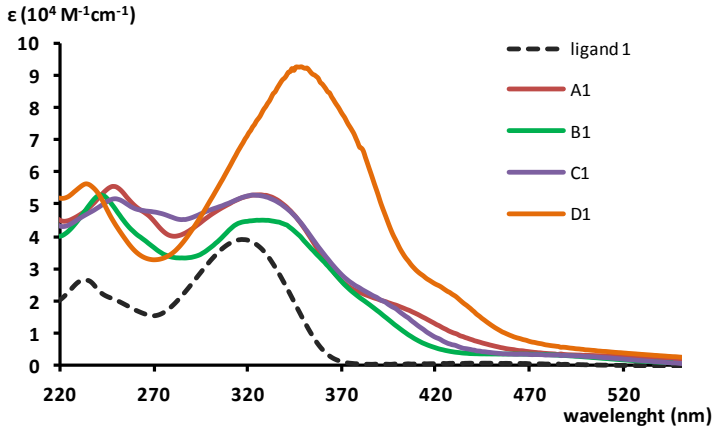

Fig. S296. UV-Vis absorption spectra of complexes **A1**–**D1** and ligand **1**.

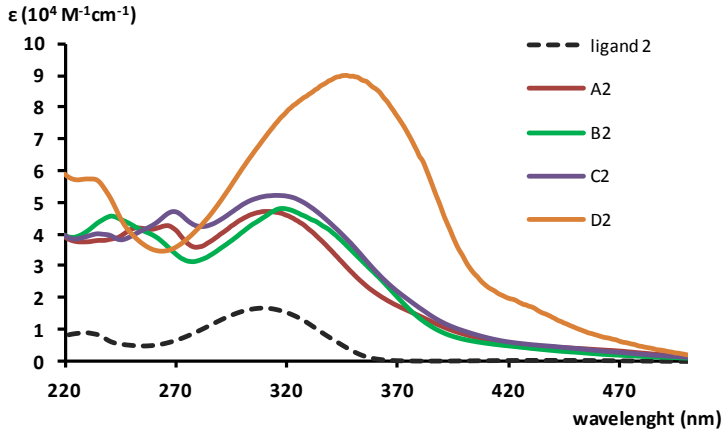

Fig. S297. UV-Vis absorption spectra of complexes **A2**–**D2** and ligand **2**.

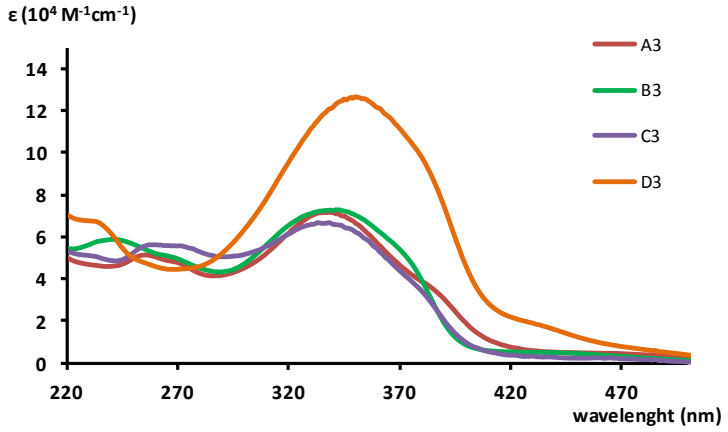

Fig. S298. UV-Vis absorption spectra of complexes **A3**–**D3**.

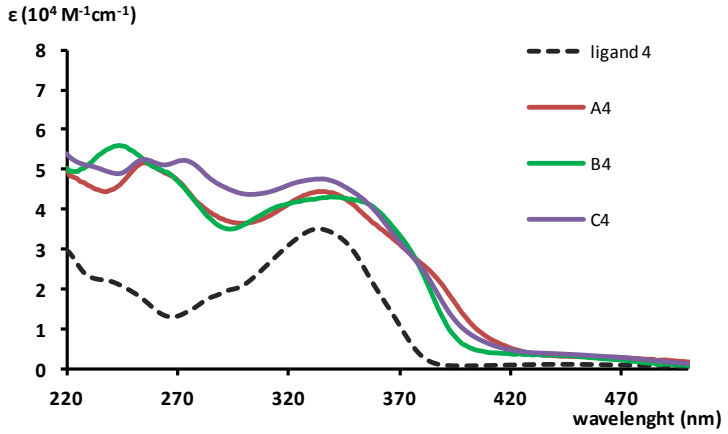

Fig. S299. UV-Vis absorption spectra of complexes **A4**–**C4** and ligand **4**.

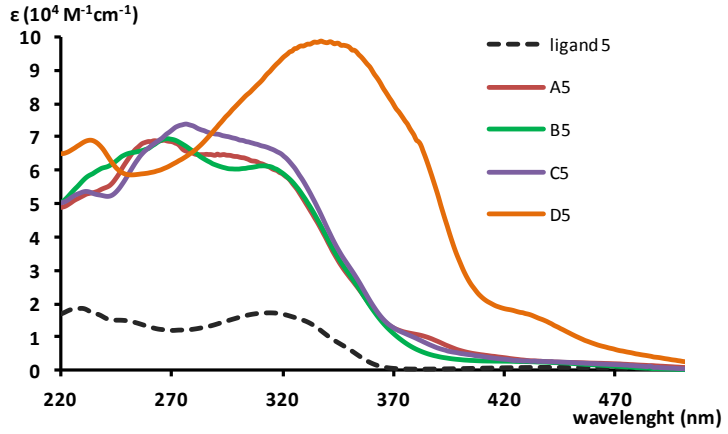

Fig. S300. UV-Vis absorption spectra of complexes **A5**–**D5** and ligand **5**.

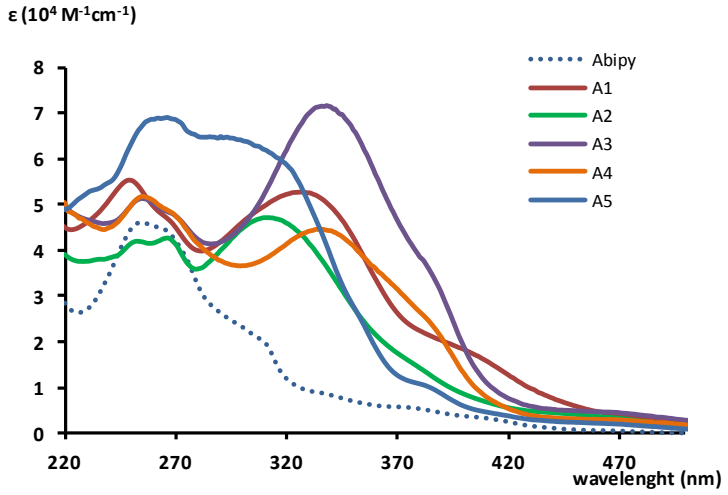

Fig. S301. UV-Vis absorption spectra of complexes **A1**–**A5**. The spectra of compound **Abipy** is also shown for comparative purposes.

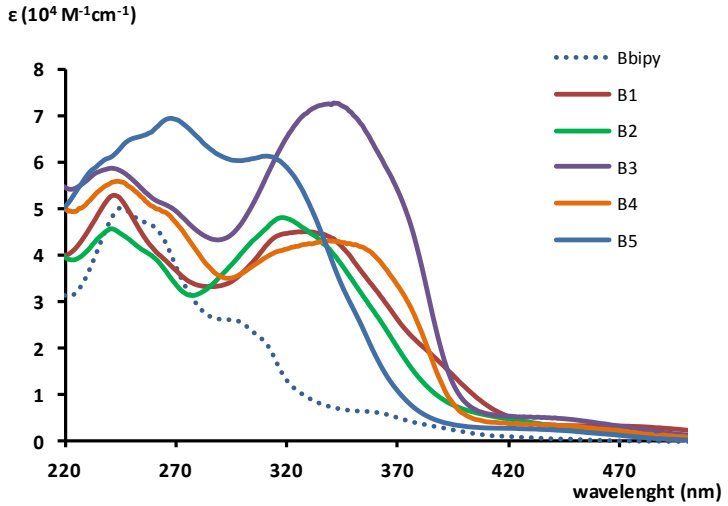

Fig. S302. UV-Vis absorption spectra of complexes **B1**–**B5**. The spectra of compound **Bbipy** is also shown for comparative purposes.

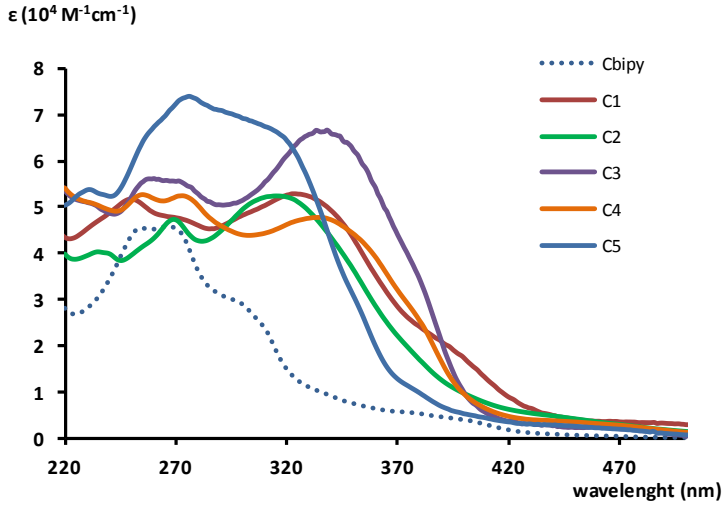

Fig. S303. UV-Vis absorption spectra of complexes **C1**–**C5**. The spectra of compound **Cbipy** is also shown for comparative purposes.

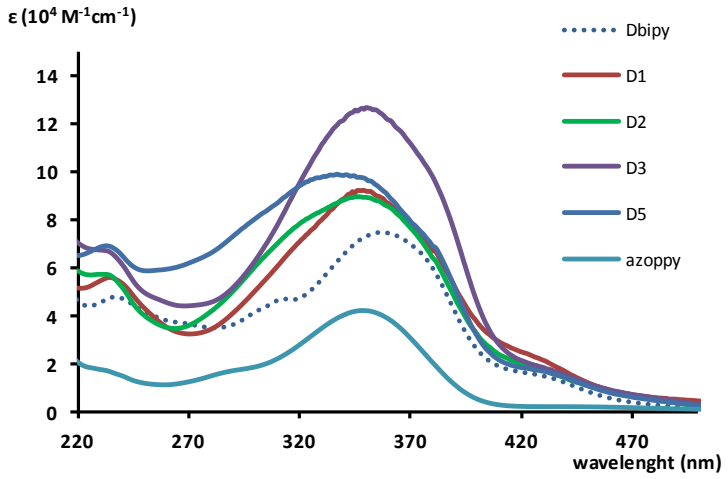

Fig. S304. UV-Vis absorption spectra of complexes **D1**–**D5**. The spectra of compound **Dbipy**, and **azoppy** = ((2-azobenzene)pyridine) are also shown for comparative purposes.

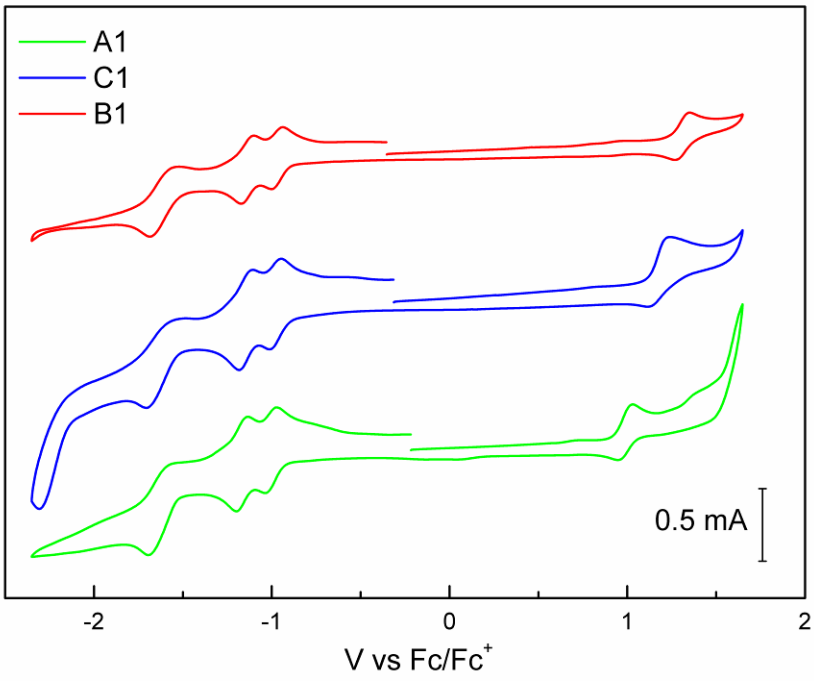

Figure S305. Cyclo-voltammograms (10^{-3} M, dry ACN) of **A1**, **B1** and **C1** containing 0.1 M $TBAPF_6$ as the supporting electrolyte, scan rate of 100 mV s^{-1}.

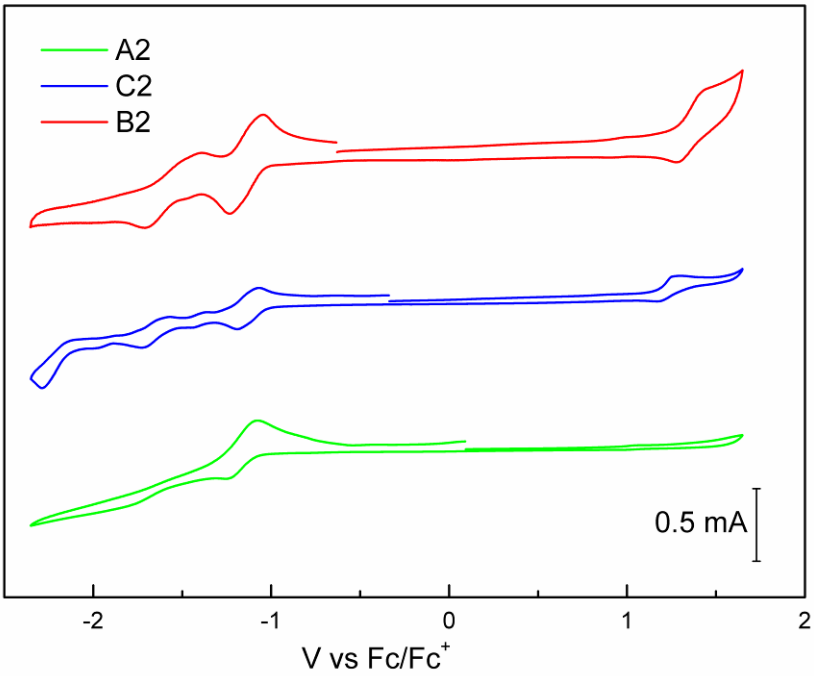

Figure S306. Cyclo-voltammograms (10^{-3} M, dry ACN) of **A2**, **B2** and **C2** containing 0.1 M $TBAPF_6$ as the supporting electrolyte, scan rate of 100 mV s^{-1}.

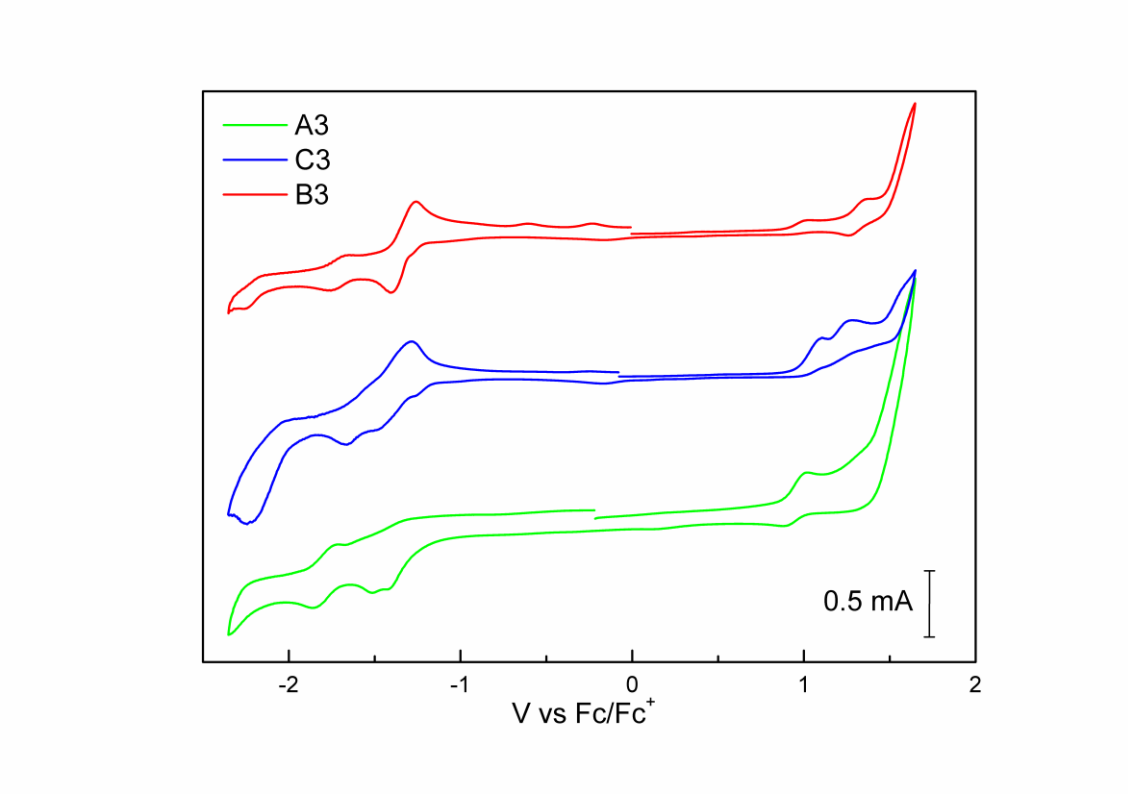

Figure S307. Cyclo-voltammograms (10^{-3} M, dry ACN) of **A3**, **B3** and **C3** containing 0.1 M $TBAPF_6$ as the supporting electrolyte, scan rate of 100 mV s^{-1}.

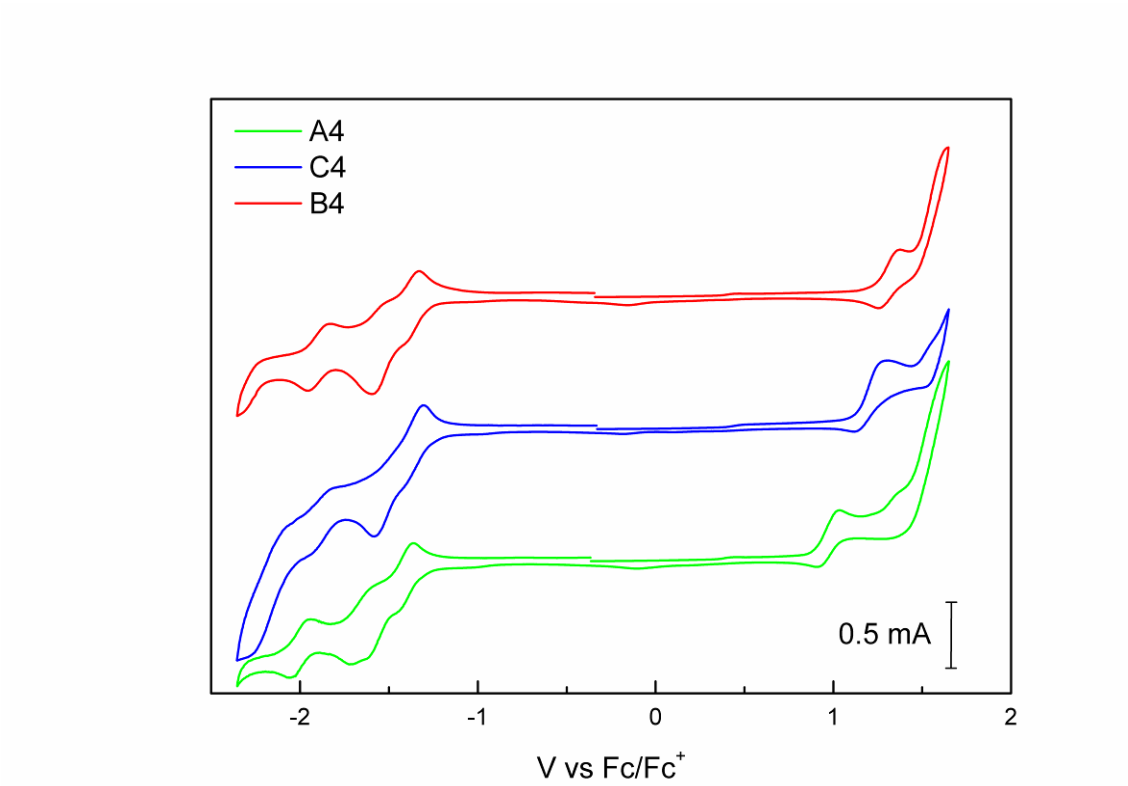

Figure S308. Cyclo-voltammograms (10^{-3} M, dry ACN) of **A4**, **B4** and **C4** containing 0.1 M $TBAPF_6$ as the supporting electrolyte, scan rate of 100 mV s^{-1}.

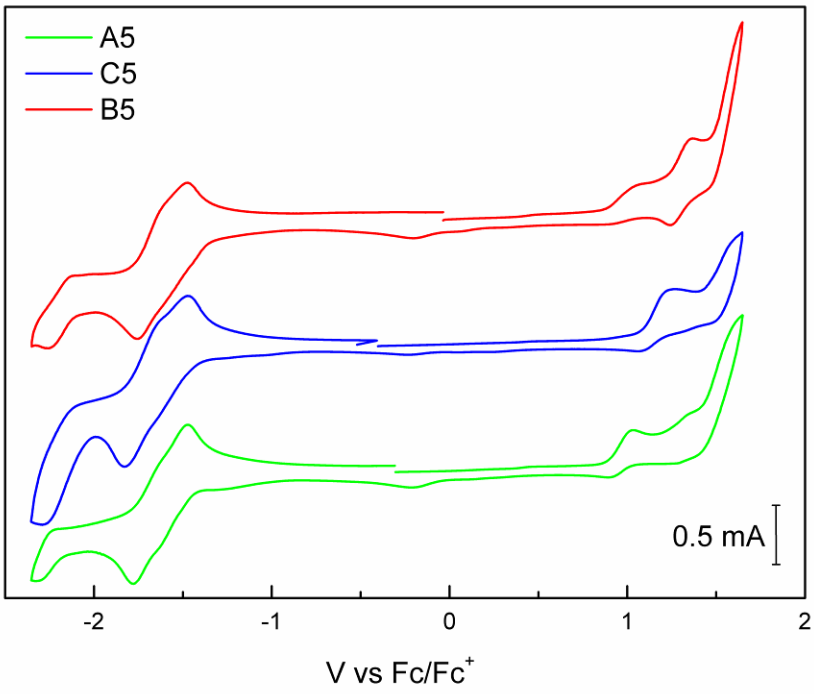

Figure S309. Cyclo-voltammograms (10^{-3} M, dry ACN) of **A5**, **B5** and **C5** containing 0.1 M $TBAPF_6$ as the supporting electrolyte, scan rate of 100 mV s^{-1}.

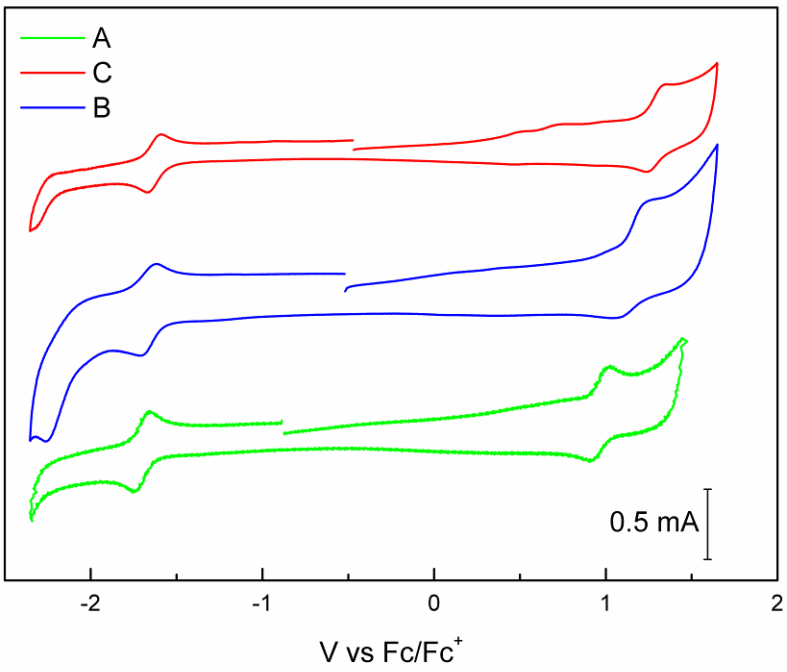

Figure S310. Cyclo-voltammograms (10^{-3} M, dry ACN) of **Abipy**, **Bbipy** and **Cbipy** containing 0.1 M $TBAPF_6$ as the supporting electrolyte, scan rate of 100 mV s^{-1}.

Table S1. Secondary MLCT transitions of complexes A, C computed at TD-CAM-B3LYP(PCM)/6-31+G*&LANL2DZ level of theory. Orbitals in italics and underlined are mainly located on the Ir(bipy) moiety or the azo moiety respectively.

	E [eV]	*f*	*transition*
A1	3.57	0.75	*HOMO-4*→LUMO (49%)
B1	3.66	0.66	*HOMO-4*→LUMO (65%)
C1	3.64	0.92	*HOMO-4*→LUMO (57%)
A2	3.83	1.16	*HOMO-3*→LUMO (30%) *HOMO-2*→LUMO+1 (25%)
B2	3.82	0.59	*HOMO*→LUMO (47%)
A3	3.67	1.12	*HOMO-3*→LUMO (44%) *HOMO-2*→LUMO+1 (38%)
B3	3.73	2.21	*HOMO-1*→LUMO (44%) *HOMO-2*→LUMO+1 (38%)
C3	3.67	1.15	*HOMO-3*→LUMO (48%) *HOMO-2*→LUMO+1 (42%)

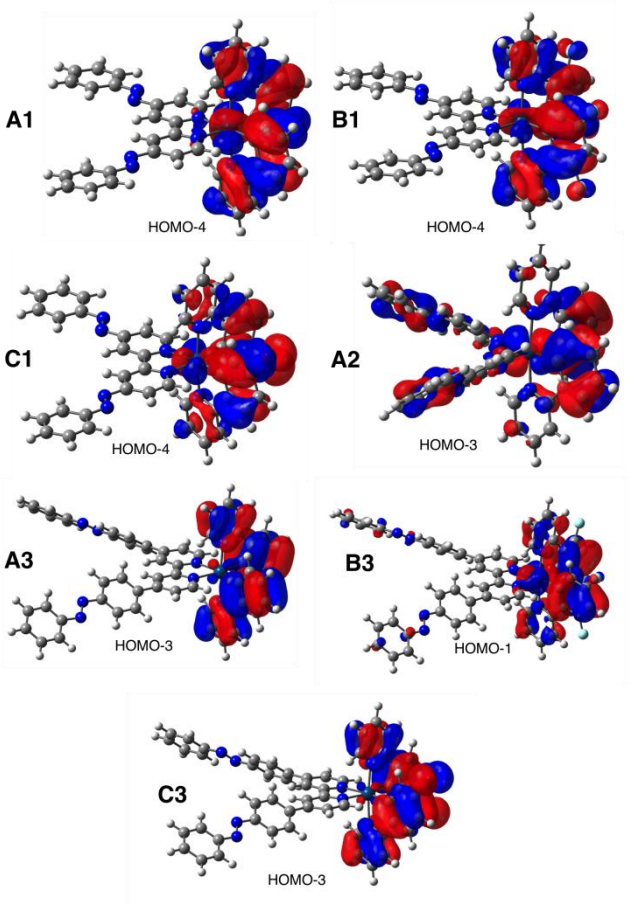

Figure S311. Orbitals AC1–3 involved on the MLCT secondary transitions

Cartesian coordinates and energy in hartrees (optimized at the CAM-B3LYP(PCM)/6-31+G*&LANL2DZ level) of all the stationary points discussed in the main text.

1 (HF= -1175.8277845)

Center Number	Atomic Number	Atomic Type	Coordinates (Angstroms) X	Y	Z
1	6	0	0.501431	0.553514	-0.018730
2	6	0	0.888552	2.816208	-0.017216
3	6	0	1.864904	0.274106	-0.022241
4	6	0	2.268438	2.639853	-0.021902
5	1	0	0.464281	3.816664	-0.015421
6	6	0	2.761529	1.340335	-0.022284
7	1	0	2.213331	-0.748852	-0.026082
8	1	0	2.945631	3.486730	-0.024419
9	6	0	-0.888552	-2.816209	-0.017210
10	6	0	-0.501431	-0.553514	-0.018728
11	6	0	-2.268438	-2.639854	-0.021893
12	1	0	-0.464281	-3.816665	-0.015416
13	6	0	-1.864904	-0.274107	-0.022235
14	6	0	-2.761530	-1.340335	-0.022274
15	1	0	-2.213331	0.748852	-0.026076
16	7	0	0.021142	1.806956	-0.015825
17	7	0	-4.181704	-1.206294	-0.028590
18	7	0	-4.590958	-0.032063	0.030257
19	6	0	-6.000805	0.130633	0.021517
20	6	0	-6.447165	1.450707	0.090004
21	6	0	-6.918412	-0.924487	-0.049735
22	6	0	-7.811422	1.724532	0.087587
23	1	0	-5.714162	2.249435	0.144372
24	6	0	-8.276879	-0.644151	-0.051491
25	1	0	-6.559619	-1.945640	-0.102512
26	6	0	-8.726115	0.677658	0.016844
27	1	0	-8.158291	2.751585	0.140722
28	1	0	-8.994301	-1.457162	-0.106450
29	1	0	-9.791529	0.886825	0.014716
30	1	0	-2.945631	-3.486731	-0.024407
31	7	0	-0.021142	-1.806957	-0.015823
32	7	0	4.181703	1.206294	-0.028604
33	7	0	4.590958	0.032062	0.030236
34	6	0	6.000805	-0.130633	0.021509
35	6	0	6.447166	-1.450707	0.089986
36	6	0	6.918413	0.924489	-0.049722
37	6	0	7.811423	-1.724531	0.087580
38	1	0	5.714162	-2.249437	0.144338
39	6	0	8.276880	0.644153	-0.051467
40	1	0	6.559619	1.945641	-0.102491
41	6	0	8.726116	-0.677656	0.016858
42	1	0	8.158291	-2.751585	0.140707
43	1	0	8.994302	1.457166	-0.106410
44	1	0	9.791530	-0.886822	0.014738

2 (HF= -588.5051537)

Center Number	Atomic Number	Atomic Type	Coordinates (Angstroms) X	Y	Z
1	6	0	3.670945	1.239519	0.170027
2	6	0	4.022545	-0.991615	-0.174518
3	6	0	2.292461	1.083835	0.193231
4	6	0	2.657672	-1.259831	-0.161015
5	1	0	4.736126	-1.798341	-0.318689
6	6	0	1.775141	-0.199936	0.017281
7	1	0	1.637922	1.932421	0.348826
8	1	0	2.283006	-2.269486	-0.289836
9	7	0	4.533334	0.231097	-0.012326
10	7	0	0.387949	-0.524581	0.028683
11	7	0	-0.371375	0.459300	-0.047767
12	6	0	-1.760590	0.169061	-0.019360
13	6	0	-2.602132	1.271591	-0.170074
14	6	0	-2.296421	-1.113124	0.150999
15	6	0	-3.982821	1.099181	-0.156919
16	1	0	-2.160157	2.254768	-0.297410
17	6	0	-3.673694	-1.277256	0.165151
18	1	0	-1.632570	-1.961086	0.271346
19	6	0	-4.518640	-0.174595	0.010802
20	1	0	-4.637259	1.956799	-0.275864
21	1	0	-4.096446	-2.268347	0.298079
22	1	0	-5.595410	-0.313246	0.023411
23	1	0	4.108636	2.224821	0.306384

3 (HF= -1637.695097)

Center Number	Atomic Number	Atomic Type	Coordinates (Angstroms) X	Y	Z
1	7	0	-1.228193	-1.010334	0.855697
2	7	0	4.695871	-0.450141	6.938666
3	7	0	4.911078	-1.435328	7.670613
4	6	0	-1.403687	-1.610852	2.032257
5	1	0	-2.338577	-2.150524	2.161289
6	6	0	-0.475763	-1.570575	3.065114
7	1	0	-0.694422	-2.067150	4.004249
8	6	0	0.713916	-0.862985	2.876381
9	6	0	0.896534	-0.234908	1.643828
10	1	0	1.803133	0.313531	1.422348
11	6	0	-0.090162	-0.330075	0.663773
12	6	0	1.744602	-0.780390	3.939845
13	6	0	2.007013	-1.882185	4.768373
14	1	0	1.464328	-2.809987	4.616647
15	6	0	2.968500	-1.816910	5.763310
16	1	0	3.170903	-2.675763	6.392061
17	6	0	3.690201	-0.633466	5.951927
18	6	0	3.437736	0.468525	5.136193
19	1	0	4.000471	1.382433	5.297889
20	6	0	2.474816	0.395169	4.137786
21	1	0	2.277117	1.266908	3.522441
22	6	0	5.918199	-1.255776	8.657382
23	6	0	6.144260	-2.353607	9.488055
24	1	0	5.556293	-3.253755	9.338116
25	6	0	7.109219	-2.284110	10.488578

26	1	0	7.282817	-3.139548	11.133867
27	6	0	7.848515	-1.116754	10.657564
28	1	0	8.602527	-1.058527	11.436678
29	6	0	7.621667	-0.018352	9.824055
30	1	0	8.200499	0.890612	9.957299
31	6	0	6.660747	-0.081018	8.824951
32	1	0	6.478425	0.765346	8.173284
33	7	0	1.228193	1.010334	-0.855697
34	7	0	-4.695871	0.450141	-6.938666
35	7	0	-4.911078	1.435328	-7.670613
36	6	0	1.403687	1.610852	-2.032257
37	1	0	2.338577	2.150524	-2.161289
38	6	0	0.475763	1.570575	-3.065114
39	1	0	0.694422	2.067150	-4.004249
40	6	0	-0.713916	0.862985	-2.876381
41	6	0	-0.896534	0.234908	-1.643828
42	1	0	-1.803133	-0.313531	-1.422348
43	6	0	0.090162	0.330075	-0.663773
44	6	0	-1.744602	0.780390	-3.939845
45	6	0	-2.007013	1.882185	-4.768373
46	1	0	-1.464328	2.809987	-4.616647
47	6	0	-2.968500	1.816910	-5.763310
48	1	0	-3.170903	2.675763	-6.392061
49	6	0	-3.690201	0.633466	-5.951927
50	6	0	-3.437736	-0.468525	-5.136193
51	1	0	-4.000471	-1.382433	-5.297889
52	6	0	-2.474816	-0.395169	-4.137786
53	1	0	-2.277117	-1.266908	-3.522441
54	6	0	-5.918199	1.255776	-8.657382
55	6	0	-6.144260	2.353607	-9.488055
56	1	0	-5.556293	3.253755	-9.338116
57	6	0	-7.109219	2.284110	-10.488578
58	1	0	-7.282817	3.139548	-11.133867
59	6	0	-7.848515	1.116754	-10.657564
60	1	0	-8.602527	1.058527	-11.436678
61	6	0	-7.621667	0.018352	-9.824055
62	1	0	-8.200499	-0.890612	-9.957299
63	6	0	-6.660747	0.081018	-8.824951
64	1	0	-6.478425	-0.765346	-8.173284

---

4 (HF= -3637.6444873)

Center Number	Atomic Number	Atomic Type	Coordinates (Angstroms) X	Y	Z
1	6	0	3.677285	-0.239252	0.066504
2	6	0	4.139885	-2.450894	0.454794
3	6	0	5.034208	0.071920	-0.035023
4	6	0	5.513381	-2.249281	0.371211
5	1	0	3.750467	-3.446521	0.650036
6	6	0	5.947143	-0.956403	0.120658
7	1	0	5.343769	1.089527	-0.230188
8	1	0	6.205557	-3.072834	0.497827
9	6	0	2.189291	3.039063	-0.462937
10	6	0	2.647184	0.828285	-0.097442
11	6	0	0.817917	2.829258	-0.389711
12	1	0	2.578699	4.036671	-0.649383
13	6	0	1.290691	0.522703	-0.012969
14	6	0	0.342562	1.536498	-0.157500
15	1	0	0.995140	-0.499061	0.188239
16	7	0	3.239737	-1.480874	0.307231
17	7	0	-5.253950	0.519065	0.252629
18	7	0	-5.708125	-0.538226	-0.225421
19	6	0	-7.110038	-0.722667	-0.081630
20	6	0	-7.618971	-1.895465	-0.640104
21	6	0	-7.964035	0.176706	0.567477
22	6	0	-8.979912	-2.174474	-0.556379
23	1	0	-6.936381	-2.577992	-1.136783
24	6	0	-9.319748	-0.107875	0.648416
25	1	0	-7.558579	1.083729	1.000062
26	6	0	-9.831347	-1.281153	0.087748
27	1	0	-9.373424	-3.087238	-0.992645
28	1	0	-9.985928	0.586565	1.151359
29	1	0	-10.893630	-1.495217	0.155890
30	1	0	0.138332	3.662212	-0.532912
31	7	0	3.093488	2.070842	-0.321177
32	6	0	-1.109384	1.248995	-0.063778
33	6	0	-1.637041	0.055628	-0.580133
34	6	0	-1.980447	2.160567	0.540036
35	6	0	-2.991558	-0.221937	-0.499523
36	1	0	-0.979123	-0.655453	-1.069764
37	6	0	-3.339203	1.885830	0.628796
38	1	0	-1.594376	3.081730	0.964543
39	6	0	-3.851619	0.697845	0.109749
40	1	0	-3.391175	-1.141992	-0.908995
41	1	0	-4.016938	2.586667	1.105807
42	35	0	7.797774	-0.590567	-0.011299

A1 (HF=-2237.3793297)

Center Number	Atomic Number	Atomic Type	Coordinates (Angstroms) X	Y	Z
1	77	0	-2.041213	-0.000001	0.000001
2	6	0	-1.423810	-0.111055	-2.975859
3	6	0	-3.048384	1.444463	-2.334141
4	6	0	-1.536672	0.238434	-4.308460
5	1	0	-0.736604	-0.882951	-2.653808
6	6	0	-3.200423	1.838101	-3.665221
7	6	0	-2.444130	1.236244	-4.657154
8	1	0	-0.925935	-0.262885	-5.049980
9	1	0	-3.913076	2.612923	-3.919017
10	1	0	-2.561267	1.539462	-5.692395
11	6	0	-3.478378	-1.410057	-0.060437
12	6	0	-3.790445	-1.988495	1.190642
13	6	0	-4.167068	-1.897625	-1.178341
14	6	0	-4.740600	-3.009668	1.308677
15	6	0	-5.113195	-2.914039	-1.063787
16	1	0	-3.965646	-1.482618	-2.161800
17	6	0	-5.404030	-3.474808	0.181073
18	1	0	-6.140944	-4.267064	0.269935
19	6	0	0.896233	-0.739393	-0.073092
20	6	0	-0.397748	-2.657721	-0.276498
21	6	0	2.063997	-1.485646	-0.133246
22	6	0	0.725596	-3.466576	-0.341280
23	1	0	-1.396571	-3.073923	-0.330855

24	6	0	1.978253	-2.869978	-0.271931
25	1	0	3.039199	-1.023292	-0.075891
26	1	0	0.630425	-4.540885	-0.446479
27	6	0	-0.397749	2.657721	0.276483
28	6	0	0.896233	0.739396	0.073065
29	6	0	0.725595	3.466578	0.341253
30	1	0	-1.396572	3.073922	0.330850
31	6	0	2.063996	1.485650	0.133206
32	6	0	1.978251	2.869982	0.271893
33	1	0	3.039198	1.023298	0.075840
34	6	0	-1.423781	0.111054	2.975854
35	6	0	-3.048360	-1.444465	2.334153
36	6	0	-1.536630	-0.238435	4.308456
37	1	0	-0.736579	0.882950	2.653796
38	6	0	-3.200386	-1.838103	3.665235
39	6	0	-2.444084	-1.236245	4.657160
40	1	0	-0.925886	0.262885	5.049971
41	1	0	-3.913036	-2.612926	3.919038
42	1	0	-2.561211	-1.539462	5.692402
43	6	0	-3.478379	1.410053	0.060452
44	6	0	-4.167059	1.897620	1.178363
45	6	0	-3.790458	1.988492	-1.190623
46	6	0	-5.113188	2.914034	1.063819
47	1	0	-3.965627	1.482613	2.161821
48	6	0	-4.740615	3.009664	-1.308649
49	6	0	-5.404035	3.474803	-0.181038
50	1	0	-6.140951	4.267058	-0.269893
51	7	0	-0.320110	-1.328736	-0.149132
52	7	0	-2.155193	0.472614	-2.012642
53	7	0	-2.155173	-0.472616	2.012645
54	7	0	3.101599	3.741667	0.348980
55	7	0	4.202583	3.159556	0.308114
56	6	0	5.346173	3.989875	0.381746
57	6	0	6.570618	3.320119	0.343465
58	6	0	5.301669	5.386368	0.487045
59	6	0	7.758060	4.041978	0.411068
60	1	0	6.574236	2.237883	0.261521
61	6	0	6.489616	6.098482	0.553508
62	1	0	4.344482	5.893442	0.515183
63	6	0	7.717343	5.429871	0.516082
64	1	0	8.710796	3.523284	0.381867
65	1	0	6.465264	7.180618	0.635080
66	1	0	8.641735	5.996747	0.569181
67	1	0	0.630423	4.540887	0.446452
68	1	0	-4.968709	-3.448400	2.275279
69	1	0	-5.629592	-3.271983	-1.950680
70	1	0	-5.629577	3.271976	1.950717
71	1	0	-4.968734	3.448396	-2.275248
72	7	0	-0.320110	1.328737	0.149117
73	7	0	3.101601	-3.741661	-0.349033
74	7	0	4.202584	-3.159550	-0.308155
75	6	0	5.346176	-3.989870	-0.381760
76	6	0	6.570620	-3.320115	-0.343465
77	6	0	5.301673	-5.386364	-0.487049
78	6	0	7.758063	-4.041975	-0.411044
79	1	0	6.574238	-2.237878	-0.261529
80	6	0	6.489620	-6.098479	-0.553487
81	1	0	4.344486	-5.893438	-0.515198
82	6	0	7.717347	-5.429868	-0.516046
83	1	0	8.710799	-3.523281	-0.381832
84	1	0	6.465269	-7.180616	-0.635051
85	1	0	8.641739	-5.996745	-0.569126

B1 (HF= -2634.2785179)

Center Number	Atomic Number	Atomic Type	Coordinates (Angstroms) X	Y	Z
1	77	0	-1.437376	-0.000101	-0.000040
2	9	0	-4.479281	3.482043	-2.543322
3	9	0	-4.478786	-3.482452	2.543551
4	9	0	-5.144199	3.358245	2.079184
5	9	0	-5.144050	-3.358855	-2.078911
6	7	0	0.276690	1.331447	0.102505
7	7	0	0.276852	-1.331461	-0.102717
8	7	0	3.813518	3.576322	0.177197
9	7	0	3.814000	-3.575838	-0.177953
10	7	0	3.699908	4.809358	0.319473
11	7	0	3.700551	-4.809061	-0.318764
12	7	0	-1.550212	0.414578	-2.023845
13	7	0	-1.549989	-0.414784	2.023776
14	6	0	0.200748	2.668737	0.179703
15	1	0	-0.797976	3.086113	0.222139
16	6	0	0.201084	-2.668756	-0.179928
17	1	0	-0.797587	-3.086266	-0.222265
18	6	0	1.316576	3.483610	0.209810
19	1	0	1.212557	4.558850	0.272592
20	6	0	1.317018	-3.483483	-0.210183
21	1	0	1.213128	-4.558734	-0.272990
22	6	0	2.572379	2.880825	0.156935
23	6	0	2.572748	-2.880536	-0.157417
24	6	0	2.655191	1.496242	0.070217
25	1	0	3.634321	1.037898	0.024248
26	6	0	2.655378	-1.495935	-0.070754
27	1	0	3.634452	-1.037457	-0.024927
28	6	0	1.488840	0.740189	0.044389
29	6	0	1.488931	-0.740038	-0.044765
30	6	0	4.908555	5.543852	0.342117
31	6	0	4.909335	-5.543323	-0.341704
32	6	0	4.763274	6.922049	0.512893
33	1	0	3.764949	7.335483	0.614429
34	6	0	4.764214	-6.921700	-0.511165
35	1	0	3.765898	-7.335435	-0.611557
36	6	0	5.889243	7.738328	0.550743
37	1	0	5.778644	8.809603	0.683718
38	6	0	5.890330	-7.737771	-0.549206
39	1	0	5.779855	-8.809182	-0.681182
40	6	0	7.155417	7.174449	0.417295
41	1	0	8.036562	7.808002	0.446187
42	6	0	7.156484	-7.173512	-0.417216
43	1	0	8.037741	-7.806902	-0.446242
44	6	0	7.298342	5.793836	0.245739
45	1	0	8.288523	5.361348	0.142114
46	6	0	7.299248	-5.792723	-0.246936
47	1	0	8.289418	-5.359946	-0.144423
48	6	0	6.181343	4.973288	0.207532
49	1	0	6.279539	3.902295	0.075474
50	6	0	6.182109	-4.972378	-0.208580
51	1	0	6.280178	-3.901253	-0.077502
52	6	0	-0.808097	-0.200558	-2.957523

53	1	0	-0.123484	-0.959117	-2.601494
54	6	0	-0.807844	0.200420	2.957385
55	1	0	-0.123304	0.959014	2.601288
56	6	0	-0.906765	0.100106	-4.303280
57	1	0	-0.286952	-0.426237	-5.019336
58	6	0	-0.906385	-0.100228	4.303155
59	1	0	-0.286557	0.426176	5.019154
60	6	0	-1.812056	1.080807	-4.693968
61	1	0	-1.920614	1.347889	-5.739938
62	6	0	-1.811584	-1.080978	4.693930
63	1	0	-1.920065	-1.348030	5.739916
64	6	0	-2.583099	1.718164	-3.734043
65	1	0	-3.291934	2.479352	-4.023386
66	6	0	-2.582649	-1.718414	3.734075
67	1	0	-3.291412	-2.479642	4.023491
68	6	0	-2.445251	1.373839	-2.386814
69	6	0	-2.444918	-1.374117	2.386828
70	6	0	-3.190404	1.940732	-1.256462
71	6	0	-3.190121	-1.941084	1.256545
72	6	0	-4.157540	2.943193	-1.340902
73	6	0	-4.157178	-2.943613	1.341091
74	6	0	-4.832249	3.442281	-0.244157
75	1	0	-5.577698	4.221200	-0.345443
76	6	0	-4.831927	-3.442786	0.244409
77	1	0	-5.577299	-4.221770	0.345771
78	6	0	-4.500286	2.891968	0.981587
79	6	0	-4.500104	-2.892480	-0.981377
80	6	0	-3.552487	1.897614	1.138804
81	1	0	-3.355082	1.521788	2.136263
82	6	0	-3.552396	-1.898055	-1.138691
83	1	0	-3.355102	-1.522238	-2.136177
84	6	0	-2.877218	1.404803	0.018956
85	6	0	-2.877085	-1.405156	-0.018909

C1 (HF= -7379.2018165)

Center Number	Atomic Number	Atomic Type	Coordinates (Angstroms) X	Y	Z
1	6	0	2.442645	-1.402178	-0.118287
2	6	0	2.767232	-1.807919	-1.431760
3	6	0	3.729621	-2.792169	-1.672394
4	6	0	4.393961	-3.397910	-0.614713
5	6	0	4.073184	-2.998862	0.678220
6	6	0	3.121497	-2.021319	0.937050
7	6	0	2.022708	-1.128918	-2.498844
8	7	0	1.120614	-0.214029	-2.057580
9	6	0	0.384569	0.480107	-2.940684
10	6	0	0.502817	0.302474	-4.306550
11	6	0	1.420087	-0.634024	-4.776825
12	6	0	2.180893	-1.350158	-3.867418
13	77	0	1.002780	-0.000337	-0.000811
14	6	0	2.443518	1.400711	0.118391
15	6	0	2.766000	1.806721	1.432288
16	6	0	3.728755	2.790288	1.674342
17	6	0	4.395471	3.395075	0.617621
18	6	0	4.076719	2.995852	-0.675785
19	6	0	3.124691	2.018992	-0.935917
20	6	0	2.018975	1.128882	2.498404
21	7	0	1.117818	0.213646	2.055887
22	6	0	0.379805	-0.479849	2.937837
23	6	0	0.494812	-0.300815	4.303847
24	6	0	1.410552	0.636520	4.775322
25	6	0	2.173596	1.351753	3.867043
26	7	0	-0.713741	1.336657	0.022291
27	6	0	-0.638706	2.674654	0.085032
28	6	0	-1.754647	3.486479	0.162671
29	6	0	-3.009524	2.879522	0.177231
30	6	0	-3.091706	1.494137	0.105783
31	6	0	-1.925133	0.741564	0.031191
32	7	0	-4.250506	3.570680	0.262010
33	7	0	-4.134605	4.805672	0.383247
34	6	0	-5.343766	5.534705	0.472702
35	6	0	-5.195957	6.913799	0.632726
36	6	0	-6.322070	7.724445	0.734813
37	6	0	-7.590923	7.154193	0.674760
38	6	0	-7.736437	5.772767	0.512671
39	6	0	-6.619289	4.957764	0.411581
40	6	0	-1.925412	-0.739646	-0.041114
41	7	0	-0.714617	-1.335603	-0.026384
42	6	0	-0.640235	-2.673835	-0.087277
43	6	0	-1.756402	-3.484923	-0.168100
44	6	0	-3.010811	-2.877012	-0.189114
45	6	0	-3.092202	-1.491459	-0.121246
46	7	0	-4.252010	-3.567031	-0.280092
47	7	0	-4.137804	-4.805091	-0.366333
48	6	0	-5.347390	-5.532625	-0.463575
49	6	0	-5.201498	-6.917298	-0.567488
50	6	0	-6.327989	-7.727183	-0.671108
51	6	0	-7.595368	-7.150364	-0.669965
52	6	0	-7.738970	-5.763216	-0.565252
53	6	0	-6.621337	-4.949077	-0.461952
54	1	0	0.359608	3.095119	0.069840
55	1	0	0.357855	-3.094802	-0.068098
56	1	0	-1.651410	4.562522	0.212449
57	1	0	-1.653775	-4.561121	-0.215775
58	1	0	-4.069725	1.031104	0.118929
59	1	0	-4.069721	-1.027616	-0.141072
60	1	0	-4.195608	7.332468	0.676209
61	1	0	-4.202258	-7.340816	-0.566201
62	1	0	-6.209352	8.796397	0.860490
63	1	0	-6.216816	-8.803564	-0.752437
64	1	0	-8.472154	7.783376	0.753558
65	1	0	-8.476893	-7.778893	-0.750813
66	1	0	-8.728758	5.335306	0.466005
67	1	0	-8.730102	-5.320598	-0.565079
68	1	0	-6.719491	3.886136	0.286365
69	1	0	-6.720050	-3.873078	-0.380986
70	1	0	-0.313120	-1.199403	2.521330
71	1	0	-0.309372	1.199309	-2.525271
72	1	0	-0.120629	-0.885970	4.976825
73	1	0	-0.111497	0.887818	-4.980377
74	1	0	1.529214	0.805912	5.840384
75	1	0	1.541751	-0.801819	-5.841810
76	1	0	2.892195	2.082586	4.216637
77	1	0	2.900688	-2.080284	-4.216016
78	1	0	5.142728	4.158948	0.797299
79	1	0	5.141002	-4.162215	-0.793361
80	1	0	2.917202	1.745689	-1.964322
81	1	0	2.912252	-1.748238	1.965168

82	1	0	3.975482	-3.100667	-2.683303
83	35	0	4.974663	-3.822808	2.142744
84	35	0	4.981615	3.818382	-2.138973
85	1	0	3.972914	3.099009	2.685608

A2 (HF= -2238.5601268)

Center Number	Atomic Number	Atomic Type	Coordinates (Angstroms) X	Y	Z
1	77	0	-0.000002	1.409036	-0.000056
2	7	0	1.602689	-0.157489	0.000481
3	7	0	4.679110	-3.020401	-0.274156
4	7	0	5.708618	-2.808872	0.395509
5	7	0	0.332289	1.514079	-2.046652
6	6	0	2.767661	0.048568	0.644410
7	1	0	2.849051	0.974419	1.200844
8	6	0	3.823022	-0.842981	0.607764
9	1	0	4.737174	-0.630209	1.146765
10	6	0	3.683042	-2.012276	-0.140835
11	6	0	2.490348	-2.226060	-0.822666
12	1	0	2.350417	-3.119459	-1.420269
13	6	0	1.482627	-1.279267	-0.725294
14	1	0	0.544700	-1.424359	-1.247133
15	6	0	6.726081	-3.787970	0.293921
16	6	0	7.876496	-3.528136	1.041050
17	1	0	7.921874	-2.620793	1.634875
18	6	0	8.938662	-4.426411	1.014766
19	1	0	9.833570	-4.225470	1.594788
20	6	0	8.846776	-5.581775	0.243055
21	1	0	9.673045	-6.285670	0.220182
22	6	0	7.693118	-5.840435	-0.503810
23	1	0	7.627856	-6.743388	-1.102797
24	6	0	6.630546	-4.949523	-0.483670
25	1	0	5.731594	-5.139967	-1.057858
26	6	0	-0.285901	0.758296	-2.968461
27	1	0	-1.018802	0.052975	-2.599248
28	6	0	-0.018032	0.861120	-4.320862
29	1	0	-0.546940	0.228374	-5.023686
30	6	0	0.934601	1.787100	-4.738077
31	1	0	1.173196	1.899501	-5.790560
32	6	0	1.578200	2.565028	-3.790079
33	1	0	2.323928	3.288348	-4.095618
34	6	0	1.268760	2.418788	-2.436734
35	6	0	1.876782	3.176521	-1.337500
36	6	0	2.857684	4.155873	-1.530419
37	1	0	3.217917	4.393853	-2.526541
38	6	0	3.382904	4.837597	-0.440454
39	1	0	4.143928	5.597626	-0.587857
40	6	0	2.920263	4.537494	0.841430
41	1	0	3.322506	5.069999	1.699250
42	6	0	1.943441	3.561454	1.029948
43	1	0	1.602301	3.355698	2.040764
44	6	0	1.402092	2.851797	-0.048555
45	7	0	-1.602174	-0.158035	-0.001878
46	7	0	-4.677630	-3.022179	0.270754
47	7	0	-5.707625	-2.809971	-0.397943
48	7	0	-0.331889	1.511944	2.046633
49	6	0	-2.767632	0.048602	-0.644740
50	1	0	-2.849728	0.975306	-1.199652
51	6	0	-3.822744	-0.843260	-0.608630
52	1	0	-4.737316	-0.629971	-1.146714
53	6	0	-3.681971	-2.013545	0.138271
54	6	0	-2.488794	-2.227934	0.819061
55	1	0	-2.348245	-3.122108	1.415358
56	6	0	-1.481403	-1.280721	0.722372
57	1	0	-0.543130	-1.426263	1.243461
58	6	0	-6.725862	-3.788125	-0.295008
59	6	0	-7.876841	-3.527427	-1.040968
60	1	0	-7.922059	-2.620155	-1.634913
61	6	0	-8.939737	-4.424799	-1.013440
62	1	0	-9.835070	-4.223201	-1.592578
63	6	0	-8.848028	-5.580119	-0.241644
64	1	0	-9.674873	-6.283306	-0.217795
65	6	0	-7.693822	-5.839630	0.504078
66	1	0	-7.628703	-6.742545	1.103139
67	6	0	-6.630519	-4.949619	0.482698
68	1	0	-5.731120	-5.140750	1.055956
69	6	0	0.287304	0.755885	2.967533
70	1	0	1.020871	0.051710	2.597414
71	6	0	0.019678	0.857166	4.320095
72	1	0	0.549382	0.224269	5.022184
73	6	0	-0.933713	1.781874	4.738421
74	1	0	-1.172107	1.893085	5.791077
75	6	0	-1.578229	2.560176	3.791342
76	1	0	-2.324447	3.282607	4.097782
77	6	0	-1.269017	2.415508	2.437773
78	6	0	-1.877734	3.173950	1.339387
79	6	0	-2.859179	4.152539	1.533437
80	1	0	-3.219464	4.389256	2.529841
81	6	0	-3.384821	4.835191	0.444255
82	1	0	-4.146251	5.594641	0.592540
83	6	0	-2.922020	4.536830	-0.837979
84	1	0	-3.324571	5.070098	-1.695180
85	6	0	-1.944636	3.561576	-1.027633
86	1	0	-1.603387	3.357203	-2.038692
87	6	0	-1.402891	2.850968	0.050049

B2 (HF=- 2635.4585829)

Center Number	Atomic Number	Atomic Type	Coordinates (Angstroms) X	Y	Z
1	6	0	1.397348	2.511428	-0.023021
2	6	0	1.896257	2.830779	-1.310004
3	6	0	2.868040	3.825820	-1.421334
4	6	0	3.369496	4.522854	-0.339353
5	6	0	2.852194	4.186407	0.898897
6	6	0	1.888350	3.211311	1.081683
7	6	0	1.321267	2.067226	-2.422987
8	7	0	0.374787	1.167237	-2.037119
9	6	0	-0.229693	0.399184	-2.956439
10	6	0	0.059335	0.479698	-4.306122
11	6	0	1.020430	1.395452	-4.718707
12	6	0	1.653040	2.189573	-3.774489
13	77	0	0.000000	1.067073	-0.000001

14	7	0	1.595916	-0.493075	0.025785
15	6	0	2.753306	-0.287943	0.684613
16	6	0	3.810226	-1.177298	0.655773
17	6	0	3.680915	-2.343722	-0.099190
18	6	0	2.495088	-2.558240	-0.792678
19	6	0	1.485138	-1.613678	-0.704289
20	7	0	4.680132	-3.349209	-0.225735
21	7	0	5.713812	-3.122535	0.432735
22	6	0	6.735668	-4.096931	0.337266
23	6	0	7.888232	-3.822597	1.076034
24	6	0	8.955028	-4.715405	1.054399
25	6	0	8.865801	-5.879241	0.295166
26	6	0	7.710300	-6.152071	-0.443865
27	6	0	6.642917	-5.267007	-0.428020
28	7	0	-1.595900	-0.493090	-0.025816
29	6	0	-2.753279	-0.287973	-0.684667
30	6	0	-3.810190	-1.177340	-0.655846
31	6	0	-3.680879	-2.343762	0.099121
32	6	0	-2.495061	-2.558269	0.792626
33	6	0	-1.485121	-1.613693	0.704258
34	7	0	-4.680082	-3.349267	0.225639
35	7	0	-5.713803	-3.122544	-0.432749
36	6	0	-6.735662	-4.096937	-0.337267
37	6	0	-7.888279	-3.822543	-1.075931
38	6	0	-8.955080	-4.715345	-1.054278
39	6	0	-8.865805	-5.879233	-0.295130
40	6	0	-7.710252	-6.152122	0.443796
41	6	0	-6.642863	-5.267065	0.427932
42	7	0	-0.374793	1.167199	2.037119
43	6	0	0.229682	0.399129	2.956427
44	6	0	-0.059350	0.479620	4.306111
45	6	0	-1.020446	1.395366	4.718709
46	6	0	-1.653054	2.189503	3.774503
47	6	0	-1.321276	2.067180	2.423000
48	6	0	-1.896268	2.830748	1.310028
49	6	0	-2.868057	3.825781	1.421374
50	6	0	-3.369517	4.522828	0.339402
51	6	0	-2.852215	4.186401	-0.898853
52	6	0	-1.888365	3.211314	-1.081653
53	6	0	-1.397357	2.511418	0.023041
54	1	0	-2.828105	0.633955	-1.248279
55	1	0	-4.717630	-0.965000	-1.206166
56	1	0	-2.362241	-3.450420	1.393600
57	1	0	-0.553615	-1.760142	1.236534
58	1	0	-7.931503	-2.908453	-1.659471
59	1	0	-9.851660	-4.503444	-1.627747
60	1	0	-9.695801	-6.578831	-0.275786
61	1	0	-7.647534	-7.061441	1.033326
62	1	0	-5.742545	-5.468160	0.996325
63	1	0	0.969844	-0.298592	2.587984
64	1	0	0.460246	-0.162731	5.007014
65	1	0	-1.278723	1.491812	5.768034
66	1	0	-2.404025	2.902645	4.079411
67	9	0	-3.370737	4.156817	2.636508
68	1	0	-4.123542	5.290333	0.462015
69	9	0	-3.317798	4.853374	-1.982286
70	1	0	-1.533214	3.015675	-2.087302
71	1	0	2.828134	0.633988	1.248219
72	1	0	4.717676	-0.964945	1.206072
73	1	0	2.362270	-3.450390	-1.393654
74	1	0	0.553624	-1.760136	-1.236549
75	1	0	7.931420	-2.908547	1.659638
76	1	0	9.851567	-4.503552	1.627949
77	1	0	9.695793	-6.578845	0.275835
78	1	0	7.647619	-7.061349	-1.033462
79	1	0	5.742640	-5.468056	-0.996494
80	1	0	-0.969856	-0.298542	-2.588005
81	1	0	-0.460264	-0.162639	-5.007034
82	1	0	1.278703	1.491917	-5.768031
83	1	0	2.404008	2.902722	-4.079388
84	9	0	3.370716	4.156878	-2.636464
85	1	0	4.123515	5.290366	-0.461954
86	9	0	3.317774	4.853367	1.982340
87	1	0	1.533200	3.015656	2.087330

C2 (HF= -7380.3822089)

Center Number	Atomic Number	Atomic Type	Coordinates (Angstroms) X	Y	Z
1	6	0	-1.393489	2.075058	0.129795
2	6	0	-1.793795	2.400849	1.442799
3	6	0	-2.755684	3.384511	1.686473
4	6	0	-3.339916	4.072110	0.631183
5	6	0	-2.938561	3.756722	-0.661957
6	6	0	-1.983554	2.782249	-0.922644
7	6	0	-1.128728	1.639951	2.506345
8	7	0	-0.216210	0.735221	2.063427
9	6	0	0.451454	-0.021938	2.948950
10	6	0	0.257156	0.080110	4.314111
11	6	0	-0.670635	1.005570	4.783834
12	6	0	-1.364649	1.785588	3.873437
13	77	0	-0.000001	0.630629	0.000010
14	7	0	-1.597610	-0.928911	0.091406
15	6	0	-2.800253	-0.722399	-0.479064
16	6	0	-3.853984	-1.609788	-0.369348
17	6	0	-3.670989	-2.774317	0.377017
18	6	0	-2.433919	-2.995212	0.972178
19	6	0	-1.433484	-2.050365	0.809993
20	7	0	-4.658798	-3.779984	0.569717
21	7	0	-5.795089	-3.456641	0.172893
22	6	0	-6.807983	-4.432738	0.331930
23	6	0	-8.078620	-4.045319	-0.097672
24	6	0	-9.147342	-4.929449	0.011690
25	6	0	-8.942129	-6.197501	0.549108
26	6	0	-7.668386	-6.583495	0.978338
27	6	0	-6.598243	-5.707790	0.873488
28	7	0	1.597595	-0.928923	-0.091378
29	6	0	2.800279	-0.722367	0.478987
30	6	0	3.854002	-1.609765	0.369265
31	6	0	3.670952	-2.774353	-0.376993
32	6	0	2.433840	-2.995291	-0.972053
33	6	0	1.433419	-2.050430	-0.809872
34	7	0	4.658745	-3.780038	-0.569686
35	7	0	5.795060	-3.456673	-0.172946
36	6	0	6.807939	-4.432789	-0.331966
37	6	0	8.078600	-4.045347	0.097543
38	6	0	9.147311	-4.929493	-0.011810
39	6	0	8.942061	-6.197582	-0.549126
40	6	0	7.668293	-6.583599	-0.978261

41	6	0	6.598162	-5.707879	-0.873419
42	7	0	0.216195	0.735205	-2.063407
43	6	0	-0.451513	-0.021925	-2.948921
44	6	0	-0.257220	0.080108	-4.314084
45	6	0	0.670610	1.005524	-4.783818
46	6	0	1.364663	1.785517	-3.873430
47	6	0	1.128746	1.639897	-2.506335
48	6	0	1.793839	2.400784	-1.442797
49	6	0	2.755753	3.384420	-1.686482
50	6	0	3.339996	4.072022	-0.631200
51	6	0	2.938626	3.756667	0.661943
52	6	0	1.983593	2.782221	0.922642
53	6	0	1.393517	2.075027	-0.129789
54	1	0	2.915120	0.199017	1.036669
55	1	0	4.798923	-1.398936	0.853357
56	1	0	2.255570	-3.890220	-1.556971
57	1	0	0.464171	-2.197878	-1.269588
58	1	0	8.210974	-3.051401	0.512905
59	1	0	10.135680	-4.629807	0.321341
60	1	0	9.773246	-6.890663	-0.635657
61	1	0	7.515267	-7.573896	-1.395682
62	1	0	5.606767	-5.996056	-1.202375
63	1	0	-1.163894	-0.726302	-2.540021
64	1	0	-0.823568	-0.553183	-4.986505
65	1	0	0.851330	1.116711	-5.847790
66	1	0	2.091891	2.508928	-4.220391
67	1	0	3.063531	3.629687	-2.697776
68	1	0	4.087421	4.835339	-0.812597
69	35	0	3.725710	4.694265	2.123410
70	1	0	1.704870	2.580205	1.950951
71	1	0	-2.915049	0.198936	-1.036835
72	1	0	-4.798869	-1.398998	-0.853528
73	1	0	-2.255692	-3.890095	1.557179
74	1	0	-0.464270	-2.197779	1.269790
75	1	0	-8.210965	-3.051402	-0.513113
76	1	0	-10.135692	-4.629781	-0.321534
77	1	0	-9.773323	-6.890570	0.635647
78	1	0	-7.515388	-7.573762	1.395839
79	1	0	-5.606868	-5.995949	1.202515
80	1	0	1.163800	-0.726355	2.540060
81	1	0	0.823468	-0.553206	4.986539
82	1	0	-0.851360	1.116768	5.847804
83	1	0	-2.091853	2.509027	4.220390
84	1	0	-3.063454	3.629800	2.697764
85	1	0	-4.087322	4.835448	0.812570
86	35	0	-3.725628	4.694314	-2.123438
87	1	0	-1.704840	2.580209	-1.950952

A3 (HF=- 2699.2390597)

Center Number	Atomic Number	Atomic Type	Coordinates (Angstroms) X	Y	Z
1	77	0	-3.415494	0.051526	0.017476
2	7	0	-1.758176	-1.358138	-0.104803
3	7	0	-1.630081	1.296447	0.135370
4	7	0	5.022588	-6.451140	-0.576100
5	7	0	5.691903	5.586050	0.490750
6	7	0	6.037133	-6.173747	0.091723
7	7	0	5.789800	6.669641	-0.116284
8	7	0	-3.507982	0.486252	-2.004840
9	7	0	-3.547608	-0.369666	2.039708
10	6	0	-1.892739	-2.685471	-0.211958
11	1	0	-2.909460	-3.058366	-0.251335
12	6	0	-1.636137	2.631731	0.226110
13	1	0	-2.612021	3.100702	0.273548
14	6	0	-0.810554	-3.545544	-0.268616
15	1	0	-0.986767	-4.612571	-0.337053
16	6	0	-0.475939	3.384386	0.271556
17	1	0	-0.548541	4.461327	0.367753
18	6	0	0.483999	-3.024637	-0.212913
19	6	0	0.762138	2.740428	0.222721
20	6	0	0.611286	-1.639017	-0.093743
21	1	0	1.598286	-1.197529	-0.067326
22	6	0	0.755462	1.347508	0.120837
23	1	0	1.695941	0.817057	0.055008
24	6	0	-0.517000	-0.829673	-0.040310
25	6	0	-0.445552	0.650075	0.076504
26	6	0	1.676078	-3.900666	-0.284200
27	6	0	2.033698	3.497850	0.276788
28	6	0	1.677326	-5.030243	-1.108276
29	1	0	0.809298	-5.263149	-1.716426
30	6	0	2.148497	4.742583	-0.360974
31	1	0	1.306931	5.144835	-0.916038
32	6	0	2.798866	-5.846395	-1.180710
33	1	0	2.809276	-6.718539	-1.826364
34	6	0	3.333461	5.458658	-0.318242
35	1	0	3.418642	6.414496	-0.821028
36	6	0	3.933591	-5.549779	-0.426851
37	6	0	4.431338	4.939100	0.376113
38	6	0	3.942864	-4.425196	0.405286
39	1	0	4.822055	-4.201621	0.997442
40	6	0	4.326306	3.706359	1.018843
41	1	0	5.183139	3.321345	1.562144
42	6	0	2.823779	-3.611411	0.469741
43	1	0	2.833485	-2.752271	1.133103
44	6	0	3.138261	2.988610	0.966210
45	1	0	3.066531	2.039797	1.487886
46	6	0	-2.802548	-0.148878	-2.954762
47	1	0	-2.150913	-0.943702	-2.615268
48	6	0	-2.788563	0.201610	2.988818
49	1	0	-2.066830	0.933035	2.648440
50	6	0	-2.898367	0.177916	-4.294461
51	1	0	-2.310040	-0.365295	-5.024534
52	6	0	-2.916003	-0.110515	4.329387
53	1	0	-2.281631	0.379188	5.058759
54	6	0	-3.760074	1.207855	-4.665196
55	1	0	-3.862810	1.494449	-5.706693
56	6	0	-3.869282	-1.055548	4.701998
57	1	0	-3.999592	-1.327771	5.744274
58	6	0	-4.488945	1.863512	-3.687018
59	1	0	-5.165307	2.664728	-3.957733
60	6	0	-4.654498	-1.644163	3.724748
61	1	0	-5.403359	-2.377506	3.997059
62	6	0	-4.355715	1.490968	-2.347787
63	6	0	-4.485515	-1.290074	2.384537
64	6	0	-5.071664	2.092893	-1.216847
65	6	0	-5.254823	-1.824273	1.254614
66	6	0	-5.974832	3.153168	-1.357481
67	1	0	-6.184588	3.579559	-2.333746

68	6	0	-6.253240	-2.795027	1.397327
69	1	0	-6.499633	-3.200177	2.374098
70	6	0	-6.614677	3.673523	-0.240419
71	1	0	-7.315026	4.496219	-0.346867
72	6	0	-6.941899	-3.252409	0.281754
73	1	0	-7.716828	-4.005048	0.389838
74	6	0	-6.347465	3.128468	1.016752
75	6	0	-6.627163	-2.734856	-0.976019
76	6	0	-5.448613	2.072717	1.153596
77	1	0	-5.264749	1.670992	2.146009
78	6	0	-5.632467	-1.769147	-1.115121
79	1	0	-5.413632	-1.386781	-2.108105
80	6	0	-4.784409	1.528675	0.046725
81	6	0	-4.917746	-1.290066	-0.009763
82	6	0	7.130166	-7.069715	-0.051623
83	6	0	7.045052	7.325120	-0.003280
84	6	0	7.116739	-8.210046	-0.864152
85	1	0	6.227155	-8.452479	-1.433432
86	6	0	7.159498	8.522995	-0.709965
87	1	0	6.309756	8.873754	-1.287247
88	6	0	8.245735	-9.014592	-0.927454
89	1	0	8.240735	-9.900088	-1.555761
90	6	0	8.348313	9.245966	-0.668448
91	1	0	8.435669	10.176876	-1.219753
92	6	0	9.387225	-8.691843	-0.187951
93	1	0	10.265755	-9.327350	-0.244107
94	6	0	9.421082	8.771466	0.081761
95	1	0	10.349859	9.332662	0.117621
96	6	0	9.397704	-7.557624	0.619661
97	1	0	10.282311	-7.304283	1.195374
98	6	0	9.303896	7.572584	0.790886
99	1	0	10.141840	7.206174	1.376106
100	6	0	8.268571	-6.746471	0.687970
101	1	0	8.253564	-5.857458	1.310701
102	6	0	8.121929	6.846269	0.752852
103	1	0	8.021482	5.916420	1.300135
104	1	0	-7.163014	-3.086996	-1.853685
105	1	0	-6.845550	3.529689	1.895597

B3 (HF= -3096.1382408)

Center Number	Atomic Number	Atomic Type	Coordinates (Angstroms) X	Y	Z
1	6	0	8.472294	6.890749	0.775305
2	6	0	7.391384	7.363629	0.021158
3	6	0	7.495703	8.565143	-0.680922
4	6	0	8.678484	9.297765	-0.636793
5	6	0	9.755244	8.829258	0.111460
6	6	0	9.648170	7.626718	0.815998
7	7	0	6.141555	6.698465	-0.094020
8	7	0	6.052652	5.611344	0.508048
9	6	0	4.796750	4.955541	0.391162
10	6	0	3.694616	5.470720	-0.299658
11	6	0	2.514639	4.746705	-0.344510
12	6	0	2.409586	3.498193	0.287457
13	6	0	3.518439	2.992906	0.972854
14	6	0	4.701335	3.718898	1.027849
15	6	0	1.143183	2.732900	0.231746
16	6	0	-0.098913	3.368684	0.284291
17	6	0	-1.254344	2.609500	0.236512
18	7	0	-1.239879	1.274385	0.139913
19	6	0	-0.050863	0.635413	0.077730
20	6	0	1.145134	1.340158	0.124504
21	77	0	-3.008924	0.020995	0.014966
22	6	0	-4.505757	-1.322800	-0.025836
23	6	0	-4.838849	-1.868013	1.240827
24	6	0	-5.846969	-2.830422	1.310413
25	6	0	-6.544284	-3.281597	0.207078
26	6	0	-6.191775	-2.724168	-1.009765
27	6	0	-5.203600	-1.767738	-1.152148
28	6	0	-0.114243	-0.843459	-0.045435
29	7	0	-1.353352	-1.377518	-0.115320
30	6	0	-1.481552	-2.705147	-0.230182
31	6	0	-0.395218	-3.559364	-0.288387
32	6	0	0.896798	-3.032994	-0.226555
33	6	0	1.017239	-1.647184	-0.100294
34	6	0	2.093002	-3.902773	-0.298920
35	6	0	2.100475	-5.030069	-1.126076
36	6	0	3.226353	-5.840036	-1.199839
37	6	0	4.358822	-5.539493	-0.444167
38	6	0	4.361583	-4.417368	0.391300
39	6	0	3.238384	-3.609454	0.456943
40	7	0	5.452843	-6.434610	-0.595147
41	7	0	6.465630	-6.152622	0.073395
42	6	0	7.563880	-7.041822	-0.071340
43	6	0	7.557160	-8.180885	-0.885747
44	6	0	8.690935	-8.978539	-0.950407
45	6	0	9.830510	-8.650142	-0.210419
46	6	0	9.834285	-7.517241	0.599099
47	6	0	8.700334	-6.712975	0.668800
48	6	0	-4.069098	-1.352230	2.379217
49	7	0	-3.136372	-0.424011	2.030805
50	6	0	-2.368772	0.144639	2.973176
51	6	0	-2.477487	-0.174737	4.313877
52	6	0	-3.420672	-1.125035	4.689727
53	6	0	-4.218302	-1.714194	3.720726
54	7	0	-3.100782	0.477772	-2.000738
55	6	0	-2.380238	-0.147696	-2.944319
56	6	0	-2.462856	0.182329	-4.284295
57	6	0	-3.327713	1.205265	-4.658040
58	6	0	-4.075228	1.854656	-3.687619
59	6	0	-3.955028	1.479462	-2.346858
60	6	0	-4.677796	2.056117	-1.206886
61	6	0	-5.601847	3.099699	-1.273795
62	6	0	-6.256047	3.607436	-0.168625
63	6	0	-5.948453	3.022121	1.047331
64	6	0	-5.043527	1.986250	1.187100
65	6	0	-4.388376	1.484665	0.058889
66	1	0	-2.495201	-3.084941	-0.275050
67	1	0	-2.231708	3.074373	0.287203
68	1	0	-0.566884	-4.626630	-0.362854
69	1	0	-0.178841	4.444588	0.385177
70	1	0	2.001878	-1.200880	-0.069549
71	1	0	2.088699	0.815654	0.056045
72	1	0	1.234330	-5.265865	-1.735765
73	1	0	1.669806	5.145755	-0.896880
74	1	0	3.241903	-6.710254	-1.847945
75	1	0	3.772566	6.429538	-0.797864

76	1	0	5.239036	-4.191026	0.984949
77	1	0	5.561464	3.337356	1.568345
78	1	0	3.243198	-2.752290	1.122875
79	1	0	3.454090	2.041077	1.489960
80	1	0	-1.726900	-0.938803	-2.600441
81	1	0	-1.654867	0.881150	2.628316
82	1	0	-1.861969	-0.354055	-5.009013
83	1	0	-1.836090	0.314097	5.037512
84	1	0	-3.422718	1.496274	-5.698948
85	1	0	-3.538211	-1.405616	5.731204
86	1	0	-4.752131	2.649086	-3.963753
87	1	0	-4.956717	-2.451148	3.998655
88	9	0	-5.899700	3.672846	-2.466720
89	9	0	-6.188908	-3.376180	2.504355
90	1	0	-6.967967	4.418703	-0.256253
91	1	0	-7.321726	-4.030078	0.296765
92	1	0	-4.862874	1.584858	2.177843
93	1	0	-4.992723	-1.383279	-2.143608
94	1	0	6.668995	-8.427700	-1.455362
95	1	0	6.642940	8.911060	-1.256661
96	1	0	8.691225	-9.863027	-1.580142
97	1	0	8.758036	10.231498	-1.184482
98	1	0	10.712827	-9.280277	-0.267676
99	1	0	10.679315	9.398030	0.149404
100	1	0	10.717399	-7.259592	1.175186
101	1	0	10.489219	7.265080	1.399721
102	1	0	8.680023	-5.825102	1.292996
103	1	0	8.379612	5.958025	1.319050
104	9	0	-6.856929	-3.143937	-2.113722
105	9	0	-6.573295	3.495902	2.152968

C3 (HF= -7841.0615953)

Center Number	Atomic Number	Atomic Type	Coordinates (Angstroms) X	Y	Z
1	77	0	2.527844	-0.011269	-0.020678
2	35	0	6.395406	3.740289	-2.462108
3	35	0	6.624406	-3.505846	2.428680
4	7	0	0.856197	-1.397741	0.069064
5	7	0	0.767455	1.262492	-0.109076
6	7	0	-5.983733	-6.431296	0.152410
7	7	0	-6.484481	5.683941	-0.027593
8	7	0	-6.958741	-6.141782	-0.567086
9	7	0	-6.518225	6.772989	0.576669
10	7	0	2.625362	0.378528	2.011210
11	7	0	2.655876	-0.391731	-2.051806
12	6	0	0.971516	-2.730011	0.128263
13	1	0	1.981570	-3.119810	0.170062
14	6	0	0.793952	2.599786	-0.160024
15	1	0	1.775220	3.055685	-0.218254
16	6	0	-0.122791	-3.576141	0.132462
17	1	0	0.038214	-4.647293	0.162766
18	6	0	-0.353961	3.371779	-0.150453
19	1	0	-0.264931	4.449654	-0.216888
20	6	0	-1.408980	-3.036053	0.067529
21	6	0	-1.601101	2.747665	-0.078186
22	6	0	-1.516120	-1.645001	0.004024
23	1	0	-2.496139	-1.188928	-0.032580
24	6	0	-1.615755	1.351993	-0.024202
25	1	0	-2.561964	0.834814	0.062716
26	6	0	-0.377081	-0.849793	0.009261
27	6	0	-0.426671	0.633880	-0.044782
28	6	0	-2.611921	-3.899801	0.069486
29	6	0	-2.859095	3.528412	-0.054178
30	6	0	-2.648893	-5.059322	0.849859
31	1	0	-1.802683	-5.323152	1.475820
32	6	0	-2.919895	4.755827	0.623441
33	1	0	-2.046217	5.126718	1.149896
34	6	0	-3.778925	-5.866784	0.855702
35	1	0	-3.817801	-6.761928	1.467878
36	6	0	-4.091662	5.493424	0.658168
37	1	0	-4.134808	6.434873	1.192323
38	6	0	-4.884744	-5.533138	0.074893
39	6	0	-5.231336	5.013247	0.004036
40	6	0	-4.858606	-4.377326	-0.712878
41	1	0	-5.716278	-4.123712	-1.324269
42	6	0	-5.181233	3.796896	-0.675449
43	1	0	-6.071153	3.441528	-1.184701
44	6	0	-3.732249	-3.570855	-0.708918
45	1	0	-3.714003	-2.686556	-1.338262
46	6	0	-4.005137	3.058158	-0.702436
47	1	0	-3.976964	2.123153	-1.252487
48	6	0	1.908375	-0.264774	2.946733
49	1	0	1.244037	-1.041485	2.590668
50	6	0	1.902417	0.206330	-2.988647
51	1	0	1.187810	0.937641	-2.633597
52	6	0	2.009238	0.032766	4.293110
53	1	0	1.411418	-0.515791	5.011284
54	6	0	2.028145	-0.080063	-4.335358
55	1	0	1.398977	0.430682	-5.054647
56	6	0	2.887551	1.039520	4.686178
57	1	0	2.994184	1.302055	5.733495
58	6	0	2.972138	-1.025919	-4.727382
59	1	0	3.100374	-1.277487	-5.774970
60	6	0	3.629008	1.703320	3.722537
61	1	0	4.318989	2.486570	4.010851
62	6	0	3.751537	-1.642613	-3.762342
63	1	0	4.493273	-2.377419	-4.049790
64	6	0	3.489851	1.360554	2.377104
65	6	0	3.584339	-1.313987	-2.416579
66	6	0	4.218359	1.972325	1.259307
67	6	0	4.347334	-1.879175	-1.297264
68	6	0	5.142603	3.008275	1.419567
69	1	0	5.366037	3.413509	2.401201
70	6	0	5.337075	-2.852985	-1.455849
71	1	0	5.588343	-3.242331	-2.437206
72	6	0	5.796707	3.542108	0.317608
73	1	0	6.514130	4.345912	0.433502
74	6	0	6.021623	-3.344181	-0.352558
75	1	0	6.790078	-4.099544	-0.467113
76	6	0	5.504718	3.019038	-0.937521
77	6	0	5.693015	-2.842273	0.902172
78	6	0	4.589791	1.989895	-1.116214
79	1	0	4.401296	1.619140	-2.117420
80	6	0	4.712688	-1.874910	1.079291
81	1	0	4.498108	-1.518004	2.080279
82	6	0	3.920494	1.442513	-0.015985
83	6	0	4.012244	-1.371128	-0.022337
84	6	0	-8.061501	-7.034331	-0.493320

85	6	0	-7.766640	7.450088	0.554403
86	6	0	-8.107818	-8.166952	0.328723
87	1	0	-7.261544	-8.404639	0.962425
88	6	0	-7.792224	8.676548	1.219694
89	1	0	-6.885190	9.031020	1.699256
90	6	0	-9.239969	-8.969473	0.319438
91	1	0	-9.281338	-9.848675	0.955179
92	6	0	-8.966493	9.422861	1.260729
93	1	0	-8.984445	10.376635	1.778540
94	6	0	-10.325450	-8.652464	-0.502262
95	1	0	-11.206887	-9.286417	-0.502761
96	6	0	-10.114521	8.941469	0.636959
97	1	0	-11.032770	9.520030	0.667182
98	6	0	-10.276869	-7.525500	-1.318580
99	1	0	-11.118064	-7.276528	-1.957754
100	6	0	-10.087222	7.712619	-0.028734
101	1	0	-10.984423	7.340153	-0.513690
102	6	0	-9.144644	-6.715700	-1.313468
103	1	0	-9.084370	-5.831971	-1.940956
104	6	0	-8.919621	6.963778	-0.073997
105	1	0	-8.889002	6.009801	-0.587026

A4 (HF= -4698.8768485)

Center Number	Atomic Number	Atomic Type	Coordinates (Angstroms) X	Y	Z
1	77	0	2.563727	-0.446593	0.060923
2	6	0	2.243186	-0.353017	-2.961840
3	6	0	2.789967	-2.442047	-2.063186
4	6	0	2.225983	-0.850555	-4.251352
5	1	0	2.039852	0.690722	-2.759470
6	6	0	2.784126	-2.996929	-3.344551
7	6	0	2.501677	-2.202545	-4.443243
8	1	0	2.001947	-0.190013	-5.080609
9	1	0	3.003702	-4.049088	-3.476346
10	1	0	2.498048	-2.631132	-5.440056
11	6	0	4.525136	0.009637	0.052870
12	6	0	5.028948	0.471765	1.289808
13	6	0	5.422240	-0.045027	-1.021420
14	6	0	6.364091	0.866596	1.434672
15	6	0	6.751755	0.346999	-0.879781
16	1	0	5.083965	-0.397832	-1.991514
17	6	0	7.228357	0.805313	0.349648
18	1	0	8.264062	1.111617	0.459595
19	6	0	0.449082	1.687355	-0.342175
20	6	0	2.558133	2.637393	-0.529480
21	6	0	-0.153284	2.926208	-0.539140
22	6	0	2.033362	3.902656	-0.736521
23	1	0	3.629057	2.472813	-0.516087
24	6	0	0.653011	4.036676	-0.738271
25	1	0	-1.228559	3.034782	-0.534153
26	1	0	2.691157	4.748941	-0.888510
27	6	0	-0.245041	-1.828035	0.325192
28	6	0	-0.330232	0.442213	-0.120485
29	6	0	-1.624840	-1.933086	0.308091
30	1	0	0.381971	-2.690372	0.519026
31	6	0	-1.718330	0.404139	-0.155784
32	6	0	-2.397984	-0.796808	0.062245
33	1	0	-2.282742	1.300147	-0.377038
34	6	0	1.827292	0.086930	2.962505
35	6	0	4.055437	0.507313	2.387696
36	6	0	2.038050	0.461815	4.276169
37	1	0	0.855415	-0.247554	2.622600
38	6	0	4.322708	0.898767	3.701207
39	6	0	3.313998	0.877552	4.649953
40	1	0	1.218674	0.426309	4.984379
41	1	0	5.321026	1.215757	3.976284
42	1	0	3.519333	1.179810	5.671661
43	6	0	3.051382	-2.377867	0.354859
44	6	0	3.329339	-3.026371	1.564914
45	6	0	3.081056	-3.164140	-0.819069
46	6	0	3.613731	-4.389616	1.610739
47	1	0	3.324246	-2.464514	2.494732
48	6	0	3.366484	-4.533892	-0.775627
49	6	0	3.633273	-5.149670	0.439980
50	1	0	3.854878	-6.211826	0.476169
51	7	0	1.792607	1.556625	-0.339848
52	7	0	2.516268	-1.121981	-1.895309
53	7	0	2.804079	0.107579	2.041040
54	7	0	-8.084000	-1.141176	-0.068654
55	7	0	-8.750352	-0.197227	0.397382
56	6	0	-10.160968	-0.354769	0.341197
57	6	0	-10.902138	0.712408	0.850444
58	6	0	-10.810762	-1.481967	-0.176388
59	6	0	-12.293143	0.660577	0.844321
60	1	0	-10.374841	1.574400	1.246995
61	6	0	-12.197796	-1.527455	-0.178868
62	1	0	-10.225500	-2.305588	-0.567951
63	6	0	-12.941787	-0.458988	0.329850
64	1	0	-12.867966	1.491713	1.240481
65	1	0	-12.706762	-2.399340	-0.578393
66	1	0	-14.026585	-0.503753	0.323807
67	1	0	-2.083386	-2.894582	0.506708
68	1	0	6.738384	1.224189	2.389009
69	1	0	7.423031	0.294544	-1.733015
70	1	0	3.823537	-4.864434	2.565676
71	1	0	3.382472	-5.128071	-1.684217
72	7	0	0.395210	-0.671442	0.119050
73	6	0	-3.877225	-0.858095	0.033596
74	6	0	-4.646133	0.201085	0.539608
75	6	0	-4.531690	-1.975854	-0.492970
76	6	0	-6.030141	0.147070	0.525926
77	1	0	-4.155822	1.066948	0.973202
78	6	0	-5.919351	-2.032056	-0.515009
79	1	0	-3.958638	-2.797988	-0.909240
80	6	0	-6.673452	-0.976146	-0.004694
81	1	0	-6.617959	0.962890	0.929028
82	1	0	-6.432868	-2.892972	-0.930555
83	35	0	-0.132625	5.729181	-1.007220

B4 (HF= -5095.77266)

Center Number	Atomic Number	Atomic Type	Coordinates (Angstroms) X	Y	Z

1	6	0	10.470346	-0.381795	0.444719
2	6	0	11.132047	-0.962915	-0.641727
3	6	0	12.521197	-0.990295	-0.655497
4	6	0	13.250829	-0.447562	0.405030
5	6	0	12.587603	0.131951	1.485546
6	6	0	11.196279	0.174833	1.500793
7	7	0	9.056129	-0.279749	0.542994
8	7	0	8.410524	-1.007492	-0.235394
9	6	0	6.997970	-0.864628	-0.161161
10	6	0	6.252084	-1.906375	-0.709994
11	6	0	4.864311	-1.867797	-0.669215
12	6	0	4.200856	-0.772697	-0.103194
13	6	0	4.966868	0.283301	0.419767
14	6	0	6.351432	0.242308	0.398417
15	6	0	2.722622	-0.716678	-0.070187
16	6	0	1.939327	-1.867806	0.055808
17	6	0	0.560758	-1.758442	0.074899
18	7	0	-0.080359	-0.588852	-0.027341
19	6	0	0.654851	0.539237	-0.155514
20	6	0	2.039524	0.500673	-0.173735
21	77	0	-2.220107	-0.316795	0.062251
22	6	0	-4.150510	0.224048	0.260694
23	6	0	-4.524074	0.558882	1.585850
24	6	0	-5.784582	1.124103	1.804347
25	6	0	-6.694739	1.374572	0.800026
26	6	0	-6.298685	1.010572	-0.475634
27	6	0	-5.074138	0.446358	-0.768730
28	6	0	-0.115359	1.806879	-0.255040
29	7	0	-1.450033	1.707102	-0.084038
30	6	0	-2.196079	2.818439	-0.131911
31	6	0	-1.666555	4.074389	-0.372888
32	6	0	-0.297679	4.170111	-0.585880
33	6	0	0.492276	3.033274	-0.516693
34	6	0	-3.507784	0.311061	2.620239
35	7	0	-2.323907	-0.133266	2.121630
36	6	0	-1.315539	-0.427296	2.955570
37	6	0	-1.416970	-0.299123	4.327857
38	6	0	-2.622418	0.149531	4.859585
39	6	0	-3.672711	0.450029	4.003154
40	35	0	0.484747	5.839315	-0.968031
41	7	0	-2.324879	-0.620330	-1.987567
42	6	0	-2.167679	0.352941	-2.902069
43	6	0	-2.220359	0.113278	-4.262317
44	6	0	-2.437395	-1.195903	-4.692233
45	6	0	-2.619602	-2.199391	-3.752148
46	6	0	-2.580272	-1.896000	-2.387649
47	6	0	-2.796550	-2.830625	-1.272537
48	6	0	-3.067243	-4.194906	-1.392502
49	6	0	-3.237670	-5.039449	-0.314441
50	6	0	-3.115811	-4.456612	0.935032
51	6	0	-2.858723	-3.116804	1.137231
52	6	0	-2.696654	-2.272581	0.030820
53	1	0	-0.060194	-2.640273	0.182667
54	1	0	2.384689	-2.851423	0.162778
55	1	0	2.600003	1.421641	-0.281020
56	1	0	-1.992026	1.350154	-2.517690
57	1	0	-2.098352	0.933400	-4.961255
58	1	0	-2.467341	-1.431754	-5.751981
59	1	0	-2.795367	-3.217322	-4.067939
60	9	0	-3.182980	-4.768176	-2.610569
61	1	0	-3.462785	-6.092558	-0.444240
62	9	0	-3.265900	-5.255644	2.016499
63	1	0	-2.792331	-2.744724	2.154634
64	1	0	-0.402904	-0.782114	2.493034
65	1	0	-0.570613	-0.549089	4.959002
66	1	0	-2.745047	0.257660	5.932569
67	1	0	-4.621540	0.784862	4.398270
68	9	0	-6.170706	1.465875	3.053814
69	1	0	-7.657298	1.835113	0.998702
70	9	0	-7.170521	1.232018	-1.481544
71	1	0	-4.846670	0.178869	-1.796478
72	1	0	-3.259755	2.686570	0.025250
73	1	0	-2.310887	4.945812	-0.397379
74	1	0	1.561126	3.103307	-0.669290
75	1	0	4.300295	-2.684950	-1.106890
76	1	0	6.767540	-2.746136	-1.166087
77	1	0	6.935498	1.060917	0.804246
78	1	0	10.558673	-1.380672	-1.462664
79	1	0	13.152325	0.557460	2.309823
80	1	0	10.659821	0.628715	2.328636
81	1	0	4.473395	1.141392	0.866887
82	1	0	13.040466	-1.435421	-1.500349
83	1	0	14.337624	-0.471372	0.383841

C4 (HF= -9840.6990776)

Center Number	Atomic Number	Atomic Type	Coordinates (Angstroms) X	Y	Z
1	6	0	-10.930095	-0.602282	0.075892
2	6	0	-11.515931	-1.464238	1.011048
3	6	0	-12.899006	-1.555157	1.080309
4	6	0	-13.701976	-0.794819	0.225204
5	6	0	-13.116817	0.061786	-0.703543
6	6	0	-11.730204	0.158756	-0.777441
7	7	0	-9.530046	-0.425516	-0.085663
8	7	0	-8.809765	-1.120753	0.656052
9	6	0	-7.410516	-0.931793	0.490356
10	6	0	-6.594984	-1.752695	1.268222
11	6	0	-5.212480	-1.652437	1.179280
12	6	0	-4.625314	-0.719998	0.318632
13	6	0	-5.455641	0.105533	-0.454868
14	6	0	-6.834696	0.003088	-0.376466
15	6	0	-3.152261	-0.605339	0.224503
16	6	0	-2.323458	-1.725684	0.309256
17	6	0	-0.951627	-1.567627	0.218880
18	7	0	-0.371005	-0.374487	0.045204
19	6	0	-1.151463	0.724610	-0.041196
20	6	0	-2.534106	0.635035	0.048165
21	77	0	1.776773	-0.034816	-0.018128
22	6	0	3.711448	0.493977	-0.192304
23	6	0	4.183431	0.581846	-1.520917
24	6	0	5.497690	0.964605	-1.802168
25	6	0	6.376518	1.268024	-0.771256
26	6	0	5.911454	1.181671	0.536465
27	6	0	4.609498	0.802092	0.835429
28	6	0	-0.438048	2.013451	-0.228070
29	7	0	0.910724	1.954515	-0.211257
30	6	0	1.619486	3.078376	-0.370191

31	6	0	1.029141	4.318162	-0.552002
32	6	0	-0.356306	4.377682	-0.574518
33	6	0	-1.103908	3.220911	-0.412633
34	6	0	3.199342	0.250135	-2.558427
35	7	0	1.971332	-0.080077	-2.080094
36	6	0	0.987870	-0.410905	-2.932542
37	6	0	1.169682	-0.431475	-4.302888
38	6	0	2.421333	-0.093376	-4.811107
39	6	0	3.437190	0.247989	-3.933281
40	35	0	-1.227696	6.029348	-0.827093
41	7	0	1.779552	-0.101430	2.051689
42	6	0	1.458527	0.930313	2.849031
43	6	0	1.476983	0.835615	4.228151
44	6	0	1.840592	-0.378758	4.804780
45	6	0	2.170698	-1.444581	3.983854
46	6	0	2.137191	-1.293109	2.597201
47	6	0	2.467749	-2.332591	1.615349
48	6	0	2.847662	-3.630369	1.968155
49	6	0	3.144174	-4.566118	0.986624
50	6	0	3.050158	-4.175345	-0.344727
51	6	0	2.676099	-2.890204	-0.714387
52	6	0	2.373028	-1.935808	0.262914
53	1	0	-0.283791	-2.419039	0.276210
54	1	0	-2.733178	-2.722007	0.425476
55	1	0	-3.140365	1.529926	0.009637
56	1	0	1.186017	1.853043	2.353109
57	1	0	1.212248	1.696872	4.829985
58	1	0	1.867377	-0.492244	5.883445
59	1	0	2.456908	-2.395552	4.415461
60	1	0	2.918375	-3.930834	3.008589
61	1	0	3.439121	-5.574389	1.252137
62	35	0	3.450791	-5.449925	-1.705547
63	1	0	2.622010	-2.639195	-1.767562
64	1	0	0.035297	-0.669535	-2.488521
65	1	0	0.345951	-0.707449	-4.950473
66	1	0	2.603231	-0.097977	-5.880693
67	1	0	4.417172	0.511093	-4.311539
68	1	0	5.855545	1.032584	-2.824421
69	1	0	7.397014	1.565578	-0.981754
70	35	0	7.104918	1.596393	1.964822
71	1	0	4.300738	0.749425	1.873270
72	1	0	2.697627	2.973452	-0.346597
73	1	0	1.642445	5.201792	-0.674270
74	1	0	-2.183428	3.267808	-0.437941
75	1	0	-4.591369	-2.287181	1.802860
76	1	0	-7.057024	-2.465650	1.943311
77	1	0	-7.470319	0.636599	-0.983266
78	1	0	-10.885183	-2.049212	1.669964
79	1	0	-13.737542	0.653761	-1.368689
80	1	0	-11.251391	0.820306	-1.492586
81	1	0	-5.017599	0.820132	-1.144582
82	1	0	-13.358879	-2.221381	1.803850
83	1	0	-14.783139	-0.872880	0.286980

GAUSSIAN 09 (FULL REFERENCE): Gaussian 09, Revision D.01, Frisch, M. J.; Trucks, G. W.; Schlegel, H. B.; Scuseria, G. E.; Robb, M. A.; Cheeseman, J. R.; Scalmani, G.; Barone, V.; Mennucci, B.; Petersson, G. A.; Nakatsuji, H.; Caricato M.; Li, X.; Hratchian, H. P.; Izmaylov, A. F.; Bloino, J.; Zheng, G.; Sonnenberg, J. L.; Hada, M.; Ehara, M.; Toyota, K.; Fukuda, R.; Hasegawa, J.; Ishida, M.; Nakajima, T.; Honda, Y.; Kitao, O.; Nakai, H.; Vreven, T.; Montgomery, J. A.; Peralta, J. E., Jr.; Ogliaro, F.; Bearpark, M.; Heyd, J. J.; Brothers, E.; Kudin, K. N.; Staroverov, V. N.; Keith, T.; Kobayashi, R.; Normand, J.; Raghavachari, K.; Rendell, A.; Burant, J. C.; Iyengar, S. S.; Tomasi, J.; Cossi, M.; Rega, N.; Millam, J. M.; Klene, M.; Knox, J. E.; Cross, J. B.; Bakken, V.; Adamo, C.; Jaramillo, J.; Gomperts, R.; Stratmann, R. E.; Yazyev, O.; Austin, A. J.; Cammi, R.; Pomelli, C.; Ochterski, J. W.; Martin, R. L.; Morokuma, K.; Zakrzewski, V. G.; Voth, G. A.; Salvador, P.; Dannenberg, J. J.; Dapprich, S.; Daniels, A. D.; Farkas, O.; Foresman, J. B.; Ortiz, J. V.; Cioslowski, J.; Fox, D. J., Gaussian, Inc., Wallingford CT, **2013**.

Compound [Ru(p-Cym)(4,4'-dinitro-2,2'-bipyridine)(Cl)]Cl. Synthesis and characterization.

SYNTHESIS

Under a N_2 atmosphere, $Ru_2(p\text{-}Cym)_2Cl_4$ (0.1 g, 0.16 mmol) and 4,4'-dinitro-2,2'-bipyridine (0.08 g, 0.326 mmol) were dissolved in 10 mL of CH_2Cl_2. The reaction mixture was refluxed for 15 h. It was cooled to room temperature and the brown solid was filtered. Yield 63%.

Elemental Analysis: calculated for ($C_{20}H_{20}Cl_2N_4O_4Ru{\cdot}2CH_2Cl_2$): C, 36.59; H, 3.35; N, 7.76. Found: C, 36.39; H, 3.19; N, 8.24.

Exact Mass: ESI-MS $[C_{20}H_{20}ClN_4O_4Ru]^+$: calculated: m/z= 517.0217, found: m/z= 517.0228.

^{1}H NMR (300 MHz, THF-d_8): δ 9.20 (d, J = 2.3 Hz, 2H, (bipy)), 9.11 (d, J = 4.8 Hz, 2H, (bipy)), 8.25 (dd, J = 2.2 Hz, J = 5.3 Hz, 2H, (bipy)), 7.11 (s, 2H, (p-Cym)), 7.10 (s, 2H, (p-Cym)), 2.87 (m, 1H, (11)), 2.31 (s, 3H, (13)), 1.25 (d, J = 6.9 Hz, 6H, (12)).

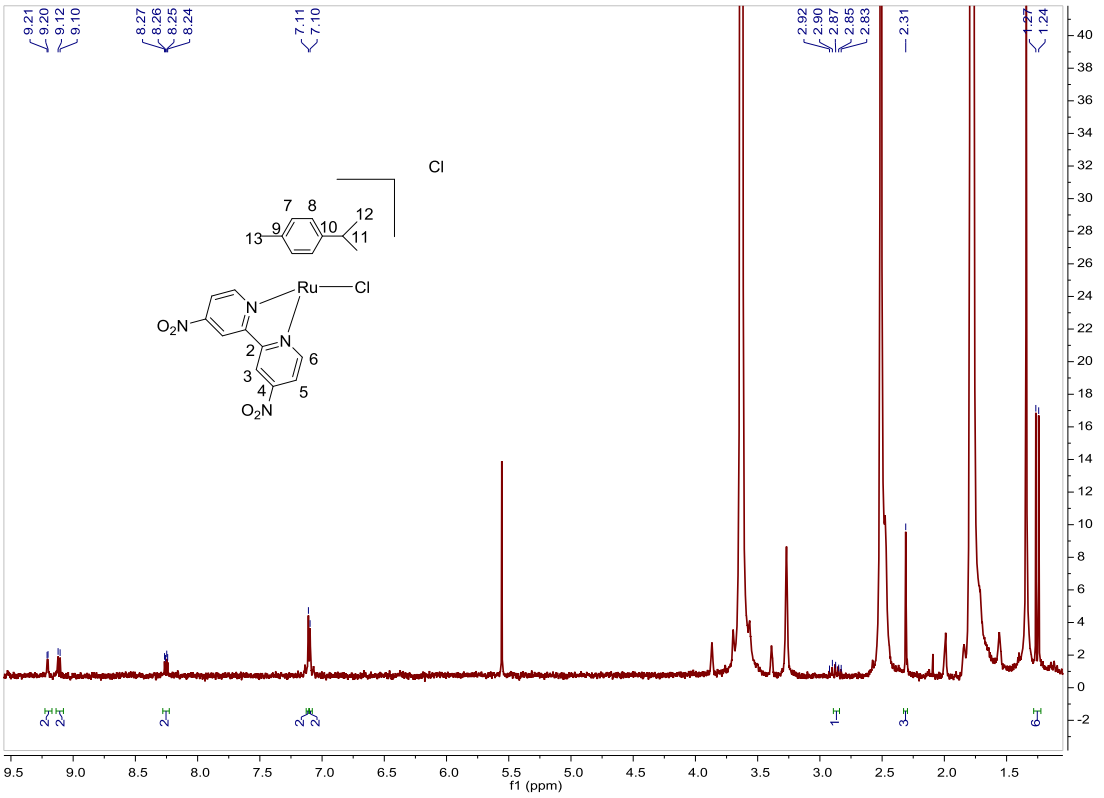

Fig. S312. ^{1}H NMR spectrum of **[Ru(p-Cym)(4,4'-dinitro-2,2'-bipyridine)(Cl)]Cl** in THF-d_8, 300 MHz.

Compound [Ru(p-Cym)(4,4'-bis(diethylphosphonate)-2,2'-bipyridine)(Cl)]Cl. Synthesis and characterization.

SYNTHESIS

Under a N_2 atmosphere, $Ru_2(p\text{-}Cym)_2Cl_4$ (0.043 g, 0.070 mmol) and 4,4'-bis(diethylphosphonate)-2,2'-bipyridine (0.060 g, 0.140 mmol) were dissolved in 4 mL of CH_2Cl_2. The reaction mixture was refluxed for 15 h. It was cooled to room temperature, the solvent was evaporated and the desired compound was obtained as a dark green solid. Yield 92%.

Elemental Analysis: calculated for ($C_{28}H_{40}Cl_2N_2O_6P_2Ru \cdot CH_2Cl_2$): C, 42.50; H, 5.17; N, 3.42. Found: C, 42.31; H, 5.46; N, 3.25.

Exact Mass: ESI-MS $[C_{28}H_{40}ClN_2O_6P_2Ru]^+$: calculated: m/z= 699.1094, found: m/z= 699.1103.

^{1}H NMR (300 MHz, $CDCl_3$): δ 10.33 (brdd, J = 4.1 Hz, J = 5.2 Hz, 2H, (6)), 8.46 (d, J = 13.4 Hz, 2H, (3)), 8.09 (ddd, J = 0.9 Hz, J = 5.5 Hz, J = 12.3 Hz, 2H, (5)), 6.56 (d, J = 6.1 Hz, 2H, (8)), 6.40 (d, J = 6.1 Hz, 2H, (7)), 4.36–4.12 (m, 8H, (14)), 2.77 (sep, J = 6.9 Hz, 1H, (11)), 2.33 (s, 3H, (13)), 1.39 (brdd, J = 7.2 Hz, J = 14.7 Hz, 12H, (15)), 1.06 (d, J = 6.9 Hz, 6H, (12)).

^{13}C NMR (75 MHz, $CDCl_3$): δ 157.46 (d, J = 12.7 Hz, 2CH, (6)), 153.39 (d, J = 13.5 Hz, $2C_{quat}$, (bipy)), 141.05 (d, J = 187.5 Hz, $2C_{quat}$, (bipy)), 129.10 (d, J = 7.5 Hz, 2CH, (5)), 124.23 (d, J = 10.5 Hz, 2CH, (3)), 105.57 (s, C_{quat}, (p-Cym)), 105.09 (s, C_{quat}, (p-Cym)), 87.64 (s, 2CH, (8)), 84.74 (s, 2CH, (7)), 63.27 (s, $4CH_2$, (14)), 30.68 (s, CH, (11)), 21.78 (s, $2CH_3$, (12)), 18.69 (s, CH_3, (13)), 15.96 (s, $4CH_3$, (15)).

^{31}P NMR (162 MHz, $CDCl_3$): δ 11.26 (s, 2P).

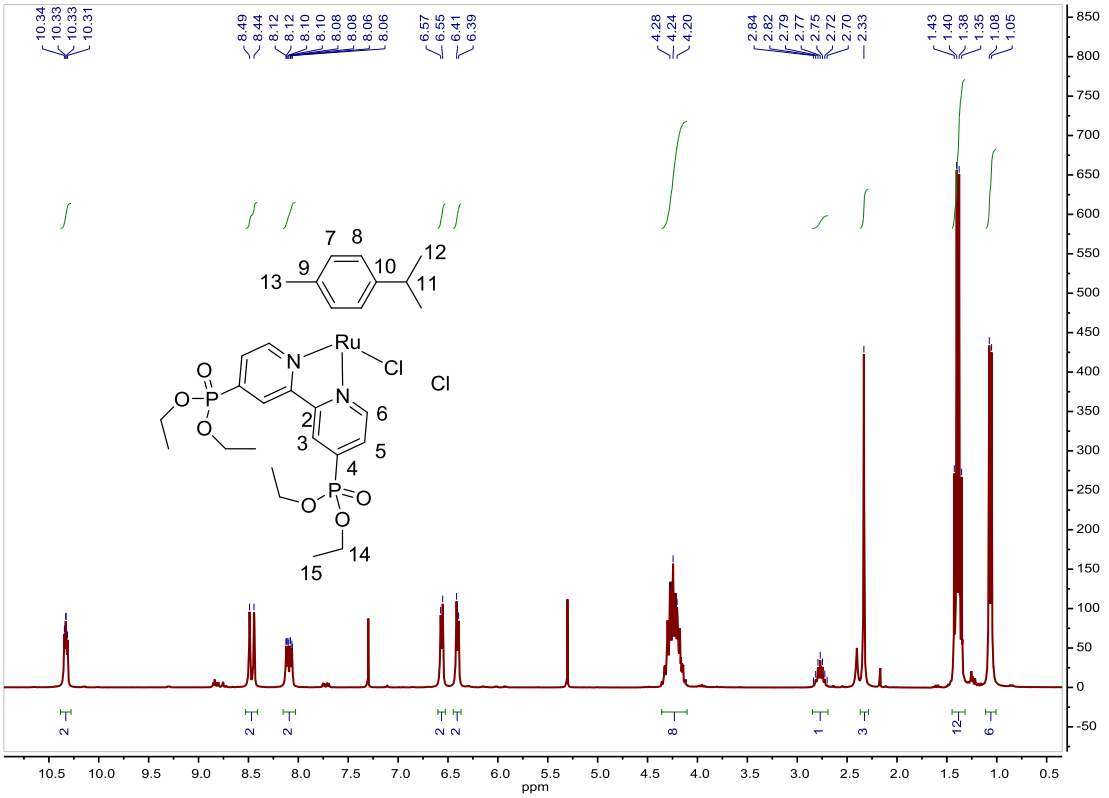

Fig. S313. ^{1}H NMR spectrum of **[Ru(p-Cym)(4,4'-bis(diethylphosphonate)-2,2'-bipyridine)(Cl)]Cl** in $CDCl_3$, 300 MHz.

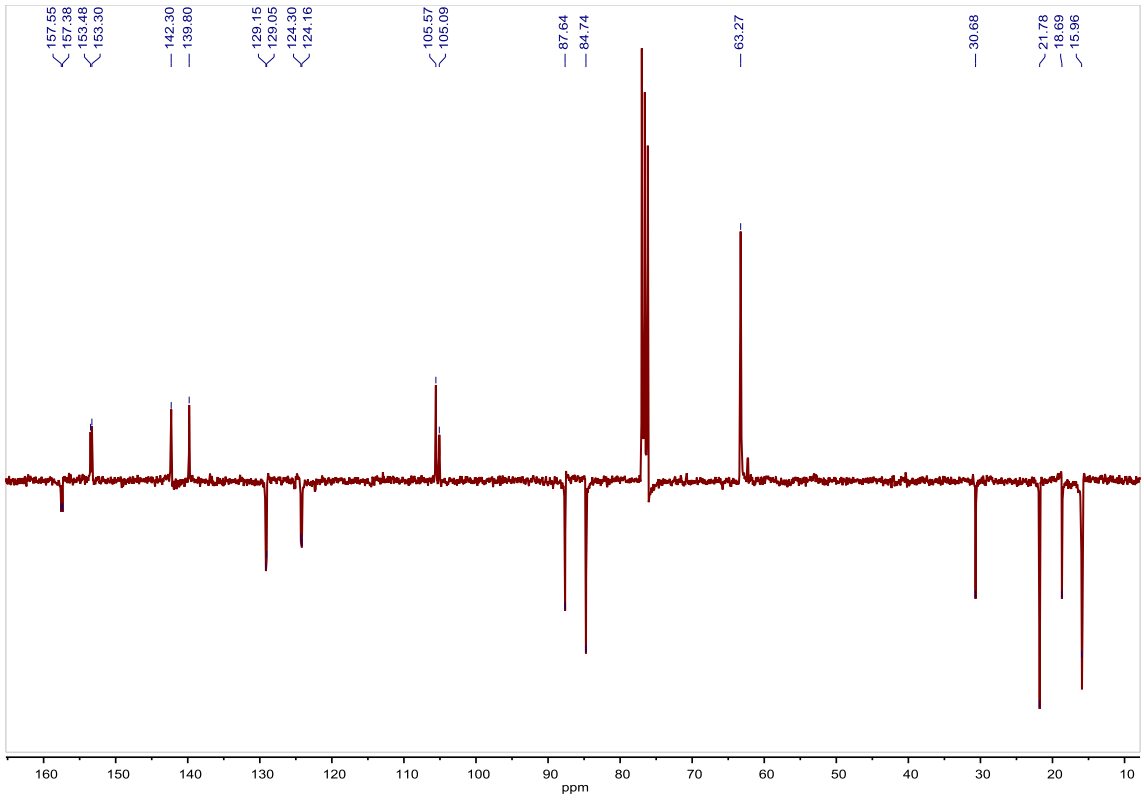

Fig. S314. ^{13}C NMR spectrum of **[Ru(p-Cym)(4,4'-bis(diethylphosphonate)-2,2'-bipyridine)(Cl)]Cl** in $CDCl_3$, 75 MHz.

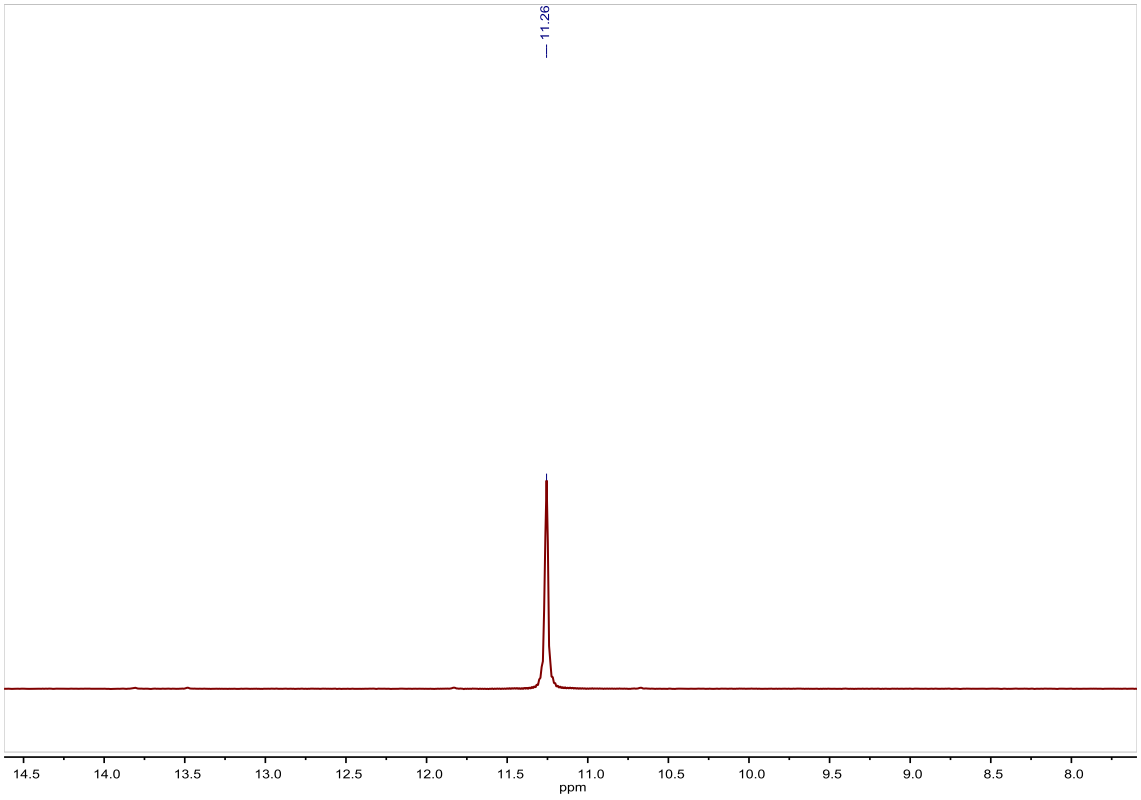

Fig. S315. ^{31}P NMR spectrum of **[Ru(p-Cym)(4,4'-bis(diethylphosphonate)-2,2'-bipyridine)(Cl)]Cl** in $CDCl_3$, 162 MHz.

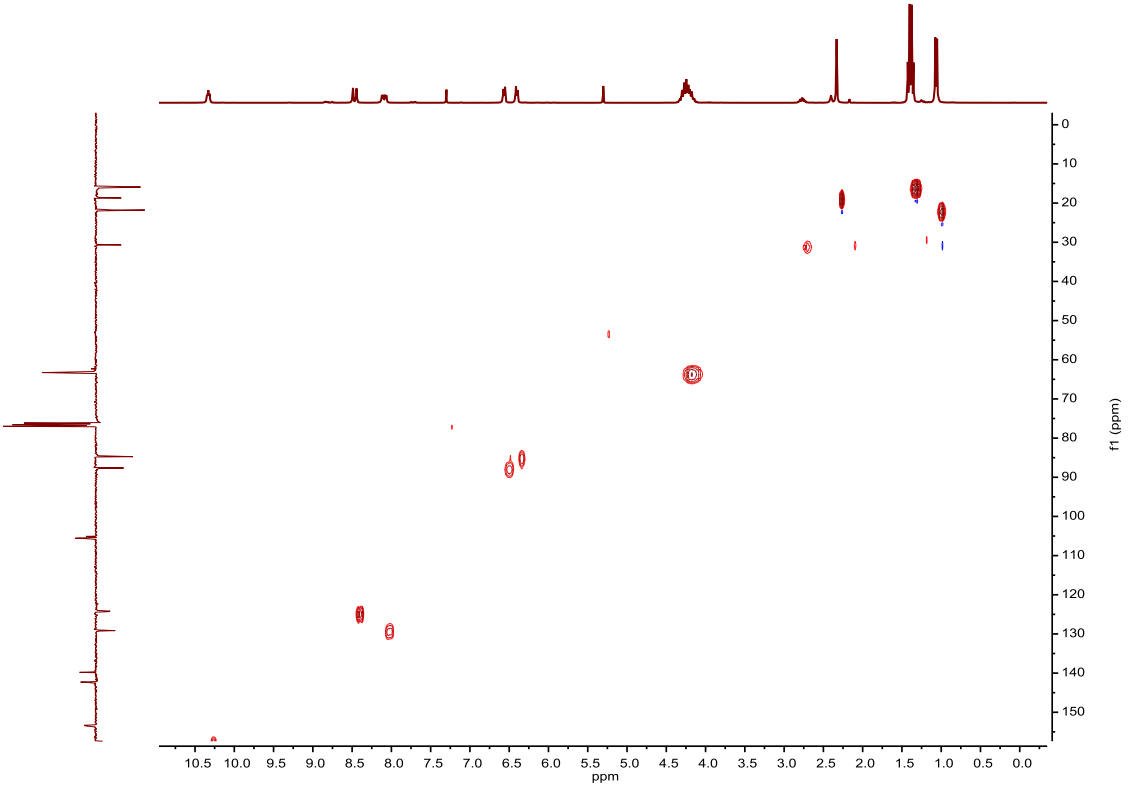

Fig. S316. HSQC NMR spectrum of **[Ru(p-Cym)(4,4'-bis(diethylphosphonate)-2,2'-bipyridine)(Cl)]Cl** in $CDCl_3$.

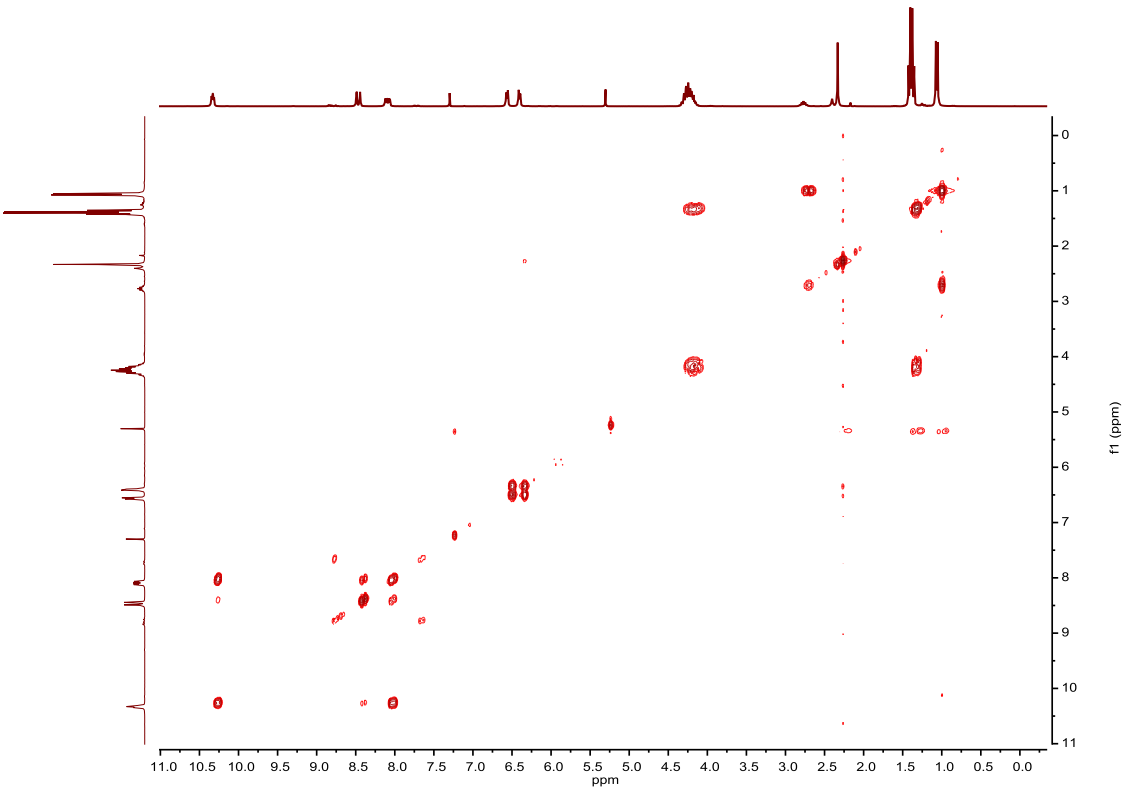

Fig. S317. COSY NMR spectrum of **[Ru(p-Cym)(4,4'-bis(diethylphosphonate)-2,2'-bipyridine)(Cl)]Cl** in $CDCl_3$.

Compound [Ru(p-Cym)(4,4'-dicarboxy-2,2'-bipyridine)(Cl)]Cl. Synthesis and characterization.

SYNTHESIS

Under a N_2 atmosphere, $[Ru(p\text{-}Cym)Cl_2]_2$ (0.188 g, 0.31 mmol) and 4,4'-dicarboxy-2,2'-bipyridine (0.15 g, 0.61 mmol) were dissolved in 10 mL of ethanol. The reaction mixture was refluxed for 15 h. It was cooled to room temperature and the orange solid that precipitated was filtered off. Yield 71%. The spectroscopic data are coincident with those described in the literature.[39]

^{1}H NMR (300 MHz, MeOD): δ 9.73 (d, J = 5.1 Hz, 2H, (6)), 9.00 (s, 2H, (3)), 8.25 (d, J = 4.6 Hz, 2H, (5)), 6.25 (d, J = 5.7 Hz, 2H, (8)), 6.01 (d, J = 5.8 Hz, 2H, (7)), 2.72 (sep, J = 6.8 Hz, 1H, (11)), 2.30 (s, 3H, (13)), 1.10 (d, J = 6.8 Hz, 6H, (12)).

^{13}C APT NMR (75 MHz, MeOD): δ 157.98 (2CH, (6)), 156.61 ($2C_{quat}$, (bipy)), 143.16 ($2C_{quat}$, (bipy)), 128.13 (2CH, (5)), 124.59 (2CH, (3)), 107.32 (C_{quat}, (p-Cym)), 106.17 (C_{quat}, (p-Cym)), 88.64 (2CH, (8)), 86.36 (2CH, (7)), 32.37 (CH, (11)), 22.34 ($2CH_3$, (12)), 18.97 (CH_3, (13)).

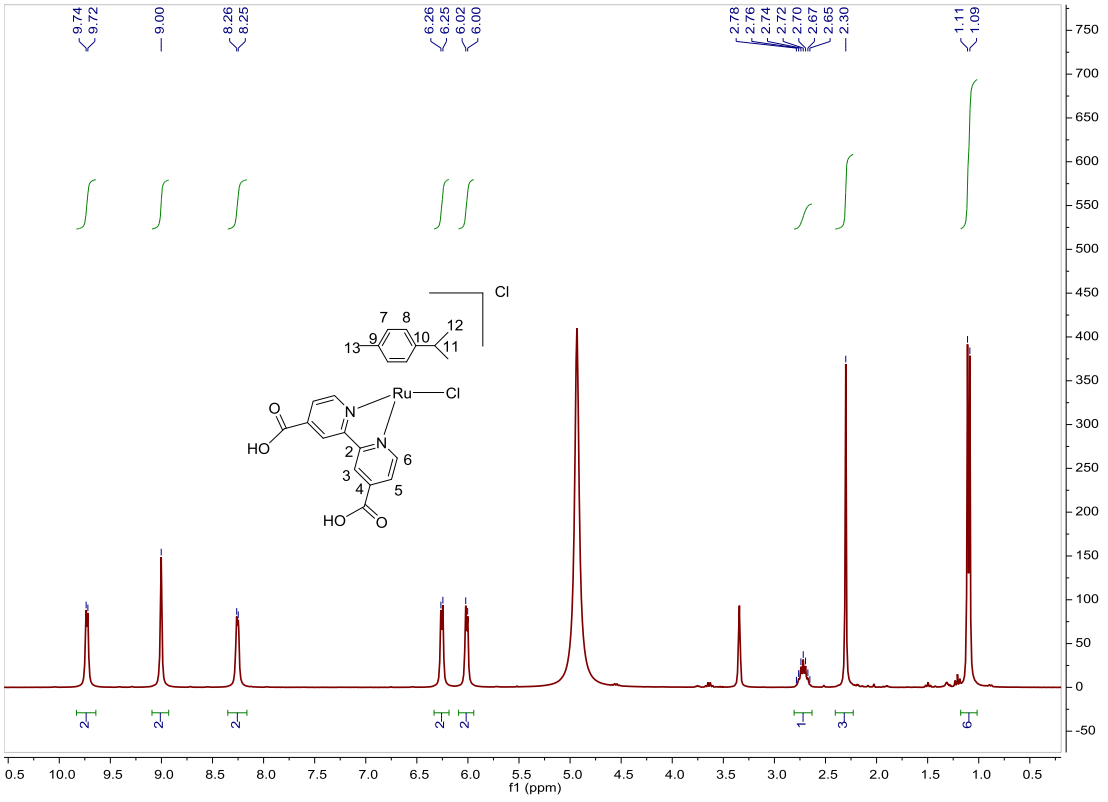

Fig. S318. ^{1}H NMR spectrum of **[Ru(p-Cym)(4,4'-dicarboxy-2,2'-bipyridine)(Cl)]Cl** in MeOD-d_4, 300 MHz.

[39] A. Kopecky, G. Liu, A. Agushi, A. G. Agrios, E. Galoppini, *Tetrahedron*, **2014**, *70*, 6271–6275.

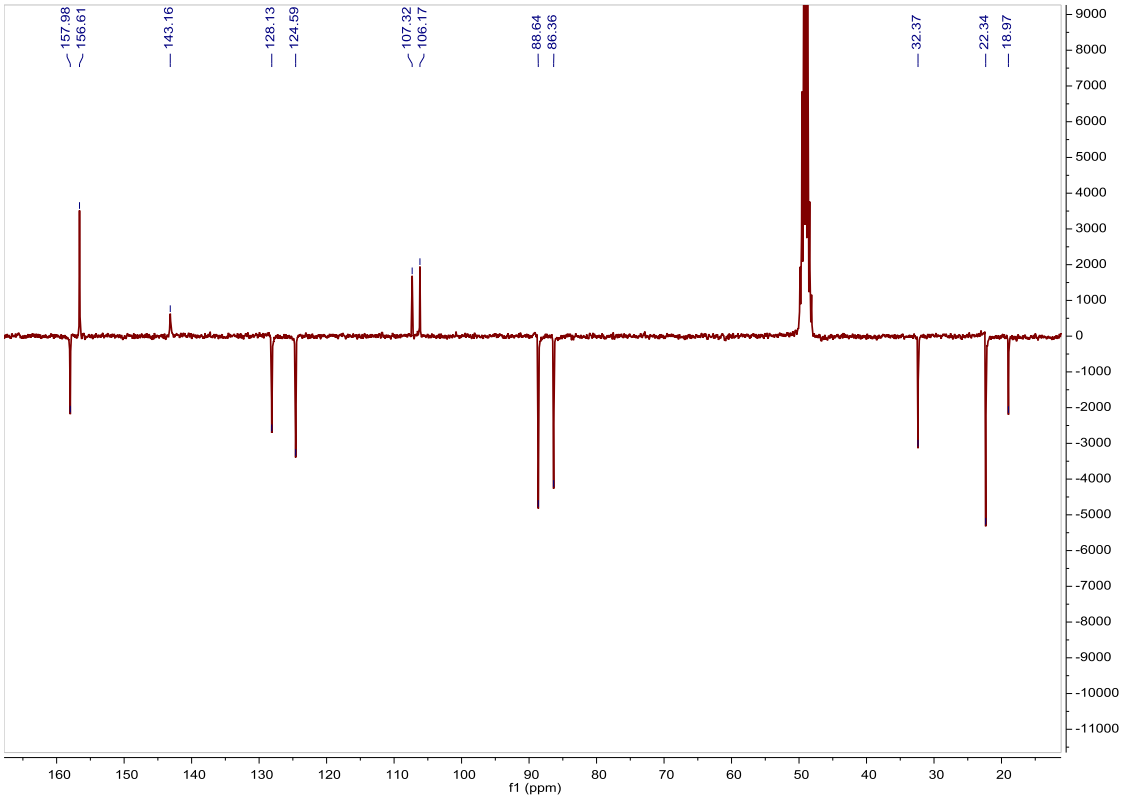

Fig. S319. ^{13}C NMR spectrum of **[Ru(p-Cym)(4,4'-dicarboxy-2,2'-bipyridine)(Cl)]Cl** in MeOD-d_4, 75 MHz.

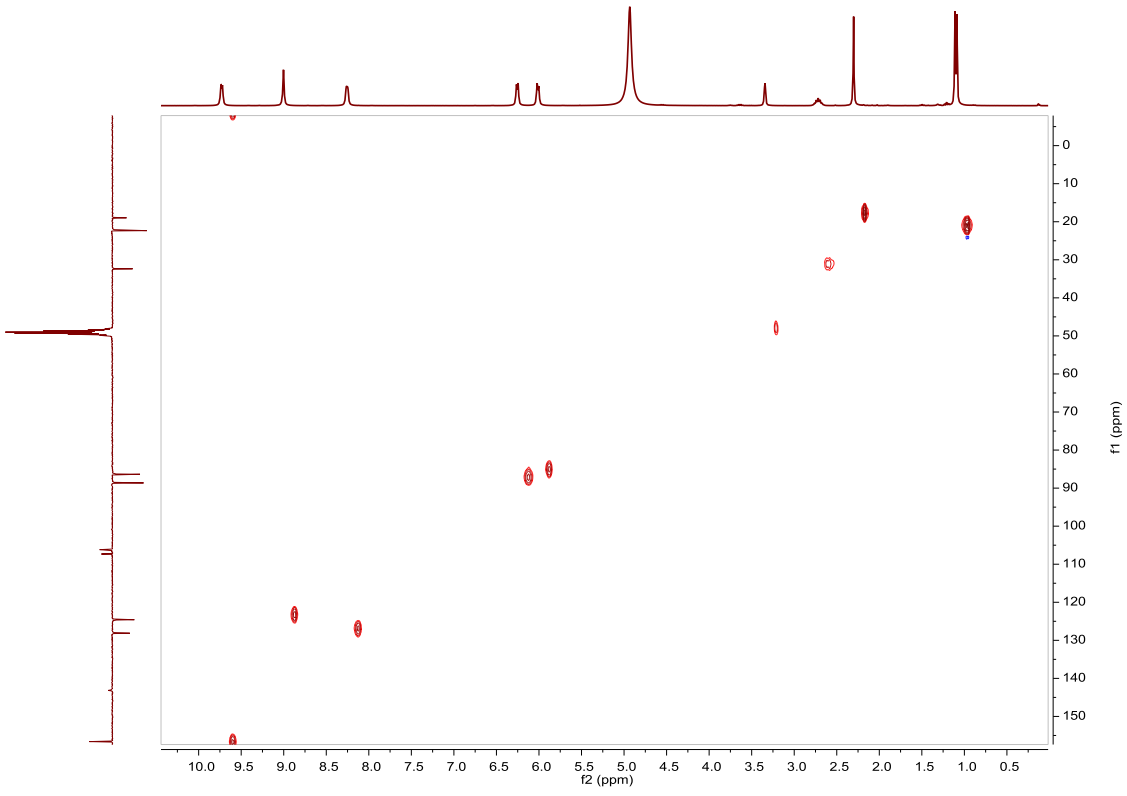

Fig. S320. HSQC NMR spectrum of **[Ru(p-Cym)(4,4'-dicarboxy-2,2'-bipyridine)(Cl)]Cl** in MeOD-d_4.

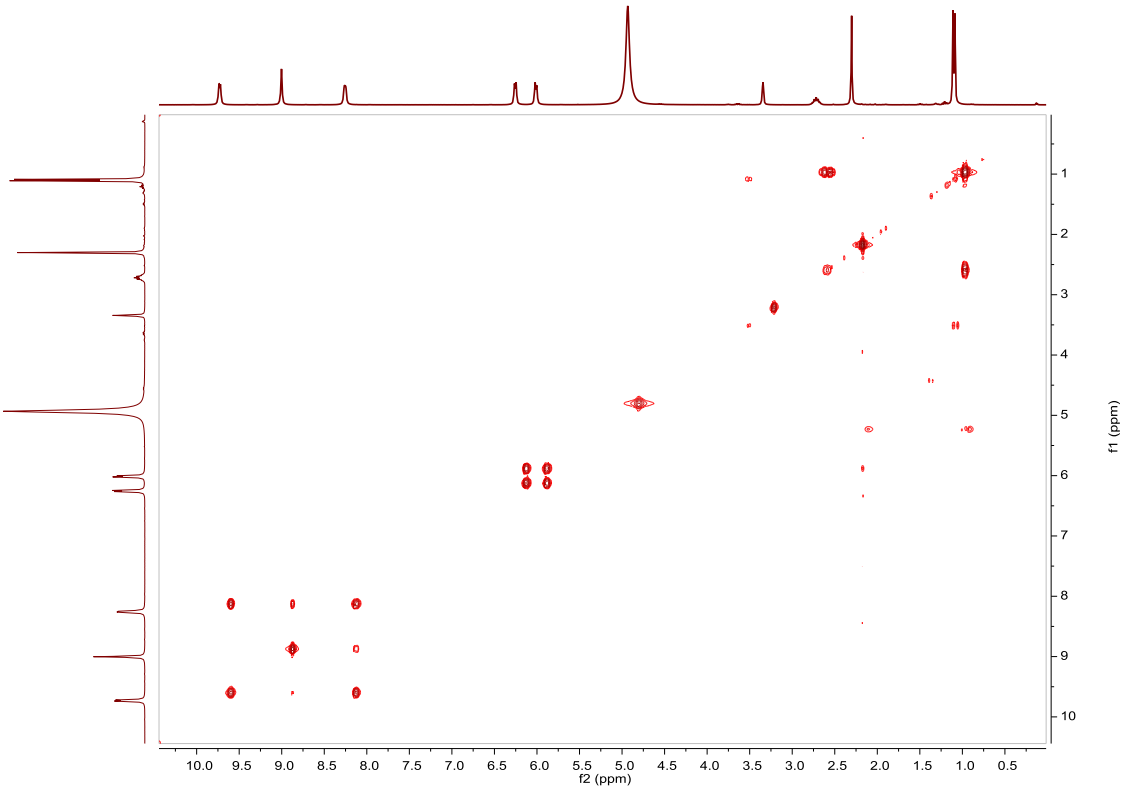

Fig. S321. COSY NMR spectrum of **[Ru(p-Cym)(4,4'-dicarboxy-2,2'-bipyridine)(Cl)]Cl** in MeOD-d_4.

Compound [Ru(p-Cym)(4,4'-bis(ethynyl)-2,2'-bipyridine)(Cl)]Cl. Synthesis and characterization.

SYNTHESIS

Under a N_2 atmosphere, $Ru_2(p\text{-}Cym)_2Cl_4$ (0.130 g, 0.214 mmol) and 4,4'-bis(ethynyl)-2,2'-bipyridine (0.087 g, 0.428 mmol) were dissolved in 10 mL of acetone. The reaction mixture was refluxed for 15 h. It was cooled to room temperature, the solvent was evaporated and the desired compound was obtained as a light brown solid. Yield 77%.

Elemental Analysis: calculated for ($C_{24}H_{22}Cl_2N_2Ru$): C, 56.48; H, 4.34; N, 5.49. Found: C, 56.44; H, 4.88; N, 5.74.

Exact Mass: ESI-MS $[C_{24}H_{22}ClN_2Ru]^+$: calculated: m/z= 475.0515, found: m/z= 475.0517.

^{1}H NMR (300 MHz, MeOD-d_4): δ 9.47 (d, J = 5.9 Hz, 2H, (6)), 8.69 (d, J = 1.8 Hz, 2H, (3)), 7.82 (dd, J = 1.7 Hz, J = 5.9 Hz, 2H, (5)), 6.16 (d, J = 6.4 Hz, 2H, (8)), 5.91 (d, J = 6.4 Hz, 2H, (7)), 4.47 (s, 2H, (15)), 2.70 (sep, J = 6.9 Hz, 1H, (11)), 2.29 (s, 3H, (13)), 1.10 (d, J = 6.9 Hz, 6H, (12)).

^{13}C NMR (75 MHz, MeOD-d_4): δ 156.79 (2CH, (6)), 156.03 ($2C_{quat}$, (bipy)), 135.84 ($2C_{quat}$, (bipy)), 130.97 (2CH, (5)), 127.64 (2CH, (3)), 106.86 (C_{quat}, (p-Cym)), 105.94 (C_{quat}, (p-Cym)), 89.63 (2CH, (15)), 88.31 (2CH, (8)), 85.92 (2CH, (7)), 80.15 (C_{quat}, (14)), 32.38 (CH, (11)), 22.32 ($2CH_3$, (12)), 18.92 (CH_3, (13)).

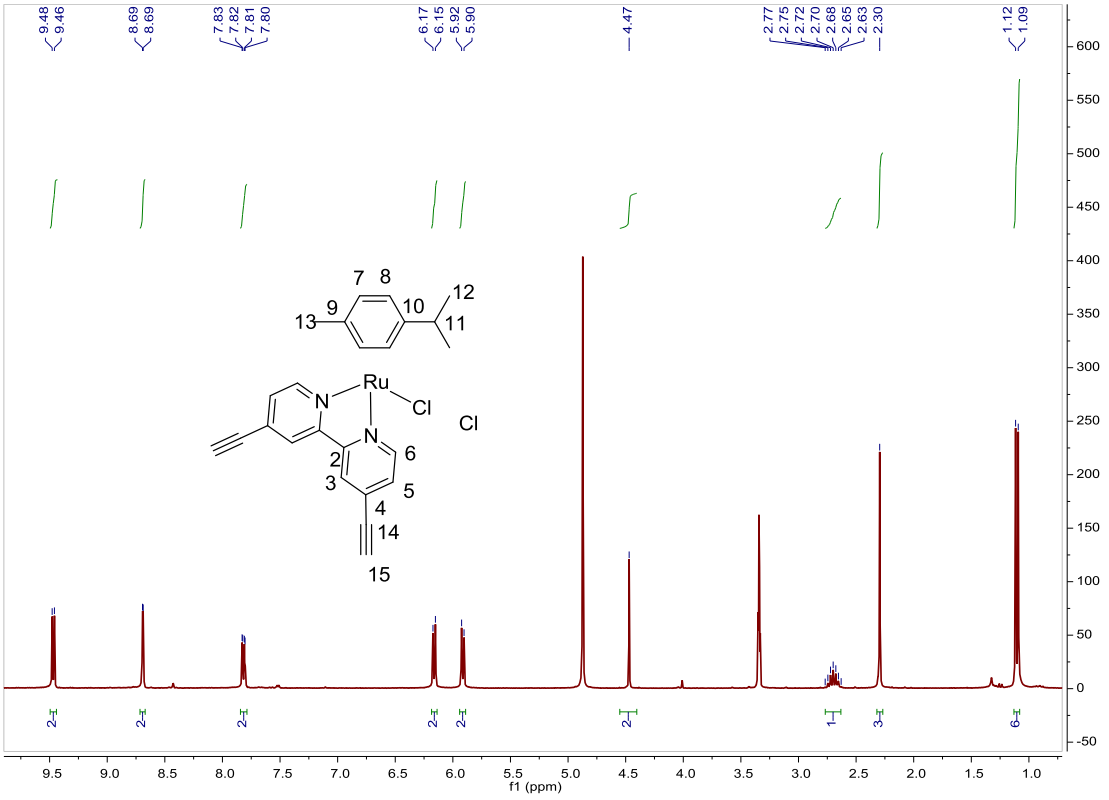

Fig. S322. ^{1}H NMR spectrum of **[Ru(p-Cym)(4,4'-bis(ethynyl)-2,2'-bipyridine)(Cl)]Cl** in MeOD-d_4, 300 MHz.

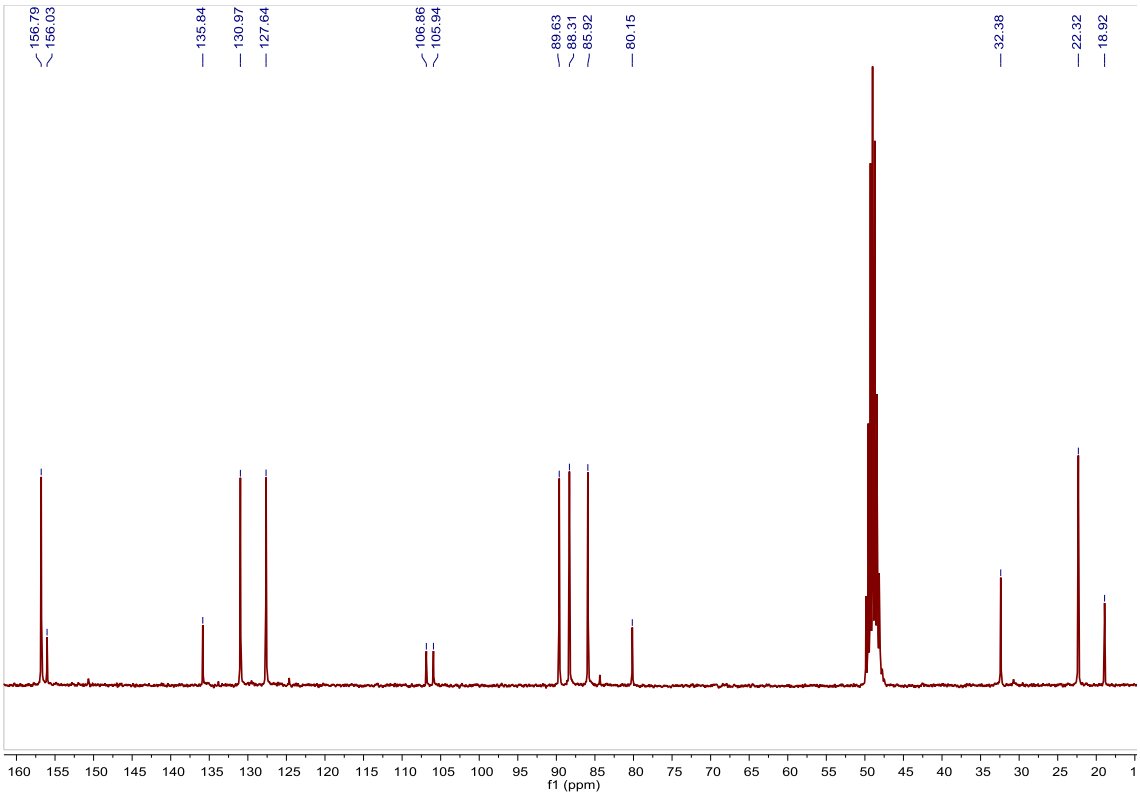

Fig. S323. ^{13}C NMR spectrum of **[Ru(p-Cym)(4,4'-bis(ethynyl)-2,2'-bipyridine)(Cl)]Cl** in MeOD-d_4, 75 MHz.

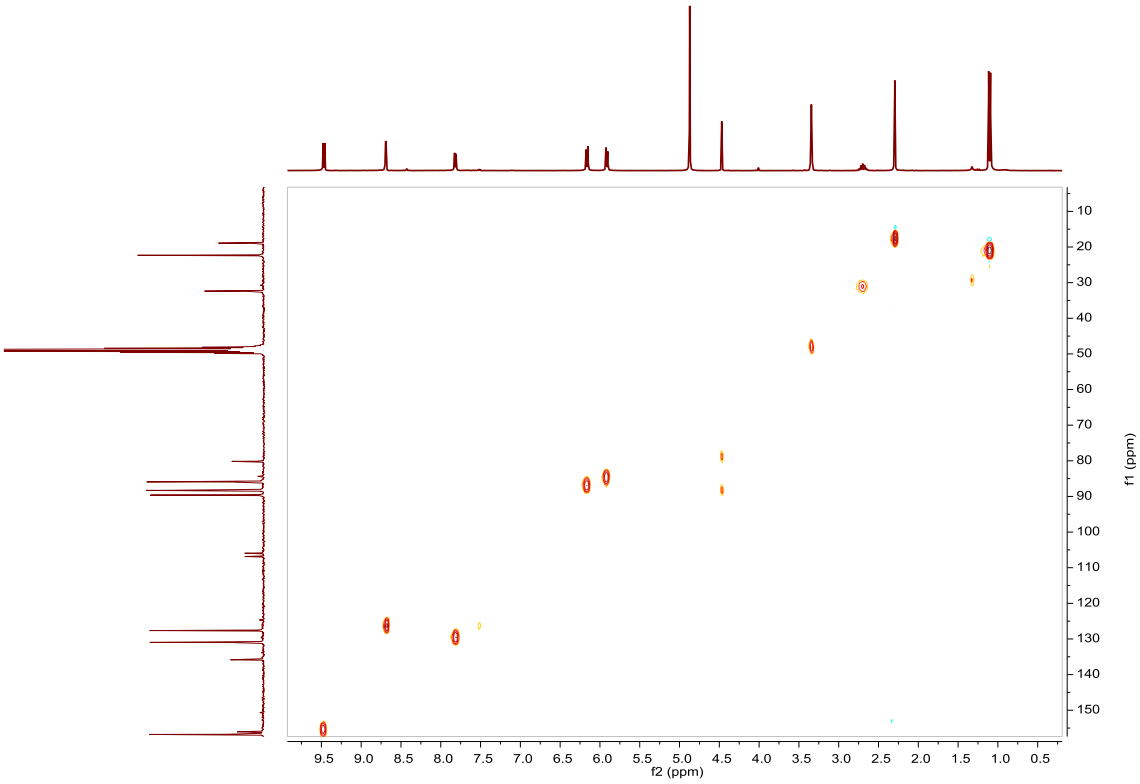

Fig. S324. HSQC NMR spectrum of **[Ru(p-Cym)(4,4'-bis(ethynyl)-2,2'-bipyridine)(Cl)]Cl** in MeOD-d_4.

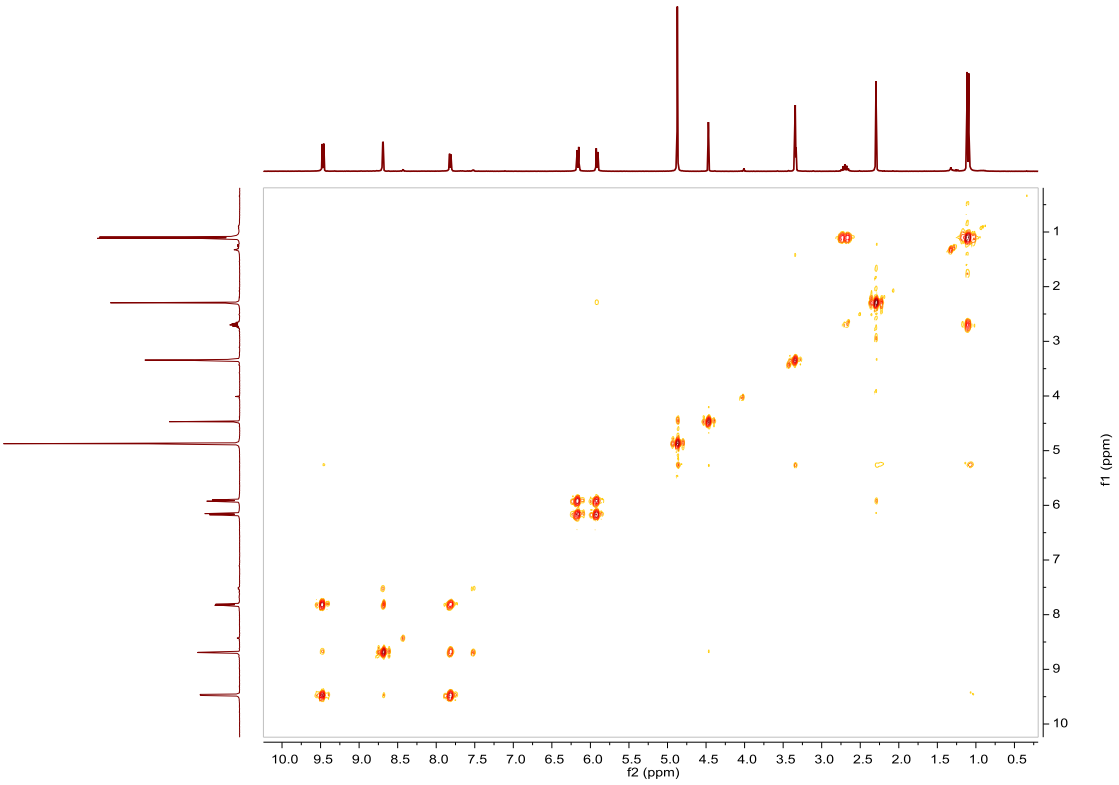

Fig. S325. COSY NMR spectrum of **[Ru(p-Cym)(4,4'-bis(ethynyl)-2,2'-bipyridine)(Cl)]Cl** in MeOD-d_4.

Compound [Ru(p-Cym)(4,4'-dibromo-2,2'-bipyridine)(Cl)]Cl. Synthesis and characterization.

SYNTHESIS

Under a N_2 atmosphere, $Ru_2(p\text{-}Cym)_2Cl_4$ (0.1 g, 0.16 mmol) and 4,4'-dibromo-2,2'-bipyridine (0.10 g, 0.32 mmol) were dissolved in 10 mL of acetone. The reaction mixture was refluxed for 15 h. It was cooled to room temperature and the yellow solid that precipitated was filtered off. Yield 85%.

Elemental Analysis: calculated for ($C_{20}H_{20}Br_2Cl_2N_2Ru$): C, 38.73; H, 3.25; N, 4.52. Found: C, 38.25; H, 3.41; N, 4.52.

Exact Mass: ESI-MS $[C_{20}H_{20}Br_2ClN_2Ru]^+$: calculated: m/z= 584.8705, found: m/z= 584.8706.

^{1}H NMR (300 MHz, MeOD-d_4): δ 9.33 (d, J = 6.1 Hz, 2H, (6)), 8.91 (d, J = 2.1 Hz, 2H, (3)), 8.05 (dd, J = 2.1 Hz, J = 6.1 Hz, 2H, (5)), 6.16 (d, J = 6.4 Hz, 2H, (8)), 5.91 (d, J = 6.4 Hz, 2H, (7)), 2.72 (sep, J = 6.9 Hz, 1H, (11)), 2.29 (s, 3H, (13)), 1.12 (d, J = 6.9 Hz, 6H, (12)).

^{13}C APT NMR (75 MHz, MeOD-d_4): δ 157.14 (2CH, (6)), 156.19 ($2C_{quat}$, (bipy)), 138.12 ($2C_{quat}$, (bipy)), 132.52 (2CH, (5)), 129.08 (2CH, (3)), 106.95 (C_{quat}, (p-Cym)), 105.70 (C_{quat}, (p-Cym)), 88.02 (2CH, (8)), 85.72 (2CH, (7)), 32.39 (CH, (11)), 22.36 ($2CH_3$, (12)), 18.91 (CH_3, (13)).

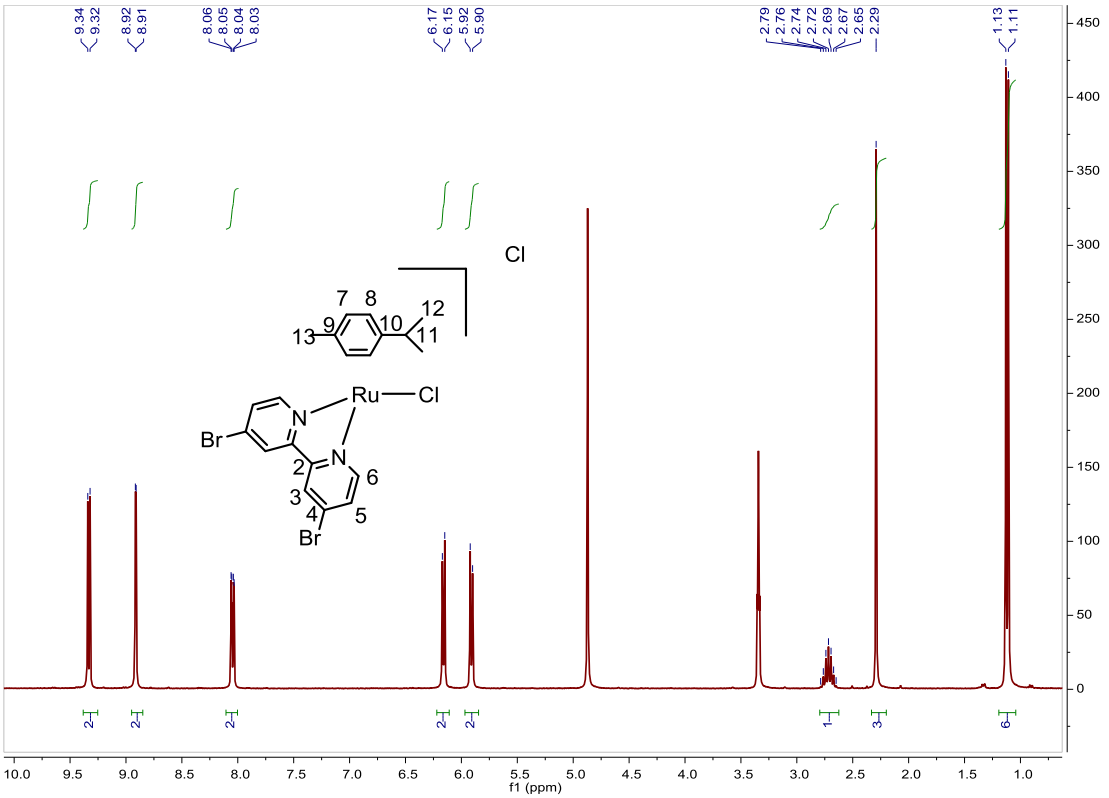

Fig. S326. ^{1}H NMR spectrum of **[Ru(p-Cym)(4,4'-dibromo-2,2'-bipyridine)(Cl)]Cl** in MeOD-d_4, 300 MHz.

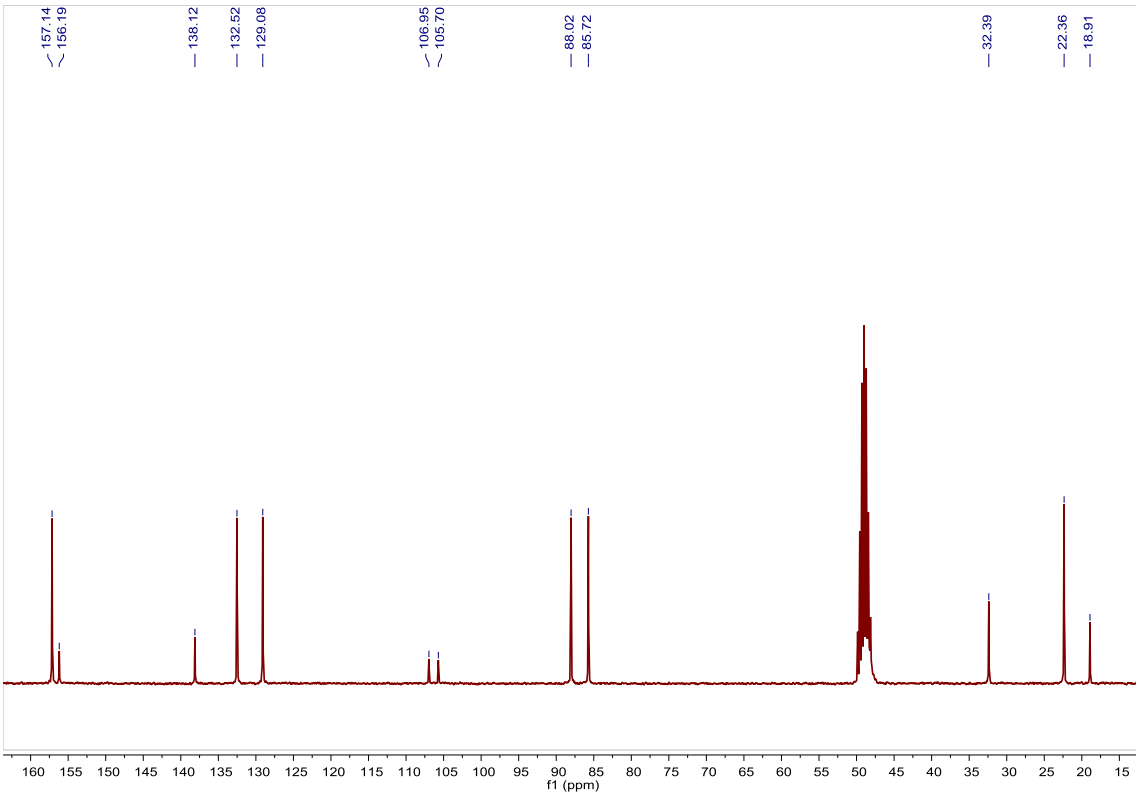

Fig. S327. ^{13}C NMR spectrum of **[Ru(p-Cym)(4,4'-dibromo-2,2'-bipyridine)(Cl)]Cl** in MeOD-d_4, 75 MHz.

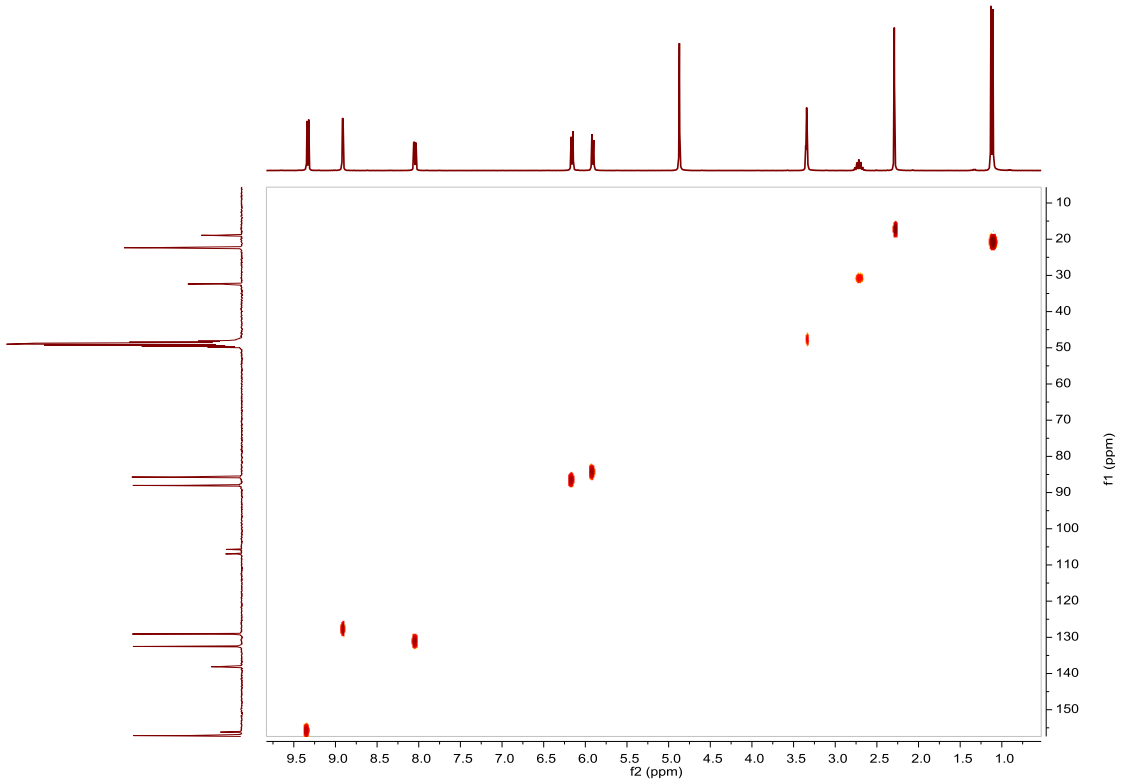

Fig. S328. HSQC NMR spectrum of **[Ru(p-Cym)(4,4'-dibromo-2,2'-bipyridine)(Cl)]Cl** in MeOD-d_4.

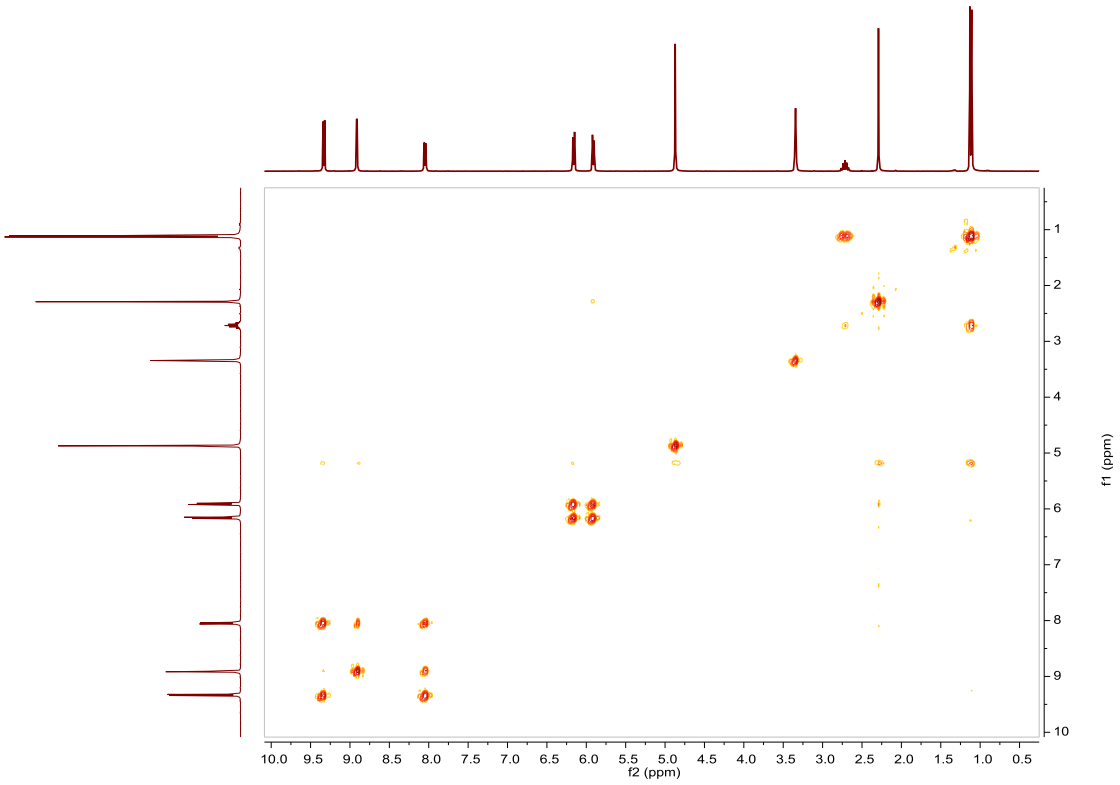

Fig. S329. COSY NMR spectrum of **[Ru(p-Cym)(4,4'-dibromo-2,2'-bipyridine)(Cl)]Cl** in MeOD-d_4.

Compound [Ru(p-Cym)(2,2'-bipyridine)(Cl)]Cl. Synthesis and characterization.

SYNTHESIS

Under a N_2 atmosphere, $Ru_2(p\text{-}Cym)_2Cl_4$ (0.350 g, 0.57 mmol) and 2,2'-bipyridine (0.178 g, 1.14 mmol) were dissolved in 20 mL of acetone. The reaction mixture was refluxed for 15 h. It was cooled to room temperature and the yellow solid that precipitated was filtered off. Yield 93%. The spectroscopic data are coincident with those described in the literature.[40]

^{1}H NMR (300 MHz, MeOD-d_4): δ 9.51 (d, J = 5.0 Hz, 2H), 8.54 (d, J = 8.1 Hz, 2H), 8.27 (ddd, J = 1.4 Hz, J = 7.9 Hz, J = 9.2 Hz, 2H), 7.80 (ddd, J = 1.3 Hz, J = 5.7 Hz, J = 7.3 Hz, 2H), 6.15 (d, J = 6.3 Hz, 2H, (p-Cym)), 5.90 (d, J = 6.3 Hz, 2H, (p-Cym)), 2.67 (sep, J = 6.9 Hz, 1H, (11)), 2.31 (s, 3H, (13)), 1.07 (d, J = 6.9 Hz, 6H, (12)).

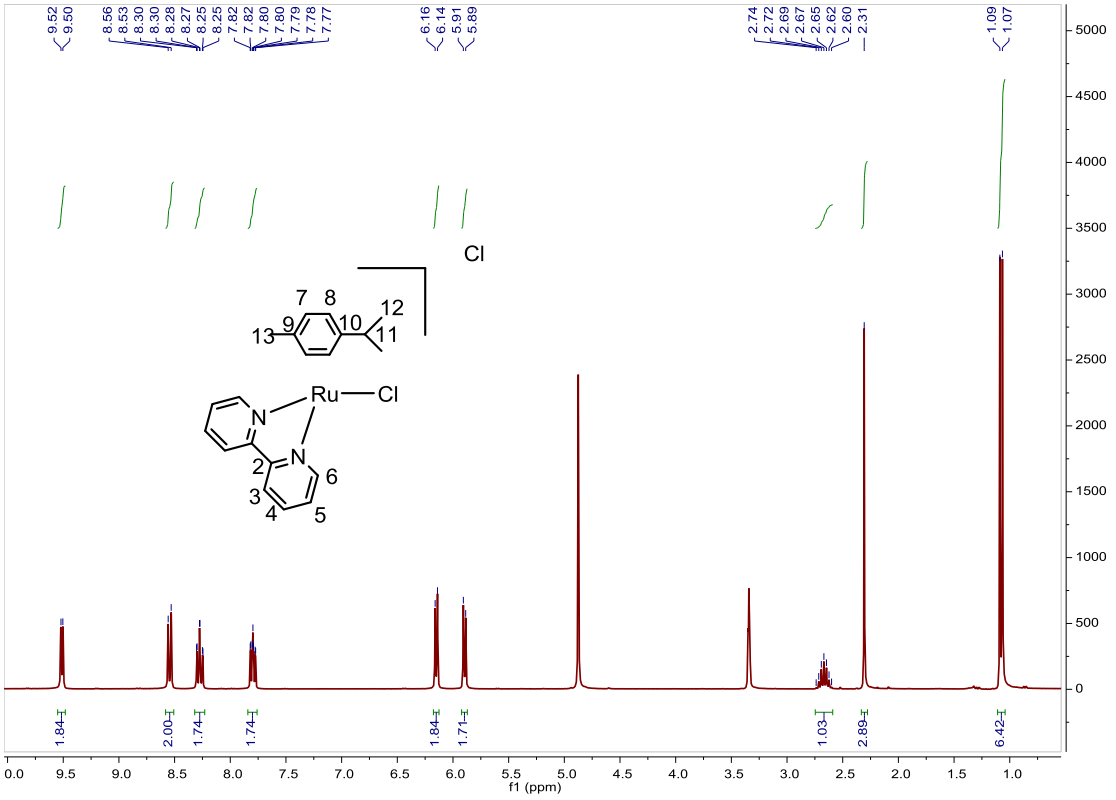

Fig. S330. ^{1}H NMR spectrum of **[Ru(p-Cym)(2,2'-bipyridine)(Cl)]Cl** in MeOD-d_4, 300 MHz.

[40] R. R. Dykeman, K. L. Luska, M. E. Thibault, M. D. Jones, M. Schlaf, M. Khanfar, N. J. Taylor, J. F. Britten and L. Harrington, *J. Mol. Catal. A: Chemical*, **2007**, *277*, 233–251.

Compound [Ru(p-Cym)(4,4'-dimethyl-2,2'-bipyridine)Cl]Cl. Synthesis and characterization.

SYNTHESIS

Under a N_2 atmosphere, $[Ru(p\text{-}Cym)Cl_2]_2$ (0.1 g, 0.16 mmol) and 4,4'-dimethyl-2,2'-bipyridine (0.06 g, 0.326 mmol) were dissolved in 10 mL of acetone. The reaction mixture was refluxed for 15 h. It was cooled to room temperature and the yellow solid that precipitated was filtered off. Yield 78%. The spectroscopic data are coincident with those described in the literature.[41]

^{1}H NMR (300 MHz, MeOD-*d*$_4$): δ 9.31 (d, J = 5.8 Hz, 2H, (6)), 8.39 (s, 2H, (3)), 7.71 (d, J = 5.7 Hz, 2H, (5)), 6.10 (d, J = 6.1 Hz, 2H, (8)), 5.85 (d, J = 6.3 Hz, 2H, (7)), 2.64 (s, 7H, (11+14)), 2.29 (s, 3H, (13)), 1.06 (d, J = 6.9 Hz, 6H, (12)).

^{13}C APT NMR (75 MHz, MeOD-*d*$_4$): δ 154.66 (2CH, (6)), 154.62 ($2C_{quat}$, (bipy)), 152.76 ($2C_{quat}$, (bipy)), 128.25 (2CH, (5)), 124.19 (2CH, (3)), 104.13 (C_{quat}, (p-Cym)), 104.03 (C_{quat}, (p-Cym)), 86.85 (2CH, (8)), 83.83 (2CH, (7)), 30.99 (CH, (11)), 20.95 ($2CH_3$, (12)), 19.91 ($2CH_3$, (14)), 17.85 (CH_3, (13)).

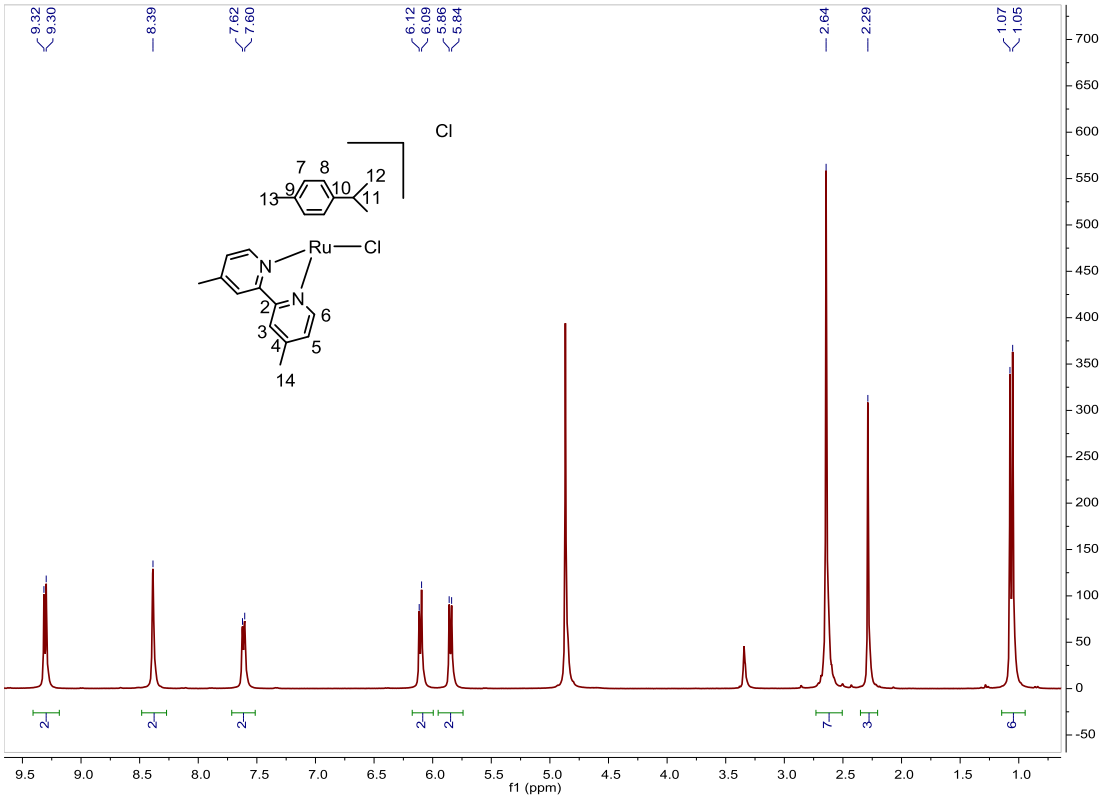

Fig S331. ^{1}H NMR spectrum of **[Ru(p-Cym)(4,4'-dimethyl-2,2'-bipyridine)Cl]Cl** in MeOD-*d*$_4$, 300 MHz.

[41] C. E. Welby, G. K. Armitage, H. Bartley, A. Wilkinson, A. Sinopoli, B. S. Uppal, C. R. Rice, P. I. P. Elliott, *Chem. Eur. J.* **2014**, *20*, 8467–8476.

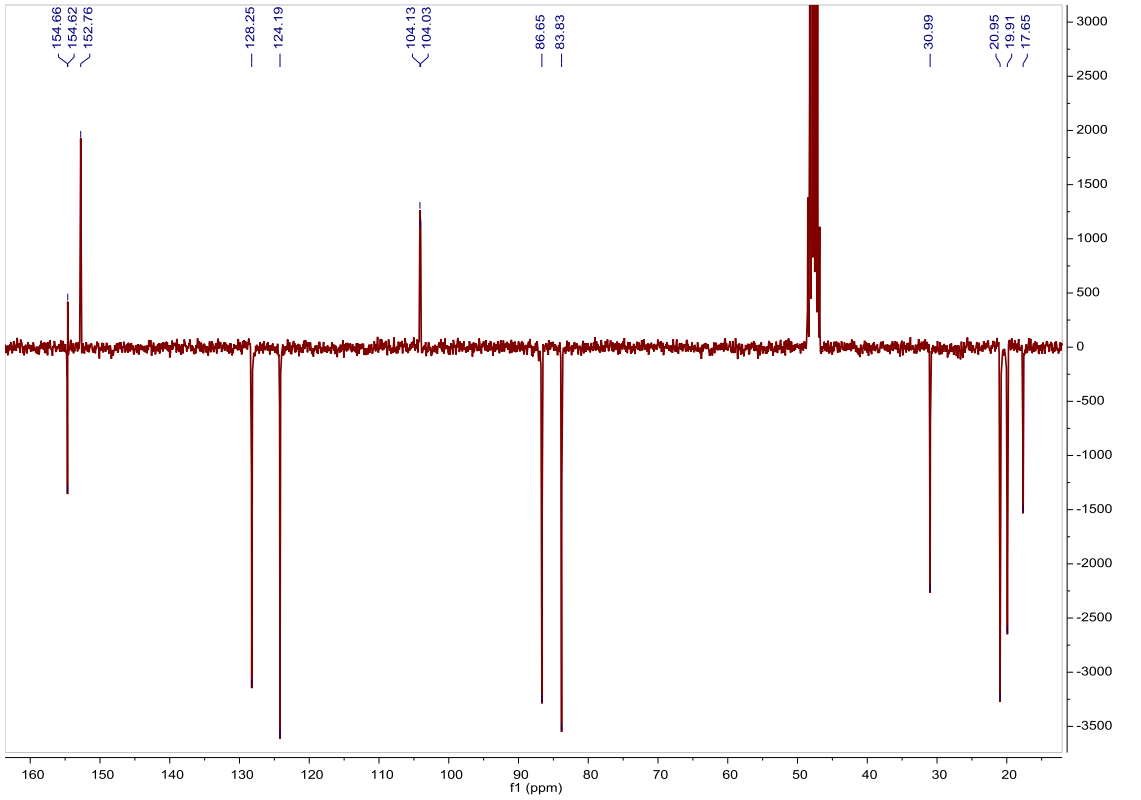

Fig S332. ^{13}C APT NMR spectrum of **[Ru(p-Cym)(4,4'-dimethyl-2,2'-bipyridine)Cl]Cl** in MeOD-d_4, 75 MHz.

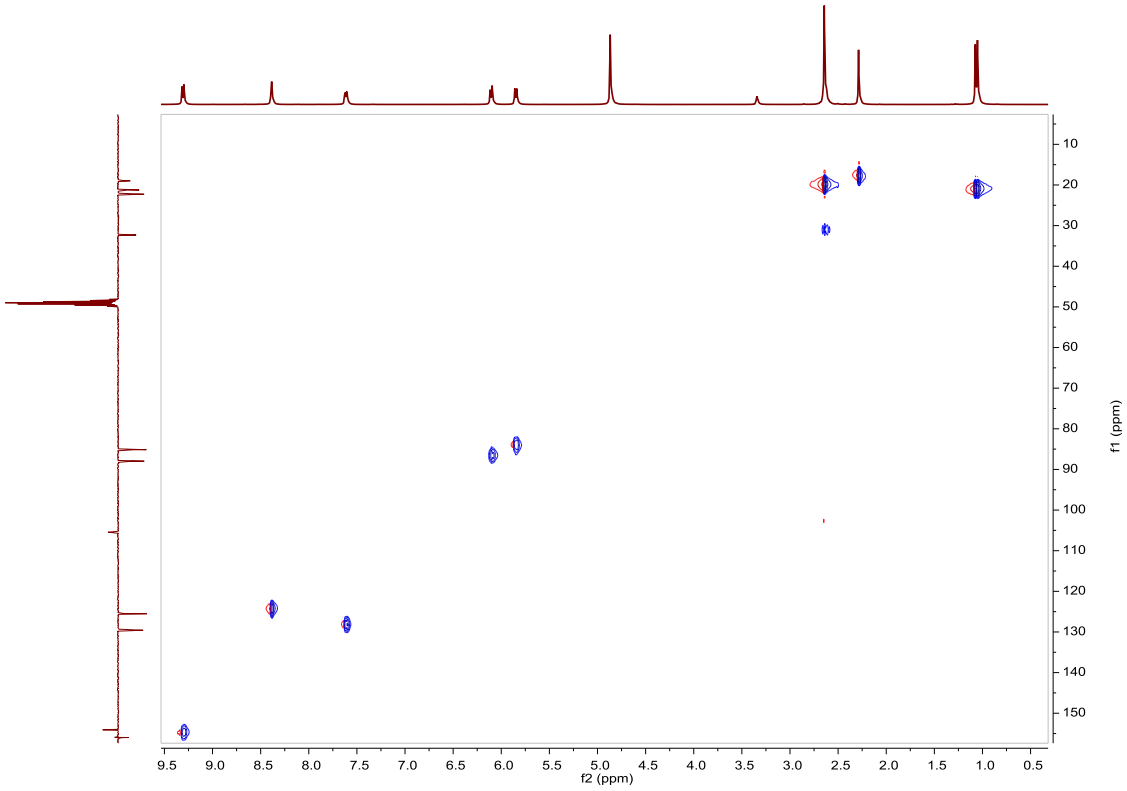

Fig S333. HSQC NMR spectrum of **[Ru(p-Cym)(4,4'-dimethyl-2,2'-bipyridine)Cl]Cl** in MeOD-d_4.

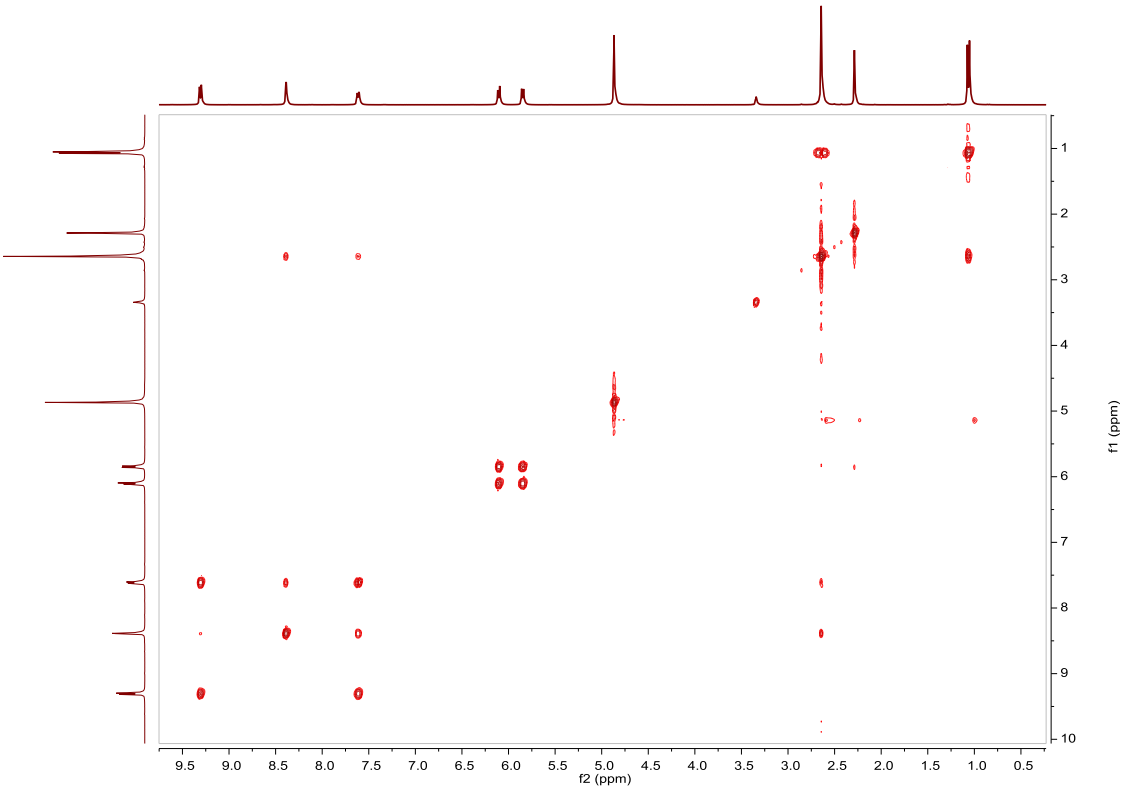

Fig S334. COSY NMR spectrum of **[Ru(p-Cym)(4,4'-dimethyl-2,2'-bipyridine)Cl]Cl** in MeOD-d_4, 300 MHz.

Compound [Ru(p-Cym)(4,4'-diazido-2,2'-bipyridine)(Cl)]Cl. Synthesis and characterization.

SYNTHESIS

Under a N_2 atmosphere, $Ru_2(p\text{-}Cym)_2Cl_4$ (0.1 g, 0.16 mmol) and 4,4'-diazido-2,2'-bipyridine (0.077 g, 0.32 mmol) were dissolved in 10 mL of acetone. The reaction mixture was refluxed for 15 h. It was cooled to room temperature and the solvent was evaporated. The product was purified by column chromatography (alumina, 100% CH_2Cl_2 to 1/100 MeOH/CH_2Cl_2). After reducing the volume of solvent of the collected fraction, the product was precipitated with ether, and obtained as a yellow solid. Yield 53%.

Elemental Analysis: calculated for ($C_{20}H_{20}Cl_2N_8Ru \cdot CH_2Cl_2$): C, 40.08; H, 3.52; N, 17.81. Found: C, 40.26; H, 3.30; N, 17.73.

Exact Mass: ESI-MS $[C_{20}H_{20}ClN_8Ru]^+$: calculated: m/z= 503.0575, found: m/z= 503.0571.

^{1}H NMR (300 MHz, MeOD-*d*$_4$): δ 9.33 (d, J = 6.3 Hz, 2H, (6)), 8.28 (d, J = 2.2 Hz, 2H, (3)), 7.48 (dd, J = 2.4 Hz, J = 6.3 Hz, 2H, (5)), 6.11 (d, J = 6.1 Hz, 2H, (8)), 5.85 (d, J = 6.1 Hz, 2H, (7)), 2.68 (sep, J = 6.9 Hz, 1H, (11)), 2.30 (s, 3H, (13)), 1.10 (d, J = 6.9 Hz, 6H, (12)).

^{13}C APT NMR (75 MHz, MeOD-*d*$_4$): δ 157.26 (2CH, (6)), 157.08 ($2C_{quat}$, (bipy)), 154.83 ($2C_{quat}$, (bipy)), 119.14 (2CH, (5)), 115.85 (2CH, (3)), 105.78 (Cquat, (p-Cym)), 105.50 (Cquat, (p-Cym)), 87.84 (2CH, (8)), 85.12 (2CH, (7)), 32.35 (CH, (11)), 22.34 ($2CH_3$, (12)), 18.97 (CH_3, (13)).

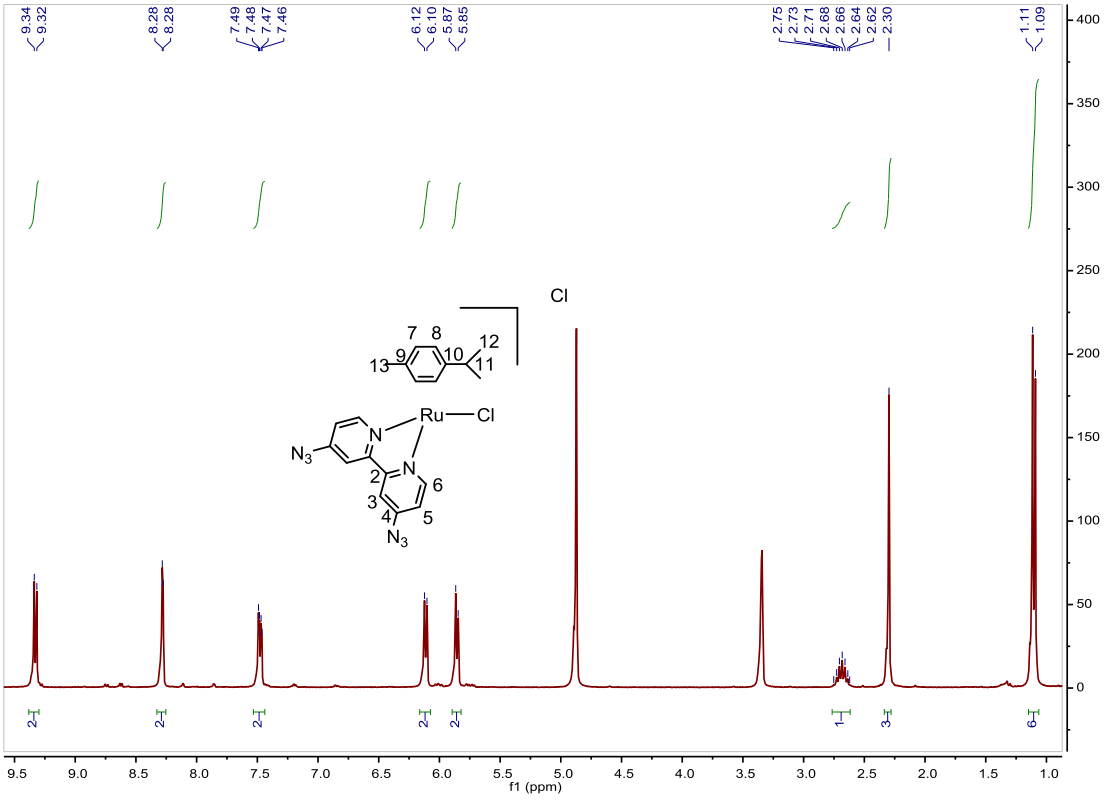

Fig. S335. ^{1}H NMR spectrum of **[Ru(p-Cym)(4,4'-diazido-2,2'-bipyridine)(Cl)]Cl** in MeOD-*d*$_4$, 300 MHz.

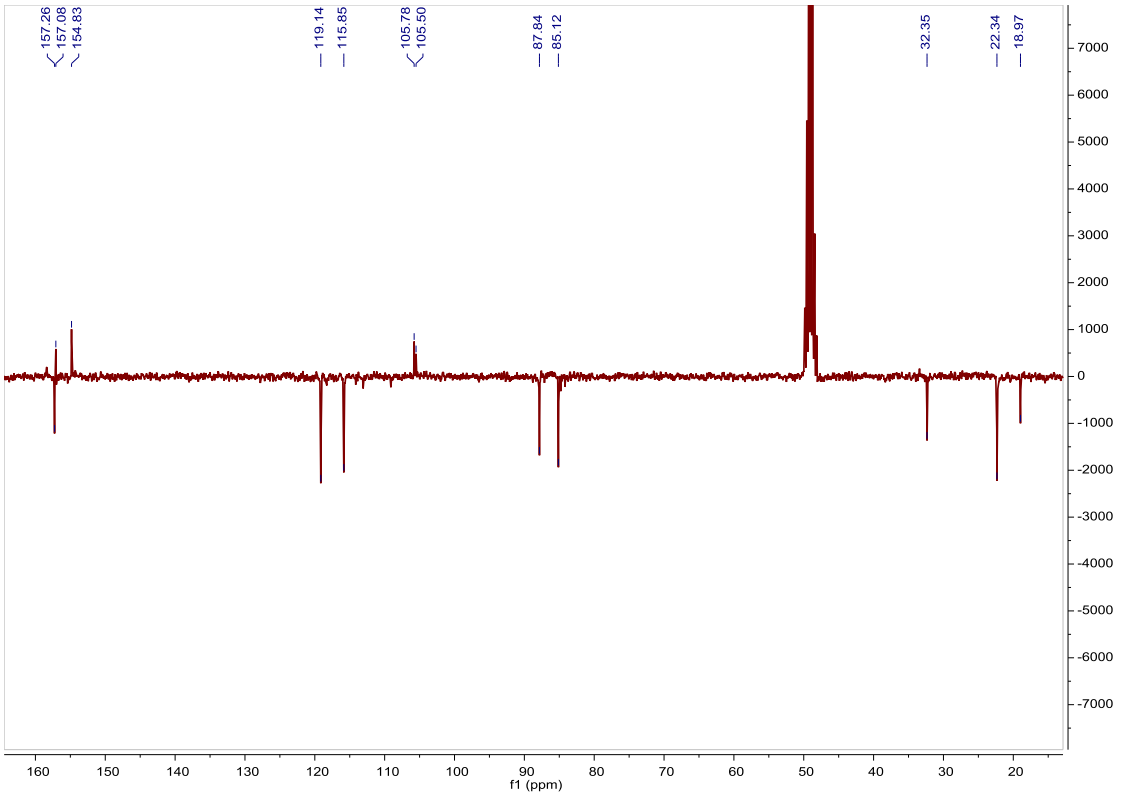

Fig. S336. ^{13}C APT NMR spectrum of **[Ru(p-Cym)(4,4'-diazido-2,2'-bipyridine)(Cl)]Cl** in MeOD-d_4, 75 MHz.

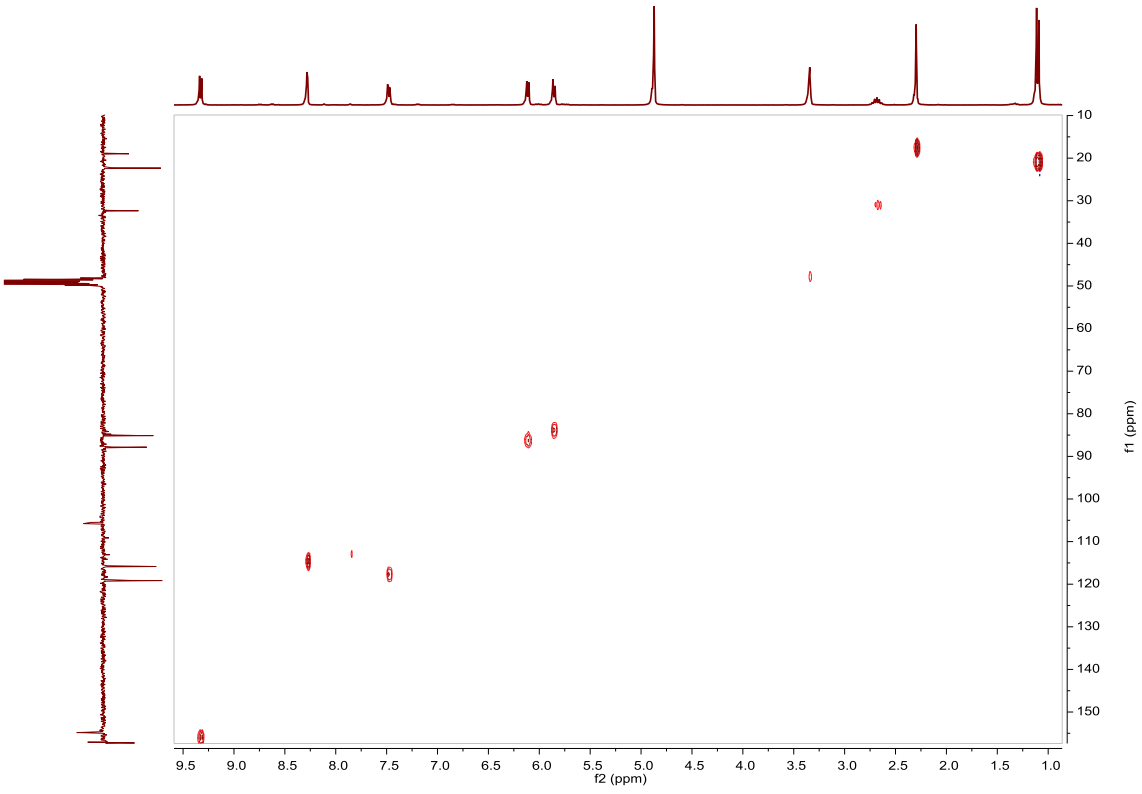

Fig. S337. HSQC NMR spectrum of **[Ru(p-Cym)(4,4'-diazido-2,2'-bipyridine)(Cl)]Cl** in MeOD-d_4.

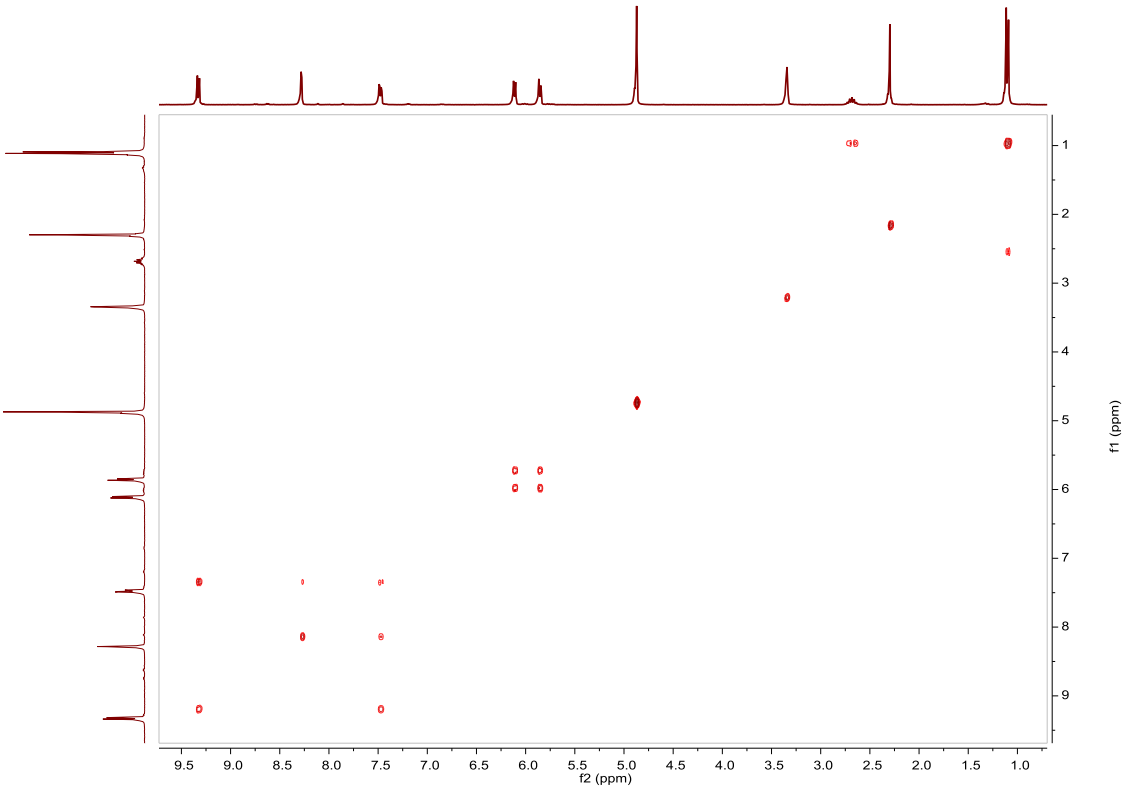

Fig. S338. COSY NMR spectrum of **[Ru(p-Cym)(4,4'-diazido-2,2'-bipyridine)(Cl)]Cl** in MeOD-d_4.

Compound [Ru(p-Cym)(4,4'-diamino-2,2'-bipyridine)(Cl)]Cl. Synthesis and characterization.

SYNTHESIS

Under a N_2 atmosphere, $Ru_2(p\text{-}Cym)_2Cl_4$ (0.1 g, 0.16 mmol) and 4,4'-diamino-2,2'-bipyridine (0.06 g, 0.326 mmol) were dissolved in 10 mL of acetone. The reaction mixture was refluxed for 15 h. It was cooled to room temperature and the brown solid that precipitated was filtered. Yield 60%.

Elemental Analysis: calculated for ($C_{20}H_{24}Cl_2N_4Ru$): C, 48.78; H, 4.91; N, 11.38. Found: C, 48.17; H, 4.88; N, 11.46.

Exact Mass: ESI-MS $[C_{20}H_{24}ClN_4Ru]^+$: calculated: m/z= 451.0765, found: m/z= 451.0768.

^{1}H NMR (300 MHz, MeOD-d_4): δ 8.70 (d, J = 6.6 Hz, 2H, (6)), 7.22 (d, J = 2.5 Hz, 2H, (3)), 6.77 (dd, J = 2.5 Hz, J = 6.6 Hz, 2H, (5)), 5.90 (d, J = 6.4 Hz, 2H, (8)), 5.63 (d J = 6.1 Hz, 2H, (7)), 2.61 (sep, J = 6.9 Hz, 1H, (11)), 2.26 (s, 3H, (13)), 1.08 (d, J = 6.9 Hz, 6H, (12)).

^{13}C APT NMR (75 MHz, MeOD-d_4): δ 158.16 ($2C_{quat}$, (bipy)), 156.61 ($2C_{quat}$, (bipy)), 155.09 (2CH, (6)), 112.55 (2CH, (5)), 107.61 (2CH, (3)), 104.12 (C_{quat}, (p-Cym)), 102.91 (C_{quat}, (p-Cym)), 87.07 (2CH, (8)), 83.93 (2CH, (7)), 32.24 (CH, (11)), 22.28 ($2CH_3$, (12)), 19.02 (CH_3, (13)).

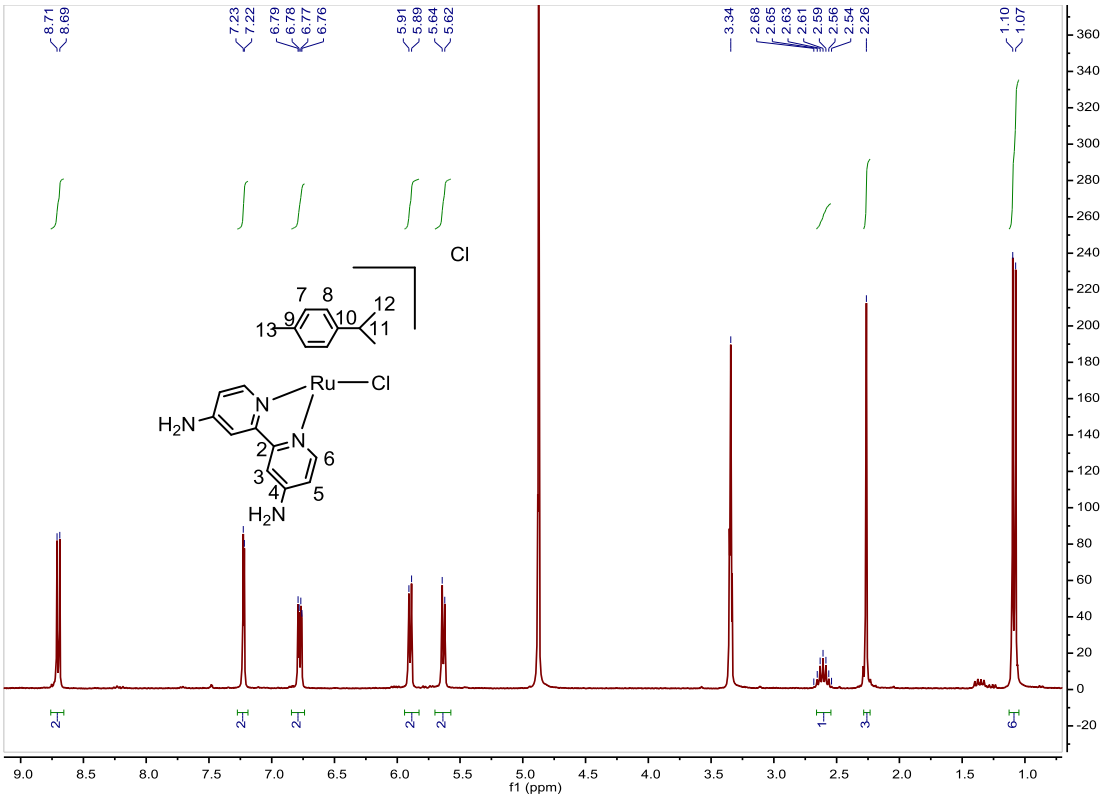

Fig. S339. ^{1}H NMR spectrum of **[Ru(p-Cym)(4,4'-diamino-2,2'-bipyridine)(Cl)]Cl** in MeOD-d_4, 300 MHz.

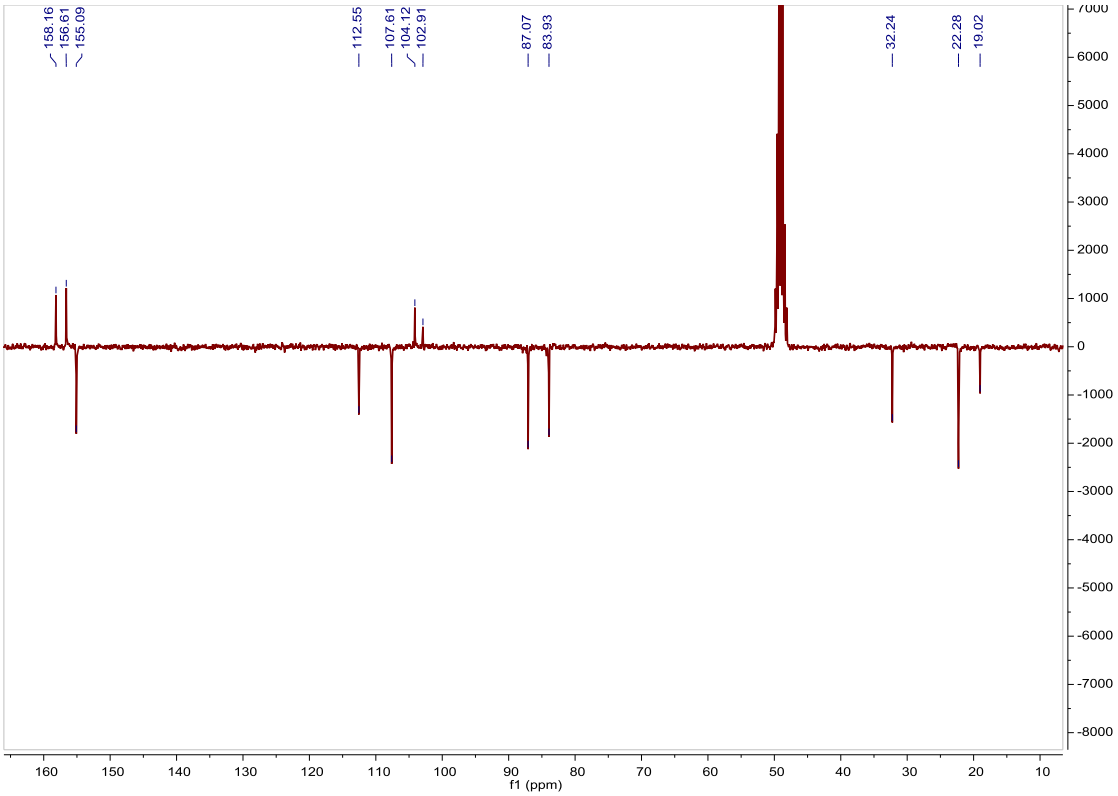

Fig. S340. ^{13}C APT NMR spectrum of **[Ru(p-Cym)(4,4'-diamino-2,2'-bipyridine)(Cl)]Cl** in MeOD-d_4, 75 MHz.

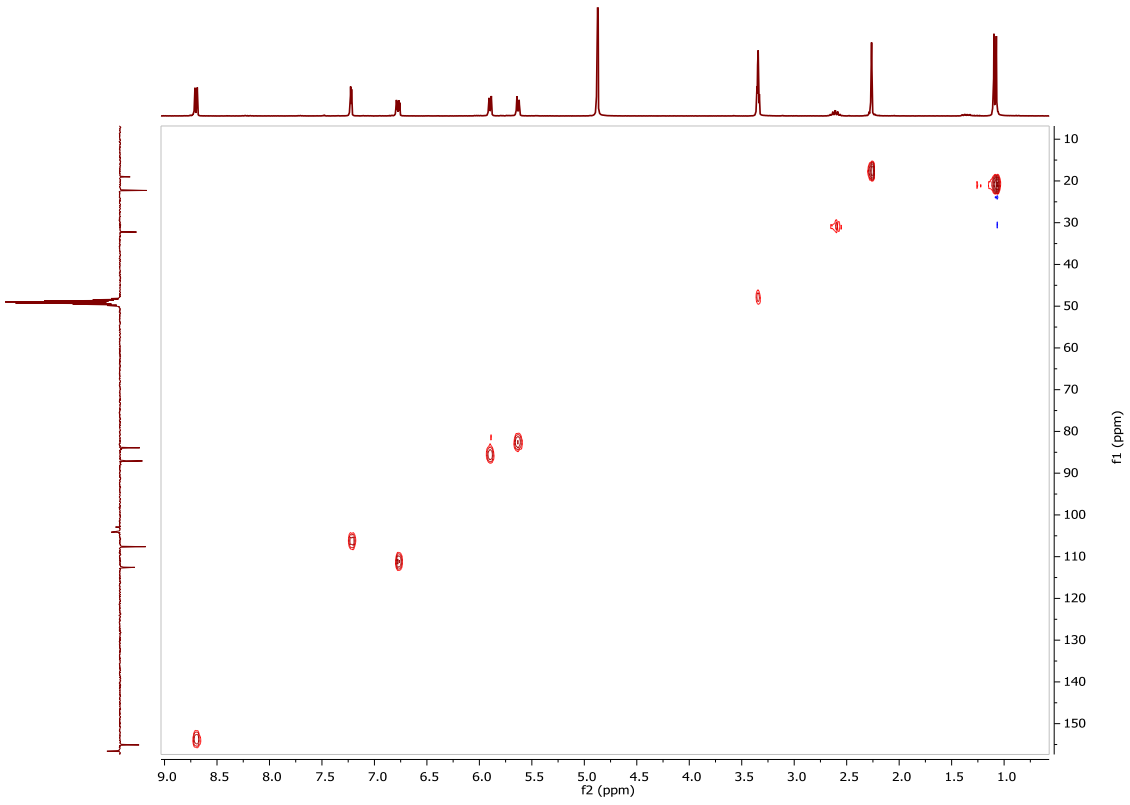

Fig. S341. HSQC NMR spectrum of **[Ru(p-Cym)(4,4'-diamino-2,2'-bipyridine)(Cl)]Cl** in MeOD-d_4.

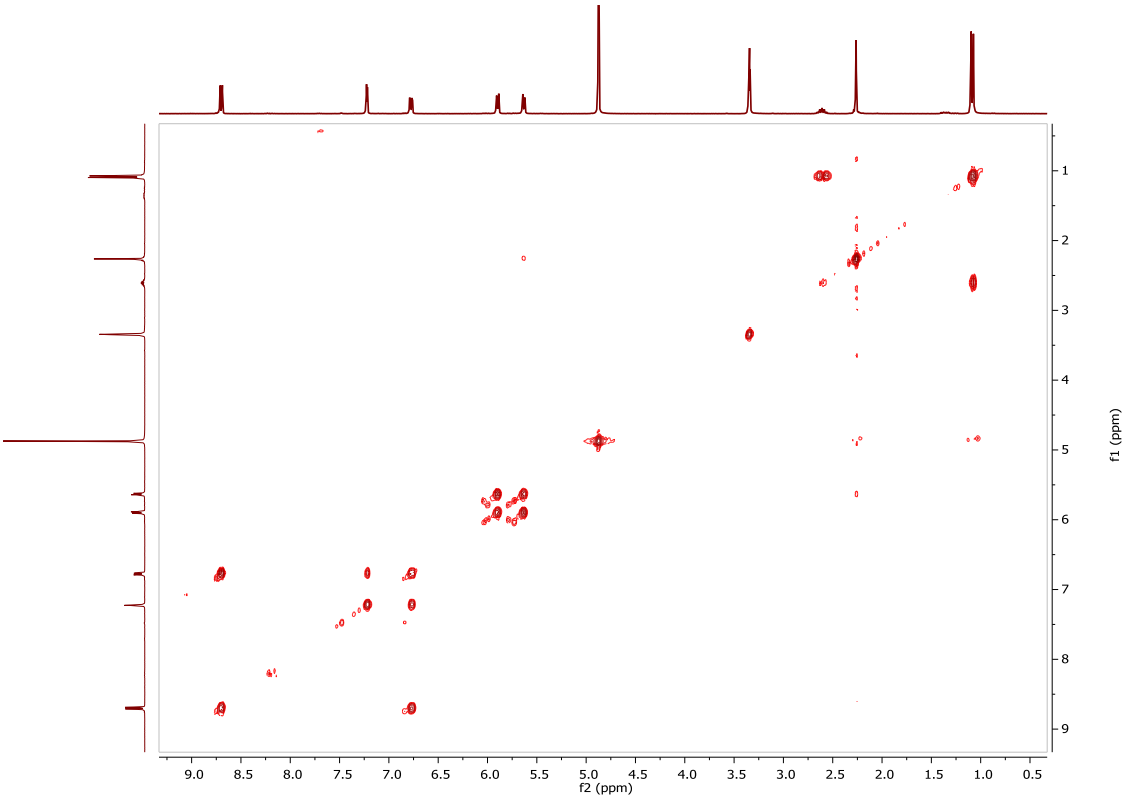

Fig. S342. COSY NMR spectrum of **[Ru(p-Cym)(4,4'-diamino-2,2'-bipyridine)(Cl)]Cl** in MeOD-d_4.

Compound [Ru(p-Cym)(4-bromo-4'-azido-2,2'-bipyridine)(Cl)]Cl. Synthesis and characterization.

SYNTHESIS

Under a N_2 atmosphere, $Ru_2(p\text{-}Cym)_2Cl_4$ (0.1 g, 0.16 mmol) and 4-bromo-4'-azido-2,2'-bipyridine (0.084 g, 0.30 mmol) were dissolved in 10 mL of acetone. The reaction mixture was refluxed for 15 h. It was cooled to room temperature, the solvent was evaporated and the desired compound was obtained after precipitated with CH_2Cl_2/Et_2O as a dark red solid. Yield 49%.

Elemental Analysis: calculated for ($C_{20}H_{20}BrCl_2N_5Ru$): C, 41.25; H, 3.46; N, 12.03. Found: C, 40.76; H, 3.63; N, 11.81.

Exact Mass: ESI-MS $[C_{20}H_{20}BrClN_5Ru]^+$: calculated: m/z= 545.9632, found: m/z= 545.9642.

^{1}H NMR (300 MHz, MeOD-*d*$_4$): δ 9.33 (d, J = 2.4 Hz, 1H, (6)), 9.31 (d, J = 2.2 Hz, 1H, (6')), 8.93 (d, J = 2.1 Hz, 1H, (3)), 8.30 (d, J = 2.5 Hz, 1H, (3')), 8.02 (dd, J = 2.1 Hz, J 6.1 Hz, 1H, (5)), 7.49 (dd, J = 2.4 Hz, J = 6.3 Hz, 1H, (5')), 6.14 (d, J = 4.3 Hz, 1H, (8)), 6.12 (d, J = 4.2 Hz, 1H, (8')), 5.88 (d, J = 4.1 Hz, 1H, (7)), 5.86 (d, J = 4.1 Hz, 1H, (7')), 2.70 (sep, J = 6.9 Hz, 1H, (11)), 2.30 (s, 3H, (13)), 1.12 (d, J = 1.9 Hz, 3H, (12)), 1.10 (d, J = 1.9 Hz, 3H, (12')).

^{13}C NMR (75 MHz, MeOD-*d*$_4$): δ 157.40 (CH, (6)), 157.03 (CH, (6')), 156.82 (Cquat, (bipy)), 156.38 (Cquat, (bipy)), 154.89 (Cquat, (bipy)), 138.04 (Cquat, (bipy)), 132.27 (CH, (5)), 128.76 (CH, (3)), 119.37 (CH, (5')), 116.16 (CH, (3')), 106.35 (Cquat, (p-Cym)), 105.59 (Cquat, (p-Cym)), 88.03 (CH, (8)), 87.83 (CH, (8')), 85.51 (CH, (7)), 85.31 (CH, (7')), 32.35 (CH, (11)), 22.36 (CH_3, (13)), 18.96 (CH_3, (12)), 15.43 (CH_3, (12')).

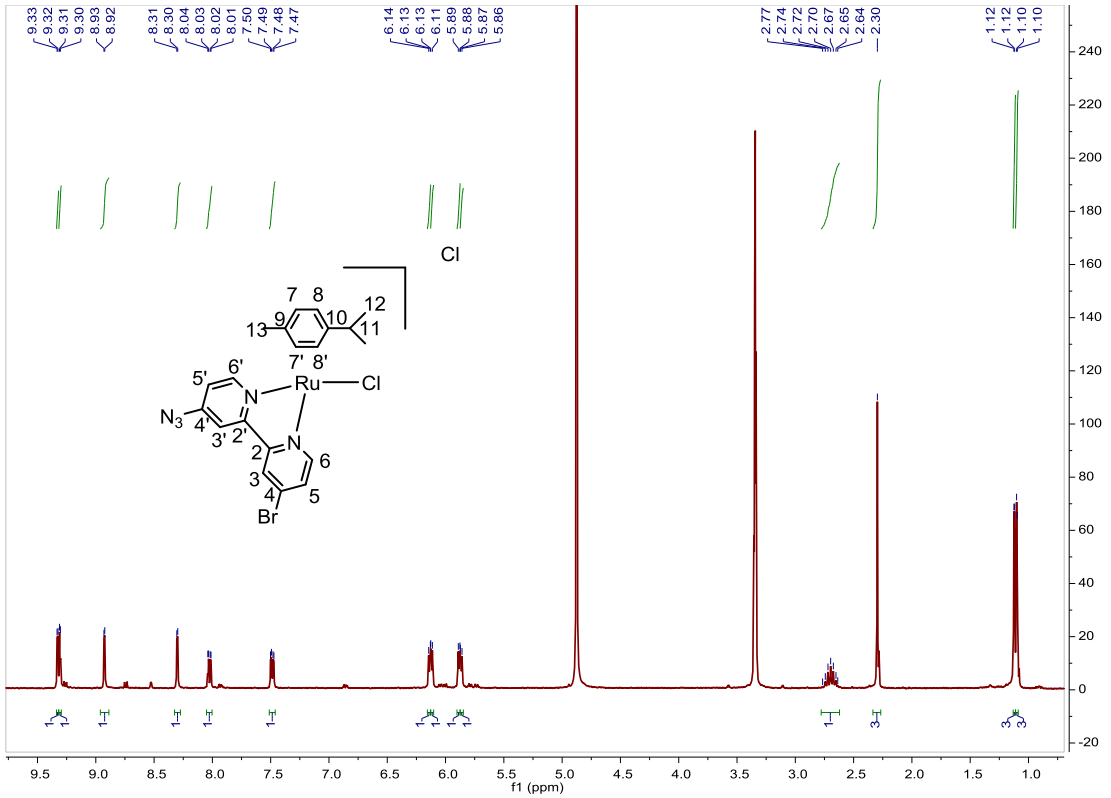

Fig. S343. ^{1}H NMR spectrum of **[Ru(p-Cym)(4-bromo-4'-azido-2,2'-bipyridine)(Cl)]Cl** in MeOD-*d*$_4$, 300 MHz.

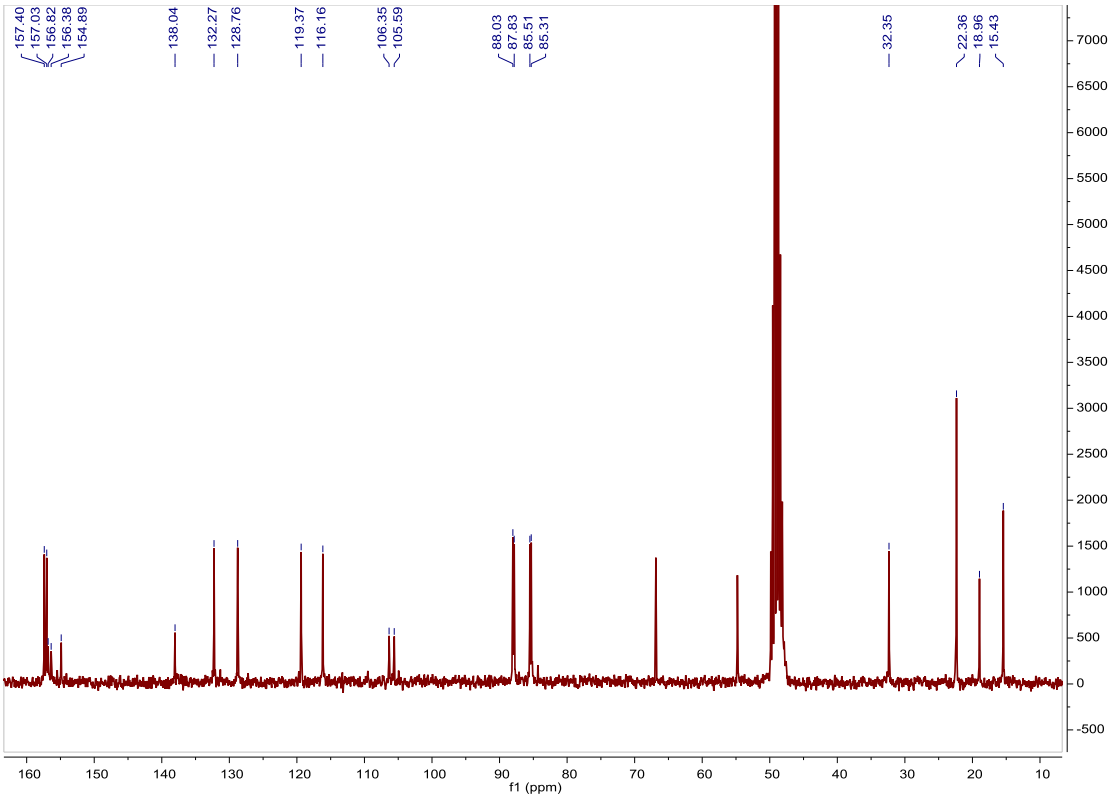

Fig. S344. ^{13}C NMR spectrum of **[Ru(p-Cym)(4-bromo-4'-azido-2,2'-bipyridine)(Cl)]Cl** in MeOD-d_4, 75 MHz.

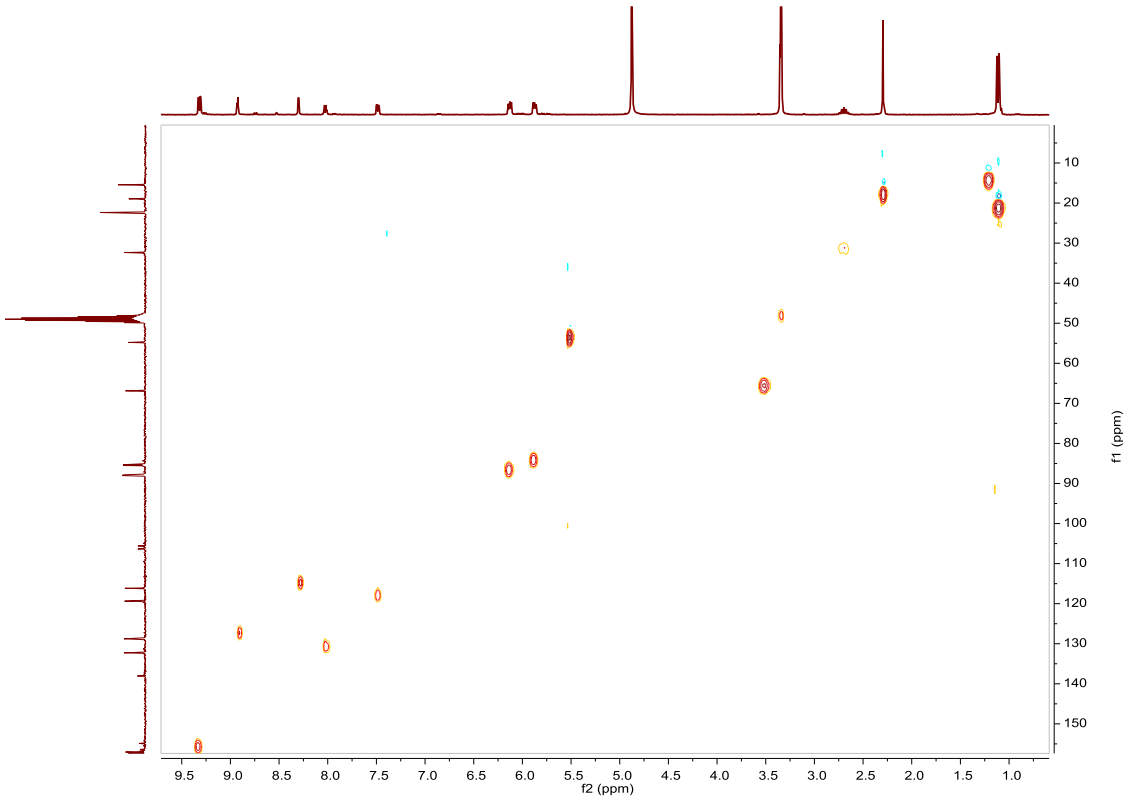

Fig. S345. HSQC NMR spectrum of **[Ru(p-Cym)(4-bromo-4'-azido-2,2'-bipyridine)(Cl)]Cl** in MeOD-d_4.

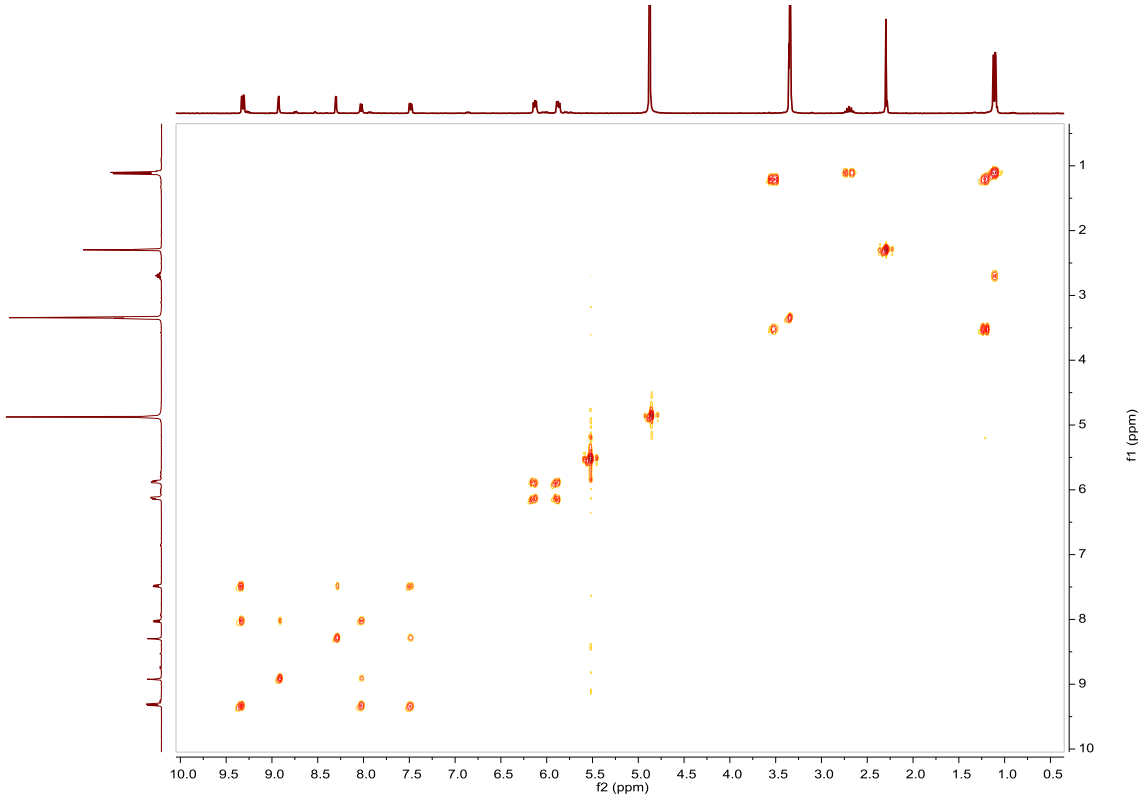

Fig. S346. COSY NMR spectrum of **[Ru(p-Cym)(4-bromo-4'-azido-2,2'-bipyridine)(Cl)]Cl** in MeOD-d_4.

Compound [Ru(p-Cym)(2,2'-bis(4-phenylazopyridine)(Cl)]Cl. Synthesis, characterization and photoisomerization studies.

SYNTHESIS

Under a N_2 atmosphere, $Ru_2(p\text{-}Cym)_2Cl_4$ (0.1 g, 0.16 mmol) and 2,2'-bis(4-phenylazopyridine) (0.119 g, 0.326 mmol) were dissolved in 10 mL of acetone. The reaction mixture was refluxed for 15 h. It was cooled to room temperature and the solid was filtered. The desired compound was obtained after precipitated with CH_2Cl_2/Et_2O as a dark red solid. Yield 73%.

Elemental Analysis: calculated for ($C_{32}H_{30}Cl_2N_6Ru{\cdot}CH_2Cl_2$): C, 52.46; H, 4.27; N, 11.12. Found: C, 52.33; H, 4.30; N, 11.09.

Exact Mass: ESI-MS $[C_{32}H_{30}ClN_6Ru]^+$: calculated: m/z= 635.1264, found: m/z= 635.1282.

^{1}H NMR (300 MHz, MeOD-d_4): δ 9.69 (d, J = 6.1 Hz, 2H, (6)), 8.98 (s, 2H, (3)), 8.19–8.04 (m, 6H, (5+15)), 7.77–7.61 (m, 6H, (16+17)), 6.24 (d, J = 6.2 Hz, 2H, (8)), 6.00 (d, J = 6.2 Hz, 2H, (7)), 2.75 (sep, J = 6.8 Hz, 1H, (11)), 2.34 (s, 3H, (13)), 1.13 (d, J = 6.9 Hz, 6H, (12)).

^{13}C APT NMR (75 MHz, MeOD-d_4): δ 160.37 ($2C_{quat}$, (bipy)), 158.42 (2CH, (6)), 157.91 ($2C_{quat}$, (bipy)), 153.73 ($2C_{quat}$, (bipy), 135.13 (2CH, (17)), 130.76 (4CH, (16)), 125.16 (4CH, (15)), 120.49 (2CH, (5)), 118.74 (2CH, (3)), 107.02 (C_{quat}, (p-Cym)), 106.04(C_{quat}, (p-Cym)), 88.47 (2CH, (8)), 86.13 (2CH, (7)), 32.34 (CH, (11)), 22.38 ($2CH_3$, (12)), 19.02 (CH_3, (13)).

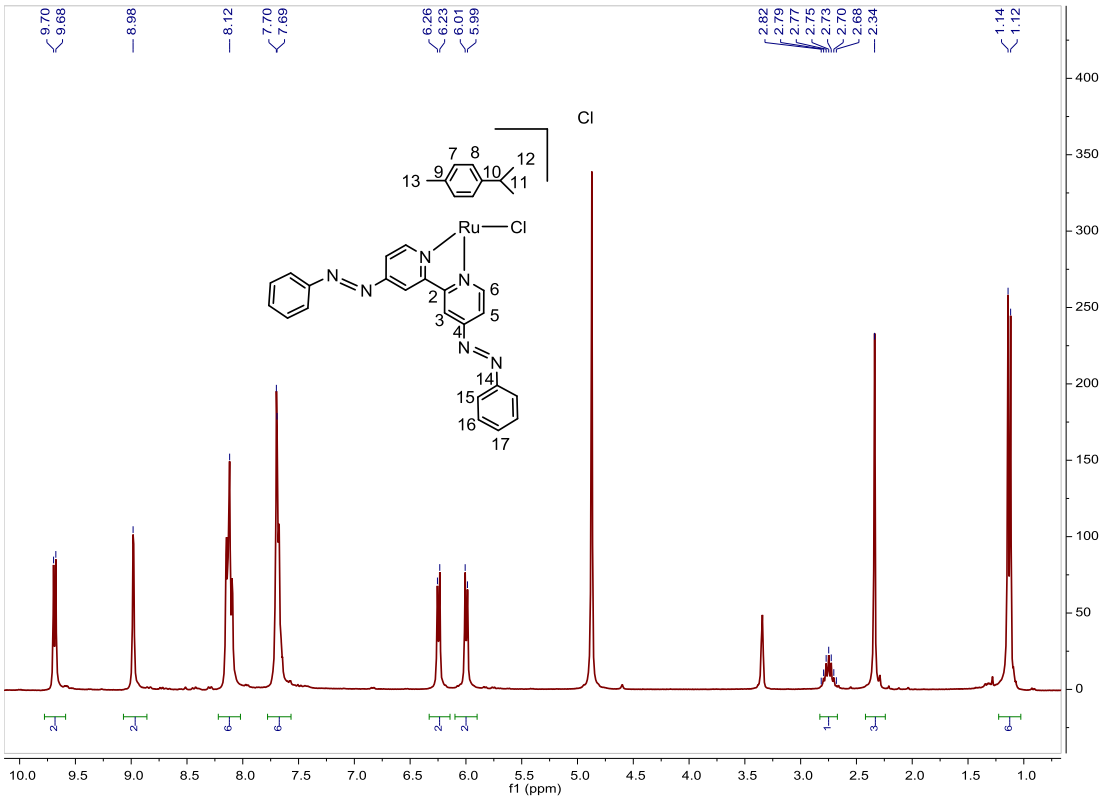

Fig. S347. ^{1}H NMR spectrum of **[Ru(p-Cym)(2,2'-bis(4-phenylazopyridine)(Cl)]Cl** in MeOD-d_4, 300 MHz.

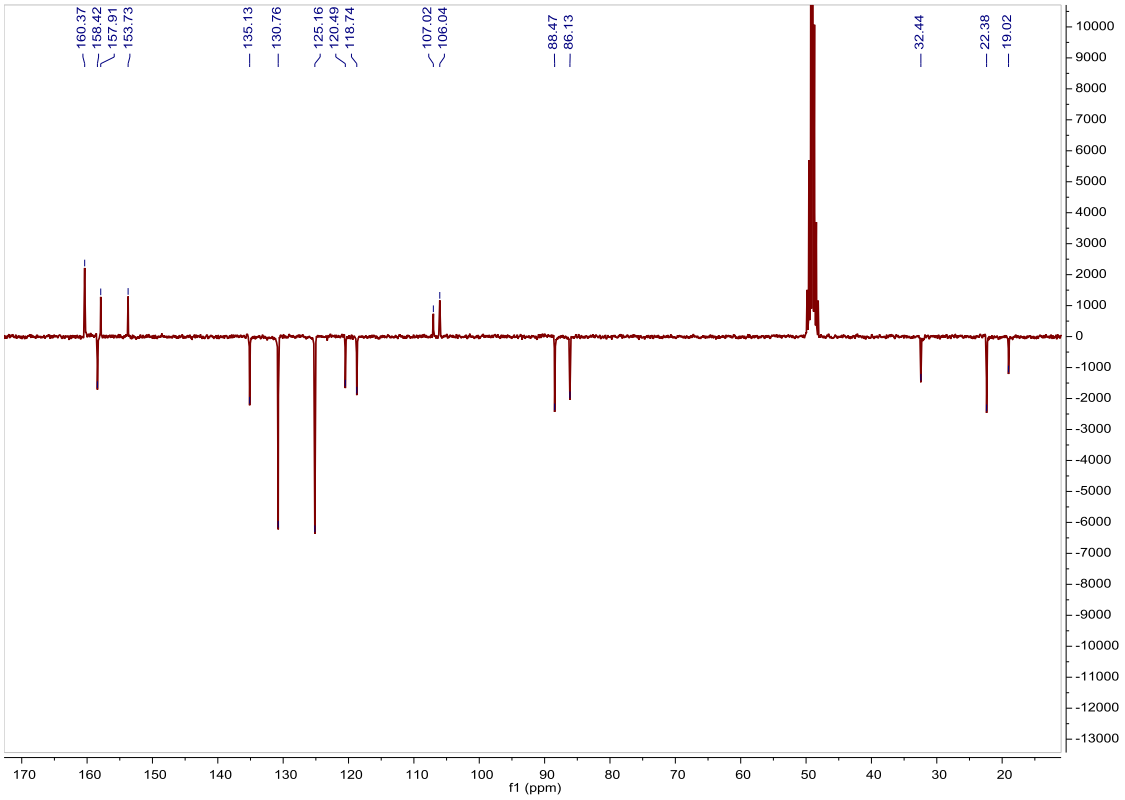

Fig. S348. ^{13}C APT NMR spectrum of **[Ru(p-Cym)(2,2'-bis(4-phenylazopyridine)(Cl)]Cl** in MeOD-d_4, 75 MHz.

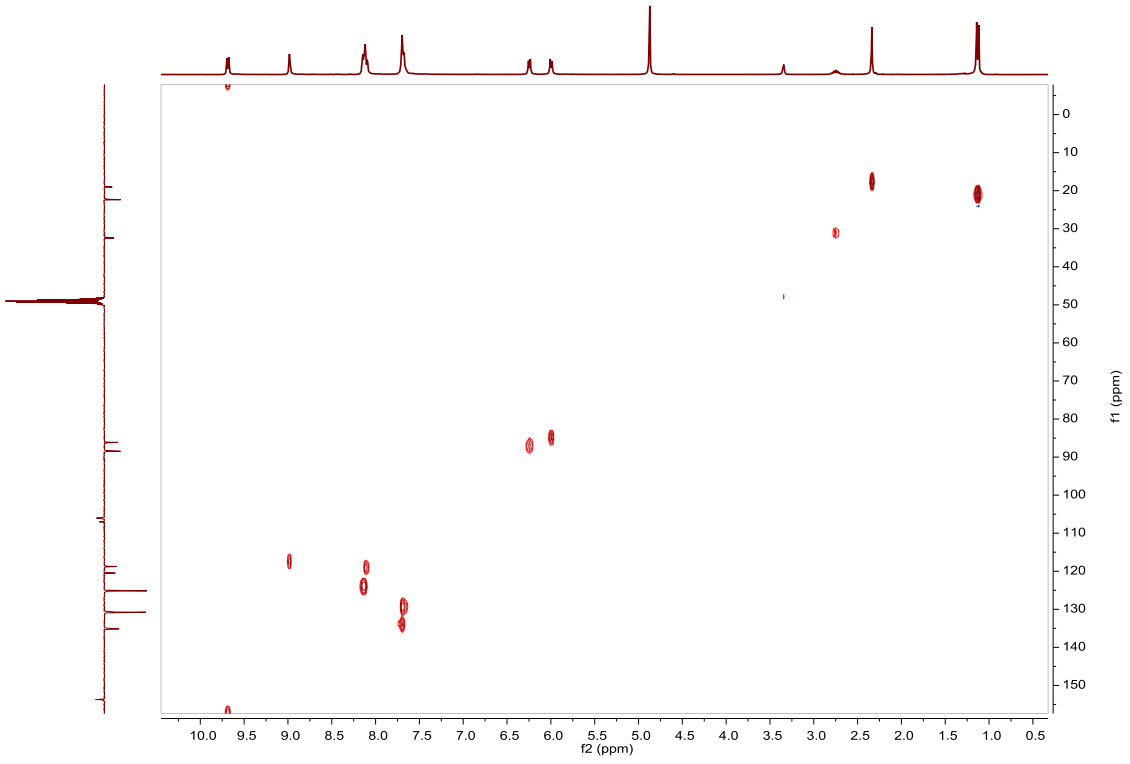

Fig. S349. HSQC NMR spectrum of **[Ru(p-Cym)(2,2'-bis(4-phenylazopyridine)(Cl)]Cl** in MeOD-d_4.

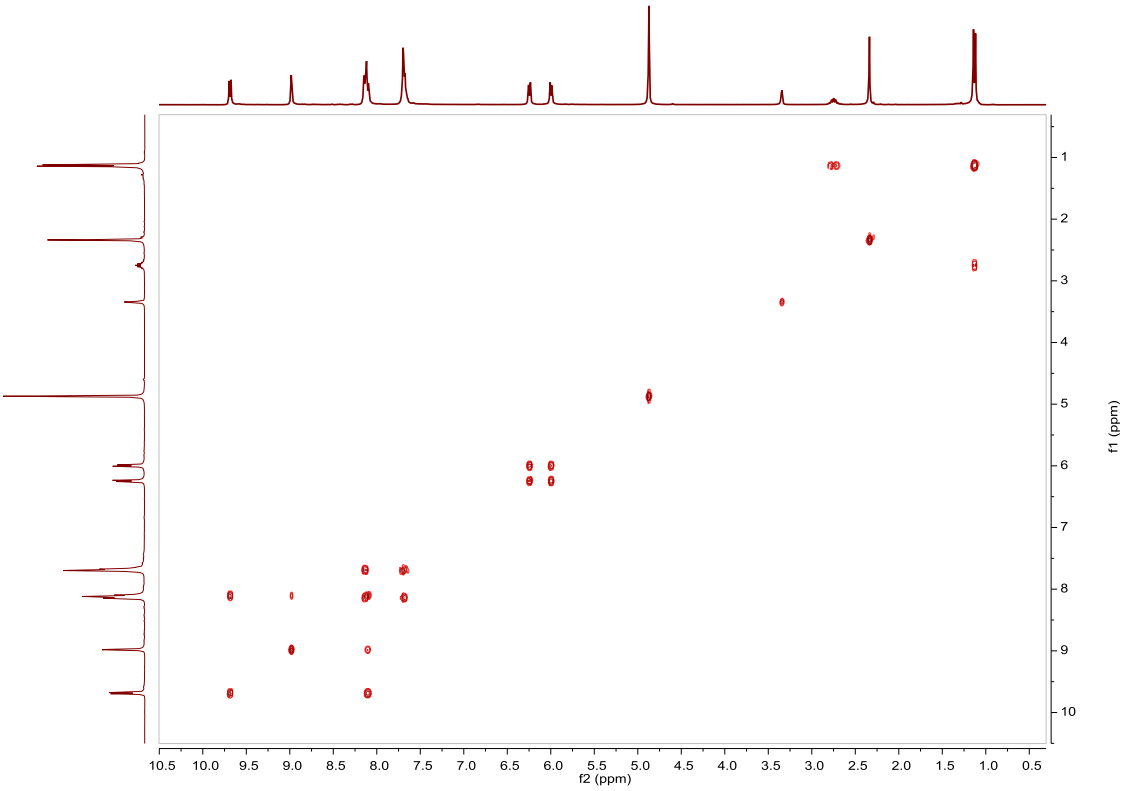

Fig. S350. COSY NMR spectrum of **[Ru(p-Cym)(2,2'-bis(4-phenylazopyridine)(Cl)]Cl** in MeOD-d_4.

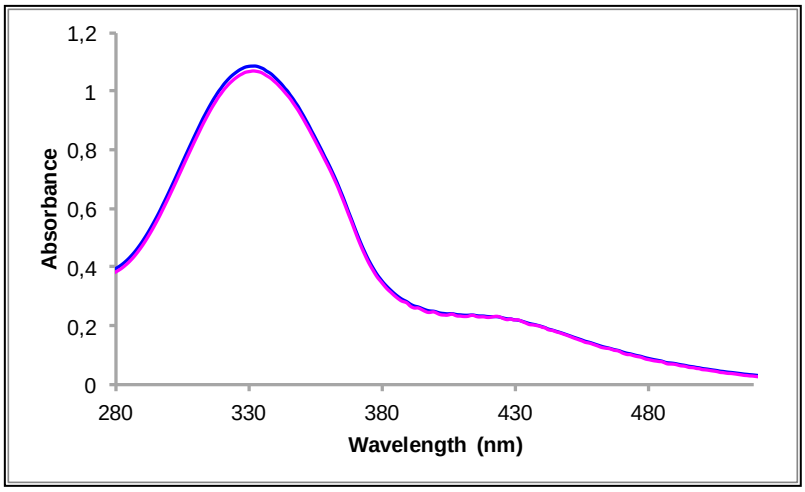

Fig. S351. UV/Vis spectra of **[Ru(p-Cym)(2,2'-bis(4-phenylazopyridine)(Cl)]Cl** in CH_3CN. Before (blue line) and after (pink line) irradiation at 316nm, $2.62 \cdot 10^{-5}$ M.

Cis to trans thermal isomerization kinetics. Due to the small degree of photoisomerization, it has been not possible to calculate k.

Compound [Ru(p-Cym)(4-phenylazopyridine)(Cl)$_2$]. Synthesis, characterization and photoisomerization studies.

SYNTHESIS

Under a N_2 atmosphere, Ru_2(p-Cym)$_2Cl_4$ (0.2 g, 0.32 mmol) and (4-phenylazopyridine) (0.117 g, 0.64 mmol) were dissolved in 20 mL of acetone. The reaction mixture was refluxed for 15 h. It was cooled to room temperature, the solvent was evaporated and the product was obtained as an orange solid. Yield 71%.

Elemental Analysis: calculated for ($C_{21}H_{23}Cl_2N_3Ru$): C, 51.54; H, 4.74; N, 8.59. Found: C, 51.51; H, 4.71; N, 8.55.

Exact Mass: ESI-MS $[C_{21}H_{23}ClN_3Ru]^+$ (M-Cl): calculated: m/z= 454.0619, found: m/z= 454.0618.

^{1}H NMR (300 MHz, $CDCl_3$): δ 9.26 (d, J = 6.9 Hz, 2H, (azopy)), 8.06–7.96 (m, 2H, (15+19)), 7.75 (d, J = 6.7 Hz, 2H, (azopy)), 7.64–7.55 (m, 3H, (16+17+18)), 5.52 (d, J = 5.7 Hz, 2H, (8)), 5.30 (d, J = 5.8 Hz, 2H, (7)), 3.06 (sep, J = 6.9 Hz, 1H, (11)), 2.17 (s, 3H, (13)), 1.37 (d, J = 6.9 Hz, 6H, (12)).

^{13}C APT NMR (75 MHz, $CDCl_3$): δ 157.12 (C_{quat}, (azopy)), 155.93 (2CH, (azopy)), 151.76 (C_{quat}, (azopy)), 132.78 (CH, (17)), 128.92 (2CH, (16+18)), 123.35 (2CH, (15+19)), 116.50 (2CH, (azopy)), 103.26 (C_{quat}, (p-Cym)), 96.88 (C_{quat}, (p-Cym), 82.58 (2CH, (8)), 81.88 (2CH, (7)), 30.24 (CH, (11)), 21.86 ($2CH_3$, (12)), 17.83 (CH_3, (13)).

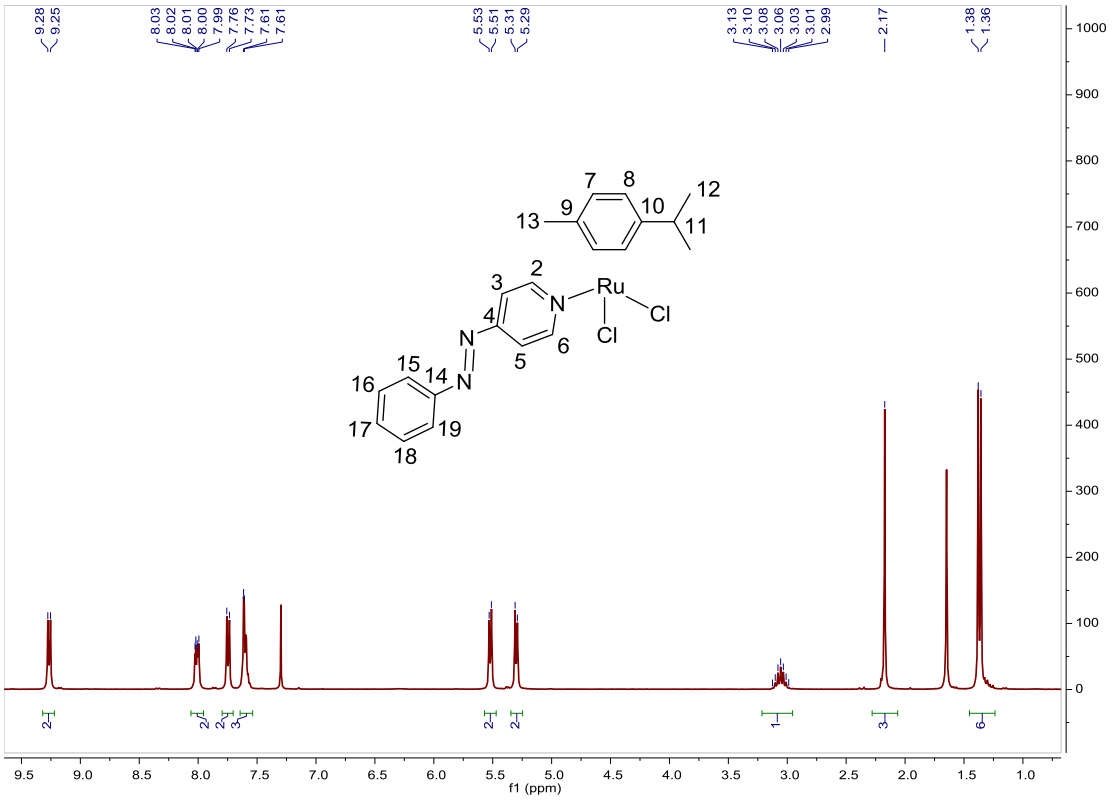

Fig. S352. ^{1}H NMR spectrum of **[Ru(p-Cym)(4-phenylazopyridine)(Cl)$_2$]** in $CDCl_3$, 300 MHz.

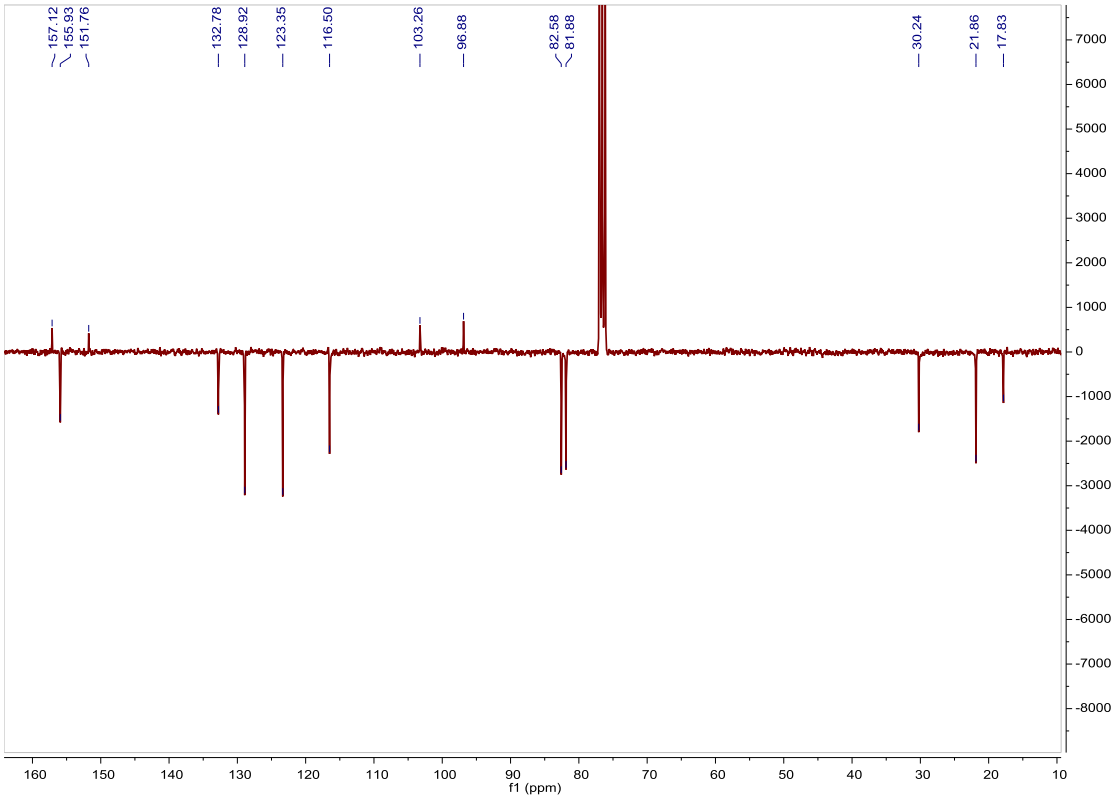

Fig. S353. ^{13}C APT NMR spectrum of **[Ru(p-Cym)(4-phenylazopyridine)(Cl)$_2$]** in $CDCl_3$, 75 MHz.

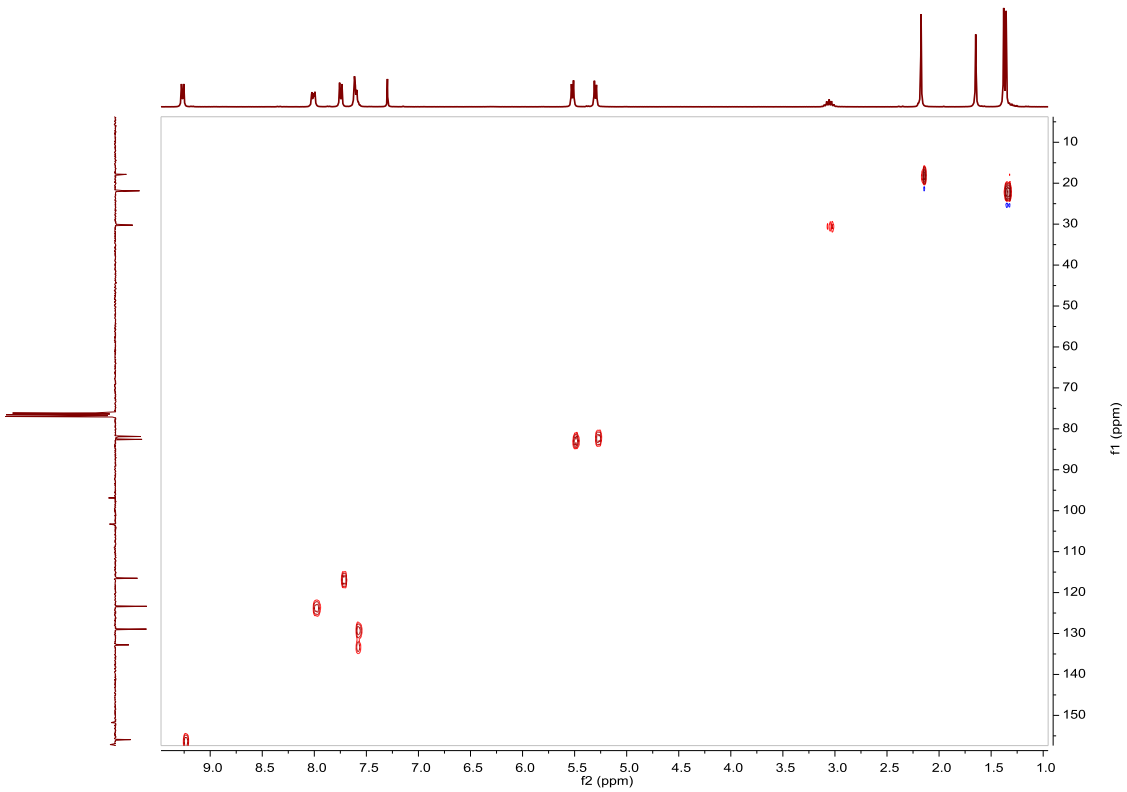

Fig. S354. HSQC NMR spectrum of **[Ru(p-Cym)(4-phenylazopyridine)(Cl)$_2$]** in $CDCl_3$.

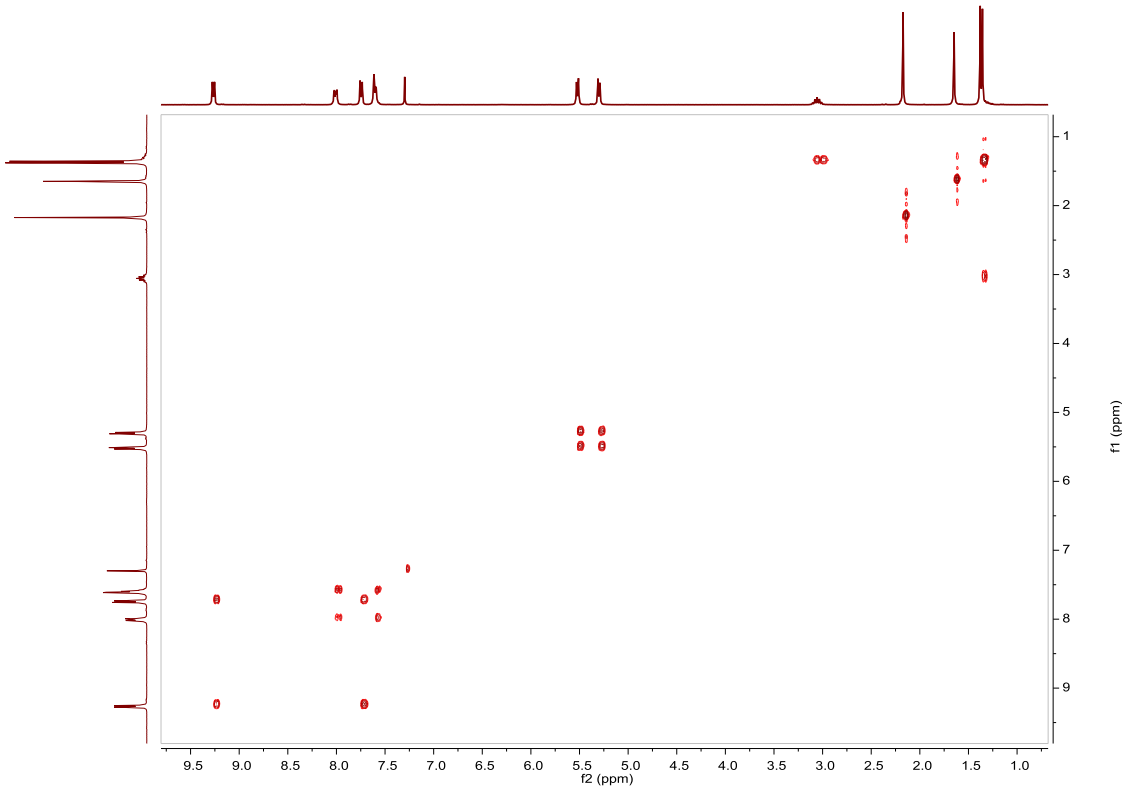

Fig. S355. COSY NMR spectrum of **[Ru(p-Cym)(4-phenylazopyridine)(Cl)$_2$]** in $CDCl_3$.

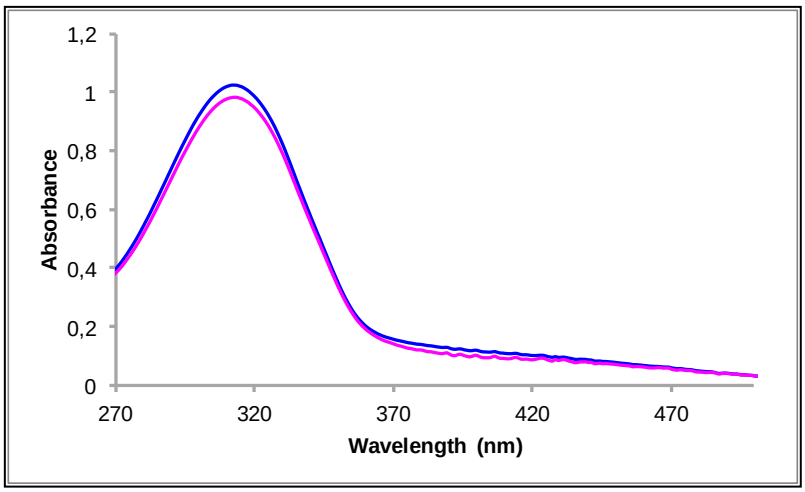

Fig. S356. UV/Vis spectra of **[Ru(p-Cym)(4-phenylazopyridine)(Cl)$_2$]** in ACN. Before (blue line) and after (pink line) irradiation at 311nm, $5.50 \cdot 10^{-5}$M.

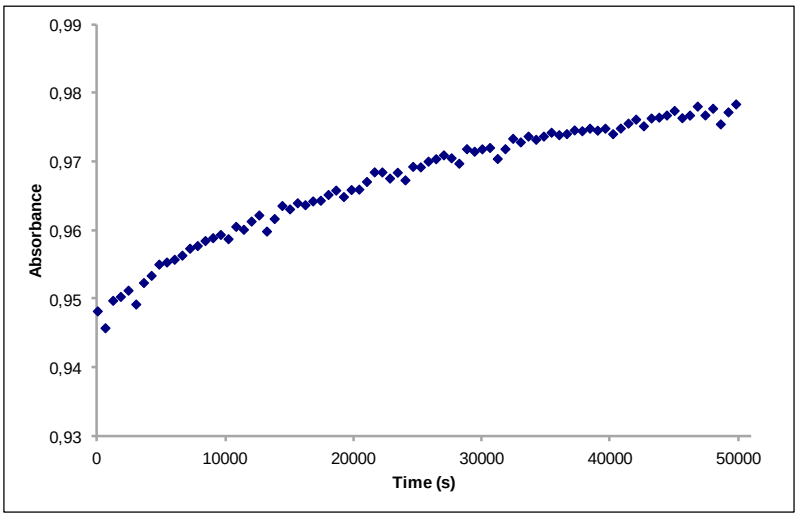

Fig. S357. Cis to trans thermal isomerization kinetics of **[Ru(p-Cym)(4-phenylazopyridine)(Cl)$_2$]**. Absorption change of the band 312nm at 338 K in ACN after irradiation at 311 nm. ($5.50 \cdot 10^{-5}$M).

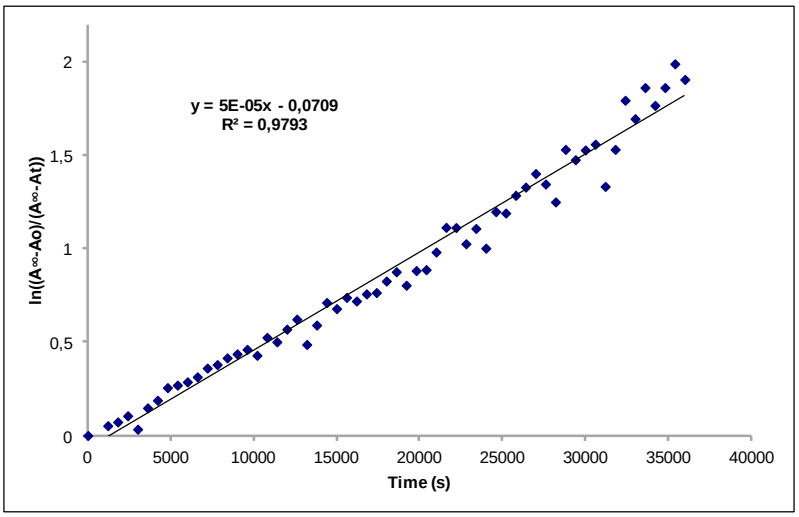

Fig. S358. Cis to trans thermal isomerization kinetics of **[Ru(p-Cym)(4-phenylazopyridine)(Cl)$_2$]**. First-order plot. k (s^{-1}) = $5.0 \cdot 10^{-5}$. Half-life (min) = 231.

Compound [Ru(p-Cym)(4-phenylazopyridine)$_2$(Cl)]PF$_6$. Synthesis, characterization and photoisomerization studies.

SYNTHESIS[42]

Under a N_2 atmosphere, [Ru(p-Cym)(4-phenylazopyridine)(Cl_2)] (0.319 g, 0.65 mmol) and AgPF6 (0.160 g, 0.63 mmol) were dissolved in 20 mL of acetone and 20 mL of methanol. The mixture was stirred for 1 h, AgCl was removed by filtration and 4-phenylazopyridine (0.119 g, 0.65 mmol) were added. The reaction mixture was stirred for 15 h and the solvent was evaporated. The product was obtained as a red solid after precipitation with acetone/ether. Yield 55%.

Elemental Analysis: calculated for ($C_{32}H_{32}ClN_6RuPF_6$): C, 49.14; H, 4.12; N, 10.75. Found: C, 49.23; H, 4.01; N, 10.59.

Exact Mass: ESI-MS $[C_{21}H_{23}ClN_3Ru]^+$ (M-L-PF_6): calculated: m/z= 454.0619, found: m/z= 454.0618.

^{1}H NMR (300 MHz, $CDCl_3$): δ 9.27 (d, J = 6.9 Hz, 4H, (azopy)), 7.97 (dd, J = 1.6 Hz, J = 7.5 Hz, 4H, (15+19)), 7.87 (d, J = 6.9 Hz, 4H, (azopy)), 7.57 (brd, J = 7.3 Hz, 6H, (16+17+18)), 6.03 (d, J = 6.1 Hz, 2H, (8)), 5.78 (d, J = 6.1 Hz, 2H, (7)), 2.67 (sep, J = 6.9 Hz, 1H, (11)), 1.86 (s, 3H, (13)), 1.23 (d, J = 6.9 Hz, 6H, (12)).

^{13}C APT NMR (75 MHz, $CDCl_3$): δ 157.66 (2C_{quat}, (azopy)), 155.29 (4CH, (azopy)), 151.74 (2C_{quat}, (azopy)), 133.09 (2CH, (17)), 128.94 (4CH, (16)), 123.47 (4CH, (15)), 118.22 (4CH, (azopy)), 102.59 (C_{quat}, (p-Cym)), 101.80 (C_{quat}, (p-Cym)), 88.49 (2CH, (8)), 81.77 (2CH, (7)), 30.45 (CH, (11)), 21.84 ($2CH_3$, (12)), 17.39 (CH_3, (13)).

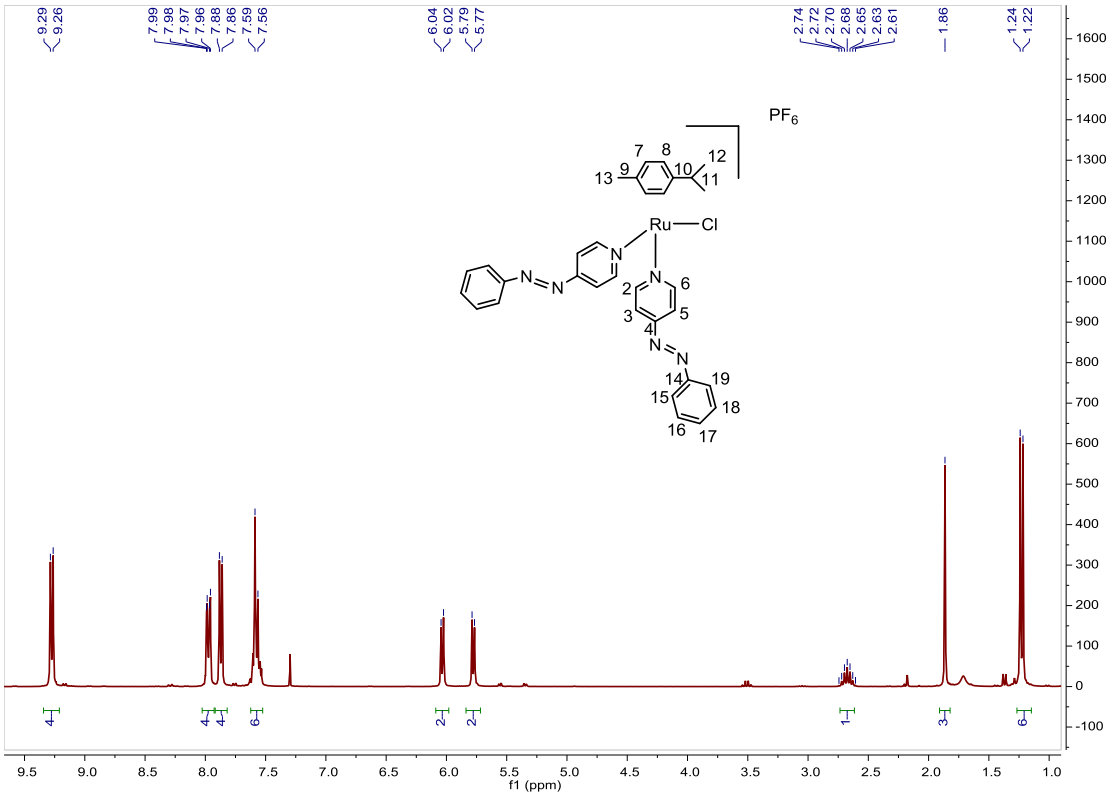

Fig. S359. ^{1}H NMR spectrum of **[Ru(p-Cym)(4-phenylazopyridine)$_2$(Cl)]PF$_6$** in $CDCl_3$, 300 MHz.

[42] S. J. Dickson, M. J. Paterson, C. E. Willans, K. M. Anderson and J. W. Steed, *Chem. Eur. J.*, **2008**, *14*, 7296–7305.

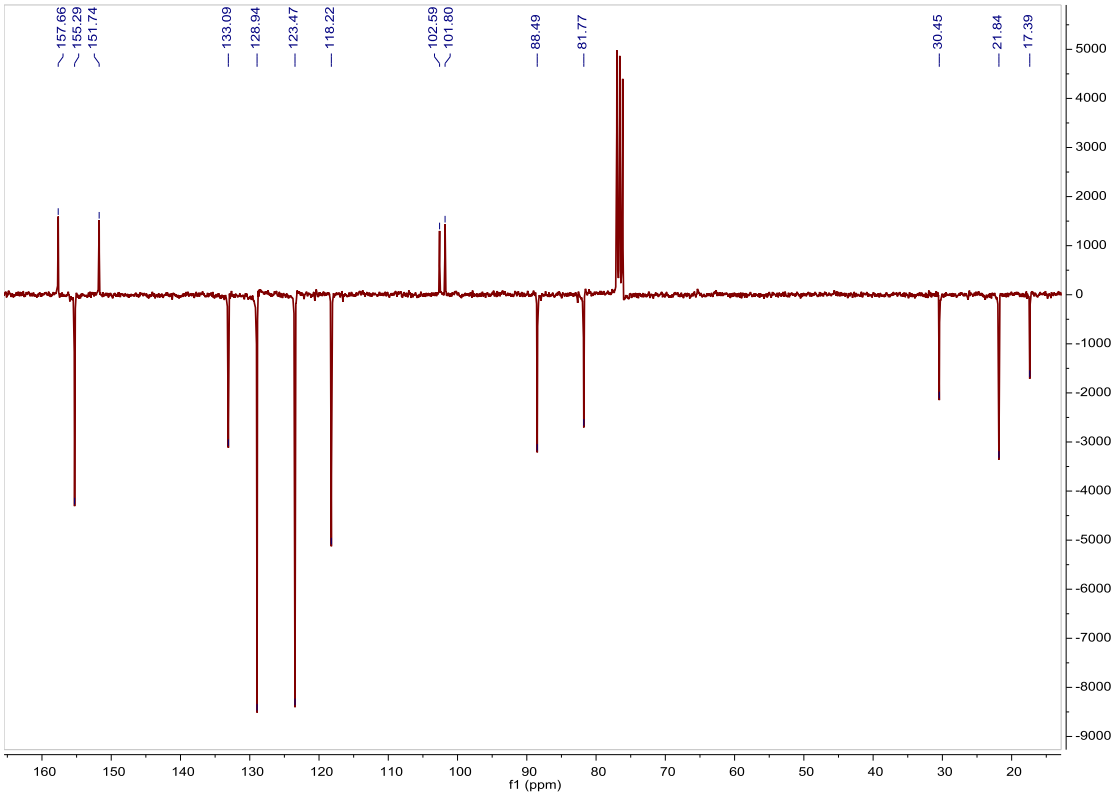

Fig. S360. ^{13}C APT NMR spectrum of **[Ru(p-Cym)(4-phenylazopyridine)$_2$(Cl)]PF$_6$** in $CDCl_3$, 75 MHz.

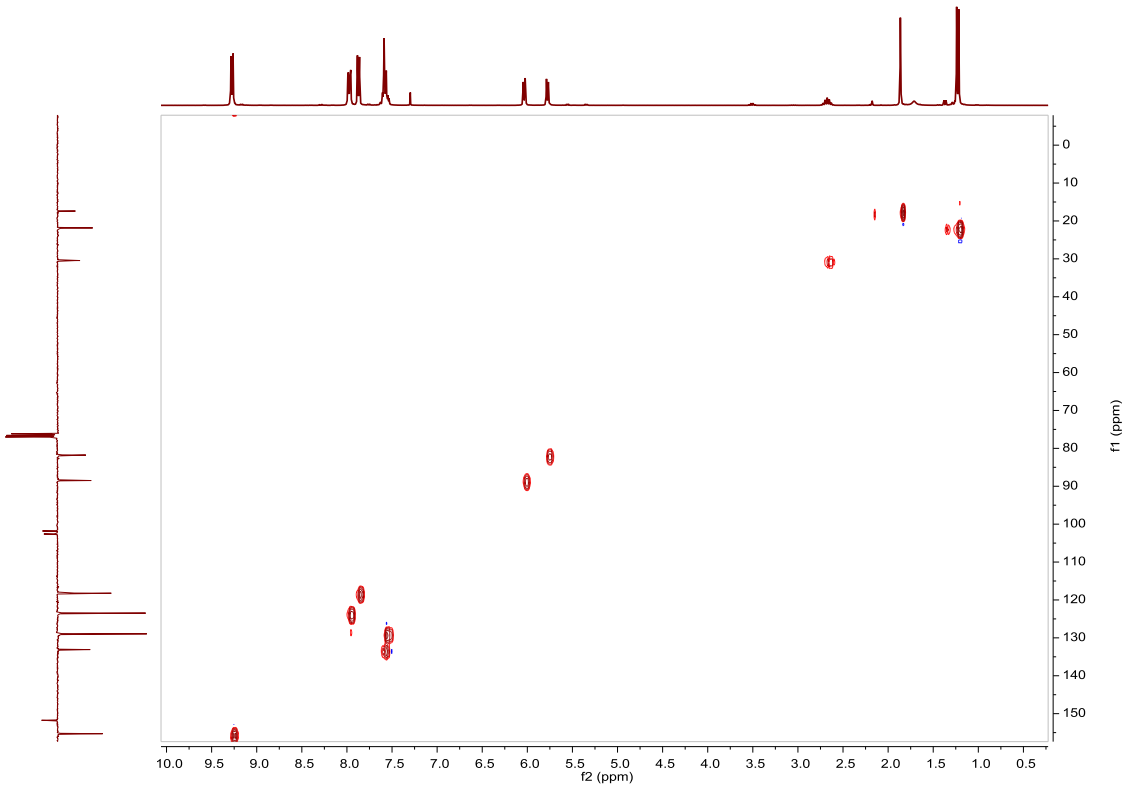

Fig. S361. HSQC NMR spectrum of **[Ru(p-Cym)(4-phenylazopyridine)$_2$(Cl)]PF$_6$** in $CDCl_3$.

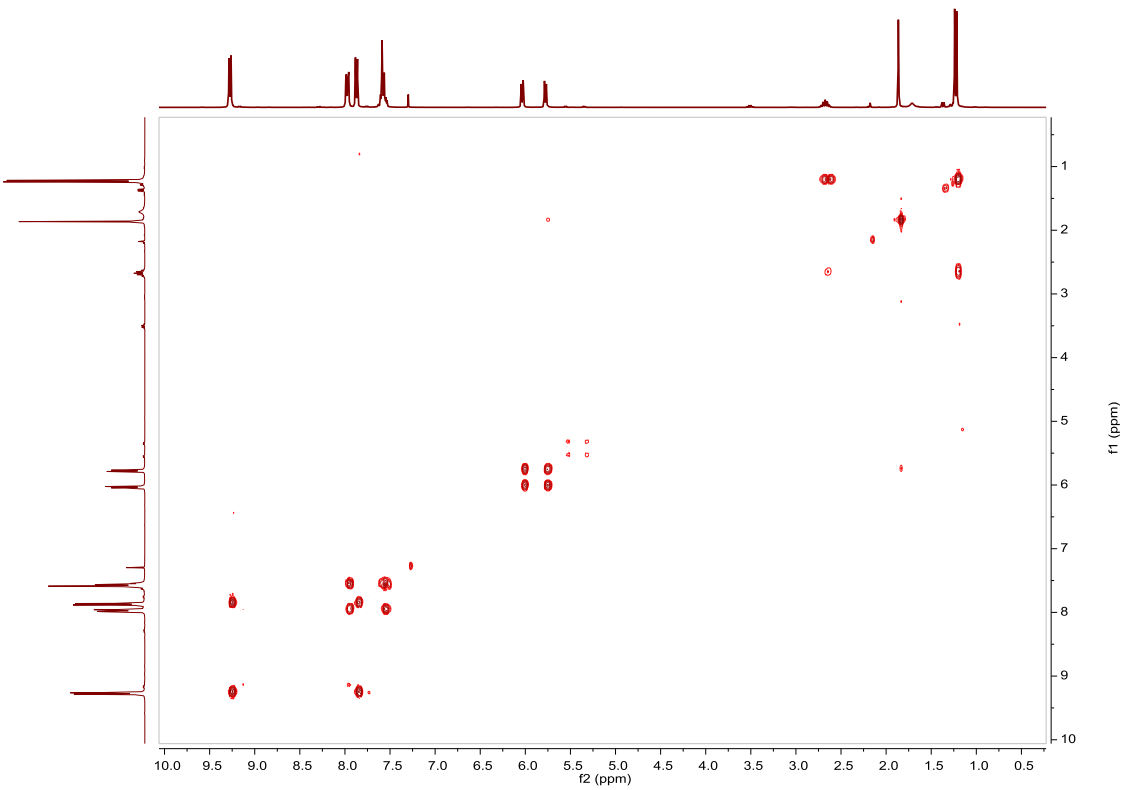

Fig. S362. COSY NMR spectrum of **[Ru(p-Cym)(4-phenylazopyridine)$_2$(Cl)]PF$_6$** in $CDCl_3$.

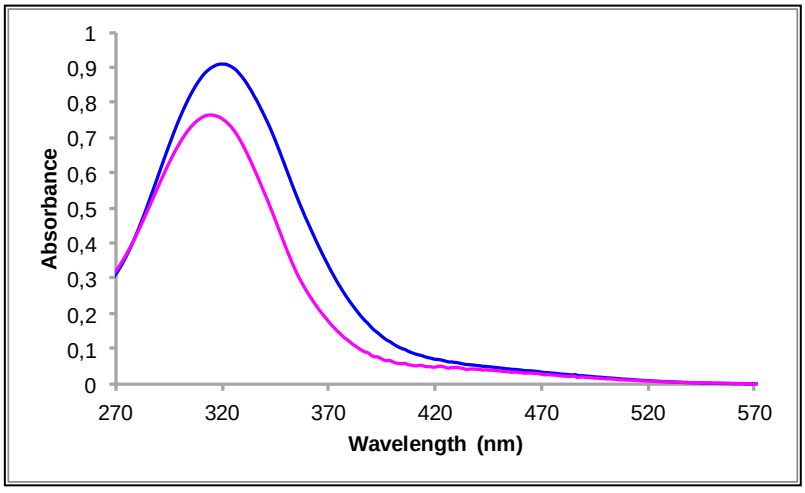

Fig. S363. UV/Vis spectra of **[Ru(p-Cym)(4-phenylazopyridine)$_2$(Cl)]PF$_6$** in ACN. Before (blue line) and after (pink line) irradiation at 347nm, $2.50 \cdot 10^{-5}$M.

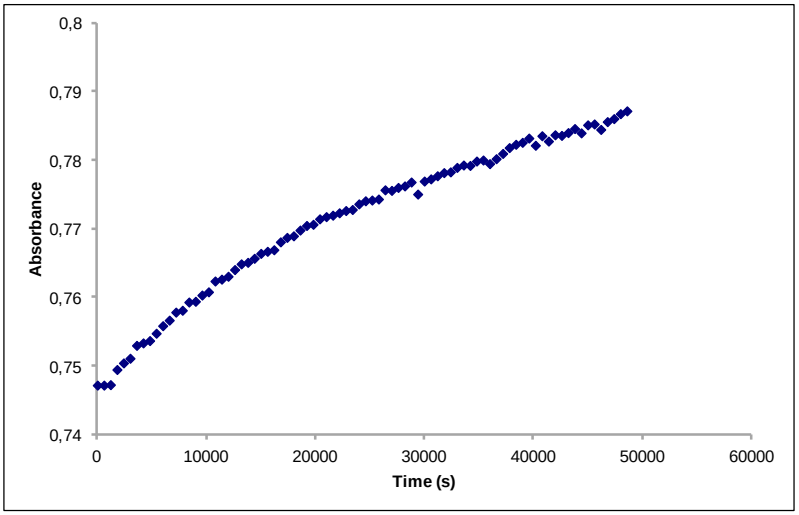

Fig. S364. Cis to trans thermal isomerization kinetics of **[Ru(p-Cym)(4-phenylazopyridine)$_2$(Cl)]PF$_6$**. Absorption change of the band 320nm at 338 K in ACN after irradiation at 347 nm. ($2.50\cdot10^{-5}$M).

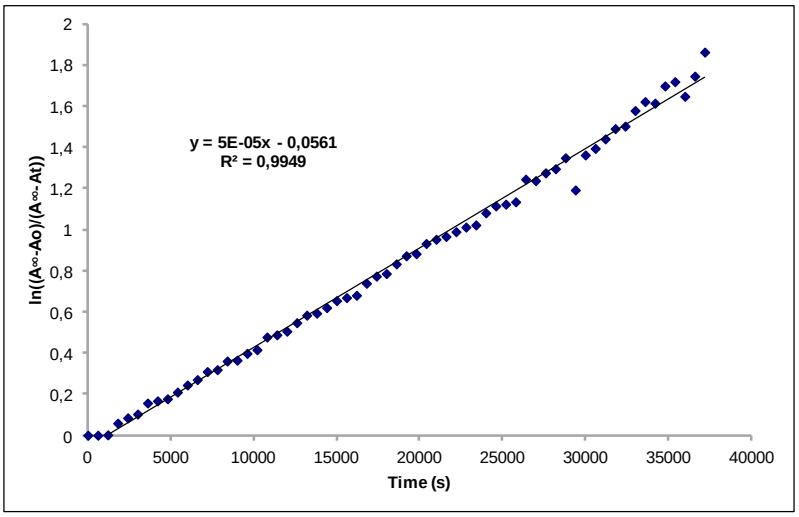

Fig. S365. Cis to trans thermal isomerization kinetics of **[Ru(p-Cym)(4-phenylazopyridine)$_2$(Cl)]PF$_6$**. First-order plot. k (s^{-1}) = $5.0\cdot10^{-5}$. Half-life (min) = 231.

Compound [Ru(p-Cym)(pyridine)$_1$(Cl)$_2$]. Synthesis and characterization.

SYNTHESIS

Under a N_2 atmosphere, Ru_2(p-Cym)$_2Cl_4$ (0.2 g, 0.32 mmol) and pyridine (53 µL, 0.65 mmol) were dissolved in 20 mL of acetone. The reaction mixture was refluxed for 15 h. It was cooled to room temperature, the solvent was evaporated and the product was obtained as an orange solid. Yield 89%. The spectroscopic data are coincident with those described in the literature.[43]

^{1}H NMR (300 MHz, CDCl$_3$): δ 9.09 (brdd, J = 1.5 Hz, J = 6.5 Hz, 2H, (2+6)), 7.78 (tt, J = 1.5 Hz, J = 7.6 Hz, 1H, (4)), 7.35 (t, J = 6.5 Hz, 2H, (3+5)), 5.48 (d, J = 5.9 Hz, 2H, (8)), 5.26 (d, J = 5.9 Hz, 2H, (7)), 3.04 (sep, J = 6.9 Hz, 1H, (11)), 2.14 (s, 3H, (13)), 1.35 (d, J = 6.9 Hz, 6H, (12)).

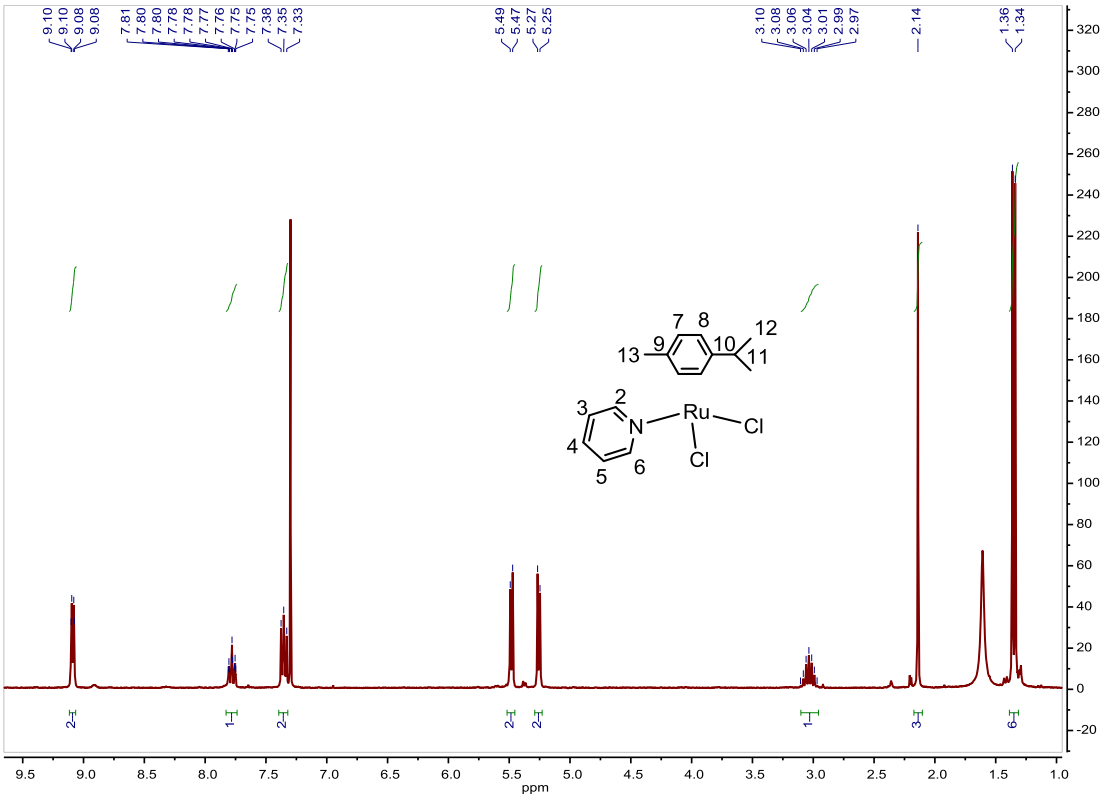

Fig. S366. ^{1}H NMR spectrum of **[Ru(p-Cym)(pyridine)$_1$(Cl)$_2$]** in $CDCl_3$, 300 MHz.

[43] C. A. Vock, C. Scolaro, A. D. Phillips, R. Scopelliti, G. Sava and P. J. Dyson, *J. Med. Chem.*, **2006**, *49*, 5552–5561.

Compound [Ru(p-Cym)(pyridine)$_2$(Cl)]PF$_6$. Synthesis and characterization.

SYNTHESIS[42]

Under a N_2 atmosphere, [Ru(p-Cym)(pyridine)(Cl_2)] (0.218 g, 0.566 mmol) and AgPF6 (0.142 g, 0.566 mmol) were dissolved in 15 mL of acetone and 15 mL of methanol. The mixture was stirred for 1 h, AgCl was removed by filtration and pyridine (0.05 mL, 0.623 mmol) were added. The reaction mixture was stirred for 4 h and the solvent was evaporated. The product was obtained as a yellow solid after precipitation with CH_2Cl_2/ether. Yield 45%.

Elemental Analysis: calculated for ($C_{20}H_{24}ClN_2RuPF_6 \cdot CH_2Cl_2$): C, 38.28; H, 3.98; N, 4.25. Found: C, 38.14; H, 4.00; N, 4.21.

Exact Mass: ESI-MS $[C_{15}H_{19}ClNRu]^+$ (M-L-PF_6): calculated: m/z= 350.0250, found: m/z= 350.0243.

^{1}H NMR (300 MHz, $CDCl_3$): δ 9.09 (brdd, J = 1.6 Hz, J = 6.6 Hz, 4H, (2+6)), 7.87 (tt, J = 1.5 Hz, J = 7.6 Hz, 2H, (4)), 7.54–7.47 (m, 4H, (3+5)), 5.94 (d, J = 6.1 Hz, 2H, (8)), 5.66 (d, J = 6.1 Hz, 2H, (7)), 2.59 (sep, J = 6.9 Hz, 1H, (11)), 1.76 (s, 3H, (13)), 1.19 (d, J = 6.9 Hz, 6H, (12)).

^{13}C NMR (75 MHz, $CDCl_3$): δ 154.14 (4CH, (2+6)), 139.03 (2CH, (4)), 126.23 (4CH, (3+5)), 102.72 (C_{quat}, (p-Cym)), 101.96 (C_{quat}, (p-Cym)), 88.71 (2CH, (8)), 81.97 (2CH, (7)), 30.83 (CH, (11)), 22.25 ($2CH_3$, (12)), 17.68 (CH_3, (13)).

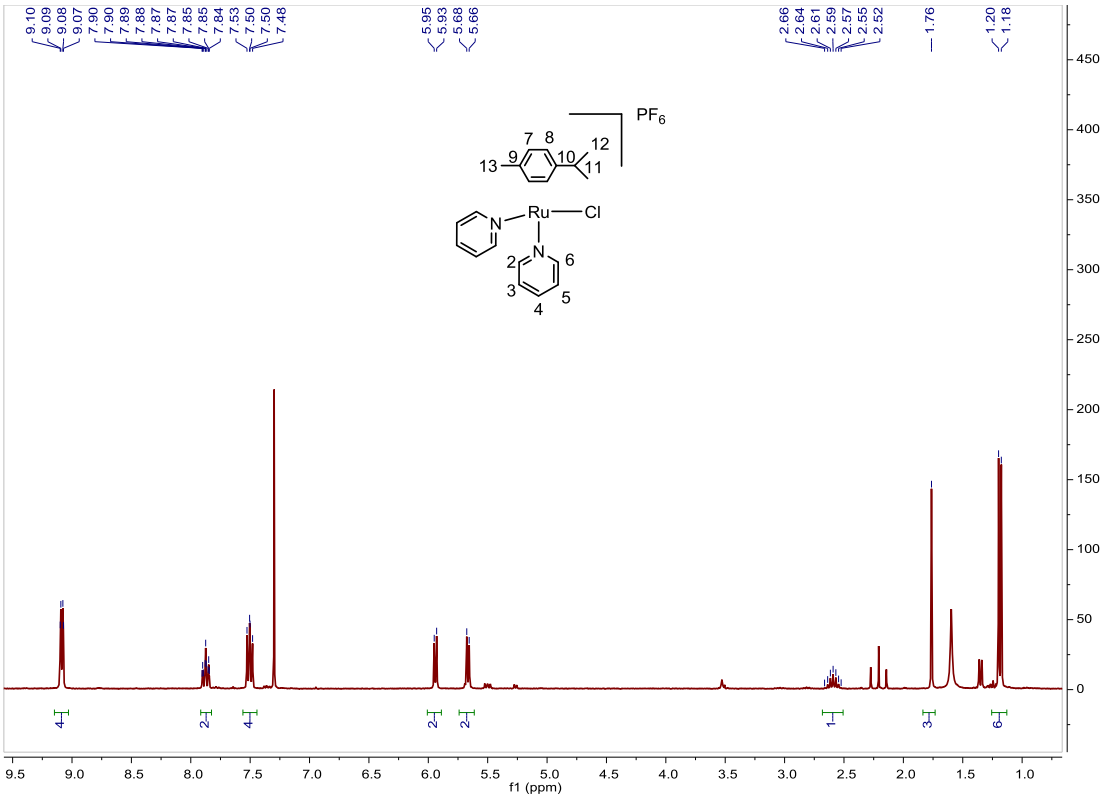

Fig. S367. ^{1}H NMR spectrum of **[Ru(p-Cym)(pyridine)$_2$(Cl)]PF$_6$** in $CDCl_3$, 300 MHz.

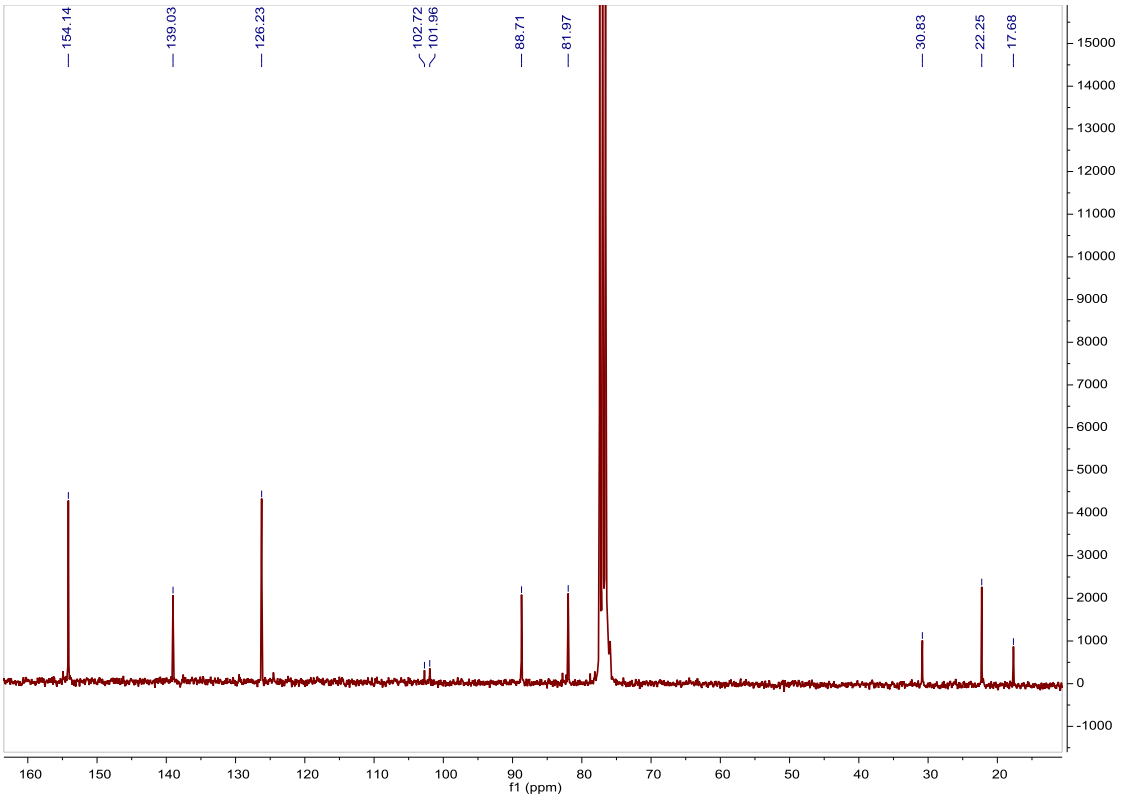

Fig. S368. ^{13}C NMR spectrum of **[Ru(p-Cym)(pyridine)$_2$(Cl)]PF$_6$** in $CDCl_3$, 75 MHz.

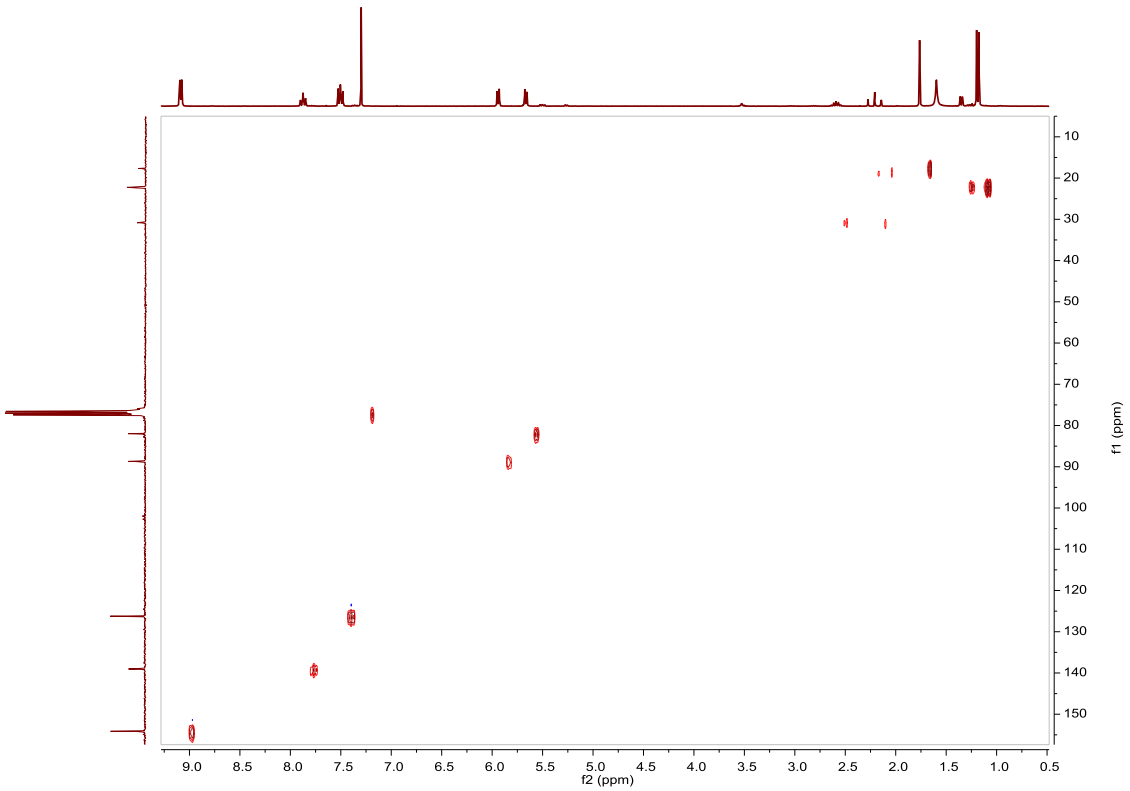

Fig. S369. HSQC NMR spectrum of **[Ru(p-Cym)(pyridine)$_2$(Cl)]PF$_6$** in $CDCl_3$.

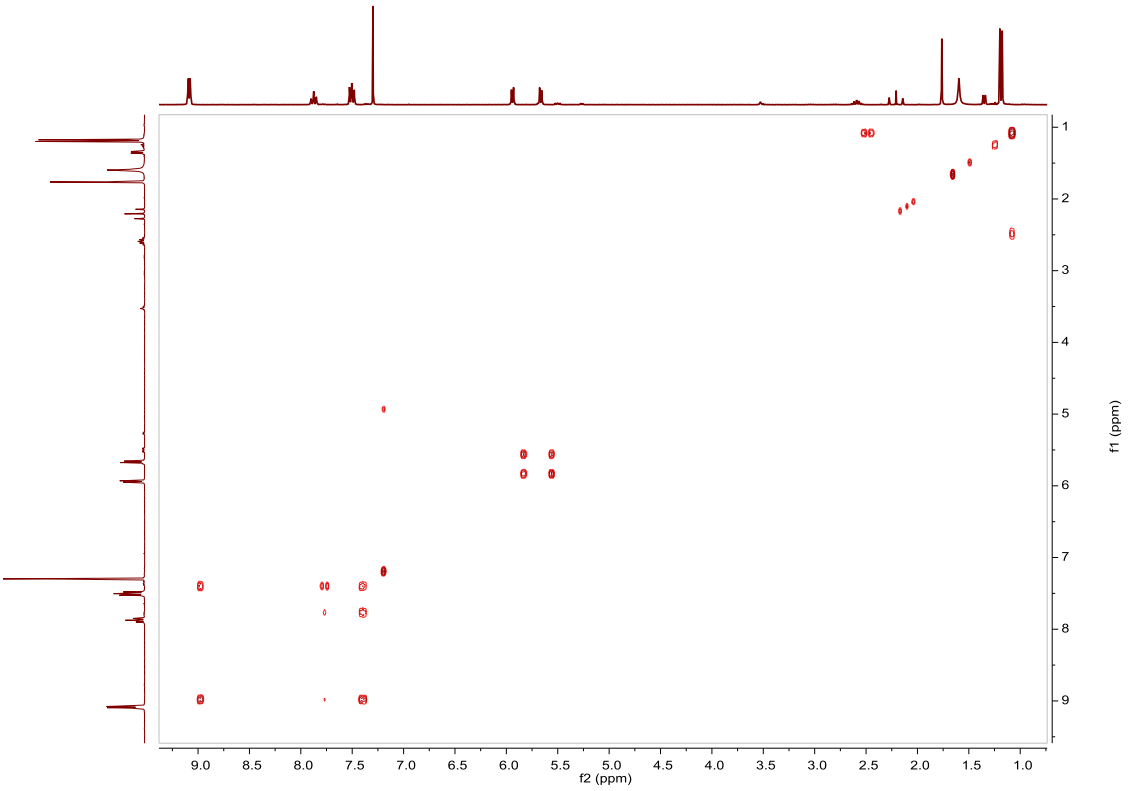

Fig. S370. COSY NMR spectrum of **[Ru(p-Cym)(pyridine)$_2$(Cl)]PF$_6$** in $CDCl_3$.

Compound [Ru(p-Cym)(4,4'-bis(*p*-azobenzene)-2,2'-bipyridine)(Cl)]Cl. Synthesis, characterization and photoisomerization studies.

SYNTHESIS

Under a N_2 atmosphere, $Ru_2(p\text{-}Cym)_2Cl_4$ (0.100 g, 0.163 mmol) and 4,4'-bis(*p*-azobenzene)-2,2'-bipyridine (0.168 g, 0.326 mmol) were dissolved in 10 mL of acetone. The reaction mixture was refluxed for 15 h. It was cooled to room temperature and the dark red solid was filtered. Yield 70%.

Elemental Analysis: calculated for ($C_{44}H_{38}Cl_2N_6Ru$): C, 64.23; H, 4.66; N, 10.21. Found: C, 63.79; H, 4.70; N, 10.13.

Exact Mass: ESI-MS $[C_{44}H_{38}ClN_6Ru]^+$: calculated: m/z= 787.1890, found: m/z= 787.1917.

^{1}H NMR (300 MHz, $CDCl_3$): δ 9.88 (brd, J = 5.5 Hz, 2H, (bipy)), 8.62 (s, 2H, (bipy)), 8.00 (m, 10H, (bipy)), 7.91 (brd, J = 7.9 Hz, 4H, (bipy)), 7.58–7.45 (m, 6H, (bipy)), 6.29 (d, J = 5.6 Hz, 2H, (8)), 6.16 (d, J = 5.4 Hz, 2H, (7)), 2.72 (sep, J = 6.8 Hz, 1H, (11)), 2.28 (s, 3H, (13)), 1.06 (d, J = 6.8 Hz, 6H, (12)).

^{13}C APT NMR (75 MHz, $CDCl_3$): δ 156.48 (2CH, (bipy)), 154.32 ($2C_{quat}$, (bipy)), 153.08 ($2C_{quat}$, (bipy)), 151.98 ($2C_{quat}$, (bipy)), 149.70 ($2C_{quat}$, (bipy)), 136.44 ($2C_{quat}$, (bipy)), 131.20(2CH, (bipy)), 128.70 (4CH, (bipy)), 128.11 (4CH, (bipy)), 125.02 (2CH, (bipy)), 123.35 (4CH, (bipy)), 122.66 (4CH, (bipy)), 120.27 (2CH, (bipy)), 104.46 (C_{quat}, (p-Cym)), 103.47 (C_{quat}, (p-Cym)), 86.87 (2CH, (8)), 84.38 (2CH, (7)), 30.66 (CH, (11)), 21.79 ($2CH_3$, (12)) 18.59 (CH_3, (13)).

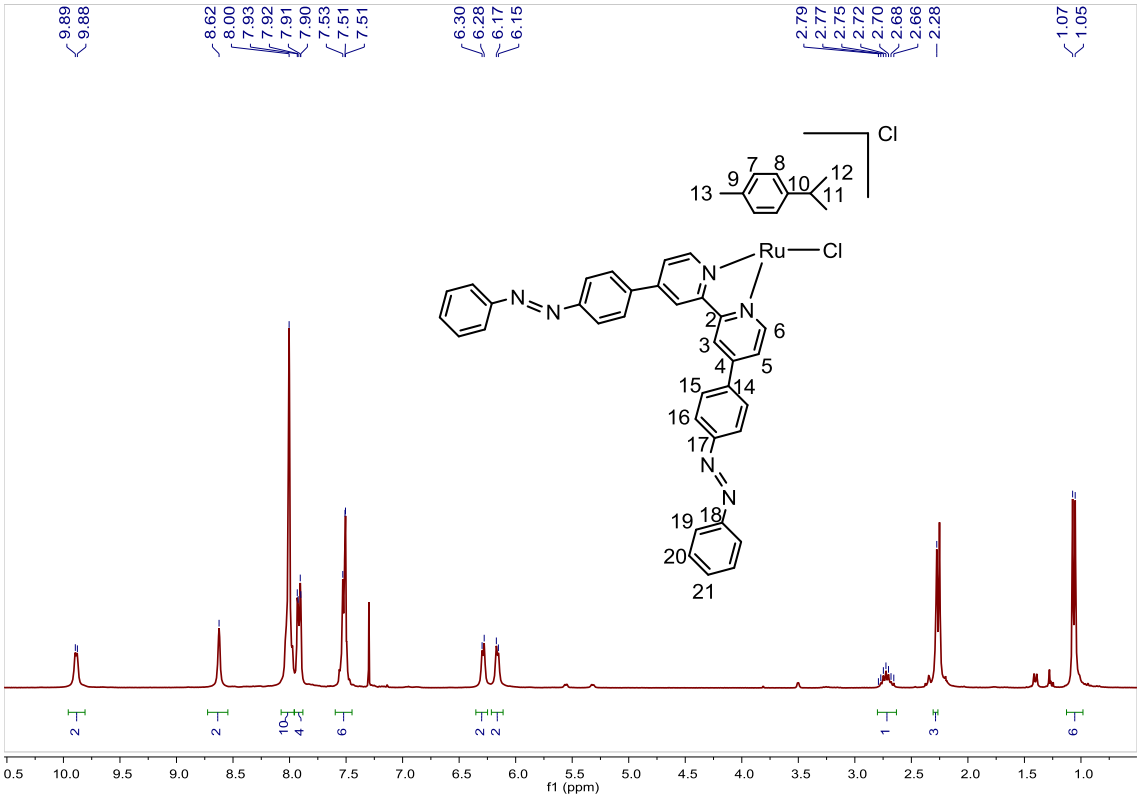

Fig. S371. ^{1}H NMR spectrum of **[Ru(p-Cym)(4,4'-bis(*p*-azobenzene)-2,2'-bipyridine)(Cl)]Cl** in $CDCl_3$, 300 MHz.

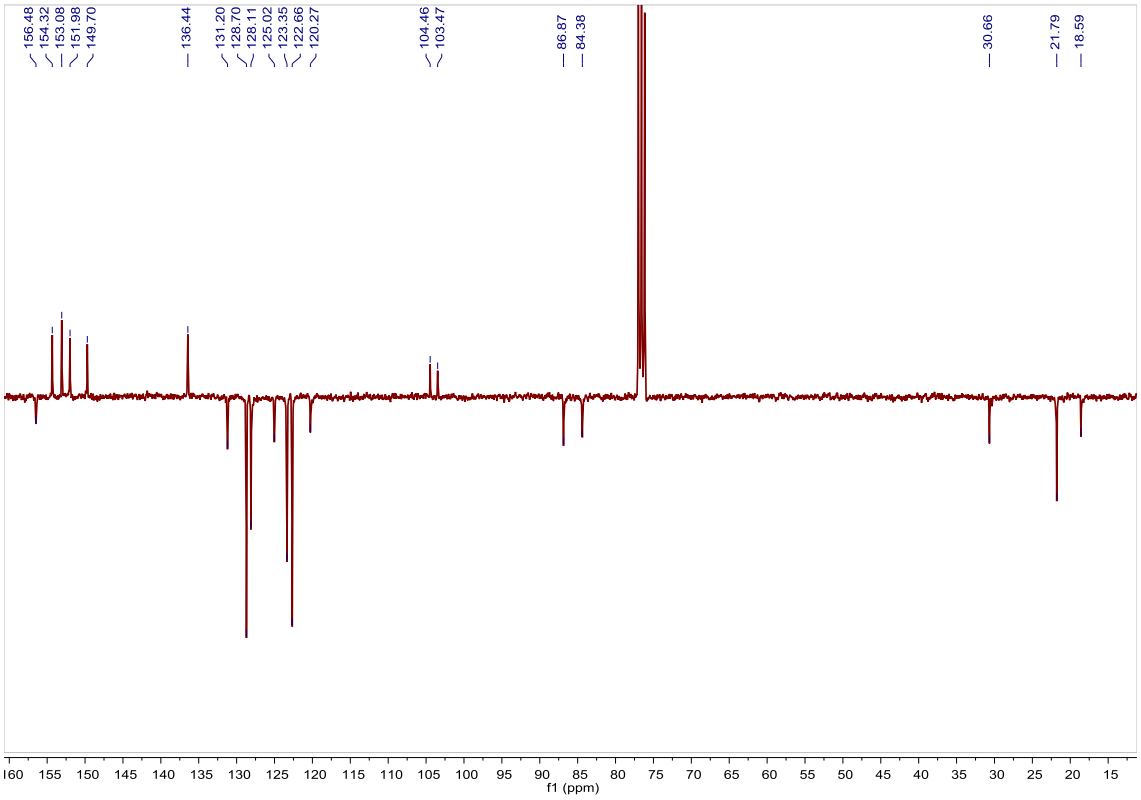

Fig. S372. ^{13}C APT NMR spectrum of **[Ru(p-Cym)(4,4'-bis(*p*-azobenzene)-2,2'-bipyridine)(Cl)]Cl** in $CDCl_3$, 75 MHz.

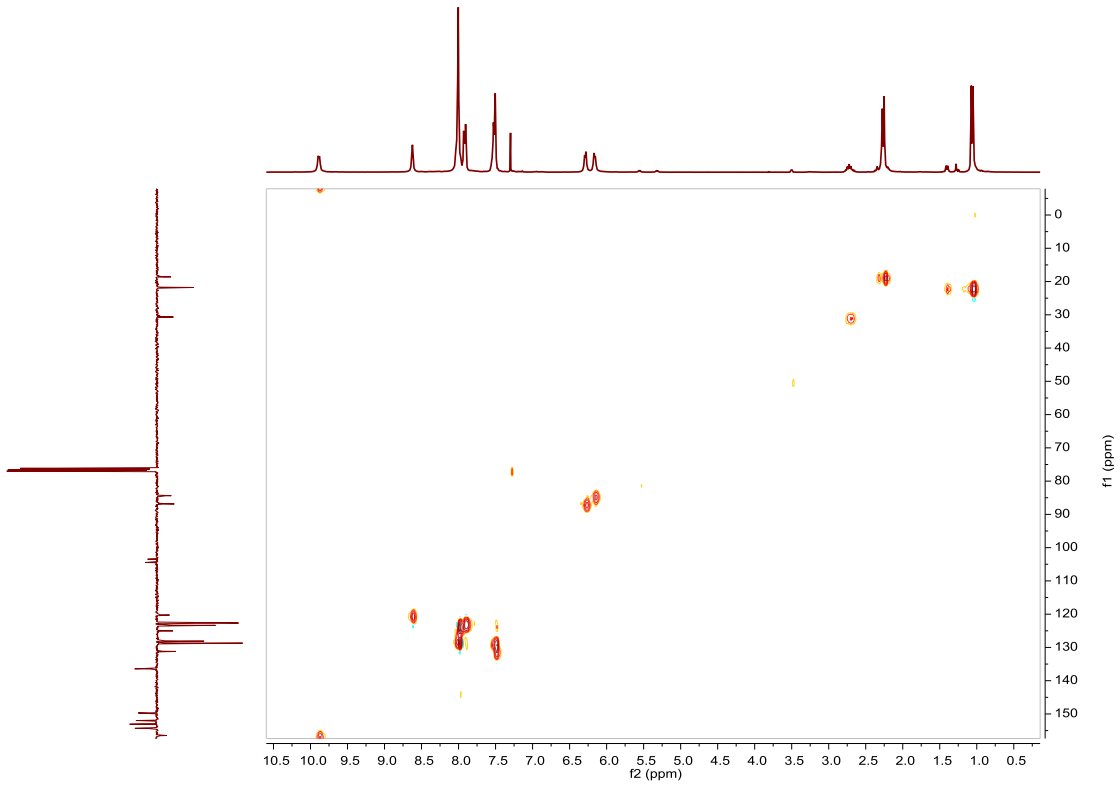

Fig. S373. HSQC spectrum of **[Ru(p-Cym)(4,4'-bis(*p*-azobenzene)-2,2'-bipyridine)(Cl)]Cl** in $CDCl_3$.

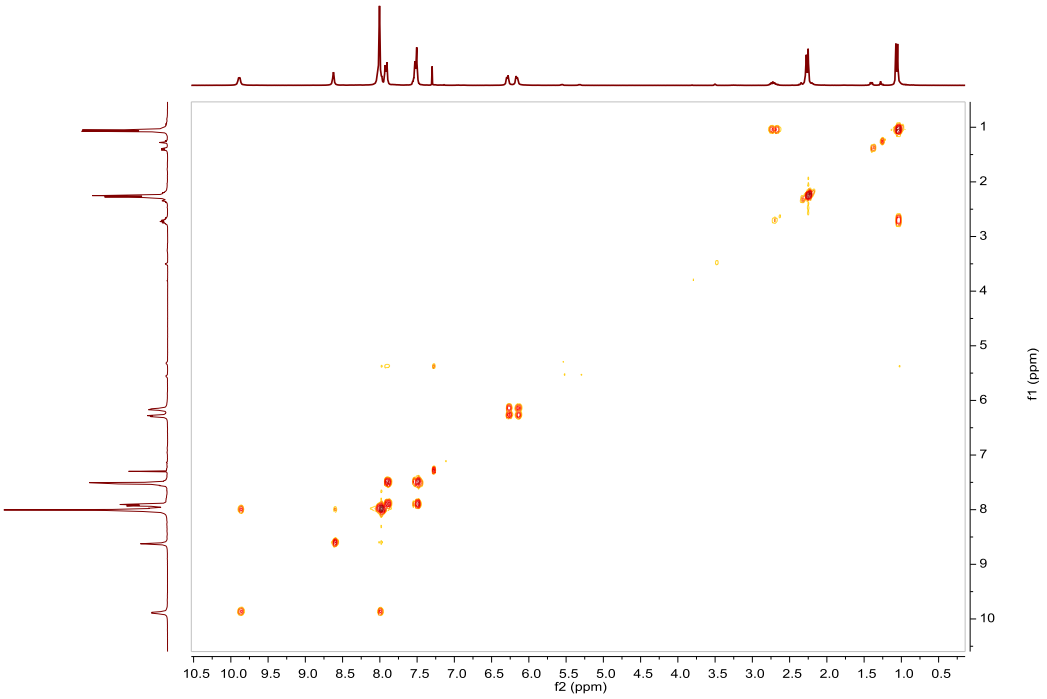

Fig. S374. COSY spectrum of **[Ru(p-Cym)(4,4'-bis(*p*-azobenzene)-2,2'-bipyridine)(Cl)]Cl** in $CDCl_3$.

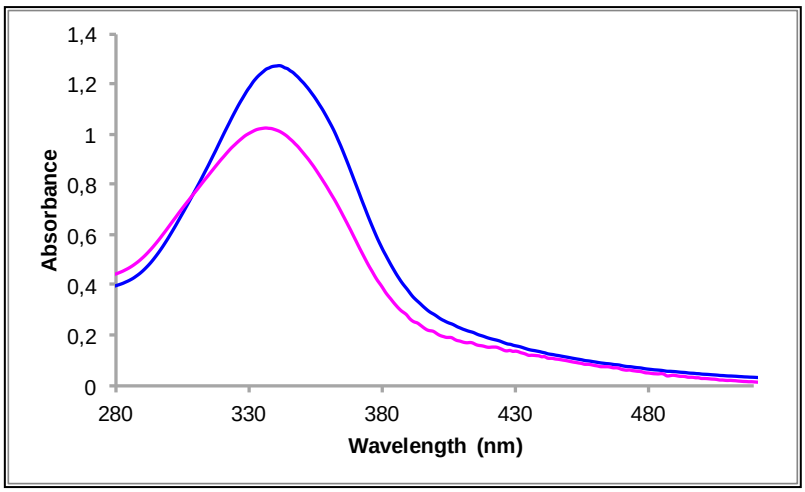

Fig. S375. UV/Vis spectra of **[Ru(p-Cym)(4,4'-bis(*p*-azobenzene)-2,2'-bipyridine)(Cl)]Cl** in ACN. Before (blue line) and after (pink line) irradiation at 350nm, $2.54 \cdot 10^{-5}$M.

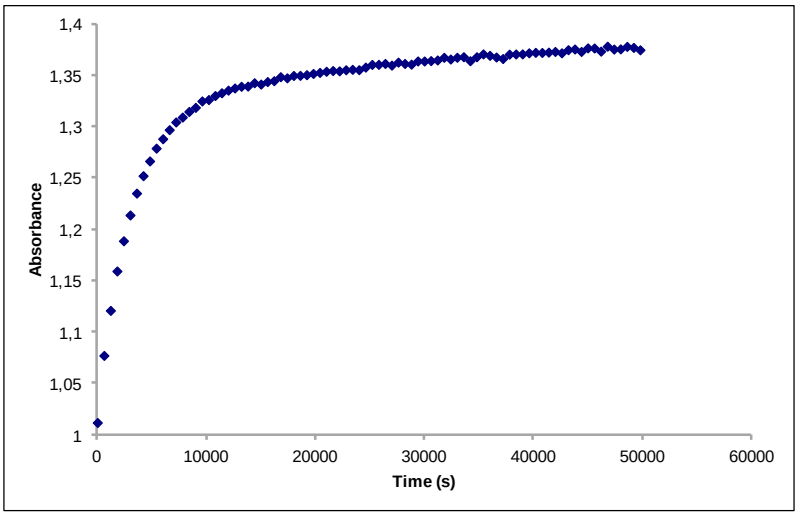

Fig. S376. Cis to trans thermal isomerization kinetics of **[Ru(p-Cym)(4,4'-bis(*p*-azobenzene)-2,2'-bipyridine)(Cl)]Cl**. Absorption change of the band 341nm at 338 K in ACN after irradiation at 350 nm. ($2.54 \cdot 10^{-5}$M).

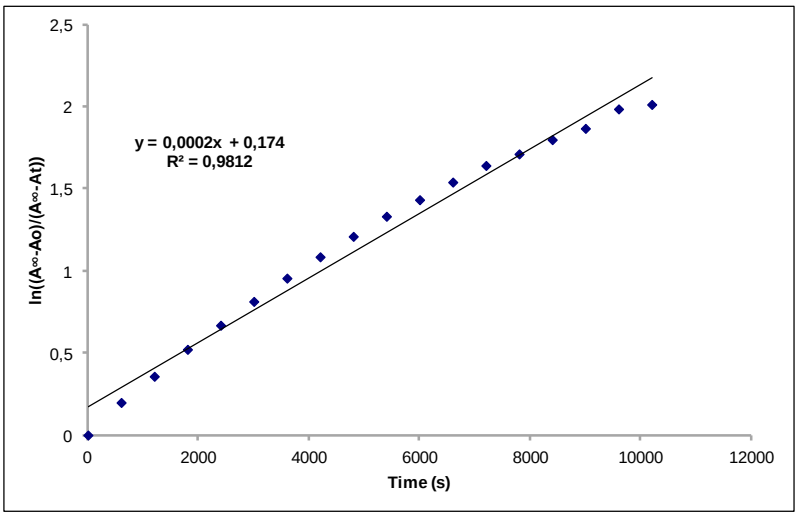

Fig. S377. Cis to trans thermal isomerization kinetics of **[Ru(p-Cym)(4,4'-bis(*p*-azobenzene)-2,2'-bipyridine)(Cl)]Cl**. First-order plot. k (s^{-1}) = $2.0 \cdot 10^{-4}$. Half-life (min) = 58.

Compound [Ru(p-Cym)(4-(*p*-azobenzene)-4'-bromo-2,2'-bipyridine)(Cl)]Cl. Synthesis, characterization and photoisomerization studies.

SYNTHESIS

Under a N_2 atmosphere, $Ru_2(p\text{-}Cym)_2Cl_4$ (0.100 g, 0.163 mmol) and 4-(*p*-azobenzene)-4'-bromo-2,2'-bipyridine (0.135 g, 0.326 mmol) were dissolved in 10 mL of acetone. The reaction mixture was refluxed for 15 h. It was cooled to room temperature and the solid was filtered. The desired compound was obtained after precipitated with CH_2Cl_2/Et_2O as an orange solid Yield 65%.

Elemental Analysis: calculated for ($C_{32}H_{29}BrCl_2N_4Ru{\cdot}CH_2Cl_2$): C, 49.15; H, 3.87; N, 6.95. Found: C, 49.04; H, 3.80; N, 6.77.

Exact Mass: ESI-MS $[C_{32}H_{29}BrClN_4Ru]^+$: calculated: m/z= 685.0308, found: m/z= 685.0334.

^{1}H NMR (300 MHz, MeOD *d_4*): δ 9.39 (d, J = 6.0 Hz, 1H, (bipy)), 9.20 (d, J = 6.1 Hz, 1H, (bipy)), 8.92 (brd, J = 1.8 Hz, 1H, (bipy)), 8.76 (brd, J = 1.5 Hz, 1H, (bipy)), 8.12–7.94 (m, 5H, (bipy)), 7.93–7.80 (m, 3H, (bipy)), 7.52–7.40 (m, 3H, (bipy)), 6.04 (m, 2H, (8+8')), 5.80 (m, 2H, (7+7')), 2.59 (sep, J = 6.9 Hz, 1H, (11)), 2.17 (s, 3H, (13)), 0.99 (d, J = 6.8 Hz, 6H, (12)).

^{13}C APT NMR (75 MHz, MeOD *d_4*): δ 157.24 (C_{quat}, (bipy)), 157.11 (CH, (bipy)), 156.98 (CH, (bipy)), 155.79 (C_{quat}, (bipy)), 155.11 (C_{quat}, (bipy)), 153.96 (C_{quat}, (bipy)), 152.07 (C_{quat}, (bipy)), 138.53 (C_{quat}, (bipy)), 138.05 (C_{quat}, (bipy)), 132.97 (CH, (bipy)), 132.11 (CH, (bipy)), 130.41 (2CH, (bipy)), 129.85 (2CH, (bipy)), 128.83 (CH, (bipy)), 126.43 (CH, (bipy)), 124.77 (2CH, (bipy)), 124.08 (2CH, (bipy)), 122.93 (CH, (bipy)), 106.64 (Cquat, (p-Cym)), 105.62 (Cquat, (p-Cym)), 88.21 (CH, (8 or 8')), 88.00 (CH, (8 or 8')), 85.87 (CH, (7 or 7')), 85.68 (CH, (7 or 7')), 32.41 (CH, (11)), 22.37 ($2CH_3$, (12)), 18.97 (CH_3, (13)).

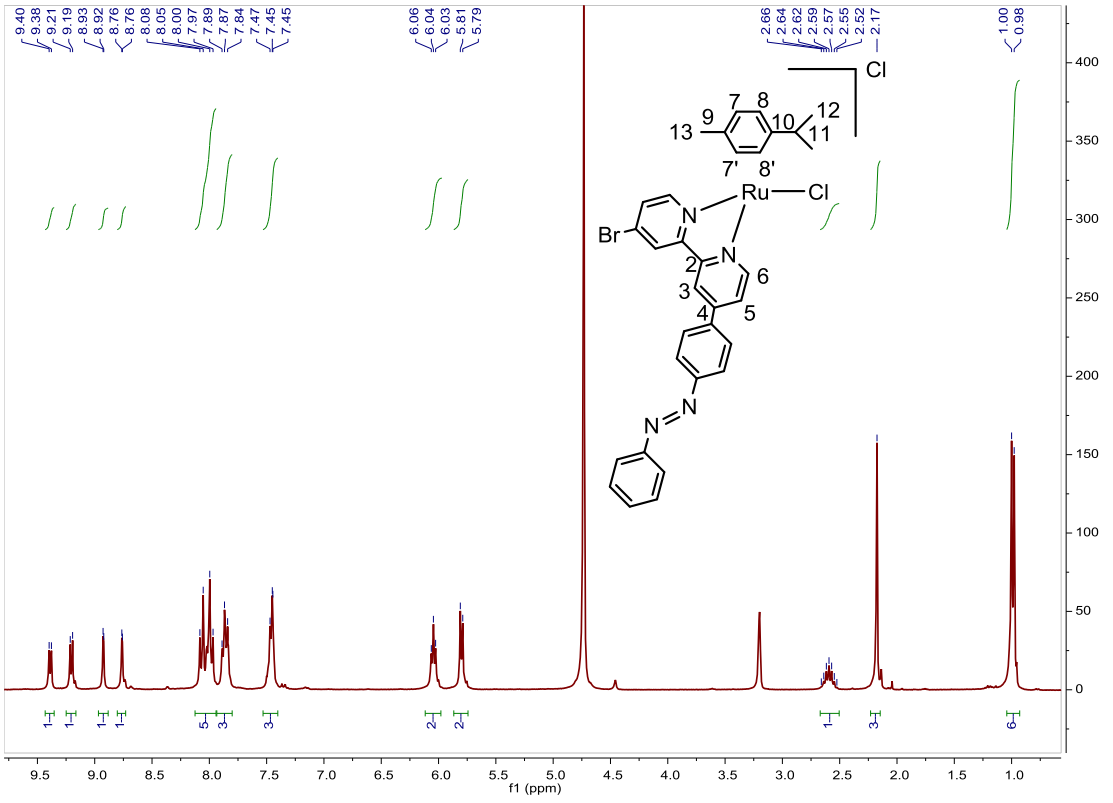

Fig. S378. ^{1}H NMR spectrum of **[Ru(p-Cym)(4-(*p*-azobenzene)-4'-bromo-2,2'-bipyridine)(Cl)]Cl** in MeOD-*d_4*, 300 MHz.

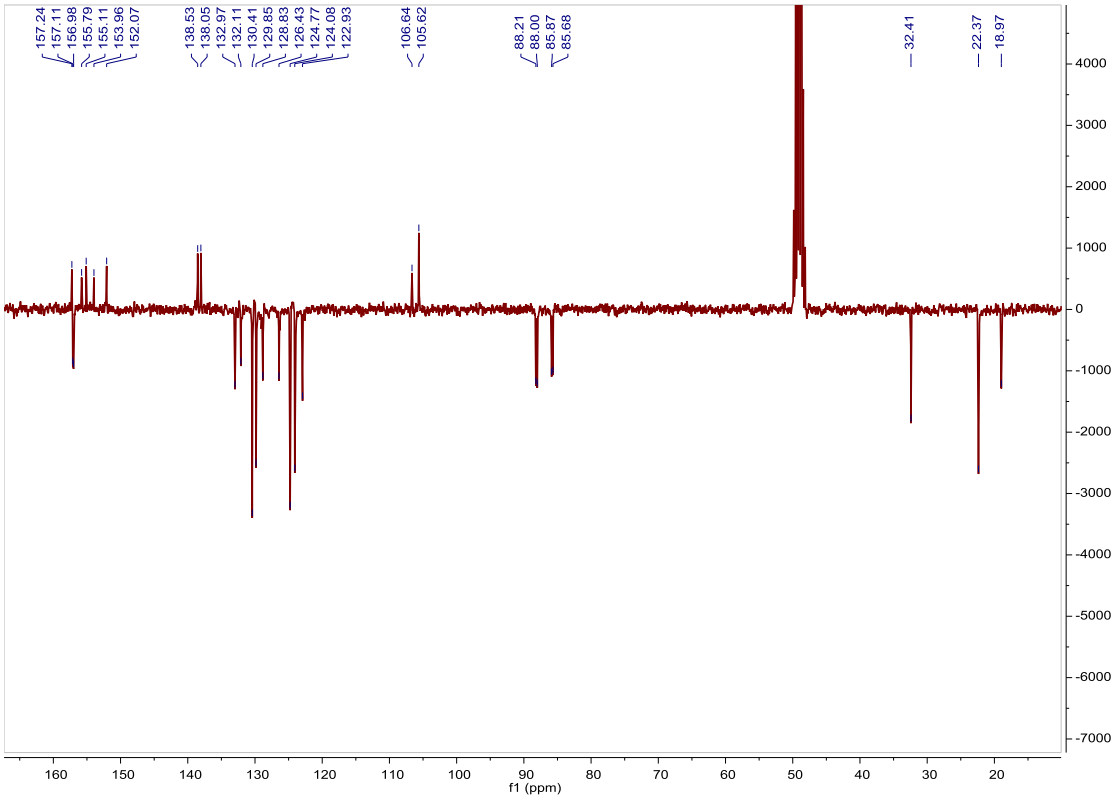

Fig. S379. ^{13}C APT NMR spectrum of **[Ru(p-Cym)(4-(*p*-azobenzene)-4'-bromo-2,2'-bipyridine)(Cl)]Cl** in MeOD-d_4, 75 MHz.

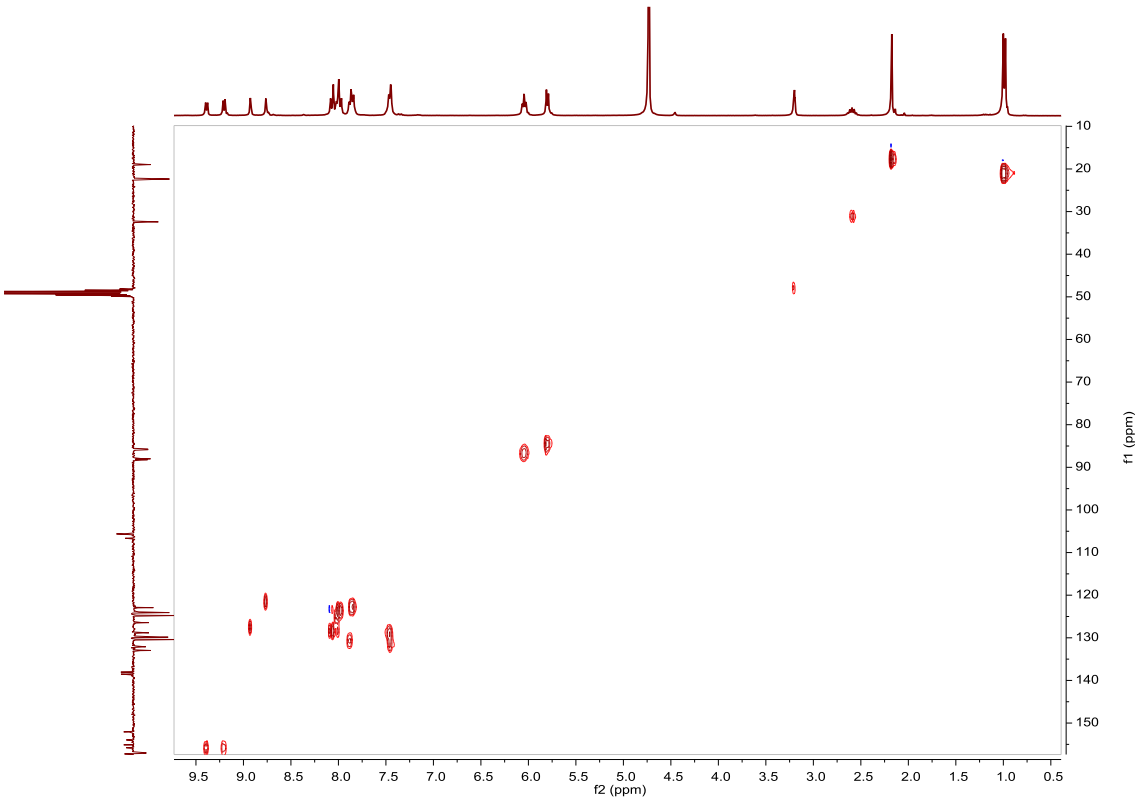

Fig. S380. HSQC NMR spectrum of **[Ru(p-Cym)(4-(*p*-azobenzene)-4'-bromo-2,2'-bipyridine)(Cl)]Cl** in MeOD-d_4.

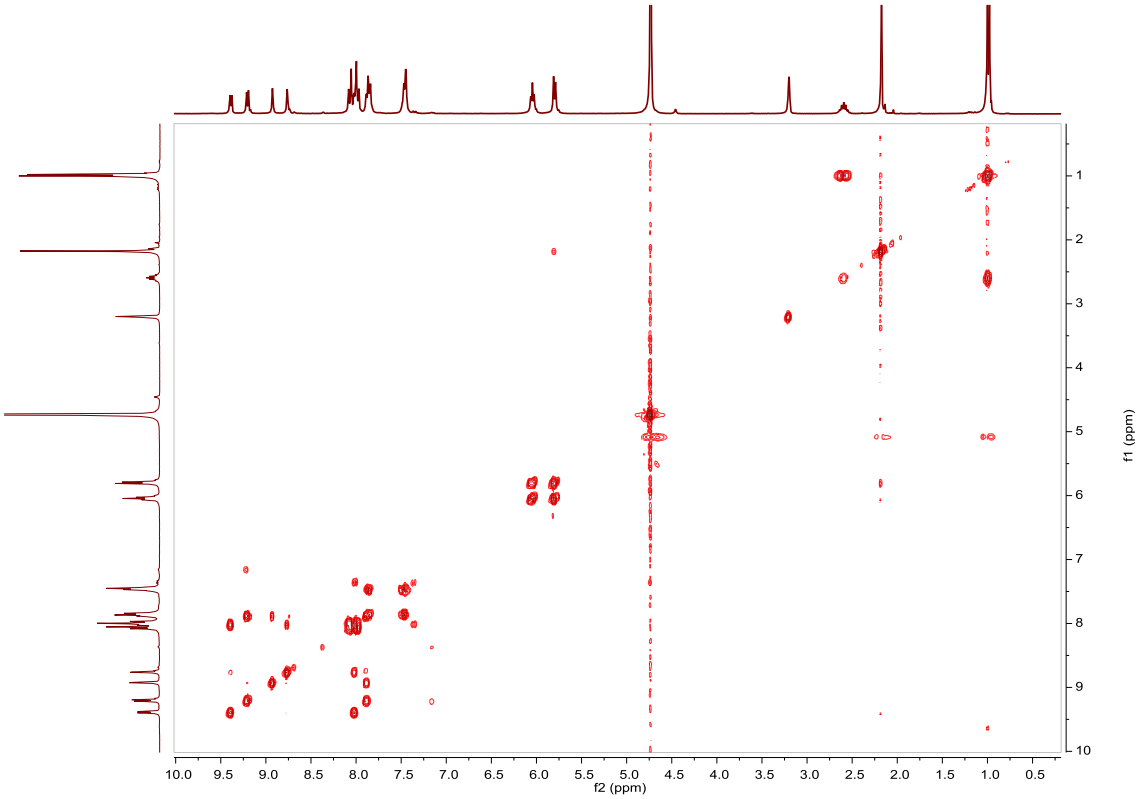

Fig. S381. COSY NMR spectrum of **[Ru(p-Cym)(4-(*p*-azobenzene)-4'-bromo-2,2'-bipyridine)(Cl)]Cl** in MeOD-d_4.

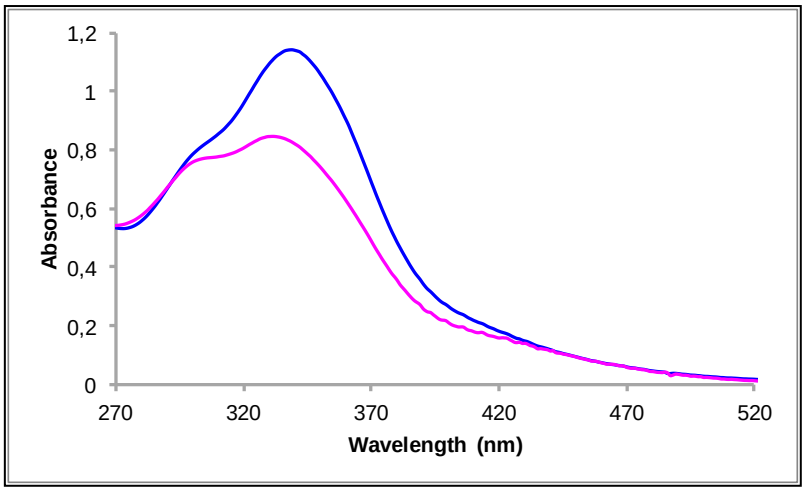

Fig. S382. UV/Vis spectra of **[Ru(p-Cym)(4-(*p*-azobenzene)-4'-bromo-2,2'-bipyridine)(Cl)]Cl** in ACN. Before (blue line) and after (pink line) irradiation at 344nm, $3.09 \cdot 10^{-5}$M.

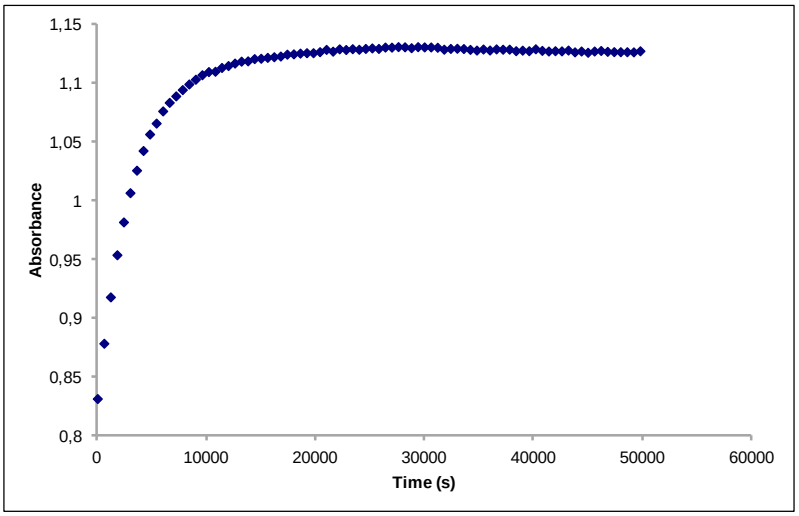

Fig. S383. Cis to trans thermal isomerization kinetics of **[Ru(p-Cym)(4-(*p*-azobenzene)-4'-bromo-2,2'-bipyridine)(Cl)]Cl**. Absorption change of the band 338nm at 338 K in ACN after irradiation at 344 nm. ($3.09 \cdot 10^{-5}$M).

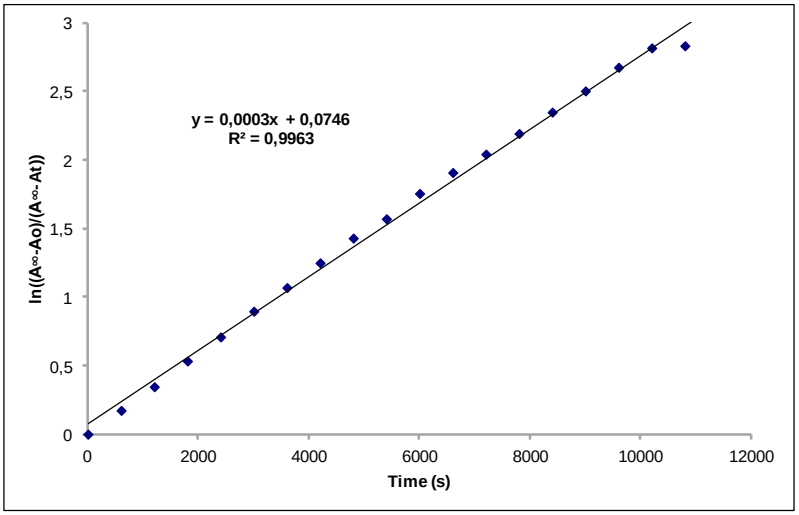

Fig. S384. Cis to trans thermal isomerization kinetics of **[Ru(p-Cym)(4-(*p*-azobenzene)-4'-bromo-2,2'-bipyridine)(Cl)]Cl**. First-order plot. k (s^{-1}) = $3.0 \cdot 10^{-4}$. Half-life (min) = 38.

Compound [Ru(p-Cym)(4,4'-bis(*m*-azobenzene)-2,2'-bipyridine)(Cl)]Cl. Synthesis, characterization and photoisomerization studies.

SYNTHESIS

Under a N_2 atmosphere, $Ru_2(p\text{-}Cym)_2Cl_4$ (0.100 g, 0.163 mmol) and 4,4'-bis(*m*-azobenzene)-2,2'-bipyridine (0.168 g, 0.326 mmol) were dissolved in 10 mL of acetone. The reaction mixture was refluxed for 15 h and ,4'-bis(*m*-azobenzene)-2,2'-bipyridine (0.168 g, 0.326 mmol) were added. It was refluxed for another 15 h. It was cooled to room temperature and the solid was filtered. The desired compound was obtained after precipitated with CH_2Cl_2/Et_2O as a brown solid. Yield 54%.

Elemental Analysis: calculated for ($C_{44}H_{38}Cl_2N_6Ru{\cdot}CH_2Cl_2$): C, 59.54; H, 4.44; N, 9.26. Found: C, 58.94; H, 4.43; N, 9.03.

Exact Mass: ESI-MS $[C_{44}H_{38}ClN_6Ru]^+$: calculated: m/z= 787.1890, found: m/z= 787.1920.

^{1}H NMR (300 MHz, $CDCl_3$): δ 9.98 (s, 2H, (bipy)), 8.51 (s, 2H, (bipy)), 8.26 (s, 2H, (bipy)), 8.13–7.86 (m, 10H, (bipy)), 7.71 (t, J = 7.2 Hz, 2H, (bipy)), 7.55–7.45 (m, 6H, (bipy)), 6.38 (s, 2H, (7 or 8)), 6.23 (s, 2H, (7 or 8)), 2.79 (m, 1H, (11)), 2.32 (s, 3H, (13)), 1.12 (d, J = 6.4 Hz, 6H, (12)).

^{13}C APT NMR (75 MHz, $CDCl_3$): δ 156.88 (2CH, (bipy)), 154.36 ($2C_{quat}$, (bipy)), 152.64 ($2C_{quat}$, (bipy)), 151.84 ($2C_{quat}$, (bipy)), 150.30 ($2C_{quat}$, (bipy)), 135.76 ($2C_{quat}$, (bipy)), 131.19 (2CH, (bipy)), 130.10 (2CH, (bipy)), 129.50 (2CH, (bipy)), 128.75 (4CH, (bipy)), 125.47 (2CH, (bipy)), 124.69 (2CH, (bipy)), 122.61 (4CH, (bipy)), 121.02 (2CH, (bipy)), 120.24 (2CH, (bipy)), 104.47 (Cquat, (p-Cym)), 103.84 (Cquat, (p-Cym)), 87.18 (2CH, (7 or 8)), 84.50 (2CH, (7 or 8)), 30.76 (CH, (11)), 21.86 ($2CH_3$, (12)), 18.72 (CH_3, (13)).

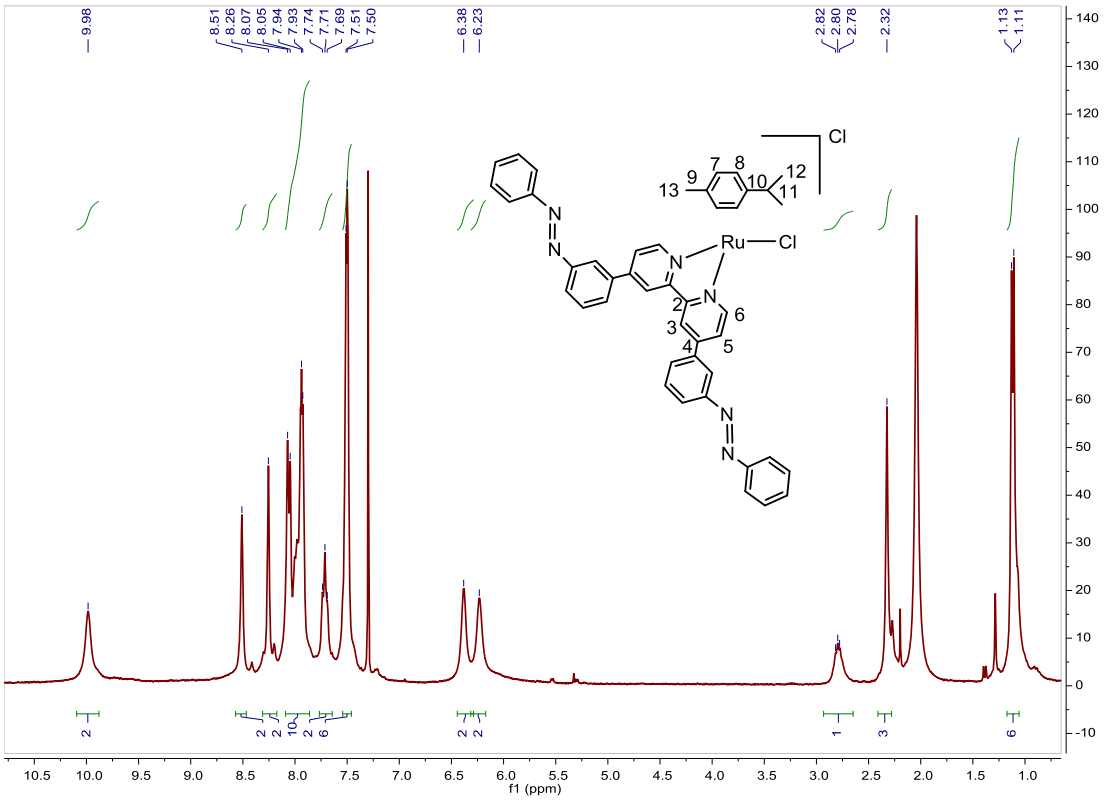

Fig. S385. ^{1}H NMR spectrum of **[Ru(p-Cym)(4,4'-bis(*m*-azobenzene)-2,2'-bipyridine)(Cl)]Cl** in $CDCl_3$, 300 MHz.

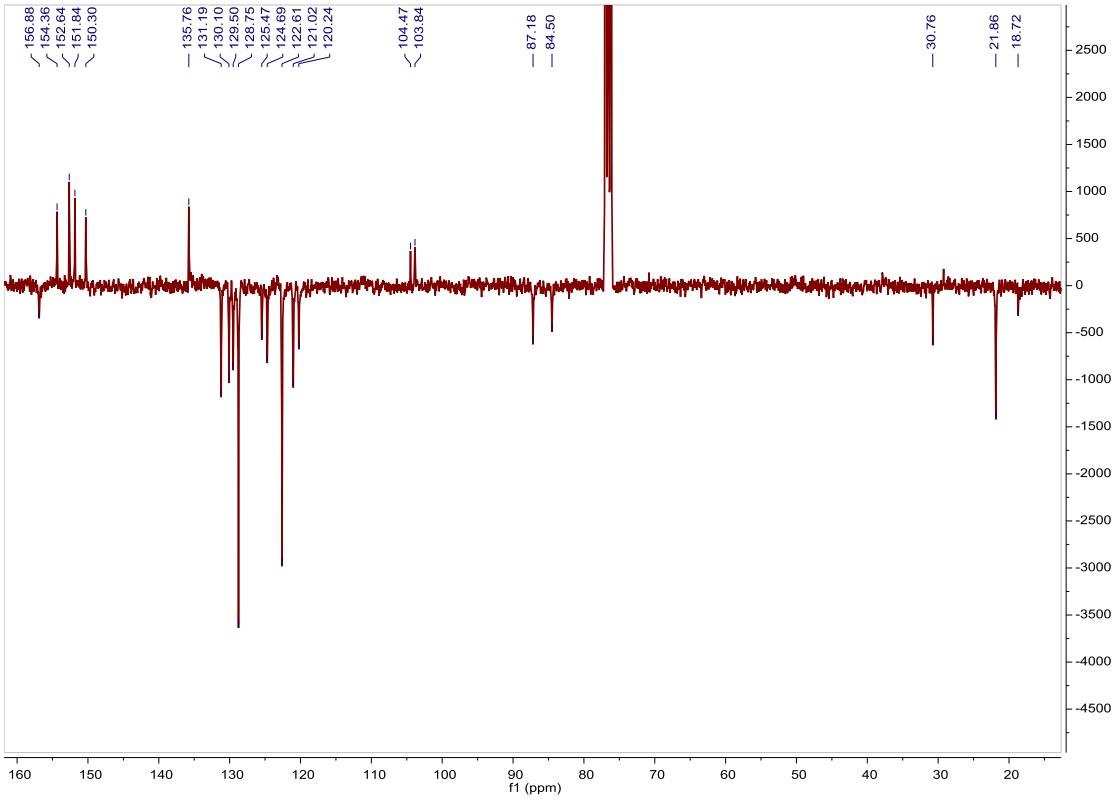

Fig. S386. ^{13}C APT NMR spectrum of **[Ru(p-Cym)(4,4'-bis(*m*-azobenzene)-2,2'-bipyridine)(Cl)]Cl** in $CDCl_3$, 75 MHz.

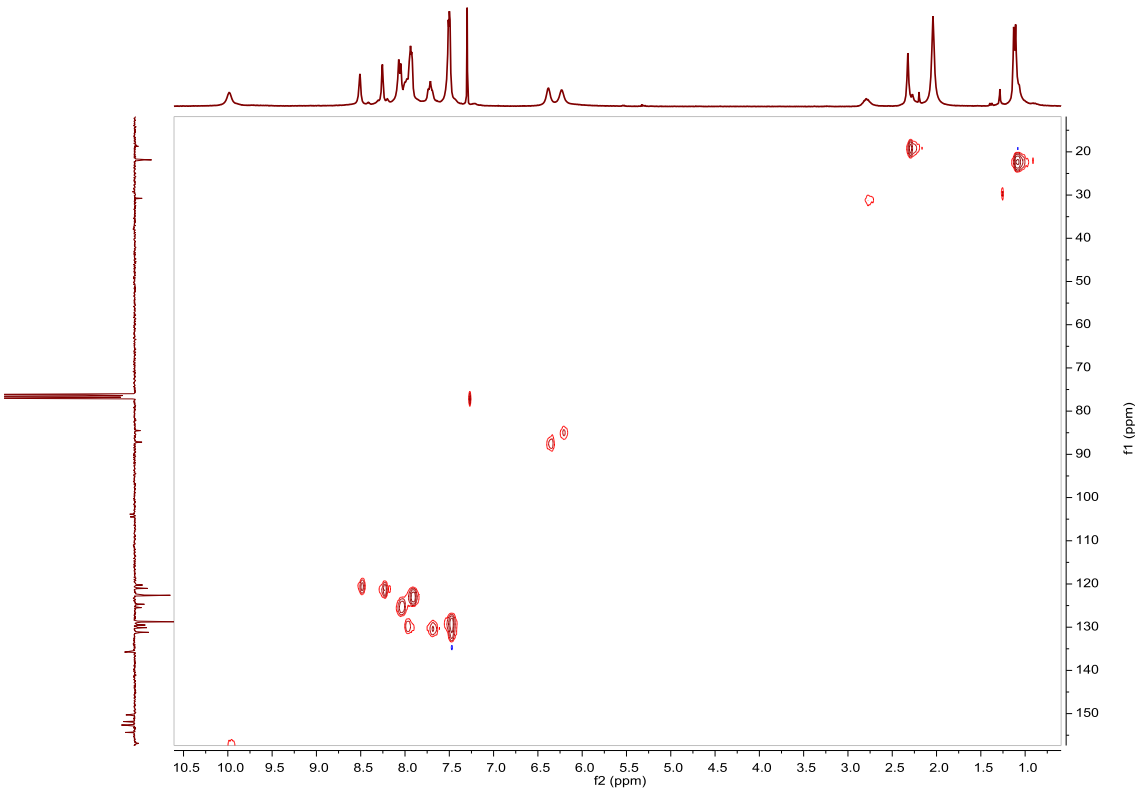

Fig. S387. HSQC NMR spectrum of **[Ru(p-Cym)(4,4'-bis(*m*-azobenzene)-2,2'-bipyridine)(Cl)]Cl** in $CDCl_3$.

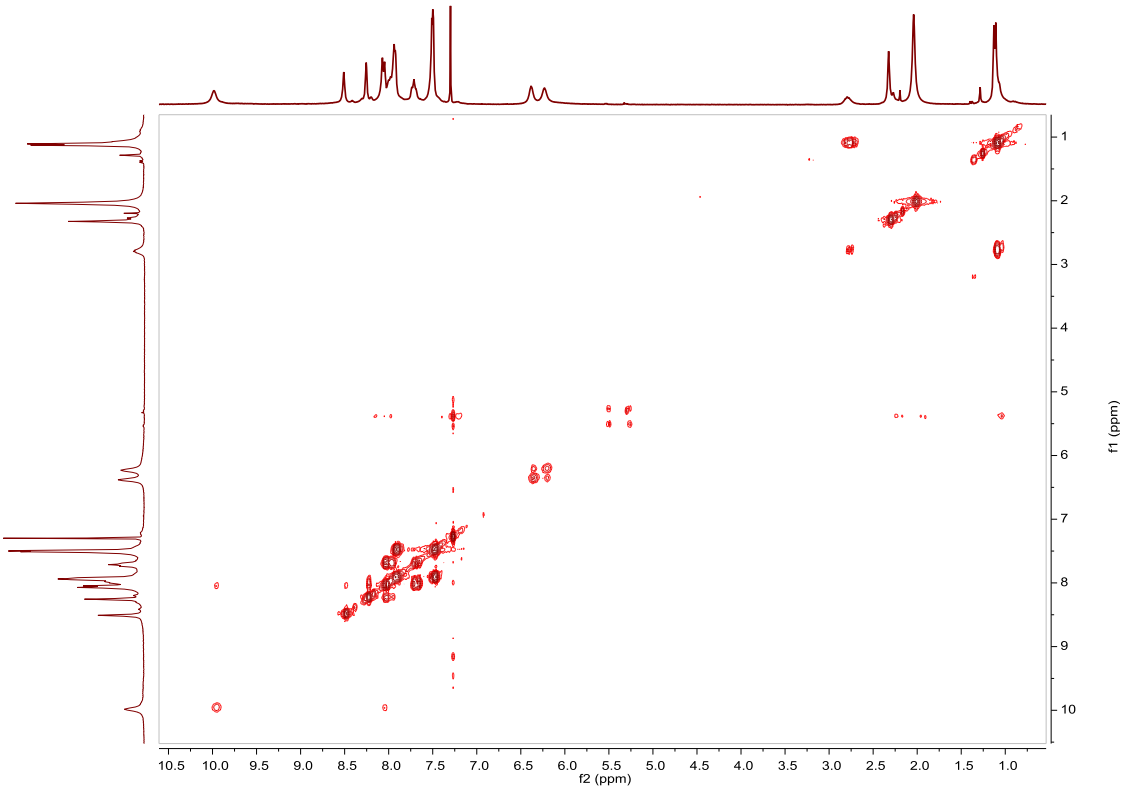

Fig. S388. COSY NMR spectrum of **[Ru(p-Cym)(4,4'-bis(*m*-azobenzene)-2,2'-bipyridine)(Cl)]Cl** in $CDCl_3$.

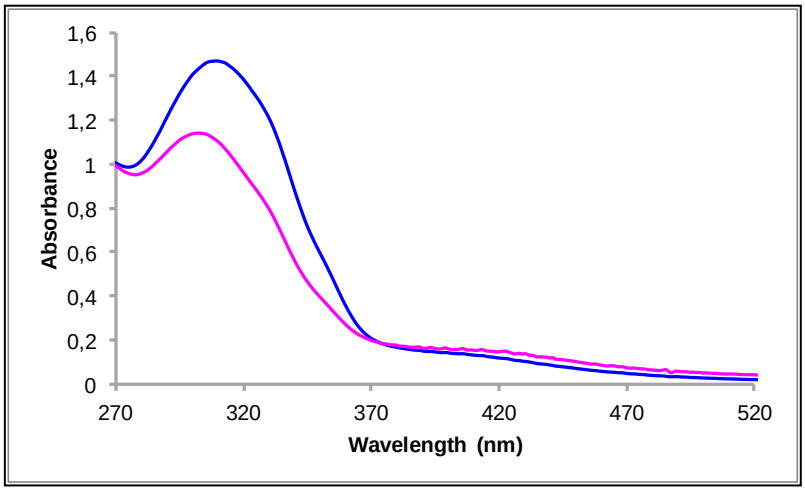

Fig. S389. UV/Vis spectra of **[Ru(p-Cym)(4,4'-bis(*m*-azobenzene)-2,2'-bipyridine)(Cl)]Cl** in ACN. Before (blue line) and after (pink line) irradiation at 322nm, $2.61 \cdot 10^{-5}$M.

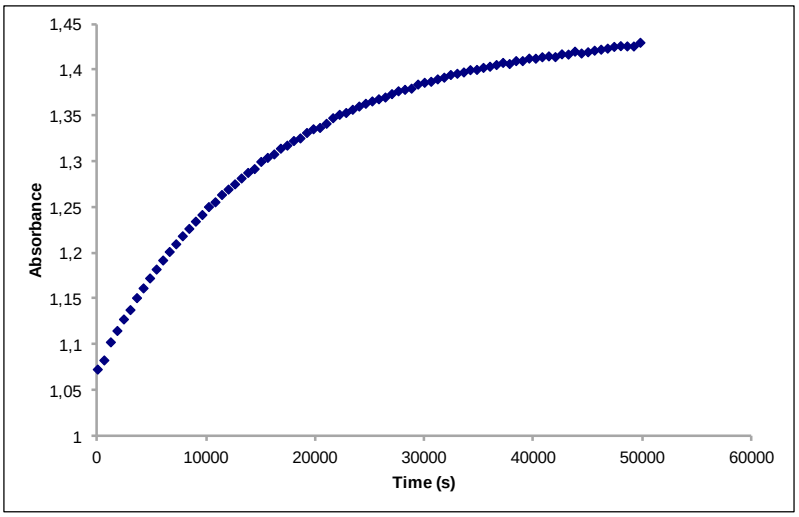

Fig. S390. Cis to trans thermal isomerization kinetics of **[Ru(p-Cym)(4,4'-bis(*m*-azobenzene)-2,2'-bipyridine)(Cl)]Cl**. Absorption change of the band 309nm at 338 K in ACN after irradiation at 322 nm. ($2.61 \cdot 10^{-5}$M).

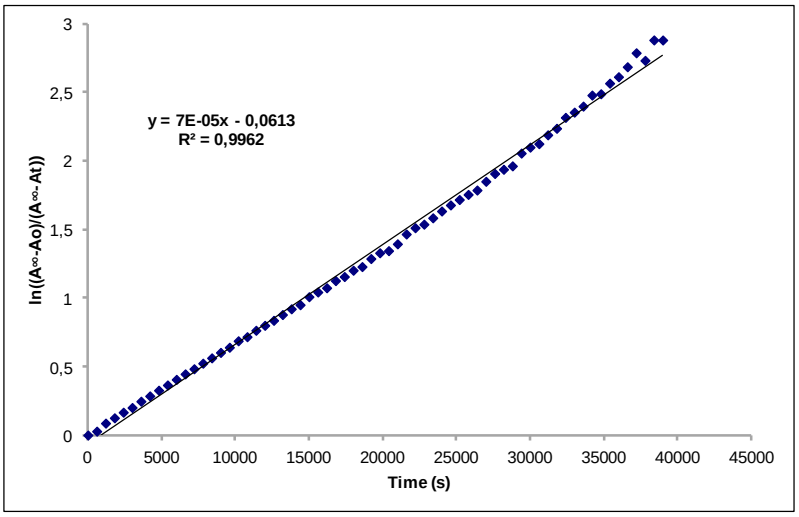

Fig. S391. Cis to trans thermal isomerization kinetics of **[Ru(p-Cym)(4,4'-bis(*m*-azobenzene)-2,2'-bipyridine)(Cl)]Cl**. First-order plot. k (s^{-1}) = $7.0 \cdot 10^{-5}$. Half-life (min) = 165.

Compound [Ru(p-Cym)(tris(*m*-phenylazobenzene)phosphine)(Cl)$_2$]. Synthesis, characterization and photoisomerization studies.

SYNTHESIS

Under a N_2 atmosphere, $Ru_2(p\text{-}Cym)_2Cl_4$ (0.100 g, 0.163 mmol) and tris(*m*-phenylazobenzene)phosphine (0.206 g, 0.359 mmol) were dissolved in 27 mL of hexane. The reaction mixture was refluxed for 15 h. It was cooled to room temperature and the solvent was evaporated. The desired compound was obtained after precipitation with CH_2Cl_2/ether as a red solid. Yield 90%.

Elemental Analysis: calculated for ($C_{46}H_{41}Cl_2N_6PRu$): C, 62.73; H, 4.69; N, 9.54. Found: C, 62.72; H, 4.96; N, 9.28.

Exact Mass: ESI-MS [M-2Cl+H]: calculated: m/z= 811.2252, found: m/z= 811.2248.

^{1}H NMR (300 MHz, $CDCl_3$): δ 8.48 (d, J = 11.0 Hz, 3H, (6)), 8.11 (t, J = 8.7 Hz, 3H, (2)), 7.90 (d, J = 7.0 Hz, 3H, (4)), 7.79 (m, 6H, (15)), 7.48 (ddd, J = 2.5 Hz, J = 7.7 Hz, J = 10.2 Hz, 3H, (3)), 7.38 (m, 9H, (16+17)), 5.27 (d, J = 6.1 Hz, 2H, (8)), 5.09 (d, J = 5.6 Hz, 2H, (7)), 2.81 (sep, J = 6.9 Hz, 1H, (11)), 1.88 (s, 3H, (13)), 1.04 (d, J = 6.9 Hz, 6H, (12)).

^{13}C APT NMR (75 MHz, $CDCl_3$): δ 151.94 (s, C_{quat}), 151.57 (d, J = 9.7 Hz, C_{quat}), 136.70 (d, J = 9.7 Hz, 3CH, (2)), 134.33 (d, J = 45.0 Hz, C_{quat}), 130.89 (s, 3CH, (17)), 128.98 (s, 3CH, (3)), 128.85 (d, J = 4.5 Hz, 3CH, (6)), 128.59 (s, 6CH, (16)), 123.44 (s, 3CH, (4)), 122.57(s, 6CH, (15)), 110.91 (s, C_{quat}), 96.54 (s, C_{quat}), 88.63 (s, 2CH, (7)), 87.07 (d, J = 5.2 Hz, 2CH, (8)), 29.87 (s, CH, (11)), 21.54 (s, $2CH_3$, (12)), 17.42 (s, CH_3, (13)).

^{31}P NMR (202 MHz, $CDCl_3$): δ 28.18 (s, 1P).

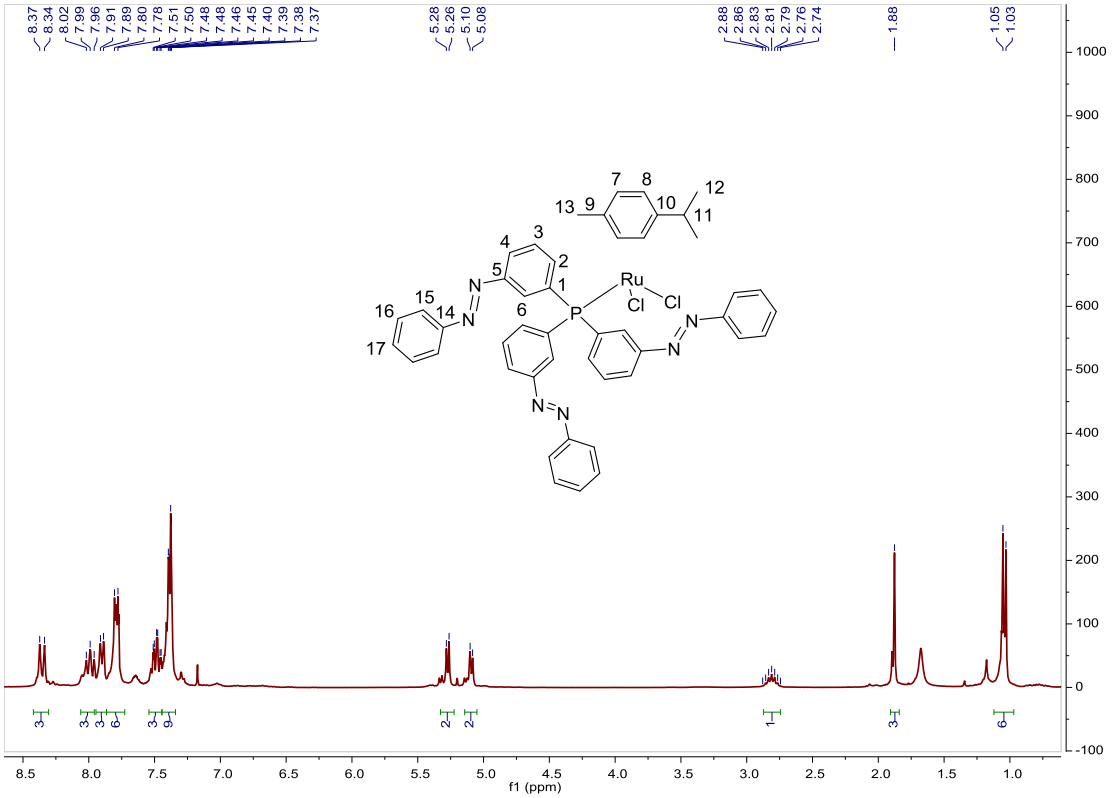

Fig. S392. ^{1}H NMR spectrum of **[Ru(p-Cym)(tris(*m*-phenylazobenzene)phosphine)(Cl)$_2$]** in $CDCl_3$, 300 MHz.

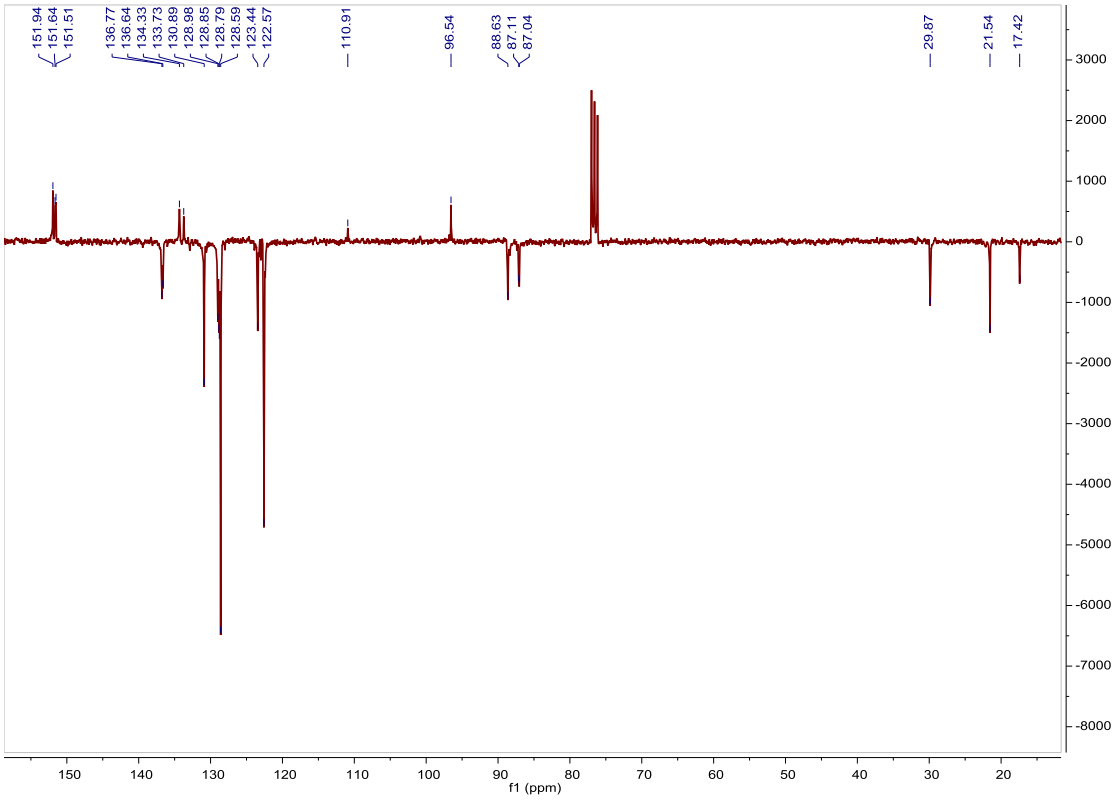

Fig. S393. ^{13}C APT NMR spectrum of **[Ru(p-Cym)(tris(*m*-phenylazobenzene)phosphine)(Cl)$_2$]** in $CDCl_3$, 75 MHz.

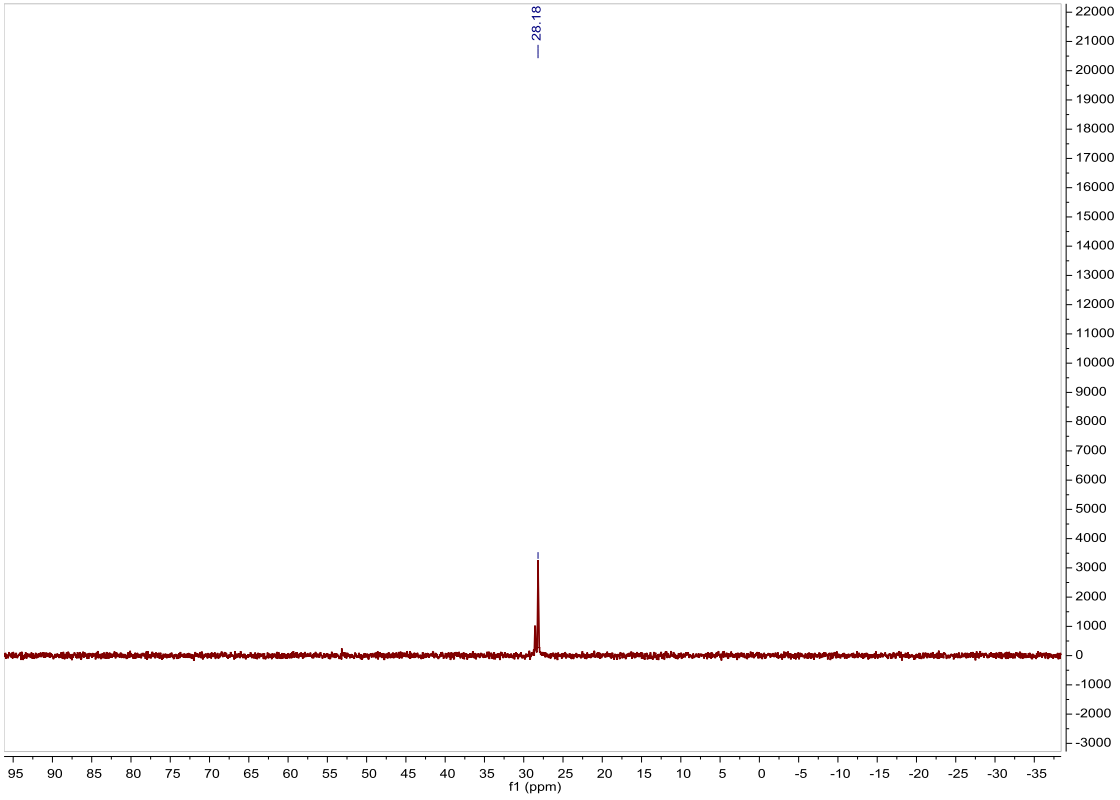

Fig. S394. ^{31}P NMR spectrum of **[Ru(p-Cym)(tris(*m*-phenylazobenzene)phosphine)(Cl)$_2$]** in $CDCl_3$, 202 MHz.

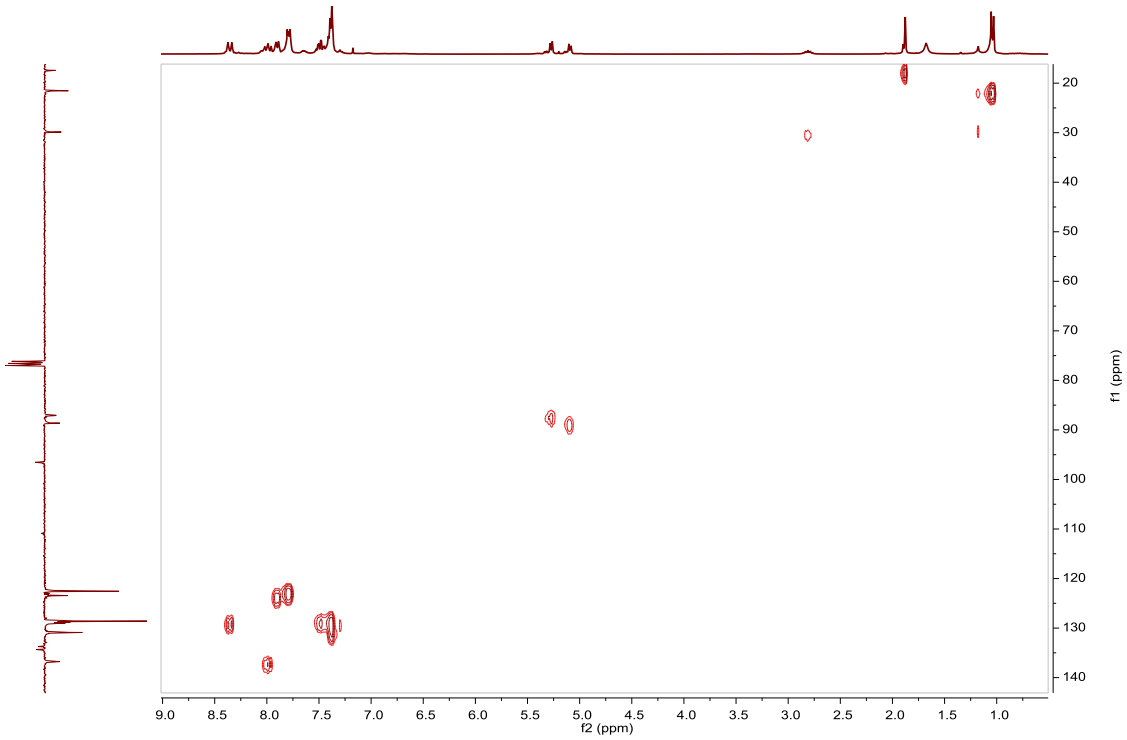

Fig. S395. HSQC NMR spectrum of **[Ru(p-Cym)(tris(*m*-phenylazobenzene)phosphine)(Cl)$_2$]** in $CDCl_3$.

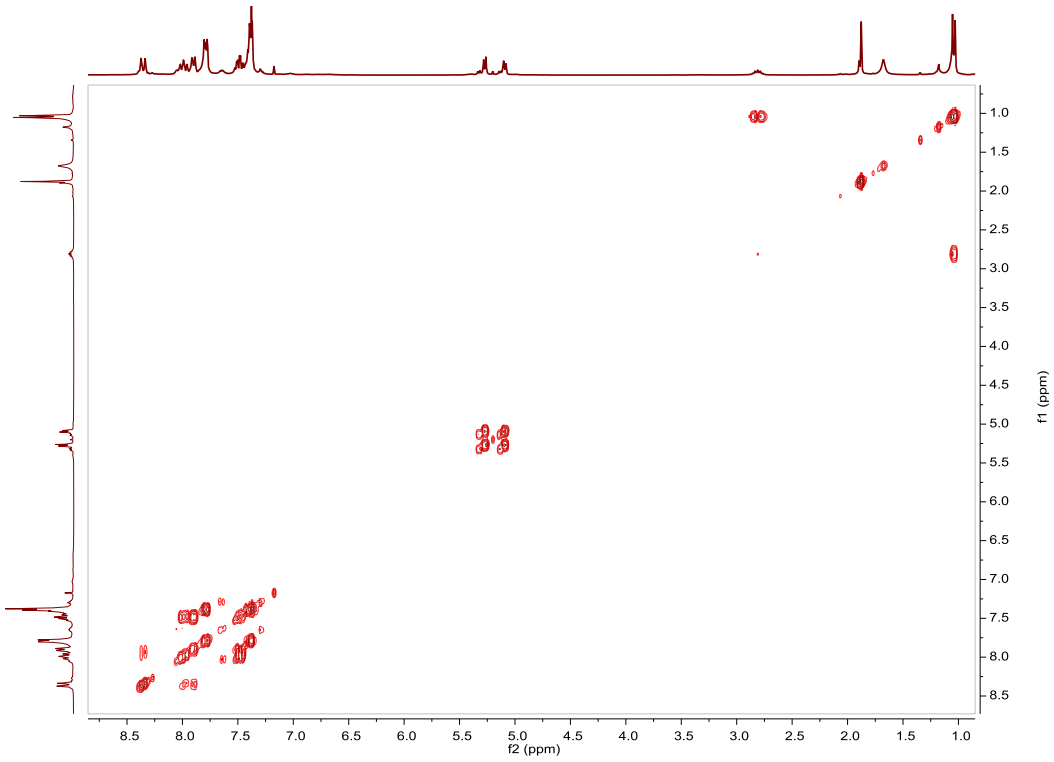

Fig. S396. COSY NMR spectrum of **[Ru(p-Cym)(tris(*m*-phenylazobenzene)phosphine)(Cl)$_2$]** in $CDCl_3$.

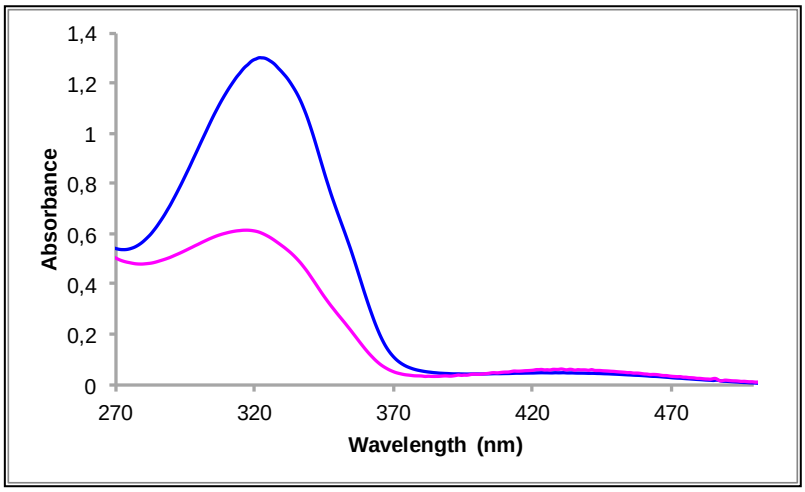

Fig. S397. UV/Vis spectra of **[Ru(p-Cym)(tris(*m*-phenylazobenzene)phosphine)(Cl)$_2$]** in ACN. Before (blue line) and after (pink line) irradiation at 324nm, 2.32·10^{-5}M.

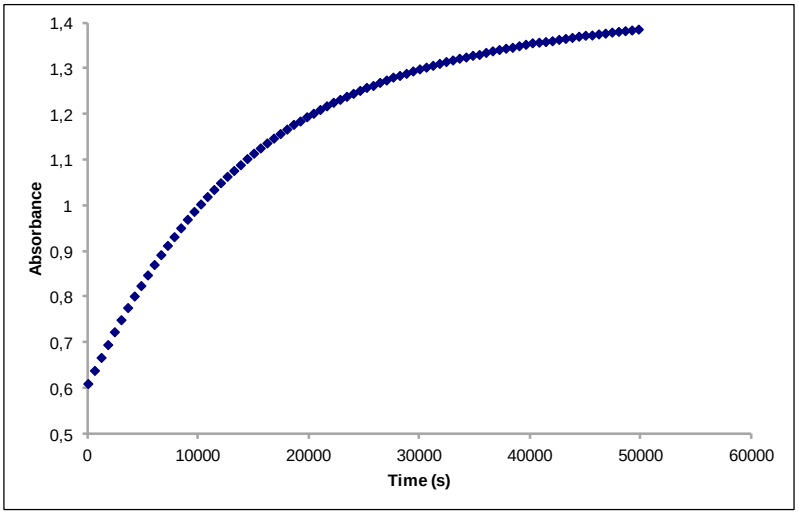

Fig. S398. Cis to trans thermal isomerization kinetics of **[Ru(p-Cym)(tris(*m*-phenylazobenzene)phosphine)(Cl)$_2$]**. Absorption change of the band 321nm at 338 K in ACN after irradiation at 324 nm. (2.32·10^{-5}M).

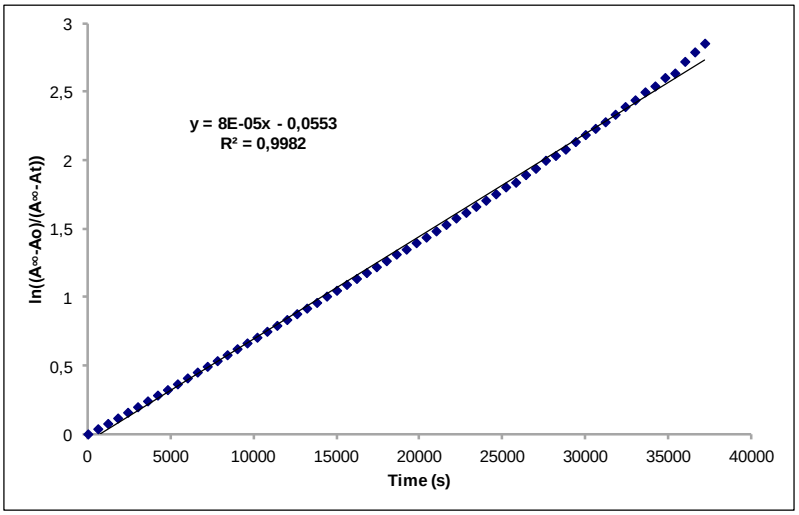

Fig. S399. Cis to trans thermal isomerization kinetics of **[Ru(p-Cym)(tris(*m*-phenylazobenzene)phosphine)(Cl)$_2$]**. First-order plot. k (s^{-1}) = $8.0 \cdot 10^{-5}$. Half-life (min) = 144.

Compound [Ru(p-Cym)(tris(*p*-phenylazobenzene)phosphine)(Cl)$_2$]. Synthesis, characterization and photoisomerization studies.

SYNTHESIS

Under a N_2 atmosphere, Ru_2(p-Cym)$_2Cl_4$ (0.11 g, 0.17 mmol) and tris(*p*-phenylazobenzene)phosphine (0.2 g, 0.348 mmol) were dissolved in 15 mL of hexane. The reaction mixture was refluxed for 15 h. It was cooled to room temperature and the red solid was filtered. Yield 95%.

Elemental Analysis: calculated for ($C_{46}H_{41}Cl_2N_6PRu$): C, 62.73; H, 4.69; N, 9.54. Found: C, 62.93; H, 4.90; N, 9.36.

Exact Mass: ESI-MS [M-2Cl+H]: calculated: m/z= 811.2252, found: m/z= 811.2229.

^{1}H NMR (300 MHz, $CDCl_3$): δ 7.97 (t, J = 8.5 Hz, 6H, (azo)), 7.82 (m, 12H, (azo)), 7.42 (m, 9H, (azo)), 5.21 (d, J = 6.1 Hz, 2H, (8)), 4.98 (d, J = 5.6 Hz, 2H, (7)), 2.83 (sep, J = 6.9 Hz, 1H, (11)), 1.85 (s, 3H, (13)), 1.06 (d, J = 6.9 Hz, 6H, (12)).

^{13}C APT NMR (75 MHz, $CDCl_3$): δ 153.58 (s, 3C_{quat}, (azo)), 152.76 (s, 3C_{quat}, (azo)), 136.22 (d, J = 45 Hz, 3Cquat, (azo)), 135.47 (d, J = 9.7 Hz, 6CH, (azo)), 131.78 (s, 3CH (azo)), 129.33 (s, 6CH, (azo)), 123.27 (s, 6CH, (azo)), 122.47 (d, J = 10.5 Hz, 6CH, (azo)), 112.07 (s, C_{quat}, (p-Cym)), 96.65 (s, C_{quat}, (p-Cym)), 89.37 (brd, J = 2.2 Hz, 2CH, (7)), 87.60 (d, J = 5.2 Hz, 2CH, (8)), 30.63 (s, CH, (11)), 22.10 (s, 2CH_3, (12)), 18.13 (s, CH_3, (13)).

^{31}P NMR (202 MHz, $CDCl_3$): δ 25.79 (s, 1P).

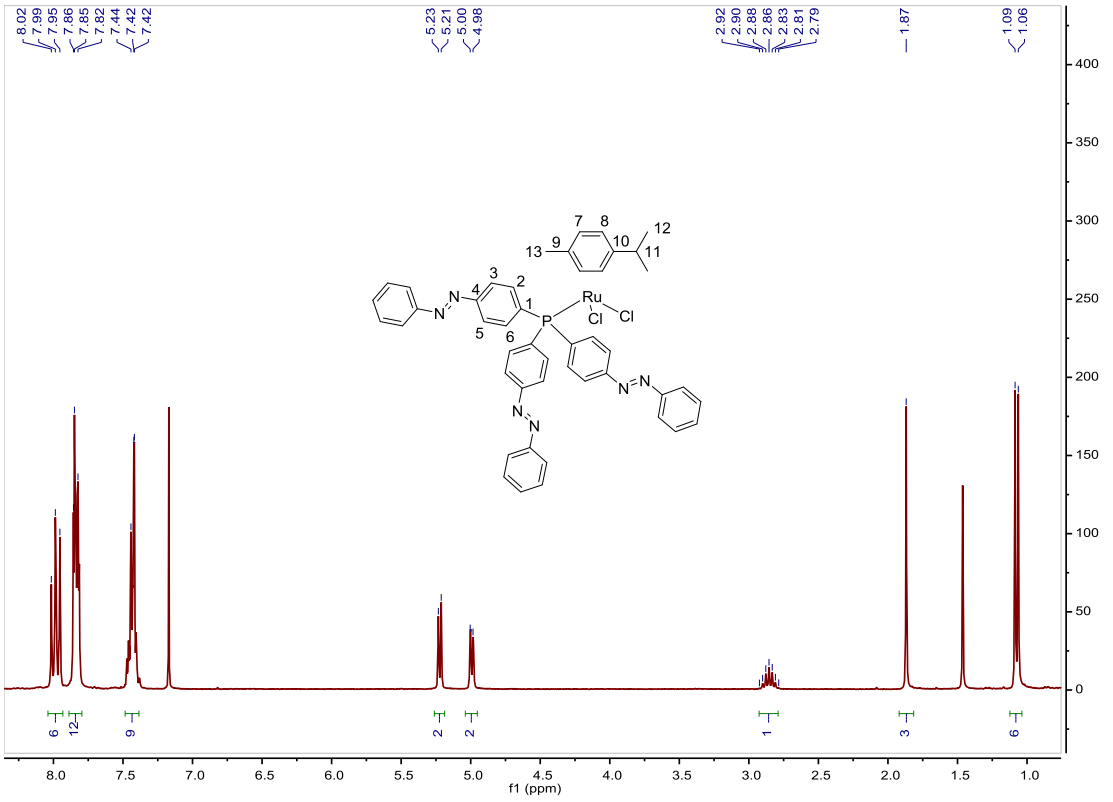

Fig. S400. ^{1}H NMR spectrum of **[Ru(p-Cym)(tris(*p*-phenylazobenzene)phosphine)(Cl)$_2$]** in $CDCl_3$, 300 MHz.

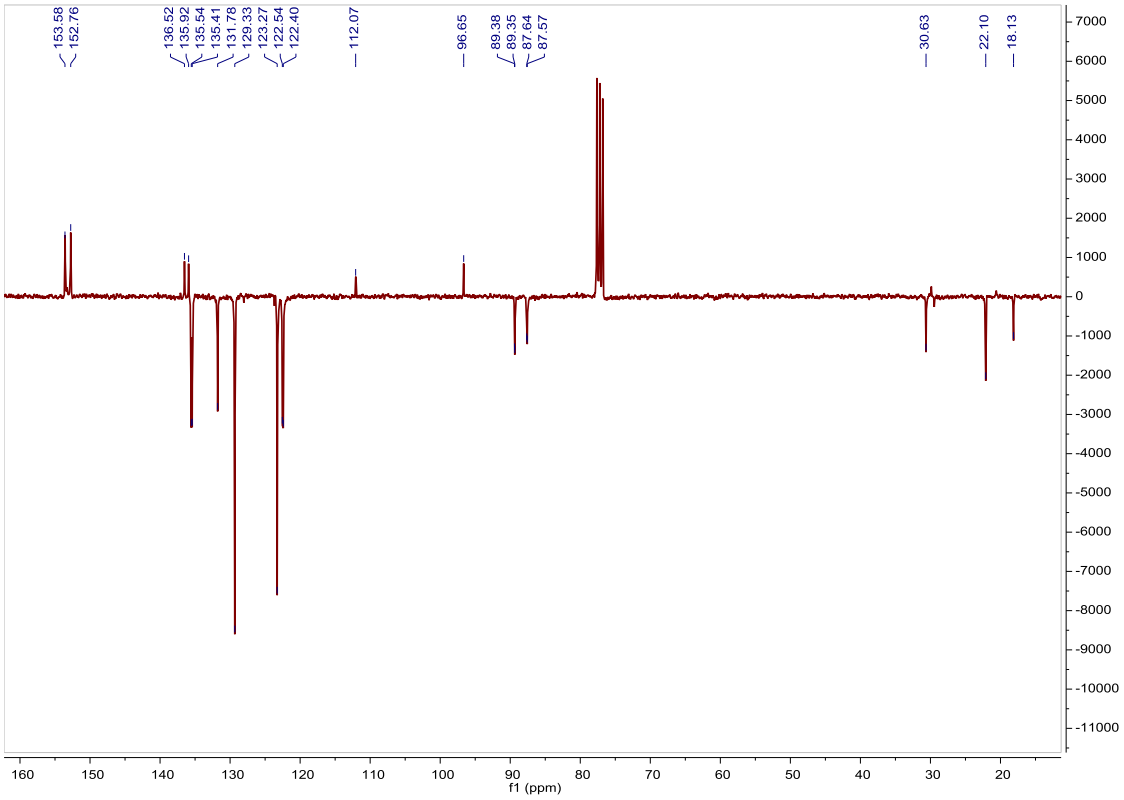

Fig. S401. ^{13}C APT NMR spectrum of **[Ru(p-Cym)(tris(*p*-phenylazobenzene)phosphine)(Cl)$_2$]** in $CDCl_3$, 75 MHz.

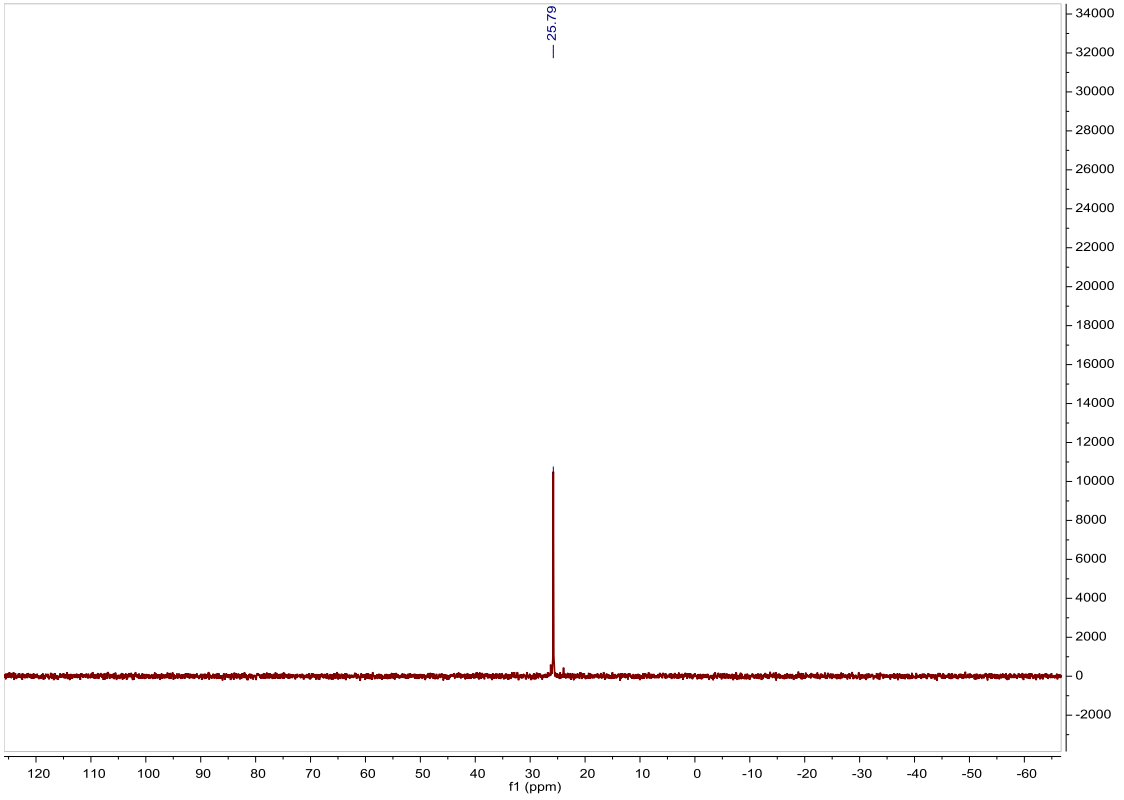

Fig. S402. ^{31}P NMR spectrum of **[Ru(p-Cym)(tris(*p*-phenylazobenzene)phosphine)(Cl)$_2$]** in $CDCl_3$, 202 MHz.

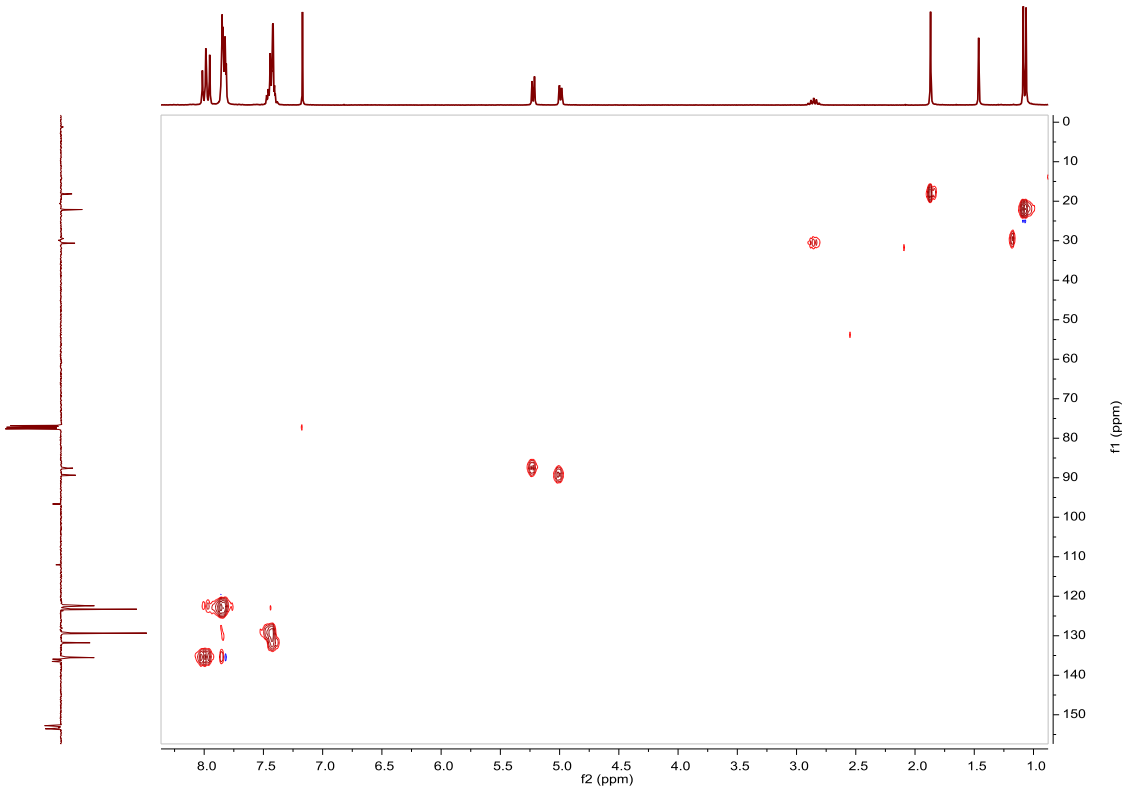

Fig. S403. HSQC NMR spectrum of **[Ru(p-Cym)(tris(*p*-phenylazobenzene)phosphine)(Cl)$_2$]** in $CDCl_3$.

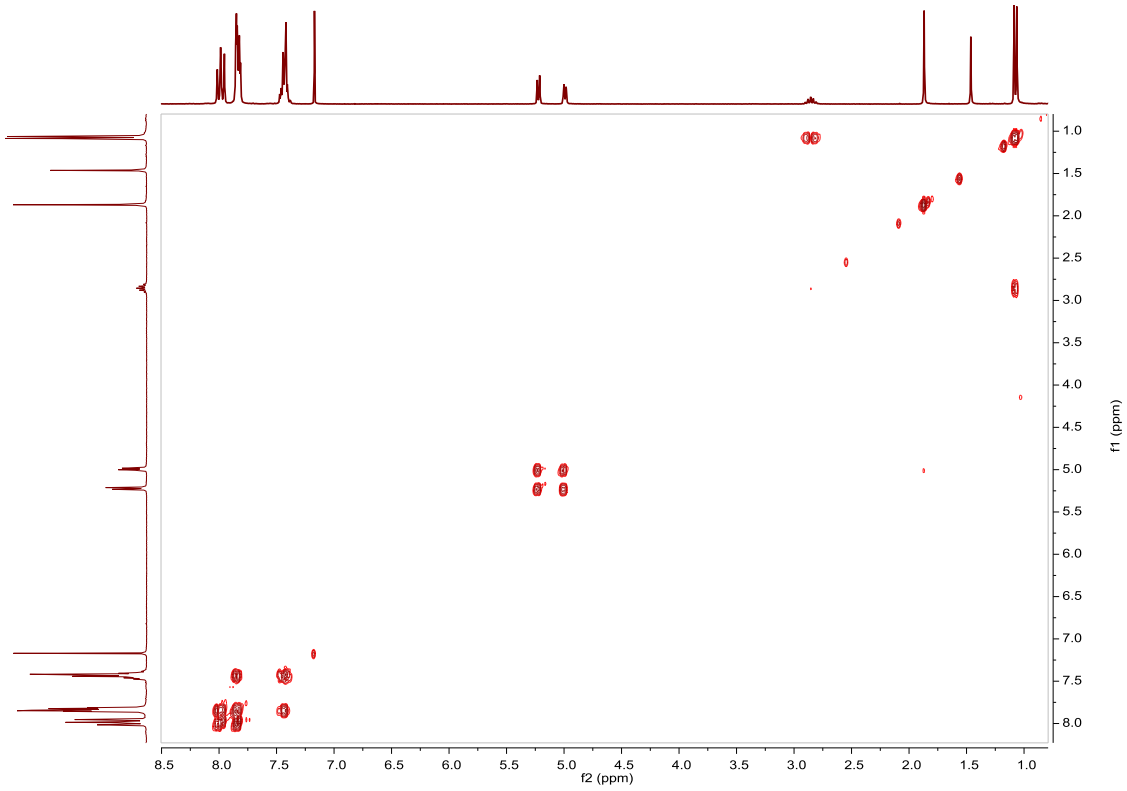

Fig. S404. COSY NMR spectrum of **[Ru(p-Cym)(tris(*p*-phenylazobenzene)phosphine)(Cl)$_2$]** in $CDCl_3$.

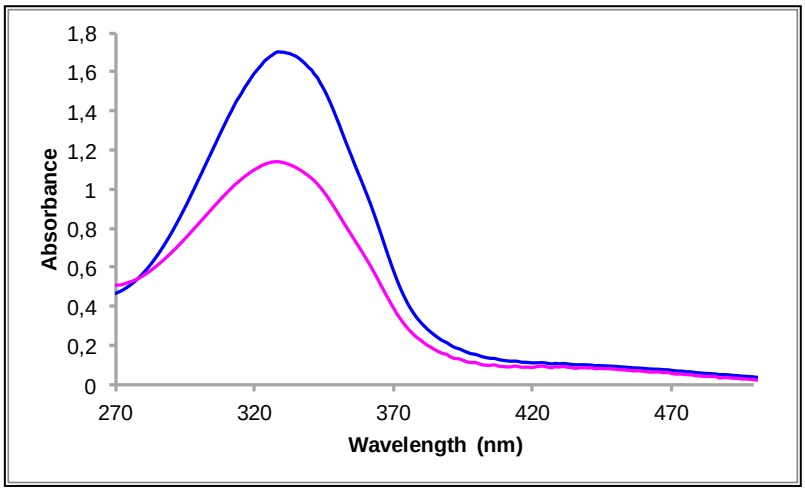

Fig. S405. UV/Vis spectra of **[Ru(p-Cym)(tris(*p*-phenylazobenzene)phosphine)(Cl)$_2$]** in ACN. Before (blue line) and after (pink line) irradiation at 334nm, 2.46·10^{-5}M.

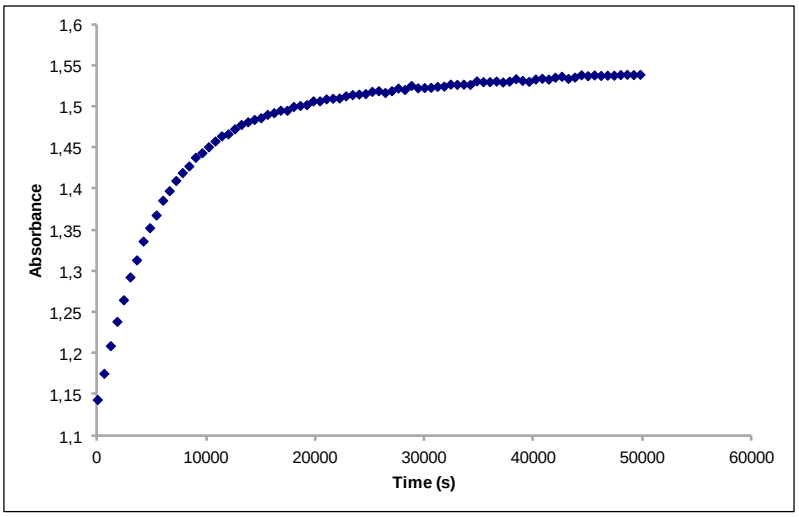

Fig. S406. Cis to trans thermal isomerization kinetics of **[Ru(p-Cym)(tris(*p*-phenylazobenzene)phosphine)(Cl)$_2$]**. Absorption change of the band 328nm at 338 K in ACN after irradiation at 334 nm. (2.46·10^{-5}M).

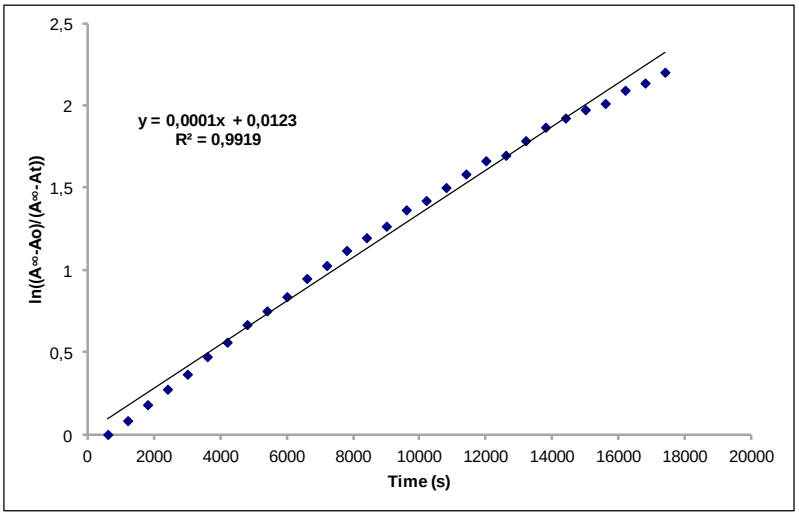

Fig. S407. Cis to trans thermal isomerization kinetics of **[Ru(p-Cym)(tris(*p*-phenylazobenzene)phosphine)(Cl)$_2$]**. First-order plot. k (s^{-1}) = $1.0 \cdot 10^{-4}$. Half-life (min) = 115.

Compound [Ru(p-Cym)(PPh_3)($Cl)_2$]. Synthesis and characterization.

SYNTHESIS

Under a N_2 atmosphere, Ru_2(p-Cym)$_2Cl_4$ (0.200 g, 0.326 mmol) and triphenylphosphine (0.171 g, 0.653 mmol) were dissolved in 15 mL of hexane. The reaction mixture was refluxed for 15 h. It was cooled to room temperature and the product was obtained as an orange solid after filtrating and washing with ether. Yield 77%. The spectroscopic data are coincident with those described in the literature.[44]

^{1}H NMR (500 MHz, $CDCl_3$): δ 7.85 (t, J = 8.7 Hz, 6H, (2+6)), 7.44–7.34 (m, 9H, (3+4+5)), 5.22 (d, J = 5.9 Hz, 2H, (8)), 5.01 (d, J = 5.9 Hz, 2H, (7)), 2.87 (sep, J = 6.9 Hz, 1H, (11)), 1.89 (s, 3H, (13)), 1.13 (d, J = 6.9 Hz, 6H, (12)).

^{31}P NMR (202 MHz, $CDCl_3$): δ 25.40 (s, 1P).

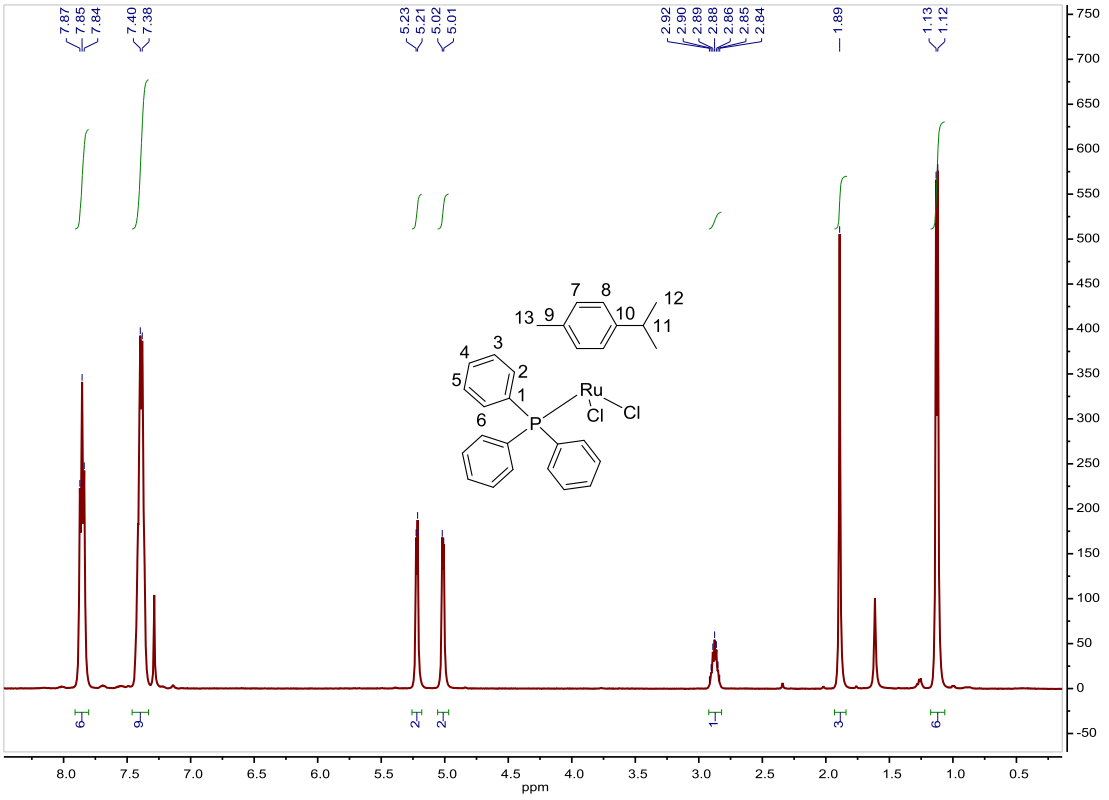

Fig. S408. ^{1}H NMR spectrum of **[Ru(p-Cym)(PPh_3)($Cl)_2$]** in $CDCl_3$, 500 MHz.

[44] E. Hodson and S. J. Simpson, *Polyhedron*, **2004**, *23*, 2695–2707.

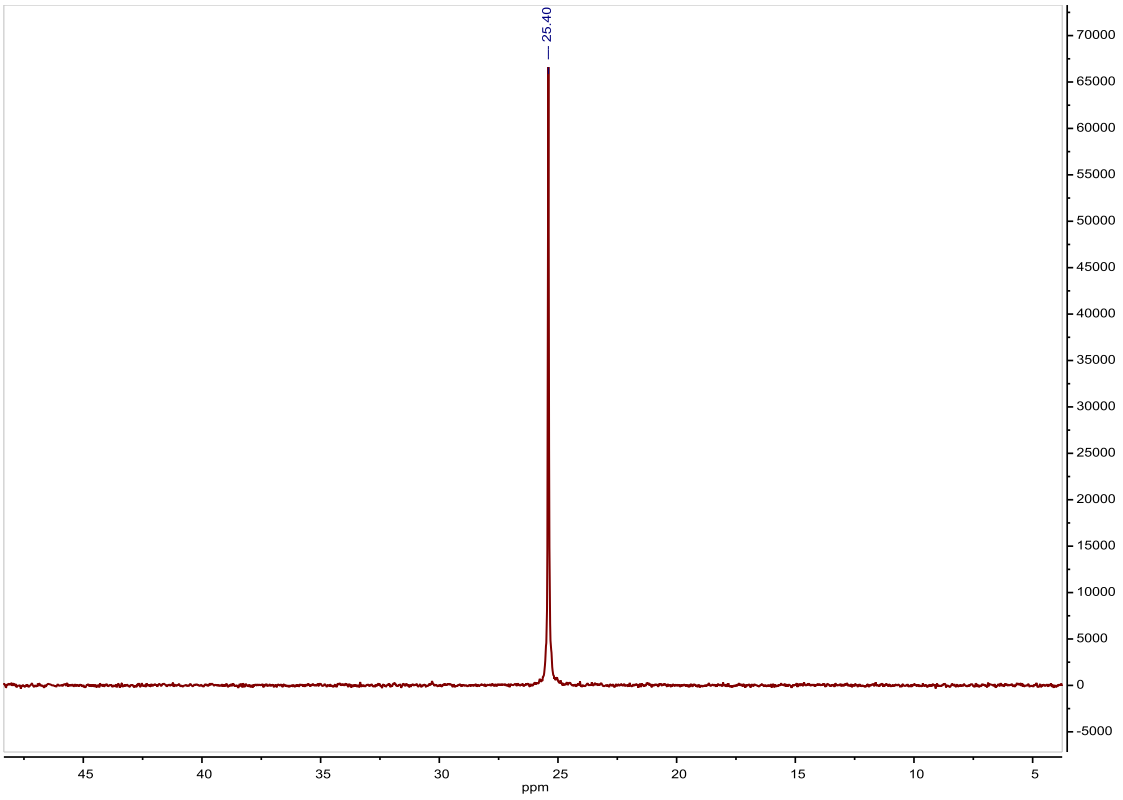

Fig. S409. ^{31}P NMR spectrum of **[Ru(p-Cym)(PPh_3)$(Cl)_2$]** in $CDCl_3$, 202 MHz.

H_3NBD_3. Synthesis and characterization.

SYNTHESIS[45]

Under a N_2 atmosphere, $NaBD_4$ (0.5 g, 11.95 mmol) and $(NH_4)_2CO_3$ (1.14 g, 11.95 mmol) were stirred in freshly distilled THF (13 mL). The reaction mixture was heated at 40 °C for 7 h and stirred at room temperature overnight. The reaction mixture was filtered through a celite path, using THF to wash the celite. The product was obtained as a white solid after sublimation at 40 °C–80 °C under vacuum. Yield 61%. The spectroscopic data are coincident with those described in the literature.

^{1}H NMR (400 MHz, THF-d_8): δ 2.11 (t, J = 41.1 Hz, NH_3).

^{11}B NMR (128 MHz, THF-d_8): δ -24.39 (s, BD_3).

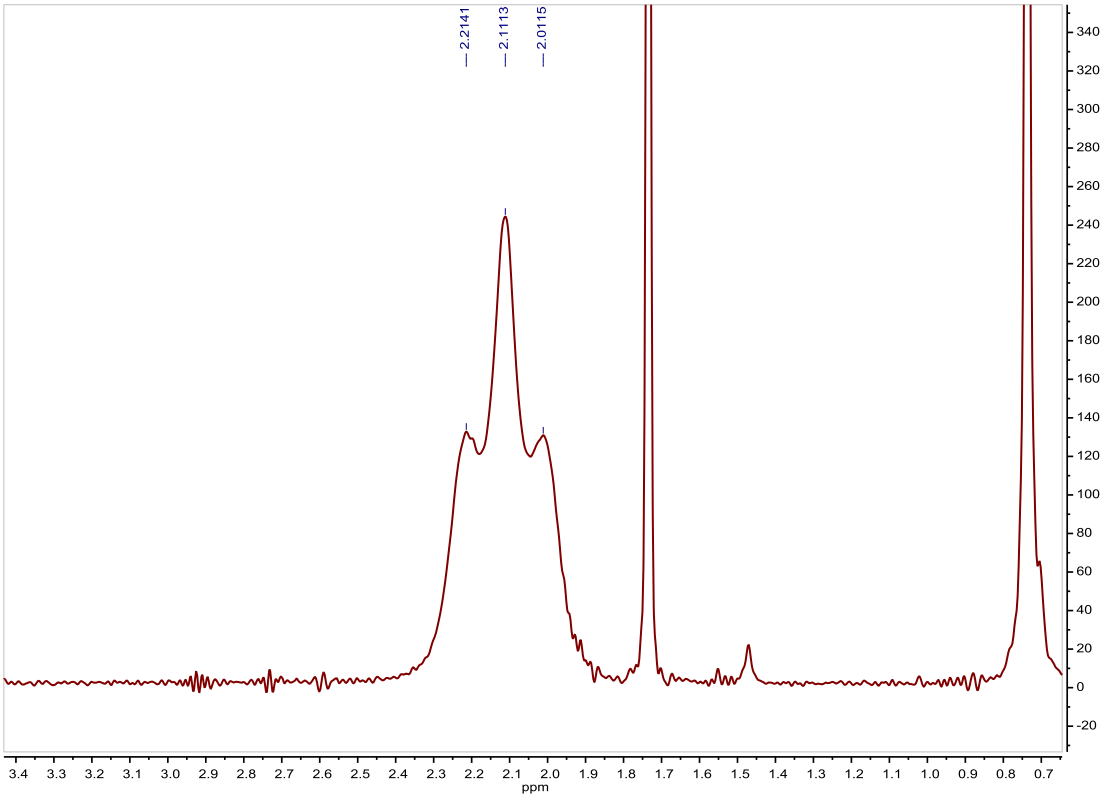

Fig. S410. ^{1}H NMR spectrum of **H_3NBD_3** in THF-d_8, 400 MHz.

[45] X. Yang, T. Fox and H. Berke, *Chem. Commun.*, **2011**, *47*, 2053–2055.

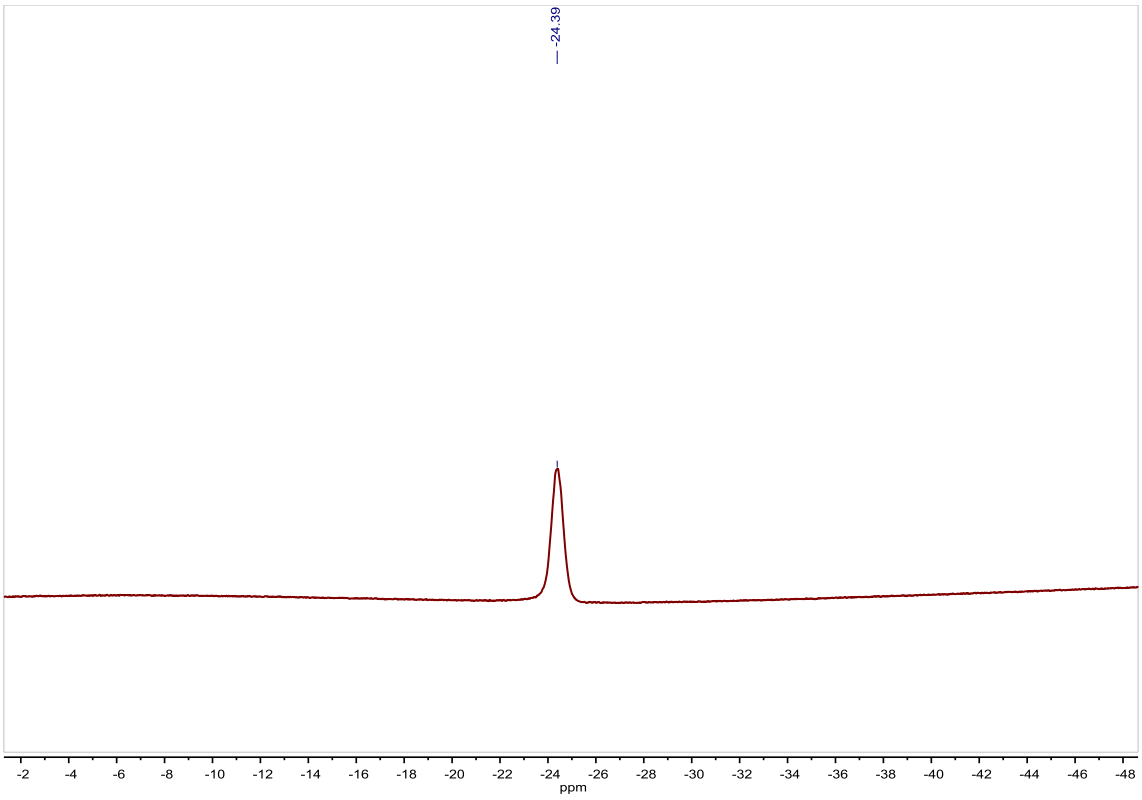

Fig. S411. ^{11}B NMR spectrum of **H_3NBD_3** in THF-d_8, 128 MHz.

Table S2. Crystal data and details of refinement for ligand **3**.

Empirical formula	$C_{34}H_{24}N_6$
Formula weight	516.61
Temperature (K)	293(2)
Wavelength (Å)	1.54184
Crystal system	Monoclinic
Space group	P21/c
Unit cell dimensions (Å / °)	a = 5.3183(4), α = 90.00 b = 9.7998(5), β = 92.498(6) c = 24.1834(15), γ = 90.00
Volume ($Å^3$)	1259.20(14)
Z	2
Calculated Density (Mg/m^3)	1.362
Absorption coefficient (mm^{-1})	0.653
F(000)	540
Theta range (°) for data collection	3.66 - 74.02
Index ranges	-6<=h<=4, -11<=k<=11, -29<=l<=29
Reflections collected	5514
Data [I>2σ(I)]	2469
Parameters	181
Restraints	0
Goodness-of-fit on F^2	1.099
Final R indices [I>2σ(I)]	R1 = 0.0475, wR2 = 0.1270
R indices (all data)	R1 = 0.0542, wR2 = 0.1311
Largest diff. peak and hole ($e/Å^3$)	0.270, -0.191

Table S3. Crystal data and details of refinement for **Aphen**.

Empirical formula	$C_{34}H_{24}F_6IrN_4P$
Formula weight	825.74
Temperature (K)	100(2)
Wavelength (Å)	0.71073
Crystal system	Triclinic
Space group	P-1
Unit cell dimensions (Å / °)	a = 15.0969(2), α = 90.00 b = 23.0030(4), β = 94.974(2) c = 18.9451(3), γ = 90.00
Volume ($Å^3$)	6554.36(18)
Z	8
Calculated Density (Mg/m^3)	1.674
Absorption coefficient (mm^{-1})	4.187
F(000)	3216
Theta range (°) for data collection	1.62 - 28.38
Index ranges	-20<=h<=19, -30<=k<=28, -25<=l<=23
Reflections collected	22666
Data [I>2σ(I)]	7459
Parameters	415
Restraints	0
Goodness-of-fit on F^2	1.063
Final R indices [I>2σ(I)]	R1 = 0.0179, wR2 = 0.0402
R indices (all data)	R1 = 0.0231, wR2 = 0.0420
Largest diff. peak and hole ($e/Å^3$)	0.913, -0.458

Table S4. Crystal data and details of refinement for **Cphen**.

Empirical formula	$C_{34}H_{22}Br_2F_6IrN_4P$
Formula weight	983.95
Temperature (K)	293(2)
Wavelength (Å)	1.54184
Crystal system	Triclinic
Space group	P-1
Unit cell dimensions (Å / °)	a = 10.42190(10), α = 90.021(2) b = 16.6122(3), β = 90.0170(10) c = 50.6413(10), γ = 92.7320(10)
Volume ($Å^3$)	8757.6(2)
Z	1
Calculated Density (Mg/m^3)	1.480
Absorption coefficient (mm^{-1})	4.957
F(000)	3728
Theta range (°) for data collection	1.72 - 28.28
Index ranges	-13<=h<=10, -22<=k<=22, -66<=l<=58
Reflections collected	68576
Data [I>2σ(I)]	38643
Parameters	1484
Restraints	147
Goodness-of-fit on F^2	1.103
Final R indices [I>2σ(I)]	R1 = 0.1102, wR2 = 0.2705
R indices (all data)	R1 = 0.1684, wR2 = 0.3073
Largest diff. peak and hole ($e/Å^3$)	1.836, -3.057

Table S5. Crystal data and details of refinement for **BbipyBr**.

Empirical formula	$C_{32}H_{18}Br_2F_{10}IrN_4P$
Formula weight	1031.51
Temperature (K)	293(2)
Wavelength (Å)	1.54184
Crystal system	Monoclinic
Space group	P21/n
Unit cell dimensions (Å / °)	a = 9.7933(3), α = 90.00 b = 22.1886(8), β = 98.771(4) c = 14.7348(6), γ = 90.00
Volume ($Å^3$)	3164.4(2)
Z	13
Calculated Density (Mg/m^3)	2.165
Absorption coefficient (mm^{-1})	12.443
F(000)	1960
Theta range (°) for data collection	3.63 - 74.05
Index ranges	-12<=h<=12, -19<=k<=27, -18<=l<=18
Reflections collected	23312
Data [I>2σ(I)]	6366
Parameters	451
Restraints	0
Goodness-of-fit on F^2	1.154
Final R indices [I>2σ(I)]	R1 = 0.0463, wR2 = 0.1012
R indices (all data)	R1 = 0.0569, wR2 = 0.1065
Largest diff. peak and hole ($e/Å^3$)	1.441, -1.318

Table S6. Crystal data and details of refinement for **CbipyBr**.

Empirical formula	$C_{32}H_{20}Br_4F_6IrN_4P$
Formula weight	1117.34
Temperature (K)	293(2)
Wavelength (Å)	1.54184
Crystal system	Monoclinic
Space group	C c
Unit cell dimensions (Å / °)	a = 12.9278(3), α = 90.00 b = 28.0093(5), β = 95.485(2) c = 11.2643(3), γ = 90.00
Volume ($Å^3$)	4060.11(16)
Z	17
Calculated Density (Mg/m^3)	1.828
Absorption coefficient (mm^{-1})	11.827
F(000)	2104
Theta range (°) for data collection	3.16 - 74.13
Index ranges	-16<=h<=13, -34<=k<=30, -13<=l<=14
Reflections collected	16221
Data [I>2σ(I)]	7096
Parameters	433
Restraints	473
Goodness-of-fit on F^2	1.066
Final R indices [I>2σ(I)]	R1 = 0.0590, wR2 = 0.1663
R indices (all data)	R1 = 0.0760, wR2 = 0.1832
Largest diff. peak and hole ($e/Å^3$)	2.560, -2.811

Table S7. Crystal data and details of refinement for **B1**.

Empirical formula	$C_{44}H_{28}F_{10}IrN_8P$
Formula weight	1081.9388
Temperature (K)	100(2)
Wavelength (Å)	0.71073
Crystal system	Monoclinic
Space group	P21/c
Unit cell dimensions (Å / °)	a = 22.4848(6), α = 90.00
	b = 9.4724(2), β = 94.080(3)
	c = 20.0655(7), γ = 90.00
Volume ($Å^3$)	4262.8(2)
Z	4
Calculated Density (Mg/m^3)	1.818
Absorption coefficient (mm^{-1})	3.385
F(000)	2288
Theta range (°) for data collection	1.82 - 26.50
Index ranges	-28<=h<=28, -9<=k<=11, -18<=l<=25
Reflections collected	31975
Data [I>2σ(I)]	8825
Parameters	604
Restraints	0
Goodness-of-fit on F^2	1.113
Final R indices [I>2σ(I)]	R1 = 0.0339, wR2 = 0.0668
R indices (all data)	R1 = 0.0423, wR2 = 0.0697
Largest diff. peak and hole ($e/Å^3$)	0.832, -2.571

Table S8. Crystal data and details of refinement for **A2**.

Empirical formula	$C_{44}H_{34}F_6IrN_8P$
Formula weight	1011.99
Temperature (K)	100(2)
Wavelength (Å)	0.71073
Crystal system	Monoclinic
Space group	C2/c
Unit cell dimensions (Å / °)	a = 17.1660(2), α = 90.00 b = 21.8245(2), β = 93.1940(10) c = 20.9858(4), γ = 90.00
Volume ($Å^3$)	7849.89(19)
Z	8
Calculated Density (Mg/m^3)	1.713
Absorption coefficient (mm^{-1})	3.516
F(000)	4000
Theta range (°) for data collection	1.76 - 26.5
Index ranges	-21<=h<=21, -27<=k<=27, -25<=l<=26
Reflections collected	24093
Data [I>2σ(I)]	8143
Parameters	597
Restraints	80
Goodness-of-fit on F^2	1.087
Final R indices [I>2σ(I)]	R1 = 0.0285, wR2 = 0.0649
R indices (all data)	R1 = 0.0359, wR2 = 0.0686
Largest diff. peak and hole ($e/Å^3$)	1.579, -1.316

Table S9. Crystal data and details of refinement for **C3**.

Empirical formula	$C_{56}H_{38}Br_2F_6IrN_8P$
Formula weight	1319.96
Temperature (K)	100(2)
Wavelength (Å)	1.54184
Crystal system	Triclinic
Space group	P-1
Unit cell dimensions (Å / °)	a = 15.2882(3), α = 85.8675(15) b = 19.3171(3), β = 83.4417(17) c = 20.0260(4), γ = 81.9153(15)
Volume ($Å^3$)	5807.62(19)
Z	4
Calculated Density (Mg/m^3)	1.505
Absorption coefficient (mm^{-1})	6.995
F(000)	2573
Theta range (°) for data collection	2.94 - 74.04
Index ranges	-18<=h<=19, -23<=k<=24, 0<=l<=24
Reflections collected	22937
Data [I>2σ(I)]	22937
Parameters	1481
Restraints	909
Goodness-of-fit on F^2	0.869
Final R indices [I>2σ(I)]	R1 = 0.0552, wR2 = 0.1696
R indices (all data)	R1 = 0.0707, wR2 = 0.1831
Largest diff. peak and hole ($e/Å^3$)	1.998, -1.121

Table S10. Crystal data and details of refinement for **A4**.

Empirical formula	$C_{44}H_{31}BrF_6IrN_6P$
Formula weight	1060.8592
Temperature (K)	100(2)
Wavelength (Å)	0.71073
Crystal system	Monoclinic
Space group	C 2/c
Unit cell dimensions (Å / °)	a = 28.2267(12), α = 90.00 b = 13.2492(3), β = 104.771(4) c = 26.6858(9), γ = 90.00
Volume ($Å^3$)	9650.2(6)
Z	8
Calculated Density (Mg/m^3)	1.460
Absorption coefficient (mm^{-1})	3.686
F(000)	4144
Theta range (°) for data collection	1.58 - 28.29
Index ranges	-37<=h<=35, 0<=k<=17, 0<=l<=35
Reflections collected	10944
Data [I>2σ(I)]	10944
Parameters	575
Restraints	450
Goodness-of-fit on F^2	1.033
Final R indices [I>2σ(I)]	R1 = 0.0790, wR2 = 0.1843
R indices (all data)	R1 = 0.1348, wR2 = 0.2031
Largest diff. peak and hole ($e/Å^3$)	3.385, -1.517

Table S11. Crystal data and details of refinement for [Ru(*p*-Cym)(**17**)Cl]Cl.

Empirical formula	$C_{24}H_{22}Cl_2N_2Ru$
Formula weight	510.4240
Temperature (K)	100(10)
Wavelength (Å)	0.71073
Crystal system	Triclinic
Space group	P -1
Unit cell dimensions (Å / °)	a = 6.9529(2), α = 92.790(6)
	b = 11.5712(7), β = 99.326(4)
	c = 16.8700(13), γ = 96.309(4)
Volume ($Å^3$)	1328.15(14)
Z	2
Calculated Density (Mg/m^3)	1.436
Absorption coefficient (mm^{-1})	0.822
F(000)	580
Theta range (°) for data collection	1.775 - 28.315
Index ranges	-6<=h<=9, -14<=k<=14, -21<=l<=21
Reflections collected	9376
Data [I>2σ(I)]	9376
Parameters	357
Restraints	24
Goodness-of-fit on F^2	1
Final R indices [I>2σ(I)]	R1 = 0.0767, wR2 = 0.1942
R indices (all data)	R1 = 0.1093, wR2 = 0.2107
Largest diff. peak and hole ($e/Å^3$)	1.555, -1.218

Table S12. Crystal data and details of refinement for [Ru(*p*-Cym)(**21**)Cl]Cl.

Empirical formula	$C_{20}H_{20}Cl_2N_8Ru$
Formula weight	544.4060
Temperature (K)	100(10)
Wavelength (Å)	1.54184
Crystal system	Triclinic
Space group	P -1
Unit cell dimensions (Å / °)	a = 9.4232(7), α = 98.121(6) b = 10.4405(5), β = 99.958(7) c = 14.3166(12), γ = 116.027(7)
Volume ($Å^3$)	1208.50(15)
Z	2
Calculated Density (Mg/m^3)	1.496
Absorption coefficient (mm^{-1})	7.419
F(000)	548
Theta range (°) for data collection	3.233 - 68.994
Index ranges	-6<=h<=11, -12<=k<=12, -17<=l<=17
Reflections collected	7871
Data [I>2σ(I)]	4398
Parameters	310
Restraints	66
Goodness-of-fit on F^2	1.139
Final R indices [I>2σ(I)]	R1 = 0.0799, wR2 = 0.2203
R indices (all data)	R1 = 0.0935, wR2 = 0.2324
Largest diff. peak and hole ($e/Å^3$)	2.462, -1.486

Table S13. Crystal data and details of refinement for [Ru(*p*-Cym)(**22**)Cl]Cl.

Empirical formula	$C_{20}H_{20}BrCl_2N_5Ru$
Formula weight	582.2890
Temperature (K)	100.01(10)
Wavelength (Å)	1.54184
Crystal system	Triclinic
Space group	P -1
Unit cell dimensions (Å / °)	a = 10.6051(8), α = 93.576(7)
	b = 10.7857(9), β = 102.190(7)
	c = 16.5095(15), γ = 107.715(7)
Volume ($Å^3$)	1742.0(3)
Z	2
Calculated Density (Mg/m^3)	1.793
Absorption coefficient (mm^{-1})	12.961
F(000)	924
Theta range (°) for data collection	2.764 - 69.99
Index ranges	-13<=h<=13, -7<=k<=13, -18<=l<=20
Reflections collected	12176
Data [I>2σ(I)]	6553
Parameters	484
Restraints	107
Goodness-of-fit on F^2	1.023
Final R indices [I>2σ(I)]	R1 = 0.0659, wR2 = 0.1708
R indices (all data)	R1 = 0.0782, wR2 = 0.1847
Largest diff. peak and hole ($e/Å^3$)	1.629, -1.492

Table S14. Crystal data and details of refinement for [Ru(*p*-Cym)(**2**)$_2$Cl]PF_6.

Empirical formula	$C_{32}H_{32}ClN_6RuPF_6$
Formula weight	782.1342
Temperature (K)	100.00(10)
Wavelength (Å)	0.71073
Crystal system	Monoclinic
Space group	P 21/c
Unit cell dimensions (Å / °)	a = 10.60258(11), α = 90 b = 12.35957(11), β = 92.8039(9) c = 26.4031(3), γ = 90
Volume (Å^3)	3455.81(6)
Z	4
Calculated Density (Mg/m^3)	1.503
Absorption coefficient (mm^{-1})	0.641
F(000)	1584
Theta range (°) for data collection	1.82 - 28.268
Index ranges	-13<=h<=14, -16<=k<=16, -34<=l<=34
Reflections collected	28098
Data [*I*>2σ(*I*)]	7880
Parameters	547
Restraints	204
Goodness-of-fit on F^2	1.063
Final R indices [*I*>2σ(*I*)]	R1 = 0.0379, wR2 = 0.0891
R indices (all data)	R1 = 0.0504, wR2 = 0.0967
Largest diff. peak and hole (e/Å^3)	0.404, -0.391